

TRANSACTIONS

American Society for Metals

VOL. XLV

1953

TECHNICAL PROGRAM AND REPORTS OF OFFICERS AMERICAN SOCIETY FOR METALS—34th ANNUAL CONVENTION, PHILADELPHIA, OCTOBER 18 to 24, 1952

FOR purposes of record and for the benefit of members who were not in attendance at the Thirty-fourth Annual Convention of the Society, held in Philadelphia, October 18 to 24, 1952, the Programs of the Technical Papers and Educational Lectures together with the Reports of Officers for 1952 are herewith published in full.

Seminar on Modern Research Techniques in Physical Metallurgy

Saturday, October 18

Benjamin Franklin Hotel, 9:30 A.M.

Metallographic Methods

Chairman: David Turnbull, General Electric Co.

Optical Microscopy, by George L. Kehl, Columbia University.

Electron Microscopy and Diffraction, by Robert D. Heidenreich, Bell Telephone Laboratories.

Intermission

Crystal Growth and Crystal Boundary Techniques, by Bruce Chalmers, University of Toronto.

Ballroom, Benjamin Franklin Hotel, 2:00 P.M.

Diffraction Methods

Chairman: Roman Smoluchowski, Carnegie Institute of Technology

X-Ray Diffraction Techniques, by Charles S. Barrett, University of Chicago.

Diffuse Scattering of X-Rays, by B. E. Warren and B. L. Averbach, Massachusetts Institute of Technology.

Intermission

Pole Figure Determinations, by A. H. Geisler, General Electric Co.

Techniques and Applications of Neutron Diffraction, by C. G. Shull, Oak Ridge National Laboratory.

Ballroom, Benjamin Franklin Hotel, 8:00 P.M.

Demonstration Lecture

Chairman: Morris Cohen, Massachusetts Institute of Technology

Electron Emission Studies of Metallurgical Problems, by Erwin W. Muller, Pennsylvania State College.

Sunday, October 19

Ballroom, Benjamin Franklin Hotel, 9:30 A.M.

Mechanical Methods

Chairman: O. T. Marzke, Naval Research Laboratory

Deformation of Single Crystals, by Earl R. Parker and Jack Washburn, University of California.

High Speed Strain Measurements, by George R. Irwin, Naval Research Laboratory.

Intermission

Internal Friction, by Professor Charles A. Wert, University of Illinois.

Ballroom, Benjamin Franklin Hotel, 2:00 P.M.

Ferromagnetic and Radioactive Methods

Chairman: Frederick Seitz, University of Illinois

Ferromagnetic Domains, by H. J. Williams, Bell Telephone Laboratories.

Radioactive Tracers, by M. B. Bever, Massachusetts Institute of Technology.

Intermission

Radioaction Damage as a Research Technique, by Sidney Siegel, North American Aviation, Inc.

Monday, October 20

Ballroom, Benjamin Franklin Hotel, 9:30 A.M.

Creep-Rupture and Recrystallization

Co-Chairmen: A. M. Bounds, Superior Tube Co.

C. L. Clark, Timken Roller Bearing Co.

Influence of Grain Size on High Temperature Properties of Monel, by Paul Shahinian and J. R. Lane, members of the Metallurgical Division, Naval Research Laboratory, Washington, D. C.

Creep and Rupture of Chromium-Nickel Austenitic Stainless Steels, by E. J. Dulis, G. V. Smith and E. G. Houston, Research Laboratory, United States Steel Co., Kearny, N. J.

Recrystallization and Grain Growth in Alpha Brass, by S. L. Channon, Kaiser Aluminum and Chemical Corp., Spokane, Wash., and H. L. Walker, Head, Department of Mining and Metallurgical Engineering, University of Illinois, Urbana, Ill.

Creep-Rupture and Recrystallization of Monel From 700 to 1700 °F, by N. J. Grant, associate professor, and A. G. Bucklin, staff member, Department of Metallurgy, Massachusetts Institute of Technology, Cambridge, Mass.

Ballroom, Convention Hall, 2:00 P.M.

High Temperature Phases

Co-Chairmen: M. A. Scheil, A. O. Smith Corp.

Otto Zmeskal, Illinois Institute of Technology

Microconstituents in High Temperature Alloys, by H. J. Beattie, Jr., physicist, and F. L. VerSnyder, metallurgist, General Electric Co., Thomson Laboratory, West Lynn, Mass.

Sigma Formation and Its Effect on the Impact Properties of Iron-Nickel-Chromium Alloys, by A. M. Talbot and D. E. Furman, Research Laboratory, International Nickel Co., Inc., Bayonne, N. J.

Mechanism of the Carburization of Some Stainless Steels, by J. B. Giacobbe, metallurgist, Superior Tube Co., Norristown, Pa.

The Electrolytic Separation and Some Properties of Austenite and Sigma in 18-8-3-1 Chromium-Nickel-Molybdenum-Titanium Steel, by T. P. Hoar, Dept. of Met., University of Cambridge, England, and K. W. J. Bowen, Research Dept., Imperial Chemical Industries, Birmingham, England.

Tuesday, October 21

Ballroom, Benjamin Franklin Hotel, 9:30 A.M.

Phase Transformation

Co-Chairmen: H. J. Elmendorf, American Steel & Wire Co.
R. I. Jaffee, Battelle Memorial Institute

- The Effect of Composition on the Temperature of Spontaneous Transformation of Austenite to Martensite in 18-8 Type Stainless Steel*, by G. H. Eichelman, metallurgist, American Brass Co., Waterbury, Conn., and F. C. Hull, manager, Metallurgical Section, Westinghouse Electric Corp., E. Pittsburgh.
- The Effect of Silicon on the Tempering of Martensite*, by A. G. Allten and P. Payson, assistant director of research, Crucible Steel Company of America, Harrison, N. J.
- The Mechanism and Kinetics of the First Stage of Tempering*, by C. S. Roberts, Metallurgical Laboratories, Dow Chemical Co., Midland, Mich., B. L. Averbach, assistant professor, and M. Cohen, professor of physical metallurgy, Massachusetts Institute of Technology, Cambridge, Mass.
- The Order-Disorder Transformation Viewed as a Classical Phase Change*, by F. N. Rhines, professor of metallurgy, and J. B. Newkirk, Carnegie Institute of Technology, Pittsburgh.

Ballroom, Convention Hall, 2:00 P.M.

Hardenability

Co-Chairmen: M. J. Day, Armour Research Foundation
Malcolm F. Hawkes, Carnegie Institute of Technology

- An End-Quench Test for Determining the Hardenability of Carburized Steels*, by F. X. Kayser, research metallurgist, R. F. Thomson, head, Metallurgy Department, and A. L. Boegehold, assistant to general manager, Research Laboratories Div., General Motors Corp., Detroit.
- The Influence of Boron on Case Hardenability in Alloy Carburizing Steels*, by C. F. Jatzak, research metallurgist, and E. S. Rowland, chief metallurgical engineer, Timken Roller Bearing Co., Canton, Ohio.
- Effect of Carbon Content on 18-4-1 High Speed Steel*, by A. H. Grobe, research metallurgist, and G. A. Roberts, chief metallurgist, Vanadium-Alloys Steel Co., Latrobe, Pa.
- Correlation of Machinability With Inclusion Characteristics in Resulphurized Bessemer Steels*, by L. H. VanVlack, process metallurgist, United States Steel Co., Pittsburgh.

Wednesday, October 22

Ballroom, Benjamin Franklin Hotel, 9:00 A.M.

A.S.M. Annual Meeting

Edward DeMille Campbell Memorial Lecture, by Dr. Cyril Stanley Smith, Director, Institute for the Study of Metals, Chicago, entitled *Microstructure*.

Chairman: Dr. John Chipman

Ballroom, Convention Hall, 2:00 P.M.

Research

Co-Chairmen: H. E. Flanders, University of Utah
J. F. Libsch, Lehigh University

- The Effect of Temperature on the Rolling Texture of Plastically Deformed Low Carbon Steel Strip*, by Norman P. Goss, Cold Metal Products Co., Youngstown, Ohio.
- Determination of Oxygen in Metals and Metal Oxides by the Isotopic Method*, by A. D. Kirshenbaum and A. V. Grosse, Research Institute of Temple University, Philadelphia.
- The Indium-Arsenic System*, by T. S. Liu, Horizons, Inc., Cleveland, and E. A. Peretti, acting head, Department of Metallurgy, University of Notre Dame, Notre Dame, Ind.

Thursday, October 23

Ballroom, Convention Hall, 9:30 A.M.

Mechanical Properties

Co-Chairmen: Alfred Bornemann, Stevens Institute of Technology
Peter Payson, Crucible Steel Co. of America

The Effect of Quenching and Tempering on Residual Stresses in Manganese Oil-Hardening Tool Steel, by H. J. Snyder, research associate, Mellon Institute of Industrial Research, Pittsburgh.

X-Ray Measurement of Residual Stress in Hardened High Carbon Steel, by A. L. Christenson, research metallurgist, and E. S. Rowland, chief metallurgical engineer, Timken Roller Bearing Co., Canton, Ohio.

The Endurance Limit of Temper-Brittle Steel, by R. D. Chapman, research metallurgist, and W. E. Jominy, chief metallurgist, Research, Chrysler Corp., Detroit.

Plastic Stress-Strain Relations of Alcoa 14S-T6 for Variable Biaxial Stress Ratios, by Joseph Marin, professor of engineering mechanics, L. W. Hu and J. F. Hamburg, Dept. of Engineering Mechanics, Pennsylvania State College, State College, Pa.

Ballroom, Convention Hall, 2:00 P.M.

Temper Brittleness

Co-Chairmen: J. W. Spretnak, Ohio State University
R. F. Thomson, General Motors Corp.

The Effect of Various Heat Treating Cycles Upon Temper Brittleness, by J. D. Jaffe and D. C. Buffum, Watertown Arsenal Laboratory, Watertown, Mass., and F. L. Carr, National Research Corp., Cambridge, Mass.

Effect of Hardness on the Level of the Impact Energy Curve for Temper-Brittle and Unembrittled Steel, by F. L. Carr, National Research Corp., Cambridge, Mass., M. Goldman, Battelle Memorial Institute, Columbus, L. D. Jaffe and D. C. Buffum, Watertown Arsenal Laboratory, Watertown, Mass.

Transverse Mechanical Properties in an SAE 1045 Forging Steel, by A. H. Grobe, research metallurgist, Vanadium-Alloys Steel Co., Latrobe, Pa., Cyril Wells, member of staff, and R. F. Mehl, director, Metals Research Laboratory, Carnegie Institute of Technology, Pittsburgh.

The Determination of the Plastic Constants of Metals by the Ultrasonic Pulse Technique, by M. B. Reynolds, Knolls Atomic Power Laboratory, General Electric Co., Schenectady, N. Y.

Friday, October 24

Ballroom, Convention Hall, 9:30 A.M.

Elevated Temperature Properties

Co-Chairmen: J. G. Jackson, William Steel Jackson & Son
V. H. Patterson, Climax Molybdenum Co.

Temperature Dependence of the Hardness of Pure Metals, by J. W. Westbrook, The Knolls, Research Lab., General Electric Co., Schenectady, N. Y.

Hardness of Various Steels at Elevated Temperatures, by F. Garofalo, P. R. Malenock and G. V. Smith, Research Laboratory, United States Steel Co., Kearny, N. J.

Some Properties of a Nodular Iron at Elevated Temperatures, by M. S. Saunders, graduate student, and M. J. Sinnott, associate professor of chemical and metallurgical engineering, University of Michigan, Ann Arbor, Mich.

Accelerated Strain Aging of Commercial Sheet Steels, by L. R. Shoenberger, research engineer, and E. J. Paliwoda, research engineer, Jones and Laughlin Steel Corp., Pittsburgh.

ASM EDUCATIONAL LECTURES*All Sessions in Ballroom, Convention Hall***Monday, October 20**

4:30 and 8:00 P.M.

Behavior of Metals at Low Temperatures

Chairman: C. W. MacGregor, University of Pennsylvania

Behavior of Single Crystals and Pure Metals, by R. M. Brick, Department of Metallurgy, University of Pennsylvania.*Influence of Mechanical Variables*, by J. R. Low, Jr., Knolls Atomic Power Laboratory, General Electric Co., Schenectady, N. Y.*Influence of Metallurgical Factors*, by C. H. Lorig, assistant director, Battelle Memorial Institute, Columbus, Ohio.**Tuesday and Wednesday, October 21 and 22**

4:30 P.M.

Gases in Metals

Chairman: I. R. Kramer, Horizon Titanium, Inc., Washington, D. C.

Fundamental Metallurgical and Thermodynamic Principles of Gas-Metal Behavior, by D. P. Smith, professor emeritus, Princeton University, Princeton, N. J.*Gases in Nonferrous Metals and Alloys*, by L. W. Eastwood, assistant director of research, Kaiser Aluminum Co., Spokane, Wash.*The Behavior of Gases in Liquid Iron and Steel*, by D. J. Carney, chief development metallurgist, United States Steel Co., Chicago.*The Behavior of Gases in Solid Iron and Steel*, by C. E. Sims, assistant director, Battelle Memorial Institute, Columbus, Ohio.**Tuesday and Wednesday, October 21 and 22**

8:00 P.M.

Metallurgical Tools for Alloy Conservation and Increased Production

Chairman: M. J. Day, Armour Research Foundation

All Lectures by J. Alfred Berger, acting department head

Department of Metallurgical Engineering, The University of Pittsburgh

*Significance of Chemical Analyses in Alloy Classification and Mechanical Properties.**Progress in Spectrography and X-Ray Diffraction Analyses and Techniques.**The Effects of Alloy Substitution on the Fundamentals of Hardening Metals.**Boron and Rare Earths in Alloy Conservation and Production.*

**ANNUAL MEETING OF
AMERICAN SOCIETY FOR METALS***Philadelphia, Wednesday, October 22, 1952—9:00 A.M.*

The annual meeting was called to order by President John Chipman. The order of business was:

1. President's address
2. Report of the Treasurer
3. Report of the Secretary
4. Presentation of ASM Teaching Awards
5. ASM Foundation for Education and Research
6. Election of officers

The report of the election of officers appears on page 26.

ANNUAL ADDRESS OF THE PRESIDENT

JOHN CHIPMAN, *President**Thirty-fourth Annual Meeting, Philadelphia, October 22, 1952*

THE past year has been one of solid accomplishment on the part of your Society. Your officers and trustees have endeavored throughout the year to emphasize and to build up the Society's educational programs. We have always been an educational society devoted to the advancement and dissemination of knowledge concerning metals. Never in the history of the Society have these objectives been overlooked. But during this past year our activities aimed at these objectives have been strengthened and broadened, with the result that our contribution to the strength of the nation is becoming daily more important.

Your education committee has been active and successful in planning educational programs for the national convention, in developing teaching aids such as motion pictures on metallurgical subjects, and in fostering educational activities of the chapters. Practically every chapter is engaged in some sort of educational program, and these programs are of more value to the practical technical man of industry than those of any other technical society. The communities in which chapters are located have come to regard the ASM chapter as the fountainhead of all knowledge on metallic subjects.

Your advisory committee on metallurgical education has initiated several new programs during the year. One has been the establishment of teaching awards for proficiency and excellence in the teaching of metallurgy in the colleges. Three awards of \$2000 each are to be made this morning to young teachers of metallurgy. You should realize that the recipients of these awards are outstanding young metallurgists who would command in industry several times the salary that their colleges can pay them.

I hope that these awards will encourage them and their colleagues to feel that the importance of their work to the national well-being is recognized and appreciated by their fellow scientists and engineers.

Another recent innovation at the collegiate level is the appropriation of funds for visiting professorships in metallurgy. It is hoped that this will make it possible for students of metallurgy to have the advantages of lectures by specialists in various phases of metallurgy and thus to broaden the teaching programs in metallurgy in many colleges in the United States and Canada.

For some years your Society has been concerned by the insufficient numbers of students of metallurgy enrolled in the colleges. We have prepared bulletins and pamphlets and have distributed these in considerable numbers in the high schools of the country with the purpose of attracting more students into metal engineering fields. It

now appears that metallurgy is not alone in its need for more recruits. In June 1951 the number of students graduating from the colleges in science and engineering was less than the demand by at least 40,000. The number of students enrolled in the engineering colleges has undergone a steady decline. In 1949 and 1950 there were about 50,000 graduates each year in the United States and Canada in engineering and scientific fields. In 1951 there were 38,000, in 1952 about 25,000. This year the number will be well under 20,000 and next year still smaller. In a world in which a nation's strength depends upon its technology, this is an alarming situation, especially when it is compared with the reported 100,000 per year in Russia.

In his visits to some 25 chapters, your President has drawn attention to the nation's need for more engineering students. Many chapters have taken an active interest in recruiting science students for the colleges and have sent representatives to the local high schools with this purpose in view. These efforts are beginning to bear fruit.

Another new activity of your Society is being carried out with the cooperation of the National Science Teachers Association. This is a contest in the high schools and junior high schools of the United States and Canada in which the student prepares a "project" related to science or engineering. A number of prizes and awards were given to students and to the schools they represent. The total amount of the awards, which together with administrative costs amounted to \$10,000, was supplied by your Society. There has been much talk about the need for more scientists, but as yet the only technical society which has given financial backing to the "Future Scientists of America Foundation" in their direct approach to junior and senior high school students is the American Society for Metals.

The growing scarcity of engineers is reflected in an increased demand for graduates of technical and vocational institutes. These schools are noncollegiate in character; many, in fact, are at the high school level. In many cases the training includes work in metals — for example, welding, heat treating, metallography and testing. Several of our chapters have maintained contacts with local schools, but by and large the Society has given them very little attention. Your trustees are convinced that there is an important job the Society can do in this field, and a new committee has been formed, with Horace Knerr as chairman, to view the problem on a nation-wide scale and recommend whatever action seems appropriate. Important results have been achieved by this committee during the year.

Thus you can see that your Society is active along the educational front from the practical man of industry or the boy in junior high school through high school or technical institute and into the colleges.

Another recent activity of your Society is the establishment of a new international journal of the science of metals. The need for such a journal has developed rapidly in recent years with the in-

creased application of physics and chemistry in the study of metals. A year ago, during the World Metallurgical Congress, a few people from each participating country were brought together to discuss the preliminary plans. As a result, a proposal was sent to metallurgical, chemical and physical societies throughout the free world. At the present moment there are 14 such societies in 11 countries cooperating with ASM, and the first issue of the new "Acta Metallurgica" under editorship of Bruce Chalmers is due to appear in January 1953. It is not expected that all members of our Society will be interested. To many it will appear too theoretical or perhaps highbrow. Nevertheless, it will be a valuable aid to high education and it will enhance the position of metallurgy among the sciences and will bring physics and chemistry to the metallurgist. For those members of ASM who want the new journal, it will be available at half price.

The officers and trustees, as usual, have been busy. There were five meetings of the board of trustees — on October 31, 1951, and on January 30, June 2, July 31 and October 21, 1952. Your President visited 25 chapters, and members of the board visited 14.

A new series of regional group meetings has been undertaken for the purpose of bringing the national organization into closer contact with individual chapters. In these meetings the chairman and vice-chairman-elect from some five to eight chapters in a district have sat down with the Secretary and usually with some member of the board of trustees in an all-day session on chapter problems. During the year the following groups participated:

PACIFIC NORTHWEST

Seattle, Portland, Vancouver, Spokane, Richland

NEW ENGLAND

Boston, Worcester, Springfield, Hartford, Providence, New Haven

ATLANTIC CENTRAL

New York, Philadelphia, Washington, Baltimore, Lehigh Valley, York

OHIO - MICHIGAN

Toledo, Detroit, Saginaw Valley, West Michigan

NORTHEASTERN OHIO - WESTERN PENNSYLVANIA

Northwest Pennsylvania, Pittsburgh, Youngstown, Warren, Canton-Massillon, Akron, Cleveland

In the month of May this year the entire membership of the Society was saddened by news of the deaths of two of our beloved past-presidents: Dr. Marcus Grossmann passed away in Pittsburgh and Dr. George B. Waterhouse in Boston. It is with the deepest regret that we record this great loss to the metallurgical profession.

For the first time the Society held a midwinter meeting. This was strictly a technical meeting for the purpose of presentation and discussion of technical papers. It was held in Pittsburgh on January 31 and February 1. The sessions were well attended and contained some valuable technical papers which have subsequently appeared in

TRANSACTIONS. The next such meeting will be in Los Angeles the week of March 23, 1953, as a part of the Western Metal Congress.

Your Society has been sweeping off the cobwebs of isolationism and has worked for the establishment of more cordial relations among the metallurgical societies of the world. Full justification of this policy is seen in the tremendous success of the World Metallurgical Congress which was held last year. You will be interested in the very attractive volume of some 835 pages published by the Society giving the full story of that meeting and containing the papers presented. The reports of European conferees will appear in another book which is scheduled to be published in the near future by the OEEC in Paris.

I have just returned from a visit to Europe in which I had the pleasure of representing ASM at a meeting of the Italian Metallurgical Association. In Italy, and in other countries that I visited, I found people enthusiastic about the World Metallurgical Congress and keenly appreciative of the part which ASM played in sponsoring and organizing it. From my conversations with many of the leading metallurgists in Europe, I can say that the prospects are bright for a second World Metallurgical Congress to be held in Europe perhaps in 1955 or 1956. I have assured them that ASM is ready to cooperate in every way to assure another conspicuously successful Congress.

And now I come to what I hope will prove to be the outstanding event of the year, the proposed establishment of the American Society for Metals Foundation for Education and Research. Your trustees have given much careful thought to the problem of how we might best insure the continued growth of our educational activities. The healthy state of our treasury during recent years has given us confidence that we have achieved that goal of early planning, a figure for total assets which is twice the annual budget. The excess above this goal we now propose to set aside in a special fund whose income can be used for purposes of education and research.

There is an additional motive, and a very practical one, for establishment of the Foundation. Recent revisions of the revenue laws have changed the status of the income of tax-exempt institutions. At the present time the net income of all tax-exempt organizations is subject to review each year by federal tax authorities. The establishment of the Foundation will provide a place where any excess income can be invested to provide future income for educational purposes. The board has studied this proposal with great care and has had the advice of competent attorneys and tax consultants. We believe it will accomplish two important objectives: (a) It will provide a mechanism for the Society's continued support of education and research in the field of metals. (b) It will safeguard a substantial portion of the Society's funds for future growth of these activities.

The proposal for establishment of the American Society for Metals Foundation for Education and Research will be presented to

you this morning. I urge you to join with the trustees in unanimously approving the proposal.

It is customary in the President's report to record the high spots of the previous meeting. You are all fully aware that the most distinctive feature of the 33rd annual convention was the First World Metallurgical Congress which accompanied it. It is an understatement to point out that this congress was sponsored solely by ASM. It was conceived in the fertile mind of your Secretary and it was brought to successful fruition by his inspired and untiring efforts.

It is appropriate to record that at the concluding banquet of the Congress three silver medals bearing the insignia of the World Metallurgical Congress were presented by ASM trustees: the first to Mr. Charles E. Wilson, director of Defense Mobilization, who delivered the principal address; the second to Dr. Zay Jeffries, Director-General of the Congress; the third to Mr. Walter Jominy, President of ASM, sponsor of the Congress. It is also appropriate to mention that the trustees presented one solid gold medal of the same design — this one to Mr. William H. Eisenman.

Other events of the 33rd annual convention included the following: the President's Medal was awarded to Arthur Focke, past-president; the Henry Marion Howe Medal was issued to Dr. B. J. Lazan of the University of Minnesota; the Sauveur Achievement Award was presented to Robert F. Mehl, director of the Metals Research Laboratory, Carnegie Institute of Technology; the ASM Medal for the Advancement of Research was presented to Gwilym Price, president of Westinghouse Electric Corporation; and the ASM Gold Medal was presented to Paul Merica, president of the International Nickel Co. The Campbell Memorial Lecture was given by Dr. C. H. Lorig of Battelle Memorial Institute.

In conclusion I wish to thank the societies that are cooperating with the American Society for Metals to make the present meeting another outstanding success. These societies are: American Welding Society; American Institute of Mining & Metallurgical Engineers, Institute of Metals Division; Society for Non-Destructive Testing. It is through this kind of cooperation that the National Metal Congress has grown into an event of major importance to the nation. We look forward to its continuance in future years.

TREASURER'S REPORT

RALPH L. DOWDELL, *Treasurer*

This report on your Society covers the fiscal year ending August 31, 1952. This was again a year of efficient operation.

The carrying value of all securities, including accrued interest, was \$1,976,351.24 on July 14, 1952. On closing the year August 31,

1952, the carrying value of all securities including accrued interest was \$1,424,210.96.

The approximate market value of securities, including accrued interest on bonds, was \$1,636,763.65 on August 31, 1952, which represents an appreciation in dollar value of about \$212,552.69.

During the year the Board of Trustees authorized a grant to the American Society for Metals Foundation for Education and Research in the amount of \$575,000.00 out of prior years' earnings and \$75,000.00 out of the current year's earnings.

The cash account was decreased \$98,187.56 from last year, so that more funds could be invested.

There has been no fundamental change in investment policy for the portfolio over the past year.

Dividends and interest earned amounted to \$78,768.31 or about 3.98%, based on the carrying value, as compared to about 4.16% for the preceding year. With a lower proportion of stocks, the yield has been slightly lowered.

Corporate stocks constitute about 30% of the total investments, while last year they constituted about 38% of the total holdings.

Total income and expense for the year ending August 31, 1952, are as follows:

INCOME AND EXPENSE

Fiscal Year ended August 31, 1952

Income	\$1,424,814.98
Expense	<u>1,266,643.90</u>
Net Income	\$ 158,171.08
Appropriated for Educational Purposes	<u>140,524.47</u>
Unappropriated Net Income	\$ 17,646.61

The approximate income and its disposition for the fiscal year ending August 31, 1952, are shown in the following tabulation:

ASM INCOME AND ITS DISPOSITION

Fiscal Year Ended August 31, 1952

	Income Per Cent	Disposition of Income Per Cent
METAL PROGRESS	40	33
Metal Exposition	26	19
Membership—Gross dues	16	
Returned to Chapters		7
Expense		3
Book Publishing	6	6
Interest and Dividends	5	
METALS HANDBOOK	4	2
METALS REVIEW	1	3
TRANSACTIONS	1	3
General Administration		12
Educational Projects		10
Miscellaneous	1	1
Added to Surplus		1
	<u>100</u>	<u>100</u>

AUDITED BALANCE SHEET

AMERICAN SOCIETY FOR METALS—August 31, 1952

ASSETS

CASH			\$ 157,438.43
SECURITIES (approximate market or redemption prices aggregate \$1,627,647.97)			
Bonds, stocks and land trust certificates—			
at cost	\$1,415,095.28		
Accrued interest	9,115.68	1,424,210.96	
CASH SURRENDER VALUE OF LIFE INSURANCE			76,713.85
NOTE AND ACCOUNTS RECEIVABLE			
Note receivable	\$ 15,000.00		
Accounts receivable:			
Advertising accounts	\$12,637.42		
National Metal Exposition—Philadelphia—October, 1952	28,653.50		
Miscellaneous	14,695.07	55,985.99	\$ 70,985.99
Less allowance for doubtful accounts		2,000.00	68,985.99
INVENTORIES—at cost or lower			
Bound or unbound publications, books, paper stock, etc.	\$ 162,622.02		
Less allowance for obsolescence	6,000.00	156,622.02	
OTHER ASSETS			
Cash advance from United States Government for expenses in connection with World Metallurgical Congress	\$ 13,459.61		
Officers, employees, and sundry accounts and deposits	21,717.26	35,176.87	
REAL ESTATE (at cost less allowances for depreciation)			50,930.47
OFFICE FURNITURE, FIXTURES, AND EQUIPMENT (at cost less allowances for depreciation)			53,040.81
DEFERRED CHARGES			
Prepaid exposition expenses:			
National Metal Exposition—Philadelphia—October, 1952	\$ 64,814.31		
Western Metal Show—Los Angeles—March, 1953	2,305.79	\$ 67,120.10	
Prepaid sundry expenses	10,074.57		
Prepaid insurance	4,322.08	81,516.75	
			<u>\$2,104,636.15</u>

The large disposition item called "Educational Projects" contains the following items of which most are for educational purposes:

ASM Foundation for Education and Research	\$64,024.47	(carrying value)
Teaching Awards and Expenses	6,500.00	
Chapter Educational Activities	5,000.00	
Second World Metallurgical Congress	15,000.00	
Program with National Science Teachers' Association	15,000.00	
ASM Visiting Lectureship	10,000.00	
Building Fund	25,000.00	
	<u>\$140,524.47</u>	

The gross income from dues was \$239,686.71 of which \$99,029.82 was returned to local chapters. The combined assets of the 82 local chapters have risen to about \$248,000 which is an increase of about \$29,000 over the previous year.

LIABILITIES, RESERVES, AND SURPLUS

LIABILITIES

Accounts payable:

For purchases, expenses, etc.	\$ 33,731.69	
Payroll taxes and taxes withheld from employees	3,592.44	
For apportionment of dues to local chapters	3,061.16	\$ 40,385.29

Advance from United States Government for expenses in connection with World Metallurgical Congress	13,459.61	\$ 53,844.90
--	-----------	--------------

INCOME APPROPRIATED FOR EDUCATIONAL PURPOSES

122,887.44

RESERVES

For METALS HANDBOOK	\$ 86,630.74	
For conventions	60,000.00	
For dues paid in advance	50,000.00	
Campbell Memorial lecture fund	15,000.00	
H. M. Howe medal fund	5,000.00	
Sauveur achievement award	5,000.00	221,630.74

DEFERRED INCOME

National Metal Exposition—Philadelphia—October, 1952	\$ 401,319.50	
Western Metal Show—Los Angeles—March, 1953	2,345.00	403,664.50

SURPLUS

Balance at September 1, 1951	\$1,778,537.62	
Add unappropriated net income for the year..	17,646.61	\$1,796,184.23
Less grant to American Society for Metals Foundation for Education and Research—Note A	493,575.66	1,302,608.57

Note A—During the year, the Board of Trustees authorized a grant to American Society for Metals Foundation for Education and Research in the amount of \$575,000.00 out of prior years' earnings and \$75,000.00 out of earnings of the current year, payable in cash or securities of equivalent value. Effective as of July 15, 1952, securities having a carrying value of \$557,550.68, and cash in the amount of \$49.45, were transferred to the Foundation, of which \$493,575.66 was charged to surplus and \$64,024.47 was charged to current earnings. However, this transaction is subject to the approval of the members voting at the annual meeting of the Society to be held October 22, 1952.

\$2,104,636.15

The income from interest earned on investments was \$78,768.31.

Both TRANSACTIONS and METALS REVIEW were distributed to the membership at a net cost to the Society of about \$44,541.97 and \$21,403.76 respectively.

The net assets of the American Society for Metals are approximately \$2,104,636.15.

This year the success of the Society is again reflected in the good management by Secretary William H. Eisenman. Your Treasurer also acknowledges the kind assistance of Secretary Eisenman, Assistant Treasurer A. A. Hess, Trust Officers A. W. Marten and W. W. Horner of the Cleveland Trust Company, members of the Finance Committee and members of the Board of Trustees of the American Society for Metals.

AUDITED INCOME AND EXPENSE STATEMENT

AMERICAN SOCIETY FOR METALS—Year ended August 31, 1952

INCOME

METAL PROGRESS—monthly publication	\$ 606,140.52
Metal Exposition	396,161.29
Memberships	141,077.49
Dividends and interest earned	78,768.31
Book sales	74,845.48
ASM METALS HANDBOOK sales	36,644.50
METALS REVIEW—monthly publication	35,388.24
Conferees to World Metallurgical Congress	18,500.00
TRANSACTIONS sales	9,657.35
General reprints	7,350.61
Discount earned	7,050.34
Microstat service	3,924.17
Sundry sales, etc.	3,709.97
Sale of purchased books	3,379.57
Increment in cash value and dividends on life insurance.....	1,891.09
Net gain on sale of securities	326.05

TOTAL INCOME\$1,424,814.98

EXPENSES

METAL PROGRESS—monthly publication	\$ 494,741.92
National Metal Exposition—Detroit—October, 1951	294,795.54
Books published	88,384.85
General expenses	67,354.68
Grant to American Society for Metals Foundation for Education and Research	64,024.47
METALS REVIEW—monthly publication	56,792.00
Memberships	53,081.27
Expenditures from appropriations	44,383.07
TRANSACTIONS	44,199.32
Secretary's office	35,463.24
ASM METALS HANDBOOK	31,419.76
Headquarters	21,739.73
Accounting department	19,620.32
World Metallurgical Congress	13,165.10
Medals, awards, and lectures	11,299.57
Winter meeting	5,966.39
National committees	5,966.25
Conferees to World Metallurgical Congress	5,206.83
Miscellaneous merchandise	4,755.79
Trustees	3,181.70
Regional conferences	2,475.69
President's office	2,432.92
Booth equipment	1,752.53
Technical books	1,676.75
Library	671.75
Research and educational contribution	500.00

TOTAL EXPENSES\$1,375,051.44

NET INCOME\$ 49,763.54

Income appropriated for educational purposes—as authorized by the Board of Trustees (\$76,500.00) less expenditures for the year (\$44,383.07) included in above expenses 32,116.93

UNAPPROPRIATED NET INCOME\$ 17,646.61

Board of Trustees,

September 29, 1952

American Society for Metals, Cleveland, Ohio.

We have examined the balance sheet of American Society for Metals as of August 31, 1952, and the related statements of income and expenses and surplus for the year then ended. Our examination was made in accordance with generally accepted auditing standards, and accordingly included such tests of the accounting records and such other auditing procedures as we considered necessary in the circumstances.

In our opinion, the accompanying balance sheet and statement of income and expenses present fairly the financial position of American Society for Metals at August 31, 1952, and the results of its operations for the year then ended, in conformity with generally accepted accounting principles applied on a basis consistent with that of the preceding year.

ERNST & ERNST
Certified Public Accountants

ANNUAL REPORT OF THE SECRETARY

W. H. EISENMAN, *Secretary*

The American Society for Metals on October 1, 1952, had a total membership of 21,599—a gain of 6.6% since last October.

Of this number 18,421 or 85.3% were regular members, 1982 or 9.2% were sustaining members, 1092 or 5% were junior members. There were 54 honorary and life members, 50 on the armed services list.

PUBLICATIONS COMMITTEE

Sixteen persons constitute the membership of the Publications Committee for 1952, under the chairmanship of W. M. Baldwin, Jr., research professor, Case Institute of Technology, Cleveland. The members of the committee and their chapter affiliation are:

W. W. Austin, Jr., Birmingham; W. E. Bancroft, Hartford; J. A. Bennett, Washington; C. L. Clark, Canton-Massillon; A. H. Geisler, Eastern New York; M. F. Hawkes, Pittsburgh; E. I. Larsen, Indianapolis; E. M. Mahla, Philadelphia; F. T. McGuire, Tri-City; Peter Payson, New York; G. C. Riegel, Peoria; C. H. Samans, Calumet; J. W. Spretnak, Columbus; L. P. Tarasov, Worcester, and Ray T. Bayless, Secretary, Cleveland.

During the year the Committee reviewed 66 papers. Of this number 41 were approved and prepared in preprint form. 30 of these are scheduled for presentation at this Convention and publication in *TRANSACTIONS* and the remaining 11 are scheduled on the program for the Western Metal Congress to be held in Los Angeles the week of March 23, 1953, and also scheduled for publication in *TRANSACTIONS*.

The Publications Committee held a meeting May 27 and 28, at which time final arrangements for the technical program for this Convention were made.

EDUCATIONAL COMMITTEE

The Educational Committee for the year 1952 was composed of the following personnel: N. J. Grant, Boston, Chairman; M. J. Day, Pittsburgh; H. Y. Hunsicker, Cleveland; I. R. Kramer, Washington; F. G. Tatnall, Philadelphia; G. M. Enos, Purdue; N. C. Jessen, Akron; Ray McBrien, Rocky Mountain; R. F. Thomson, Detroit, and Ray T. Bayless, Secretary, Cleveland.

This Committee held one formal meeting on November 29, 1951, at which time the educational lectures for this Convention were arranged as well as those for the 1953 Convention. These lectures are:

1952

1. "Behavior of Metals at Low Temperatures"—3-lecture series by:
R. M. Brick, University of Pennsylvania
J. R. Low, Jr., General Electric Co.
C. H. Lorig, Battelle Memorial Institute
2. "Gases in Metals"—4-lecture series by:
D. P. Smith, Princeton University
L. W. Eastwood, Kaiser Aluminum Co.
D. J. Carney, United States Steel Co.
C. E. Sims, Battelle Memorial Institute
3. "Metallurgical Tools for Alloy Conservation and Increased Production"—4-lecture series by:
J. Alfred Berger, University of Pittsburgh

1953

1. "Fatigue."
2. "Surface Protection Against Wear."
3. "Surface Protection Against Corrosion."

The motion picture film entitled "Heat Treatment of Steels" is still in the process of preparation by Ohio State Research Foundation, under the guidance of Prof. J. O. Lord.

ADVISORY COMMITTEE ON METALLURGICAL EDUCATION

Members are: Alfred Bornemann, Stevens Institute of Technology, Chairman; D. S. Eppelsheimer, Missouri School of Mines; F. M. Klayer, Louisville; V. N. Krivobok, New York; J. L. Libsch, Lehigh Valley; C. K. Lockwood, Montreal; W. E. Mahin, Chicago; J. P. Nielsen, New York; W. O. Philbrook, Pittsburgh; E. C. Wright, Birmingham; J. B. Austin, Rep. of ASM Board of Trustees.

The President covered the activities of this committee in his report.

ASM TECHNICAL COMMITTEES ADVISORY TO THE NAVY

The program has continued through which the Society assists the U. S. Navy in technical problems relating to conservation of scarce metals. In cooperation with the Minerals and Metals Advisory Board in Washington, ASM has now established a total of five technical advisory committees, each dealing with metal conservation in a different unit of naval equipment. In each instance, the ASM committee has been able to recommend ways and means for conserving scarce metals, either through substitution of one alloy for another or by a change in processing procedure or design.

Conservation of scarce metal has been widely discussed in indus-

try, Government and the press during the past year. ASM members, better than other groups, understand the importance of conservation. But most important, ASM members have the high technical competence to deal with conservation at the engineering level and to make final decisions which result directly in conservation of scarce metal without sacrifice of the functional performance of operating equipment. Thus these ASM members represent the highest authority on the actual feasibility of conservation in any instance. The Society is proud of the example which these members are setting through the work of the ASM advisory committees.

METALS HANDBOOK COMMITTEE

Demand for the current edition of the METALS HANDBOOK has continued at a high level, and an additional 10,000 copies were printed in June of 1952. The HANDBOOK Committee held no meetings during the year.

SPECIAL LIBRARIES ASSOCIATION

For the third consecutive year the Metals Section of the Special Libraries Association is holding its fall regional meeting in conjunction with the National Metal Congress. The purpose of the meeting is to discuss matters of literature handling and documentation that are of mutual interest to both librarians and metallurgists.

The Section is also sponsoring a booth at the National Metal Exposition, designed as a miniature working library and reference service.

Three sessions have been held on Monday afternoon, October 20, and on Tuesday morning and afternoon, October 21. The first meeting on "New Horizons in Literature Searching" was planned primarily to discuss the work of a Special Libraries Association Committee on international standardization in literature classification, and to assess the possibilities of machine techniques for literature searching.

The committee's work is based on the well-established ASM-SLA classification system designed by a joint committee of the two societies four years ago.

The papers on Tuesday covered such subjects as availability of research reports, how to obtain unclassified material from the Government, foreign-language literature and translations, and the relationship between technical research, management and library services.

TRANSACTIONS

Since the last National Metal Congress, Vol. 44 and Vol. 44A of TRANSACTIONS were published and distributed to the membership

in April 1952. Vol. 44 totals 1232 pages and constitutes 61 articles with their discussions. It contains all of the papers presented at the October 1951 Convention held in Detroit, together with the papers presented at the Midwinter Meeting held in Pittsburgh on January 31 and February 1, 1952, and also interim papers received during the year that were not presented at a convention. The president, secretary and treasurer's reports for 1951 and other current items of record were included in Vol. 44 together with a report of the Convention.

Vol. 44A contains the 12 papers (335 pages) presented at the seminar on "Metal Interfaces" held on Saturday and Sunday, October 13 and 14, 1951, during the National Metal Congress and Exposition, Detroit. This seminar was sponsored by the American Society for Metals, the subject being selected by a committee appointed by the Board of Trustees. The personnel of this committee was: J. H. Hollomon, Chairman; J. B. Austin, R. M. Brick, Morris Cohen, M. Gensamer, L. R. Jackson, L. K. Jetter, O. Marzke, D. McCutcheon, E. R. Parker and Clarence Zener.

Preparation and coordination of the series of subjects and solicitation of speakers were carried on by R. M. Brick.

PREPRINTS

Forty-one papers were prepared in preprint form and distributed to those members of the Society who requested them.

This includes thirty papers presented at this Metal Congress, and eleven papers which will be among those presented at the Western Metal Congress.

The total number of pages for the 1952 preprints is 738. A total of 45,000 preprint copies was distributed free to the membership.

METAL PROGRESS

The number of editorial pages, 680, is fairly constant over the years. Revenue advertising has shown a gratifying improvement, due to intensive work by the expanded number of representatives in the field noted in last year's report.

While a considerable amount of editorial space has been given to the production, properties and uses of the "new" metals like titanium, zirconium, and thorium (including a notable summary of the metallurgical problems involved in the construction of atomic power plants), this is warranted by today's trends in metal progress and only points up the continued attention given to such timely topics as boron-treated and other alloy steels, heat treatment, and heat and corrosion resistant metals and alloys.

Two issues were almost pre-empted by the World Metallurgical Congress—one containing the papers contributed by overseas con-

ferees. Another issue contained four important papers on the manufacture, rolling and heat treatment of deep drawing sheet. Considerable attention has been given during the year to the metallurgical problems of the foundry.

Early in the calendar year 1952 some additions were made to the editorial staff. Marjorie R. Hyslop (editor of *METALS REVIEW* since 1934) was made managing editor of *METAL PROGRESS*, with responsibility for getting out the magazine. Floyd E. Craig was employed as director of art and typography. E. C. Wright, long with National Tube Co. and now head of the department of metallurgical engineering at the University of Alabama, accepted appointment as consulting editor for *METAL PROGRESS* in the field of steel refining and manufacture.

METALS REVIEW

METALS REVIEW, during the 12 months from October 1951 through September 1952; published a total of 700 pages—an increase of 68 pages over the preceding 12 months. This increase reflects the general progress and expansion of the Society. Space devoted to news of chapter activities, doings of members, and headquarters actions remains about the same as in the past.

Specific figures are as follows:

News	197 pages or 28%
ASM Review of Metal Literature.....	375 pages or 55%
Miscellaneous	128 pages or 13%

The pages devoted to miscellaneous matters include the employment service, meeting calendars, and advertising.

The Society again published in the February issue the biographies and photographs of the junior members to assist them in obtaining employment during the coming year.

The Metal Show section was published in September.

In February 1952 the staff was expanded by the appointment of Betty Bryan as associate editor. Miss Bryan was formerly an editorial assistant for both *METALS REVIEW* and *METAL PROGRESS*.

It should be borne in mind that the splendid work of Battelle Memorial Institute, which produces for the ASM (for publication in *METALS REVIEW*) the annotations of technical articles in the field of metals in some 800 world publications, is collected and indexed annually in a bound volume.

Some libraries with indexing services available to industry offer some of the various subject headings covered by *METALS REVIEW*, but the subscription price for this coverage duplicating *METALS REVIEW* subjects would be \$410.00 per year.

The 8th volume of the REVIEW OF METAL LITERATURE was published this year, containing over 10,000 annotations, and made available to members.

These eight volumes constitute the most thorough, up-to-date and complete literature service for the last eight years that is available any place in the world.

BOOKS

During the past year, a total of 25,827 books published by the Society was sold to members and others. This figure includes 1837 copies of the 1948 METALS HANDBOOK.

During this period 7 titles were added to the publication list. These are:

TRANSACTIONS of the ASM, Vol. 44
How to Organize for Success—By W. H. Eisenman
Metal Interfaces—Seminar by 12 authors
Residual Stress Measurement—By 4 authors
Elements of Hardenability—By M. A. Grossmann
Review of Metal Literature—Vol. 8
Proceedings of the 1951 World Metallurgical Congress

Following titles are now in preparation:

Cast Bronze—By Harold J. Roast
Revision of "Principles of Heat Treatment"—By M. A. Grossmann
Revision of "Engineering Alloys"—By N. E. Woldman

The three educational lectures presented at this convention will also be available in book form. They are:

Behavior of Metals at Low Temperatures
Gases in Metals
Metallurgical Tools for Alloy Conservation and Increased Production

A number of the books published by the Society were made available to junior members of the Society at a greatly reduced cost, the purpose being to bring the price of the books within the range of the students' ability to purchase.

SEMINAR ON MODERN RESEARCH TECHNIQUES IN PHYSICAL METALLURGY

The Seminar on Modern Research Techniques in Physical Metallurgy this year was an outstanding success. It was divided into five important and interesting sessions with the meeting room filled to capacity. This interest is a great compliment to the Committee and the seminar speakers and assures a continuance of this important annual event.

The Committee on arrangements consisted of the following personnel:

R. M. Brick, Philadelphia, Chairman; Harvey Brooks, Boston;

Bruce Chalmers, Ontario; Morris Cohen, Boston, Coordinator; L. K. Jetter, Oak Ridge; O. T. Marzke, Washington; E. R. Parker, Golden Gate; A. D. Schwope, Columbus; Frederick Seitz, Peoria; Roman Smoluchowski, Pittsburgh, and David Turnbull, Eastern New York.

The papers presented during this seminar will be available in book form at a later date.

JUNIOR MEMBERSHIP

The junior members of the ASM, and other students whose course requirements provided for work in metallurgy, have been given an eight-page booklet which contains data sheets reproduced from METAL PROGRESS and other items of information of interest to the young engineer.

These were distributed through the heads of the metallurgical departments and through the deans of engineering.

JUNIOR EMPLOYMENT

In the February issue of METALS REVIEW, all ASM junior members completing their metallurgical work in June were introduced to the members of the Society and to many others by having published their pictures, biography and other items of information relative to their availability for future employment.

An additional service was organized this year for the summer employment of metallurgical and other engineering students in the United States and Canada.

The summer employment service was designed to assist engineering students who are members of the ASM. However, all engineering students were urged to make use of the jobs listed if they wished to do so.

There was no charge to either the student or the employer for this ASM summer service which offered 1858 job opportunities.

LOSANA GOLD MEDAL

It is a pleasure to report that the president of the Society, Dr. John Chipman, was the recipient of the Losana Gold Medal presented by the Italian Metallurgical Society on September 20 this year.

We have been informed the medal was given in recognition not only of Dr. Chipman's achievements in the field of metallurgy but also in appreciation of the cordial reception the Italian conferees received when they attended the first World Metallurgical Congress.

NATIONAL METAL CONGRESS

The National Metal Congress now in session speaks for itself. It is again the united effort of four national technical societies whose combined programs have for years constituted an epoch in the number and quality of the papers on the researches and investigations in the metals industry. These are—

The American Society for Metals
American Institute of Mining & Metallurgical Engineers
Institute of Metals Division
American Welding Society
Society for Non-Destructive Testing.

YOUNG ENGINEERS' DAY

As related in the President's report, the Society and all the chapters have been energetically active in endeavoring to increase enrollment in engineering schools. The American Society for Metals, as the engineering society of the metals industry, accepts its full share of responsibility in endeavoring to supply adequate engineering talent for the industry. The ASM realizes that the metals industry is the largest employer of all types of engineers and produces 40% of the income of the nation's economy.

Furthermore, the Society recognizes that approximately 50% of all students now enrolled in engineering schools will find employment and their life's work in the metals industry. Consequently, it was determined that a great advantage would be gained if the engineering students within 150 miles of the convention city could be brought in contact with the exhibitors and the exhibits in the National Metal Exposition.

Invitations were extended, through the president and the dean of engineering, with follow-up contact work carried on by a representative of the Society, to the following schools for the students in all branches of engineering to be the guests of the Society on Friday, October 24:

Brooklyn Polytechnic Institute
Catholic University of America
City College of New York
Columbia University
Drexel
George Washington University
Lafayette University
Lehigh University
Johns Hopkins
Manhattan College
New York University
Newark College of Engineering
Penn State

Pratt Institute
Swarthmore
St. Joseph College
Stevens Institute of Technology
Temple University
University of Delaware
University of Maryland
University of Pennsylvania
University of Virginia
Villanova
Princeton
Rutgers
Annapolis

The invitation received a most cordial reception, and approximately 2500 engineering students—1700 from outside Philadelphia—will visit and study the exposition on October 24, Friday.

The Society will absorb the expense of bus transportation, and the Young Engineers will be the guests of the Society at a buffet luncheon served at the Exposition.

NATIONAL METAL EXPOSITION

The National Metal Exposition continues to grow and grow, not only in size but quality. One needs but to travel the miles of aisles and observe the displays, to recognize that more and more a visit to the Metal Show is a *must* for every metal producing and fabricating metals engineer.

The Metal Show is recognized as an institution not only by manufacturers who display their products but by executives and the engineering staffs that use their products.

This year there are two new features to the Metal Show in addition to Young Engineers' Day.

The first is an endeavor to dress up the Show. Decorating four large halls for a Metal Show has always been a terrific problem. Cloth, the old standby for some 33 years, is giving way this year to the beginning of a new decor scheme in which metals and pictorial presentation of metal progress constitute the decorative media. This year is "only the beginning"—and while some cloth has been used, you may expect that each year from now on will show more and more the decorative and artistic possibilities of "dear old Metal."

The second innovation is the red carpet. It's being used on the basis that nothing is too good for the comfort of the customer (the members and the visitors to the Metal Show) and also to ease your way along the two miles of aisles in the Show. So the ASM is delighted to roll out the royal carpet for its royal guests.

And so pass the years of the ASM in an ever-changing degree of accomplishment but always in a forward and advancing direction. The past year has been no exception since it recorded unbelievable and significant achievements in every field of endeavor to which the ASM has turned its attention. If I should try to enumerate them I would again be repeating the statements of the record of achievement already presented.

I trust you have been aware that this record is your record. You and you alone by your faithful and conscientious devotion to your Society have made it possible. Your continued support and cooperation will guarantee even greater accomplishments in the years to come.

Presentation of ASM Teaching Awards

Established in 1952 by action of the Board of Trustees of the ASM, the purpose of the \$2000 award for teachers of metallurgy is to recognize the young teacher of metallurgy by encouraging his ability and accomplishments, and, additionally, as a result of the teacher's wider acceptance and prestige, to attract more graduates to the teaching of metallurgy, and a greater enrollment of students in departments of metallurgy.

By following through with these purposes, it is hoped that the need for engineering skill in American industries will be more nearly satisfied.

Winners of the first of these annual awards were Joseph W. Spretnak, associate professor of metallurgy at Ohio State University; Arthur A. Burr, associate professor of metallurgical engineering at Rensselaer Polytechnic Institute; and Robert D. Stout, professor in the department of metallurgy at Lehigh University. Each of these three awardees received a check in the amount of \$2000 and a scroll.

PRESIDENT'S REMARKS

ON THE ESTABLISHMENT OF THE AMERICAN SOCIETY FOR METALS
FOUNDATION FOR EDUCATION AND RESEARCH

The Board of Trustees received on January 31 from Secretary Eisenman a written report suggesting the creation of a separate foundation dedicated to the advancement of the technology of metals through educational activities and research; that the matter received consideration at the meetings of the Board of Trustees on January 30 and June 2 of this year (1952). At the meeting on June 2, the members of the Board expressed themselves as favoring such a foundation, to which the Society would make a substantial contribution during the current year and might make further contributions as conditions may justify in the future. The Society's legal and tax counsel were thereupon authorized to formulate a detailed plan for the creation of such a foundation.

Articles of Incorporation and a Code of Regulations for the proposed foundation were presented to a special meeting of the Board of Trustees held on July 31, 1952. After extended consideration of the matter, the Board of Trustees at that time approved the creation of the foundation and authorized the transfer to it of securities valued at \$650,000. Of this amount \$75,000 was charged to income for the year ended August 31, 1952.

The foundation, which has been named "American Society for Metals Foundation for Education and Research", was incorporated in the State of Ohio under date of August 1, 1952. The corporate

purpose of the foundation, as stated in its Articles of Incorporation, is

* * * "to provide for the advancement and dissemination of scientific knowledge, particularly with respect to the technology of metals, for the use and benefit of the public at large, either through educational activities and research carried on by the Foundation or through the support of educational and research activities in established organizations and institutions."

The Articles of Incorporation provide that the property of the Foundation shall be held as an endowment fund in perpetual trust for the purpose stated above, and that the income from the property of the Foundation shall be used exclusively for such purpose.

The management of the Foundation is vested in a board of five trustees consisting of the President and four most recent Past Presidents of the American Society for Metals, who are to serve for five-year terms on a rotating basis, one being added each year. The Board of Trustees is authorized from time to time to determine the specific use to which the income of the Foundation shall be devoted, within its corporate purpose as stated above. In the event of the dissolution of the Foundation, the Board of Trustees is required to dispose of its assets, in trust, to further its stated purpose, without preference in favor of any member, officer or trustee, upon such terms and conditions, consistent with its purpose, as the Board shall determine.

It was the sense of the Board of Trustees, at the meeting on July 31, that the contribution of \$650,000 to the foundation should receive the approval of the membership of the Society, by affirmative action of a majority of the members present and voting at this annual meeting October 22, 1952. The contribution was made, therefore, upon the condition that such approval should be forthcoming.

The Board hopes to receive the unanimous approval of the membership. I now request the Secretary to present the resolution confirming action by the Board at its meeting on July 31, 1952.

The Secretary read the following resolution and moved its adoption:

RESOLVED, that the action taken by the Board of Trustees of American Society for Metals at its meeting on July 31, 1952, authorizing the creation of an educational and research foundation to be known as "American Society for Metals Foundation for Education and Research", be and the same hereby is ratified and approved.

The motion being duly seconded was unanimously adopted by the meeting.

Past President Walter E. Jominy in accepting the funds for the establishment of this Foundation from Secretary Eisenman said:

"I am honored to receive these funds in the name of the

AMERICAN SOCIETY FOR METALS FOUNDATION FOR EDUCATION AND RESEARCH.

"This is the beginning of a most worthy enterprise, one that I am sure we will be proud of. So far as I know this is the first time that a technical society has been able from its own funds, to endow a research foundation.

"Since we will use only the income from these securities, there will not be much to spend until the end of the year. We are having a meeting of the Trustees of the Foundation tomorrow morning to formulate policies and consider any suggestions. If any of you have ideas of worth-while projects please communicate them to one of the trustees. Their names have been published in METALS REVIEW and I will read them here—John Chipman, Ralph Wilson, Arthur Focke, Harold Work and myself.

"We will do our utmost to see to it that the income from these securities will be spent for the worthy purposes set forth in our Charter."

In presenting to Past-President Walter E. Jominy an order for the funds establishing the ASM Foundation for Education and Research, Secretary Eisenman said:

"On behalf of American Society for Metals, I hand you herewith an order on the Cleveland Trust Company, of Cleveland, Ohio, directing it to deliver to you the securities set forth on the list of securities designated Schedule A hereto attached and made a part hereof.

"These securities are being delivered to you in satisfaction of the grants aggregating \$650,000 authorized by the Board of Trustees of American Society for Metals on July 31, 1952, and are being delivered to you in accordance with the terms and subject to the limitations contained in the resolution of the Board of Trustees of the Society authorizing the grants, which were that the delivery of these securities is made upon the condition that said grants be approved by the members of American Society for Metals by vote of a majority of the members present and voting at this annual meeting of its members.

"This condition has now been fulfilled, and I have the authority to present these funds to the Foundation."

ELECTION OF OFFICERS

PRESIDENT CHIPMAN: We will now proceed with the election of officers. Complying with the Constitution, I appointed in March 1952 the following nominating committees, selected from the list of candidates suggested by the eligible chapters prior to March 1, 1952.

Chairman—Gilbert E. Doan—Lehigh Valley Chapter
W. B. Cheney—Fort Wayne Chapter R. T. Waddington—Western Ontario Chapter
J. W. Queen—New Jersey Chapter
Howard E. Boyer—Springfield Chapter Gilbert S. Schaller—Puget Sound Chapter
A. B. Wilder—Pittsburgh Chapter
H. H. Heinisch—Toledo Chapter J. Y. McClure—North Texas Chapter

The Nominating Committee met in Chicago on May 20, 1952, and made the following nominations for the various offices:

FOR PRESIDENT

Ralph L. Wilson, Director of Metallurgy,
Timken Roller Bearing Co., Steel & Tube Div., Canton, Ohio, for 1 year.

FOR VICE-PRESIDENT

James B. Austin, Director, Research Laboratories,
U. S. Steel Co., Kearny, N. J., for 1 year.

FOR TRUSTEE

Harry B. Knowlton, Chief Engineer, Materials Engineering,
International Harvester Co., Chicago, for 2 years.

A. O. Schaefer, Vice-President in Charge of Engineering
and Manufacturing, Midvale Co., Philadelphia, for 2 years.

FOR SECRETARY

A committee of past-presidents of the ASM nominated
William H. Eisenman, Cleveland, for 2 years.

I have been informed by the Secretary that no additional nominations have been received prior to July 15, 1952, for any of the vacancies appearing on the Board of Trustees; consequently the nominations were closed. I now call upon the Secretary to carry out the provisions of the Constitution in respect to the election of officers.

SECRETARY EISENMAN: Conforming with the provisions and requirements of the constitution of the American Society for Metals, I hereby cast the unanimous vote of the members for the election of the aforementioned candidates who were nominated May 20, 1952.

The President then introduced the newly elected officers. The President-elect then said a few words of acceptance.

PRESIDENT CHIPMAN: Has anyone present anything to bring before the meeting for the good of the Society? If not, then a motion to adjourn is in order. Motion made and carried.

At 10:30 a.m. President Chipman called the Campbell Memorial Lecture Meeting to order and proceeded with his introduction of the twenty-seventh Campbell Memorial Lecturer, Dr. Cyril Stanley Smith, who presented his lecture entitled "Microstructure". This is published in full in this volume of the TRANSACTIONS (page 533).

ASM ANNUAL DINNER

PHILADELPHIA—OCTOBER 23, 1952

On Thursday evening, October 23, members and guests assembled in the Ballroom of the Benjamin Franklin for the Annual Dinner of the Society. The attendance was in excess of 500.

Those persons seated at the speakers' table were: A. M. Bounds, Superior Tube Co., Norristown, Pa.—Chairman, Philadelphia Chapter, ASM; J. W. Spretnak, Ohio State University, Columbus—Recipient of ASM Teaching Award; A. A. Burr, Rensselaer Polytechnic Institute, Troy N. Y.—Recipient of ASM Teaching Award; Harry B. Knowlton, International Harvester Co., Chicago—Trustee-Elect, ASM; Noah A. Kahn, New York Naval Shipyard, New York—President, Society for Non-Destructive Testing; A. O. Schaefer, Midvale Co., Philadelphia—Trustee-Elect, ASM; Ralph L. Dowdell, University of Minnesota, Minneapolis—Treasurer, ASM; James B. Austin, United States Steel Co., Kearny, N. J.—Trustee, ASM; H. J. French, International Nickel Co., New York—Past-President, ASM; Cleo F. Craig, American Telephone and Telegraph Co., New York—Recipient of 1952 ASM Medal for the Advancement of Research; John C. Warner, Carnegie Institute of Technology, Pittsburgh—Principal Speaker; John Chipman, Massachusetts Institute of Technology, Cambridge—President of ASM and Recipient of 1952 Sauveur Achievement Award; Albert E. White, University of Michigan, Ann Arbor—Past-President of ASM; Robert F. Mehl, Carnegie Institute of Technology, Pittsburgh—Recipient of 1952 ASM Gold Medal; Ralph L. Wilson, Timken Roller Bearing Co., Canton, Ohio—Vice-President and President-Elect, ASM; Walter E. Jominy, Chrysler Corp., Detroit—Recipient of 1952 ASM Past-President's Medal; Cyril Stanley Smith, Institute for the Study of Metals, University of Chicago, Chicago—1952 Campbell Memorial Lecturer; N. A. Nielsen and E. M. Mahla, E. I. duPont de Nemours and Co., Wilmington, Del.—Recipients of 1952 Howe Medal; James T. MacKenzie, American Cast Iron Pipe Co., Birmingham, Ala.—Trustee, ASM; J. B. Johnson, Wright-Patterson Air Force Base, Dayton—Trustee, ASM; George A. Roberts, Vanadium-Alloys Steel Co., Latrobe, Pa.—Trustee, ASM; Harry W. Ghenn, American Viscose Corp., Marcus Hook, Pa.—Secretary, Philadelphia Chapter, ASM; W. H. Eisenman—Founder Member and Secretary, ASM.

Presentation of President's Medal

The annual presentation of the President's Medal was made by John Chipman to Walter E. Jominy, the thirty-first president, who served the Society so ably in 1951.

Presentation of Howe Medal

In honor of Dr. Henry Marion Howe, the distinguished scientist, often called the dean of American metallurgists, the Board of Trustees in 1922 established the first of its medals. The rules governing the award of this medal make the provision that it be awarded to the author or authors of the paper judged of highest merit, presented

before the ASM and published during any one year in the TRANSACTIONS of the Society.

The 1952 award was made to the authors of the paper entitled "Carbide Precipitation in Type 304 Stainless Steel—An Electron Microscope Study" which was published in Vol. 43 of TRANSACTIONS, 1951, page 290. The authors who were honored are E. M. Mahla and N. A. Nielsen. They were each presented with a certificate, a gold medal and a bronze replica.

Edward deMille Campbell Memorial Lecture

In 1926 the Society established the Edward deMille Campbell Memorial Lecture and each year since that time has invited a distinguished scientist to present this lecture. The 1952 lecturer was Dr. Cyril Stanley Smith, Director, Institute for the Study of Metals, University of Chicago, and to commemorate this lecture a scroll certifying to that event was presented to Dr. Smith.

Honorary Membership

It was announced that an Honorary Membership in the ASM was conferred on Dr. Cecil Henry Desch of England.

Albert Sauveur Achievement Award

In 1934 the Board of Trustees established an award consisting of a metal plaque and certificate in honor of Dr. Albert Sauveur, distinguished metallurgist and for many years an honorary member of the ASM. The purpose of this award is to recognize a metallurgical achievement which has stood the test of time and stimulated others along similar lines to the extent that a marked basic advance has been made in the metal arts and sciences. The 1952 candidate was John Chipman, Head, Department of Metallurgy, Massachusetts Institute of Technology, who was presented by Dr. A. E. White, following the reading of the citation of Dr. Chipman's accomplishments. Past-president Jominy then conferred the award.

Conferring of the ASM Medal for the Advancement of Research

The 1952 ASM Medal for the Advancement of Research was awarded to Cleo F. Craig, President of the American Telephone and Telegraph Co., in recognition of his consistent sponsorship, foresight, and influence in financing and prosecuting metallurgical research, which have helped substantially to advance the arts and sciences relating to metals.

In presenting Mr. Craig, H. J. French read the citation engrossed on the scroll which accompanies the medal. President Chipman then conferred the award. The citation is:

Metallurgical research forms an important part of the basic scientific studies carried on by the Bell System for the advancement of electrical communications. Cleo F. Craig, during his long service in the System as an engineer and as an executive in the management of operating and engineering activities, has taken keen interest in the improvement and extension of communication through research. As a member of the Board of Directors of Bell Telephone Laboratories for over eight years and subsequently as President of the American Telephone and Telegraph Company, he has supported and promoted metallurgical research by giving his active encouragement and approval to the Laboratories' programs.

Metallurgical advances have been made in magnetic alloys having permeabilities manyfold greater than were previously available. Economies in storage battery operation and improvements in cable sheath manufacture and performance have come from studies in lead alloys. Alloys have been developed which give long service in the billion electrical relay contacts in the telephone system and alloys which give great stability and other unique merit to vacuum tubes and electrical filtering devices. In the field of semiconductors, the application of metallurgical research methods to the preparation of germanium and silicon of extreme purity and of very precisely controlled impurity have formed an essential base for the invention and development of the transistor.

Conferring of Gold Medal of ASM

The Gold Medal of the ASM, established in 1943, recognizes the recipient for outstanding metallurgical knowledge and great versatility in the application of science to the metal industry, as well as exceptional ability in the diagnosis and solution of diversified metallurgical problems. President Chipman presented Robert F. Mehl, Head, Department of Metallurgy, Carnegie Institute of Technology, as the candidate for the 1952 award. In presenting him, Dr. Chipman read the citation engrossed on the scroll which accompanies the medal. President Chipman then conferred the medal award upon Dr. Mehl. The citation is as follows:

For twenty years Robert F. Mehl has exerted a powerful influence on the development of metallurgical education and fundamental research in the United States. His long tenure at the Carnegie Institute of Technology has been marked by a steady flow of well-educated undergraduates into the mills and laboratories of the metal industry, and an amount of research performed under his direction by graduate students, research assistants and faculty associates which has set standards and

defined trends in physical metallurgy that are well recognized in the profession.

In 1944 this influence was extended to South America, where, in Brazil, Dr. Mehl lectured for some time, both at the University of Sao Paulo and before the Brazilian Institute of Metals.

His own major researches began in 1931 with the initiation of comprehensive studies of Widmanstätten structures to determine the mechanisms by which solid-to-solid transformations occur in metals, and these have played an important part in the theoretical study of age-hardening phenomena (matters also intently studied by his laboratory).

Somewhat allied to these studies is his detailed investigation of the structure and mode of formation of pearlite, reported as a Campbell Memorial Lecture before the American Society for Metals in 1941. This had been preceded by fundamental studies on diffusion, crystal nucleation and grain growth, and all of these studies have had an important bearing on our present understanding of the microconstituents and the hardenability of steel.

It is difficult to imagine what the metallurgy of today would be like if it had not had the influence of Mehl and Mehl-trained men. The indirect influence which he has exerted on industrial metallurgy through the medium of his former students is even greater than his direct contributions. As an example of his direct and personal contributions to practical metallurgy may be cited the investigations he made for the Metallurgical Advisory Board during the late war. This work has been competently appraised as "probably the most important war-time contribution to gun tube manufacture from the standpoint of cost and time-saving, smooth production and clear understanding of the physical test results."

In 1950 the National Research Council of the National Academy of Sciences, in response to requests from the Armed Services, decided to set up a new Metallurgical Advisory Board. To lead this Board, especially in its formative years, they needed the services of the very best man that the metallurgical profession in this country could supply. Their choice of Robert F. Mehl for chairman of this important board has been fully justified by the Board's subsequent accomplishments. Those who have had the pleasure of serving on this Board under Mehl's leadership, during his leave of absence from Carnegie Institute of Technology, to handle this governmental assignment, can attest to the fact that he is not only an outstanding metallurgist but a competent organizer and a capable leader.

Address of the Evening

President Chipman then presented Dr. John C. Warner, President of Carnegie Institute of Technology, who was the main speaker of the evening. The title of his talk was "Freedom, Scholarship, and Centers of Learning", printed in full herewith:

FREEDOM, SCHOLARSHIP AND CENTERS OF LEARNING

Among the great intellectual and creative achievements of mankind we must count as one of the greatest the development of that tremendous body of knowledge known as natural science, including the methodology of science. Everyone agrees on the substantial contribution which the applications of natural science have made to the health and material welfare of mankind, but I believe natural science and its methods have played an equally important role through the contribution they have made toward liberating the mind of man from bondage to superstition, mysticism, and the dogmas of theology and politics. Indeed it seems impossible that philosophy, religion, the fine arts, the humanities, and the social sciences could have led us to a generally satisfying set of moral, ethical, spiritual and aesthetic values without the liberalizing influence of science which has given us natural, in place of supernatural, explanations of phenomena. Throughout recorded history, improvements in our understanding of natural phenomena have seemed to come hand in hand with improvements in our understanding and appreciation of things of the spirit, of man's relation to man, his relation to his universe, and his relation to society through political, social and economic organizations.

For many centuries great minds have held that the goal of civilization should be the betterment of mankind through the elevation of the individual. As you know, progress toward this goal has not been rapid and continuous—it has been slow and irregular. We have records of periods of brilliant intellectual and creative achievement among certain peoples. In these periods substantial progress was made toward our goal. On the other hand, we have knowledge from history of long periods, such as the Dark Ages, in which superstition, mysticism, and authority again ruled the mind of man, and the few who dared to continue the search for truth were persecuted outcasts—truly voices crying in the wilderness. These golden ages in the history of civilization resulted from brilliant intellectual and creative achievements in great centers of learning—in Athens, Alexandria, and Rome, then—after almost 1000 years—in Northern Italy, France, the British Isles and finally in almost all of Western Europe—more recently in the United States and in various members of the British Commonwealth of Nations.

What conditions are necessary for the establishment and growth of great centers of learning and the consequent great bursts of intel-

lectual and creative achievement? First of all, scholars and creative artists must have intellectual freedom—and I believe the prerequisite freedoms are best and most concisely stated in the Bill of Rights of our Constitution. Secondly, they must be respected by society—their fellow citizens must place value on their achievements. A corollary would say that our scholars and artists must have such support as will eliminate undue worry about providing the necessities of life for them and their families.

But the prime prerequisite is intellectual freedom. We in our time have seen the consequences of Fascist and Communist regimes on the physical and biological sciences, and we are conscious of a perversion of all scholarship in the humanities and social sciences. There has been a comparable deterioration in the creative arts—this story is told dramatically in a recent book “The Taming of the Arts” by Jelagin, a Russian violinist who is now fortunately a member of the Houston Symphony Orchestra. These regimes violate every principle in the Bill of Rights and no center of learning can exist in a society under the control of the Fascist or Communist Apparatus.

Centers of learning can develop and flower only in free societies—which protect our basic freedoms in the manner they have been protected in the constitutional monarchies and republics of the West. Thus, to progress toward our goal of improving the lot of mankind we must join with our colleagues in the other free countries to encourage learning by insuring intellectual freedom and providing adequate support for real scholars and creative artists. Our country by reason of its great resources, its youth, and its traditions has a special obligation and a special opportunity in this regard. Indeed, my confidence in the view that eventually all people on this earth will enjoy freedom will be determined to a great extent by how well we meet our obligations and seize our opportunity.

Let us then examine our situation concerning scholarly and creative work in centers of learning in this country—the past, the present, and the near future.

The Past: From the beginning, we have enjoyed the essential freedoms, not only in theory but in practice. No people under the sun have enjoyed greater individual liberty and opportunity. There was no lack of intellectual freedom but we did not until the present century give proper encouragement and support to scholars. We were too preoccupied with the economic and political development of a continent and we heaped honors and rewards upon our industrial and political leaders. To a great extent we still relied on Europe for new knowledge in the sciences and the humanities, and for new ideas and movements in the fine arts. Many of you are familiar with the foundation and growth of important centers of learning in this country following World War I. At least you are familiar with the rapid

growth of basic research and graduate education in the physical sciences during this period. With increasing frequency, important discoveries in science were made by Americans. I believe we can claim a similar flowering in the social sciences, the humanities, and the fine arts. Fortunately, we were well along on our way when World War II intervened and our scholars served us magnificently in that struggle.

So much for the past—How about the present and the near future?

The Present and the Near Future: I believe we have reasons for concern in two general areas: The first of these arises from what seem to me to be threats to our basic freedoms, and hence a threat to that prime prerequisite for scholarly and creative work, intellectual freedom. The second arises out of questions concerning our attitudes toward scholarly work and the nature of the support we have for it in America. In the second case I shall confine my remarks primarily to the physical sciences.

The Threats to Our Freedoms: Without discussing the serious external threat to our free way of life from aggressive world communism in the hands of the men in Moscow, what internal threats to our freedom can we discern? They are numerous, but I would like to mention four or five of them which to me seem especially important.

(1) The first of these arises from our reaction to the greatest of the external threats—communist aggression. Our desire to stop this aggression and our desire to protect our free institutions against attack through infiltration and subversion has set off a wave of red-hunting, loyalty-oath swearing, and guilt-by-association which, in this country, has never been equaled in scope and has rarely been equaled in intensity. Many of our freedoms are threatened, and for some persons essential freedoms undoubtedly have already been violated. The situation presents the difficult but basic problem—how can we protect our free institutions without violating the basic rights of the individual? I believe part of the problem arises from failure to recognize the difference between heresy and conspiracy. The communist ideology is a heresy that we need not fear when it is openly, and not secretly, professed, advocated, and debated. Our deep-seated faiths in the dignity of man and in our free institutions constitute the most powerful ideas in the world. They are more than a match in the open idea market for the communist ideology. On the other hand, the communist movement from Lenin to Stalin is much more than a heresy; it is a conspiracy. It is a secret, underground movement which seeks to attain its ends, not by the normal political and educational processes, but by undermining the very conditions required if opposing views are to be free to compete for acceptance. Although we must defend the honest heretic, conspiracy cannot be tolerated in a free society. But I don't know of a single subversive engaged in the communist conspiracy who has been weeded out by the application of the noncommunist oath. We must weed them out by intelligent action in our own organizations and institutions. I am confident that our

colleges and universities can keep their own houses in order—so can business enterprises—so can the labor organizations—so can the branches, subdivisions and departments of local, state, and national government and they can do this better if not hampered by ineffective legislation, which often undermines rather than protects our freedom.

(2) Another threat to our freedoms stems from the steadily increasing centralization of political as well as economic power in the Federal Government. Such concentration of power is not *per se* a threat to our freedoms. It might not threaten our freedoms if we could safely assume that we will maintain that delicate balance and separation of powers provided in the framework of our Government by the Constitution, and that our elected and appointed officials will unfailingly make intelligent decisions for the common good. However, we have already seen some freedoms sold for promises of security, we have seen certain segments of our people given advantages at the expense of other segments in exchange for political support, and we have steadily seen more and more of the control of private institutions and enterprises transferred to Government. Frankly, I don't know how much planning and control we can have without a significant abridgment of individual liberty—and certainly we must expect and applaud social and political changes in our institutions which keep them in harmony with the realities of each age. I do know, however, that any system of planning and control which requires the Congress to enact such vague legislation that a bureaucracy must be established to finish the legislative job, administer the law, and sit in judgment on alleged infractions, will inevitably infringe upon our most precious individual rights and freedoms. In performing these functions a bureaucrat must pass judgment on the ends to which our society shall be directed, and a bureaucrat, who determines the ends of government and decides who conforms to them, is far along the path to being a dictator.

(3) The third threat to our freedoms which I wish merely to mention is an indirect one but, nevertheless, a real one. As the most powerful free nation in the world our declared purpose is to develop enough military and economic strength to defend western civilization, in the hope that a society which respects the dignity of the individual will survive. Yet we have operated during the past 15 to 20 years under fiscal policies which generate such powerful inflationary pressures that they could lead to economic chaos and the consequent loss of the very values we propose to defend. And chaos breeds dictators.

(4) I see a fourth threat to our freedoms in the existing low state of public morality and lack of integrity in public office. There is an alarming tendency to take bribes, overlook misdemeanors in office, and to spread the big lie and then so support it by propaganda that the public believes it to represent the truth.

(5) Finally, I must speak of a threat to our freedoms stemming from a method of teaching which is prevalent in too many of our colleges and secondary schools. This method requires students to memorize, repeat, and submit to the authority of a text book or a lecturer.

Submission to indoctrination by authority is not proper education for those who are to assume responsibility for citizenship in a democracy. Some great educational leaders have recognized this threat to our freedoms and have insisted that proper teaching must develop students to be self-reliant in learning and in the application of knowledge to the solution of the real problems which they encounter in their professions and as citizens. Some real progress has been made and the idea is getting strong support in at least a few centers of learning. This type of teaching is difficult and expensive, and I fear the financial difficulties of our colleges, brought about by the inflationary pressures, will encourage educators to seek economies by having teachers simply pour factual information into students in large classes. Society must find a way to give our good colleges and universities the support they need to prepare their students for independent responsible citizenship.

These threats to our freedoms have their roots in the confusion of the times which result, I believe, from the growing complexity of the problems before society. These problems are so complex that they are no longer amenable to solution by precedent, opinion, hunch, or surmise. These problems with increasing frequency have technical aspects which make it necessary for us to rely more and more on our scholars and professional people for aid in their solution. Consider for example the problems about atomic energy which faced us following Hiroshima: international control—government vs. private control—potential civilian uses and applications—what information should be held secret for purposes of security—security clearance of personnel—and a host of other problems. I doubt that any member of the Congress or of the executive branch of the Government or of the judiciary possessed the basic knowledge needed to propose solutions, and the scientists and engineers of necessity were called upon to help solve these public problems.

To preserve our freedoms we must pay whatever price is required to work our way out of the confusion resulting from past mistakes and to find sound solutions to our problems. One price of freedom may involve some sacrifice of national sovereignty as we have known it in the past. Perhaps we must set our sights on a world culture, a worldwide expanding economy and a world at peace under world law.

Attitudes Toward and Support for Scholarly Work: Why should we be concerned about our attitudes toward scholarly work and the support we have for it? (I have previously indicated that I would confine my remarks on this subject primarily to the physical sciences.) I shall proceed by posing some definite questions and discussing them.

(1) Is the present and prospective substantial support for university research really of the right kind to develop great centers of learning? Most of this support is through contracts with Government agencies—to a great extent the Armed Services and the Atomic Energy Commission; some is through contracts with industries and

trade associations; and a relatively small percentage of it is "free money"—gifts, grants and regular university income—which can be used at the discretion of the university and its scholars to support such fundamental research as at the time is considered most important. The last kind of support is really the right kind. With "free money", the scholar can be supported in following up any interesting and potentially fruitful observation or idea, even though it may very drastically change the specific nature of his research. University contract research covers the range from the purely applied to the purely basic, but all of it in a sense is project research—proposals must be submitted and progress reports must be written at regular intervals. Contracts for the purely applied are of no aid to a university in meeting its obligations as a center of learning. Those supporting basic research have been of great help and we should be thankful for them in a period when "free money" has been so scarce in university budgets. It is surprising and greatly to the credit of some of the Government agencies, especially the Office of Naval Research, that we have had substantial support through contracts for basic research. However, this form of support for basic research is not the best kind for various reasons: in the first place a proposal outlining a definite field of research must be submitted; support if granted is for too limited a period and there is always the question of whether the contract will be renewed; the support when granted cannot be used to follow up important observations and ideas if they lead very far afield from the original proposal; and no board, committee, agency administrator, or the scholar himself can predict ahead of time the most fruitful direction a scholarly investigation will take.

Although we must give great credit to the Government agencies that have had the wisdom to fill the post-war vacuum in support of fundamental research, it does seem strange that the major support has come from the Armed Services. If fundamental research is to be supported by tax money, why not through the National Science Foundation with grants of essentially free money to institutions and individual scholars? I am sure that all privately endowed, independent universities and institutes of technology would prefer to get "free money" from their alumni, from private individuals and from private industry rather than from any Government agency, including the National Science Foundation.

(2) Do our scholars and potential scholars in the physical sciences and engineering, and our university administrations have the proper aims, ambitions, ideals, and attitudes in the search for new knowledge and new ideas? In a few institutions the answer is pretty close to "Yes", and these are the greatest centers of learning in America. Too often the university administration has the wrong aims, ambitions, and attitudes—it may use "free money" potentially available for the support of scholarly work for frills, for messianic projects in higher education, or for fine buildings which are intellectually sterile inside. Then, too, I believe many university administrations have not made a proper effort to get free money through gifts and grants to support scholarly work—oftentimes rationalizing the lack of effort

by pointing to the ease of getting support for research from Government agencies or on projects sponsored by industry. I must make an exception as far as the construction and operation of great tools for nuclear research are concerned. I do not believe any university, certainly not the privately endowed universities, could under present circumstances find enough free money to finance these operations. In addition, I might express the opinion that a university administration which sets up and promotes an applied research institute or experiment station, and stops at that, is not fulfilling the institution's obligation as a center of learning.

Some of our good scholars in the physical sciences do have the proper aims, attitudes and ideals. These scholars, oftentimes with only modest support of the right kind, have been responsible for great intellectual achievements. But many of our scholars and potential scholars have been weaned away from pure science to the applied, and some have yielded to the temptation of building research empires through Government and industrial contracts—they become administrators and promoters of team research directed toward some fairly definite practical end, or the group is engaged in filling in the gaps in some area of knowledge which is needed in application. Useful as such work may be, it is no substitute for new generalizations, new ideas and new comprehensive theories, which to me constitute the essence of new science. It seems to me that new science comes primarily as a result of individual intellectual effort, not usually from project research or team research. If much new science, in the sense that I have used the term, has resulted from the very substantial support presumably given to basic research since World War II, I am not aware of it.

Then, too, I have the impression that too many of our potentially great scientists are yielding to the strong pressures on them to take leave from their university posts to engage in applied research; some are under great pressure to live a life of intellectual chaos by running from committee meeting to committee meeting from coast to coast, even including missions and meetings abroad. The situation poses the difficult problem of just where the able scientist's duty lies in view of the present world situation. Each must, of course, make up his own mind, taking into account how the best long-range result can be accomplished. But I feel sure that the present situations and practices do not represent our best effort at meeting our obligation and seizing our opportunity to establish great centers of learning in America.

In the long run, emergency or no emergency, war or no war, we can serve humanity best by preserving intellectual freedom and by supporting and honoring real scholarly and creative achievement.

CONFIDENTIAL TECHNICAL MEETING ON REFRACTORY TYPE MATERIALS FOR HIGH TEMPERATURE APPLICATIONS

November 24 and 25, 1952—Hotel Carter—Rainbow Room, Cleveland, Ohio

This two-day confidential meeting, sponsored by the American Society for Metals with the cooperation of the National Advisory Committee for Aeronautics, was attended by more than 400 persons, who had obtained military clearance to participate. Assisting in the arrangements for this meeting were the members of the committee appointed by President John Chipman. These persons are as follows: Roger A. Long, committee chairman; Ray T. Bayless, committee secretary; G. M. Ault, W. L. Badger, K. M. Bartlett, Howard Cross, A. W. F. Green, J. J. Harwood, Willson Hunter, J. B. Johnson, E. G. Pekarek, B. Pinkel, J. C. Redmond, Howard Scott, L. F. Yntema and W. H. Eisenman.

Morning Session—November 24 (9:30 A.M.–12:00 Noon)

Main Subject: *Molybdenum and Its Alloys*

Chairman: Dr. W. M. Baldwin, Jr., Case Institute of Technology

Arc Cast Molybdenum and Molybdenum-Base Alloys—Their Manufacture, Fabrication and Properties, by R. M. Parke, General Electric Co. (10 min.)

Sintered Molybdenum and Molybdenum-Base Alloys—Their Manufacture, Fabrication and Properties, by Howard Scott, Westinghouse Electric Co. (10 min.)

Related Discussion (5 min. each)

- (a) *Fabrication Procedures for Molybdenum*, by L. F. Yntema, Fansteel Metallurgical Corp.
- (b) *Fabrication of Arc Cast Molybdenum Sheet*, by J. S. Sohn and H. Hanick, Wright Aeronautical Co.
- (c) *Effect of Controlled Swaging on Properties of High Purity Commercial Molybdenum Metal*, by K. Dike, NACA.

Panel Session on Above Subjects* (30 Minutes)

The Elevated Temperature Properties of Molybdenum and Molybdenum-Base Alloys, by Howard Cross, Battelle Memorial Institute. (10 min.)

Protective Coatings for Molybdenum or Molybdenum-Base Alloys, by Ralph Wehrmann, Fansteel Metallurgical Corp. (15 min.)

Related Discussion (5 min. each)

- (a) *Protective Coatings on Molybdenum Intended for Use as Turbine Engine Components*, by P. Turner and K. M. Bartlett, Thompson Products, Inc.
- (b) *NBS Ceramic Type Coatings for Molybdenum*, by D. G. Moore, National Bureau of Standards.
- (c) *Cladding of Molybdenum*, by R. I. Jaffee, Battelle Memorial Institute.

Panel Session on Above Subjects* (30 Minutes)

— Recess 12:15 o'clock for Luncheon —

Afternoon Session—November 24 (1:30–5:00 P.M.)

Main Subject: *Ceramics and Intermetallics*

Chairman: Winston Duckworth, Battelle Memorial Institute

*Panel sessions were made up of chairman as moderator and all speakers.

Ceramic Bodies for Use at Elevated Temperatures and Their Evaluations, by R. F. Geller, Bureau of Standards. (15 min.)

Related Discussion (5 min. each)

- (a) *Negative Coefficients of Thermal Expansion in Ceramic Materials*, by F. K. Davey, Rutgers University.
- (b) *Refractory Materials for High Temperatures*, by G. M. Butler, Carborundum Co., or staff member.
- (c) *Ceramic Bodies for Use at Elevated Temperatures and Their Evaluation—Discussion on Stress Rupture Testing*, by Tom Shevlin, Ohio State University.
- (d) *Lithium Aluminosilicate Refractories*, by Bartram Dilks, Jr., Stupakoff Ceramic and Mfg. Co.
- (e) *Thermal Expansion Effects in Refractory Bodies*, by N. P. Thielke, Pennsylvania State College.
- (f) *Comments as to the Use of Ceramic Type Materials in High Temperature Applications*, by H. Z. Schofield, Battelle Memorial Institute.

Panel Session on Above Subjects* (30 Minutes)

Intermetallics—New Type Refractory Alloys, by Louis Marchi or staff member, Armour Research Foundation. (15 min.)

Molybdenum Disilicide, Properties at Elevated Temperatures, by W. Maxwell, NACA. (10 min.)

Titanium Disilicide, Properties at Elevated Temperatures, by R. Long, NACA. (10 min.)

Combinations of Carbides and Borides—Powder Ceramics, by Gordon Findley, Norton Co. (10 min.)

Related Discussion (5 min. each)

- (a) *Intermetallics by Powder Metallurgy—Structural Consideration*, by George Stern, American Electro Metals.
- (b) *Application of the Electrical Sintering Method to the Preparation of Ceramics and Intermetallics*, by F. V. Lenel, Rensselaer Polytechnic Institute.

Panel Session on Above Subjects* (30 Minutes)

Evening Session—November 24 (8:00–10:00 P.M.)

Main Subject: *Uses and Application of Refractory Type Materials*

Chairman: Colonel Paul F. Nay, U. S. Army Air Force, Chief Propulsion Branch, Office of Deputy Chief of Staff, Development

Problems Relating to the Usage of Refractory Materials in High Temperature Applications, by R. Paris, WADC. (15 min.)

Turbine Operation With Refractory Type Materials, by G. C. Deutsch and A. J. Meyer, NACA. (15 min.)

Related Discussion (5 min. each)

- (a) *Rocket Nozzle Materials*, by W. R. Sheridan, Bell Aircraft.
- (b) *Jet Engine Materials—Future Trends and Requirements*, by R. Thielemann, Pratt & Whitney Aircraft.
- (c) *Problems Involved in the Operation of Coated Molybdenum Turbine Buckets*, by E. G. Pekarek, Thompson Products.
- (d) *Thermal Shock*, by S. Manson, NACA.

Panel Session on Above Subjects* (60 Minutes)

Morning Session—November 25 (9:00 A.M. – 12:00 Noon)

Main Subject: *Ceramics and Intermetallics With Metal Additions*

Chairman: Dr. John T. Norton, Massachusetts Institute of Technology

Theoretical Structure of Refractory Materials for Elevated Temperature Applications, by John T. Norton. (15 min.)

Additions of Metals or Alloys to Base Ceramic Type Materials, by Tom Shevlin, Ohio State University. (10 min.)

Infiltration of Intermetallic Type Bodies, by Claus G. Goetzel, Sintercast Corp. (10 min.)

Related Discussion (5 min. each)

- (a) *Fabrication of Titanium Carbide Ceramals by Infiltration Techniques*, by R. Gurnick, NACA.
- (b) *The Oxidation of Titanium Carbide With Metal Additions and the Forming of Dense Silicon Carbide*, by J. R. Tinkelpaugh, N. Y. State College of Ceramics.
- (c) *Modified Chromium—Alumina Metal Ceramics*, by H. R. Spendelow, Jr., Union Carbide and Carbon.
- (d) *Metal and Silicide Bonded Titanium Diboride*, by D. Bennett, University of Illinois.

Panel Session on Above Subjects* (30 Minutes)

- Recent Developments in Titanium Carbide Alloys and Properties*, by J. C. Redmond, Kennametal, Inc. (15 min.)
- Elevated Temperature Properties of Zirconium Boride Alloy*, by Frank W. Glaser, American Electro Metals. (10 min.)
- Some Effects of Metal Additions to Molybdenum Disilicides*, by J. Jenkins, NACA. (10 min.)

Related Discussion (5 min. each)

- (a) *Comments on Molybdenum Silicides*, by R. Wehrmann, Fansteel Metallurgical Corp.
- (b) *Cast Titanium Carbide and Nickel Alloys*, by R. B. Fisher, Battelle Memorial Institute.
- (c) *Titanium Carbide Base Alloys Containing Chromium*, by W. L. Havekotte, Firth-Sterling Steel Co.
- (d) *Research, Directed by Office of Naval Research*, by J. J. Harwood, Office of Naval Research.
- (e) *Some Recent Oxidation Problems of Ceramic-Metal Materials*, by F. C. Robertshaw, Jr., General Electric.

Panel Session on Above Subjects* (25 Minutes)

Session Closes at 12:00 Noon for Luncheon

1:25 P.M.—Board Buses for NACA

Tour and Inspection of NACA, Lewis Flight Propulsion Laboratory, at 2:15–4:30 P.M. including the following:

- (a) Materials Research Building and Laboratories
- (b) Metallurgical Development Laboratories
- (c) Full Scale Jet Engine Research Facilities
- (d) 8' x 6" Supersonic Wind Tunnel

CREEP AND RUPTURE OF CHROMIUM-NICKEL AUSTENITIC STAINLESS STEELS

BY E. J. DULIS, G. V. SMITH AND E. G. HOUSTON

Abstract

Supplementing results previously reported (1),¹ creep and rupture test data are presented for AISI Grades 304L, 304L (high N), 316L, 316 Cb, and 303; test results of additional heats of 304, 321 and 347 are also given. The observed changes in microstructure and in certain room temperature mechanical properties brought about by creep test exposure are described.

AS A RESULT of restrictions on the use of some elements ordinarily added to the conventional austenitic stainless steels of the 18 Cr-8 Ni type and of new applications of these steels for elevated temperature service, considerable interest has arisen in the properties of the recent modifications of these steels. The investigation reported herein is a continuation of a study of creep and rupture of austenitic 18 Cr-8 Ni steels, with and without various other alloying elements, the initial part of which covered the four conventional types, 304, 321, 316, and 347, and was reported in an earlier publication (1). Also included in the present paper are data on additional heats of the conventional types.

MATERIALS AND PROCEDURE

The steels used in this investigation were received in the form of hot-rolled bars. Pertinent data on the composition, heat treatments and resulting hardness, and grain size of the various steels are given in Table I. The chemical analyses were made on samples from the tested bars of each steel. Steels A, C and D were tested in both creep and creep-rupture, whereas Steels B, E and H were "spot"-tested in creep only, and Steels F, G and I were tested in creep-rupture only.

Heat treatments prior to machining consisted either of annealing, i.e., rapid cooling from the range 1900 to 2000 °F (1040 to 1095 °C), or annealing followed by stabilizing for some of the titanium and columbium steels, i.e., heating to 1550 or 1600 °F (845 or 870 °C) for 2 hours. Only Steels D (316 Cb) and H (321) were tested after both heat treatments. After the initial heat treatments, Steels

¹ The figures appearing in parentheses pertain to the references appended to this paper.

A paper presented before the Thirty-fourth Annual Convention of the Society, held in Philadelphia, October 18 to 24, 1952. The authors, E. J. Dulis, G. V. Smith and E. G. Houston, are associated with the Research Laboratory, United States Steel Company, Kearny, N. J. Manuscript received April 10, 1952.

A, B, C and H consisted of austenite and delta ferrite (H also contained titanium carbide); Steel D contained austenite and carbide after annealing, and austenite, carbide and sigma after stabilizing; and Steel E was austenitic with stringers of a nonmetallic selenium compound. Steels F, G and I initially consisted of austenite, austenite and titanium carbide, and austenite and columbium carbide, respectively.

The test methods for measuring creep (0.5-inch diameter specimens) and creep-rupture (0.25-inch diameter specimens) have been described in detail in an earlier publication (2). Other mechanical tests such as hardness, tensile and notch impact were made in accordance with accepted practices. Notch-impact specimens, machined from creep specimens after test, were, of necessity, two-thirds standard size; consequently, this size was used also for all test specimens. Duplicate notch-impact tests were made for specimens which had been tested in creep, and at least three specimens were tested for the initial condition.

Magnetic permeability measurements, at room temperature, of specimens before and after creep test were made with an apparatus described by Sosman and Austin (3).

Creep and creep-rupture specimens were examined before and after test to study the microstructural changes which occur with time at elevated temperatures; the mode of fracture of the creep-rupture specimens was also investigated by this method. Differentiation of the various phases (austenite, carbide, sigma and ferrite) by microscopic means was accomplished by techniques described in an earlier publication (4).

X-ray diffraction patterns were used in some instances to identify constituents or to corroborate microscopic identifications. Chromium $K\alpha$ radiation was used throughout.

MECHANICAL TESTS

The occurrence of creep during service at elevated temperatures makes it necessary to choose the working stress within two limitations: (a) that the total deformation not exceed a specific value, depending on the application; and (b) that fracture (rupture) does not occur. (Limiting the total creep does not necessarily insure that fracture will not occur, for fracture under prolonged loading may occur with considerably reduced deformation.)

Thus an evaluation of the creep characteristics of metals involves, on one hand, determination of the relation between total creep, stress and temperature, and on the other, between rupture-time, stress and temperature. Whereas the latter information is directly available from the familiar plots of stress versus time to rupture at different temperatures, total creep is not so easily obtained, due to the com-

Table I
Identification, Chemical Composition, Heat Treatment, Grain Size and Hardness of Steels

Steel Type	Chemical Analyses										Others	Before Test— ASTM Grain Size	Heat Treatment °F
	C	Mn	P	S	Si	Cr	Ni	Mo	Cb†	Ti†			
A 304L	0.03	0.65	0.010	0.019	0.54	19.50	10.22	N-0.031 Al-0.003 Al(Al ₂ O ₃)-0.002	4-7	135 1900 Q
B 304L (High N)	0.03	1.48	0.018	0.024	0.67	19.38	7.14	N-0.161 Al-0.003 Al(Al ₂ O ₃)-0.001	3-5	196 1900 Q
C 316L	0.03	1.50	0.013	0.027	0.34	17.46	10.70	2.20	N-0.030 Al-0.004 Al(Al ₂ O ₃)-0.001	2-5	132 2000 Q
D 316Cb	0.05	0.77	0.018	0.006	0.36	18.50	14.19	2.45	0.49	...	N-0.063 Al-0.018 Al(Al ₂ O ₃)-0.008	4-8	(1) 2000 Q (2) 2000 Q + 1600 A.C.
E 303	0.07	0.86	0.142	0.019	0.35	17.66	9.47	Se-0.30 Cu-0.02 Zr-0.01	5-7	164 1900 Q
F 304	0.05	0.53	0.008	0.005	0.61	18.53	10.12	N-0.041 Al-0.002 Al(Al ₂ O ₃)-0.001	4-7	138 1900 Q
G 321	0.07	0.52	0.021	0.003	0.39	17.97	10.40	0.58	N-0.010 Al-0.088 Al(Al ₂ O ₃)-0.002	8	142 1900 Q + 1550 Q
H 321	0.049	0.56	0.022	0.008	0.50	18.21	11.21	0.60	N-0.011 Al-0.182 Al(Al ₂ O ₃)-0.004	6-8 6-8	(1) 1950 Q (2) 1950 Q + 1600 A.C.
I 347	0.06	1.43	0.018	0.006	0.44	17.80	11.16	...	0.77	...	N-0.045 Al-0.059 Al(Al ₂ O ₃)-0.001	8-9	1900 Q + 1550 Q
J* 347	0.06	1.61	0.016	0.006	0.32	18.12	11.10	...	0.78	...	N-0.068 N-0.011	7, 8	1950 Q
K* 321	0.05	0.53	0.017	0.010	0.41	17.60	10.81	0.42	N-0.011	8	143 1900 A.C.
L* 321	0.09	0.46	0.012	0.007	0.63	18.56	11.29	0.34	...	5-8	164 1950 Q
M* 304	0.05	0.28	0.015	0.009	0.44	18.38	10.12	N-0.053	3-5	142 1900 Q
N* 316	0.08	1.63	0.017	0.014	0.37	17.76	12.47	2.55	N-0.061	4-6	145 2000 Q
O* 347	0.08	1.27	0.015	0.009	0.60	18.04	10.83	...	0.69	6-8	189 1950 Q

*Tests on these steels reported in Ref. 1.

†Steel
G
H
I
J

Cb/C
....
....
12.8
13.0

Ti/C
8.3
12.2
....
....

†Steel
K
L
O

Ti/C
8.4
3.8
....

Cb/C
....
....
8.6

Table II
Summary of Creep and Creep-Rupture Test Results

Steel	Type	Treatment °F	Stress for Creep Rate of 0.0001% Per Hour (1000 psi) — °F						Stress for Rupture in 1000 Hours (1000 psi) — °F					
			900	1050	1100	1200	1300	1500	900	1050	1100	1200	1300	1500
A	304L	1900 Q	9.7 ^a	6.8 ^b	3.4 ^a	1.5	18.8	11.3 ^d	6.8	3.0
B	304L	1900 Q (High N)	17.8	10.0 ^b	5.9	1.2
C	316L	2000 Q	14.1 ^a	8.2 ^b	4.8 ^a	1.56	26.9	17.3 ^d	11.7	4.6
D	316 Cb	2000 Q	25.5	15.2 ^b	9.1	3.4	42.0	27.8 ^d	18.7	5.4
D	316 Cb	2000 Q + 1600 A.C.	30.0	16.0 ^b	8.1	2.8	40.0	24.5 ^d	15.0	5.4
E	303	1900 Q	22.5	12.0 ^b	6.2	1.8
F	304	1900 Q	36.0 ^a	16.5 ^a	12.2 ^b	7.2 ^a	48.5	27.0	21.0 ^d	14.0
G	321	1900 Q + 1550 Q	39.0 ^a	26.0 ^a	19.0 ^b	12.7 ^a	48.5	32.0	25.8 ^d	18.0
H	321	1950 Q	21.3	12.0 ^b	7.1	1.4
H	321	1950 Q + 1600 A.C.	18.0	10.0 ^b	5.4	1.1
I	347	1900 Q + 1550 Q	36.5	31.0 ^b	22.0	50.0	40.0	34.0 ^d	26.0
J ^c	347 ^c	1950 Q	27.0	8.0	1.8	36.0	13.2	4.5
K ^c	321 ^c	1900 A.C.	16.0	4.6	0.85	26.0	10.0	3.8
L ^c	321 ^c	1950 Q	21.0	7.8	2.7
M ^c	304 ^c	1900 Q	13.0	5.2	2.1	22.0	9.2	4.2
N ^c	316 ^c	2000 Q	26.0	9.7	3.2	33.0	17.0	7.1
O ^c	347 ^c	1950 Q	27.0	8.0	1.8

Steel	Type	Treatment °F	Time for Beginning of Tertiary Creep at Stress Causing Creep Rate of 0.0001% Per Hour (1000 Hours) — °F						Extrapolated Per Cent Elongation at Rupture in 10,000 Hours — °F					
			900	1050	1100	1200	1300	1500	900	1050	1100	1200	1300	1500
A	304L	1900 Q	60.0	20.0	10.0	7.0	9.5	6.0
B	304L	1900 Q (High N)
C	316L	2000 Q	>100.0	100.0	32.0	44.0	28.0	14.0
D	316 Cb	2000 Q	30.0	178.0	7.0	1.0	3.0	30.0
D	316 Cb	2000 Q + 1600 A.C.	5.0	50.0	20.0	26.0	54.0	2.5
E	303	1900 Q
F	304	1900 Q	9.0	38.0	33.0	20.0	16.0	12.0
G	321	1900 Q + 1550 Q	118.0	5.0	3.2	40.0	28.0	20.0
H	321	1950 Q
H	321	1950 Q + 1600 A.C.
I	347	1900 Q + 1550 Q	1.8	4.5	<1.0	29.0
J ^c	347 ^c	1950 Q	20.0	3.0	9.0	24.0	28.0	9.5
K ^c	321 ^c	1900 A.C.	7.0	7.0	40.0	4.0	7.0	6.0
L ^c	321 ^c	1950 Q
M ^c	304 ^c	1900 Q	100.0	45.0	30.0	10.0	23.0	16.0
N ^c	316 ^c	2000 Q	10.0	25.0	70.0	2.5	30.0	20.0
O ^c	347 ^c	1950 Q

^aExtrapolated from Stress Versus Minimum Creep Rate Curve. ^bInterpolated from Temperature Versus Stress for Minimum Creep Rate of 0.0001% Per Hour. ^cData for these steels taken from Ref. 1. ^dInterpolated from Temperature Versus Stress for Rupture in 1000 Hours.

plicated course of the creep versus time curve. As described in an earlier publication (1), however, total creep (C_t) can be expressed for times prior to beginning of tertiary or accelerating creep, as the sum of the intercept (C_0) on the creep ordinate, of the minimum creep rate slope, and the product of minimum creep rate (\dot{C}_m) and time (t), or:

$$C_t = C_0 + \dot{C}_m t$$

Equation 1

Thus total creep can be computed if the relations between stress and (a) intercept C_0 , (b) minimum creep rate \dot{C}_m , and (c) time for

beginning of tertiary creep are known. Such plots are given herein whenever sufficient data were obtained.

Specific comparisons of the steels are also afforded by tabulating or plotting values of stress to cause rupture in 1000 hours and the stress to cause a minimum creep rate of 0.0001% per hour (i.e., the commonly reported 1% per 10,000 hours "creep strength").

Creep and creep-rupture test results are given in graphical form in Figs. 1 to 15 and are summarized in Table II; for comparison with the properties of the conventional grades, data previously reported are included in Table II. Because, in our experience, the data plotted on double logarithmic scales have given a more nearly linear relation than when plotted on semilogarithmic coordinates, the former type of graph was used for Figs. 1 through 7; on the other hand, semilogarithmic coordinates proved best for showing the variation of creep rate and creep-rupture strengths with temperature, Figs. 8, 9 and 10. Variations of the minimum creep rate intercept with stress were plotted on linear coordinates, Figs. 11 to 15.

Creep-Rupture and Creep Strength

The variations with stress² of the time to rupture and of minimum creep rate are given in A and B of Figs. 1 to 7. Since Steels B, E and H were spot-tested only, the minimum creep rate data, Fig. 7, are in some cases meager; in several instances lines were drawn through single points either parallel to the lines of similar steels or by conservatively judging the slopes from known trends. The relations between stress and rupture-time or minimum creep rate are essentially linear on log-log coordinates, as previously observed for similar steels (1), and thus suited to extrapolation within limits; in the case of the rupture-time data, it is, of course, necessary that the second slope be attained.

Stresses to produce rupture in 1000 hours or to cause minimum creep rates of 0.0001% per hour at each test temperature, from Figs. 1 to 7, are given in Table II and plotted in Figs. 8, 9 and 10; also, data for nontest temperatures were obtained by interpolation in Figs. 8, 9 and 10 in some cases and are included, in Table II, for comparison.

In terms of the stress to cause rupture in 1000 hours, Steel D (316 Cb) in both the annealed and stabilized conditions was the strongest at 1100 °F (595 °C) of the steels studied in this or the previously reported investigation (1). At 1300 °F (705 °C) annealed 316 Cb was again strongest, with regular Type 316 only slightly weaker; stabilized 316 Cb was third strongest. At 1500 °F (815 °C) regular 316 had attained first position, with annealed or

² All tests were made with constant load; thus the stress varied with deformation during test. This change in stress is relatively insignificant, however, for stresses and deformations of the magnitude encountered in most service.

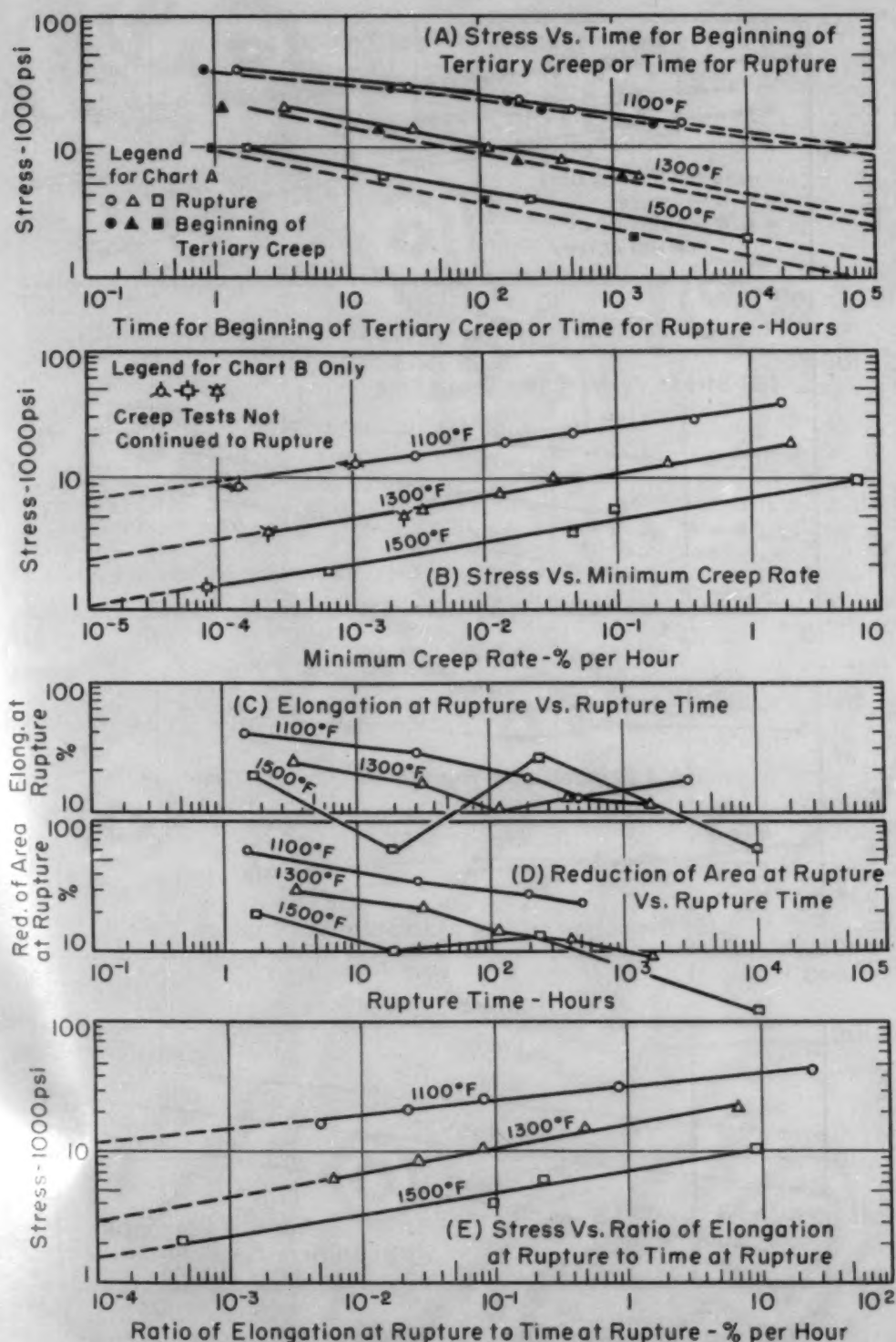


Fig. 1—Properties of Steel A (304L).

stabilized 316 Cb slightly weaker. Of the remaining steels tested in creep-rupture, Steel I (347) was the next strongest at 1100 and 1200 °F (595 and 650 °C) (the highest temperature of test for Steels F, G and I in this study), followed by Steels C (316L), G (321),

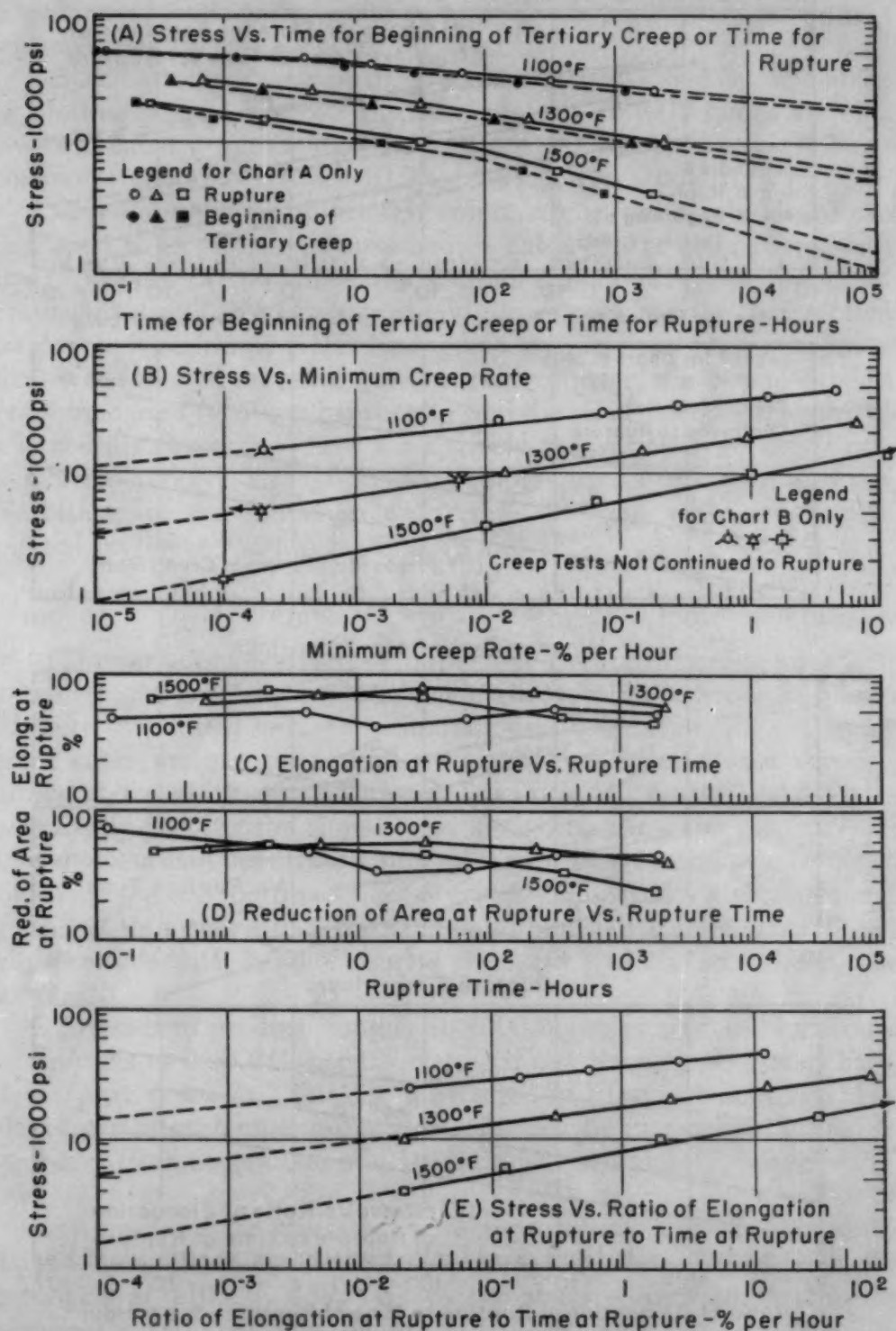


Fig. 2—Properties of Steel C (316L).

F (304), and, lastly, A (304L). It is interesting to note that the addition of molybdenum to low carbon 18-8 raises the creep-rupture strength so that it compares quite favorably with the conventional

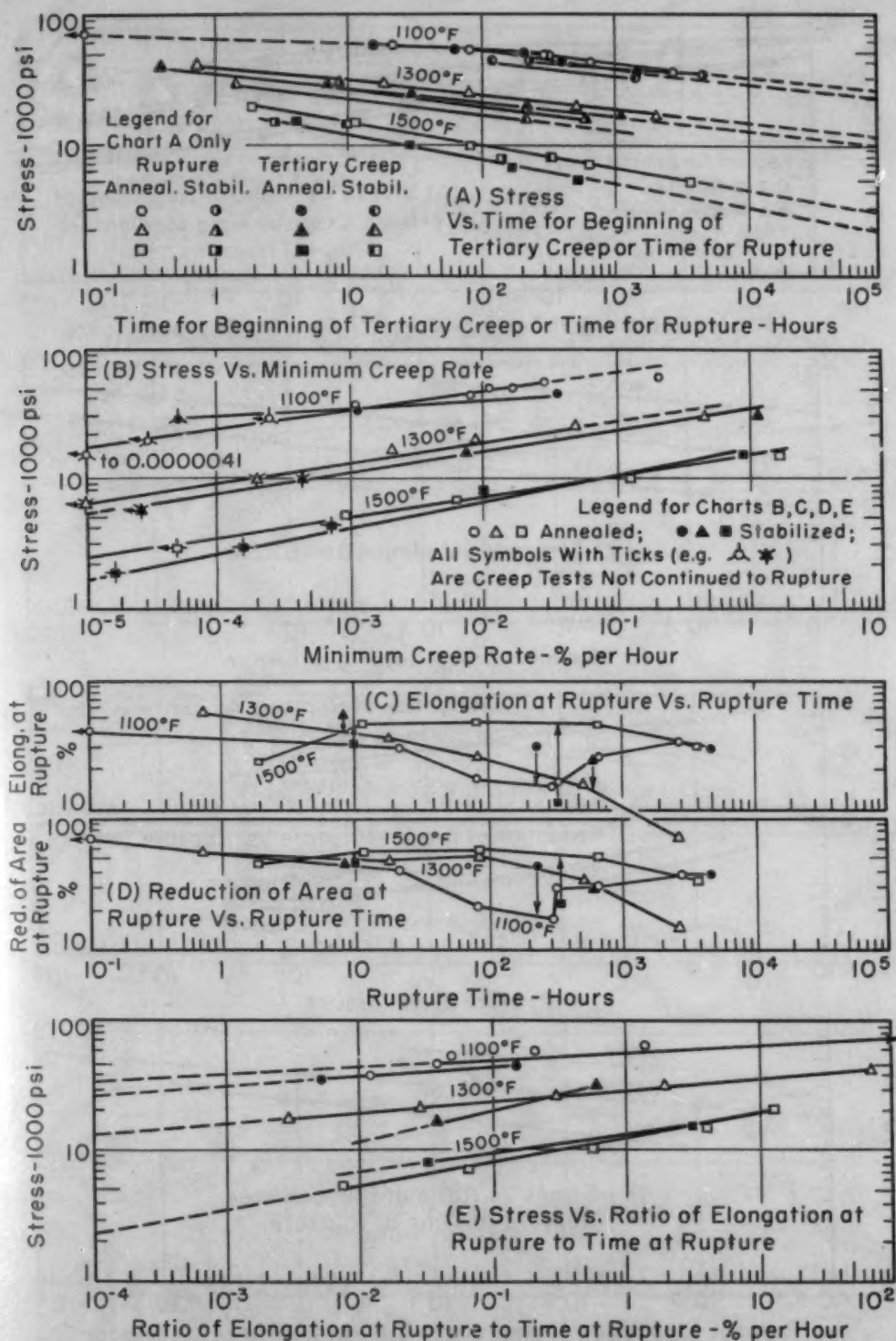


Fig. 3—Properties of Steel D (Type 316 Cb).

grades, other than 316, particularly at 1300 and 1500 °F (705 and 815 °C).

In terms of the stress to cause a minimum creep rate of 0.0001% per hour (frequently termed 1% per 10,000 hours) at 1100 °F

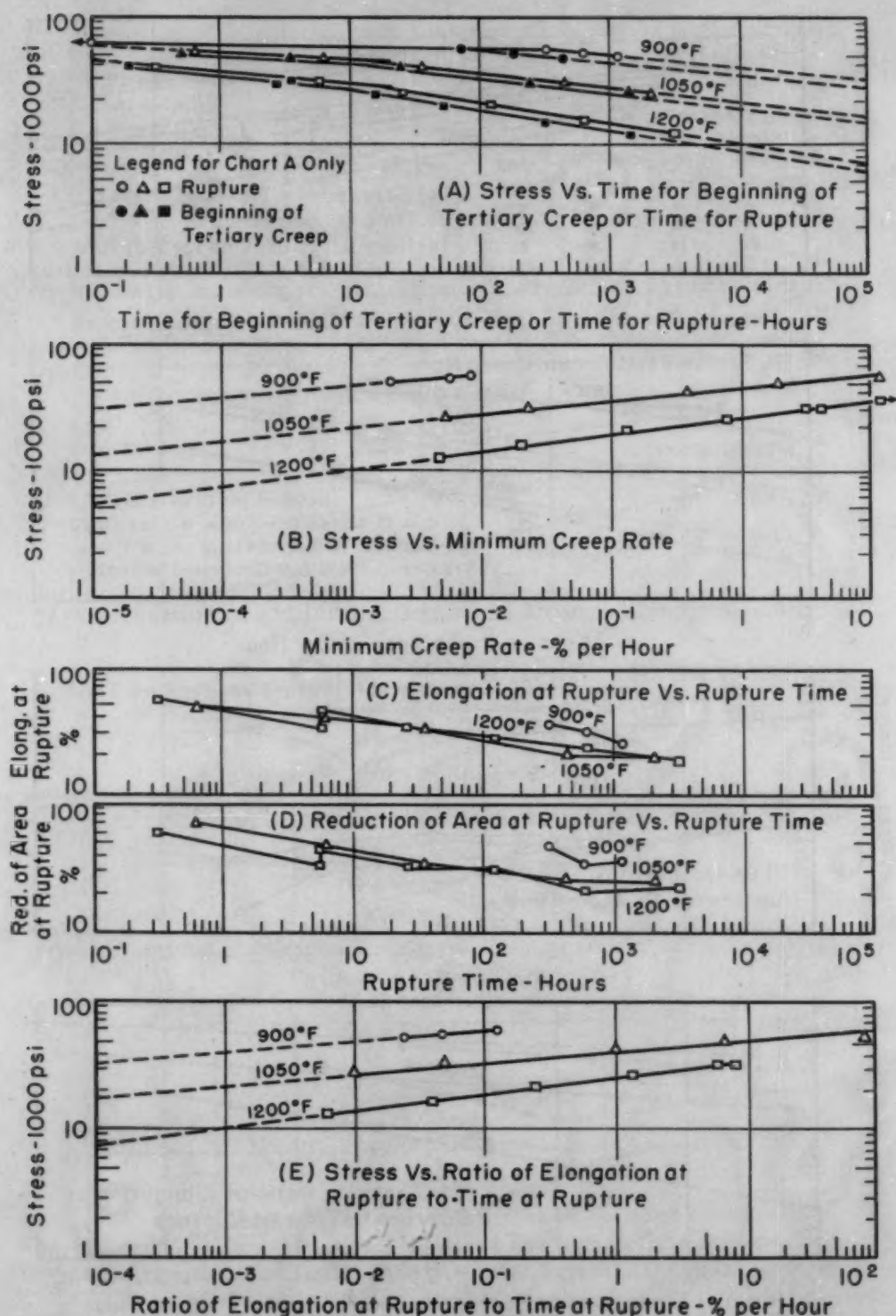


Fig. 4—Properties of Steel F (Type 304).

(595 °C), the molybdenum (excluding the low carbon grade) and columbium-containing steels were strongest. These were followed in decreasing strengths by Steel E (303) (22,500 psi); Steels H (321) (21,300 psi) and L (321) (21,000 psi); Steel B (304L, high N)

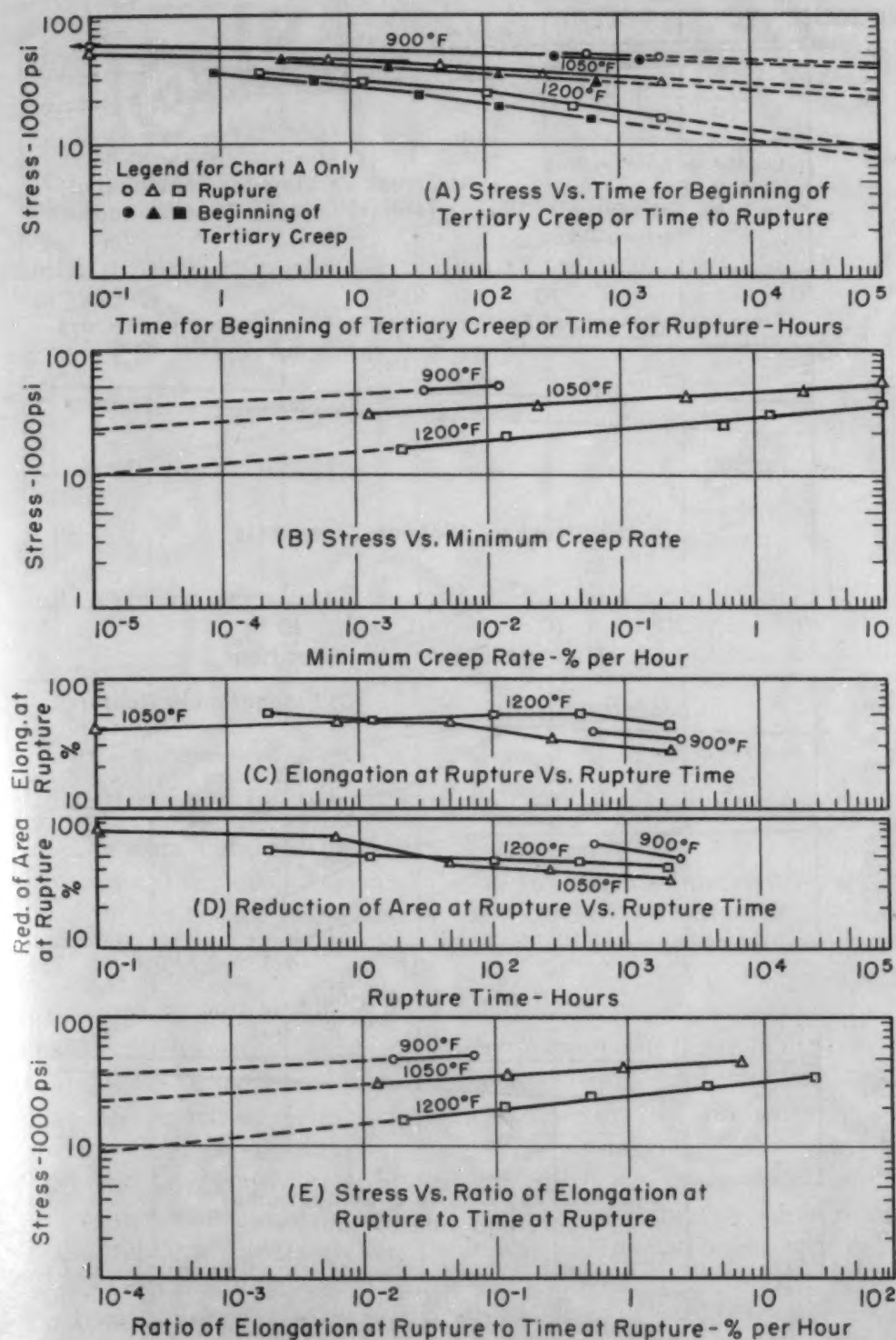


Fig. 5—Properties of Steel G (Type 321).

(17,800 psi); Steel C (316L) (14,100 psi); Steels F (304) (12,200 psi) and M (304) (13,000 psi); and finally Steel A (304L) which had a creep-rate strength of 9700 psi. With increasing temperature beyond 1200 °F (650 °C), the Type 347 grades weakened rapidly

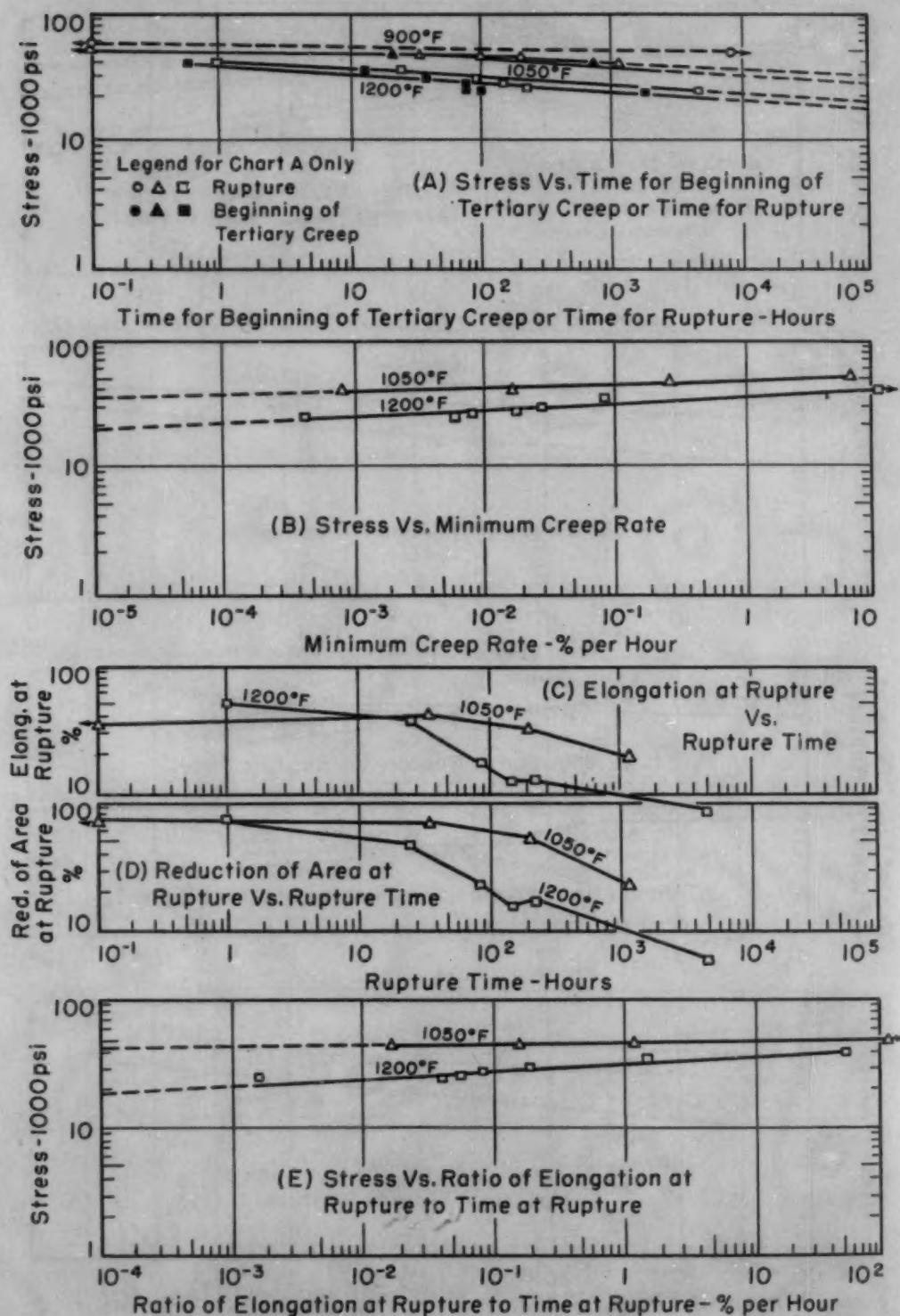


Fig. 6—Properties of Steel I (Type 347).

and the molybdenum-containing grades 316 and 316 Cb became strongest. Type 304L was least strong at 1100 and 1300 °F (595 and 705 °C) but two heats of 321, H and K, were weakest at 1500 °F (815 °C).

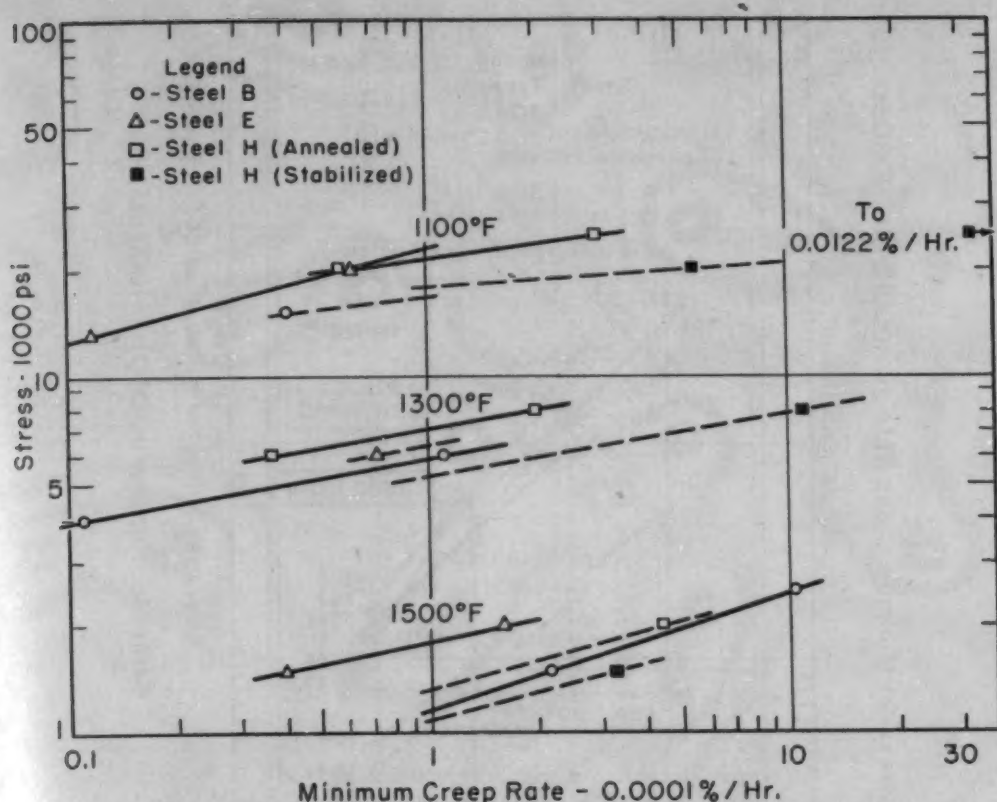


Fig. 7—Relation Between Stress and Minimum Creep Rate for Steels B (304L, High N), E (303), and H (321).

The data obtained in the present investigation, when compared with those previously reported, are of interest in regard to the variation in strength of nominally identical grades. As shown in Fig. 8, the two Type 304 heats showed excellent agreement in both creep and rupture strengths within the range of overlapping test temperatures. On the other hand, as shown in Fig. 10, there appears to be considerable variation in creep strength from one heat of Type 321 to another; in rupture (two heats only, one annealed, the other stabilized), good agreement is indicated within the limited range of overlap. Similar good agreement in creep-rupture may be noted for Type 347, but again one heat was annealed, the other stabilized; in creep rate two heats of annealed Type 347 steel showed quite similar results, while a third stabilized heat was slightly stronger within the range of overlapping tests.

It is of interest to note that the heat of Type 321 steel which showed the greatest creep strength at 1500 °F (815 °C) of any of the stabilized grades was that having the least ratio of titanium to carbon, but the converse is not true.

Whereas the previous study (1) had suggested that stabilization heat treatment produced only negligible differences in strength from the annealed condition, the tests on Type 321 Steel H of the present

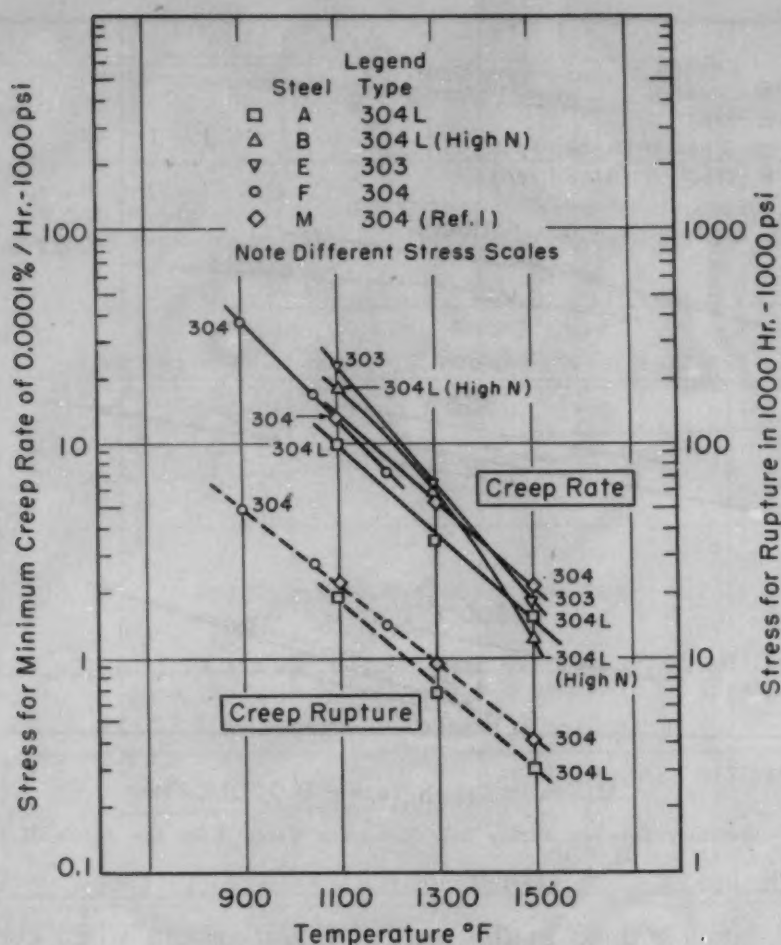


Fig. 8—Variation of Creep and Rupture Strengths of Steels A, B, E, F and M With Temperature. See also Figs. 9 and 10.

investigation show a slightly deleterious effect of stabilization on creep-rate strength. Stabilization heat treatment of 316 Cb Steel D also resulted in slightly inferior creep-rate strength at 1300 and 1500 °F (705 and 815 °C), and creep-rupture strength at 1300 °F (705 °C), but not otherwise. As discussed later, sigma developed during stabilization of this steel.

Carbon is very effective in improving creep strength at all temperatures, Fig. 8. Thus the substitution of 0.03% carbon Type 304L for the stabilized grades (321 or 347) in elevated temperature service must be done with caution. Nitrogen is similarly effective at 1100 and 1300 °F (595 and 705 °C) and, in fact, develops greater strength in the 0.03% carbon-type alloy than is possessed by standard Type 304, but it is deleterious at 1500 °F (815 °C). The free-machining grade, Type 303, which is probably not widely used at elevated temperatures, proves to be superior to standard Type 304 at 1100 °F (595 °C), but little different at 1300 or 1500 °F (705 or 815 °C).

Carbon content is important in Type 316 as well as in Type 304;

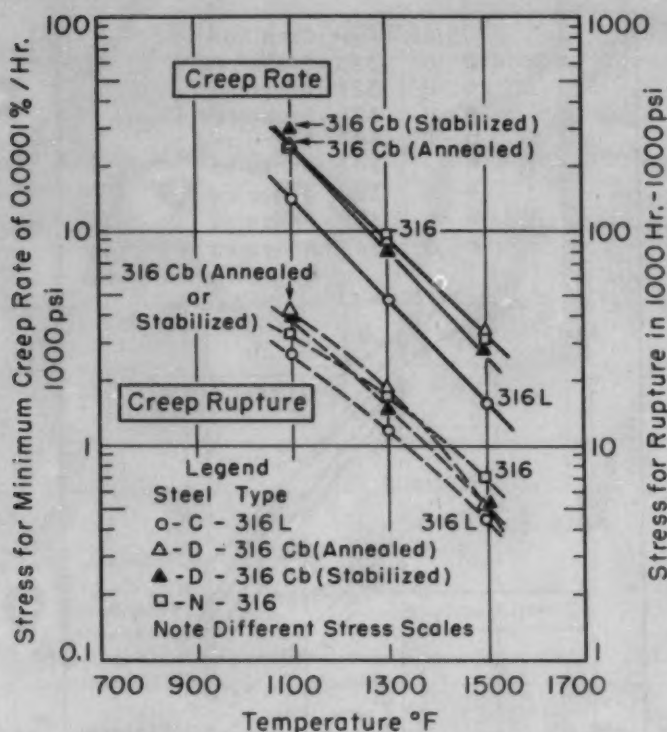


Fig. 9—Variation of Creep and Rupture Strengths of Steels C, D and N With Temperature. See also Figs. 8 and 10.

the 0.03% carbon Type 316 steel, i.e., 316L, is significantly weaker in both creep rate and creep-rupture strength, Fig. 9. The addition of columbium may either weaken or strengthen Type 316 steel, depending on the test temperature and the strength criterion of interest.

It is difficult to draw any general conclusions regarding the relative strengths of Types 321 and 347, Fig. 10, due partly to the variation among the different heats of 321. Type 347 does appear, however, to be consistently superior in the intermediate temperature range about 1100 °F (595 °C).

An important factor to be considered in comparing strength properties of these steels is grain size; in general, the stabilized grades (321 and 347) are fine-grained, whereas the remainder are fairly coarse-grained. As elevated temperature strength is affected by grain size, the alloying effects will, in part at least, be influenced by grain size differences.

Minimum Creep Rate Intercept Deformation, C_0

Variations with stress of the intercept, C_0 , of the minimum creep rate on the extension ordinate are given in Figs. 11 to 15 for all steels except those spot-tested in creep rate only, in which case the data were too meager. The form of the curves is quite similar to that previously reported for several austenitic steels (1). Although some

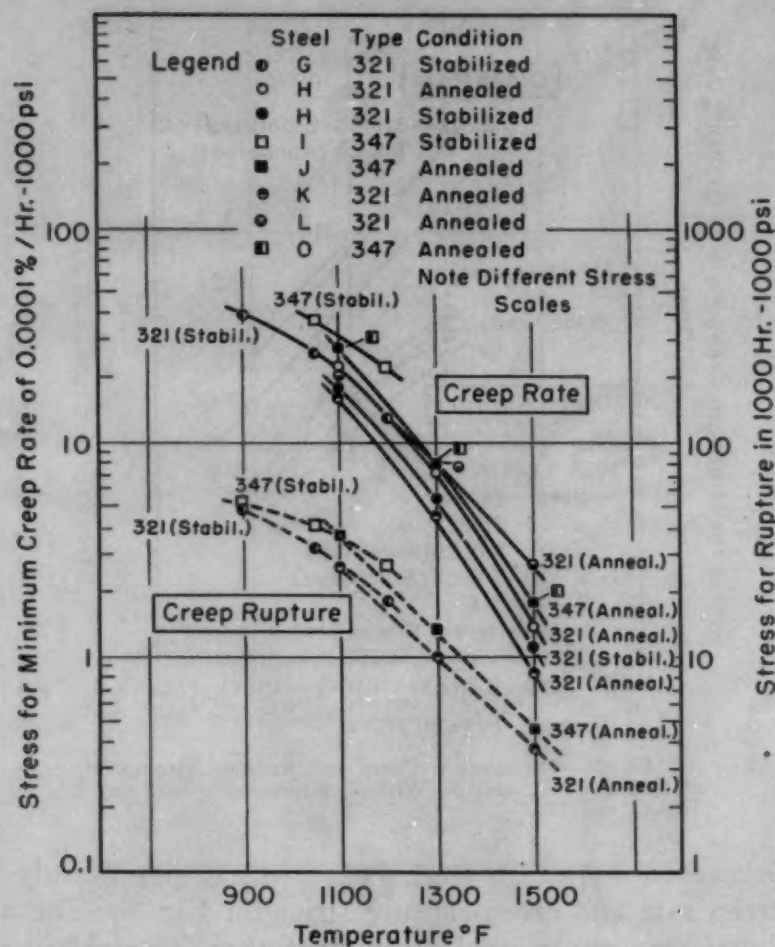


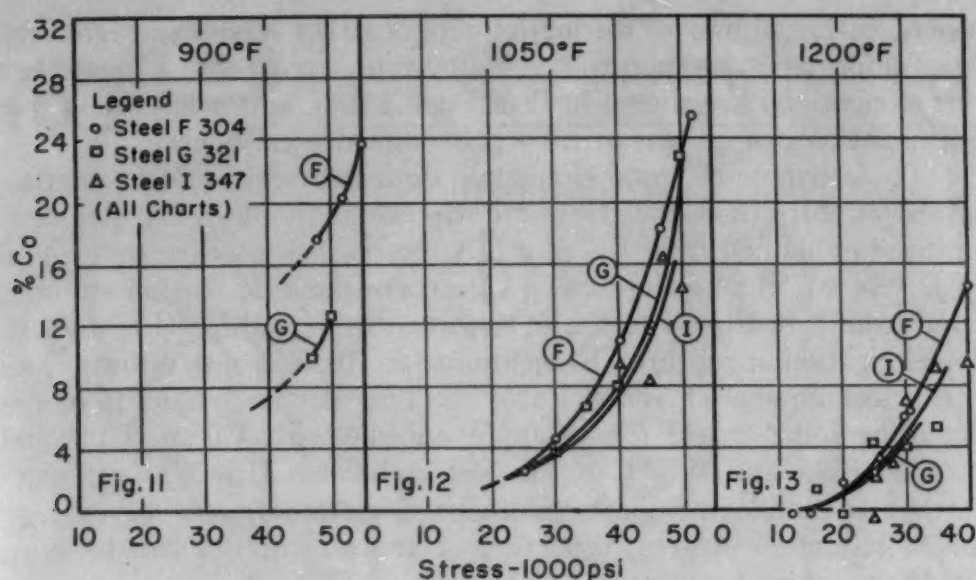
Fig. 10—Variation of Creep and Rupture Strengths of Steels G, H, I, J, K, L and O With Temperature. See also Figs. 8 and 9.

scatter exists in the data, a reasonably good approximation of C_0 can be obtained for calculating the total deformation by Equation 1, as previously described.

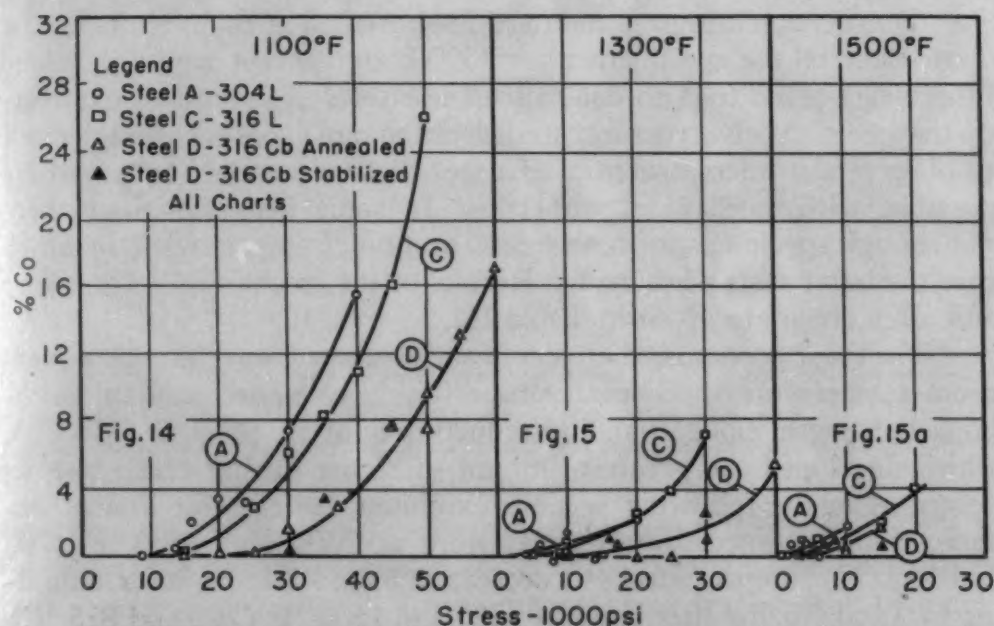
Beginning of Tertiary Creep

Stress versus time for beginning of accelerated or tertiary creep for the steels tested in creep-rupture is shown graphically in 'A' of Figs. 1 to 6; the relationship is similar to that between stress and rupture time, the two curves being substantially parallel. Times for beginning of tertiary creep at stresses which give a creep rate of 0.0001% per hour (a rate widely used for reporting creep strength) are given in Table II.

It is important to remember that the relationship given in Equation 1 for calculating total creep is valid only when the time involved is less than that for beginning of accelerating rate of creep.



Figs. 11, 12, 13—Variation of Creep Intercept, C_o , With Stress at 900, 1050 and 1200 °F (480, 565 and 650 °C).



Figs. 14, 15, 15a—Variation of Creep Intercept, C_o , With Stress at 1100, 1300 and 1500 °F (595, 705 and 815 °C).

Elongation and Reduction of Area at Fracture

As shown in C and D of Figs. 1 to 6, the variation of elongation or reduction of area with time for rupture is generally irregular and not suitable for extrapolation to longer rupture times. However, a method of determining elongation or reduction of area by extrapolation to long times for rupture was developed at this Laboratory and previously reported (1). Briefly, this technique is based on the exist-

ence of a straight line for the log-log plot of stress versus average creep rate (deformation at rupture divided by time at rupture). These data (for elongation) are shown in E of Figs. 1 to 6, and it is evident that extrapolation can be performed with reasonable confidence.

To determine the total elongation or reduction of area at rupture for any rupture time, the stress for rupture at the designated time to rupture is obtained from the plot of stress versus rupture time, A of Figs. 1 to 6. The average creep rate corresponding to this stress is found from E of Figs. 1 to 6, and this quantity is multiplied by time to give elongation at rupture. Elongations for 10,000-hour rupture times by this technique are given in Table II. The very low values to be expected in some cases, for example annealed 316 Cb at 1100 and 1300 °F (595 and 705 °C) (but not stabilized 316 Cb), are noteworthy. By employing similar plots, i.e., log stress versus log average rate of reduction of area, reduction of area at rupture can be computed for any rupture time.

Mechanical Properties After Test

Tensile, notch-impact and hardness tests, all at room temperature, were made on the specimens after 3000-hour (except where indicated otherwise) creep tests to determine the effects of creep test exposure on the steels. Microstructural studies of the same specimens were made to observe the microstructural changes and to correlate them, where possible, with mechanical properties. In some instances there were not enough specimens for both tensile and notch-impact tests, in which case the latter tests were made. Results of the mechanical tests before and after creep are given in Table III.

The most pronounced effects of the creep exposure on subsequent room temperature mechanical properties were a decrease in notch-impact strength, elongation, and reduction of area. Steel D (316 Cb), which developed the greatest amount of sigma during creep test, as described in the following section, exhibited the greatest loss of impact strength, especially after exposure at 1300 and 1500 °F (705 and 815 °C); impact strength decreased from 45 ft-lbs after annealing to 9 and 7 ft-lbs after creep at 1300 and 1500 °F (705 and 815 °C) (2/3 size specimens). A similar decrease in impact strength occurred during creep tests in this steel when given an initial stabilizing heat treatment. In the initial quenched (i.e., annealed) condition, no sigma was present, whereas in the stabilized condition some sigma was observed; impact strengths were accordingly 45 ft-lbs in the quenched and 34 ft-lbs in the stabilized condition. Elongations and reductions of area also showed appreciable decreases on exposure at 1300 or 1500 °F (705 or 815 °C). The same general behavior was previously found for Steel N (316) (1).

Steel C (316L) showed a marked decrease in impact strength

Table III
Hardness, Tensile Properties and Notch Impact Strength at Room Temperature
Before and After Creep Test^a

Steel	Type	Initial Heat Treatment	Creep Test Temp., °F	DPH Hardness	0.2% Offset Yield Strength (1000 psi)	Tensile Strength	Elongation % in 2 In.	Red. of Area %	² / ₁₆ Size Charpy Notch Impact ^b (ft-lb)
A	304L	Q	Orig. Material	135	29.2	78.3	64.5	75.7	47.0
A	304L	Q	1100	139	33.7	80.2	60.0	72.1	39.0
A	304L	Q	1300	147	26.2	79.4 ^d	62.0	72.1	26.0 ^e
A	304L	Q	1500	135	32.5
B	304L (High N)	Q	Orig. Material	181	46.1	99.0	63.5	77.2	50.0
B	304L (High N)	Q	1100	178	41.5
B	304L (High N)	Q	1300	177	42.0	95.8	63.0	70.0	42.0
B	304L (High N)	Q	1500	173	43.4	94.8 ^a	57.0	59.6	42.0
C	316L	Q	Orig. Material	132	31.3	77.2	63.5	77.0	49.5
C	316L	Q	1100	146	38.0
C	316L	Q	1300	151	26.95	77.7	60.5	66.9	37.5 ^f
C	316L	Q	1500	140	15.0
D	316 Cb	Q	Orig. Material	156	48.2	87.6	46.0	71.2	45.5
D	316 Cb	Q	1100	165	57.5	93.8	39.0	64.5	30.5
D	316 Cb	Q	1300	205	54.2	101.3	38.1	9.0
D	316 Cb	Q	1500	180	38.1	92.5 ^g	19.0	21.6	7.0
D	316 Cb	Q + S	Orig. Material	192	42.8	87.4	46.0	70.4	34.0
D	316 Cb	Q + S	1100	196	25.5
D	316 Cb	Q + S	1300	206	42.8	102.9	29.5	43.0	8.5
D	316 Cb	Q + S	1500	207	36.1	92.6	31.5	39.6	7.0
E	303	Q	Orig. Material	164	40.1	93.0	58.5	68.3	34.5
E	303	Q	1100	204	49.55	103.9	45.0	63.4	19.0
E	303	Q	1300	171	21.0
E	303	Q	1500	163	36.15	93.4	55.0	64.1	24.0
H	321	Q	Orig. Material	131	33.5	81.5	53.0	75.9	53.0
H	321	Q	1100	162	50.1	86.3 ^h	46.0	69.7	47.0
H	321	Q	1300	152	33.5	81.1	47.5	71.2	25.0
H	321	Q	1500	140	41.0
H	321	Q + S	Orig. Material	132	33.5	82.7	51.0	74.5	44.0
H	321	Q + S	1100	138	46.6	82.5 ⁱ	40.0	48.7	20.5 ^j
H	321	Q + S	1300	139	4.0 ^k
H	321	Q + S	1500	130	25.4	72.4	27.0	30.5	19.0

^aCreep test for 3000 hours duration except where noted. ^bAverages of 3 specs. before creep and 2 after creep. All values were in good agreement except H (Q + S) 1500 where the values were 33 and 5 ft-lbs. ^c2088-hour test. ^d2688-hour test. ^e2088-hour test. ^f460-hour test. ^g2304-hour test. ^h2016-hour test. ⁱ408-hour test. ^j1848-hour test. ^k1704-hour test.

after the 1500 °F (815 °C) creep test. After test at 1500 °F (815 °C), this steel was found to contain considerable sigma. The decrease in impact strength of Steel E (303) during creep test at each temperature is attributable to formation of both carbides and sigma. It is of interest to note that Steels A (304L) and B (304L, high N) showed comparatively little change in properties.

Steel H (321) after test showed a decrease in impact strength which was generally proportional to the amount of sigma which formed. The pronounced decrease in impact strength of this steel after creep exposure at all temperatures for initially stabilized specimens was not explainable from examination of the microstructure.

Hardness and strength were also affected by creep-test exposure and, as with the impact strength, changes were greatest with 316 Cb

(annealed); hardness increased from 156 DPH as-annealed to 205 DPH after exposure at 1300 °F (705 °C), with corresponding changes in yield and tensile strengths.

MICROSTRUCTURAL STUDIES

Microstructures before and after 3000-hour creep tests at 1100, 1300 and 1500 °F (595, 705 and 815 °C) for all of the steels except F (304), G (321), and I (347)³ are shown in Figs. 16 to 19; these latter steels were tested in creep-rupture only at 900, 1050 and 1200 °F (480, 565 and 650 °C), and microstructures after the longest test times are given in Fig. 20. The observed changes are summarized in Table IV.

Steel A (304L) (Fig. 16 a-d) when quenched from 1900 °F (1040 °C) consists of austenite and a very slight amount of delta ferrite, the latter confined to a region near the bar center. During creep test at 1100 °F (595 °C) an almost continuous grain boundary precipitate of carbide formed and the delta ferrite partially transformed to sigma, austenite, and carbide.⁴ After the tests at 1300 and 1500 °F (705 and 815 °C), the carbides appeared to coalesce, transformation of delta ferrite to sigma proceeded further with increased test temperature, and some large, clear sigma particles were found. It is not possible to state with certainty whether sigma forms only from delta ferrite or also from austenite. As reported earlier (1), nitrogen absorption from the atmosphere was observed, especially at higher test temperatures. The Type 304L high-nitrogen Steel B (Fig. 16 c-h) quenched from 1900 °F (1040 °C) showed an austenitic matrix and a very few delta ferrite particles. During test at 1100 °F (595 °C), grain boundary carbides and possibly nitrides precipitated and the delta ferrite appeared to be partially transformed. The pronounced increase in magnetic permeability of this specimen (see following section) was not accompanied by observable change in the microstructure. Following tests at 1300 and 1500 °F (705 and 815 °C), the grain boundary precipitate coalesced and the delta ferrite appeared to have transformed to a greater extent.

Steel C (316L) (Fig. 17 a-d) contained a slight quantity of delta ferrite in most, but not all, sections, after quenching from 2000 °F (1095 °C). After exposure at 1100 °F (595 °C) for 3000 hours there was observed a grain boundary precipitate of carbide (though possibly containing some sigma), and partial transformation of the delta ferrite. As with Type 304L, carbide (Cr_{23}C_6), but not sigma, was detected by X-ray diffraction examination of this alloy

³ Microstructures of other heats of these steels tested at 1100, 1300 and 1500 °F (595, 705 and 815 °C) for 3000 hours are shown and described in Ref. 1.

⁴ X-ray diffraction tests (Ref. 5) confirmed the presence of the carbide Cr_{23}C_6 in this steel when heated for 10,000 hours at 1050 and 1200 °F (565 and 650 °C). Sigma was not detected; that forming from the small amount of delta ferrite was not sufficient to cause detectable diffraction.

Table IV
Changes of Microstructure During Creep or Rupture Test Exposure

Steel	Type of Steel	Extra Constituents Initially Present	Exposure Temperature, °F					
			900	1050	1100	1200	1300	1500
A	304L	Delta Ferrite			{Carbide Sigma*		{Carbide Sigma*	{Carbide, Nitride Sigma*
B	304L (High N)	Delta Ferrite			{Carbide (Nitride?) Sigma*		{Carbide (Nitride?) Sigma*	{Carbide (Nitride?) Sigma*
C	316L	Delta Ferrite			{Carbide Sigma*		{Carbide Sigma*	{Carbide, Nitride Sigma*
D	316 Cb	{Carbide Sigma†			{Carbide Sigma (?)		{Carbide Sigma	{Carbide Sigma
E	303	Se compound			{Carbide Sigma (?)		{Carbide Sigma	{Carbide Sigma
F	304	{Carbide Strain lines	{Carbide Nitride		{Carbide Nitride		
G	321	Carbide	Carbide	{Carbide Sigma (?)		{Carbide Sigma		
H	321	{Delta Ferrite Carbide			{Carbide Sigma*		{Carbide Sigma*	{Carbide Sigma*
I	347	Carbide	Carbide	{Carbide Sigma (?)		{Carbide Sigma		

*Forms partly or perhaps wholly from delta ferrite. †After stabilizing.

*Forms partly or perhaps wholly from delta ferrite. †After stabilizing.

heated for 10,000 hours at 1050 or 1200 °F (565 or 650 °C) (5). The 1300 °F (705 °C) specimen exhibited larger carbides and sigma particles in the grain boundaries and partially transformed delta ferrite. Complete delta-to-sigma transformation and grain boundary sigma and carbide growth were found in the 1500 °F (815 °C) specimen. X-ray diffraction patterns of specimens after 3000 hours at 1500 °F (815 °C) showed sigma to be present in the 316L and 316 Cb steels, while the chi (7) or X (8) phase (having the structure of alpha manganese) was found in the regular Type 316. The similarity between the X-ray diffraction patterns of sigma and chi, and unfamiliarity with chi at the time, caused us to mistake chi for sigma in previous studies (1, 4); however, closer examination of the differentiation has now led us to conclude that chi rather than sigma had been formed in the 316 steel, N, tested in creep at 1500 °F (815 °C). It is interesting to note that only the 316 steel that contained a normal carbon content formed the chi phase. Our studies to date have revealed only sigma in 316L and 316 Cb; of course, the carbon in 316 Cb is no doubt combined with Cb to form the stable CbC. Chemical analysis of the chi phase reported by Forgeng (8) indicates it contains 24.6% chromium, 19.3% molybdenum, 4.3% nickel, 0.57% carbon, with the remainder believed to be iron.

Microstructures of Steel D, 316 Cb, before and after creep tests are shown in Fig. 18 for both the initial 2000 °F (1095 °C) quench and 2000 °F (1095 °C) quench plus 1600 °F (870 °C) air-cool heat treatments. As quenched, the microstructure consists of austenite containing fine undissolved carbides within the grains and at the grain boundaries, and typical large CbC-CbN particles (9). The quenched and stabilized steel showed, in addition to the general fine carbide precipitate, fairly large sigma particles predominantly at grain junctions and boundaries; a few stringers of sigma containing small pools of austenite were also exhibited in banded regions which contained abundant large CbC-CbN particles and presumably higher columbium and/or molybdenum to give regions of a composition which transforms to sigma plus austenite during the 2 hours at 1600 °F (870 °C). The microstructural changes during creep tests at 1100, 1300 and 1500 °F (595, 705 and 815 °C) were substantially the same for the steels after the two different initial heat treatments. After tests at 1100 °F (595 °C) an almost continuous grain boundary precipitate of fine carbides and possibly sigma formed, which was too fine to enable differentiation. The 1300 and 1500 °F (705 and 815 °C) specimens contained abundant sigma particles as well as carbides; the latter specimens exhibited coarser particles.

Free machining 18-8 Steel E (Fig. 17 e-h) when quenched from 1900 °F (1040 °C) showed austenite and nonmetallic stringers of presumably a selenium compound. After 3000 hours at 1100 °F

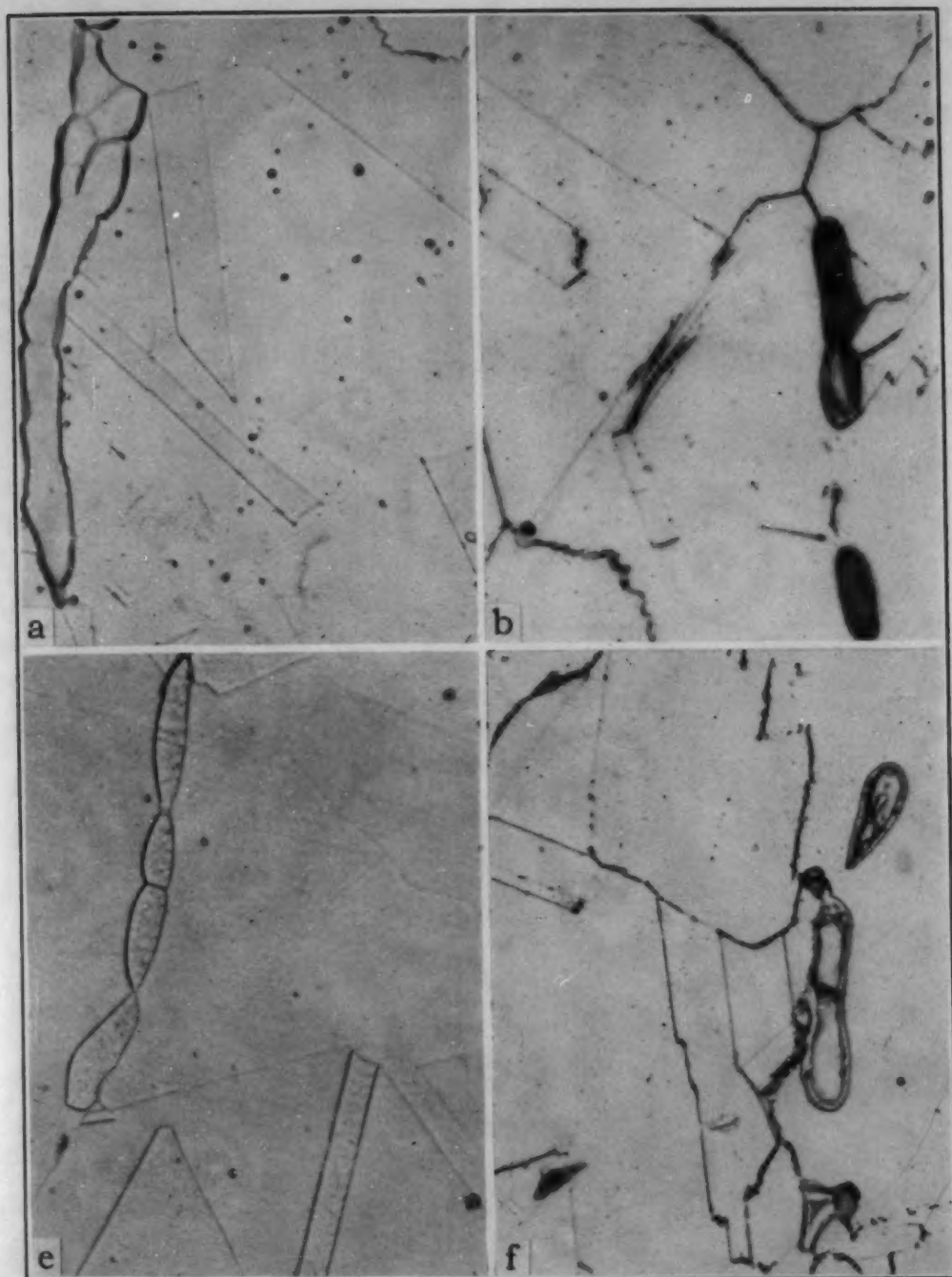


Fig. 16—Microstructure of Steels A and B Before and After Creep Test at Indicated Temperatures for 3000 Hours Except C Which Was Tested for 2088 Hours. Picric-HCl etch. $\times 1000$. Specimens (a), (b), (c) and (d)—Steel A, Type 304L; Specimens (e), (f), (g) and (h)—Steel B, Type 304L (High in N); Specimens (a) and (c)—quenched; (b) and (f)—1100 °F.

(595 °C) a grain boundary and general precipitate of carbide and possibly sigma was exhibited. The creep-test exposure of 1300 and 1500 °F (705 and 815 °C) caused the precipitate to coalesce to somewhat coarser carbides and fairly large sigma particles. Sigma appears to be associated with the inclusions as well as occurring separately.

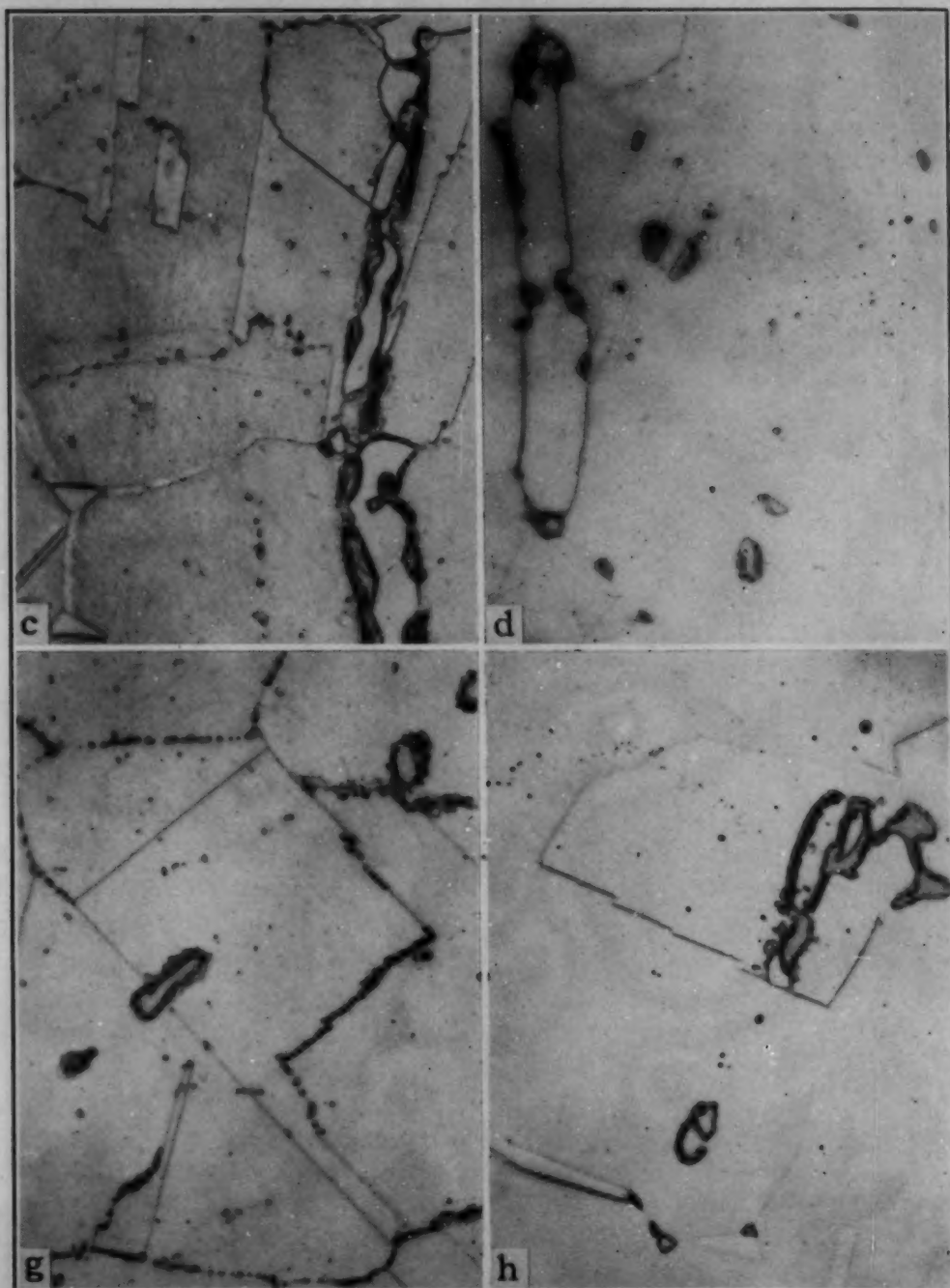


Fig. 16—Microstructure of Steels A and B Before and After Creep Test at Indicated Temperatures for 3000 Hours Except C Which Was Tested for 2088 Hours. Picric - HCl etch. $\times 1000$. Specimens (a), (b), (c) and (d)—Steel A, Type 304L; Specimens (e), (f), (g) and (h)—Steel B, Type 304L (High in N); Specimens (c) and (g)—1300 °F; (d) and (h)—1500 °F.

Whereas the as-quenched steel was paramagnetic, a slight increase in permeability was noted after 3000 hours at 1100 °F (595 °C); microscopic evidence of the ferrite phase was not found.

Steel H, Type 321 (Fig. 19), initially contained undissolved carbides and delta ferrite after both the 1950 °F (1065 °C) quench and

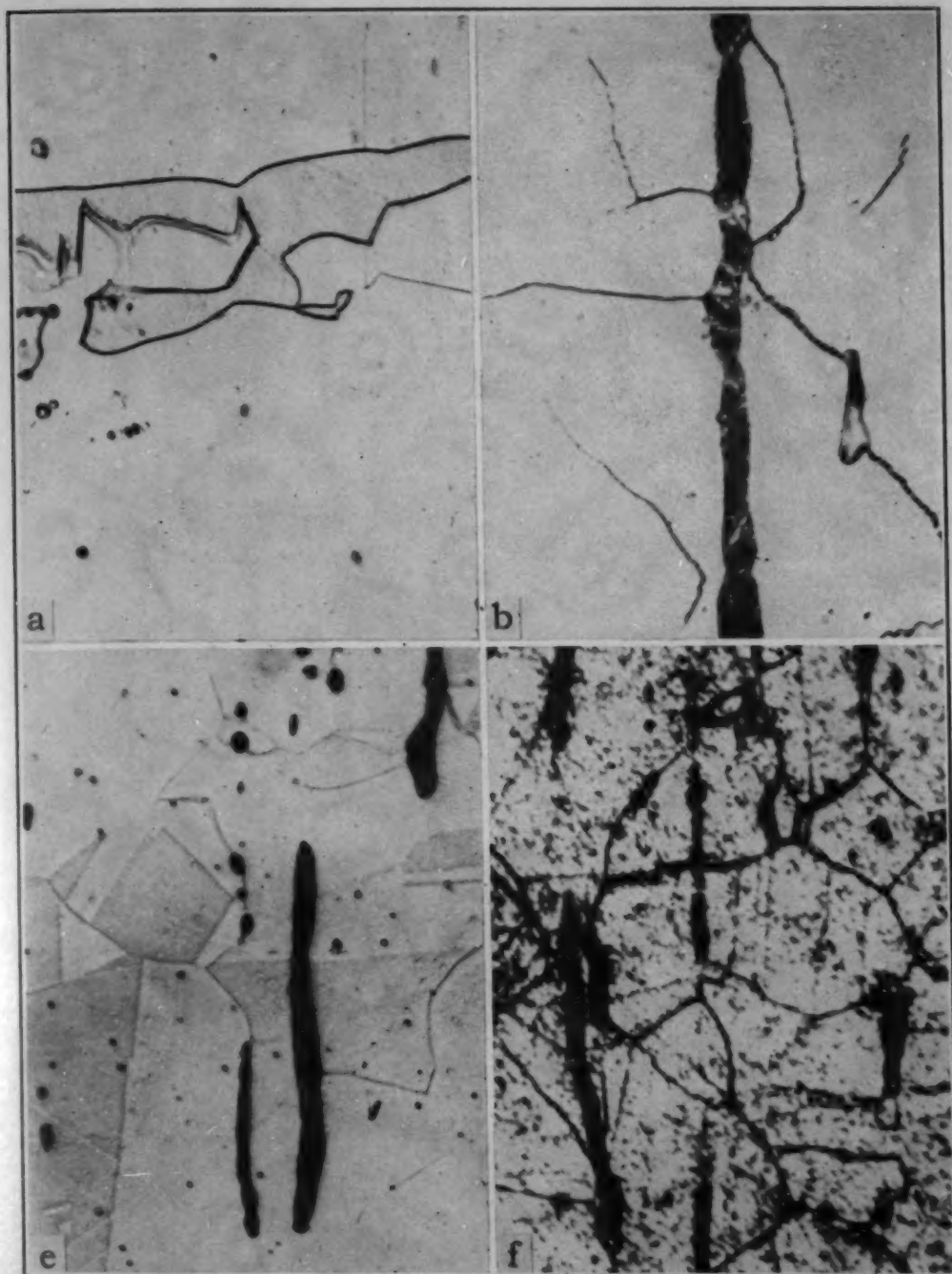


Fig. 17—Microstructure of Steels C and E Before and After Creep Tests at Indicated Temperatures for 3000 Hours Except C, the Test Time of Which Was 480 Hours. Picric-HCl etch. $\times 1000$. Specimens (a), (b), (c) and (d)—Steel C, Type 316L; Specimens (e), (f), (g) and (h)—Steel E, Type 303; Specimens (a) and (e)—quenched; (b) and (f)—1100°F.

1950 °F (1065 °C) quench plus 1600 °F (870 °C) air-cool heat treatments. As this steel contained more titanium and had a higher Ti : C ratio than steels of the same type previously reported (1), the delta ferrite was not unexpected, in contrast to its absence in the two steels previously studied. The difference in initial heat treatments for

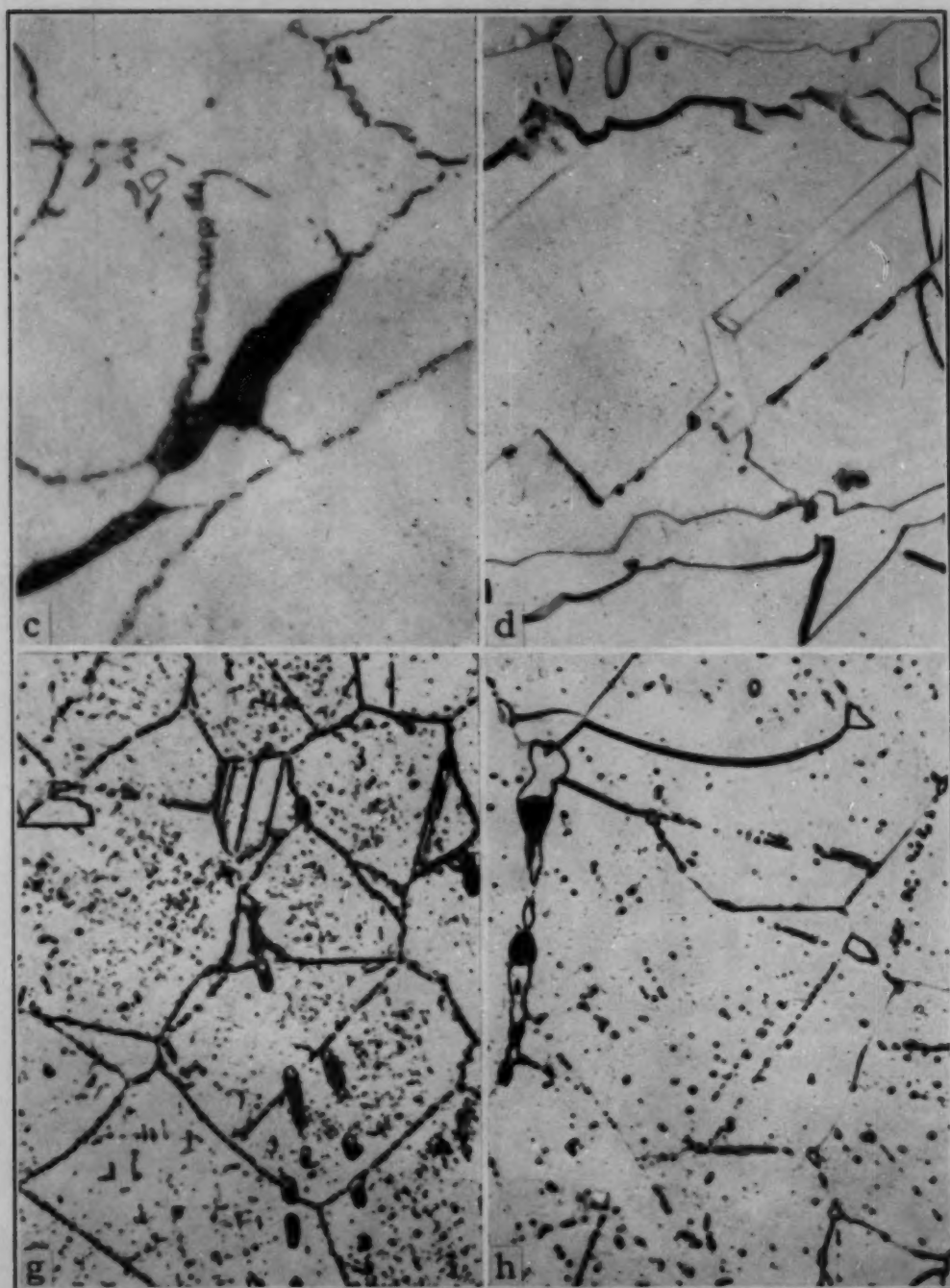


Fig. 17—Microstructure of Steels C and E Before and After Creep Tests at Indicated Temperatures for 3000 Hours Except C, the Test Time of Which Was 480 Hours. Picric-HCl etch. $\times 1000$. Specimens (a), (b), (c) and (d)—Steel C, Type 316L; Specimens (e), (f), (g) and (h)—Steel E, Type 303; Specimens (c) and (g)—1300 °F; (d) and (h)—1500 °F.

Steel H did not appear to influence the subsequent microstructure after creep exposure. Undissolved carbides did not coalesce substantially, and sigma formed both from the austenite and delta ferrite after creep exposures of 1100, 1300 and 1500 °F (595, 705 and 815 °C); the amount of sigma was greatest after the 1300 °F (705 °C) ex-

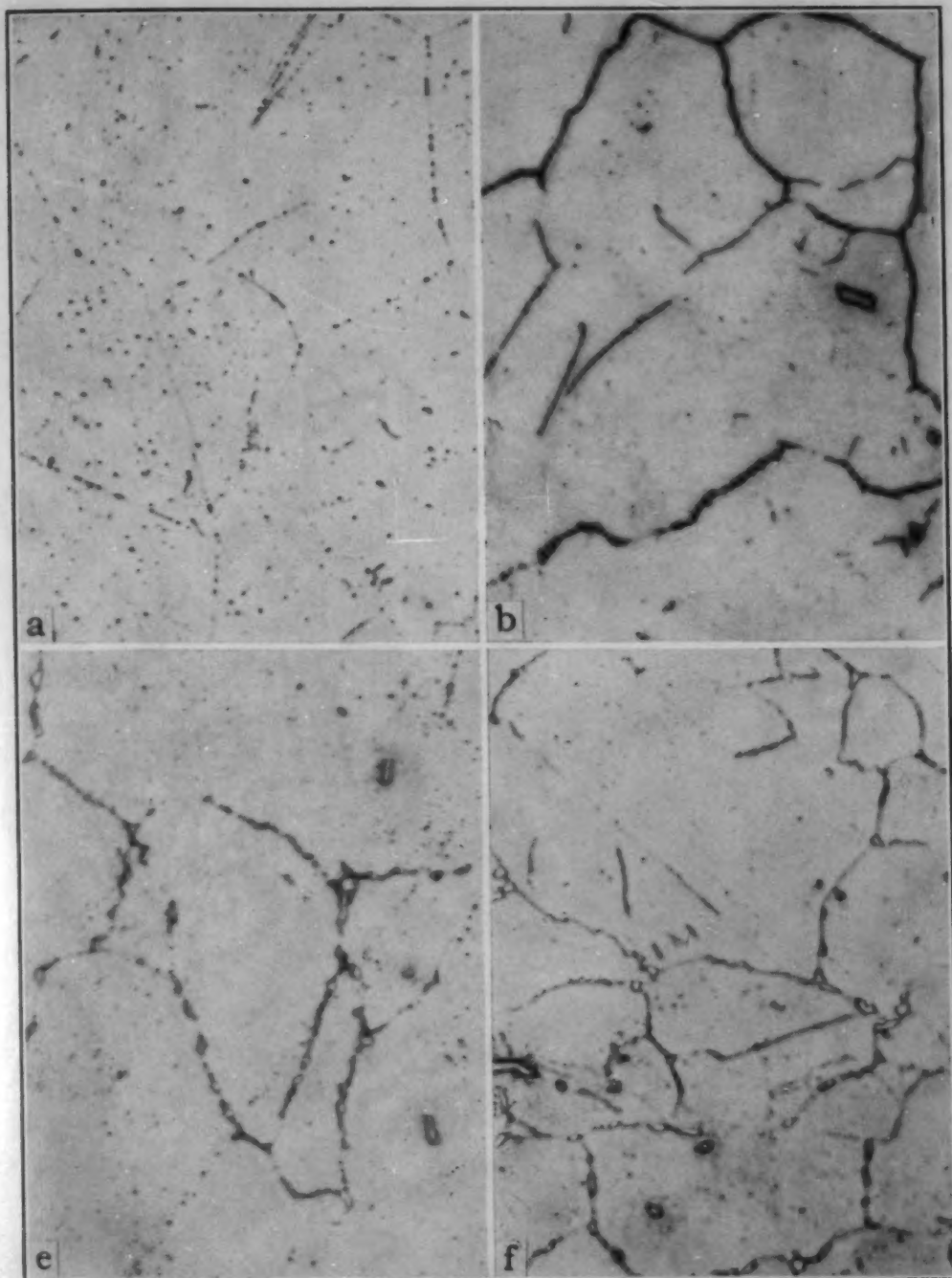


Fig. 18—Microstructure of Steel D (18-8-Mo-Cb) Before and After Creep Tests at Indicated Temperatures for 3000 Hours. Figs. a-d were initially quenched from 2000 °F (1095 °C) and Figs. e-h were quenched from 2000 °F and air-cooled after 2 hours at 1600 °F (870 °C). Sigma particles are shown in e before creep test. Picric-HCl etch. $\times 1000$. Specimens (a), (b), (c) and (d)—Steel D, Type 316 Cb, initially quenched; Specimens (e), (f), (g) and (h)—Steel D, Type 316 Cb, initially quenched and stabilized; Specimens (a) and (e)—before test; (b) and (f)—1100 °F.

posure and least after the 1100 °F (595 °C) exposure; the size of particles increased with temperature. Some delta ferrite particles apparently remained untransformed after exposure at each test tempera-

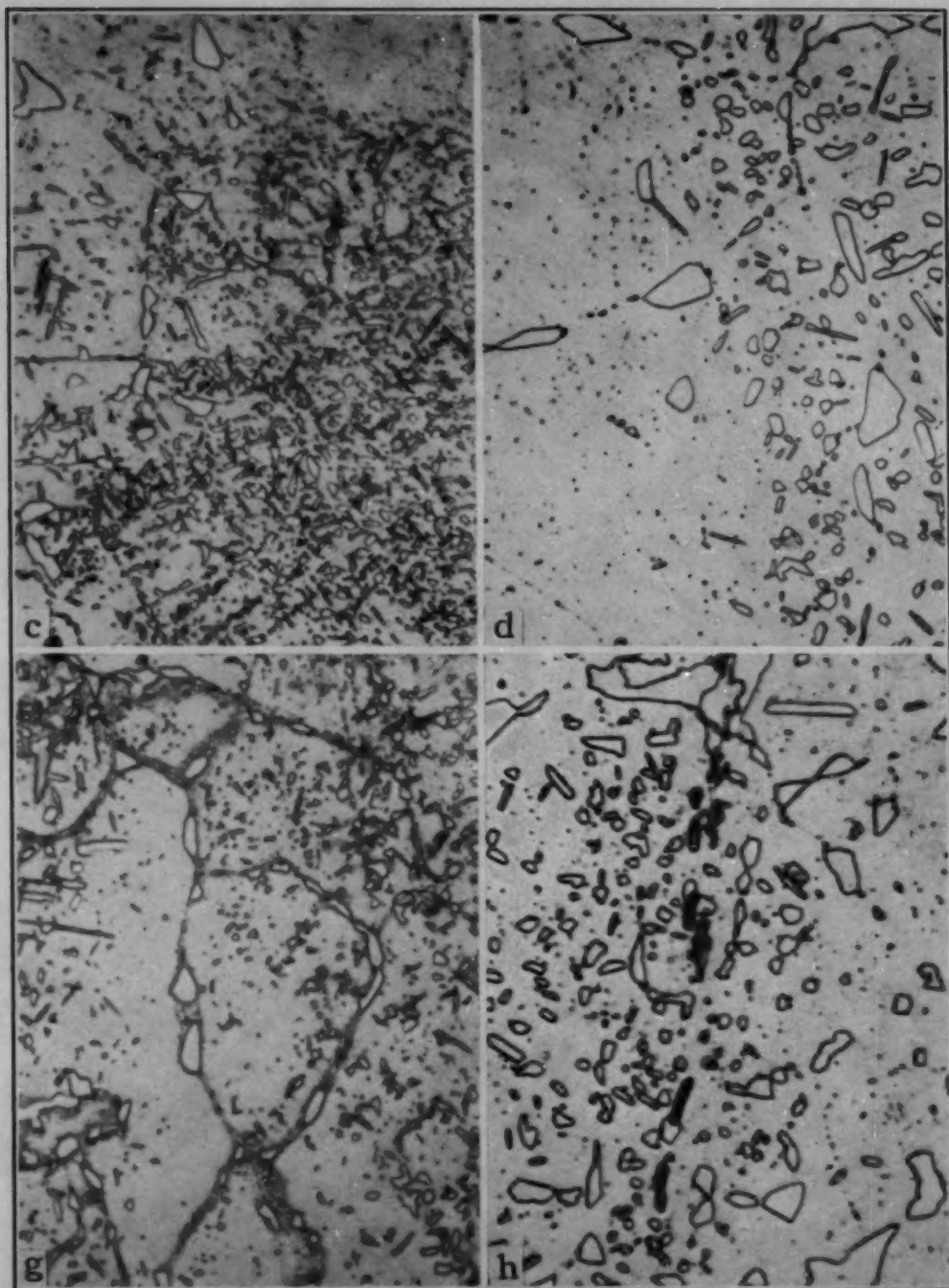


Fig. 18—Microstructure of Steel D (18-8-Mo-Cb) Before and After Creep Tests at Indicated Temperatures for 3000 Hours. Figs. a-d were initially quenched from 2000 °F (1095 °C) and Figs. e-h were quenched from 2000 °F and air-cooled after 2 hours at 1600 °F (870 °C). Sigma particles are shown in e before creep test. Picric-HCl etch. $\times 1000$. Specimens (a), (b), (c) and (d)—Steel D, Type 316 Cb, initially quenched; Specimens (e), (f), (g) and (h)—Steel D, Type 316 Cb, initially quenched and stabilized; Specimens (c) and (g)—1300 °F; (d) and (h)—1500 °F.

ture. This surprising observation was confirmed by magnetic permeability measurements.

The creep-rupture specimens tested, generally for less than 3000 hours, showed the progressive development of the microstructures ob-

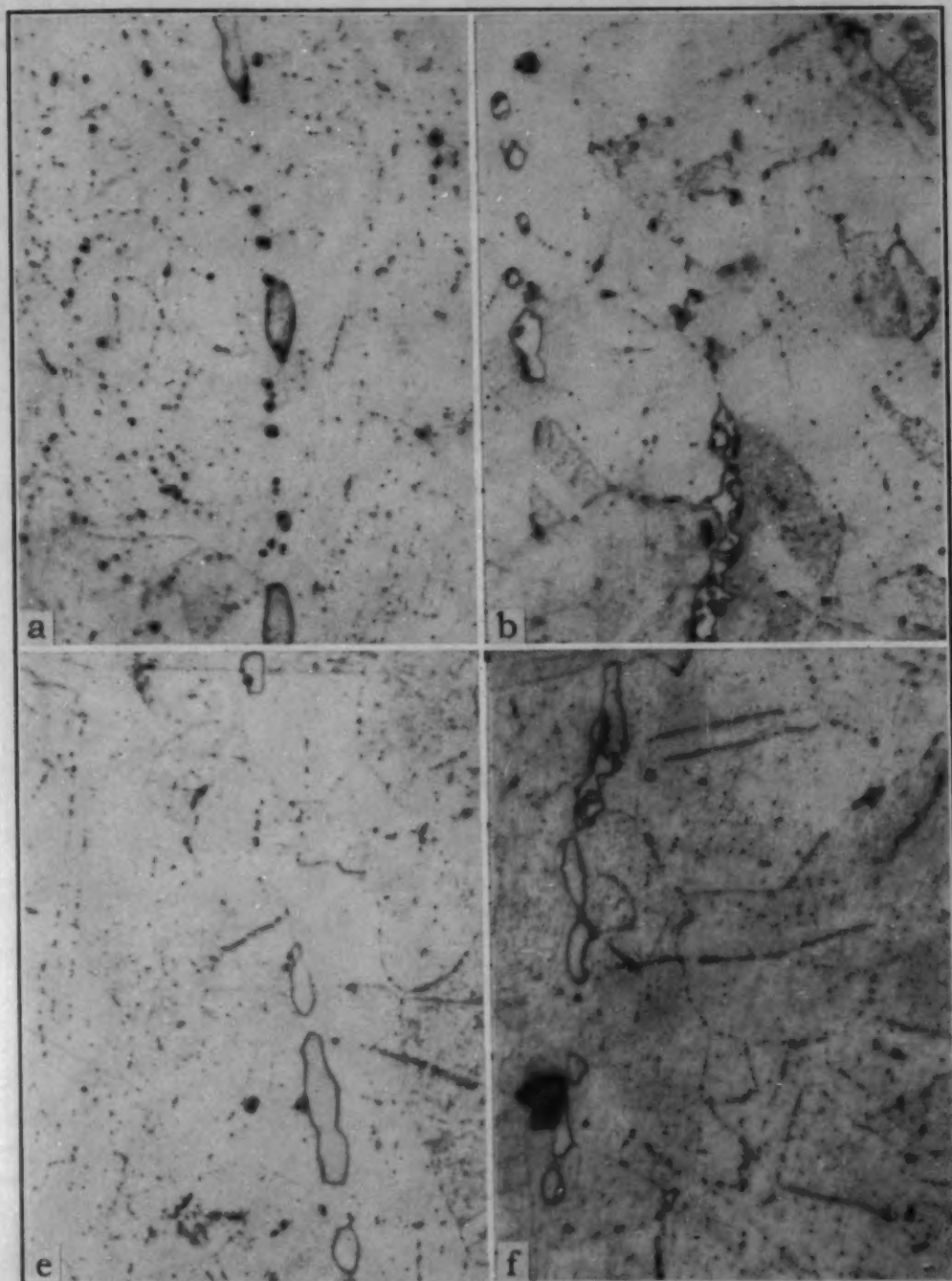


Fig. 19—Microstructure of Steel H (18-8 Ti) Before and After Creep Tests at Indicated Temperatures for 3000 Hours Except in f and g, the Test Times Being 1848 and 1704 Hours Respectively. Picric-HCl etch. $\times 1000$. Specimens (a), (b), (c) and (d)—Steel H, Type 321, initially quenched; Specimens (e), (f), (g) and (h)—Steel H, Type 321, initially quenched and stabilized; Specimens (a) and (e)—before test; (b) and (f)—1100 °F.

served after the 3000-hour creep tests. In addition, the formation of chromium nitrides, as a Widmanstätten or pearlitic-like phase, was found in specimens of Steels A (304L) and C (316L) after long-time creep-rupture tests at 1500 °F (815 °C), and in Steel F (304) after tests at 1050 and 1200 °F (565 and 650 °C).

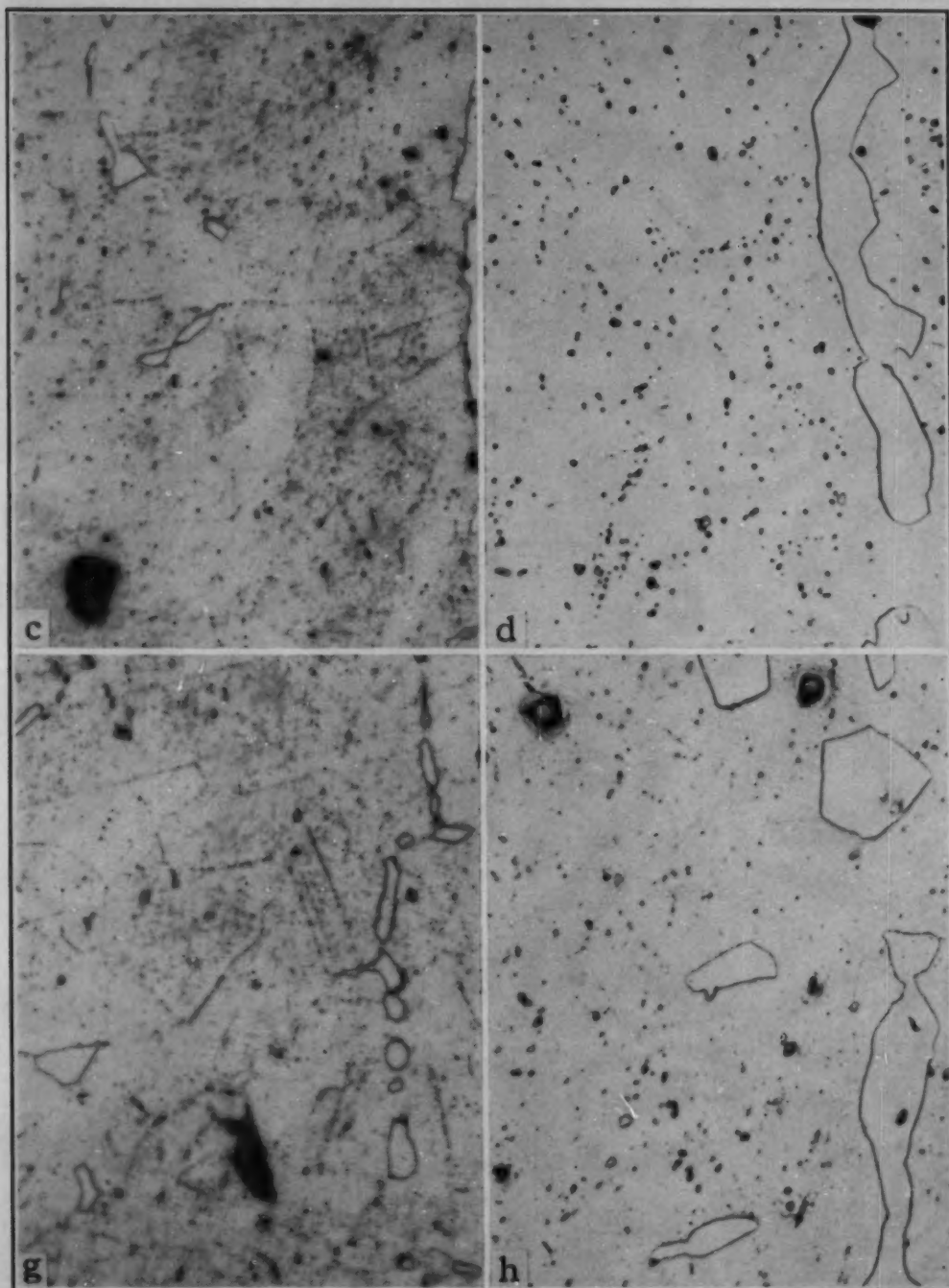


Fig. 19—Microstructure of Steel H (18-8 Ti) Before and After Creep Tests at Indicated Temperatures for 3000 Hours Except in f and g, the Test Times Being 1848 and 1704 Hours Respectively. Picric-HCl etch. $\times 1000$. Specimens (a), (b), (c) and (d)—Steel H, Type 321, initially quenched; Specimens (e), (f), (g) and (h)—Steel H, Type 321, initially quenched and stabilized; Specimens (c) and (g)—1300 °F; (d) and (h)—1500 °F.

Mode of fracture was generally similar to that described in detail previously for austenitic steels (1), i.e., intergranular fracture tends to occur with high test temperature and slow strain rate, while transgranular fracture is more apt to occur at lower test temperature and

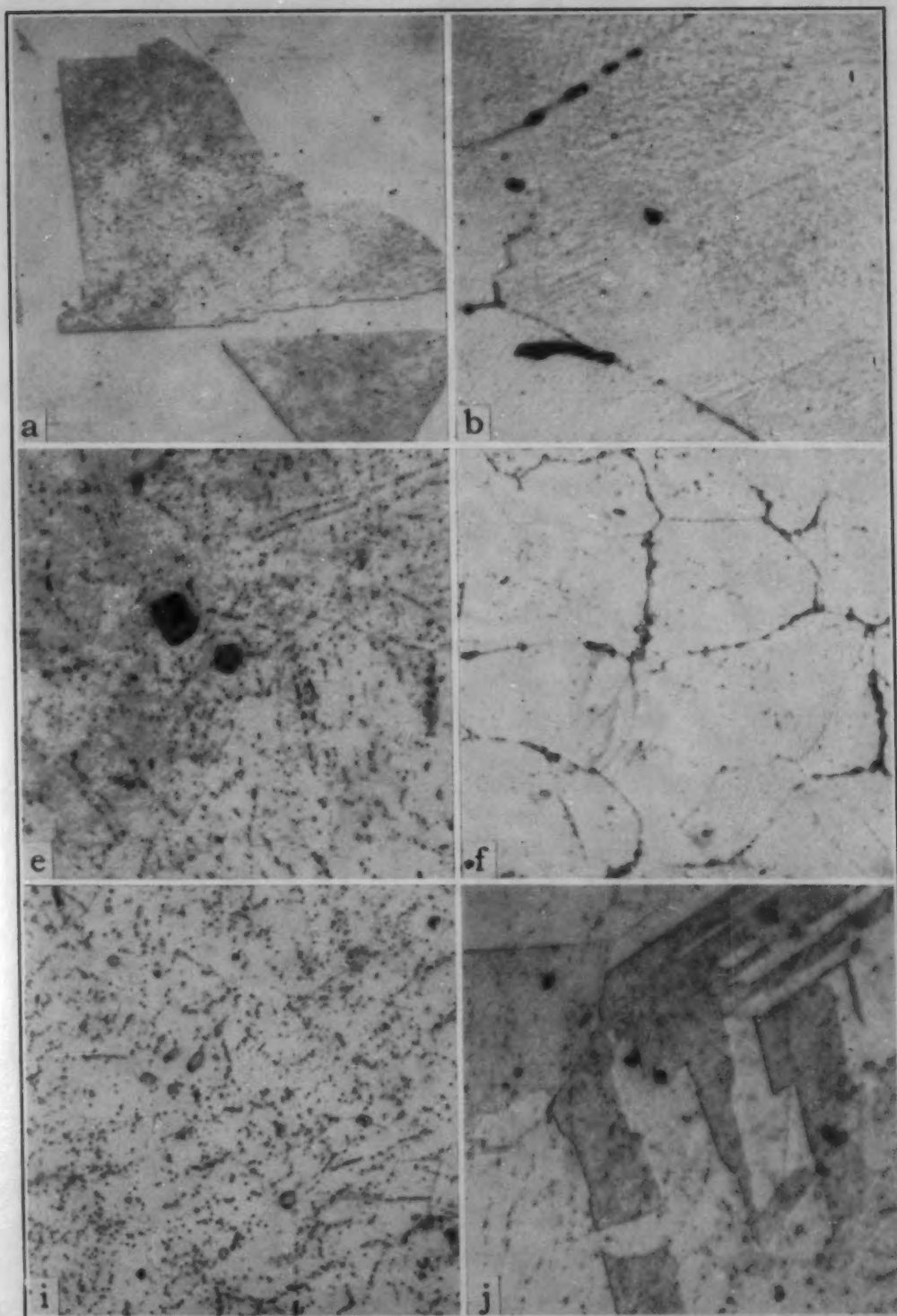


Fig. 20—Steels F (304), G (321) and I (347) Before and After Long Creep-Rupture Tests at 900, 1050 and 1200 °F (480, 565 and 650 °C); F Tested for 1079 Hours at 900 °F, 1972 Hours at 1050 and 2987 Hours at 1200 °F; G, 2052 Hours at 900 °F, 2145 Hours at 1050 °F and 2124 Hours at 1200 °F; I, 8300 Hours at 900 °F, 1150 Hours at 1050 °F and 4522 Hours at 1200 °F. Picric-HCl etch. $\times 1000$. Specimens (a), (e) and (i)—annealed; (b), (f) and (j)—900 °F.

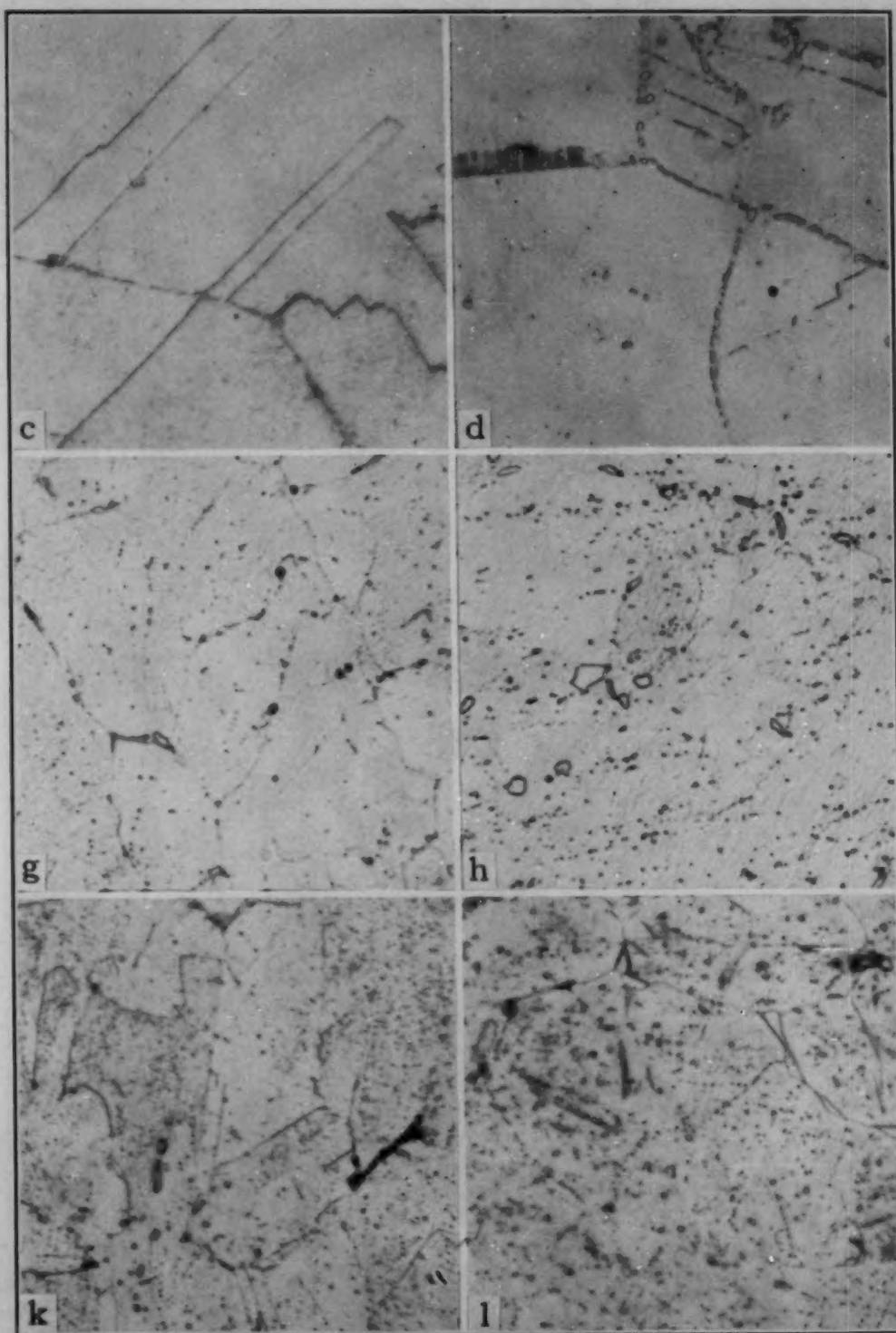


Fig. 20—Steels F (304), G (321) and I (347) Before and After Long Creep-Rupture Tests at 900, 1050 and 1200 °F (480, 565 and 650 °C); F Tested for 1079 Hours at 900 °F, 1972 Hours at 1050 and 2987 Hours at 1200 °F; G, 2052 Hours at 900 °F, 2145 Hours at 1050 °F and 2124 Hours at 1200 °F; I, 8300 Hours at 900 °F, 1150 Hours at 1050 °F and 4522 Hours at 1200 °F. Picric-HCl etch. $\times 1000$. Specimens (c), (g) and (k)—1050 °F; (d), (h) and (l)—1200 °F.

faster strain rate; both types of fracture may be found at each test temperature, depending on the strain rate (rupture time).

The association of change in fracture type with the break in the curve of log stress versus log time for rupture, the greater slope portion corresponding to intergranular fracture, was indicated to be substantially valid, but the transition from transgranular to intergranular fracture was found to be gradual rather than abrupt as the curves suggest, thus confirming previous observations (1).

Microstructures of Steels F (304), G (321) and I (347) tested in creep-rupture at 900, 1050 and 1200 °F (480, 565 and 650 °C) are shown in Fig. 20. Strain markings were noted in Steel F tested at 900 °F (480 °C),⁵ the markings being more pronounced at shorter rupture times (higher strain rates) than those shown in Fig. 20. Precipitation and coalescence of carbide in this steel with increasing test temperature are shown in Fig. 20 b, c, d; a pearlitic-like structure, presumably nitrides, was also found associated with the general intergranular cracking of impending rupture in 1050 and 1200 °F (565 and 650 °C) specimens. Figs. 20 e to h show for Steel G the increase in quantity and size of sigma particles as the exposure temperature increased. Figs. 20 i to l show the microstructural changes in Steel I during test; after 900 °F (480 °C) for 8300 hours some of the grains appear darkened by a precipitation of submicroscopic particles, and after 4522 hours at 1200 °F (650 °C) large sigma particles were found at grain boundaries and grain junctions.

MAGNETIC PERMEABILITY STUDIES

As austenite, sigma, and chromium carbide are paramagnetic, magnetic permeability tests provide a sensitive measure of relative amounts of ferrite which may be present initially as delta ferrite or which may be induced by the long-time heat treatment of the creep-test exposure. Induced ferrite found by this method was difficult, if not impossible, to detect by metallographic means; in addition, metallographic identification of delta ferrite was substantiated by the magnetic tests. The results for creep-test specimens before and after creep are given in Table V. Completely austenitic alloys have a permeability of approximately 1.003, and the presence of sigma or chromium carbide does not increase this permeability.

Permeabilities of Steels A (304L), B (304L, high N), C (316L) and H (321), before and after creep test, indicate that a slight amount of delta ferrite was originally present and partially transformed to a nonmagnetic phase during the long-time exposure at the test tem-

⁵ The appearance of strain markings suggests the possibility of a different mode of plastic deformation at this lower test temperature than that for the tests at higher temperatures.

Table V
Magnetic Permeabilities Before and After Creep Tests^a

Steel	Type	Original Heat Treatment	Test Temperature °F	Magnetic Permeability
A	304L	Q	Orig. Material	1.0104
A	304L	Q	1100	1.0062
A	304L	Q	1300 ^b	1.0082
A	304L	Q	1500	1.0068
B	304L (High N)	Q	Orig. Material	1.0095
B	304L (High N)	Q	1100	1.163
B	304L (High N)	Q	1100 + (-105) [†]	1.238
B	304L (High N)	Q	1300	1.0091
B	304L (High N)	Q	1500	1.0030
C	316L	Q	Orig. Material	1.0619
C	316L	Q	1100	1.0334
C	316L	Q	1300 ^c	1.0264
C	316L	Q	1500	1.0040
D	316 Cb	Q	Orig. Material	1.0040
D	316 Cb	Q	1100	1.0037
D	316 Cb	Q	1300	1.0039
D	316 Cb	Q	1500	1.0040
D	316 Cb	QN	Orig. Material	1.0033
D	316 Cb	QN	1100	1.0034
D	316 Cb	QN	1300	1.0038
D	316 Cb	QN	1500	1.0039
E	303	Q	Orig. Material	1.0032
E	303	Q	1100	1.0225
E	303	Q	1300	1.0063
E	303	Q	1500	1.0052
H	321	Q	Orig. Material	1.0166
H	321	Q	1100	1.0092
H	321	Q	1300	1.0068
H	321	Q	1500	1.0083
H	321	QN	Orig. Material	1.0222
H	321	QN	1100 ^d	1.0076
H	321	QN	1300 ^e	1.0112
H	321	QN	1500	1.0077

^a3000 hours except as indicated. ^bCreep test of 2088-hour duration. ^c480 hours. ^d1848 hours. ^e1704 hours. [†]Quenched in dry ice at -105 °F for 15 minutes.

peratures; Steels B and C were substantially paramagnetic after the 1500 °F (815 °C) test.

Steel B (304L, high N) showed a pronounced increase in permeability after test at 1100 °F (595 °C). The extent of the increase suggests a transformation of the martensitic type on cooling from the test temperature, a phenomenon described in detail for an 18 Cr-8 Ni steel in Ref. 6. Presumably, the chemical composition of the austenite became unbalanced, due to the formation of chromium nitride and carbide, the resultant lowering of the chromium content of the matrix being such as to permit the martensite reaction to occur. Tests on the 1100 °F (595 °C) specimen showed a permeability of 1.163 before and 1.238 after an immersion into dry ice at -105 °F, indicating further transformation of a martensitic type on cooling to subatmospheric temperature. The permeability of the 1300 °F (705 °C) specimen indicated some ferrite to be present which was

not observed in the microstructure; the 1500 °F (815 °C) specimen was paramagnetic.

Steel E (303) was initially paramagnetic and showed its highest permeability after test at 1100 °F (595 °C); the steel was also slightly magnetic after creep tests at 1300 and 1500 °F (705 and 815 °C).

The permeability of Steel D (316 Cb) remained constant at the paramagnetic level, indicating no initial delta or induced ferrite during creep test.

SUMMARY AND CONCLUSIONS

The principal findings of the investigation are:

1. With regard to reproducibility of properties in the same nominal grade, excellent agreement was obtained with Type 304, slight scatter was observed with Type 347, whereas Type 321 showed relatively wide scatter in respect to creep rate, but only slight scatter in respect to creep-rupture strength. Relatively few heats of each grade were tested, however, and it is possible that tests of additional heats may indicate variations not encountered in this investigation.

2. Whereas previous study had indicated little difference in strength between annealed or stabilized Type 321, or between annealed or stabilized Type 347, Type 321 Steel H of the present study was slightly inferior in the stabilized condition. Stabilization heat treatment of 316 Cb slightly decreased creep-rate strength at 1300 and 1500 °F (705 and 815 °C) and creep-rupture strength at 1300 °F (705 °C).

3. The extra low carbon (0.03 max.) grades of Types 304 and 316, i.e., 304L and 316L, are significantly weaker in creep than the corresponding standard carbon grades. Nitrogen addition to 304L raises the strength at 1100 and 1300 °F (595 and 705 °C) so that it exceeds that of 304; however, at 1500 °F (815 °C) nitrogen is ineffective.

4. No general statement regarding the relative strengths of 321 and 347 can be made other than that Type 347 does appear to be superior in the intermediate range at about 1100 °F (595 °C).

5. Free-machining 18-8, Type 303, and Type 304 have substantially the same creep strengths at 1100, 1300 and 1500 °F (595, 705 and 815 °C).

6. Study of the effect of creep-test exposure on notch-impact strength, hardness and tensile properties showed that notch-impact strength was most affected. Greatest decrease in impact strength was observed in 316 Cb. Relatively slight changes were observed in 304L with or without high nitrogen.

7. Sigma formation and carbide precipitation were the principal microstructural changes observed. Sigma formed most rapidly (even during stabilizing heat treatment) and most plentifully (up to 15%) in Type 316 Cb. In contrast, Type 321 Steel H showed no sigma

after stabilization heat treatment, even though containing delta ferrite, and some delta ferrite apparently persisted untransformed throughout the 3000-hour creep test. Sigma was observed in all of the low carbon (0.03) grades but probably formed from delta ferrite.

8. Nitrogen absorption from the atmosphere, as previously observed, was encountered.

ACKNOWLEDGMENTS

W. B. Seens and W. L. Jensen made the room temperature mechanical tests and K. G. Carroll and D. S. Miller aided in the X-ray diffraction studies.

References

1. G. V. Smith, E. J. Dulis and E. G. Houston, "Creep and Rupture of Several Chromium-Nickel Austenitic Stainless Steels", *TRANSACTIONS, American Society for Metals*, Vol. 42, 1950, p. 935-980.
2. G. V. Smith, W. G. Benz and R. F. Miller, "Creep and Creep-Rupture Testing", *Proceedings, American Society for Testing Materials*, Vol. 47, 1947, p. 615-638.
3. R. B. Sosman and J. B. Austin, "An Apparatus for Measuring the Magnetic Susceptibility of Liquids and Solids at High Temperatures", *Journal, Washington Academy of Sciences*, Vol. 25, 1935, p. 15-32.
4. E. J. Dulis and G. V. Smith, "Identification and Mode of Formation and Re-Solution of Sigma Phase in Austenitic Fe-Cr-Ni Steels", *ASTM Special Technical Publication* 110, 3-37 (1950).
5. G. V. Smith, W. B. Seens, H. S. Link and P. R. Malenock, "Microstructural Instability of Steels for Elevated Temperature Service", *Proceedings, American Society for Testing Materials*, Vol. 51, 1951, p. 895.
6. E. J. Dulis and G. V. Smith, "Ferrite Formation Associated With Carbide Precipitation in 18 Cr-8 Ni Austenitic Stainless Steel", *TRANSACTIONS, American Society for Metals*, Vol. 44, 1952, p. 621.
7. K. W. Andrews, "A New Intermetallic Phase in Alloy Steels", *Nature*, Dec. 10, 1949, p. 1015.
8. W. D. Forgeng, "The Sigma Phase Investigation Program of Subcommittee VI of A10, ASTM", Union Carbide and Carbon Research Laboratory, Inc., report presented at ASTM Annual Meeting, June 1950.
9. E. J. Dulis and G. V. Smith, "Identification of Inclusions in Austenitic 18 Cr-8 Ni-Cb (Type 347) Steel", *TRANSACTIONS, American Society for Metals*, Vol. 44, 1952, p. 877.

THE EFFECT OF COMPOSITION ON THE TEMPERATURE OF SPONTANEOUS TRANSFORMATION OF AUSTENITE TO MARTENSITE IN 18-8-TYPE STAINLESS STEEL

BY G. H. EICHELMAN, JR., AND F. C. HULL

Abstract

The effect of composition on the temperature at which the martensitic transformation begins in 18-8-type stainless steels during cooling was determined by dilatometric measurements and can be expressed by a simple linear equation. The relative effectiveness of the additions, in their normal composition ranges, in lowering the M_s temperature increases in the following order: silicon, manganese, chromium, nickel, carbon and nitrogen. M_s changes caused by carbide precipitation can be used as a sensitive means for determining the solubility of carbon in stainless steel.

INTRODUCTION

CONSIDERABLE attention has been given in the past to the microstructure of austenitic stainless steels, the stability of the phases present in these steels and the effects of amount and distribution of the phases on properties and behavior of the material in service. For example, when stainless steel is used as a welding electrode, a composition producing a certain percentage of ferrite in the weld deposit has been considered as beneficial in reducing weld cracking and in increasing the creep resistance of the weld at elevated temperatures. However, for stainless steel applications involving highly corrosive solutions, a fully austenitic structure may be preferred to one containing ferrite. The presence of ferrite is also undesirable in steels to be used at elevated temperatures for extended periods of time because of the accelerating effect of ferrite on sigma phase formation and the resulting impairment of room temperature ductility and toughness.

Completely stable austenitic steels possess many desirable characteristics. Their single-phase, face-centered-cubic crystal structure permits difficult hot forming operations, and the absence of transformation during deformation gives them good cold fabrication properties. They have high resistance to corrosion, excellent ductility at subzero temperatures and useful nonmagnetic characteristics.

A paper presented before the Thirty-fourth Annual Convention of the Society, held in Philadelphia, October 18 to 24, 1952. Of the authors, G. H. Eichelman, Jr., is connected with the American Brass Co., Waterbury, Conn., formerly research engineer, Westinghouse Research Laboratories, and F. C. Hull is manager, Metallurgical Section, Westinghouse Research Laboratories, East Pittsburgh, Pa. Manuscript received May 16, 1952.

Austenite instability can have beneficial effects, however, as illustrated by the process recently developed by Ziegler and Brace (1).¹ Stainless steel alloys in which austenite transforms to martensite during rolling or wire drawing at subzero temperatures can be produced with unusually high tensile strengths, particularly if the material is aged at 750 °F (400 °C) after deformation.

Studies of austenite stability reported in the literature have been confined mainly to the effect of composition on ferrite formation, the effect of composition on corrosion behavior and indirectly on the phases present, and the effect of composition on transformation induced by deformation. In spite of its commercial and theoretical significance, however, there are no data in the literature directly relating the composition of austenitic stainless steels to their M_s temperatures. In order to permit a better understanding of the behavior of stainless steels during fabrication and in service, and to assist in designing alloy compositions to suit specific applications, the following study of the effects of composition on the austenite-to-martensite transformation was undertaken. A specific practical objective of the research was to provide a means of calculating the M_s temperature of an alloy from its composition.

LITERATURE REVIEW

"Stability of austenite" is a general concept that has been used to express different things by different people. In a strict sense, a stable austenite is one which, at a given temperature, is thermodynamically stable. It is the equilibrium phase, regardless of the extreme measures and long holding times that may be required to establish such a state. This term has been applied more loosely to refer to wrought or cast alloys in which (a) no delta ferrite is present or forms during holding at elevated temperatures, that is, ferrite that does not transform to austenite on cooling; (b) no martensitic ferrite forms from austenite on cooling; or (c) no martensitic ferrite formation is induced by plastic deformation at a given temperature.

The effect of alloying additions on austenite stability is generally expressed in chromium or nickel equivalents, depending on whether they are ferrite or austenite stabilizers. This classification is based on the tendency for a single element when added to iron to close or open the gamma loop. In respect to (delta) ferrite formation at high temperatures, nickel, manganese, carbon and nitrogen are austenite stabilizers, and chromium and silicon are ferrite formers. Confusion may arise from the fact that all of the above elements increase the stability of austenite with respect to M_s , the temperature of spontaneous martensite formation on cooling, or M_d , the highest temperature at which martensite will form if the austenite is plastically

¹The figures appearing in parentheses pertain to the references appended to this paper.

deformed. When applying alloy element equivalents reported in the literature, it is therefore important to know how they were obtained and what they mean.

An initially austenitic structure is metastable down to the M_s or M_d temperatures, even though these temperatures are considerably below the solubility limit of ferrite in austenite. Owen and Liu (2) in their work on the ferrite plus austenite field of the iron-nickel system at equilibrium found it necessary to produce martensite first in order to have low nickel ferrite and high nickel austenite form by diffusion at temperatures within the ferrite plus austenite field. De-

Table I
Chromium and Nickel Equivalents Determined by Various Investigators
for Wrought Stainless Steels

Basis of Evaluation	Tendency to Form Delta Ferrite			Corrosion Resistance
	Thielemann (3)	Fleischman (4)	Binder, Brown and Franks (5)	Binder, Brown and Franks (5)
Reference				
Element				
Carbon	-40	-30	-23
Nitrogen	-20
Nickel	-3	-1	-0.8	-0.7
Manganese	-2	-0.5
Titanium	+7.2
Silicon	+5.2
Columbium	+4.5
Molybdenum	+4.2	+2 Cr	+1.4	+2.25
Chromium	+1	+Cr*	+1	+1
	(+) Increases the amount of delta ferrite. (-) Decreases the amount of delta ferrite.			(+) Increases corrosion resistance. (-) Decreases corrosion resistance.
Basis of Evaluation	Martensite Transformation Induced by Deformation	Temperature of Spontaneous Martensite Formation		
		Post and Eberly (6)	Scott (7)	This Work
Reference				
Element				
Carbon	+35		+30	+27
Nitrogen	+27
Nickel	+1		+1	+1
Manganese	+0.5		+2.5	+0.55
Titanium
Silicon	+0.45
Columbium
Molybdenum	+1.5 Cr	
Chromium	+Cr*		+0.68
	(+) Lowers the M_d temperature.		(+) Lowers the M_s temper- ature.	

*The relationships between the effects of chromium and nickel were not given.

formed austenite would not decompose to ferrite and austenite of different compositions, regardless of temperature or time. From a practical viewpoint, considering the difficulties involved in attaining true equilibrium in stainless steels, other criteria of austenite stability are useful.

Various methods have been described in the literature for determining the chromium and nickel equivalents for the elements found in stainless steels. The reported results of several investigations have been listed in Table I. Thielemann (3) calculated the equivalents by the weight per cent of the element combined with iron to completely close the gamma loop. These values for binary alloys are in reasonable agreement with those determined experimentally for stainless steels. The factors obtained by Newell and Fleischman (4) for stainless steels are based on the elimination of delta ferrite. Binder, Brown and Franks (5) measured the per cent ferrite by a modified magne gage in specimens annealed 10 minutes at 1970 °F (1075 °C) and air-cooled to room temperature. Incidentally, in the absence of additional information, this method would not distinguish between delta ferrite formed during annealing and martensite produced on cooling. However, the latter authors confirmed metallographically that delta ferrite was present.

Post and Eberly (6) used the "breaking point" in the plot of permeability versus tensile strength for specimens previously cold-rolled varying degrees. These data depend upon the temperature of the M_d point relative to room temperature and might therefore be expected to also predict the approximate relative effects of the alloying elements on M_s temperatures. The nickel equivalents of manganese and carbon were determined by Scott (7) for nickel-manganese-iron alloys using M_s temperature measurements. The absence of chromium in his alloys may account for the high equivalent assigned to manganese.

There is need for information concerning the effect of carbide and nitride precipitation on the transformation of austenite to martensite. In the literature it is implied that carbide precipitation at an elevated temperature induces ferrite formation at that temperature. Although this is a possibility in certain composition ranges, in some of the standard 18-8 grades it is more likely that carbide precipitation raises the M_s temperature above room temperature, and martensite forms on cooling after aging, as described by Dulis and Smith (8). Their work, however, did not evaluate the quantitative effect of aging on the M_s temperature.

EXPERIMENTAL PROCEDURE

Low carbon ferrochromium, Armco iron, and electrolytic nickel were used in the induction melting furnace charge. The heats were deoxidized with 0.3% calcium-silicon and then additions of electrolytic manganese, commercially pure silicon and lump graphite were made. For Heats 6600 to 6865 of Table II, two ingots $1\frac{1}{4}$ by $1\frac{1}{4}$ by 11 inches were chill-cast from each heat. After the installation of a larger rolling mill, only one ingot $2\frac{3}{4}$ by $2\frac{3}{4}$ by 10 inches was

chill-cast from each heat. The small ingots were rolled from 2100 °F (1150 °C) to 1/2-inch diameter bar stock by alternate reductions of area of 15 to 20% and anneals for 5 minutes. The large ingots were rolled from 1900 °F (1040 °C) by alternate reductions and anneals to 5/8-inch diameter bar stock.

The samples for chemical analyses of the small ingots were taken from near the ends of the bars that were originally the bottoms of

Table II
Chemical Analyses and M_s Temperatures of Chromium-Nickel Stainless Steels

Heat No.	Homogenized 1 Hour at 2300 °F (1250 °C), ASTM Grain Size No. 1-2						M _s Temperatures, °F	
	Cr	Ni	Mn	Si	C	N	Measured*	Calculated
12% Cr, Variable Ni								
6696	11.9	9.7	1.39	0.42	0.025	0.034**	+174	+140
6940†	12.33	10.04	1.28	0.45	0.034	0.062	+32	-35
6908	12.24	10.25	1.33	0.42	0.030	0.039**	+4	+28
6909	12.26	10.30	1.46	0.40	0.032	0.045**	-55	-10
6903	12.18	12.04	1.36	0.47	0.031	0.032	-170	-150
6600	11.7	14.8	1.25	0.33	0.052	0.035	< -452	-479
14% Cr, Variable Ni								
6865‡	14.38	9.06	1.21	0.36	0.008	0.034	+10	+90
6866‡	14.63	10.60	1.21	0.37	0.004	0.030	-60	-75
17% Cr, Variable Ni								
6697	16.8	6.1	1.33	0.49	0.027	0.048	+156	+121
6902	17.30	7.56	1.33	0.49	0.031	0.050	-60	-95
6625	16.7	10.2	1.42	0.46	0.023	0.042	< -320§	-297
6625V	16.6	10.2	0.63	0.46	0.011	0.017	-50	-138
6626	16.8	10.2	1.38	0.37	0.023	0.084**	< -320§	-423
6627	17.0	10.1	1.29	0.42	0.110	0.038	< -320	-598
Variable C								
6694	12.0	10.0	1.31	0.42	0.023	0.036	+114	+104
6695	12.0	10.0	1.28	0.39	0.105	0.038	-82	-144
6699	16.8	6.1	1.32	0.48	0.026	0.047**	+132	+128
6700	16.8	6.1	1.31	0.44	0.107	0.053	-78	-42
Variable Mn								
6939	12.13	10.13	1.32	0.43	0.030	0.059	-18	-11
6904	12.35	10.15	3.20	0.44	0.026	0.033	-68	-51
6905	12.21	10.11	5.03	0.50	0.031	0.035	-142	-171
Variable Si								
6941	10.28	12.15	1.36	1.01	0.048	0.027	-110	-82
6906	10.46	12.00	1.42	1.42	0.036	0.027	-143	-38
6942	10.24	12.05	1.39	1.96	0.038	0.028	-97	-90
6907	10.46	12.11	1.37	2.58	0.028	0.020	-110	-80

*Determined during cooling from 2000 °F (1095 °C).

**Nitrogen bubbled through the melt.

†Half the iron charged after the ferrochromium and nickel additions.

‡Electrolytic chromium charged.

§Previous heat remelted under vacuum.

|| Above -320 °F according to magne gage measurements.

|| Below -452 °F according to magne gage measurements after 20 minutes in liquid helium.

the ingots. The large ingots were sampled at the middles of the bars produced by rolling. The surface of the samples was machined off to a depth of 1/16 inch to remove oxides and decarburized metal, and the remaining stock was milled into chips. The chemical analyses of the heats are recorded in Table II.

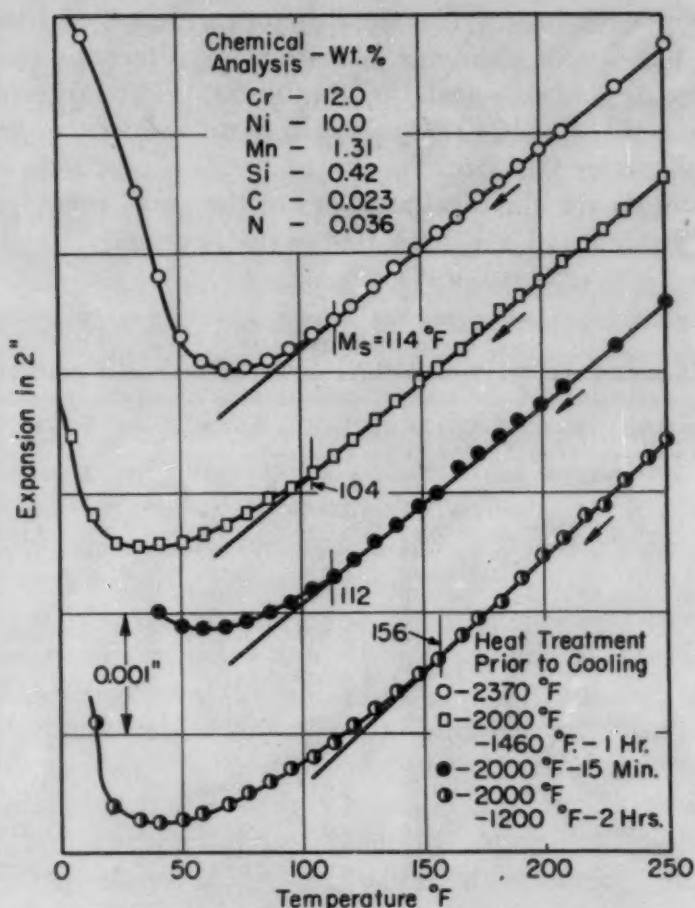


Fig. 1—The Effect of Carbide Precipitation on the Beginning of Transformation in Stainless Steel, Heat No. 6694.

The beginning of transformation upon cooling was determined by dilatometer measurements. The formation of martensite from austenite is accompanied by an increase in volume so that the beginning of transformation on cooling is detected as a change in slope when the change in length during cooling is plotted against temperature. The dilatometer used in this investigation consisted of a quartz tube closed at one end with a flat ground quartz plug to support the test specimen. A quartz push-rod with a rounded end placed inside the tube rested on one of the flat ground ends of the metal specimen. The difference in length between the tube and the push-rod was determined by the deflection of a dial gage graduated in 0.0001 inch and read to one-fourth of a division. The tube containing the specimen and push-rod was placed in a vertical tube furnace for solution treating and aging, and then removed from the furnace and air-cooled to approximately 400 °F (205 °C) to prevent carbide precipitation at temperatures in the range of 1500 to 1000 °F (815 to 540 °C).

A controlled cooling rate was maintained between temperatures

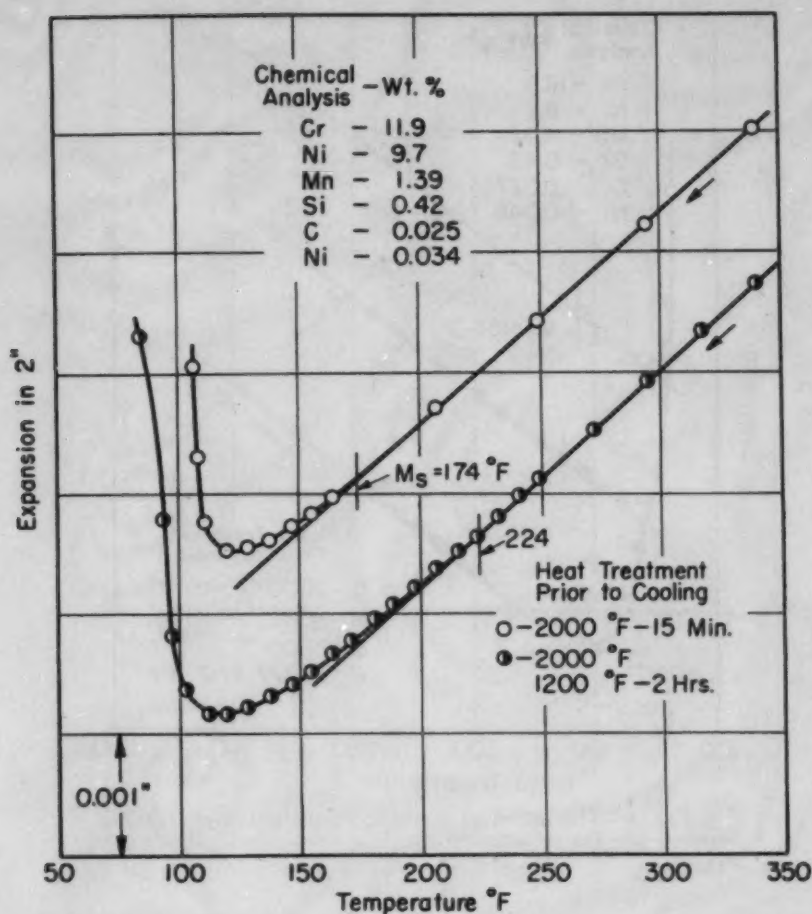


Fig. 2—The Effect of Carbide Precipitation on the Beginning of Transformation in Stainless Steel, Heat No. 6696.

of $+200^\circ\text{F}$ ($+95^\circ\text{C}$) and -320°F (-195°C) by slowly adding liquid nitrogen to the bottom of a thermos bottle in which the dilatometer tube was suspended, the cooling medium surrounding the tube being gaseous nitrogen formed by boiling of the liquid nitrogen. Several trial runs were made with thermocouples attached to the top and bottom of the specimen to determine the effect of cooling rate on the thermal gradient of the specimen. With cooling rates of 4°F per minute or less, the thermal gradient was reduced to a negligible value. Accurate temperature measurements were attained by spot welding the ends of the 7.5-mil diameter thermocouple wires to the surface of the specimen midway between the ends. The specimen, therefore, was part of the junction, thus eliminating any thermal gradient between the junction of the thermocouple and the surface of the specimen.

Dilatometer specimens $\frac{3}{8}$ inch in diameter and 2 inches long were machined from bar stock that had been annealed for 1 hour at 2300°F (1260°C) to homogenize the material and produce a uniform ASTM grain size of No. 1-2. For the M_s determinations,

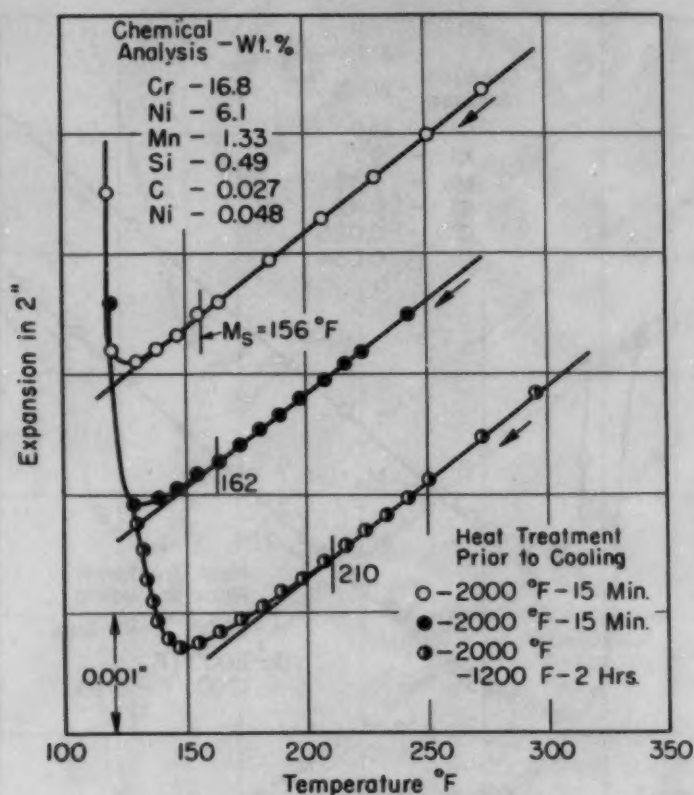


Fig. 3—The Effect of Carbide Precipitation on the Beginning of Transformation in Stainless Steel, Heat No. 6697.

the specimens were reheated, usually to 2000 °F (1095 °C), prior to cooling. All contraction curves for a given heat were obtained by successive runs on the same specimen. To assure that a solution treatment at 2000 °F (1095 °C) for 15 minutes was sufficient to redissolve the carbides precipitated by the aging treatments, the M_s temperature was redetermined for the solution-treated condition before subsequent aging treatments. The close agreement of the M_s temperatures after these two solution treatments showed that the carbides were redissolved by solution treating at 2000 °F (1095 °C) for 15 minutes and that the loss of carbon during the elevated temperature treatments was below the limits that could be detected by the dilatometric results. The 2000 °F (1095 °C) treatment also eliminated any effects due to partial transformation to martensite on the previous cooling. Sample analyses were made on Heats 6696 and 6700 to determine the effect of the various heat treatments during dilatometer measurements on the carbon contents. The results were as follows:

Heat No.	Weight Per Cent Carbon		
	Heat Analyses	Specimen Analyses After Dilatometer Tests	Difference in Composition
6696	0.025	0.020	-0.005
6700	0.107	0.115	+0.008

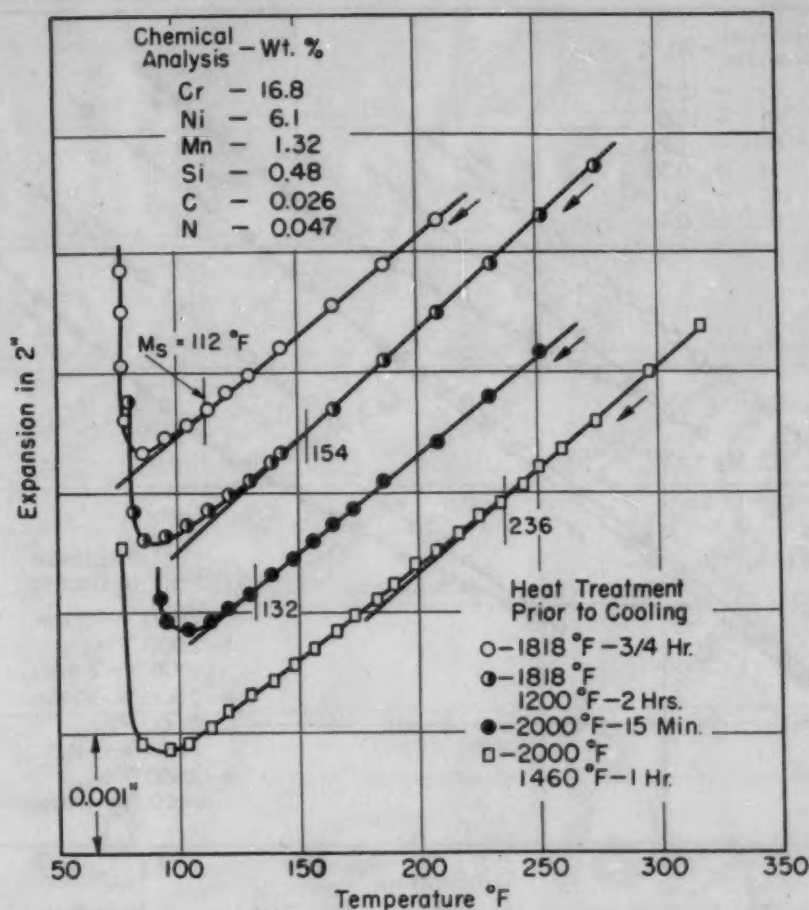


Fig. 4—The Effect of Carbide Precipitation on the Beginning of Transformation in Stainless Steel, Heat No. 6699.

The chemical analyses show no significant change in the carbon contents during the tests, since the differences are less than the probable error in the chemical analysis.

DISCUSSION OF RESULTS

Of the various alloy compositions investigated, the majority of the alloys transformed spontaneously above liquid nitrogen temperature, -320°F (-195°C). The M_s temperatures observed are recorded in Table II, and the contraction curves for several of these alloys are given in Figs. 1 to 7. The accuracy of the M_s values obtained depends upon the uniformity of temperature distribution along the length of the specimen, the cooling rate from the solution treating temperature, the cooling rate at the time transformation begins, and the sensitivity of the change in length measurements. From the various figures it can be seen that the M_s temperatures could be reproduced to within 10 to 20°F . Martensite formation was verified by metallographic examination, X-ray diffraction studies, electrical resistance, magnetic and density measurements, as well as by the dis-

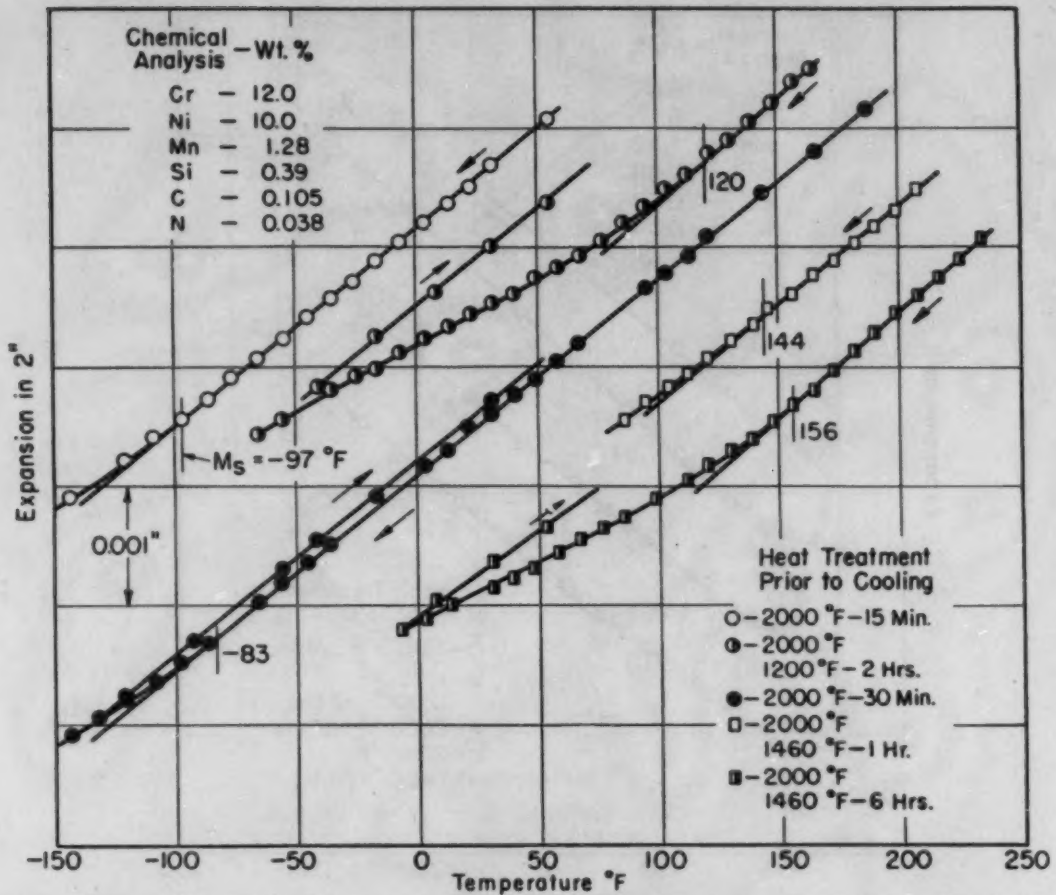


Fig. 5—The Effect of Carbide Precipitation on the Beginning of Transformation in Stainless Steel, Heat No. 6695.

placement of the expansion curve from the contraction curve to show a net increase in length.

The problem of determining the effect of composition on the M_s temperature would be simplified if it were possible to melt a series of alloys in which everything except manganese, for example, was kept constant. Actually, unavoidable differences in melting practice and recoveries led to variations in the base composition while a major change in a given element was being studied. By selecting heat compositions carefully, however, it was possible to get approximate correction factors for each of the elements. When the approximate correction factors were applied to the M_s versus composition curves for each element, closer factors were obtained. By a series of successive approximations, the final factors were derived.

Carbon and nitrogen are strong austenite stabilizers, making it necessary to correct for even the small compositional variations that exist within the present series of alloys. The effect of these elements on the M_s temperature was determined in two series of alloys with the same chromium, nickel, manganese and silicon contents and variable carbon plus nitrogen. Actually carbon was the principal variable,

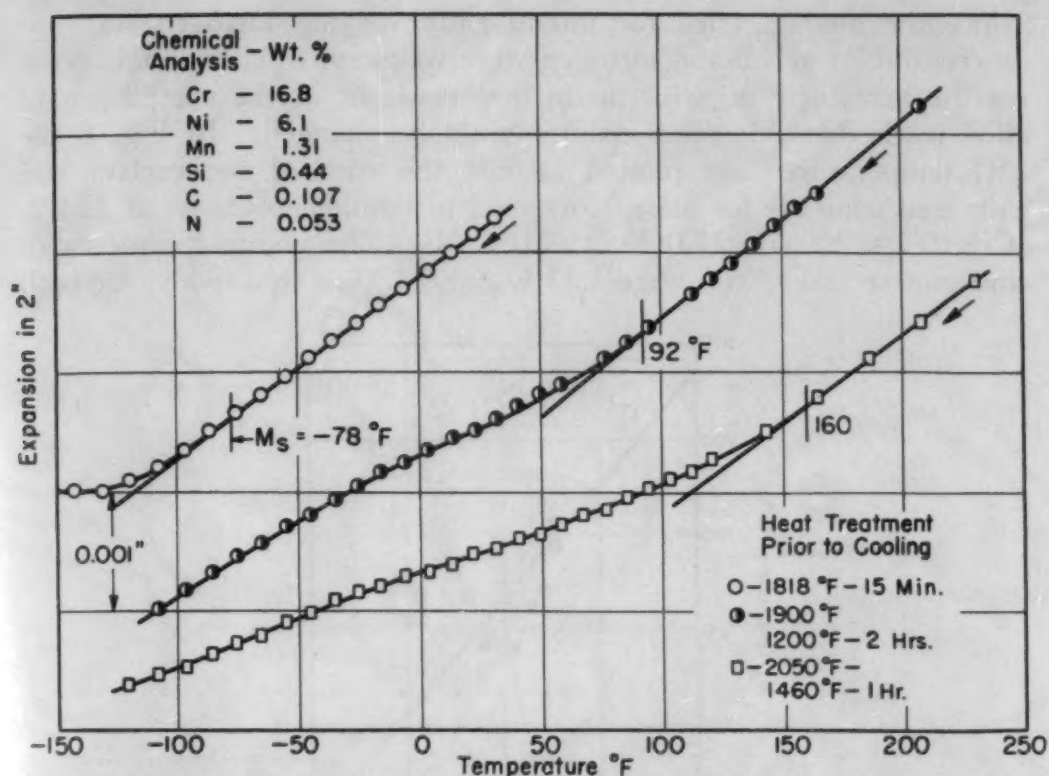


Fig. 6—The Effect of Carbide Precipitation on the Beginning of Transformation in Stainless Steel, Heat No. 6700.

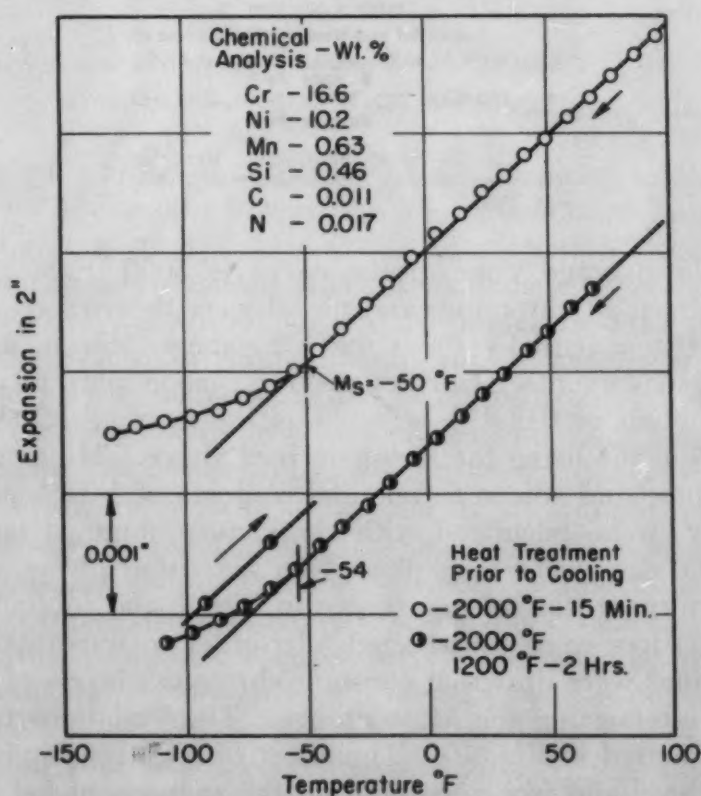


Fig. 7—Effect of Carbide Precipitation on the Beginning of Transformation in Stainless Steel, Heat No. 6625V.

since the method tried for intentionally varying nitrogen was unsuccessful. Carbon and nitrogen were weighted equally at this point in the investigation, with no further evidence at the completion of this work that this relationship should be changed. In Fig. 8 the M_s temperatures are plotted against the sum of the carbon and nitrogen contents for alloys corrected to nominal contents of 12.0% Cr, 10.2% Ni and 17.0% Cr, 7.0% Ni. The nominal contents of manganese and silicon were 1.33% and 0.47%, respectively, for both

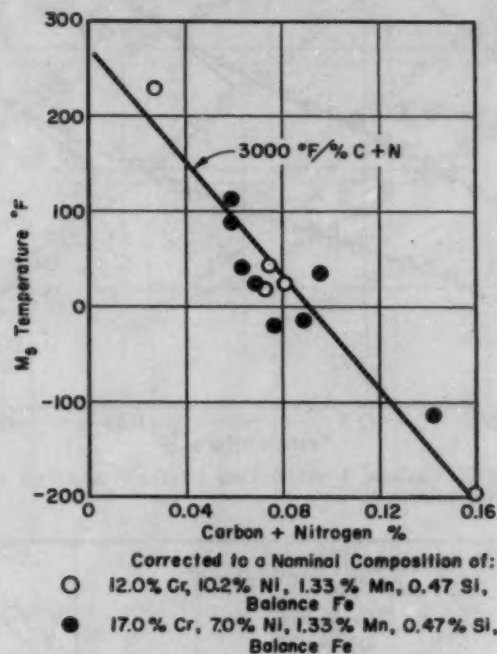
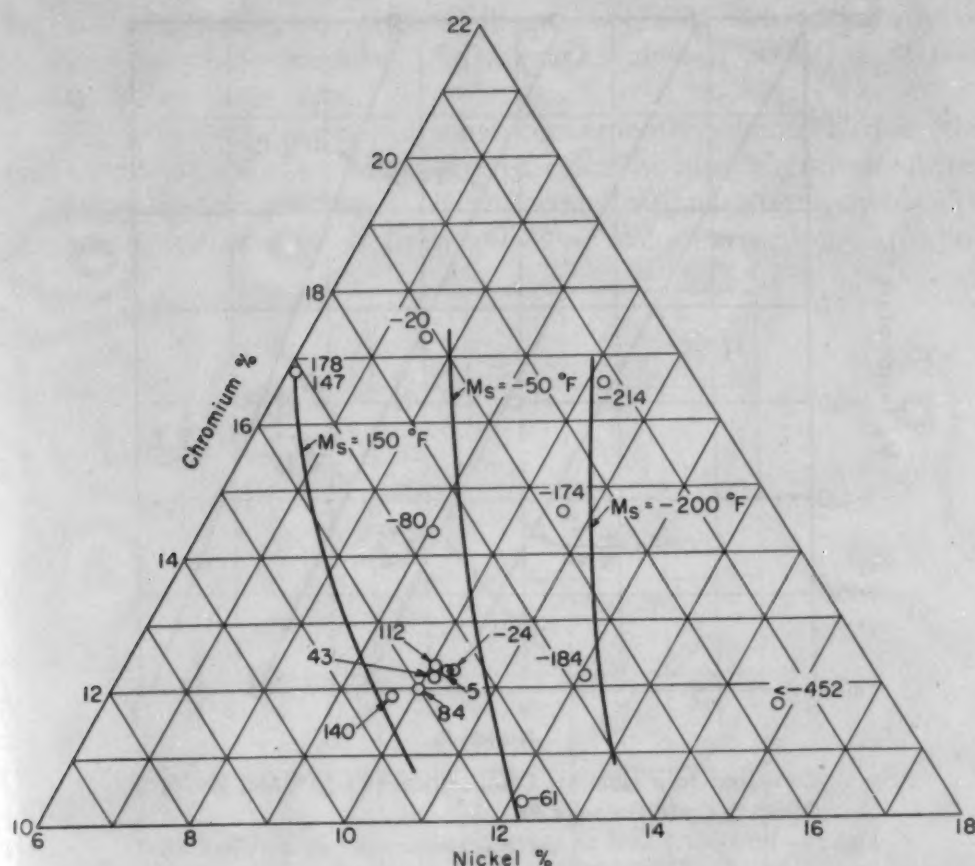


Fig. 8—Effect of Carbon Plus Nitrogen on the M_s Temperature of Stainless Steel.

series. The average slope of the curve is $3000^{\circ}\text{F}/\% (\text{C} + \text{N})$.

The effects of chromium and nickel were determined in a series of alloys with essentially the same manganese, silicon, and carbon plus nitrogen contents. Corrections for carbon plus nitrogen to a nominal content of 0.068%, which was the average content for the series, were made using the factor derived above. Minor corrections for manganese and silicon to nominal contents of 1.33% and 0.47%, respectively, were calculated with the factors obtained later in this paper. The data were then plotted on a portion of an iron-nickel-chromium ternary diagram, as shown in Fig. 9, and contours of equal M_s temperatures were constructed. In order to illustrate the effect of nickel, lines were drawn at constant chromium levels of 11, 13, 15 and 17%, intersecting the M_s contours. The variations of M_s with nickel are plotted in Fig. 10. The effect of nickel depends upon the chromium level and vice versa, but on the average, nickel lowers the M_s temperature about $110^{\circ}\text{F}/\% \text{Ni}$. A similar procedure was fol-



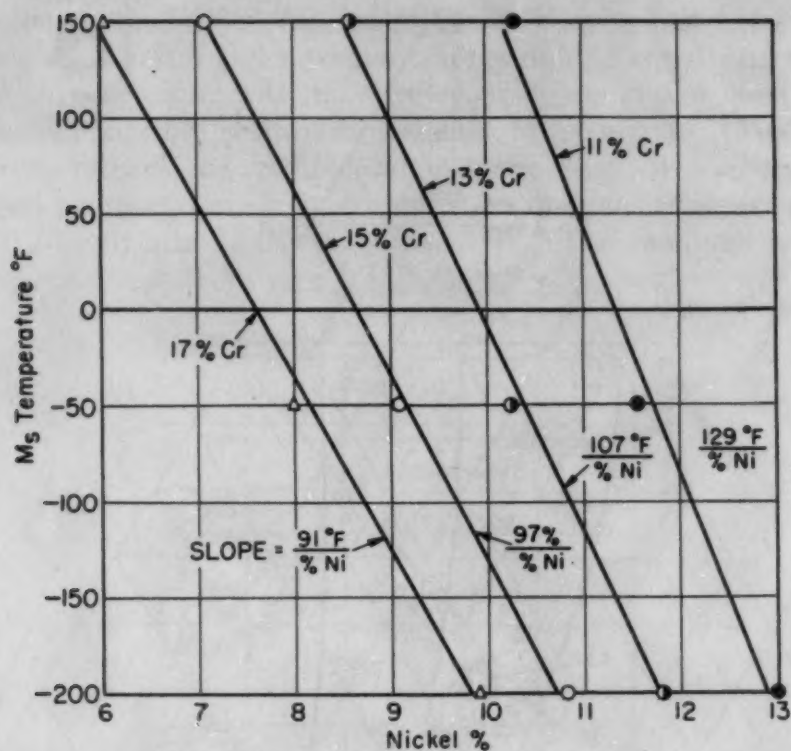
Corrected to a Nominal Composition of 1.33% Mn, 0.47% Si, 0.068% C+N and Balance Fe.

Fig. 9— M_s Temperatures of Chromium-Nickel Stainless Steels.

lowed to get the effect of chromium at several nickel levels as shown in Fig. 11. Chromium lowers the M_s temperature approximately $75^\circ\text{F}/\% \text{Cr}$.

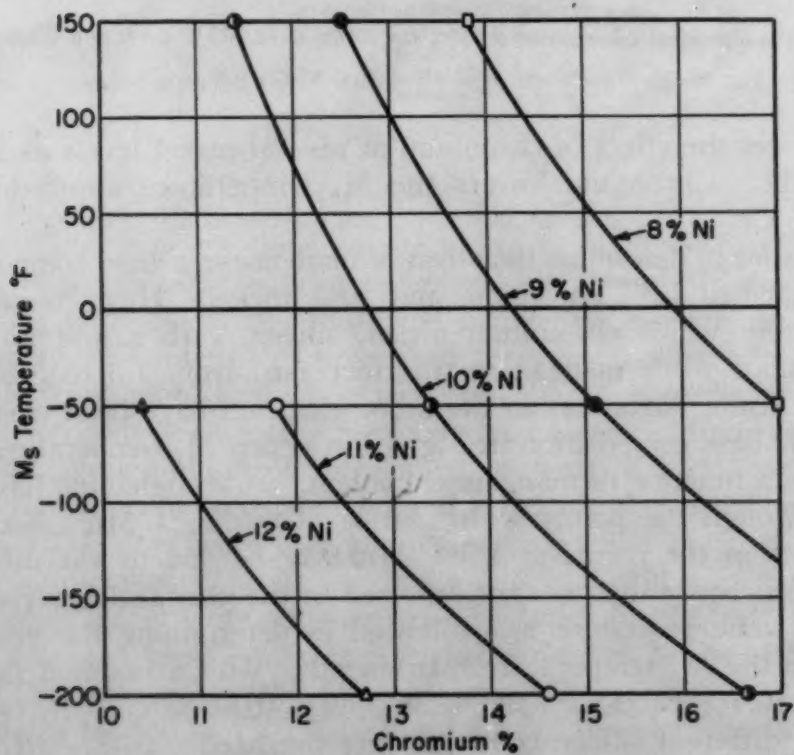
In order to determine the effect of manganese, a base composition was selected of 12% chromium and 10% nickel. Heats were then compared in which chromium, nickel, silicon, carbon and nitrogen were similar, while manganese was increased from 1.3 to 3.20 and 5.03%. Minor variations in the other elements have been corrected to a single base composition in Fig. 12 in which M_s temperatures are plotted as a function of manganese content. A straight line has been drawn through the points with a slope of $60^\circ\text{F}/\% \text{Mn}$. Some of the scatter in the points at 1.3% Mn may be due to variations in melting procedure that are not reflected in the chemical analyses.

The same procedure was followed in determining the effect of silicon on the M_s temperature. In an alloy with a nominal composition of 10.4% Cr, 12.1% Ni, 1.38% Mn, 0.063% C + N, balance iron, five different silicon contents were prepared: 0.47, 1.01, 1.42, 1.96 and 2.58% silicon. In Fig. 13 measured M_s temperatures, corrected for minor variations from the nominal composition, are



Corrected to a Nominal Composition of 1.33% Mn, 0.47% Si, 0.068% C+N, Balance Fe.

Fig. 10—Effect of Nickel on the M_s Temperature of Stainless Steel.

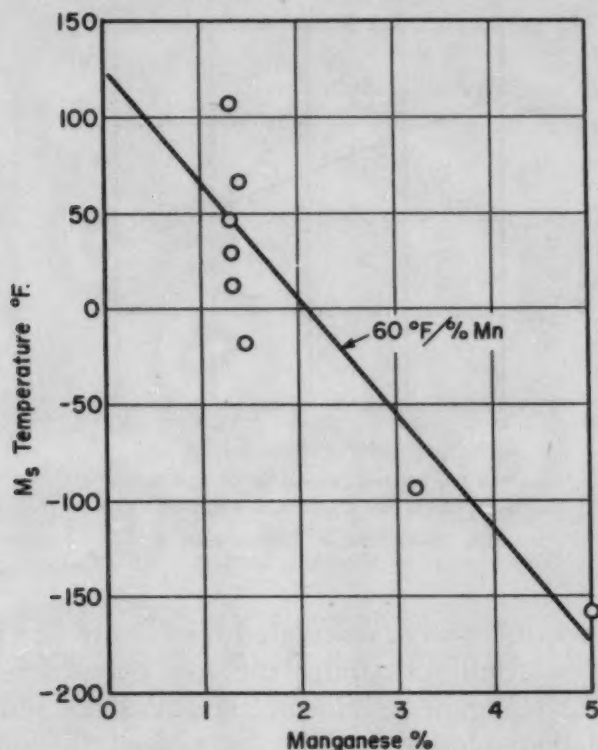


Corrected to a Nominal Composition of 1.33% Mn, 0.47% Si, 0.068%, Balance Fe.

Fig. 11—Effect of Chromium on the M_s Temperature of Stainless Steel.

plotted versus silicon content. Silicon lowers M_s less than any of the other alloying elements. An average value of $50^\circ\text{F}/\% \text{Si}$ was obtained from these data.

The previous results are most conveniently summarized in the form of an equation enabling one to calculate the M_s temperatures of 18-8-type stainless steels if the compositions are known. To establish a reference point from which to make corrections, an alloy



Corrected to a Nominal Composition of 12.2% Cr,
10.1% Ni, 0.43% Si, 0.072% C + N, Balance Fe.

Fig. 12—Effect of Manganese on the M_s Temperature of Stainless Steel.

was selected that had an M_s temperature of 0°F and a nominal composition in about the middle of the composition range investigated.

Element	Wt. %
Chromium	14.6
Nickel	8.9
Manganese	1.33
Silicon	0.47
Carbon + Nitrogen	0.068
Iron	Balance

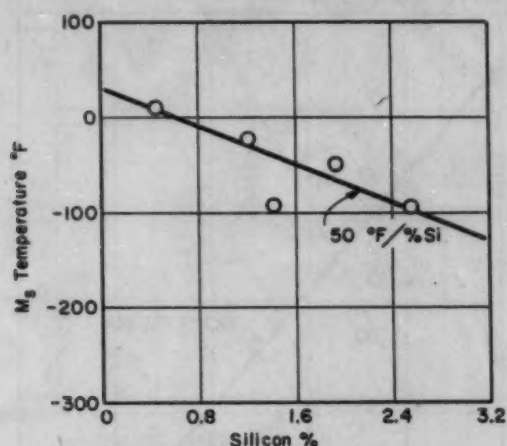
Within the compositional limits in weight per cent of

10 to 18	chromium	0.004 to 0.12	carbon
6 to 12	nickel	0.01 to 0.06	nitrogen
0.6 to 5.0	manganese	Balance	iron,
0.3 to 2.6	silicon		

it has been assumed for simplicity that the M_s temperature is a

linear function of each alloying element and that the effect of each element is additive and independent of the level of the other elements. The M_s temperatures in degrees Fahrenheit for alloys in the composition range studied are then given approximately by the following equation in which compositions are expressed in weight per cent:

$$M_s = 75 (14.6 - \text{Cr}) + 110 (8.9 - \text{Ni}) + 60 (1.33 - \text{Mn}) + 50 (0.47 - \text{Si}) + 3000 (0.068 - [\text{C} + \text{N}])$$



Corrected to a Nominal Composition of 10.4 % Cr, 12.1 % Ni, 1.38 % Mn, 0.063 % C + N, Balance Fe

Fig. 13—Effect of Silicon on the M_s Temperature of Stainless Steel.

The M_s temperatures were calculated for twenty-five of the heats using the above equation containing the five correction factors for chromium, nickel, manganese, silicon, and carbon plus nitrogen. These data were then plotted in Fig. 14 against the measured M_s temperatures and show an average deviation of only 37 °F in the calculated from the measured values. It was previously pointed out that the reproducibility of the M_s temperatures in a given specimen was ± 10 to 20 °F as determined by the procedure followed in this investigation. The accuracy of the chemical analysis also has a considerable effect on the M_s temperature, as may be seen by applying the above factors to the limits of error of the analyses estimated by the analytical laboratory.

Element	Typical Composition Per Cent	Limit of Error Per Cent	Possible Variation in M_s Due to Error in Analysis, °F
Chromium	13	± 0.1	± 7
Nickel	9	± 0.04	± 4
Manganese	1.3	± 0.05	± 3
Silicon	0.5	± 0.01	± 1
Carbon	0.04	± 0.01	± 30
Nitrogen	0.04	± 0.005	± 15

In Table I, for example, although Heats 6697 and 6699 are practically identical in composition, there is a difference of 24 °F in the

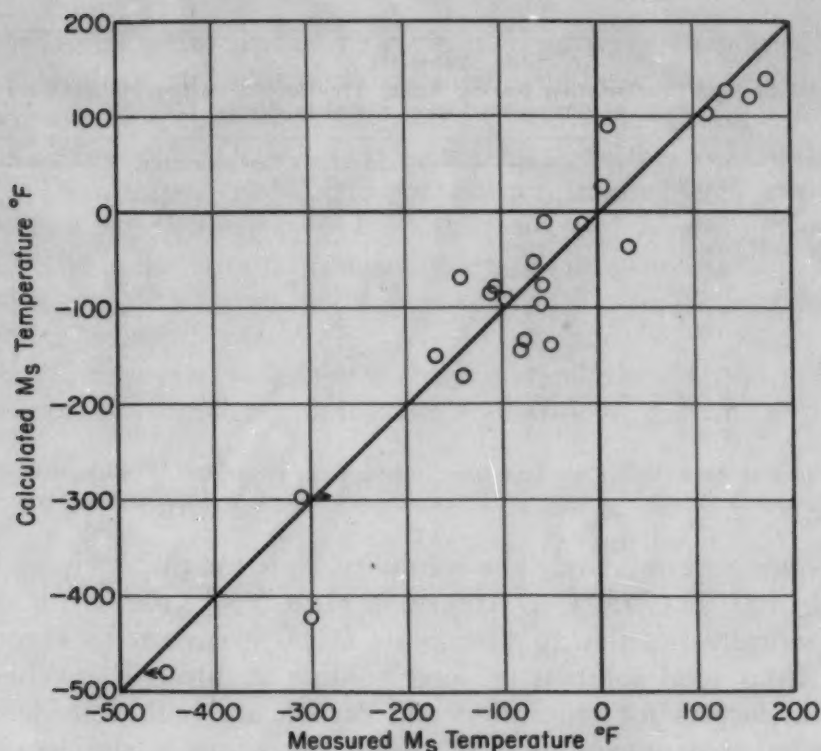


Fig. 14—Measured M_s Temperature Versus M_s Calculated by the Equation: $M_s = 75 (14.6\text{-Cr}) + 110 (8.9\text{-Ni}) + 60 (1.33\text{-Mn}) + 50 (0.47\text{-Si}) + 3000 (0.068\text{-[C + N]})$.

M_s temperatures. The M_s temperature could be determined more accurately by electrical resistance measurements, but the data did not warrant greater accuracy in view of the effect chemical analysis alone has on the results.

Data pertaining to the effect of composition on the M_s temperature would not be complete without including the effect of carbide precipitation. Alloys of high and low carbon were selected for study. The nitrogen contents of all the heats studied have been assumed to be within the solubility limit of nitrogen in stainless steels. The aging treatments employed were 1 hour at 1460 °F (795 °C) and 2 hours at 1200 °F (650 °C). Thermal contraction curves obtained for specimens aged at 1200 °F and specimens aged at 1460 °F are shown in Figs. 1 to 7. M_s temperatures observed after aging are recorded in Table III.

The removal of carbon and chromium from solid solution and the precipitation of these elements at the grain boundaries as chromium carbide during aging at these temperatures produced an increase in the M_s temperature that varied with the amount of carbide precipitated. Aging an alloy such as Heat 6625V with carbon content below the solubility limit at 1200 °F (650 °C) does not affect the M_s temperature. Careful examination of the contraction curves of the alloys containing 0.023 to 0.027% carbon will show that these

Table III
Effect of Carbide Precipitation During Aging Treatments on the M_s Temperatures of Chromium-Nickel Stainless Steels

Heat No.	Weight Per Cent Carbon	Measured M_s Temperatures, °F			
		2000 °F 15 Min.	2000 °F,† 1460 °F— 1 Hr.	2000 °F 15 Min.	2000 °F,† 1200 °F— 2 Hrs.
6625V	0.011	-50	-54
6694	0.023	+114	+104	+112	+156
6695	0.105	-82	+144, +156*	-97	+120
6696	0.025	+174	+224
6697	0.027	+156	+226 ?	+162	+210
6699	0.026	+132	+236	+112	+154
6700	0.107	-78	+160	...	+92
6909	0.032	-55	-40	-60	+40
6939	0.030	-18	+36
6940	0.034	+32	...	+36	+100

*6 Hours at 1460 °F. †Cooled to aging temperature from 2000 °F without holding.

contents are approximately the solubility limit for carbon in stainless steels at 1460 °F (795 °C). Hence, in Heat 6695 (Fig. 5), it should be theoretically possible to precipitate 0.080% carbon as chromium carbide from solid solution by long holding at 1460 °F. When the correction factors for chromium and carbon are both considered, it is estimated that precipitation of $Cr_{23}C_6$, as occurs in stainless steels (9), should raise the M_s temperature 4250 °F/% C precipitated. For the above example, this amounts to 340 °F. Experimentally, the increase in M_s was found to be 253 °F, which is in satisfactory agreement with the calculated value, considering the fact that 6 hours at 1460 °F is obviously insufficient to permit much chromium diffusion from the centers of the grains toward the boundaries which were depleted of chromium by carbide precipitation, and is probably even too short to reduce the carbon content throughout the grain to its equilibrium solubility. The sensitivity of this method of detecting small changes in the carbon content in solid solution should be a useful tool for measuring carbon solubility.

CONCLUSIONS

M_s temperatures of twenty-five heats of stainless steel of selected composition have been determined in order to evaluate the effect of each alloying element in suppressing the austenite-to-martensite transformation. The conclusions based on these data are limited to alloys that fall within the following composition limits in weight per cent:

10 to 18	chromium	0.3 to 2.6	silicon
6 to 12	nickel	0.004 to 0.12	carbon
0.6 to 5.0	manganese	0.01 to 0.06	nitrogen
	Balance		iron

1. The relative effectiveness of the elements in lowering the M_s temperature increases in the following order: silicon, manganese, chromium, nickel and carbon or nitrogen.

2. The effect of the alloying elements in weight per cent on the M_s temperature in degrees Fahrenheit can be calculated approximately with the equation: $M_s = 75 (14.6 - \text{Cr}) + 110 (8.9 - \text{Ni}) + 60 (1.33 - \text{Mn}) + 50 (0.47 - \text{Si}) + 3000 (0.068 - [\text{C} + \text{N}])$.

3. The nickel equivalents of silicon, manganese, chromium, carbon and nitrogen are 0.45, 0.55, 0.68, 27, and 27, respectively.

4. The precipitation of carbides results in an increase in the M_s temperature which varies with the amount of carbon and chromium removed from solid solution.

5. M_s changes caused by carbide precipitation can be used as a sensitive means for determining the solubility of carbon in stainless steel.

ACKNOWLEDGMENTS

The writers are indebted to Messrs. D. Spring, C. P. Mueller and J. P. Webb for making the alloys and for assisting in the rolling operations. Thanks are also extended to the analytical section of the Chemical Department and the chemical laboratory of Materials Engineering for the chemical analysis.

References

1. N. A. Ziegler and P. H. Brace, "Hardening of Austenitic Stainless Steels by Mechanical Working at Sub-Zero Temperatures", *Proceedings, American Society for Testing Materials*, Vol. 50, 1950, p. 861.
2. E. A. Owen and Y. H. Liu, "Further X-Ray Study of the Equilibrium Diagram of the Iron-Nickel System", *Journal, Iron and Steel Institute*, Vol. 163, 1949, No. 3, p. 132.
3. R. H. Thielemann, "Some Effects of Composition and Heat Treatment on the High Temperature Rupture Properties of Ferrous Alloys", *Proceedings, American Society for Testing Materials*, Vol. 40, 1940, p. 788.
4. W. D. Newell and M. Fleischman, U. S. Patent 2,118,683 (May 24, 1938).
5. W. O. Binder, C. M. Brown and Russell Franks, "Resistance to Sensitization of Austenitic Chromium-Nickel Steels of 0.03% Max. Carbon Content", *TRANSACTIONS, American Society for Metals*, Vol. 41, 1949, p. 1301.
6. C. B. Post and W. S. Eberly, "Stability of Austenite in Stainless Steels", *TRANSACTIONS, American Society for Metals*, Vol. 39, 1947, p. 868.
7. H. Scott, Unpublished data.
8. E. J. Dulis and G. V. Smith, "Ferrite Formation Associated With Carbide Precipitation in 18 Cr-8 Ni Austenitic Stainless Steel", *TRANSACTIONS, American Society for Metals*, Vol. 44, 1952, p. 621.
9. E. M. Mahla and N. A. Nielsen, "Carbide Precipitation in Type 304 Stainless Steel—An Electron Microscope Study", *TRANSACTIONS, American Society for Metals*, Vol. 43, 1951, p. 290.

DISCUSSION

Written Discussion: By W. S. Eberly, Metallurgical Department, Carpenter Steel Co., Reading, Pa.

The authors are to be commended for devising and applying a rapid and easy experimental procedure for studying the transformation of an

iron-chromium-nickel austenite (face-centered cubic lattice) to a ferritic (body-centered cubic lattice) type of iron-chromium-nickel structure. The empirical formula derived in their discussion of results applies well to the analysis limits considered in this work. Their element equivalents agree well with those already published.

In reviewing the data presented in this paper, the thought was kept in mind as to how well the results would agree with published literature associated with the stability of iron-chromium-nickel austenite at room temperature when subjected to cold work.

Data published in the authors' paper indicate that the elements carbon, nitrogen, nickel, manganese, silicon and chromium lower the M_s tem-

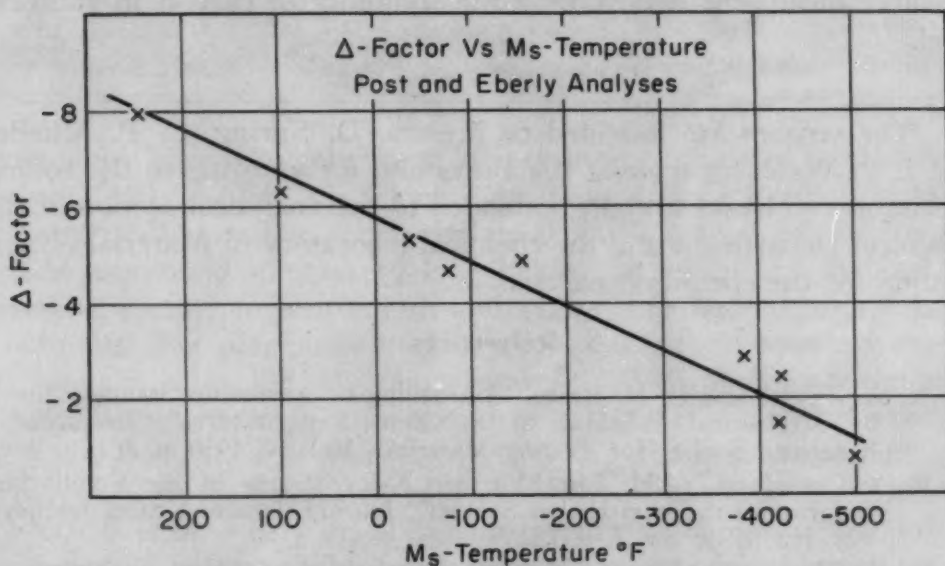


Fig. 15—Delta Factor Versus M_s Temperature. Post and Eberly analyses.

perature for all analyses within the ranges studied in this work. Even though the elements chromium and silicon are generally assumed to be ferrite-forming elements, they will lower the M_s point as long as the chromium plus silicon percentage, expressed as chromium alone, does not exceed 20%. That is to say, these analyses fall on the lower side of the knee in the phase diagram.

These data were compared with the work of Post and Eberly.² For comparing the data, analyses studied in each undertaking were expressed in the M_s value and Δ value.

When plotting the M_s values versus the Δ values, for the chemical analyses shown in the paper by Post and Eberly, the comparison is a fairly good linear relationship, as shown in Fig. 15. The comparison of Eichelman and Hull M_s values versus Δ values does not produce a good linear relationship. When the analyses are broken into their respective groups for the variables studied, such as 12% Cr—variable Ni, 14% Cr—variable Ni, variable carbon and variable manganese, one finds that a degree of linearity is established with lines at different levels. Is there an explanation for this behavior? See Fig. 16.

²C. B. Post and W. S. Eberly, "Stability of Austenite in Stainless Steels", TRANSACTIONS, American Society for Metals, Vol. 39, 1947, p. 868.

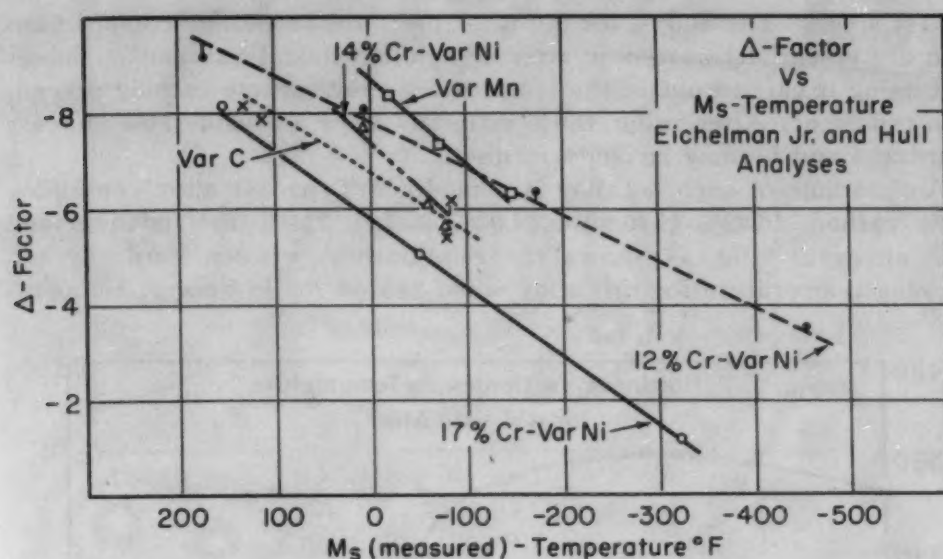


Fig. 16—Delta Factor Versus M_s Temperature. Eichelman, Jr., and Hull analyses.

Even though a slow cooling rate, of the order of 4 °F, or less, per minute, was employed in this study, it would be very interesting to have a knowledge of whether rates of the order of 1 °F per hour, or lower, would produce the same results.

Another point of interest would be a knowledge of the magnetic susceptibility of the various specimens after the test. Actually, it is assumed that the higher the M_s point, the higher the magnetic susceptibility, providing all specimens were cooled to the same temperature when studying the expansion properties.

Written Discussion: By A. J. Lena and J. A. Ferree, Research Laboratory, Allegheny Ludlum Steel Corp., Brackenridge, Pa.

The data which the authors have presented should find considerable use in the evaluation of the stability of the common stainless steels and in the development of new alloys. We were particularly glad to see that the influence of nitrogen was taken into consideration, for it has been an all too common practice in the past to neglect this element and its effect on the structural stability and properties of stainless steels. We would like to ask the authors if they have investigated the influence of grain size on the M_s point. This was not a factor in this paper because the initial homogenization temperature produced a coarse grain size (ASTM No. 1-2) which should have remained constant throughout subsequent heat treatments. In general, we are more interested in the properties of fine-grain steels, and it has been shown by other investigators that decreasing the grain size depresses the M_s point. Conceivably, this could introduce an error in the M_s calculation for a fine-grain steel from the equation which Eichelman and Hull have derived. The effect, however, may be quite small and perhaps the error would be less than that introduced by errors in chemical analysis.

The rise in the M_s temperature accompanying the precipitation of carbides may account for some of the changes in properties which have been attributed to age hardening in some of the so-called age hardening

stainless steels. The alloys, for the most part, are borderline compositions which are essentially austenitic after a "solution heat treatment". Subsequent aging is carried out in the temperature range where carbide precipitation can occur. After aging, these materials show a considerable increase in hardness and become strongly magnetic.

An example of such an alloy is a modified Type 431 alloy containing 0.093% carbon, 16.92% chromium, 4.02% nickel, 2.29% molybdenum and 0.05% nitrogen. Fig. 17 shows the relationship between hardness and hardening temperature for this alloy when heated for $\frac{1}{2}$ hour at tempera-

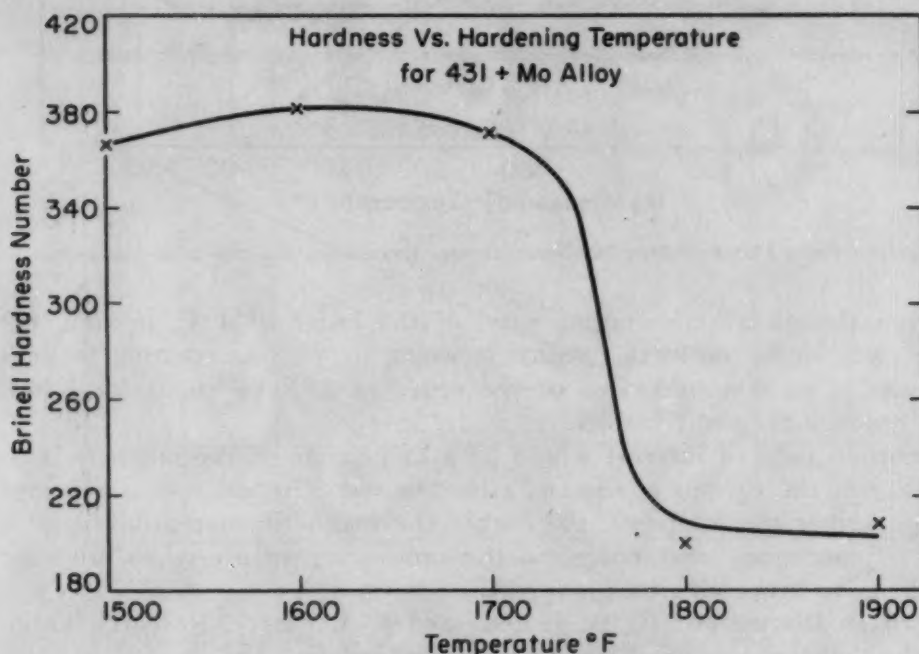


Fig. 17—Hardness Versus Hardening Temperature for 431 + Mo Alloy

ture and air-cooled to room temperature. The rapid decrease in hardness at 1800 °F is due to solution of carbides with a resultant lowering of the M_s temperature to below room temperature. The alloy in this condition is essentially nonmagnetic as measured with a hand magnet, whereas it is strongly magnetic when cooled from temperatures below 1800 °F. The effect of aging time at 1300 °F on the room temperature hardness of specimens previously annealed at 1800 °F is shown in Fig. 18. The hardness begins to increase after aging for as short a time as 2 minutes and reaches a maximum in 10 minutes or less. The structure of this alloy which prior to aging was almost completely austenitic is now essentially martensitic (with some free ferrite), as can be seen in Fig. 19. The carbide precipitation which occurs during this short-time aging appears to be primarily at grain boundaries, as was observed by Eichelman and Hull, and this fact raises an interesting academic question. In the short aging time of 10 minutes at 1300 °F, it is not conceivable that carbon and chromium would diffuse sufficiently fast to achieve homogeneity, and therefore the centers of the grain should have a lower M_s temperature than the grain boundaries. However, the martensite forms throughout the grains as shown in

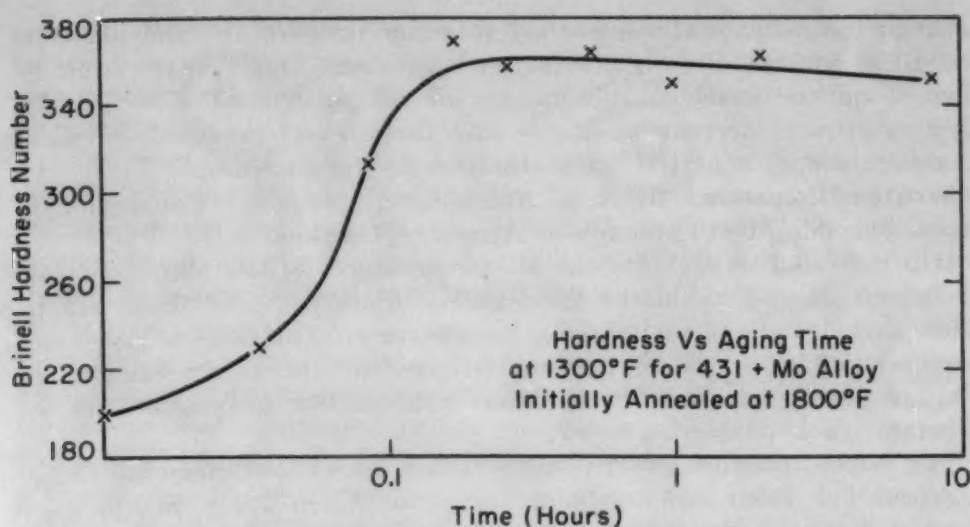


Fig. 18—Hardness Versus Aging Time at 1300 °F for 431 + Mo Alloy Initially Annealed at 1800 °F.

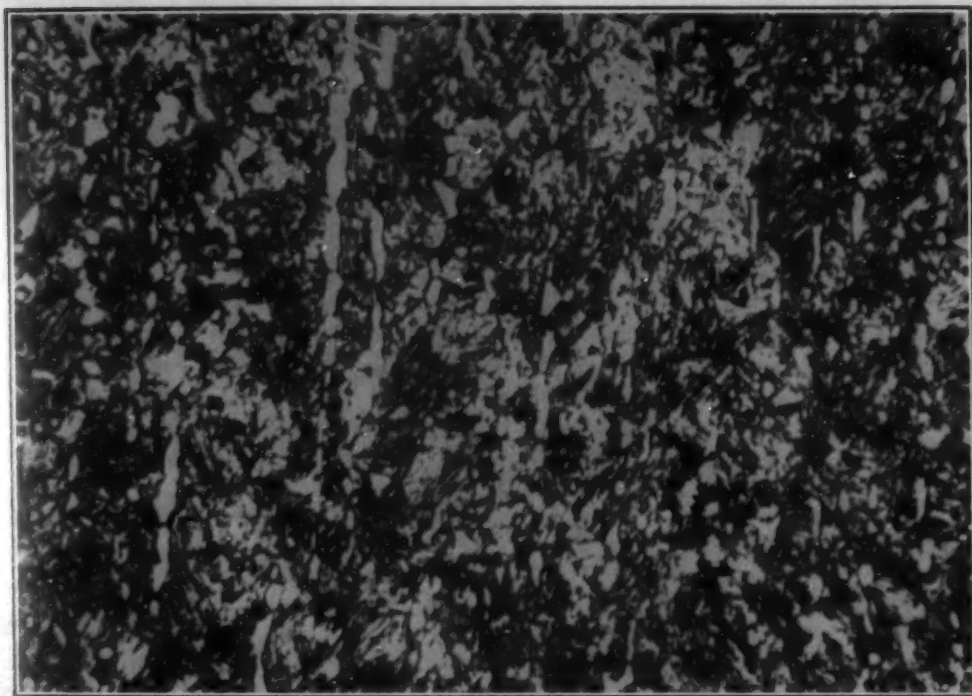


Fig. 19—431 + Mo Alloy Annealed at 1800 °F, ½ Hour, Air-Cooled, and Aged for 10 Minutes at 1300 °F.

Fig. 19. Does this mean that martensite is being nucleated at the grain boundaries where the M_s point is above room temperature, in which case the martensite shear must carry it through the grain where the composition is such that the M_s point is normally below room temperature, or does it mean that the M_s point is raised by the precipitation of submicroscopic carbides within the grain?

We have also found that the cooling rate from the annealing temperature has some effect on the M_s temperature. When the 431 + Mo alloy is air-cooled from 1800 °F, the hardness is 200 BHN and the alloy is non-

magnetic; but when water-quenched to room temperature, the hardness is 250 BHN and the alloy is moderately magnetic. This perhaps could be explained on the basis of stabilization of the austenite by air cooling with a subsequent decrease in M_s or that the stresses produced by water quenching produce a partial transformation of the austenite.

Written Discussion: By A. E. Nehrenberg, supervisor, Research Laboratory, Crucible Steel Company of America, Harrison, N. J.

It is now well known that the M_s temperatures of low alloy constructional steels can be calculated from composition, provided there are no residual carbides at the austenitizing temperature. The present paper represents what I believe to be the first attempt to extend such calculations to stainless steels of the 18-8 type, and I should like to congratulate the authors for their pioneering work.

The factors proposed by the authors for the various elements except manganese are about twice as large as those which apply to low alloy steels.³ I recognize the fact that the effect of an element on the M_s temperature is not necessarily linear over a very wide range of composition, but I would expect the factors to be smaller, rather than larger as the authors' data would seem to suggest, when the concentration of an element is increased to relatively high levels.

In the case of carbon, for example, Grange and Stewart⁴ in the closure of their paper have shown that above about 0.9% the effect of carbon on the M_s temperature departs from linearity. The factor for carbon decreases with increasing carbon above 0.9%. Also, at the 12% chromium level the factor for chromium amounts to 25 °F/1% Cr⁵ compared with a factor of 40 for lower levels of chromium.⁶

Rickett and his associates⁷ recently published data on the effect of variations in carbon in the range 0.02 to 0.16% on the M_s temperature of 12% chromium steels, and concluded that for this range of carbon the factor amounts to 1355 °F/1% C. In similar work carried out in our own laboratory we have confirmed that the carbon factor for 12% chromium steels of low carbon content is of this order of magnitude. The authors' factor for variations in carbon in this range on the M_s temperature of 18-8-type stainless steels is about twice this value.

It may be that the authors' factors are high because they reflect not only an effect on the true M_s temperature, but, in addition, an effect on the amount of stabilization occurring during cooling at the constant rate employed in their experiments. Stabilization during cooling above the M_s temperature can proceed very rapidly as Klier and Troiano have reported.⁷ In their work, in which a metallographic technique was employed, special precautions were necessary to assure that stabilization was avoided in their determination of M_s temperatures for chromium steels of varying carbon

³P. Payson and R. A. Grange, "The Temperature Range of Martensite Formation in Steel", ASM METALS HANDBOOK, 1948 Edition, p. 611-612.

⁴R. A. Grange and H. M. Stewart, "The Temperature Range of Martensite Formation", *Transactions, American Institute of Mining and Metallurgical Engineers*, Vol. 167, 1946, p. 467-501.

⁵R. L. Rickett, W. F. White, C. S. Walton and J. C. Butler, "Isothermal Transformation, Hardening, and Tempering of 12% Chromium Steel", *TRANSACTIONS, American Society for Metals*, Vol. 44, 1952, p. 138-175.

⁶A. E. Nehrenberg discussion of Reference 2.

⁷E. P. Klier and A. R. Troiano, "Ar' in Chromium Steels", *Transactions, American Institute of Mining and Metallurgical Engineers*, Vol. 162, p. 175-185.

content. In fact, in the case of one of their alloys, Klier and Troiano reported that stabilization occurred so rapidly that they were not able to obtain what they considered to be a reliable M_s temperature for one of their alloys.

The possibility that stabilization might have occurred during the authors' experiments could be checked by ascertaining the effect of cooling rate on the M_s temperature. If the M_s temperature is independent of cooling rate, it can be concluded that stabilization is absent. Do the authors have any data on the effect of cooling rate on the M_s temperature of the steels studied?

Finally, since martensite can be formed in 18-8-type stainless steels by plastic deformation at temperatures above the M_s , and since cold working is commonly employed in the fabrication of steels of this type, will the authors elaborate on their comments concerning the practical value of a knowledge of the M_s temperatures obtained for some definite cooling rate? Would not a knowledge of the M_a temperatures, that is, the temperatures above which martensite cannot be formed by plastic deformation, be more useful?

Written Discussion: By J. J. Heger, research associate, United States Steel Co., Pittsburgh.

The equation determined by Messrs. Eichelman, Jr., and Hull for the M_s temperature in 18-8 type of stainless steels will be quite useful to those who are engaged in developing age-hardenable stainless steels. Many of these steels must undergo an austenite-to-martensite transformation before an aging reaction occurs, and quantitative data on the effect of composition on the temperature at which this transformation takes place have been needed. We hope that the authors plan to continue their studies and obtain quantitative information on the effect of other elements such as titanium, molybdenum, aluminum and columbium and also extend their studies so as to include the determination of the M_r temperature.

We are, indeed, pleased to note the good correlation illustrated in Fig. 14 between the calculated M_s temperature and the measured M_s temperature. However, we believe that this correlation may be somewhat misleading because the heats represented in Fig. 14 are the heats from which data were obtained to establish the M_s equation. We suggest that the authors determine the correlation between the calculated and measured M_s temperatures on a number of additional heats. Until this is done we must consider the authors' equation as being only approximate.

Authors' Reply

The authors appreciate the interest of the persons who contributed to the value of the paper through their constructive discussions. Some of the questions raised can be answered; others will require further investigation by workers in this field.

The authors have no explanation for the good agreement between the Δ -Factor and M_s for Post and Eberly's steels (Fig. 15) and the relatively poor agreement between the Δ -Factor and measured M_s for the steels of this paper (Fig. 16).

Magnetic susceptibility was not determined in the course of our investigation. The specimens were not all cooled to the same temperature dur-

ing the dilatometer runs, so that measurements on the samples now would not be significant.

Mr. Eberly asked about the effect of rates of cooling less than 1 °F per hour on M_s . Kulin and Speich⁸ published results on isothermal transformation studies of one of our steels, Heat 6865. With a cooling rate of 1 to 2 °C per minute, the M_s temperature was -7 °C. A specimen was cooled at this rate to -5 °C without transformation, reheated to room temperature, cooled to -1.5 °C and held. Fig. 8 of their paper shows the isothermal transformation of martensite that occurred above M_s . Thus, in this Cr-Ni stainless steel, it appears that an extremely slow cooling rate would result in a slightly higher observed M_s temperature and not a much lower M_s as might be expected from stabilization effects that occur in chromium steels, as described in Mr. Nehrenberg's discussion.

The M_s temperature of Heat 6694 was determined dilatometrically for several cooling rates with the following results:

Cooling Rate Between 200 and 100 °F, °F/min.	M_s Temperature °F
2	107
4	114
8	118
20	95

At least in the range of cooling rates from 2 to 20 °F per minute, there is no evidence of stabilization of austenite at the slower rates.

There is another aspect of cooling rate that is related to internal stresses, and their effect on martensite formation, rather than to stabilization. An example of this is cited by Dr. Lena and Mr. Ferree. Mr. G. H. Eichelman and Dr. K. Goldman, at our laboratory, have determined the effect of quenching velocity from the annealing temperature on the M_s temperature in 0.10-inch diameter wires of Heat 6865. Cooling from room temperature to the M_s transformation was at a rate of 3 °F per minute. As illustrated in Fig. 20, higher residual stresses resulting from a drastic quench can raise the M_s by as much as 30 °F, as has also been observed by Kulin, Cohen and Averbach.⁹

Dr. Lena and Mr. Ferree properly point out that grain size has an influence on the M_s temperature. This effect has been investigated on wires of Heat 6865 using an electrical resistance method for determining M_s . As shown in Fig. 20, decreasing grain size lowers M_s about 8 °F for every ASTM Grain Size Number.

The rapid increase of room temperature hardness of the 431 + Mo alloy when aged at 1300 °F would indeed lead to nonuniform composition throughout the grains. We favor the view that martensite forms first at the carbon and chromium depleted grain boundaries and that stresses produced by this transformation induce further martensite formation throughout the grains.

Mr. Nehrenberg has asked for an elaboration of the practical value of M_s temperatures, since in cold fabricated steels a knowledge of the M_s temperatures would be more useful. On the basis of some information in

⁸S. A. Kulin and G. A. Speich, "Isothermal Martensite Formation in an Iron-Chromium-Nickel Alloy", *Transactions, American Institute of Mining and Metallurgical Engineers*, Vol. 194, p. 258.

⁹S. A. Kulin, Morris Cohen and B. L. Averbach, "Affect of Applied Stress on the Martensite Transformation", *Journal of Metals*, June 1952, p. 661.

the literature, we now believe that there is a correlation between M_s and M_d . Bloom, Goller and Mabus¹⁰ determined a "cold work hardening factor" (related to the area under a stress-strain curve) of a variety of stainless steels in compression. When this factor is plotted versus M_s temperature calculated by our formula, there is a break in the curve at 500 to 600 °F below room temperature. If the calculated M_s is more than about 600 °F below room temperature, the only effect of plastic deformation is work hardening of the austenite. If the M_s is less than 600 °F below room

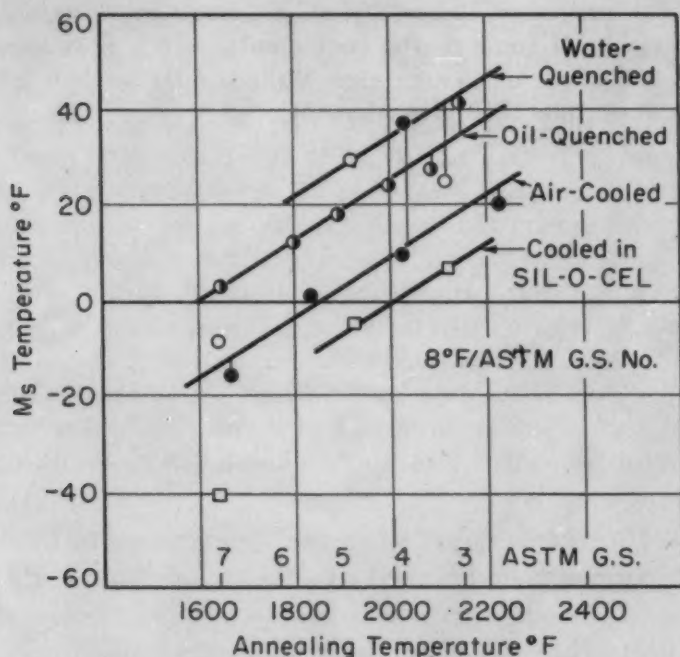


Fig. 20—The Effect of Annealing Temperature and Quenching Rate on the M_s Temperature of Stainless Steel. Heat 6865.

temperature, plastic deformation results in both work hardening of austenite and transformation to martensite and an apparent increased rate of work hardening of the steel. This behavior indicates that M_s is 500 to 600 °F lower than M_d .

Magnetic permeability data of Post and Eberly¹¹ for annealed stainless steels show a sudden increase when M_s calculated by our equation is higher than room temperature. For cold-worked steels the break is 650 °F below room temperature, confirming the above relationship between M_s and M_d .

Post and Eberly's tensile data on steels cold-reduced 62.5% in thickness have been plotted versus calculated M_s temperatures. For steels with 0.04–0.07% C, the break is again 650 °F below room temperature.

Ziegler and Brace¹² determined hardnesses of eleven compositions of stainless strip rolled to 75% reduction in thickness at room temperature

¹⁰F. K. Bloom, G. N. Goller, P. G. Mabus, "The Cold Work Hardening Properties of Stainless Steels in Compression", *TRANSACTIONS, American Society for Metals*, Vol. 39, 1947, p. 843.

¹¹Reference 6 in paper.

¹²Reference 1 in paper.

and at liquid nitrogen temperature. Breaks in hardness versus calculated M_s curves occurred 600 °F below the working temperature employed for rolling.

M_s temperatures of several stainless steels have been given by Tisinai and Shortsleeve.¹² For compositions in which the carbon was completely soluble, the measured values agree reasonably well with those calculated by our equation.

The fact that M_s calculations on so many sets of data correlate well with experimentally determined M_s and M_d temperatures gives us added confidence in the utility of the equation, although more exhaustive tests may require revision of some of the coefficients. To a first approximation it appears that the effect of elements on M_d is similar to their effect on M_s and that M_d is about 600 °F higher than M_s .

¹²Discussion of Reference 8 in paper.

AUSTENITE STABILITY AND CREEP-RUPTURE PROPERTIES OF 18-8 STAINLESS STEELS

BY JACK K. Y. HUM AND NICHOLAS J. GRANT

Abstract

Two series of simple unstabilized 18-8 chromium-nickel steels were tested, one a carbon series from 0.001 to 0.18% and the second a nitrogen series from 0.005 to 0.176%. The effect of these composition changes on the structure and the effect of structure on the creep-rupture properties were then studied. Creep-rupture tests were run from 1000 to 1300 °F (540 to 705 °C) for rupture times of 3 seconds to about 1000 hours. Over these carbon and nitrogen ranges large differences in rupture strength and creep resistance are noted, the rupture strength going through a minimum and the creep rate through a maximum. The effects of carbon and nitrogen are compared and assist in explaining the strength theory proposed. In these unstabilized steels, the amount of carbide or nitride is shown to be the most important strengthening effect in the usual carbon and nitrogen ranges.

THE need to understand better the constitution of 18-8-type stainless steels and the stability of the various structures as a function of time, temperature, and strain is great. The expansion of the jet engine, gas turbine and allied fields calls for utilization of the lower alloyed steels of practical high temperature significance. There is little doubt that the quantities of cobalt, nickel, molybdenum, columbium, tungsten and other elements for large-scale turbine production cannot be obtained. Accordingly, more judicious application of lower alloyed steels must be the answer; but this can be accomplished only if the effects of composition on structure and the effects of structure on the high temperature mechanical properties are much more completely known.

It was with this thought in mind that the present research as part of a more extensive program was undertaken. It was planned, first, to study the effect of composition on the constitution and stability of the simple 18-8 steels and, secondly, to study the effect of the structure on the creep and stress-rupture properties.

Based on a thesis submitted in partial fulfillment of the requirements for an Sc.D. degree.

Of the authors, J. K. Y. Hum was formerly research assistant, Department of Metallurgy, Massachusetts Institute of Technology, Cambridge, Mass., now with Bechtel International, San Francisco, Calif., and Nicholas J. Grant is associate professor of metallurgy, Massachusetts Institute of Technology, Cambridge, Mass. Manuscript received February 11, 1952.

EXPERIMENTAL PROCEDURE

Because of the almost complete lack of data on the role of structure in the 18-8-type steels on the creep and stress-rupture behavior in the temperature range 1000 to 1300 °F (540 to 705 °C) it appeared desirable to start with the most simple compositions. Accordingly, two series of 18-8 steels were made, namely: (a) a low nitrogen series of increasing carbon content from 0.001 to 0.18% carbon; (b) a low carbon series of increasing nitrogen content from 0.005 to 0.176% nitrogen.

Thirteen 6-pound ingots (numbers 6 to 21) and three 15-pound ingots (numbers 28 to 30) were induction-melted under helium to control nitrogen pick-up and to decrease oxidation losses. Two 10-pound high purity vacuum-melted ingots (numbers 31 and 33) were supplied by the National Research Corporation.

Because of the current interest in the extra low carbon stainless steels, one heat of Elc 304 (Heat 32) was included, and was obtained from the U. S. Steel Co. as 1/2-inch forged bars.

Table I lists the heat analyses. The nitrogen values were obtained by wet methods. Manganese and silicon were each less than 0.10% and are not carried in the table.

All ingots were forged to 1/2-inch rounds at a maximum temperature of 2200 °F (1205 °C). Creep-rupture bars with a 0.25-inch diameter by 1.25-inch gage length were machined from these bars.

Table I
Compositions of 18-8 Carbon and Nitrogen Series

Carbon Series					Nitrogen Series				
Heat No.	Per Cent				Heat No.	Per Cent			
	C	N ₂	Cr	Ni		N ₂	C	Cr	Ni
18	0.18	0.040	19.25	7.86	6, 7, 14*	0.176	0.036	18.85	7.87
30	0.14	0.049	19.47	7.83	8	0.132	0.032	18.97	7.88
16	0.12	0.050	19.26	8.03	9	0.097	0.036	18.78	7.88
29	0.067	0.029	18.74	7.68	10	0.067	0.030	18.42	7.92
15	0.050	0.035	18.69	7.82	11, 13*	0.050	0.035	18.96	7.93
33	0.038	0.004	19.40	8.00	33	0.004	0.038	19.40	8.00
31	0.001	0.005	16.54	9.07	31	0.005	0.001	16.54	9.07

Elc Type 304 (Heat 32): 18.57% Cr, 10.20% Ni, 0.036% C, 0.034% N₂.

*These heats were so close in composition for all elements that they could be grouped.

Prior to creep-rupture testing, all bars were solution-treated for 1 hour at 2050 °F (1120 °C) followed by a water quench.

Creep-rupture tests were run in equipment previously described, which more than adequately meets ASTM specifications. The creep-rupture tests were conducted at temperatures of 1000, 1200 and 1300 °F (540, 650 and 705 °C). This is the temperature range of maximum interest for load-carrying applications for the 18-8 steels and

also the range in which the ferrite is the least stable. Creep-rupture tests were run at stresses which yielded rupture times from about 0.001 to 1000 hours.

The complete program of testing was as follows:

1. After solution treatment, samples from each heat were checked at room temperature for ferrite and austenite contents by means of magnetic measurements, X-rays, and metallography.
2. Solution-treated samples from each alloy were heated in sealed Vycor tubes for 1560 hours at 1000 °F (540 °C), for 1000 hours at 1200 °F (650 °C), and for 700 hours at 1400 °F (760 °C). They were then checked for ferrite and austenite contents by the same three methods listed above, at room temperature.
3. Solution-treated samples from each heat were cold-worked 30%. They were then heated in the same way for the same times and temperatures and checked for ferrite and austenite as in items 1 and 2.
4. Specimens were tested in creep-rupture as discussed above and were then checked for ferrite and austenite at room temperature by the usual X-ray, magnetic and metallographic means.

After each creep-rupture test, one piece of the specimen was heavily electropolished to remove the oxide skin and also to remove the outer worked surface which may have resulted from handling. The polished specimen was then mounted in a Norelco X-ray spectrometer, in a holder similar to one described by Norton (1).¹ The only modification was to increase the rotational speed of the specimen to 120 rpm. This high speed made it possible to obtain a fair average value of ferrite, since it was discovered from the initial tests that there was a difference in ferrite content in different areas around the periphery of the specimen. Chromium radiation was used in all measurements. The specimen was so placed in the apparatus that the X-ray beam would strike the uniformly elongated section instead of the fracture zone, since excessive necking at the point of fracture would influence the readings unduly. The (110) line was used to measure the ferrite, whereas the (111) line was used to measure the retained austenite (1-4).

The X-ray determinations were used as the primary measure of the quantities of ferrite and austenite present. To determine if simple magnetic measurements were of any value, a Magnegage, which registers the pull required to remove a calibrated magnet from the surface of the specimen, was utilized. To calibrate the Magnegage, compacts of mixed iron and copper powders were prepared and checked by X-ray measurements. Values of ferrite versus dial reading of the Magnegage were then obtained for three magnets which permitted virtually complete coverage from 0 to 100% ferrite.

¹The figures appearing in parentheses pertain to the references appended to this paper.

Measurements were made both near the fracture as well as on the uniformly elongated section. Except in the case of the very short-time creep-rupture tests, the X-ray and Magnegage values for ferrite were uniformly different by a value of about 10 to 15%, the Magnegage giving in all instances the higher values of ferrite. Lineal analysis for ferrite was also tried but was completely unsuccessful.

EXPERIMENTAL RESULTS

Creep-Rupture Tests—Carbon Series—Fig. 1 shows the solution-treated structures of the carbon series of alloys which are representative of the starting structures for the creep-rupture tests. Where 100% austenite was obtained from X-ray measurements, the Magnegage showed only about 97%. This is probably due to a small amount of surface ferrite due to polishing of the samples. From these photo-

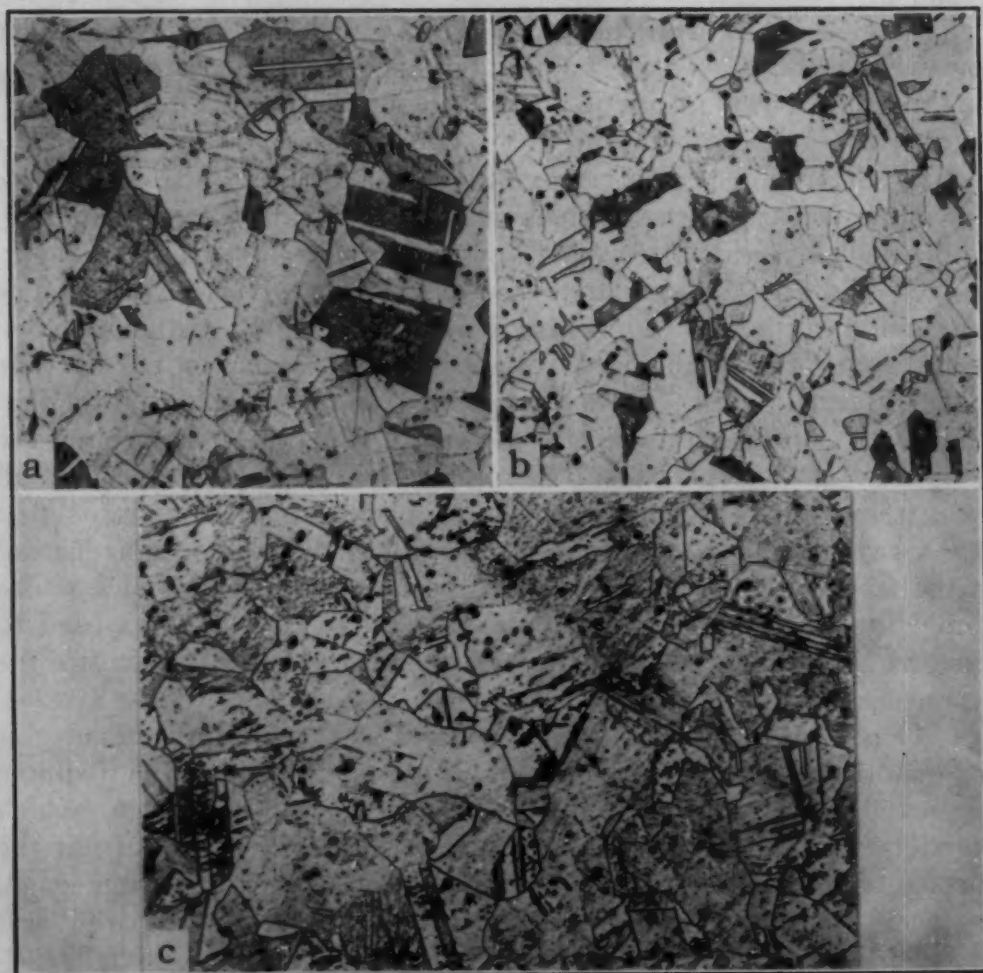


Fig. 1—Structures of Solution-Treated Alloys in Carbon Series. Water-quenched from 2050 °F. 15% oxalic acid, electrolytic etch. $\times 100$. (a)—Alloy 18, 0.18% carbon, 0.04% nitrogen, 100% austenite. (b)—Alloy 16, 0.12% carbon, 0.05% nitrogen, 100% austenite. (c)—Alloy 15, 0.05% carbon, 0.035% nitrogen, 97% austenite.

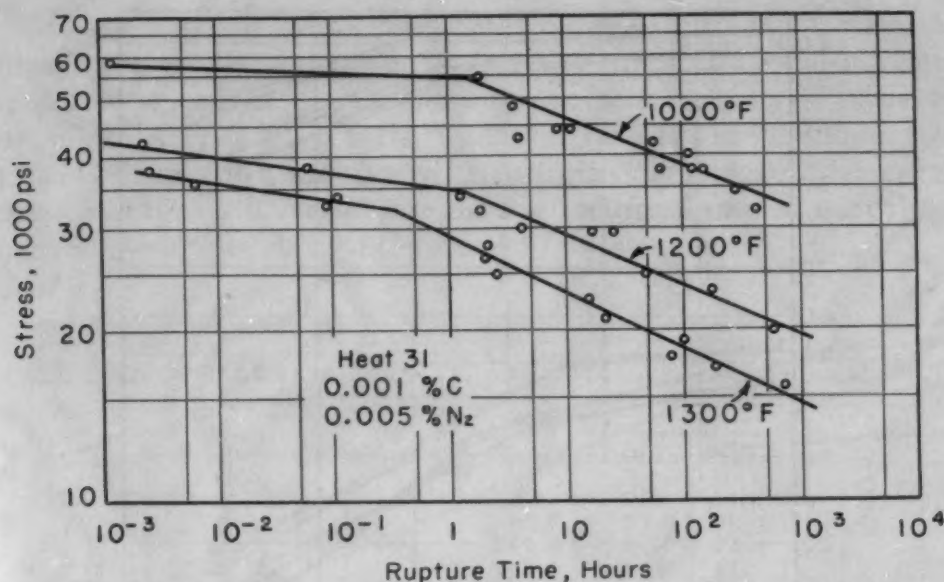


Fig. 2—Log-Log Plot of Stress Versus Rupture Life for Alloy No. 31, 1000, 1200 and 1300 °F.

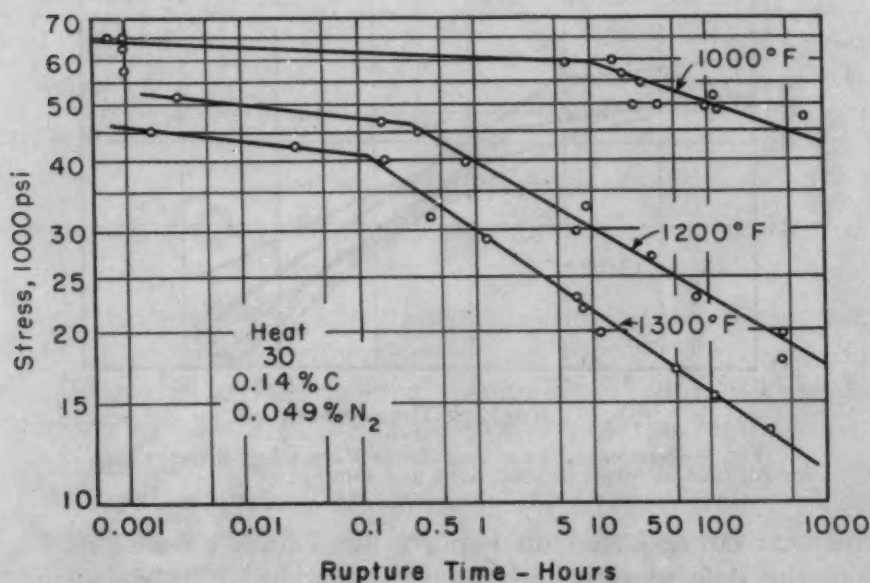


Fig. 3—Log-Log Plot of Stress Versus Rupture Life for Alloy No. 30, 1000, 1200 and 1300 °F.

micrographs and those of Fig. 7, it is evident that the grain size from alloy to alloy was quite uniform.

Figs. 2 and 3 show typical log stress - log rupture-life plots for two of the carbon series alloys. Such plots were obtained for all of the alloys in the carbon series but, for the sake of brevity, are not included here. All of the stress-rupture tests are summarized in Fig. 4, showing the relationship among the various carbon alloys at all three test temperatures.

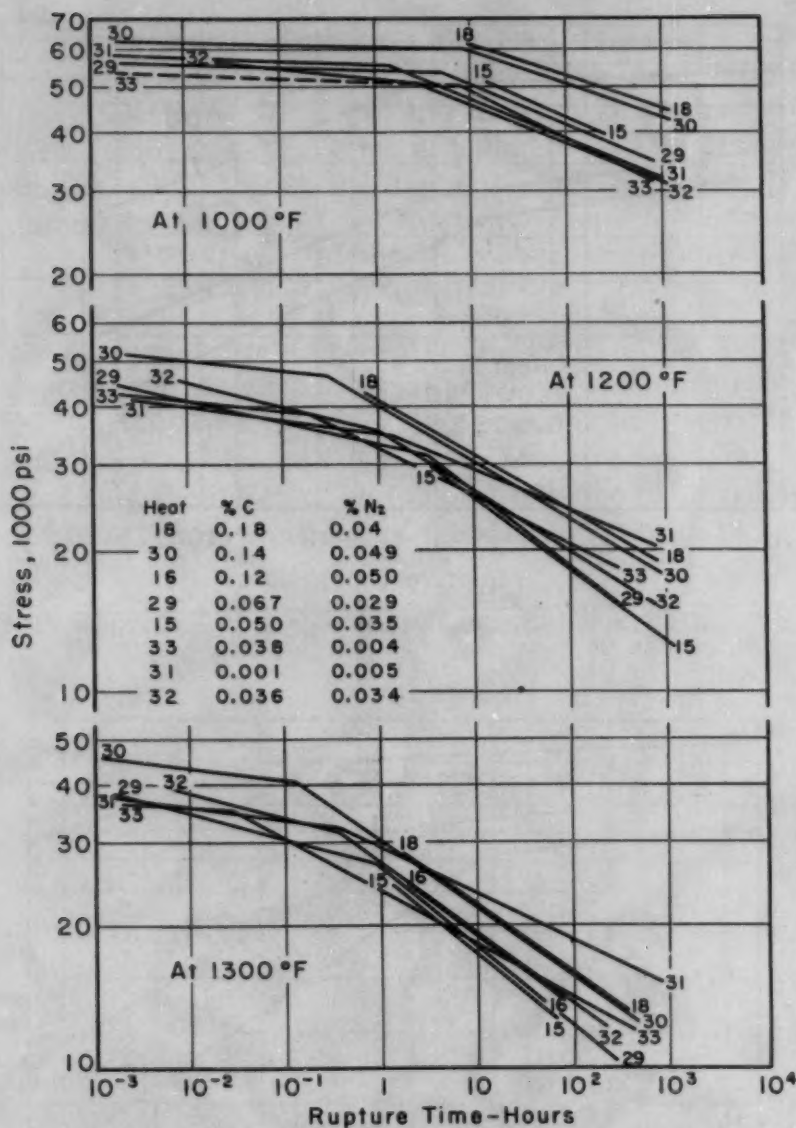


Fig. 4—Summary Plot of Log Stress Versus Log Rupture Life for All Carbon Alloys at 1000, 1200 and 1300 °F.

The best curve based on rupture-life values as well as on the nature of the deformation and fracture was drawn. In one or two instances, due to too few points, the curves were not capable of being drawn very accurately. This is especially true of those curves in Fig. 4 (also in Figs. 6, 8, and 9) which cover only a short range of rupture times. In all instances where the break in the curves is shown, it was definitely determined that intercrystalline cracking was present in the creep-rupture bar, and became more severe at higher temperatures and longer rupture life.

Fig. 5 is a typical log-log plot of stress versus minimum creep rate, for Alloy 30. Again similar plots were obtained for all the alloys, and these are summarized in one master plot, Fig. 6, for the three test temperatures.

Creep-Rupture Tests—Nitrogen Series—In a similar way individual log-log data plots were obtained of rupture life and minimum creep rate against stress for the nitrogen series of alloys. The test temperatures again were 1000, 1200 and 1300 °F (540, 650 and 705 °C). Typical solution-treated structures of nitrogen alloys are shown in Fig. 7. Two of these nitrogen alloys, 7 and 9, were 100% austenitic, whereas Alloy 11 showed 97% austenite.

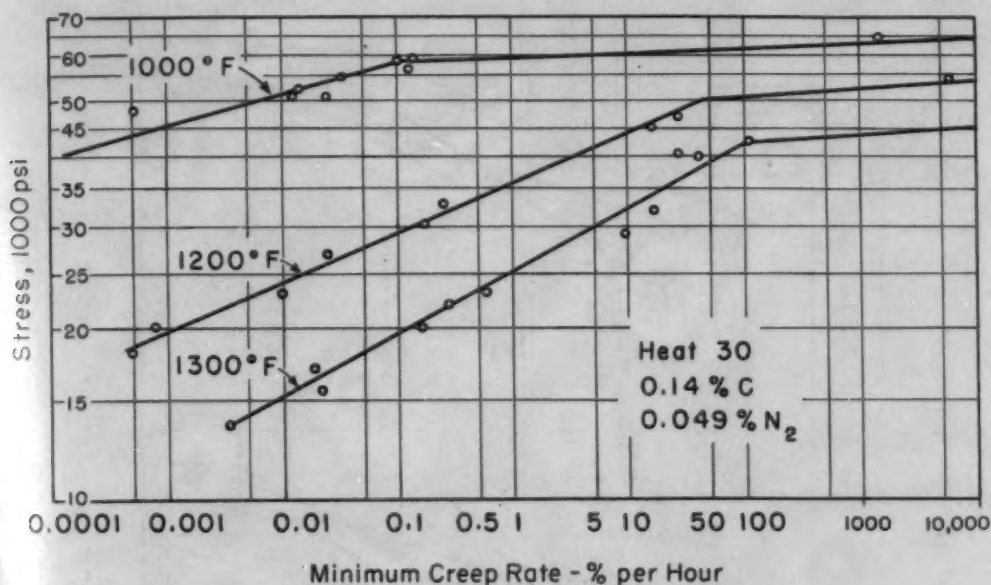


Fig. 5—Log-Log Plot of Stress Versus Minimum Creep Rate for Alloy No. 30.

Fig. 8 is the master plot summarizing the log stress – log rupture-life data at all three temperatures, and Fig. 9 is the master plot summarizing the log stress – log minimum creep rate data for the nitrogen series of alloys. Fractures were of the high temperature intercrystalline type beyond the break in these curves.

Effect of Carbon and Nitrogen on the Creep-Rupture Properties—If one selects various stress levels at each temperature from Fig. 4, in such a way that the selected stresses intersect all curves beyond the equicohesive transition (the breaks in the curves shown in Fig. 4), one obtains the curves shown in Fig. 10. Fig. 10 shows the high temperature rupture life as a function of carbon plus nitrogen content for the carbon series of alloys for selected values of stress and temperature. The small and fairly constant nitrogen content of the carbon series of alloys gave smoother curves when added to the carbon content. It will be shown later that there is valid reason to add the carbon and nitrogen at low values of either element in each series.

It is extremely interesting to note the minima in the curves of Fig. 10. The actual minimum shifts to a higher carbon (plus nitrogen) value with decreasing stress (longer rupture life). From this

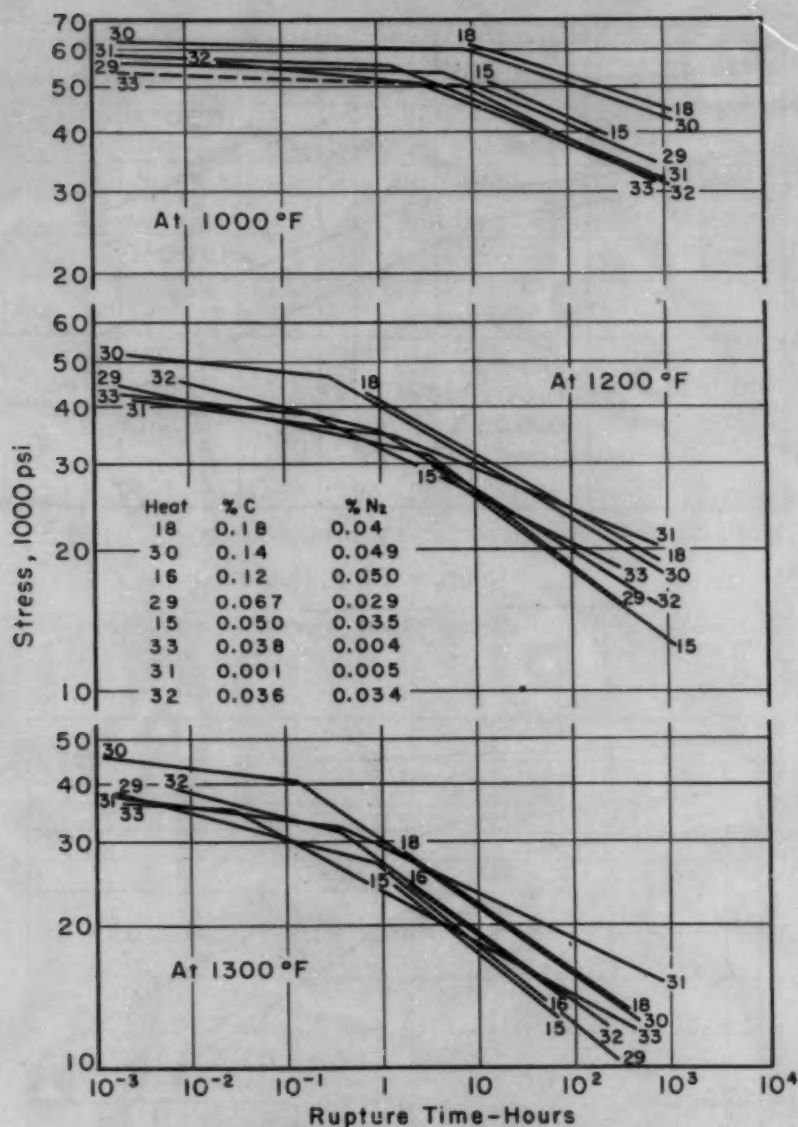


Fig. 4—Summary Plot of Log Stress Versus Log Rupture Life for All Carbon Alloys at 1000, 1200 and 1300 °F.

The best curve based on rupture-life values as well as on the nature of the deformation and fracture was drawn. In one or two instances, due to too few points, the curves were not capable of being drawn very accurately. This is especially true of those curves in Fig. 4 (also in Figs. 6, 8, and 9) which cover only a short range of rupture times. In all instances where the break in the curves is shown, it was definitely determined that intercrystalline cracking was present in the creep-rupture bar, and became more severe at higher temperatures and longer rupture life.

Fig. 5 is a typical log-log plot of stress versus minimum creep rate, for Alloy 30. Again similar plots were obtained for all the alloys, and these are summarized in one master plot, Fig. 6, for the three test temperatures.

Creep-Rupture Tests—Nitrogen Series—In a similar way individual log-log data plots were obtained of rupture life and minimum creep rate against stress for the nitrogen series of alloys. The test temperatures again were 1000, 1200 and 1300 °F (540, 650 and 705 °C). Typical solution-treated structures of nitrogen alloys are shown in Fig. 7. Two of these nitrogen alloys, 7 and 9, were 100% austenitic, whereas Alloy 11 showed 97% austenite.

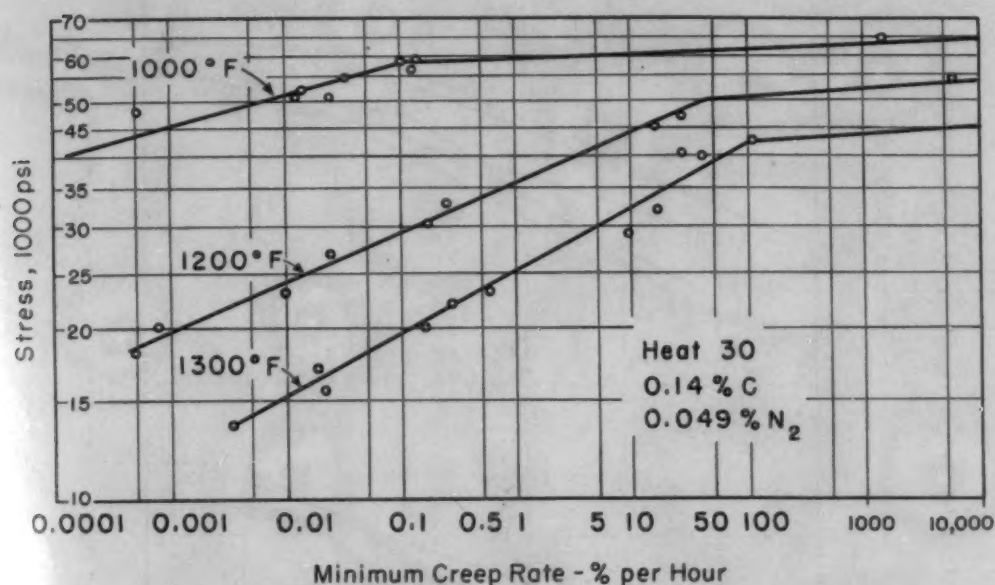


Fig. 5—Log-Log Plot of Stress Versus Minimum Creep Rate for Alloy No. 30.

Fig. 8 is the master plot summarizing the log stress – log rupture-life data at all three temperatures, and Fig. 9 is the master plot summarizing the log stress – log minimum creep rate data for the nitrogen series of alloys. Fractures were of the high temperature intercrystalline type beyond the break in these curves.

Effect of Carbon and Nitrogen on the Creep-Rupture Properties—If one selects various stress levels at each temperature from Fig. 4, in such a way that the selected stresses intersect all curves beyond the equicohesive transition (the breaks in the curves shown in Fig. 4), one obtains the curves shown in Fig. 10. Fig. 10 shows the high temperature rupture life as a function of carbon plus nitrogen content for the carbon series of alloys for selected values of stress and temperature. The small and fairly constant nitrogen content of the carbon series of alloys gave smoother curves when added to the carbon content. It will be shown later that there is valid reason to add the carbon and nitrogen at low values of either element in each series.

It is extremely interesting to note the minima in the curves of Fig. 10. The actual minimum shifts to a higher carbon (plus nitrogen) value with decreasing stress (longer rupture life). From this

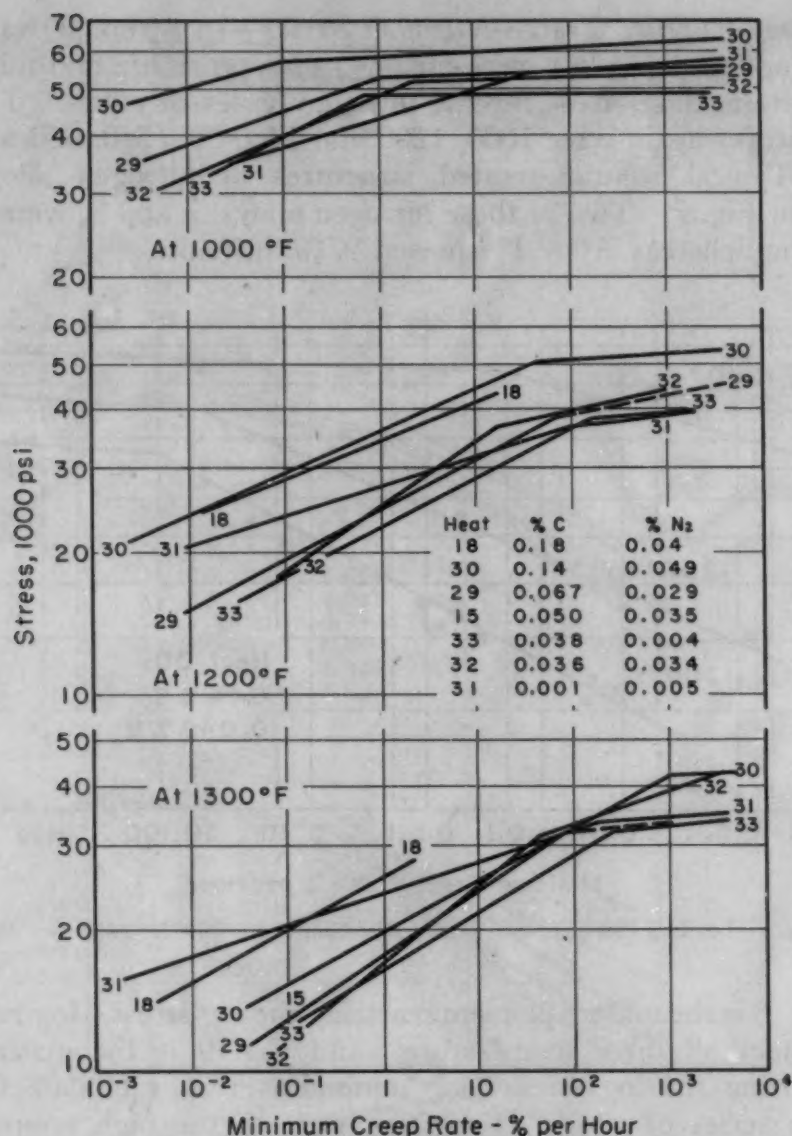


Fig. 6—Summary Plot of Log Stress Versus Log Minimum Creep Rate for All Carbon Alloys at 1000, 1200 and 1300 °F.

plot, it is evident that the very lowest carbon plus nitrogen alloy is the strongest, this superiority becoming more obvious as the stress decreases or as the temperature increases up to 1300 °F (705 °C). In the range of 0.006 to about 0.097% carbon plus nitrogen, depending on stress and temperature, the strength is the lowest. As the carbon (plus nitrogen) increases to values greater than about 0.09, the rupture life at all temperatures increases, then tends to level off at the higher carbon values.

Fig. 11 is a similar plot for the nitrogen series of alloys, based on selected temperatures and stresses from Fig. 8. Again, as in the carbon series (Fig. 10), there is a minimum in rupture life at intermediate values of nitrogen (plus carbon), with the very low nitrogen

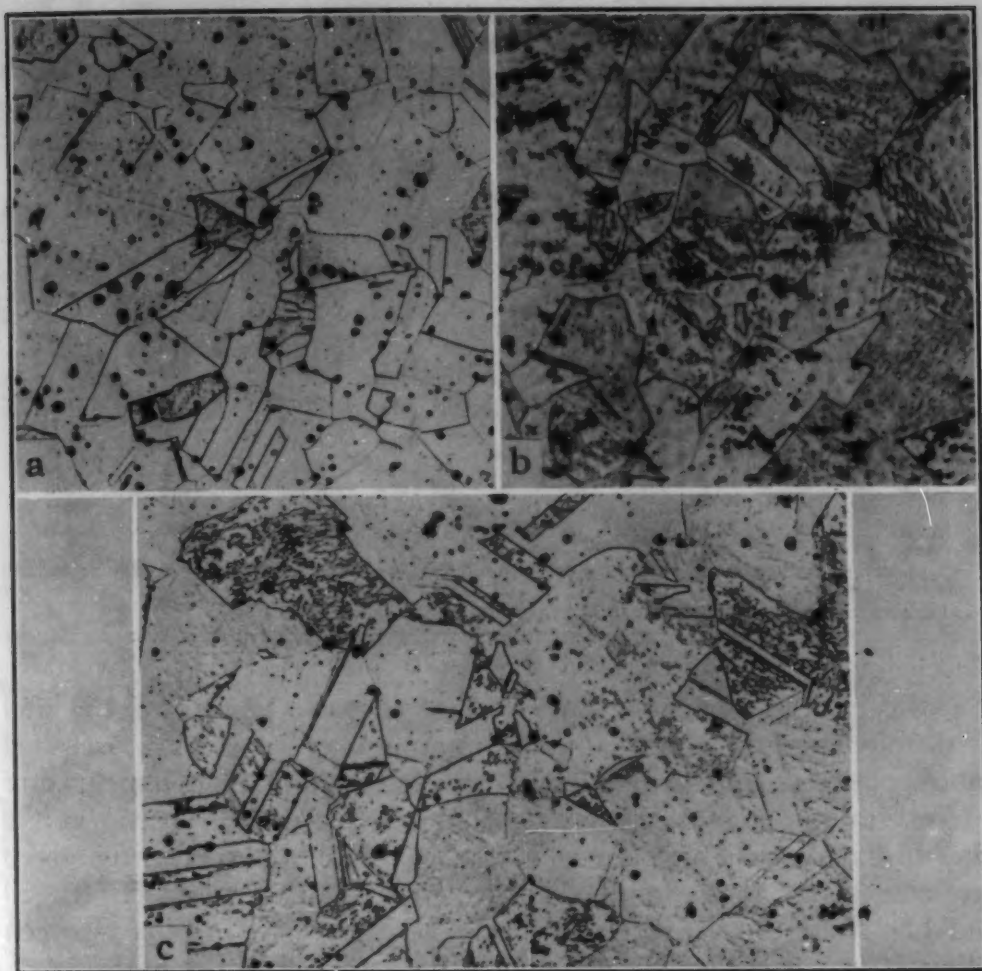


Fig. 7—Structures of Solution-Treated Alloys in the Nitrogen Series. Water-quenched from 2050 °F. 15% oxalic acid, electrolytic etch. $\times 100$. (a)—Alloy 7, 0.174% nitrogen, 0.032% carbon, 100% austenite. (b)—Alloy 9, 0.097% nitrogen, 0.036% carbon, 100% austenite. (c)—Alloy 11, 0.05% nitrogen, 0.029% carbon, 97% austenite.

plus carbon alloy being very strong. The higher nitrogen alloys, as is true of the carbon alloys, increase in strength with increasing nitrogen (plus carbon) beyond the minimum values. Table II lists the rupture-life values (taken from the individual log stress versus log rupture-life curves for each alloy) used in obtaining Figs. 10 and 11. These individual point values were not shown, to avoid confusion among the many curves and points.

It will be noted from Table II that the minimum in the rupture-life curves shown in Figs. 10 and 11 does not occur for any one alloy. Depending on the selected stress and temperature, the minimum rupture life is shown for alloys with up to 0.097% carbon plus nitrogen or nitrogen plus carbon. Furthermore, the minimum is determined by more than one point in most instances. This lends support to the evidence that the noted minima are not based on the erratic behavior of any one particular alloy in these two series of alloys.

Table II
Rupture-Life Values at Selected Temperatures and Stresses Represented in Figs. 4 and 8.
These Values Used to Determine Curves of Figs. 10 and 11

Alloy No.	C + N ₂ %	At 1000 °F		At 1200 °F		At 1300 °F	
		50,000 psi	40,000 psi	30,000 psi	20,000 psi	25,000 psi	15,000 psi
31	0.006	4.0*	60.0*	7.0	750.0	4.5	750.0
33	0.042	8.0	75.0	2.0*	130.0	0.6*	50.0
15	0.085	16.0	250.0	3.5	50.0*	1.0	20.0*
29	0.096	13.0	180.0	4.0	55.0	1.4	30.0
16	0.170	11.0	1.7	45.0
30	0.189	210.0	2800.0	11.0	320.0	3.7	130.0
18	0.220	270.0	3000.0	14.0	500.0	4.0	150.0
NITROGEN SERIES							
31	0.006	4.0*	60.0	7.0	750.0	4.5	750.0
33	0.042	8.0	75.0	2.0*	130.0	0.6*	50.0
11, 13	0.085	†	55.0	3.5	70.0	1.0	25.0*
10	0.097	5.0	50.0*	...	50.0*	1.1	35.0
9	0.136	35.0	250.0	2.5	55.0
8	0.164	55.0	500.0	3.5	80.0
6, 7, 14	0.212	50.0	450.0	9.5	400.0	6.0	95.0

*Italic figure represents the alloy with the lowest rupture life in the particular carbon or nitrogen series.

†Fractured on loading. Rupture life less than 0.001 hour.

Figs. 12 and 13 show the effect of carbon (plus nitrogen) and of nitrogen (plus carbon) on the minimum creep rates at selected values of stress and temperature (which result in high temperature intercrystalline fracture). Maxima in the creep rates occur at the intermediate carbon and nitrogen levels. These maxima in the creep rate correspond to the minima in the rupture-life curves of Figs. 10 and 11. Whereas the strength of the very low carbon plus nitrogen Alloy 31 was equal to or greater than the strength of the high carbon and nitrogen alloys, the creep resistance of the high carbon alloys appears to be the best.

The effect of variations in the carbon or nitrogen content is appreciably greater on the minimum creep rate of these 18-8 alloys than on the rupture life, the creep rate changing by a factor of 100 or more over fairly small carbon or nitrogen composition ranges.

This effect on the creep rate and on the nature of the creep curve is possibly best illustrated in Figs. 14 and 15 which show actual creep-rupture curves at 20,000 psi and 1200 °F (650 °C) for each of the carbon and each of the nitrogen alloys, respectively. These creep-rupture curves are shown only up to the first 70 hours. It is obvious that both carbon and nitrogen beyond about 0.12% increase the rupture life and creep resistance of 18-8 alloys considerably, the effect of the carbon on the improved creep resistance being much greater than the effect of the nitrogen (compare alloys of similar carbon and nitrogen content in Figs. 14 and 15). Alloy 31 (0.006% carbon plus nitrogen) shows creep resistance comparable to that of the better high carbon and high nitrogen alloys. Whereas the intermediate carbon plus nitrogen alloys show very little second-stage creep, the high

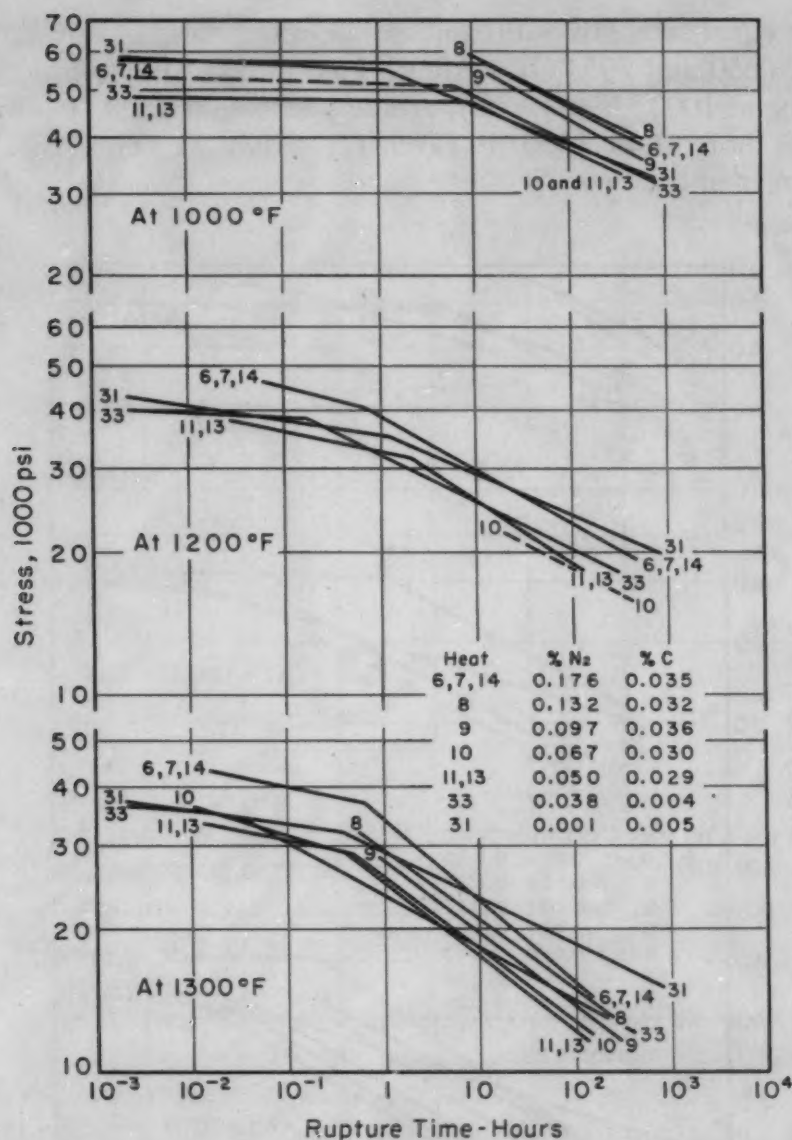


Fig. 8—Summary Plot of Log Stress Versus Log Rupture Time for All Nitrogen Alloys From 1000, 1200 and 1300 °F.

carbon and high nitrogen alloys as well as Alloy 31 show extended second-stage creep.

A comparison of stress for rupture of 10, 100 and 1000 hours at 1000, 1200 and 1300 °F (540, 650 and 705 °C) is given in Table III for alloys of comparable carbon (plus nitrogen) content and nitrogen (plus carbon) content.

Values are also listed for Alloys 31, 33 and the commercial Elc Type 304 for the purpose of additional comparisons.

Again it is evident that the high carbon alloys are stronger than alloys of equivalent nitrogen content. On the other hand, when the carbon or nitrogen levels are of the order of about 0.10% and lower, the carbon alloys are stronger only at 1000 °F (540 °C), but are

of about equal strength with comparable nitrogen alloys at 1200 and 1300 °F (650 and 705 °C). Alloy 31 and even Alloy 33, which are not strong at 1000 °F (540 °C), are very strong at 1200 °F (650 °C) and even more so at 1300 °F (705 °C), Alloy 31 being very much the stronger of the two.

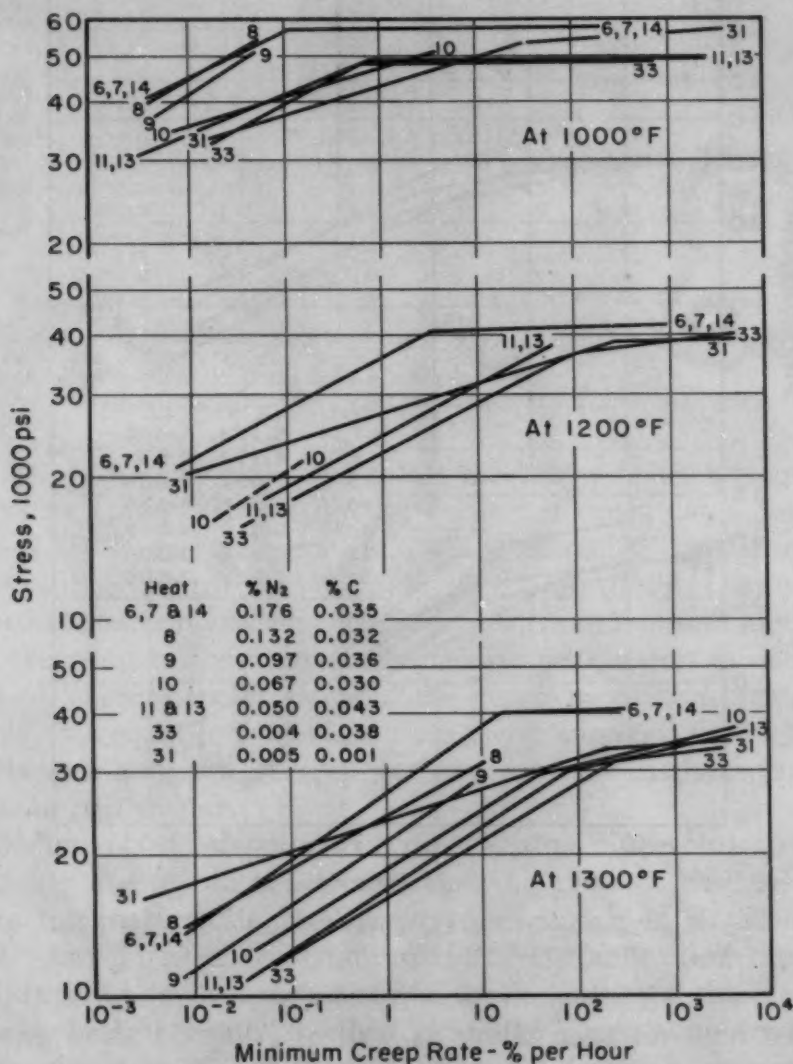


Fig. 9—Summary Plot of Log Stress Versus Log Minimum Creep Rate for All Nitrogen Alloys From 1000, 1200 and 1300 °F.

Strength values and creep rates are only of partial significance unless ductility values are also known. This is especially true for the 18-8 types of alloys, since they are subject to carbide and nitride precipitation which may result in embrittlement. Table IV lists ranges of values of both elongation (in 1.25 inches) and reduction of area. The ductility in the long-time creep-rupture tests is generally less than in the short-time tests; the values shown in Table IV

Table III
Comparative Stresses for Specified Rupture Times for Carbon and Nitrogen Alloys at
1000, 1200 and 1300 °F (540, 650 and 705 °C)

Alloy No.	C + N ₂ %	Temp. °F	Stress for Rupture Life			Alloy No.	C + N ₂ %	Temp. °F	Stress for Rupture Life		
			10 Hrs.	100 Hrs.	1000 Hrs.				10 Hrs.	100 Hrs.	1000 Hrs.
18	0.220	1000	62,000	52,500	45,000	7*	0.212	1000	56,500	46,000	35,000
		1200	31,000	24,000	18,000			1200	29,000	22,000	17,000
		1300	21,500	15,800	11,500			1300	22,500	15,000	10,200
30	0.189	1000	59,000	51,000	43,000	8	0.164	1000	57,000	46,500	36,000
		1200	30,000	23,000	17,000			1200
		1300	21,200	15,500	11,200			1300	20,700	14,500	11,000
29	0.096	1000	51,000	41,000	34,000	10	0.097	1000	47,000	36,500	30,000
		1200	25,000	18,500	12,700			1200	(23,500)	18,000	14,500
		1300	18,000	11,800	7,500			1300	18,000	12,000	8,000
15	0.085	1000	52,000	42,000	11†	0.085	1000	47,000	36,500	30,000
		1100	25,000	18,200	12,500			1200	25,000	18,500	14,000
		1300	17,500	11,600	7,000			1300	17,500	11,200	7,000
33	0.042	1000	48,500	38,500	31,000						
		1200	24,500	20,500	16,000						
		1300	18,500	14,000	11,000						
31	0.006	1000	46,000	38,500	31,500						
		1200	29,000	24,000	19,500						
		1300	23,000	18,000	14,800						
32	0.070	1000	45,000	37,500	31,700						
		1200	26,000	19,500	14,500						
		1300	19,000	13,500	9,000						

*Actually 6, 7, 14. †Actually 11, 13.

are to be read accordingly, even though appreciable scatter in individual tests was evident. From Table IV, which shows ductility values for comparable nitrogen and carbon contents, several interesting trends may be noted which support data already presented and some yet to follow.

1. For carbon alloys from about 0.085% carbon plus nitrogen or more, there is a decrease in ductility with increasing carbon. This decrease is very severe in the longer-time tests at 1200 and 1300 °F (650 and 705 °C).

2. The nitrogen alloys are similarly embrittled but not as severely as the carbon alloys. For example, Alloys 11 (13) and 10 show higher values than Alloys 15 and 29, at comparable carbon and nitrogen values. This is in line with smaller amounts of nitride precipitation than carbide precipitation noted at comparable alloying levels, as in Fig. 22.

3. Of interest is the sustained high ductility of the strong Alloy 31 (and 33) in spite of increasing temperature or rupture life.

4. Similarly, Alloy 32, the Elc 304 stainless steel, remains ductile with its increased nickel content and only 0.070% carbon plus nitrogen.

Austenite-Ferrite Transformation—To serve as a base line for comparison, Figs. 16 and 17 show the amount of retained austenite for the solution-treated and quenched alloys, and after long-time exposure at 1000, 1200 and 1400 °F (540, 650 and 760 °C) in simple

exposure tests. These figures are for the carbon and the nitrogen series respectively and are based on X-ray determinations made at room temperature after careful surface preparation to avoid surface ferrite transformation.

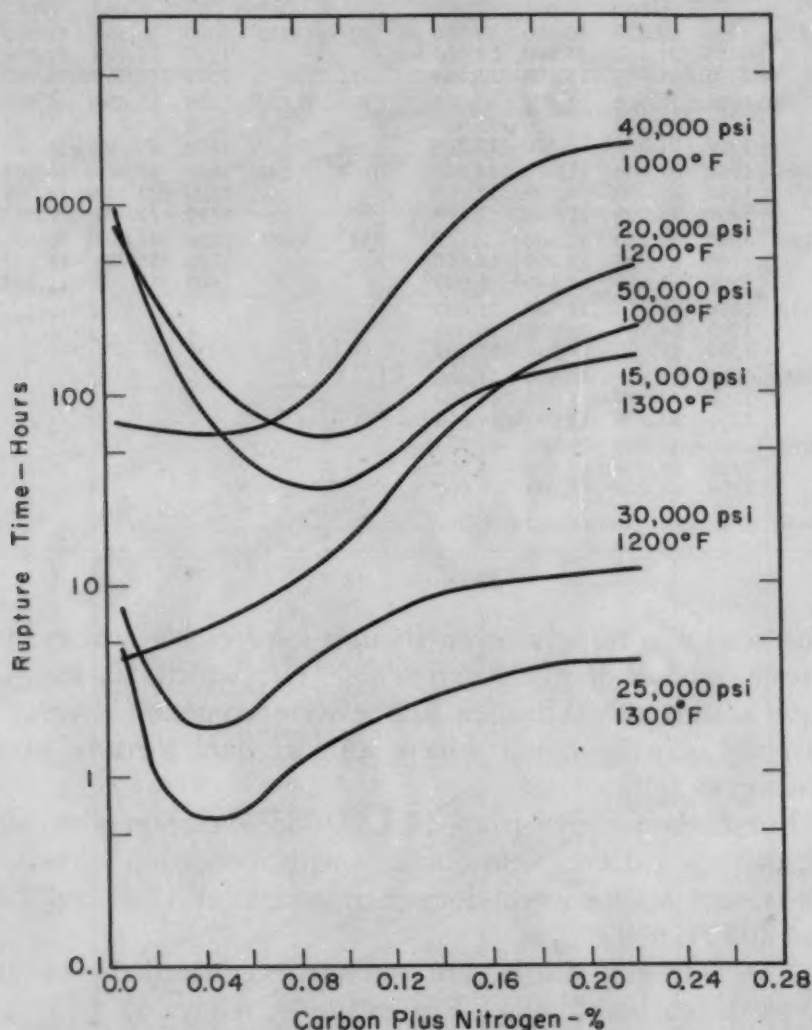


Fig. 10—Variation in Rupture Life as a Function of Carbon Plus Nitrogen Content for Carbon Alloys at Selected Temperatures and Stress Levels for High Temperature-Type Deformation. (See Table II for values.)

The individual points for these curves and in the subsequent figures are omitted to avoid complication. Actually, the point scatter was not as good as might be desired; however, this was not attributed to any fault in the X-ray measurements but to the fact that four readings at 90 degrees to each other around the circumference of a specimen gave a fairly wide range of values of ferrite and austenite. To minimize this, the specimens were rotated, giving much improved reproducibility but still resulting in very measurable scatter from test piece to test piece. This is apparently due to the instability of the

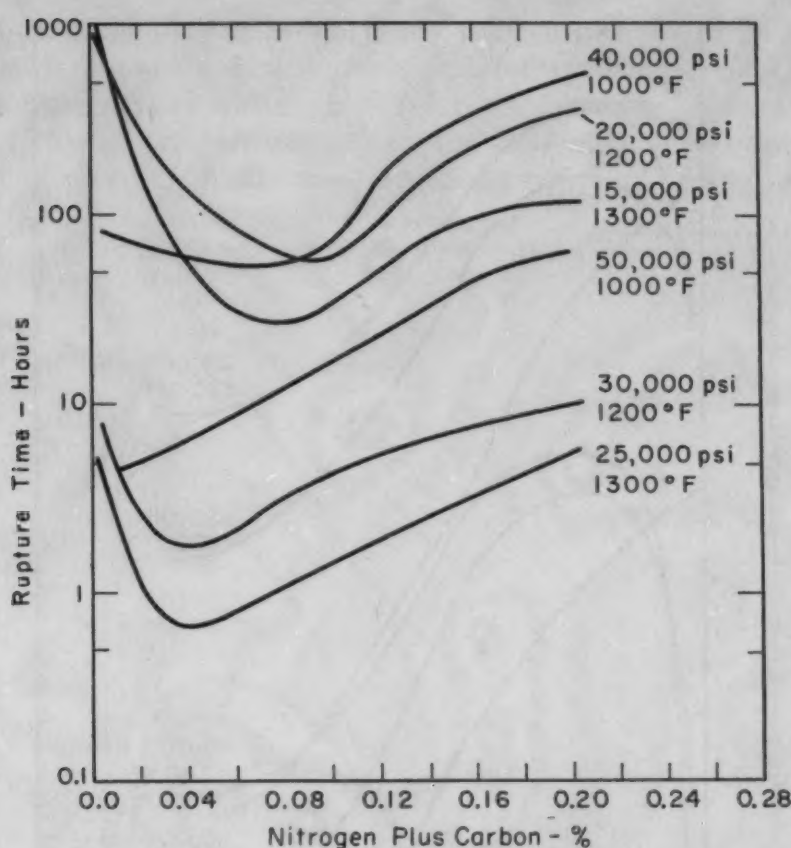


Fig. 11—Variation in Rupture Life as a Function of Nitrogen Plus Carbon Content for Nitrogen Alloys at Selected Temperatures and Stress Levels for High Temperature-Type Deformation. (See Table II for values.)

Table IV
Ductility Values From Stress-Rupture Tests at 1000 to 1300 °F (540 to 705 °C)

Alloy No.	Carbon Series			Temp. °F	Alloy No.	Nitrogen Series		
	C + N ₂ %	Elong. %	Red. of Area, %			N ₂ + C %	Elong. %	Red. of Area, %
18	0.220	15-34	16-29	1000	6, 7, 14	0.212	13-27	12-23
		5-14	2-17	1200			3-24	7-23
		2-7	2-8	1300			2-23	4-18
30	0.189	6-50	18-57	1000	8	0.164	11-28	14-30
		5-24	2-45	1200		
		3-28	3-39	1300			5-16	6-13
29	0.096	16-39	19-64	1000	10	0.097	14-66	15-39
		5-28	12-36	1200			17-28	8-30
		6-27	6-26	1300			10-34	10-33
15*	0.085	11-40	20-27	1000	11, 13	0.085	19-51	15-42
		6-20	5-26	1200			16-27	14-25
		1300			8-29	12-31
33	0.042	27-44	33-75	1000	32	0.070	17-50	20-57
		42-70	40-70	1200			20-38	22-47
		31-64	40-75	1300			20-40	20-39
31	0.006	23-50	48-67	1000				
		20-50	26-76	1200				
		19-40	42-75	1300				

*Based on more limited data.

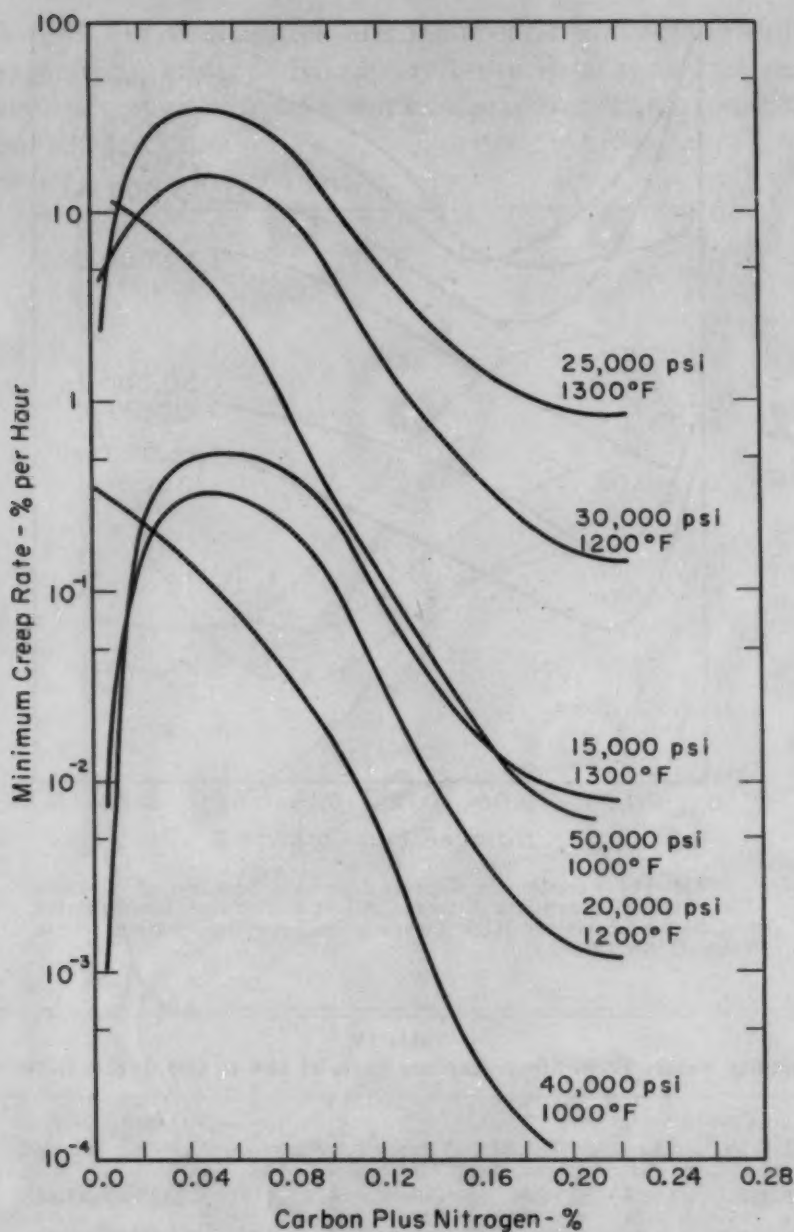


Fig. 12—Variation in Minimum Creep Rate as a Function of Carbon Plus Nitrogen Content for Carbon Alloys at Selected Temperatures and Stresses for High Temperature-Type Deformation.

austenite in these unstabilized alloys and to some anisotropy of deformation, especially at the surface of the test bars.

Figs. 18 and 19 are for the carbon and nitrogen series of alloys respectively, and show the effect of 30% cold reduction of the solution-treated steels on the amount of ferrite to form due to subsequent heating to temperatures of 1000, 1200 and 1400 °F (540, 650 and 760 °C) for long periods of time similar to those used to obtain the data of Figs. 16 and 17.

Working curves of "per cent ferrite versus rupture life" were

drawn for each alloy tested at each temperature in creep-rupture. From such curves a few interesting and revealing temperature-rupture time curves were selected for the purpose of showing the effect of stress (or creep strain) on the amount of ferrite formed as a result of creep-rupture testing (measurements made at room tem-

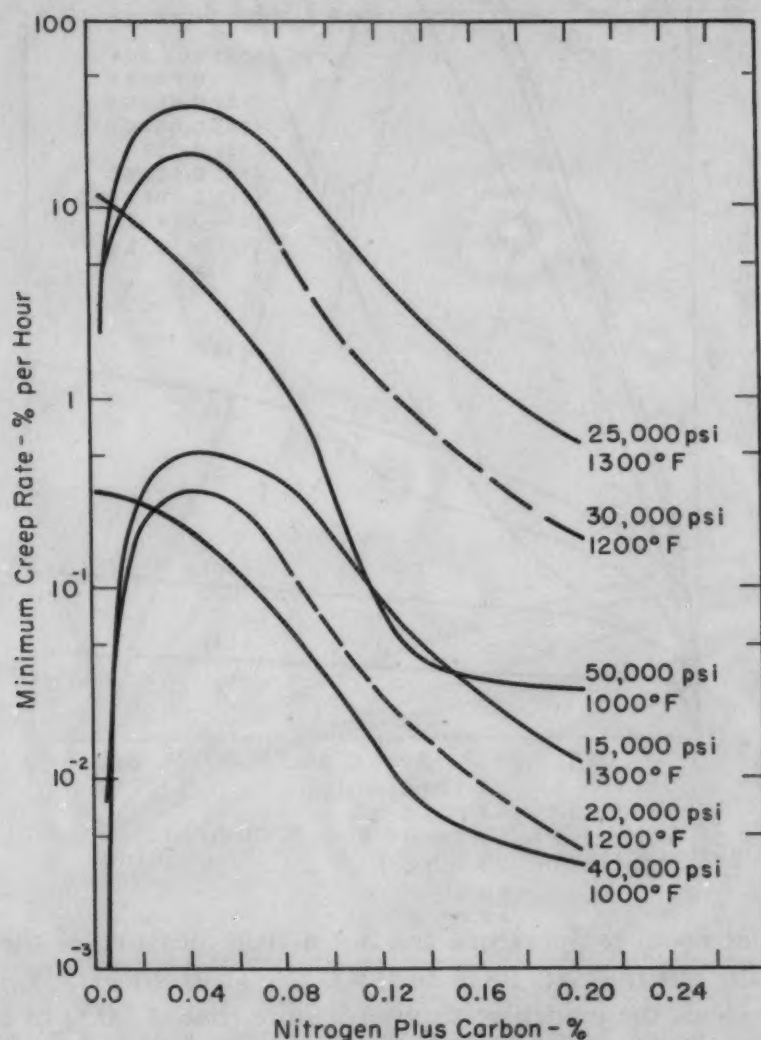


FIG. 13—Variation in Minimum Creep Rate as a Function of Nitrogen Plus Carbon Content for Nitrogen Alloys at Selected Temperatures and Stresses for High Temperature-Type Deformation.

perature) as compared to the amount found after the usual static time-temperature heating tests. Figs. 20 and 21 compare retained austenite for the carbon and nitrogen series respectively for several different combinations of rupture time and temperature compared to other treatments.

DISCUSSION

It must be pointed out that the values of ferrite and austenite as

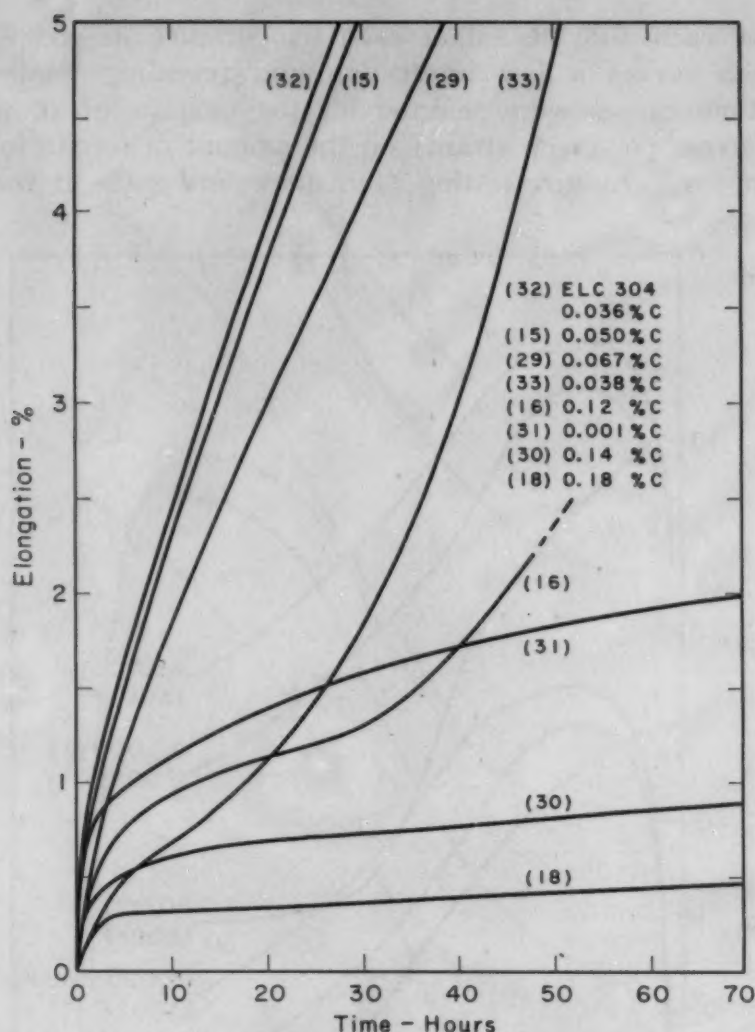


Fig. 14—Creep Curves for First 70 Hours of Test for Carbon Alloys at 20,000 Psi, 1200 °F.

measured at room temperature are not a true measure of the ferrite or austenite existing at 1000 to 1300 °F (540 to 705 °C). For 18-8-type steels the evidence is quite definite that at 1000 to 1300 °F (540 to 705 °C) the ferrite which is noted at room temperature is not very stable and transforms to austenite on heating, re-forming ferrite on cooling at temperatures below about 200 to 500 °F (6, 7, 8). In instances where an alloy shows up to 30% ferrite after quenching from the solution temperature (such as Alloys 31 and 33), it is not known what the austenite-ferrite relationships are after reheating to 1000 to 1300 °F (540 to 705 °C) under the various test conditions used here. It is expected, however, that the changes which occur at 1000 to 1300 °F, such as carbide or nitride precipitation, predispose the alloy for the transformation to ferrite on cooling to room temperature. Accordingly, this room temperature ferrite is then an approximate measure of other changes occurring at the actual reheat

temperature. Some ferrite is, of course, present at temperatures of 1000 to 1300 °F (8); this quantity probably increases with an increase in the quantity of ferrite which is noted at room temperature following solution treatment.

It is entirely unfortunate that tests were not made at tempera-

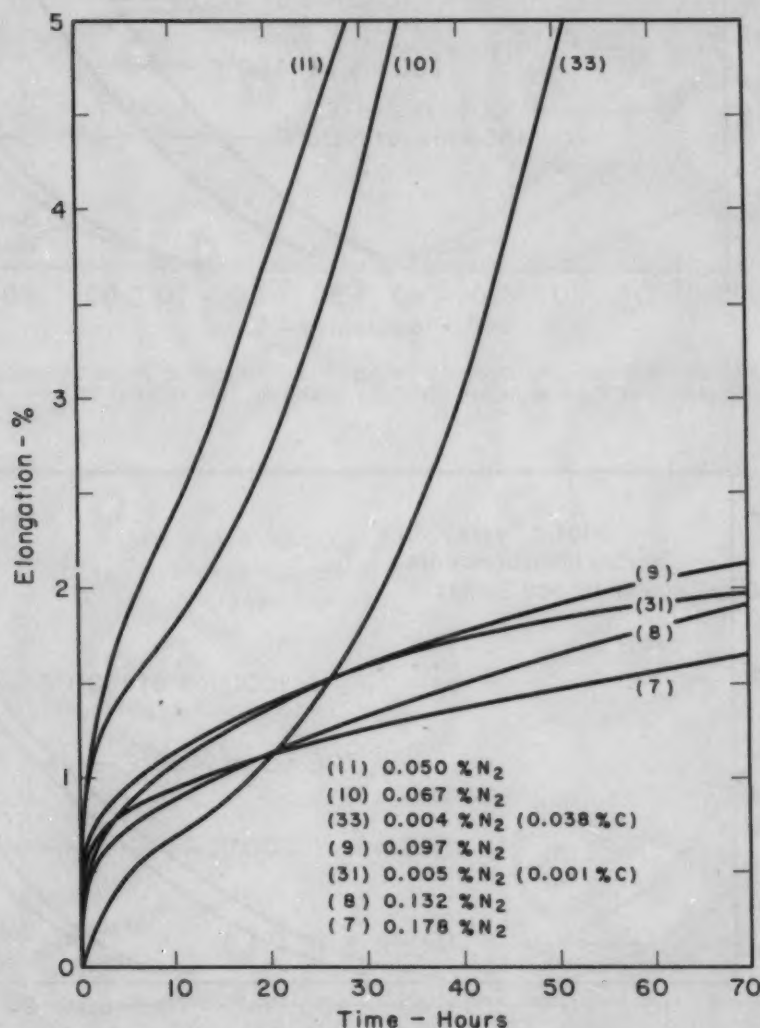


Fig. 15—Creep Curves for First 70 Hours of Test for Nitrogen Alloys at 20,000 Psi, 1200 °F.

tures of 1000 to 1300 °F (540 to 705 °C) to determine actual quantities of ferrite present at each temperature.

Figs. 16 and 17 show that after static time-temperature heating tests at 1000 to 1300 °F (540 to 705 °C) the amount of room temperature ferrite increases with increasing reheat temperature compared to the solution-treated state, until a maximum is reached for some temperature above about 1300 °F (705 °C), although this was not determined accurately. By the time 1400 °F (760 °C) is reached, these alloys re-enter the stable austenite field, resulting in an increase

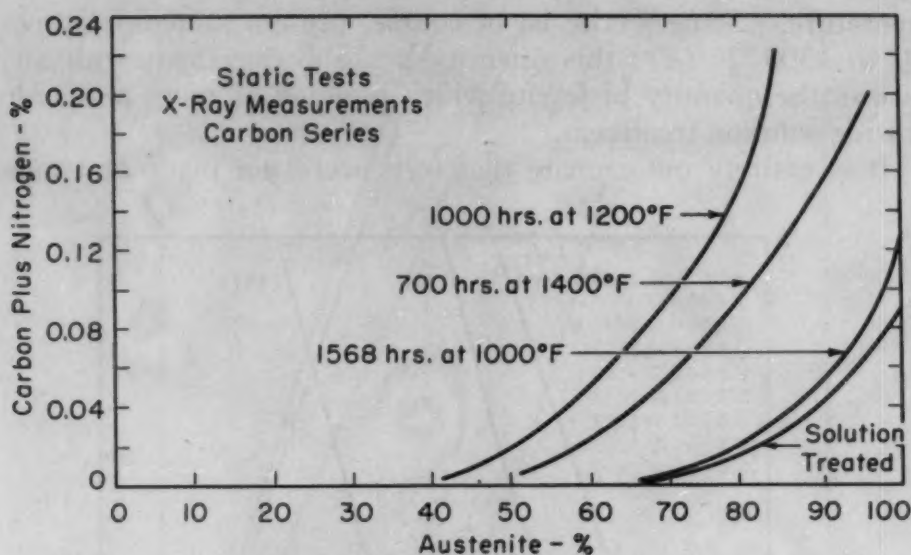


Fig. 16—Approximate Decrease in Austenite Content at Room Temperature After Exposure of Carbon Alloys for Long Times at 1000 to 1400 °F.

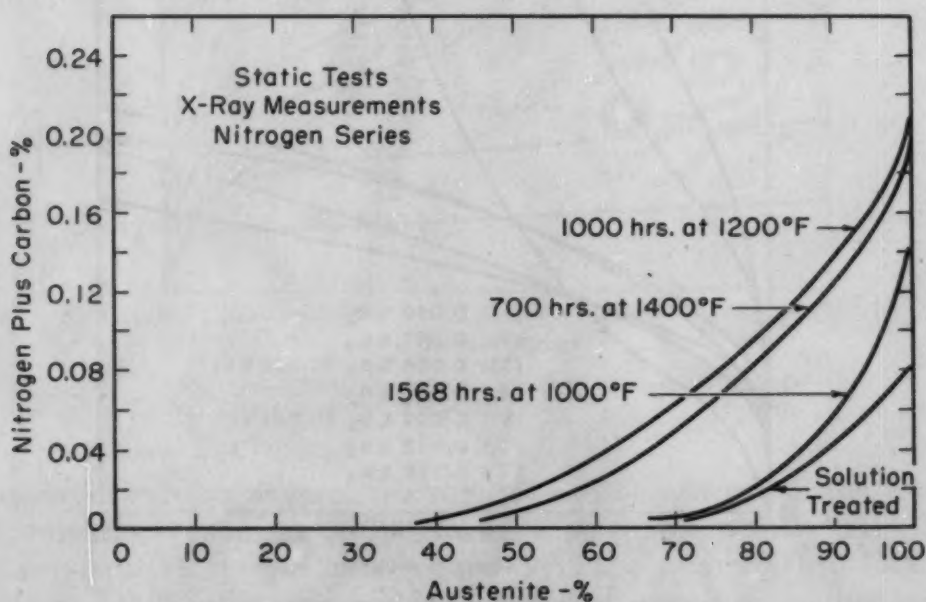


Fig. 17—Approximate Decrease in Austenite Content at Room Temperature After Exposure of Nitrogen Alloys for Long Times at 1000 to 1400 °F.

in the amount of austenite. After 1568 hours at 1000 °F (540 °C) the increase in ferrite is quite small, the stability of the austenite being fairly good and of similar amount for both carbon and nitrogen alloys. After 1000 hours at 1200 °F (650 °C), however, there is an increase of the order of 20 to 30% in the room temperature ferrite content over that measured for the solution-treated condition or after mere exposure at 1000 °F (540 °C). A very important effect, previously noted by other investigators in a more qualitative way, is that the

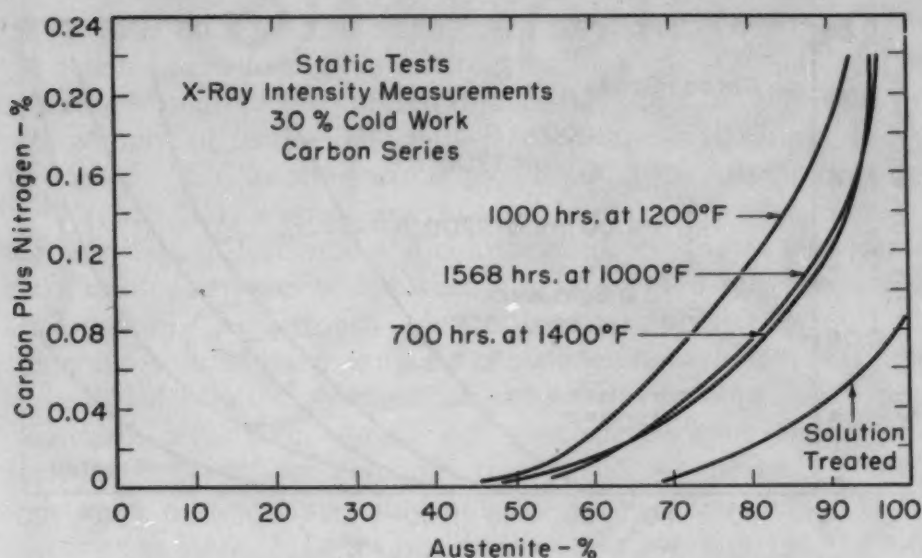


Fig. 18—Approximate Effect of 30% Cold Work on Austenite Content of Prior Solution-Treated Alloys Due to Exposure for Long Periods of Time at Temperatures of 1000 to 1400 °F.

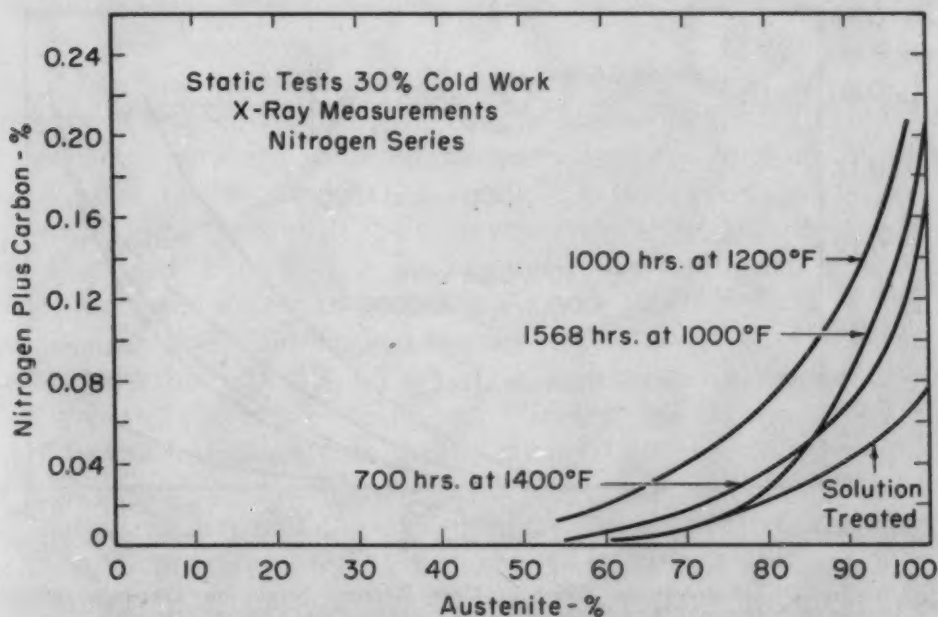


Fig. 19—Approximate Effect of 30% Cold Work on Austenite Content of Prior Solution-Treated Alloys Due to Exposure for Long Periods of Time at Temperatures of 1000 to 1400 °F.

austenite in the high nitrogen alloys is appreciably more stable than in the carbon alloys. At about 0.20% carbon plus nitrogen and after 1000 hours at 1200 °F (650 °C), the nitrogen alloys show almost 100% austenite, whereas the carbon alloys show about 20% ferrite (see Figs. 16 and 17). At the lower carbon and nitrogen contents of the order of 0.08% or less, the amount of ferrite formed is about the same for either the carbon or the nitrogen alloys.

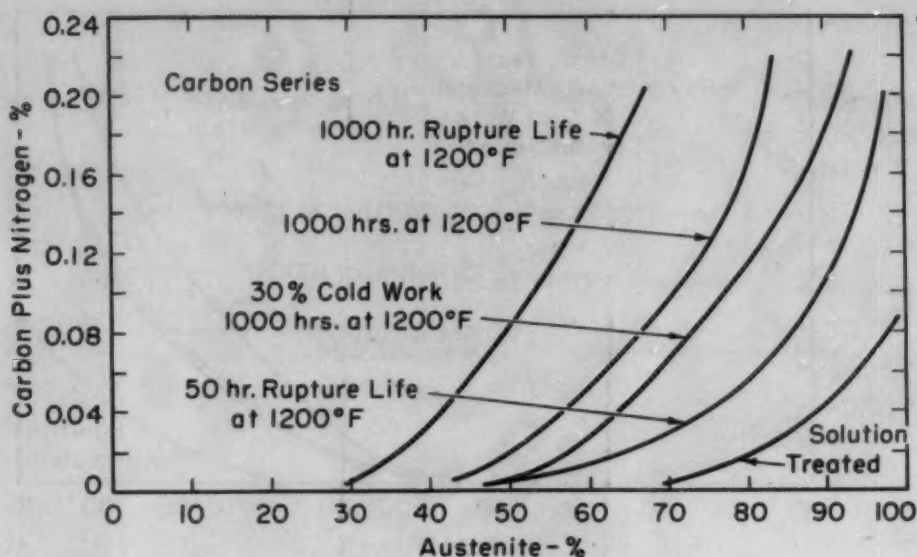


Fig. 20—Approximate Effect of Creep-Rupture Strain on Promotion of Ferrite in Carbon Alloys Showing Large Increase Over Other Treatments.

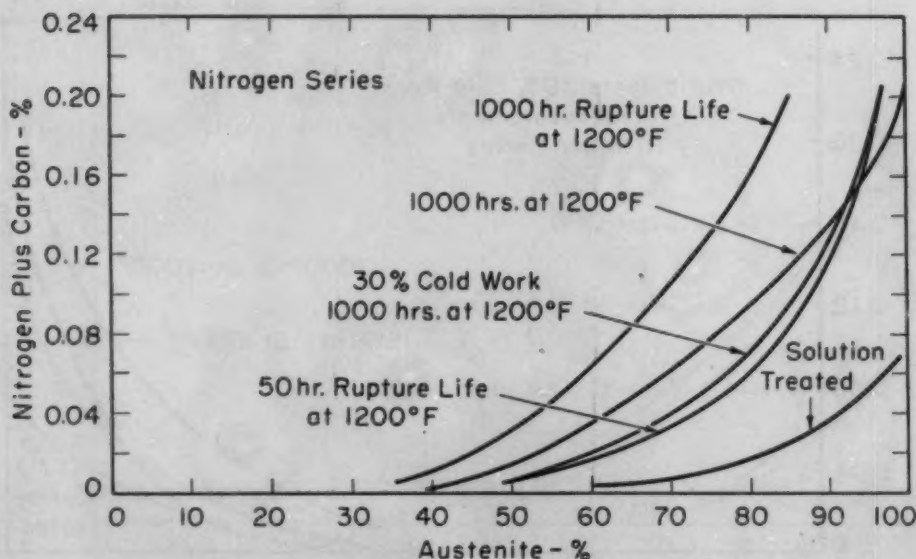


Fig. 21—Approximate Effect of Creep-Rupture Strain on Promotion of Ferrite in Nitrogen Alloys Showing Large Increase Over Other Treatments.

Fig. 22 shows a series of photomicrographs of representative carbon and nitrogen alloys after exposure of the solution-treated samples at 1200 °F (650 °C) for 1000 hours. It will be noted that the amount of carbide precipitated in the high carbon Alloy 18 is appreciably greater than the amount of nitride precipitated in the high nitrogen Alloy 7. This difference is notably less in comparing the carbon Alloy 15 (0.05% carbon) with the nitrogen Alloy 11 (0.05% N₂).

This increased amount of carbide precipitate probably accounts

for the greater strength and better creep resistance of the high carbon alloys as compared to the high nitrogen alloys.

It was somewhat unexpected to note the effect of 30% cold work on the amount of ferrite found after reheating to 1000 and 1200 °F (540 and 650 °C), as shown in Figs. 18 and 19. After reheating to 1200 °F (650 °C), within experimental limits, there was very little, if any, increase in ferrite in the cold-worked test pieces as compared to the annealed samples which were simply exposed for an equal time at temperature. This would indicate that at 1200 °F (650 °C) these alloys come to about the same ferrite-austenite-carbide (or nitride) balance in 1000 hours, whether one starts with an annealed structure or one with 30% cold work. For shorter reheating times, of the order of 100 hours, for example, this would not be true, since the cold-worked alloys would undoubtedly show more ferrite. After 1568 hours at 1000 °F (540 °C), on the other hand, due to the longer time needed for precipitation of the carbide or nitride, the 30% cold-worked sample showed more ferrite than the solution-treated specimen. This increase in ferrite was greater at the higher carbon and nitrogen levels and was somewhat larger for carbon alloys (Fig. 18) than for nitrogen alloys (Fig. 19).

When one accomplishes the metal deformation at the test temperature in a creep-rupture type of test, instead of through cold work at room temperature followed by reheating, the amount of ferrite found after testing at 1200 °F (650 °C) is appreciably larger, as shown in Figs. 20 and 21. For a relatively short rupture life of 50 hours at 1200 °F (650 °C), the amount of ferrite formed is less than after unstressed exposure for 1000 hours at 1200 °F (650 °C) of the annealed or 30% cold-worked specimens; however, after 1000 hours rupture life at 1200 °F (650 °C), the increase in ferrite is large compared to the other treatments. Again the carbon alloys show more ferrite formation than do the nitrogen alloys.

Strength Considerations—Two things were fairly clear from the curves shown and the measurements made. First, the increase in room temperature ferrite for any alloy after testing at a given temperature was uniform with increasing rupture time; and for a given rupture time the increase in ferrite with increasing test temperatures up to 1300 °F (705 °C) was also uniform. Secondly, the amount of ferrite increased continuously with decreasing carbon or nitrogen for each different treatment, whether after static exposure, after cold work, or after rupture testing. In spite of these observations of the uniform change in ferrite, there is clear evidence from Figs. 10 to 15 that these stainless steels go through a minimum in rupture strength and a maximum in creep rate with increasing carbon or nitrogen. In Fig. 10 all the alloys which yield the curve shown for 1200 °F (650 °C) and 20,000 psi contain ferrite, the quantity

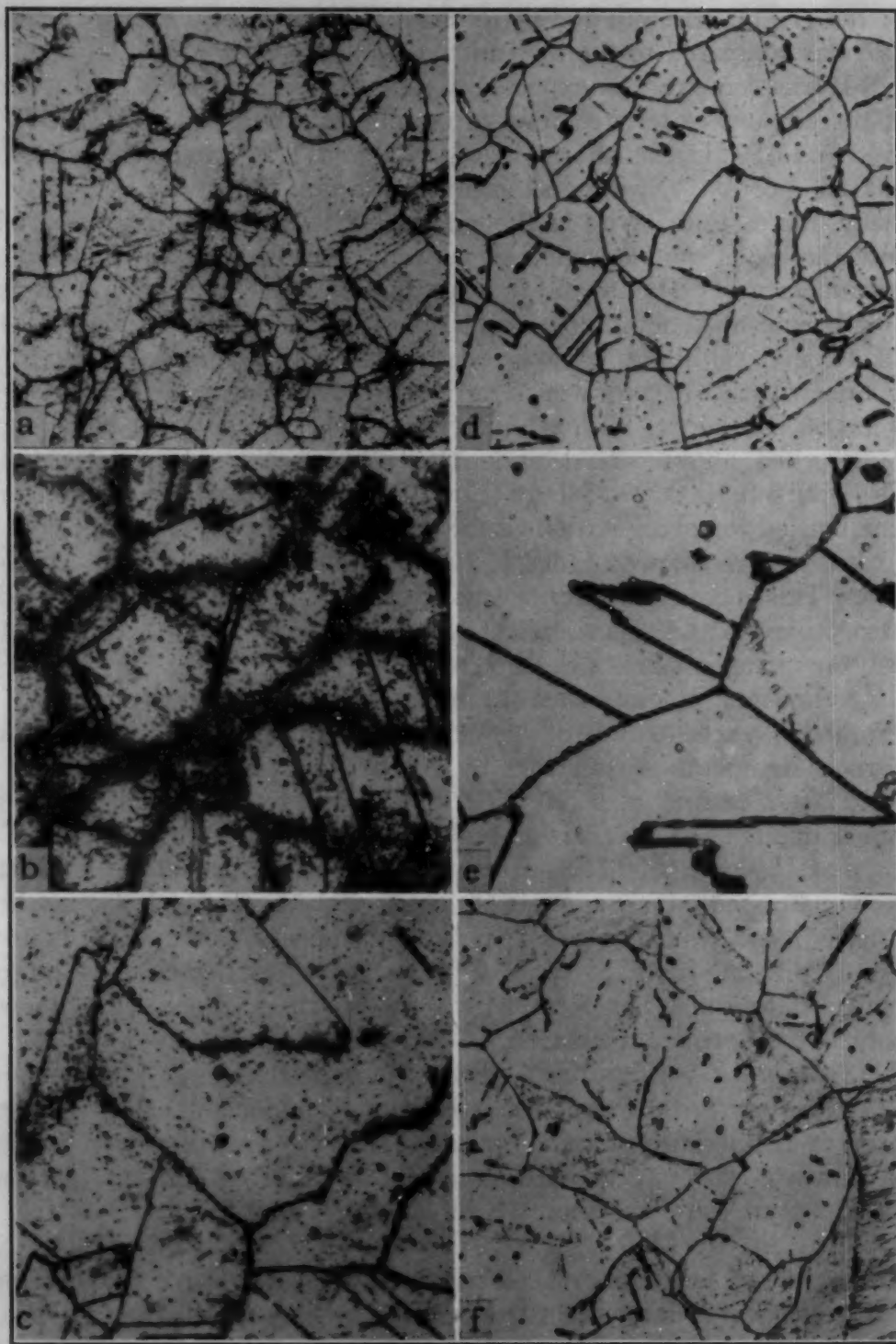


Fig. 22—Microstructures of Solution-Treated 18-8 Stainless Steels After Reheating for 1000 Hours at 1200 °F. 15% oxalic acid, electrolytic etch.

Carbon Series

- (a)—Alloy 18, 0.18% carbon. $\times 100$.
(b)—Alloy 16, 0.12% carbon. $\times 500$.
(c)—Alloy 15, 0.05% carbon. $\times 500$.

Nitrogen Series

- (d)—Alloy 7, 0.174% nitrogen. $\times 100$.
(e)—Alloy 8, 0.132% nitrogen. $\times 500$.
(f)—Alloy 11, 0.05% nitrogen. $\times 100$.

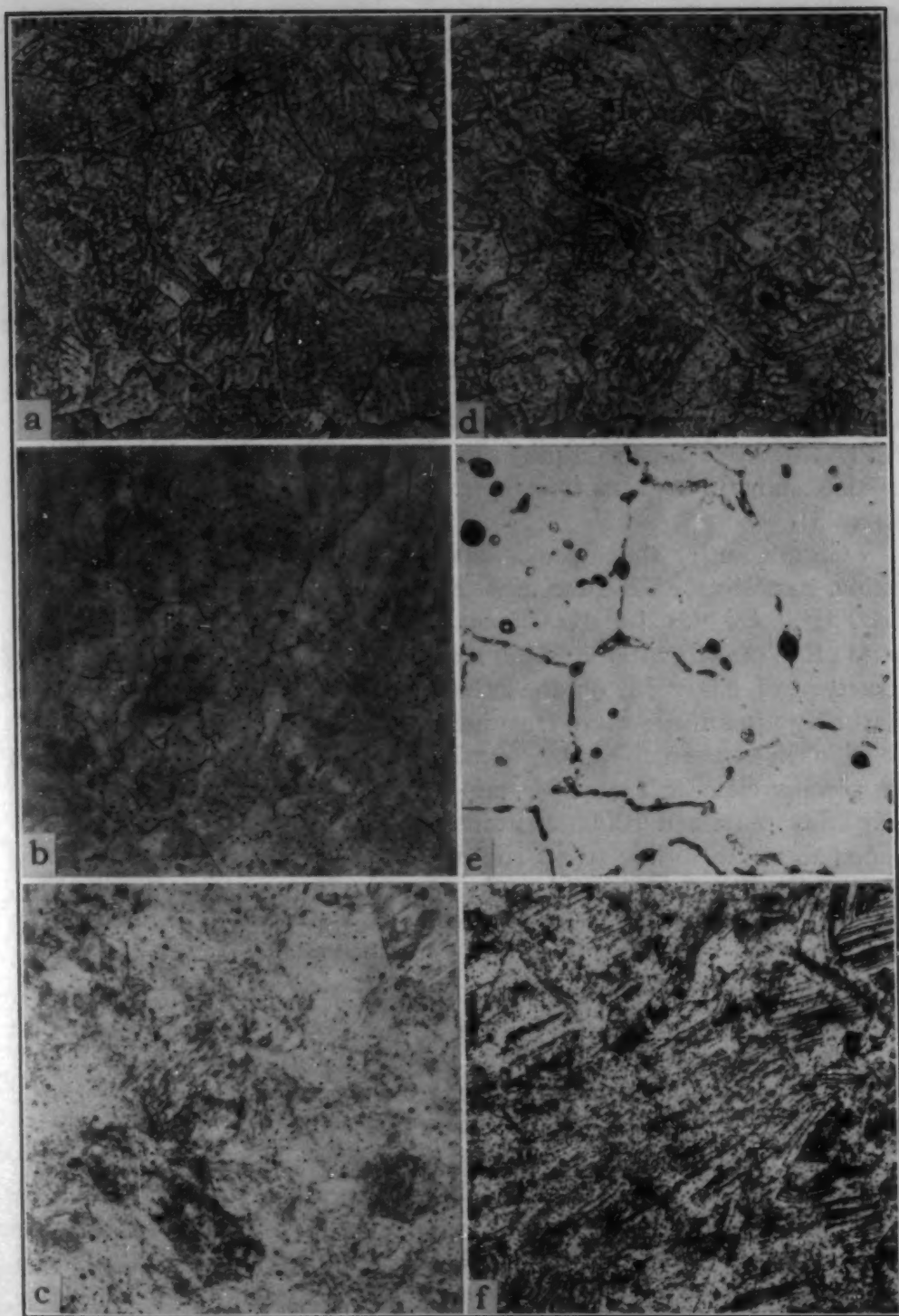


Fig. 23—Photomicrographs Showing Stability of Acicular Ferritic Structure of Alloy 31, Compared to Alloy 33. 15% oxalic acid, electrolytic etch. (a)—Alloy 31, solution-treated. $\times 100$. (b)—Alloy 31, reheat 700 hours at 1400 °F. $\times 100$. (c)—Alloy 31, 30% cold work, reheat 1000 hours at 1200 °F. $\times 100$. (d)—Alloy 33, solution-treated. $\times 100$. (e)—Alloy 33, reheat 700 hours at 1400 °F. $\times 500$. (f)—Alloy 33, 30% cold work, reheat 1000 hours at 1200 °F. $\times 100$.

decreasing regularly with increasing carbon content. Accordingly, one could suggest that the ferrite alone is responsible for the observed minimum. One might state that increasing carbide and nitride precipitation is responsible for the increased strength and creep resistance at higher carbon and nitrogen contents beyond the inflection point in the curves of Figs. 10 to 13. Metallographic evidence indicates that this is correct. The higher strength and creep resistance of high carbon alloys over high nitrogen alloys can then be explained also by the greater amount of precipitation in high carbon alloys (see Fig. 22a and 22d). The only possible explanation of the high rupture strength and creep resistance shown by the very low carbon, low nitrogen alloys is the acicular form of the ferrite. This structure is shown in Fig. 23 for the solution-treated condition of Alloy 31. Alloy 33 (0.042% carbon plus nitrogen versus 0.006% for Alloy 31) is also shown, its structure approaching the acicular structure of Alloy 31.

Significantly, the acicular structure of Alloy 31 is extremely stable, persisting even after 30% cold work followed by reheating to 1200 °F (650 °C) for 1000 hours, and after 700 hours reheat at 1400 °F (760 °C) after solution treatment, as shown in Fig. 23. The structure of Alloy 33, on the other hand, is not stable and changes markedly after these same treatments.

To strengthen the above explanation, the creep-rupture data of the commercial Elc Type 304 stainless steel were utilized. This alloy (No. 32) remained 100% austenitic after all of the treatments mentioned above, including stress-rupture testing up to 1300 °F (705 °C). If one plots the data for this Alloy 32 (0.036% carbon plus 0.034% N₂) in Figs. 10 to 13, the rupture-life and creep-rate values fall almost exactly on these same curves which are plotted on the basis of the carbon plus nitrogen content (instead of ferrite content). Accordingly, this 18 Cr-10 Ni stainless steel with 100% austenite has about equal strength to an 18-8 grade of equal carbon plus nitrogen content but with appreciable ferrite, the determining factor being the carbide and nitride quantities.

If the above is correct, then one could explain the shape of the curves shown in Figs. 10 to 13 by the composite curve drawn in Fig. 24. The bottom curve indicates the course of the rupture-life values (dashed curve) if the ferrite at these low carbon and nitrogen contents were not in the stable acicular form. The entire increase with increasing carbon and nitrogen is then due to carbide and nitride precipitation, and not to ferrite formation.

Closer examination of Table III indicates that if one desires high temperature strength for 18-8 applications, barring other restrictions such as corrosion, there is a carbon plus nitrogen range near 0.03 to 0.10% which gives the lowest rupture strength and creep

resistance. The presence of ferrite need not be detrimental to the creep-rupture properties.

Alloys of 0.006 or even 0.010% carbon plus nitrogen are not readily made except by vacuum melting and casting; accordingly, reproduction of an alloy similar in composition to Heat 31 and with its properties would be difficult. It does suggest, however, that alloys

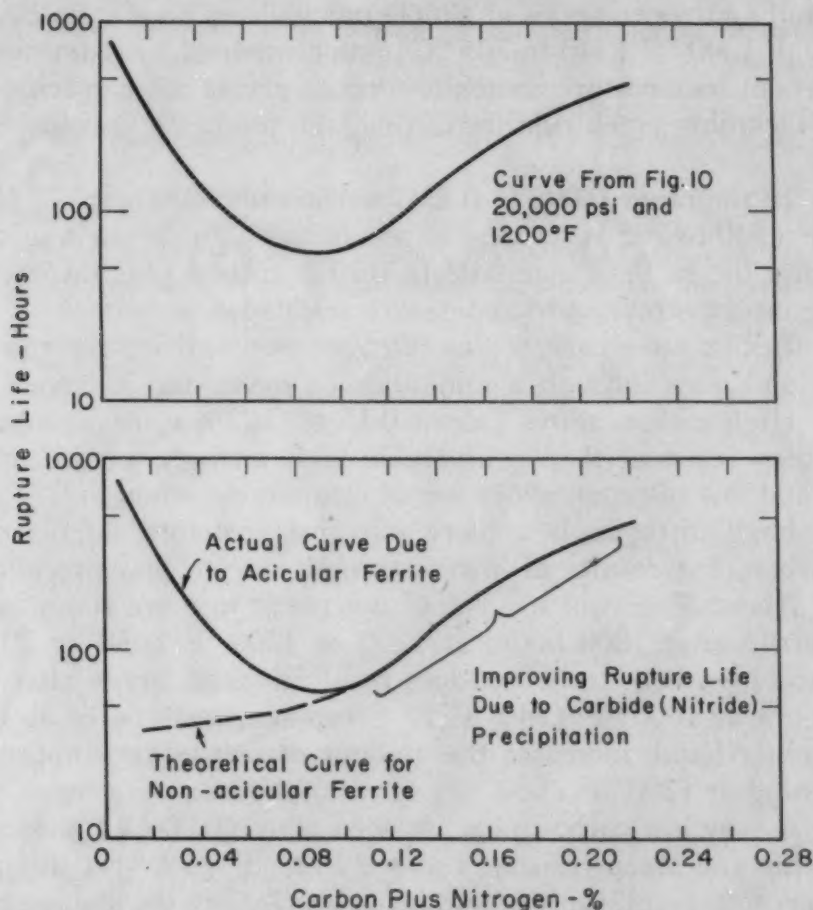


Fig. 24—Composite Curve Showing Contribution of Acicular Ferrite and of Carbide or Nitride to High Temperature Strength of 18-8 Alloys.

of adjusted nickel and chromium content which would give the stable acicular ferrite structure might prove to be of great value for high creep-rupture properties.

While the nitrogen content of the 18-8 stainless steels is practically never given as a chemically analyzed quantity when purchasing or applying such steels, this research shows that the nitrogen plays a similar role as carbon, especially at the usual nitrogen levels under about 0.05%. Its contribution to the strength and creep resistance at high temperatures is important, especially since it will determine whether one has a strong or weak alloy. Unfortunately, it appears

that in the Elc Type 304 stainless grade the carbon plus nitrogen content results in low rupture life (see Table III) and relatively low creep resistance.

CONCLUSIONS

Based on studies of the creep-rupture properties of a carbon series and a nitrogen series of simple unstabilized 18-8 stainless steels at 1000 to 1300 °F (540 to 705 °C), supplemented by determinations of the room temperature austenite-ferrite balance after specific treatments, including creep-rupture testing, the following conclusions are made:

1. In the range 0.005 to 0.22% carbon plus nitrogen, at 1000 to 1300 °F (540 to 705 °C), these experimental alloys show a minimum in rupture life in the range 0.03 to 0.10% carbon plus nitrogen, depending on the stress and temperature selected.
2. In this same carbon plus nitrogen range, the creep resistance is poor and goes through a minimum (a maximum in creep rate).
3. High carbon alloys (about 0.15 to 0.22%) are stronger and more creep resistant than comparable high nitrogen alloys, but low carbon and low nitrogen alloys are of comparable strength.
4. High nitrogen is a more effective austenite stabilizer than high carbon, but results in lower strength due to less precipitation.
5. About 30% cold work does not result in more room temperature ferrite after 1000 hours at 1200 or 1300 °F (650 or 705 °C) than uncold-worked steels, but does result in more ferrite after about 1500 hours at 1000 °F (540 °C). Creep-rupture type of straining, on the other hand, increases the amount of ferrite very appreciably after testing at 1200 °F (650 °C) for 1000 hours.
6. A very low carbon plus nitrogen alloy (0.006%) shows high rupture life and creep resistance above 1000 °F (540 °C) in spite of a high ferrite content, the strength being ascribed to the stable acicular form of the ferrite.
7. At carbon and nitrogen contents greater than those giving minimum strength, the strength improvement is due to the increased amounts of precipitation of carbide or nitride.
8. Nitrogen is an important alloying element and essentially equivalent to carbon in controlling high temperature strength properties in the usual range of chemical values.

ACKNOWLEDGMENTS

The authors are indebted to the Bureau of Ships for sponsorship of this research and for permission to publish. Thanks are also expressed to Mrs. Gloria Johnson for extensive metallographic work and to Ralph Kimble for assisting in the creep work.

References

1. J. T. Norton, "A Technique for Quantitative Determination of Texture of Sheet Metals", *Journal of Applied Physics*, Vol. 19, December 1943, p. 1176.
2. "Internationale Tabellen zur Bestimmung von Kristall-strukturen", Zweiter Band, Gebrüder Borntraeger, Berlin, 1935, p. 556.
3. A. Taylor, "An Introduction to X-Ray Metallography", Chapman and Hall, Ltd., London, 1945.
4. C. S. Barrett, "Structure of Metals", McGraw-Hill, London, New York, 1943.
5. W. O. Binder, C. M. Brown and Russell Franks, "Resistance to Sensitization of Austenitic Chromium-Nickel Steels of 0.03% Max. Carbon Content", *TRANSACTIONS, American Society for Metals*, Vol. 41, 1949, p. 1301.
6. H. H. Uhlig, "The Role of Nitrogen in 18-8 Stainless Steel", *TRANSACTIONS, American Society for Metals*, Vol. 30, 1942, p. 947.
7. R. Buehl, J. H. Hollomon and J. Wulff, "Magnetic Analysis of Transformations in a Cold-Worked 18-8 Alloy", *Transactions, American Institute of Mining and Metallurgical Engineers*, Vol. 140, 1940, p. 368.
8. E. J. Dulis and G. V. Smith, "Ferrite Formation Associated With Carbide Precipitation in 18 Cr-8 Ni Austenitic Stainless Steels", *TRANSACTIONS, American Society for Metals*, Vol. 44, 1952, p. 621.

MECHANISM OF THE CARBURIZATION OF SOME STAINLESS STEELS

By J. B. GIACOBBE

Abstract

A theory of carburization of alloy steels postulates that pure, solid carbon per se cannot supply soluble or diffusible carbon to the metal surface. An "oxidizing potential" created by carbon dioxide or water vapor must exist in order that nascent carbon may be generated as a result of the formation and subsequent dissociation of carbon monoxide.

In this investigation, it is shown that certain austenitic stainless steels of the 18-8 variety can absorb carbon from high purity graphite under a vacuum of the order of 10^{-4} millimeters of mercury. Under these conditions it is believed that the gaseous phase or "oxidizing potential" plays a minor role in the mechanism of carburization. On the other hand, contact pressure between the solid carburizer and the metal surface exerts a pronounced influence on the rate of carburization, the higher the pressure, the greater the carbon absorption. This is explained on the basis of "contact catalysis" lowering the energy of formation of carbides at the metal surface which, on absorption and dissociation, provide the necessary carbon for diffusion in the austenite.

IN pack or solid carburizing, it is generally believed that a gaseous phase such as carbon dioxide or water vapor, which creates an "oxidizing potential", must be present in the solid, carbonaceous medium in order that carbon transfer to the metal surface may occur (1).¹ Under high vacuum, where the concentration of this gaseous phase would be extremely low, it has been reported that carburization of steels proceeds very slowly if at all (2). To check the validity of the "oxidizing potential" theory, a series of experiments was undertaken in which the "carburizing" reaction was carried out under high vacuum, using high purity graphite as the solid carburizer in contact with the metal surface. Because of their high affinity for carbon at temperatures in excess of 1400 °F (760 °C), austenitic stainless steels of the 18-8 variety were used to permit the detection

¹The figures appearing in parentheses pertain to the references appended to this paper.

This paper is based on a thesis submitted to Lehigh University in partial fulfillment of the requirements for the degree of Master of Science in Metallurgical Engineering.

A paper presented before the Thirty-fourth Annual Convention of the Society, held in Philadelphia, October 18 to 24, 1952. The author, J. B. Giacobbe, is plant metallurgist, Superior Tube Co., Norristown, Pa. Manuscript received August 27, 1951.

of the slightest trace of carbon absorption. A temperature of 1900 °F (1040 °C) was arbitrarily used for all tests in this investigation, inasmuch as this is the minimum temperature generally used in commercial annealing of these alloys.

EXPERIMENTAL PROCEDURE

The carburizing reactions were carried out in austenitic stainless steel tubes, $\frac{1}{2}$ inch OD by 0.035 inch wall by 42 inches long, welded at one end and attached at the open end to a vacuum apparatus as shown in Fig. 1. With the aid of a long-handled spoon, high purity graphite was placed between two preflattened surfaces of the tube as shown at "B", Fig. 1. Upon withdrawing the spoon, the tube

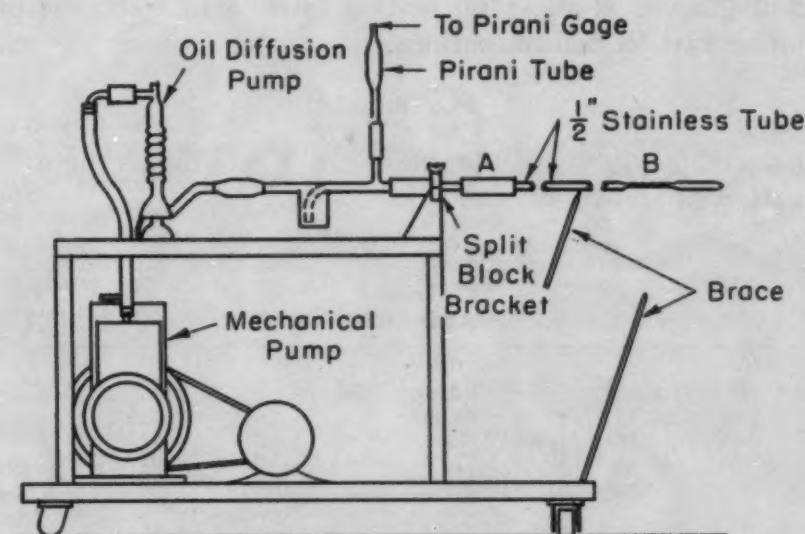


Fig. 1—Schematic Diagram of Apparatus Used.

was quickly attached to the vacuum apparatus at "A" with high vacuum hose and pumped down to a pressure of 1.2 to 2.0×10^{-4} millimeters of mercury. After approximately 6 hours under this vacuum, during which time adsorbed surface oxygen would be released (3), a compression load was applied at "B" by means of a universal tensile tester of 20,000 pounds capacity. This was done primarily to obtain close contact between the metal surface and the high purity graphite but, as will be pointed out later, the pressure was found to have a pronounced effect on the rate of carburization.

After releasing the load, and with the vacuum system still pumping, the tube was guided into an "atmosphere-controlled" muffle furnace operating at a temperature of 1900 ± 10 °F (1040 °C). In all tests the reaction area "B" was held at temperature for a period of 60 minutes.

The tubular muffle, a 27% chromium-iron alloy, 1 inch ID by

0.065 inch wall was provided with a water-cooled coil at the entrance end in order to obtain the necessary cooling when withdrawing the stainless steel tube from the heating zone at the end of the heating cycle. Several blank runs (without graphite) showed that this arrangement cooled the stainless steels used in this investigation sufficiently rapidly to obtain a structure free from intergranular carbide precipitation as determined by metallographic examination at a magnification of 1000 diameters.

The "atmosphere", either dissociated ammonia or argon, introduced at the back end of the muffle, provided an adequate blanket of gas over the tube during the carburizing cycle.

At the end of each test the tube was sectioned at "B" and examined for degree of carburization. One of the flat surfaces was used for metallographic studies and boiling nitric acid tests, the other for quantitative carbon determinations.

MATERIALS

The composition of the stainless steel tubing used in this investigation is shown in Table I.

Table I
Analyses of Steels

AISI Type	C	Cr	Ni	Mn	Si	P	S	Mo	Cb
316	0.04	16.80	13.40	1.90	0.32	0.025	0.012	2.40	0.00
347	0.06	18.33	12.24	1.80	0.44	0.014	0.013	0.17	0.79
304	0.06	18.88	10.42	1.76	0.43	0.027	0.013	0.03	0.00

Each of the tubes was treated in the following manner before testing:

1. Pickle in a solution of 10% by volume nitric acid-7% by volume hydrofluoric acid heated to approximately 150 °F (65 °C).
2. Rinse in running hot water.
3. Pickle in a 1:1 hydrochloric acid solution at the same temperature.
4. Rinse in dilute ammonia water.
5. Rinse in running water and swab with wet cotton.
6. Rinse with CP acetone.
7. Rinse with CP ether.

Following this cleaning cycle one end of each tube was flattened and welded to form a vacuum-tight closure.

High purity graphite was obtained through the courtesy of the National Carbon Company. As will be seen from the following analysis, this material, identified by National Carbon Company as Sample 2301, was selected as being the most desirable because of its low impurity content.

	Per Cent
Calcium	0.04
Silicon	0.02
Iron	0.02
Titanium	0.01
Vanadium	0.005
Aluminum	0.002
Magnesium	0.002
Maximum Ash	0.20

The approximate composition and degree of impurities present in the gases used for muffle atmosphere are shown in Table II.

Table II
Approximate Analyses of Gases

Gas	H ₂	N ₂	CO	CO ₂	CH ₄	O ₂	% Purity
Dissoc. Ammonia	75.0%	25.0%	None	None	None	None
Argon*	20 ppm	0.1%	20 ppm	99.9
Argon†	Nil	Nil	Nil	Nil	Nil	Nil	99.999

*"Commercially pure", analysis furnished by supplier.

†"Highest purity argon obtainable", analysis furnished by supplier.

The dissociated ammonia after passage over activated alumina showed a dew point of -50°F (-45.5°C) or less and was of sufficiently high purity to permit heating the stainless to 1900°F (1040°C) without the slightest trace of discoloration. No purification, of course, was needed for the special high purity argon, but the "commercially pure" argon was passed over oxidized copper to convert hydrocarbons to water and CO_2 , and then over reduced copper to remove oxygen (4).

RESULTS

The experimental data for each series of tests are shown in Table III. It is to be noted that in each test the vacuum always decreased during heating, indicating a release of adsorbed gases, but then quickly dropped back to some low value when argon or air was used in the muffle. With dissociated ammonia in the muffle the pressure remained at some higher level, indicating diffusion of hydrogen through the stainless tube wall.

In Table IV are reported the depth of carburization, depth of grain boundary precipitate, total carbon content and corrosion rates in boiling 65% nitric acid for each test. All metallographic specimens except those of Type 347 stainless were etched with the reagent developed by Kahn et al (5).² The solution was diluted 1:1 with

*Kahn's Reagent—	Ethyl Alcohol	65.0 cc
	Water	16.7 cc
	Nitric Acid	0.7 cc
	Hydrochloric Acid ...	17.5 cc
	Picric Acid	0.8 gm
	Copper Sulphate	6.7 gm

Table III

Test	Description of Tests—60 Minutes at 1900 °F (1040 °C) With H.P.G.*			Vacuum Data (Pressure, mm Hg (Corrected)— Max. Attained)		
	AISI Alloy	Muffle Atmosphere	Compressive Stress, psi	Before Heating × 10 ⁻⁴	During Heating 1900 °F (1040 °C)	End of Heating Cycle
<i>Series 1</i>						
1	304	Dissoc. NH ₃	6900	2.0	0.12	0.12
2	304	Dissoc. NH ₃	6900	3.5	0.12	0.11
3	347	Dissoc. NH ₃	6900	2.0	0.11	0.09
4	316	Dissoc. NH ₃	6900	1.8	0.12	0.12
5	316	Dissoc. NH ₃	6900	1.4	0.11	0.11
6	316	Dissoc. NH ₃	6900	2.0	0.12	0.11
<i>Series 2</i>						
7	316	Argon	6900	1.4	0.11	3.4 × 10 ⁻⁴
8	316	Air	6900	1.4	0.13	1.6 × 10 ⁻⁴
9	316	Air	6900	1.5	0.17	1.6 × 10 ⁻⁴
10†	316	Air	6900	1.6	0.17	3.3 × 10 ⁻⁴
11†	316	Air	6900	2.0	0.20	6.0 × 10 ⁻⁴
12†	316	Air	6900	3.5	0.20	3.8 × 10 ⁻⁴
<i>Series 3 (Oxidized Tubes)</i>						
13	316	Air	6900	1.4	0.22	1.6 × 10 ⁻⁴
14	316	Air	6900	1.4	0.17	3.4 × 10 ⁻⁴
15	316	Argon	6900	1.4	0.18	3.4 × 10 ⁻⁴
<i>Series 4</i>						
16	316	Dissoc. NH ₃	0	1.5	0.12	0.12
17	316	Dissoc. NH ₃	1750	1.5	0.12	0.11
18	316	Dissoc. NH ₃	36000	1.4	0.12	0.11
19	316	Argon	0	1.5	0.19	27.0 × 10 ⁻⁴
20	316	Argon	36000	1.4	0.22	1.8 × 10 ⁻⁴
21	316	Argon	36000	1.4	0.22	1.6 × 10 ⁻⁴

*H.P.G. = High purity graphite, Sample 2301.

†Vacuum system purged with "highest purity argon" obtainable.

ethyl alcohol to retard etching speed. The Type 347 specimens were etched electrolytically in 10% oxalic acid. Transverse sections of all test specimens were taken for metallographic mounts.

In the first series of tests with dissociated ammonia in the muffle and a preload of 20,000 pounds (6900 psi compressive stress) applied at "B", the carbide zone formed in Type 316, Type 347 and Type 304 stainless after 60 minutes contact with high purity graphite at 1900 °F (1040 °C) is shown by the micrographs in Figs. 2 to 7, inclusive. It is evident that Type 316 stainless (Figs. 2 and 3) absorbs the greatest amount of carbon, and Type 347 (Figs. 4 and 5) the least. The average depth of the carbide zone in Type 316 stainless is 0.012 inch, whereas there appears to be no gross carburization of Type 347 stainless. Instead a slow etching zone extending to a depth of approximately 0.010 inch is observed. Type 304 (Figs. 6 and 7) is intermediate with carburization to a depth of 0.004 inch. Total carbon content and corrosion rates show the same relationship for the three stainless steel grades, Table IV. Because in this series of tests there was considerable diffusion of hydrogen through the stainless tube during the carburizing cycle, it is possible that the reaction

Table IV
Carburizing in High Purity Graphite, 60 Minutes at 1900 °F (1040 °C)

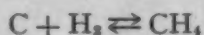
Test	AISI Alloy	Muffle Atmosphere	Compressive Stress at "B" psi	Depth of Carburization Inches Max.	Depth G.B.* Inches	Total Carbon %	Av. Corrosion Rate Boiling 65% HNO ₃ , ipm
<i>Series 1</i>							
1	304	Dissoc. NH ₃	6900	0.004	0.016	0.34	0.019†
2	304	Dissoc. NH ₃	6900	0.004	0.016	0.32	0.017
3	347	Dissoc. NH ₃	6900	?	None	0.09	0.003†
4	316	Dissoc. NH ₃	6900	0.013	0.022	0.43	0.029†
5	316	Dissoc. NH ₃	6900	0.014	0.022	0.45
6	316	Dissoc. NH ₃	6900	0.010	0.020	0.41
<i>Series 2</i>							
7	316	Argon	6900	0.005	0.017	0.45	0.019
8	316	Air	6900	0.006	0.017	0.30	0.020
9	316	Air	6900	0.009	0.020	0.38	0.020
10‡	316	Air	6900	0.008	0.018	0.53	0.032
11‡	316	Air	6900	0.010	0.026	0.55	0.022
12‡	316	Air	6900	0.011	0.023
<i>Series 3 (Oxidized Tubes)</i>							
13	316	Air	6900	0.001	0.011
14	316	Air	6900	0.003	0.010
15	316	Argon	6900	0.004	0.012
<i>Series 4</i>							
16	316	Dissoc. NH ₃	0	0.00	0.008	0.08	0.002
17	316	Dissoc. NH ₃	1750	0.04	0.005
18	316	Dissoc. NH ₃	36000	0.014	0.022	0.65	0.034
19	316	Argon	0	0.00	0.006	0.06	0.001
20	316	Argon	36000	0.014	0.022	0.62
21	316	Argon	36000	0.014	0.022	0.62

*G.B.—Grain boundary.

†Base corrosion rate obtained on blank runs approximately 0.001 ipm.

‡Vacuum system purged with "highest purity argon".

was influenced by the formation of methane in accordance with the following reaction:



To obviate this difficulty the second series of tests was made with Type 316 stainless under the same conditions with respect to time, temperature, preload and carburizing agent, but argon and air instead of dissociated ammonia were used as muffle atmosphere. The micrograph in Fig. 8 shows that considerable carbon is still absorbed with air as a muffle atmosphere, even though the "gas" pressure, except for momentary rise to 0.11 millimeters of mercury, remained low throughout the carburizing cycle. An average depth of carburization of 0.007 inch was recorded under these conditions. With an argon atmosphere in the muffle, the depth of carburization was 0.005 inch. Actually the increase in total carbon content was somewhat greater in the argon test, 0.45% carbon as compared to an average of 0.34% carbon for the run with air in the muffle.

The possibility was also considered that residual oxygen in the stainless tube at the low pressure of 2×10^{-4} millimeters of mercury might react with the graphite to form CO, and create an "oxidizing

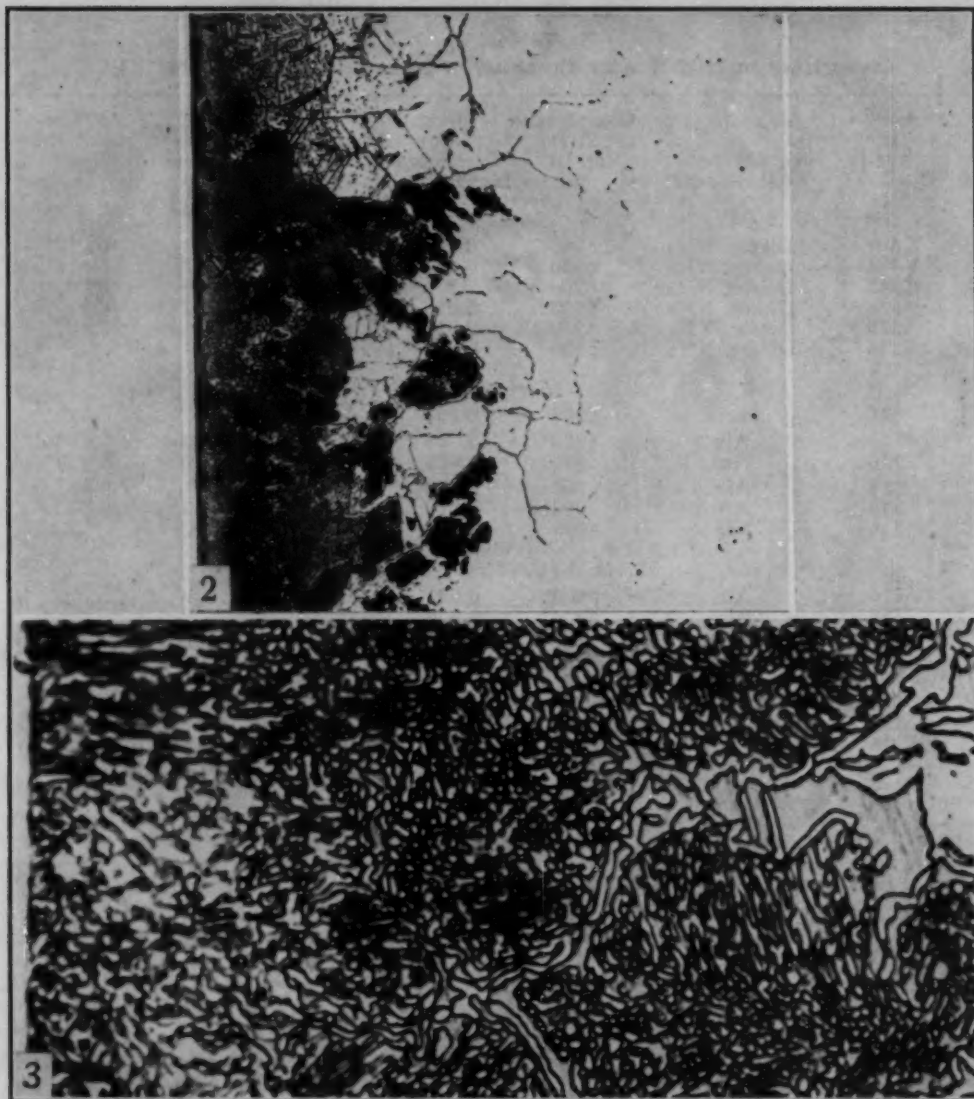


Fig. 2—Type 316, 60 Minutes at 1900 °F (1040 °C) With High Purity Graphite. Dissociated ammonia in muffle. $\times 100$.

Fig. 3—Type 316, Same as Fig. 2. $\times 1000$.

potential" which would influence the course of the carburizing reaction. Therefore, to reduce the oxygen partial pressure to as low a value as possible, several tests were made in which the stainless tube and vacuum system, after assembly, were repeatedly purged after each pump-down with "the highest purity argon obtainable". In all other respects the test conditions were identical to those described for Tests 8 and 9 in Series 2, i.e., 20,000 pounds (6900 psi) preload, air in muffle and 60 minutes at temperature. The carbide zone thus formed is shown by the micrograph in Fig. 9. There appears to be a slight increase in the depth of carburization, when compared with the results of Tests 8 and 9 (Fig. 8), from an average of 0.0075 inch to an average of approximately 0.010 inch. An in-

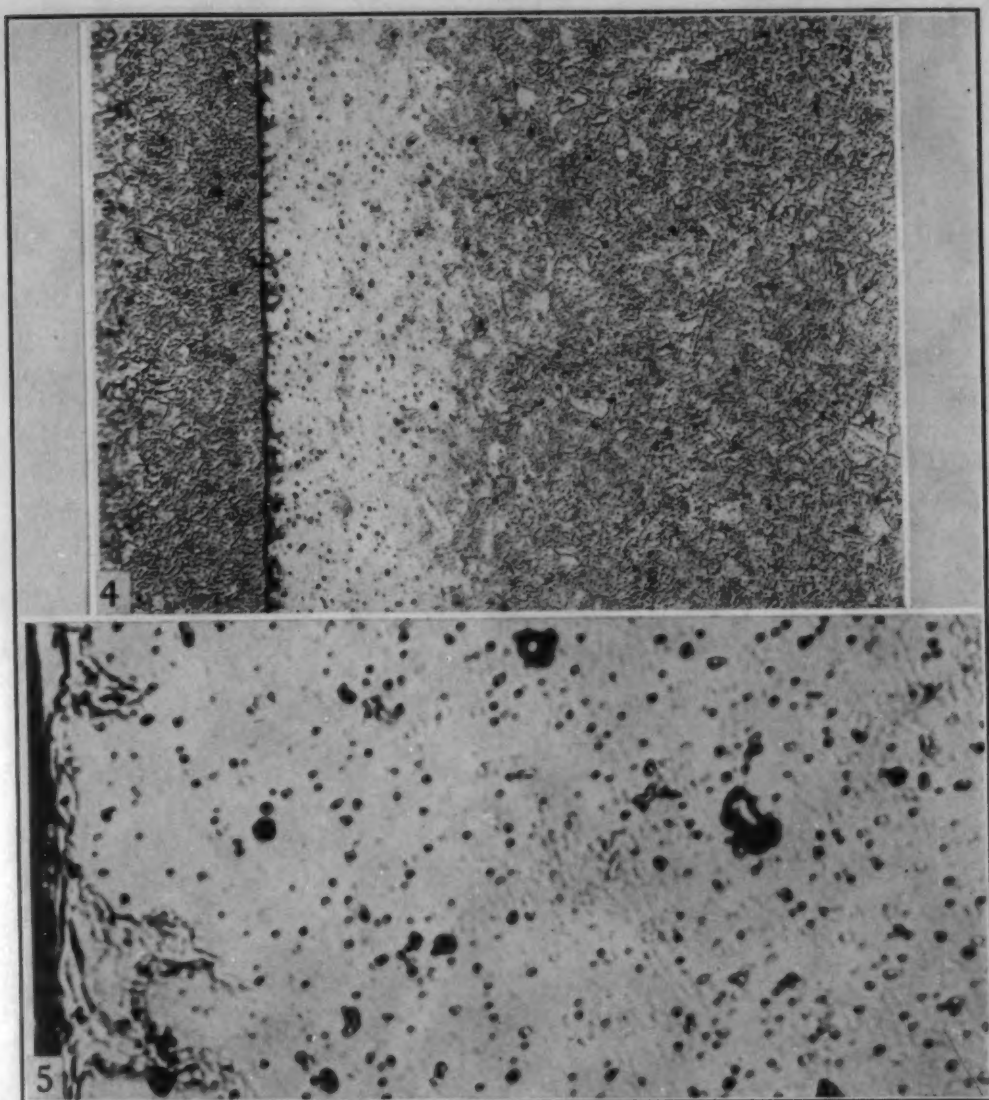


Fig. 4—Type 347, 60 Minutes at 1900 °F (1040 °C) With High Purity Graphite. Dissociated ammonia in muffle. $\times 100$.

Fig. 5—Type 347, Same as Fig. 4. $\times 1000$.

crease in the average total carbon content from 0.34% to 0.54% corroborates this observation. Thus, it is evident that the formation of a carbide zone in Type 316 stainless steel can occur without the benefit of an "oxidizing potential".

A third series of tests was performed under the usual conditions of time, temperature, preload and vacuum, except that the stainless surface was preoxidized at 1900 °F (1040 °C) with high purity hydrogen saturated with water vapor at 75 °F (25 °C). These tests were made primarily to determine whether an oxide film hinders or accelerates the rate of carbon absorption, particularly from the standpoint of the "oxidizing potential" theory, since, obviously, oxygen is available under these conditions. As shown by the photograph in

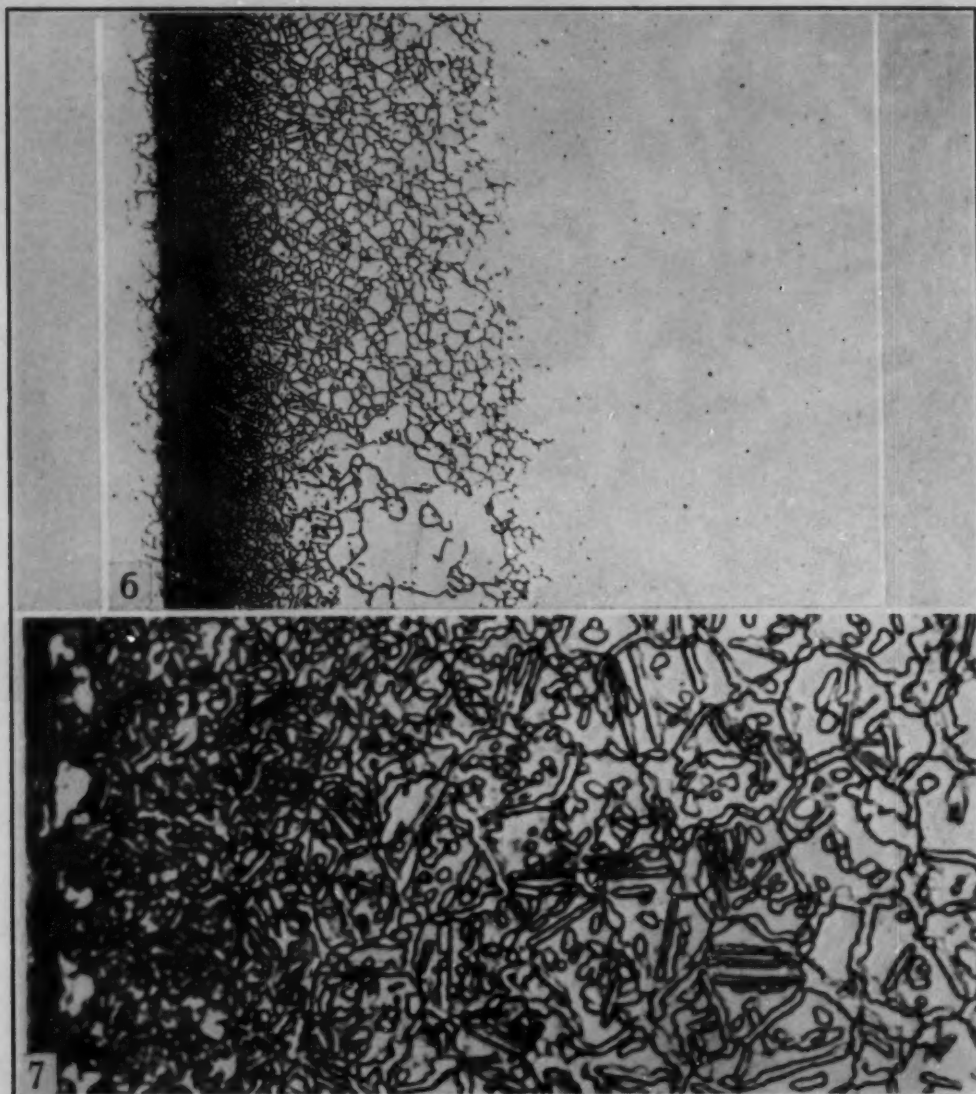


Fig. 6—Type 304, 60 Minutes at 1900 °F (1040 °C) With High Purity Graphite. Dissociated ammonia in muffle. $\times 100$.

Fig. 7—Type 304, Same as Fig. 6. $\times 1000$.

Fig. 10 and the data in Table IV, carbon absorption was erratic if not negligible. Where the oxide was reduced, penetration to a maximum depth of approximately 0.004 inch was observed.

On the assumption that this erratic behavior was due to the nonuniform "packing" of the graphite between the flattened metal surfaces, a fourth and final series of tests was made varying only the preload in area "B" from 0 to 36,000 psi. Using "oxide-free" Type 316 tubes, the results obtained are shown by the micrographs in Figs. 11 and 12. With an initial compressive stress of zero, there is very little carbon penetration, only enough in fact to produce a shallow intergranular carbide network to a depth of 0.008 inch. The total carbon content was only 0.08% as compared to 0.04% of the

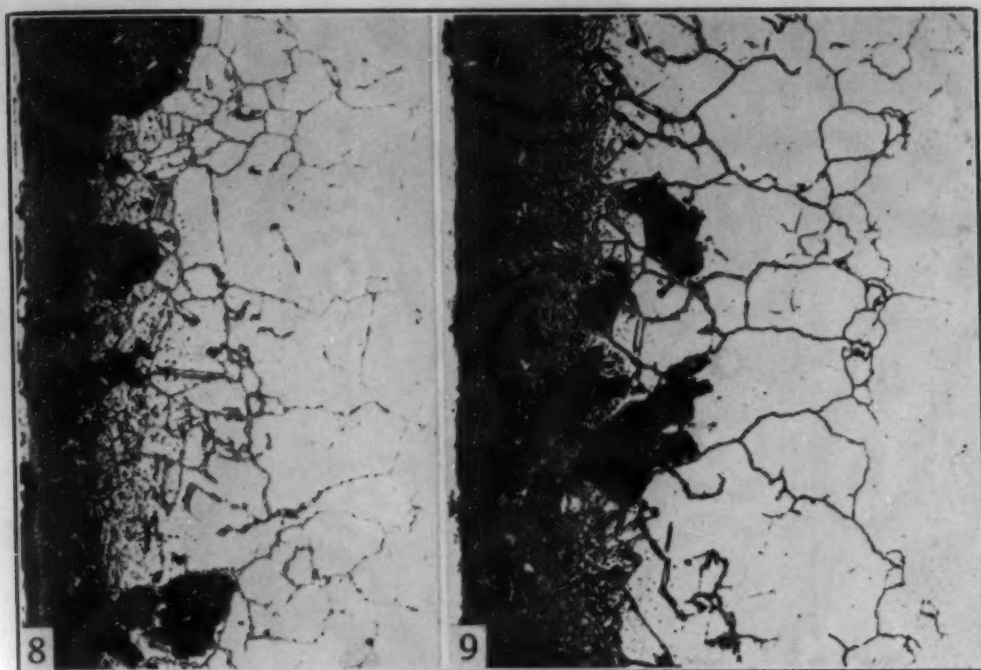


Fig. 8—Type 316, 60 Minutes at 1900 °F (1040 °C) With High Purity Graphite. Air in muffle. $\times 100$.

Fig. 9—Type 316, 60 Minutes at 1900 °F (1040 °C) With High Purity Graphite. Vacuum system purged with highest purity argon. $\times 100$.

original tube. On the other hand, with an initial unit stress of 36,000 psi, a large increase in total carbon content to approximately 0.63% was found and a dense, carbide zone extending to a depth of 0.014 inch was formed as shown in Fig. 12. The highest corrosion rate, 0.034 ipm, was recorded for this test. Since substantially the same results were obtained with either dissociated ammonia or argon in the muffle during the carburizing cycle, it is apparent that hydrogen influences only slightly the course of the reaction, while pressure, i.e., contact pressure between the graphite and the metal surface, exerts a pronounced effect on the carburizing reaction.

The results of several of the more significant tests are summarized by the chart in Fig. 13. The close correlation between depth of carburization and corrosion rates is evident.

DISCUSSION

During the carburizing reaction, using *solid* carburizers, a carbon transfer agent is assumed which delivers atomic or nascent carbon to the surface of the metal. For example, in commercial carburizing compounds, it has been postulated that carbon dioxide released from a metallic carbonate is the agent responsible for the formation of nascent carbon in accordance with the reactions:

1. $\text{CO}_2 + \text{C (Solid)} \rightleftharpoons 2\text{CO}$
2. $2\text{CO} \rightleftharpoons \text{CO}_2 + \text{C (Nascent on the steel surface)}$

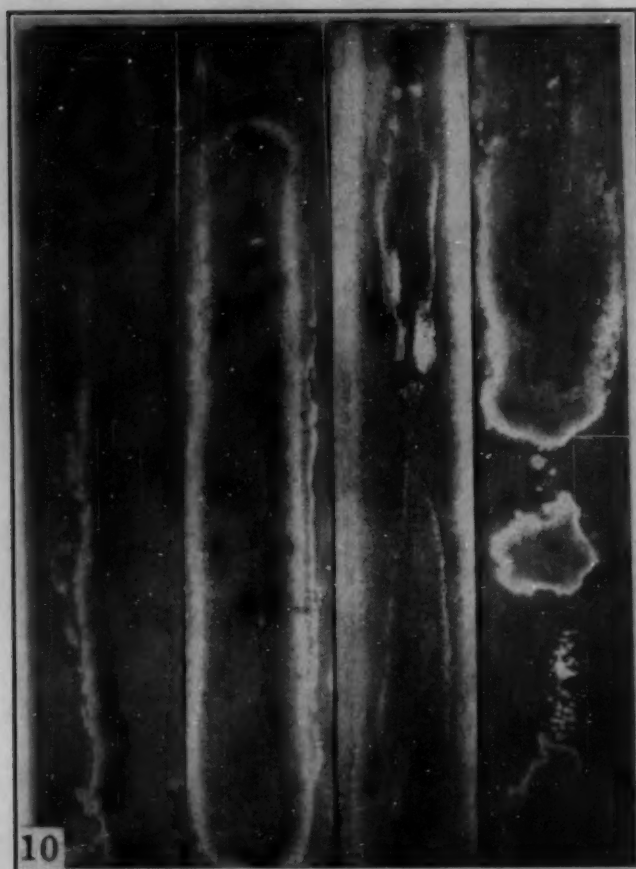


Fig. 10—Type 316, Series 3, 60 Minutes at 1900 °F (1040 °C) With High Purity Graphite. Surface oxidized prior to carburizing. Approximate actual size.

Thus, if the concentration of carbon dioxide and in turn carbon monoxide were held to a very low value, the rate of carburization should also be low. This, in fact, was found to be true in the fourth series of tests where very little carbon was absorbed by Type 316 stainless in contact with high purity graphite under high vacuum at a temperature of 1900 °F (1040 °C). However, the degree of carburization was greatly affected by the pressure placed on the graphite and the metal surface prior to heating. With zero pressure, only a shallow carbide network was formed to a depth of approximately 0.007 inch (Fig. 11). This grain boundary network was fairly continuous and was evidently precipitated during the cooling cycle. Although detrimental to corrosion resistance, this represents only a mild form of carburization.

On the other hand, with a high unit pressure of 36,000 psi applied to the carbon and metal surface *prior* to heating, a dense carbide zone extending to a depth of 0.014 inch resulted (Fig. 12). Under high magnification this zone has the appearance of "nodular pearlite" surrounded by massive carbides in the grain boundaries,

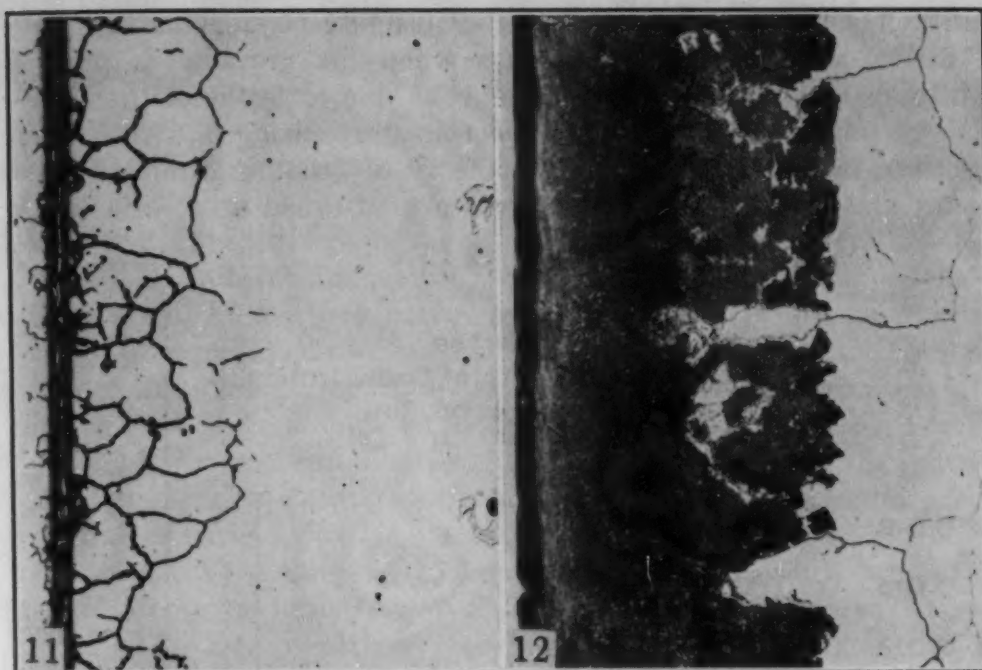


Fig. 11—Type 316, 60 Minutes at 1900 °F (1040 °C) With High Purity Graphite. Zero compressive stress. Dissociated ammonia in muffle. $\times 100$.

Fig. 12—Type 316, 60 Minutes at 1900 °F (1040 °C) With High Purity Graphite. 36,000 psi compressive stress. Dissociated ammonia in muffle. $\times 100$.

which may be explained as follows: Because of the high alloy content of 18-8 stainless steel, the limit of solid solubility of carbon in the austenite at 1900 °F (1040 °C) is quite low (approximately 0.20% as compared to approximately 1.4% for iron-carbon alloys). On account of the high affinity of chromium and molybdenum for carbon, this saturation value is quickly reached and precipitation of complex carbides begins at the surface. Since the carbides are more highly alloyed than the austenite with which they are in equilibrium, the austenite now has greater capacity for carbon and will continue to take up increasing amounts at the surface. Diffusion will occur from this high carbon level to successfully lower layers where the same cycle of carbide precipitation will occur as soon as a particular layer has been supersaturated with respect to carbon. As a result of this continued precipitation of carbides, a two-phase structure is formed at 1900 °F (1040 °C) consisting of complex carbides and saturated austenite low in chromium and molybdenum, but high in nickel and carbon. On cooling to room temperature the saturated austenite transforms to the observed structure resembling "nodular pearlite".

The initial, high contact pressure of 36,000 psi between the graphite and the metal evidently promotes a high rate of carbon absorption at the surface which, in turn, brings about a high rate of diffusion inward, inasmuch as the diffusion coefficient increases

with increasing carbon content in the austenite (6). This high rate of carbon absorption which occurs when the graphite is pressed tightly against the metal surface may be due to "contact catalysis". This possibility of a catalytic effect in carburizing has also been described by Schlumpf (2). The theory of "contact catalysis" postulates that when molecules or atoms are adsorbed at a surface, the

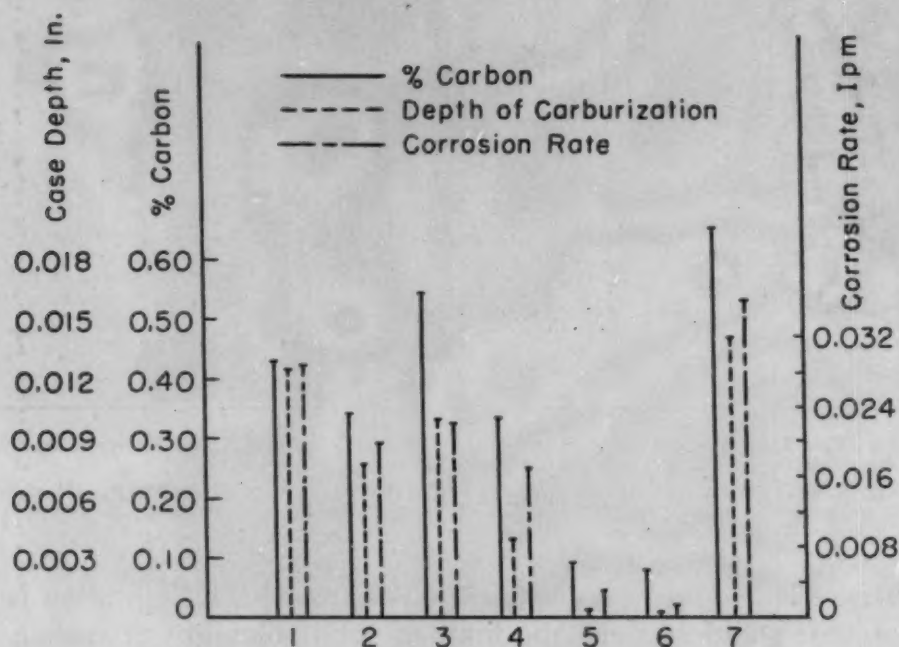


Fig. 13—Results Obtained on Oxide-Free Tubes Carburized in High Purity Graphite, 60 Minutes at 1900 °F (1040 °C).

1. Type 316, XNH₃* in muffle, 6900 psi.
2. Type 316, air in muffle, 6900 psi.
3. Type 316, air in muffle, 6900 psi, system purged with highest purity argon before carburizing.
4. Type 304, air in muffle, 6900 psi.
5. Type 347, XNH₃ in muffle, 6900 psi.
6. Type 316, XNH₃ in muffle, 0 psi.
7. Type 316, XNH₃ in muffle, 36,000 psi.

*Dissociated ammonia.

energy of activation is lowered for the formation of new compounds (7), e.g., alloy carbides. Thus, with increasing contact pressure, a greater number of carbon atoms from the graphite may be adsorbed at the metal surface which can react directly with the chromium and molybdenum in the steel to form carbides. In this manner the entry of carbon into austenite would not have to follow the sequence C (solid) → CO → C (nascent) as required by the "oxidizing potential" theory, but would be brought about simply by the reaction $C(\text{solid}) + xM \rightleftharpoons M_xC$ as a result of contact catalysis. Under equilibrium conditions the formation and decomposition of alloy carbides at the surface would produce the necessary carbon for solution in the austenite.

SUMMARY AND CONCLUSIONS

This investigation was undertaken to study the factors affecting carbon absorption by austenitic chromium-nickel steels of the 18-8 variety and to investigate the validity of the "oxidizing potential" theory as applied to pack or solid carburizing. Using high purity graphite as the carburizing agent, tests were conducted at 1900 °F (1040 °C) in a vacuum of the order of 10^{-4} to 10^{-3} millimeters of mercury and in the presence of hydrogen at a pressure of approximately 0.12 millimeter of mercury. The effect of contact pressure between the carburizing compound and the metal surface was also investigated. The results led to the following conclusions:

1. Austenitic, chromium-nickel stainless steels of the 18-8 variety can absorb carbon from "solid" carburizers, even though the partial pressure of carbon dioxide and water vapor is held to an extremely low value. The observed carbon absorption apparently cannot be explained on the basis of the "oxidizing potential" theory.

2. The rate of carbon absorption of this class of steels under a high vacuum is drastically reduced by the presence of an oxide film on the metal surface.

3. Provided the surface oxide film of the stainless steel is decomposed or broken down under vacuum, carbon absorption, in the reduced gas phase, increases with an increase in contact pressure between the solid carburizer and the metal surface. As a result of this pressure, adsorbed carbon at the surface may react directly with chromium and molybdenum to form carbides which, under equilibrium conditions, provide the necessary carbon for entry into the austenite. The direct formation of carbides is attributed to the lowered energy of activation (as a result of surface or contact catalysis) for the formation of new compounds at the surface of the metal.

ACKNOWLEDGMENTS

The author wishes to acknowledge the kind assistance and guidance given to him by Dr. Gilbert E. Doan, Lehigh University, in carrying out this investigation. Thanks are also due to A. M. Bounds of Superior Tube Company for his suggestions and constructive criticism throughout the project.

References

1. C. R. McCloskey and J. H. Loux, "A Theory of the Mechanics of Carburization", *Steel Processing*, January 1946, p. 53-56.
2. R. W. Schlumpf, *METALS HANDBOOK*, American Society for Metals, 1939, p. 1037-1042.
3. M. G. Fontana, "Surface Studies of Metals from the Corrosion Standpoint", *National Association of Corrosion Engineers*, Vol. 3, 1947, p. 567-579.

4. L. S. Darken, "Diffusion of Carbon in Austenite with a Discontinuity in Composition", American Institute of Mining and Metallurgical Engineers, T.P. 2443, September 1948.
5. W. Kahn, H. Oster and R. Wachtell, "Investigation of a Type of Failure of 18-8 Stabilized Stainless Steel", TRANSACTIONS, American Society for Metals, Vol. 37, 1946, p. 567-585.
6. R. F. Mehl, "Preface to Diffusion", American Institute of Mining and Metallurgical Engineers, T.P. 1658, January 1944.
7. S. Glasstone, *Textbook of Physical Chemistry*, D. Van Nostrand Co., Inc., Second Edition, 1946, p. 1126-1154.

DISCUSSION

Written Discussion: By John J. B. Rutherford, Tubular Products Division, The Babcock & Wilcox Co., Beaver Falls, Pa.

Mr. Giacobbe has presented a thought-provoking paper on a subject of vital interest to all who process stainless steels. As is so often the case, it stirs up many new ideas, possibly more than it establishes.

The interpretation of the effect of pressure on carburization is interesting but not entirely complete. It should be noted that the pressure was applied prior to heating. From the knowledge of creep and relaxation effects at elevated temperatures, it is well established that the pressure during the carburizing cycle would be considerably less than originally applied. There is the possibility that high pressure at ambient temperatures somehow broke down the adsorbed oxygen layer on the metal surface, to render it more susceptible to carburization on subsequent heating. We would like to know if the carburized case was uniform around the inner periphery of the tube where pressure was applied.

Carburization has been observed in stainless steels at cracks and abutting surfaces, after service in heating petrochemicals. These cracks were assumed to catalyze a reaction which did not occur at the open surface. Mr. Giacobbe has come closer to an explanation of this phenomenon.

Written Discussion: By Elmer Gammeter, director of laboratories, Globe Steel Tubes Co., Milwaukee, Wis.

The author's interesting study of the mechanism of carburization will be of value to those concerned with the process of carburization as well as those who are trying to avoid it in processing austenitic stainless steels. It is on this latter phase that I would like to comment, as this is of much interest in the austenitic stainless fields, since heretofore little systematic study has been made. Producers of stainless steel products in these grades have always been concerned with the avoidance of carburization which, of course, impairs corrosion resistance.

In processing austenitic stainless steel tubes considerable care is used to avoid contamination by drawing compounds, cleaners, lubricants, etc., which usually contain carbon and, if present during annealing, will cause "carbon pick-up" or carburization. Many efforts to study this phenomenon have resulted in somewhat erratic results. Using the actual lubricants directly in contact with test surfaces does not necessarily follow the pattern of contaminated surfaces existing after drawing with lubricants still embedded or drawn into the surface areas.

Mr. Giacobbe's results are of much interest in covering the effect of direct solid carburization with and without pressure. In his data we noted

that the Type 347 absorbed the least amount and that the corrosion rate in nitric acid was only slightly impaired. Since, on some occasions in tube production, Type 347 shows a greater tendency to "carbon pick-up" than other grades, we were somewhat surprised at this result.

Without endeavoring to cover extensive details, we made a series of tests on 304, 316, 347 and 321, using relatively pure graphite within a closed but not sealed steel container. After 60 minutes at 1950 °F (1065 °C) the samples were quenched and the maximum depths of grain boundary precipitation were 0.004, 0.010, 0.001 and 0.001 respectively, which rather parallels the author's findings.

In regard to the etching technique, we would like to ask the author if he found any specific advantage to the Kahn reagent. Our brief study indicated no tangible difference between this and the normal electrolytic 10% sodium cyanide etch that we use.

In our opinion the paper offers a good nucleus for further study to establish more information on the "carbon pick-up" problem involved in production processing of austenitic stainless steels.

Mr. Giacobbe is to be congratulated on this interesting and informative paper on an important subject.

Written Discussion: By M. E. Carruthers, supervising metallurgist, Research Laboratories, Armco Steel Corp., Middletown, Ohio.

Mr. Giacobbe's paper is of interest to those of us concerned with the stainless steels because carbon plays such an important role in the corrosion resistance of these steels. There are, no doubt, many present who are familiar with the deterioration of stainless surfaces that have not been adequately cleaned of drawing compounds and other contaminants before annealing and pickling.

While our experiences with the carburization of stainless steels have not been surrounded with exactly the same conditions as described by the author, the results of some of our own experiments may be of interest.

In one experiment, cold-rolled Type 304 strip of composition 0.056% carbon, 18.31% chromium and 9.05% nickel was chemically cleaned and exposed to the flow of a mixture of carefully scrubbed and purified hydrogen carrying 0.044% methane. After 23 hours exposure at 2050 °F, the surfaces remained untarnished, yet carbon content had increased from 0.056 to 0.16%. This experience would seem to substantiate the author's postulation that methane can carburize stainless steel under conditions wherein water vapor and other oxygen-containing gases are reduced to very low concentrations.

The author found that oxide films tended to hinder the rate of carbon absorption during short exposure to conditions that were carburizing to clean surfaces. We have noted this effect during experimental carburization of Type 410 stainless steel by the pack method. Shallow and non-uniform case depth resulted except when oxide films were minimized by using moisture-free compounds and by pre-flushing air from the system.

In another case, we observed that Type 316 stainless steel heated for 3 hours at 1950 °F was not appreciably surface-carburized in an atmosphere of partially burned natural gas of composition 5.4% CO₂, 0.2% O₂, 12.1% CO, 17.4% H₂, 0.4% CH₄ with dew point 128 °F. It is highly probable here, too, that the oxide film interfered with carburization.

In closing, we wish to commend Mr. Giacobbe on the content of this paper. His conclusion regarding the mechanics of carburization under the special conditions described is a valuable contribution to our knowledge of the behavior of stainless steels.

Author's Reply

The author wishes to extend his sincere thanks to Messrs. Rutherford, Gammeter and Carruthers for their written discussions of this paper.

Replying to Mr. Rutherford, the pronounced effect of pressure on the rate of carburization, even though the pressure is applied *prior* to heating, is attributed largely to the intimate contact developed between the carburizing compound and the metal surface. As Mr. Rutherford points out, the actual pressure existing during the carburizing cycle at elevated temperatures is small as, in fact, it is when the load is released *prior* to heating. However, because the carbon is thoroughly embedded in the microscopic fissures and pores of the metal surface, which in this instance was a pickled surface, it is felt that "contact catalysis" increases the rate of reaction between the carbide-forming elements and the carbon itself. As a corollary to this it might be interesting to study the rate of carburization of a highly polished surface under otherwise similar conditions.

In answer to Mr. Rutherford's specific question, the carburized case was quite uniform around the inner periphery of the tube where pressure was applied.

Mr. Gammeter's observation is indeed interesting to those of us who have attempted to carburize stainless steel by simply coating the surface with drawing compound and annealing in the conventional manner. Usually little or no "carbon pickup" occurs; however, if a cold drawn tube is annealed without thoroughly removing the drawing compound severe carburization may result.

Although Mr. Gammeter is somewhat surprised at the low rate of carbon absorption of Type 347 stainless steel, it is noted that his data corroborates the author's findings that Type 347 absorbs the least amount of carbon, Type 316 the greatest amount, and Type 304 an intermediate amount under a given set of conditions.

No effort was made to critically compare Kahn's reagent with the standard electrolytic 10% sodium cyanide etch. Both developed the same microstructure although it was felt that better delineation was obtained with the Kahn reagent.

Mr. Carruthers' data provide further evidence that the "oxidizing potential" theory does not necessarily apply to the carburization of austenitic stainless steels of the 18-8 variety. All indications are that moisture in the carburizing medium retards the rate of carbon absorption. For the types of stainless steels under consideration, the rate of formation of surface oxide even under mildly oxidizing conditions is very rapid at elevated temperatures. If conditions favor the formation of this oxide film, then there is little likelihood that carburization can occur even though such constituents as carbon monoxide and methane are present in the gaseous phase. It is the writer's experience, however, that under reducing conditions methane and carbon monoxide can completely destroy the corrosion resistance of Type 304 and Type 316 stainless steels.

CREEP-RUPTURE AND RECRYSTALLIZATION OF MONEL FROM 700 TO 1700 °F

BY NICHOLAS J. GRANT AND ALBERT G. BUCKLIN

Abstract

Extensive creep-rupture tests were made on wrought Monel at temperatures from 700 to 1700 °F and for rupture times from about 0.001 to 2700 hours. Tests were made on the annealed, 30% cold-worked and 75% cold-worked structures. Recrystallization data were obtained for Monel cold-worked from 4 to 70% and annealed from 0.5 to 500 hours at temperatures from 800 to 1700 °F (425 to 925 °C). Correlation of recrystallization data from static tests was attempted with hardness changes and equicohesion values from stress-rupture tests. Recrystallization is evident at much lower temperatures and shorter times in creep-rupture bars than is predicted from static tests. It is shown that the Grant and Bucklin method of graphically extrapolating and interpolating short-time stress-rupture data holds for Monel. Experimentally determined values of equicohesion are given for 30% cold-worked Monel.

THE research which is discussed in this report is a continuation of studies at the Massachusetts Institute of Technology of the behavior of metals and alloys under conditions of strain at elevated temperatures. Previous publications were concerned with a complex age-hardenable, heat-resistant alloy (1),¹ and with the behavior of aluminum as a function of purity (2, 3). This report deals with the single-phase Monel alloy in the temperature range 700 to 1700 °F (370 to 925 °C).

The specific aims of this research were:

1. To obtain creep-rupture data for one of the Monel alloys.
2. To study the role of cold work on the creep-rupture behavior of Monel.
3. To relate, if possible, the recrystallization data for Monel with the creep-rupture behavior.
4. To confirm or adjust the suggested graphical method of

¹The figures appearing in parentheses pertain to the references appended to this paper.

A paper presented before the Thirty-fourth Annual Convention of the Society, held in Philadelphia, October 18 to 24, 1952. Of the authors, Nicholas J. Grant is associate professor, Department of Metallurgy, and Albert G. Bucklin is staff member, Metallurgy Department, Massachusetts Institute of Technology, Cambridge, Mass. Manuscript received January 9, 1952.

extrapolating short-time creep-rupture data suggested by Grant and Bucklin (1).

Monel of the following composition—67% nickel, 30% copper, 1.5% iron, 1% manganese, and 0.15% carbon—was selected as the test material because it is a single-phase nonage-hardenable alloy in which the known instabilities (under varying conditions of temperature, time and strain) would be: (a) the transition from low-temperature-type behavior to high-temperature-type; (b) recrystallization; (c) oxidation.

Other complicating structural or chemical instabilities would thus be avoided, permitting an easier realization of the aims listed above.

EXPERIMENTAL PROCEDURE

To determine the recrystallization behavior of Monel, cold-worked bar stock was first annealed for 30 minutes at 1500 °F (815 °C), and was then cold-worked from 4 to 75% reduction of area by cold swaging. Time-temperature recrystallization data were then obtained, using hardness, metallography, resistivity, and X-ray measurements. Times up to 500 hours were used to obtain as extensive data as possible.

For the creep-rupture tests annealed Monel and two grades of cold-worked Monel were used; namely, 30 and 75%. The annealed bars were also heat treated for ½ hour at 1500 °F (815 °C) prior to testing. While this did not yield a dead soft condition, it did keep the grain size within desired limits.

Creep-rupture tests were run from about 0.001 to 2700 hours at temperatures from 700 to 1700 °F (370 to 925 °C). The test bars were 0.250 inch in diameter by 1.25 inches gage length. The testing equipment has been described elsewhere (1) and readily meets ASTM requirements for all measurements. For the short-time tests, a hydraulic loading jack was used to permit rapid loading without significant impact on the test bar. In all instances, the specimens were brought up to temperature as rapidly as possible and were held there no more than 10 to 20 minutes prior to loading.

EXPERIMENTAL RESULTS

Fig. 1 shows the microstructures of the starting materials in the annealed, 30 and 75% cold-worked conditions. The annealed and 75% reduced Monel are of the same initial grain size, whereas the 30% reduced Monel is somewhat finer grained, being of a different lot of material, but of the same composition. The annealed grain size is about 0.03 millimeter in diameter.

The data from the stress-rupture tests are listed in Table I. The results of these tests are shown graphically in Figs. 2 to 4 in

Table I
Stress-Rupture Test Results

Load × 1000 psi	Life Hrs.	Creep Rate %/Hr.	Elongation %	Red. in Area %	Hardness* Rockwell "B"
30% Cold-Worked					
700°F					
110	0.025	~240.0	10.8	63.3	103-104
100	6.70	1.90	14.1	43.5	103-103
95	87.9	0.066	15.7	43.4	103-105
90	140.0	0.044	30.4	28.4	102-102
80	472.0	0.0016	†	11.8	104-102
900°F					
90	0.0011	<20,000	21.1	52.8	101-102
85	0.003	<4,500	13.5	54.8	102-101
82	0.046	110.0	12.1	34.4	104-101
80	0.081	36.0	12.2	26.9	102-100
70	0.56	8.4	9.7	19.2	102-100
55	2.45	~0.80	3.2	4.0	103-102
50	4.50	<0.55	2.5	3.5	100- 98
45	23.7	<0.14	3.5	4.8	102- 98
40	93.5	0.029	2.5	3.3	102- 98
35	344.0	0.015	7.7	7.8	102- 93
1000°F					
80	0.0016	<9,300	14.8	41.9	102-102
75	0.008	<1,500	12.4	27.3	101- 99
70	0.036	84.0	20.5	22.2	102- 97
60	0.13	35.0	7.5	10.0	97- 96
60	0.17	40.0	6.6	14.1	101-100
50	0.95	<9.3	8.8	17.2	101- 96
40	2.68	0.96	2.5	6.3	97- 95
40	3.38	~1.30	4.0	6.2	101- 94
30	36.9	0.14	9.8	14.4	101- 94
25	157.0	0.083	15.0	22.6	97- 82
1100°F					
67.5	0.002	<7,000	14.1	30.9	101- 99
65	0.003	<6,000	18.2	31.6	99- 96
60	0.012	<1,700	21.0	40.9	103- 96
55	0.065	~290	23.9	36.0	97- 93
50	0.12	44.0	15.8	19.0	97- 93
50	0.19	62.4	20.3	20.5
45	0.40	<40.0	16.2	20.0	97- 91
40	0.72	<17.5	12.6	26.5	96- 88
35	2.5	<2.70	6.7	11.6	95- 87
30	7.38	<3.40	25.0	43.2	75- 88
					95- 88
25	19.8	<0.86	17.2	20.6	†80-85-77
20	34.8	<0.63	21.9	37.8	73- 78
					85- 81
10	925	0.011	14.6	35.1	68- 64
1200°F					
47.5	0.0017	<10,000	17.5	43.9	99- 94
43.35	0.0056	< 2,700	15.2	43.8	100- 94
35	0.064	130.0	19.5	46.3	97- 92
30	0.217	96.0	52.5	45.3	91- 87
25	0.75	~15.0	38.4	44.2	90- 85
20	3.60	<8.0	30.8	35.0	82- 75
15	19.5	<0.90	17.7	23.0	78- 71
10	57.8	<0.24	13.5	18.4	79- 70
10	64.1	~0.18	16.8	15.1	73- 65
7.5	97.5	~0.07	16.1	14.0	72- 59
7.1	123.0	0.051	9.8	12.4	72- 65
5	564.0	0.014	12.8	10.9	61- 57
2.5	2547.0	0.0045	18.0	9.1	61- 54
1300°F					
35	0.0036	<14,000	52.0	40.0	98- 94
20	0.49	43.0	31.2	41.7	92- 86
10	12.4	<1.30	16.2	16.8	75- 65
5	67.3	0.13	15.3	11.6	75- 65
2.2	459.0	0.017	10.1	9.3	77- 63

*First hardness values are highest readings; second readings in fracture area.

† $\frac{1}{4}$ -inch gage length, broke in fillet.

‡First value is in threaded section.

Table I—(Continued)
Stress-Rupture Test Results

Load × 1000 psi	Life Hrs.	Creep Rate %/Hr.	Elongation %	Red. in Area %	Hardness* Rockwell "B"
30% Cold-Worked					
1500°F					
20	0.0064	<4,000	24.6	36.0	79- 82
15	0.05	290	14.8	28.2	81- 84
10	0.40	28.0	23.4	19.7	80- 66
3.7	7.43	<1.90	14.3	10.5	72- 59
0.5	2750	extremely oxidized		
1700°F					
15	0.003	<13,000	38.6	33.6	80- 67
10	0.027	860	28.8	22.6	74- 72
7	0.10	130	16.9	16.2	72- 69
3	1.45	<7.0	10.6	7.7	64- 59
0.8	81.8	0.088	badly oxidized		61- 52
75% Cold-Worked					
900°F					
85	0.021	~270	13.7	51.5	96- 98
75	2.51	2.0	20.0	57.0	100- 99
74	3.50	~1.6	20.9	73.8	99- 98
70	4.50	0.83	12.6	55.8	100- 98
50	151.3	0.020	5.6	6.9	100- 97
45	424.0	0.007	6.0	5.5	98- 96
1100°F					
65	0.027	~67.0	23.0	72.2	102-101
55	0.22	18.5	8.1	67.4	101- 98
50	0.35	12.0	17.2	68.1	101- 98
40	0.78	~5.0	27.4	68.9	96- 97
30	2.68	~2.1	53.3	74.4	94- 96
15	162.0	0.18	43.5	55.3	81- 79
1300°F					
30	0.018	<1950	35.0	58.0	92- 89
23.6	0.117	336	90.0	75.0	85- 81
20	0.18	160	64.5	65.2	85- 79
12.4	3.7	<7.2	26.9	39.4	75- 67
10	13.5	~1.7	55.7	36.6	62- 57
7	81.7	0.34	18.0	30.3	64- 61
Annealed					
700°F					
75	<0.001	<42,000	41.9	72.5	184-100-101
75	<0.001	<42,000	41.5	73.0	179- 99-100
70	125.8	0.13	43.5	68.3	183- 98-100
900°F					
65	0.0033	<13,000	45.2	71.3	173- 93- 99
60	0.154	130	45.9	62.1	181- 95- 97
57	0.67	<66	44.4	44.6	174- 96- 96
50	14.7	0.88	31.7	36.4	175- 91- 93
45	232.6	0.02	23.9	22.6	175- 88- 92
1100°F					
50	0.0022	<20,000	43.5	64.2	179- 89- 92
45	0.038	< 1,400	54.8	63.3	177- 91- 92
40	0.40	63.0	56.5	58.0	177- 85- 88
35.7	1.11	14.0	44.8	51.2	174- 86- 89
30	7.53	~1.4	35.5	38.0	175- 84- 86
25	98.0	0.21	29.7	28.3	174- 79- 79
20	277.0	0.094	31.7	29.3	175- 77- 78
15	2714.0	0.0075	32.2	33.2	171- 74- 71
1300°F					
30	0.028	860	54.0	47.2	175- 88- 80
25	0.21	130	50.4	41.5	176- 86- 81
20	1.96	16.4	39.3	37.7	175- 79- 78
15	5.58	3.2	27.7	174- 78- 75
10	22.0	0.56	28.1	27.9	168- 68- 64
5	769	0.02	24.6	16.2	160- 59- 50

‡First value is in threaded section.

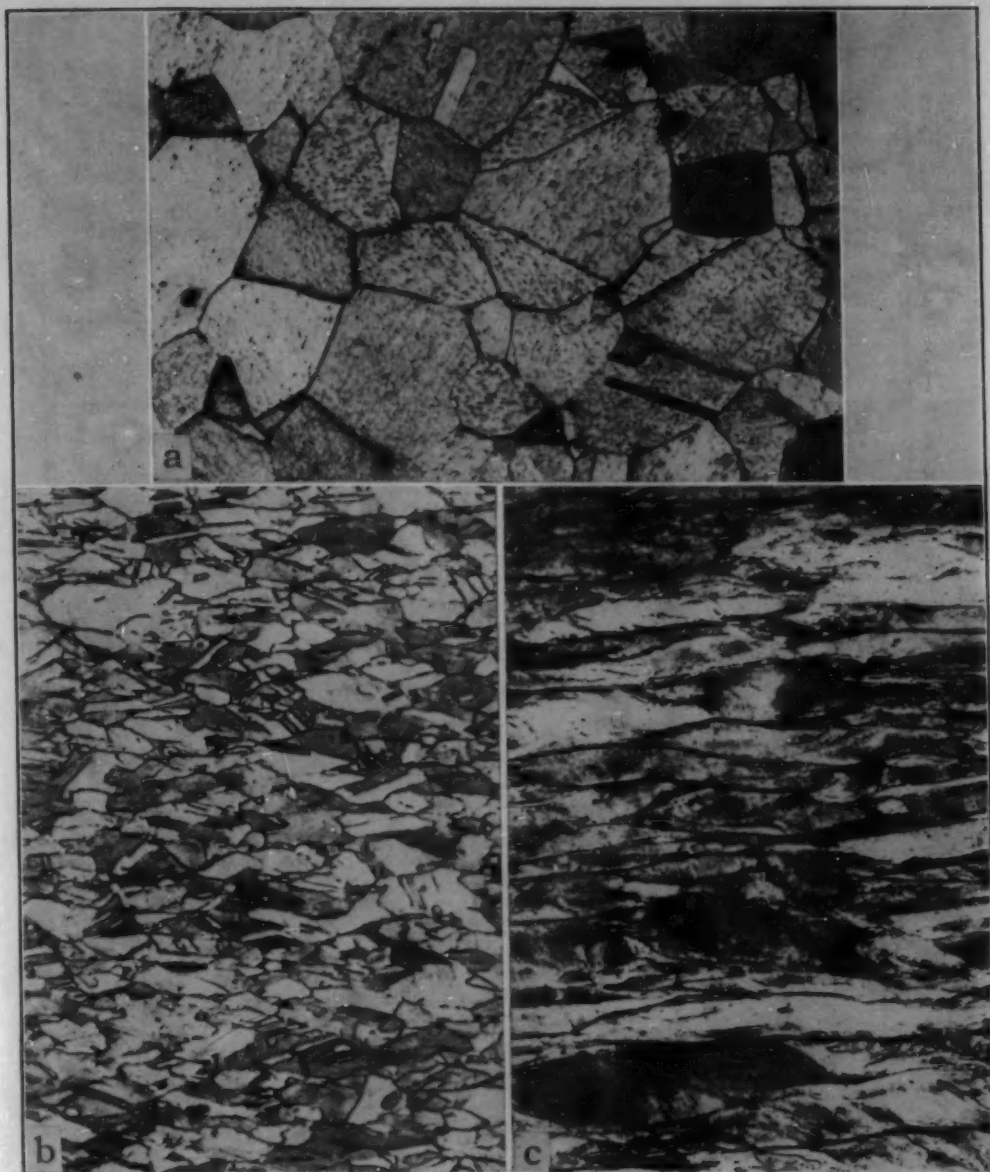


Fig. 1—Original Grain Structures (Longitudinal Sections) Prior to Testing. All at $\times 250$. Carapella's etch. (a) Annealed one-half hour at 1500°F (0.03 mm. diameter grain size). (b) 30% cold work. (c) 75% cold work.

log-log plots of stress versus rupture life. Following the same procedure used in previous work (1), the best straight-line segments were drawn through the points. The breaks in the curves are based not only on the individual points, but also on the nature of the fracture (transcrystalline or intercrystalline), on the mode of deformation, and on observable instabilities such as recrystallization or oxidation.

It will be noted in Figs. 2 to 4 that most of the data were obtained for the 30% cold-worked material. A series of breaks in the straight lines of Figs. 2 to 4 are noted at zones A, B, C, D. It

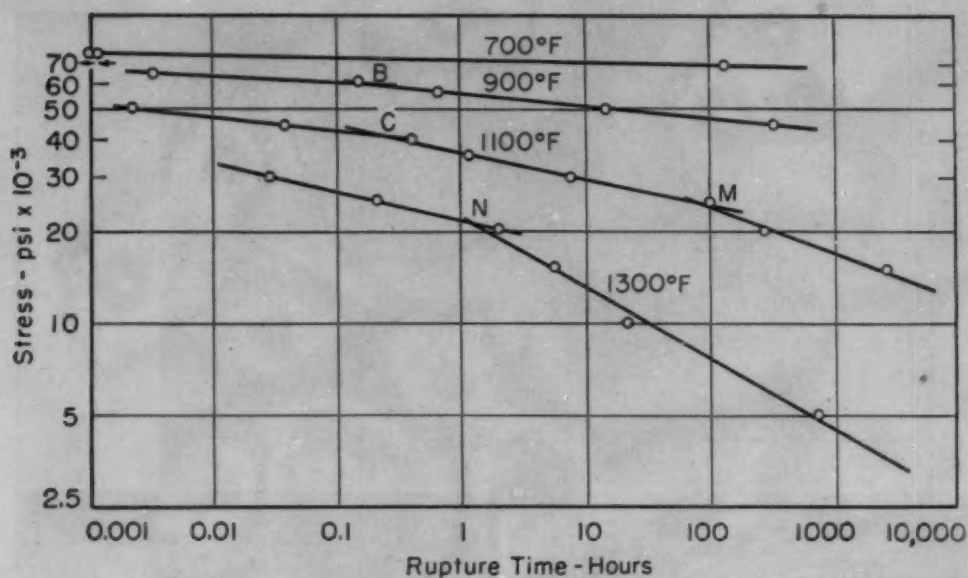


Fig. 2—Log Stress Versus Log Rupture Life Plot for Annealed Monel at 700 to 1300°F.

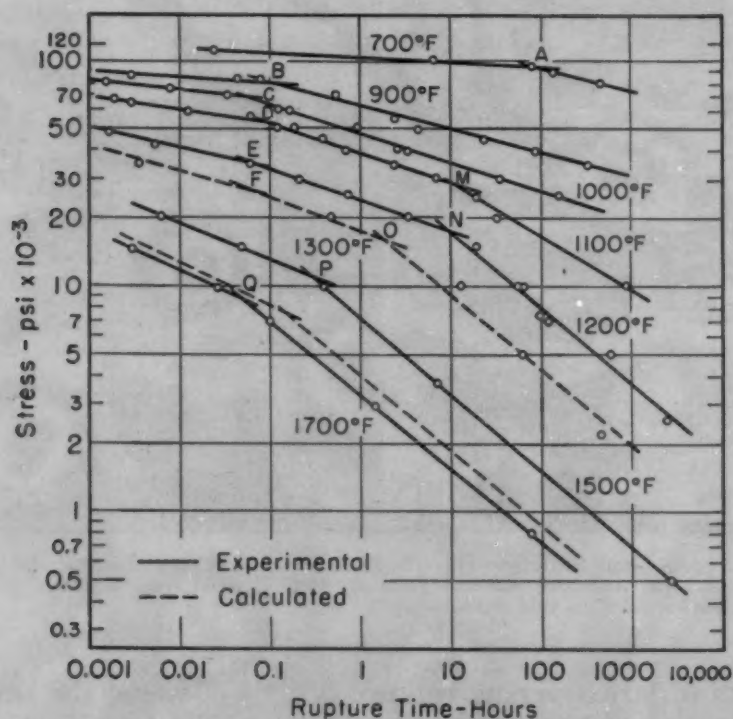


Fig. 3—Log Stress Versus Log Rupture Life Plot for 30% Cold-Worked Monel at 700 to 1700°F.

was determined by these breaks in the curves and checked metallographically that these are zones where Monel is changing from low-temperature (transcrystalline)-type fracture to high-temperature (intercrystalline)-type fracture. As noted previously (1), this is not a sharp break, but this method of plotting permits a rather close demarcation of the time-temperature-stress relationship for the first

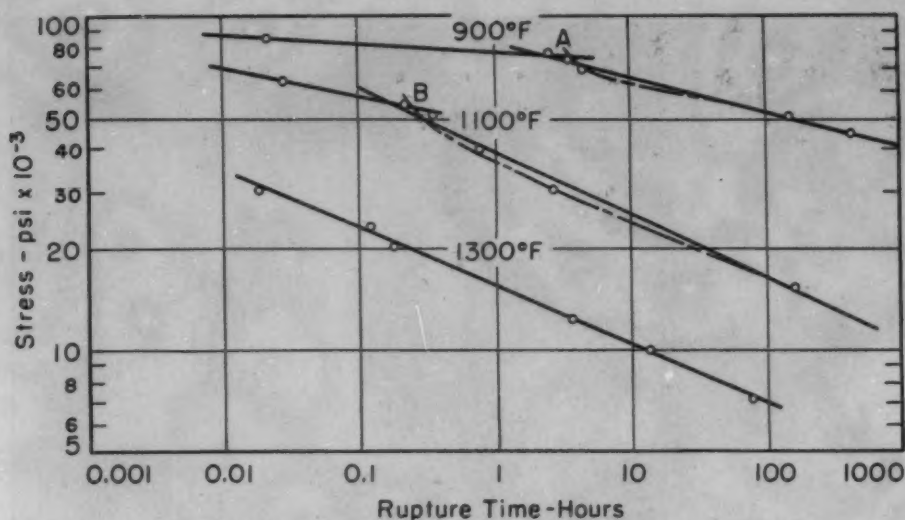


Fig. 4—Log Stress Versus Log Rupture Life Plot for 75% Cold-Worked Monel at 900 to 1300°F. Dashed lines show alternate choice of curves.

evidence of intercrystalline cracking, even though the rest of the fracture may be transcrystalline due to the increased stress (and strain rate) because of diminution of cross sectional area. It must be emphasized that only the curves of Fig. 3 are considered to be quite accurate with respect to the slopes and the breaks in the curves which are shown, whereas the curves of Figs. 2 and 4 are considerably less accurate, due to the smaller number of test points.

A second set of breaks in the curves is shown in these same three figures, generally represented by the letters MNOPQ. It was thought, at first, that the breaks in the log-log curves represented by these letters could be ascribed to oxidation, which progressively and materially decreases the test cross section by intergranular oxidation, resulting in decreased rupture life; however, this was not the case. Table II shows the rupture life values at each temperature for the points MNOP for the annealed and the two cold-worked structures, taken from Figs. 2, 3, and 4.

Since the effect of cold work on the rate of oxidation is probably small, except insofar as it affects grain size and intergranular oxidation, cold work should not affect the incidence of oxidation damage.

Therefore, it follows that in the case of 30% cold-worked material, but especially in the case of the 75% cold-worked Monel, the

Table II
Approximate Rupture Time Values at Slope Changes MNOP in Figs. 2, 3, 4*

	900°F	1100°F	1300°F
Annealed	> 1000 hours	75 hours	1 hour
30% cold-worked	> 1000 hours	10 hours	2 hours
75% cold-worked	> 1000 hours	?	?

*Holding time of 10 to 20 minutes at temperature prior to loading.

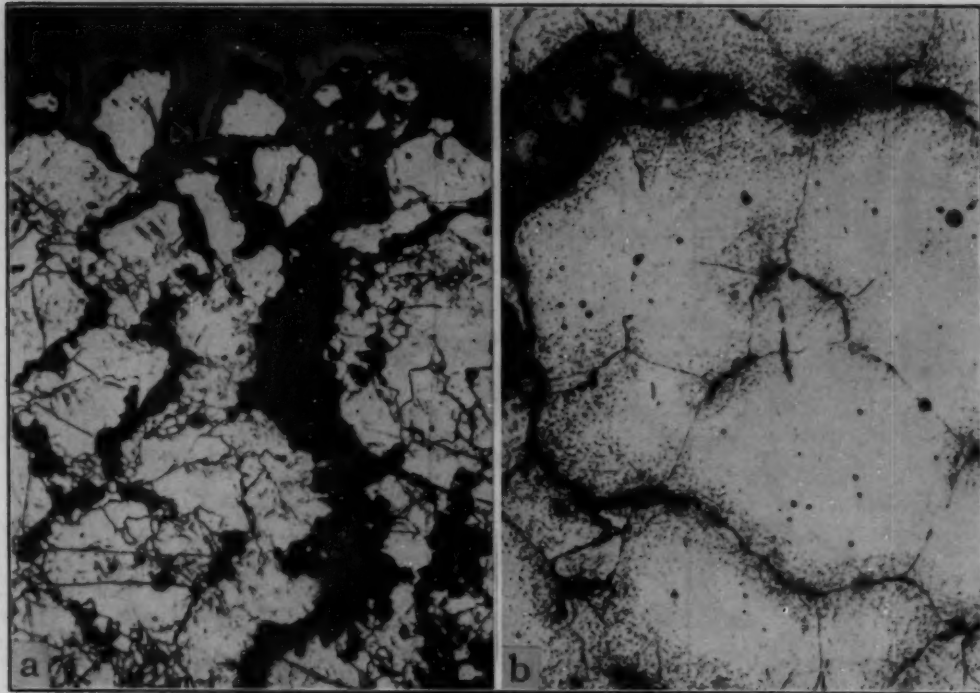


Fig. 5—Oxide Penetration in Monel During Creep-Rupture Testing. (a) Annealed Monel after 2700 hours at 1100°F and 15,000 psi. $\times 150$. Electrolytic H_3PO_4 etch. (b) 30% cold-worked Monel after 82 hours at 1700°F and 800 psi showing internal oxidation and grain boundary penetration. $\times 150$. Electrolytic H_3PO_4 etch.

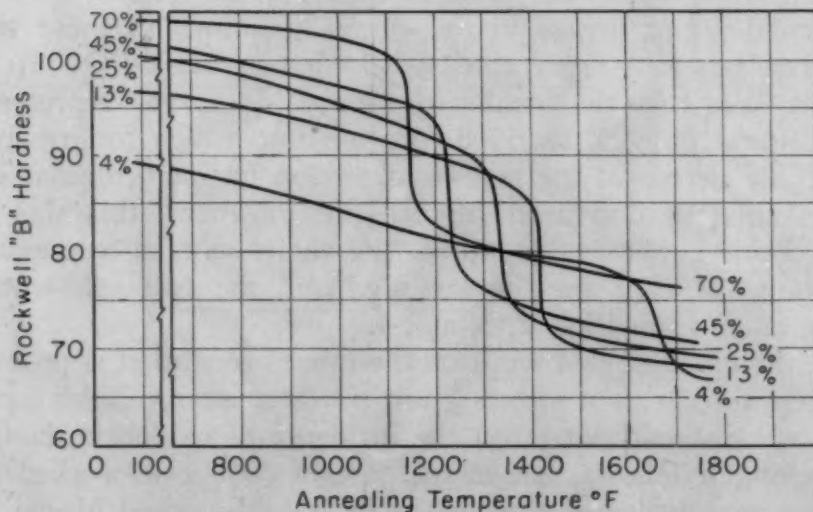


Fig. 6—Recrystallization Curves for Monel (Based on Hardness) After Holding $\frac{1}{2}$ Hour at Temperature. 4 to 75% cold work.

positions MNOP are being affected by a recrystallization phenomenon which first begins to be noted beyond the zones ABCD. Accordingly, the MNOP instability regions of Fig. 3 which may in part be ascribed to an obvious intergranular oxidation effect are simultaneously being affected by a continuing recrystallization process which in part controls the location of these zones and the slopes of the lines.

For the 75% cold-worked material (Fig. 4) where the recrystallization process is more rapid, due to the larger amount of cold work, instability regions associated solely with oxidation cannot be detected, since the oxidation effect is overshadowed by the large effects of recrystallization on the rupture life of the material.

Up to temperatures of about 900 °F (480 °C), Monel has very good long-time oxidation resistance. From 900 to about 1300 °F

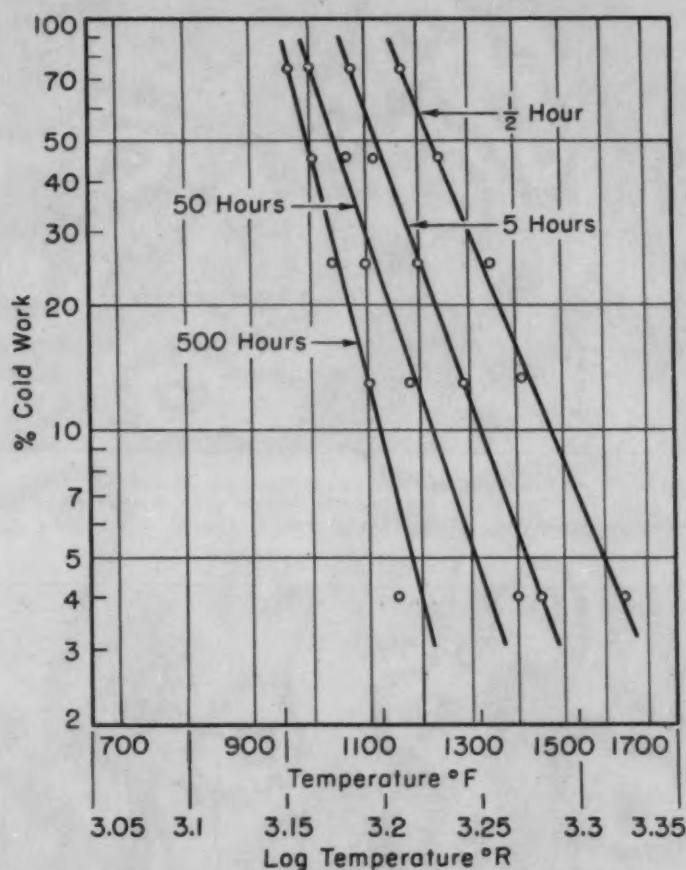


Fig. 7—Plot of Cold Work Versus Temperature for Recrystallization of Monel for Times of 0.5, 5, 50, and 500 Hours.

(480 to 705 °C), the surface scale is still thin and very adherent, but grain boundary penetration of oxide is quite evident and is complexly related to intercrystalline cracking during creep-rupture testing. Above 1500 °F (815 °C), the bulk oxide grows rapidly but still remains adherent and apparently quite dense; however, the oxide is poorly protective.

Fig. 5 shows two photomicrographs of oxide penetration. Fig. 5a shows adherent surface oxide after 2700 hours at 1100 °F (595 °C) as well as intergranular penetration. Fig. 5b shows oxide penetration at 1700 °F (925 °C). Note the large amount of internal oxidation in the grains near the boundary regions.

To obtain more information on the role of the recrystallization

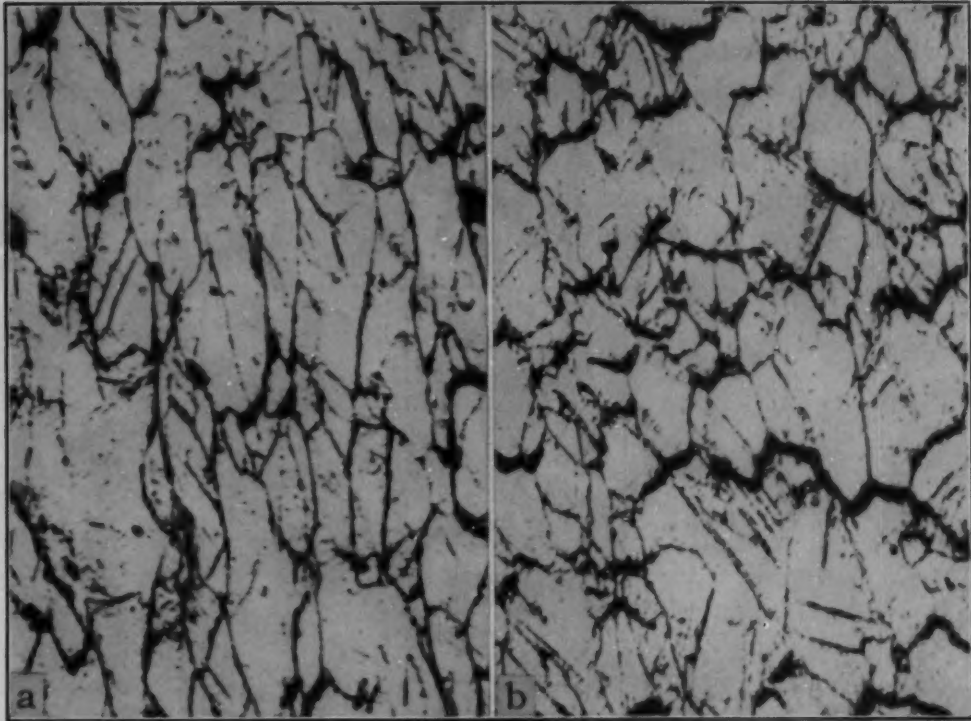


Fig. 8—Intercrystalline Cracking of 30% Cold-Worked Monel at 700°F. $\times 750$. Electrolytic H_3PO_4 etch. (a) 140 hours rupture life, 90,000 psi. Reduction of area, 28%. (b) 472 hours rupture life, 80,000 psi. Reduction of area, 11.8%.

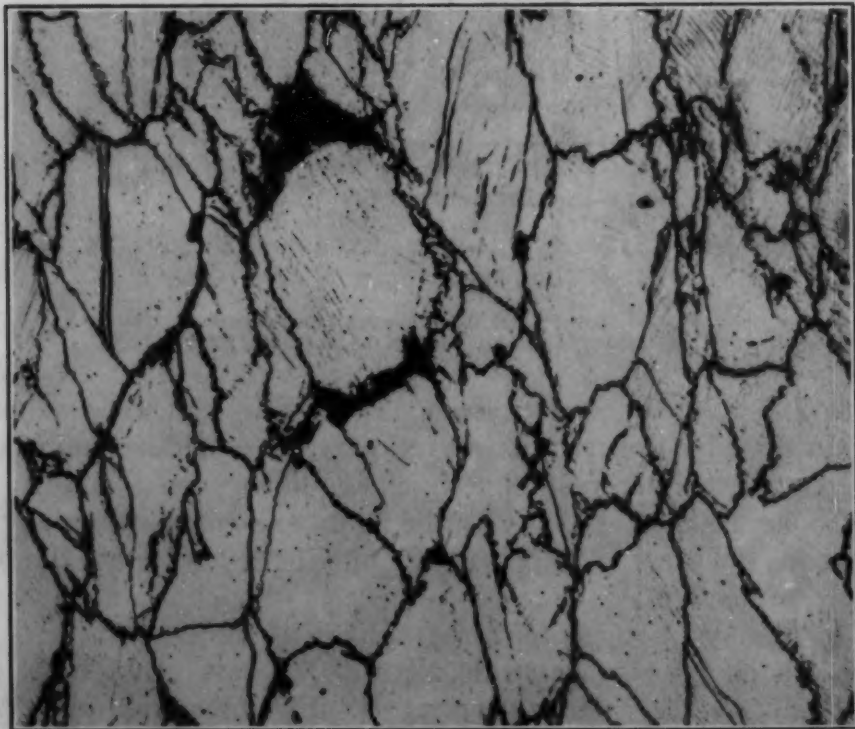


Fig. 9—Structure at Point Removed From Fracture in Test at 700°F, 472 Hours Rupture Life for 30% Cold-Worked Monel. Note very fine structure at grain boundaries. $\times 1200$. Electrolytic H_3PO_4 etch.

process on the creep-rupture properties and on any possible relationship between recrystallization (as measured by hardness) and equicohesion, which is represented by the instability located by the letters ABCD, static time-temperature recrystallization data were obtained after various degrees of cold work and are shown in Figs. 6 and 7. Fig. 6 shows the hardness versus temperature plot for cold-worked Monel after holding $\frac{1}{2}$ hour at temperature. Similar sets of curves were obtained for annealing times of 5, 50, and 500 hours for the same amounts of cold work. Because of the large number of points involved, the individual values are omitted. Recrystallization is defined in this instance as the point of inflection of the curves shown in Fig. 6.

Fig. 7 summarizes the recrystallization time in a log-log plot of per cent cold work versus temperature. The recrystallization data shown in Fig. 7 were checked metallographically and by X-ray measurements of line intensity. Since the agreement by these methods was very good, the values need not be given here.

From Fig. 7 one would not expect that recrystallization would occur much below 900 °F (480 °C) and definitely not below 800 °F (425 °C) in a period of 1000 hours or more, even after extremely severe cold work. Yet, after examination of test bars at the fracture zone and even at points removed from the fracture in those tests which were run at 700 °F (370 °C) and yielded rupture times greater than about 100 hours, there is very good evidence of the start of recrystallization at the grain boundaries. Incidentally, from Fig. 3 it will be noted that the equicohesion break at 700 °F (370 °C) for 30% cold-worked Monel is at about 100 hours (designated by the letter A). Fig. 8 shows the unmistakable evidence of intergranular cracking at 700 °F (370 °C) for both the 140- and the 470-hour rupture life tests (both beyond the equicohesion zone), the 470-hour test showing more of the intercrystalline cracks.

While both Figs. 8a and 8b show a rough grain boundary appearance, there are too many intercrystalline cracks to show the grain boundary detail clearly at a magnification of 750. Accordingly, Fig. 9, of the rupture bar at 700 °F (370 °C) and 470 hours rupture life, shows the structure at a magnification of 1200. There is unmistakable evidence of a fine new grain structure at the grain boundaries.

Clear evidence of the progress of recrystallization noted above is shown in Fig. 10. Figs. 10a and 10b show the 900 °F (480 °C) structures of the 30 and 75% cold-worked alloys respectively at $\times 500$ at a point removed from the fracture. The 30% cold-worked structure (Fig. 10a) shows the similar grain boundary roughening noted in Fig. 9, but at a more advanced stage. Fig. 10b (75% cold work) is at a still more advanced stage, to the extent that a fine

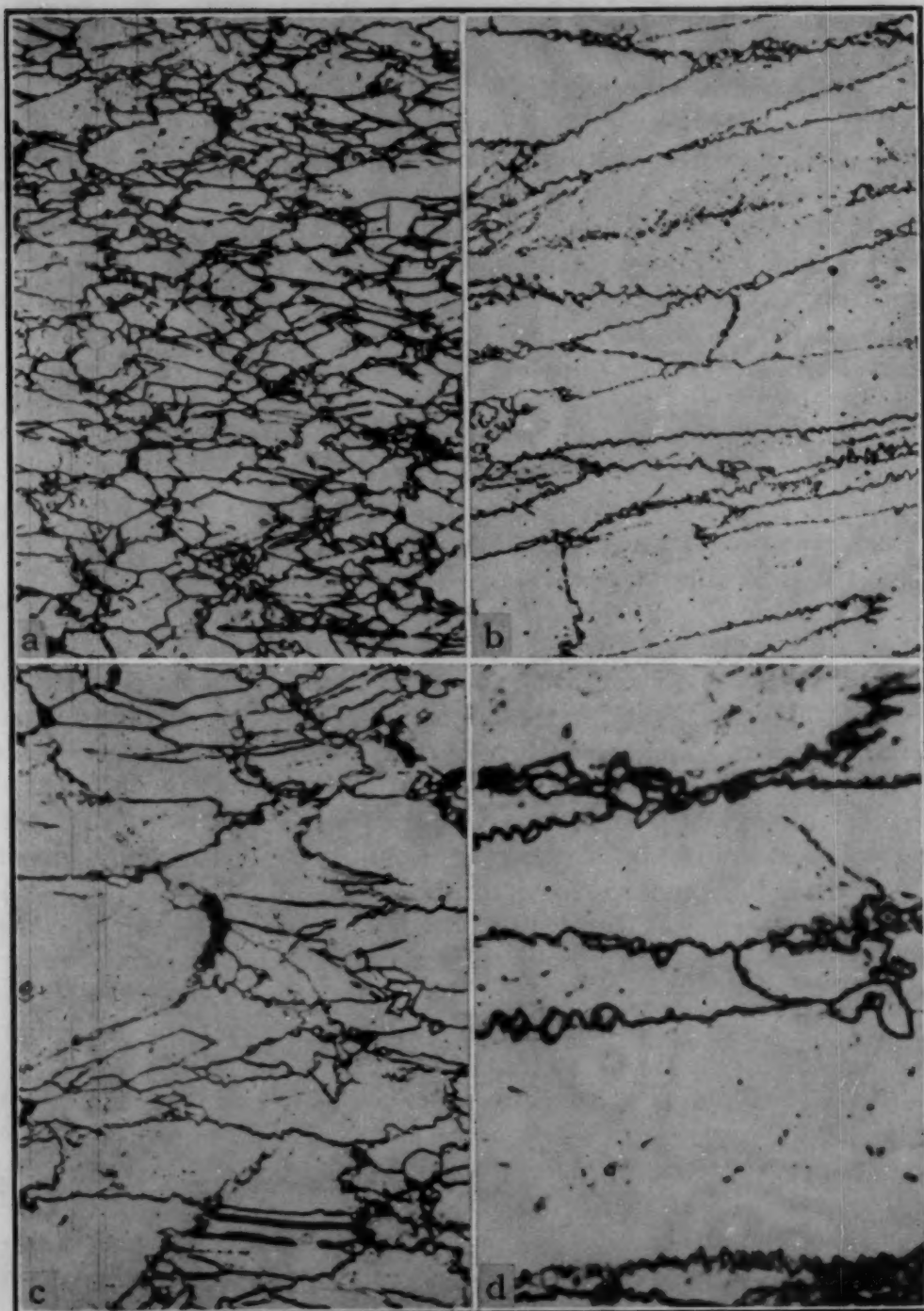


Fig. 10—Advanced Grain Boundary Recrystallization During Creep-Rupture Testing at 900°F. Electrolytic H_3PO_4 etch. (a) 30% cold work. 344 hours rupture life. $\times 500$. (b) 75% cold work. 424 hours rupture life. $\times 500$. (c) 30% cold work. 344 hours rupture life. $\times 1200$. (d) 75% cold work. 424 hours rupture life. $\times 1000$.

new grain structure is plainly evident at the grain boundaries. Figs. 10c and 10d are higher magnifications of the same structures clearly revealing recrystallization.

Fig. 11 shows this recrystallization process in the late stages of

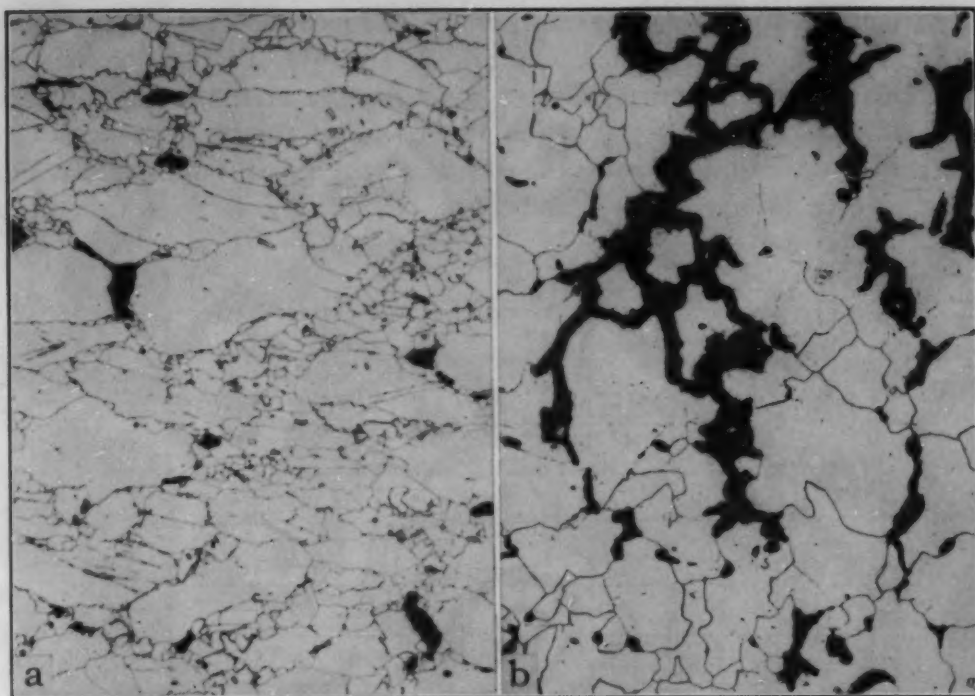


Fig. 11—Final Stages of Grain Boundary Recrystallization During Creep-Rupture Testing at 1300°F. $\times 150$. Electrolytic H_2PO_4 etch. (a) Annealed Monel after 0.028 hours (1.7 minutes). (b) Annealed Monel after 769 hours. Recrystallization complete.

completion. Fig. 11a shows the size of the new grains in annealed Monel at $\times 150$, after testing at 1300°F (705°C) for a rupture time of 1.7 minutes (0.028 hour). Fig. 11b is the same material at 1300°F (705°C) after a rupture time of 769 hours. Recrystallization is now complete. Please note the severe intercrystalline cracking.

From this series of photomicrographs it is quite evident that in creep-rupture testing, recrystallization can occur at much lower temperatures and shorter times than would be anticipated from static recrystallization studies. Furthermore, it also appears that the equicohesive instability (change from transcrystalline to intercrystalline fracture) is associated with the first tendency for recrystallization (defined in a broad sense).

If one compares in one plot: (a) The points of equicohesion for the 30% cold-worked Monel (from Fig. 3); (b) the recrystallization time for similar temperatures and cold work; and (c) the time for a distinct softening of the tested stress-rupture bars (measured both at the fracture and at a point well removed from the fracture), the interesting comparison shown in Fig. 12 results. This figure clearly illustrates the effect of strain (imposed in a creep-rupture test) on the softening and recrystallization of Monel, the effect being to speed up the softening process and to promote recrystallization by a large factor.

It is possible now to examine Fig. 4 more closely. At 900 and 1100 °F (480 and 595 °C) (letters A and B), there is consistent evidence that the rupture life decreases sharply at the transition, and then appears to recover (dashed line). This might be ascribed to the rapid formation of fine new grains at the grain boundary, which causes early failure at these stresses. At still lower stresses these

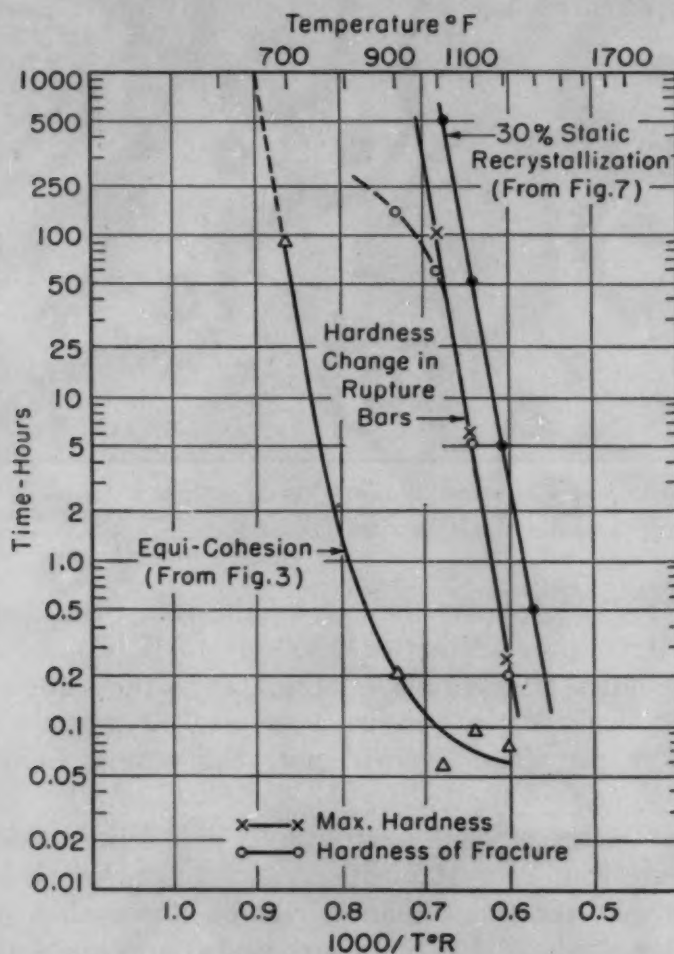


Fig. 12—Comparison of the Time-Temperature Relationships for 30% Cold-Worked Monel. (a) Static recrystallization (from Fig. 7); (b) equicohesion (from Fig. 3); (c) hardness change of ruptured test bars.

new grains have an opportunity to grow before fracture occurs, resulting in a partial recovery of the curve; but it will be noted from Fig. 4 that the slope is steep, due to the existence of this finer grain size at the old grain boundaries (see Figs. 10b and 10d).

From the viewpoint of increasing the strength of Monel through cold working, Table III compares the stress for the 10, 100, and 1000-hour rupture times from 900 to 1300 °F (480 to 705 °C). It is not recommended that strength comparisons also be made among the three grades of Monel shown in Figs. 2, 3, and 4 because of differences in initial grain size, which would affect the recrystallization be-

Table III
Effect of Cold Work on Stress for Rupture (in psi)

	At 900°F		
	10 Hours	100 Hours	1000 Hours
Annealed	51,000	46,000	43,000
30% cold-worked	70,000	60,000	45,000
	At 1100°F		
	10 Hours	100 Hours	1000 Hours
Annealed	30,000	24,000	17,000
30% cold-worked	35,000	25,000	14,000
	At 1300°F		
	10 Hours	100 Hours	1000 Hours
Annealed	13,000	8000	4500
30% cold-worked	15,000	8000	4000

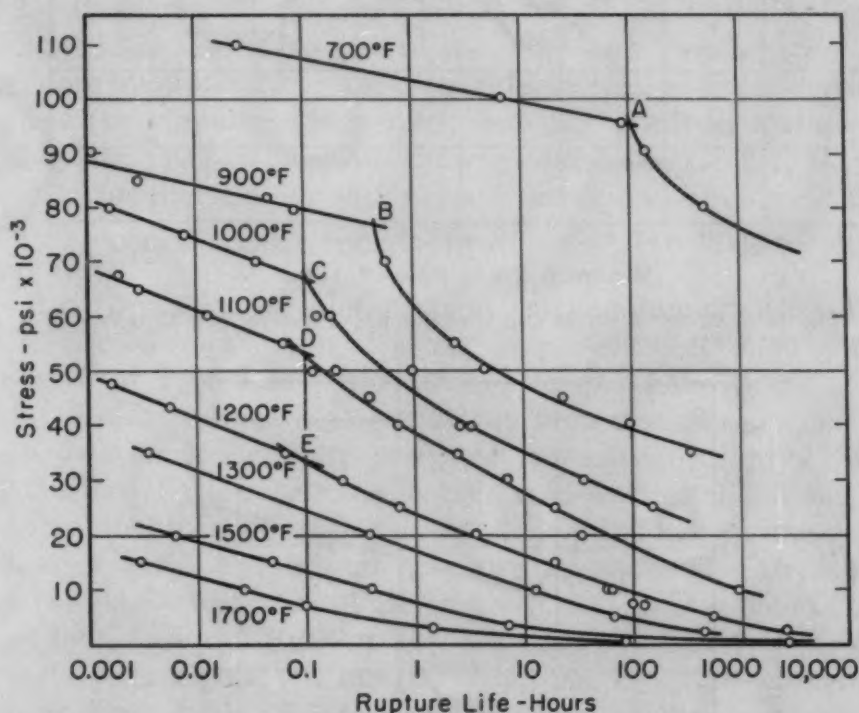


Fig. 13—Semi-Log Plot of Stress Versus Rupture Life for 30% Cold-Worked Monel From 700 to 1700°F.

havior and thereby the strength of the different grades of Monel. Fortunately, some bar stock was available, half of which was annealed and half cold drawn 30%, which permits a comparison of rupture strength of the annealed and 30% cold-worked conditions, at 900 to 1300°F (480 to 705°C). These results are shown in Table III.

From Table III it is obvious that 30% cold work effectively strengthens Monel at 900°F (480°C) for a period of more than 1000 hours. The curves intersect at about 2000 hours. At 1100°F (595°C) the benefits of 30% cold work are lost in 200 hours. At 1300°F (705°C) and higher, the annealed and 30% cold-worked values are about the same over the entire rupture-life range, any

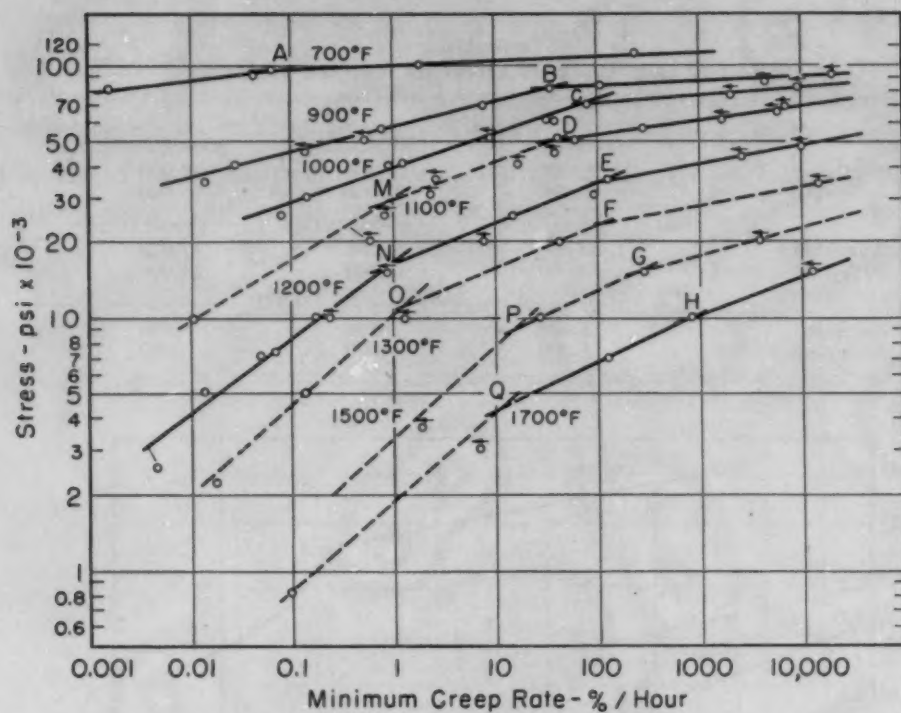


Fig. 14—Log Stress Versus Log Minimum Creep Rate for 30% Cold-Worked Monel From 700 to 1700°F.

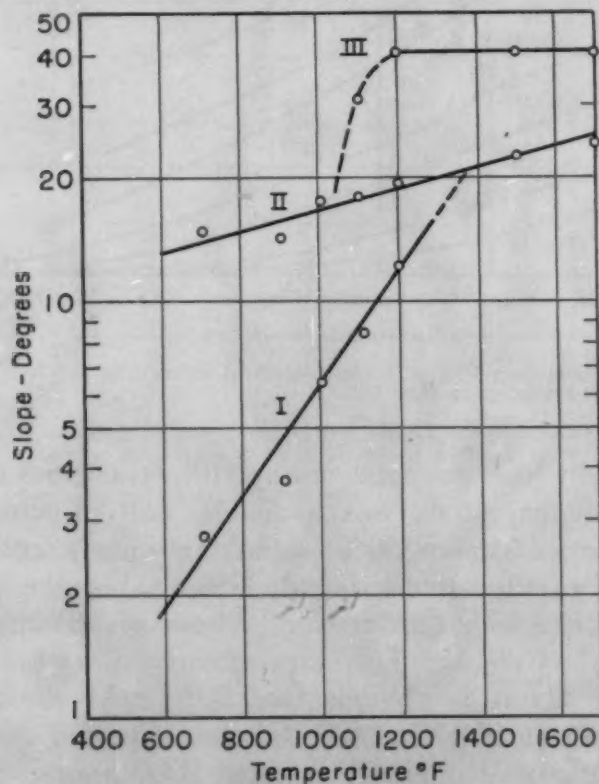


Fig. 15—Slopes of Straight-Line Segments From Fig. 3 Versus Test Temperature.
I. Segments to left of ABCD.
II. Segments between ABCD and MNOP.
III. Segments to right of MNOP.

difference being due to grain size or composition. Recrystallization is complete after several hours at 1300 °F (705 °C) and results in similar grain size for both grades.

Examination of the ductility data in Table I show a definite decrease in ductility at the equicohesion break. This is true for the true ductility (1) as well as for total ductility. Where the data are available, it was shown that the true ductility decreases with increasing rupture time and with increasing temperature, beyond the instability designated by ABCD in Fig. 3. These results bear out the experimental evidence of a ductility decrease similarly noted for the complex high temperature Ni-Cr-Co-Fe-base alloy S590 (1) and for three grades of aluminum (2).

Fig. 13 is a semi-log plot of the same data shown in Fig. 3 and once more shows that the semi-logarithmic plot of stress versus rupture life (or minimum creep rate) does not result in a straight line for the data (1, 2, 4) beyond the equicohesion zone (A, B, C, D). The data for the semi-log plot beyond the equicohesive zone are best fitted by a curve which approaches but does not intersect the zero stress axis.

Fig. 14 is a log-log plot of stress versus minimum creep rate for the 30% cold-worked condition and is presented to show the creep resistance of Monel as a function of temperature, stress and cold work. Similar curves have previously been discussed in detail (1). Creep data on Monel were previously reported by Betty, Eiselstein and Huston (5) for the annealed and cold-worked conditions.

One of the purposes of this research was to check the graphical method of extrapolating and interpolating short-time stress-rupture data (based on tests from 0.01 to about 200 to 500 hours) as proposed by Grant and Bucklin (1). Monel, a relatively simple alloy, appeared to be a good test metal. Using the 30% cold-worked stress-rupture data of Fig. 3, the complete stress-rupture curves at 1300 and 1700 °F (705 and 925 °C) were calculated and are shown as the dashed curves of Fig. 3. Experimental tests were subsequently run and the points at 1300 °F (705 °C) are shown, fitting the calculated curve almost perfectly. Since the fit is good, the experimental curve was omitted for clarity.

There was a very small difference at 1700 °F (925 °C) between the experimental and calculated curves, the agreement being very good.

The data used to calculate these curves are shown in Figs. 15 and 16. The reader is referred to Reference 1 for an explanation of the procedures for obtaining and using these curves.

This work therefore serves as a confirmation of the proposed graphical method of extrapolating relatively short-time creep-rupture test data through the utilization of the log-log plot of stress against

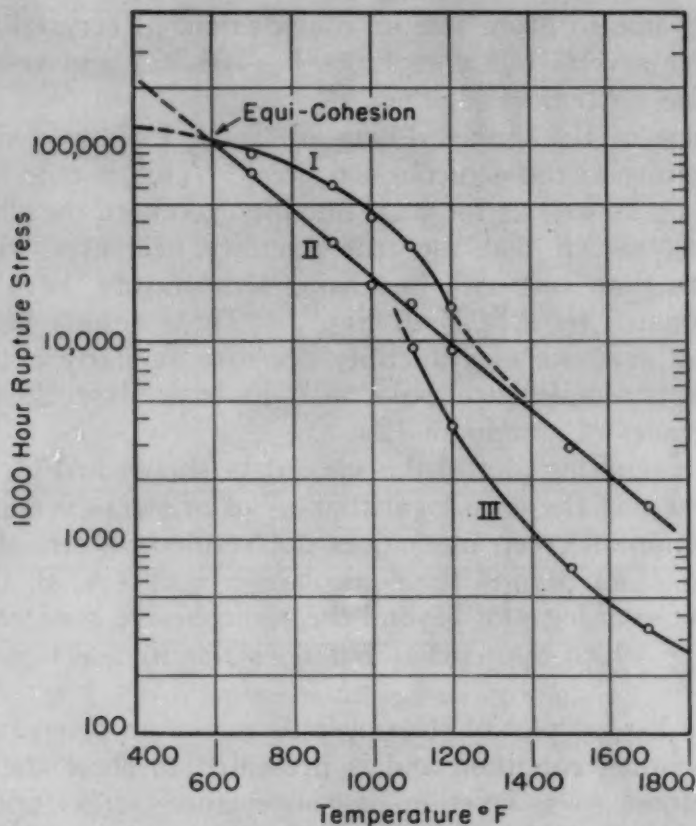


Fig. 16—Plot of Stress for 1000 Hours Rupture Life Versus Temperature. Curves I and II determine a point of equicohesion.

- I. Strength of grains, using segments to left of ABCD.
- II. Strength of grain boundaries, using segments between ABCD and MNOP.
- III. Strength based on oxidation and recrystallization, segments to right of MNOP.

rupture life which serves to locate zones of instability in the alloy as a function of time, temperature and stress.

It is interesting to point out that Curves I and II of Fig. 16 represent the 1000-hour rupture-life stresses of the grain (Curve I) and of the grain boundary (Curve II). The intersection of these two curves determines, therefore, an experimental equicohesive temperature for the conditions which fix this graph. This same graph further suggests a theoretical strength for the grain boundary at room temperature (for a 1000-hour rupture life) through the extrapolation of Curve II. As the higher temperatures are approached, the trend of Curve I indicates that the strength of the grain decreases and approaches the strength of the grain boundary region.

Since equicohesion is more rigorously defined as a function of the strain rate or for a given strain rate (6), Fig. 17 was drawn from the data of Fig. 14, plotting the stress for a constant strain rate of 0.1% per hour versus temperature. Again curves for the grain (I) and for the grain boundary (II) are obtained, the intersection

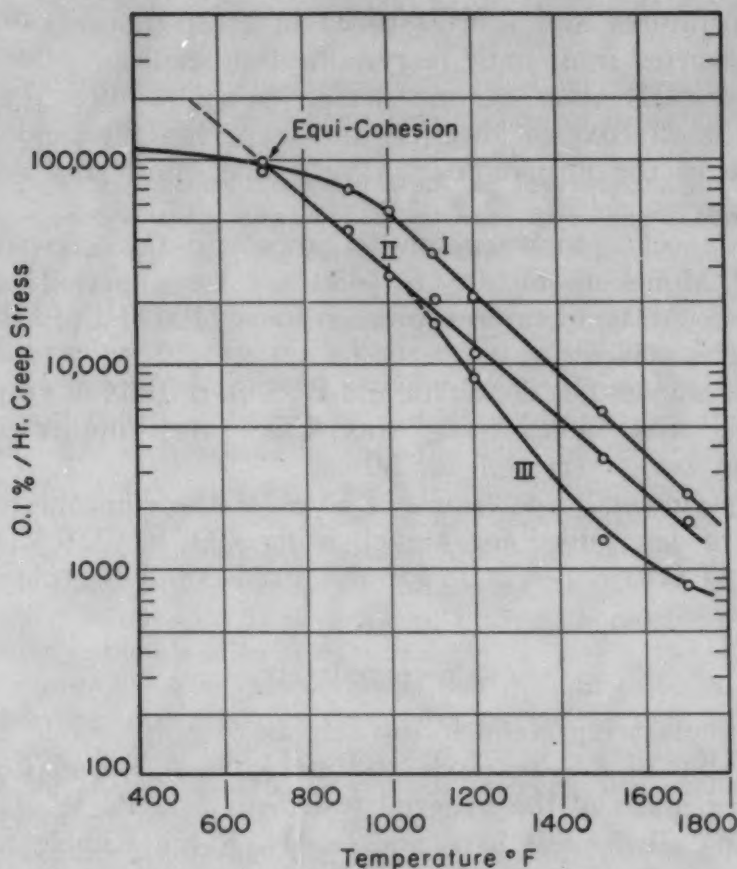


Fig. 17—Plot of Stress for a Creep Rate of 0.001 per Hour Versus Temperature. Curves I and II determine a point of equicohesion. Curves I, II and III are similarly defined as in Fig. 16.

of which defines the equicohesive temperature of Monel for a strain rate of 0.001 per hour.

SUMMARY AND CONCLUSIONS

1. Creep-rupture data for Monel in the annealed, 30 and 75% cold-worked conditions have been obtained for temperatures from 700 to 1700 °F (370 to 925 °C) and for rupture times up to about 2700 hours.

2. Recrystallization data have been obtained for Monel for cold-work reductions up to 70% and for recrystallization times from 0.5 to 500 hours.

3. The instabilities which decrease the long-time creep and rupture properties of Monel are the incidence of intercrystalline fracture, oxidation, and recrystallization.

4. Time-temperature relationships for recrystallization as measured by hardness changes do not serve as accurate indications of the onset of intercrystalline cracking in creep-rupture testing of Monel; and, coincidentally, evidence of recrystallization is present at much

lower temperatures and shorter times in creep-rupture tests than could be predicted from static recrystallization studies.

5. Recrystallization occurs during creep-rupture testing of Monel and is effective in lowering the creep resistance and rupture life because of the formation of a very fine grain size along the grain boundaries.

6. 30% cold work effectively improves the creep-rupture strength of Monel up to 900 °F (480 °C) for a period of about 2000 hours. At temperatures greater than 1100 °F (595 °C) no benefit at all is evident.

7. It is shown that the Grant and Bucklin method of graphically extrapolating and interpolating short-time creep-rupture data is effective and works very well for Monel.

8. Experimentally determined values of the equicohesive temperatures are determined for Monel, being 700 °F (370 °C) for a strain rate of 0.10% per hour for this grade of 30% cold-worked Monel.

ACKNOWLEDGMENT

The authors are grateful to the Bureau of Ships, Code 343, for the sponsorship of this research, to International Nickel Company for supply of much of the material tested, to Mr. E. W. LaRocca for machining all the test bars, and to Mr. Ralph Kimble for performing most of the creep-rupture tests.

References

1. N. J. Grant and A. G. Bucklin, "On the Extrapolation of Short-Time Stress-Rupture Data", *TRANSACTIONS, American Society for Metals*, Vol. 42, 1950, p. 720-761.
2. I. S. Servi and N. J. Grant, "Creep and Stress-Rupture Behavior of Aluminum as a Function of Purity", *Journal of Metals, Transactions, American Institute of Mining and Metallurgical Engineers*, Vol. 3, No. 10, October 1951, p. 909.
3. I. S. Servi and N. J. Grant, "Structure Observations of Aluminum Deformed in Creep at Elevated Temperatures", *Journal of Metals, Transactions, American Institute of Mining and Metallurgical Engineers*, Vol. 3, No. 10, October 1951, p. 917.
4. I. S. Servi and N. J. Grant, "Creep and Stress-Rupture as Rate Processes", *Journal, Institute of Metals*, Vol. 80, September 1951, p. 33.
5. B. B. Betty, H. L. Eiselstein and F. P. Huston, Jr., "Creep Properties of Cold-Drawn Monel and Inconel", *Transactions, American Institute of Mining and Metallurgical Engineers*, Vol. 161, 1945, p. 441-454.
6. Z. Jeffries, "Effect of Temperature, Deformation and Grain Size on the Mechanical Properties of Metals", *Transactions, American Institute of Mining and Metallurgical Engineers*, Vol. 60, 1919, p. 474.

DISCUSSION

Written Discussion: By Henry E. Frankel, metallurgist, High Temperature Alloys Branch, Metallurgy Division, Naval Research Laboratory, Washington, D. C.

The paper represents a careful study of recrystallization phenomena occurring under static conditions and also while in the process of being strained. However, there appears to be discrepancies which the authors can perhaps clear up.

According to the authors in a previous work,² breaks occurring in log stress-log rupture time curves indicate points at which the mode of fracture changes or points at which structural changes such as oxidation or recrystallization occur. In Figs. 2 and 3, two breaks are frequently encountered. The first breaks indicate the first evidences of intercrystalline fracture. The authors ascribe a relationship between recrystallization phenomena and equicohesion. The second break is described as being affected by a recrystallization phenomenon which first begins to be noted beyond the zones ABCD. Thus it is intimated that there is a single major cause for the two breaks. It is wondered if the authors have observed this phenomenon in metals other than monel.

The second break in the curve was first thought to be caused by oxidation, but the authors stated that this was not the case (their seventh page). However, on the next page, it is stated that the MNOP regions may "in part be ascribed to an obvious intergranular oxidation effect". These statements appear to be contradictory.

The authors show that the 75% cold-worked material recrystallizes more rapidly than the other specimens. If there is a relation between the equicohesive point and recrystallization, the break in a log stress-log rupture time curve should appear at shorter times the more a specimen is prestrained. Then the break for the 75% cold-worked material should occur at a shorter time than for the 30% cold-worked material and the latter should exhibit a break at a shorter period of time than the annealed metal. However, at 900 °F, for example, the 75% cold-worked material exhibits the break at 5 hours, the 30% cold-worked at 0.1 hour, and the annealed at 0.3 hour. Have the authors an explanation for this discrepancy?

Written Discussion: By Donald N. Frey, Ford Motor Co., Dearborn, Mich.

This paper proved to be most interesting and informative and, accordingly, the writer wishes to congratulate the authors for the fine work. The following points for further discussion are submitted for the authors' consideration and possible comment.

The discontinuities labeled M, N, O, P and Q in Fig. 3 do not appear in Fig. 13. From this the question is raised as to whether the discontinuities M, N, O, P and Q can be considered real or rather somewhat as artifacts of the plotting method.

The authors also note on their thirteenth page that equicohesive instability is associated with the first tendency for recrystallization—"defined in a broad sense". Also Fig. 12 tends to point out only a limited relationship between the breaks in Fig. 3 and recrystallization. It is suggested,

²See Reference 1 of paper.

therefore, that a more direct relationship between "equicohesive instability" or loss of strength and pre-recrystallization recovery might exist. For example,³ it is shown that relaxation by annealing of internal stresses (as measured by X-ray diffraction line widths) results in reduction in creep resistance of previously cold-worked metals. This relaxation phenomenon is a pre-recrystallization one, and might be expected to affect rupture resistance in a similar manner.

Lastly, the same shapes of rupture curves as are shown in Fig. 13 are found for rather diverse materials not necessarily cold-worked (see, for example, curves for age-hardened Inconel-X).⁴ The question then is raised as to whether any relationship at all exists between discontinuities such as those labeled A, B, C, D, E and F in Fig. 3 and recrystallization following cold work.

Written Discussion: By Joseph R. Lane, Metallurgy Division, Naval Research Laboratory, Washington, D. C.

It is gratifying to find that where the Grant-Bucklin data overlap that obtained by Mr. Shahinian and myself,⁵ the agreement is generally satisfactory. As noted on the fourteenth page of our paper, we found a tendency for the log stress-log rupture life plots to curve downward at high temperatures. It is quite likely that the grain boundary recrystallization described by Grant and Bucklin is at least a factor in this behavior. Additional close examination of our specimens confirms that recrystallization can occur in a specimen put on test in an annealed condition, as shown in Fig. 18.

In a previous work by these authors,⁶ it was shown that the equicohesion breaks in the log stress-log rupture life curves, in the two alloys reported, varied widely and continuously with temperature. This is to be expected because of the relation between temperature and strain rate. However, the breaks in the curves for monel, especially in the case of the 30% cold-worked alloy, occurred at approximately the same time at all temperatures. Have the authors any explanation for this effect?

The observation by Grant and Bucklin that recrystallized grains are formed during creep-rupture possibly may be used to determine the true stress involved. The extensive fissuring which usually occurs near high temperature-type fractures renders an estimate of the deformation based on the dimensions of the specimen unreliable. Work by Walker,⁷ Wensch and Walker,⁸ and Channon and Walker,⁹ shows that a logarithmic relation exists between the recrystallized grain size and the square root of the deformation. While their data involve only cold deformation, it is suggested that such a relationship might be used to indicate the localized

³D. N. Frey and J. W. Freeman, "Fundamental Effects of Cold Working on the Creep Resistance of an Austenitic Alloy", *Journal of Metals*, Vol. 3, No. 9, 1951, p. 755.

⁴D. N. Frey, J. W. Freeman and A. E. White, "Fundamental Aging Effects Influencing High-Temperature Properties of Solution-Tested Inconel-X", National Advisory Committee for Aeronautics, Technical Note 2385, 1951.

⁵Paul Shahinian and J. R. Lane, "Influence of Grain Size on High Temperature Properties of Monel", published in this volume of TRANSACTIONS.

⁶See Reference 1 of paper.

⁷H. L. Walker, "Grain Size Produced by Recrystallization and Coalescence in Cold-Rolled Cartridge Brass", University of Illinois Experiment Station Bulletin No. 359, 1945.

⁸G. W. Wensch and H. L. Walker, "Recrystallization and Grain Growth of Nickel", TRANSACTIONS, American Society for Metals, Vol. 44, 1952, p. 1186.

⁹S. L. Channon and H. L. Walker, "Recrystallization and Grain Growth in Alpha Brass", published in this volume of TRANSACTIONS.

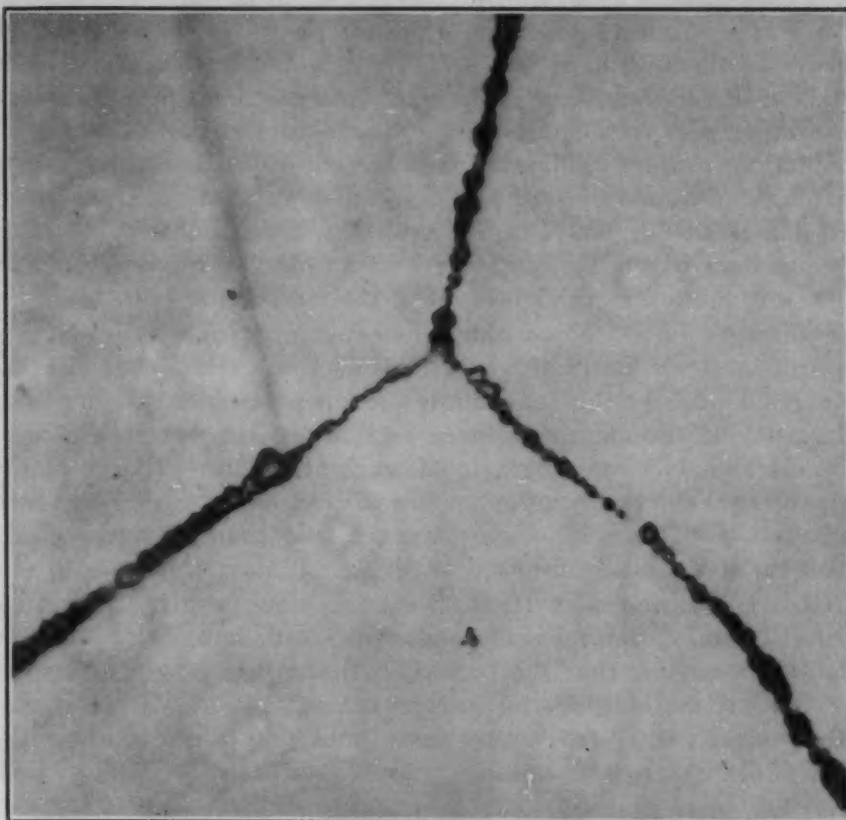


Fig. 18—Grain Boundary Recrystallization in a Monel Stress-Rupture Specimen After 45 Hours at 900 °F and 45,000 psi. $\times 1500$.

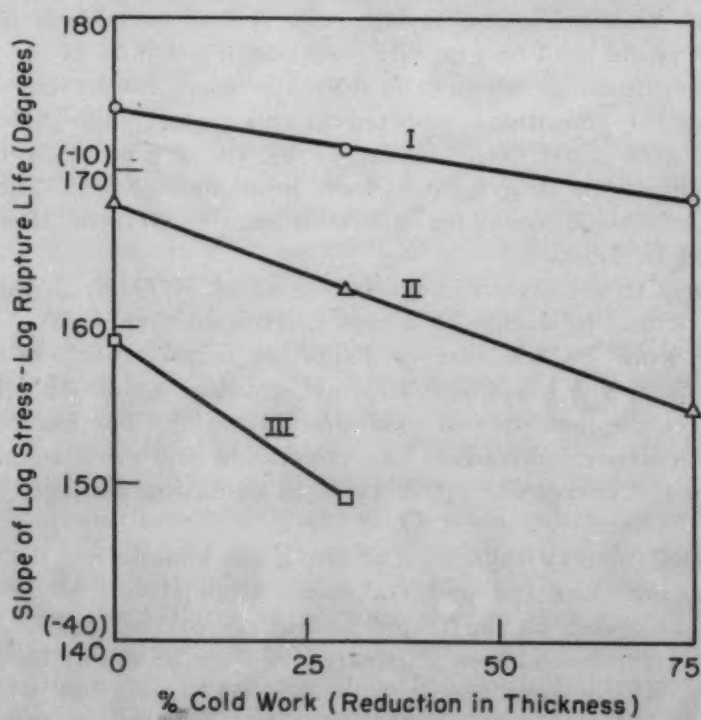


Fig. 19—Influence of Cold Work on Slope of Log Stress - Log Rupture Life Curves for Monel at 1100 °F. Original data from Grant and Bucklin.

stress in a creep-rupture specimen at those points at which recrystallization occurs. In establishing such a curve, it would be necessary to change the criterion of recrystallized grain size from the size of the grains when the material is just completely recrystallized to the size of the grains at the completion of recrystallization in only two dimensions (i.e., continuous grains along the boundaries of the original large grains). The recrystallized grain size of our 900 °F specimen⁵ was approximately 0.00025 millimeter, equivalent to the residual stress of an extremely great deformation (over 100% reduction in thickness using the curves⁶ for brass).

The authors have shown that their extrapolation procedure works well in still another material, monel. It is interesting that the method can be carried even farther and allow for material with varying amounts of cold work. If the slopes of three sections of the log stress-log time curves are drawn as a function of cold work (the 1100 °F curve is given in Fig. 19), the necessary correction to Fig. 15 can be made for any intermediate amount of cold work. Unfortunately, adequate data to include this additional variable would rarely be available.

Written Discussion: By H. H. Bleakney, metallurgist, Department of Mines and Technical Surveys, Ottawa, Ont., Canada.

The authors argue that the breaks in the curves of Fig. 3 at A, B, C, D, E, F are attributable to the intercrystalline cracks which are typical of so many metals in creep-rupture tests; and they argue that the breaks at M, N, O, P, Q are attributable to recrystallization. The evidence is somewhat less than convincing in both cases.

The intercrystalline cracking associated with the breaks in the curves at A, B, C, D, E, F takes place so much more rapidly in this monel than in other metals that one suspects the influence of an additional agency. Such an agent might well be graphite. Although graphite is not found in monel at temperatures at which it is normally used, its presence is to be expected under the conditions reported in this paper. The fissures seen in Fig. 11 could be most easily explained by the presumption that they originated at thin films of graphite at the grain boundaries. Such a presumption might also account for the wide scatter of reduction of area values reported in Table I.

With respect to the breaks in the curves at M, N, O, P, Q, the authors dismiss intergranular oxidation as a factor. However, they say "Since the effect of cold work on the rate of oxidation is probably small, except insofar as it affects the grain size and intergranular oxidation, cold work should not affect the incidence of oxidation damage." The exception contained in this sentence contradicts the conclusion and even suggests that these breaks in the curves are attributable to oxidation damage. Table II supports that opinion.

With respect to recrystallization at the grain boundaries, the evidence falls short of being clear and unmistakable. Monel frequently displays a highly mixed grain size, as illustrated in Fig. 1b of the paper. The fine grains shown at the boundaries illustrated in Fig. 10 might be the remnants of grains which were originally somewhat larger, but which have been consumed by their neighbors almost to the point of extinction. However, even if the fine grains shown at the boundaries in Fig. 10 are in fact the products of recrystallization, they appear to be much too few to ac-

count for the very marked breaks in the curves at M, N, O, P, Q. Moreover, it is highly debatable that recrystallization has a life-shortening effect in creep-rupture tests. Evidence indicates that the opposite is true. When a metal is susceptible to intercrystalline cracking, such cracking is more serious in shortening the creep-rupture life than the temporary acceleration of the creep rate caused by recrystallization. Greenwood has reported that of four samples of lead which differed only in heat treatment, the only one which displayed an intercrystalline fracture was that one which had not recrystallized during the test.

Authors' Reply

The authors are pleased with the extensive discussion of the paper and for the contributions from the discussers.

First, regarding Mr. Frankel's discussion, the two breaks in the curves of Fig. 2 are not ascribed to a single cause. The first break is associated with the incidence of grain boundary deformation and fracture. For Monel, it so happens that this is the same point for the first evidence of recrystallization. However, recrystallization is not the cause of the break. The noted recrystallization is probably the result of the extensive grain boundary deformation which becomes operative at about this particular temperature, time, and stress. This is, incidentally, the first evidence of such recrystallization phenomenon that we have observed in creep-rupture studies, which in the past have included several grades of aluminum, stainless steels, and many nickel and cobalt based super-alloys.

The second break is due "in part" to obvious oxidation. In part, the break is also due to a simultaneous and continuing recrystallization effect. Thus, the break in the curve cannot be associated with a single instability. Such overlapping instabilities have been proposed and discussed in a previous paper (2).

In the recrystallization of cold-worked metals, during creep testing, the simple advent of recrystallization cannot alone be considered. There are also the effects of the rate of growth of new grains and the orientation of such new grains. In the case of Monel, important preferred orientation effects become evident as recrystallization occurs. Accordingly, the complex effects noted during creep studies are admittedly poorly understood.

Regarding Dr. Frey's discussion, the discontinuities MNOP in Fig. 3 do not appear in Fig. 13 because the semi-log method of plotting crowds the stresses at low values, for example, between 100 and 1000 psi. Thus, a change in stress from 1000 to 100 psi is a 10-fold change similar to the 10-fold change from 1000 to 10,000 psi; however, the space allotted on a semi-log basis to these two ranges of values is vastly different.

Such crowding does not permit observations of slope changes due to instabilities, even if they do occur. It is for this reason, if for no other, that the double-log plots are preferable since they permit the necessary stress scale expansion to view the incidence or continued role of instabilities on the creep rate or rupture life of materials at low stresses.

Pre-recrystallization or recovery phenomena play an important role in the shape of the curves, but these effects would be expected to produce changes in slope before the instability ABCD becomes operative. Thus

the slopes of the log stress-log rupture life curve at the left of the zone ABCD should be examined instead of those to the right. Cold work is certainly not a prerequisite for obtaining discontinuity ABCD. Equi-cohesion is prevalent in all face-centered cubic metals and alloys (except for high purity materials) regardless of prior history or treatment.

Regarding Dr. Lane's discussion, no explanation for poor line-up of equi-cohesion breaks as a function of temperature can be offered. Dr. Lane's calculations confirm our beliefs that the deformation at the grain boundary when the equi-cohesion temperature is reached can be and is extremely large. We wish to thank Dr. Lane for the other valuable contributions and his discussion.

While Mr. Bleakney expresses extensive doubts regarding many of our experimental results, it appears that he is quite willing to do extensive "presuming", without offering any supporting evidence. We clearly admit hesitancy regarding some of the noted effects but at least we do present evidence and reasons for such evidence. We believe the burden of the proof lies with Mr. Bleakney to show first the evidence of the presence of graphite, and second to show its effects along the lines he suggests. It is virtually impossible to conceive or to show how the graphite (which, while it may be there, was not noted to exist) could account for any of the changes in behavior, or why graphite would produce discontinuities in the curves as a function of time and temperature. We wonder if Mr. Bleakney observed that all of the materials prior to testing or cold working had been annealed at 1500 °F to equalize them in every way possible.

The role of oxide has already been discussed above. Mr. Bleakney's suggestion that many thousands of grain fragments survived the recrystallization or annealing treatment of 1500 °F (far above the temperature necessary for complete recrystallization, measured in any sense of the word), and began to grow again only after creep deformation, is difficult to consider. Recrystallized grain boundaries indicate that these fine new crystals formed during the deformation process. While these grains are extremely fine and abundant at the old grain boundaries, they materially weaken the load-carrying capacity of the Monel as shown in the paper and result in the sharp discontinuity. We are pleased to have the confirming work of Lane and Shahinian in the preceding paper, not only showing the fine new crystals at the grain boundary (Fig. 18 of the discussion) but also their evidence of the weakness of the fine-grained structure.

INFLUENCE OF GRAIN SIZE ON HIGH TEMPERATURE PROPERTIES OF MONEL

BY PAUL SHAHINIAN AND JOSEPH R. LANE

Abstract

To evaluate the effect of grain size on flow and fracture as influenced by temperature, wrought Monel, a single-phase alloy, was used. Specimens of two heats were tested in creep-rupture at 700, 900, 1100 and 1300 °F (370, 480, 595 and 705 °C), and at stresses ranging from 7000 to 65,000 psi. The test temperatures permitted the observation of low temperature as well as high temperature behavior, and the transition from one type to the other. The grain sizes, which ranged from 0.024 to 0.78 mm. average diameter, were obtained by cold work and recrystallization.

Time-to-rupture, minimum creep rate, total elongation, and reduction-in-area curves were drawn showing their relationship to grain size. The results show an optimum grain size range for maximum rupture time at 1100 and 1300 °F (595 and 705 °C), temperatures which are above the "equicohesive" temperature. Below 1100 °F (595 °C), the finest grain size specimens generally had the greatest rupture life. There is an optimum grain size for lowest minimum creep rate at 900 and 1100 °F (480 and 595 °C), but not at 700 or 1300 °F (370 or 705 °C). Total elongation and reduction in area generally increase with a decrease in grain size when above the equicohesive temperature. Below that temperature, the changes in these quantities with grain size are small and more erratic. It was found that rupture lives and creep rates of separate heats of the same nominal composition varied significantly, especially at the lower temperatures.

INTRODUCTION

THE BEHAVIOR of metals and alloys at elevated temperatures depends upon metallurgical factors such as grain size, crystal structure, composition and microstructure in addition to external factors such as temperature and atmosphere. It was the object of this study to evaluate more completely the influence of grain size on

A paper presented before the Thirty-fourth Annual Convention of the Society, held in Philadelphia, October 18 to 24, 1952. The authors, Paul Shahinian and Joseph R. Lane, are members of the Metallurgy Division, Naval Research Laboratory, Washington, D. C. Manuscript received April 10, 1952.

flow and fracture characteristics of Monel in the belief that fundamental information obtained from such a study should be valuable in the development of metals and alloys for greater strength and resistance to creep at elevated temperatures.

A search of the literature showed that numerous workers had studied grain size influence on creep behavior of metals. While the results of investigations on this subject are varied and often inconclusive, in general it is agreed that coarse-grained material is more creep-resistant than fine-grained material at high temperatures while the reverse is true at low temperature. The lack of control over variables other than grain size detracts from the value of much of the work.

One of the earliest investigations on this subject is that of Clark and White (1)¹ on brass and bronze alloys. Their results, obtained from upstep loading creep tests, showed that fine-grained brass is more resistant to creep than coarse-grained below a certain temperature range, and that above this range, the reverse is true. Only two grain sizes were studied in their work. Burghoff et al (2) observed greater creep resistance of coarse-grained copper alloys over fine-grained at elevated temperatures, and Hanson and Sandford (3) made similar observations on alloys of tin. The influence of specimen size as well as grain size of copper was considered by Parker and Riisness (4) and they concluded that creep rate is independent of grain size; early data which indicated an optimum grain size for minimum creep rate was later attributed to oxidation of the small diameter test bar. Hanson (5) presented data showing an optimum grain size for maximum rupture life and also for minimum creep rate for pure tin. His data are limited, however, in that tests were made at only one temperature and stress. From studies on creep of virgin lead at room temperature, McKeown (6) found coarse-grained material to be more creep-resistant than fine-grained.

Weaver (7) concluded that for steel an optimum grain size exists for maximum creep strength. He tested several heats of SAE 4340 of various grain sizes in creep at 840 °F (450 °C). Because of variations in composition and heat treatment of the steels involved, even though a uniform microstructure was indicated, the results did not appear to be conclusive. Further work by Weaver (8) with the composition variable eliminated produced similar results. Other investigators of the influence of grain size on steels have reported greater creep resistance of coarse-grained over fine-grained at elevated temperatures; for example, White and Clark (9), Cross and Lowther (10, 11), Thielemann (12), Miller (13), and Clark and Freeman (14).

Grant (15) found that coarse-grained cobalt-chromium alloys

¹The figures appearing in parentheses pertain to the references appended to this paper.

are strongest at high temperatures. However, in some cases, very wide scatter was obtained in the testing of specimens in which the grains were so large that grain orientation became significant.

For a discussion in greater detail and a more extensive review of the literature on this subject, reference is made to the work of Smith (16).

PROCEDURE

Preparation of Specimens. An attempt has been made in this study to eliminate as many external variables as feasible, and to cover a broad range of grain sizes and temperature and stress levels. To eliminate the effect of precipitation or transformation variables, a single-phase alloy, Monel, was used. This alloy was annealed at temperatures higher than the testing temperature to reduce the possibility of grain growth during test and to produce a stable microstructure. This work was done on two separate heats. A greater range of stresses was covered with the first heat; the second was used primarily to check reproducibility. The first heat, designated as "F", was received in the cold-rolled condition in the form of $\frac{3}{4}$ -inch square rods. The second heat, designated as "L", was in the form of $\frac{5}{8}$ -inch rounds. Chemical compositions are shown in Table I.

Table I
Chemical Compositions of Two Monel Heats

Heat	Ni	Cu	Fe	Mn	Co	C	Si	Cr	S
F	65.08	29.63	3.25	1.01	0.56	0.19	0.19	0.04	0.04
L	65.05	30.53	2.54	0.90	0.43	0.20	0.30	0.01	0.04

The wide range of grain sizes essential for this investigation was produced by annealing the as-received bars at various temperatures, or by cold working of the bars followed by annealing. Table II lists the treatments used in obtaining the various grain sizes. Severe oxidation above 1600 °F (870 °C) prompted the use of vacuum annealing above that temperature. The testing of specimens which had been either air or vacuum-annealed at 1400 °F (760 °C) and below showed that there was no effect of annealing atmosphere. However, for further insurance, a considerable amount of the surface was removed in the machining of the bars. Chemical analyses made before and after the various heat treatments showed the composition to be unchanged by the treatment, within analytical error.

Measurement of Grain Size. Determinations of grain size were made by counting the number of grains intersected by lines $\frac{1}{4}$ -inch long scribed on the specimen. The product of the counts on two such lines at right angles yielded the number of grains per $\frac{1}{16}$ square inch. These values were then converted to the average grain diameter, in

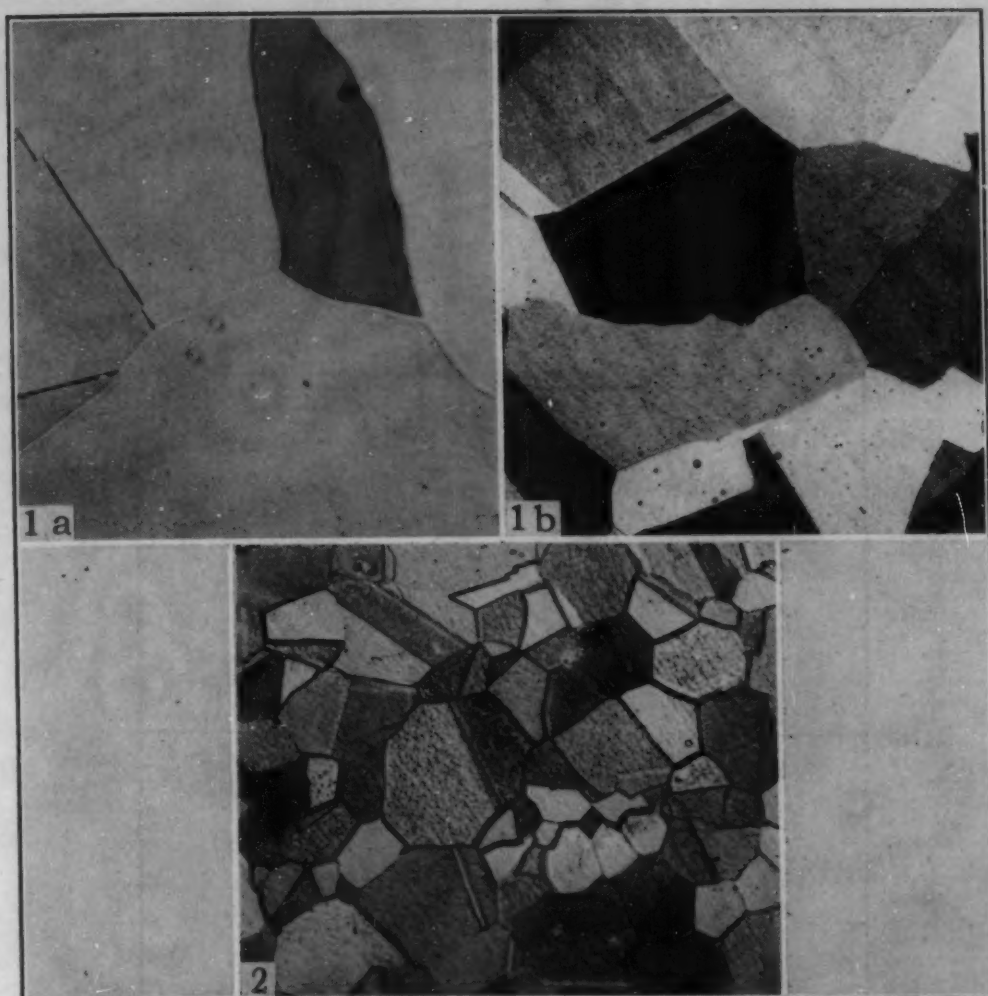
Table II
Heat Treatments and Resultant Grain Sizes

Designation	Treatment	Average Grain Diam., mm.	Grains per $\frac{1}{4}$ -Inch Diam. Cross Sectional Area of Specimen
HEAT F			
RA	Vacuum-annealed at 2300°F for 2 hours	0.779	52
SA	Vacuum-annealed at 2200°F for 3 hours	0.705	64
TC	Vacuum-annealed at 2100°F for 3 hours	0.345	266
M	Cold-rolled and annealed at 1850°F	0.230	600
TA	Vacuum-annealed at 1925°F for 3 hours	0.214	690
MO	Cold-rolled and annealed at 1700°F	0.178	1,000
TD	Vacuum-annealed at 2020°F for 3 hours	0.171	1,080
TB	Vacuum-annealed at 1925°F for 3 hours	0.153	1,370
U	Annealed at 1400°F for 24 hours	0.0635	7,850
V	Annealed at 1300°F for 1 hour, cold-rolled to 50% reduction in area, annealed at 1400°F for 24 hours	0.0240	55,100
HEAT L			
DS	Vacuum-annealed at 2200°F for 1 hour	0.376	224
DT	Vacuum-annealed at 1950°F for 4 hours	0.267	445
DD	Vacuum-annealed at 1825°F for 4 hours	0.125	2,040
DU	Vacuum-annealed at 1450°F for 4 hours	0.0435	16,700

millimeters, and to the number of grains in the cross section of a $\frac{1}{4}$ -inch round specimen. As a check, measurements were made by counting the number of grains in a known area on the ground glass of a metallograph. Grain size determinations were made both on the bar stock after final heat treatment and on fractured specimens after test. The microstructures of the coarsest and finest grain size specimens are shown in Figs. 1 and 2.

Testing Conditions. The specimens employed in the tests were $\frac{1}{4}$ inch diameter by $1\frac{1}{4}$ inch gage length and were machined from the centers of the bars. These were tested in single-lever constant-load creep-rupture machines of Naval Research Laboratory design. Specimen temperature, measured by a chromel-alumel thermocouple tied to the center, was maintained to within $\pm 2^\circ\text{F}$. Previous surveys indicated the temperature gradient along the gage length of the specimen to be no more than 1°F . Tests were conducted at 700, 900, 1100 and 1300°F (370, 480, 595 and 705°C), and at stresses ranging from 7000 to 65,000 psi. Extension of the specimen was autographically recorded from the loading lever deflection, giving an elongation versus time curve. In addition periodic readings were taken from a dial gage and recorded. After test, fractured specimens were examined microscopically for evidence of grain growth, changes in microstructure and type of fracture. There were no detectable changes in grain size or microstructure. Creep-rupture tests were run at temperatures below as well as above the "equicohesive" temperature so that the change in type of fracture normally encountered could be observed.

Tests were made which indicated that the prolonged heating at

Fig. 1a—Coarse-Grained Monel (RA, Heat F). $\times 250$.Fig. 1b—Coarse-Grained Monel (RA, Heat F). $\times 25$.Fig. 2—Fine-Grained Monel (V, Heat F). $\times 250$.

test temperatures had no apparent effect on grain growth. In these tests, no significant changes of grain size were noted when samples of each grain size were heated at 1300 °F (705 °C) for 1000 hours. This is the highest temperature to be applied during the testing. Data, shown in Table III, indicate that the influence of oxidation on tests does not appear to be significant.

Table III
Effect of Atmosphere on Creep-Rupture at 1300 °F and 9000 Psi

Average Grain Diam., mm.	Hours to Rupture		Preoxidized at 1300 °F for 200 hrs.
	Regular	Copper Plated	
0.779	108	100.6
0.705	156.6, 142.2	146.3	147.5
0.214	225.2, 178.3	237.8	203.5
0.0635	148	164.7	158.5
0.0240	68.9, 65, 66.2	71.2	62

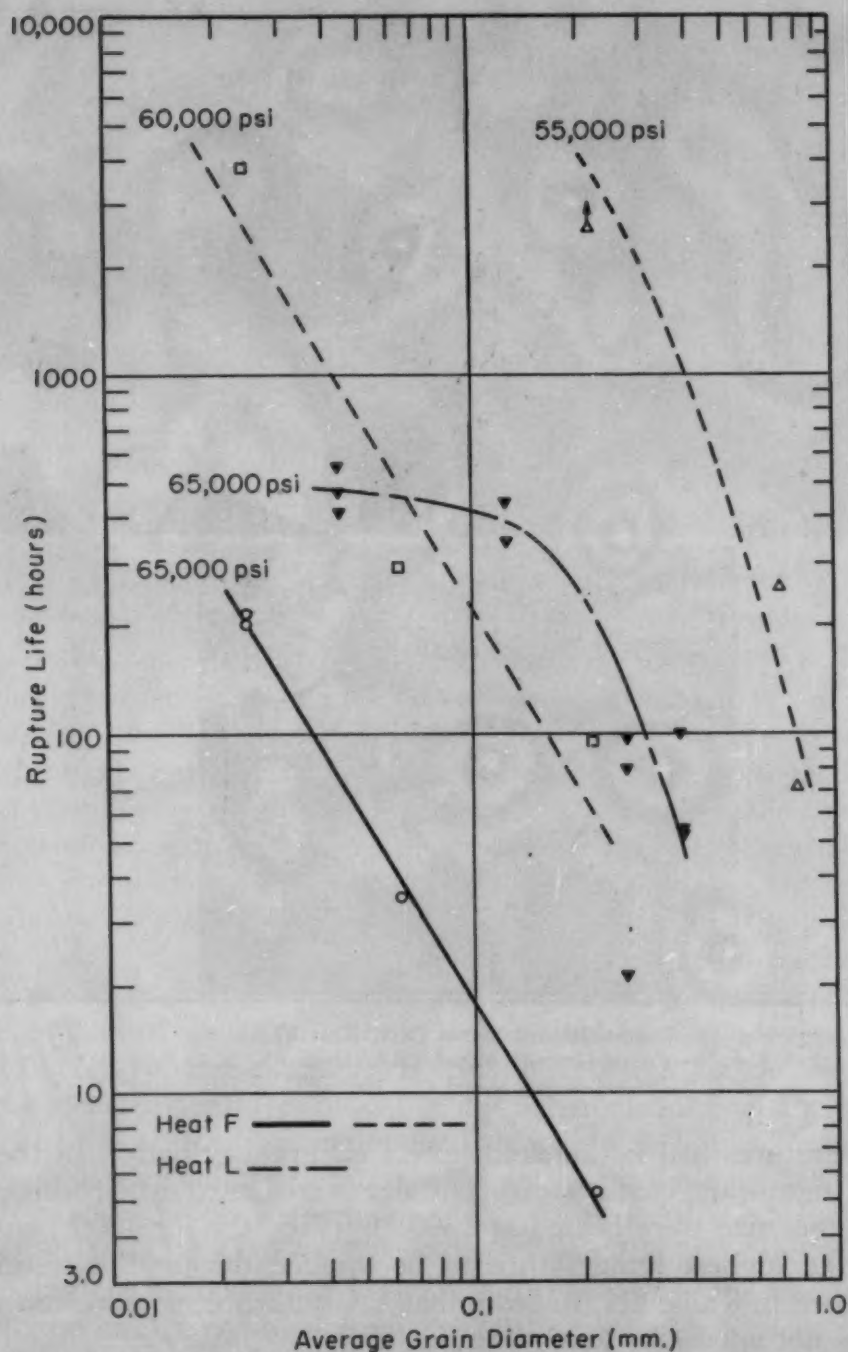


Fig. 3—Variations of Rupture Life With Grain Size of Monel at 700 °F (370 °C).

DISCUSSION AND RESULTS

Grain Size Effect on Rupture Life and Creep Rate. The results of the rupture testing are given in Table IV. From these results, the curves in Figs. 3 to 6 were drawn relating rupture life to grain size at the four test temperatures. It can be seen from Fig. 3 that at the lowest temperature the rupture life increases rapidly as the

Table IV
Creep-Rupture Results

Temp. °F	Stress psi	Specimen No.	HEAT F					Type of Fracture
			Average Grain Diam., mm.	Rupture Time, Hrs.	Min. Creep Rate in./in./ 1000 Hrs.	Elonga- tion, %	Red. in Area, %	
700	65,000	RA 6	0.779	<0.1	...	52	62	Transcrys.
		SA 6	0.705	<0.1	...	48	51	Transcrys.
		TA 6	0.214	5.3	4.7	56	69	Transcrys.
		U 6	0.0635	35.0	1.2	54	70	Transcrys.
		V 6	0.0240	201.6	0.73	52	66	Transcrys.
		V 6X	0.0240	217.7	0.87	51	67	Transcrys.
	60,000	RA 1	0.779	<0.1	...	49	55	Transcrys.
		SA 1	0.705	<0.1	...	43	50	Transcrys.
		TA 1	0.214	95.0	0.43	54	59	Transcrys.
		U 1	0.0635	290.5	0.51	50	54	Transcrys.
		V 1	0.0240	3831.0	0.017	36	30	Transcrys. and Intercrys.
900	55,000	RA 12	0.779	71.0	1.1	51	59	Transcrys.
		SA 12	0.705	255.4	0.36	49	58	Transcrys.
		TA 12	0.214	2544+	0.0021	28+	..	Unbroken
	43,000	RA 14	0.779	0.63	94.4	38	25	Transcrys.
		SA 14	0.705	0.60	78.7	32	20	Transcrys.
		TA 14	0.214	6.6	20.4	36	28	Transcrys.
		U 14	0.0635	13.1	12.6	39	37	Transcrys.
		V 14	0.0240	15.1	11.4	40	35	Transcrys.
		TC 14	0.345	2.0	52.5	32	36	Transcrys.
		TB 14	0.153	11.3	14.2	35	33	Transcrys.
	40,000	RA 7	0.779	0.32	101.0	27	28	Transcrys. and Intercrys.
		SA 7	0.705	0.58	62.0	27	23	Transcrys. and Intercrys.
		TA 7	0.214	21.5	4.5	33	26	Transcrys. and Intercrys.
		U 7	0.0635	34.2	3.4	30	27	Transcrys. and Intercrys.
		U 7X	0.0635	28.9	4.6	31	28	Transcrys. and Intercrys.
		V 7	0.0240	36.3	3.6	33	28	Transcrys. and Intercrys.
		V 7X	0.0240	36.5	3.5	32	29	Transcrys. and Intercrys.
		M 7	0.230	7.7	4.7	21	24	Transcrys. and Intercrys.
		MO 7	0.178	24.6	1.7	23	23	Transcrys. and Intercrys.
		MON 7	0.178	24.6	4.1	23	25	Transcrys. and Intercrys.
		TC 7	0.345	11.0	7.5	27	26	Transcrys. and Intercrys.
		TB 7	0.153	30.8	4.4	28	30	Transcrys. and Intercrys.
		TB 71	0.153	29.9	4.5	29	28	Transcrys. and Intercrys.
35,000		RA 9	0.779	2.3	9.2	21	21	Intercrys.
		SA 9	0.705	3.1	13.2	22	15	Intercrys.
		TA 9	0.214	502.2	0.065	18	16	Intercrys.
		U 9	0.0635	168.2	0.36	17	17	Intercrys.
		U 9X	0.0635	140.7	0.40	18	15	Intercrys.
		V 9	0.0240	150.0	0.62	22	19	Intercrys.
		V 9X	0.0240	131.7	0.72	22	20	Intercrys.
		V 9XX	0.0240	146.7	0.44	23	19	Intercrys.
		M 9	0.230	69.5	0.40	16	21	Intercrys.
		MO 9	0.178	74.6	0.42	15	18	Intercrys.
		MO 91	0.178	71.0	0.44	15	16	Intercrys.
		TC 9	0.345	69.9	0.72	20	23	Intercrys.
		TD 9	0.171	193.0	0.26	19	19	Intercrys.
		TD 9X	0.171	373.7	0.11	20	19	Intercrys.
		TB 9	0.153	188.6	0.42	22	26	Intercrys.
		TB 91	0.153	176.4	0.42	22	27	Intercrys.
	32,000	RA 16	0.779	6.7	3.9	17	13	Intercrys.
		SA 16	0.705	7.3	2.8	18	19	Intercrys.
		TA 16	0.214	1949.0	0.020	18	18	Intercrys.
		U 16	0.0635	436.7	0.065	13	11	Intercrys.
		V 16	0.0240	373.0	0.20	20	16	Intercrys.
		TC 16	0.345	350.9	0.083	17	19	Intercrys.
		TC 16X	0.345	187.6	0.099	18	31	Intercrys.
		TD 16	0.171	1114.0	0.045	18	15	Intercrys.
		TB 16	0.153	1013.0	0.056	19	19	Intercrys.

Table IV—(Cont.)
Creep-Rupture Results

HEAT F								
Temp. °F	Stress psi	Specimen No.	Average Grain Diam., mm.	Rupture Time, Hrs.	Min. Creep Rate in./in./ 1000 Hrs.	Elonga- tion, %	Red. in Area, %	Type of Fracture
1100	25,000	RA 3	0.779	0.2	165.0	13	9	Intercrys.
		SA 3	0.705	0.5	54.0	14	13	Intercrys.
		TA 3	0.214	21.7	4.5	31	24	Intercrys.
		TA 3X	0.214	24.2	2.8	30	33	Intercrys.
		U 3	0.0635	24.5	3.5	18	20	Intercrys.
		U 3.	0.0635	17.6	5.2	19	16	Intercrys.
		U 3X	0.0635	16.8	4.6	17	15	Intercrys.
		V 3	0.0240	19.4	8.8	35	29	Intercrys.
		V 3.	0.0240	13.7	12.1	34	27	Intercrys.
		V 3X	0.0240	13.9	11.7	30	25	Intercrys.
		TC 3	0.345	21.9	5.6	26	31	Intercrys.
	20,000	RA 13	0.779	1.8	5.8	9	7	Intercrys.
		SA 13	0.705	2.8	3.0	8	4	Intercrys.
		TA 13	0.214	220.5	0.32	16	10	Intercrys.
		TA 13X	0.214	212.7	0.33	19	18	Intercrys.
		U 13	0.0635	244.5	0.43	18	15	Intercrys.
		U 13X	0.0635	200.4	0.43	17	15	Intercrys.
		U 13XX	0.0635	228.3	0.44	18	14	Intercrys.
		V 13	0.0240	135.0	1.58	42	31	Intercryst.
		V 13X	0.0240	129.5	1.5	42	33	Intercryst.
		V 13XX	0.0240	123.4	1.58	37	34	Intercryst.
		TC 13	0.345	114.5	0.46	16	17	Intercryst.
		TB 13	0.153	210.6	0.46	26	24	Intercryst.
	17,800	RA 11	0.779	24.8	0.61	7	3	Intercryst.
		SA 11	0.705	6.5	1.1	9	3	Intercryst.
		TA 11	0.214	617.0	0.13	14	17	Intercryst.
		U 11	0.0635	699.5	0.17	23	19	Intercryst.
		V 11	0.0240	326.0	0.63	46	37	Intercryst.
		TC 11	0.345	417.7	0.17	14	12	Intercryst.
1300	15,000	RA 15	0.779	2.8	8.0	8	4	Intercryst.
		SA 15	0.705	1.8	9.4	5	3	Intercryst.
		SA 15X	0.705	2.8	6.7	6	3	Intercryst.
		TA 15	0.214	6.7	13.6	18	14	Intercryst.
		U 15	0.0635	9.5	11.5	26	20	Intercryst.
		V 15	0.0240	5.9	41.7	52	40	Intercryst.
		M 15	0.230	7.8	9.0	14	15	Intercryst.
	12,000	RA 8	0.779	22.6	2.1	11	4	Intercryst.
		SA 8	0.705	28.3	1.9	12	9	Intercryst.
		TA 8	0.214	40.7	3.2	22	14	Intercryst.
		TA 8X	0.214	65.6	3.2	21	15	Intercryst.
		U 8	0.0635	34.8	3.9	23	17	Intercryst.
		V 8	0.0240	19.3	10.6	54	36	Intercryst.
		V 8X	0.0240	17.8	9.8	37	28	Intercryst.
		M 8	0.230	45.7	2.0	17	9	Intercryst.
		TD 8	0.171	50.1	4.5	26	22	Intercryst.
		TB 8	0.153	37.3	5.3	19	22	Intercryst.
	9,000	RA 4	0.779	108.0	0.44	8	5	Intercrys.
		SA 4	0.705	156.6	0.46	16	6	Intercrys.
		SA 41	0.705	142.2	0.56	11	9	Intercrys.
		TA 4	0.214	225.2	0.73	24	16	Intercrys.
		TA 4X	0.214	178.3	0.94	23	15	Intercrys.
		U 4	0.0635	148.0	0.94	28	19	Intercrys.
		V 4	0.0240	68.9	1.81	50	32	Intercrys.
		V 4X	0.0240	65.0	2.2	45	29	Intercrys.
		V 4XX	0.0240	66.2	1.3	48	31	Intercrys.
		M 4	0.230	227.2	0.59	20	11	Intercrys.
	7,000	TC 4	0.345	165.6	0.83	18	14	Intercrys.
		TD 4	0.171	181.1	1.1	22	21	Intercrys.
		TB 4	0.153	178.7	0.97	20	15	Intercrys.
		RA 10	0.779	162.0	0.23	10	5	Intercryst.
		SA 10	0.705	341.2	0.20	10	4	Intercryst.
		TA 10	0.214	481.1	0.23	18	12	Intercryst.
		U 10	0.0635	418.3	0.36	28	17	Intercryst.
		V 10	0.0240	142.7	1.1	39	27	Intercryst.
		V 10X	0.0240	163.4	0.87	38	25	Intercryst.

Table IV—(Cont.)
 Creep-Rupture Results

Temp. °F	Stress psi	Specimen No.	HEAT L		Rupture Time, Hrs.	Min. Creep Rate in./in./ 1000 Hrs.	Elonga- tion, %	Red. in Area, %	Type of Fracture
			Average Grain Diam., mm.						
700	65,000	DS 6	0.376		99.6	0.75	47	56	Transcryst.
		DS 61	0.376		54.1	9.0	54	64	Transcryst.
		DS 62	0.376		53.7	2.36	51	64	Transcryst.
		DT 6	0.267		82.0	1.68	55	59	Transcryst.
		DT 61	0.267		20.8	0.79	51	69	Transcryst.
		DT 62	0.267		97.3	0.90	49	59	Transcryst.
		DD 6	0.125		344.0	0.328	46	51	Transcryst.
		DD 61	0.125		440.4	0.131	44	54	Transcryst.
		DU 6	0.0435		476.0	0.197	45	59	Transcryst.
		DU 61	0.0435		415.0	0.23	46	60	Transcryst.
		DU 62	0.0435		561.7	0.197	45	58	Transcryst.
	45,000	DS 20	0.376		7.0	5.82	28	30	Transcrys. and Intercryst.
		DS 201	0.376		10.7	3.3	23	26	Transcrys. and Intercryst.
		DS 202	0.376		5.1	8.74	25	24	Transcrys. and Intercryst.
		DT 20	0.267		21.0	1.94	24	26	Transcrys. and Intercryst.
		DT 201	0.267		20.4	2.57	24	23	Transcrys. and Intercryst.
		DT 202	0.267		18.6	2.04	26	24	Transcrys. and Intercryst.
		DD 20	0.125		30.7	1.55	23	23	Transcrys. and Intercryst.
		DD 201	0.125		50.9	0.728	25	23	Transcrys. and Intercryst.
		DD 202	0.125		30.4	1.80	24	25	Transcrys. and Intercryst.
		DU 20	0.0435		46.8	2.38	34	31	Transcrys. and Intercryst.
		DU 201	0.0435		45.1	2.43	34	33	Transcrys. and Intercryst.
		DU 202	0.0435		29.1	3.54	34	35	Transcrys. and Intercryst.
		DU 203	0.0435		45.7	2.77	33	34	Transcrys. and Intercryst.
	40,000	DS 7	0.376		52.4	0.473	20	18	Transcrys. and Intercryst.
		DS 71	0.376		61.0	0.328	17	15	Transcrys. and Intercryst.
		DS 72	0.376		37.7	0.485	23	20	Transcrys. and Intercryst.
		DT 7	0.267		89.2	0.291	19	15	Transcrys. and Intercryst.
		DT 72	0.267		90.7	0.225	20	19	Transcrys. and Intercryst.
		DD 7	0.125		212.3	0.131	18	20	Transcrys. and Intercryst.
		DD 71	0.125		287.7	0.082	16	15	Transcrys. and Intercryst.
		DD 72	0.125		303.4	0.098	20	19	Transcrys. and Intercryst.
		DU 7	0.0435		259.0	0.23	22	20	Transcrys. + Intercryst.
		DU 71	0.0435		330.6	0.164	23	20	Transcrys. + Intercryst.
		DU 72	0.0435		294.2	0.197	23	23	Transcrys. + Intercryst.
1100	28,000	DS 5	0.376		6.8	9.23	23	28	Intercryst.
		DT 5	0.267		12.2	7.72	27	31	Intercryst.
		DD 5	0.125		11.3	9.18	28	31	Intercryst.
		DD 51	0.125		13.4	10.15	30	27	Intercryst.
		DU 5	0.435		10.3	14.0	31	29	Intercryst.
		DS 3	0.376		31.2	1.31	14	15	Intercryst.
	25,000	DS 31	0.376		34.8	1.41	17	14	Intercryst.
		DS 32	0.376		28.3	1.36	16	19	Intercryst.
		DS 33	0.376		24.5	1.80	16	15	Intercryst.
		DT 3	0.267		41.4	1.31	18	19	Intercryst.
		DT 31	0.267		44.8	1.21	18	23	Intercryst.
		DT 32	0.267		49.3	1.26	20	20	Intercryst.
		DT 33	0.267		45.6	1.02	20	21	Intercryst.

Table IV—(Cont.)
Creep-Rupture Results

Temp. °F	Stress psi	Specimen No.	HEAT L					Type of Fracture
			Average Grain Diam., mm.	Rupture Time, Hrs.	Min. Creep Rate in./in./ 1000 Hrs.	Elonga- tion, %	Red. in Area, %	
1100	25,000	DD 3	0.125	44.2	1.85	23	23	Intercryst.
		DD 31	0.125	48.8	1.46	18	19	Intercryst.
		DD 32	0.125	56.6	1.21	21	24	Intercryst.
		DD 33	0.125	55.6	1.75	23	20	Intercryst.
		DU 3	0.0435	50.6	2.62	28	26	Intercryst.
		DU 31	0.0435	46.8	2.96	28	25	Intercryst.
		DU 32	0.0435	44.0	3.20	29	26	Intercryst.
		DU 33	0.0435	44.5	3.30	29	27	Intercryst.
1300	15,000	DS 15	0.376	8.8	6.02	12	14	Intercryst.
		DS 151	0.376	9.8	5.87	12	17	Intercryst.
		DT 15	0.267	12.8	6.40	14	14	Intercryst.
		DT 151	0.267	14.5	5.44	17	12	Intercryst.
		DT 152	0.267	17.6	6.55	18	17	Intercryst.
		DD 15	0.125	13.0	10.5	22	19	Intercryst.
		DD 151	0.125	13.3	10.6	23	17	Intercryst.
		DU 15	0.0435	9.7	18.65	33	26	Intercryst.
		DU 151	0.0435	9.7	18.95	35	28	Intercryst.
	9,000	DS 4	0.376	186.5	0.525	14	9	Intercryst.
		DS 41	0.376	187.3	0.525	16	9	Intercryst.
		DS 42	0.376	179.2	0.525	14	9	Intercryst.
		DT 4	0.267	206.8	0.557	20	11	Intercryst.
		DT 41	0.267	198.0	0.492	18	9	Intercryst.
		DT 42	0.267	207.5	0.622	18	11	Intercryst.
		DD 4	0.125	201.3	0.917	28	18	Intercryst.
		DD 41	0.125	175.4	1.08	29	18	Intercryst.
		DD 42	0.125	181.0	0.945	27	20	Intercryst.
		DU 4	0.0435	100.8	1.31	35	25	Intercryst.
		DU 41	0.0435	100.0	1.21	38	24	Intercryst.
		DU 42	0.0435	95.7	0.827	38	25	Intercryst.

grain size decreases. On the other hand, at high temperatures (Figs. 5 and 6), the longest rupture life corresponds to an intermediate grain size.

The magnitude of the grain size effect at low temperatures can be illustrated by the specimens tested at 700 °F (370 °C) and 60,000 psi. The coarse-grained specimen fractured on loading, whereas the finest-grained specimen of the same heat lasted 3831 hours.

A change in the effect of grain size on rupture time occurred at 900 °F (480 °C). Behavior at the high stresses (40,000 and 43,000 psi) was similar to that at 700 °F (370 °C), while at the low stresses (32,000 and 35,000 psi) there appeared to be an optimum grain size for maximum rupture life. On the basis of the nature of the fracture (indicated in Table IV) as well as the results of the rupture tests, this temperature of 900 °F (480 °C) appears to be approximately the equicohesive temperature for Monel. At this temperature, the fracture was both transcrystalline and intercrystalline. Below 900 °F (480 °C), failure occurred by transcrystalline fracture, with the exception of one long-time test, while above this temperature all fractures were intercrystalline.

At high temperatures (Figs. 5 and 6) an optimum grain size effect is clearly indicated. The optimum grain size range is different for each temperature and is also affected by the stress; in no case

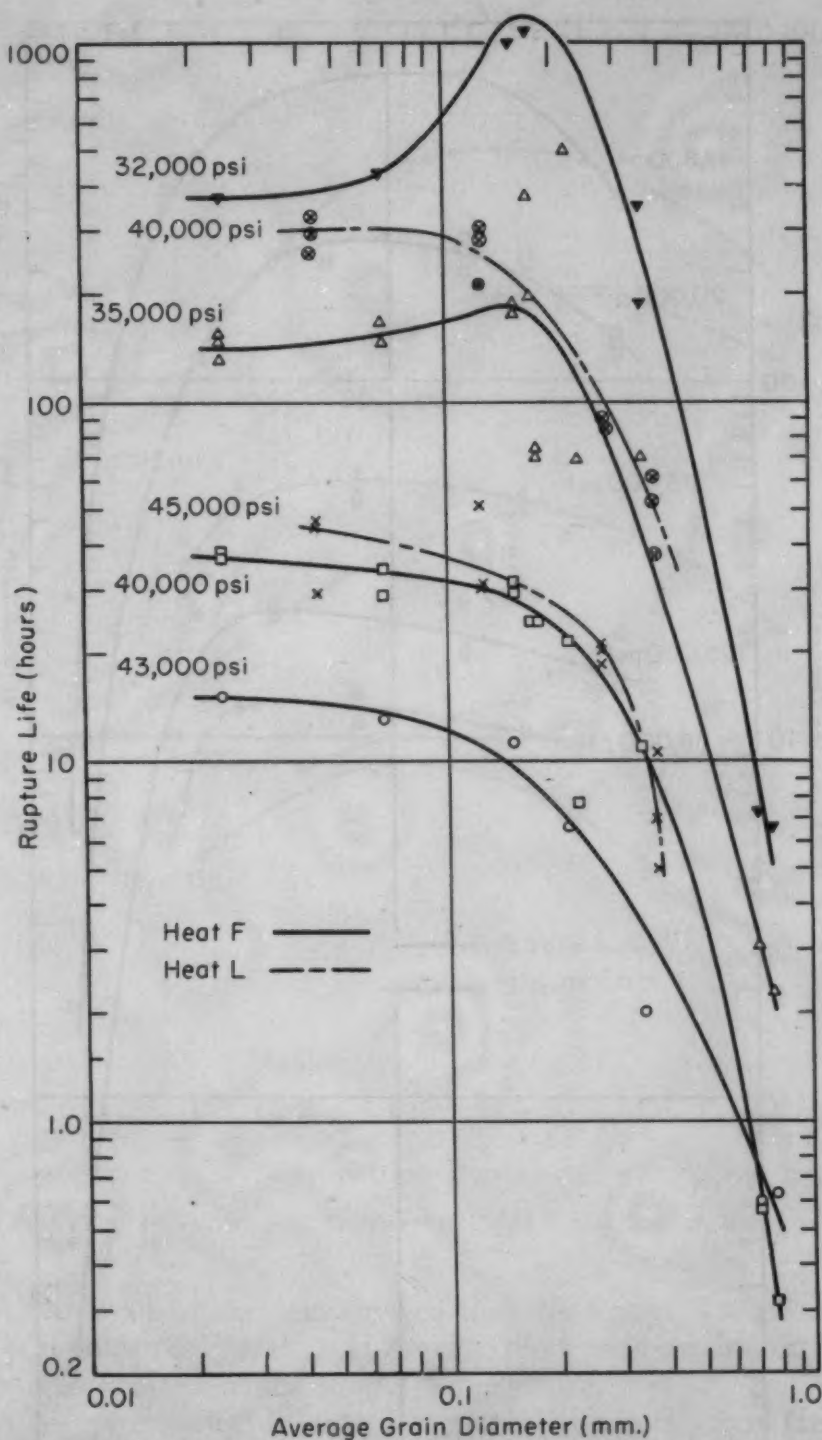


Fig. 4—Variation of Rupture Life With Grain Size of Monel at 900 °F (480 °C).

was the optimum grain size the coarsest size tested. The increase in the optimum grain size with increasing temperature as was found here for rupture life is similar to results obtained by Weaver (8) on creep strength.

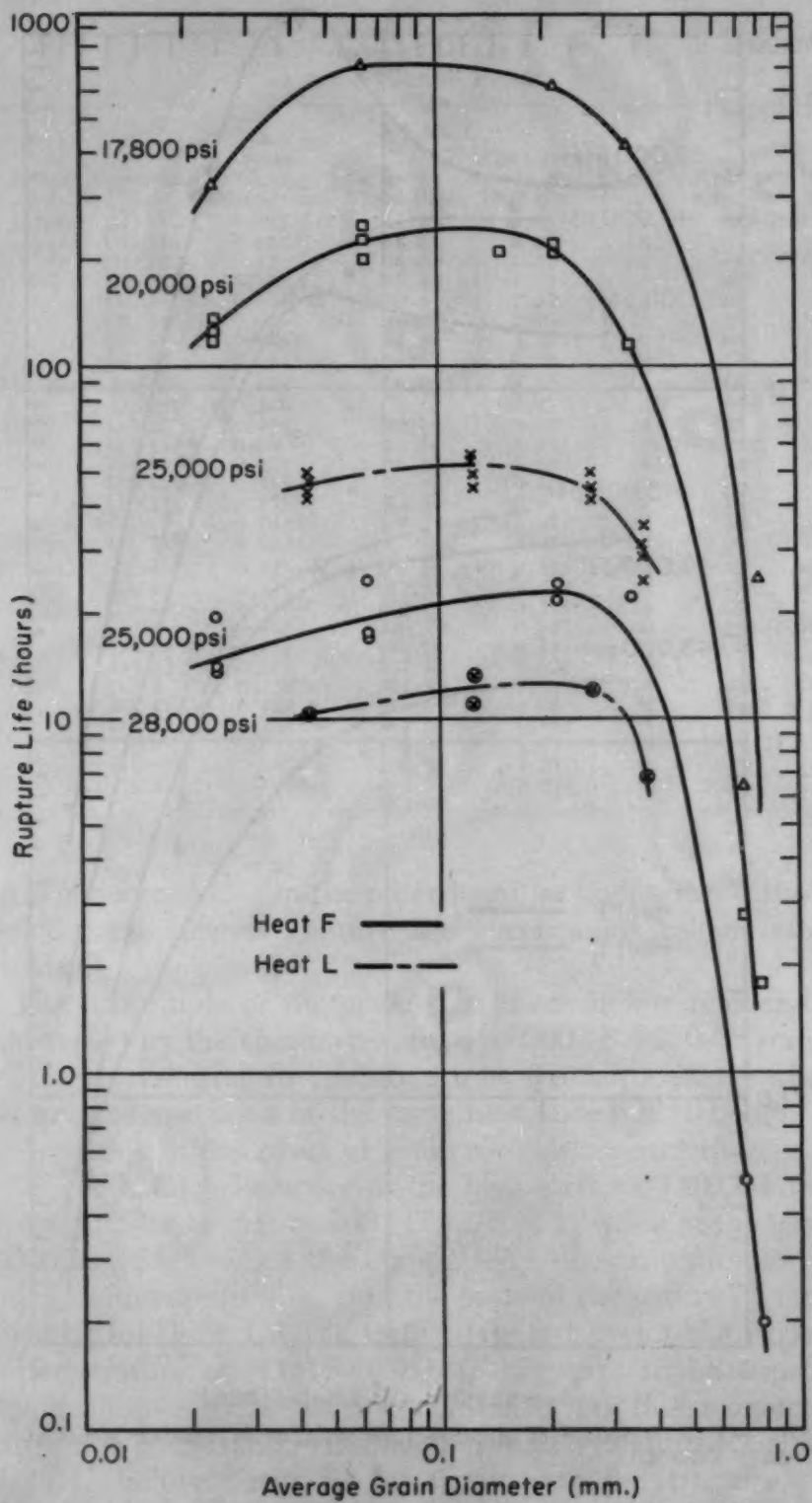


Fig. 5—Variation of Rupture Life With Grain Size of Monel at 1100 °F (595 °C).

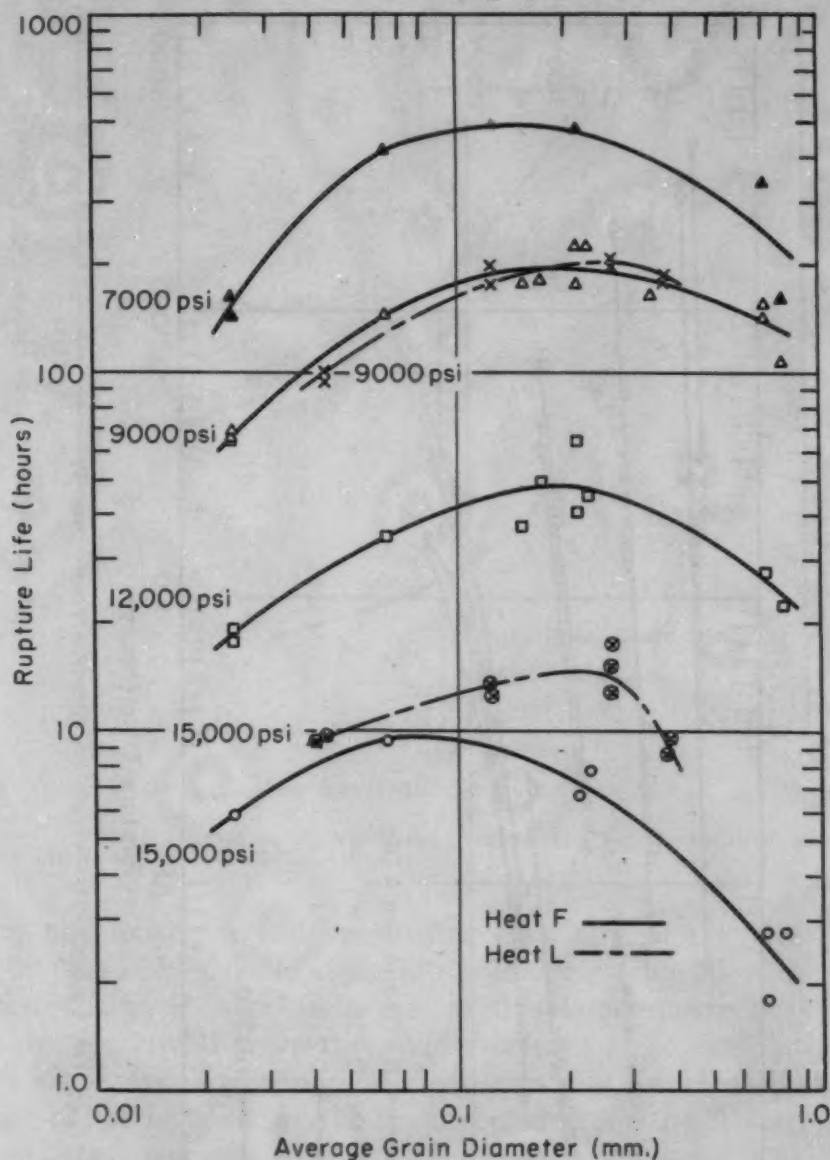


Fig. 6—Variation of Rupture Life With Grain Size of Monel at 1300 °F (705 °C).

An analysis of the data showed that the scatter was of the same degree at all stress levels. However, there was an indication that scatter was greatest at the lowest temperature.

A log stress – log rupture life plot of the data from Heat F is shown in Fig. 7. At the highest temperature the lines tend to curve downward and are not straight as usually found on log-log plots. This tendency to depart from a straight line is greatest with the coarsest grain specimens.

The minimum-creep-rate values, like the rupture lives, showed an optimum grain size effect at many combinations of temperature and stress. The plots for the four temperatures are shown in Figs.

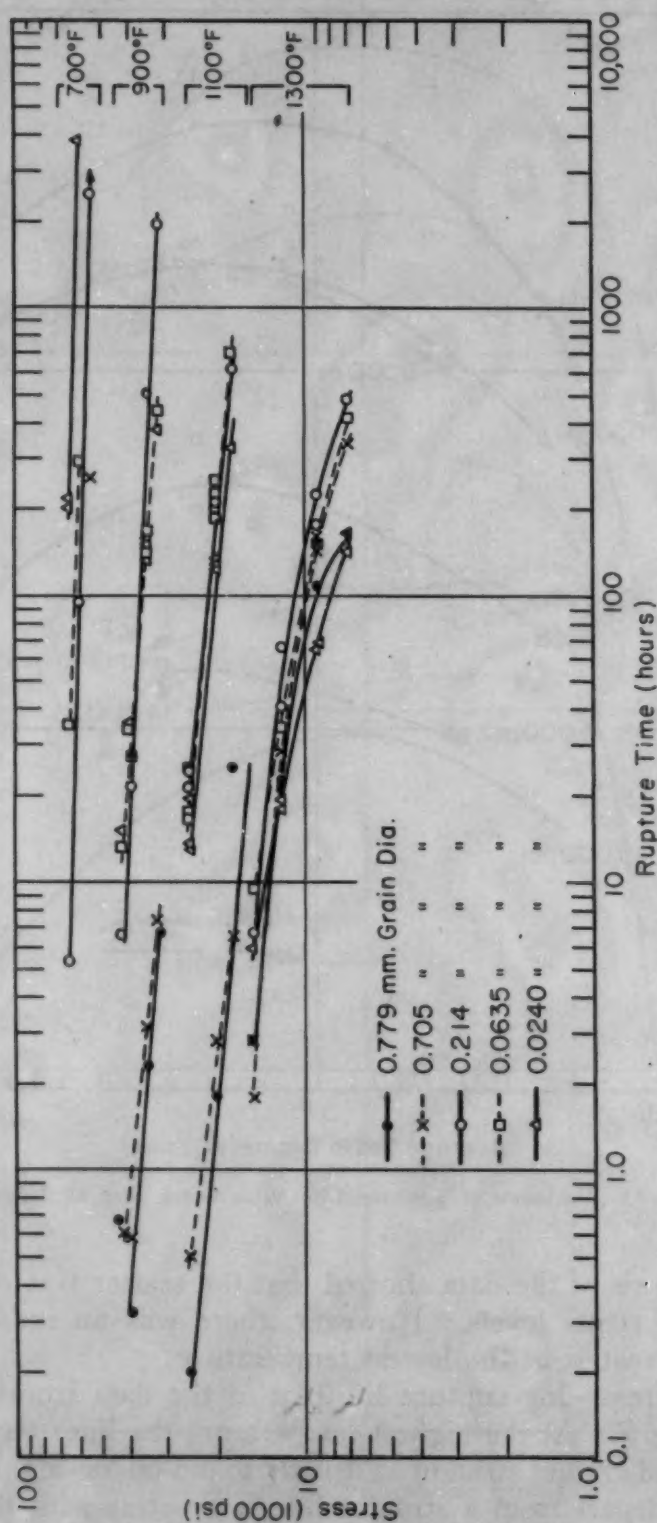


Fig. 7—Log Stress Versus Log Rupture Time—Heat F.

8 to 11. The optimum effect was observed at all stresses tested at 1100 °F (595 °C), and, with two exceptions, at 900 °F (480 °C). At 700 °F (370 °C), an optimum grain size for the lowest creep

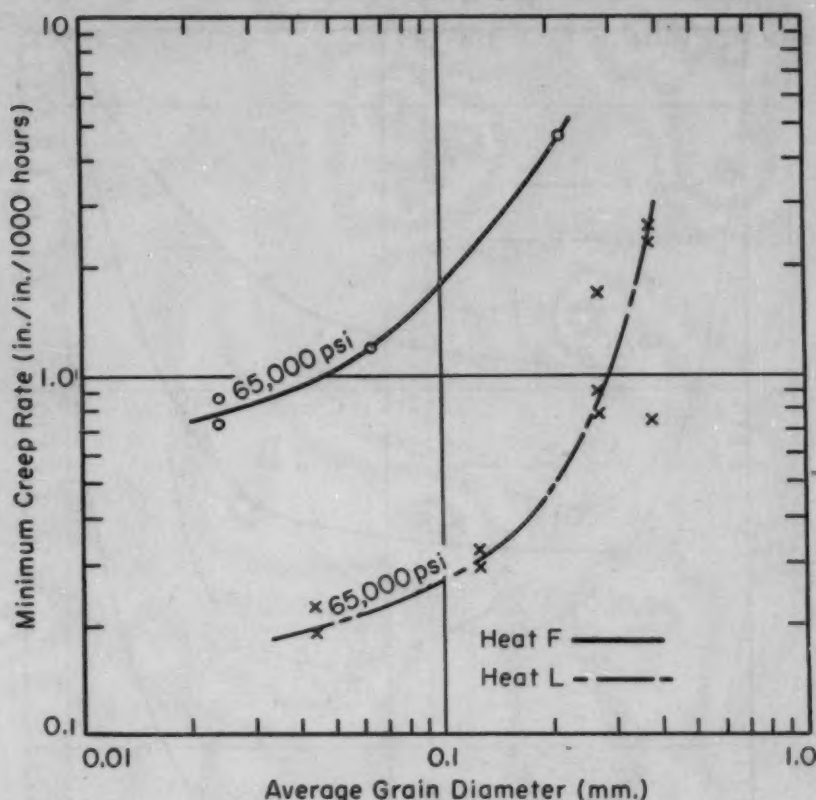


Fig. 8—Variation of Minimum Creep Rate With Grain Size of Monel at 700 °F (370 °C).

rate, if one exists, would be smaller than any of the sizes tested. At 1300 °F (705 °C), the creep rate was decreasing up to the largest size tested, and it is possible that at this temperature an optimum grain size for lowest creep rate might exist at some even larger size.

A log stress – log minimum creep rate plot for Heat F is shown in Fig. 12; it is what would be expected from the log stress – log rupture time curves.

Ductility as Influenced by Grain Size and Temperature. Figs. 13, 14, 15 and 16 show the change in total elongation (elongation at fracture) with grain size and stress for the various testing temperatures. At 700 and 900 °F (370 and 480 °C), the elongation varies only moderately with grain size; an optimum grain size is suggested by the data at 700 °F (370 °C), while at 900 °F (480 °C) there is a slight decrease with increasing grain size. The elongation increases with an increase in stress. In general, at 1100 and 1300 °F (595 and 705 °C), the decrease in elongation with increasing grain size is much more pronounced. An anomalous behavior was observed with Heat F at 25,000 psi for which no explanation is apparent. The elongation at these temperatures decreased from 35 to 50% at the finest grain size to 5 to 15% for the coarsest size.

Reduction-in-area data, Table IV, followed the pattern of total

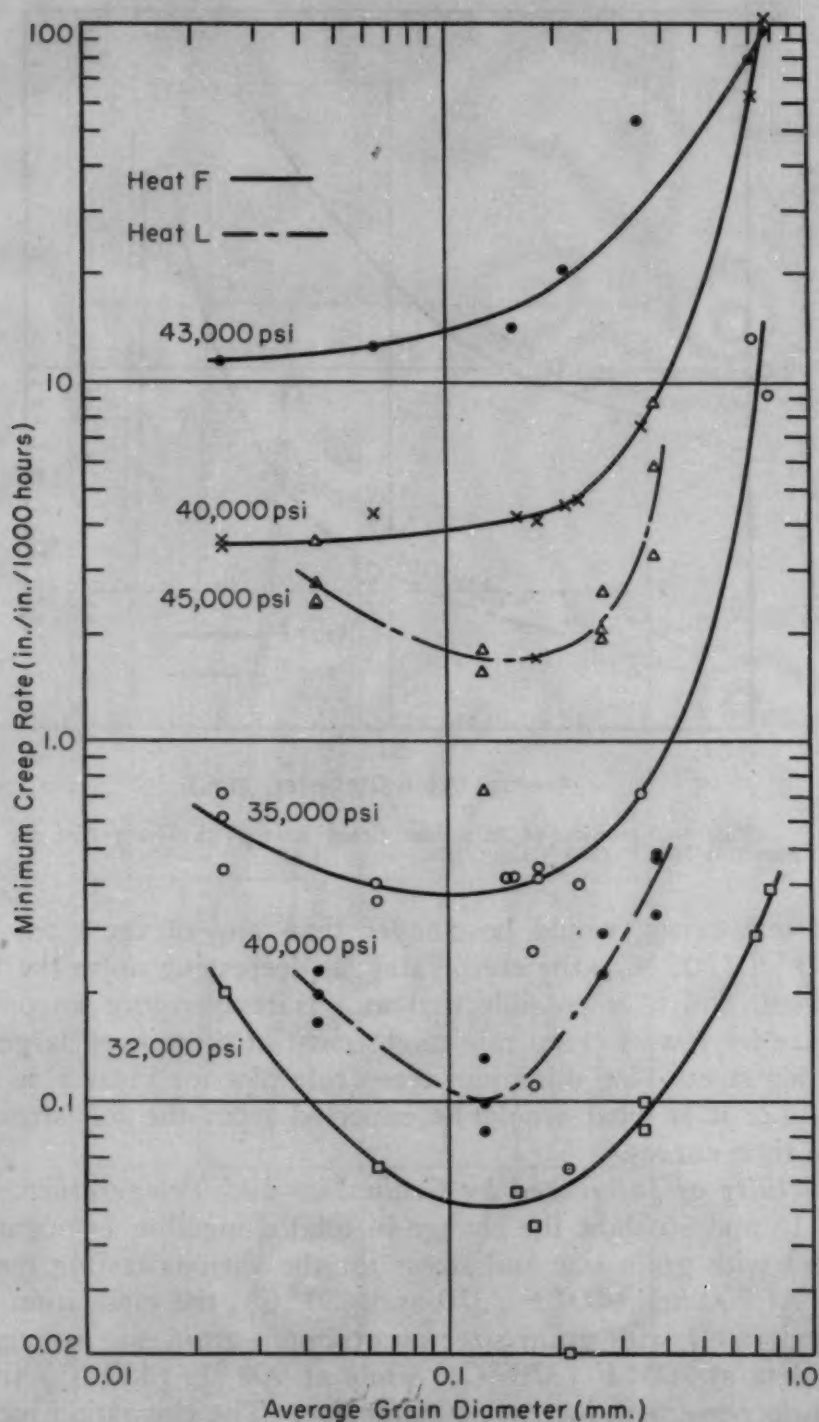


Fig. 9—Variation of Minimum Creep Rate With Grain Size of Monel at 900 °F (480 °C).

elongation values, with both having about the same numerical value in the equicohesive range. However, below this range (900 to 1100 °F), the per cent reduction-in-area was generally greater than the per cent total elongation, while above the range the reverse was true.

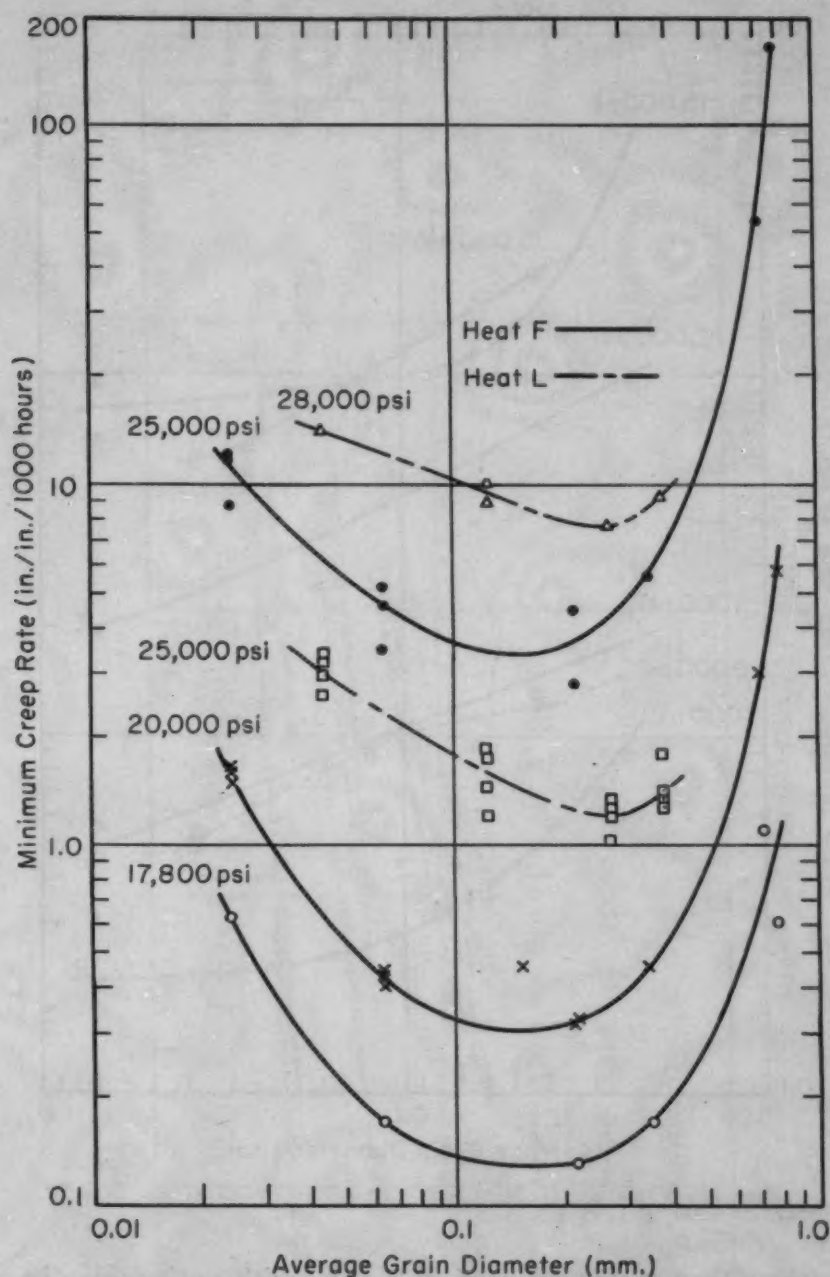


Fig. 10—Variation of Minimum Creep Rate With Grain Size of Monel at 1100 °F (595 °C).

Influence of Composition. The two heats, L and F, varied slightly in composition as shown in Table I. However, this small difference in composition resulted in sizable variations in rupture life, creep rate, and elongation. The effects due to difference in heats are much greater at low temperatures than at high temperatures and may be of the same magnitude as the grain size effect.

CONCLUSIONS

1. At low temperatures, grain size has a pronounced influence

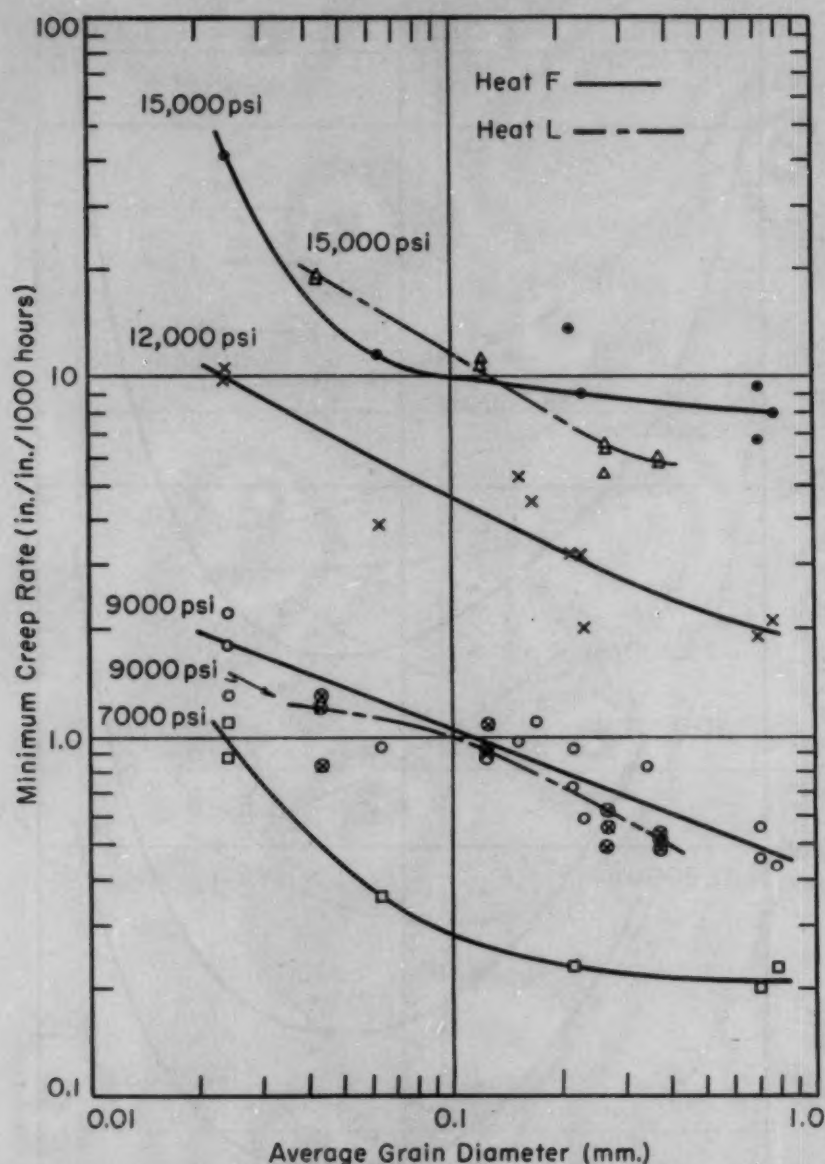


Fig. 11—Variation of Minimum Creep Rate With Grain Size of Monel at 1300 °F (705 °C).

on time-to-rupture and creep rate of Monel, with an increase in grain size producing shorter rupture times and higher creep rates.

2. At high temperatures, there is an optimum grain size for maximum rupture time.

3. There may or may not be an optimum grain size for the lowest minimum creep rate depending on the temperature and stress. At 900 and 1100 °F (480 and 595 °C) there is an optimum grain size, but at 1300 °F (705 °C) the minimum creep rate decreases with increase in grain size.

4. The influence of grain size on total elongation is small below the equicohesive temperature, but above the equicohesive temperature, total elongation generally increases with decrease in grain size. Also,

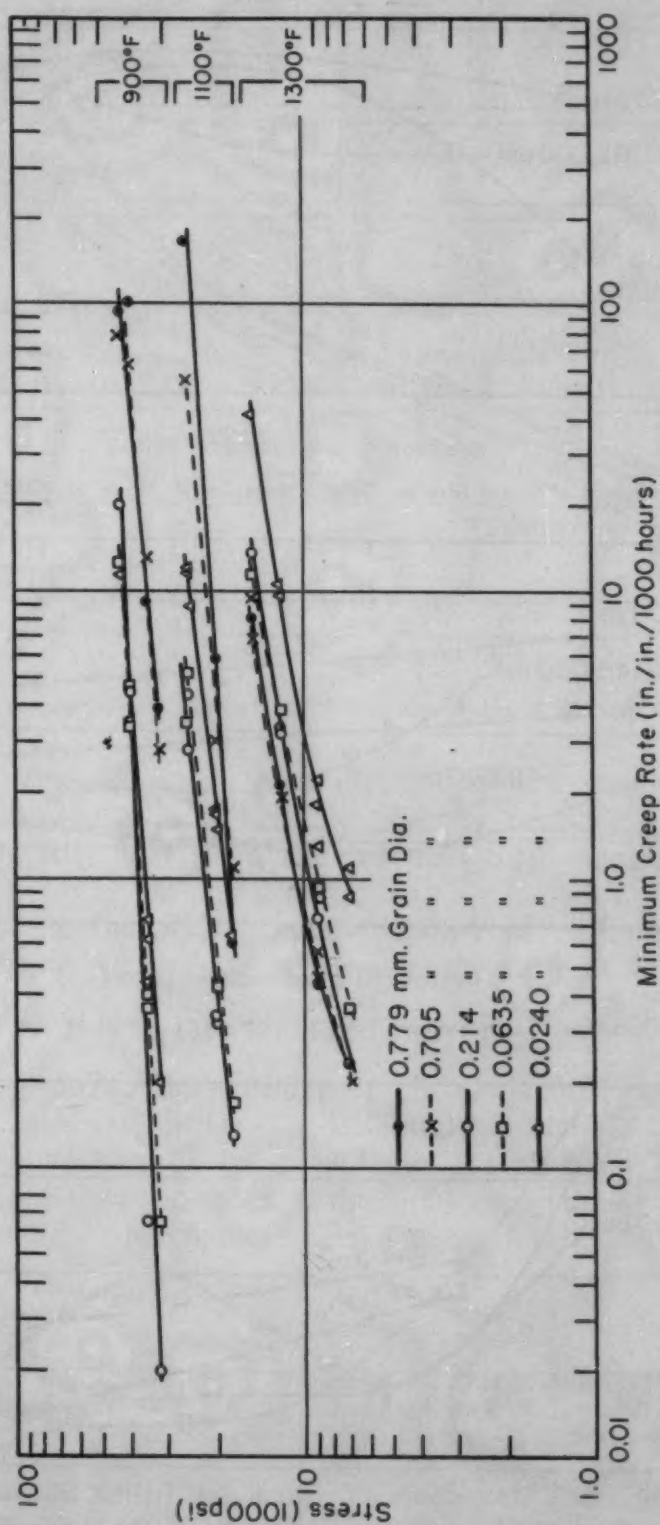


Fig. 12—Log Stress Versus Log Minimum Creep Rate—Heat F.

above the equicohesive temperature, the elongation of fine-grained Monel increases with increase in temperature.

5. Reduction-in-area values vary with grain size in the same

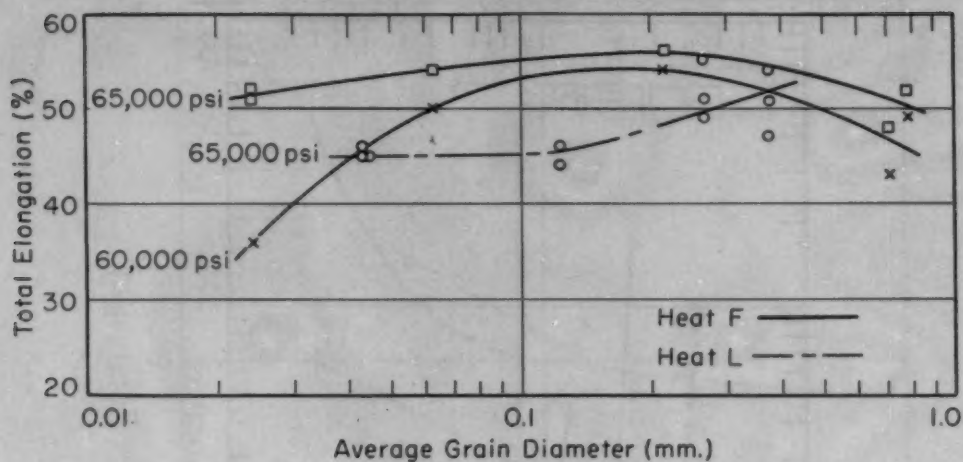


Fig. 13—Influence of Grain Size on Total Elongation of Monel at 700 °F (370 °C).

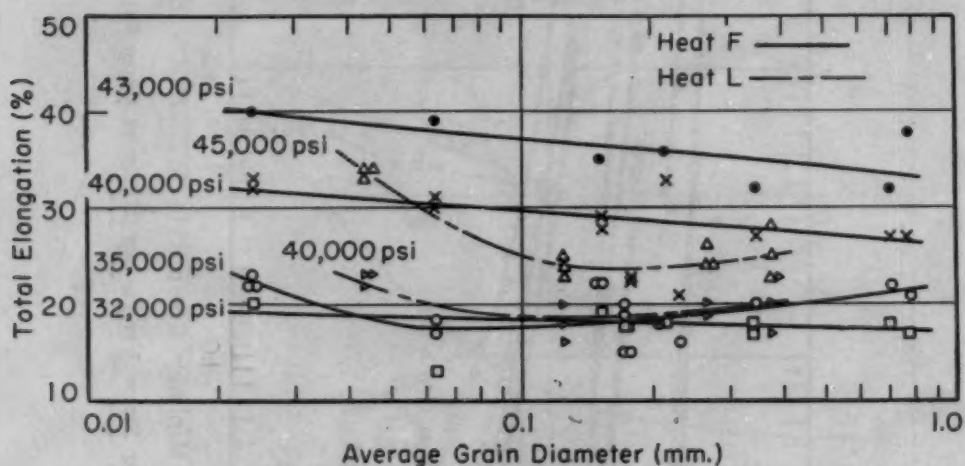


Fig. 14—Influence of Grain Size on Total Elongation of Monel at 900 °F (480 °C).

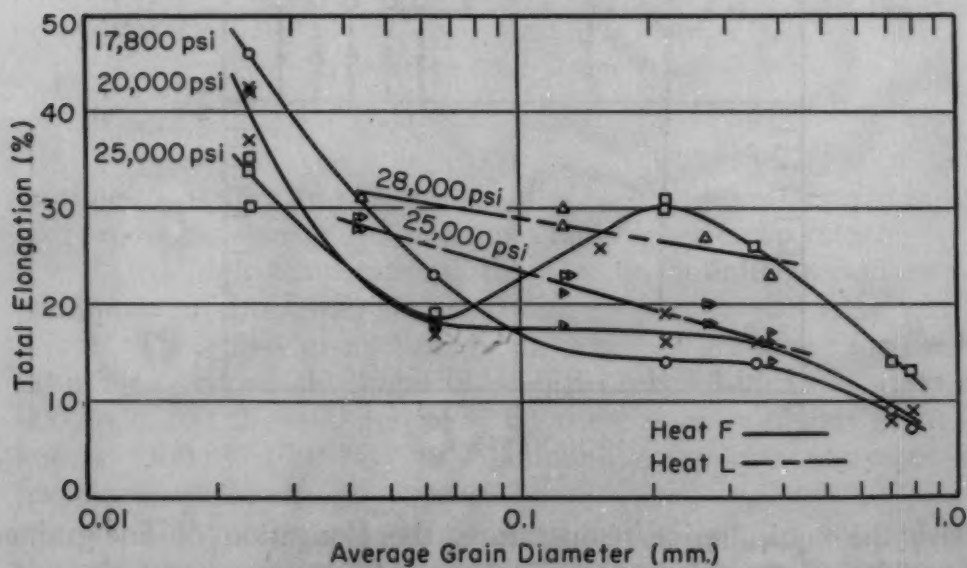


Fig. 15—Influence of Grain Size on Total Elongation of Monel at 1100 °F (595 °C).

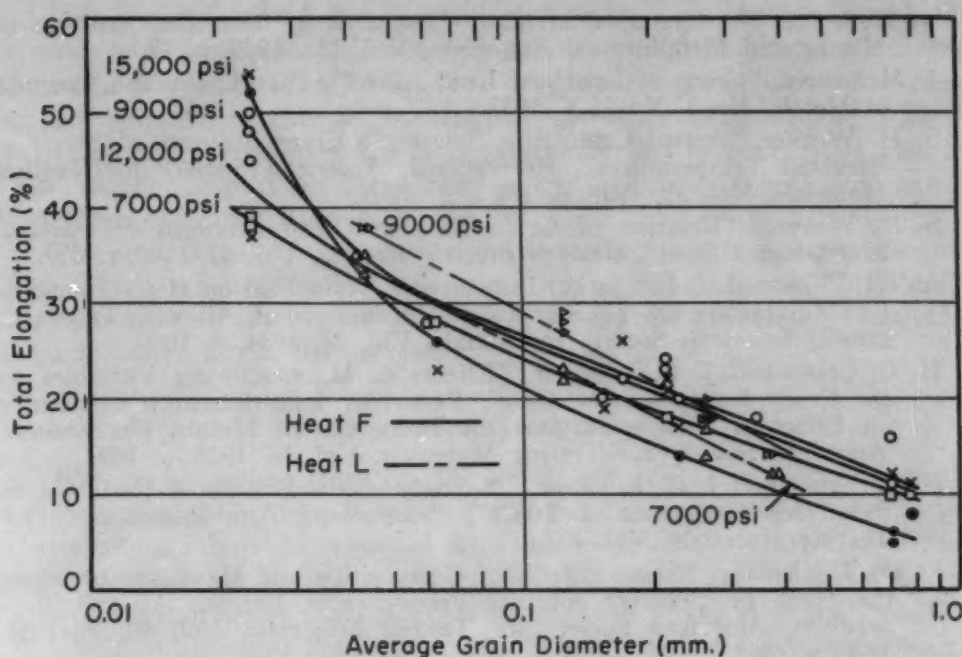


Fig. 16—Influence of Grain Size on Total Elongation of Monel at 1300 °F (705 °C).

manner as total elongation. Generally, at low temperatures, the per cent reduction-in-area is higher than the per cent total elongation, whereas at high temperatures the per cent total elongation is the higher.

6. The influence of different heats on rupture time and creep rate is significant, particularly at lower temperatures.

ACKNOWLEDGMENT

This program was inaugurated by Dr. D. J. Blickwede, and the results were reviewed by Dr. O. T. Marzke. The tests were conducted by Mr. William O. Baker and Mr. Joseph Fiege. Mr. Donaldson prepared most of the metallographic specimens, and Dr. S. Thompson of the Mechanics Division conducted the statistical analysis.

References

1. C. L. Clark and A. E. White, "Influence of Recrystallization Temperature and Grain Size on the Creep Characteristics of Non-Ferrous Alloys", *Proceedings, American Society for Testing Materials*, Vol. 32, 1932, p. 492.
2. H. L. Burghoff, A. I. Blank and S. E. Maddigan, "The Creep Characteristics of Some Copper Alloys at Elevated Temperatures", *Proceedings, American Society for Testing Materials*, Vol. 42, 1942, p. 668.
3. D. Hanson and E. J. Sandford, "The Creep of Tin and Tin Alloys", *Journal, Institute of Metals*, No. 1, Vol. LXII, 1938.
4. E. R. Parker and C. F. Riisness, "Effect of Grain Size and Bar Diameter on Creep Rate of Copper at 200 °C", *Transactions, American Institute of Mining and Metallurgical Engineers*, Vol. 156, 1944, p. 117.

5. D. Hanson, "The Creep of Metals", *Transactions*, American Institute of Mining and Metallurgical Engineers, Vol. 133, 1939, p. 15.
6. J. McKeown, "Creep of Lead and Lead Alloys", Part I, *Journal*, Institute of Metals, No. 1, Vol. LX, 1937.
7. S. H. Weaver, "Actual Grain Size Related to Creep Strength of Steels at Elevated Temperatures", *Proceedings*, American Society for Testing Materials, Vol. 38, 1938, p. 176.
8. S. H. Weaver, "Relation of Grain Size to Creep Strength of Carbon-Molybdenum Steel", *General Electric Review*, Vol. 43, 1940, p. 357.
9. A. E. White and C. L. Clark, "Influence of Grain Size on High Temperature Characteristics of Ferrous and Non-Ferrous Alloys", *TRANSACTIONS*, American Society for Metals, Vol. 22, 1934, p. 1069.
10. H. C. Cross and J. G. Lowther, "Effects of Manufacturing Variables on the Creep Resistance of Steels", Report of Joint Research Committee on Effect of Temperature on the Properties of Metals, *Proceedings*, American Society for Testing Materials, Vol. 38, 1938, p. 149.
11. H. C. Cross and J. G. Lowther, "A Study of the Effects of Variables on the Creep Resistance of Steels", *Proceedings*, American Society for Testing Materials, Vol. 40, 1940, p. 125.
12. R. H. Thielemann, "Some Effects of Composition and Heat Treatment on the High Temperature Rupture Properties of Ferrous Alloys", *Proceedings*, American Society for Testing Materials, Vol. 40, Part II, 1940, p. 788.
13. R. F. Miller, "Effect of Deoxidation Practice on Creep Strength of Carbon-Molybdenum Steel at 850 and 1000 °F", *Transactions*, American Society of Mechanical Engineers, Vol. 65, 1943, p. 309.
14. C. L. Clark and J. W. Freeman, "The Apparent Influence of Grain Size on the High Temperature Properties of Austenitic Steels", *TRANSACTIONS*, American Society for Metals, Vol. 38, 1947, p. 148.
15. N. J. Grant, "Structural Variations in Gas Turbine Alloys Revealed by the Stress Rupture Tests", *TRANSACTIONS*, American Society for Metals, Vol. 39, 1946, p. 335.
16. G. V. Smith, "Properties of Metals at Elevated Temperatures", McGraw-Hill Book Co., Inc., 1950, p. 277.

DISCUSSION

Written Discussion: By C. S. Roberts, Metallurgical Laboratories, The Dow Chemical Company, Midland, Mich.

From the study of a single-phase alloy of commercial use the authors have revealed both practical and fundamental aspects of the grain size effect. In fact, there is some information of basic value which remains to be extracted in the future from their findings.

The existence of a minimum in the secondary creep rate as a function of grain size for zinc tested at 95 °C and for aluminum tested at 200 °C was proved by Crussard.² Although he is little quoted in our literature, he was probably the first to explain clearly this variation and to use it to illustrate the predicted transition of the major deformation process from the boundary to the grain as the volume-to-boundary-area ratio increased. At the optimum grain size, each process is of equal importance in controlling the minimum creep rate. This comprehensive experimental study certainly has confirmed his findings and his analysis.

²C. Crussard, "The Influence of Grain Size on Creep Rate", *Comptes rendus*, Vol. 219, 1944, p. 681.

It is general knowledge that the deformation at the grain boundary becomes more important as creep rate decreases and temperature increases. The authors' results show an increase of optimum grain size with decreasing minimum creep rate at constant temperature (Fig. 9) and with increasing temperature at constant minimum creep rate (Figs. 9 and 10). Thus, in this respect also, the results are in harmony with our general knowledge of deformation in creep.

The analysis of the cooperation between the various deformation processes which are necessary to preserve intercrystalline continuity during creep should be made eventually. These curves and similar ones should be of quantitative use in the problem.

Authors' Reply

We are pleased to learn of this short paper of Crussard. A more detailed discussion by him is given in *Metal Treatment* (Charles Crussard, "Creep and Fatigue as Affected by Grain Boundaries", *Metal Treatment*, Vol. XIV, Autumn 1947). A minimum in the creep-rate versus grain size curve was reported as early as 1939 by Hanson (Reference 5).

The interaction of temperature, minimum creep rate and optimum rate as suggested by Dr. Roberts would conform to the general understanding of this subject, but we feel that his conclusion concerning a change in optimum grain size with minimum creep rate is not fully justified on the basis of our data.

RECRYSTALLIZATION AND GRAIN GROWTH IN ALPHA BRASS

BY S. L. CHANNON AND H. L. WALKER

Abstract

Cold-rolled commercially pure 70/30 cartridge brass samples of different initial grain sizes were annealed isothermally at various temperatures for various times. The recrystallized grain size "r" was independent of the temperature of annealing, and was related to the degree of deformation "d" by the equation

$$\log r = nd^{1/2} + \log m$$

where "n" is constant and "m" is a function of initial grain size. Initial grain size "i" was related to the recrystallized grain size "r" by the equation

$$r = bi^a$$

where "a" is constant and "b" is a function of deformation. Grain growth in commercially pure brass was shown to be a continuous process up to annealing times of 10^7 seconds, but the presence of impurities interrupted the growth process. An equilibrium grain size was not definitely established up to 10^7 seconds.

The heat of activation for recrystallization decreased with increasing deformation and decreasing initial grain size, reaching a lower limit of 41 kilocalories per mole. The "quasi-heat of activation" for average grain growth in this material was 61 kilocalories per mole and was essentially independent of prior deformation or initial grain size.

INTRODUCTION

A COMPLETE review of the literature on recrystallization and grain growth would be superfluous, since excellent reviews have been written by various authors, of whom the most recent have been Mehl (16),¹ Anderson (17) and Burke (13).

¹The figures appearing in parentheses pertain to the references appended to this paper.

This paper represents part of a thesis submitted by S. L. Channon in partial fulfillment of the requirements for the degree of Doctor of Philosophy at the University of Illinois, February 1951.

A paper presented before the Thirty-fourth Annual Convention of the Society, held in Philadelphia, October 18 to 24, 1952. Of the authors, S. L. Channon, formerly graduate research assistant, University of Illinois, is now associated with the Physical Metallurgy Department, Division of Metallurgical Research, Kaiser Aluminum and Chemical Corp., Spokane, Wash., and H. L. Walker is head, Department of Mining and Metallurgical Engineering, University of Illinois, Urbana, Ill. Manuscript received January 18, 1952.

In a previous investigation (1), it was found that, when cold-worked brass of a particular initial grain size was annealed isothermally, the recrystallized grain size "r" decreased with increasing deformation "d" according to the relation

$$\log r = nd^{\frac{1}{n}} + \log m$$

where "n" and "m" are constants. Greis and Esser (18) and Schroeder and Matthaes (19) made the only quantitative study of the effect of initial grain size on the critical deformation, but no information was given concerning the effect of initial grain size on the recrystallized grain size. The present work was undertaken to determine whether the above equation was valid for brasses with different initial grain sizes and to determine the effects of deformation and initial grain size on the recrystallized grain size and heat of activation for recrystallization.

Several investigators (1, 12, 13) have studied grain growth in cartridge brass, with particular reference to the equilibrium grain size. It was concluded that apparently an equilibrium grain size was reached at long annealing times, since the grain growth curves tend to level off at a constant grain size. The authors believed that further data were required at very long annealing times to definitely establish whether an equilibrium grain size existed.

MATERIALS

The brass used in this investigation was Test Lot 590 of commercially pure cartridge brass supplied by Western Cartridge Company, East Alton, Ill. The analysis of this material is shown in Table I.

Table I
Analysis of Brass

Element	Weight, %
Copper	70.16
Lead	0.026
Iron	0.020
Phosphorus	Nil
Tin	Nil
Zinc	Balance

The rolling schedule was designed to produce strips of constant thickness for experimental annealing.

In Table II, the deformations, initial grain sizes and code symbols of the material which formed the basis of the investigation are listed.

It was intended that the grain size levels for the materials would be 0.100 and 0.010 millimeter respectively, but, during processing, coils A and C were found to have initial grain sizes of 0.068 milli-

meter, and coils E, R and T had initial grain sizes of 0.066 millimeter. Coils B, D and F had markedly different initial grain sizes, 0.012, 0.004 and 0.006 millimeter respectively.

Table II
Deformation and Initial Grain Size of Brass

Coil Code Symbol	Deformation (Reduction of Thickness) %	Grain Size Found by Jeffries Method* mm.	Hardness	
			RH	V.H.N.
A	20.5	0.068	111	...
B	20.5	0.012	117	...
C	40.4	0.068	117	...
D	40.4	0.004	120	...
E	61.8	0.066	120	...
F	61.8	0.006	122	...
R	90.2	0.066	...	264
S	90.2	0.006	...	260
T	94.5	0.066	...	269
U	Slightly greater than 90.2	0.006	...	260

*Average of at least 6 separate grain counts.

EXPERIMENTAL PROCEDURE

Annealing—A liquid salt bath was found to be the most suitable specimen heating medium, since this provided a fast rate of heating of the specimen to the bath temperature, and dezincification and corrosion of the specimens were only slight. The molten salt was contained in a steel pot about 12 inches deep and 5 inches diameter which was suspended in a Hevi-Duty Type HD-612 8-Kilowatt Pot Furnace. The temperature of the salt pot was controlled by a chromel-alumel thermocouple with the hot junction in the vicinity of the heating coils of the furnace, and the cold junction incorporated in a Leeds and Northrup Micromax Model C potentiometric controller. This method of control produced a uniform temperature in the salt bath in spite of temperature fluctuations of $\pm 10^{\circ}\text{F}$ in the heating coil zone.

The true annealing time represents the time at which the specimen was annealed after reaching the temperature of the bath. The

Table III
Heating Times at Various Temperatures

Temperature $^{\circ}\text{C}$	Time for Specimen to Reach Bath Temperature Seconds
300	32
350	30
400	29
500	25
550	23
600	21
650	19
700	16

heating times for specimens of 0.062 inch thickness are shown in Table III. Heating times for specimens of 0.016 and 0.009 inch thickness were not determined.

Hardness Measurements—The course of recrystallization was followed by both hardness determinations and metallographic examination. The Rockwell hardness testing machine (H scale) was used to detect the relative changes in hardness produced by cold working and subsequent annealing of the specimens of 0.062 inch thickness. These numbers are only relative, since Rockwell H numbers above 100 are not considered reliable for absolute hardness measurements. A minimum of three hardness readings was made on each specimen.

Hardness measurements were made on the material of 0.016 and 0.009 inch thickness with the Vickers hardness testing machine using a 1-kilogram load.

Grain Size Determination—Specimens were electrolytically polished in an aqueous solution of 550 grams per liter of orthophosphoric acid and etched in a mixture of 6 parts of a 50% ammonium hydroxide solution with 1 part of 3% hydrogen peroxide.

Microstructures were recorded directly on Kodabromide paper. Ten photomicrographs were taken on each specimen and the grain size was determined by the Jeffries (2) method of inscribing a circle of 79.8 millimeters diameter on the photomicrograph and counting the number of grains entirely included within the circle plus one-half of the number of grains intersected by the circle. The magnification was selected so that at least 50 grains were included in the circle whenever possible. An attempt was made to measure grain sizes in very fine-grained material by the use of X-ray diffraction patterns but this was unsuccessful, since the grain size which it was desired to measure was within the range of 10^{-3} to 10^{-6} cm, in which it is very difficult to estimate grain sizes from diffraction patterns (3).

Isothermal Recrystallization Anneal—Specimens about 1.5 inches in length were sheared from strips, labeled according to the classification in Table IV, and annealed at 300, 350, 400, 500, 600 and 700 °C (570, 660, 750, 930, 1110 and 1290 °F) for the specimens A, B, C, D, E and F, and 250, 300 and 365 °C (480, 570 and 690 °F) for the specimens R, S, T, U. Several preliminary samples were annealed at various times, e.g., 1, 2, 4, 8, 16, 32, 64, etc. (seconds, minutes or hours). The hardness changes in these samples served to indicate the approximate time interval in which recrystallization was complete. Additional specimens were then annealed for various times at closer intervals within this range in order to locate more accurately the time at which recrystallization was complete.

Specimens in the region of complete recrystallization were then prepared for microscopic examination. The presence of slip lines and bent twin interfaces indicated that the material was still in the

strained condition. When the evidence of strained metal had disappeared, recrystallization was considered to be complete. In some cases, the exact time for complete recrystallization was very difficult to determine because the recrystallization process is time-dependent and the changes in microstructure take place rather slowly, particularly at low temperature. A series of photomicrographs was made of specimens which were annealed for various times at constant temperature in the region of recrystallization and, by careful study of these photomicrographs in conjunction with the hardness-time curves, it was possible to determine the time for complete recrystallization fairly accurately.

Isothermal Grain Growth Anneal—Specimens were supported by Nichrome wire in groups in the salt bath in the same manner as for the recrystallization anneal, and subjected to long annealing times up to 128 days at temperatures of 400, 500, 600 and 700 °C (750, 930, 1110 and 1290 °F). Since the objective in this work was to investigate the effects of very long annealing time at various temperatures, a wide range of annealing times was used. Following the annealing operations, all specimens were prepared for microscopic examination and 8 to 10 photomicrographs were taken of different areas of each specimen. Grain counts were then made on the majority of these microstructures, but, in cases where no apparent difference was observed between specimens representing two adjacent times, one set of photographs was eliminated from the tedious counting operation. No hardness measurements were made on the grain growth specimens.

It was found that the corrosive attack of the salt on the specimens at temperatures of 700 °C (1290 °F) and above was excessive. For this reason, salt bath annealing of specimens was not carried out beyond 6 days at 700 °C (1290 °F).

EXPERIMENTAL RESULTS

Isothermal Recrystallization—At high temperature, recrystallization was complete within a very short time after the specimens were placed in the salt—in many cases, before the specimens had reached the bath temperature. Annealing times shorter than those required for the specimen to reach the bath temperature were prefixed with a minus sign to distinguish them from times at the temperature of the bath.

The times and temperatures at which recrystallization of the different materials was complete were found by comparing the hardness-time curves and the microstructures of specimens A, B, C, D, E and F. The microstructures of specimens R, S, T and U were not examined because of the difficulty of mounting, preparing and examining specimens of this thin material of extremely small

Table IV
Times and Temperatures for Complete Recrystallization

Specimen	Temperature °C	Time for Complete Recrystallization* Seconds	Hardness at Complete Recrystallization	Grain Sizes at Complete Recrystallization*
	300	Greater than 4,000,000
A	350	400,000	93 R _H
	400	30,000	93 R _H	0.030 ₂
	500	240	98 R _H	0.029 ₅
	600	-15	92 R _H	0.033 ₇
	300	300,000	102 R _H	0.012 ₀
B	350	15,000	101 R _H
	400	960	102 R _H	0.012 ₂
	500	-25	102 R _H	0.013 ₅
	600	-10	100 R _H	0.012 ₈
	300	400,000	103 R _H	0.012 ₀
C	350	20,000	102 R _H
	400	1,900	103 R _H	0.015
	500	16	104 R _H	0.013 ₂
	600	-15	100 R _H	0.013 ₄
	300	3,000	112 R _H	0.002 ₇
D	350	150	111 R _H
	400	12	112 R _H	0.002 ₀
	500	-10	112 R _H	0.002 ₀
	600	-5	109 R _H	0.002 ₀
	300	40,000	108 R _H	0.007 ₈
E	350	1,500	107 R _H
	400	120	109 R _H	0.007 ₅
	500	-10	108 R _H	0.007 ₈
	600	-6	108 R _H	0.007 ₈
	300	800	115 R _H	0.002 ₄
F	350 R _H
	400	2	113 R _H	0.002 ₁
	500	-8	114 R _H	0.002 ₂
	600	-5	110 R _H	0.002 ₄
	250	20,000	155 V.H.N.
R	300	500	165 V.H.N.
	365	13	165 V.H.N.
	250	14,000	165 V.H.N.
S	300	350	170 V.H.N.
	365	12	165 V.H.N.
	250	9,000	165 V.H.N.
T	300	250	170 V.H.N.
	365	7.5	180 V.H.N.
	250	6,000	190 V.H.N.
U	300	200	185 V.H.N.
	365	7	185 V.H.N.

*Minus sign before the time indicates that recrystallization was complete before the specimen reached the bath temperature. Long times for complete recrystallization are expressed as powers of 10, since it is difficult to obtain a more accurate determination on a logarithmic time scale. Grain sizes are the average of at least six grain counts.

grain size. The times for complete recrystallization of these specimens were determined on the basis of the hardness curves supported by X-ray diffraction patterns.

The hardness-time curves (forty-seven in number) have been omitted here in order to save publishing space. From these curves (20), it was generally observed that the hardness after recrystallization was higher the greater the deformation, the lower the annealing temperature and the finer the initial grain size. The times for complete recrystallization at different temperatures for different materials are listed in Table IV. The annealing time for complete recrystallization was shorter the higher the deformation, the higher the annealing temperature and the smaller the initial grain size.

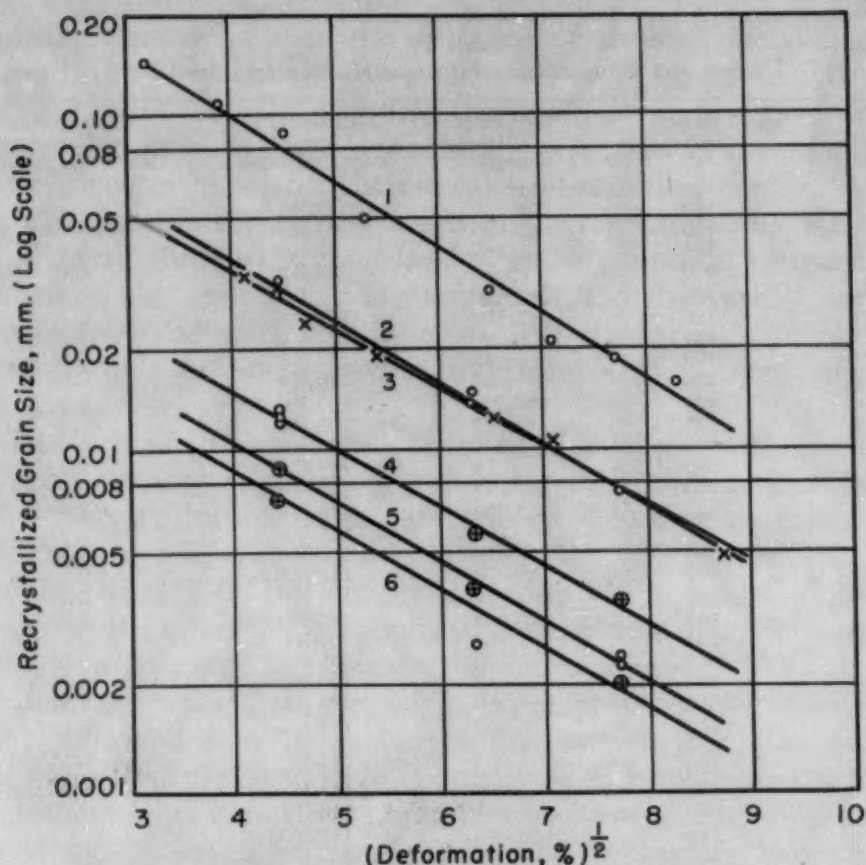


Fig. 1—Relation Between Recrystallized Grain Size and Deformation for Brass of Different Initial Grain Sizes.

Curve 1	Initial grain size 0.53 mm. [Walker (1)]
Curve 2	Initial grain size 0.066 mm.
Curve 3	Initial grain size 0.053 mm. [French (4)]
Curve 4	Initial grain size 0.012 mm.
Curve 5	Initial grain size 0.006 mm.
Curve 6	Initial grain size 0.004 mm.

When the grain size at complete recrystallization (Table IV) is plotted on a logarithmic scale as a function of the square root of the deformation, Curves 2, 4, 5 and 6 of Fig. 1 are obtained. For purposes of comparison, the data of Walker (1), for material of 0.53 millimeter initial grain size (Curve 1), and French (4), for material of 0.053 millimeter initial grain size (Curve 3), are plotted in the same figure. Curve 2 represents the data obtained in this investigation for material with an initial grain size of 0.066 millimeter. This curve has approximately the same slope as Curves 1 and 3 and lies in the expected position between these curves. At each of the three deformations (20.5, 40.4 and 61.8%), the grain size at which recrystallization was complete was found to be the same for all the annealing temperatures used in this investigation. Material "A" showed slight deviation in the grain size at the three temperatures, 400, 500 and 600 °C (750, 930 and 1110 °F), but this may be attributed to experimental error, since it is difficult to meas-

ure a representative area in coarse-grained material. It may be concluded from these data that the recrystallized grain size is independent of the temperature of annealing. This observation has been confirmed by several other investigators (1, 5, 6).

It has been found (1) that the general equation relating the coordinates of Fig. 1 may be expressed as:

$$\log \text{ grain size} = \log m + n \sqrt{\text{percentage deformation}}$$

The equation for Curve 1 is:

$$\log \text{ grain size} = -0.193 \sqrt{\text{percentage deformation}} - 0.235$$

and for Curve 3 is:

$$\log \text{ grain size} = -0.168 \sqrt{\text{percentage deformation}} - 0.796$$

It was also found, by plotting the data of Eastwood, Bousu and Eddy (5) in the same manner, that a similar relation existed for brasses of different compositions. The numerical value of the slope "n" was larger with decreasing zinc content.

The equation for Curve 1 was also calculated by the authors of this paper, using the method of least squares, and the values of "n" and "log m" were found to be essentially identical with those shown above. The equation for Curve 2, calculated by the method of least squares, is as follows:

$$\log \text{ grain size} = -0.176 \sqrt{\text{percentage deformation}} - 0.731$$

These data show a definite relationship between the recrystallized grain size and the deformation.

The material which was supplied in the fine-grained condition was found to have a different initial grain size at each of the deformation levels investigated. Thus it was not possible to show the effect of deformation on the recrystallized grain size in the fine-grained material because only one point could be plotted for each initial grain size. The experimental results are plotted as open circles on Curves 4, 5 and 6 in Fig. 1.

From these experimental data and those of Curves 1, 2 and 3, it was found that, for a constant deformation, a linear relationship existed between the recrystallized grain size and the initial grain size when plotted on a logarithmic scale (Fig. 2). Furthermore, at different deformations, the straight lines were approximately parallel. Extrapolation and interpolation of these lines enabled recrystallized grain sizes to be found for a particular initial grain size and deformation. These values of recrystallized grain size were then plotted in Fig. 1, as shown by the crossed circles, and Curves 4, 5 and 6 were thus obtained. The slope and intercept of these curves cannot be determined with great accuracy, since they are merely "derived"

curves which were plotted to indicate the trend in the effect of very fine grain sizes on the recrystallized grain size.

The empirical relation between recrystallized grain size and initial grain size may be expressed as:

$$\log (\text{recrystallized grain size}) = a \log (\text{initial grain size}) + \log b$$

where $\log b$ is a function of the deformation. The slope of Curves 4, 5 and 6 indicates that these lines are parallel. However, it has

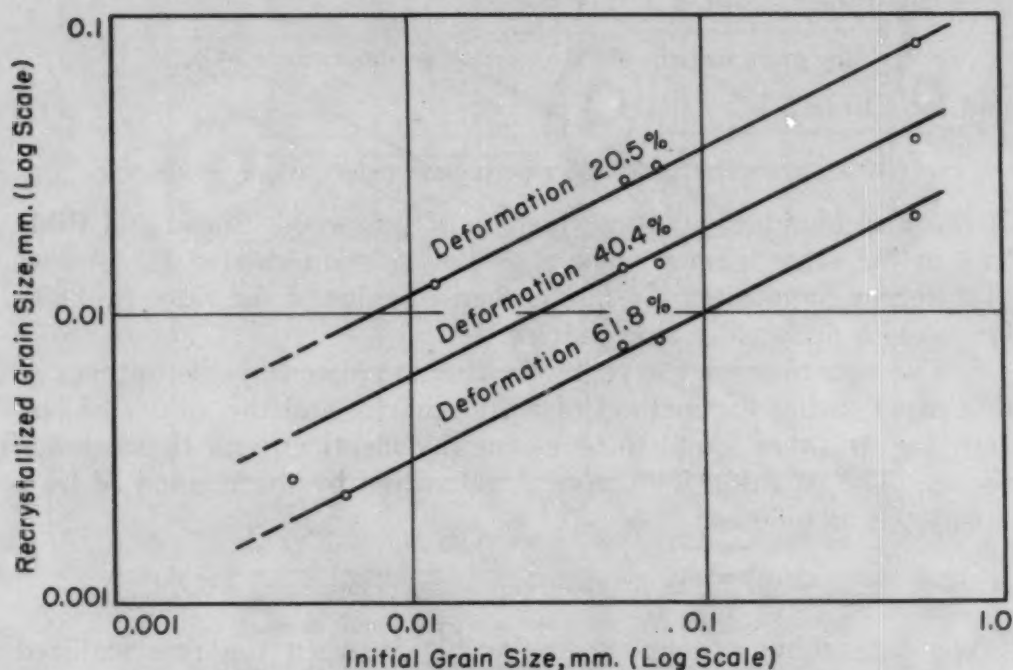


Fig. 2—Relation Between Initial Grain Size and Recrystallized Grain Size for Different Values of Prior Deformation.

been stated by Wood (7) that there is a limiting crystallite size which is produced by cold working a metal. He stated that this is of the order of 10^{-4} cm. This suggested that Curves 4, 5 and 6 should reach a lower limit for the recrystallized grain size which would correspond with the limiting crystallite size.

Heat of Activation for Recrystallization—Cold working has been shown to result in storage of energy in a metal, thus increasing its potential energy. The cold-worked material may then be represented by the metastable position on the energy curve in Fig. 3. The annealed condition may be represented by the stable position. When the amount of cold working increases, more energy should be stored in the material, thus moving the metastable position to a higher potential energy level. Assuming the potential level of the energy barrier is constant, a smaller activation energy, U_0 , would be required to enable the atoms in the metastable state to pass over the hump to the stable state. As the amount of cold working is in-

creased, the activation energy is reduced, since less additional energy is required from other sources (e.g., thermal energy) to bring about the transformation.

Anderson and Mehl (8) found a decrease in the heats of activation for nucleation, nucleus growth and recrystallization with increasing deformation in aluminum. Cook and Richards (9) observed

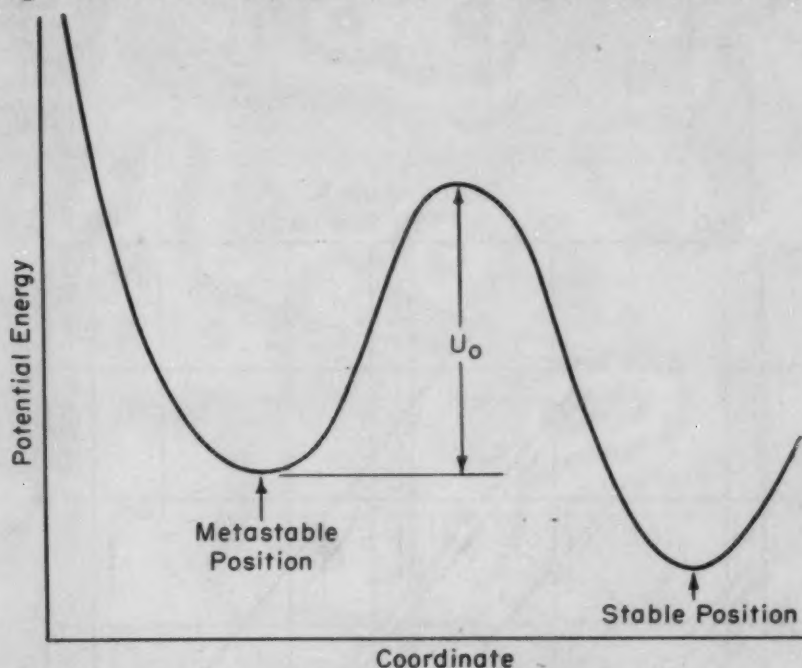


Fig. 3—Schematic Representation of the Concept of Activation Energy. The metastable position of an atom corresponds to the cold-worked state and the stable position corresponds to the annealed state of the metal. U_0 is the energy hump or activation energy which must be overcome in passing from the cold-worked state to the annealed state. (15)

the same result in copper, and Wensch (10) found this to be true for nickel.

The time and temperature for complete recrystallization are related by the Arrhenius equation

$$\ln \frac{t_1}{t_2} = \frac{Q}{R} \left(\frac{1}{T_1} - \frac{1}{T_2} \right)$$

where t_1 and t_2 are the times required for a given amount of reaction at absolute temperatures T_1 and T_2 , Q is the heat of activation in kilocalories per mole, and R is the gas constant. It must be emphasized that the heat of activation for recrystallization calculated from the slopes of curves in Fig. 4 is the heat of activation for the combined process of nucleation and nucleus growth.

The times and temperatures for complete recrystallization obtained in this investigation are plotted in Fig. 4. The times plotted here are the times for which the specimens were at the temperature of the salt bath. Curves 1 to 9 represent different amounts of deformation or different initial grain sizes. The key to these curves

Table V
Heat of Activation for Recrystallization

Curve	Specimen	Prior Deformation %	Initial Grain Size mm.	Heat of Activation Kilocalories per Mole
1	A	20.5	0.068	48.8
2	C	40.4	0.068	44.5
3	B	20.5	0.012	43.8
4	E	61.8	0.068	42.8
5	D	40.4	0.004	42.4
6	R	90.2	0.066	41.5
7	S	90.2	0.006	40.85
8	T	94.5	0.066	41.00
9	U	90.2	0.006	40.80

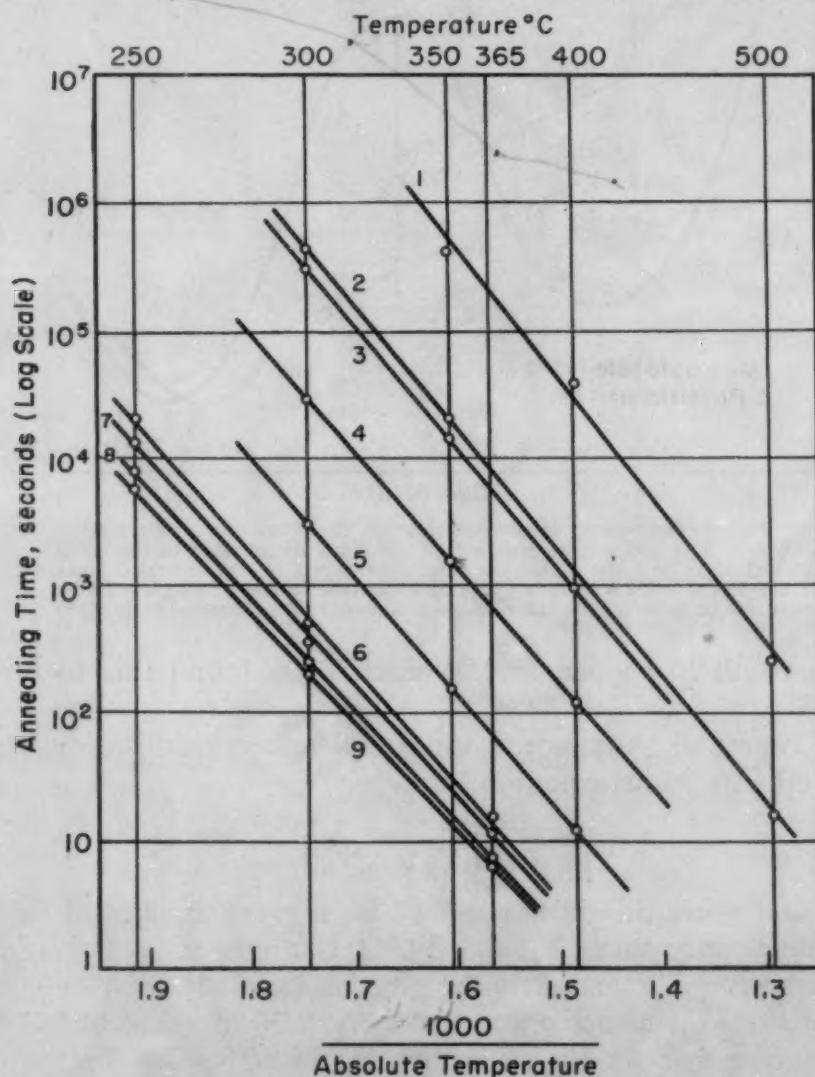


Fig. 4—Times and Temperatures for Complete Recrystallization.
(For the key to these curves, see Table V.)

and the heat of activation associated with each curve is shown in Table V. In Fig. 5, plotted from the data in Table V, a decrease in the heat of activation is observed with increasing deformation and decreasing initial grain size.

The heat of activation which appears in the Arrhenius equation, therefore, should not be expressed as a constant but as a function of deformation and initial grain size such that

$$\ln \frac{t_1}{t_2} = \frac{Q \text{ (deformation, initial grain size)}}{R} \left(\frac{1}{T_1} - \frac{1}{T_2} \right)$$

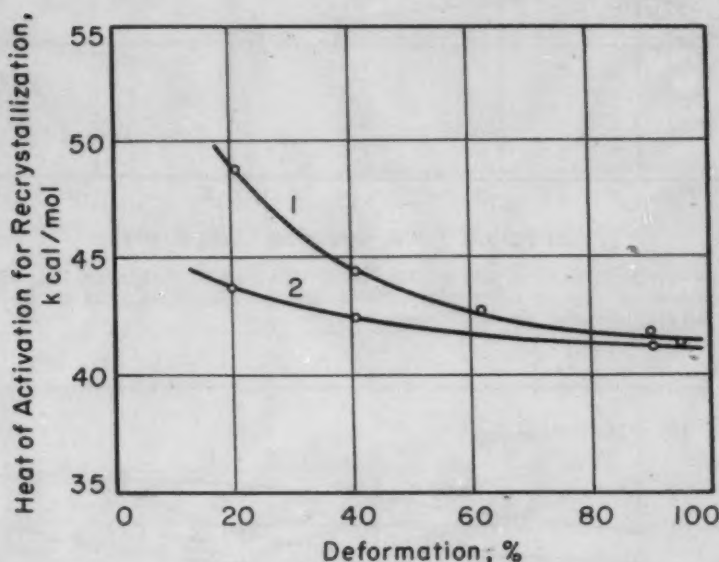


Fig. 5—Effect of Deformation and Initial Grain Size on Heat of Activation for Recrystallization of Brass. Curve 1 is for brass of initial grain size 0.066 millimeter; curve 2 is for brass with grain size of 0.010 to 0.004 millimeter.

The heat of activation appears to approach a minimum value of approximately 41 kilocalories per mole, irrespective of the initial grain size. It is interesting to note that this value is in very close agreement with the values of heats of activation for volume diffusion and for viscous slip at grain boundaries in alpha brass found by Kê (11) to be about 40 kilocalories per mole.

Isothermal Grain Growth—The grain growth data shown in Figs. 6 to 12 require very little comment. The curves representing growth of specimens with different initial conditions annealed at 600 °C (1110 °F) illustrated in Fig. 6 show that the grain size reached after approximately 10^3 to 10^4 seconds is the same, regardless of the initial condition of the material. The rate of growth seems to be slower in this region and then increases again beyond 10^4 seconds, finally becoming slower at 10^7 seconds. The grain sizes when recrystallization is just complete are shown merely to illustrate the rapid rate of growth of the fine-grained and more severely deformed specimens in the earlier annealing stages. The slow rate of growth at about 10^4 seconds may have been due to the obstructing effect of impurities, which were either agglomerated or dissolved at longer annealing times. The series of curves at 600 °C (1110 °F)

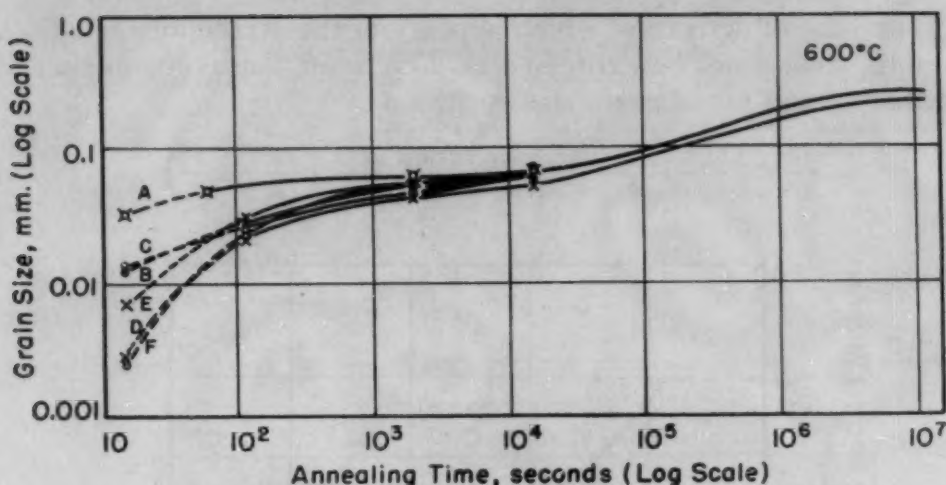


Fig. 6—Grain Growth at 600°C. Points A, B, C, D, E, F show the recrystallized grain size of the six materials. The grain size reaches almost a common value for all specimens at about 10^6 seconds.

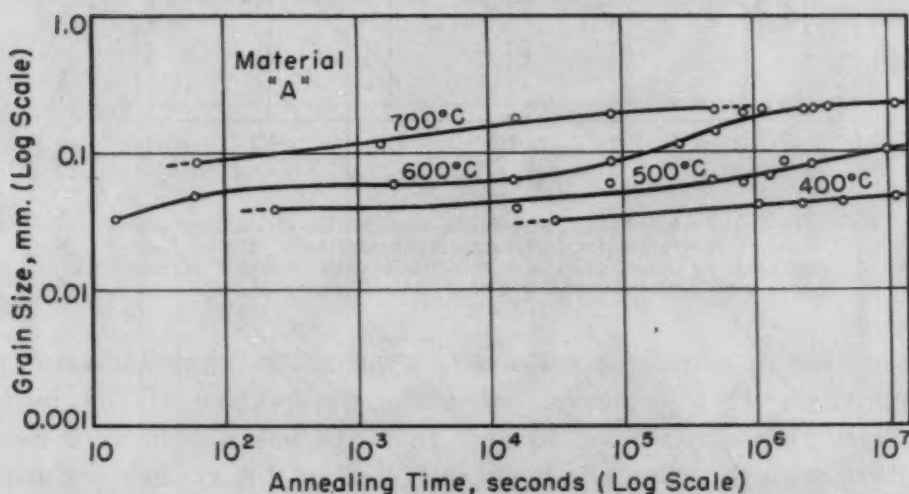


Fig. 7—Grain Growth Curves of Material "A" (Deformation 20.5%, Initial Grain Size 0.068 Millimeter) at Various Temperatures.

was the only series which showed this effect rather markedly. It was faintly visible in the curves at 500°C (930°F).

The curves of Figs. 6 to 12 illustrate the effect of temperature on the grain growth of a particular material. The grain size reached in a certain annealing time is larger the higher the temperature of annealing.

The grain growth curves did not show very definite evidence of the existence of an equilibrium grain size at the higher annealing temperatures. The 600 and 700°C (1110 and 1290°F) curves tend to level out at the grain size reached, but this evidence is not sufficiently conclusive for any definite statement to be made regarding the equilibrium grain size.

In Fig. 6, the rate of growth at 600°C (1110°F) appears to

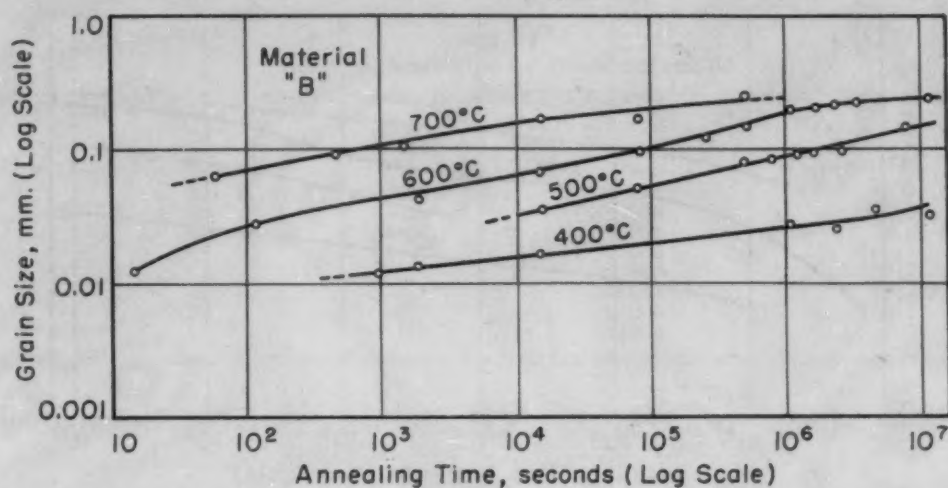


Fig. 8—Grain Growth Curves of Material "B" (Deformation 20.5%, Initial Grain Size 0.012 Millimeter) at Various Temperatures.

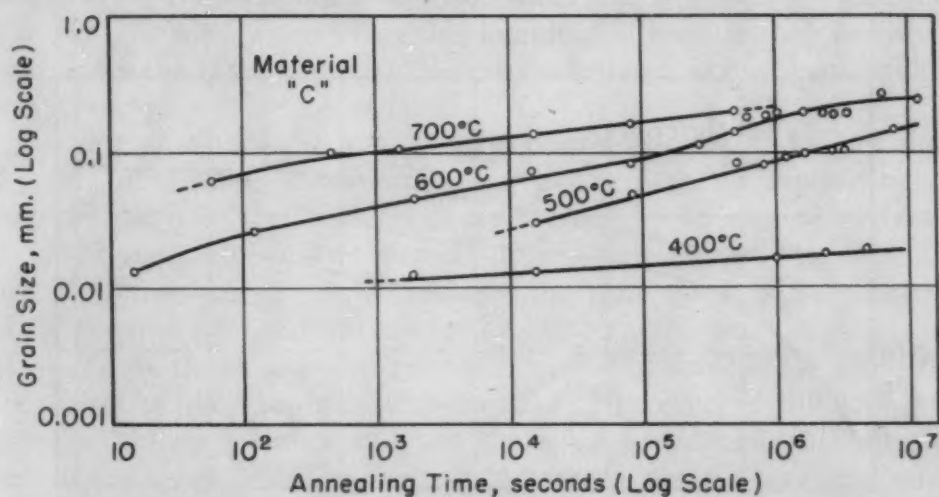


Fig. 9—Grain Growth Curves of Material "C" (Deformation 40.4%, Initial Grain Size 0.068 Millimeter) at Various Temperatures.

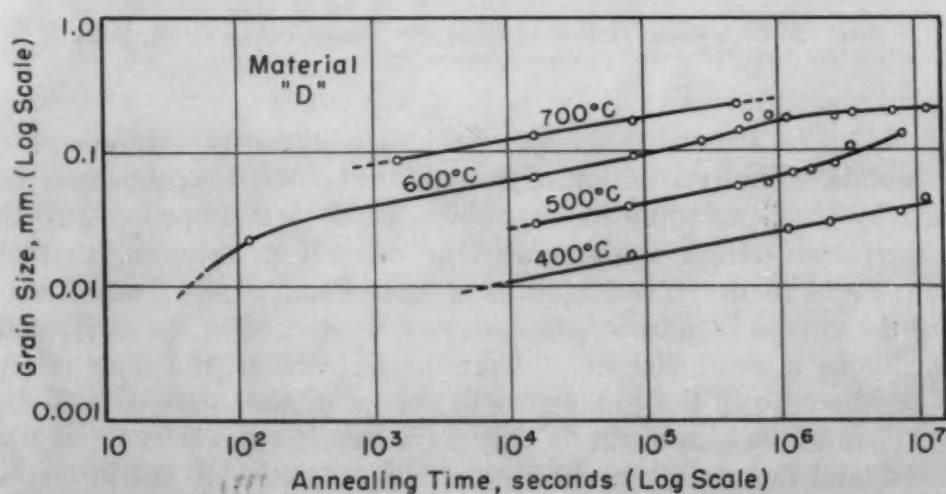


Fig. 10—Grain Growth Curves of Material "D" (Deformation 40.4%, Initial Grain Size 0.004 Millimeter) at Various Temperatures.

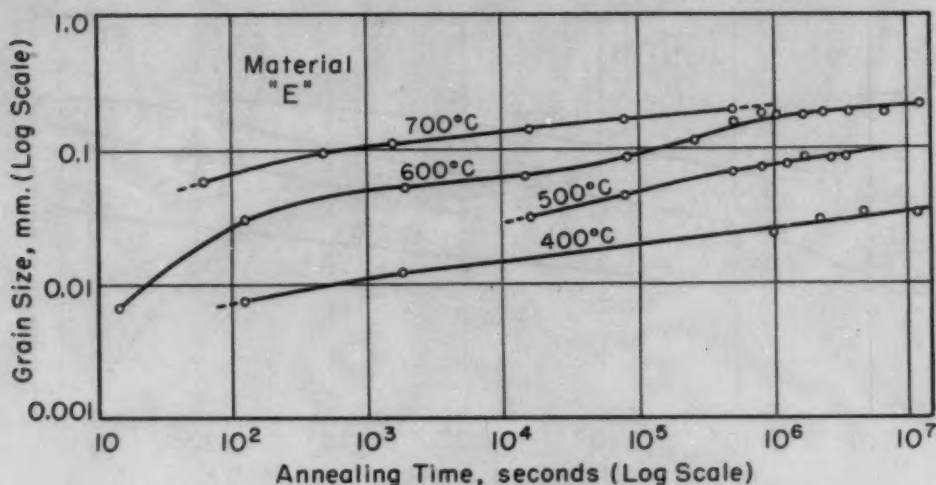


Fig. 11—Grain Growth Curves of Material "E" (Deformation 61.8%, Initial Grain Size 0.066 Millimeter) at Various Temperatures.

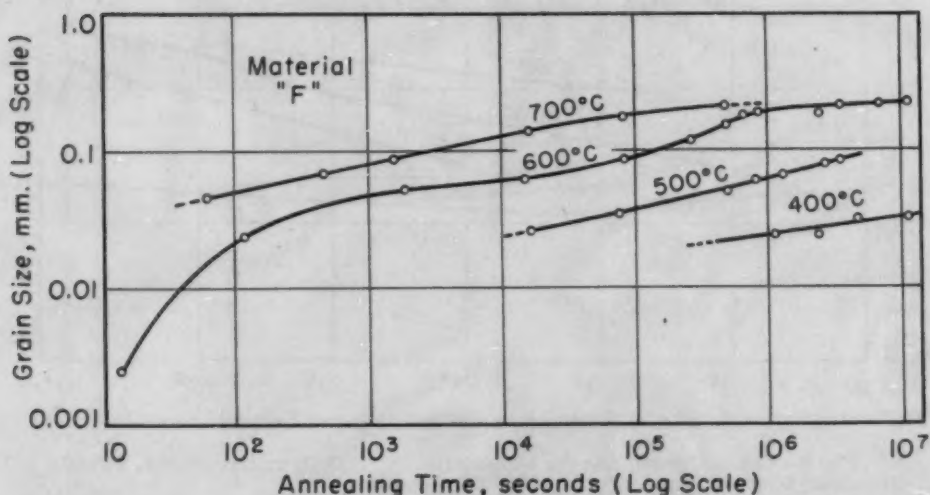


Fig. 12—Grain Growth Curves of Material "F" (Deformation 61.8%, Initial Grain Size 0.006 Millimeter) at Various Temperatures.

decrease up to about 10^4 seconds, and then increases again beyond 10^4 seconds. The retardation of growth at about 10^4 seconds may be caused by small amounts of impurities which first impeded growth and then were either agglomerated or taken into solution, so that growth could then proceed again at a more rapid rate. The flattening of the curves is quite small, and may, at first sight, be attributed to variations in grain size determinations. However, the same effect may be observed in the grain growth curves of the specimens A, B, C, D, E and F, which suggests that the effect is characteristic of the material, and the grain size determinations are probably not in error.

It was proposed by Beck and his associates (12) that a straight-line relationship describes grain growth completely when the log-

Table VI
Heats of Activation for Grain Growth

Curve	Specimen	Prior Deformation %	Initial Grain Size mm.	Heat of Activation Kilocalories per Mole
1	A	20.5	0.066	59.9
2	B	20.5	0.012	64.8
3	C	40.4	0.066	53.6
4	C	40.4	0.066	63.7
5	D	40.4	0.004	58.2
6	E	61.8	0.066	59.4
7	F	61.8	0.006	60.5
8	F	61.8	0.006	59.2

arithm of the average grain diameter, D , is plotted against the logarithm of the annealing time. The equation is:

$$D - D_0 = Kt^n$$

where D_0 is the recrystallized grain size, and K and n are constants. The present work shows that this simple relationship may not always hold, since the 600 °C (1110 °F) curve deviates from the straight line at approximately 10^5 seconds.

Heat of Activation for Grain Growth—Burke (13) has shown that the time and temperature for grain growth for alpha brass, at least up to 700 °C (1290 °F), are related by a heat of activation.

The most convenient method of determining the heat of activation for grain growth is to measure the time taken for a grain size of D to grow from an initial size of D_0 , e.g., the recrystallized grain size. These times are then plotted on a logarithmic scale against the reciprocal of the absolute temperature. However, individual grains grow at different rates and are therefore associated with different heats of activation. The heat of activation for the average rate of grain growth for all grains should then be described as a "quasi-heat of activation". In the following discussion concerning grain growth, the prefix "quasi" has been omitted but is implied. Due to the non-linearity of the grain growth curve at 600 °C (1110 °F), it was difficult to select a grain size level at which the times and temperatures gave a linear plot with the above coordinates. This is illustrated by plotting times and temperatures at two different grain size levels for specimens C and F (Curves 3 and 4, and 7 and 8, respectively, in Fig. 13). The key to these curves and the calculated heats of activation are listed in Table VI.

There is apparently no significant effect of deformation and initial grain size on the heat of activation for grain growth. The scatter of these results is within the experimental error, since it is very difficult to locate times exactly at very long annealing times. The average of these calculated heats of activation is approximately 61 kilocalories per mole.

This value agrees very well with the heat of activation of 64

kilocalories per mole and 60 kilocalories per mole found by Burke (13), and 61.5 kilocalories per mole found by Beck, Towers and Manly (12) for grain growth in commercially pure alpha brass. It is expected that the heat of activation for grain growth would be greater than that for recrystallization, since the recrystallization process is aided by the deformation energy stored in the material after cold work. In the case of grain growth, the energy for grain

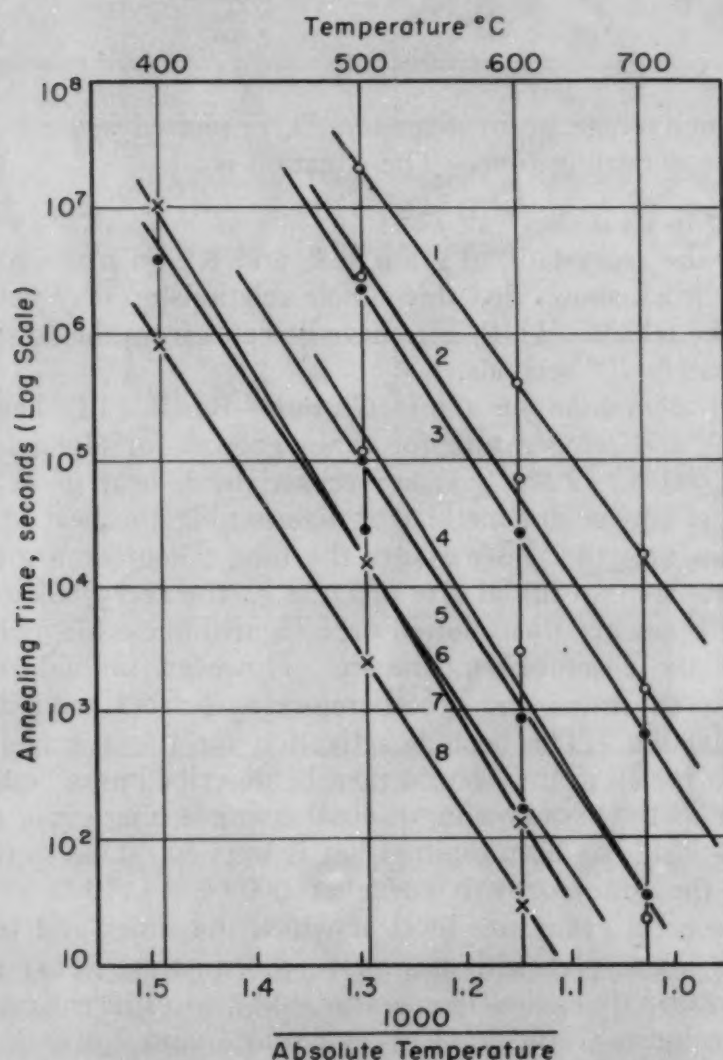


Fig. 13—Times and Temperatures for Growth to a Particular Grain Size. The grain sizes for each curve were approximately 0.010 millimeter, varying slightly for the different curves. (For the key to these curves, see Table VI.)

boundary migration must originate almost entirely from thermal energy and partly from surface energy of the grains. In the presence of inhibiting materials such as insoluble impurities, additional energy must be provided to overcome the resistance of these impurities. It would be expected, then, that a pure material should have a lower

heat of activation for grain growth. Burke (13) has found a heat of activation of approximately 40 to 42 kilocalories per mole for grain growth in high purity brass. This is a close agreement with the values of 46 kilocalories per mole reported by Jenkins (14) for diffusion of zinc in 70/30 alpha brass, and of 40 kilocalories per mole reported by Kê (11) for grain boundary relaxation and reorientation of zinc atoms in a brass of the same composition.

CONCLUSIONS

From the results of isothermal recrystallization and grain growth data obtained in this investigation, the following conclusions may be drawn:

1. The recrystallized grain size was found to be independent of the temperature of annealing.

2. The relation between recrystallized grain size "r" and deformation, "d", i.e.,

$$\log r = nd^{1/2} + \log m$$

was confirmed in this investigation for materials of different initial grain sizes. In addition, it was found that "m" is a function of the initial grain size.

3. The relation between initial grain size "i" and recrystallized grain size "r" may be expressed by the equation

$$r = bi^a$$

where "b" is a function of the deformation.

4. The heat of activation for recrystallization was found to decrease with increasing deformation and decreasing initial grain size, reaching a lower limit of approximately 41 kilocalories per mole, which compares favorably with values of 40 kilocalories per mole quoted for heat of activation for volume diffusion and for viscous slip at grain boundaries in alpha brass.

5. The grain size after long annealing time is essentially independent of the amount of prior deformation and initial grain size.

6. The slope of the grain growth curves at 600 °C (1110 °F) appears to decrease and then increase again after further annealing for longer times. This effect is believed to be due to the agglomeration or dissolution of impurities which then allow growth to continue. The slope of the grain growth curves is approximately the same at different annealing temperatures.

7. Within the limits of annealing times investigated, the grain size was still increasing with increasing time, but appeared to be approaching an equilibrium grain size. An equilibrium grain size was not definitely established in the commercial brass investigated. For practical purposes, grain growth may be regarded as a con-

tinuing process, at least for annealing temperatures below 700 °C (1290 °F) and annealing times shorter than 128 days.

8. The heat of activation for grain growth in this material was found to be 61 kilocalories per mole, and was independent of the prior deformation or initial grain size.

ACKNOWLEDGMENT

The authors are indebted to the University of Illinois Engineering Experiment Station for making this research possible through the appointment of a research assistantship, and to Western Cartridge Company, who supplied the material.

References

1. H. L. Walker, "Grain Sizes Produced by Recrystallization and Coalescence in Cold-Rolled Cartridge Brass", Engineering Experiment Station, Bulletin No. 359, University of Illinois, Urbana, Ill.
2. Z. Jeffries, American Society for Testing Materials' Standards, Part 1, 1927, p. 780-782.
3. G. L. Clark, "Applied X-Rays", McGraw-Hill Book Company, 1940.
4. R. S. French, "Grain Growth and Recrystallization of 70/30 Cartridge Brass", *Transactions*, American Institute of Mining and Metallurgical Engineers, Vol. 156, 1944, p. 195.
5. L. W. Eastwood, A. E. Bousu and C. T. Eddy, "Recrystallization and Grain Growth in Cold-Worked Polycrystalline Metals", *Transactions*, American Institute of Mining and Metallurgical Engineers, Vol. 117, 1935, p. 246.
6. L. W. Eastwood, R. W. James and R. F. Bell, "Some Aspects of the Recrystallization of Aluminum and Aluminum Alloys", *Transactions*, American Institute of Mining and Metallurgical Engineers, Vol. 133, 1939, p. 124.
7. W. A. Wood, "The Lower Limiting Crystallite Size and Internal Strains in Some Cold-Worked Metals", *Proceedings*, Royal Society, Series A, Vol. 172, 1939, p. 231-241.
8. W. A. Anderson and R. F. Mehl, "Recrystallization of Aluminum in Terms of Rate of Nucleation and Rate of Growth", *Transactions*, American Institute of Mining and Metallurgical Engineers, Vol. 161, 1945, p. 140-167.
9. M. Cook and T. L. Richards, "Observations on the Rate and Mechanism of Recrystallization in Copper", *Journal*, Institute of Metals, Vol. 73, 1947, p. 1.
10. G. W. Wensch and H. L. Walker, "Recrystallization and Grain Growth of Nickel", *TRANSACTIONS*, American Society for Metals, Vol. 44, 1952, p. 1186.
11. T. S. Kê, "Viscous Slip Along Grain Boundaries and Diffusion of Zinc in Alpha Brass", *Journal of Applied Physics*, Vol. 19, March 1948, p. 285.
12. P. A. Beck, J. Towers, Jr., and W. D. Manly, "Grain Growth in 70/30 Brass", *Metals Technology*, Vol. 15, February 1948, T.P. No. 2326.
13. J. E. Burke, "Some Factors Affecting Rate of Grain Growth in Metals", *Transactions*, American Institute of Mining and Metallurgical Engineers, Vol. 180, 1949, p. 73-91.
14. Ivor Jenkins, "Surface Effects During Annealing of 70/30 Brass", *Journal*, Institute of Metals, Vol. 73, 1947, p. 641.
15. C. Zener, "Role of Statistical Mechanics in Physical Metallurgy", *Seminar on Thermodynamics in Physical Metallurgy*, American Society for Metals, 1950, p. 16.

16. R. F. Mehl, "Recrystallization", METALS HANDBOOK, 1948 Edition, American Society for Metals.
17. W. A. Anderson, "Recrystallization of Aluminum in Terms of Rate of Nucleation and Rate of Growth", Doctoral Dissertation, Carnegie Institute of Technology, Pittsburgh, 1947.
18. H. Greis and H. Esser, "Über Einkristalle aus Eisen", *Archiv für das Eisenhüttenwesen*, Vol. 2, 1929, p. 749.
19. A. Schroeder and K. Matthaes, *Metallwirtschaft*, Vol. 20, 1941, p. 631.
20. S. L. Channon, "Recrystallization and Grain Growth Phenomena in Cartridge Brass", University Microfilms (Ann Arbor, Mich.), Publication No. 2713, 192 pages.

DISCUSSION

Written Discussion: By Glen W. Wensch, Technical Division, U. S. Atomic Energy Commission, Wilmington Area Office, Wilmington, Del.

The authors have shown the dependence of the heat of activation for recrystallization upon the degree of prior deformation. This dependence was recently observed in the study of "Recrystallization Kinetics of Tantalum" as shown below:

Deformation (Cold Rolling)	H (Kcal/mole)
40 ²	124 ²
80	97

On the authors' seventeenth page they state that insoluble impurities may increase the heat of activation for grain growth. This idea is not disputed, but it is felt that the particle size of the impurity is an important consideration in its ability to hinder grain boundary migration. Would the authors be kind enough to present their comments?

The authors are to be commended for presenting valuable data of a type not available previously.

Written Discussion: By Raymond G. Crawford, furnace engineer, Chase Brass and Copper Co., Waterbury, Conn.

I am very much interested in this subject, particularly in a relationship between time and temperature for small increments of time. I have just realized that the question of whether or not there is an equilibrium grain size for a prolonged heating time fits into my particular interest by the assumption of a theory which I should appreciate comments upon.

The entire grain growth pattern could be considered a problem of inertia. This would apply from recrystallization to apparent equilibrium. Up to the point of recrystallization, the action seems more like a physical property of the metal with governing conditions set up by the previous deformation and grain size of the metal. In this regard I should like to know if a stressed metal could be heated so rapidly that melting would occur prior to recrystallization. It seems to me that this could not happen. However, beyond this point it appears quite evident that application of heat must be accompanied by an increment of time for a change in grain size. It therefore seems that the heat is the activating force applied to the grain mass, giving them a rate of size change which could be likened to acceleration so that all factors would apply in the formula $F = ma$.

²G. W. Wensch, K. B. Bruckart and R. H. Deidler, "Recrystallization of Tantalum", *Journal of Metals*, American Institute of Mining and Metallurgical Engineers, June 1952, p. 596.

On the basis of this theory, there would not be a resulting grain size equilibrium until such time as internal resistance cancelled the heating force. An apparent equilibrium could be reached when the mass became sufficiently large and the rate of grain size change would be made very small. The internal resistive forces could be impurities, as shown in the paper, which during the action might actually create a different characteristic mass and alter the characteristic of the declining rate of change. Physical size limitations of the metal might also set up resistive forces which influence the apparent equilibrium.

My particular interest is concerned with how much change in force is equivalent to a change in time and whether this relationship is constant.

I realize that this discussion is not directly concerned with this fine paper and in this regard can only say that I very greatly appreciate the work and presentation of Messrs. Channon and Walker. I should be happy if they would offer some comment, no matter how brief their limited time permits.

Authors' Reply

We wish to thank Dr. Wensch for his data on tantalum confirming the fact that the heat of activation for recrystallization decreases with increasing deformation.

The effect of composition and impurities on the grain growth of metals has long been a subject of discussion but is still not completely understood. The most recent summary of the effects of impurities on the annealing characteristics of brass has been compiled by Burghoff.

The grain size reached at a particular time and temperature is larger in pure brass than in commercial brass. Impurities which are in solid solution have a minor effect on grain growth, but the undissolved impurities seem to exert a pronounced influence. Jeffries and Archer pointed out that a given amount of a second phase is most efficient in hindering growth if it is present in a finely divided form. We believe this is true.

Occasionally, however, the second-phase impurities which appear to inhibit grain growth coalesce or enter into solution at higher temperatures and longer times. When this occurs, the obstruction to grain growth is partially or wholly removed and grain growth may continue. This has been very nicely demonstrated by Beck, Holzworth and Sperry in their studies of grain growth in an alloy of aluminum with 1.00% manganese.

Mr. Crawford's comments are appreciated. In reply to his question concerning the possibility of obtaining melting in a stressed metal prior to recrystallization, we have observed, in our work, that specimens annealed at 700 and 800 °C were fully recrystallized before the specimens reached the temperature of the salt bath. Recrystallization occurred in a matter of 5 seconds or so in those specimens, the time being shorter with greater prior deformation. On the basis of these observations we do not believe it is possible to melt a strained metal before recrystallization occurs.

With respect to the limitations of physical size of the specimen on the grain growth, we did observe, in some of our specimens, that the grains extended across the entire width of the specimen. When this occurs, growth is inhibited in one direction and further growth must take place in the other two directions in the specimen.

TEMPERATURE DEPENDENCE OF THE HARDNESS OF PURE METALS

BY J. H. WESTBROOK

Abstract

A long-standing problem in high temperature metallurgy has been the temperature dependence of the strength of metals. The rich literature covering the hardness of pure metals as a function of temperature has been reviewed and some generalizations made. These led to an approximate method for calculating the hardness of a pure metal as a function of the test temperature, crystal structure, specific heat, and heats of fusion and transformation. The method has approximate validity from near absolute zero to about half the absolute melting point.

HARDNESS, as it is most commonly measured, is simply the resistance of a material to plastic deformation by indentation. Extensive engineering use is made of this property because it is such a simple test to make, can be made quickly, and requires but a small specimen, the only specification for which is that there be at least one plane surface. Justification for such use rests upon the many correlations established between hardness and various engineering properties.¹ The relation between hardness and yield point has been shown by Tabor (1)² for a variety of metals. Janitzky and Baeyertz (2) have found a linear relation between the tensile strength and Brinell hardness of quenched and tempered alloy steels. Bens (3) has demonstrated that a close relationship exists between hot hardness and time to rupture for chromium-base alloys at 870 °C (1600 °F). Relations have also been found between hardness and certain electrical and magnetic properties (4, 5, 6).

On the other hand, hardness measurements have only rarely been employed in scientific studies³ because of the objections that the hardness test involves a complex state of stress, that it measures

¹Several excellent books and monographs are available on the subject of hardness and hardness measurement. Particularly to be recommended are O'Neill (7) for a comprehensive analytical treatment and Williams (8) for his extensive bibliography.

²The figures appearing in parentheses pertain to the references appended to this paper.

³The few instances of such published work have been reviewed by O'Neill (7) and Smith (9).

A paper presented before the Thirty-fourth Annual Convention of the Society, held in Philadelphia, October 18 to 24, 1952. The author, J. H. Westbrook, is associated with the General Electric Research Laboratory, The Knolls, Schenectady, N. Y. Manuscript received March 13, 1952.

not one but several properties, and that the hardness values obtained cannot be identified with dimensional properties. Still, in spite of the difficulties in analyzing exactly the factors which determine the hardness number, it is remarkable in its close correlation with the most fundamental atomic and crystalline properties. For example, a relation has been found between the hardness of pure metals and their compressibility (7). Still other relations between hardness and atomic properties have been found by Lazarev (10) and others (11, 12, 13).

There are two potential applications of hardness measurements in scientific studies which as yet have not been sufficiently explored. These are the problem of the effect of temperature on the mechanical behavior of metals and the problem of the theory of alloying. It is the purpose of this paper to examine the first of these with the aid of the considerable data to be found in the literature. The application of hardness measurements to the theory of alloying will be treated separately (14, 15).

QUALITATIVE OBSERVATIONS

As is usually the case, most of the significant qualitative observations of the temperature dependence of hardness were made by the earliest investigators. The rather rapid decrease in hardness of metals with increasing temperature has been known to metal workers since ancient times. Quantitative measurements of hardness at elevated temperatures, however, apparently date from some researches of Brinell (16), early in the present century. It has been observed for some time that in general the higher the melting point of a pure metal, the higher the hardness at a given temperature. The room temperature hardness values of a number of pure annealed metals are plotted against their absolute melting points in Fig. 1. The data were taken from the 1948 ASM Metals Handbook (17) and Smithells' "Metals Reference Book" (18). In cases of discrepancy the lower value was plotted. As may be seen from Fig. 1 and as Ludwik (19) observed from some of his own results, the hardness-melting point relationship is not quite this simple. Thus, Ludwik found that plotting hardness data against the homologous temperature⁴ does not give complete equilibration. (See Fig. 2.)

One may also note from almost any plot of hardness data over a wide temperature range (see Fig. 2 for example) that hardness falls off sharply at first with temperature and more and more slowly as the temperature approaches the melting point. Further, it has been observed (19) that the hardness of all metals is still appreciable

⁴A homologous temperature is a temperature having the same relative value for different metals. This concept was introduced by Ludwik, who defined a homologous temperature scale whose values are the ratios of the test temperatures to the melting point when expressed in absolute degrees. $T_h = T/T_{mp}$ ($^{\circ}K$).

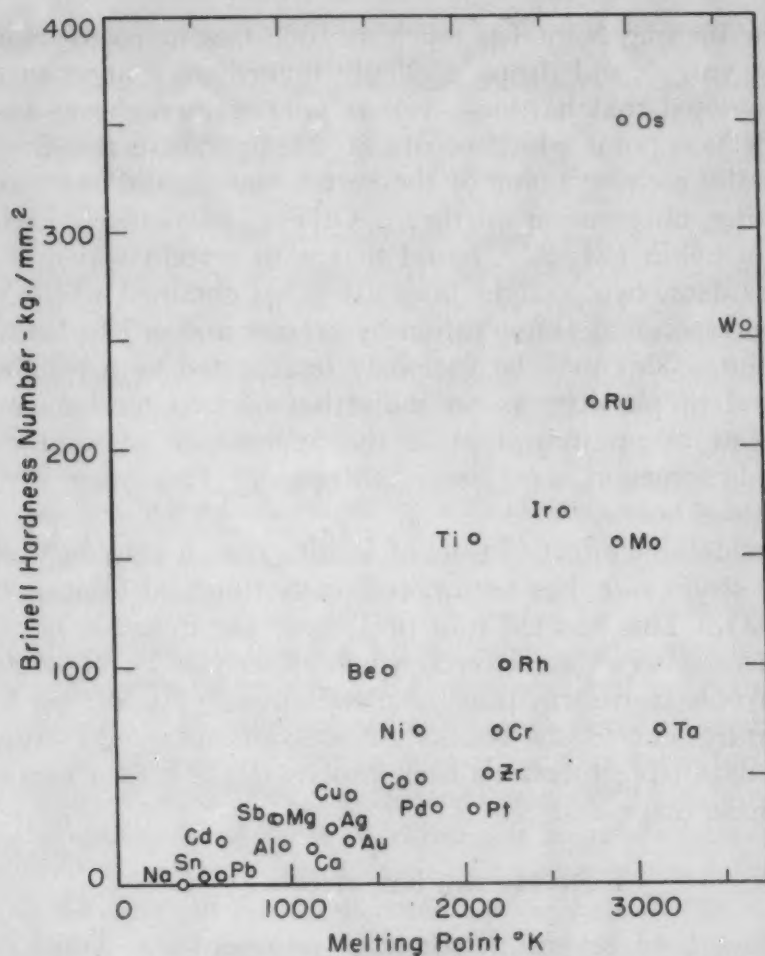


Fig. 1—Room Temperature Hardness of Pure Metals as a Function of Melting Point. Handbook Data 1949.

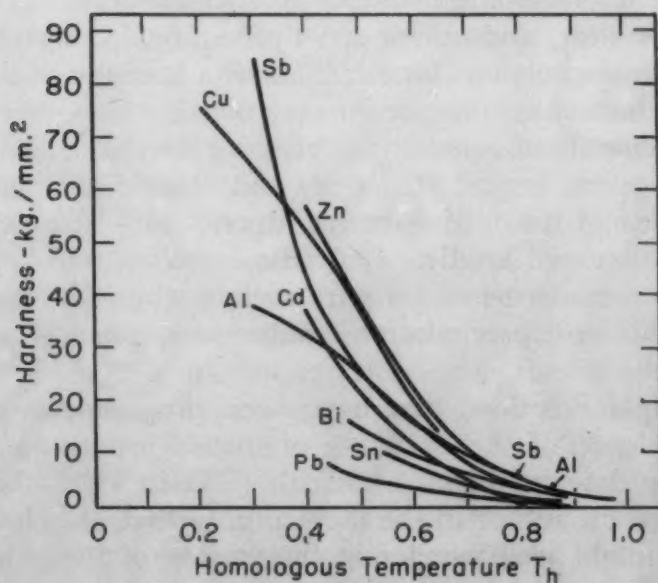


Fig. 2—Hardness of Pure Metals as a Function of the Homologous Temperature, $T_h = \frac{T}{T_{mp}}$ °K. (After Ludwik.)

very near the melting point (as much as 10% that at room temperature in some cases) and drops suddenly immediately upon melting.

Ludwik noted that hardness versus temperature curves usually show an inflection point which occurs at a temperature roughly proportional to the melting point of the metal, but he did not explore this interesting observation further. Others, particularly Schwab (20) and Shishokin (21, 22), found that with certain ways of plotting hardness data, two straight lines are often obtained which cross at a point corresponding (observation by present author) to Ludwik's inflection point. This may be variously interpreted as a peculiarity of the method of plotting, as an indication of two mechanisms of deformation, or as an indication of the appearance of a new and extraneous phenomenon, e.g., recrystallization. This point will be further discussed below.

The considerable effect of time of loading, i.e., a combined effect of strain and strain rate, has been noted many times, at least as early as Kürth (23). This has led to a preference for dynamic hardness testing in cases where time effects would otherwise be appreciable. Finally, allotropic transformations in metals usually appear on hardness-temperature curves as breaks or discontinuities. Hardness-temperature data have therefore been proposed (21) as a means of estimating phase diagrams.

FUNCTIONAL RELATIONS

There have been several attempts to represent the temperature dependence of the hardness of metals analytically—some based on theoretical derivations, some deduced by analogy with equations for elastic or plastic flow, and others strictly empirical. Many of these are rather simple expressions for hardness as a function of the testing temperature with constants unique for each metal, while other attempts aim for more generalized equations expressing hardness as a function of the melting point, crystal structure, and other fundamental constants, as well as of the testing temperature. The success of these efforts will be discussed briefly. Only those studies will be included which relate to measurements on pure metals where effects of non-equilibrium conditions, precipitation reactions, etc., can be presumed not to appear.

The principal functions that have been proposed for the temperature dependence of the hardness of metals are summarized in Table I. These date from that of Kürth (23) in 1909, the earliest found by the present author in the literature, to that of Schwab (20) in 1949. One might well wonder at the variety of the expressions, not only from the standpoint of the quantitative values predicted but also from that of the implied functional relations. These differences are really not too surprising, however, when the crudity of the early

Table I
Principal Functions Proposed for Temperature Dependence of the Hardness of Metals

Date	Investigator	Experimental Technique on Which Function Is Based	Proposed Function	Implied Linear Dependence	Reference
1909	Kürth	steel ball	$H = H_0 - ct L^{(n-2)/n}$	$H \sim T$	(23)
1916	Ludwik	90° steel cone	$H = H_0 \left(1 - a \frac{T}{T_{mp}}\right)$	$H \sim T$	(19)
1921	Waizenegger	data of Kürth	$H = b (T_{mp} - T)^{4/5}$	$H^{5/4} \sim T$	(24)
1923	Ito	steel ball	$\log H = \log H_0 + aT$ where $a = \frac{2.5}{T_{mp}} - 0.00145$	$\ln H \sim T$	(25)
1930	Shishokin	steel ball	$H = Ae^{-at}$	$\ln H \sim T$	(21)
1949	Schwab	steel ball	$H = A - B \sqrt{T}$	$H \sim T^{1/2}$	(20)
1949	Schwab	steel ball	$H = \frac{1}{Ae^{-\epsilon_1/T} + Be^{-\epsilon_2/T}}$	$\ln H \sim 1/T$	(20)

H = hardness. H_0 = hardness at absolute zero. T = test temperature, °K. T_{mp} = melting point, °K. t = test temperature, °C. L = load in kgs. $n, a, b, c, \alpha, A, B, \epsilon_1, \epsilon_2$ = constants.

hot hardness tests is considered and when cognizance is taken of the limited temperature range of the data obtained by many of the experimenters. Also, the experimental data used in deriving the empirical equations or offered in support of the theoretical derivations were obtained from tests that differed considerably from one another.

Notwithstanding these objections, it is still of interest to attempt anew a semiempirical formulation of an expression for the temperature dependence of hardness based on the best of the existing hardness data. It is of interest, first, because of the possibility of predicting with such an expression the hardness of a metal over a considerable temperature range from data obtained over a limited range, or perhaps directly from such basic properties as crystal structure and melting point. Secondly, a satisfactory functional relation for the temperature dependence of hardness may yield important implications useful in analyzing the results of more rigorous tests. Finally, looking ahead somewhat, it is hoped to compare the functional form of the temperature dependence of the hardness of metals with that for materials of other atomic bond types, provided a satisfactory general expression for metals can be found.

Returning to the equations previously proposed, it may be noted that several of these are not so different as they might seem at first. If the equations of Waizenegger and Ito-Shishokin are expanded, polynomials of the form $A - BT + CT^2 - DT^3 + \dots$ are obtained. Thus Ludwik's and Kürth's equations are merely approximations embodying the first two terms of such a series. Intuitively one would feel that an exponential expression of the type proposed by Ito and independently by Shishokin is the more reasonable one. Support for this is found in the semiempirical equation proposed by Hollomon and Lubahn (26) for the flow stress of metals as a func-

Table II

Investigator	Reference	Technique	Metals Studied				°C Temp. Range
			FCC β Co	BCC Mo, Cr W, Fe	HCP α Co	Other	
Grossmann and Bain	(29)	Brinell 10/3000/30*†					-150/ 500
Ludwik	(19)	Steel cone 90°/5-1000/15	Al, Cu Pb		Zn Cd	Bi, Sn, Sb	20/ 600
Ito	(25)	Brinell 10/300-1000/30	Al, Ag, Cu, Pb, Ni		Zn Cd Mg	Sn, Bi, Sb	-50/ 150
Shishokin	(21, 22)	Brinell 9.52/9.9/1800	Pb Ag	β Ti	Zn Cd α Ti	Bi, Sn	0/300
Inokuty	(30)	Brinell 10/40-1000/20	Al, Cu	Fe	Zn	Sn	-200/ 200
Engl and associates	(31, 32, 33)	Cone 120°/10-150/60 (diamond < 600 °C) (sapphire > 600 °C)	Cu, Ni	Mo, W			-200/ 1900
Bens	(3)	Diamond pyramid 136°/10/15		Cr, Fe, W, Mo			20/ 900
Schwab	(20)	Brinell 6.5/35.6/60	Cu, Ag		Zn Cd		20/ 450
Schwinning and Fischer	(34)	Brinell 10/250/30	Al				-80/ 200
Guillet	(35)	Brinell† 10/500/30	Cu				20/ 1000
Freeman	(36)	Brinell 10/500/30			Zn		20/ 200
Kessler and Hansen	(37)	Diamond pyramid 136°/10.47/15		Mo			20/ 900
Kürth	(23)	Brinell 10/20-1500/60-3600	Cu, Ag, Ni, Al	Zn	Sn		-80/ 500
Ham	(49)	Diamond pyramid‡ 136°/10/15		Mo, W, Fe			-180/ 900
Nachtigall	(50)	Diamond pyramid‡ 136°/10/15		Mo, W			-100/ 800

*Following the convention for reporting hardness data the diameter of the ball is given in mm; the load in kgs. and the time of loading in secs. In the case of cone or diamond pyramid tests the angle of the cone or face angle of the pyramid is given in the place of the ball diameter.

†Loading data not given. Assumed to be standard Brinell values.

‡Loading data not given. Assumed to be standard Vickers values.

tion of temperature, which states that at constant strain and strain rate, the logarithm of stress should vary linearly with temperature. They have shown that such a relation holds for the Boas and Schmid data for the creep of aluminum (27). Carreker (28) has found similar good agreement with their equation for platinum over a wide range of experimental conditions.

This exponential expression was then tested with the best of the hardness data available in the literature. In view of the host of hardness tests used in the past, some basis had to be determined for selection of data for this analysis. The type of test chosen was a static indentation test wherein the results are expressible in terms of the load per unit contact area of impression in kg/mm². Even within this relatively narrow classification there are considerable variations in geometry of indenter, load, and rate and time of loading. These variations will be largely ignored in the following analysis,

since the aim is only a first-order approximation of the generalized behavior of metals. The sources of the selected data are summarized in Table II. Good straight-line plots were obtained in almost every instance. Several representative plots are shown in Figs. 3a to 3d.

It may well be argued that log-hardness versus reciprocal temperature plots of the sort proposed by Schwab give equally good straight lines in many instances, at least over the relatively narrow temperature range of the available data. However, Schwab's equa-

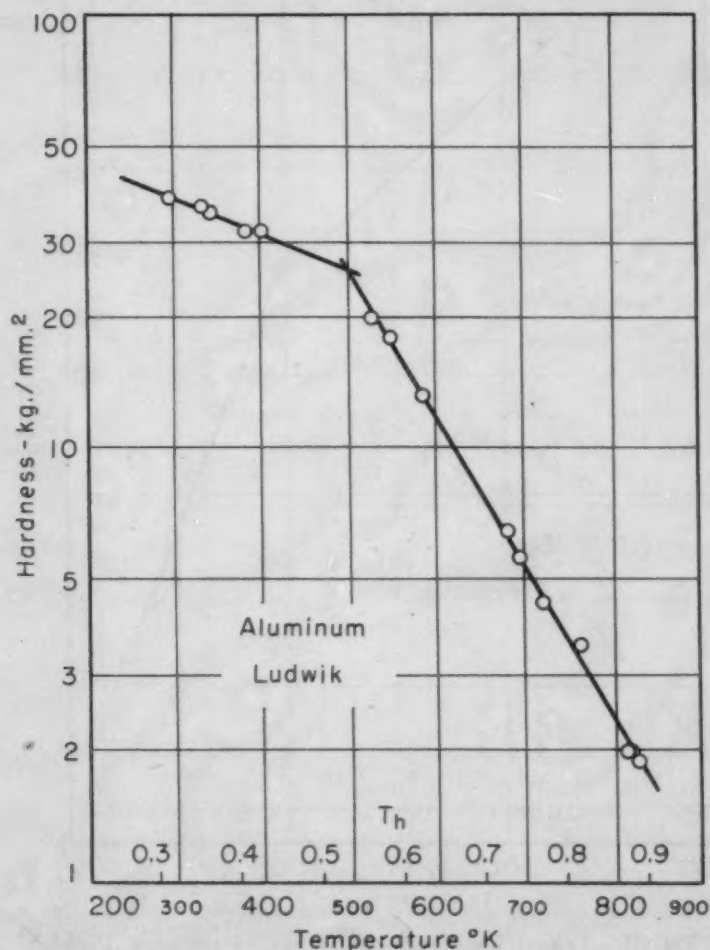


Fig. 3a—Typical Log Hardness Versus Temperature Plots of Hot Hardness Data.

tion predicts infinite hardness at the absolute zero of temperature and a finite hardness at infinite temperature, which does not seem reasonable. The Ito-Shishokin equation, on the other hand, predicts finite hardness at absolute zero and zero hardness at infinite temperature. Further, several sets of data give definite curves rather than straight lines when plotted against reciprocal temperature. A typical example is shown in Fig. 4 for the data of Grossmann and Bain (29) on molybdenum.

If we now examine the breaks found in the group of plots represented by Figs. 3a to 3d, we may attempt to determine whether these result from a metallurgical change in state, the deformation mechanism, or the method of plotting itself. It was first observed that the breaks were of two types: an abrupt vertical discontinuity or a sudden change in slope with no discontinuity. Those of the first type may be identified in almost every case with known allotropic trans-

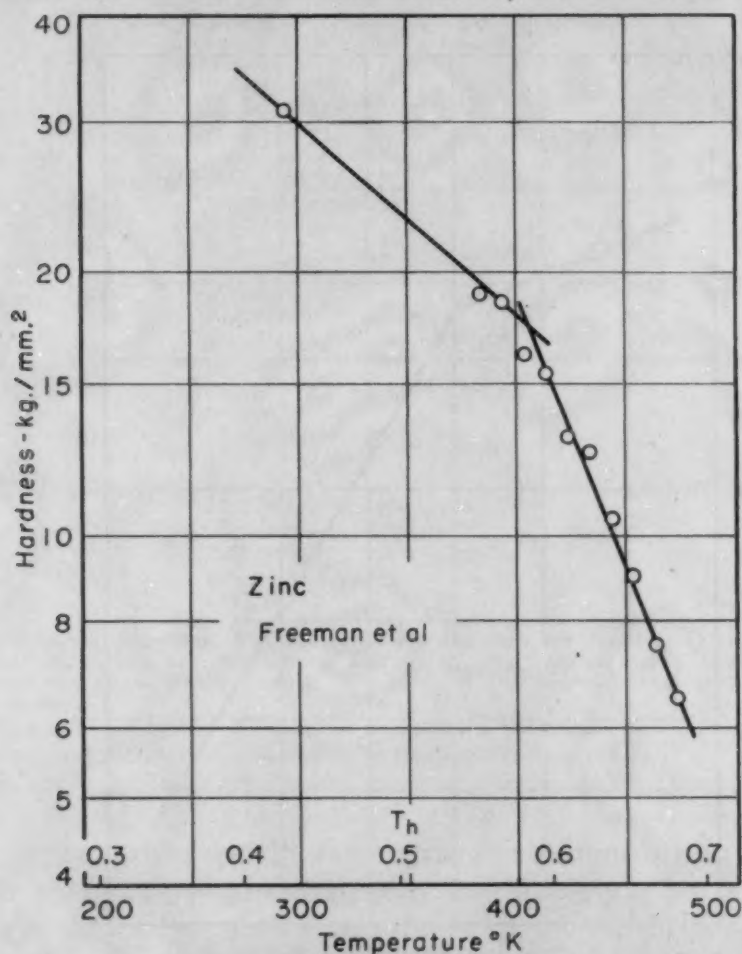


Fig. 3b—Typical Log Hardness Versus Temperature Plots of Hot Hardness Data.

formations; a typical example is given in Fig. 5. A break involving a change in slope always occurs at about $0.55 T_{mp}$, the absolute melting point.⁵ The possibility of identifying breaks of this second type with allotropic changes is obviated on two counts: the nature of the discontinuity is unlike that usually found for such changes, and, further, all metals obviously do not show allotropy at $0.55 T_{mp}$.

A correlation of these hardness-temperature plots with tensile

⁵It is presumed that purity, grain size, strain rate, etc., affect the exact value of this homologous temperature. See further below.

data also lends support to the deformation mechanism idea for explanation of the slope change at $0.55 T_{mp}$ and causes one to reject the trivial possibility of the method of plotting. For example, Fig. 6 compares data for the variation of stress with temperature at approximately constant strain and strain rate from tensile tests on copper by Nadai and Manjoine (38) with data of Ludwik (19) for the hot

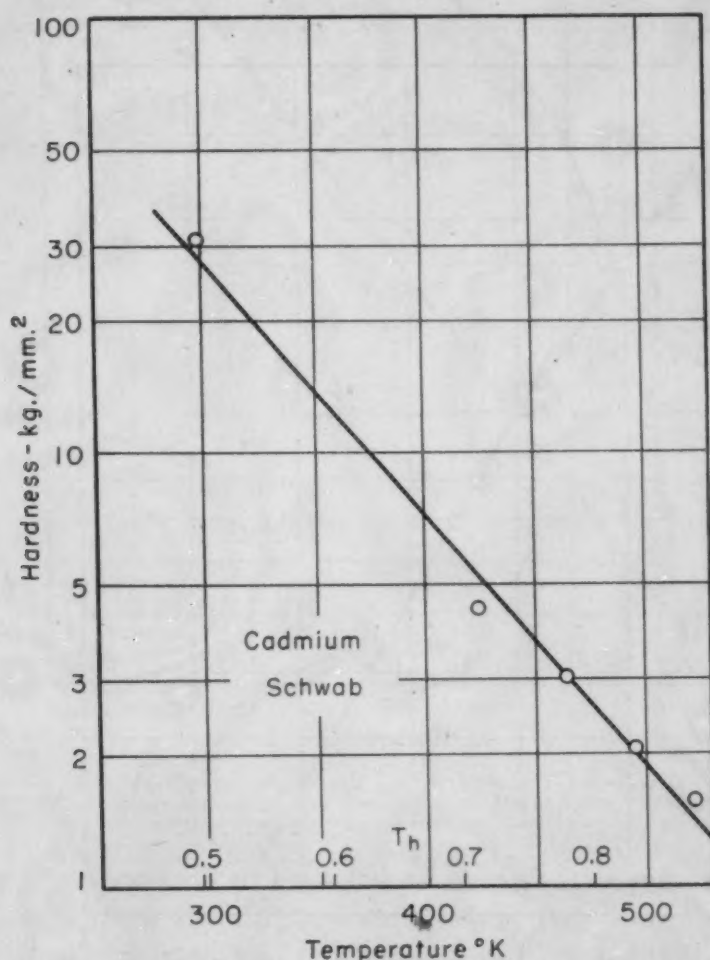


Fig. 3c—Typical Log Hardness Versus Temperature Plots of Hot Hardness Data.

hardness of the same material. In the case of creep and tensile tests, such breaks frequently have been interpreted (26, 39, 40, 41) as an indication of two mechanisms of flow, one at low temperatures, one at high temperatures. This hypothesis has often [see for example (26)] been extended to say that the high temperature mechanism is probably one of grain rotation, a process which has been shown (41-44) to occur at high temperatures, while the low temperature mechanism is slip. There is not much doubt that grain boundary flow frequently occurs; but that it is very likely not the primary mechanism of high temperature deformation can be seen from Fig. 7

in which are replotted the data of Engl and Heidtkamp (31) for single and polycrystalline copper as log hardness versus temperature. The single-crystal data show breaks in the log hardness - temperature curves just as do the polycrystalline data. Engl and Heidtkamp sought for evidence of recrystallization in their single crystals by metallographic examination of sections taken through their hardness indentations. No such evidence was found in specimens tested below

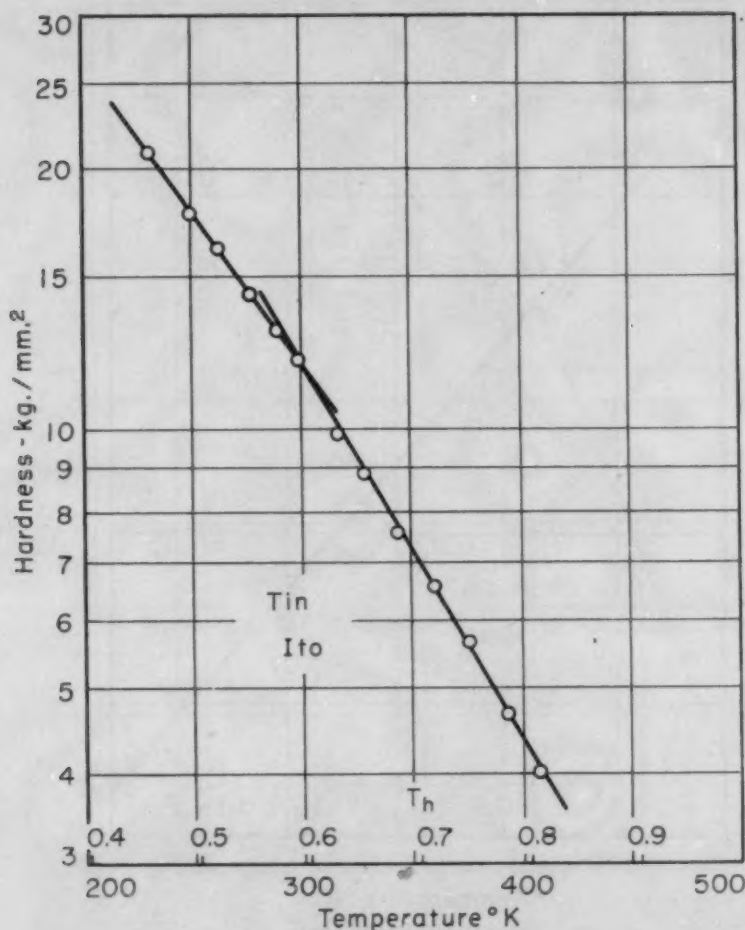


Fig. 3d—Typical Log Hardness Versus Temperature Plots of Hot Hardness Data.

about 1000 °K, although recrystallization was detected in specimens tested at 1050 °K and above. Explanation for the observed breaks in the log hardness - temperature curves must lie other than in recrystallization or grain boundary flow.

The slight differences between the single and polycrystalline copper data of Fig. 7 are attributed by Engl and Heidtkamp to the fact that their single crystal contained 2% silver. The observed behavior is in accord with the results of Servi and Grant (41) who have shown that impurities tend to raise the temperature of transition

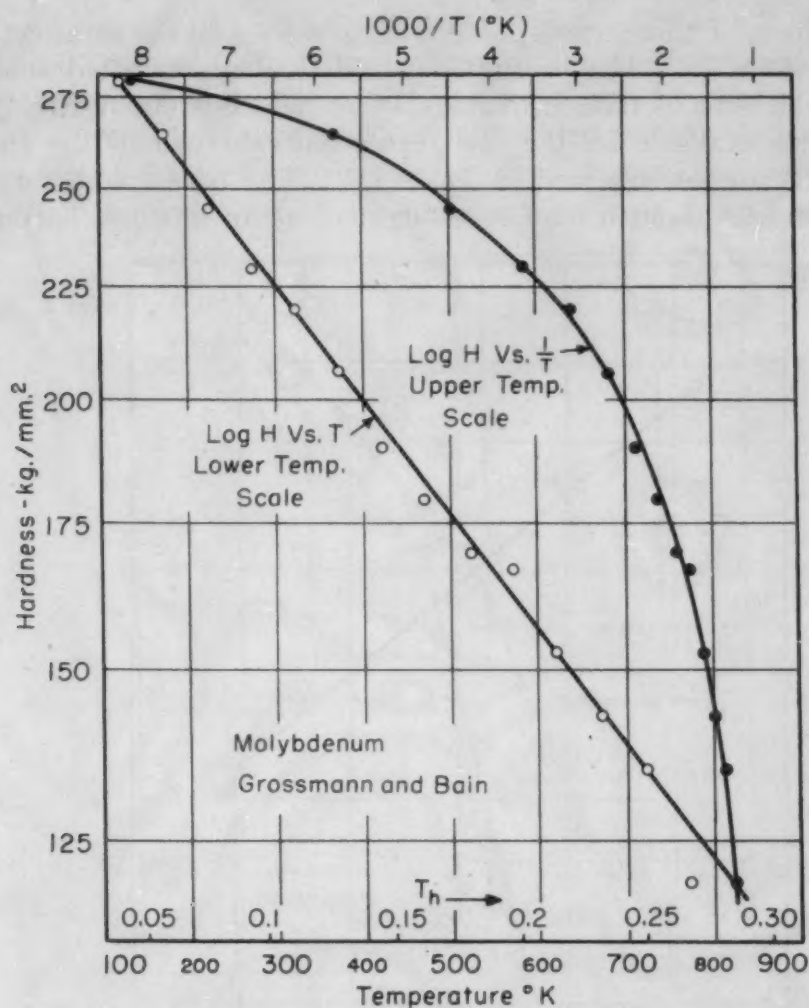


Fig. 4—Comparison of the Log H Versus T and Log H Versus $1/T$ Representations of the Temperature Dependence of Hardness.

from low temperature to high temperature behavior.⁶

Summarizing the findings thus far, it has been shown that the temperature dependence of hardness is well represented by a function of the form $H = Ae^{-BT}$ where the constants A and B have one set of values at low temperatures, and another set of values at high temperatures, possibly indicative of two deformation mechanisms.

FUNDAMENTAL CORRELATIONS

It is now of interest to study the data more closely and seek a correlation between the constants A and B and fundamental physical parameters. At this point we will confine our attention to the low temperature region where we know the deformation mechanism and

⁶Servi and Grant also find that increasing strain rate increases the transition temperature. The effects of grain size and other variables are as yet unresolved. The effects of such variables on the transition temperature in hardness tests are to be explored further in other papers (14, 15).

where effects of time, atmosphere, etc., are least likely to affect the experimental data. The constants A and B were evaluated analytically for all sets of data in Table II, for which at least five good points were available on the low temperature branch of the curve. The results are summarized in Table III. The constant A for this low temperature branch may be thought of as an intrinsic hardness,

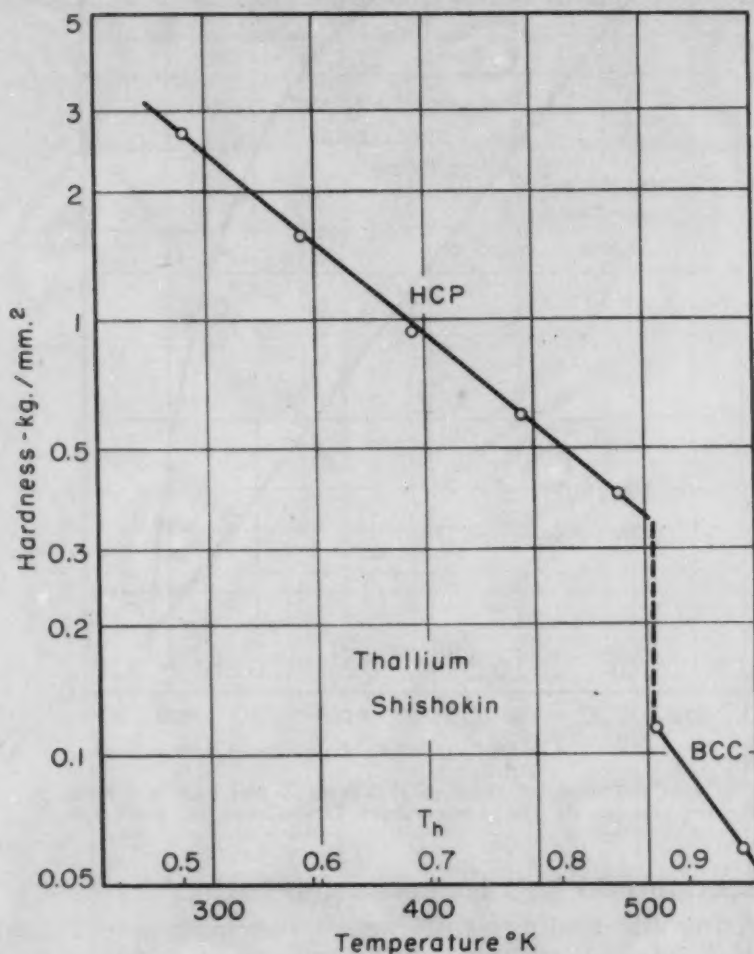


Fig. 5—Typical Example of a Log H Versus T Plot Showing an Allotropic Transformation.

i.e., the extrapolated hardness at absolute zero. The constant B determined from the slopes of this portion of the curve may be thought of as the thermal coefficient of hardness.

One might expect A to be a measure of the inherent strength of the interatomic bond in the metal lattice. If this is so, A should be roughly proportional to the absolute melting point. An approximately equivalent and more satisfying correlation might be found with an energy parameter. Since the flow process is one in which only displacement of one part of the lattice relative to another occurs rather than actual rupture, the "thermal energy of melting" should be a better measure of the resistance to flow than would the true

cohesive energy. The term, "thermal energy of melting", is used to mean the heat content of liquid metal at the melting point and will be designated by the symbol Θ_{imp}^7 . To test this hypothesis, absolute values of these heat contents were calculated for the various metals by graphical integration from the specific heat equations of Kelley (45, 46) supplemented where necessary by data from Quill (47).

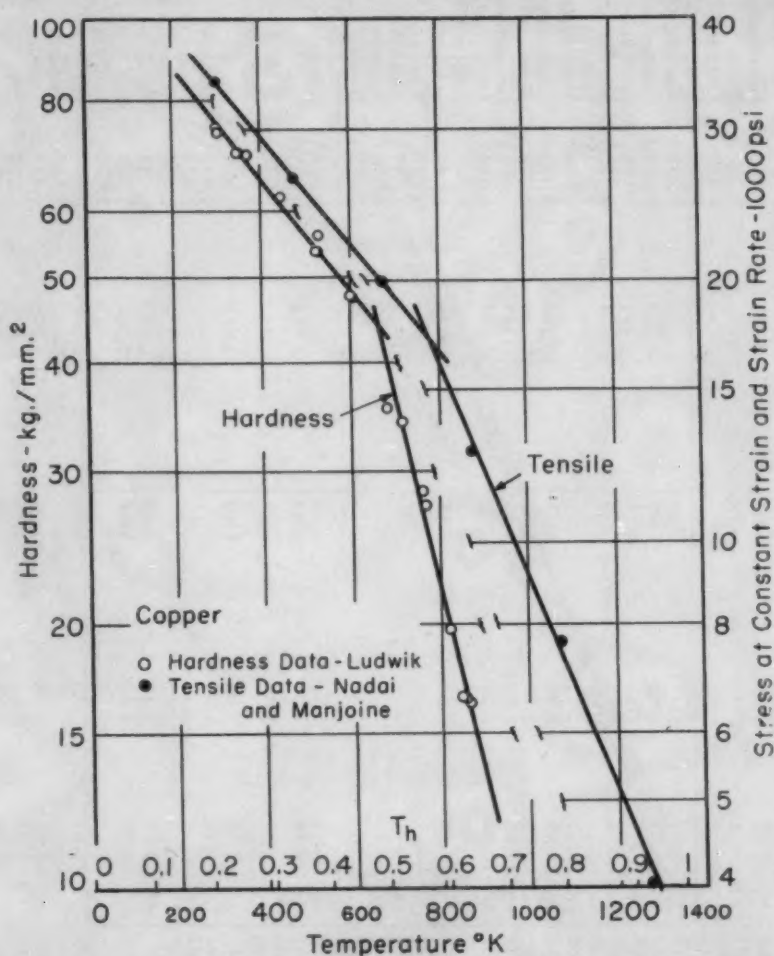


Fig. 6—Correlation Between the Temperature Dependence of Hardness (Ludwik) and of Tensile Strength (Nadai and Manjoine) for Pure Copper.

These results are also summarized in Table III and are plotted against the A values for the same metals in Fig. 8. The corresponding plot of A values versus the absolute melting points is shown in Fig. 9.

It will be observed that the two plots show practically the same relationships. In both cases the data fall into natural groups according to their crystal structure. Within each group, A tends to increase approximately linearly with increasing binding energy. Reasonably, the curves pass through the origin, those representing the least sym-

⁷ Θ is used for heat content, rather than the conventional H , to eliminate confusion with the hardness symbols using H .

Table III
Summary of Hardness-Temperature Data

Correlation of the Constants of the Low-Temperature Branches of the Log Hardness - Temperature Curves With Thermal Energy Parameters

Metal	T_{mp} (°K)§	$\frac{1000}{T_{mp}}$ (°K ⁻¹)	A (kg/mm ²)	-1000B (°K ⁻¹)	$(\theta_{imp})^{*†}$ (kcal/mol)	$\theta_{T_{mp}/2}$ (kcal/mol)	$\bar{C}_p = \frac{\theta_{T_{mp}/2}}{T_{mp}/2}$ (cal/°K)	$P = \frac{\bar{C}_p}{\theta_{imp}}$ (°K ⁻¹)	$Q = \frac{-1000B}{\ln A}$ (°K ⁻¹)	Investigator	Refer- ence
W	3655	0.274	510	1.464	33.6†	9.20	5.04	0.150	0.235	Grossmann and Bain	29
			349	0.627	0.107	Bens	3
			192	0.786	0.150	Engl and Folmer	32
			294	1.140	0.200	Ham	49
			220	0.614	0.1093	Nachtigall	50
Mo	2893	0.346	323	1.233	26.6†	8.66	5.99	0.225	0.214	Grossmann and Bain	29
			172	0.844	0.164	Engl and Folmer	32
			101	0.403	0.0875	Kessler and Hansen	37
			116	0.445	0.0935	Ham	49
			126	0.466	0.0962	Nachtigall	50
Cr	2193	0.466	206	0.287	21.55	6.70	6.11	0.284	0.0539	Grossmann and Bain	29
			171	1.94	18.85	5.79	6.34	0.336	0.378	Ham	49
			213	0.237	17.66	3.92†	5.50†	0.312	0.0442	Grossmann and Bain	29
			99.0	0.386	16.62	5.26	6.09	0.367	0.0841	Ito	25
			107	1.039	0.222	Engl and Katz	33
Cu	1357	0.739	68.9	0.708	11.34	3.52	5.19	0.458	0.167	Ito	25
			64.9	0.957	0.230	Engl and Katz	33
			117	1.473	0.309	Ludwik	19
			65.8	1.630	0.390	Inokuty	30
			65.6	1.305	0.312	Guillet	35
Ag	1233	0.813	54.9	1.695	0.423	Schwab	20
			59.4	1.498	0.366	Kürth	23
			45.4	0.841	10.54	3.37	5.47	0.518	0.221	Ito	25
			35.4	1.404	0.395	Schwab	20
			25.6	1.093	0.338	Shishokin	22
Al	933	1.070	66.7	2.41	7.88	2.05	4.40	0.559	0.574	Ito	25
			65.1	1.843	0.442	Ludwik	19
			38.0	1.502	0.415	Inokuty	30
			52.0	1.912	0.485	Schwinn and Fischer	34
			99.6	2.92	7.54	2.16	4.69	0.622	0.636	Ito	25
Mg	903	1.108	115	2.555	10.06	2.29	5.08	0.506	0.539	Ito	25
			55.1	6.93	1.096	Ludwik	19
			263	4.92	6.61	1.55	4.48	0.679	0.885	Ito	25
			128	2.73	0.563	Inokuty	30
			35.1	5.47	4.81	1.58	5.26	1.095	1.547	Ito	25
Pb	600	1.667	236	6.63	4.81	1.41	4.75	0.988	1.218	Ito	25
			594	1.683	1.350	Ito	25
			544	1.840	5.64	1.36	5.00	0.887	1.350	Ito	25
			135	8.08	4.55	1.11	4.41	0.969	1.642	Ito	25
			505	1.980	1.969	Inokuty	30

§ Melting points from Smithells (18). * Except as noted, calculated by C_p equations of Kelley (45, 46). † θ is used for heat content rather than the conventional H , to eliminate confusion with the hardness symbols using H . ‡ Obtained by graphical extrapolation from data in Quill (47). § To avoid the heat of transition and break in the $C_p(T)$ curve which occurs in cobalt just below 0.5 T_{mp} , \bar{C}_p was calculated from data for the range from 0 °K to the transition temperature, 713 °K.

metric structures having the greater slope. Of particular interest is the fact that the elongated c/a ratio of cadmium and zinc compared to the normal close-packed c/a ratio is sufficient to place these metals on a separate curve. The points for bismuth, antimony, and tin are not to be associated with any of the curves shown, for these metals have rhombohedral and tetragonal structures. With the exception of the two refractory metals, molybdenum and tungsten, the scatter

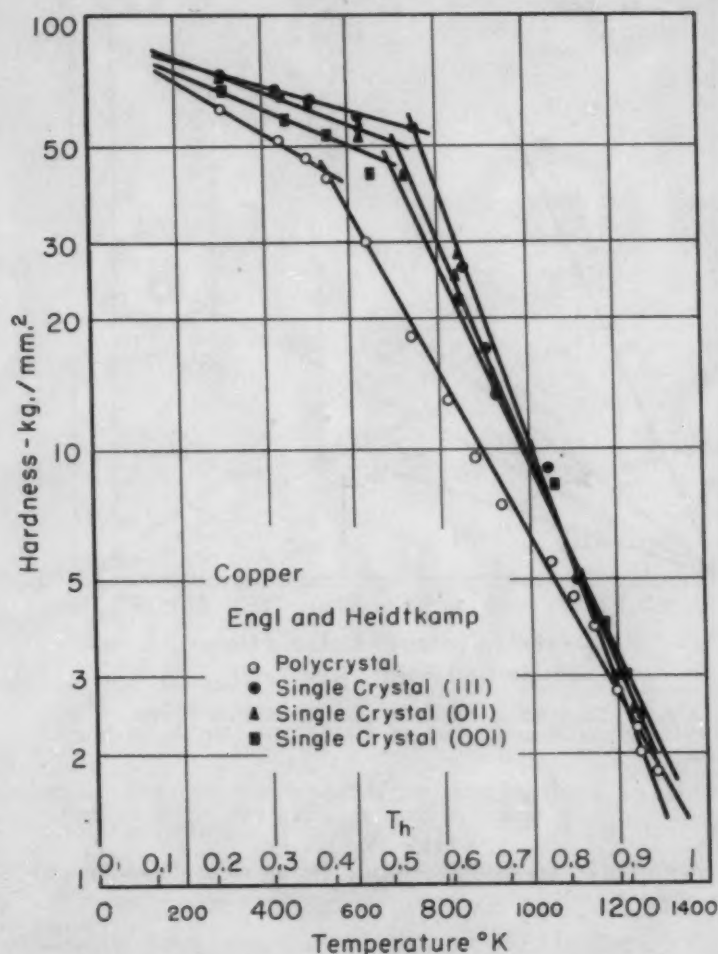


Fig. 7—Temperature Dependence of Hardness in Single and Polycrystalline Copper. Data of Engl and Heidtkamp replotted on semilogarithmic scale.

in the data of various investigators is remarkably small, considering the dissimilarity in the tests and the probable variation in purity of the metals tested. The considerably wider scatter in the case of molybdenum and tungsten is not unexpected because of the difficulty in preparing these metals (chromium as well) in high purity form. The marked effects of small quantities of impurities on the hardness of refractory metals can be illustrated by some data on the room temperature hardness values of several grades of "pure" titanium (48), as shown in Table IV. The only inconsistency in Figs. 8

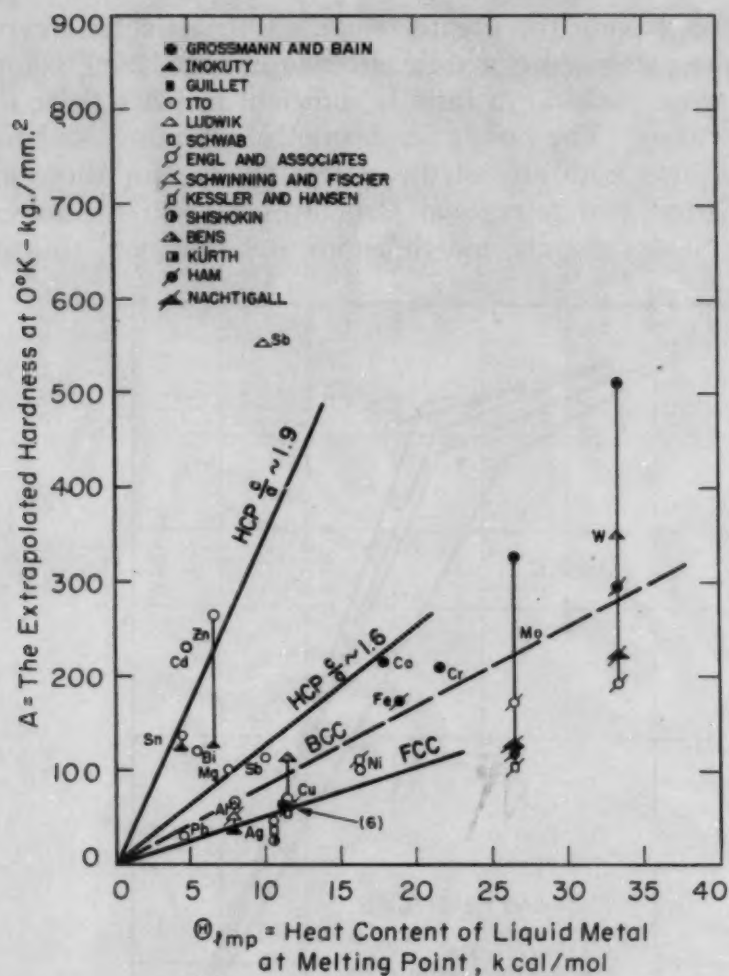


Fig. 8—Correlation Between the Constant A (From $H = Ae^{-BT}$) and the Heat Content of Liquid Metal at the Melting Point.

Table IV
Effect of Purity on Room Temperature Hardness of Titanium (48)

Grade	Approximate Purity %	Typical Hardness VPN
Iodide	99.95	90
Dupont L	99.8	145
Dupont Standard	99.6	165
Dupont H	99.5	195
Dupont HH	99.4	225

and 9 for which there is no apparent explanation is the discrepancy between the values for antimony found by Ludwik and by Ito.

In analyzing the data obtained for the slopes of the log hardness-temperature curves, we might begin with the observation of Ito (25) and of Shishokin (21) that an inverse relation exists between this slope and the melting point. Further study is required, since Ito did not recognize the fact that the slope changes as one crosses from

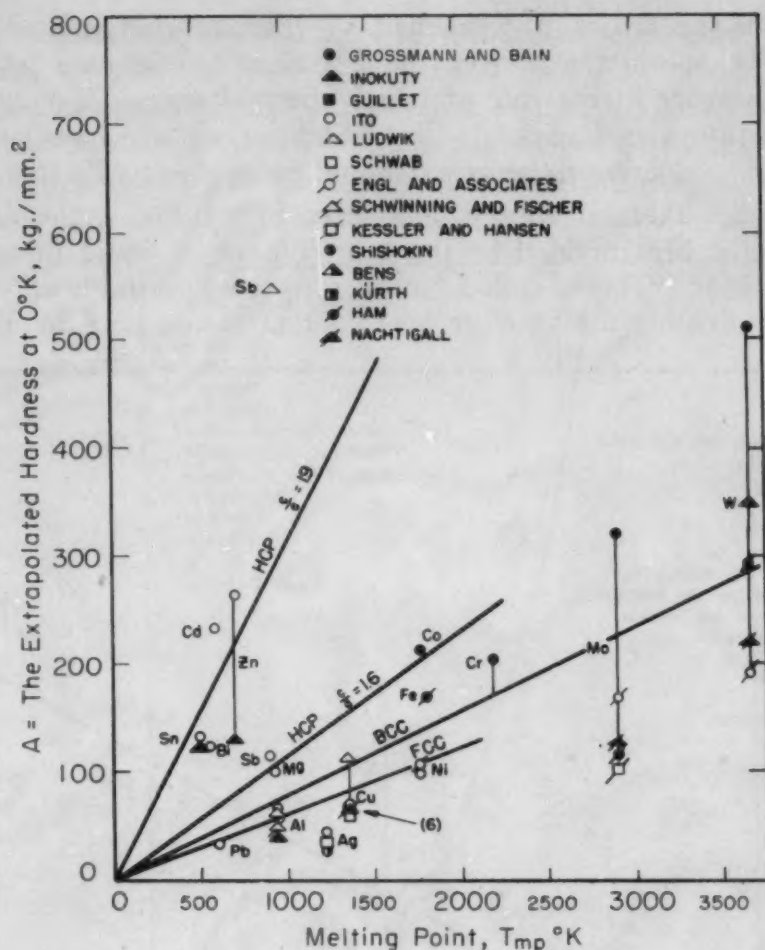


Fig. 9—Correlation Between the Constant A (From $H = Ae^{-BT}$) and the Absolute Melting Point, T_{mp} .

the region of the low temperature mechanism to that of the high temperature mechanism. Shishokin noted this in some cases but apparently did not realize the generality of the phenomenon. In addition, it would be desirable to place this empirical relationship on a somewhat more fundamental basis than the melting point. It may also be seen from Fig. 10, which plots slope versus reciprocal melting point from the data of Table III, that the Ito-Shishokin reciprocal melting point relation is not an entirely satisfactory one, since, if the data for the lower melting point metals are valid, the plot seems to indicate that metals with melting points above 1615 °K should show *zero or positive slope*. Actually, W, Mo, Cr, Co, and Ni all show finite *negative values of slope*. Hence, a somewhat more complex function is indicated.

In seeking a correlation for the A values, use was made above of the thermal energy required for melting as a measure of the resistance to flow. One might therefore expect to find a relationship between the slope (B) of the log hardness - temperature plot, i.e., the

rate at which the lattice is weakened by thermal energy, and the mean effective specific heat over the pertinent temperature range, which is a measure of the rate at which thermal energy is built up as the temperature is increased. Inasmuch as we are considering different metals, relative parameters should be devised. To this end we will define a thermal energy parameter $P = \bar{C}_p / \Theta_{\text{imp}}$, the mean effective specific heat divided by the heat content of liquid metal at the melting point. The so-called "mean effective specific heat" was computed by dividing the absolute heat content at one-half the abso-

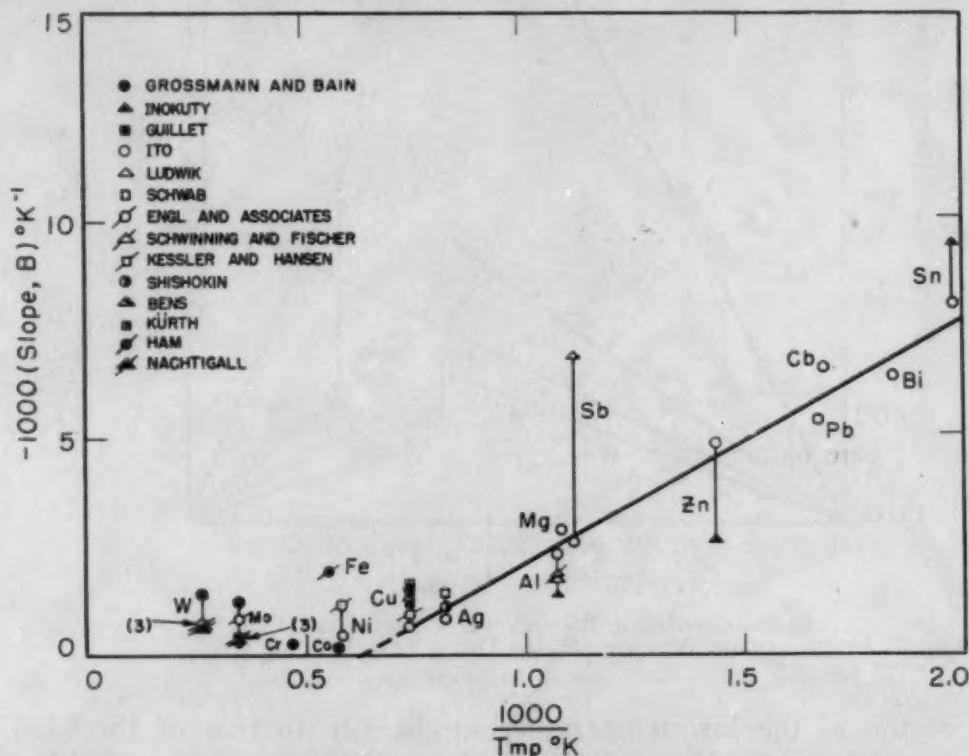


Fig. 10—Correlation Between the Constant B (From $H = Ae^{-BT}$) and the Reciprocal Melting Point, $1/T_{\text{mp}}$.

lute melting point (obtained by graphical integration as above) by half the absolute melting point. Thus, the parameter P is the fraction of the thermal energy required for melting which is added per degree temperature rise. Another parameter Q , designated as the slope parameter, will be defined as $Q = \text{slope } |B| / \ln A$. It is thus the fractional hardness change relative to the intrinsic hardness that occurs per degree temperature rise. The various terms used in the computation of these two parameters are summarized in Table III.

Fig. 11 shows the result of plotting the calculated values of P and Q from Table III against each other. The correlation is considered to be fairly good. Only one point falls very far from a smooth curve drawn through the group of points and the origin. The curve is drawn through the origin since it seems reasonable

that if there could be a case where there were no change in thermal energy with temperature, there should also be no change in hardness with temperature. The stray point is that derived from Ludwik's data on antimony, which was already suspected as being anomalous (see Figs. 8 and 9). It is now clear that the proper representation of the data in Fig. 10 is a curve, concave upward, passing through

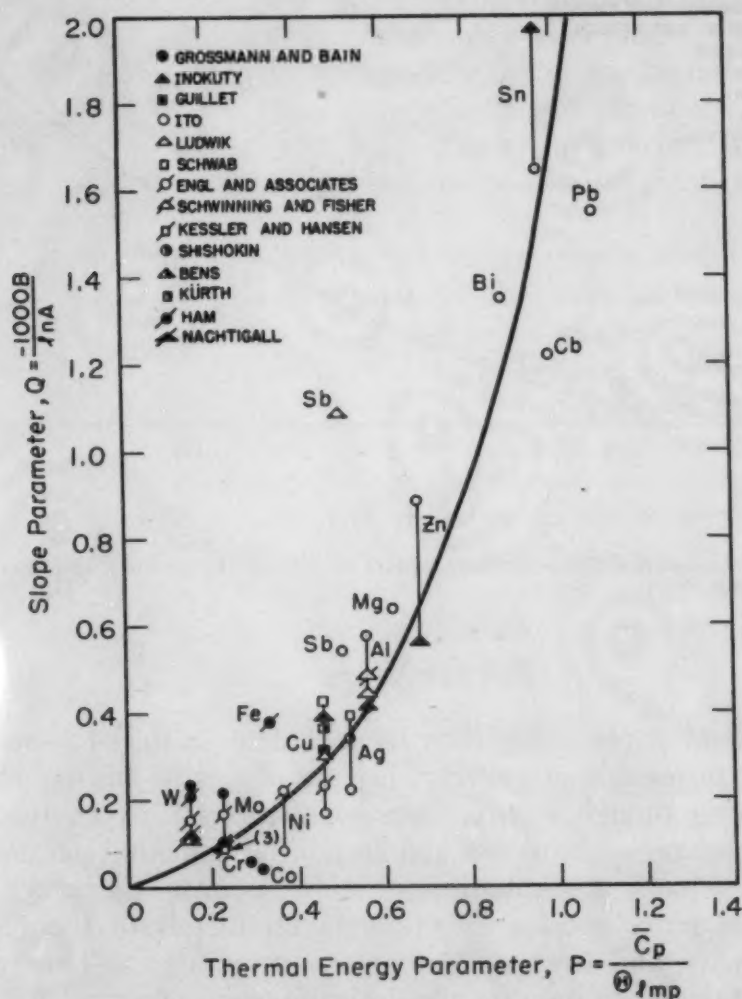


Fig. 11—Correlation Between a Thermal Energy Parameter $P = \frac{\bar{C}_p}{\theta_{1mp}}$ and a Slope Parameter $Q = \frac{1000B}{\ln A}$

the origin. In other words, a hypothetical metal of infinitely high melting point would show zero slope in the log hardness – temperature plot. Fig. 10 is redrawn in this fashion in Fig. 12.

The scatter of the points in Fig. 11 is too great to permit the application of curve-fitting techniques in order to establish an exact relation between the parameters P and Q . However, judging from the shape of the smooth curve as drawn in Fig. 11, it appears that a hyperbolic equation of the form $Q = P/(a + bP)$ is more likely than a parabolic or logarithmic relation.

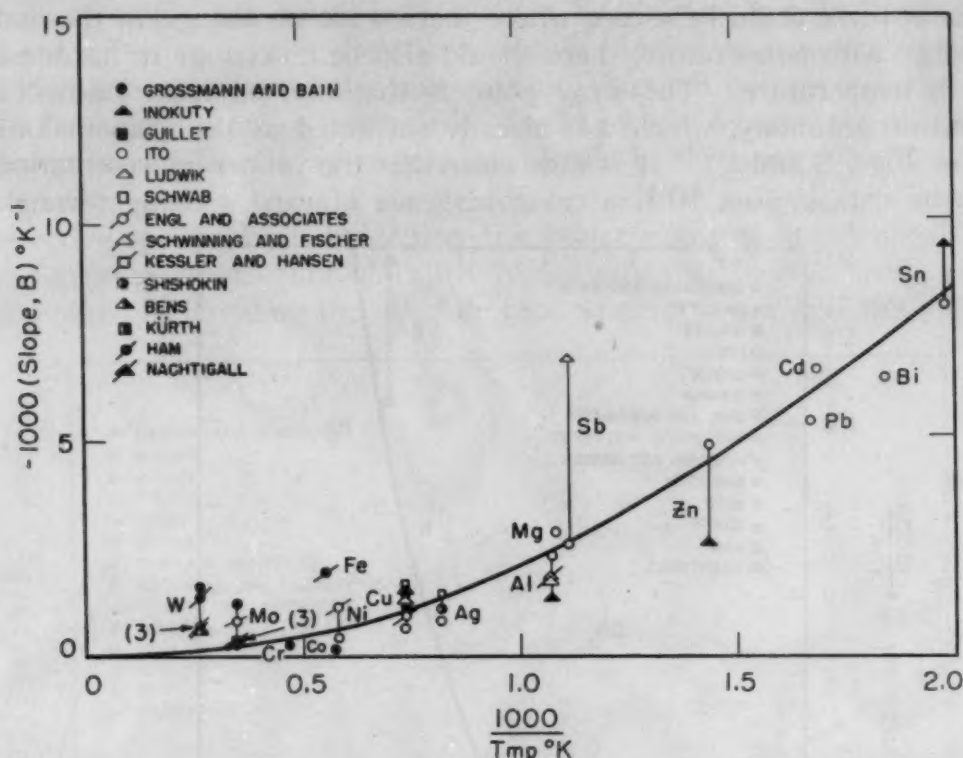


Fig. 12—Correlation Between the Constant B (From $H = Ae^{-BT}$) and the Reciprocal Melting Point.

FUTURE WORK

The present paper using data from widely scattered sources in the literature on metals of varying degrees of purity has established some interesting though approximate correlations between the temperature dependence of hardness and certain fundamental parameters. We must now seek confirmation or refutation of these relations from new and more precise experiments on metals of the highest obtainable purity and over wide temperature ranges. The results presented in this paper indicate the desirability of selecting, for such experiments, metals representative of each of the common crystal structures. Within each group of structures the metals selected should cover the widest possible range of melting points. For example, we might choose, in the FCC group, metals ranging from Pb (m. p. 327 °C) to Ir (m. p. 2454 °C), in the BCC group, Li (m. p. 180 °C) to W (m. p. 3382 °C) and in HCP, Tl (m. p. 300 °C) to Re (m. p. 3167 °C). It would be desirable, if possible, to make these tests on single crystals in order to avoid grain size effects. In all cases the temperature range to be studied would be based upon the homologous temperature scale. An experimental program along these lines is now underway; results of these studies will be published in forthcoming papers.

SUMMARY

It has been shown that the temperature dependence of the hardness of pure metals is well represented by a function of the form $H = Ae^{-BT}$ where the constants A and B have one set of values at low temperatures, where slip is the primary deformation mechanism, and another set of values at high temperatures, where viscous flow or some as yet unidentified mechanism predominates. The transition between low and high temperature behavior in the indentation hardness test is related to the absolute melting point of the metal, occurring at approximately $0.55 T_{mp}$. Purity, grain size, strain rate and other variables presumably affect its position slightly on the temperature scale.

Within the low temperature range, the constant A is simply related to the crystal structure and the thermal energy of melting defined as the heat content of liquid metal at the melting point. The A values for a given thermal energy of melting are found to increase with decreasing symmetry in the crystal structure. Within the same temperature range, the constant B is related in a somewhat complex way to the rate of change of heat content with increasing temperature. It is thus possible to calculate (at least approximately) the hardness of a pure metal as a function of temperature up to about half the absolute melting point if the crystal structure, specific heat, and heats of fusion and transformation are known. A new experimental program based on these results is proposed.

ACKNOWLEDGMENT

The author is indebted to many of the members of the Metallurgy and Ceramics Division of the General Electric Research Laboratory, particularly Mr. J. D. Nisbet and Dr. W. R. Hibbard, for their helpful discussion and criticism of this analysis. Thanks are also due Mrs. M. Doyle and Miss Nancy Weaver of this laboratory for performing most of the computations.

References

1. D. Tabor, "A Simple Theory of Static and Dynamic Hardness", *Proceedings*, Royal Society, London, A, Vol. 192, 1948, p. 247.
2. E. J. Janitzky and M. Baeyertz, "The Marked Similarity in Tensile Properties of Several Heat Treated SAE Steels", *METALS HANDBOOK*, American Society for Metals, Cleveland, 1939, p. 515.
3. F. P. Bens, "Hardness Testing of Metals and Alloys at Elevated Temperatures", *TRANSACTIONS*, American Society for Metals, Vol. 38, 1947, p. 505.
4. C. Barus, "On the Probability of an Inherent Relation of the Electrical Resistance and Hardness of Steel", *Physical Review*, Vol. 30, 1910, p. 347.
5. C. Barus and V. Strouhal, "The Electrical and Magnetic Properties of the Iron Carburets", *Bulletin*, U. S. Geological Survey, No. 14, House

- Miscellaneous Document, 2nd Session 48th Congress, Vol. 16, 1884-5, p. 597.
6. S. R. Williams, "A Correlation Between the Mechanical Properties and the Magnetostrictive Effects of Ferromagnetic Substances", *TRANSACTIONS, American Society for Steel Treating*, Vol. 5, 1924, p. 562.
 7. H. O'Neill, *Hardness of Metals and Its Measurement*, Sherwood Press, Cleveland, 1934.
 8. S. R. Williams, *Hardness and Hardness Measurements*, American Society for Metals, Cleveland, 1942.
 9. G. V. Smith, "Strain Hardening—Effects of Alloying Elements and Microstructure", from *Cold Working of Metals*, American Society for Metals, Cleveland, 1949.
 10. P. Lazarev, "Relationships Between Hardness and Properties of the Elements", *Bulletin, Academy of Sciences, Russia*, Vol. 6, 1918, p. 1259; *ibid.*, 1918, p. 2241; *ibid.*, 1919, p. 1005.
 11. J. Innes, "Mechanics of Solidity", *Nature*, Vol. 106, 1921, p. 377.
 12. C. Benedicks, "Derivation of Planck's Energy Distribution Law from the Agglomeration Hypothesis; A Simple Relation Between Hardness and Vibration Frequency", *Annalen der Physik*, Vol. 42, 1913, p. 133.
 13. V. D. Kuznetzow, "Mechanical Properties as a Function of the Ionic Radii", *Journal of Physical Chemistry, USSR*, Vol. 6, 1935, p. 813.
 14. W. R. Hibbard, "Strength Properties of Solid Solutions" (in preparation).
 15. J. D. Nisbet and J. H. Westbrook, "Temperature Dependence of the Strength of Alloys, I" (in preparation).
 16. J. A. Brinell, "Researches on the Comparative Hardness of Acid and Basic Open Hearth Steel at Various Temperatures by Means of Ball Testing", *Iron and Steel Magazine*, Vol. 9, 1905, p. 16-19.
 17. *METALS HANDBOOK*, American Society for Metals, Cleveland, 1948.
 18. C. J. Smithells, *Metals Reference Book*, Interscience Publishers, New York, 1949.
 19. P. Ludwik, "The Variation of the Internal Friction of Metals with Temperature", *Zeitschrift für physikalische Chemie*, Vol. 91, 1916, p. 232.
 20. G. M. Schwab, "Some New Aspects of the Strength of Alloys", *Transactions, Faraday Society*, Vol. 45, 1949, p. 385.
 21. V. P. Shishokin, "The Hardness and Fluidity of Metals at Different Temperatures", *Zeitschrift für anorganische Chemie*, Vol. 189, 1930, p. 263.
 22. V. P. Shishokin, "The Relation Between Chemical Composition and the Thermal Coefficient of Plastic Deformation", *Bulletin, Academy of Sciences, USSR, Class des sci. math. et natur.*, 1937, p. 1341.
 23. A. Kürth, "Investigations on the Effect of Heat on the Hardness of Metals", *Zeitschrift des Vereins deutscher Ingenieure*, Vol. 53, 1909, p. 85, 209.
 24. F. Waizenegger, "Contribution on Hardness Testing", *Zeitschrift des Vereins deutscher Ingenieure*, Vol. 65, 1921, p. 824.
 25. K. Ito, "The Hardness of Metals as Affected by Temperature", *Tohoku Science Reports*, Vol. 12, 1923, p. 137.
 26. J. Hollomon and J. Lubahn, "The Flow of Metals at Elevated Temperatures", *General Electric Review*, February and April, 1947.
 27. W. Boas and E. Schmid, "The Dependence of Crystal Plasticity on Temperature", *Zeitschrift für Physik*, Vol. 71, 1931, p. 703.
 28. R. Carreker, "Plastic Flow of Platinum Wires", *Journal of Applied Physics*, Vol. 21, 1950, p. 1289.
 29. M. A. Grossmann and E. C. Bain, *High Speed Steel*, 1931, p. 87, J. Wiley, New York City, data taken from private communication from E. S. Davenport and W. P. Sykes.
 30. T. Inokuty, "Thermal Brittleness of Metals", *Tohoku Science Reports*, Vol. 17, 1928, p. 817.

31. J. Engl and G. Heidtkamp, "Temperature Dependence of the Cone Hardness of Metals, I", *Zeitschrift für Physik*, Vol. 95, 1935, p. 30.
32. J. Engl and J. Folmer, "Temperature Dependence of the Cone Hardness of Metals, II", *Zeitschrift für Physik*, Vol. 98, 1936, p. 702.
33. J. Engl and J. Katz, "Temperature Dependence of the Cone Hardness of Metals, III", *Zeitschrift für Physik*, Vol. 106, 1937, p. 1.
34. W. Schwinning and F. Fischer, "Investigation of the Effect of Temperature on the Notch Toughness and Hardness of Aluminum Alloys", *Zeitschrift für Metallkunde*, Vol. 22, 1930, p. 1.
35. L. Guillet, "The Variation of the Hardness of Alloys of Copper with Temperature", *Revue de Metallurgie*, Vol. 21, 1924, p. 295.
36. V. R. Freeman et al, "Pure Zinc at Normal and Elevated Temperatures", *Science Papers*, Bureau of Standards, No. 522, Vol. 20, 1926, p. 661.
37. H. D. Kessler and M. Hansen, "A Study of Arc-Melted Molybdenum-Rich Chromium-Molybdenum Alloys", *Transactions*, American Society for Metals, Vol. 42, 1950, p. 1008.
38. A. Nadai and M. J. Manjoine, "High Speed Tension Tests at Elevated Temperatures", Parts II and III, *Transactions*, American Society of Mechanical Engineers, Vol. 63, 1941, p. A-77.
39. S. Dushman, "Cohesion and Atomic Structures", *Proceedings*, American Society for Testing Materials, Vol. 29, Part II, 1929, p. 7.
40. N. J. Grant and A. G. Bucklin, "On the Extrapolation of Short-Time Stress-Rupture Data", *TRANSACTIONS*, American Society for Metals, Vol. 42, 1950, p. 720.
41. I. S. Servi and N. J. Grant, "Creep and Stress Rupture Behavior of Aluminum as a Function of Purity", *Journal of Metals*, Vol. 3 (10), October 1951, p. 909.
42. W. Rosenhain and J. Humphrey, "The Crystalline Structure of Iron at High Temperatures", *Proceedings*, Royal Society (London), Vol. 83, 1909, p. 200.
43. D. Hanson and M. A. Wheeler, "Deformation of Metals Under Prolonged Loading—Part I, Flow and Fracture of Aluminum", *Journal*, Institute of Metals, Vol. 45, 1931, p. 229.
44. H. F. Moore, B. B. Betty and C. W. Dollins, "The Creep and Fracture of Lead and Lead Alloys", *University of Illinois Bulletin*, 1935, p. 272.
45. K. K. Kelley, "Contributions to the Data on Theoretical Metallurgy", X, Bulletin No. 476, U. S. Bureau of Mines, 1949.
46. K. K. Kelley, "Contributions to the Data on Theoretical Metallurgy", XI, Bulletin No. 477, U. S. Bureau of Mines, 1949.
47. L. L. Quill, "Chemistry and Metallurgy of Miscellaneous Materials, Thermodynamics", McGraw-Hill, New York City, 1950.
48. P. C. Rossin, Private communication.
49. J. L. Ham, "An Introduction to Arc Cast Molybdenum and Its Alloys", *Transactions*, American Society of Mechanical Engineers, Vol. 73 (6), August 1951, p. 723.
50. E. Nachtigall, "Behavior of Molybdenum and Tungsten in the Low and Medium Temperature Ranges", *Powder Metallurgy Bulletin*, Vol. 6 (1), 1951, p. 26.

DISCUSSION

Written Discussion: By W. Chubb, Battelle Memorial Institute, Columbus, Ohio. 1177

The author is to be complimented upon his critical analysis of the hot-hardness data available in the literature. His selection of the log-

hardness-temperature representation of these data is to be especially commended.

It is especially interesting to note that the author has noticed a relation between the melting point of pure metals and the inflection point in the log-hardness-temperature curves. There also seems to be some relationship between the extrapolated hardness of the metals at 0 °K and the heat content of the molten metals at their melting point.

While these relationships probably have some basis in the physical nature of metals, it should be pointed out that there are exceptions to the inflection point-melting point relation. At any event, it is well known that zirconium (m.p. 2100 °K) and titanium (m.p. 2090 °K) have allotropic transformations at approximately $0.55 T_{mp}$ (1136 and 1158 °K respectively). One would not expect another basic change in the coherency of the metals very close to these temperatures. However, numerous hot-hardness tests on zirconium at Battelle Memorial Institute have established the existence of an inflection point in the log-hardness-temperature curve at about 710 °K or $0.34 T_{mp}$. It also should be noted that this point is not really a point on the hot-hardness curve; it is obtained by extrapolation of the straight-line portions of the curve which extend to within 20 or 30 degrees of the inflection point. Near the inflection point, there is a transition zone where the graph changes slope gradually.

Another interpretation of the transition zone around the inflection point is that it represents a temperature range below which cold working takes place during the time of the hardness test and above which hot working takes place. Certainly, it represents a change in atomic mobility or freedom within the solid. If processes taking place at temperatures just above the inflection point cannot be associated with recrystallization, then at least they should be associated with stress relief during the time of the hardness test.

Written Discussion: By Donald N. Frey, Ford Motor Company, Dearborn, Mich.

The writer of this discussion very much enjoyed reading and thinking upon the points put forth in this paper. Accordingly, he wishes to congratulate the author for this excellent paper.

As a further point for discussion, are there sufficient data for any analysis of the temperature variation of hardness above the $0.5 T_{mp}$ transition point? If so, what are the results?

Written Discussion: By J. T. Waber and F. W. Schonfeld, staff members, Los Alamos Scientific Laboratory, University of California, Los Alamos, N. M.

In his extremely interesting paper, the author rejects the tentative suggestion made by Hollomon and Lubahn (Ref. 26) that the grain boundary rotation accounts for, or strongly affects, the high temperature behavior of metals. The rejection is based on Fig. 7. The present writers submit the idea that highly strained single crystals behave similarly to polycrystalline specimens, and hence the rejection may not be necessary. In support of this idea, Fig. 13 illustrates the different temperature dependences (of the critical shear stress) of strained and unstrained single crystals, respectively.

In an unpublished study, using Schwab plots, the present writers have

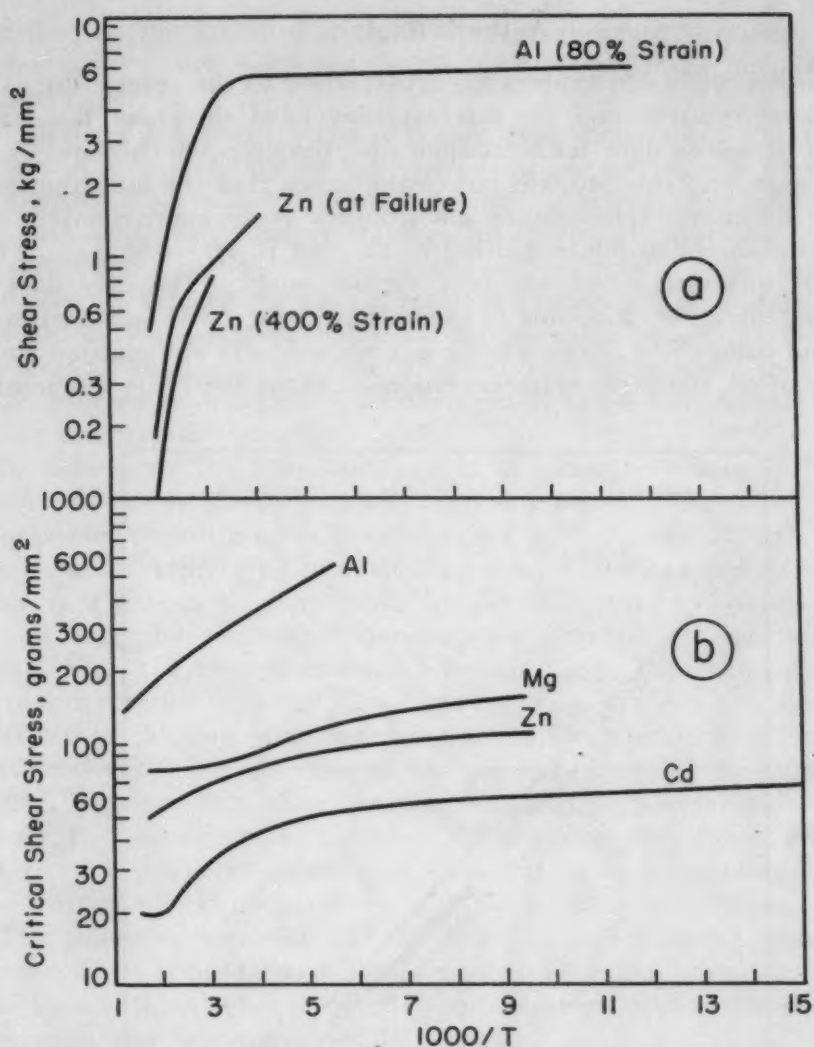


Fig. 13—Temperature Dependence of Shear Stress in Strained and Unstrained Crystals. (Redrawn from data of W. Boas and E. Schmid, *Zeitschrift für Physik*, Vol. 61, 1930, p. 767, and of E. Schmid and W. Fahrenhorst, *Zeitschrift für Physik*, Vol. 64, 1932, p. 845.)

observed that tensile data as well as hardness data show the same changes in slope in the vicinity of $0.6 T_m$. Fig. 13a is reminiscent of our Schwab plots of hardness and tensile data.

There is independent evidence that the grain boundary slip and grain rotation begin to occur in the vicinity of $0.6 T_m$ (depending slightly on strain rate, etc.) and there is some evidence that these phenomena affect tensile and compressive strengths at test temperatures higher than this critical temperature when the strain is not too large.

The orientation differences between subgrains in a heavily deformed single crystal are perhaps large enough that the further strain behavior is essentially "polycrystalline". Hence it appears injudicious to dismiss grain rotation on the basis of Fig. 7 alone, since severe local deformation is produced in any conventional hardness test.

Author's Reply

The author wishes to express his appreciation to the several discussers for their kind remarks and the interest they have shown in this paper. Dr. Chubb describes data for zirconium and titanium which show exceptions to the general rule brought out in the paper that the inflection point on the log hardness-temperature plots occurs at an approximately constant fraction of the absolute melting point, that is, at $\sim 0.55 T_{mp}$. These findings are interesting and will bear further study. The only data for titanium and zirconium available to the author show too wide a scatter for analysis and comparison. The situation is undoubtedly complicated by the occurrence of an allotropic transformation at about the same temperature

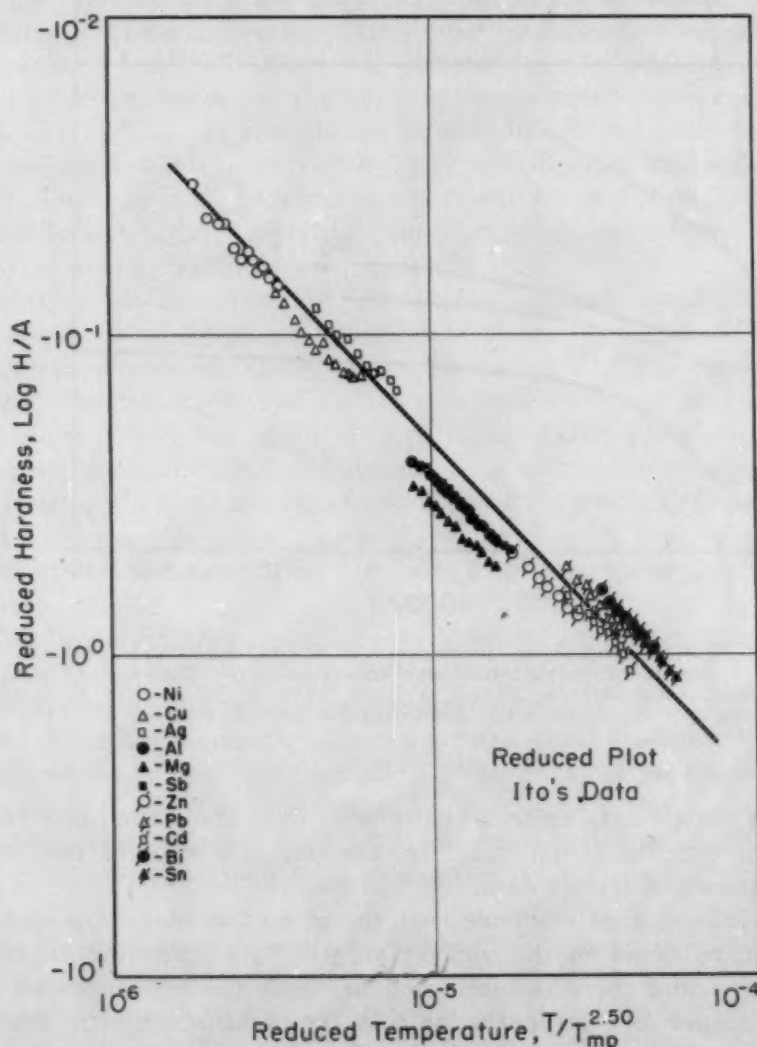


Fig. 14

range. However, in contrast to Dr. Chubb's view, the author does not believe that the occurrence of one such change in lattice coherency would necessarily obviate the possibility of a change of another type. The author agrees with Dr. Chubb that the inflection point is not a true point, but is

obtained by extrapolation of straight-line segments into a transition region. This feature was not very clear in the particular figures included in the published paper.

Both Dr. Chubb and Messrs. Waber and Schonfeld discuss the possible mechanisms involved in the "high temperature" region of the hardness plots. All agree that this region is one of increased atomic mobility; the question lies in the exact ways in which the atoms move. Although recrystallization must be ruled out, recovery or stress relief may play a major role. In rejecting the grain rotation hypothesis, the author intended to discard only the notion that gross movement of grains at the original grain boundaries is a primary mechanism. It is quite likely that subgrain formation or polygonization of strained grains has a considerable effect on the high temperature behavior.

In answer to Dr. Frey, analysis of the hardness data for the high temperature region ($>0.5 T_{mp}$) has been attempted. The slope of the log hardness-temperature plots in this region yielded correlations with melting point and thermal energy of melting similar to those found for the low temperature region, however, with considerably greater scatter. No correlations could be established between the constant A and fundamental parameters in the high temperature region. It is felt that this result is due to differences between tests (purity, strain-rate, time, etc.) whose effects are much more pronounced at the high temperatures. These variations, particularly in the case of the constant A , which establishes the hardness level and thus the transition temperature, are evidently sufficient to mask the fundamental relations. It is hoped that these will become clear when a sufficient amount of data has been accumulated from the current experimental program.

The following analysis may serve as an indication of what may be expected when accurate data for several pure metals have been obtained. It has been established that hardness-temperature data in the low temperature range may be represented by

$$H = Ae^{-BT} \quad (1)$$

We may then write

$$\ln \frac{H}{A} = -BT \quad (2)$$

where B was shown roughly to be a function of reciprocal melting point. This function is of the type

$$B = \frac{K}{T_{mp}^n} \quad (3)$$

Substituting this in (2), we obtain

$$\ln \frac{H}{A} = -K \frac{T}{T_{mp}^n} \quad (4)$$

Thus by plotting $\ln H/A$ versus T/T_{mp}^n we should obtain a reduced plot in which hardness data for all pure metals fall on a single straight line. We can only expect good results in a plot of this sort when the effects of variations in testing technique have been minimized, i.e., by examining the

data of a single worker. Of the various previous investigators, Ito gives data for the greatest number of pure metals. A reduced plot was therefore prepared from his data and is shown in Fig. 14. A log-log representation was chosen because of the breadth of range of variables. While the logarithmic plot tends to improve the appearance of the correlation, the result is still interesting.

THE EFFECT OF DISPERSIONS ON THE TENSILE PROPERTIES OF ALUMINUM-COPPER ALLOYS

By R. B. SHAW, L. A. SHEPARD, C. D. STARR AND J. E. DORN

Abstract

The plastic properties of aluminum-copper alloys were correlated with the mean free path between the hard CuAl_2 particles dispersed in the alpha solid solution phase. The true stress-true plastic strain curves for the various dispersions formed a homologous series, the yield strength and the rate of strain hardening increasing uniformly with decreasing mean free path between the CuAl_2 particles in the alpha solid solution. These results were found to be valid over the entire range of conditions that were examined, covering test temperatures of 78 to 295 °K, and compositions of 3, 4 and 5% copper in high purity aluminum. The present observations are in qualitative agreement with those made by Gensamer et al on the correlation between the mean free ferrite path and the tensile properties of heat treated steels. A small quantitative difference, however, was detected between the present results and those obtained by Gensamer; whereas Gensamer found that the flow stress decreased linearly with the logarithm of the mean free ferrite path in steels, the results on CuAl_2 dispersions in an alpha solid solution of copper in aluminum suggest that the logarithm of the flow decreases linearly with the logarithm of the mean free path between the CuAl_2 particles. None of the recent dislocation theories for plastic deformation in polyphase systems are in complete quantitative harmony with either the former observations on steels or the present observations on aluminum-copper alloys.

INTRODUCTION

THE significant effect of dispersions of hard constituents embedded in a soft ductile phase on the plastic properties of polyphase alloys was uncovered shortly following the introduction of metallurgical microscopy early in the history of scientific physical metallurgy. Over the intervening years, extensive practical use was made of the knowledge that the yield strengths of polyphase alloys could be improved solely by refining the dispersion of the hard con-

A paper presented before the Eighth Western Metal Congress of the Society, held in Los Angeles, March 23 to 27, 1953. Of the authors, R. B. Shaw, L. A. Shepard and C. D. Starr are research engineers, and J. E. Dorn is professor of metallurgy, University of California, Berkeley, Calif. Manuscript received May 29, 1952.

stituent in the soft ductile phase. But in spite of the recognized technological importance of this subject, no systematic study of the effects of dispersions on the plastic properties of alloys was made until 1942 when Gensamer and his colleagues (1)¹ first reported their investigations on the effect of dispersions of carbides in ferrite on the plastic properties of steels. Since that time, several theories based on the concept of dislocations have been formulated to predict

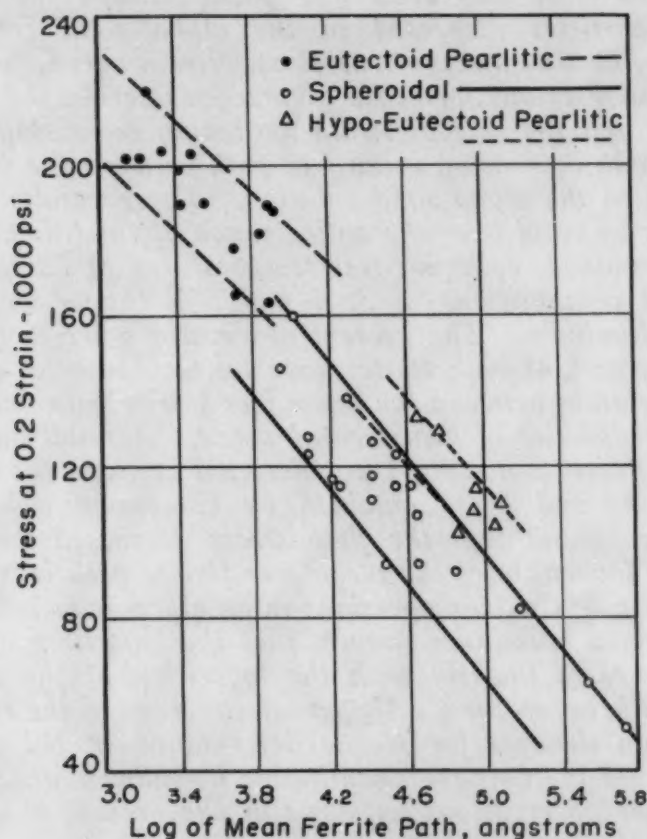


Fig. 1—The Effect of the Mean Distance Between Particles on the Flow Stress of Steels. (After Gensamer.)

the effect of dispersions of hard particles on the plastic properties of alloys. Inasmuch as the current predictions based on the properties of dislocations are not in complete quantitative harmony with the sole experimental data now available, the details of their formulation are highly suspect and they have no justifiable practical value. Apparently two types of investigations are required in order to formulate a more complete understanding of the important effects of dispersions on the plastic properties of polyphase alloys: (a) More extensive information is needed on the actual effects of dispersions on plastic properties and (b) a more realistic theory of the effects

¹The figures appearing in parentheses pertain to the references appended to this paper.

of dispersions on the behavior of dislocations is required. The present research was undertaken in an attempt to help satisfy the first need by analyzing the effect of dispersions of CuAl_2 on the plastic properties of aluminum-copper alloys. It will prove helpful, however, to review the existing knowledge on dispersions before recounting the details of the present investigation.

A summary of the essential observations of Gensamer et al (1, 2) on the effect of dispersions on the deformation strengths of a series of steels is reproduced in Fig. 1 where the deformation strength at a plastic strain of 0.20 is given as a function of the average distance between the carbide particles dispersed in the ferrite phase. The recorded data apply to various steels that had about the same percentage of minor chemical components and differed principally relative to their carbon content and heat treatment. Whereas the pearlites were produced by isothermal decomposition of austenite, the spheroidites were obtained by tempering martensite. These data reveal that, within a rather broad scatter band, the flow strength of dispersions of carbides in ferritic steels decreases linearly with the logarithm of the mean ferrite path independent of carbon content or type of dispersion, be it entirely lamellar or lamellar islands in ferrite, or spheroidal. When the individual scatter bands for eutectoid pearlitic, hypoeutectoid pearlitic, and the various spheroidal dispersions are separately demarked, as shown in Fig. 1, however, the spheroidal dispersions appear to give slightly lower deformation strengths at strains of 0.20 than is given at the same mean free ferrite path for the pearlitic types of dispersions. In view of the recognized difficulties in measuring the mean ferrite paths, this difference might well be attributed to scatter in the data.² On the other hand, additional data will shortly be presented to illustrate that real differences in the plastic properties of pearlitic and spheroidal dispersions do in fact exist. Thus Gensamer's data suggest that the deformation strength of steels at 0.20 strain decreases linearly with the logarithm of the mean ferrite path independent, within the scatter band, of carbon content; but the level of the deformation strength at a given mean ferrite path might be slightly greater at a strain of 0.20 for pearlitic than for spheroidal dispersions.

It is well known that a wide variety of steels obey the empirical stress - plastic strain relationship

$$\sigma = A \epsilon^n$$

Equation 1

where

σ = the true deformation stress

ϵ = the true plastic strain

A = the deformation stress at unit strain

n = the strain hardening index.

²Since this investigation was completed, a report has appeared by Roberts et al (3) on the effects of dispersions of carbides on the plastic properties of plain carbon steels and pure irons. Their data for the carbon steels agreed well with the earlier findings of Gensamer.

Since A and n are constants for any given specimen of steel, they serve to characterize its plastic properties. If, for a given class of steels, n is a single-valued function of A , that class of materials is said to provide an homologous series of stress-strain curves. Although A might increase from specimen to specimen in that class, n will also change systematically so that an entire homologous family of stress-strain curves are obtained in the homologous series of steels. Conversely, if n is not a single-valued function of A within a group of steels, intersecting stress-strain curves will be obtained and the group is nonhomologous. Obviously the plastic properties of dispersions can be correlated uniquely with the mean ferrite path only within an homologous series.

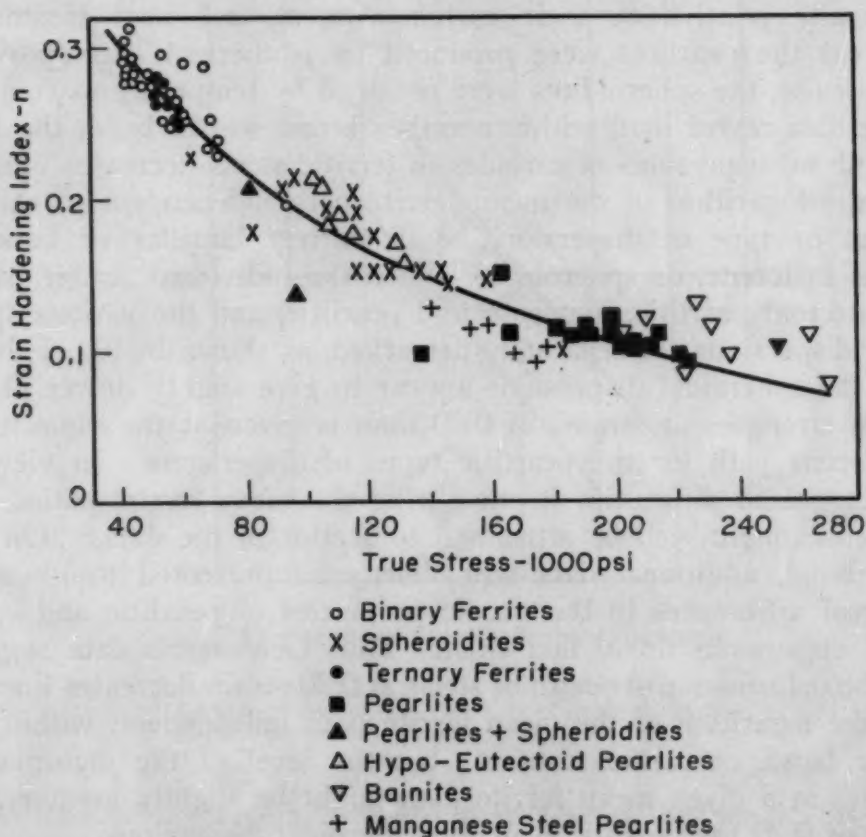


Fig. 2—Correlation of Strain Hardening Index, n , With the Deformation Stress at a Strain of 0.20 (4). (After Gensamer.)

Reference to Fig. 2 reveals that, in general, the strain hardening index decreases uniformly with increasing values of the deformation strength at a strain of 0.20 for a wide variety of steels. This suggests that within the scatter band obtained these steels form an homologous series of alloys. But upon closer inspection of the data, certain well-documented differences between the various types of

steels become evident. For example, the strain hardening index, n , for bainites is greater than that for manganese steel pearlites at the same deformation strength. Although the initial crude analysis suggested that all of the steels represented form an homologous series of alloys, a more refined analysis suggests that the various groups of steels represented in Fig. 2 are somewhat unique.

Bain's data (5) on the effect of dispersions on the plastic properties of a eutectoid steel are given in Fig. 3. These data clearly reveal that, for the same hardness values, the proof stress, breaking

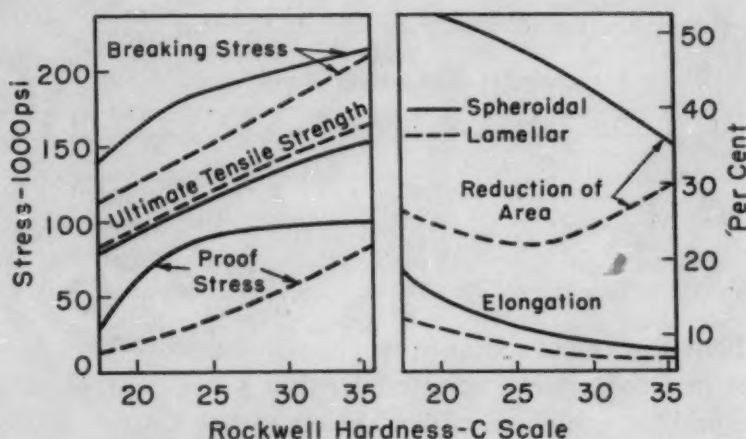


Fig. 3—The Influence of Structure on the Tensile Properties of a Eutectoid Steel. (After Bain.)

stress and tensile strength for the pearlitic structures are distinctly different from those for the spheroidal dispersions. Consequently, the pearlitic and spheroidal dispersions cannot fall into a single homologous series of alloys just as the bainites and the manganese steel pearlites also exhibit distinctly different sets of homologous properties. These deductions insist that the type of structure as well as its dispersion must influence the plastic properties of polyphase alloys. Thus the plastic properties of an alloy containing a hard phase dispersed in a soft ductile phase cannot depend only on the mean path between the hard constituents in the ductile phase but it must also be dependent on the type of structure. The investigations by Gensamer et al reveal that the mean free ferrite path is the more important factor for correlating the plastic properties of steels, and that it is probably the unique factor for a given type of structure.

TEST MATERIALS

Inasmuch as rather extensive data are now available on the plastic properties of steels, it seemed to be desirable to investigate some other polyphase alloy system in order to broaden the basis of our knowledge on the effects of dispersions of a hard constituent in

a soft ductile phase on its plastic properties. The aluminum-copper system was selected for this objective in view of the existing correlatable data on the plastic properties of various alpha solid solutions of aluminum, including the aluminum-copper alpha solid solutions (6). Alloys containing about 3, 4 and 5% of copper by weight as shown in Table I were prepared from high purity aluminum cast into an ingot, homogenized, hot and cold-rolled to 12-inch wide sheet 0.100 inch thick, and finally annealed.³ The various dispersions of CuAl_2 in the aluminum-copper alpha solid solution were then developed in the alloys by special sequences of heat treatments.

Table I
Chemical Composition of the Alloys

Nominal Per Cent by Weight Cu	Per Cent Weight Alloying Component				
	Chemical Analysis Cu	Spectrochemical Analysis			
		Si	Fe	Mn	Zn
3	3.05	0.002	0.002	trace	0.0004
4	4.03	0.002	0.002	0.001	0.0004
5	5.05	0.003	0.002	0.002	0.0006

The heat treatments that were finally employed to develop the dispersions of CuAl_2 were selected so that good control of auxiliary variables could be achieved. In addition to the degree of dispersion, the following factors were considered to be important in evaluating the plastic properties of the aluminum-copper alloys:

1. Grain size of the alpha phase.
2. Composition of the alpha phase.
3. Uniformity of the dispersion, particularly the absence or only nominal presence of grain boundary precipitation.
4. Single type of almost spheroidal dispersion.

The heat treatments which were finally selected for use can be generalized as follows:

A. The as-received alloys were solution heat treated and homogenized for 72 hours at 540 °C (1005 °F) and water-quenched.

B. The alloys were then cold-rolled 30% preliminary to a recrystallization treatment at 540 °C (1005 °F) to provide a constant final grain size of the alpha solid solutions. Unfortunately additional grain growth took place during the subsequent precipitation treatments. Consequently the time at the recrystallization and grain growth temperature had to be controlled for the various alloys and dispersions so that the final alpha solid solution grain size would be identical for all specimens. The grain size for the 3% very coarse dispersion, however, was somewhat larger than that of the other alloys, and therefore the data for the 3% very coarse dispersion were not included in the final analysis.

³All alloys and analyses were furnished by courtesy of the Aluminum Company of America Research Laboratories.

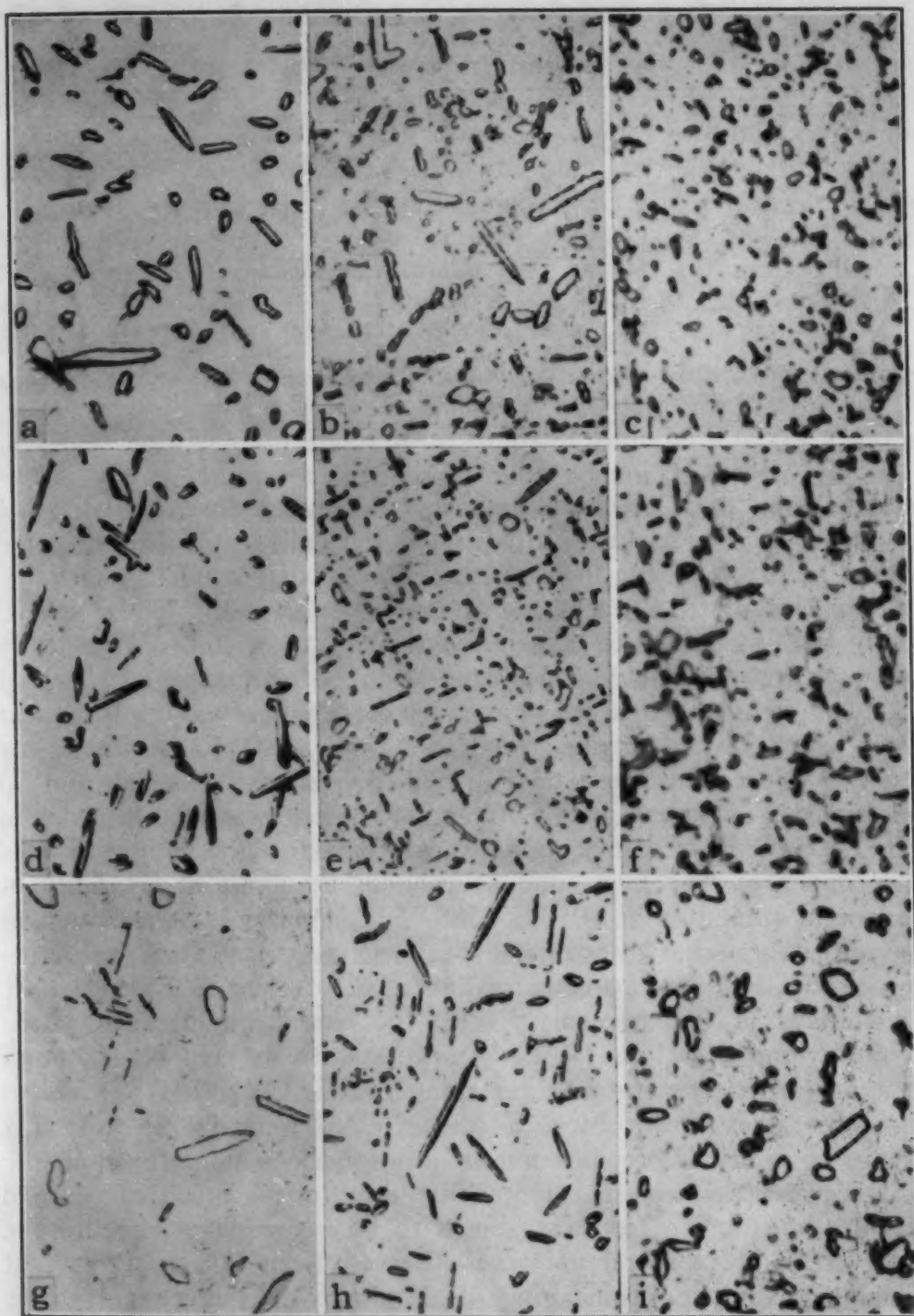


Fig. 4—Photomicrographs of CuAl_2 Dispersions. Specimens a, b, c—5.05% copper-aluminum alloys. Specimens d, e, f—4.03% copper-aluminum alloys. Specimens g, h, i—3.05% copper-aluminum alloys. Specimens a, d, h—Coarse dispersion, $\times 573$. Specimens b, e—Medium dispersion, $\times 1060$. Specimens c, f—Fine dispersion, $\times 2227$. Specimen g—Very coarse dispersion, $\times 885$. Specimen i—Medium dispersion, $\times 2227$.

C. The recrystallization treatments were followed by appropriate aging treatments. In selecting the aging treatments it was

Table II
Heat Treatments for Dispersions of CuAl₂*

Designation % Cu Dispersion	Recrystallization		Preliminary Aging Treatment				Grain Size† grains/mm
	Time Min.	Temp. °C	Time Hrs.	Temp. °C	Time Hrs.	Temp. °C	
3-VC	2¼	540 W.Q.	24	465	0.8
3-C	2¼	540 W.Q.	24	455	2.3
3-M	3	540 W.Q.	¼	455	W.Q. and 3	350	2.4
4-C	2¼	540 W.Q.	24	465	2.4
4-M	2½	540 W.Q.	½	440	A.C. and 3	350	2.3
4-F	1¼	540 W.Q.	0.025	415	W.Q. and 3	350	2.3
5-C	4	540 W.Q.	1	525	2.3
5-M	3¼	540 W.Q.	1	500	2.2
5-F	2½	540 W.Q.	0.025	525	W.Q. and 1	400	2.1

*Symbols: VC = very coarse; C = coarse; M = medium; F = fine; W.Q. = water-quenched; A.C. = air-cooled. †By intercept method.

necessary to avoid conditions which would result in excessive grain boundary precipitation or a strongly crystallographically oriented plate-like precipitation, in order to obtain a fairly random dispersion of particles of CuAl₂ that approximated spheroids. Thus, special aging treatments had to be selected for each alloy and dispersion in order to approximately achieve the described results.

D. Finally the material was given a preliminary aging treatment after which it was furnace-cooled to 305 °C (580 °F) and aged for 2 days. Specimens were then machined from the material, and an additional 2-day aging at 305 °C (580 °F) was practiced in order to remove the effects of machining and to establish the composition of the copper in the alpha solid solution at the limit of solubility of copper in aluminum at 305 °C (580 °F). Precision lattice constant measurements on a series of the specimens suggested that the resulting alpha solid solutions contained about 0.19 atomic per cent copper which was in fair agreement with the extrapolated results from solubility investigations (7, 8). Since specimens held for 1 month at atmospheric temperature after aging at 305 °C (580 °F) exhibited the same stress-strain curve as those tested immediately following aging, no effect of precipitation at atmospheric temperatures on the plastic properties was detected. Furthermore, the effect of possible strain aging during test was shown to be insignificant because the same trends of dispersions were observed from 298 to 78 °K, at which temperature strain aging of aluminum does not occur. The actual heat treatments which were used to develop the various dispersions are given in Table II.

Typical microstructures obtained by the above heat treatments are shown in Fig. 4. In general they exhibit only nominal grain boundary precipitation and fairly uniformly distributed dispersions of CuAl₂. A few of the dispersions as shown for the 4-M dispersion, however, exhibited more plate-like than spheroidal type of precipitate.

CALCULATION OF MEAN FREE PATH

In order to reduce the experimental tedium of actually measuring the mean free path in the alpha solid solution between the particles of CuAl_2 , an approximate method was developed for estimating this quantity from easily obtained metallographic data. Two assumptions, that are only approximately in harmony with the observed microstructures, were made for the purpose of facilitating the analysis: First, the dispersed phase was assumed to consist of uniform spheres, and secondly, it was assumed that the spheres of the intermetallic compound were uniformly dispersed in the alpha solid solution. To a good first-order approximation, therefore, each intermetallic compound of uniform radius r can be conceived to be located at the center of a spherical domain of uniform radius R representing the volume of the particle of the intermetallic compound and its associated solid solution. The calculation of the volumetric mean free path between particles then reduces to a simple problem of geometrical probabilities as follows:

(a) *Frequency of Distribution of Lines in Space*—As shown in Fig. 5 the probability that any line, l , be oriented in the range ϕ to $\phi + d\phi$ to a fixed reference direction, Z , is proportional to the area of a unit reference sphere within the selected range of angles. Thus the well-known relation

$$P(\phi \text{ to } \phi + d\phi) = \frac{\sin \phi d\phi}{\int_0^{\pi/2} \sin \phi d\phi} = \sin \phi d\phi \quad \text{Equation 2}$$

is obtained.

(b) *Average Length of Line in a Sphere*—According to Equation 2 the average length of a line in a spherical domain of radius R is given by

$$\bar{l} = \int_0^{\pi/2} l \sin \phi d\phi$$

Since Fig. 6 reveals that

$$l = 2R \cos \phi$$

the average length of a line in a sphere is

$$\bar{l} = \int_0^{\pi/2} 2R \cos \phi \sin \phi d\phi = R \quad \text{Equation 3}$$

(c) *Probability of a Line Striking a Particle in the Center of a Spherical Domain*—As shown in Fig. 7 the probability, P , of a line in a spherical domain of radius R striking a spherical particle of radius r at the center of the domain is equal to the area of a unit reference sphere included in the range of ϕ from zero to ϕ_1 .

Consequently

$$P = \int_0^{\phi_1} \sin \phi \, d\phi = 1 - \cos \phi_1 = 1 - \frac{\sqrt{R^2 - r^2}}{R} = 1 - \sqrt{1 - \left(\frac{r}{R}\right)^2}$$

Equation 4

(d) *Mean Path*—The number of particles intersected per unit length of a line is equal to the average number of domains intersected per unit length times the probability, P , that a line in a domain will

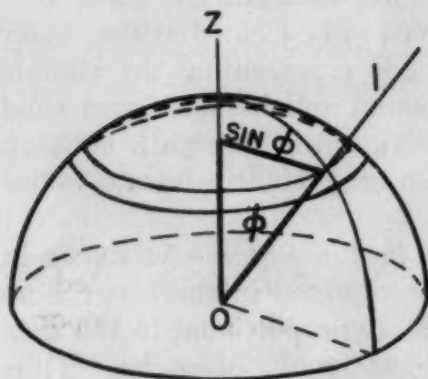


Fig. 5—Frequency of Distribution of Lines in Space.

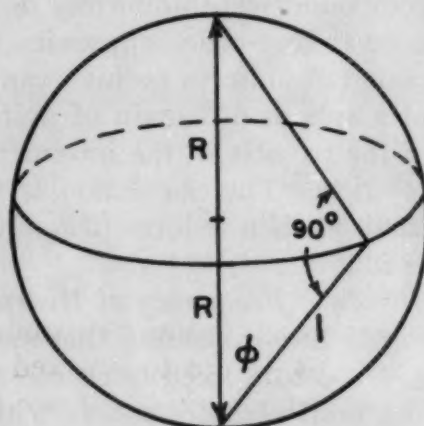


Fig. 6—Average Length of Line in a Sphere.

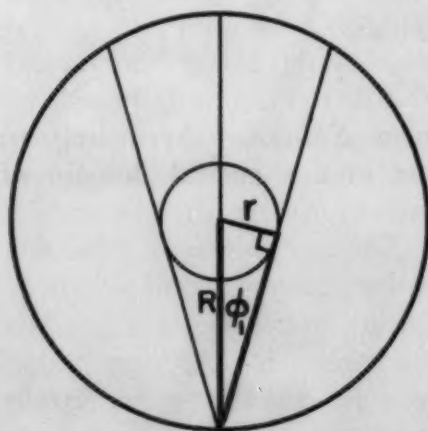


Fig. 7—Probability of a Line Striking a Particle.

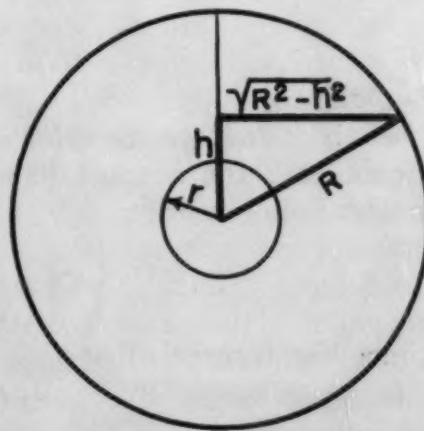


Fig. 8—Average Number of Particles per Unit Area of Polish.

strike a particle. Since the average length of a line in a domain is R , the number of domains intersected per unit length of a line is $1/R$ and therefore the number of particles N_p of radius r intersected per unit length is

$$N_p = \frac{1}{R} \left\{ 1 - \sqrt{1 - \left(\frac{r}{R}\right)^2} \right\}$$

Equation 5

Then the average distance between the centers of particles is

$$\frac{1}{N_p} = \frac{R}{\left\{ 1 - \sqrt{1 - \left(\frac{r}{R}\right)^2} \right\}} \quad \text{Equation 6}$$

and therefore the volumetric mean free path between particles is

$$\text{V.M.F.P.} = \frac{R}{\left\{ 1 - \sqrt{1 - \left(\frac{r}{R}\right)^2} \right\}} - r = R \left\{ \frac{1}{1 - \sqrt{1 - \left(\frac{r}{R}\right)^2}} - \frac{r}{R} \right\} \quad \text{Equation 7}$$

where r is the mean path in the particle.

(e) *Evaluation of R and r* —The values of R and r for determining the V.M.F.P. are easily established from the composition and metallographic inspection of the specimen. As shown in Fig. 8, for all sections of the domain from $h = 0$ to r a particle is seen, whereas for sections from $h = r$ to R no particles are obtained. Thus the number of particles observed per unit area on a plane of polish is

$$N = \frac{\int_0^r dh}{\int_0^R \pi (R^2 - h^2) dh} = \frac{3r}{2\pi R^2} \quad \text{Equation 8}$$

Furthermore the ratio of the volume of the particle to that of the surrounding domain is

$$f = \frac{4/3 \pi r^3}{4/3 \pi (R^3 - r^3)} = \frac{1}{\left(\frac{R}{r}\right)^3 - 1} \quad \text{Equation 9}$$

Whereas N can be determined directly from counts of the number of particles per unit area on a plane of polish, f can be evaluated from the known composition, phase diagram, and the density of the two phases. Assuming a density of $\rho = 4.35$ for CuAl_2 , a density of 2.73 for the alpha solid solution and assuming the alpha solid solution contained 0.194 atomic per cent copper the values of f given in Table III were obtained for the present alloys.

Table III
Volumetric Ratios of CuAl_2 to the Alpha Solid Solution

Weight % Copper	f
8.05	0.0323
4.03	0.0453
5.05	0.0595

Table IV
Mean Free Path Determination

Disper- sion	Test Tem- perature	No. Particles in 5-cm. Diameter Circle		N $\times 10^{-4}$	f	V.M.F.P. in cm.	P.M.F.P. in cm.
		Magni- fication					
5% C	78 °K	375 \times	51	36.1	0.0595	0.0091	0.000502
	135	375 \times	82	58.4	0.0595	0.0071	0.000395
	194	725 \times	23	62.9	0.0595	0.0069	0.000381
	295	725 \times	23	58.9	0.0595	0.0071	0.000389
5% M	78 °K	573 \times	71	118.9	0.0595	0.0051	0.000277
	135	573 \times	65	108.5	0.0595	0.0052	0.000290
	194	725 \times	62	167.3	0.0595	0.0042	0.000234
	295	725 \times	60	160.6	0.0595	0.0043	0.000239
5% F	78 °K	2227 \times	302	7616.7	0.0595	0.00062	0.0000346
	135	2227 \times	280	7061.8	0.0595	0.00065	0.0000359
	194	2227 \times	354	8928.2	0.0595	0.00058	0.0000319
	295	2227 \times	276	6960.9	0.0595	0.00065	0.0000362
4% C	78 °K	573 \times	57	95.0	0.0453	0.0065	0.000400
	135	573 \times	57	95.5	0.0453	0.0065	0.000400
	194	573 \times	58	96.7	0.0453	0.0064	0.000395
	295	573 \times	66	106.3	0.0453	0.0061	0.000379
4% M	78 °K	1060 \times	307	1754.3	0.0453	0.00151	0.000093
	135	1060 \times	262	1497.2	0.0453	0.00163	0.000100
	194	1060 \times	336	1920.0	0.0453	0.00144	0.000088
	295	1060 \times	306	1365.7	0.0453	0.00171	0.000103
4% F	78 °K	2227 \times	256	6456.0	0.0453	0.00078	0.0000484
	135	2227 \times	256	6456.0	0.0453	0.00078	0.0000484
	194	2227 \times	256	6450.0	0.0453	0.00078	0.0000484
	295	2227 \times	240	6053.0	0.0453	0.00081	0.0000500
3% VC	78 °K	855 \times	36	71.9	0.0323	0.0088	0.000600
	135	855 \times	32	62.9	0.0323	0.0095	0.000641
	194	855 \times	28	55.9	0.0323	0.0101	0.000680
	295	855 \times	26	51.9	0.0323	0.0104	0.000706
3% C	78 °K	1060 \times	93	533.1	0.0323	0.00325	0.000220
	135	1060 \times	79	452.0	0.0323	0.00353	0.000239
	194	1060 \times	93	532.6	0.0323	0.00326	0.000295
	295	573 \times	198	330.5	0.0323	0.00413	0.000280
3% M	78 °K	2227 \times	208	5246.0	0.0323	0.00104	0.0000702
	135	2227 \times	223	5624.0	0.0323	0.0010	0.0000678
	194	2227 \times	241	6078.0	0.0323	0.00096	0.0000652
	295	2227 \times	277	6986.0	0.0323	0.00090	0.0000608

The various data used to calculate the V.M.F.P. in the alpha solid solution domain are shown in Table IV. The test temperature given in column 2 refers to the temperature at which the plastic properties were evaluated, as will be described in the next section of this report. The V.M.F.P. was evaluated by simultaneous solutions of Equations 8 and 9 following introduction of the determined values of N and f shown in columns 5 and 6.

The macroscopic plastic behaviors of isotropic polycrystalline aggregates are known to approach those of amorphous materials. To within the approximations of this analogy, the effect of dispersions of CuAl_2 on the plastic properties of the aluminum-copper alpha solid solution should be similar to the effect of dispersions of steel balls in wax on the plastic properties of the wax. This analogy suggests that the plastic properties of dispersions in polycrystalline aggregates be correlated in terms of the volumetric mean free path between the hard particles of the dispersed phase. From the crystallographic viewpoint, however, it might be presumed that the hard

particles of the dispersed phase restrain the passage of dislocations. If the dislocations are presumed to be confined to migrate along a slip plane, it appears as if the plastic properties of the dispersion alloy should be correlated with the mean path between the dispersed particles on that plane. Assuming that the dispersion is random, the mean free path between the particles on a slip plane would be identical with the mean free path measured on any plane of polish of the specimen. The planar mean free path, however, will be simply related to the volumetric mean free path, for the case of random dispersions of spheroids. Consequently, when the plastic properties correlate with the volumetric mean free path they will correlate similarly with the planar mean free path.

The estimation of the planar mean free path can be based on the same approximations used to estimate the volumetric mean free path. It will be assumed that each particle forms the center of a circular domain on the plane of polish. Thus from Equation 8 the area of this domain is

$$\pi R'^2 = \frac{1}{N} = \frac{2\pi R^3}{3r}$$

whence the average radius of the circular domain becomes

$$R' = \sqrt{\frac{1}{\pi N}} = \sqrt{\frac{2}{3} \frac{R^3}{r}} \quad \text{Equation 10}$$

Furthermore the average radius r' of the particle on a plane of polish is directly obtained from the average cross sectional area of the spherical particle of radius r , namely

$$\pi r'^2 = \frac{\int_0^r \pi (r^2 - h^2) dh}{\int_0^r dh}$$

whence

$$r' = \sqrt{2/3} r \quad \text{Equation 11}$$

As shown by analogy to Fig. 7, the probability that a random line through the circular domain of radius R strikes a particle of radius r is

$$P = \frac{\int_0^{\phi_1} d\phi}{\int_0^{\pi/2} d\phi} = \frac{2}{\pi} \arcsin \frac{r'}{R'} \quad \text{Equation 12}$$

And the mean length of a line in the circular domain of radius R' by analogy to Fig. 6, is

$$\bar{l} = \frac{2}{\pi} \int_0^{\pi/2} l \, d\phi = \frac{2}{\pi} \int_0^{\pi/2} 2R' \cos \phi \, d\phi = \frac{4}{\pi} R' \quad \text{Equation 13}$$

Thus the number of particles intercepted by a unit length of line is given by

$$\frac{2}{\pi} \arcsin \frac{r'}{R'} \times \frac{1}{\bar{l}} = \frac{1}{2R'} \arcsin \frac{r'}{R'}$$

Consequently the average distance between centers of particles on a plane of polish is

$$\frac{2R'}{\arcsin \frac{r'}{R'}}$$

But by Equation 13 the average length of the line through a particle is $4r'/\pi$ whence the planar mean free path is approximated by

$$\text{P.M.F.P.} = \frac{2R'}{\arcsin \frac{r'}{R'}} - \frac{4r'}{\pi} \quad \text{Equation 14}$$

In the above evaluation, R' can be determined directly from the number of particles observed per unit area on the plane of polish as given by Equation 10. The value of r' , as shown by Equation 11, is equal to $\sqrt{2/3}r$ and is thus evaluable by simultaneous solutions of Equations 8 and 9. The planar mean free path deduced in this way is given in the last column of Table IV.

STRESS-STRAIN DATA

True stress-true plastic strain data were obtained for each alloy and heat treatment previously recorded over a range of temperatures from 78 to 295 °K. The tensile specimen axes from which these data were obtained were selected to be in the rolling direction. Since the details of such tests have already been reported (6) they will not be repeated here. The results of these tests are recorded in Figs. 9 to 12. In addition the true stress-true plastic strain curves for a supersaturated alpha solid solution of aluminum containing 0.50 weight per cent of copper are also reported.

DISCUSSION OF RESULTS

Although the true stress-true plastic strain curves for binary ferrites and dispersions of carbides in ferrite can be fairly accurately represented by the previously discussed empirical relationship $\sigma = A\epsilon^n$, binary alpha solid solutions of aluminum give distinctly different types of stress-strain curves. The reported stress-strain curves for alloys consisting of dispersions of CuAl_2 in an alpha solid solution of aluminum also deviated from the proposed empirical relationship

in a manner that was in harmony with the behavior of binary alpha solid solutions of aluminum. Consequently the data for the dispersion alloys could not be analyzed in terms of parameters of a simple empirical equation.

A review of the stress-strain curves of Figs. 9 to 12 reveals that the finer dispersions exhibit higher values of the initial deformation strength and also slightly higher rates of strain hardening. In fact the initial deformation strength and the rate of strain hardening is appreciably greater than those of the supersaturated alpha solid solution containing 0.50 weight per cent copper.

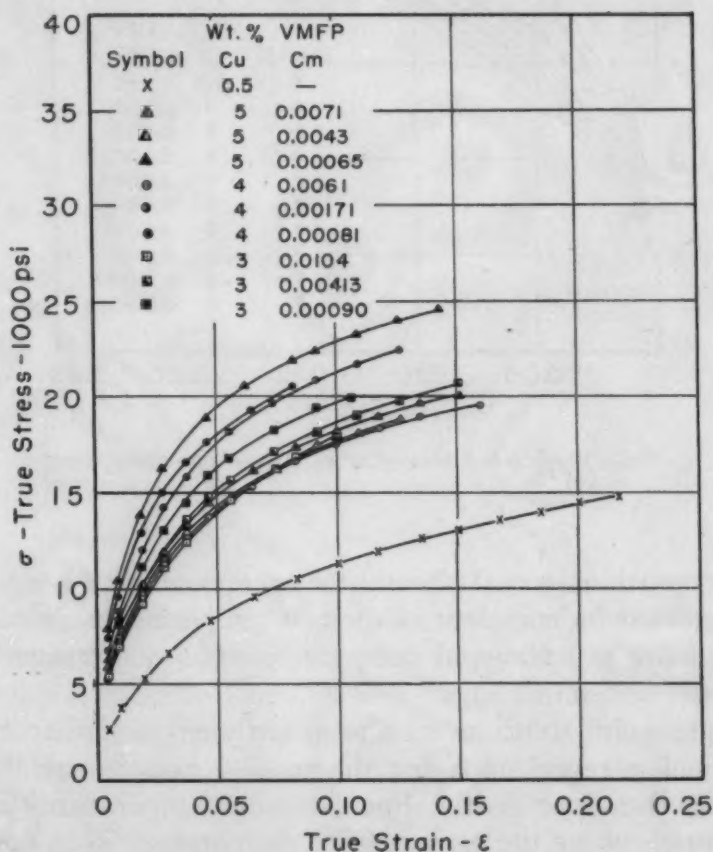


Fig. 9—Stress-Strain Curves for Aluminum-Copper Alloys at 295 °K.

The uniform trends of the stress-strain curves with dispersion suggest that they exhibit homologous plastic properties. In order to check this point further, the difference in the deformation stresses at $\epsilon = 0.10$ and 0.02 was plotted as a function of the deformation stress at $\epsilon = 0.02$ as shown in Fig. 13. Similar data (6) were also plotted for high purity aluminum, and a series of alpha solid solutions of copper and magnesium in aluminum. These data reveal that the strain hardening of the dispersion alloys increases linearly with the de-

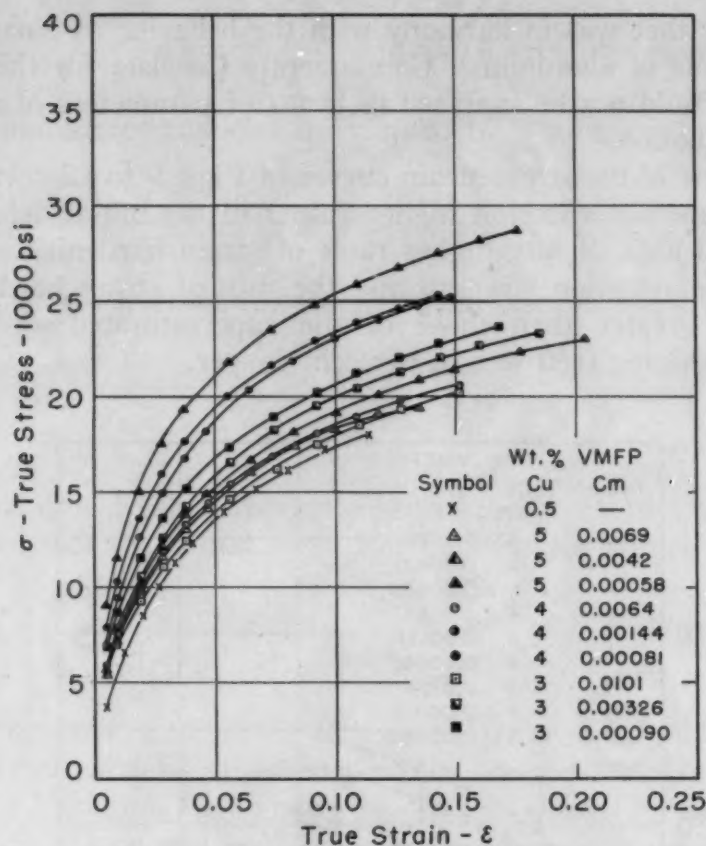


Fig. 10—Stress-Strain Curves for Aluminum-Copper Alloys at 194 °K.

formation strength at $\sigma = 0.02$, and that the slope of the $\sigma_{0.10} - \sigma_{0.02}$ versus $\sigma_{0.02}$ plot is independent of the test temperature. Thus, within the spread of the experimental data, the various dispersions do form an homologous series of alloys.

The alpha solid solutions of aluminum yield a similar trend but exhibit a much steeper slope for the $\sigma_{0.10} - \sigma_{0.02}$ versus $\sigma_{0.02}$ line. Furthermore, the slope of the line is quite temperature-dependent, decreasing in slope as the temperature decreases. This trend is in harmony with the previously reported effect of solid solution alloying in that the maximum effect of alloying on the rate of strain hardening is observed in the vicinity of room temperature. Consequently, it must be inferred that the strain hardening for the dispersion alloys is a quantitatively dissimilar function of the deformation strength from that which applies to alpha solid solutions. Each class of alloys, alpha solid solutions or dispersions, form a distinctly different homologous series.

Gensamer's data on steels might suggest that in the present example, also, the deformation strength at some specified strain should decrease linearly with the mean free path between the par-

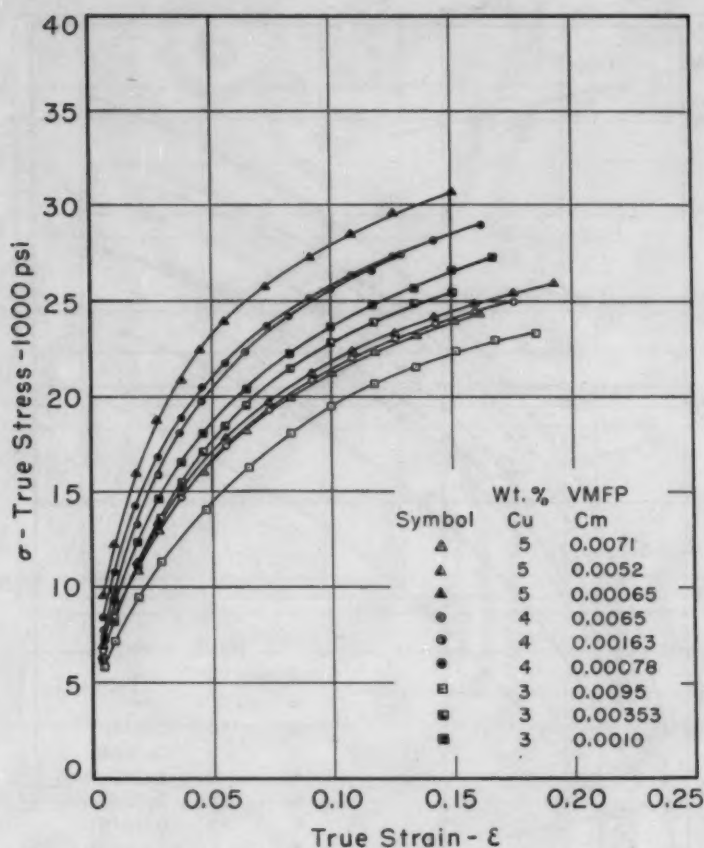


Fig. 11—Stress-Strain Curves for Aluminum-Copper Alloys at 135 °K.

ticles. Although the qualitative trend of decreasing deformation strength with increasing planar mean free path between the CuAl_2 particles was observed, the σ versus logarithm of M.F.P. relationship was curvilinear. When, however, the data were plotted as the logarithm of σ versus the logarithm of M.F.P., within a rather narrow scatter band, a linear relationship was obtained as shown in Figs. 14 and 15. These data suggest that the correlations between the plastic properties and the dispersions might be based either on the volumetric or the planar mean free path. In fact the slopes of the logarithm of the stress versus the logarithm of the mean free path curves are the same for both the volumetric and the planar measures of the mean free path.

In a single homologous series of alloys, the deformation strength will be a function of any suitable measure of the dispersion. Consequently, from the purely phenomenological viewpoint, no special significance can be ascribed to the fact that the deformation strength correlates with the mean free path between the dispersed hard particles in a given homologous series of alloys. From a theoretical viewpoint, however, dispersions of hard constituents might be visual-

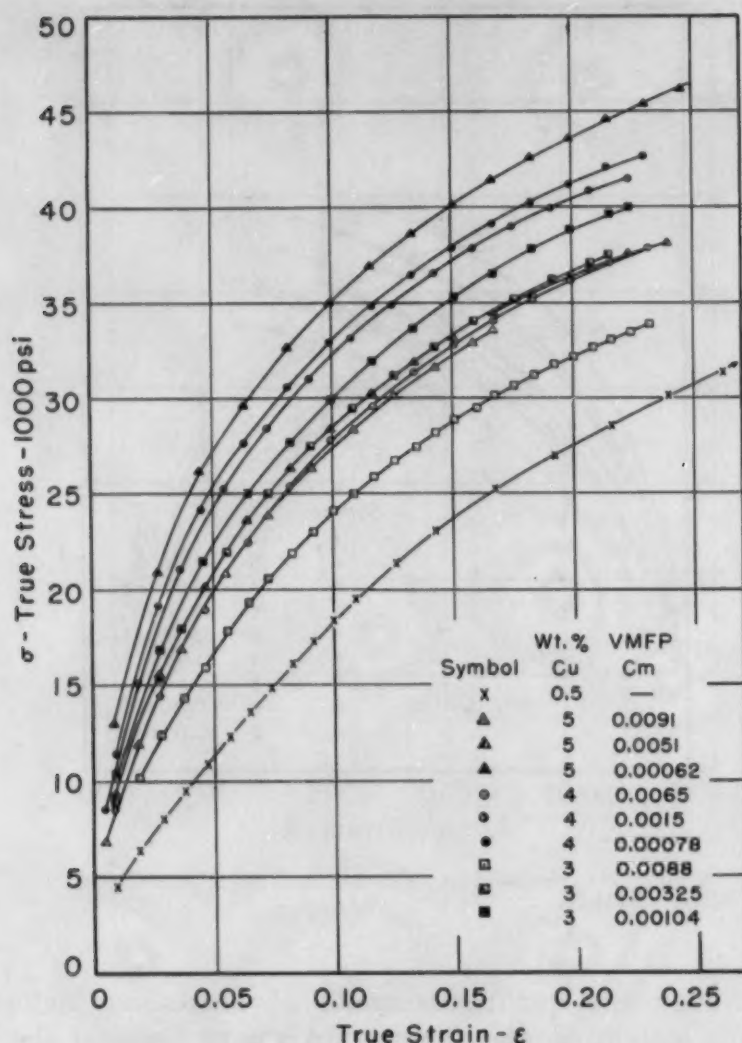


Fig. 12—Stress-Strain Curves for Aluminum-Copper Alloys at 78°K.

ized as barriers to the migration of dislocations. For example, Orowan (9) estimates that the yield strength of a uniformly dispersed system should be

$$\sigma = A' / \text{P.M.F.P.} \quad \text{Equation 15}$$

where A' is some constant and P.M.F.P. is the planar mean free path between the hard particles. The correlation between the data for Figs. 14 and 15 reveal that a similar relationship

$$\sigma = A / \text{V.M.F.P.} \quad \text{Equation 16}$$

should apply to the volumetric mean free path. Of course Orowan's equation might not apply to all types of dispersions, such as for example the pearlites, since it was predicated on the hypothesis of a uniform distribution of fine particles. The data obtained by Gen-

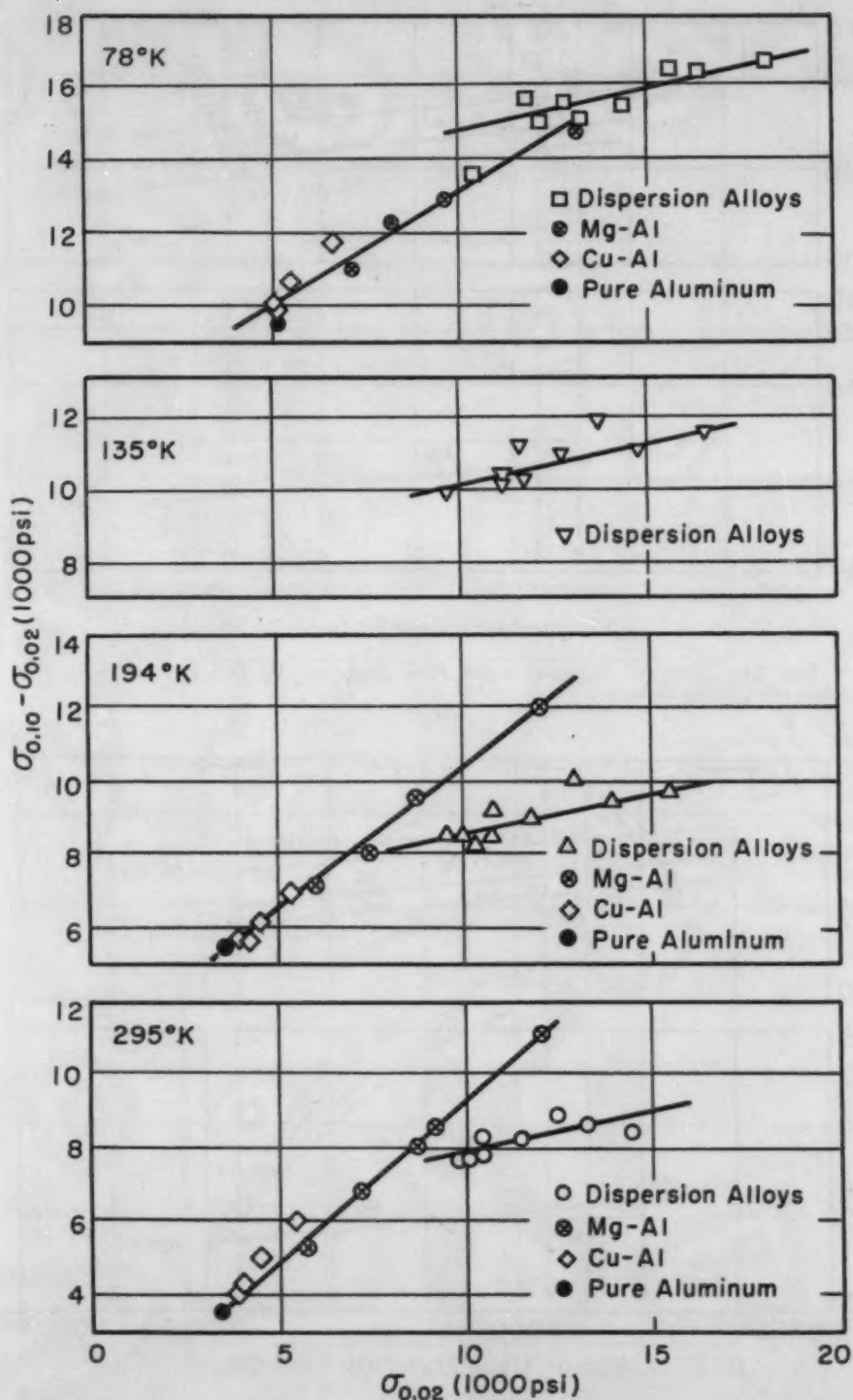


Fig. 13—Comparison of Strain Hardening and Deformation Strength of Dispersions of CuAl_2 and Solid Solutions of Aluminum Which Reveals That the Dispersion Alloys Form a Homologous Series.

samer for steels clearly reveal that the Orowan relationship is invalid for pearlites. Orowan's theory, if sufficiently representative of the facts, should correlate reasonably well with Gensamer's data for

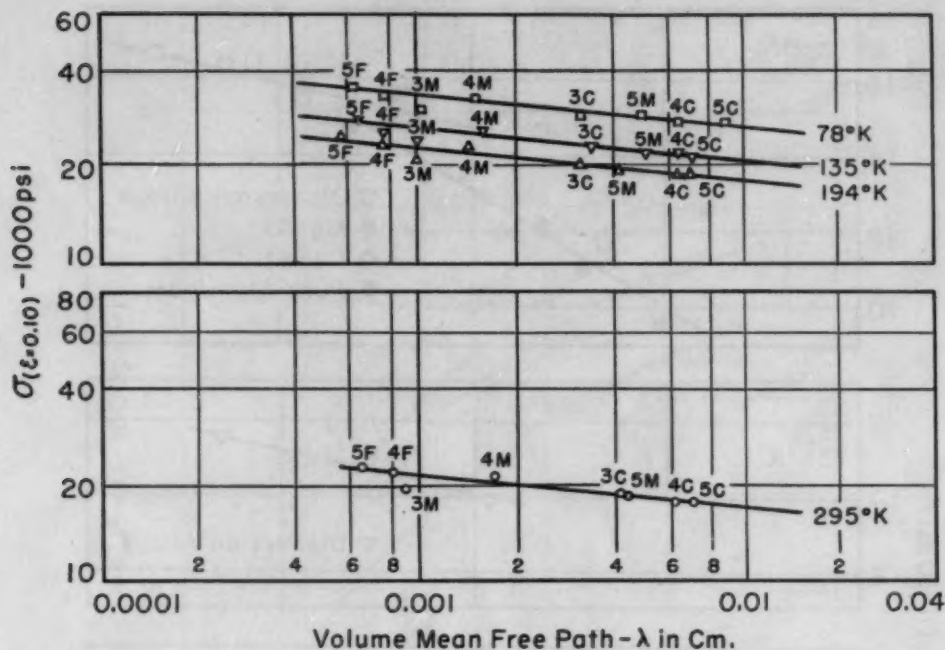


Fig. 14—Effect of Volume Mean Free Path on the Deformation Stress of Aluminum-Copper Alloys.

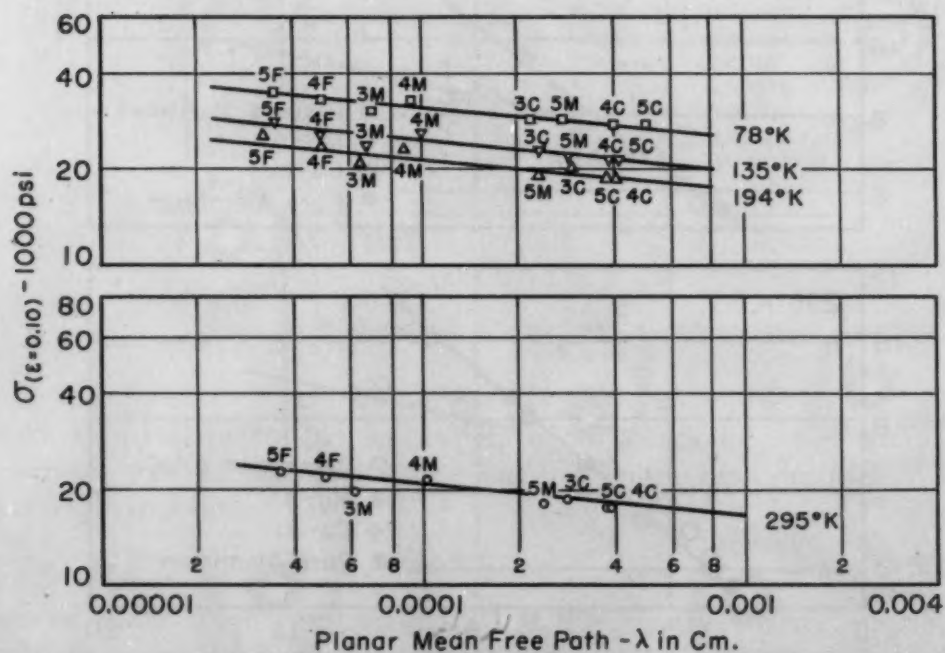


Fig. 15—Effect of Planar Mean Free Path on the Deformation Stress of Aluminum-Copper Alloys.

spheroidal dispersion of carbides in ferrite as well as with the present data on dispersions of CuAl_2 in aluminum. Since the data for the aluminum-copper alloys exhibit small quantitative differences from those pertaining to steels, Orowan's theory cannot be expected to agree with both sets of data. Actually Orowan's theory is in

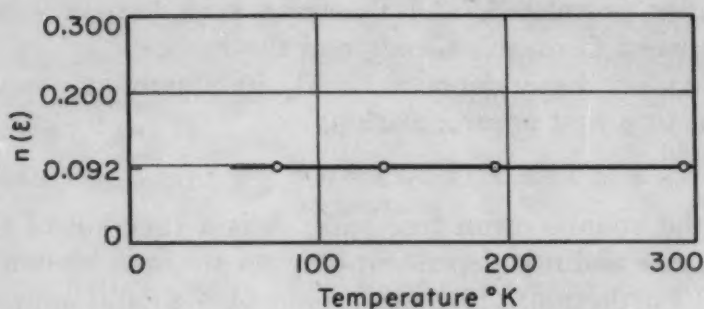


Fig. 16—Effect of Temperature on the Parameter $n(\epsilon)$ at a True Strain of $\epsilon = 0.10$.

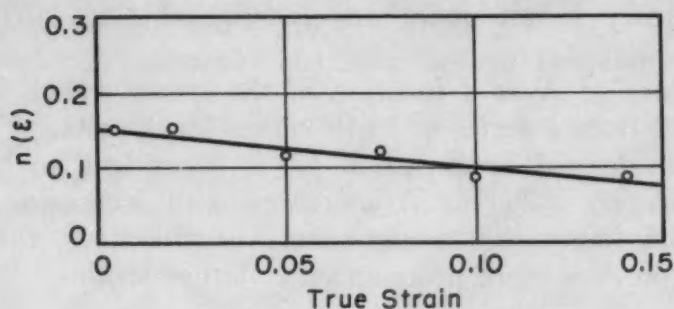


Fig. 17—Effect of True Strain on the Parameter $n(\epsilon)$.

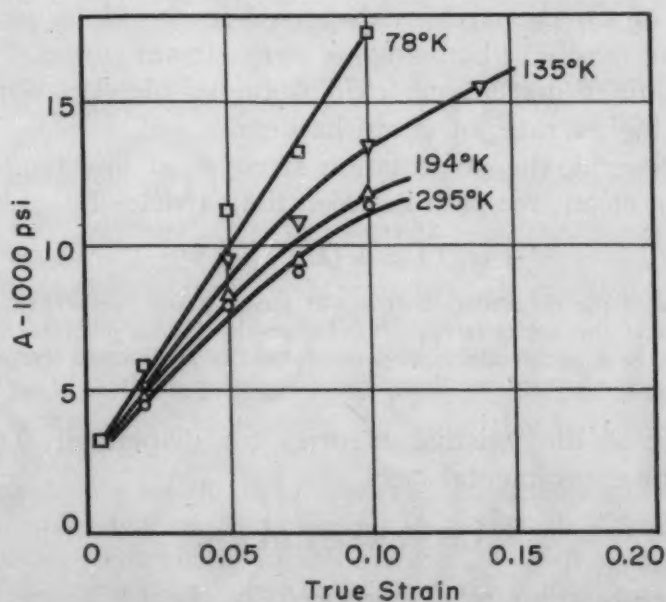


Fig. 18—Effect of Temperature and Strain on the Parameter $A(\epsilon, T)$.

closer harmony with the aluminum-copper alloy data than with those on steels. But the aluminum-copper alloy data in Fig. 14 reveal that the volumetric mean free path does not enter Equation 16 in the

simple manner postulated, and illustrate even here a serious discrepancy between Orowan's theory and the facts.

The data on dispersions of CuAl_2 in aluminum-copper alloys suggest that, to a first approximation,

$$\sigma(\epsilon, T) = A(\epsilon, T) \lambda^{-n(\epsilon)} \quad \text{Equation 17}$$

where λ is the volume mean free path, A is a function of the strain and temperature and n is dependent only on strain as shown by Figs. 16 and 17. Furthermore, the magnitude of n should approach 1 at the initiation of yielding (at $\epsilon_p = 0$) if Equations 16 and 17 are compatible. Although n does increase with decreasing strain, it appears to approach a limiting value of only 0.15. Consequently, Orowan's theory is not quantitatively applicable to fairly uniform dispersions.

The values of A as a function of the strain shown in Fig. 18 were obtained from a series of $\log \sigma$ versus $\log \lambda$ plots. The magnitude of A , as defined by Equation 17, is dependent on both strain and temperature. Whereas A increases with increasing strain, it decreases with increasing temperature. Furthermore, the effect of temperature on A is more pronounced at larger strains.

CONCLUSIONS

1. Alloys of aluminum-copper containing a more or less random distribution of CuAl_2 particles dispersed in the alpha phase yield a self-consistent family of homologous stress-strain curves.
2. The finer dispersions exhibit higher deformation strengths and slightly higher rates of strain hardening.
3. In general, the deformation strength at low temperatures is related to the mean free path between the particles by

$$\sigma(\epsilon, T) = A(\epsilon, T) \lambda^{-n(\epsilon)}$$

where σ is the deformation stress at strain ϵ and temperature T .

λ is the mean free path between the CuAl_2 particles.

$A(\epsilon, T)$ is a parameter that depends on the strain and temperature.

$n(\epsilon)$ is a parameter that depends only on strain.

4. None of the existing theories for dispersion strengthening agree with the experimental facts.

ACKNOWLEDGMENTS

This investigation was sponsored by the Office of Naval Research. The authors wish to thank the O.N.R. staff for their support and cooperation throughout the course of this investigation.

The authors express their sincere appreciation to the Aluminum Company of America for furnishing the alloys used in this investigation.

In addition they wish to thank S. Frederick for his assistance

in preparing the alloys, C. Wiseman for his assistance in the testing program, O. D. Sherby for his advice, suggestions, and assistance during this investigation, and Mrs. G. Pelatowski for the preparation of the figures.

References

1. M. Gensamer, E. B. Pearsall, W. S. Pellini and J. R. Low, Jr., "Tensile Properties of Steel", *TRANSACTIONS, American Society for Metals*, Vol. 30, 1942, p. 983.
2. M. Gensamer, "Strength and Ductility", *TRANSACTIONS, American Society for Metals*, Vol. 36, 1946, p. 30.
3. C. S. Roberts, R. C. Carruthers and B. L. Averbach, "The Initiation of Plastic Strain in Plain Carbon Steels", *TRANSACTIONS, American Society for Metals*, Vol. 44, 1952, p. 1150.
4. G. V. Smith, "Properties of Metals at Elevated Temperatures", McGraw-Hill Book Company, 1950.
5. E. C. Bain, *The Alloying Elements in Steel*, American Society for Metals, 1939.
6. J. E. Dorn, P. Pietrokowsky and T. E. Tietz, "The Effect of Alloying Elements on the Plastic Properties of Aluminum Alloys", *Transactions, American Institute of Mining and Metallurgical Engineers*, Vol. 188, 1950, p. 933.
7. R. H. Brown, W. L. Fink and M. S. Hunter, "Measurements of Irreversible Potentials as a Metallurgical Research Tool", *Transactions, American Institute of Mining and Metallurgical Engineers*, Vol. 143, 1941, p. 165.
8. E. C. Elwood and J. M. Silcock, "The Lattice Spacings of Solid Solutions of Copper in Aluminum", *Journal, Institute of Metals*, Vol. 74, 1948, p. 457.
9. E. Orowan, Discussion, "Symposium on Internal Stresses", Institute of Metals, London, 1947, p. 451.

DISCUSSION

Written Discussion: By F. R. Morral, head, X-ray Department, Kaiser Aluminum & Chemical Corp., Spokane, Wash.

It is always encouraging to be informed that facts found for one type of material, such as steel, are operating in an equivalent manner for other engineering materials. The authors are to be thanked for this study on aluminum alloys.

The explanations for the facts, however, are often challenging. A new approach is suggested by Skimmer in *Metal Industry*, Oct. 31, 1952, p. 340. The author's comments on this editorial, as well as the applicability of Röhner's theory (*Journal, Institute of Metals*, Vol. 73, p. 285-321, discussion p. 768-785, 1947), might be pertinent at this time.

Written Discussion: By J. H. Westbrook, Metallurgy Research Department, General Electric Co., Research Laboratory, Schenectady, N. Y.

The authors have presented a paper of fundamental significance to our understanding of the microstructural dependence of mechanical properties. Their careful analysis of the mean free path and the excellence of the data obtained are particularly to be commended. The writer wishes to

call the authors' attention to a paper by Unckel⁴ which was apparently overlooked in their literature survey. Although his analysis is less elegant and his data somewhat less precise than those of the authors, Unckel presents the results of quantitative experiments on the effects of microstructure (particularly interphasal spacing) on the mechanical properties of many different types of alloys. The alloys which he treated include eutectoid and hypoeutectoid steels, $\alpha + \beta$ brasses, Cu-W, copper-graphite, Al-Si and SbSn in tin.

The authors have related the deformation strength, σ , to the mean free path between particles, λ , by

$$\sigma = A\lambda^{-n}$$

where A and n depend respectively on strain and temperature, and on strain alone. It is of no consequence that this expression was not based upon a theoretical analysis or even that it does not include all of the factors for which the ultimate theory must account (e.g., shape, distribution, etc.), for empiricisms have value in their own right. However, the above expression, although representing the data adequately, seems somewhat illogical. That is, for an infinite distance between particles, i.e. pure matrix phase, the authors' expression would predict zero strength. A simple semi-logarithmic relation as originally put forward by Gensamer et al (1) is apparently not correct either, for Roberts et al (3) encountered difficulty in fitting their datum point for high purity iron to such a function. Unckel, on the other hand, proposes an expression of the form

$$\sigma = Ae^{-B\lambda} + C$$

It will be observed that this expression predicts finite strengths at both zero and infinite spacing. Thus, the strength of the particulate phase is given by $A + C$ and that of the matrix by C .

The writer has tested the data of Shaw et al as well as that of earlier workers (1), (2), (3) for conformance with Unckel's function and finds that in all cases the fit with this function is as good as, or better than, that found for the expression proposed by the original authors. The available data, therefore, do not necessarily indicate a difference in kind in the microstructural dependence of strength in pearlitic steels and $\text{CuAl}_2 + \text{Al}$ alloys. The data of Roberts et al for the high purity irons are now explicable—the matrix yield strength is evidently very close to the 15,000-psi value shown for both "Puron" and the very high purity National Research iron. The data were fitted to the Unckel expression by a least squares analysis, temporarily omitting the datum point for the National Research iron. The matrix yield strength was found to be 14,650 psi as predicted, and that of cementite approximately 115,000 psi; a not unreasonable value.

Fig. 19 shows the results of a similar treatment for a portion of the authors' data for CuAl_2 particles in Al ($T = 78^\circ\text{K}$; $\epsilon = 0.10$). A value of 36,600 psi for the flow stress of CuAl_2 is found and 27,500 psi for the solid solution matrix; again reasonable values. A further consequence of this type of analysis is the conclusion that, beyond a certain spacing, hard particles add insignificantly to the strength of the matrix. This is intuitively

⁴H. Unckel, "The Dependence of Mechanical Properties on Structure in Two-Phase Alloys", *Metal*, Vol. 5, 1951, p. 446.

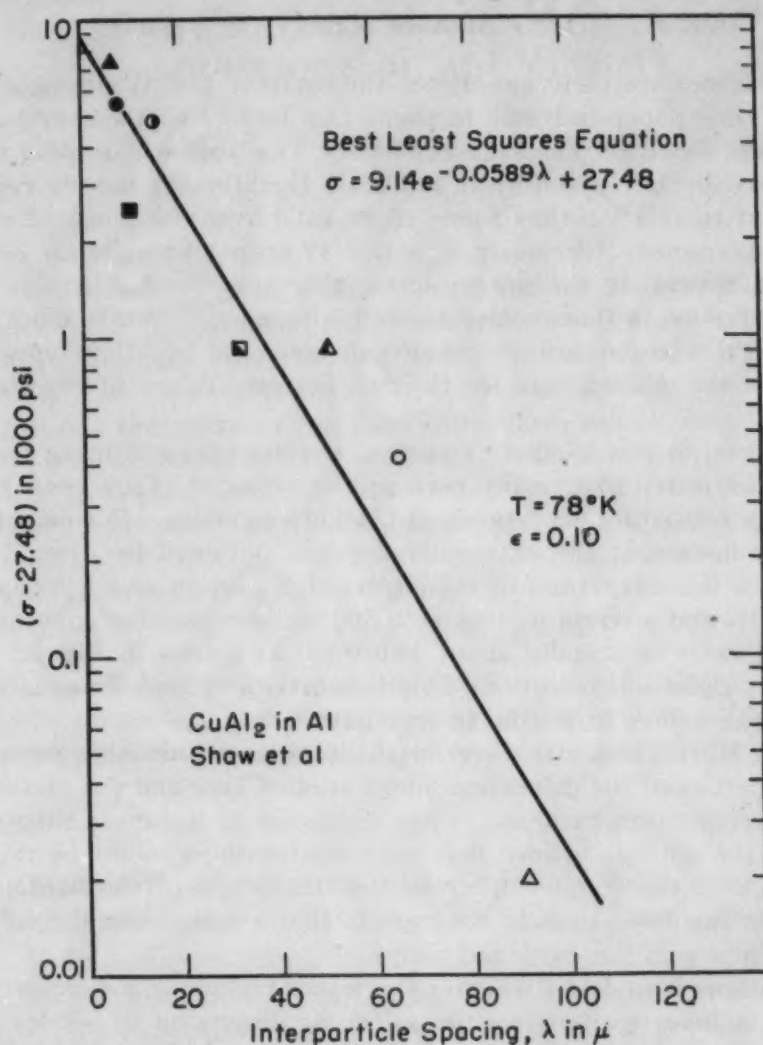


Fig. 19—Best Least Squares Equation.

satisfying. If the level of significance is arbitrarily set at 1% of the base strength of the matrix, we find the critical spacing for CuAl₂ in Al to be 59 μ and for the steels of Roberts et al, 46 μ . The values are surprisingly close together. The scatter in the data of Unckel and those of Gensamer was considered to be too great to warrant further analysis. The writer has not completed the analysis of the CuAl₂-Al data to ascertain the dependence of the Unckel constants A, B and C on the other measured variables, strain and temperature.

It is to be hoped that the present paper will stimulate further experimental studies which will permit a proper accounting of all the pertinent variables, both the microstructural factors—the amount, size, shape and distribution of the second phase; and the physical factors, the properties of the matrix and embedded phase—ductility, strength, work hardening capacity, crystallographic misfit, interfacial energy and interfacial bond strength. Considerable ingenuity will be required to select experimental systems in which these many factors can be effectively separated and studied.

Authors' Reply

The authors sincerely appreciate the interest Mr. Westbrook has expressed in their paper and wish to thank him for the supplemental analyses he has made based on Unckel's equation. The authors' original analyses were admittedly solely empirical and their Equation 17 merely represents the simplest correlation they found to be valid over the range of variables that were examined. Obviously Equation 17 cannot be valid for either the pure alpha matrix or the pure intermetallic compound. In this respect Unckel's equation, although also tainted with empiricism, is more acceptable. But there are an infinite number of empirical equations which could equally give the desired data for the two extreme values of the mean free path.

Therefore, to test Unckel's equation, a wider range of mean free paths than were subjected to scrutiny here will be required. Care must be exercised in any premature acceptance of Unckel's equation. For example, Mr. Westbrook finds that the extrapolated value, obtained by using Unckel's equation, for the flow stress of the alpha solid solution of copper in aluminum at 78 °K and a strain of 10% is 27,500 psi, whereas the experimentally determined value is actually about 18,000 psi as shown in Fig. 12 for the 0.5% copper alpha solid solution. This suggests that Unckel's equation also fails for large values of the mean free path.

As Mr. Morral suggests, there might be some relationship between the plastic properties of the dispersion alloys studied here and the plastic properties of precipitation-hardened states discussed in Rohmers theory. But at present the authors believe that such relationships might be rather remote in view of the distinct differences in the origin of the hardening resulting from the dispersions in contrast to that arising from the coherency stresses in precipitation-hardened alloys.

The authors also doubt whether the tracer technique for oxygen would be helpful in investigations on the effect of dispersion of oxides on the plastic properties of alloys since the dispersion hardening is related to the mean free path between the dispersed particles rather than the percentage of the dispersed phase.

EFFECT OF ALLOYING ELEMENTS ON GRAIN BOUNDARY RELAXATION IN ALPHA SOLID SOLUTIONS OF ALUMINUM

BY C. DEAN STARR, E. C. VICARS, A. GOLDBERG AND J. E. DORN

Abstract

Small additions of zinc, silver, copper and germanium that form alpha solid solutions with aluminum have no significant effect on the resistance to grain boundary relaxation. Accordingly, the activation energy, Q , for these alloys is the same as for pure aluminum which was found to be 38,000 calories per mole. The activation energy for Al-Mg alloys, however, increases linearly from 38,000 calories per mole at 0% magnesium to 54,000 calories per mole for 1.617 atomic % magnesium. The grain boundary relaxation was correlated by means of the relation

$$G/G_u = f \{ A D^{1.86} \nu e^{Q/RT} \}$$

where A = parameter dependent on composition; D = grain diameter; ν = frequency of vibration; Q = activation energy; R = gas constant; T = absolute temperature.

INTRODUCTION

EXTENSIVE investigations have already been made on grain boundary relaxations by Zener (1),¹ Kê (2), and others. Nevertheless, little is known about the effects of solid solution alloying on the relaxation phenomenon. On the basis of a single damping capacity test, Kê (3) suggested that as much as 1/2% copper in alpha solid solution does not materially alter the grain boundary relaxation in aluminum. Köster (4), however, has reported that the temperature at which grain boundaries first begin to relax in aluminum decreases appreciably as the purity of aluminum increases from 99.6 to 99.998% aluminum. The present investigation was initiated to uncover the effect of alloying on grain boundary relaxations in alpha solid solutions of aluminum.

MATERIALS AND TECHNIQUES

The shear modulus relaxation method was selected in preference to the damping capacity for evaluating grain boundary relaxations.

¹The figures appearing in parentheses pertain to the references appended to this paper.

A paper presented before the Eighth Western Metal Congress of the Society, held in Los Angeles, March 23 to 27, 1953. Of the authors, C. Dean Starr and A. Goldberg are research engineers, E. C. Vicars is a graduate student, and J. E. Dorn is professor of physical metallurgy, University of California, Berkeley, Calif. Manuscript received March 28, 1952.

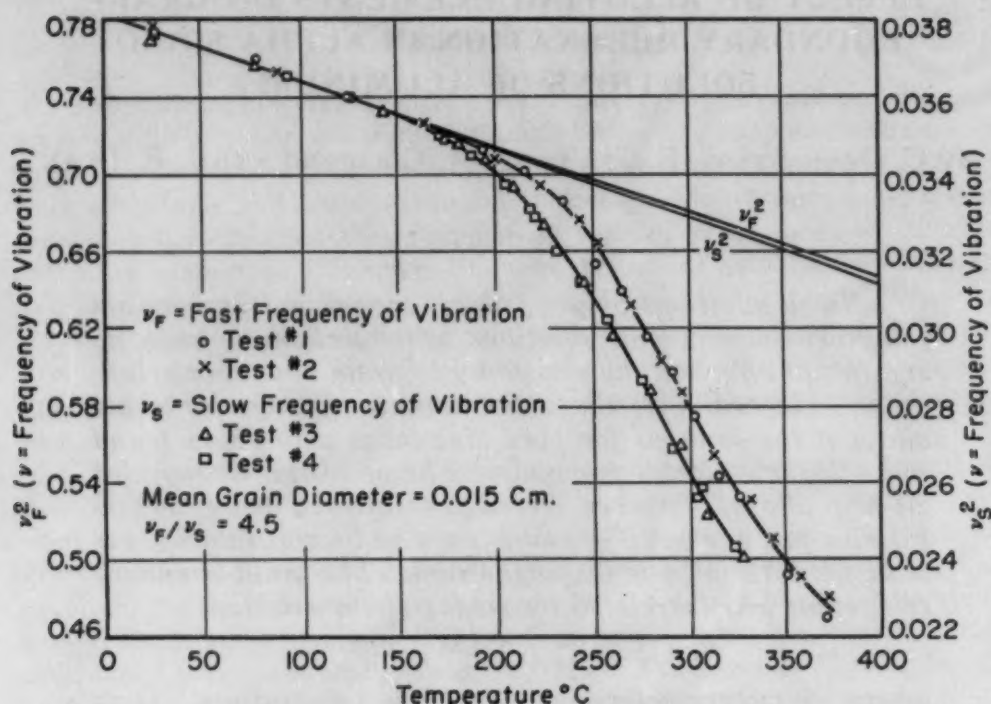


Fig. 1—Effect of Frequency of Vibration on Grain Boundary Relaxation in Pure Aluminum.

A torsion pendulum consisting of a wire specimen (~ 0.036 inch in diameter and ~ 18 inches in length) was mounted in a vertical temperature-controlled tube furnace. The chemical compositions of the alloys are given in Table I. Cold drawn wire specimens were recrystallized in situ in the furnace, to provide various grain sizes, as recorded in Table II. All grains were equiaxed and exhibited only normal variations from the mean grain diameter.

The mean frequency of oscillation of the torsion pendulum was determined at a series of temperatures from the mean period of the pendulum. During any test run, the temperature of the specimen was maintained uniform and constant to better than $\pm 0.5^\circ\text{C}$.

EXPERIMENTAL RESULTS

Typical experimental results are illustrated in Fig. 1. Two different inertia bars were used to obtain the two slightly different frequencies, ν_F and ν_S . The data were plotted as frequency squared versus temperature, since the shear modulus, G , is directly proportional to the square of the frequency of a given torsion pendulum. Thus, up to slightly above 150°C (300°F) the shear modulus was observed to decrease linearly with an increase in temperature in complete harmony with theory and previous investigations. Kê has clearly demonstrated that the abnormally high decrease in G with increasing temperature slightly above 150°C (300°F) and in the

Table I
Chemical Analyses of Alloys

Alloying Element	Atomic %	Weight % of Residual Impurities				
		Silicon	Iron	Copper	Magnesium	Manganese
Aluminum C	0	0.004	0.003	0.004	0.0004	0.001
Magnesium	0.554	0.003	0.003	0.007
	1.617	0.003	0.004	0.006
Copper	0.029	0.003	0.004	0.0006	0.001
	0.054	0.003	0.004	0.0007	0.001
	0.101	0.003	0.003	0.0006	0.001
Zinc	0.211	0.004	0.004	0.006	0.001
	0.402	0.004	0.005	0.006	0.001
	0.755	0.004	0.005	0.006	0.001
Germanium	0.015	0.004	0.004	0.006	0.001
	0.033	0.004	0.004	0.006	0.001
	0.082	0.003	0.005	0.007	0.001
	0.145	0.003	0.006	0.007	0.001
Silver	0.025	0.003	0.005	0.006	0.001
	0.053	0.003	0.005	0.006	0.001
	0.100	0.003	0.005	0.007	0.001

range of frequencies employed is attributable to anelastic grain boundary relaxations.

Zener has shown that inasmuch as grain boundary relaxation depends upon thermal activation,

$$G/G_u = \frac{\nu^2}{\nu_u^2} = f \{ \nu e^{Q/RT} \} \quad \text{Equation 1}$$

for a given alloy and grain size

where G = observed shear modulus

G_u = unrelaxed modulus

ν^2 = observed frequency squared

ν_u^2 = linearly extrapolated value of the frequency squared, assuming no relaxation

R = gas constant

T = absolute temperature

Q = activation energy

Thus an increase in frequency causes the relaxation to first occur at a somewhat higher temperature. This relationship permits an experimental evaluation of the activation energy; for the same percentage relaxation (e.g., $G/G_u = 0.85$) and two frequencies of test

$$\nu_1 e^{Q/RT_1} = \nu_2 e^{Q/RT_2} \quad \text{Equation 2}$$

and Q is determinable. As shown in Fig. 2, the activation energy for grain boundary relaxation in the high purity aluminum under scrutiny here was about 38,000 calories per mole. This value is somewhat higher than that of 32,000 calories per mole obtained by Kê from shear modulus studies and only slightly higher than the 34,500 calories per mole value Kê estimated from damping capacity investigations.

On the basis of damping capacity studies, Kê suggested that an

Table II
Heating Cycles and Mean Grain Diameters for Aluminum Solid Solution Alloys

Alloying Element	Atomic %	Heat Treatment		Mean Grain Diameter (cm.)
		Time (hrs.)	Temp. (°C)	
Aluminum C		1½	325	0.005
		4	400	0.010
		8	425	0.015
		4	500	0.034
		5	550	0.077
Magnesium	0.554	1½	325	0.008
		4	400	0.015
		4	500	0.060
		5	550	0.063
		8	425	0.021
Copper	1.617	5	550	0.059
	0.029	5	550	0.077
	0.054	5	550	0.072
	0.101	5	550	0.077
Zinc	0.211	5	550	0.100
	0.402	5	550	0.072
	0.755	5	550	0.067
Germanium	0.015	5	550	0.056
	0.033	5	550	0.077
	0.082	5	550	0.067
	0.145	5	550	0.083
Silver	0.025	5	550	0.091
	0.053	5	550	0.067
	0.100	5	550	0.067

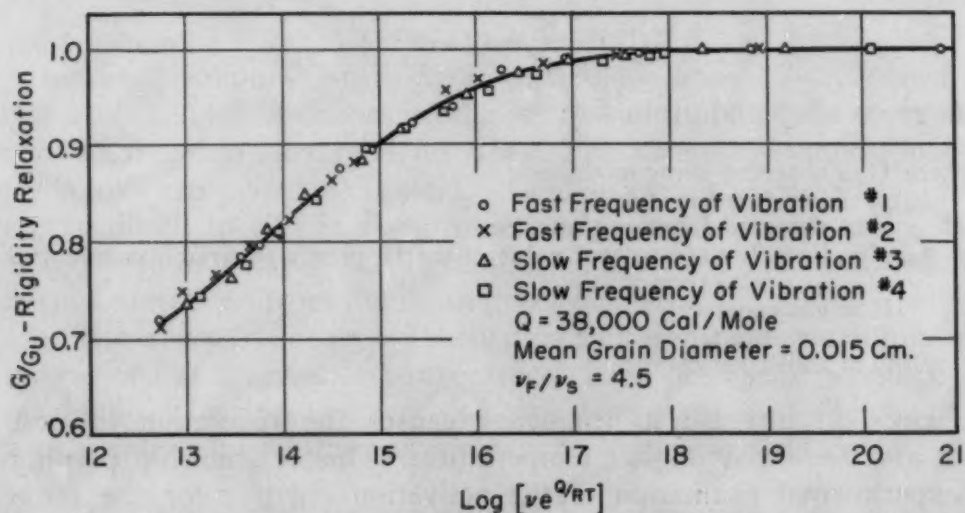


Fig. 2—Correlation of Frequency, Energy of Activation and Temperature for Grain Boundary Relaxation in Pure Aluminum.

increase in the mean grain diameter, D , shifted the relaxation temperature to higher values, consonant with the thought that

$$G/G_u = f(D^m \nu e^{Q/RT}) \quad \text{Equation 3}$$

where $m = 1$. Actually Kê's own data suggest that m is nearer 1.5 than 1. In order to compare the grain boundary relaxations of the various alloys and grain sizes under consideration here, this ambiguity had to be resolved. As shown in Fig. 3, the best value for m

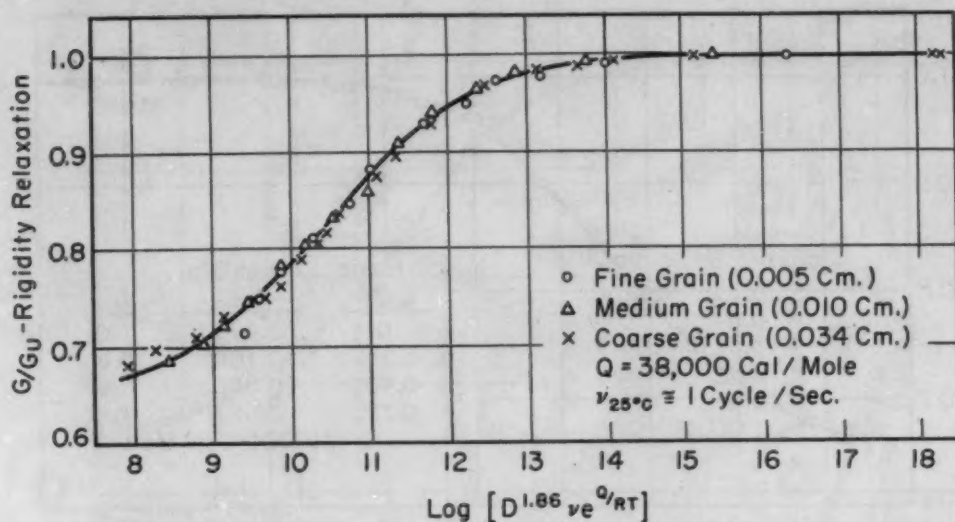


Fig. 3—Correlation of Grain Size, Frequency, Energy of Activation and Temperature for Grain Boundary Relaxation in Pure Aluminum.

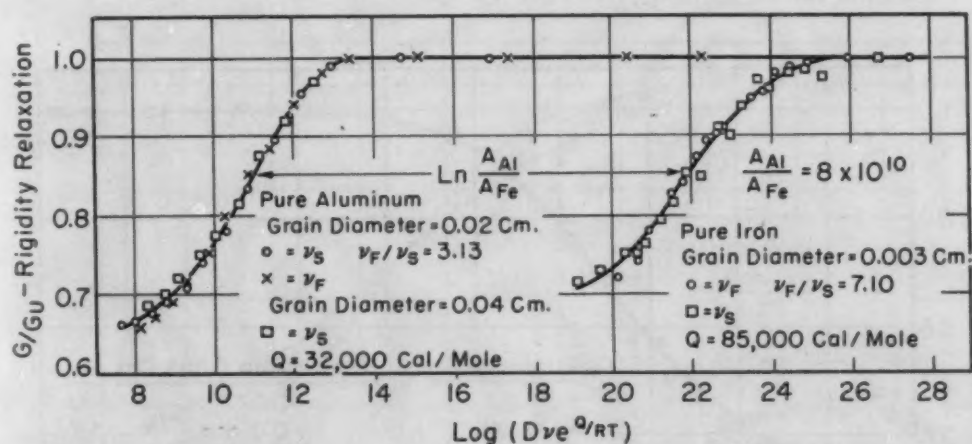


Fig. 4—Grain Boundary Relaxation of Pure Aluminum and Pure Iron as a Function of the Parameter ($D\nu e^{Q/RT}$). (Data by Kê.)

was observed to be about 1.86. Additional confirmation of the nominal validity of this choice for m will be given later in the discussion on relaxations in the alloy containing 0.554 atomic % magnesium.

It must be recognized that Equation 3 permits analyses and comparisons of grain boundary relaxations in a single metal or alloy. A new activation energy, however, may be found for each metal or alloy. In addition, another factor associated with the mechanism and entropy of activation for relaxation will enter the analysis. Therefore, in general,

$$G/G_u = f \{ A D^m \nu e^{Q/RT} \} \quad \text{Equation 4}$$

where Q and A are functions of the composition. This relationship is

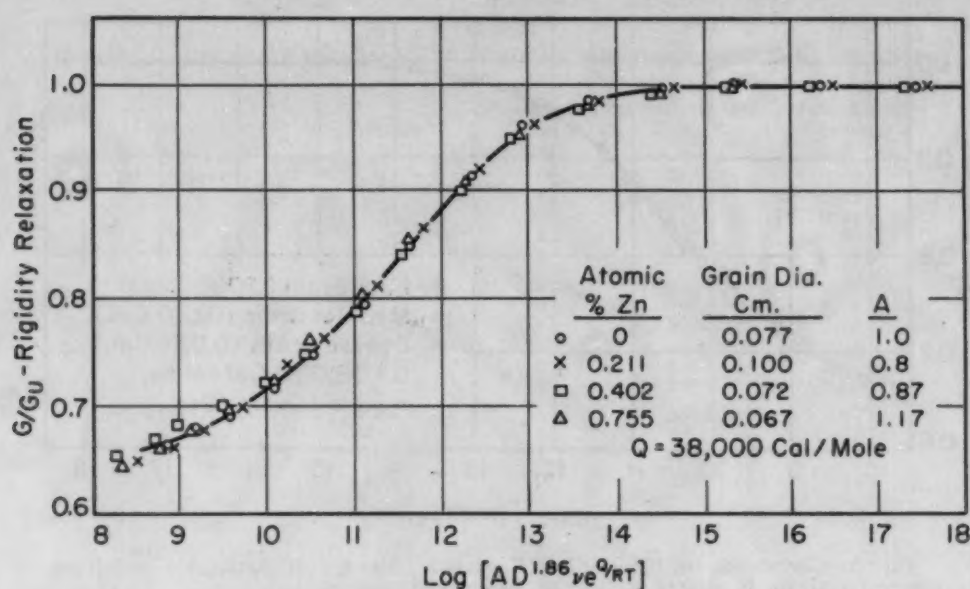


Fig. 5—Rigidity Relaxation in Aluminum and Aluminum-Zinc Alloys as a Function of the Parameter ($AD^{1.86} \nu e^{Q/RT}$).

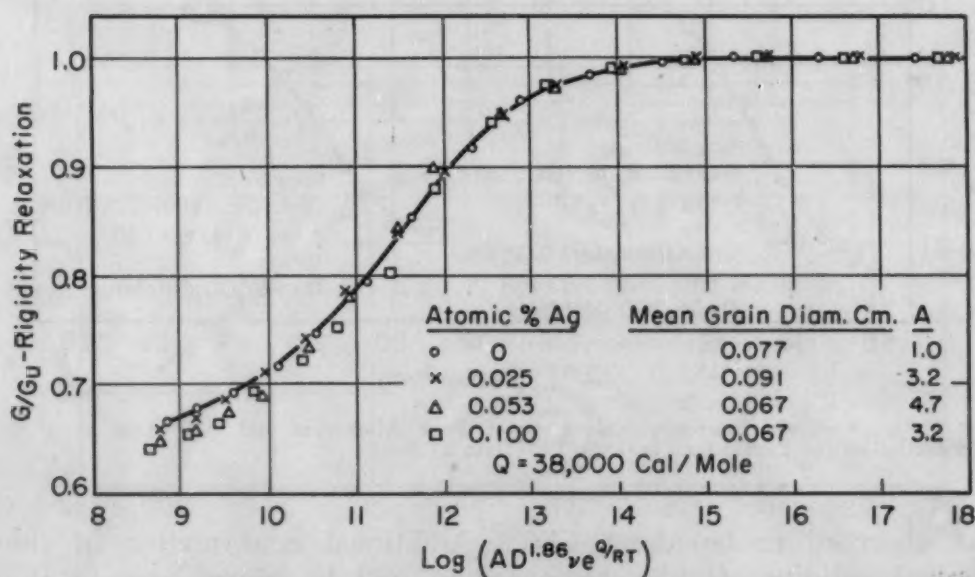


Fig. 6—Rigidity Relaxation in Pure Aluminum and Aluminum-Silver Alloys as a Function of the Parameter ($AD^{1.86} \nu e^{Q/RT}$).

illustrated in Fig. 4, where it is shown that A_{Al} is about $8 \times 10^{10} A_{Fe}$. Thus A might be very sensitive to alloying. Throughout the remainder of this report, all analyses will be based on Equation 4 using $m = 1.86$ and taking A for pure aluminum to be unity.

The relaxation data for Al-Zn, Al-Ag, Al-Cu and Al-Ge alloys are correlated in Figs. 5 to 8, respectively. In all cases the activation energy was determined by equating the argument of Equation 4 for the various conditions of test at $G/G_u = 0.85$. In all of these cases

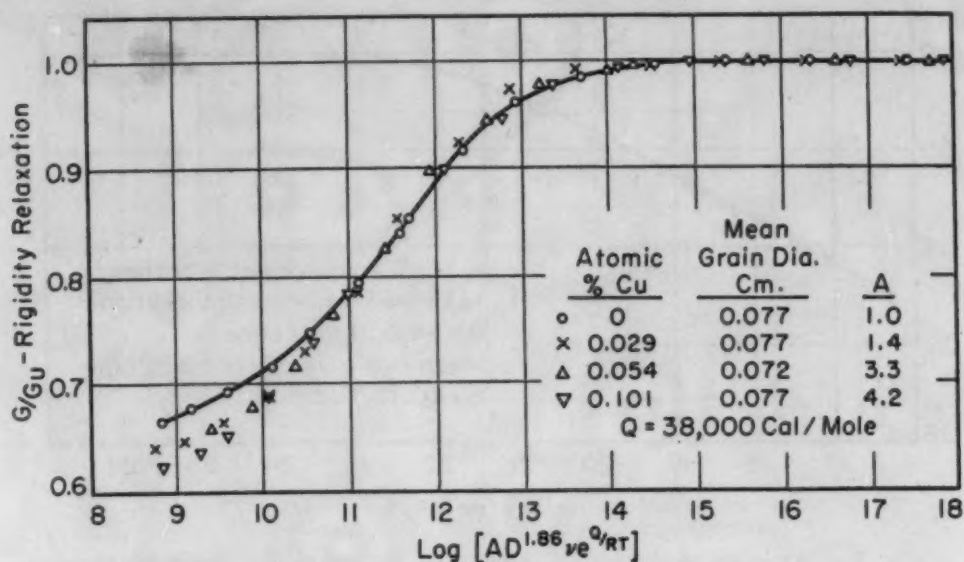


Fig. 7—Rigidity Relaxation of Pure Aluminum and Aluminum-Copper Alloys as a Function of the Parameter ($AD^{1.86} \nu e^{Q/RT}$).

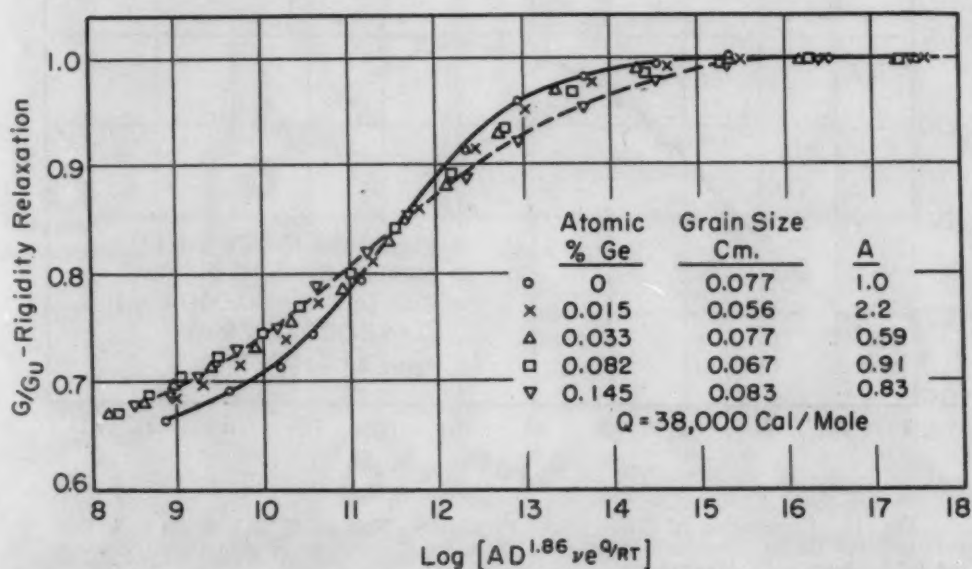


Fig. 8—Rigidity Relaxation in Pure Aluminum and Aluminum-Germanium Alloys as a Function of the Parameter ($AD^{1.86} \nu e^{Q/RT}$).

the alloying additions had practically no effect on either A or the activation energy Q . It is significant to note that the relaxation band for Al-Ge alloys increased with increasing alloy content. In contrast, the relaxation bands for Al-Cu and Al-Ag appear to have contracted slightly with increase in the percentage of the addition element.

Although the preceding data suggest that the activation energy for grain boundary relaxation and the parameter A are insensitive to minor alloying additions, the data obtained for the Al-Mg series reveal that small magnesium additions have substantial effects on

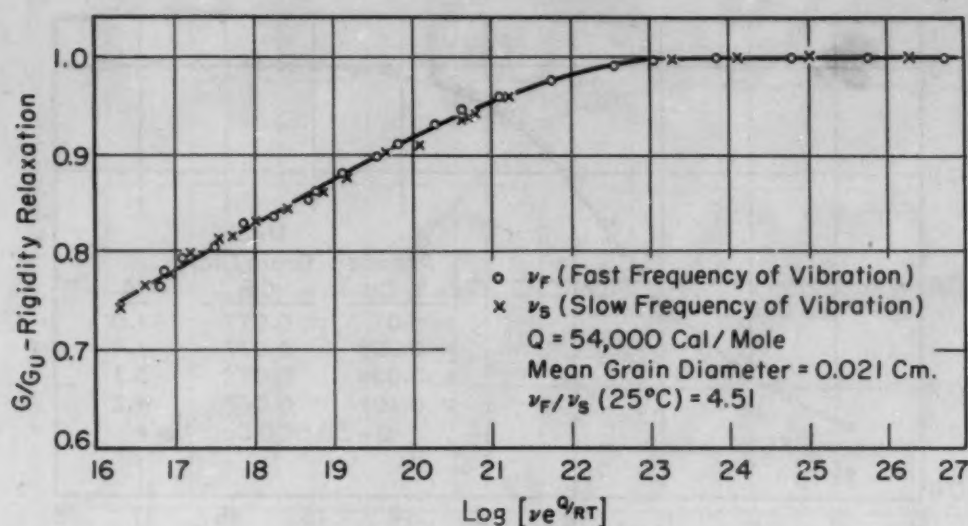


Fig. 9—Correlation of Frequency, Energy of Activation and Temperature for Grain Boundary Relaxation in a Solid Solution of Aluminum Containing 1.617 Atomic % Magnesium.

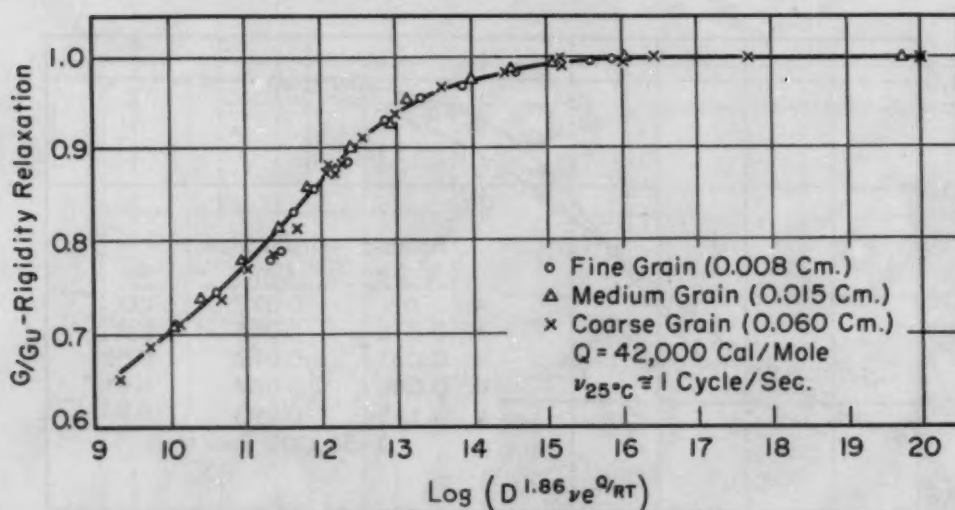


Fig. 10—Correlation of Grain Size, Frequency, Energy of Activation and Temperature for Grain Boundary Relaxation in a Solid Solution of Aluminum Containing 0.554 Atomic % Magnesium.

grain boundary relaxations in aluminum. The series of tests on the 1.617 atomic % magnesium alloy, recorded in Fig. 9, were obtained by using two slightly different inertia bars. These data reveal that the activation energy for this alloy is about 54,000 calories per mole. The series of tests on the 0.554 atomic % magnesium alloy, which are correlated in Fig. 10, were obtained on specimens of different grain sizes. This alloy had an activation energy for grain boundary relaxation of about 42,000 calories per mole. As shown by the data in Fig. 11, magnesium increases the activation energy for grain boundary relaxation in aluminum. The consistent trends observed here further confirm the nominal validity of $m = 1.86$.

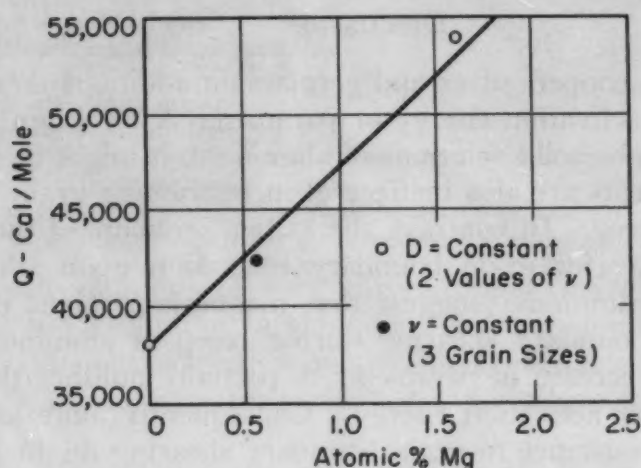


Fig. 11—Effect of Addition of Magnesium to Pure Aluminum on the Activation Energy for Grain Boundary Relaxation.

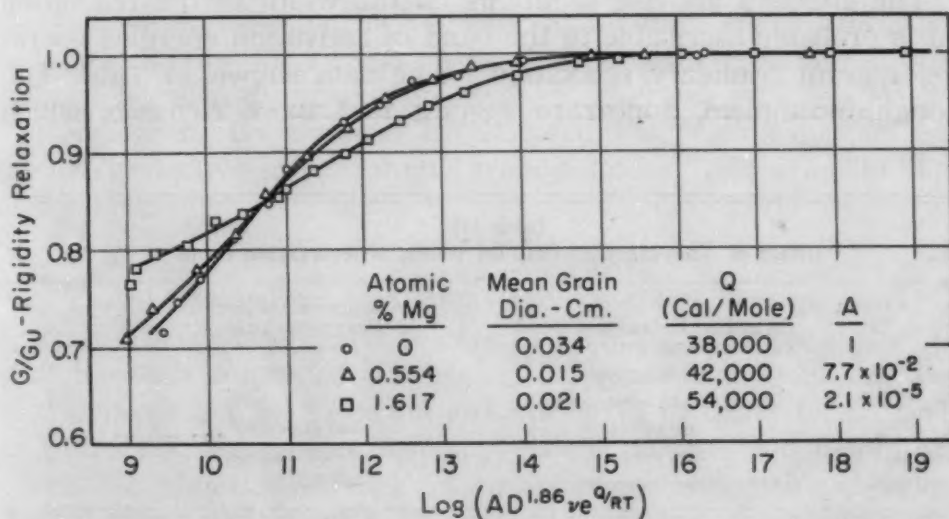


Fig. 12—Rigidity Relaxation in Pure Aluminum and Aluminum-Magnesium Alloys as a Function of the Parameter $(AD^{1.86}\nu e^{Q/RT})$.

A comparison of the grain boundary relaxation phenomenon in the Al-Mg alloys can now be made with high purity aluminum on the basis of the previously established activation energies, as shown in Fig. 12. These data reveal that A decreases precipitously as the magnesium content increases. Furthermore, the relaxation band appears to increase with increasing magnesium content. Part of this effect is attributable to the higher activation energy exhibited by the higher magnesium content alloys. The observed spreading of the relaxation band, however, is much greater than that ascribable solely to the increase in activation energy.

DISCUSSION

Since zinc, copper, silver and germanium additions do not materially alter the activation energy or parameter A for grain boundary relaxation in alpha solid solutions of aluminum, it might be presumed that these elements are also ineffectual in restraining grain boundary shear during creep. In contrast, the rather pronounced increases in activation energy for grain boundary relaxation upon additions of magnesium to aluminum suggest that magnesium might effectively restrain grain boundary shearing during creep of aluminum alloys. But the rapid decrease in parameter A partially nullifies the advantages of a higher activation energy. Consequently, only modest increases in the resistance to grain boundary shearing might be anticipated from alpha solid solution additions of magnesium to aluminum. Perhaps more effectual locking against grain boundary shearing during creep can be secured by promoting grain boundary precipitation of an intermediate phase.

The effect of alloying additions on the width of the relaxation band is probably ascribable to the band of activation energies operative for grain boundary relaxation. The data shown in Table III, although incomplete, appear to suggest that those elements which

Table III
Effect of Alloying Elements on Width of Relaxation Band

Alloy	Width of Relaxation Band (as compared with pure Al)	Change in Lattice Parameter per Atomic %	Valency
Copper	contraction	-0.00495	1
Silver	very slight contraction	0	1
Zinc	no effect	-0.00068	2
Magnesium	increase	+0.00363	2
Germanium	large increase	+0.00138	4

have greater atomic radii than aluminum expand the relaxation band, whereas elements having smaller atomic radii than aluminum contract the band. This trend, however, is not quantitative and other factors are undoubtedly pertinent. Furthermore, it is not yet clear as to why a narrower band of activation energies for grain boundary relaxation should be obtained with a larger alloying element and a smaller band with smaller alloying elements than the host.

CONCLUSIONS

1. Grain boundary relaxation among alloys can be compared by means of the functional relationship

$$G/\bar{G}_a = f \{ A D^m \nu e^{Q/RT} \}$$

where G = shear modulus

G_u = unrelaxed shear modulus

R = gas constant

T = absolute temperature

D = mean grain diameter

m = constant (~ 1.86 for aluminum and aluminum solid solution alloys investigated)

Q = activation energy for grain boundary relaxation

A = parameter dependent on structure and composition

2. Small additions of zinc, silver, copper and germanium that form alpha solid solutions in aluminum have no significant effect on A or Q . Thus the activation energy for grain boundary relaxation is about 38,000 calories per mole for these alloys as well as pure aluminum.

3. The activation energy for grain boundary relaxation for Al-Mg alloys increases almost linearly with magnesium content from 38,000 calories per mole for high purity aluminum to about 54,000 calories per mole for the 1.617 atomic % magnesium alloy.

4. Additions of zinc to aluminum do not change the width of the relaxation band of high purity aluminum; silver and copper additions narrow the relaxation band, whereas magnesium and germanium broaden the relaxation band.

5. Among the elements investigated, magnesium appears to be the most effective in restraining grain boundary relaxation in aluminum alloys.

ACKNOWLEDGMENTS

This investigation was sponsored by the Office of Naval Research. The authors desire to express their appreciation to the ONR staff for their continued interest and support throughout the course of this investigation. The authors also wish to thank O. D. Sherby and A. T. Robinson for their suggestions, advice, and helpful criticisms; W. Holden and M. Fein for assistance in securing the experimental data; and Mrs. G. Pelatowski for the preparation of the figures. In addition, one of us (E.C.V.) wishes to express his appreciation to the U. S. Naval Post Graduate School for their assistance during this investigation.

References

1. C. Zener, "Elasticity and Anelasticity of Metals", 1948, University of Chicago Press.
2. T'ing-Sui Kê, "Stress Relaxations Across Grain Boundaries in Metals", *Physical Review*, Vol. 72, 1947, p. 41.
3. T'ing-Sui Kê, "Internal Friction of Metals at Very High Temperatures", *Journal of Applied Physics*, September 1949.
4. W. Köster, "Über eine Sondererscheinung im Temperaturgang von Elastizitätsmodul und Dämpfung der Metalle Kupfer, Silber, Aluminum und Magnesium", *Zeitschrift für Metallkunde*, Vol. 39, 1948.

PROPERTIES OF SOME HYDROGEN-SINTERED, BINARY MOLYBDENUM ALLOYS

By W. L. BRUCKART, M. H. LACHANCE, C. M. CRAIGHEAD
AND R. I. JAFFEE

Abstract

From a study conducted on alloys representing 18 different binary types, data are presented showing the effects of these additions on the fabricability, room-temperature mechanical properties, and hot hardness to 800 °C. Results of this investigation indicate that aluminum, cobalt, chromium, iron, silicon, and tungsten are the most effective alloying additions.

INTRODUCTION AND SCOPE OF INVESTIGATION

WHEN properly protected against oxidation, wrought unalloyed molybdenum possesses desirable strength properties above 1600 °F. As a result, molybdenum is becoming important as a structural material for very high-temperature use, and efforts are being made to improve the strength properties still further by alloying. As the initial phase of an alloy-development program with this objective, the work reported here concerns a study of binary molybdenum alloys. The effects of binary additions on the fabricability, room-temperature mechanical properties, and hardness to 800 °C (1470 °F) were evaluated. Protection against oxidation was not included as a part of this program, but was the subject of a separate investigation (1).¹ Nevertheless, observations on the oxidation characteristics of the alloys were made during fabrication. When compared with the unalloyed base, none of the alloys had sufficiently better oxidation characteristics to be noticeable. In addition to the unalloyed molybdenum controls, a total of eighteen groups of binary alloys were evaluated. These include alloying additions of aluminum, boron, beryllium, carbon, columbium, cobalt, chromium, iron, indium, manganese, nickel, phosphorus, sulphur, silicon, tin, tantalum, thorium, and tungsten.

Efforts to make alloys containing columbium and tantalum were unsuccessful because of hydrogen contamination during sintering.

¹The figures appearing in parentheses pertain to the references appended to this paper.

A paper presented before the Eighth Western Metal Congress of the Society, held in Los Angeles, March 23 to 27, 1953. Of the authors, W. L. Bruckart and M. H. LaChance are principal metallurgists, C. M. Craighead is assistant supervisor, and R. I. Jaffee is supervisor in the Nonferrous Physical Metallurgy Division at Battelle Memorial Institute, Columbus, Ohio. Manuscript received June 3, 1952.

Since alloys containing titanium, zirconium, or vanadium would probably behave in the same way, these additions were not studied either.

EXPERIMENTAL METHODS

Materials

The molybdenum powder used in this investigation was purchased from the Fansteel Metallurgical Corporation. Its particle size ranged from 2 to 10 microns, with approximately 30% of the particles having a diameter of 3 microns.

All alloying powders were of high purity and were finer than 325 mesh. The majority of the alloys were made by blending the elemental powders with molybdenum. In some cases, master-alloy powders were more desirable than the elemental additions. Such powders were prepared by arc melting, crushing, and sieving.

Preparation, Sintering, and Fabrication

The steps taken to produce the test specimens are outlined in Fig. 1. Pressing was done at room temperature in a single-acting steel die of $\frac{1}{2}$ by 7-inch cavity section. Bars of $\frac{1}{4}$ or $\frac{1}{2}$ -inch thickness were formed. The sintering temperature was governed by the fusion point of the alloy, and the bars were sintered at a temperature just below the melting point of the alloy. Weight and density measurements were made to check the effectiveness of sintering.

Breakdown rolling was done at 1250 °C (2280 °F) whenever possible. However, some of the alloys required temperatures as high as 1600 °C (2910 °F). After both the breakdown and final rolling operations, descaling was done in a nitrate-nitrite salt bath for 30 seconds at 425 °C (800 °F).

Evaluation

With the exception of elevated-temperature hardness measurements, all mechanical-properties data were from room-temperature tests. The standard condition for testing was as-finish-rolled at 1250 °C (2280 °F) to 0.040 inch and annealed for $\frac{1}{2}$ hour at 1100 °C (2010 °F) in hydrogen.

A sintered bar, when reduced to 0.040-inch thickness, usually would produce enough metal for at least two tensile specimens. Bend-ductility and hardness specimens were made from the balance of the strip and from the undeformed ends of the tensile specimens.

Tensile Properties

Tensile testing was done using specimens 4 to 4½ inches long by $\frac{1}{2}$ inch wide, having a reduced section 1.25 inches long by 0.250 inch wide. Thickness was 0.040 inch, and gage length was 1 inch.

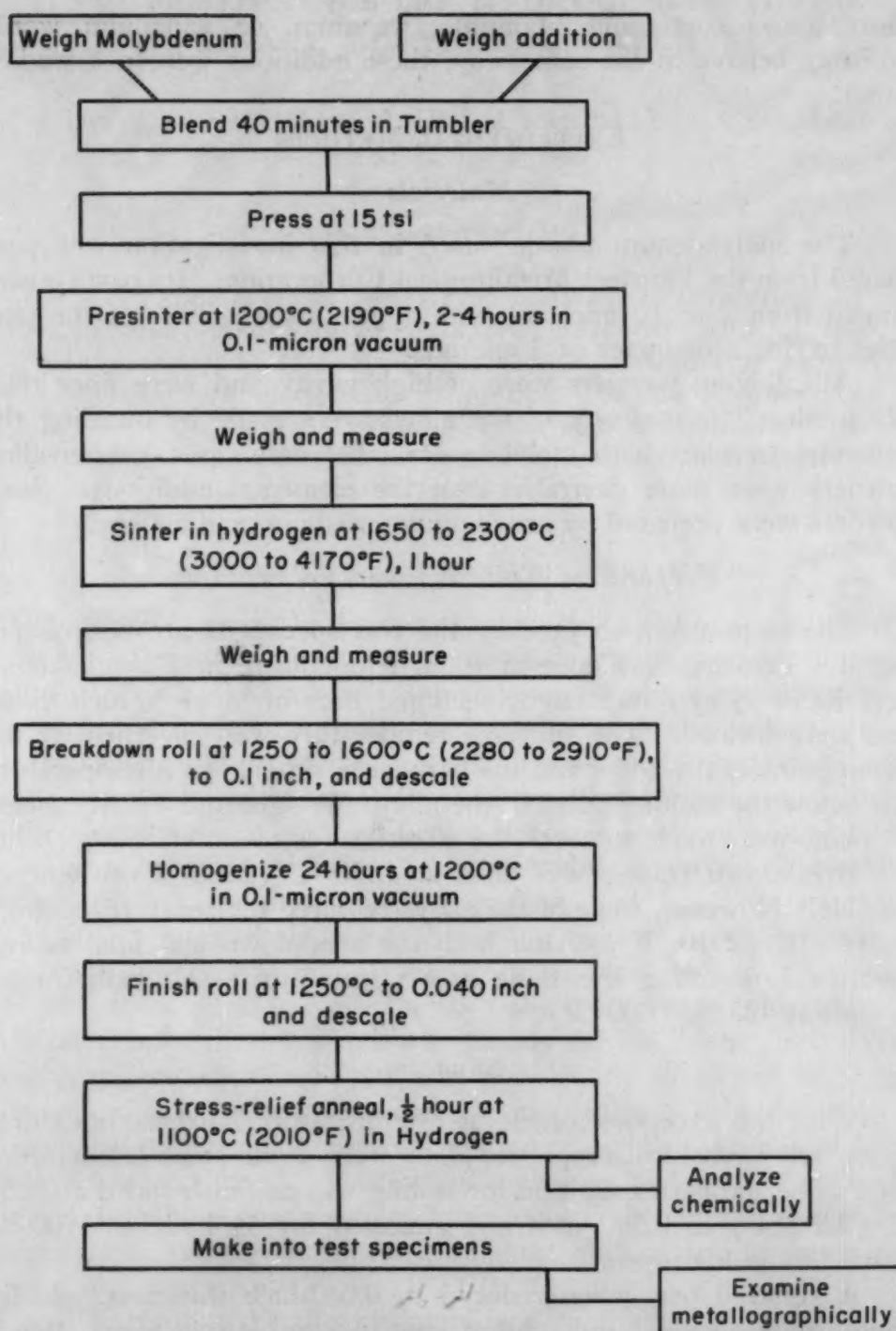


Fig. 1—Diagram of Steps Followed in Processing Experimental Binary Molybdenum Alloys.

Stress-strain data were obtained with SR-4 strain gages at a strain rate of 0.016 inch per inch per minute.

Vickers Hardness

Room Temperature—Vickers 10-kg. hardness was measured on

both longitudinal and transverse sections of each specimen. The data reported are the averages of five impressions on each specimen.

Elevated Temperature—Vickers 10-kg. hardness data were obtained from five impressions made on the surface of one specimen of each alloy. The temperatures were room temperature, and 200, 500, and 800 °C (390, 930, and 1470 °F). A diamond penetrator and an argon-atmosphere furnace mounted on a movable anvil were used for this phase of the investigation.

Bend Ductility

A special bend test (2) was used to evaluate the formability of the molybdenum alloys at room temperature. Duplicate specimens $\frac{1}{2}$ inch wide by at least $\frac{3}{4}$ inch long were prepared. The 105-degree bend was made at right angles to the rolling direction with punches of successively smaller radius. The results, expressed in terms of the thickness of the specimens, are reported as the smallest radius around which the specimen could be bent without cracking. For example, a 0.040-inch specimen bent over a $\frac{3}{64}$ -inch radius (0.0469 inch) is said to be capable of 1.2T bend; for a 0.100-inch specimen, a $\frac{3}{64}$ -inch radius would be a 0.5T bend.

RESULTS

Composition of Test Materials

A complete chemical analysis was made of the molybdenum base. The samples for analysis were taken from the strip after the final annealing treatment. Table I gives the amount of impurities present and the methods used in their determination.

Table I
Results of Chemical Analysis of Wrought Unalloyed Fansteel Molybdenum

Element	Amount Present %	Determined by
Molybdenum	99.95	Difference
Hydrogen	0.0002	Vacuum fusion, precision $\pm 0.0003\%$
Oxygen	0.007	Vacuum fusion, precision $\pm 0.002\%$
Nitrogen	0.009	Vacuum fusion, precision $\pm 0.004\%$
Carbon	0.009	Combustion
Sulphur	0.005	Wet analysis
Phosphorus	0.005	Wet analysis
Nickel	<0.01	Wet analysis
Silicon	0.01	Wet analysis
Manganese	<0.001	Spectrography
Iron	<0.001	Spectrography
Chromium	n.d.	Spectrography
Aluminum	<0.001	Spectrography
Copper	<0.001	Spectrography
Thorium	n.d.	Spectrography

Table II gives the intended compositions of all of the alloys prepared and the results of chemical analyses where available. The alloys containing nickel, thorium, and tungsten were not analyzed,

Table II
Compositions and Fabrication Behavior of Alloys Prepared

Alloy	Concentration of Addition, % (Balance Mo)			Breakdown-Rolling Behavior			
	Intended	Analyzed	Retention	1250°C	1400°C	1500°C	1600°C
Molybdenum	G†
Mo-Al	0.01	G
	0.10	0.085	85	G
	0.25	0.21†	84	G
	0.50	0.43†	86	F
	1.00*	0.74†	74	...	F	G	...
	1.50*	1.26	84	G	...
	2.00*	1.69	85	F	...
Mo-B	0.01	G
	0.025	G
	0.05	G
	0.10	G
	0.25	0.14	56	G
	0.50	0.26	52	G
	1.00	0.8	80	G	...	G	G
Mo-Be	0.01	G
	0.025	F
	0.05	G
	0.10	F	...	G	...
	0.25	0.27	100	G
Mo-C	0.10*	0.01	10	G
	0.20*	0.01	5	G
	0.40*	0.02	5	G
	1.00*	0.56	56	F
	1.50*	0.84	56	F
Mo-Co	0.01	G
	0.10	0.09	90	G
	0.25	0.23	92	F
	0.30	0.27	90	...	G
	0.40	0.35	88	...	G (1450°C)	NG	NG
Mo-Cr	0.25	0.06	25	G
	0.50	0.41	82	F	G
	0.75	0.71	95	P	G
	1.00	0.93	93	...	G
	2.00	1.81	91	...	G
Mo-Fe	0.01	F
	0.10	0.14	100	G
	0.25	0.31	100	F
	0.30	0.33	100	...	F (1450°C)
	0.40	0.44	100	...	F

*Elements added in master alloy form: Al as Mo + Al; C as Mo₂C; P as MoP + Mo; S as MoS₂; Si as MoSi₂ + Mo.

†Good—no difficulty in rolling, no edge or surface cracks.

Fair—no difficulty in rolling, slight edge or surface cracks.

Poor—difficult to roll, specimen obtainable despite cracks.

Bad—difficult to roll, no specimen obtainable.

NG—complete loss.

†	In Solution, %	Inclusions, %
0.25 Al	0.07	0.14
0.50 Al	0.18	0.25
1.00 Al	0.64	0.40

because it was felt that the retention of these additions should be good.

Although the hydrogen-sintering atmosphere was dried in all cases, carbon tended to be removed through decarburization from the traces of moisture in the sintering atmosphere. Extra precautions were taken to keep the atmosphere dry in the case of the two Mo-C

Table II—(Continued)
Compositions and Fabrication Behavior of Alloys Prepared

Alloy	Concentration of Addition, % (Balance Mo)			Breakdown-Rolling Behavior			
	Intended	Analyzed	% Retention	1250°C	1400°C	1500°C	1600°C
Mo-In	0.05	0.03	60	G
	0.10	0.03	30	G
	0.25	0.03	12	G
	0.50	0.03	6	G
Mo-Mn	0.01	G
	0.10	0.014	14	F	G
	0.25	0.06	24	P	G
	0.50	0.24	48	...	G
	1.00	0.54	54	...	G
	1.50	0.81	54	...	G
Mo-Ni	0.02	G
	0.05	G
	0.075	G
	0.10	P†
Mo-P	0.05*	<0.005	<10	NG	G
	0.10*	0.018	18	...	F
Mo-S	0.05*	0.033	67	G
	0.10*	0.067	67	G
	0.25*	0.03- 0.16‡	..	G
Mo-Si	0.01	G
	0.10	0.07	70	G
	0.25	0.18	72	G
	0.30*	0.20	67	...	G
	0.50*	0.42	84	NG	...	B	G
Mo-Sn	0.10	0.03	30	G
	0.25	0.10	40	G
	0.50	0.13	26	G
Mo-Th	0.10	G
	0.25	G
	0.50	G
	0.75	G
	1.00	G
Mo-W	2.5	G
	5.0	G
	7.5	G
	10.0	G
	12.5	G
	15.0	G
	20.0	G
	30.0	F (1300°C)
	40.0	F (1300°C)

*Elements added in master alloy form: Al as Mo + Al; C as Mo₂C; P as MoP + Mo; S as MoS₂; Si as MoSi₂ + Mo.

†Too brittle to test.

‡Results of chemical analysis varied widely.

alloys containing nominally 1.0 and 1.5% carbon, and the retention of carbon was markedly better, as is apparent in Table II.

In the case of indium, nearly all of the addition was lost because the sintering temperature was above its boiling point (about 2000 °C). For the same reason, retentions of tin and phosphorus were low also.

Sintering and Fabrication Behavior

Vacuum presintering was done without difficulty, except for the Mo-2.5 Al and Mo-5.0 Al alloys made using an elemental aluminum addition. A reaction occurred in these two alloys during pre-

sintering which resulted in the bars becoming swollen and non-metallic in appearance. Use of a molybdenum-aluminum master alloy eliminated this difficulty in the Mo-2.5 Al alloy. The Mo-5.0 Al alloy was not remade. An unusual behavior was observed at about 1400 °C (2550 °F) in the sintering process with bars containing 0.5% or higher silicon. These bars had an irregular surface, suggesting a local reaction between the components. Substitution of a Mo-Si master alloy eliminated this effect.

The sintering temperature was 2040 °C (3700 °F)² for all compositions except those listed below:

Composition	Sintering Temperature
Mo-30 W	2140 °C (3885 °F)
Mo-40 W	2240 °C (4065 °F)
Mo-50 W	2300 °C (4170 °F)
Mo-1 Be, Mo-C (from 0.4 to 1.5%)	1850 °C (3650 °F)
Mo-B (from 0.5 to 1.0%)	1800 °C (3270 °F)
Mo-2 Si	1750 °C (3180 °F)
Mo-2 B	1650 °C (3000 °F)

All of the sintered bars were between 90 and 95% of ideal density, and had shrunk between 10 and 14% in length and between 30 and 40% in volume.

The breakdown-rolling behavior of the alloys is given in Table II. Alloys containing between 0.25 and 0.5 silicon, between 0.25 and 0.4 cobalt, and above 20 tungsten demonstrated erratic breakdown-rolling behavior. Although properties have been obtained from these alloys, attempts to reproduce the alloys often have met with failure. After the 24-hour recrystallization anneal, the final rolling operation was conducted from 0.1 inch to 0.040 inch at 1250 °C (2280 °F). Without exception, the alloys that could be breakdown-rolled could be finish-rolled at 1250 °C (2280 °F) with good results.

Based on the data given in Table II, the range of molybdenum base binary compositions that can be fabricated to strip form by powder-metallurgy methods was found to be as follows:

Aluminum	Up to 1.69% Al
Boron	Up to 0.8% B
Beryllium	Up to 0.25% Be
Carbon	Up to 0.84% C
Cobalt	Up to 0.35% Co, erratic above 0.25% Co
Chromium	Up to 1.8% Cr
Iron	Up to 0.4% Fe, erratic above 0.25% Fe
Indium	At least up to 0.03% In
Manganese	At least up to 0.8% Mn
Nickel	Up to 0.075% Ni
Phosphorus	Up to 0.02% P
Sulphur	At least up to 0.1% S
Silicon	Up to 0.4% Si, erratic above 0.2% Si
Tin	At least up to 0.13% Sn
Thorium	At least up to 1% Th
Tungsten	Up to 40% W, erratic above 20% W

²Surface temperature, black-body temperature would be about 2300 °C (4170 °F).

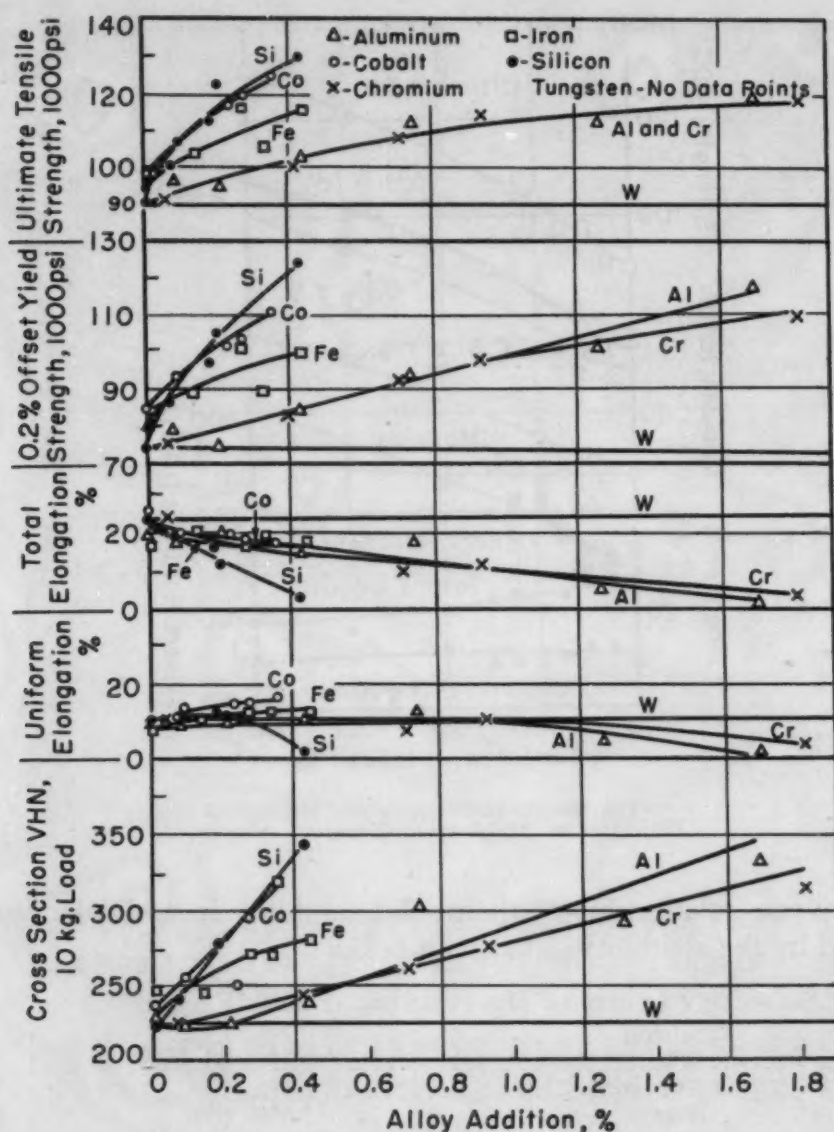


Fig. 2—Effects of Alloying Additions on the Mechanical Properties of Molybdenum.

Mechanical Properties

Strength and Hardness—Averages of the tensile and hardness data obtained on molybdenum and its alloys in this study are given in Table III. Six of the sixteen alloying elements studied appeared to be superior to the others, and data on these are plotted in Fig. 2. A separate plot of the Mo-W alloy strength-composition data is given in Fig. 3 in order that the effect of tungsten may be seen over the full range investigated.

The order of strengthening effect is seen to be: silicon, cobalt, iron, aluminum, chromium, and tungsten. Except for the Mo-Al alloys, the strengthening and hardening effects of these six elements

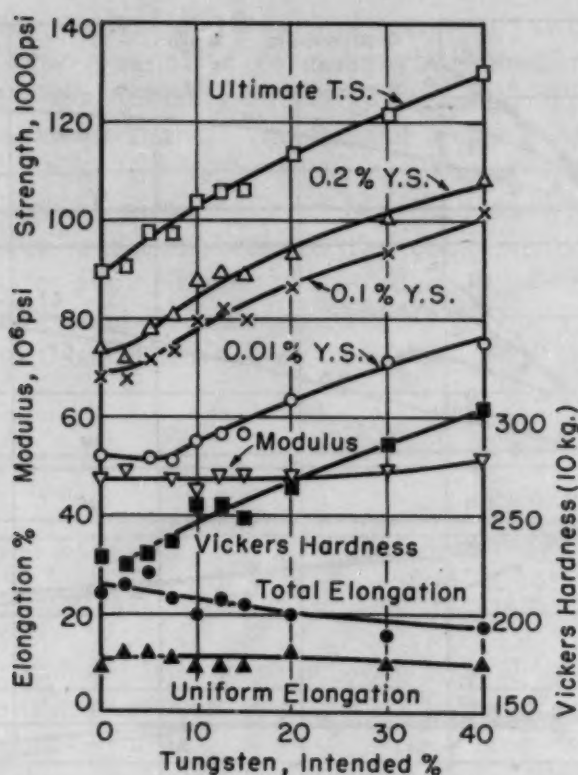


Fig. 3—Room-Temperature Mechanical Properties of Molybdenum-Tungsten Alloys.

are in inverse relationship to their solid solubility in molybdenum, as indicated by the solubility data given below:

SOLUBILITY LIMITS IN MOLYBDENUM AT 2000 °F (1095 °C)

Silicon	0.2% (3)
Cobalt	0.55% (3)
Aluminum	1.4% (3)
Iron	2.65% (3)
Chromium	100% (4)
Tungsten	100% (4)

Although both chromium and tungsten are completely soluble in molybdenum, the existence of a minimum in the solidus curve in the Mo-Cr system at about 75% chromium indicates a tendency to form terminal solid solutions. From this consideration, it is reasonable that chromium has a lower tendency than tungsten to form solid solutions with molybdenum and is a more effective strengthener. Concerning the effect of aluminum, a portion of the aluminum addition was believed to be oxidized (cf. Table II); hence, the solid-solution strengthening effect should be greater than is indicated by the curves, which are based on total aluminum content.

As would be expected, silicon, which is the most effective strengthener, causes the greatest decrease in ductility, as measured by total elongation, while tungsten has the least effect. The four

Table III
Average Room-Temperature Mechanical Properties of Binary Molybdenum-Base Alloys

Composition* Intended	Offset Yield Strength, psi		Tensile Strength, psi	Elongation, %		Modulus, 10 ⁶ psi	Minimum Bend Radius†	Cross-Section VHN (10-Kg. Load)	No. of Specimens Tested
	0.01%	0.1%		Uniform	Total				
Molybdenum	51,900	68,900	73,900	9	24	47.5	OT to >6T	226	10
0.01 Al	52,600	74,800	80,800	8	19	45.6	OT to >6T	228	4
0.10 Al	51,800	72,300	95,400	8	18	47.0	1.2T	222	4
0.25 Al	51,700	68,900	74,200	9	20	48.9	1.9T	224	3
0.50 Al	64,800	77,200	83,500	10	15	48.7	1.2T to >6T	238	4
1.00 Al	71,100	90,100	93,000	12	18	45.9	1.5T	303	2
1.50 Al	75,600	99,800	100,900	4	5	44.4	>6T	291	2
2.00 Al	94,600	113,700	116,800	1	1	45.7	>6T	332	2
0.01 B	42,600	68,500	75,600	10	32	45.3	OT to >6T	247	2
0.025 B	43,200	64,700	71,000	10	34	41.2	4.6T to >6T	238	2
0.05 B	43,400	63,800	69,800	10	27	42.2	1.2T to >6T	236	2
0.10 B	41,900	69,100	75,900	11	33	45.1	OT to >6T	246	2
0.25 B	50,800	72,200	76,500	6	7	47.5	>6T	232	2
0.50 B	52,300	73,200	78,200	8	10	43.1	2.3T to >6T	252	2
1.00 B	49,800	67,400	72,100	1	1	39.6	>6T	260	1
0.01 Be	51,200	67,500	72,700	12	24	45.8	4.6T to >6T	234	2
0.025 Be	53,000	73,500	79,700	10	26	44.4	OT to >6T	237	2
0.05 Be	51,200	66,700	70,200	11	30	46.0	0.8T	220	2
0.10 Be	51,900	71,600	76,800	9	13	48.6	1.2T to >6T	242	2
0.25 Be	69,600	88,900	92,100	5	5	45.0	1.2T to >6T	262	2
0.10 C	53,600	78,600	83,600	9	26	46.8	OT	244	2
0.20 C	52,800	76,400	84,000	8	26	43.7	OT	240	4
0.40 C	68,200	82,800	86,100	12	24	46.3	2.3T to >6T	251	2
1.00 C	47,600	80,800	85,300	4	6	46.8	>6T	271	2
1.50 C	60,200	79,500	82,800	1	1	44.0	>6T	271	1
0.01 Co	62,500	77,000	84,000	9	26	47.1	OT	236	4
0.10 Co	87,900	92,700	92,900	13	21	47.6	0.1T	254	4
0.25 Co	96,100	101,100	101,200	14	20	48.8	OT to >6T	251	4
0.30 Co	92,600	102,700	103,100	14	19	47.7	3.1T to >6T	296	2
0.40 Co	99,600	109,700	110,400	16	18	45.3	1.2T to >6T	319	2
0.25 Cr	59,300	71,000	74,500	11	25	46.0	OT to >6T	225	4
0.50 Cr	66,100	78,700	82,400	10	16	48.6	OT to >6T	242	6
0.75 Cr	74,000	89,300	92,100	7	10	48.7	OT to >6T	261	3
1.00 Cr	77,200	95,200	108,900	10	12	48.8	OT to >6T	277	6
2.00 Cr	99,700	107,500	108,700	4	4	46.8	>6T	315	2
0.01 Fe	58,000	76,400	84,000	7	17	46.4	0.2T	247	4
0.10 Fe	71,400	85,300	88,000	10	21	47.8	OT	246	4
0.25 Fe	89,400	99,200	100,400	12	17	48.0	1.5T	272	3
0.30 Fe	73,700	87,000	89,500	12	20	48.6	0.3T	270	2
0.40 Fe	86,700	98,400	99,300	12	18	47.2	0.4T	281	2

*Balance molybdenum.

†B = R/T; R = Radius of bend in inches; T = Thickness of specimens in inches.

Table III—(Continued)
Average Room-Temperature Mechanical Properties of Binary Molybdenum-Base Alloys

Composition* Intended	Composition* Actual	Offset Yield Strength, psi		Tensile Strength, psi	Elongation, %		Modulus, 10 ⁶ psi	Minimum Bend Radius†	Cross-Section VHN (10-Kg. Load)	No. of Specimens Tested
		0.01%	0.1%		Uniform	Total				
0.05 In	0.03	60,600	71,500	85,000	9	26	49.3	1.5T	215	2
0.10 In	0.03	49,200	69,600	83,200	7	15	51.0	1.6T to >6T	228	2
0.25 In	0.03	55,500	69,300	85,200	11	35	49.8	OT	219	2
0.50 In	0.03	53,900	66,200	81,500	11	31	48.5	4.6T to >6T	222	2
0.01 Mn	...	54,000	69,200	93,400	10	21	47.7	OT	231	2
0.10 Mn	0.014	58,400	73,000	91,800	9	22	48.6	OT to >6T	232	6
0.25 Mn	0.06	57,700	71,700	90,400	12	25	48.3	OT to >6T	233	6
0.50 Mn	0.24	57,800	72,900	90,400	11	13	46.4	>6T	226	2
1.00 Mn	0.54	67,800	84,700	104,600	11	16	46.7	0.8T to >6T	268	2
1.50 Mn	0.81	74,000	95,600	110,700	4	4	48.8	1.2T to >6T	322	2
0.02 Ni	...	65,500	78,800	97,100	11	26	47.6	1.6T to >6T	225	2
0.05 Ni	...	76,700	81,500	88,200	8	10	48.2	1.2T to >6T	232	4
0.075 Ni	77,600	1	1	48.5	6T	225	1
0.05 P	0.005	62,600	72,200	85,400	10	25	47.6	OT	218	2
0.10 P	0.018	68,900	85,600	98,500	13	27	48.3	OT	235	2
0.05 S	0.033	59,100	74,700	84,500	7	27	48.1	4.6T to >6T	235	2
0.10 S	0.067	48,300	69,600	81,500	7	23	47.9	0.8T to >6T	224	2
0.25 S	0.03-	39,000	68,200	85,400	7	23	47.7	OT	224	2
0.01 Si	0.16	56,100	76,000	93,500	9	25	50.5	0.6T	223	4
0.10 Si	0.07	77,600	85,500	100,600	11	20	49.9	OT	241	4
0.25 Si	0.18	82,800	96,500	112,600	12	17	53.1	0.1T	277	2
0.30 Si	0.20	89,300	101,500	122,300	10	12	50.5	0.8T	281	2
0.50 Si	0.42	100,300	121,800	130,000	1	3	45.6	>6T	345	2
0.10 Sn	0.03	50,900	65,100	79,700	8	29	47.4	4.6T to >6T	221	2
0.25 Sn	0.10	54,700	68,600	84,500	11	24	51.8	4.6T	222	2
0.50 Sn	0.13	64,000	74,200	88,300	13	24	47.6	2.3T	224	2
0.10 Th	...	50,600	67,300	92,100	10	21	45.1	OT to >6T	223	4
0.25 Th	...	49,700	67,900	94,100	8	19	45.7	OT to >6T	224	4
0.50 Th	...	57,400	77,200	100,500	8	21	45.5	1.4T	231	4
0.75 Th	...	61,600	80,200	102,600	7	17	46.3	1.5T	245	4
1.00 Th	...	58,300	74,100	95,300	9	22	45.5	OT	235	6
2.5 W	...	49,100	67,500	90,200	12	26	49.5	OT to >6T	224	4
5.0 W	...	51,500	71,900	97,500	12	28	50.6	OT to >6T	230	4
7.5 W	...	51,100	73,200	97,800	11	23	47.4	OT to >6T	232	6
10.0 W	...	55,300	79,400	103,500	9	20	45.6	OT to >6T	251	6
12.5 W	...	56,800	82,000	105,900	9	23	48.3	1.6T to >6T	251	6
15.0 W	...	56,100	79,800	106,200	9	22	48.3	2.3T to >6T	249	4
20.0 W	...	63,500	86,800	113,100	12	16	47.9	2.3T	264	2
30.0 W	...	71,400	93,500	121,300	10	10	49.5	>6T	287	2
40.0 W	...	75,100	101,700	130,200	10	18	52.2	>6T	305	2

*Balance molybdenum.

†B = R/T; R = Radius of bend in inches; T = Thickness of specimens in inches.

Table IV
Bend Ductility of Molybdenum-Base Alloys*

Alloy Group	Excellent	Good	Bend Rating† Fair	Poor	Erratic
Mo					All
Mo-Al		to 1.0 Al		1.5, 2.0 Al	
Mo-B					All
Mo-Be		0.05 Be			All others
Mo-C	0.1, 0.15, 0.2 C			1.0, 1.5 C	0.3, 0.4 C
Mo-Co	0.01, 0.1 Co			0.4 Co	All others
Mo-Cr				2.0 Cr	All others
Mo-Fe	0.01, 0.1 Fe	0.25, 0.3, 0.4 Fe		0.5 Fe	
Mo-In					All
Mo-Mn	0.01 Mn			0.5 Mn	All others
Mo-Ni				0.075 Ni	All others
Mo-P	0.05, 0.1 P				
Mo-S	0.25 S				All others
Mo-Si	0.1, 0.25 Si	0.01, 0.3 Si		0.5 Si	
Mo-Sn		0.5 Sn	0.25 Sn		0.1 Sn
Mo-Th	1.0 Th	0.5, 0.75 Th			0.1, 0.25 Th
Mo-W			12.5, 20 W	30, 40 W	All others

*Compositions given are the amounts added. For actual analyses see Table III.

†Excellent: 0T to 0.3T; Good: 0.4T to 1.6T; Fair: 2.0T to 4.6T; Poor: >4.6T; Erratic: bends ranging from 0T to >6T within the same bar.

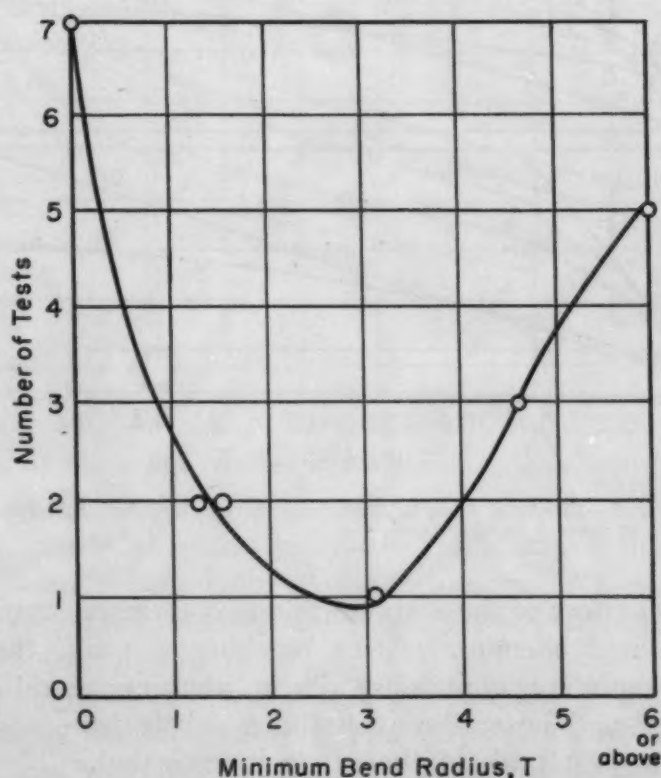


Fig. 4—Distribution of Bend-Ductility Data for the Wrought Molybdenum Strip Specimens.

remaining elements, cobalt, chromium, aluminum, and iron, show little difference in their relative effects, and the total elongations fall more or less on a common line between the curves for silicon and tungsten.

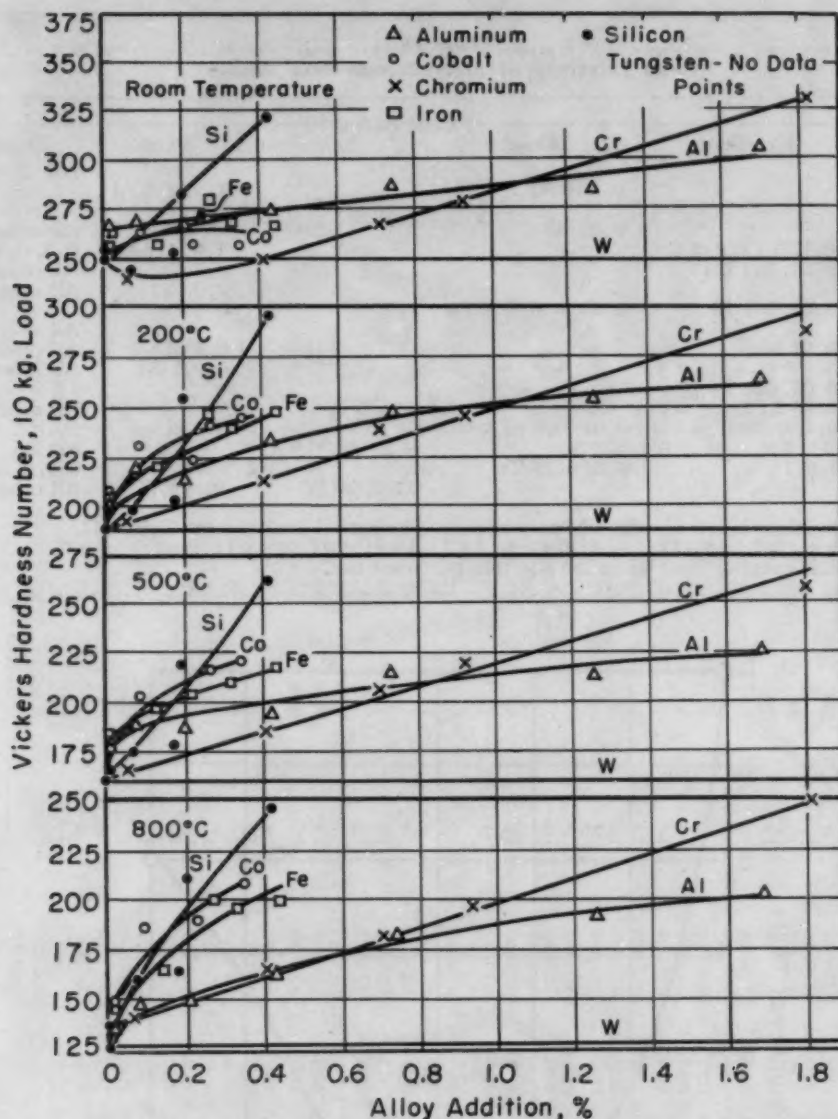


Fig. 5—Effects of Alloying Additions on the Hardness of Molybdenum at Several Temperatures.

The initial effect of these six additions is to increase the uniform elongation of molybdenum. After reaching a peak, the uniform elongation of the alloys containing silicon, aluminum, and chromium tends to decrease. Those alloys containing cobalt, iron, and tungsten do not show such a peak in the range investigated. The fact that all of these materials were rolled at 1250 °C to 60% reduction, which undoubtedly corresponds to different levels of internal strain in the various specimens, probably has a bearing on this observation.

Bend Ductility—Bend-ductility data are given in Table III. A classification of these data according to behavior is given in Table IV. Unalloyed molybdenum has erratic bend ductility at room temperature under the fabrication and test conditions used. It usually shows

either very good or poor bend ductility. Twenty bend tests on various runs of experimentally produced molybdenum strips produced the distribution shown in Fig. 4. However, as shown in Table IV, some of the alloying additions improved the erratic bend characteristics of unalloyed molybdenum. These additions were carbon, cobalt, iron, manganese, phosphorus, silicon, and thorium. Most of these elements are good deoxidizers, which may account for this result.

Hot Hardness—The hardness data taken at room temperature and 200, 500, and 800 °C (390, 930, and 1470 °F) are listed in

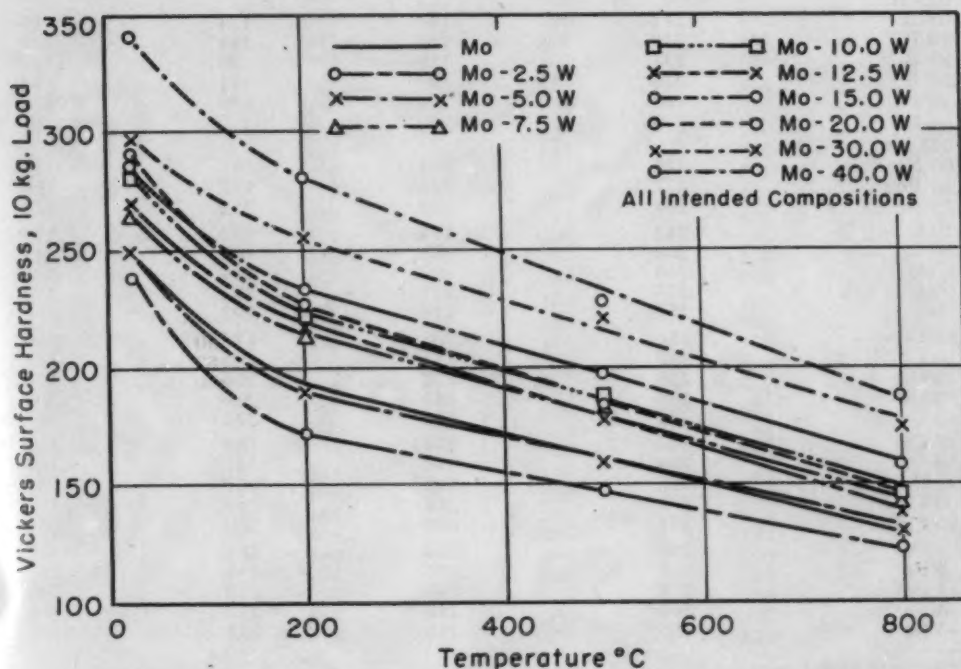


Fig. 6—Hot Hardness of Molybdenum-Tungsten Alloys.

Table V. Hardness versus alloy concentration for those alloys containing silicon, cobalt, iron, chromium, aluminum, and tungsten is shown in Fig. 5. Hot-hardness data for the entire range of Mo-W alloys are shown in Fig. 6.

In the temperature range from 200 to 800 °C (390 to 1470 °F), the maximum workable alloy concentrations produced hardening in the same order as was found in the strength-versus-composition comparison, although at concentrations of less than 0.2%, the relative hardening effectiveness of silicon is less than that of cobalt, iron, or aluminum. Fig. 6, which refers to the alloys with tungsten, is typical of the effect of temperature on hardness for all of the alloys. The greatest drop in hardness occurs between room temperature and 200 °C. Beyond that temperature, the loss in hardness is roughly linear. Although the data are limited to 800 °C (1470 °F), this linear drop

Table V
Average Hot-Hardness Values for Binary Molybdenum Alloys
 (Vickers Hardness, 10-Kg. Load)

Intended Composition*	Room Temperature	Surface Hardness		
		200 °C	500 °C	800 °C
Molybdenum	249	189	163	128
0.01 Al	265	203	179	137
0.10 Al	268	221	191	148
0.25 Al	261	215	185	149
0.50 Al	275	234	196	163
1.00 Al	288	248	216	182
1.50 Al	287	255	215	193
2.00 Al	306	265	228	203
0.01 B
0.025 B
0.05 B	212	141	124	99
0.10 B	230	166	144	121
0.25 B	234	150	130	110
0.50 B	233	167	141	118
1.00 B	263	220	180	155
0.01 Be
0.025 Be
0.05 Be	224	164	141	124
0.10 Be	272	227	197	159
0.25 Be	295	246	211	178
0.10 C	243	174	152	121
0.20 C	266	212	183	141
0.40 C	246	192	164	139
1.00 C	276	221	192	173
1.50 C	251	218	192	166
0.01 Co	256	208	178	150
0.10 Co	262	231	205	182
0.25 Co	258	224	206	190
0.30 Co	270	241	219	200
0.40 Co	256	245	222	209
0.25 Cr	240	194	168	142
0.50 Cr	250	214	187	165
0.75 Cr	273	240	207	183
1.00 Cr	281	247	222	197
2.00 Cr	332	290	260	251
0.01 Fe	263	206	181	145
0.10 Fe	257	221	198	165
0.25 Fe	279	246	218	200
0.30 Fe	269	240	212	196
0.40 Fe	266	248	218	199

*Balance molybdenum.

in hardness is believed to continue at least to the recrystallization range.

Microstructure

A metallographic examination was made on each specimen in both longitudinal and transverse sections. Three general types of microstructure were observed: (a) single-phase elongated grain structures, sometimes partly equiaxed; (b) single-phase elongated grain structure containing scattered inclusions strung out in the rolling direction; (c) two-phase structures containing a molybdenum compound as the second phase in a matrix of elongated grains. Examples of these types are given in Figs. 7-9.

Aluminum—Mo-Al alloys had structures similar to that shown in Fig. 8a. The grains were elongated, and scattered inclusions

Table V—(Continued)
Average Hot-Hardness Values for Binary Molybdenum Alloys
(Vickers Hardness, 10-Kg. Load)

Intended Composition*	Room Temperature	Surface Hardness		
		200 °C	500 °C	800 °C
0.05 In	233	165	144	123
0.10 In	230	158	126	104
0.25 In	233	177	146	126
0.50 In	219	166	131	117
0.01 Mn
0.10 Mn
0.25 Mn	233	173	156	129
0.50 Mn	227	178	154	139
1.00 Mn	233	198	176	149
1.50 Mn	240	208	179	159
0.02 Ni	255	196	172	145
0.05 Ni	245	204	181	163
0.075 Ni	243	202	185	163
0.05 P	249	189	164	146
0.10 P	242	186	162	142
0.05 S	232	146	126	105
0.10 S	227	141	121	106
0.25 S	264	181	151	128
0.01 Si	255	190	168	137
0.10 Si	243	199	177	161
0.25 Si	253	204	181	165
0.30 Si	283	254	221	212
0.50 Si	322	297	262	247
0.10 Sn	230	146	130	104
0.25 Sn	221	158	133	117
0.50 Sn	232	172	153	130
0.10 Th	258	190	165	126
0.25 Th	254	183	161	125
0.50 Th	261	210	181	136
0.75 Th	269	212	184	142
1.00 Th	264	199	169	135
2.5 W	238	170	147	122
5.0 W	249	190	160	130
7.5 W	264	212	181	142
10.0 W	282	221	187	145
12.5 W	268	217	180	139
15.0 W	286	232	197	157
20.0 W	289	225	183	146
30.0 W	298	254	220	173
40.0 W	341	281	237	187

*Balance molybdenum.

increased in amount with aluminum content. From the chemical analyses and metallographic study, these inclusions are believed to be aluminum oxide.

Boron—Alloys containing 0.1% or less boron showed a single-phase structure of elongated grains. Alloys with an intended 0.25% or more boron showed particles of a boride phase, as shown in Fig. 9a. Such a structure may account for the low ductilities of the Mo-B alloys in the higher boron range.

Beryllium—A second phase was observed in all alloys containing beryllium. This phase appeared to increase with beryllium content and may be an oxide (Fig. 8b).

Carbon—The microstructure of the 0.01% (actual analysis) carbon alloy consisted of a single phase with elongated grains. There was considerably more fibering of the grains along the surface

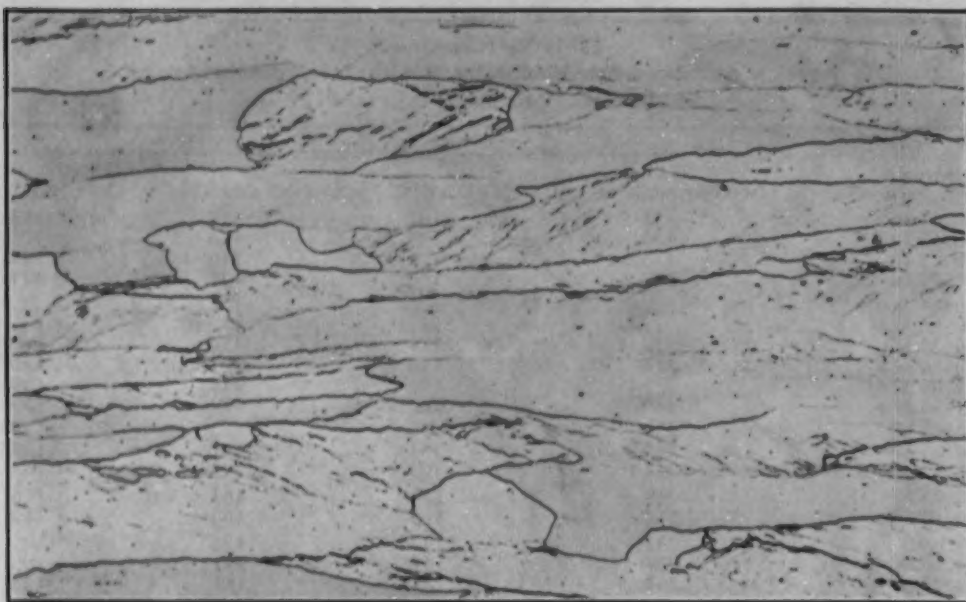


Fig. 7—Longitudinal Section of Unalloyed Molybdenum. $\times 250$.

of the strip than in the center. Molybdenum carbide was observed in the specimen analyzing 0.02% carbon. This phase is shown in Fig. 9b, where the carbide exists as a series of white rounded particles strung out in the rolling direction.

Cobalt—Evidence of partial recrystallization was observed in the Mo-Co alloys analyzing 0.23% or more cobalt. The typical structure of these alloys is shown in Fig. 10. At 0.1% cobalt, or lower, the typical, elongated-grain structure of unalloyed molybdenum was found.

Chromium—All Mo-Cr alloys showed a single-phase structure of elongated grains.

Iron—Single-phase structures were observed in all Mo-Fe alloys studied. Medium-sized, elongated grains were observed in the centers of the strips, while the fibering was finer toward the surface.

Indium—All the Mo-In alloys were composed of a single-phase structure containing a mixture of elongated and equiaxed grains, showing partial recrystallization.

Manganese—All of the alloys containing less than 0.54% manganese appeared to be single-phase solid solutions. However, alloys with 0.54 and 0.81% manganese showed some elongated inclusions (see Fig. 8c). The exact nature of this phase is not known, but it appears to be nonmetallic and possibly is an oxide of manganese.

Nickel—All of the Mo-Ni alloys showed only a single phase consisting of fibered or elongated grains.

Phosphorus—The Mo-P alloys were all partially recrystallized, single-phase structures. Some grain-size refinement was observed with an increase in phosphorus content.

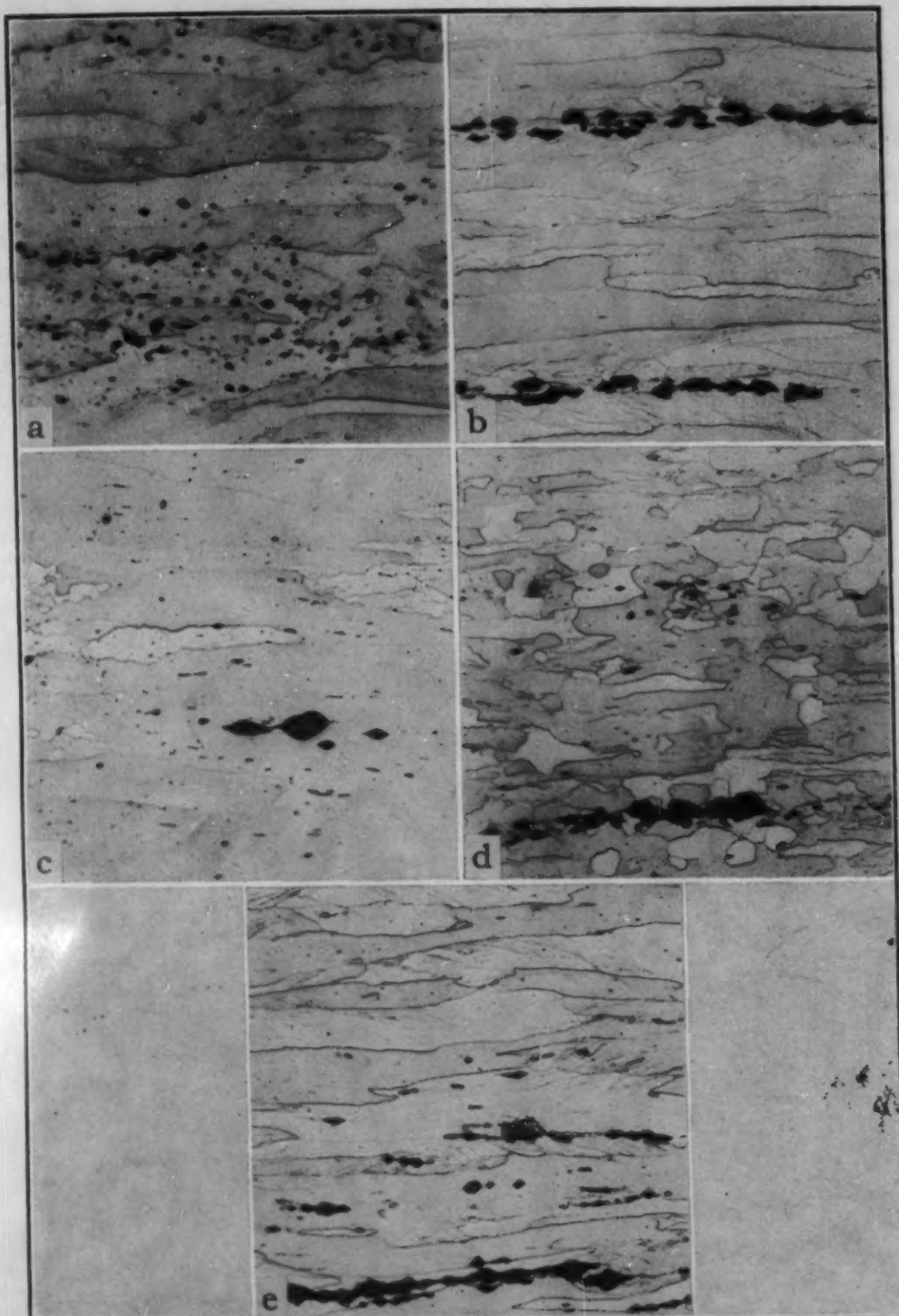


Fig. 8—Longitudinal Sections of Molybdenum-Base Alloys Showing Types of Inclusions. $\times 250$. (a) Mo-0.43 Al; (b) Mo-0.25 Be; (c) Mo-0.54 Mn; (d) Mo-0.18 Si; (e) Mo-1.0 Th.

Sulphur—The Mo-S alloys were composed of coarse, fibered grains, and showed some recrystallization along the edges of the section. However, as the sulphur content was increased, the recrystallization became less noticeable.

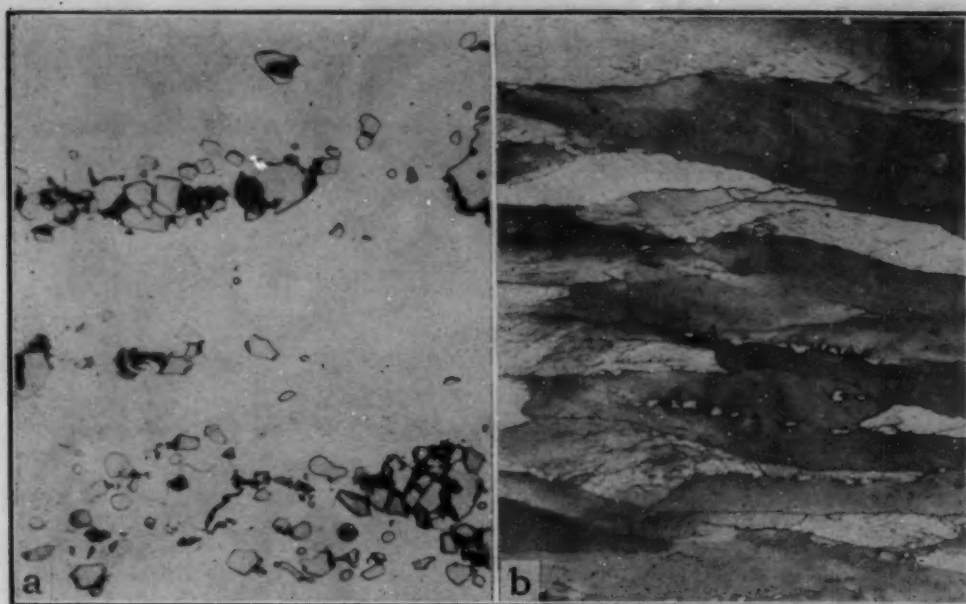


Fig. 9—Longitudinal Sections of Molybdenum-Boron and Molybdenum-Carbon Alloys Showing Second Phases. $\times 500$. (a) Mo-0.8 B showing boride phase; (b) Mo-0.02 C showing carbide phase.

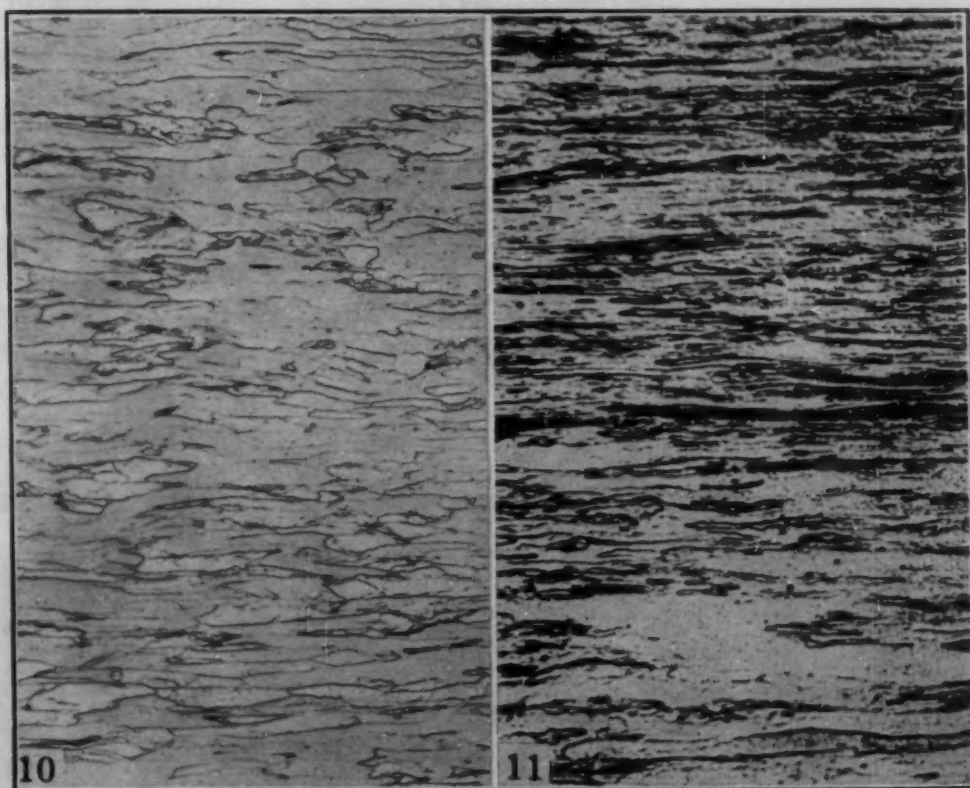


Fig. 10—Longitudinal Section of Mo-0.23 Co Alloy, Showing Partial Recrystallization.

Fig. 11—Longitudinal Section of Mo-12.5 W Alloy Showing Nonuniform Fibering. Both photomicrographs $\times 250$.

Silicon—Equiaxed grains increasing in amount with the silicon content were observed in the Mo-Si alloys. The specimens containing 0.18% silicon, or more, were observed to contain inclusions, as

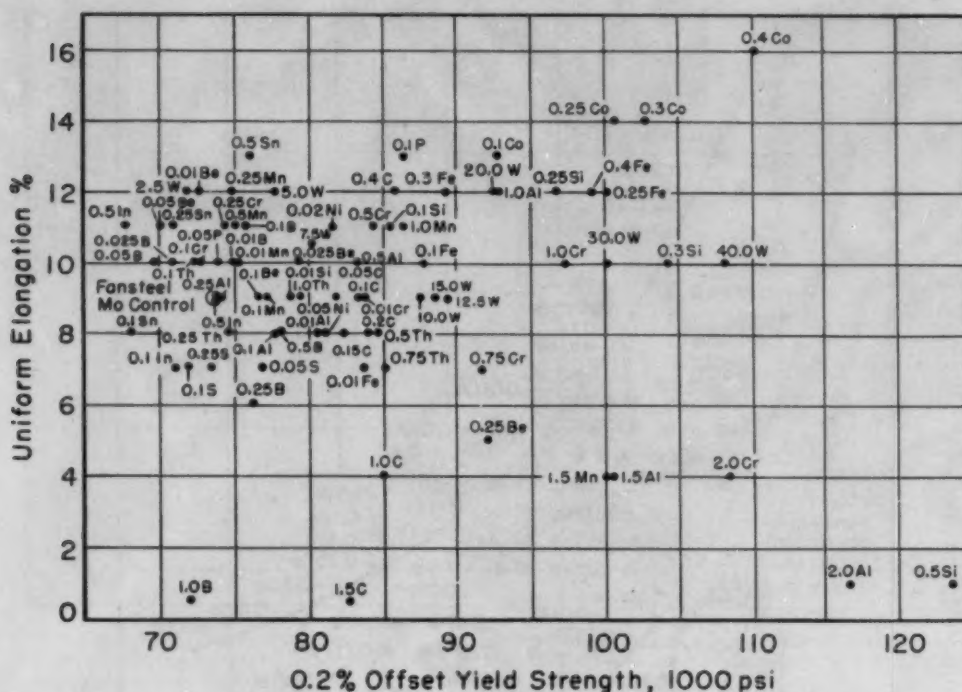


Fig. 13—Yield Strength Versus Uniform Elongation for Molybdenum-Base Alloys.

phased fibered grains. Most of these alloys had a nonuniform structure in which bands of finely fibered material coexisted with medium to coarse elongated grains (Fig. 11).

Correlations

For the six best binary alloy groups, correlation plots of strength, elongation, and hardness versus composition have been presented and discussed in a previous section of this paper. General correlations of strength and elongation, strength and hardness, and hardness anisotropy are given in Figs. 12 to 16 and are discussed below.

Strength-Elongation Correlation—Since total elongation usually decreases as strength increases, comparisons of strength-composition curves or ductility-composition curves will tell little about the alloys with optimum properties until the two are combined. One such combination is given in Fig. 12 for tensile strength and total elongation. The strength-elongation data are shown as points representing the intended compositions. In general, there is a trend toward increasing strengths being accompanied by decreased elongation. The alloys which have highest elongation for a given strength, a position nearest the upper curve on the plot, are the most desirable, although all of those between the two curves shown may be considered as having satisfactory strength-elongation combinations. The best combinations of tensile strength and total elongation obtained from all of the alloys studied are given in the tabulation on the next page by their intended compositions in order of decreasing strength level:

Addition Elements, Weight %	Tensile Strength, 1000 Psi	0.2% Offset Yield Strength, 1000 Psi	Vickers Hardness	Elongation, % in 1 Inch
40 W, 0.4 Co, 30 W	120-130	100-115	300-325	14-18
0.25 Co, 20 W, 0.3 Co, 0.4 Fe, 0.25 Fe	110-120	90-100	275-300	18-20
12.5 W, 15 W, 0.1 Co, 0.1 Fe, 0.5 Th	100-110	80-90	250-275	20-24
5 W, 0.01 C, 0.01 Co, 0.02 Ni, 0.025 Be	95-100	75-80	240-250	24-28
0.1 B, 0.01 B, 0.025 B, 0.05 Be	85-90	70-75	210-225	30-35

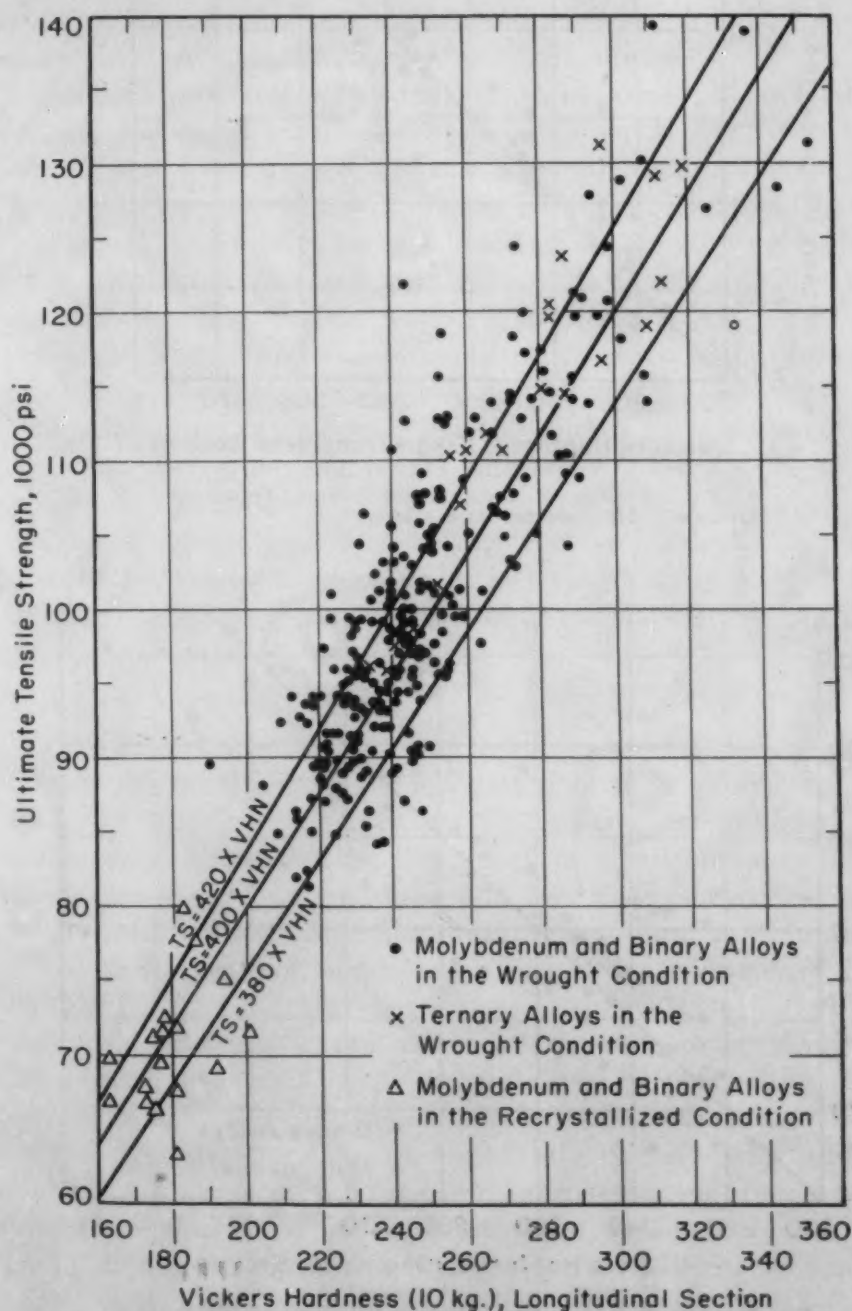


Fig. 14—Tensile Strength Versus Vickers Hardness for Molybdenum-Base Alloys.

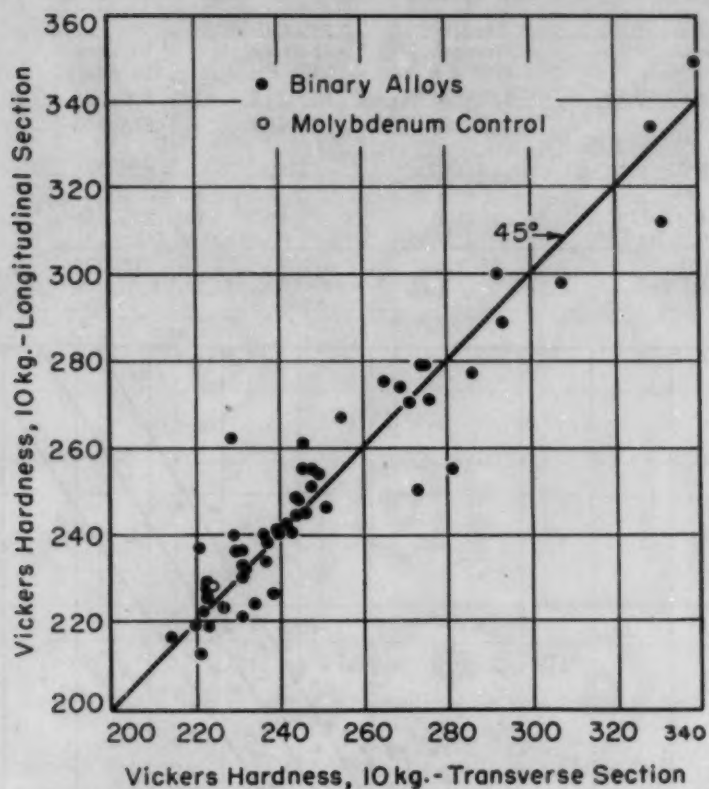


Fig. 15—Plot of Longitudinal Versus Transverse Hardness of Molybdenum-Base Alloys.

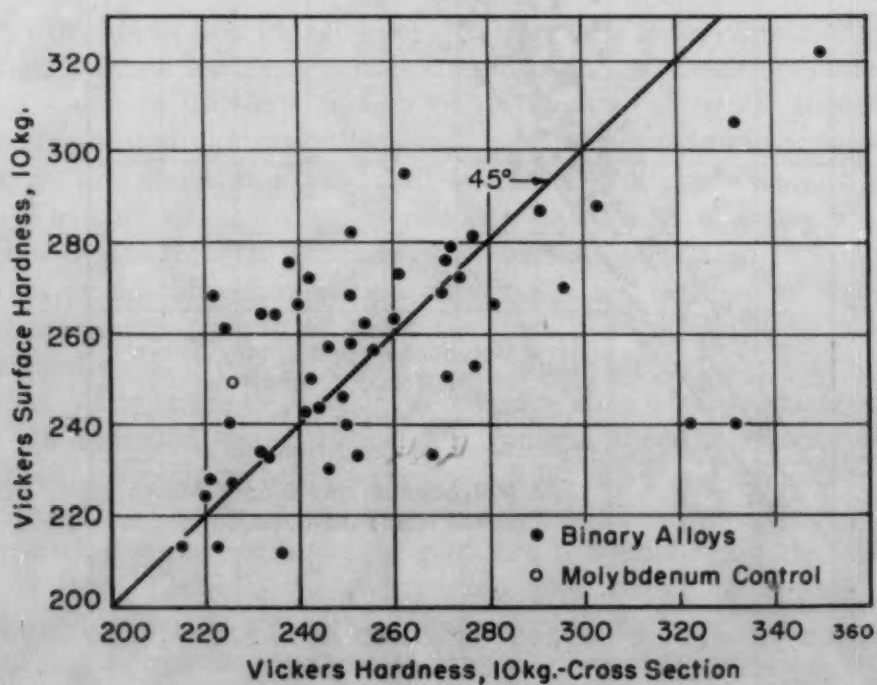


Fig. 16—Plot of Surface Versus Section Hardness of Molybdenum-Base Alloys.

It is worth noting that the binary alloys with tungsten are high up in each strength-level group.

Fig. 13 is a plot of yield strength versus uniform elongation of all of the binary alloys investigated, given as points representing the intended compositions. Uniform elongation and yield strength are two important design factors. It is surprising to note that uniform elongation tends to increase with the yield strength. This indicates that molybdenum alloys are considerably superior to unalloyed molybdenum in this respect. Outstanding alloys, those with the highest yield strengths and uniform elongations, are as follows: 0.4 cobalt, 40 tungsten, 0.3 cobalt, 0.25 iron, and 0.25 silicon.

Ultimate Strength-Hardness Correlation—A correlation between hardness and tensile strength is shown in Fig. 14. Included in this figure are hardness-tensile strength data for some ternary molybdenum-base alloys, and for some binary molybdenum-base alloys which were completely recrystallized prior to testing. Although there is considerable scatter, the bulk of the points lie close to a line whose equation is: $\text{Tensile Strength} = 400 \times \text{VHN}$.

Hardness Anisotropy—No anisotropy was found to exist between hardness measurements on longitudinal and transverse sections of molybdenum or its alloys. Fig. 15 shows that, within the limits of experimental error, all points fall fairly close to the line of no anisotropy (45 degrees).

Further comparison between the surface hardness and the average of the section hardnesses (Fig. 16) shows more scatter than was found in the comparison above, but no consistent anisotropy was detected.

CONCLUSIONS AND DISCUSSION

The data presented on molybdenum-base alloys prepared by hydrogen sintering permit an evaluation of their probable usefulness and service behavior at temperatures below the recrystallization range. Potency of alloying, that is, the ability of small amounts of alloying addition to strengthen molybdenum, has been shown to be in the order silicon, cobalt, iron, aluminum, chromium, and tungsten, for the six most effective additions. This order of potency has been shown to hold for Vickers hardness up to 800 °C (1470 °F), which is below the recrystallization range. However, for service, the merit of an alloy is measured by the magnitude of its properties, not by the economy of alloying. On this basis, tungsten, which may be alloyed in large concentrations, is the most effective alloying addition for molybdenum, despite its small unit strengthening response. Considering the over-all strength of alloys possessing adequate ductility, Fig. 12 demonstrates that the most effective alloying additions³ are: (a) 40 tungsten, (b) 0.4 cobalt, (c) 30 tungsten, (d) 0.3 cobalt,

³These are amounts of the additives, not retained contents.

(e) 0.25 cobalt, (f) 0.25 iron, (g) 0.4 iron, (h) 1 chromium, (i) 20 tungsten, and (j) 0.25 silicon. If the alloys that are hard to fabricate and are erratic in their fabrication behavior are eliminated, the most effective alloying additions are: (a) 0.25 cobalt, (b) 0.25 iron, (c) 1 chromium, (d) 20 tungsten, (e) 0.25 silicon, and (f) 1 aluminum. These alloy additives all fabricate readily and have strengths above 110,000 psi and elongations above 10%.

ACKNOWLEDGMENTS

The authors wish to express their appreciation to J. B. Johnson and the U. S. Air Force for permission to publish the results of work obtained at Battelle Memorial Institute under Contract No. AF 33(038)-12641. They also are indebted to Jack A. Taynor and Richard D. Mico, who performed a large part of the experimental work, and to R. D. Buchheit and George Wheeler for preparation of the metallographic specimens.

References

1. W. L. Bruckart and R. I. Jaffee, "Cladding of Molybdenum for Service in Air at Elevated Temperature", *TRANSACTIONS, American Society for Metals*, Vol. 44, 1952, p. 176.
2. C. M. Craighead, O. W. Simmons and L. W. Eastwood, *Transactions, American Institute of Mining and Metallurgical Engineers*, Vol. 188, 1950, p. 485.
3. J. L. Ham, "Arc-Cast Molybdenum-Base Alloys", First Annual Report on Project NRO31-331, Climax Molybdenum Company of Michigan, April 1, 1950.
4. *METALS HANDBOOK*, American Society for Metals, 1948.

DISCUSSION

Written Discussion: By M. Semchyshen, Climax Molybdenum Co., Detroit.

The authors of this paper are to be commended for their contribution to the fast-accumulating body of engineering data on molybdenum and molybdenum-base alloys. For the alloys that can be compared we find fairly good agreement between these data and data obtained in our laboratory on cast and wrought alloys produced by arc melting, although we have data for only a few of the alloys in comparable structural conditions.

During the fabrication of the alloys studied by Mr. Bruckart and his co-workers, the alloys were rolled from 0.1 inch to 0.040 inch at 1250 °C (2280 °F). Subsequent stress relieving for ½ hour at 1100 °C (2010 °F) did not place all of the alloys in one structural condition. Some of the alloys were partially recrystallized and some stress-relieved as a result of the heat treatment. The degree of recrystallization affects tensile properties and hardness. For this reason we find it advisable to process the alloys so as to produce only one structural condition when comparing the alloying effects of various elements. In our exploratory evaluations of molybdenum-base alloys, we compared the alloys in the fully recrystallized condition, because molybdenum and molybdenum-base alloys are being

considered for service in a temperature range at which recrystallization may occur in service.

We would like to comment briefly upon the alloying effects of beryllium and thorium. It is our experience that the alloying effects of these elements is lost to the extent that formation of stable oxides of beryllium and thorium occurs. In the case of beryllium, large increases in hardness could be obtained with beryllium contents of the order of 0.05%, if oxidation of the beryllium was largely avoided. We agree that the second phases described by the authors in the molybdenum-beryllium and molybdenum-thorium systems could be oxide. Perhaps an analysis such as that made on the molybdenum-aluminum system should have been applied to the molybdenum-beryllium and molybdenum-thorium systems also, in order to bring out the alloying effects.

In evaluating the molybdenum-tungsten alloys, it should be borne in mind that, although they appear in the group having the highest strength, the higher strength is required to offset the increased density if the material is to be subjected to high centrifugal forces. If we allow for the greater density of the 20 and 40% tungsten alloys, they are not so promising, with respect to increased strength, as some of the other alloy systems.

Written Discussion: By Harry B. Goodwin, Battelle Memorial Institute, Columbus, Ohio.

There are three important problems to be solved before molybdenum-base alloys can be used for construction of heat engines. These are (a) finding suitable means of protection against oxidation, (b) increasing room-temperature ductility, especially of weldments, to make fabrication less difficult, and (c) developing alloys which retain more strength at higher temperatures for longer times than unalloyed molybdenum and which still have satisfactory ductility.

The authors of this paper have undoubtedly begun the most comprehensive effort to date on the last problem. Since the paper does not include the high temperature creep and creep-rupture properties of the alloys, the results must be considered as preliminary. It is to be hoped that the authors will soon publish information on the high temperature properties.

It would be interesting to have comparable data on similar alloys prepared by arc casting. In those few cases where enough data is available to make a comparison, the effects of alloys are quite similar. Yet it is known that the properties of arc-cast molybdenum are more adversely affected by oxygen than those of powder metallurgy molybdenum.

Only a few minor points of comment can be made on the paper itself. The specimens were tested in a wrought condition after being finish-rolled at identical temperatures. Rolling specimens of different composition at the same temperature may produce, in effect, varying amounts of cold work and this may affect the properties. This difficulty could hardly be avoided, but it should be borne in mind when evaluating the results. The use of intended rather than actual compositions in the text and figures is somewhat confusing. Also, it would add to the value of the data if oxygen and possibly nitrogen contents of all the alloys, after rolling, were given. These are known to affect the properties of pure molybdenum very greatly when present in extremely small quantities and they must have some effect on the alloys. They could possibly explain some of the erratic

bend-test results. Data on bend-test strain rate would also be desirable.

On the whole, the paper is certainly a major contribution to the metallurgy of molybdenum. An excellent job has been done of summarizing and organizing a large mass of detail into an understandable and comprehensive whole, and of discovering the underlying patterns.

Written Discussion: By J. D. Nisbet, Metallurgy Research Department, General Electric Co., Schenectady, N. Y.

It might be premature to list the order of hardening caused by alloying elements added to molybdenum, as the authors did in this paper, in view of the fact that several variables apparently could not be adequately controlled. In describing the hardening effects caused by adding one element to another, the following well-known factors must be recognized: (a) the effect of deoxidation, (b) the effect of strain hardening, and (c) the effect of precipitation.

The authors talk about the possible deoxidation effect caused by small additions of reactive elements, and they suggest that this might have some effect upon the properties. The deoxidizing effect of small quantities of reactive elements added to base elements of the molybdenum type might have a greater effect upon the properties of the base material by virtue of removing oxygen than the effect associated with the particular alloying ingredient added. Lacy and Gensamer showed that ferrite could be softened by adding small quantities of chromium. An interpretation of this effect was that ferrite was softened more by removing residual oxygen than it was hardened by adding chromium in solution. Certainly the principle is applicable here and it is unfortunate that this effect could not be isolated.

The recrystallization temperature of pure molybdenum is about 1100 °C and some unpublished research indicates that molybdenum-base alloys of the type studied might have recrystallization temperatures ranging up to 1500 °C. Therefore, when the alloys studied by the authors of this paper were finish-rolled at a temperature of 1250 °C and lower, they would be cold-worked and by different amounts because of differences in recrystallization temperatures from one alloy to another. Subsequently, the annealing temperature of 1100 °C, according to the photomicrographs shown, did not cause recrystallization. Therefore, it is reasonable to expect that the alloys studied were cold-worked or strain-hardened different amounts, and it is suggested that the strain hardening effect might well have been more important than the so-called "effect of alloying".

According to photomicrographs in the paper, several of the alloys studied contained second phases. One would expect, then, a large effect of heat treatment on the properties of these materials because of wide variations in the structure, and, here again, the conditions for testing the alloys would not be comparable in that their response to heat treatment would not be the same. Work in this field has indicated that molybdenum-base alloys of the type studied show precipitation hardening. Therefore, the two-phase alloys could develop a wide range of properties, depending upon how they are treated.

The three factors above, if not controlled, lead to erratic results and one would expect some difficulty in reproducing the properties reported here if slight changes were made in the melting, fabricating, or heat treat-

ing practices. I would like to know whether the authors agree that these three factors might have masked the so-called "order of hardening" listed for the alloying elements studied.

Authors' Reply

The authors thank Messrs. Semchyshen, Goodwin and Nisbet for their detailed discussion. All of these gentlemen have commented on the fact that the alloys were compared after a common fabrication history, in which different degrees of strain hardening presumably were involved. This is true. There really is no recognized way in which cold-worked materials can be produced with identical degrees of internal strain. Hence, we used the most simple method of comparison. In defense of this procedure, we would like to point out that molybdenum and its alloys are used in the fibered or cold-worked condition, which possesses a considerable advantage in strength over the recrystallized condition both at room temperature and at anticipated service temperatures (up to 1800 °F). We felt that the results would have greater utility if the condition of testing corresponded to commercial practice.

The correlation found between strengthening and solubility fitted the Lacy-Gensamer generalization found for ferrites; namely, that the greater the solubility for a substitutional solute the less is the lattice distortion and strengthening effect. This was an obvious indication from the data. In answer to Mr. Nisbet's point about the effect of different strain hardenability in the various alloys, we can refer to our companion paper, "Recrystallization of Wrought Hydrogen-Sintered Molybdenum and Its Alloys". In this paper it is shown that after complete recrystallization the same approximate order of strengthening is found; namely, cobalt, silicon, aluminum, iron, chromium and tungsten. Deoxidation effects need to be separated from solid-solution strengthening effects, as Mr. Nisbet points out. We have considered that after the initial softening, presumably caused by deoxidation, the solid-solution strengthening effect takes hold. It is this latter effect that we have considered in comparing relative hardening by the various solutes. Concerning possible precipitation of the second phases noted by Mr. Nisbet, all of these phases with the exception of the boride phase are believed to be oxides of the added metal. Therefore, little or no precipitation based on these phases is expected. All in all, we believe that our data substantiate for molybdenum alloys the Lacy-Gensamer type of correlation with solid solubility.

We are indebted to Mr. Semchyshen for his comments on the disposition of beryllium and thorium in molybdenum alloys as they are ordinarily produced by powder metallurgy or arc casting techniques. In further substantiation of the indication that the second phase in the Mo-Th alloys is probably an oxide of thorium, we have recently measured the Knoop hardness of this phase in the Mo-1 Th alloy. The phase is very hard, above 1000 Knoop. Metallic thorium is very soft, below 100 Knoop; hence, the phase is probably an oxide.

The strain rate used in the bend test was not controlled for most of the specimens tested. A hand arbor press supplied the force to bend the specimens. For a few alloys the strain rate was controlled at 0.5 inch per minute, using a testing machine. This made a notable improvement in the consistency of the bend-test results.

RECRYSTALLIZATION OF WROUGHT HYDROGEN-SINTERED MOLYBDENUM AND ITS ALLOYS

BY M. H. LACHANCE, W. L. BRUCKART, C. M. CRAIGHEAD
AND R. I. JAFFEE

Abstract

The recrystallization characteristics of hydrogen-sintered molybdenum prepared from four commercial powders are compared. Using one of these powder types as a base material, the effects of twelve alloying elements on the recrystallization characteristics were investigated. The smallest recrystallized grain sizes were observed in alloys containing boron, carbon, cobalt, and silicon. As might be expected, the change in mechanical properties most definitely associated with recrystallization was the loss of hardness and of strength. The tensile ductility of unalloyed molybdenum was generally higher in the recrystallized than in the wrought condition. Addition of elements with strong affinities for oxygen resulted in alloys having higher ductilities when recrystallized than were obtained with recrystallized unalloyed molybdenum.

The annealing temperature-recrystallization characteristics of the various alloys were evaluated. In general, those alloy additions with the highest solubility most effectively retarded recrystallization. A notable exception was the Mo-0.1 Si alloy. The solubility of silicon in molybdenum is very low, but this alloying addition effectively retarded recrystallization. Nickel and cobalt additions were observed to accelerate recrystallization.

INTRODUCTION AND SCOPE

THE RECRYSTALLIZATION of strain-hardened molybdenum alloys is accompanied by a decrease in both elevated- and room-temperature strengths. Because of the importance of maintaining the strength of molybdenum at a high level for its use as a high temperature material, an investigation was conducted to determine the alloying elements which would increase the thermal requirements for recrystallization most effectively.

The effect of addition elements on the recrystallization of alloys is related to their solid solubility in the base metal, to the manner in

A paper presented before the Eighth Western Metal Congress of the Society, held in Los Angeles, March 23 to 27, 1953. Of the authors, M. H. LaChance and W. L. Bruckart are principal metallurgists, C. M. Craighead is assistant supervisor, and R. I. Jaffee is supervisor, Nonferrous Physical Metallurgy Division, Battelle Memorial Institute, Columbus, Ohio. Manuscript received July 21, 1952.

which nucleation is affected by secondary or inclusion phases, and to the influence of such elements on strain hardenability.

The effect of the individual addition elements on strain hardening was not known; therefore, for purposes of evaluation, all the alloys were given the same fabrication treatment prior to final annealing.

Unalloyed hydrogen-sintered molybdenum (fabricated from powders from four commercial sources) was investigated. Using one of these powder grades as the alloy base, the effects of twelve binary additions were investigated at the following addition levels:

Alloying Element	Addition Levels, Weight %
Aluminum*	0.1, 0.5, and 1.0
Boron	0.1, 0.5, and 1.0
Beryllium	0.1
Carbon*	0.05, 0.2 and 0.4
Cobalt*	0.1 and 0.25
Chromium*	0.5 and 1.0
Iron*	0.1, 0.25, and 0.4
Manganese	0.5 and 1.0
Nickel	0.02 and 0.05
Silicon*	0.1 and 0.25
Thorium	0.25 and 0.75
Tungsten	10.0 and 20.0

*Elements added as master-alloy powders are indicated by asterisks.

A specimen of each composition was fabricated to sheet and evaluated as indicated by asterisks in the following tabulation:

Data Obtained	As-Rolled† Condition	Final Annealing Temperature‡				
		1000 °C (1830 °F)	1100 °C (2010 °F)	1200 °C (2190 °F)	1300 °C (2370 °F)	1400 °C (2550 °F)
Metallographic	*	*	*	*	*	*
Vickers hardness	*	*	*	*	*	*
Tensile test	*	*	*	*	*	*

†Rolled to 0.040-inch sheet, 60% reduction at 1000 °C (1830 °F).

‡Annealed in hydrogen for 30 minutes.

EXPERIMENTAL METHODS

Materials

The four types of molybdenum powder used in this study are referred to as Types A, B, C, and D, rather than by trade names. All were of commercial purity. Results of chemical analyses are given in Table I.

The powders were finer than 325 mesh, with the following particle-size distribution:

Type of Molybdenum Powder	Particle-Size Range, Microns	Greatest Number of Particles Diameter, Microns	% of Total
A	2-10	3	30
B	1-12	2	19
C	1-8	1	27*
D	1-14	2	25†

*52% at 1 to 2 microns.

†54% at 1 to 2 microns.

When alloys made with elemental additions failed to fabricate, the addition of alloying elements in the form of master-alloy powders

Table I
Results of Chemical Analysis of Molybdenum Produced From Powder Obtained
From Various Sources
 (Specimens Were Taken From Rolled and Annealed Strip)

Type of Molybdenum Powder	Impurity Elements, %						
	H ^a	N	O ^b	C ^c	S ^d	P ^e	Ni ^f
A	0.0002	0.007 ^g	0.009	0.009	0.005	0.005	<0.01
B	0.00019	0.0007 ^d	0.0025	0.01	0.005	<0.005	n.d.
C	0.0004	0.004 ^e	0.009	0.01	0.006	<0.01	n.d.
D	0.00023	0.0014 ^d	0.005	0.01	0.005	<0.005	<0.01

Type of Molybdenum Powder	Impurity Elements, %						
	Si ^g	Mn ^h	Fe ⁱ	Cr ^j	Al ^k	Cu ^l	Th ^m
A	0.01	<0.001	<0.001	<0.001	<0.001	n.d.
B	<0.01	<0.005	<0.005	<0.001	<0.005	<0.03	n.d.
C	0.05	<0.001	<0.01	<0.01	<0.001	<0.001	n.d.
D	<0.01	<0.005	<0.01	<0.001	<0.005	<0.01	n.d.

^aVacuum-fusion analysis; precision $\pm 0.0003\%$. ^bVacuum-fusion analysis; precision $\pm 0.002\%$. ^cVacuum-fusion analysis; precision $\pm 0.004\%$. ^dVacuum-fusion analysis; precision $\pm 0.0004\%$. ^eSpectrographic analysis. ^fWet analysis. ^gCombustion.

proved to be advantageous. Binary master alloys were made with compositions chosen so as to form either intermetallic compounds or alloys with minimum melting points. Intended and actual compositions of the six master alloys used are as follows:

Master Alloy	Intended Composition, %	Actual Composition, %	Iron-Impurity Pickup,* %
Mo - Al [†]	36 Al	55.1	0.1
Mo - C [‡] (Mo ₂ C)	5.9 C	6.68	0.1
Mo - Co [†]	63 Co	40.9	0.21
Mo - Cr [†]	75 Cr	74.1	0.14
Mo - Fe [†]	65 Fe	61.8
Mo - Si [§] (MoSi ₂)	36.9 Si	30.0

*From grinding process, after magnet treatment.

[†]Vacuum arc-melted from presintered mixtures.

[‡]Fused in carbon crucible under argon.

[§]Ball-milled from fused ingots made by arc melting under argon.

In this paper, intended compositions will be used to refer to all alloys except those containing carbon. For the Mo-C alloys, actual compositions will be given. Typical analyses are tabulated below. Except for the analyses of the Mo-C alloys, these data were obtained from another phase of the investigation (1).¹

Composition, %		Retention, %	Composition, %		Retention, %
Intended	Actual		Intended	Actual	
0.5 Al	0.43	86	0.5 Cr	0.41	82
1.0 Al	0.74	74	1.0 Cr	0.93	93
0.1 B	0.05	50	0.1 Fe	0.14	100
0.5 B	0.26	52	0.25 Fe	0.31	100
1.0 B	0.8	80	0.4 Fe	0.44	100
0.05 C*	0.04	80	0.5 Mn	0.24	48
0.2 C*	0.05	25	1.0 Mn	0.54	54
0.4 C*	0.1	25	0.1 Si	0.07	70
0.1 Co	0.09	90	0.25 Si	0.18	72
0.25 Co	0.23	92			

*An asterisk indicates that the alloy addition was made in the form of master-alloy powder.

¹The figures appearing in parentheses pertain to the references appended to this paper.

It will be noted that carbon retention in two of the alloys was only 25%. This probably resulted from the decarburizing action of small amounts of moisture in the hydrogen sintering atmosphere. Numerous oxide inclusions were observed in the microstructures of the Mo-Al alloys. Detailed chemical analyses confirmed that an insoluble constituent was present, as shown by the following results:

Intended	Composition, %		
	Soluble	Actual Insoluble	Total
0.25 Al	0.07	0.14	0.21
0.5 Al	0.18	0.25	0.43
1.0 Al	0.64	0.10	0.74

A similar type of analysis for the Mo-0.25 Si alloy probably would show the presence of insoluble silica, since an inclusion phase was visible in the microstructure. No analyses were conducted for the alloys with nickel, thorium, or tungsten, but the retention of these elements would be expected to be high.

Preparation of Specimens

The steps followed in preparing the test specimens are shown graphically in Fig. 1. After compacting and presintering, the bars were sintered by resistance heating in a hydrogen atmosphere. Normally, a surface temperature of 2040 °C (3705 °F) was maintained for 1 hour. This is about 2200 °C (3990 °F) true temperature. Because of the lower solidus temperatures of the Mo-B and Mo-C alloys, they were sintered at a surface temperature of 1800 °C (3270 °F). Volume and weight measurements were made before and after sintering. When shrinkage and sintered density were lower than normal, the bar was resintered. The alloys, in general, had volume shrinkages ranging from 28 to 44%, with densities of 91 to 99% of theoretical.

The sintered bars were reduced to 50% of their original thickness by hot rolling. Scale was removed then by immersion in a nitrate-nitrite bath operated at 425 °C (795 °F). Following a recrystallizing anneal, the bars were finish-rolled to a thickness of 0.04 inch. These materials furnished the stock for final annealing at the following temperatures: 1000, 1100, 1200, 1300 and 1400 °C (1830, 2010, 2190, 2370 and 2550 °F). The annealing time was 30 minutes at temperature.

Evaluation

Preparation for Metallographic Examination—Longitudinal and transverse sections were examined metallographically. A Forstmann cloth was used for polishing, as follows:

Abrasive	First Polish	Final Polish
	Linde B—chromic acid slurry	Linde B
Pressure	Heavy	Light
Etchant	—	Murakami's Reagent

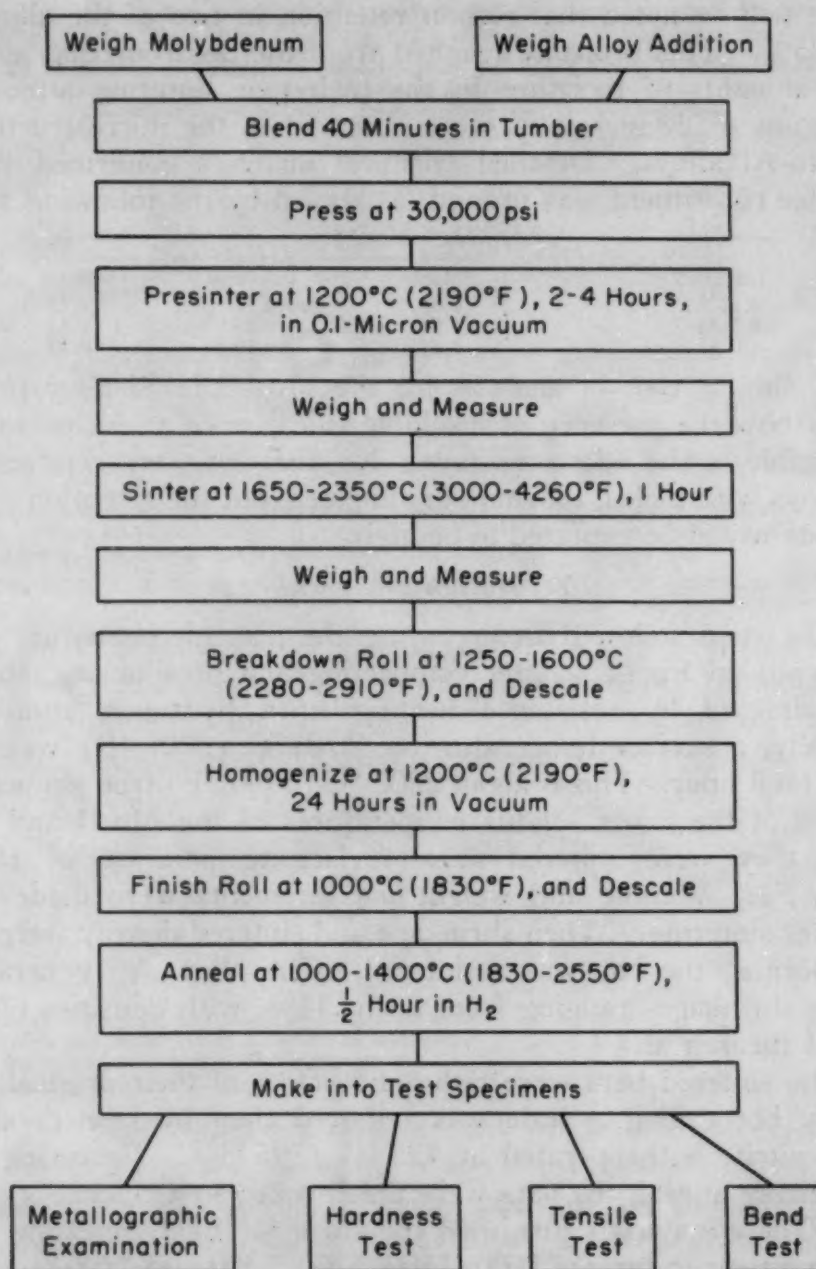


Fig. 1—Diagram of Steps Followed in Producing Experimental Molybdenum and Molybdenum Binary Alloys.

Mechanical-Property Tests

Vickers Hardness—Five Vickers hardness impressions (10-kg. load) were made on longitudinal sections of the rolled strip. The data are reported as average hardnesses.

Tensile Properties—The tensile properties were determined on 0.04-inch thick sheet specimens having 1.0 by 0.25-inch gage sections. SR-4 gages were used for strain measurements.

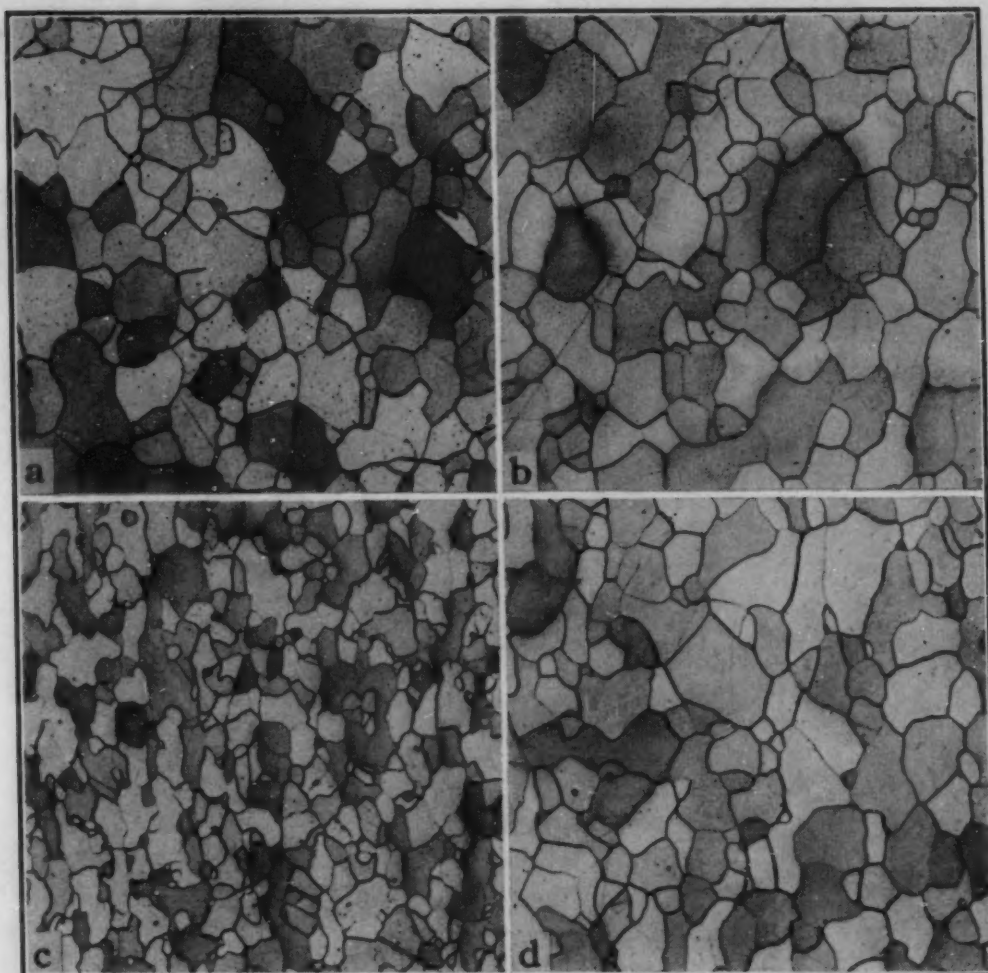


Fig. 2—Grain Size of Molybdenum Fabricated From Various Commercial Powders. Pretreatment: Rolled from 0.2 to 0.1 inch at 1250 °C, annealed at 1200 °C (2190 °F) for 24 hours and finish-rolled to 0.04 inch at 1000 °C (1830 °F). Annealing Time: ½ hour at 1400 °C (2550 °F). Average grain diameter (a) Type A, 0.045 mm.; (b) Type B, 0.045 mm.; (c) Type C, 0.025 mm.; (d) Type D, 0.040 mm. All $\times 100$. Etch: Murakami's Reagent.

Unalloyed Molybdenum

Grain Size—The recrystallized grain sizes of the four types of molybdenum studied were determined by the Jefferies' planimetric method (2) on specimens annealed for 30 minutes at 1400 °C (2550 °F). This anneal produced complete recrystallization with little or no visible grain growth. Photomicrographs upon which the grain counts were conducted are shown in Fig. 2.

The results of the grain size determinations are as follows:

Type of Molybdenum Powder Used	Number of Grains per Square mm.	Average Grain Diameter, mm.
A	550	0.045
B	488	0.045
C	1796	0.025
D	634	0.040

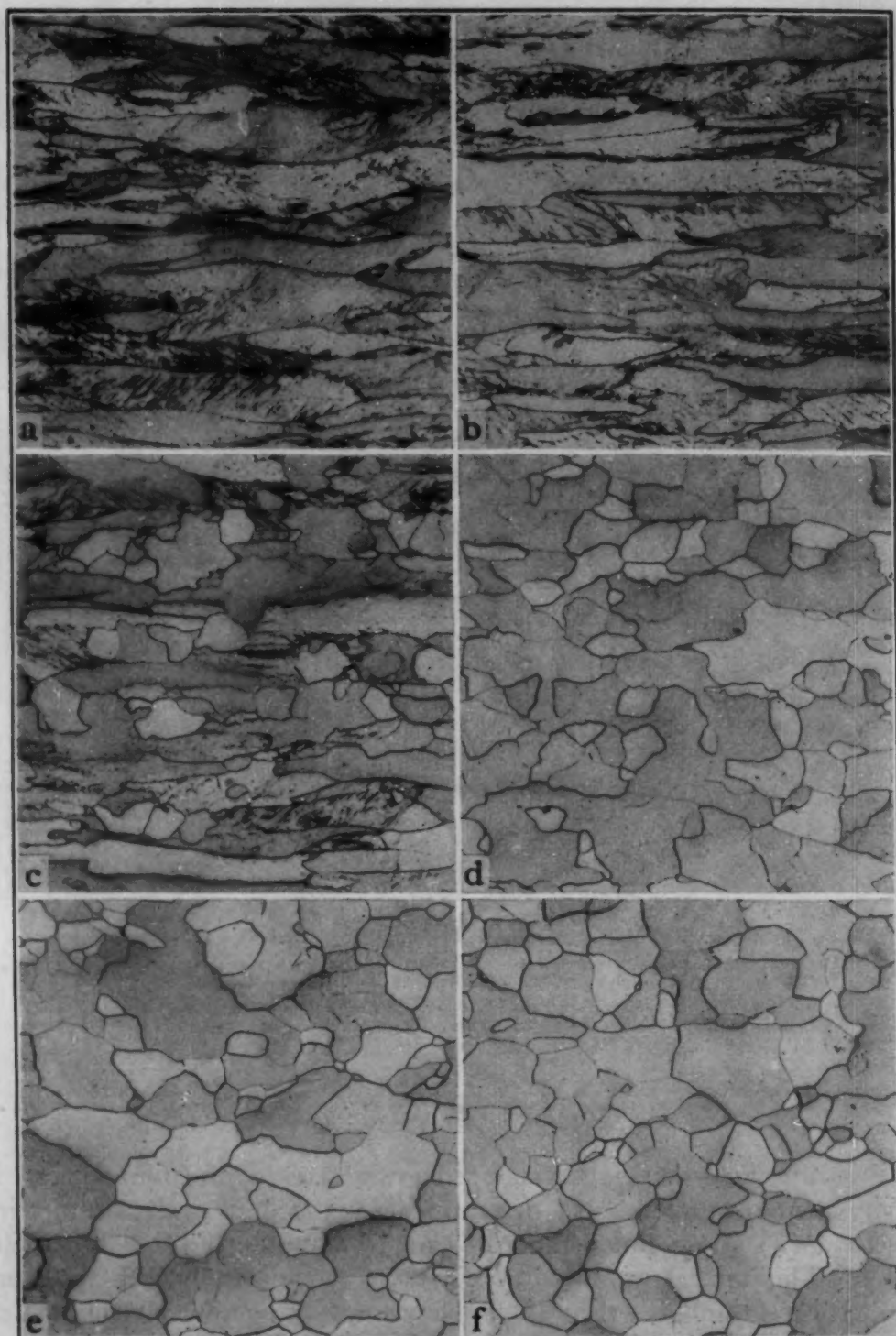


Fig. 3—Effect of Annealing Temperature on Microstructure of Hydrogen-Sintered Molybdenum (Type A). (a) No anneal; (b) 1000 °C; (c) 1100 °C; (d) 1200 °C; (e) 1300 °C; (f) 1400 °C. Annealing time: $\frac{1}{2}$ hour; Etch: Murakami's Reagent. $\times 100$.

Chemical analyses (Table I) showed that Type C molybdenum contained approximately five times as much silicon as did the other three grades. Since grain refinement was noted when silicon was

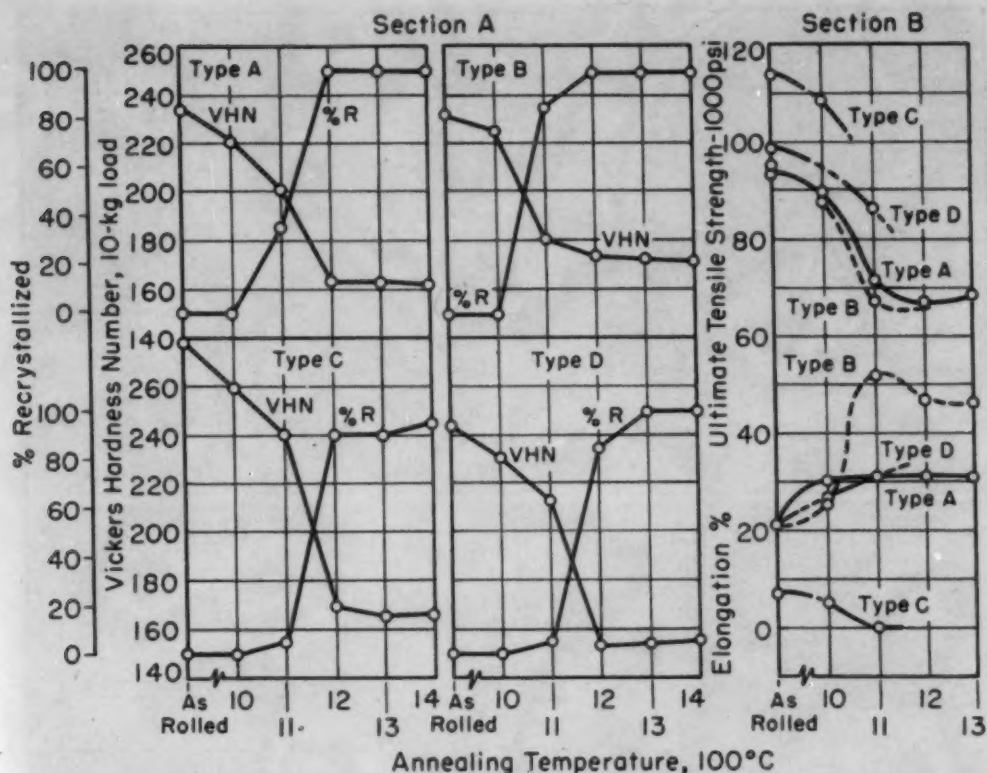


Fig. 4—Effect of Annealing on Recrystallization and Mechanical Properties of Unalloyed Molybdenum (Hydrogen-Sintered From Powders Obtained From Four Commercial Producers).

alloyed with Type A molybdenum, the very fine grain size of the Type C grade is attributed to its silicon content.

Recrystallization Characteristics—A series of micrographs of Type A molybdenum (alloy base used for all binary alloys) is shown in Fig. 3. Annealing for 30 minutes at 1000 °C (1830 °F) did not initiate recrystallization. Recrystallized grains are visible in the specimen annealed at 1100 °C (2010 °F). The structures resulting from annealing at 1200, 1300 and 1400 °C (2190, 2370 and 2550 °F) are recrystallized completely but show little or no grain growth with increased annealing temperature.

Data showing the degree to which the four types of molybdenum recrystallized (when annealed for 30 minutes at various temperatures) are plotted in Fig. 4, Section A. Here it is seen that the recrystallization versus annealing-temperature curves for Types A and B are very similar. However, Types C and D were sluggish in their response to annealing.

The differences among the four grades of unalloyed metal were not so pronounced as were the variations in recrystallization behavior when effective alloy additions were made to Type A molybdenum.

The reluctance of Type C to recrystallize fully (even at 1400 °C), as well as its very fine grain size, is ascribed to its higher silicon

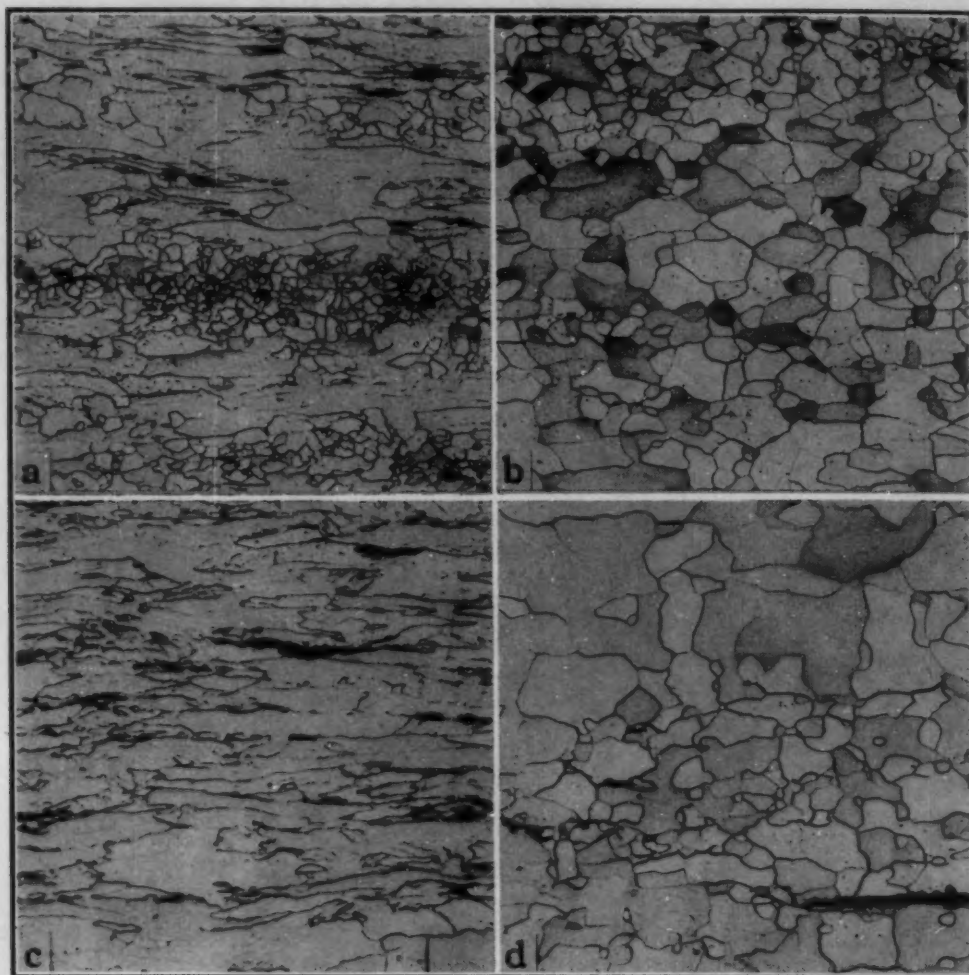


Fig. 5—Photomicrographs of Typical Solid Solution-Type Alloys of Molybdenum Showing Two Stages of Recrystallization. (a) Mo-0.25 Co, 1100 °C; (b) Mo-0.25 Co, 1400 °C; (c) Mo-20.0 W, 1200 °C; (d) Mo-20.0 W, 1400 °C. Annealing time: ½ hour; Etch: Murakami's Reagent. $\times 100$.

content (0.05%, as compared with 0.01% for the other grades).

Initial recrystallization of all four types of molybdenum investigated occurred between 1000 and 1100 °C (1830 and 2010 °F). Except for the retention of fibering at the surface of Type C, complete recrystallization of all four grades was observed after annealing for 30 minutes at 1300 °C (2370 °F). No grain growth was observed after annealing at 1400 °C (2550 °F).

The effects of recrystallization on the tensile properties of the four types of molybdenum are shown in Fig. 4, Section B. Strength curves for Types A and B, like the recrystallization curves for these two materials, are almost coincident. However, Type B, when completely recrystallized, had the highest ductility. In the fibered condition, the strengths of Types C and D molybdenum were higher than those of Types A and B. Type C molybdenum, with the highest strength and lowest ductility, was so brittle in the recrystallized con-

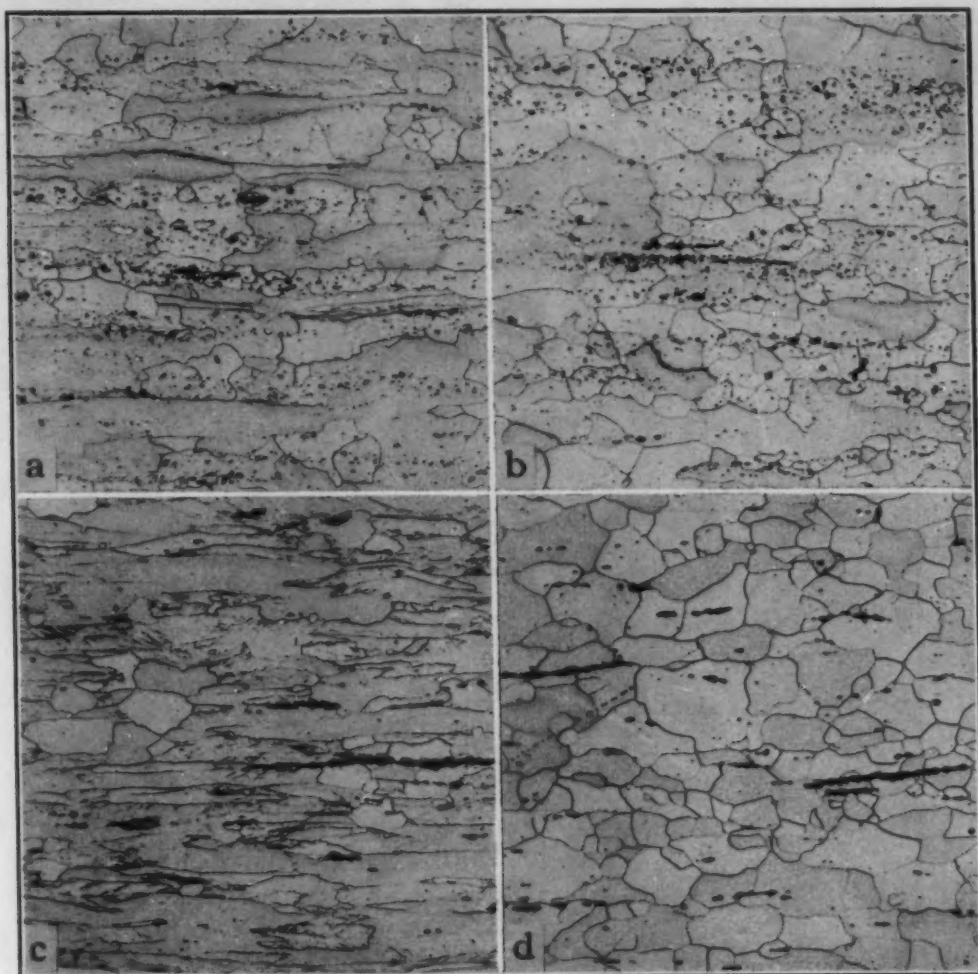


Fig. 6—Photomicrographs of Typical Oxide-Containing Alloys of Molybdenum Showing Two Stages of Recrystallization. (a) Mo-0.5 Al, 1200 °C; (b) Mo-0.5 Al, 1300 °C; (c) Mo-0.75 Th, 1100 °C; (d) Mo-0.75 Th, 1200 °C. Annealing time: ½ hour; Etch: Murakami's Reagent. $\times 100$.

dition that tensile data could not be obtained.

Binary Alloys of Molybdenum

Microstructure—For purposes of discussion, the alloys may be divided into groups. The first group is composed of binary alloys of the solid solution type, namely Mo-Co, Mo-Cr, Mo-Fe, Mo-Ni and Mo-W. Typical microstructures representing solid solution alloys are those of Mo-0.25 Co and Mo-20 W shown in Fig. 5. Each alloy is shown at an intermediate stage of recrystallization and at a stage where recrystallization essentially is completed.

The second group of binary alloys is composed of Mo-Al, Mo-Be, Mo-Mn, Mo-Si and Mo-Th, which contained nonmetallic inclusions presumed to be oxides. Photomicrographs of Mo-0.5 Al and Mo-0.75 Th, representing the oxide-containing alloys, are shown in Fig. 6.

Alloys of molybdenum and carbon contained a carbide phase

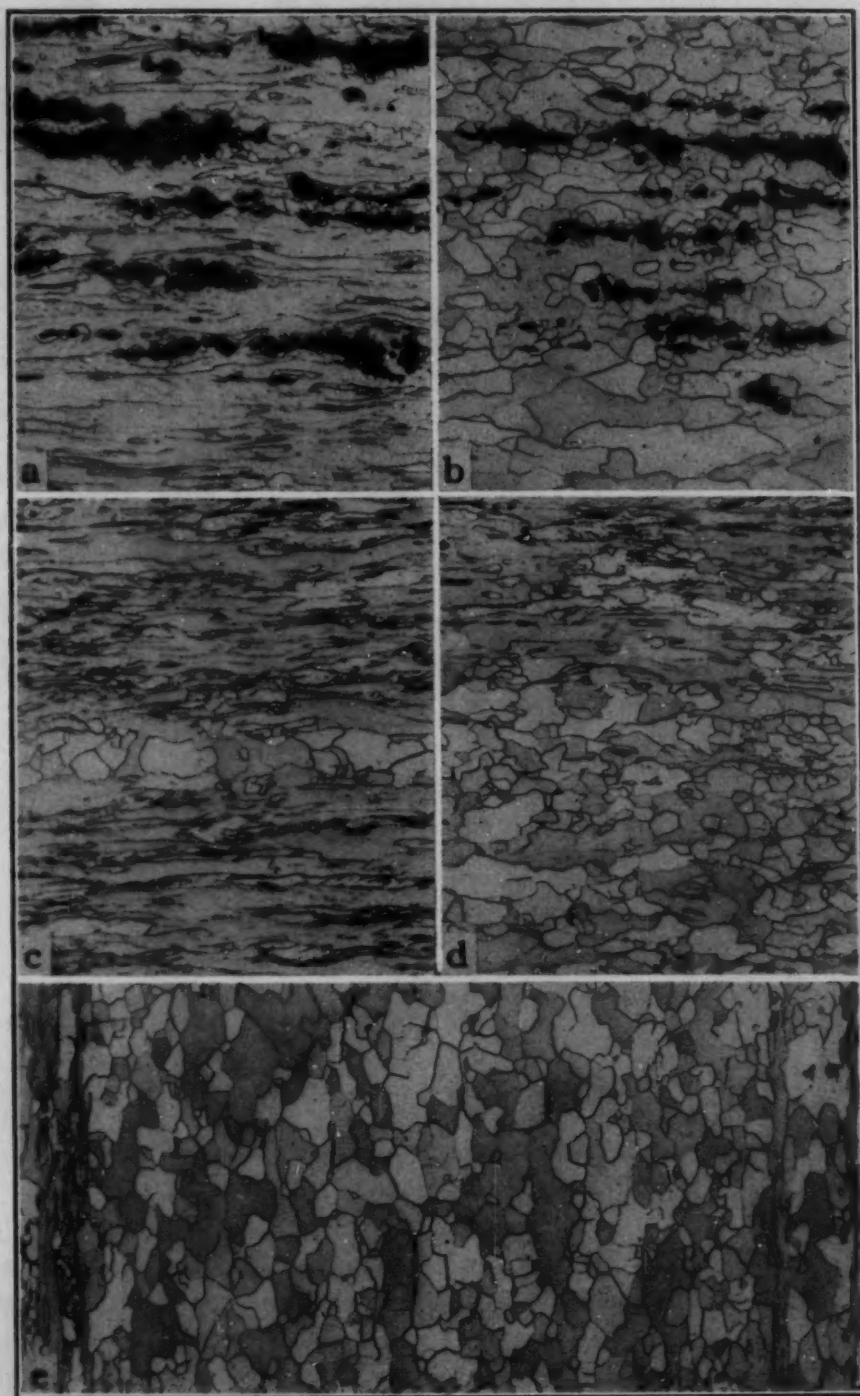


Fig. 7—Photomicrographs of Mo-B and Mo-Si Alloys Showing, Respectively, Two and Three Stages of Recrystallization. (a) Mo-0.5 B, 1100 °C; (b) Mo-0.5 B, 1300 °C; (c) Mo-0.1 Si, 1200 °C; (d) Mo-0.1 Si, 1300 °C; (e) Mo-0.1 Si, 1400 °C. Annealing time: $\frac{1}{2}$ hour; Etch: Murakami's Reagent. $\times 100$.

(Mo_2C), and those of molybdenum and boron contained a boride phase. The microstructure of the Mo-0.5 B alloy at two stages of recrystallization is shown in Fig. 7. In these photomicrographs, the dark areas are voids formerly occupied by the boride phase. Etching,

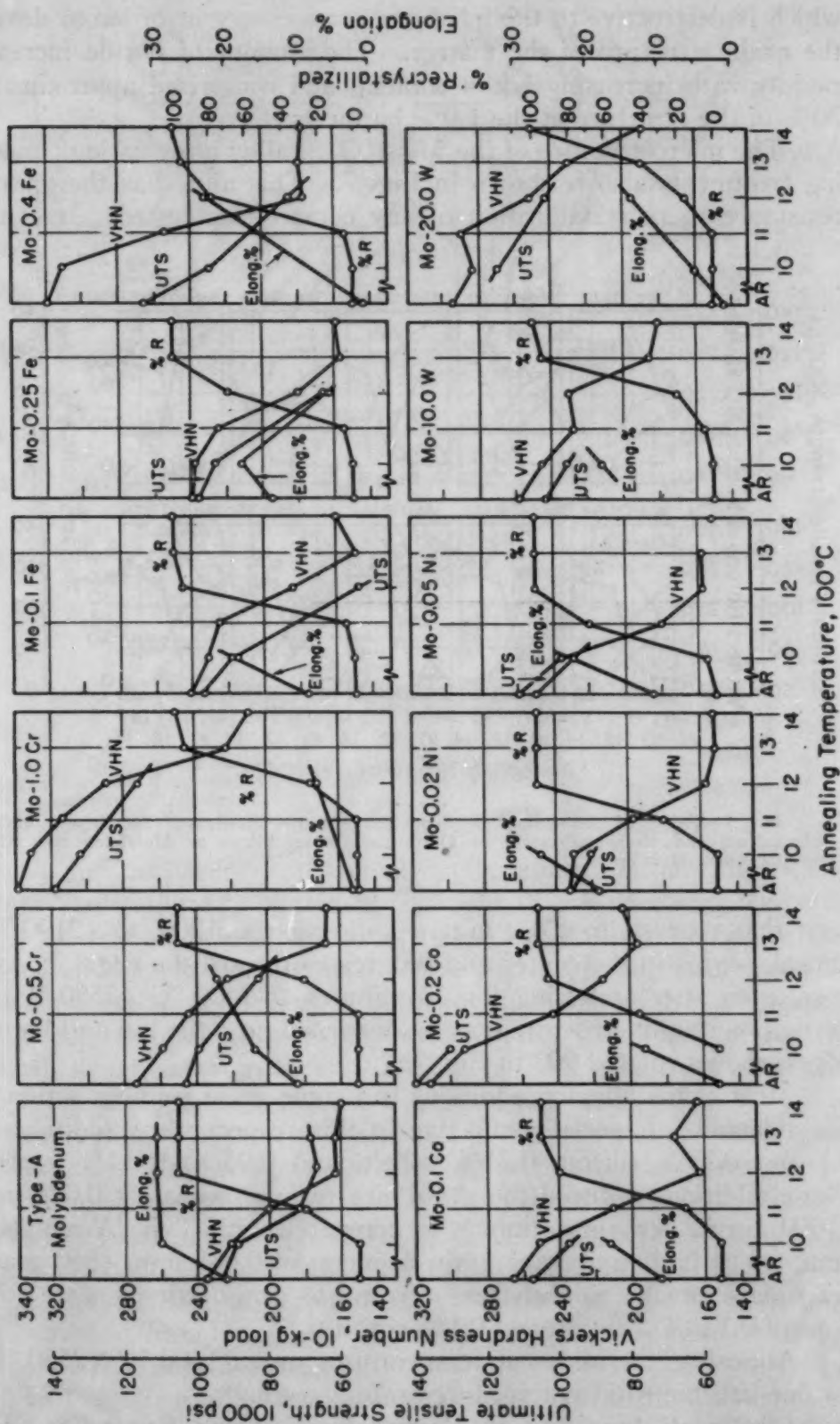


Fig. 8—Effect of Annealing on Room-Temperature Hardness, Tensile Strength, Elongation, and Recrystallization of Solid Solution-Type Alloys of Molybdenum. Annealing time, 30 minutes.

which is destructive to this phase, was necessary in order to develop the grain structure of the matrix. The amount of boride increased rapidly with increasing boron content, and comprised approximately 30% of the structure at the 1.0% boron level.

The microstructure of the Mo-0.1 Si alloy after various annealing treatments also is shown in Fig. 7. This alloy has the greatest resistance to recrystallization of any composition tested. It can be

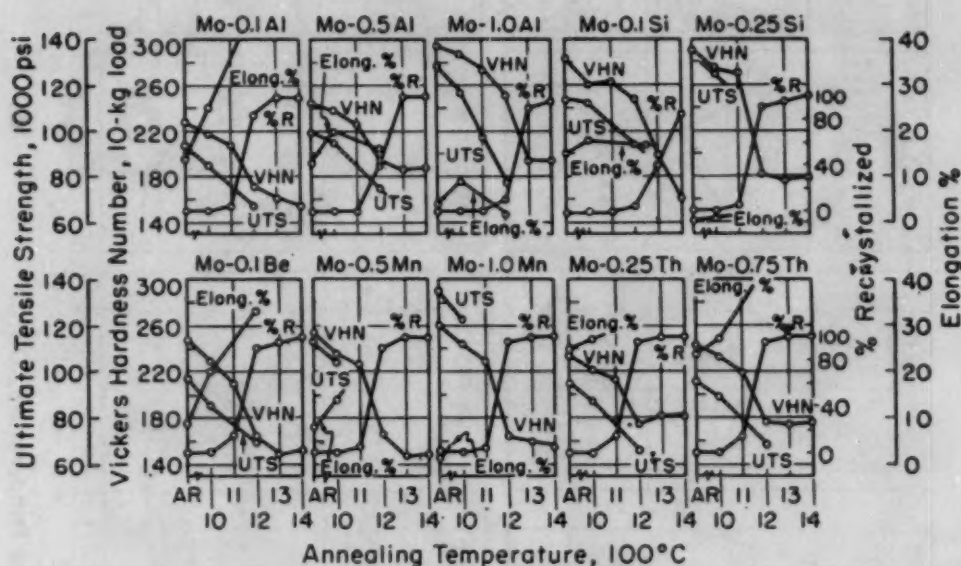


Fig. 9—Effect of Annealing on Room-Temperature Hardness, Tensile Strength, Elongation, and Recrystallization of Oxide-Containing Alloys of Molybdenum. Annealing time, 30 minutes.

seen that recrystallization, initiated during the 1200 °C (2190 °F) anneal, begins in the center and progresses toward the edges. However, even after annealing for 30 minutes at 1400 °C (2550 °F), a partially wrought structure may be discerned near the top and bottom edges, shown rotated 90° in Fig. 7e.

Most of the alloying additions had some grain refining action on molybdenum. Especially effective in this respect were additions of 0.1 and 0.25% silicon, 0.25% cobalt, and 0.05 and 0.1% carbon. These additions reduced the grain size to approximately 0.025 mm. (1600 grains per square mm.), as compared with Type A molybdenum, which had an average grain diameter of 0.045 mm. (550 grains per square mm.). Slightly less effective as grain refiners were additions of 0.1 to 1% boron and 0.1% cobalt.

Annealing the alloys at temperatures up to 1400 °C (2550 °F) for one-half hour did not produce grain growth.

Effects of Annealing on Recrystallization and Properties—The effects of annealing the various alloys at temperatures ranging from 1000 to 1400 °C (1830 to 2550 °F) are shown in Figs. 8, 9 and 10.

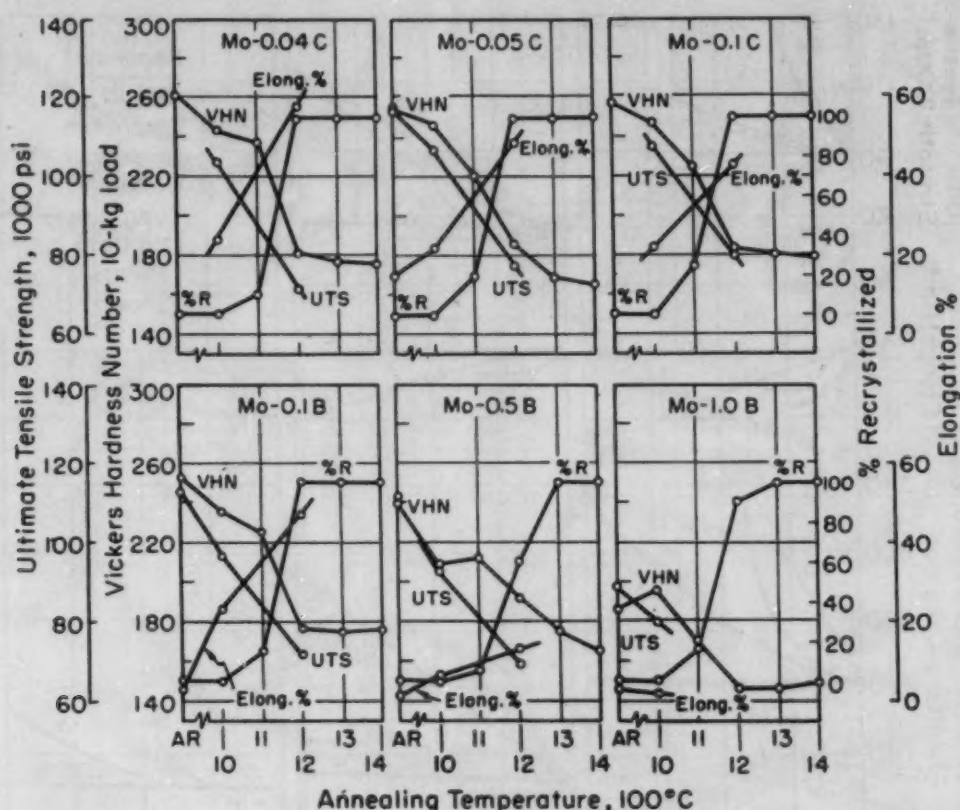


Fig. 10—Effect of Annealing on Room-Temperature Hardness, Tensile Strength, Elongation, and Recrystallization of Molybdenum Alloys Containing a Second Phase. Annealing time, 30 minutes.

The changes in hardness, tensile strength, elongation, and the extent of recrystallization are plotted as functions of the annealing temperature. It will be noted that, in all cases, hardness and strength decreased and elongation increased before any recrystallization could be detected metallographically. Following their initial drop, hardness and strength decreased markedly with increasing amounts of recrystallized structure. Once recrystallization was essentially complete (90% or more) there was little change in hardness.

Figs. 11 and 12 show the relationship between alloy concentration and mechanical properties after three different annealing treatments: (a) as annealed at 1000 °C (1830 °F), where no recrystallization occurs, (b) as annealed at 1200 °C (2190 °F), where the structures are partially recrystallized, and (c) as annealed at 1400 °C (2550 °F), where recrystallization is complete. Alloys of the solid solution type are shown in Fig. 11 and those containing a second phase, or oxide inclusions, are shown in Fig. 12.

In Fig. 11, it will be observed that the general level of hardness increase of the alloys over unalloyed molybdenum decreased as recrystallization proceeded. Also, there was much less initial hardening effect of alloying in the completely recrystallized condition than in

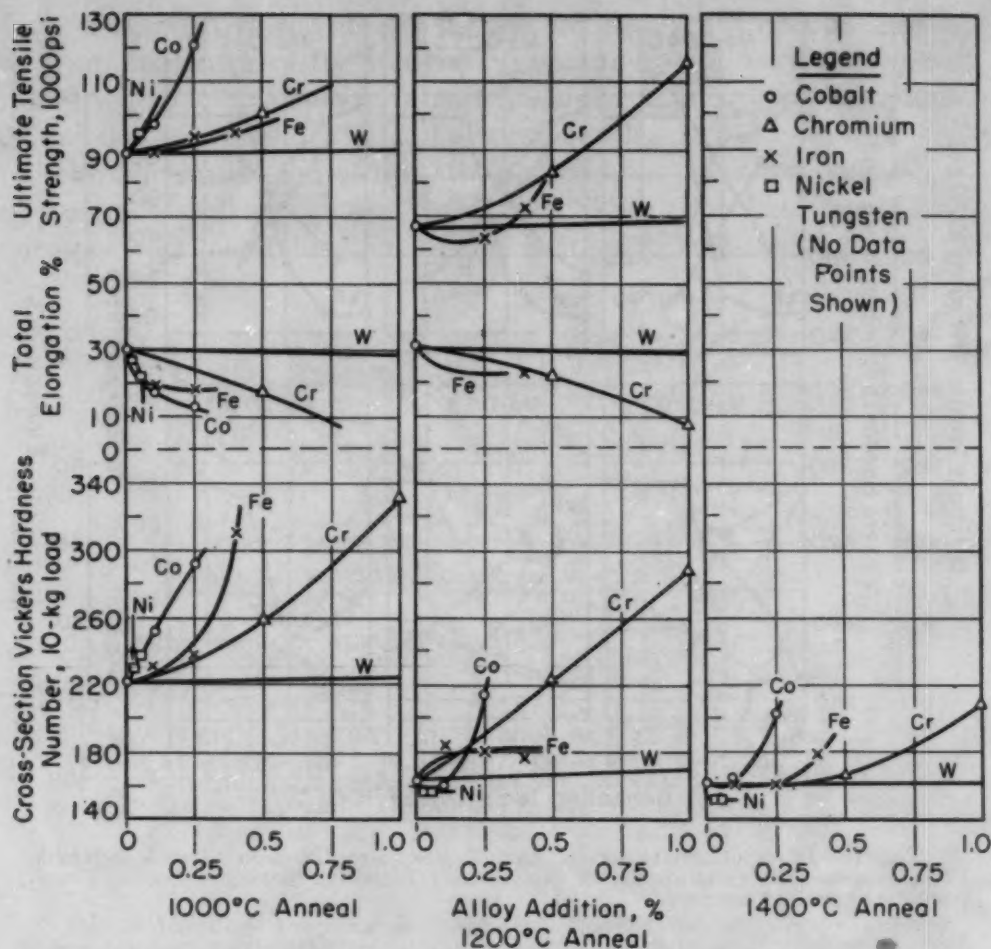


Fig. 11—Effect of Annealing on Room-Temperature Mechanical Properties of Solid Solution-Type Alloys of Molybdenum.

the fibered condition. The hardness-composition curves for alloys of cobalt, chromium, and tungsten occupy the same relative positions as do the strength-composition curves.

After annealing at 1000 °C (1830 °F) (fibered condition), cobalt and nickel were the most effective solid solution hardeners, followed by iron, chromium and tungsten. This is the order of increasing solubility in molybdenum. In the 1400 °C-annealed condition (fully recrystallized), the same order of hardnesses prevails except for the decreased hardness of the nickel alloys. The tensile data, although limited, correlate reasonably well with the hardness data. Elongation data for the alloys in the 1000 °C-annealed condition show that cobalt, nickel and iron, the most effective strengtheners, produce slightly less ductile alloys. Chromium and tungsten produced higher ductilities commensurate with their strengthening effects. This same relative order of ductility prevailed for the 1200 °C (2190 °F) condition, although no tensile data were obtained for the Mo-Co and Mo-Ni alloys.

For alloys containing second phases or oxide inclusions (Fig.

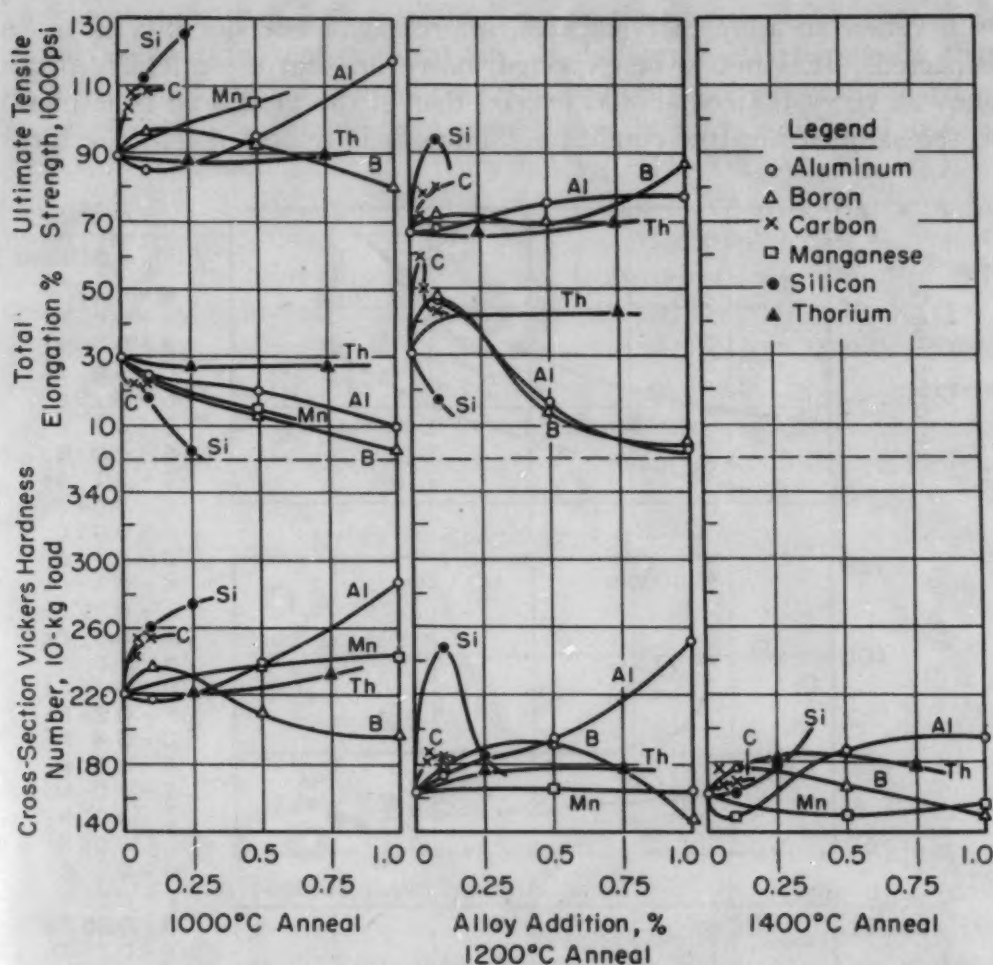


Fig. 12—Effect of Annealing on Room-Temperature Mechanical Properties of Molybdenum Alloys Which Contain a Secondary Phase or Oxide Inclusions.

12), the same general effects may be noted, i.e., the hardness-composition curves occupy the same relative positions as do the strength-composition curves. The most effective strengthener was silicon; it also produced the lowest ductilities. The hardness of the Mo-0.25 Si alloy as annealed and partially recrystallized appears to be quite low. Examination of Fig. 9, however, will show that this alloy was recrystallized more completely by the 1200 °C (2190 °F) anneal than was the 0.1% silicon alloy.

Several alloys (Fig. 12) had excellent tensile ductility in the 1200 °C-annealed condition. Elongation data for these alloys in both the wrought and recrystallized conditions are as follows:

Alloy Addition, %	Annealed at 1000 °C (1830 °F)		Annealed at 1200 °C (2190 °F)	
	% Recrystallized	Elongation, %	% Recrystallized	Elongation, %
None	0	30	100	31
0.1 Al	0	25	85	46
0.1 Be	0	20	90	33
0.75 Th	0	27	95	42
0.1 B	0	23	100	47
0.04 C	0	22	100	59
0.05 C	0	22	100	49
0.1 C	0	22	100	43

When an alloy recrystallizes, improved tensile ductility is to be expected. It is not to be expected, however, that the ductility of an alloy as recrystallized should exceed that of the unalloyed base metal in the same strain-free condition. Thus, it is indicated that the fore-

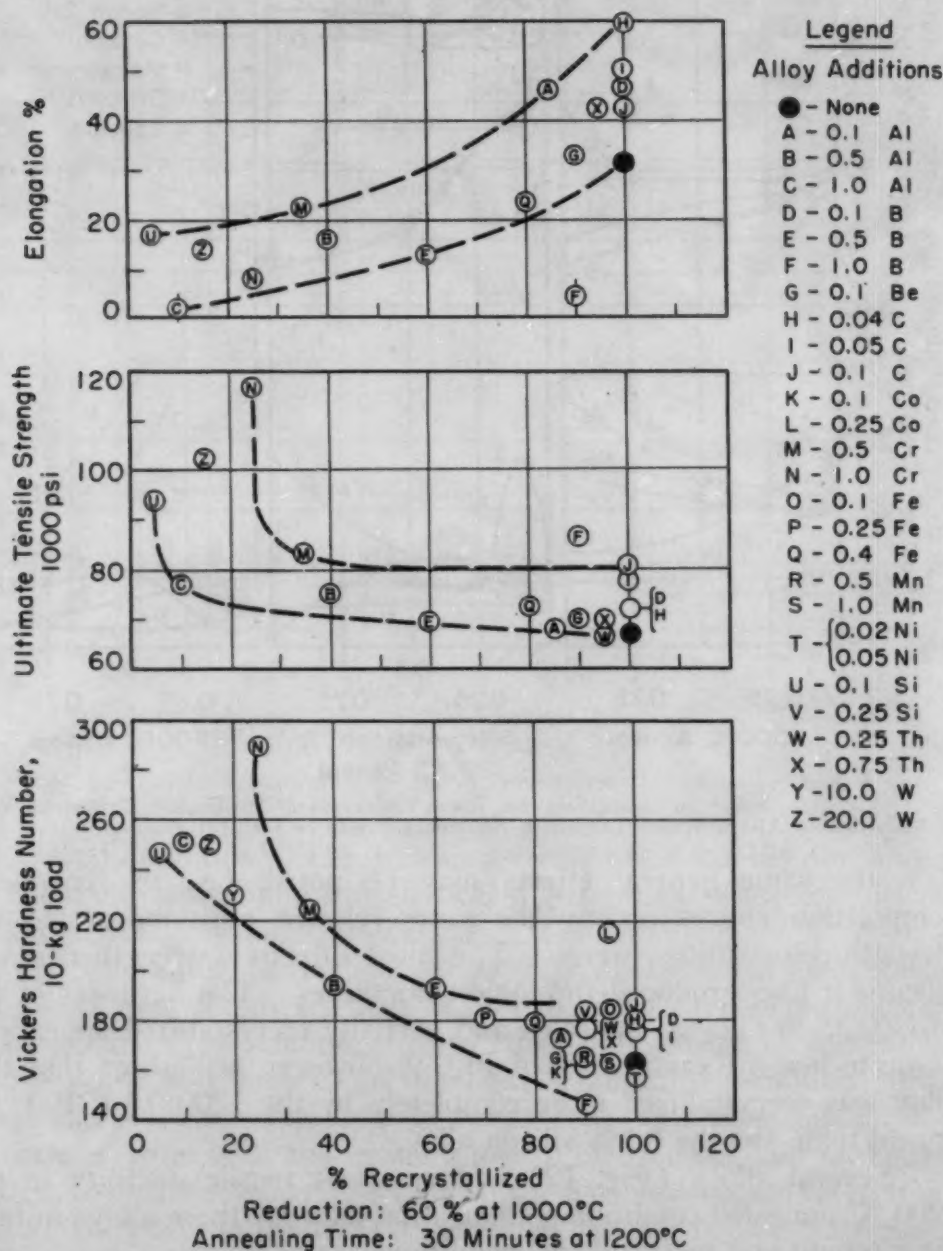


Fig. 13—Relationships Between Mechanical Properties and Per Cent Recrystallization of Binary Molybdenum Alloys.

going alloy additions react with certain impurities in the molybdenum, resulting in improved ductility.

In Fig. 13, data for the 1200 °C-annealed condition have been replotted in order to show the relationships between recrystallization

and mechanical properties, as well as to classify those compositions most resistant to recrystallization. This figure clearly shows that alloys in the initial stages of recrystallization were generally harder, stronger, and less ductile than were alloys in more advanced stages. The superior ductility of the recrystallized Mo-0.1 Al, Mo-0.1 B, Mo-0.1 Be, Mo-C, and Mo-0.75 Th alloys cited earlier can be observed readily.

Taking the alloys as they appear from left to right in Fig. 13, the following compositions were recrystallized least by the 1200 °C (2190 °F) anneal: Mo-0.1 Si, Mo-1.0 Al, Mo-20.0 W, Mo-10.0 W, Mo-1.0 Cr, Mo-0.5 Cr and Mo-0.5 Al. It is of interest to note that tungsten, chromium and aluminum, all of which effectively retarded recrystallization, have appreciable solubility in molybdenum.

SOLUBILITY LIMITS IN MOLYBDENUM AT 1095 °C (2000 °F)

Element	Solubility, %
Tungsten	100 (3)
Chromium	100 (3)
Iron	2.65 (4)
Aluminum	1.4 (4)
Cobalt	0.55 (4)
Nickel	0.5 (4)
Silicon	0.2 (4)

The retarding effect of tungsten, chromium and aluminum on recrystallization became more pronounced with increasing alloy concentration in a manner which is normal for solid solutions. The retarding effect of silicon, however, is difficult to explain, since it was greater at an intermediate, rather than at a higher, concentration. This was confirmed further by examining two additional silicon alloys, Mo-0.1 Si and Mo-0.20 Si (given 90% reduction at 1050 °C (1920 °F) and annealed at 1000, 1100, 1200, 1300 and 1400 °C). The recrystallization of Mo-0.1 Si was again definitely more sluggish than that of Mo-0.2 Si.

In another phase of the research program (1), nonmetallic inclusions observed with 0.25% silicon (0.18 actual) were absent from the microstructure when 0.1% silicon (0.07 actual) was added. The data indicated that a small amount of silicon in solid solution is extremely potent in retarding recrystallization; however, this retarding effect is reduced greatly with the appearance of the inclusion phase.

Alloys with the greatest tendency to recrystallize were those containing nickel and cobalt. There is no apparent explanation for this effect.

The presence of secondary or inclusion phases appeared to have no consistent effect on the recrystallization behavior of molybdenum alloys. As mentioned previously, the inclusion phase in the silicon alloys may have tended to accelerate recrystallization. Increasing

aluminum content, on the other hand, resulted in an abundance of inclusions and a retardation of recrystallization. Increasing the thorium content from 0.25 to 0.75% increased the quantity of the inclusion phase, but had no apparent effect on recrystallization. The presence of the Mo_2C and boride phases had no apparent effect on the threshold temperature of recrystallization.

CONCLUSIONS

1. Silicon, tungsten, chromium and aluminum are effective in retarding recrystallization when alloyed with molybdenum.
2. No growth of the recrystallized grains is apparent for annealing temperatures up to 1400°C (2550°F). This pertains to both unalloyed molybdenum and the binary alloys investigated.
3. Most of the binary additions investigated have a grain-refining effect. The greatest refinement is produced by additions of silicon, carbon, cobalt and boron.
4. Recrystallization generally decreased strength and hardness and increased ductility. Small additions of aluminum, beryllium, boron, carbon and thorium resulted in increased ductility.
5. The general hardness level, as well as the initial increase in hardness resulting from alloying, was greater in the fibered than in the recrystallized condition.
6. The presence of inclusion phases had no consistent effect on the recrystallization of the alloys.

ACKNOWLEDGMENTS

The authors express their appreciation to J. B. Johnson and the United States Air Force for permission to publish the results of work obtained at Battelle Memorial Institute under Contract No. AF-33(038)-12641. They also are indebted to Jack A. Taynor and Richard D. Mico, who performed much of the experimental work, and to R. D. Buchheit and George Wheeler for the preparation of the metallographic specimens.

References

1. W. L. Bruckart, M. H. LaChance, C. M. Craighead and R. I. Jaffee, "Summary Report on Investigation of Molybdenum and Molybdenum-Base Alloys Made by Powder-Metallurgy Techniques to Office of Air Research", June 30, 1951 (Contract No. AF-33(038)-12641).
2. "ASTM Standards", Nonferrous Metals Section, 1949, p. 1088.
3. METALS HANDBOOK, American Society for Metals, 1948.
4. J. T. Ham, "Arc-Cast Molybdenum-Base Alloys", First Annual Report on Project NR031-331, Climax Molybdenum Company of Michigan, April 1, 1950.

THE EFFECT OF TEMPERATURE ON THE ROLLING TEXTURE OF PLASTICALLY DEFORMED LOW CARBON STEEL STRIP

BY NORMAN P. GOSS

Abstract

Some of the factors which influence the texture of cold-rolled steel strip are well recognized and have been adequately studied. However, the effect of temperature on the deformation texture has been neglected. With the introduction of increased rolling speeds and increased reductions, the temperature of rolling may be an important factor.

A series of samples was rolled in a sequence of initial temperatures, ranging from 32 to 800 °F. All other variables such as number of passes and total reduction were kept the same throughout the entire series. X-ray diffraction patterns were taken by the "reflection" method with the X-ray beam transverse to the rolling direction. The intensity minima and maxima were measured with a microphotometer. The intensity measurements show that with decrease in the temperature of rolling, the maxima of a diffraction pattern increase in intensity while the minima decrease in intensity. With increase in the temperature of rolling, the reverse change takes place. At the higher temperature (700 °F) the original low temperature texture (001) [110] has been replaced by a new texture, (110) [001], in which the maxima and minima of the two textures have interchanged positions. At an intermediate temperature the texture simulates that of random orientation.

THE TEXTURE of low carbon strip steel as produced by cold rolling at ordinary temperatures has been adequately studied by X-ray methods and is fully described in the literature (1).¹ While some of the factors which influence the texture of cold-rolled sheet are well recognized, the effect of the temperature of deformation has been almost entirely neglected (2). However, with the introduction of the four-high rolling mill, the increased rolling speeds and reductions possible over that of the two-high mill, the temperature at which the rolling is performed may well be a very important factor.

¹The figures appearing in parentheses pertain to the references appended to this paper.

A paper presented before the Thirty-fourth Annual Convention of the Society, held in Philadelphia, October 18 to 24, 1952. The author, Norman P. Goss, is consultant, The Cold Metal Products Company, Youngstown, Ohio. Manuscript received February 13, 1952.

The experimental work of Andrade and Tsien (3) has shown that for body-centered metals the slip mechanism changes with rise in temperature, while Nadai (4) has pointed out that the slip mechanism is profoundly influenced by the temperature of deformation. Hanawalt (5) has shown that the preferred orientation texture of extruded magnesium alloys depends on the temperature of the extruded metal.

In a study of the rolling texture of a large number of samples rolled on a four-high mill taken directly from production, considerable variation in the degree of preferred orientation was observed. This variation was in many instances too large in magnitude to be satisfactorily explained by the factors to which such variations in texture are usually attributed. The total reduction and the number of passes as well as the roll diameter and the tension applied were practically the same for all the samples. Initially, in the operation of a cold rolling mill, the temperature of the sheet and rolls is quite low; however, as the rolling progresses the temperature of the strip and rolls rises, and, depending on the manner of cooling and the nature of the coolant, the temperature of the strip may attain rather high values. Temperatures as high as 500 °F (260 °C) have been reported in the literature. It was with this fact in mind that a series of low carbon steel strip samples was rolled in a sequence of temperatures.

EXPERIMENTAL PROCEDURE

Preparation of Samples. The material used for the samples was annealed hot strip with an initial thickness of 0.113 inch. The chemical composition was as follows:

C	0.10%	Mn	0.35%	Ni	0.09%
Si	0.005%	Cu	0.11%	S	0.033%
Mo	0.009%	P	0.009%	Cr	0.05%

All of the samples (approximate dimension 1 by 1¼ inches) were given seven successive passes with long dimension in rolling direction on a small laboratory mill with a total reduction of 72%. Previous to each pass the sample was heated or cooled to a specified temperature and held at that temperature for a period of 2 minutes. For the lower temperatures an ice bath and boiling water were used, while for the higher temperatures the samples were heated in an open furnace. These temperatures are recorded in Table I as the "initial temperature" of the sample. The temperature on leaving the rolls, designated as "exit temperature", was measured for samples 3, 4, 5, 6, 7 and 8. The "exit temperature" for samples 1 and 2 was estimated. The "mean temperature" of rolling is the mean of the "initial temperature" of the sample on entering the rolls, and the temperature of the sample on leaving the rolls, or "exit temperature".

Table I
Rolling Temperatures

Sample	Initial Temperature °F	Exit Temperature °F	Mean Temperature of Rolling °F
1	70	...	130
2	32	60	45
3	212	175	180
4	300	220	260
5	400	265	330
6	500	325	410
7	600	400	500
8	700	525	610
9	800	630	715

The "mean temperature" of rolling is recorded in column four of Table I.

Sample 1 is a control sample which was rolled at room temperature. No attempt was made to have this sample return to the temperature of the room between successive passes, and the passes were made in rapid succession.

X-Ray Diffraction Patterns. X-ray diffraction patterns were taken of all of the samples using the "reflection" method. This method possesses several advantages over the transmission method since it requires no special preparation other than a possible surface etch of the sample. The absorption of the X-rays by the sample definitely determines the thickness of the sample examined. In this method of obtaining a diffraction pattern, a well-defined X-ray beam is incident on the surface of the sample at a definitely determined angle, usually the Bragg angle for an important atomic plane. In the arrangement used, the plane of the incident and the reflected X-ray beam was normal to the rolling direction and the incident beam made an angle of 10 degrees with the surface of the sample. This arrangement is often known as the transverse direction and sometimes designated by the symbol T-10. The number 10 designates an angle of 10 degrees as the angle of incidence for $\text{MoK}\alpha$ radiation on the (110) planes of iron. This particular arrangement was chosen, as the diffraction pattern shows a higher degree of preferred orientation than in either of the so-called parallel (P) or normal (N) directions. It is often the most informative one for the study of preferred orientation. The most significant of the X-ray diffraction patterns are shown in Fig. 1 and are presented in the sequence of the rolling temperatures as listed in Table I.

Microphotometer Data. An examination of the diffraction patterns obtained from the samples rolled at various initial temperatures shows quite clearly that the maxima and minima of the diffraction rings change in intensity and position as the temperature of rolling is increased. In order that these changes in intensity with temperature of rolling may be made more evident, as well as comparisons

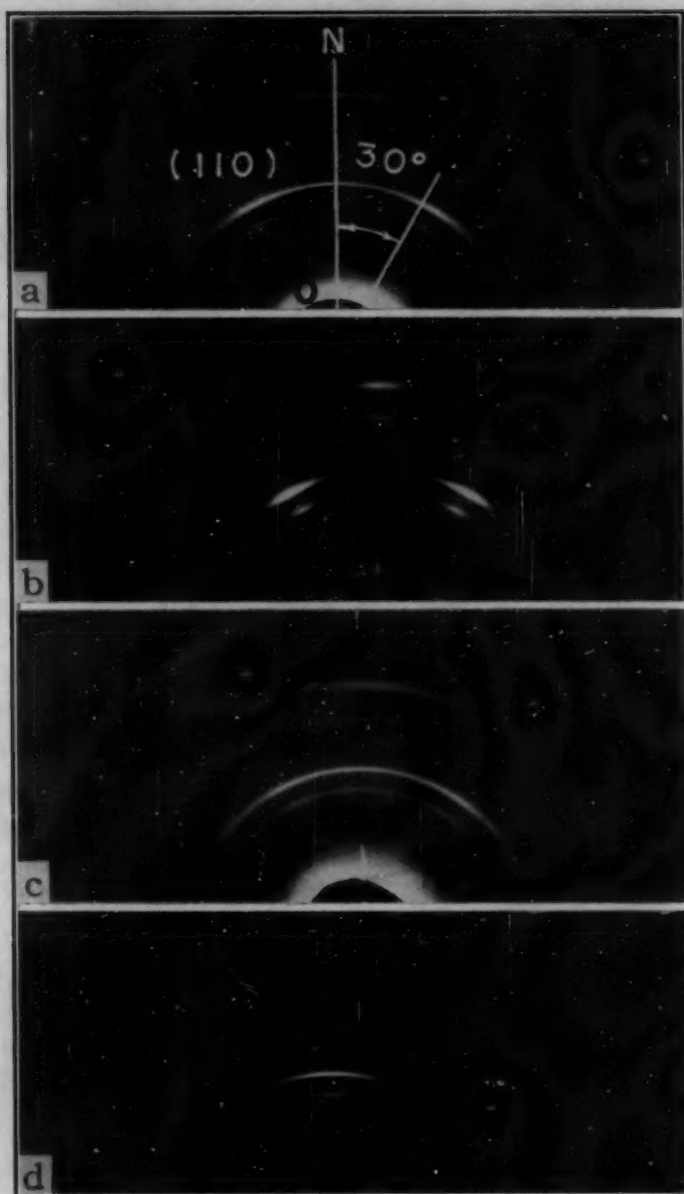


Fig. 1—Most Significant Diffraction Patterns in the Sequence of Rolling Temperatures as Listed in Table I. (a) Sample 1, rolled at room temperature; (b) Sample 2, rolled at 32 °F; (c) Sample 5, rolled at 400 °F; (d) Sample 8, rolled at 700 °F. All patterns were taken in the transverse direction with the surface of the specimen set at an angle of 10 degrees with direction of X-ray beam.

at various temperatures be made more readily, the intensity of the diffraction rings was measured by means of a Leeds and Northrup microphotometer. The diffraction pattern is symmetrical with respect to a vertical line ON drawn through the center of the pattern. Measurements were taken at every 5-degree interval considering the intersection of this line with the (110) diffraction ring as the zero position. The region of maximum intensity occurs at an angle of

30 degrees for the patterns taken at the lower rolling temperatures.

While such intensity measurements were made on the diffraction patterns of all the prepared samples, only those patterns and their microphotometer measurements are presented which have special sig-

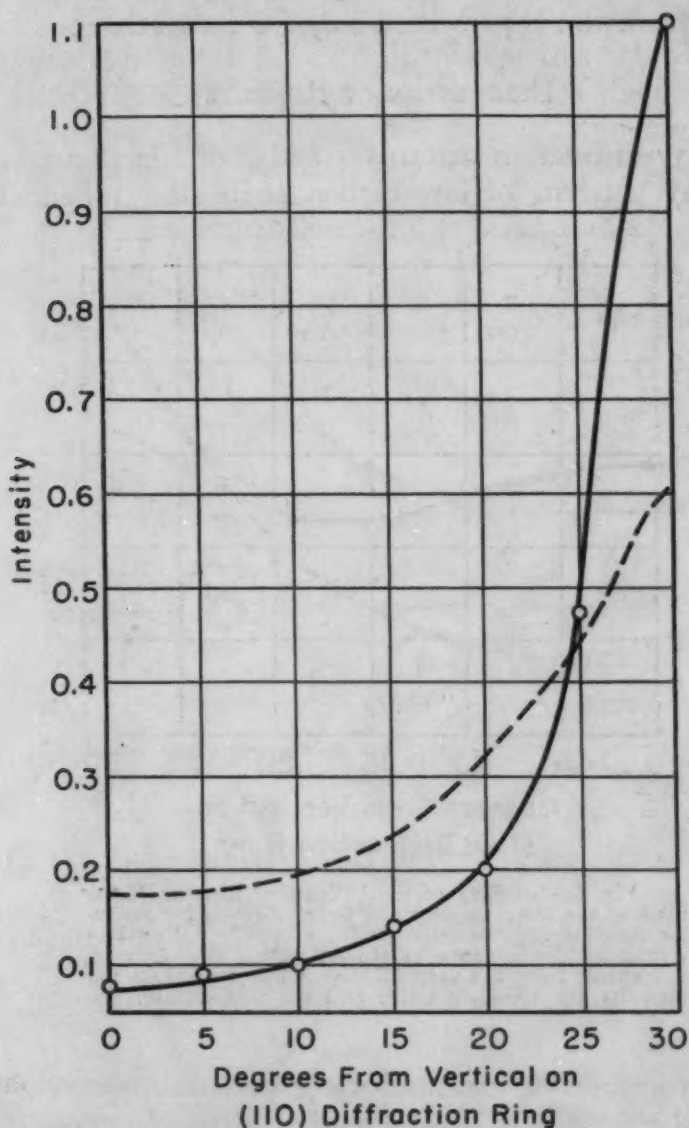


Fig. 2—Intensity of the Diffraction Ring as Measured by the Microphotometer Plotted Against the Angular Reading for Specimen Rolled at 32°F. Full line represents the intensity of the diffraction ring at various angles from the vertical. Dash line represents the intensity for specimen rolled at room temperature.

nificance. Since the photographic density at any portion of a diffraction ring is directly related to the number of grain fragments properly oriented for reflection, the microphotometer readings are a direct measure of the number of grain fragments oriented in a specific direction.

In the solid line curves of Figs. 2, 3, and 4, the intensity of the diffraction ring as measured by the microphotometer is plotted as ordinate against the angular reading as abscissa for the initial temperatures of 32, 400, and 700 °F. On each of the figures the dashed curve represents the variation in intensity for the sample rolled at room temperature and is presented only for comparison.

DISCUSSION OF RESULTS

The X-ray diffraction patterns 1 and 2 of Fig. 1 are representative of X-ray patterns of low carbon strip steel rolled at low or

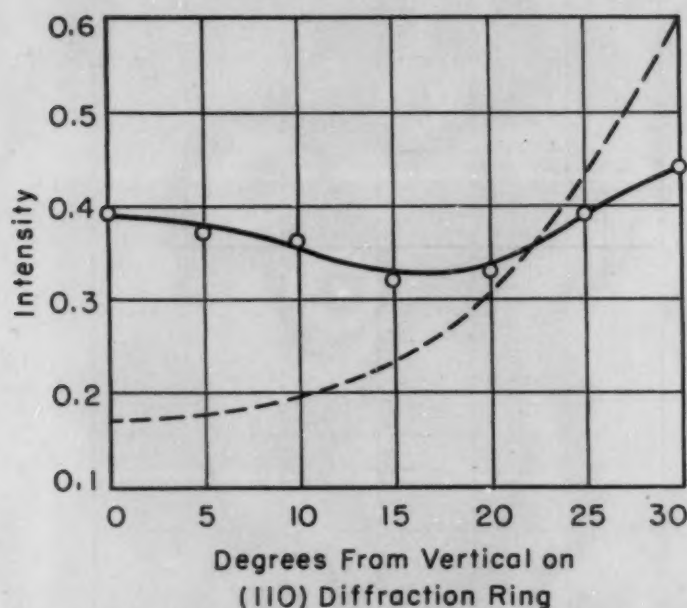


Fig. 3—Intensity of the Diffraction Ring as Measured by the Microphotometer Plotted Against the Angular Reading for Specimen Rolled at 400 °F. Full line represents the intensity of the diffraction ring at various angles from the vertical. Dash line represents the intensity for specimen rolled at room temperature.

room temperatures. The maxima of the pattern make angles of 30 degrees with the vertical. However, the intensity curves of Fig. 2 show that the maxima for the sample 2 rolled at an initial temperature of 32 °F is approximately twice as large in magnitude as for the sample 1 rolled at room temperature; also that the minimas have the inverse relationship. The areas under the two intensity curves are approximately the same. At these rolling temperatures the (001) planes tend to lie in the rolling plane and the [110] direction tends to coincide with the rolling direction.

The full-line intensity curve of Fig. 3 taken from the diffraction pattern of sample 5, which was rolled at an initial temperature of 400 °F, has two maximas. One of these is in the normal position of

30 degrees and the other in the zero position. These maximas of intensity are nearly equal in magnitude though the one at 30 degrees from the vertical is somewhat greater. The minimum of intensity has shifted from the zero position to that of approximately 15 degrees, and is not much less in magnitude than the maximas. If the grain fragments were oriented at random the intensity curve would be a straight line. It is thus quite evident that for this rolling temperature (400 °F initial) the texture approaches that of a random orientation. The dashed curve is for the sample rolled at room temperature and is again included for comparison.

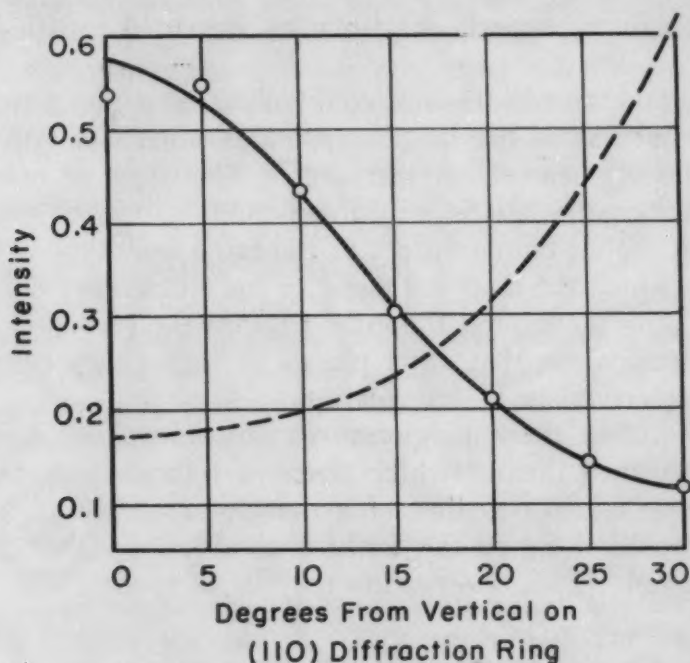


Fig. 4—Intensity of the Diffraction Ring as Measured by the Microphotometer Plotted Against the Angular Reading for Specimen Rolled at 700 °F. Full line represents the intensity of the diffraction ring at various angles from the vertical. Dash line represents the intensity for specimen rolled at room temperature.

The full-line intensity curve for sample 8, rolled at an initial temperature of 700 °F, is shown in Fig. 4. The maxima now occur in the 0 degree position and the minima at 30 degrees. This is a complete reversal of the maxima and minima from that obtained at room temperature as can be seen in comparing the full line with the dashed curve. At this temperature of rolling the (110) planes of the grain fragments lie predominantly in the rolling plane, and the [001] direction of the grain fragments in the rolling direction. This texture agrees with the one observed by Goss (6) in the hot rolling of iron, and might well be called the "warm rolling" texture of low carbon steel in contrast to that obtained by the usual "cold rolling".

The cold rolling texture is designated by (001) [110] and the

"warm rolling" by (110) [001]. These textures are simply related since by rotation of the space lattice of the first texture through 90 degrees around a $[\bar{1}10]$ at a $[1\bar{1}0]$ direction as axis, the second texture will be obtained. The intermediate temperatures of rolling thus represent a transition from the (001) [110] texture to the (110) [001] texture. This transition satisfactorily explains why "warm rolling" in a definite temperature range may give a texture simulating that of random orientation.

SUMMARY

An analysis of the experimental results presented justifies certain conclusions:

1. That as the temperature of cold rolling, at a given reduction, is lowered below that of the "ordinary temperature" of rolling, the degree of preferred orientation increases. The type of orientation texture does not change but is only intensified.

2. That at higher temperatures of rolling, a new type of texture is developed in which the diagonal plane of the elementary cube tends to lie in the rolling plane, and the cube edge in the direction of rolling. It is quite apparent that other planes at higher temperature are effective in the mechanism of deformation.

3. That between these temperatures of cold rolling there is a range of temperature during which there is a transition from the usual cold rolling texture to that of a new "warm rolling" texture. During this transition range the texture obtained simulates that of random orientation. This observation may be of considerable practical significance.

ACKNOWLEDGMENTS

Acknowledgments are made to Wm. Brenner, Jr., for carrying out the necessary rollings, and to Edward N. Nelson for taking the X-ray diffraction patterns, both of The Cold Metal Products Company Laboratory.

References

1. C. Barrett, "Structure of Metals", McGraw-Hill Book Company, New York City, p. 381-419.
2. R. M. Brick, "Cold Working of Metals", American Society for Metals, 1951, p. 106.
3. E. N. DaC. Andrade and L. C. Tsien, *Proceedings*, Royal Society, Vol. (A) 163, 1927, p. 1.
4. A. L. Nadai, "Theory of Flow and Fracture of Solids", McGraw-Hill Book Company, p. 62.
5. Wayne T. Sproull, "X-Rays in Practice", 1946, p. 456. ASTM Symposium on Radiography and X-Ray Diffraction, 1936, p. 321.
6. N. P. Goss, "Structural Changes in Low Carbon Steels Produced by Hot and Cold Rolling", *TRANSACTIONS*, American Society for Metals, Vol. 29, 1941, p. 20.

DISCUSSION

Written Discussion: By G. L. Clark, University of Illinois, Department of Chemistry, Urbana, Ill.

There seems to be no question concerning the validity of these results and the interpretation. This paper is illustrative of the fact that some of the fields of investigation, longest known and most frequently studied, still provide opportunity for remarkably excellent fundamental and practical research work. It would naturally occur to people interested in rolling steel to observe quantitatively the effect of temperature, but apparently this variable has not been previously studied except in a very incidental manner.

The question naturally arises as to whether, at the intermediate temperatures where the texture simulates that of random orientation, the resultant rolled sheet has different properties in the sense that there can be considerably greater reduction without intermediate anneals. It is this very type of random orientation maintained during deformation that has been sought by application of opposed tensions and compressions, control of compositions and otherwise. It would of course be exceedingly interesting and valuable if the author could disclose whether or not the sheet with random orientation actually has any markedly different property form itself that displays fiber patterns by X-ray diffraction. It is generally true in all physical chemical processes that any system will set up a maximum resistance to further change, in this case a preferred orientation against further deformation. The mechanism and the energy involved in producing essentially random texture at intermediate temperatures are, therefore, of extraordinary significance. If this is true, then, further heat treatment should give a completely different result in terms of grain size and grain orientation than would be the case in a highly fibered condition.

The author is to be congratulated for finding an important new area in a supposedly exhaustively-known subject. It is clearly evident that considerably more work on this discovery with X-rays, optical and electron microscopy, and mechanical and chemical tests, such as corrosion, will be eminently worth-while.

Written Discussion: By R. L. Davidson, associate director, Research Laboratories, Armco Steel Corp., Middletown, Ohio.

This paper by Mr. Goss is an interesting addition to the knowledge of deformation textures. The writer would like to point out a similar effect in which the temperature of cold reduction affects the degree of orientation in oriented silicon steel. This relationship was demonstrated in the writer's laboratory a number of years ago and resulted in the issuance of two patents.

One of the interesting features learned there was that the difference in degree of orientation produced by different temperatures of cold reduction was noticeable after subsequent recrystallization at elevated temperature. Another observation was that the effects of cold reduction at various temperatures depended in a very critical manner upon the composition of the steel, especially with respect to manganese.

It would be interesting to know if slight changes in manganese or other features of composition in the carbon steel used in this paper would have such a critical effect.

It perhaps does not need to be pointed out that the new type of orientation postulated was arrived at from a single intensity maximum on a single X-ray diffraction ring. While this new orientation seems to be compatible with the diffraction patterns shown, it would have been more definitely established if a complete stereographic pole figure had been constructed. This would have required a number of diffraction patterns made with the X-ray beam at various angles to the sheet, or the newer methods utilizing direct-reading X-ray apparatus. It would seem worth-while to substantiate the new orientation by one of these more rigorous methods.

Written Discussion: By G. M. Sinclair, Metallurgical and Ceramic Department, Westinghouse Research Laboratories, East Pittsburgh, Pa.

Mr. Goss has clearly demonstrated a most important effect of temperature on the rolling textures obtained in low carbon steel strip. It is rather surprising that these considerable differences in texture may result from relatively small changes in the rolling temperature; this emphasizes the importance of close control of this variable during production. While it is desirable to process sheet for deep drawing purposes so as to reduce preferred orientation to a minimum, quite the opposite is true in the production of magnetically "soft" sheet, such as the silicon-irons, which one would expect to be similarly influenced by rolling temperature. To obtain optimum magnetic properties a high degree of preferred orientation is usually desirable, since the ease of magnetization varies with the orientation of the crystal lattice. Mr. Goss' work is thus of interest as a possible means of control for either mechanical or magnetic properties. A point of importance, however, is the fact that in the case of either deep drawing or magnetically-soft sheet the metal is normally used in the annealed or recrystallized condition for best results. In view of this I should like to ask Mr. Goss if he has been able to extend his work to include a study of the textures obtained after recrystallization of the rolled strip.

Author's Reply

The author appreciates the fine discussions of this paper. These have added much to a better understanding of the subject matter.

Dr. Clark asked whether any physical tests had been made on the cold-reduced strip which exhibited a substantial random orientation. So far very few tests have been made on the physicals of the strip plastically deformed at various temperatures, in the range of 150 to over 700 °F. However, from the meager data obtained so far, it seems that certain properties will be altered, others will not be affected.

In reply to Dr. Davidson, I wish to say that the conclusions arrived at in this paper complied with all the requirements of the pole figure method. The method used is in line with that of De Barr and Roberts² and J. K. Wood³. The method was originally proposed by Davey, Nitchie and Fuller.⁴ In this method one requires only three X-ray exposures. These are made in the P, T and N (normal to surface) directions. The X-ray

²A. E. De Barr and B. Roberts, "Texture of Rolled Sheets", *Journal, Iron and Steel Institute*, March 1950, p. 285.

³*Journal of Applied Physics*, Vol. 19, 1949, p. 784.

⁴"Determining Orientation of Crystals in Rolled Metal From X-Ray Patterns Taken by Monochromatic Pin Hole Method", Tech. Pub. 243, American Institute of Mining and Metallurgical Engineers.

exposures in the P and T directions are made at some Bragg angle, in this case 10 degrees. All (110) planes which lie parallel to the surface of the sheet are in a position to reflect. From these P and T X-ray exposures, one can easily determine the orientations present, and the intensity as well.

In this paper the X-ray patterns made in the T direction were the only ones presented for the reasons stated in the text. However, the X-ray data taken were sufficient for the construction of the complete pole figure.

It was shown in another paper⁴ that the hot and cold rolling orientation textures are quite different; however, the transition temperature from the hot to the cold rolling texture was not determined at that time.

The comments of Mr. Sinclair are indeed appreciated, especially his reference to the marked effect a small change in rolling temperature may have upon the intensity of the orientation. It may be recalled by many of the early workers in this field, that at times one would observe great variations in the intensity of the X-ray diffraction pattern of strip and wire given the same reduction and under the same conditions. However, the temperature at which the metal was worked was not taken into consideration. The case in point here is the tremendous difference in the orientation texture when rolling at 32 °F and room temperature.

Some work has been done on the "temperature effect" in relationship to the residual orientation texture after annealing below A_3 (low carbon strip steel). The results show that a wide range of recrystallization textures are possible. The temperature at which a metal is rolled can control the intensity of the residual orientation texture after annealing. Under certain warm rolling conditions random orientations of the grains may be obtained. The warm rolling technique is without question related to the deep drawing characteristics after heat treatment. The warm rolling of metals and alloys should have a marked effect upon the with and cross grain properties of cold-reduced strip. It is quite likely that warm rolling of metals will gradually find many useful applications in the field of rolling, drawing and forming.

ACCELERATED STRAIN AGING OF COMMERCIAL SHEET STEELS

BY L. R. SHOENBERGER AND E. J. PALIWODA

Abstract

The effect of natural strain aging on the hardness and tensile characteristics of some rimmed and stabilized steels was determined. Variations in the behavior of rimmed steels were ascribed principally to ferrite grain size and degree of skin rolling. In the strain aging of aluminum-killed and vanadium-rimmed steels, the nitrogen not combined with aluminum or vanadium assumes an important position as shown by its relationship to proportional limit changes.

An accelerated strain aging test using gradient heating was developed to predict the course of age hardening and to estimate the rate and severity of yield point return during aging.

INTRODUCTION

THE strain aging of sheet and strip after skin rolling has long been recognized as an important factor in the ultimate drawability of steel. Skin rolling is performed primarily to eliminate the yield point which is associated with stretcher strain markings during forming. Changes that occur in the period between skin rolling by the producer and fabrication by the consumer result in yield point return and embrittlement of the steel.

A few steels have been developed in which strain aging is effectively inhibited, but only two—aluminum-killed and vanadium-rimmed—are commercially important (1, 2).¹ Since both are more expensive to produce, control of strain aging of ordinary rimmed steels and development of a low-cost stabilized steel are desirable. Present information regarding the strain aging of skin-rolled steels is limited, however, and there is no satisfactory means for measuring the actual strain aging characteristics of temper-rolled material.

NATURAL AGING

Natural aging of a number of rimmed, aluminum-killed, and vanadium-rimmed steels was measured by means of hardness and

¹The figures appearing in parentheses pertain to the references appended to this paper.

A paper presented before the Thirty-fourth Annual Convention of the Society, held in Philadelphia, October 18 to 24, 1952. The authors, L. R. Shoenberger and E. J. Paliwoda, are research engineers in the Metallurgical Research Division, General Technical Department, Jones & Laughlin Steel Corporation, Pittsburgh. Manuscript received April 16, 1952.

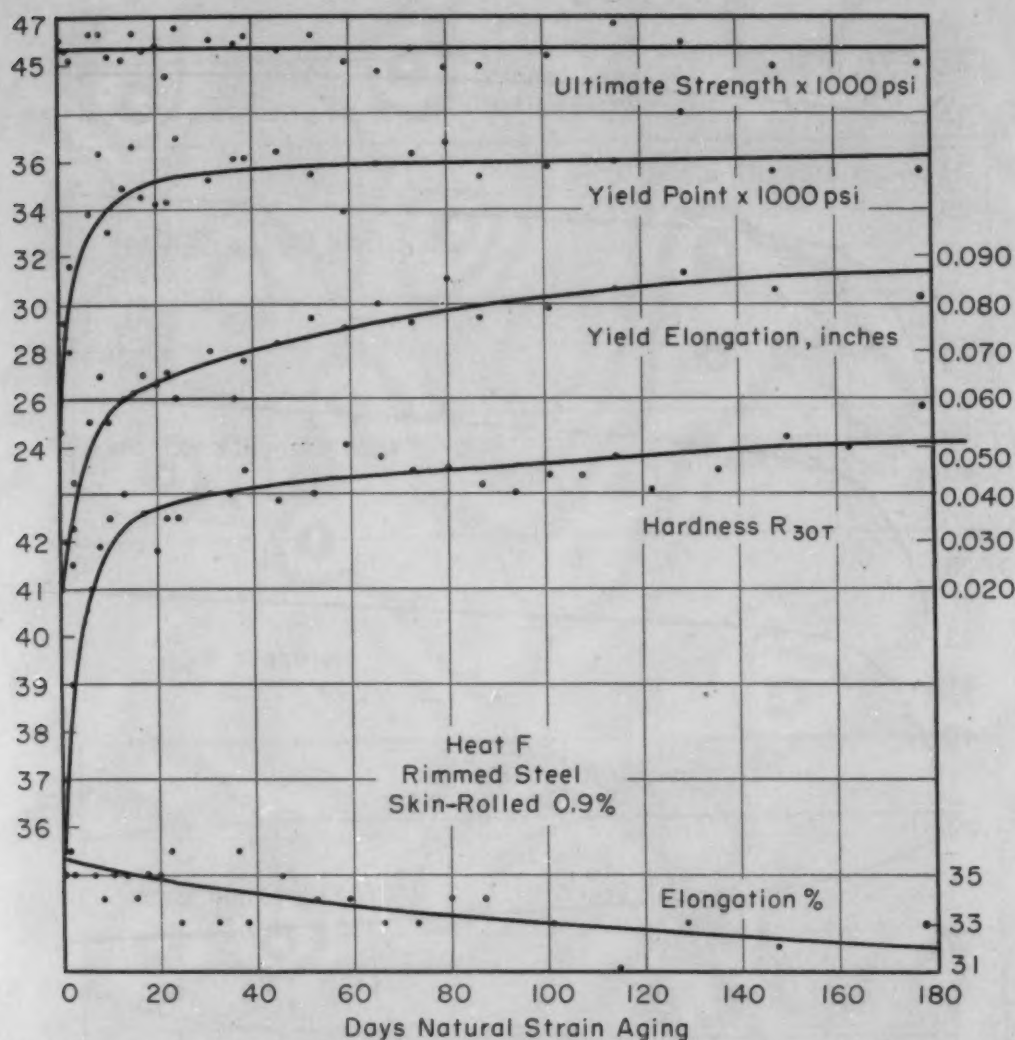


Fig. 1—Changes in Mechanical Properties of Skin-Rolled Rimmed Steel During Natural Strain Aging.

tensile tests. Chemical composition limits of these steels are shown in Table I.

Table I
Chemical Composition Limits

Type	C	Mn	P	S	Si	Al	V
Rimmed	0.03/0.06	0.25/0.37	0.004/0.009	0.010/0.037	0.01	0.003/0.005
V-Rimmed	0.04/0.05	0.28/0.35	0.006/0.011	0.025/0.026	0.01	0.003/0.004	0.022/0.037
Al-Killed	0.05/0.06	0.25/0.29	0.003/0.010	0.029/0.036	0.02/0.04	0.021/0.038
Type	Total Nitrogen		Soluble Nitrogen		Uncombined Nitrogen*		
Rimmed	0.003/0.005		0.003/0.005		0.003/0.005		
V-Rimmed	0.004/0.005		0.001/0.003		0.001/0.003		
Al-Killed	0.005/0.007		0.005/0.007		0.0002/0.0024		

*Nitrogen not combined as AlN or VN.

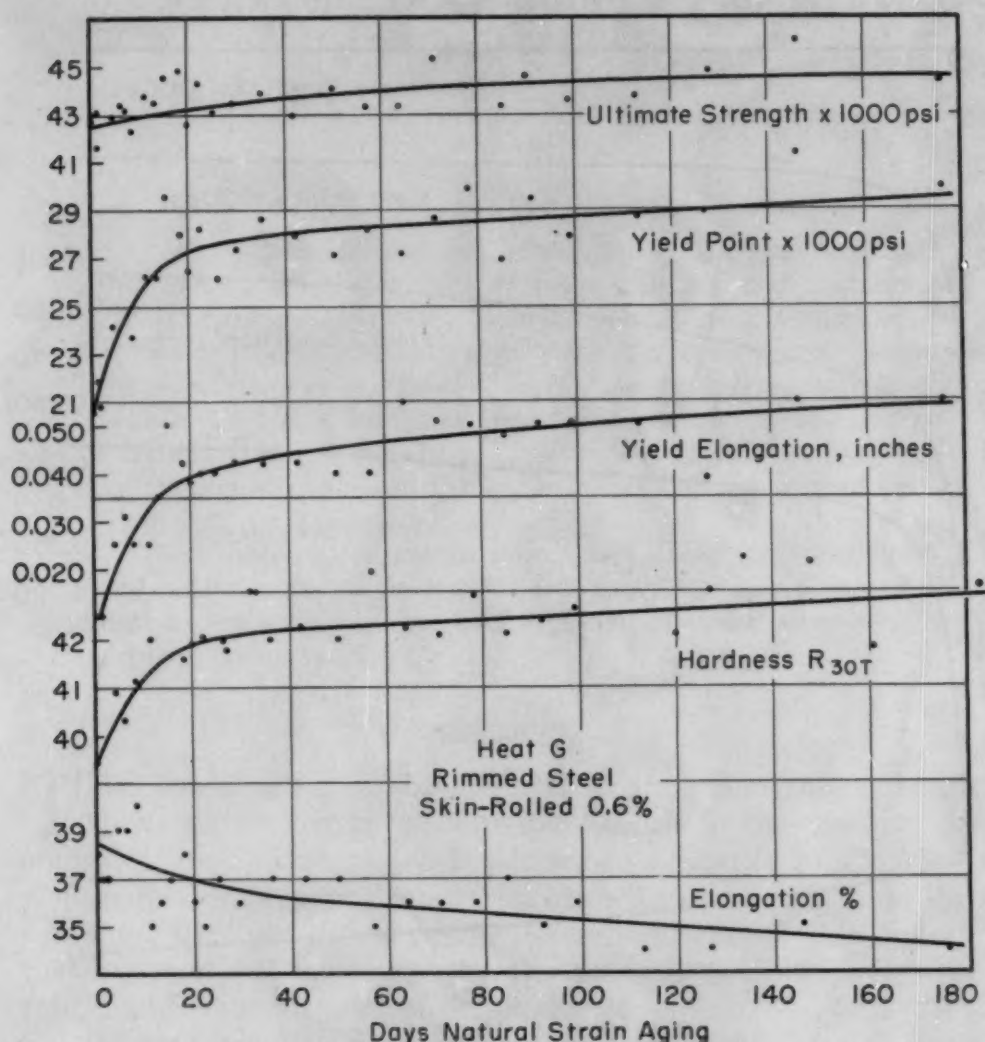


Fig. 1—Changes in Mechanical Properties of Skin-Rolled Rimmed Steel During Natural Strain Aging.

Samples were selected from center portions of skin-rolled sheets and mechanical properties were determined within 8 hours after rolling. Subsequently, 10 to 20 hardness impressions and a tensile test were made periodically for 6 months as the steels strain-aged at room temperature (65 to 85 °F or 20 to 30 °C). Typical examples of the aging characteristics of several steels are illustrated in Figs. 1 and 2.

Factors Affecting Aging of Rimmed Steels

Considerable variations in the aging characteristics of rimmed and stabilized steels were noted, and attempts were made to ascertain the significant variables. Chemical composition, ferritic grain size, and degree of skin rolling were considered to be important factors. However, deviations in chemical composition of the ordinary rimmed steels tested did not appear to influence strain aging behavior.

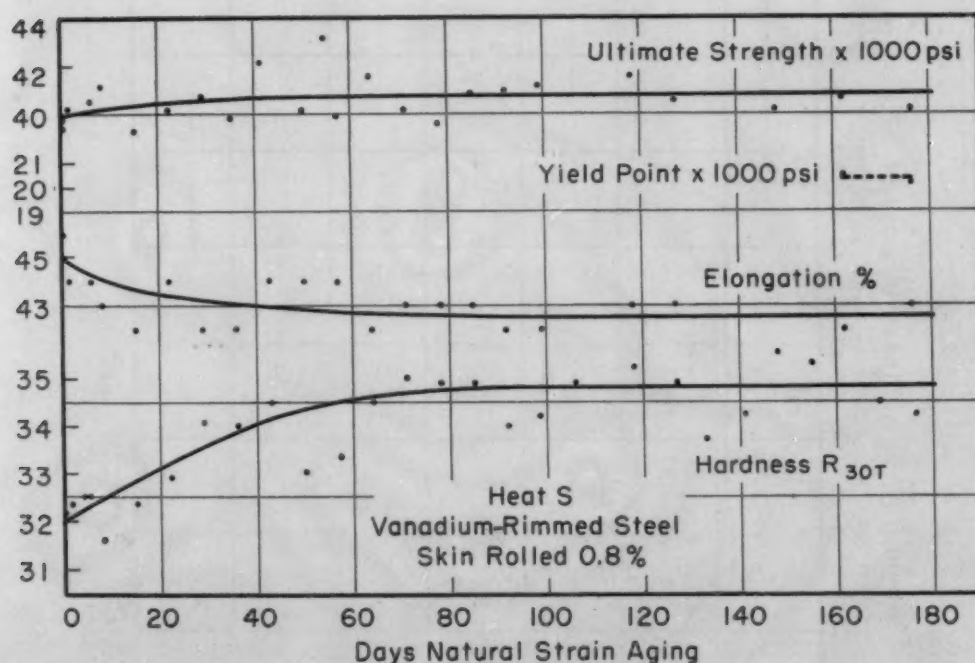
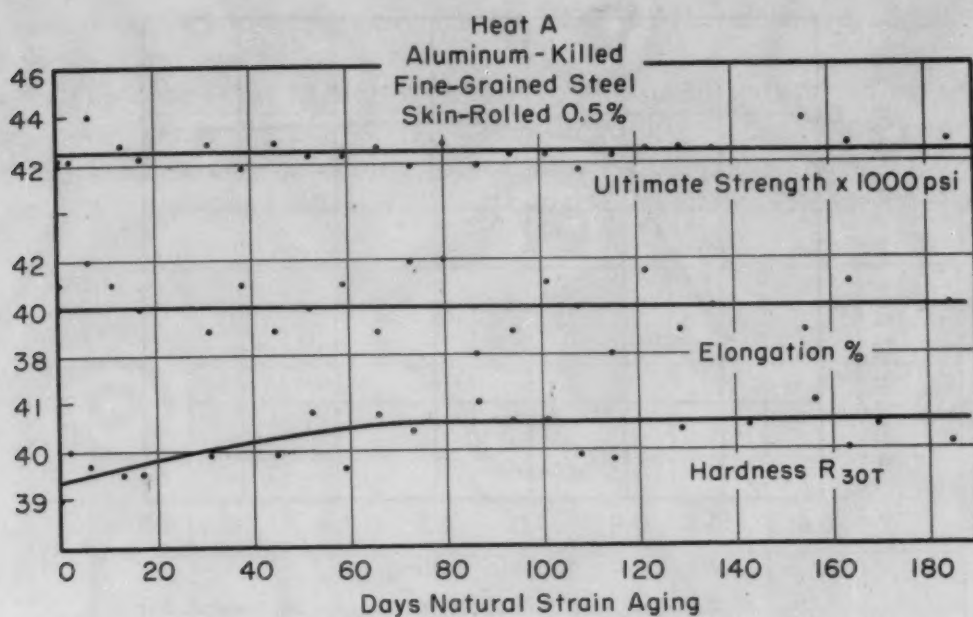


Fig. 2—Changes in Mechanical Properties of Skin-Rolled Stabilized Steel During Natural Strain Aging.

Ferrite grain size measurements were made by the intercept method ($\times 200$); and where grain size differences existed between rim and core, consideration was given to the proportions in deriving an average intercept grain size. The range of average grain sizes in the rimmed steels varied from 4.5 to 7 by ASTM standards.

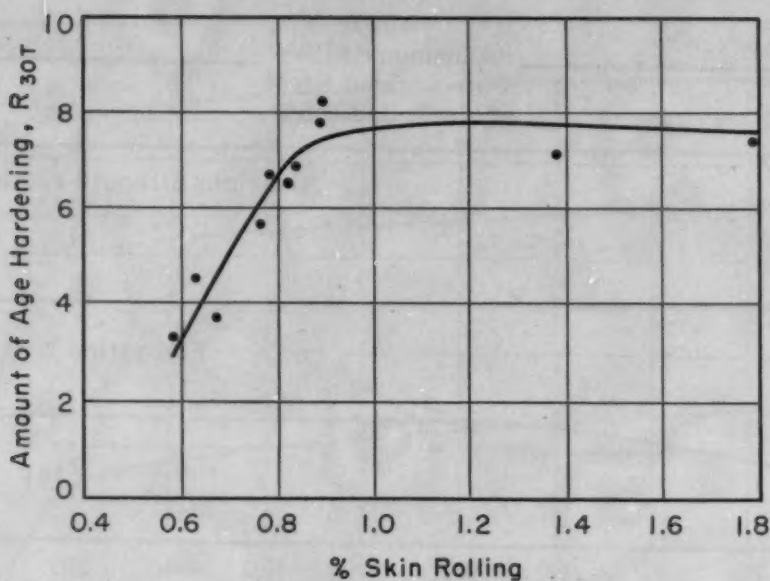


Fig. 3—Effect of Skin Rolling on the Amount of Natural Age Hardening Occurring in 6 Months Aging of Rimmed Steels.

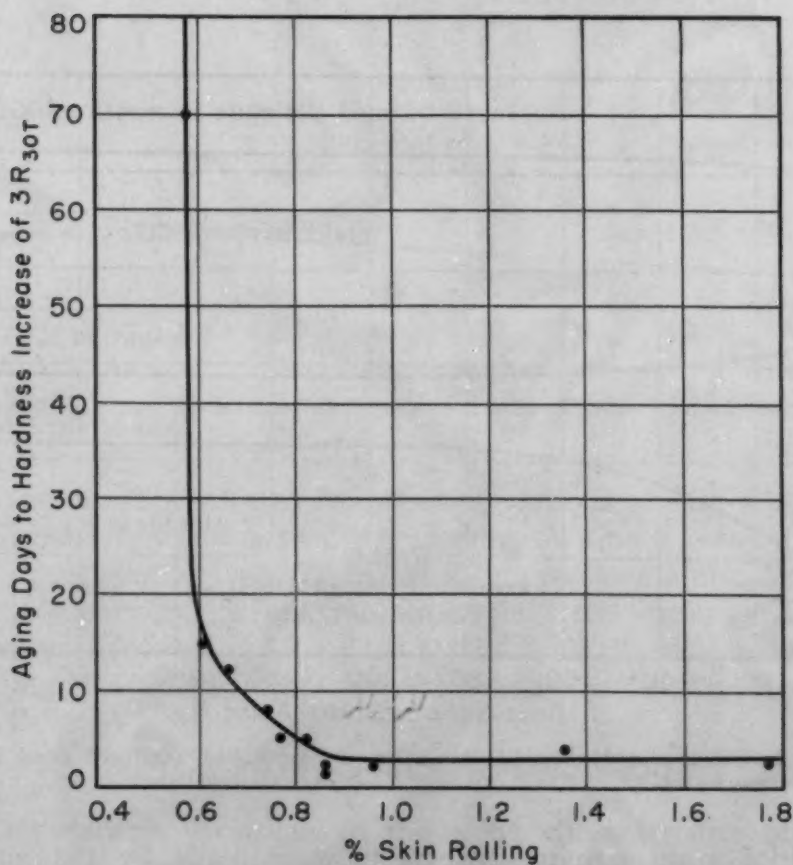


Fig. 4—Effect of Skin Rolling on the Rate of Natural Age Hardening in Rimmed Steels.

The general hardness levels of rimmed steels before and after aging proved to be mainly a function of ferrite grain size. Smaller-

grained steels were relatively harder, both in the freshly skin-rolled and the aged conditions.

The change in hardness during 6 months of natural aging was associated with the degree of skin rolling (Fig. 3). In this work, the amount of age hardening increased with temper rolling to 0.8%. Skin rolling 0.8 to 1.8% did not appear to further influence the degree

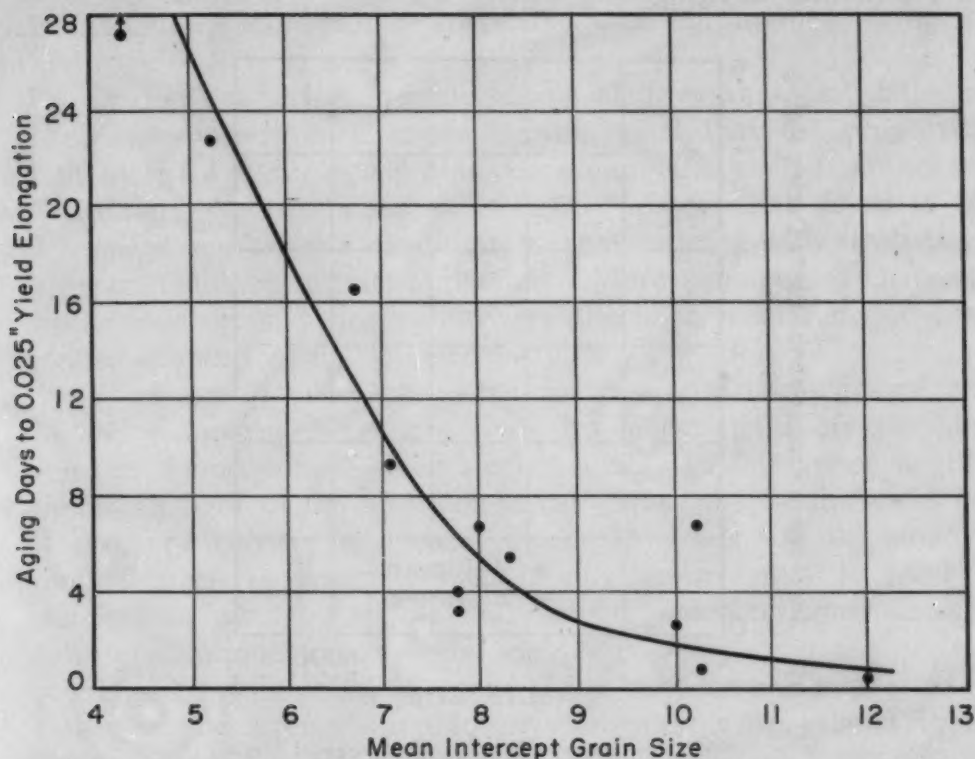


Fig. 5—Rate of Yield Elongation Increase Is Faster in Smaller-Grained Rimmed Steels.

of age hardening. Faster rates of age hardening were noted in rimmed steels that were temper-rolled more than 0.8% (Fig. 4).

Greater amounts of yield elongation after 6 months aging were observed in finer-grained material, which is in agreement with findings of other investigators (3, 4, 5). The speed of tensile testing, in this instance, was 0.05 inch per minute and the yield elongation value employed is for a standard 2-inch gage length.

Faster rates of yield elongation return were observed in ordinary rimmed steels having small ferrite grains (Fig. 5). These steels were skin-rolled from 0.6 to 1.8%. Data for several samples of the same heat, which were skin-rolled various amounts, suggest a minor retarding action by the more severe skin rolling operations, but results are not conclusive. Jevons, however, noted that increased skin rolling (1 to 10%) impeded the rate of yield elongation return (4).

A yield point returned for all rimmed steels within 3 days after skin rolling. A similar observation was made by Sachs (6). Yield

point increased markedly during aging in a manner similar to yield elongation return. An increase of about 1800 psi in yield point was accompanied by a return of 0.010 inch yield elongation. Higher as-aged yield points and tensile strengths were related to finer-grained material. Tensile strength of the steels was comparatively unaffected by strain aging, the increase in strength seldom exceeding 2500 psi after 6 months of aging.

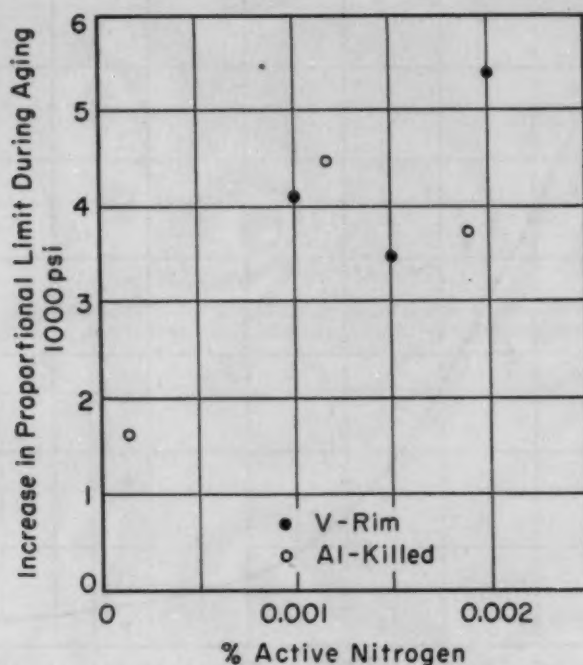


Fig. 6—Greater Changes in Proportional Limit During Natural Aging Occurred in Stabilized Steels With Greater Active Nitrogen Contents:

Attempts to relate elongation data with mechanical and chemical characteristics of the steels were not completely successful.

Factors Affecting the Aging of Stabilized Steels

Both ferrite grain size and degree of skin rolling are probably significant in the production of stabilized sheet and strip steels, but nitrogen assumes an important position not found in rimmed steels. Large portions of the nitrogen contents of stabilized material are combined as aluminum or vanadium nitrides by suitable alloy additions and heat treatment (7, 8). The remainder of the nitrogen in aluminum-killed and vanadium-rimmed steels is arbitrarily designated as active or uncombined nitrogen, and is usually low. These active nitrogen contents varied from 0.0002 to 0.0024% in steels employed in this investigation (Table I).

Since nitrogen has been regarded as one of the possible causes of aging (9, 10), efforts were made to ascertain the significance of

uncombined nitrogen in stabilized steels. Due to the apparent interdependence of a number of factors in strain aging, no clear-cut solution was obtained. For example, higher hardness (freshly skin-rolled and strain-aged) was observed for stabilized materials with relatively high, active nitrogen contents. The influence of grain size on the hardness of this material could not be determined due to differences in grain shape (elongated versus equiaxed). Degree of age hardening could not be correlated with uncombined nitrogen in this work.

During the periodic tensile testing of three aluminum-killed and three vanadium-rimmed steels, it was noted that the proportional limit increased with aging time, paralleling the yield point increase of ordinary rimmed material. Higher proportional limits in both skin-rolled and as-aged conditions were associated with steels having large uncombined nitrogen contents. More pronounced changes in proportional limit during aging were also observed for material with greater amounts of uncombined nitrogen (Fig. 6).

A return of yield was noted for two vanadium-rimmed steels (3 and 6 months) despite active nitrogen contents comparable to those of the aluminum-killed steels tested. This behavior might be viewed in light of the effect of ferrite grain size on the yield point of ordinary rimmed material. Since the grain size of vanadium-rimmed steels is generally fine, it may be necessary to fix larger amounts of nitrogen to obtain nonaging characteristics similar to those of aluminum-killed steels.

Despite differences in grain shape, test results suggested that higher tensile strength and lower elongation were related to finer ferrite grains in stabilized steels.

GRADIENT STRAIN AGE TESTING

The influence of strain aging on the hardness and yield point behavior of commercially produced sheet and strip varies and depends on a number of factors including grain size, degree of skin rolling and uncombined nitrogen. Consequently, it appears desirable to evaluate both age hardening and yield point characteristics in any strain aging test. The dependence of strain aging on time and temperature was utilized in this investigation in an effort to devise a quantitative accelerated aging test applicable to all grades of strip steel.

Immediately after skin rolling, samples ($\frac{1}{2}$ inch by 14 inches) were heated for various lengths of time in a gradient furnace similar to that used by Halley (11). In this furnace, Globars are located near the end of the muffle, and a thermal gradient is produced by virtue of their position. The furnace was modified slightly, in that closed Inconel tubes were positioned in the muffle to shield test

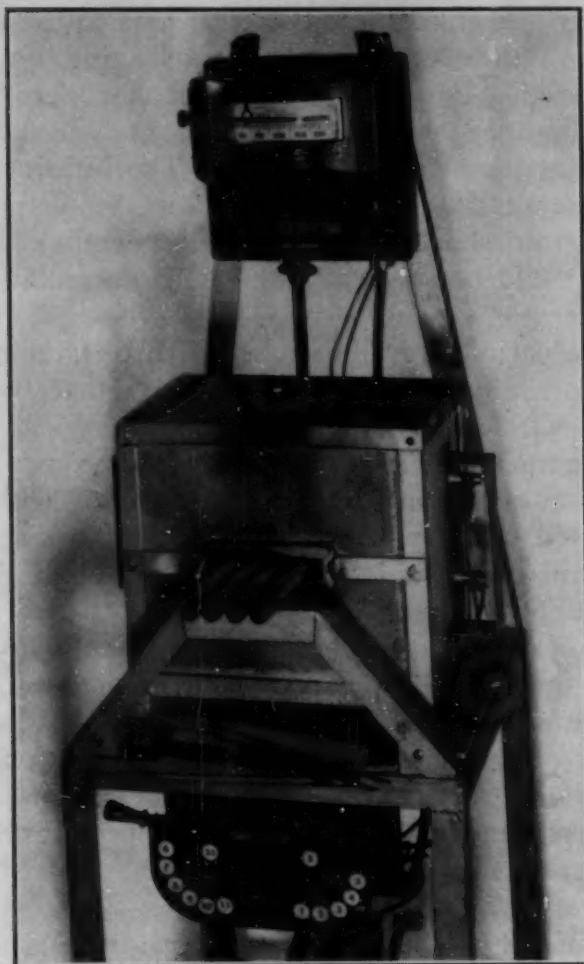


Fig. 7—Gradient Furnace Used for Accelerated Age Hardening and Strain Line Testing.

specimens from drafts and to extend the thermal gradient. These tubes protruded about 8 inches as illustrated in Fig. 7.

Thermocouples were employed to establish the temperature gradient, but this procedure did not prove satisfactory. As an alternate method, "Tempilstiks" were used to obtain reference temperatures (Fig. 8). The temperature ranges selected were approximately 100 to 500 °F (40 to 260 °C) for rimmed steels and 125 to 600 °F (50 to 315 °C) for stabilized steels. All testing was completed within 10 hours after skin rolling.

Age Hardening

Three or more Rockwell T-30 impressions were made at selected intervals along the length of the gradient-treated sample. The average hardness at each location was compared to the hardness of the same steels after natural aging for various lengths of time. Thus, a relationship was empirically derived between time and temperature

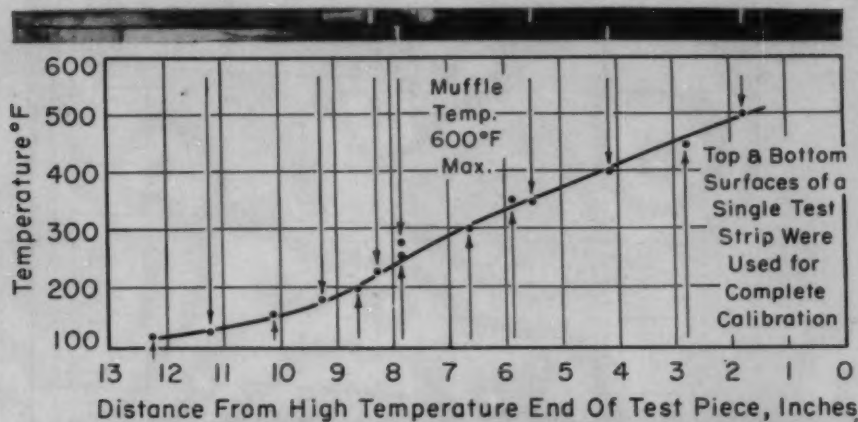


Fig. 8—Calibration of Furnace Temperature Gradient From Fusion of Tempilstik Markings.

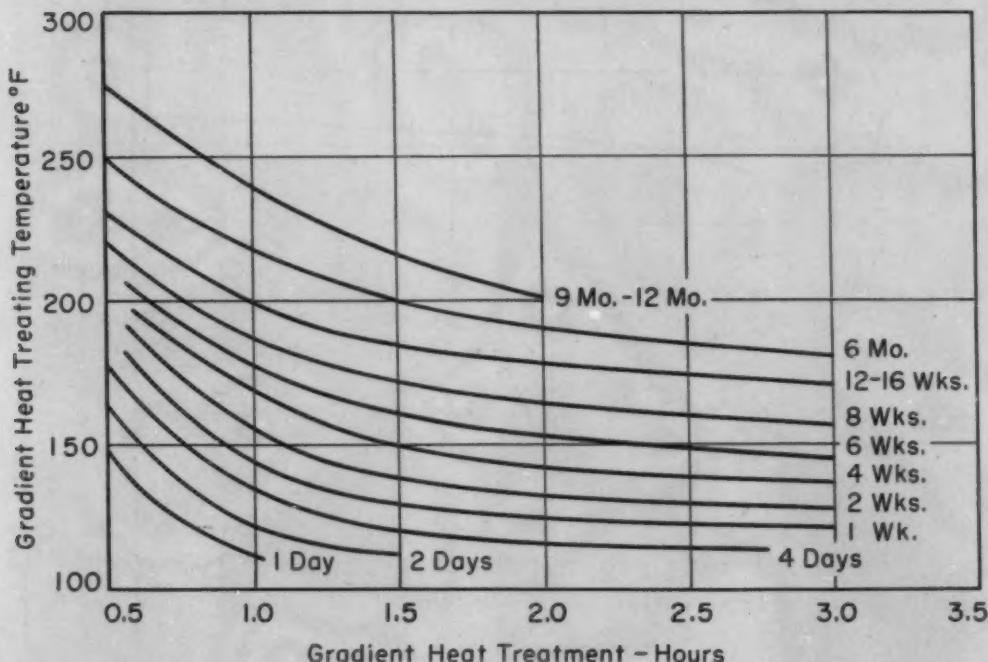


Fig. 9—Interpretation Graph Used to Correlate Gradient Age Hardening Data With Natural Age Hardening.

of gradient heat treatment and time of strain aging at room temperature (65 to 85 °F or 20 to 30 °C). This correlation, shown in Fig. 9, was employed to predict the age hardening characteristics of sheet steels. For example, an estimate of the hardness of material aged 6 months can be obtained by heat treating at 200 °F (95 °C) for 1½ hours or at 250 °F (120 °C) for ½ hour. These values would be the same under ideal conditions, but in practice it is desirable to use an average of several such "equivalent" values for each point in constructing a predicted hardness curve.

Comparisons of actual and predicted age hardening trends for

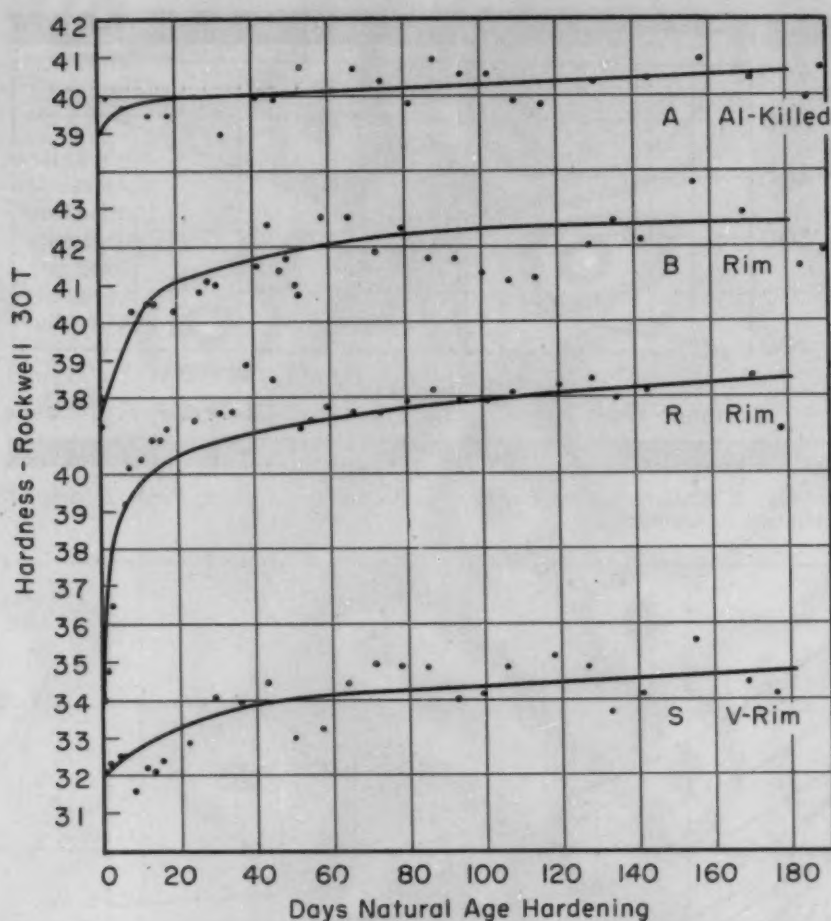


Fig. 10—Typical Predicted Age Hardening Curves (Solid Lines) Shown With Average Hardness Values (Points) Obtained During Natural Strain Aging.

several steels are indicated in Fig. 10. In about 70% of the tests made, the actual and predicted hardness values for 6 months of natural aging agreed within ± 1 Rockwell T-30.

Yield Point Behavior

A variation in test procedure was developed to measure yield point behavior of strip steels. Samples were cut to the dimensions previously mentioned, but added care was taken to obtain a $\frac{1}{2}$ -inch parallel section. After gradient heating for 1 hour, these strips were polished with 240-grit abrasive to aid in observation of the formation of strain lines. The samples were deformed in tension at 0.5 inch per minute.

At about 400 to 500 pounds load, a network of light strain markings could be seen rising from the low temperature end of the specimen. Shortly thereafter, this network consolidated rather sharply into a wave and proceeded upward. The origin of this wave was marked as it appeared, and the corresponding temperature was

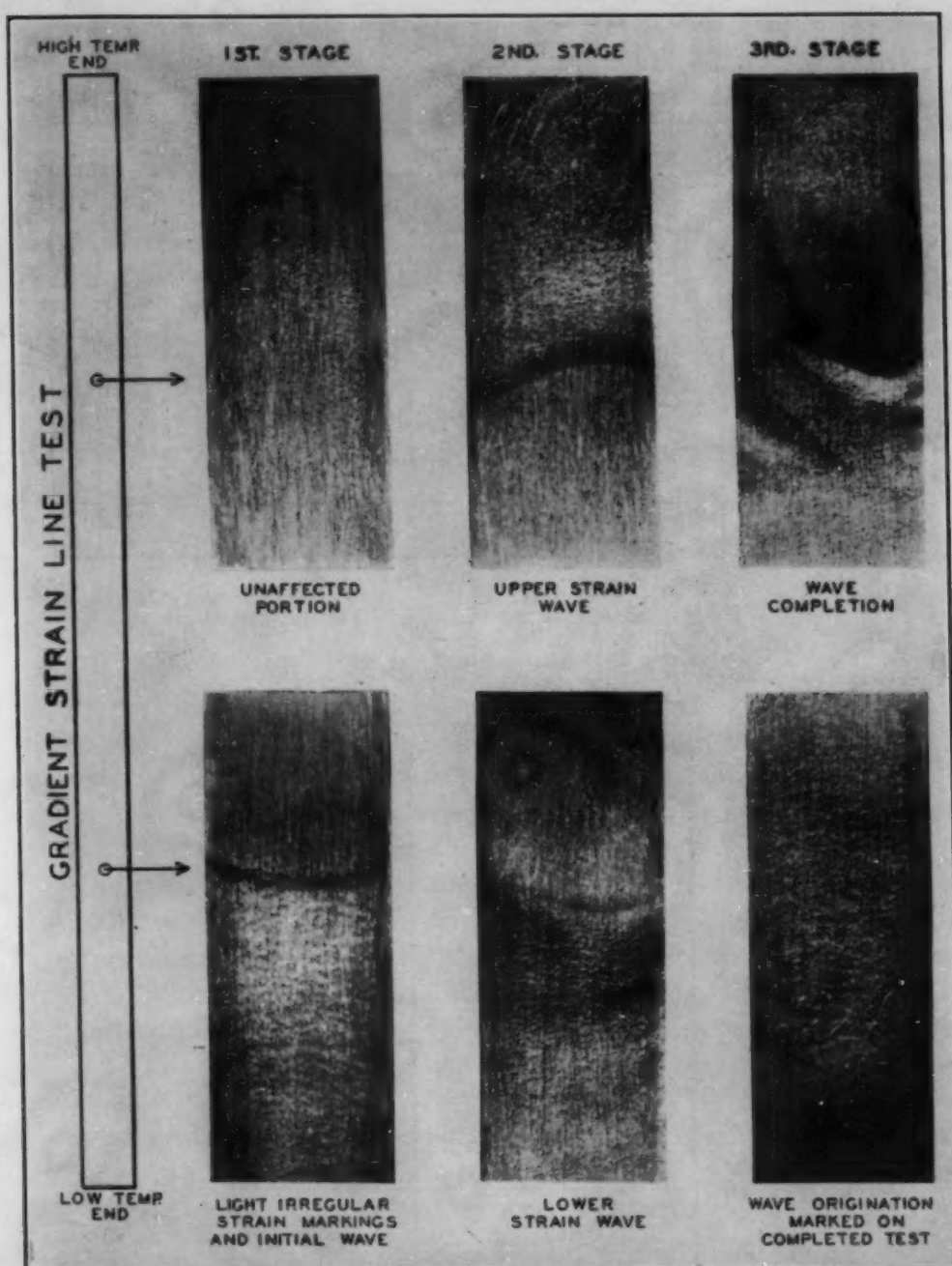


Fig. 11—Strain Wave Action During Stretching of Gradient Test in Tensile Machine.

determined from the calibration curve. At some higher load, a strain wave formed at the high temperature end of the sample and moved downward to meet the lower wave. The appearance of the strain markings and action during testing are illustrated in Fig. 11.

The average wave origination values for ordinary rimmed steels ranged from 120 to 205 °F (50 to 95 °C). Two vanadium-rimmed steels, which showed a return of the yield point after 3 and 6 months aging, had wave origination values of 260 and 345 °F (125 and 175

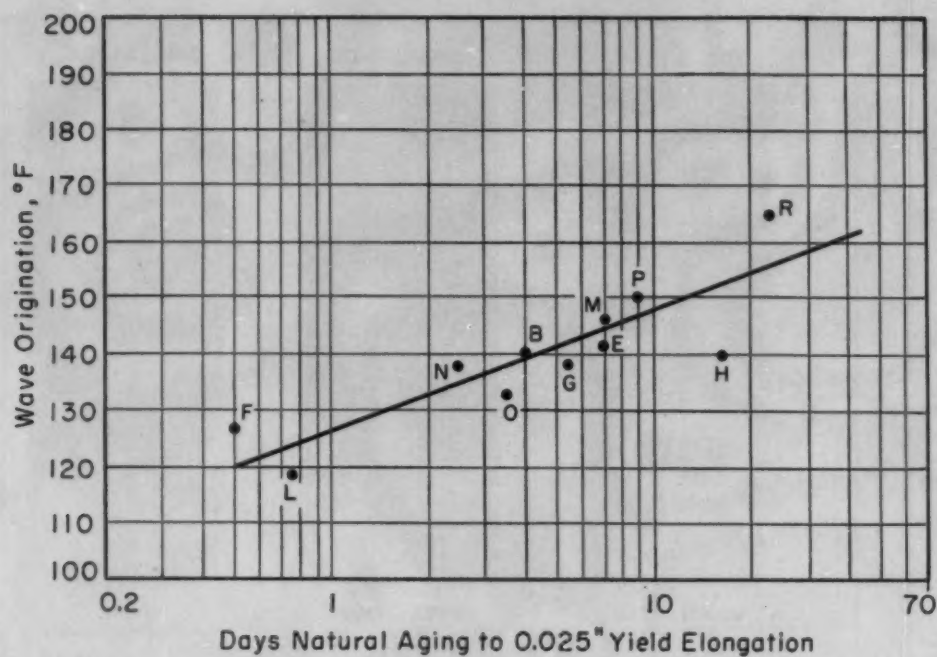


Fig. 12—Relationship Between Rate of Yield Return and Strain Wave Origination Temperature.

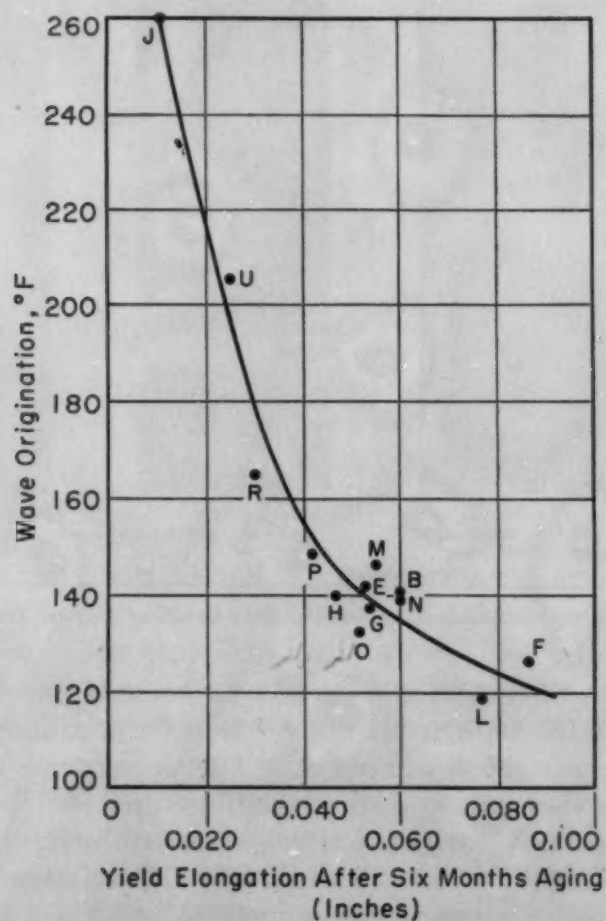


Fig. 13—Correlation Between Wave Origination Temperature and the Amount of Yield Elongation After 6 Months Natural Strain Aging.

°C), respectively. The remaining stabilized steels showed values ranging from 440 to 505 °F (225 to 265 °C).

Wave origination in gradient-treated samples was believed to approximate some value of yield elongation, since the latter has been associated with stretcher straining during drawing or pressing. This correlation was determined empirically. It was found that the temperature which produced strain wave origination in gradient-treated specimens was related to natural aging time required for about 0.025 inch yield elongation in a 2-inch gage length (Fig. 12).

The severity of yield elongation in steels after 6 months natural aging was associated with the wave origination temperature as shown in Fig. 13. It can be noted that gradient strain age testing can be employed to estimate yield point behavior as well as the age hardening tendencies of strip steels.

SUMMARY

The strain aging of a number of commercial strip steels was determined by means of hardness and tensile tests. Variations in aging characteristics of ordinary rimmed steels were attributed primarily to the effect of ferrite grain size and skin rolling. Increases in the latter (to 0.8%) resulted in more pronounced age hardening characteristics. Smaller ferrite grains were associated with generally higher levels of hardness, faster rates of yield point increase and greater yield elongation after aging.

Both factors probably influence the strain aging of stabilized steels, but in this work a large portion of the heat-to-heat variation in strain aging was apparently governed by the amount of uncombined nitrogen. Higher hardness values in the freshly skin-rolled or aged conditions and larger increases in proportional limits were observed in stabilized steels with the greater uncombined nitrogen contents.

An aging test was developed, utilizing gradient heat treated samples and employing time-temperature relationships to obtain varying degrees of accelerated aging. These time-temperature relationships were correlated with aging at room temperature. By this means, accurate predictions can be made of the age hardening characteristics of freshly skin-rolled sheet and strip steels.

The rate and severity of yield return can be predicted by determining the aging temperature necessary to produce strain waves in gradient-treated samples as they are stretched in a tensile machine. The temperature that initiates the strain wave is a measure of the rate and severity of yield point return.

References

1. H. W. Graham and S. L. Case, "Sensitivity Controlled Steel and the Manufacture Thereof", U. S. Patent No. 2,174,740.

2. S. Epstein, U. S. Patent No. 2,356,450, Aug. 22, 1944.
3. J. Winlock and R. W. E. Leiter, "Some Factors Affecting the Plastic Deformation of Sheet and Strip Steel and Their Relation to Deep Drawing Qualities", *TRANSACTIONS, American Society for Metals*, Vol. 25, 1937, p. 163.
4. J. D. Jevons, "The Metallurgy of Deep Drawing and Pressing", John Wiley and Sons, 1946, p. 211, 238.
5. A. N. Holden, "Dislocation Collision and the Yield Point of Iron", *Journal of Metals*, Vol. 4, February 1952, p. 182.
6. G. Sachs, "Principles and Methods of Sheet Metal Fabricating" (Book), Reinhold Publishing Co., 1951.
7. H. K. Work and G. H.ENZIAN, "Effect of Deoxidation on the Strain-Sensitivity of Low Carbon Steels", *Transactions, American Institute of Mining and Metallurgical Engineers*, Vol. 162, 1945, p. 723.
8. H. F. Beeghly, "Determination of Aluminum Nitride Nitrogen in Steel", *Analytical Chemistry*, Vol. 21, December 1949, p. 1513.
9. W. Eilender, H. Cornelius and H. Knuppel, *Archiv für das Eisenhüttenwesen*, Vol. 8, May 1935, p. 507.
10. S. Harper, "Precipitation of Carbon and Nitrogen in Cold-Worked Alpha Iron", *Physical Review*, Vol. 83, Aug. 15, 1951, p. 709.
11. J. W. Halley, "Grain Growth Inhibitors in Steel", *Transactions, American Institute of Mining and Metallurgical Engineers*, Vol. 167, 1946, p. 224.

DISCUSSION

Written Discussion: By C. W. Beattie, R. L. Kenyon and R. H. Heyer, Armco Steel Corp., Middletown, Ohio.

Studies of strain aging are always of interest because of the continuing use of large tonnages of rimmed steel sheets.

Investigations at Armco of aging of both rimmed and aluminum-killed steels have resulted in data which supplement those in the paper. These tests include various degrees of cold rolling up to 10%, room temperature aging up to 21 years, and accelerated aging at 212 and 400 °F.

Results pertaining to stretcher straining of low carbon rimming steel are summarized in Table II. These data are taken from tests which were reported in part in 1933.² The room temperature aging tests were carried further to a total time of 16 years. The elevated temperature tests were made in an oil bath thermostatically controlled to ± 2 °F.

Table II
Time for Return of Stretcher Straining in Tensile Test Specimens After Cold Rolling Low Carbon Rimming Steel

Cold Rolling, %	Approximate Time for Return of Stretcher Straining at Various Aging Temperatures		
	Room Temp.	212 °F	400 °F
1	1 month	10 min.	1 min.*
2	3 months	30 min.	1 min.*
3	6 months	3 hrs.	1 min.*
6	16 years	1 day	5 min.*
10	†	3 days	10 min.

*Immersed in 400 °F oil bath for total time of 1 minute—sample required 1 minute to come to temperature.

†No stretcher straining at 16 years.

²R. O. Griffis, R. L. Kenyon and R. S. Burns, "Aging of Mild Steel Sheets", *Yearbook, American Iron and Steel Institute*, 1935, p. 142.

In the authors' Fig. 9, 1 month of room temperature aging is equivalent to about 30 minutes at 212 °F. The Griffis, Kenyon, Burns data for 1% temper rolling show 1 month of room temperature aging to be equivalent to 10 minutes at 212 °F. It is not clear from the paper what amount of cold rolling was applied to the authors' samples. Their method of heating the samples raises a question as to whether specific test locations on the specimens were held at a uniform temperature for the indicated lengths of time. These factors should be clarified before a direct comparison of the data is made.

The Griffis, Kenyon, Burns data for greater amounts of cold rolling are in agreement with a statement in the paper that increased temper rolling increases the time required for the return of stretcher straining. This agrees with years of practical experience in producing sheets for specific applications.

The mechanical properties of the rimmed steel (results not tabulated) changed up to 3 months of room temperature aging, but there was little change between 3 months and 16 years.

A better understanding of Fig. 5 of the paper is obtained when the normal relationship between grain size and yield point elongation in the dead soft condition is taken into account. Coarse-grained steel may have little more than 1.25% (0.025 inch in 2-inch gage length) yield elongation before temper rolling; therefore would naturally take a long time to return to this level after temper rolling and aging. On the other hand, a fine-grained steel, which may have 5.0% yield point elongation initially, would only have to regain one-fourth of this in order to age to the level used in Fig. 5; hence the time required would naturally be much less than in the case of the coarse-grained steel.

Our tests of aluminum-killed stabilized steels over a period of 21 years have shown no change in mechanical properties from those of the fresh temper-rolled samples, even though accelerated aging indicated lack of complete stability at 400 °F. We note in the authors' Fig. 10 the slight increase in hardness in room temperature aging of their aluminum-killed steel. While we have observed a similar result in some of our tests, the tensile properties, including yield point, per cent elongation, and yield point elongation, do not show any change whatever. Typical results for our aluminum-killed stabilized material temper-rolled ½% are shown in

Table III
Mechanical Properties of Aluminum-Killed Stabilized Steel Aged at Room Temperature After Temper Rolling ½%

Aging Time	Yield Str. psi.	Tensile Str. psi.	Elong. in 2 Inches %	Y.P. Elong. %	RB
Fresh	25,850	44,900	43.5	0.0	41
1 week	25,700	44,200	43.5	0.0	41
1 month	23,900	44,600	42.0	0.0	42.5
3 months	24,800	44,550	43.0	0.0	42.5
6 months	24,550	44,500	43.5	0.0	43
1 year	25,750	45,200	44.5	0.0	42
2 years	25,100	45,200	43.5	0.0	43
5 years	24,100	45,250	44.0	0.0	43
10 years	25,050	44,600	43.5	0.0	43.5
15 years	24,400	43,600	44.0	0.0	43
21 years	24,700	44,650	45.0	0.0	43.5

Table III. Similar results were obtained after rolling 1, 1½, 2, and 2½%.

Additional data correlating aging and yield point return for four aluminum-killed stabilized steels are given in Table IV. In the case of materials 83 and 88 which developed a slight return of yield point elongation after 15 years, no significant change in the yield point or other tensile properties was found, nor was there any tendency toward development of stretcher straining.

Table IV
Effect of Room Temperature and Accelerated Aging on Yield Point Return of Aluminum-Killed Stabilized Steels

Material	Temper Rolling %	Yield Point Elongation After Aging at Various Temperatures					
		Room Temp.		212 °F		400 °F	
		Time	Y.P. El., %	Time	Y.P. El., %	Time	Y.P. El., %
79	1	15 yrs.	0	6 days	0	10 min.	0
83	¾	5 yrs.	0	1 day	0.7	1 min.	1.0
	¾	15 yrs.	0.7	6 days	0.7	10 min.	2.6
87	¾	15 yrs.	0	6 days	0.4	1 min.	0.6
	¾					10 min.	1.5
88	½	15 yrs.	0.5	6 days	0.4	1 min.	0.8
	½					10 min.	2.6

We do not find mention in the paper of processing variables, which have long been known to have a strong influence on strain aging characteristics. It was disclosed in the Hayes-Griffis patent³ that annealing temperature and cooling rate were also important factors in the production of nonaging (stabilized) killed steels.

Written Discussion: By N. H. Polakowski, Metallurgical Department, University College, Swansea, England.

The comprehensive data presented in the paper will undoubtedly prove of use to those engaged in the manufacture and testing of sheet steel. It would be helpful, however, if the authors could specify in some detail the condition of their temper rolling, such as: diameter and surface condition of rolls, whether the material was skin-passed in sheared lengths or in coils, and whether it was leveled after rolling. All these factors may affect to a certain extent the mechanical characteristics of the sheet both before and after aging.

The writer's own experience lends support to Jevons' statement that increasing severity of temper rolling retards the return of a jogged yield point upon aging. Unfortunately, this advantage is largely offset by the relatively small residual ductility of a low carbon sheet which has been rolled 5% or more and aged afterwards. For many purposes this will certainly be regarded as a major defect.

The shape of the curve in Fig. 5 is interesting. It appears as if its slope is uniform as long as the grain size is less than 8, but that it becomes asymptotic for still finer-grained material. In this connection the writer would be grateful for the authors' comment on the following points:

(a) Was the yield point completely eliminated by temper rolling in all the samples, including the two lowest ones (grain 10 and 12) prior to the aging experiments?

³A. Hayes and R. O. Griffis, U. S. Patent No. 2,069,758, Feb. 9, 1937, "Ferrous Metal and Process for Producing Same".

(b) Could the authors reproduce the grain size versus yield elongation diagram in the as-annealed condition for this batch of steels?

It is appropriate to recall that some years ago Andrew and Lee (*Journal, Iron and Steel Institute*, Vol. 145, 1942, p. 153) have produced curves of a very similar shape (loc. cit. Figs. 34 and 35). The "knee" on their diagrams corresponds to 50/60 grains per linear millimeter, this being equivalent to No. 8/9 on the ASTM scale. While this agreement with the present results may be a matter of coincidence, it is not unlikely that it may contain something of importance for the understanding of the fundamental nature of the yield point effect in carbon steel.

Authors' Reply

We wish to express our appreciation to Messrs. Beattie, Kenyon and Heyer, and to Mr. Polakowski for their interesting discussions.

The samples employed in this work were obtained from 20-inch wide center portions of sheets (0.030 to 0.050 inch thick) that had been box-annealed at 1300 °F for 25 to 40 hours. The sheets were skin-rolled 0.4 to 1.8% in a four-high mill with 20-inch diameter grit-blasted work rolls and roller leveled immediately upon emerging from the temper mill. Tensile tests were made within 6 hours after skin rolling. Several of the steels exhibited slight yield points including the two samples with intercept grain sizes of 10 and 12. We cannot state with certainty, however, whether the yield points had been incompletely eliminated by skin rolling or had appeared during the few hours before the initial tensile tests were made.

The correlations of natural and accelerated strain aging shown in Fig. 9 of the text and Table II of the discussion differ mainly because the test results in Fig. 9 are based on total heat treating time. We have found in calibrating the furnace that test strips of 0.030 to 0.050 inch thickness require about 15 to 20 minutes to adequately assume the temperature gradient. The nature of gradient furnace heating causes differences in the time at which various points along test strips attain proper temperature. The method used at Armco is better adapted to precise temperature measurement.

The alternate explanation offered by the discussers in regard to Fig. 5 is stated in terms which might be considered capacity of yield point elongation or stretcher strain susceptibility. This interpretation suggests that slightly increased grain size of rimmed steels is desirable from the standpoints of degree and rate of yield elongation return. Their interpretation for Fig. 5 could also apply to Fig. 4 in which rate of age hardening is plotted.

There are no data available concerning the as-annealed yield elongation values for this series of steels. In other work, we have found that large yield elongation values are generally associated with rimmed steels having fine ferrite grains.

The stability of aluminum-killed steels is widely recognized. Changes in hardness of naturally aged material are small—often insignificant. In the stabilized steels tested, a change in the proportional limit occurred. This increase appeared related to the amount of nitrogen not combined with aluminum or vanadium. Greater changes in the stress-strain characteristics were noted in steels with larger amounts of active nitrogen.

SOME PROPERTIES OF A NODULAR IRON AT ELEVATED TEMPERATURES

BY M. S. SAUNDERS AND M. J. SINNOTT

Abstract

Short-time tensile data over the temperature range of 800 to 1200 °F (425 to 650 °C) are presented for a typical nodular iron in two conditions: as-cast and partially annealed. Elevated temperature impact data for various exposure times over the same temperature range are presented. Stress-rupture data at 1200 °F (650 °C) for the iron in both conditions are included. Comparison is made with the same properties of killed carbon steel and with carbon-molybdenum steel. From the data, it appears that the properties of the nodular iron are comparable in some respects to the properties of the steels.

PUBLISHED data on the high temperature properties of cast irons are very meager, principally because of lack of interest in a material which possesses negligible plasticity. This in itself is not too severe a drawback to its use, since in many applications the metal may not be required to undergo any plastic deformation during installation or use, but lack of good reproducibility coupled with low impact strength necessitates the use of low design stress which militates against the use of cast iron. The appearance of nodular cast iron should change this picture to some degree because of its ability to plastically deform, even in the as-cast condition. Since data on the behavior of the nodular cast irons at elevated temperatures were not available, it was felt that some indication of its properties should be obtained for possible use in engineering applications.

It is obvious that nodular iron is by its nature a more complex material than steel. Structurally, it is somewhat comparable in that it may consist of ferrite, pearlite, cementite, tempered structures and transformation products, but in addition it contains nodular graphite. The amount and the distribution of this graphite can and does vary quite markedly. In addition, the chemical analysis of this type of iron can be varied over considerable limits and this can be expected to affect the properties. In view of these facts, it should be emphasized that the results presented in this paper are merely indicative of part of the range of values that might be obtained, and they can-

A paper presented before the Thirty-fourth Annual Convention of the Society, held in Philadelphia, October 18 to 24, 1952. Of the authors, M. S. Saunders is a graduate student, Metallurgical Engineering, and M. J. Sinnott is associate professor, Chemical and Metallurgical Engineering, University of Michigan, Ann Arbor, Mich. Manuscript received April 8, 1952.

not be said to represent either the optimum or the minimum properties for all types and treatments of nodular iron.

MATERIAL

All of the data presented in this paper were obtained from the same billet of a nodular nickel-iron. The billet shape and analysis are shown in Fig. 1. The billet was supplied by a commercial foundry, and the melting practice, method of gating, etc., is unknown. Prior to delivery, the billet had been slowly heated to 600 °F (315 °C), held for 48 hours, then slowly cooled; presumably this was a stress-relief treatment.

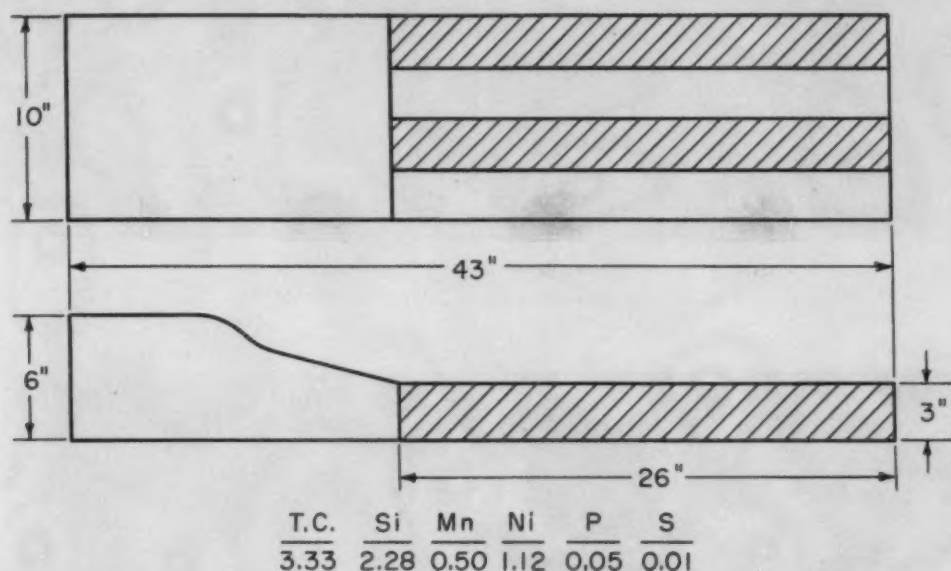


Fig. 1—Nodular-Iron Casting. Cross-hatched areas were machined into test specimens.

The section size of this casting is somewhat larger than sizes for which room temperature test data are readily available, but it was believed to be better to investigate material from the same casting rather than to try to prepare similar specimens from a series of smaller castings. The material used for testing was taken from the sections that are cross-hatched in Fig. 1. The analysis of this iron shows that the manganese, nickel and phosphorus contents are a little higher than is usual in nodular irons but not enough to invalidate the test results.

The microstructure of this material, termed the "as-cast" in this paper, is shown in Figs. 2 and 3. It is chiefly a pearlitic structure with some areas of ferrite occurring adjacent to the graphite nodules. The casting, in spite of its size, was remarkably uniform and showed no excessive bull's-eye patterns as might have been expected.

It was initially intended to evaluate this iron in the as-cast and

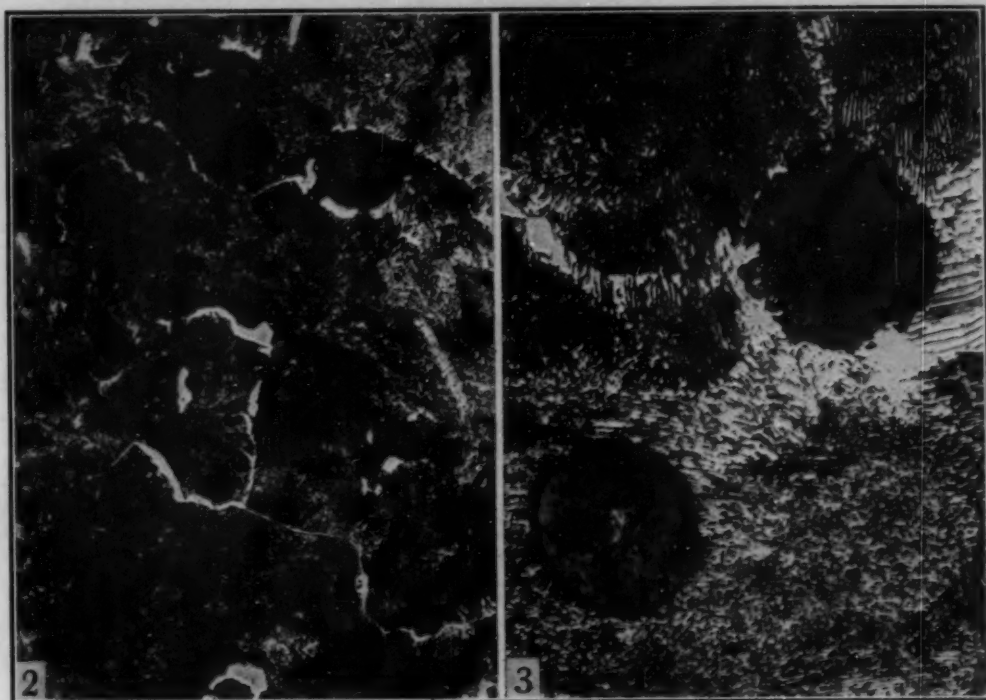


Fig. 2—As-Cast Structure. Picral etch. $\times 100$.

Fig. 3—As-Cast Structure. Picral etch. $\times 500$.

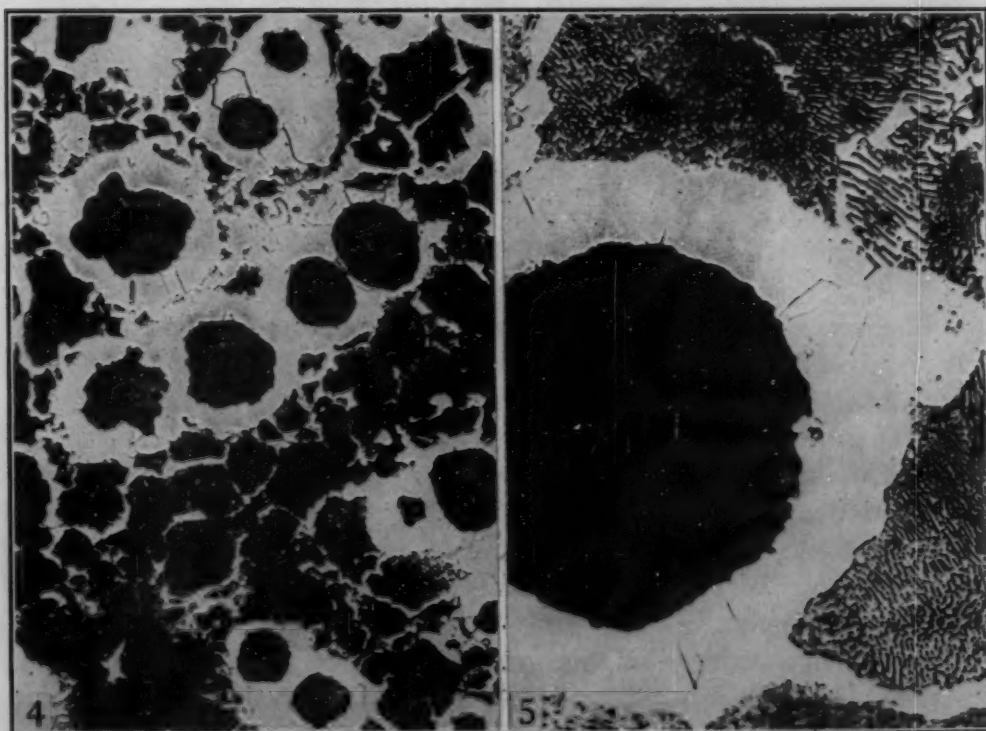


Fig. 4—Partially Annealed Structure. Picral etch. $\times 100$.

Fig. 5—Partially Annealed Structure. Picral etch. $\times 500$.

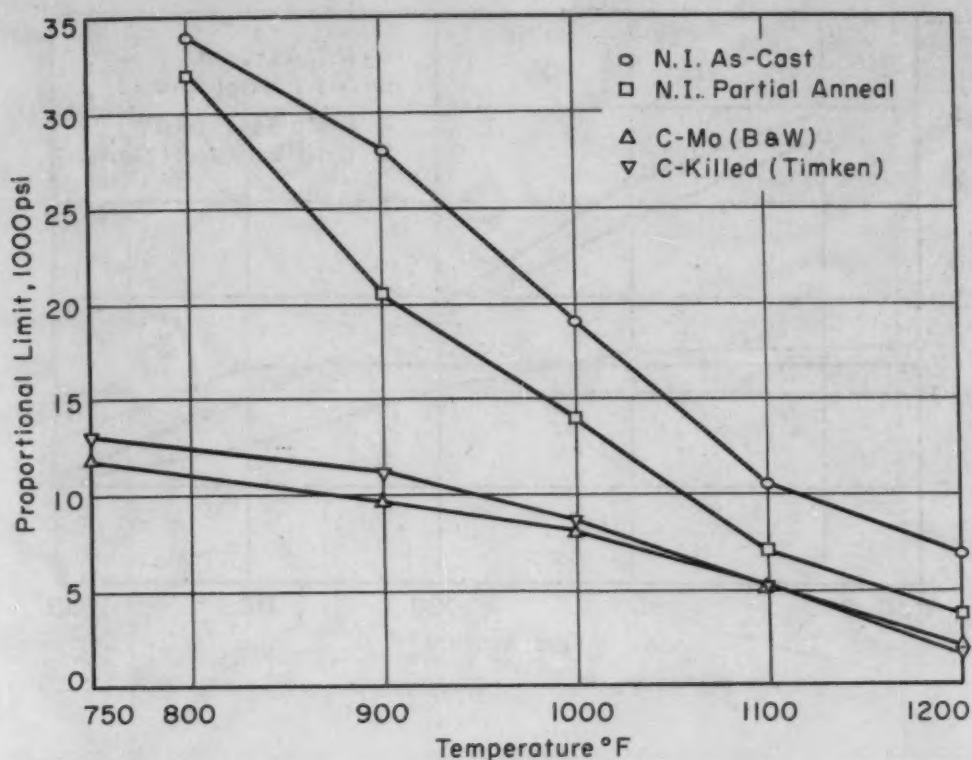


Fig. 6—Proportional Limit Versus Temperature.

as the fully annealed material. To obtain a fully annealed structure the iron was heated to 1650 °F (900 °C), held for 4 hours, furnace-cooled 50 °F per hour to 1200 °F (650 °C), then furnace-cooled to room temperature. This treatment produced the structures of Figs. 4 and 5. This is only a partially annealed structure, but since the work was exploratory it was decided to test the material in this condition.

EXPERIMENTAL PROCEDURES

The following tests on the nodular iron in the as-cast and partially annealed conditions were performed:

Tensile Tests at 80, 800, 900, 1000, 1100 and 1200 °F
(25, 425, 480, 540, 595 and 650 °C)

Impact Tests at 80, 800, 1000 and 1200 °F (25, 425, 540 and 650 °C)
for exposure periods of 1, 100 and 1000 hours.

Stress-Rupture Tests at 1200 °F (650 °C).

Tensile Tests

All tensile tests were carried out on standard 0.505-inch diameter test specimens. The room temperature stress-strain data were obtained with SR-4 strain gages, while the elevated temperature test data were obtained by the use of a modified Martens type of optical

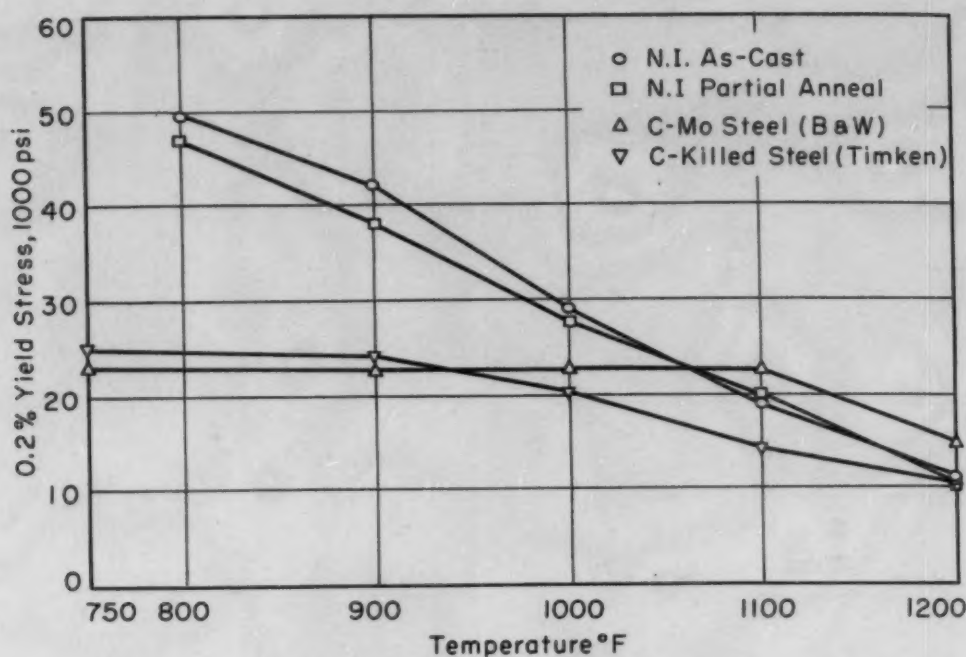


Fig. 7—Yield Stress Versus Temperature.

Table I
Summary of Tensile Test Data

Material	Test Temp. °F	Prop. Limit psi	0.2% Yield psi	Ult. Str. psi	% Elong. in 2 Inches	% R. A.	Young's Mod. psi × 10 ⁶	Brinell Hard- ness
As-Cast	70	46,250	59,750	74,900	3.0	...	25.00	245
As-Cast	800	34,000	50,000	72,800	3.0	4.4	20.25	...
As-Cast	900	28,000	42,000	51,000	1.0	...	19.85	...
As-Cast	1000	19,000	29,000	40,600	3.0	5.5	13.60	...
As-Cast	1100	11,000	19,000	28,800	6.5	7.5	11.70	...
As-Cast	1200	7,000	11,700	17,550	11.0	14.0	5.71	...
Part. Ann.	70	35,000	61,500	80,000	2.5	...	25.00	216
Part. Ann.	800	32,000	46,700	73,400	4.5	5.0	22.10	...
Part. Ann.	900	20,500	37,700	48,200	3.0	3.0	19.55	...
Part. Ann.	1000	14,000	28,000	41,100	3.5	4.5	14.70	...
Part. Ann.	1100	7,000	19,200	27,300	6.0	6.0	12.45	...
Part. Ann.	1200	4,000	11,000	14,900	11.0	11.0	5.70	...
Full Anneal	70	33,000	49,750	63,600	6.0	7.0	25.00	116

extensometer. The sensitivity of measurement in both types is on the order of three millionths of an inch per inch. With minor exceptions, the tests were carried out in accordance with the specifications given in ASTM E-21-43 which governs the procedure to be used in making short-time tensile tests.

Table I presents the pertinent data obtained or derived from this series of tensile tests. The various mechanical properties are plotted as functions of temperature in Figs. 6 to 9. For comparative purposes the similar data on carbon-molybdenum steel (1)¹ and carbon-killed steel (2) are included in these plots.

¹The figures appearing in parentheses pertain to the references appended to this paper.

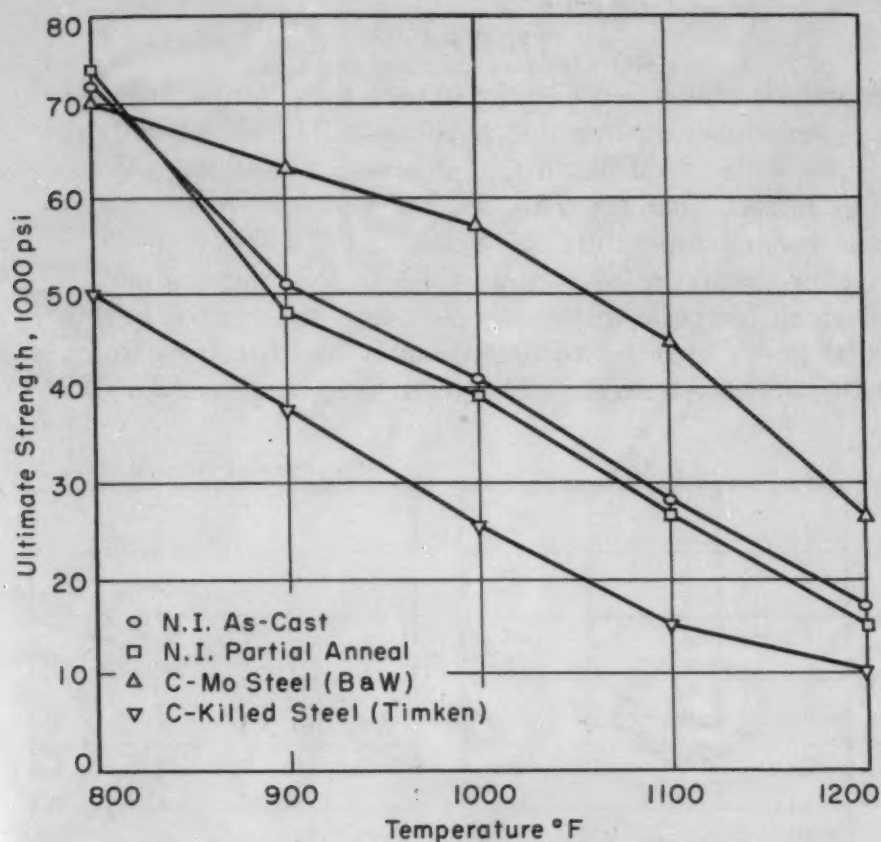


Fig. 8—Ultimate Strength Versus Temperature.

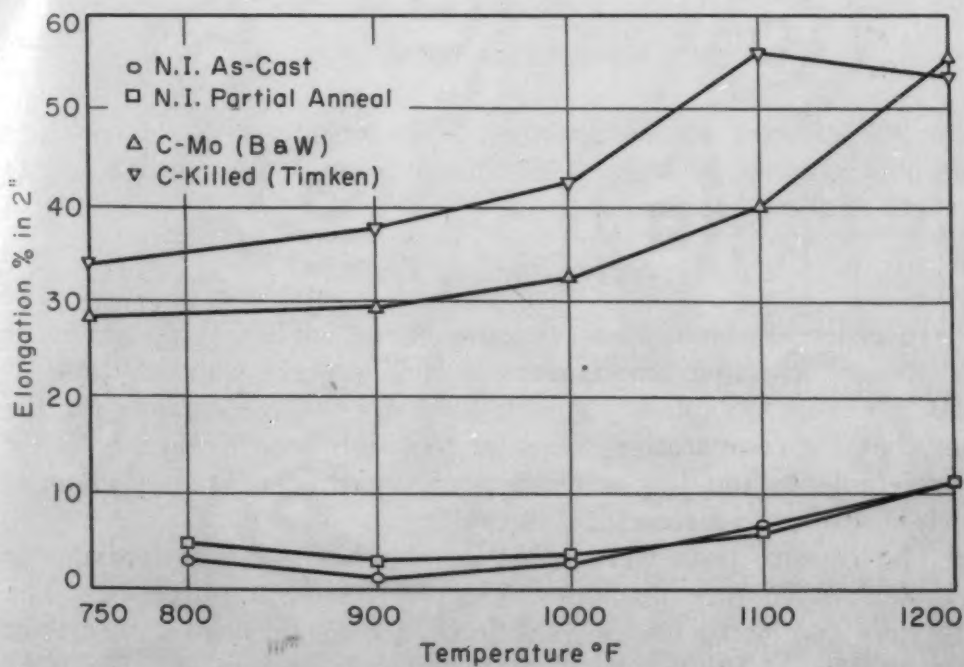


Fig. 9—Per Cent Elongation Versus Temperature.

Impact Tests

Standard unnotched Charpy impact bars, 10 by 10 by 55 millimeters, were made up for test purposes. The unnotched bars were used, since it has been found that this type of specimen is more sensitive to impact changes than the notched specimens. Tests were made at room temperature, 800, 1000 and 1200 °F (425, 540 and 650 °C) on both the as-cast and on the partially annealed irons. The elevated temperature tests were made after exposure for 1, 100 and 1000 hours in order to determine if structural instability would affect the impact strength. The tests were made on an Olsen ma-

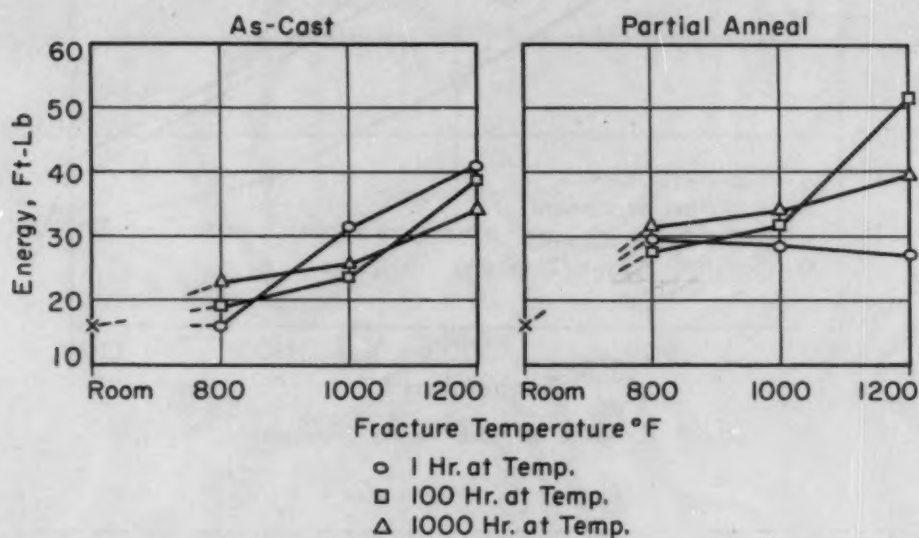


Fig. 10—Impact Strength Versus Temperature.

chine set adjacent to the furnaces. The results of these tests are presented graphically in Fig. 10. Each point is the average impact strength of three specimens.

Stress-Rupture Tests

In order to obtain some measure of the load-carrying ability of the irons at elevated temperatures, stress-rupture data at 1200 °F (650 °C) were obtained. This is an extreme temperature for the irons, but for comparative purposes too high a temperature of test is preferable to too low a temperature, particularly in a material which is subject to a structural instability.

The rupture tests were made on standard 0.505-inch diameter specimens in rupture machines designed for such purposes. The tests were conducted under conditions of constant load rather than constant stress. The results of these tests are presented in Table II and the stress-rupture curves are given in Fig. 11.

Table II
Stress-Rupture Data at 1200 °F (650 °C)

Material	Stress psi	Frac. Time hrs.	% Elong. in 2 Inches	% R. A.	Brinell Hardness
Part. Ann.	14,900	STT	11.0	11.0	195
Part. Ann.	8,500	5.2	29.5	19.0	156
Part. Ann.	6,000	13.7	13.0	11.5	142
Part. Ann.	4,500	22.6	17.5	9.5	130
Part. Ann.	3,000	284.4	19.0	7.5	126
Part. Ann.	2,700	404.8	15.0	10.0	118
Part. Ann.	2,400	1,272.0	15.0	17.2	120
As-Cast	17,550	STT	11.0	14.0	212
As-Cast	10,500	2.8	26.0	19.4	156
As-Cast	9,800	7.0	12.0	16.0	160
As-Cast	6,000	46.0	15.5	17.0	135
As-Cast	4,900	38.0	5.7	7.5	152
As-Cast	4,200	110.0	18.0	16.0	135
As-Cast	3,020	830.0	8.0	5.0	135

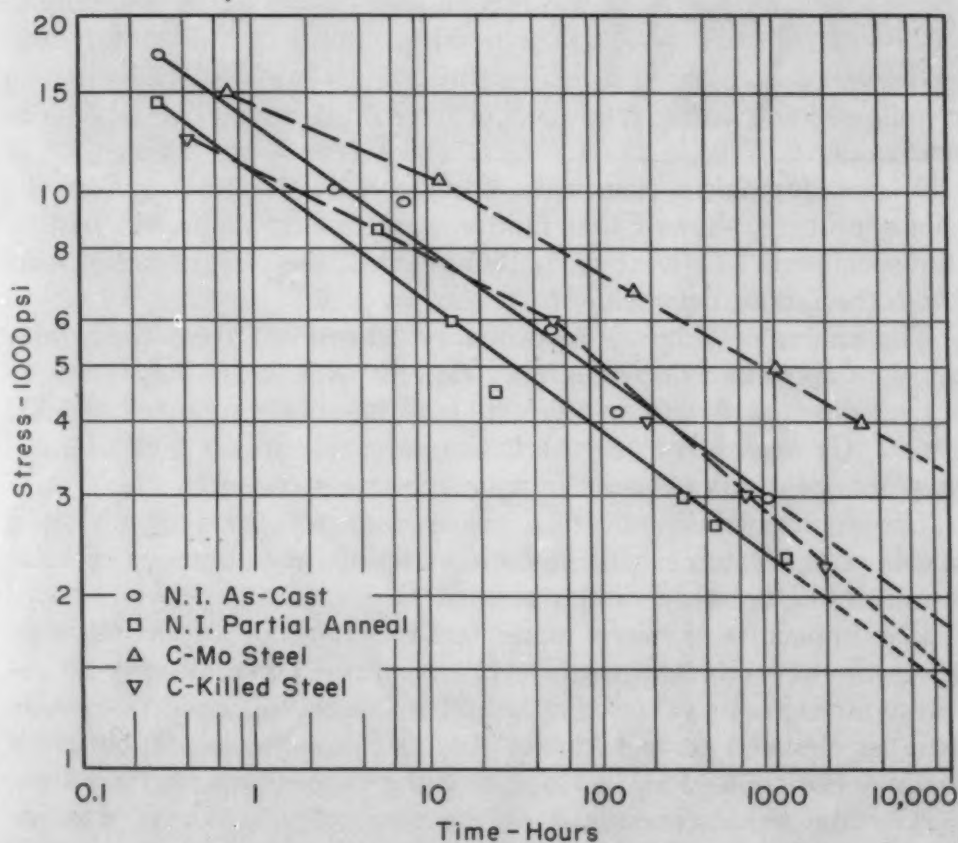


Fig. 11—Stress-Rupture Curves at 1200 °F (650 °C).

DISCUSSION OF RESULTS

The data on the tensile properties of the nodular irons are somewhat misleading. It would appear that the proportional limit and 0.2% yield strengths are considerably better than the same properties of the steels. While this is true, it should be realized that the nod-

ular irons are not stable and that if held for a sufficiently long time period, particularly at the higher temperatures, it would break down to graphite and ferrite and show a lower strength. None of the short-time tensile structures showed any indication of graphitization during this test, but specimens used to test impact strength and rupture strength did show this structural instability.

The ductility of the material as measured by the per cent elongation in 2 inches is obviously lower than the similar values for the steels and appears to reach a minimum at 900 °F (480 °C). The room temperature ductility of this material is lower than the normal values for nodular irons, and this can be traced to the higher manganese and phosphorus content of the iron. Vennerholm et al (3) report that ductility is decreased if the manganese content exceeds 0.30% or if the phosphorus content exceeds 0.04%. It is believed that the lower ductilities at the higher temperatures are traceable to this same cause. In any case a pearlitic matrix would not be expected to show a great deal of ductility. The per cent reduction in area followed the same trend as that developed in the per cent elongation values.

A metallographic examination of each of the fractures of the tensile specimens showed that failure was transcrystalline in nature. In the specimens that were partially annealed, the path of failure was through the ferrite network.

The values of Young's modulus as determined from the stress-strain data appear to decrease more rapidly with increasing temperature than do similar data on steels (4). The values reported at 1200 °F (650 °C) are not of very high accuracy, due to the lack of sufficient points below the elastic limit on the stress-strain curve.

The reproducibility of the tensile data was very good, since duplicate samples were run on both materials at a number of temperatures and gave very similar results.

The impact tests were made for the purpose of determining whether the effect of temperature or structural instability would reduce the strength to values that would make the material unsuitable for use at elevated temperatures. In all cases the impact strength of the material showed an increase over the room temperature values. Generally the values increased as the temperature of test was increased from 800 to 1200 °F (425 to 650 °C) and showed no minimum in the range of 900 to 1000 °F (480 to 540 °C) as do the carbon-molybdenum and carbon-killed steel. Since these tests were on unnotched bars, the impact values should not be compared directly with the values obtained on steel notched bars.

The time held at temperature did not seem to affect the impact strength of the as-cast material to any appreciable extent. This is somewhat surprising in view of the fact that the structures at the



Fig. 12—Fracture Structure, As-Cast Iron, 830 Hours at 1200 °F (650 °C). Picral etch. $\times 250$.

end of the stated holding periods, particularly at 1200 °F (650 °C), were different. The specimen held for 1 hour was pearlitic, the one held for 100 hours was mostly ferritic but did have some pearlite present, and the specimen held for 1000 hours was completely ferritic. The partially annealed specimens showed essentially the same impact strength as the as-cast material except that the specimens held for 1 hour at temperature did not show an increase in strength with an increase in temperature at the 1200 °F (650 °C) level. This was probably due to the ferritic network which did not have an opportunity to grow.

Rupture data at 1200 °F (650 °C) are probably not of too much value from a design standpoint, but because the nodular iron eventually reaches an equilibrium structure at this temperature it enables one to compare its properties with other materials. From the stress-rupture plots it is apparent that the partially annealed iron does not have the load-carrying ability of the as-cast iron, although the difference is not great. There are two possible explanations for this behavior: one is grain size and the other is the degree of structural instability. The prior heat treatment given the partially annealed iron refined the grain size and resulted in a weaker material. The prior treatment also produced a material which was relatively more unstable than the as-cast structure and subsequent testing at 1200 °F (650 °C) allowed the structure to proceed more rapidly to its equi-

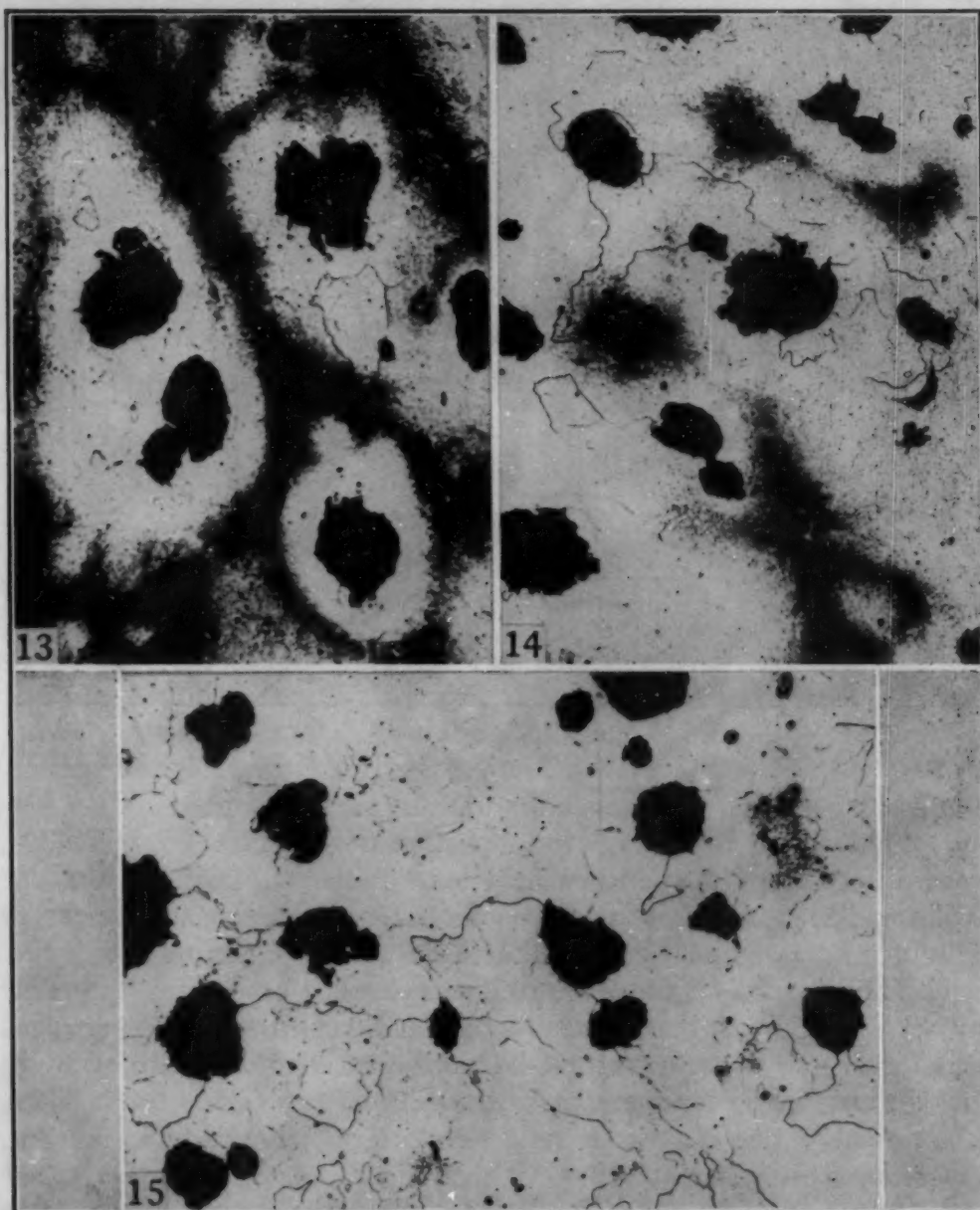


Fig. 13—Structure of As-Cast Iron Rupture Specimen, 2.8 Hours at 1200 °F (650 °C). Picral etch. $\times 100$.

Fig. 14—Structure of As-Cast Iron Rupture Specimen, 7 Hours at 1200 °F (650 °C). Picral etch. $\times 100$.

Fig. 15—Structure of As-Cast Iron Rupture Specimen, 830 Hours at 1200 °F (650 °C). Picral etch. $\times 100$.

librium during testing. Metallographic examination showed that both of these factors had influenced the results.

General scaling at 1200 °F (650 °C) was severe in both conditions, but it was of a uniform type of attack with oxygen penetration to the graphite nodules occurring to a minor extent. No intergranular oxidation occurred, but failure was intergranular as is shown in Fig. 12.

The structural instability that occurred in both conditions was the disappearance of the pearlite during testing at 1200 °F (650 °C). This occurred first in the areas surrounding the graphite nodules and was complete after 10 to 15 hours at temperature and under stress. Spheroidization of the pearlite did not occur prior to its diffusion and breakdown to ferrite and graphite. To indicate the process of this breakdown, several photomicrographs of the as-cast rupture specimens are shown in Figs. 13, 14 and 15. The rupture specimens had less pearlite remaining after exposure to temperature than the impact specimens held for the same time periods. This would indicate that the stress assists in the breakdown of the pearlite. This same structural instability occurs at lower temperatures but not to the same degree, as could be noted from examination of the impact specimens.

The ductility of the materials under long-time exposure under stress showed considerable improvement over these same values as determined from the short-time tensile tests. This is due to the disappearance of the pearlitic matrix. There is some variability in the actual values of individual tests, but this is to be expected in a heterogeneous system.

CONCLUSIONS

Except for ductility, the nodular iron tested has short-time tensile properties that are equal to or better than similar properties in carbon-molybdenum or carbon-killed steels.

The high temperature impact strength of the nodular iron is better than the room temperature strength but is not as good as the steels.

The stress-rupture strength at 1200 °F (650 °C) is comparable to that obtainable in carbon-molybdenum or carbon-killed steels.

References

1. "Digest of Steels for High Temperature Service", Timken Roller Bearing Company, Canton, Ohio, 5th Edition, 1946.
2. "Properties of Carbon and Alloy Steel Tubing for High Temperature-High Pressure Service", The Babcock & Wilcox Tube Company, Beaver Falls, Pa. Technical Bulletin 6-D, 5th Edition.
3. C. W. Andrews, "Effect of Temperature on the Modulus of Elasticity", *METAL PROGRESS*, Vol. 58, 1950, p. 85.
4. G. Vennerholm, H. N. Bogart and R. B. Melmoth, "Nodular Iron", *Journal*, Society of Automotive Engineers, Vol. 58, 1950, p. 31.

DISCUSSION

Written Discussion: By R. E. Savage, metallurgist, Development and Research Division, The International Nickel Co., Inc., New York.

The authors have presented an excellent as well as a very informative paper on the mechanical properties of ductile iron at elevated temperatures.

The data presented in this paper should do much to stimulate further research with ductile iron in the elevated temperature field of metallurgy.

I should like to discuss the value given by the authors for the elongation of fully annealed ductile iron at 70 °F. The authors have shown the per cent elongation in 2 inches of the fully annealed ductile iron which they tested at 70 °F to be 6.0%. This value is given in Table I, entitled "Summary of Tensile Test Data". This value is far below the average value normally obtained for annealed ductile iron. Large tonnages of ductile iron are currently being produced commercially. Extensive mechanical tests have been made on annealed ductile iron having the following range of chemical composition which includes the chemical composition of the ductile iron used in this investigation:

	Carbon	Silicon	Manganese	Phosphorus	Nickel
Annealed Ductile Iron	3.3-3.8	2.2-2.8	0.25-0.75	0.10 max.	0.5-2.0

The mechanical tests made at room temperature gave the following range of mechanical properties for the range of ductile iron chemical compositions listed above:

	Tensile Strength in psi	Yield Point in psi	Elongation % in 2 Inches	Brinell Hardness
Annealed Ductile Iron	65-75,000	50-60,000	17-23%	140-180

These data would indicate that there is some reason other than chemical composition which is responsible for the low value of elongation reported by the authors for the fully annealed ductile iron tested at room temperature.

Since all test bars used in this investigation were machined from the same billet of ductile iron, it is quite possible that the billet was not composed of sound metal throughout its entire length. If internal porosity or shrinkage is present in certain areas of the billet, it would undoubtedly be a contributing factor to the low value of elongation of annealed ductile iron at room temperature as reported by the authors. Elongation is one of the mechanical properties which is greatly affected by small amounts of internal shrinkage.

Written Discussion: By Harry Majors, Jr., California Research and Development Co., Livermore, Calif.

This paper is a welcome addition to our increasing knowledge on the properties of nodular cast iron. As time goes by, the need will increase for a more systematic method of obtaining properties of new materials for evaluation in engineering design.

At room temperature the optimum properties of nodular nickel iron are obtained with this approximate chemical composition in the as-cast condition: carbon, 3.25 to 3.5%; silicon, 2.0%; manganese, 0.42 to 0.80%; phosphorus, 0.10%; nickel, 1.58 to 1.95%; magnesium, 0.07 to 0.10%.

Would the authors hazard a guess if such a composition is beneficial for optimum properties at elevated temperatures?

What is the influence of the nickel addition upon the elevated temperature properties?

Written Discussion: By Charles R. Wilks, metallurgist, American Brake Shoe Co., Mahwah, N. J.

With little previously published information on the properties of nodular irons at elevated temperatures, this paper, reporting exploratory

studies, should serve to stimulate further work along similar lines.

American Brake Shoe Co. has in progress a testing program to obtain creep and stress-rupture properties of ferritic, pearlitic, and austenitic nodular irons in the temperature range of 600 to 1000 °F. A technical paper on this work is planned for next year.

The stress-rupture properties reported by the authors appear consistent with those which we have obtained, when due consideration is given to the markedly higher hot strength of pearlite in contrast to ferrite where temperatures are sufficiently low and/or rupture times sufficiently short that the pearlitic matrix remains essentially stable and graphitization is negligible. Under such conditions, a partially annealed (i.e. partly pearlitic, partly ferritic) nodular iron would be expected to be stronger than a fully annealed or ferritic type, but weaker than a fully pearlitic grade. This is confirmed by comparison of short-term rupture strengths (such as the stresses to produce rupture in 10 hours or less), although little more than qualitative comparisons can be made because of the necessity of extended extrapolation of our test data to the higher temperature used by the authors.

Consideration of 100-hour and 1000-hour rupture strengths of their partially annealed and our fully ferritic material, the latter by extrapolation, suggests however that the time required to reach the equilibrium condition completely, the result of complete graphitization of any pearlite present initially, may extend well beyond the 10 to 15 hours indicated by the authors on the basis of metallographic examination. The 100-hour rupture strength of the partially annealed material is still very much higher than we estimate would obtain for a fully annealed grade, although the difference is not as great as prevailed in the 10-hour rupture strengths. The 1000-hour rupture strengths, however, are essentially comparable, the extrapolated value for our fully annealed type being only slightly lower than that indicated for the partially annealed material. A growth test at 1200 °F to show the progress of graphitization would be extremely enlightening, provided that oxidation does not becloud the issue.

Graphitization proceeds more slowly of course at 1000 °F as compared to 1200 °F. Only the most incipient stages of breakdown of the pearlite were evident in a stress-rupture specimen which fractured in 12.8 hours (and, in addition, was at temperature for 28 hours before loading). After an 1800-hour creep test on a companion specimen, however, the matrix was substantially ferritic. A 1000 °F growth test now in progress suggests that graphitization will be nearly complete in 1200 to 1400 hours.

The progressive weakening effect of this graphitization on the hot strength of pearlitic nodular iron is noteworthy. Comparison of pearlitic and ferritic nodular iron [both heat treated at 1650 °F, the former normalized (air-cooled) and the latter annealed (slow furnace cool with arrest at 1300 °F), so that comparable ferritic grain sizes should obtain in both conditions] showed that at the higher stresses associated with short fracture times (less than 24 hours), the pearlitic matrix persists and is markedly stronger than the ferritic material. Where there is sufficient time for graphitization to be effectively completed such as occurred in the lower-stress creep test that was discontinued after 1800 hours, the second-stage or minimum creep rate for the originally pearlitic grade differs only slightly

from that which obtains at the same stress for the grade which was ferritic at the start of the test. Graphically, there is a marked departure from linearity in the stress-rate plot for the pearlitic grade, and none for the ferritic grade. Tests are now in progress to substantiate the present indications that at stresses which will produce rates of the order of 0.0001% per hour (the basis of the customary limiting creep strength values), there will be no significant difference in the strength of the two grades.

At 800 °F, graphitization would be expected to proceed at a very slow rate. No evidence of graphitization was observed in a pearlitic specimen that was creep-tested at 800 °F for 1561 hours.

Authors' Reply

The authors would like to thank those who have so kindly contributed to the discussion of this paper.

Mr. Savage does have a point in that the ductility of the fully annealed iron is considerably less than values on such irons that have been published. On the other hand one of the larger commercial producers of this material has made a practice of casting test bars with each heat of this material and testing these bars in the as-cast and as the completely annealed material. His results show considerably lower values for ductility than those reported by Mr. Savage and are in line with the value we have reported. In the foundry tests, as well as in ours, internal shrinkage may have been a factor since the samples were not examined in a detailed fashion for this defect.

In answer to Mr. Majors' question the authors would say that in this material, as is the case with steels, the composition is only one of the many variables that might affect the high temperature strength. Generally one would not expect to find that an analysis which yields optimum properties at one temperature level would also yield optimum properties at other levels; particularly if there is an appreciable difference between the two temperatures. On the basis of our knowledge of the behavior of nickel in steels we would say that nickel is a ferrite strengthener at elevated temperatures but in these nodular irons it also assists in the breakdown of the carbide and from this standpoint it undoubtedly weakens the iron to the extent that this occurs.

The comments and data of Mr. Wilks are very welcome and the authors are looking forward to the publication of what is obviously a more extensive investigation than they attempted.

HARDNESS OF VARIOUS STEELS AT ELEVATED TEMPERATURES

BY F. GAROFALO, P. R. MALENOCK AND G. V. SMITH

Abstract

A hot hardness tester of the static loading type is described and the testing techniques developed are discussed. A number of different steels, including various types of 18 Cr-8 Ni stainless, plain carbon steels and an 8 Cr-1 Mo steel, have been tested at temperatures ranging from room temperature to 1500 °F. The results appear to indicate a general relation between hot hardness and creep- or creep-rupture strength, which, to a first approximation, is independent of structure or test temperature. A similar relation is observed between hot hardness and the ultimate tensile strength in short-time hot tensile tests.

WITH the ever-increasing demand for alloys to withstand higher and higher temperatures there exists a need for rapid, inexpensive tests to provide some indication of the probable mechanical properties and, under certain conditions, the performance of various materials at elevated temperatures. One such important property is hot hardness. The test methods which have been employed in determining hot hardness may be classified into two types, static and dynamic. The most important differences between these two types are rate of loading and duration of full load. In the dynamic test the loading is of impact nature and of extremely short duration, whereas in the static test, loading is much slower and the duration is at least of the order of seconds. Since the mechanical behavior of metals in the plastic range at elevated temperatures is greatly affected by the rate and duration of loading, it is not surprising that no correlation is found between results of these two methods.

Since the beginning of the century a great deal of work has been done on the hot hardness of various alloys (1-10)¹; however, a great deal of confusion has arisen because of lack of standardization of equipment or testing techniques. Little or no standardization has been achieved in dynamic hot hardness testing and it becomes impossible to correlate results of different dynamic hardness testers. A certain degree of standardization is evident in recent years among test methods of the static loading type.

¹The figures appearing in parentheses pertain to the references appended to this paper.

A paper presented before the Thirty-fourth Annual Convention of the Society, held in Philadelphia, October 18 to 24, 1952. The authors, F. Garofalo, P. R. Malenock and G. V. Smith, are associated with the Research Laboratory, United States Steel Co., Kearny, N. J. Manuscript received April 10, 1952.

Various refinements in determining hot hardness by the static loading method have been made since the early work of Brinell (1), in which the specimen was heated to the desired temperature and tested in a hardness tester whose indenter and anvil remained at room temperature. Large errors were undoubtedly introduced in the results obtained in this manner, since the sample was not only chilled in the contact area by the indenter but also lost heat to its surroundings. By heating both sample and indenter, these errors have been minimized; however, other difficulties, such as softening and scaling of the indenter, have been encountered. Tungsten carbide balls or Vickers-type diamond indenters have been found to give satisfactory service under certain conditions, while scaling of the sample has been minimized by testing under vacuum (9) or inert atmosphere (8).

Although these refinements make it possible to determine hot hardness with essentially the same accuracy and degree of reproducibility as in room temperature hardness testing (8, 9), it should be noted that further standardization is needed, especially concerning the duration of load application (14).

APPARATUS

The present apparatus enables the determination of the hot hardness of metals by heating both specimen and indenter² to the desired temperature in a virtually inert atmosphere, and by means of an automatic mechanism applying a deadweight load onto the indenter while in contact with the specimen. Following the loading cycle of fixed duration, the load is removed automatically. By rotating the cylindrical specimen after each loading and unloading cycle a number of impressions (maximum of 18) can be made at temperature while preserving the inert atmosphere. Following cooling to room temperature and removing the specimen from the apparatus, the hardness is measured as in the standard Vickers test. A photograph of the apparatus is shown in Fig. 1a and a schematic diagram in Fig. 1b.

The screw jack assembly, Fig. 1b, has a coarse adjustment which serves to elevate the rotating stage and anvil supporting the specimen until the liquid metal³ seal is formed at the lower end of the furnace tube. The fine adjustment elevates the specimen into testing position. The anvil is seated in the top of the screw jack assembly with its center of rotation slightly offset from the axis of the screw jacks. Since the indenter is aligned with the axis of the screw jacks, a series of impressions can be made on the specimen about its center by rotating the stage.

²A standard Vickers-type diamond indenter mounted with a high temperature binding agent was used initially, but was replaced, for reasons discussed later, by a sapphire indenter of the same type.

³Cerrolow, melting point 117 °F (see Metals Handbook, 1948 Edition, page 744), is used as the seal for test temperatures above 700 °F. Below this temperature mercury is used.

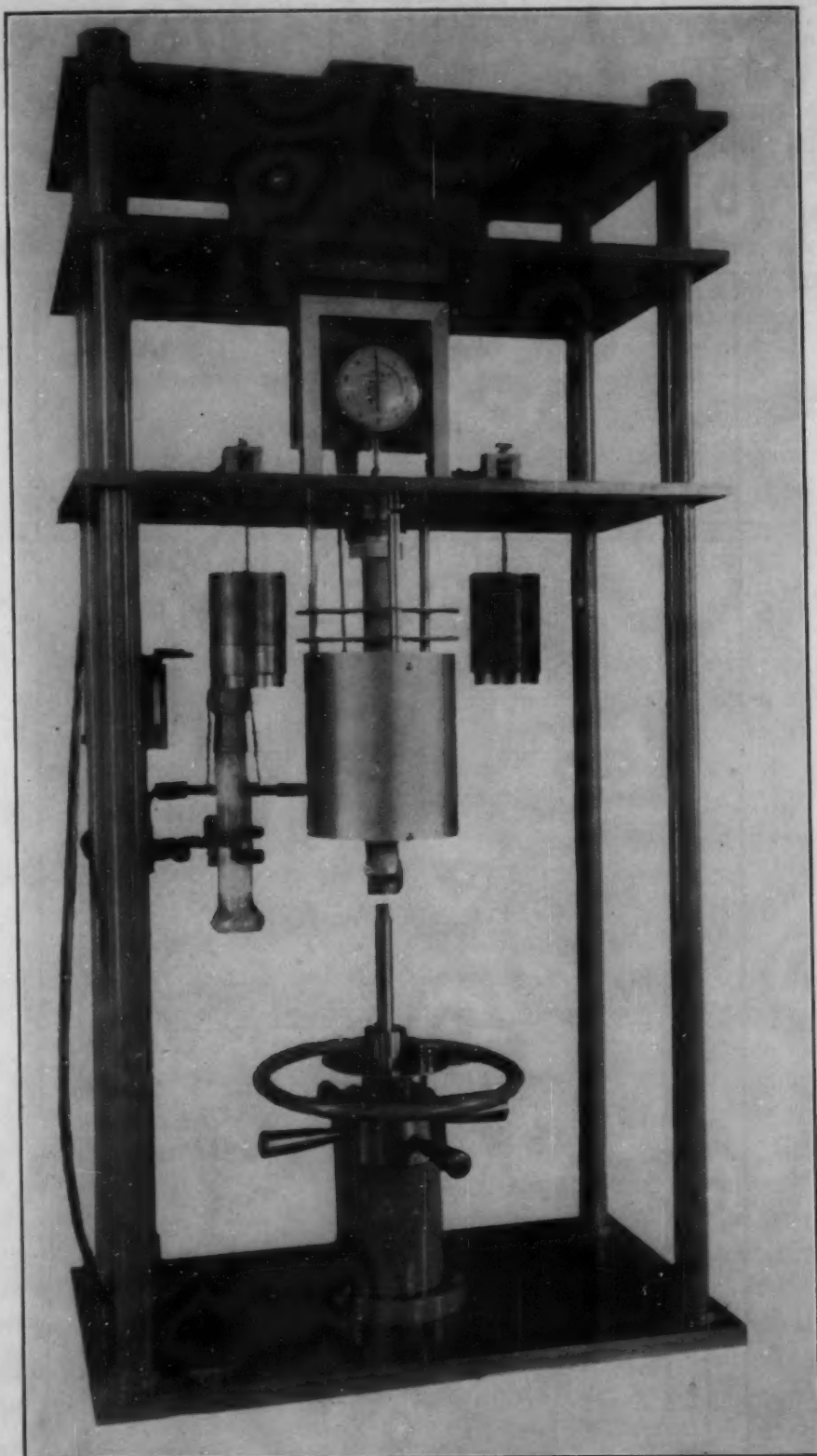


Fig. 1a—Photograph of Hot Hardness Tester

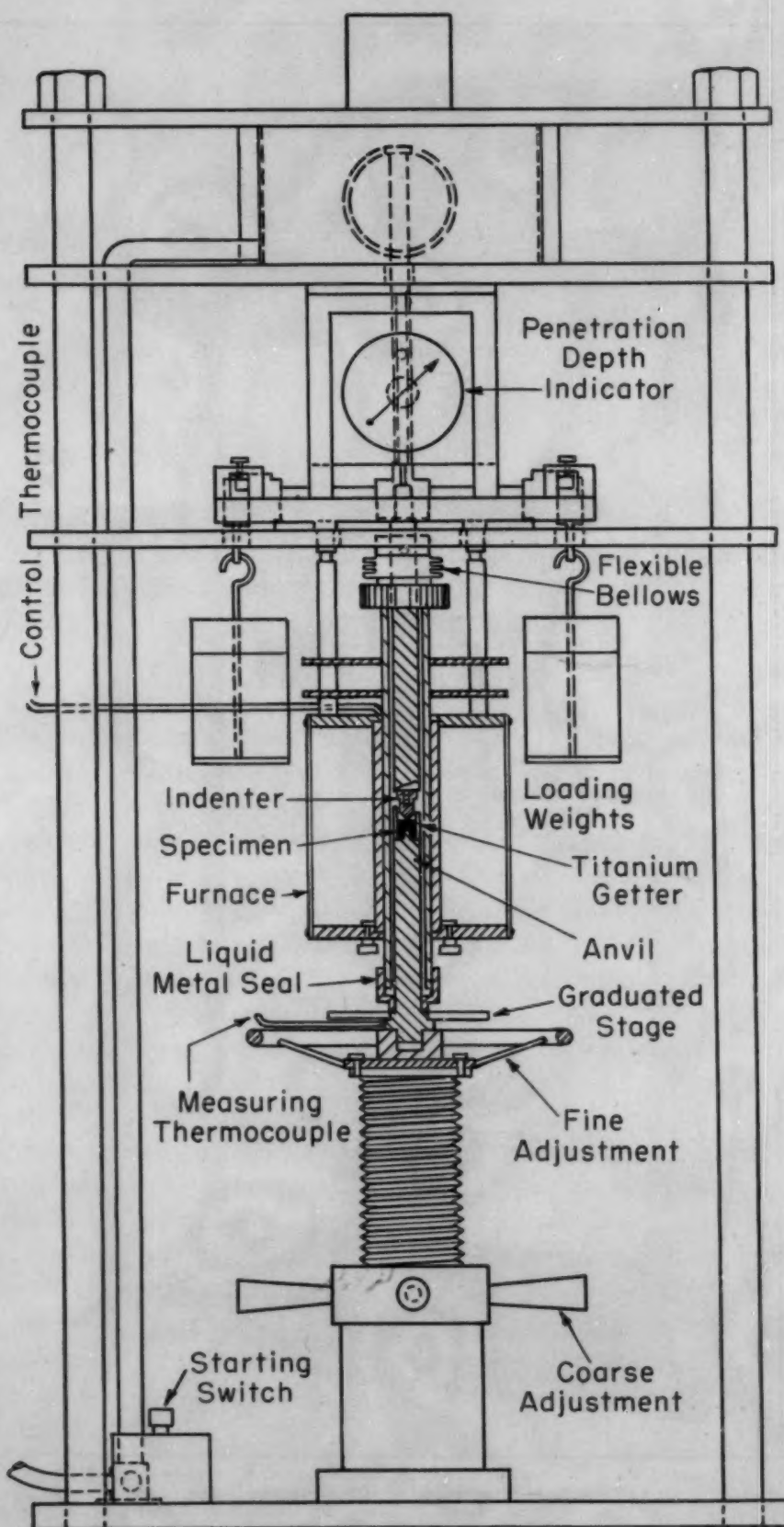


Fig. 1b—Schematic Sketch of Hardness Tester Shown in Fig. 1a.

The furnace utilizes a nichrome heating element wound about an alundum tube making up the core of the furnace or test chamber. Sil-o-cel is used as an insulating medium between heating unit and outer shell. A control thermocouple is located in a groove on the side of the alundum tube with its outlet through the top end plate of the furnace shell. Two stainless steel fins mounted above the furnace protect the loading mechanism and penetration indicator from undue radiation. The test chamber is attached to the indenter stem through a flexible bellows, which permits transmission of the load, without significant loss, to the specimen while preserving the atmosphere within the test chamber.

A virtually inert atmosphere (98% helium and 2% hydrogen) is employed in combination with a titanium "getter" immediately surrounding the specimen. The mixture enters the heating chamber at an inlet above the bellows after leaving the purification train, which consists of an Ascarite⁴ tower for removal of CO₂, a furnace heated tube (held at 915 °F) containing copper gauze, and a dehydrating tower of P₂O₅. A flow meter which precedes the purification train indicates the rate of flow of gas entering the purification train. The small amount of hydrogen and the titanium "getter" were added because it was not possible otherwise consistently to preserve a bright surface on stainless steel, especially at lower test temperatures. The temper film of oxide that formed in the absence of hydrogen and titanium was, however, probably too thin to affect hardness, as judged from the absence of any difference in hardness at room temperature with and without such a film. It is believed that the small amount of hydrogen exerts no deleterious effect, except possibly on carbon steel at higher temperatures than that tested. It should also be noted that purified tank helium without added hydrogen or a titanium "getter" was sufficient to preserve a bright surface on plain carbon steel.

The electrically actuated loading mechanism permits a loading and unloading cycle of 1 minute each, total load on the specimen being applied for approximately 1¼ minutes. On depressing the starter-switch the timing control cam is set in motion, applying the load through a lever system which removes the knife-edge support from the loading yoke. Total load includes the weights on the loading pans as well as the weight of the housing assembly of the indenter and is applied directly onto the indenter stem. The penetration depth indicator is incorporated into the apparatus to determine when the indenter has contacted the specimen, and to serve as a qualitative evaluation of hardness change at temperature.

TEST PROCEDURE

The cylindrical test specimens are ½ inch in length and 7/16 to

⁴NaOH deposited on asbestos particles.

10/16 inch in diameter with a center hole (3/16 inch in diameter and 6/16 inch deep) for anchoring over the anvil pin. The test surface of each specimen is polished by accepted metallographic techniques to a degree suitable for microscopic examination. The test surface is maintained parallel to the base throughout the polishing operation.

Following the surface preparation, three impressions are made with the hot hardness tester at room temperature, the diagonals measured with the standard Vickers optical measuring unit, and three additional impressions, for purposes of comparison, are made with the standard Vickers hardness machine having a loading time of $\frac{1}{2}$ minute. These impressions are made at approximately the same distance from the center of the specimen as those made with the hot hardness tester. The scatter of measurements of the hot hardness tester is about the same as for the Vickers at room temperature, and somewhat less, numerically, at elevated temperatures. The specimen is then positioned on the anvil of the hot hardness tester and a thermocouple spot-welded to the test surface at a point along the arc formed by the room temperature impressions. This thermocouple is set in a groove in the anvil stem and emerges from beneath the liquid metal seal cup. A slit titanium tube, $\frac{5}{8}$ inch in length and 11/16 inch inside diameter, is placed about the specimen, effectively serving as a "getter" for any residual oxygen remaining in the system. The anvil assembly, which includes the liquid metal seal cup and rotating stage, is then positioned in the recessed screw block and when using Cerrolow in the seal cup this alloy is melted by external heating with a small resistance furnace before the anvil is raised by means of the coarse adjustment screw. For tests above 700 °F (370 °C) the Cerrolow alloy remains liquid during test as a result of heat flow along the anvil.

The furnace chamber is flushed with purified gas mixture for several hours and the furnace heated to the desired temperature. The specimen is held at temperature for approximately $\frac{1}{2}$ hour before any impressions are made.

Following temperature stabilization the anvil is raised by means of the fine adjustment screw until the depth gage indicates (by 0.0001-inch motion) contact between specimen and indenter. The initial impression is then made without further adjustments by depressing the starter-switch. To maintain the desired distance between impressions (minimum distance usually given as $2\frac{1}{2}$ times the diagonal of an impression) (11) when testing at room or elevated temperature, the stage, which is indexed with numbered positions from 0 to 24 over 360°, is rotated a fixed amount after each impression. Following the first impression the anvil is lowered, usually by one or more turns on the fine adjustment screw, the stage turned to the new position and

Table I
Description of 18 Cr - 8 Ni Austenitic Stainless Steels

Code	Type	Heat Treatment	Composition—(Per Cent)*							Other Elements
			C	Mn	P	S	Si	Ni	Cr	
A1	18-8 (304L)									
	Low C	1900 °F-½ hr.-W.Q.	0.030	0.65	0.010	0.019	0.54	10.22	19.50
A2	18-8 (304)	1900 °F-½ hr.-W.Q.	0.050	0.28	0.015	0.009	0.44	10.12	18.38
A3	18-8 (304)									
	Low C, High N	1900 °F-½ hr.-W.Q.	0.030	1.48	0.018	0.024	0.67	7.14	19.38	0.15 N
A4	18-8-Mo (316L)									
	Low C	2000 °F-½ hr.-W.Q.	0.030	1.50	0.013	0.027	0.34	10.70	17.46	2.20 Mo
A5	18-8-Mo (316)	2000 °F-½ hr.-W.Q.	0.090	1.63	0.017	0.014	0.37	12.47	17.76	2.55 Mo
A6	18-8-Mo-Cb	2000 °F-½ hr.-W.Q.	0.050	0.77	0.018	0.006	0.36	14.19	18.50	2.45 Mo, 0.51 Cb
A7	18-8-Ti (321)	{ 1950 °F-½ hr.-W.Q., or 1900 °F-½ hr.-A.C.	0.050	0.53	0.017	0.010	0.41	10.81	17.61	0.42 Ti
A8	18-8-Ti (321)		0.085	0.48	0.012	0.007	0.61	11.28	18.50	0.33 Ti, 0.11 Cu
A9	18-8-Ti (321)	1950 °F-½ hr.-W.Q.	0.049	0.56	0.022	0.008	0.50	11.21	18.21	0.60 Ti, 0.18 Cu
A10	18-8-Cb (347)	1950 °F-½ hr.-W.Q.	0.080	1.27	0.015	0.009	0.61	10.83	18.04	0.69 Cb
A11	18-8-Cb (347)	1950 °F-½ hr.-W.Q.	0.060	1.61	0.016	0.006	0.57	11.10	18.12	0.78 Cb

*Check analysis on all except Steel A8.

the procedure repeated until at least seven impressions are made. In all tests a 10-kilogram load is used at room temperature and a 5-kilogram load at elevated temperatures. The temperature, measured before and during each loading, has not been observed to vary more than 5° during a series at any temperature up to 1500 °F.

After completion of all impressions the specimen is allowed to cool to approximately 250 °F; when using Cerrolow in the seal cup it has now solidified and is remelted before the specimen is removed from the apparatus. The diagonals of each impression made at temperature are then measured with the standard Vickers optical measuring unit and an average diamond pyramid hardness computed. Very little error is encountered because of thermal contraction of the diagonals in cooling from test temperature to room temperature (9).

It is, of course, possible to maintain a specimen at elevated temperature for an extended period, measuring the hardness at intervals.

MATERIALS

The chemical composition and type of all test steels are given in Tables I and II. The particular heat treatment for each of the austenitic steels is given in Table I. These steels were annealed in the range 1900 to 2000 °F (1040 to 1095 °C) for ½ hour followed by water quenching except for Steel A7 which was also tested after air cooling from 1900 °F (1040 °C). The plain carbon steels were normalized by heating to 1650 °F (900 °C) for ½ hour and cooling in air, whereas the 8 Cr - 1 Mo steel (Table II) was cooled from 1700 °F (925 °C) at a rate of 50 °F per hour.

Table II
Description of Ferritic Steels

Code	Type	Composition—(Per Cent) ^a								Other Elements	Main Deoxidizer ^b Lb. per Ton
		C	Mn	P	S	Si	Al	Al ₂ O ₃	N		
B1	Capped open-hearth	0.07	0.45	0.006	0.020	0.005	0.004	None
B2	Capped Bessemer	0.08	0.38	0.079	0.037	0.005	0.013	None
B3	Si-Ti killed open-hearth	0.19	0.47	0.009	0.028	0.18	0.005	0.002	0.006	0.002 Ti	10 FeSi, 6 FeCTi
B4	Si-Al-Ti killed open-hearth	0.16	0.48	0.008	0.022	0.20	0.004	0.002	0.005	0.003 Ti	10 FeSi, 4 FeCTi, 0.5 Al
B5	Si-Al killed open-hearth	0.15	0.47	0.011	0.023	0.19	0.007	0.003	0.006	0.001 Ti	10 FeSi, 1 Al
B6	Si-Al killed open-hearth	0.24	0.86	0.013	0.021	0.023	0.033	0.009	8.4 FeSi, 1.8 Al
B7	Si-Al killed open-hearth	0.16	0.51	0.013	0.020	0.16	0.035	0.006	0.009	7 FeSi, 2 Al
B8	Si killed open-hearth	0.27	0.52	0.016	0.025	0.22	0.006	0.006	7.7 FeSi
B9	Si-Al killed Bessemer	0.14	0.54	0.074	0.022	0.18	0.025	0.013	6.8 FeSi, 3.4 Al
B10	Si-Al killed Bessemer	0.13	0.48	0.087	0.029	0.21	0.047	0.020	10 FeSi, 3 Al
B11	Si-Al killed Bessemer	0.15	0.46	0.088	0.018	0.22	0.024	0.005	0.022	10 FeSi, 2.5 Al
B12	Al killed Bessemer	0.18	0.51	0.077	0.022	0.03	0.066	0.020	3.4 Al
B13	8% Cr-1% Mo	0.10	0.38	0.015	0.013	0.32	8.21 Cr 1.06 Mo	

a. Check analysis on all steels; absence of value indicates no determination made.

b. FeSi refers to ferrosilicon; FeCTi refers to ferrocobalt-titanium; Al to aluminum.

Hardness tests at 1100, 1300 and 1500 °F (595, 705 and 815 °C) were made on the series of eleven quenched austenitic stainless steels described in Table I; Steel A7 from this series was also cooled in air from 1900 °F (1040 °C) and tested at 400, 700, 900, 1100, 1300 and 1500 °F (205, 370, 480, 595, 785 and 815 °C). The series of twelve plain carbon steels described in Table II was tested at 850 °F (455 °C). Steels B7 and B12 were tested also at 300, 400, 500 and 700 °F (150, 205, 260 and 370 °C). The 8 Cr - 1 Mo Steel B13 was tested at 300, 500, 800, 1000, 1200 and 1400 °F (150, 260, 425, 540, 650 and 760 °C). A separate specimen was used for each temperature.

HARDNESS TESTING AT ROOM TEMPERATURE

As mentioned previously, the hardness of all specimens tested at elevated temperatures was determined initially at room temperature on both the hot hardness tester and Vickers hardness machine. These room temperature tests led to some interesting observations.

Influence of Specimen Preparation—In a number of initial tests on austenitic stainless steels it was found that the hardness depends to a great extent on the machining operations preceding the metallographic polish, even when the polished surface seemingly is free of

any disturbed metal layer. For example, when a specimen is cut with a band saw and the test surface faced in a lathe, the hardness after polishing is usually greater than when a similar specimen is first sectioned with a cut-off wheel and surface ground before polishing. Differences up to 60 DPH have been observed in some cases. Stainless steels of the 18-8 type are known to harden very readily upon straining and therefore it is not surprising that rough machining causes strain hardening in these steels to an appreciable depth. Other metals

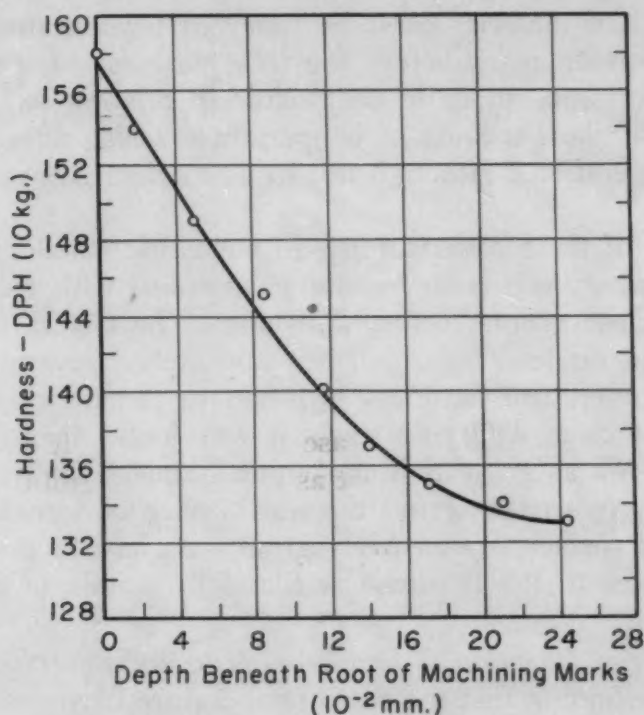


Fig. 2—Variation of Hardness of Steel A9 (Type 321) With Depth Beneath Root of Machining Marks Following Rough Machining of Test Surface.

behave in a similar manner (12) except perhaps in degree or depth of strain hardening.

Fig. 2 gives some indication of the effect of machining on hardness of an austenitic stainless steel. In this case a specimen of Steel A9 (Type 321) was cut with a band saw, faced in a lathe and the test surface ground on a lead lap until all machining marks were no longer visible. The sample was then alternately polished and etched several times and upon examination, following the final etch, no trace of a disturbed metal layer was observed. Hardness impressions made on the surface, using the Vickers hardness tester, resulted in hardness values for a surface just beneath the root of the machining marks. The average of these values is shown as the first experimental point in Fig. 2. The specimen was then ground on lead laps, polished, and etched a number of times until the additional points shown in Fig. 2

were obtained. Each point on this graph represents the average of three hardness values. After each polishing operation, but before etching the sample, the diagonals of the previous impressions were measured and the thickness of the metal layer removed was then computed from the relation: $d = 0.143 (D_1 - D_2)$, where d is the thickness removed, D_1 the average diagonal before grinding and D_2 the average diagonal after grinding. The depth beneath the root of the machining marks is then the cumulative sum of d .

The results in Fig. 2 show that approximately 20×10^{-2} mm. (0.008 inch) of material must be removed beyond the root of the deepest machining mark before the true hardness of the material is obtained. The importance of this factor in relation to hot hardness testing is that the hardness at temperature is also affected by prior machining operations, although not to as marked degree as at room temperature.

In view of these observations, all austenitic stainless steel specimens for hot hardness testing are first sectioned with a cut-off wheel and then surface ground before polishing. The test surface is alternately ground on lead laps, polished and etched several times until the room temperature hardness is found to remain essentially constant. In the case of ferritic steels it was found that the depth of hardening is not as great as in austenitic stainless steels; thus it was not necessary to surface grind the test surface of ferritic steels, but the machined surface is alternately ground on lead laps and polished several times until the hardness is found to remain at essentially a constant level.

Influence of Duration of Loading—A second observation of some interest is the finding that the room temperature hardness determined on the Vickers hardness machine is usually greater (see Tables III and V) than the room temperature hardness determined for the same specimen by means of the hot hardness tester. This difference is particularly noticeable in the austenitic stainless steels. Since the duration of full load in the hot hardness tester ($1\frac{1}{4}$ minutes) is greater than in the Vickers hardness tester ($\frac{1}{2}$ minute), this behavior is attributed to the greater amount of creep which may occur during the longer time of loading in the hot hardness tester (13). Since creep results in a larger impression, an apparent lower hardness value is observed.

The effect of time of loading on hardness at room temperature is illustrated for one austenitic steel (Type 321) in Fig. 3. The hot hardness tester was used, since it is possible to vary the time of loading within wide limits by merely stopping and starting the actuating mechanism of the tester at predetermined time intervals.

Curves I and II in Fig. 3 show the effect of loading time on two specimens of the same steel. In both of these samples, following

Table III
Hardness of 18 Cr-8 Ni Stainless Steels at 75, 1100, 1300 and 1500 °F

(Average of Seven Measurements)							
		Room Temperature Hardness—DPH (10 kg.)		Hardness at 1100 °F	Hardness at 1300 °F	Hardness at 1500 °F	
Code	Type	Specimen	Vickers Machine	Hot Hardness Tester	DPH (5 kg.)	DPH (5 kg.)	DPH (5 kg.)
A1	18-8 (304)	1	143	140	84.6
A1	Low C	2	145	140	64.5
A1	3	139	136	37.2
A2	18-8 (304)	1	134	131	76.4
A2	2	133	131	65
A2	3	141	136	43.1
A3	18-8 (304)	1	177	172	92.1
A3	Low C	2	173	165	77.5
A3	High N	3	178	174	51.2
A4	18-8-Mo (316)	1	135	133	82.6
A4	Low C	2	142	140	74.3
A4	3	143	136	48.5
A5	18-8-Mo (316)	1	148	146	94.7
A5	2	147	143	83.4
A5	3	144	135	57.6
A6	18-8-Mo-Cb	1	162	161	111
A6	2	163	161	96.1
A6	3	158	156	57
A7	18-8-Ti (321)*	1	145	144	90.7
A7	2	146	140	72.9
A7	3	142	138	46
A8	18-8-Ti (321)	1	149	148	98.4
A8	2	144	143	75.1
A8	3	151	139	48.1
A9	18-8-Ti (321)	1	142	135	100.5
A9	2	137	133	79.7
A9	3	140	138	60.7
A10	18-8-Cb (347)	1	186	181	111
A10	2	189	182	91.4
A10	3	183	173	53
A11	18-8-Cb (347)	1	165	162	105
A11	2	163	162	83.6
A11	3	161	160	49.1

*Water-quenched from 1950 °F.

facing on a lathe, enough material was removed by grinding on lead laps so that the test surface was just beneath the root of the deepest machining mark. The difference in the hardness level in the two curves is a result possibly of differences in amount of material removed during the grinding operation. The test results for Curves I and II show that for the same time of loading ($\frac{1}{2}$ minute) the Vickers tester and hot hardness tester give essentially the same hardness values; however, as the time of loading is increased, a sharp drop in the hardness is observed before levelling-off at about $1\frac{1}{2}$ minutes. Thus an appreciable difference is found between the Vickers tester, employing a loading time of $\frac{1}{2}$ minute, and the hot hardness tester, employing a loading time of $1\frac{1}{4}$ minutes.

By further polishing the above two samples until considerable material was removed from the test surface, an appreciable drop in hardness resulted and in addition the hardness of the two samples for the various loading times was similar. These results for both samples are shown as Curve III. Again in this case, the Vickers and hot

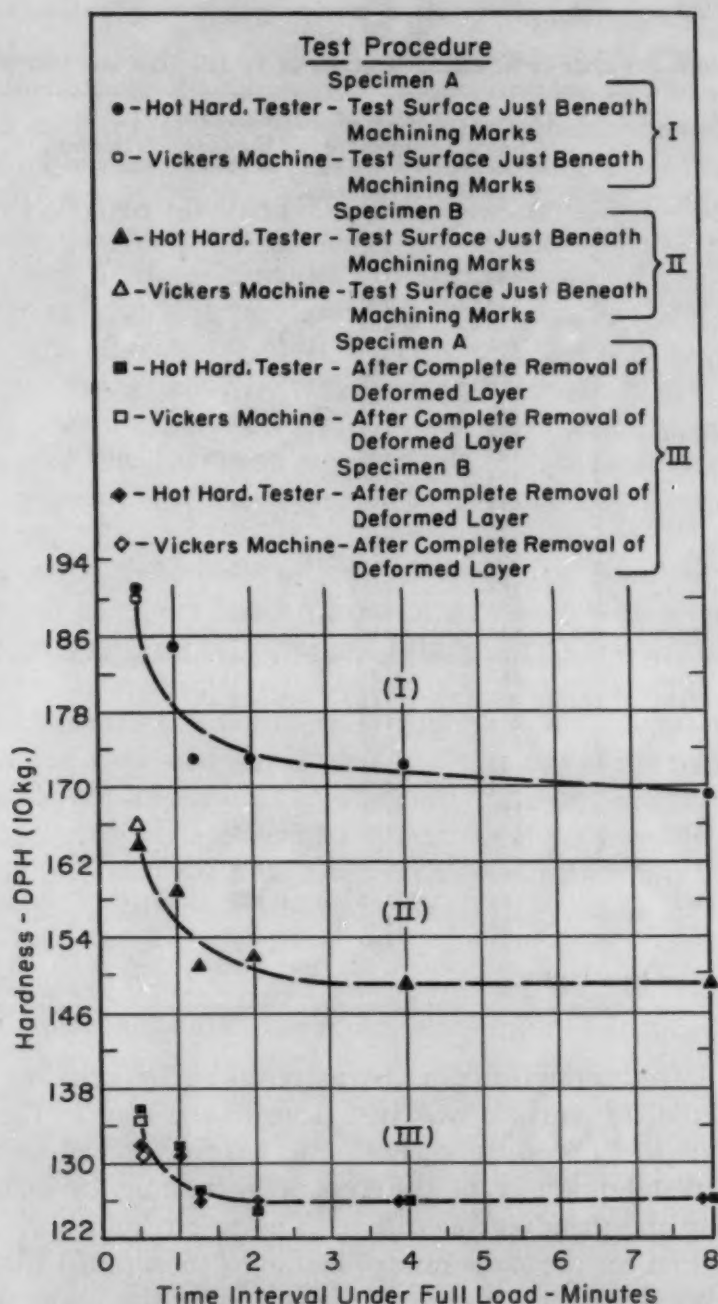


Fig. 3—Variation of Hardness With Time of Loading at Room Temperature, Steel A9 (Type 321).

hardness testers give similar values for the same loading time, but as the loading time is increased the hardness drops sharply before leveling-off. It should be noted that in this instance the drop is approximately half of that shown in Curves I and II which occurred before removal of the strain hardened metal layer. Apparently this layer not only affects the hardness level at room temperature but also tends to magnify the effect of time of loading. It would seem that further standardization of hardness testing for improved precision not only

at elevated temperature but also at room temperature is indicated. The time of loading for room temperature testing should be constant for all testers, and, as indicated from the results reported here, to be free from the effect of loading times of short duration for loads of 5 or 10 kilograms, should be of the order of 2 minutes. At elevated temperature the problem is more complex, since the loading time, to be within the level part of the curve, is known to vary with temperature and material (14). Thus a constant loading time might not be adequate for a number of materials and test temperatures. Further work on this phase of hot hardness testing is indicated. Further standardization for both room and elevated temperature testing should also be concerned with the adoption of an accepted procedure for surface preparation, especially in the case of materials which strain harden readily.

A similar study of several ferritic alloys in the range of hardness of 100 to 200 DPH showed only a slight dependence of hardness on testing time. Within this range, the hardness for a loading time of $\frac{1}{2}$ minute did not exceed by more than 7 DPH numbers the hardness for a loading time of up to 8 minutes.

HARDNESS TESTING AT ELEVATED TEMPERATURES

Steels A1 to A11, which include various types of 18 Cr-8 Ni stainless steels, were tested at 1100, 1300 and 1500 °F (595, 705 and 815 °C). The test results are given in Table III. These results show that the hardness of the test steels at each of the three test temperatures covers a considerable range. The results for Steel A7 when air-cooled from 1900 °F (1040 °C) are included in Table IV.

The initial tests on these steels at elevated temperatures were made with a regular Vickers-type diamond indenter cemented to its holder with a special high temperature binding material. The diamond indenter gave adequate service at 1100 and 1300 °F (595 and 705 °C), but not at 1500 °F (815 °C), where, after a dozen or so impressions, the portion of the indenter tip which penetrated the test material began to show signs of disintegration. The indenter tip seemingly dissolved away, leaving an irregular or jagged, truncated surface. It is very likely that the large affinity of chromium-rich austenite for carbon favored diffusion of carbon from the indenter to the metal in the area of contact. Evidently, the effect of the factors influencing this type of diffusion was minimized by lowering the temperature to 1300 or 1100 °F (705 or 595 °C) where no visible attack resulted.

Various attempts to prevent direct contact between the diamond indenter and test material by electrodepositing on the surface a layer of copper on which was superimposed a silver flash coating, or covering of the test surface with gold foil, were not successful. The indenter penetrated both silver and copper coatings, while the gold foil

Table IV
Hardness of Various Ferritic and Austenitic Stainless Steels at Temperatures
Between 75 and 1500 °F

Temperature, °F	(Average of at Least Seven Measurements)				
	Hardness—DPH*				
	Steels				
	A 7†	A 10	B 7	B 11	B 13
75	154	179	123	143	144
300	113	146	132
400	125	...	124	156	...
500	114	154	119
700	109	...	102	130	...
800	107
850	80.3	105	...
900	99.5
1000	88.6
1100	93.7	111
1200	49.2
1300	70.5	91.4
1400	20.3
1500	44.7	53

*A 5-kilogram load was used at temperatures except at 75 °F when a 10-kilogram load was used.

†Air-cooled from 1900 °F.

broke up into small particles, offering little protection to the diamond indenter.

Failure of these attempts led to the adoption of a sapphire indenter. The first indenter of this type gave indications, after several test runs at 1500 °F (815 °C), of developing in the region of the tip striations or faults which were oriented in a direction favorable to a high resolved shear stress. The regularity of these faults suggested the possibility of their being along certain crystallographic planes, perhaps parallel to the basal or cleavage planes⁵. In a second sapphire indenter the basal planes of the crystal were found, from X-ray diffraction, to be inclined between 42 and 49 degrees to the base of the pyramid, an orientation for which the resolved shear stress is at its maximum. All tests on the austenitic steels at 1100, 1300 and 1500 °F (595, 705 and 815 °C) were made with this indenter without any development of striations or faults despite the apparently unfavorable orientation. This indenter was also used in making all other tests reported.

The results obtained on all ferritic steels are reported in Tables IV and V. Whereas the results indicate that hot hardness of the carbon steels at 850 °F (Table V) depends on melting and deoxidation practices, as well as on chemical composition, and no doubt other factors such as grain size and microstructure, it is difficult to generalize about individual effects because of the simultaneous variation of many factors. It does appear possible to state that Bessemer steels are harder than open-hearth steels of similar composition and deoxidation practice, presumably a consequence primarily of higher nitrogen and phosphorus.

⁵The crystal structure of sapphire (Al_2O_3 - α) is rhombohedral.

Table V
Hardness of Carbon Steels at 75 and 850 °F

(Average of Seven Measurements)				
Code	Type	Room Temperature		Hardness at 850 °F DPH (5-kg.)
		Hardness	DPH (10 kg.)	
		Vickers Machine	Hot Hardness Tester	
B1	Capped open-hearth	87.8	88.2	61
B2	Capped Bessemer	116	113	88.1
B3	Si-Ti killed open-hearth	116	120	87.1
B4	Si-Al-Ti killed open-hearth	108	111	81.4
B5	Si-Al killed open-hearth	113	112	82.6
B6	Si-Al killed open-hearth	146	143	94.2
B7	Si-Al killed open-hearth	118	120	80.3
B8	Si killed open-hearth	135	132	97.7
B9	Si-Al killed Bessemer	129	126	91.6
B10	Si-Al killed Bessemer	130	128	93.8
B11	Si-Al killed Bessemer	143	140	105
B12	Al killed Bessemer	126	126	90.3

RELATION BETWEEN HARDNESS AND STRENGTH AT ELEVATED TEMPERATURES

The hardness test at room temperature has been used not only as a research tool but has been employed extensively as a material control test. In the latter role it has proved of great value as a time-saving as well as nondestructive test for estimating the strength of various alloys. It would seem that a similar relation might exist between hardness and "short-time" strength at elevated temperatures. Recent results (9) indicate the existence of such a relation which may lead to the use of the hot hardness test as an important sorting tool for high temperature alloys.

Further evidence of the existence of a relation between hardness and strength at elevated temperatures is given in Figs. 4, 5 and 6. In Fig. 4 is shown a plot of the hardness against the stress for rupture⁶ in 1, 100 or 1000 hours for several of the stainless steels tested at 1100, 1300 and 1500 °F (595, 705 and 815 °C), and for all of the carbon steels tested at 850 °F (455 °C). These results seem to indicate that the relation between hardness and strength is independent of structure or temperature within the limits investigated. It should be observed that the amount of scatter seems to be least for the 1-hour rupture strength results and increases as the time to rupture increases. Moreover, as creep-rupture time decreases, the concave curve tends to straighten out, approaching a linear relationship. This is not surprising since, as the time to rupture approaches that of the short-time tensile test, the creep-rupture strength approaches the ultimate tensile strength, which, when plotted against hot hardness, as in Fig. 5, reveals a linear relationship with little scatter. The experimental points in Fig. 5 correspond to all the hardness values reported in Table IV. These results indicate that the linear relationship between ultimate

⁶The creep-rupture results for some of the stainless and all of the carbon steels have been reported previously (15, 16).

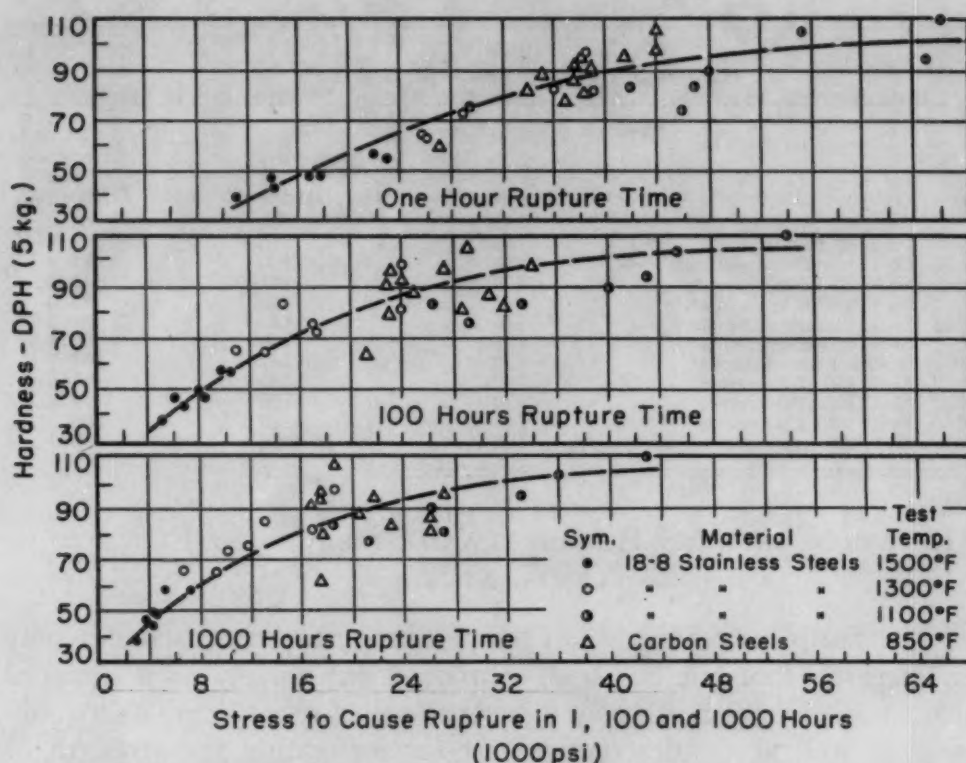


Fig. 4—Relation Between Hot Hardness and Creep-Rupture Strength for 18 Cr-8 N Stainless and Carbon Steels.

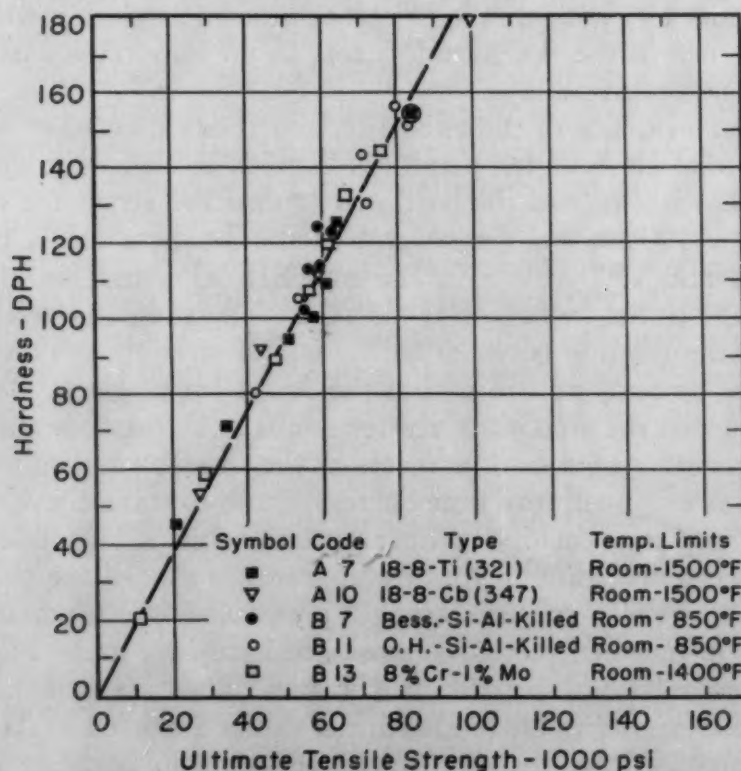


Fig. 5—Relation Between Hot Hardness and Ultimate Tensile Strength for Several Ferritic and Austenitic Steels.

tensile strength and hot hardness is independent of structure or temperature within the limits investigated. In Fig. 6 is shown a plot of the hardness against the creep strength (stress causing a creep rate of 1% per 10,000 hours) for all stainless steels tested at 1100, 1300 and 1500 °F (595, 705 and 815 °C) and all carbon steels tested at

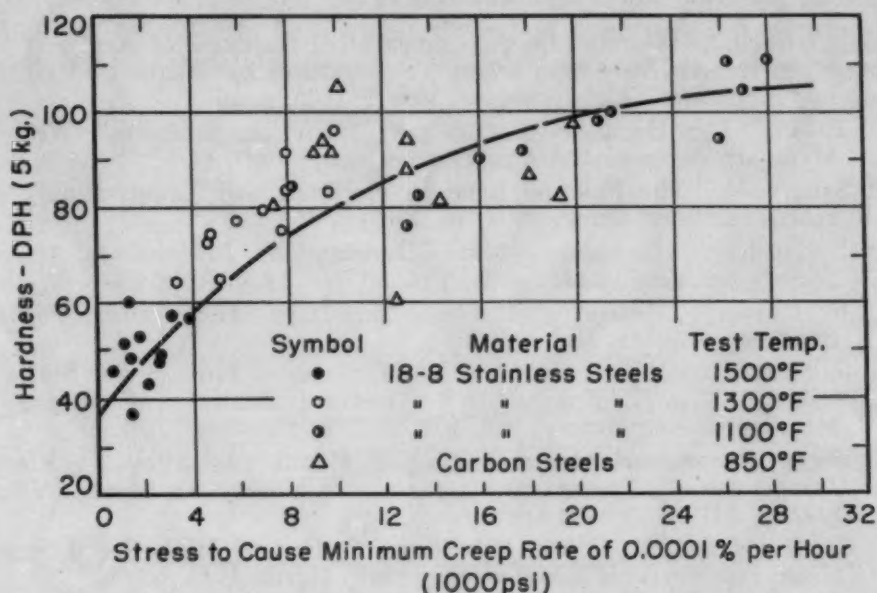


Fig. 6—Relation Between Hot Hardness and Creep Strength of 18 Cr-8 Ni Stainless and Carbon Steels.

850 °F (455 °C). The relation in Fig. 6 is very similar to that observed in Fig. 4. The curve is again concave downward.

SUMMARY

A static loading type, hot hardness tester of new design is described in this paper, and the testing techniques, including several observations on specimen preparation and effect of duration of loading, are discussed. A number of different steels including various types of 18 Cr-8 Ni stainless, capped and killed open-hearth and Bessemer steels, and one ferritic 8 Cr-1 Mo steel have been tested at temperatures ranging from 75 to 1500 °F (24 to 815 °C). The test results indicate a relationship between hot hardness and the stress to cause rupture in 1, 100 or 1000 hours (Fig. 4). The scatter of experimental points is least for the 1-hour rupture time and greatest for the 1000-hour rupture time. A linear relationship between hardness and ultimate tensile strength is found for test temperatures up to 1500 °F (815 °C) (Fig. 5). A relationship between hot hardness and stress to cause a creep rate of 1% per 10,000 hours (Fig. 6) has also been observed. In all cases the relationship appears to be independent of structure as well as temperature within the limits investigated.

ACKNOWLEDGMENTS

The authors gratefully acknowledge the assistance of H. S. Link and S. Zirinsky in the experimental work and of Q. Henderson, who directed the construction of the apparatus.

References

1. J. A. Brinell, "Researches on the Comparative Hardness of Acid and Basic Open-Hearth Steel at Various Temperatures by Means of Ball Testing", *Iron and Steel Magazine*, Vol. 9, 1905, p. 16.
2. F. Robin, "The Hardness of Steels at High Temperatures", *Revue de Metallurgie*, Vol. 5, 1908, p. 893.
3. F. Sauerwald, "The Relation Between Hardness and Temperature", *Zeitschrift für Metallkunde*, Vol. 16, 1924, p. 315.
4. I. H. Cowdrey, "Hardness by Mutual Indentation", *Proceedings, American Society for Testing Materials*, Vol. 30, No. II, 1930, p. 23.
5. J. F. Kayser, "Measuring Hardness at High Temperatures", *METAL PROGRESS*, Vol. 23, No. 3, 1933, p. 50.
6. O. E. Harder and H. A. Grove, "Hot Hardness of High Speed Steels and Related Alloys", *Transactions, American Institute of Mining and Metallurgical Engineers*, Vol. 105, 1933, p. 88.
7. E. Fetz, "Dynamic Hardness Testing of Metals and Alloys at Elevated Temperatures", *TRANSACTIONS, American Society for Metals*, Vol. 30, 1942, p. 1419.
8. E. C. Bishop and M. Cohen, "Hardness Testing of High Speed Steel at High Temperatures", *METAL PROGRESS*, March 1943, p. 413.
9. F. P. Bens, "Hardness Testing of Metals and Alloys at Elevated Temperatures", *TRANSACTIONS, American Society for Metals*, Vol. 38, 1947, p. 505.
10. A. Brenner, "Microhardness Tester for Metals at Elevated Temperatures", *Journal of Research, National Bureau of Standards*, Vol. 46, No. 2, February 1951, p. 126.
11. H. O'Neill, "The Hardness of Metals and Its Measurement", Chapman and Hall, Ltd., London, 1934.
12. F. C. Hull and H. R. Welton, "Work Hardened Surfaces of Fatigue Specimens", *METAL PROGRESS*, Vol. 48, December 1945, p. 1287.
13. R. H. Heyer, "Hardness Conversion Relationships", *Proceedings, American Society for Testing Materials*, Vol. 42, 1942, p. 708.
14. H. S. Avery, "Hot Hardness of Hard-Facing Alloys", *Welding Journal*, Vol. 29, July 1950, p. 552.
15. G. V. Smith, E. J. Dulis and E. G. Houston, "Creep and Rupture of Several Chromium-Nickel Austenitic Stainless Steels", *TRANSACTIONS, American Society for Metals*, Vol. 42, 1950, p. 935.
16. G. V. Smith and E. J. Dulis, "Effect of Manufacturing Practice on Creep and Creep-Rupture Strength of Low Carbon Steel", *Proceedings, American Society for Testing Materials*, Vol. 49, 1949, p. 584.

DISCUSSION

Written Discussion: By Philip C. Miller, The Babcock & Wilcox Co., Research and Development Dept., Alliance, Ohio.

One of the most interesting findings of the authors is that they have observed a relationship between hot hardness and the stress to cause rupture in 1, 100, or 1000 hours as well as between hot hardness and stress to

cause a creep rate of 1% per 10,000 hours. In this connection it is pertinent to point out that a relationship between hot hardness and what is described as long-term stability has also been reported by Russian investigators.⁷

Similar studies were conducted at the Research and Development Center of The Babcock & Wilcox Co. at Alliance, Ohio. Instead of employing hot hardness per se as criterion of high temperature behavior, we used the depth of penetration versus time under a given load at various tem-

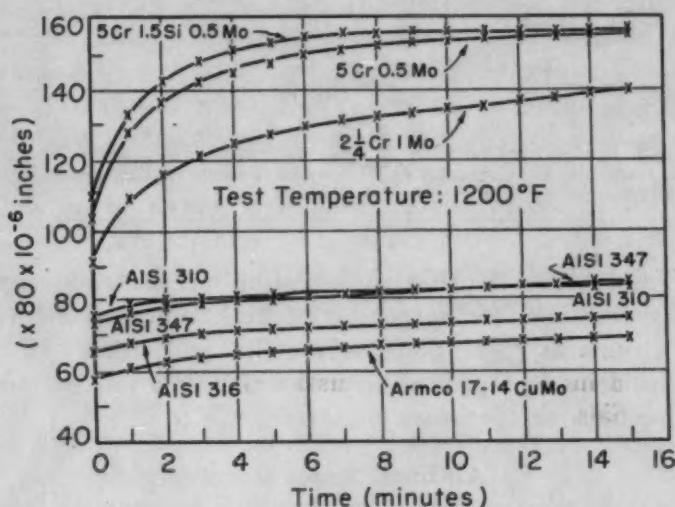


Fig. 7—Graph Showing the Depth-of-Penetration Curves at 1200 °F for the Following Materials: Armco 17-14 CuMo, AISI 316, AISI 310, AISI 347, 2.25 Cr-1 Mo, 5 Cr-0.5 Mo, and 5 Cr-1.5 Si-0.5 Mo.

peratures. For this purpose we modified a standard Rockwell hardness testing machine by equipping it with a suitable furnace operating in a purified argon atmosphere. Specimen and indenter temperature was controlled within 0 to +3 °F. A standard diamond penetrator, mounted on a stabilized zirconia shaft, was used. Testing was carried out by applying a load of 60 kg. in the usual manner and taking a first dial reading on the Rockwell A scale, which was used as "zero minute" point. Subsequent readings were taken every following minute for a total period of 15 minutes. At the end of 15 minutes, a final reading was taken and the load removed. The dial setting after removal of the load was used for calculating the depth of penetration from "zero minutes" to 15 minutes. One division change of the Rockwell scale equaled 80×10^{-6} inch lineal movement of the indenter.

We studied in this manner various high temperature alloys generally used in steam plant service and obtained a remarkable correlation between the depth of penetration versus time curves and the corresponding creep and stress-rupture curves. This is illustrated by Fig. 7, showing the depth-of-penetration curves at 1200 °F for the following materials: Armco 17-14 CuMo, AISI 316, AISI 310, AISI 347, 2.25 Cr-1 Mo, 5 Cr-0.5 Mo, and

⁷I. L. Mirkin, et al, Zavodskaya Laboratory, 1949, No. 9, p. 1080; see also *Metallurgia*, September 1950, p. 207 and 208.

5 Cr-1.5 Si-0.5 Mo. The stress-rupture and creep strength properties of these alloys, given in Table VI, are seen to arrange themselves in the same order as the depth-of-penetration curves.

Table VI

	Stress-Rupture Strength at 1200 °F (10,000 hours)	Creep Strength at 1200 °F (1% El. in 10,000 hours)
1. 17-14 CuMo	25,500	19,000†
2. 16-13-3	16,500†	12,000†
3. 18-8 Cb	15,500	11,400
4. 25-20	12,000†	7,400
5. Croloy 2¼	5,000	4,175
6. Croloy 5	4,500*	2,600*
7. Croloy 5 Si	3,600	1,600

*R. F. Miller and J. J. Heger, ASTM Special Technical Publication No. 100.

†W. F. Simmons and H. C. Cross, ASTM Special Technical Publication No. 124. All other values were determined by The Babcock & Wilcox Co.

The high temperature depth-of-penetration versus time curves may eventually lend themselves for screening of high temperature alloys, but much more work remains to be done before this and similar methods can be looked upon as reliably reproducing and indicating the sustained load-carrying ability of high temperature materials.

Authors' Reply

Mr. Miller's results are a welcome addition to, as well as confirmation of, our findings.

MICROCONSTITUENTS IN HIGH TEMPERATURE ALLOYS

BY H. J. BEATTIE, JR., AND F. L. VERSNYDER

Abstract

With the complementary use of microstructural studies and X-ray diffraction analysis of electrolytically separated residues, the microconstituents of iron-base, cobalt-base and nickel-base high temperature alloys were studied. The techniques used are described in detail. The results show, in particular, some of the effects of titanium and molybdenum as alloying additions.

The occurrence and suggested mode of formation of titanium carbonitride in a nickel-base age-hardenable alloy were determined and are described in detail. Conclusions applicable to most air-melted titanium-containing alloys are drawn.

The intermetallic compounds M_2Ti and Fe_2Al were identified and discussed.

A new phase $CrMoN_x$ was observed and identified. Its crystallography is discussed.

The second Brillouin zone is considered for the complex carbides M_6C and $M_{23}C_6$ with the resulting determination of the ratio of electron to metal atom capacity of about 7:1 for these two carbides.

INTRODUCTION

IN recent years much excellent research work has been done on the ternary and quaternary systems on which most high temperature alloys are based. Reference to the transactions of the technical societies in the last three years will yield papers too numerous to list here. However, the researches have not as yet reached the stage of determining much more complex systems, nor has much work been published on the effects of the multitude of minor alloying additions to high temperature alloys. Therefore, it becomes important to study the complex commercial alloys as possible sources of information regarding the microconstituents to be expected, the phase relationships involved, and the effect of the minor alloying additions on high temperature alloys. Work has been done in this field (1-3)¹; how-

¹The figures appearing in parentheses pertain to the references appended to this paper.

A paper presented before the Thirty-fourth Annual Convention of the Society, held in Philadelphia, October 18 to 24, 1952. Of the authors, H. J. Beattie is physicist, and F. L. VerSnyder is metallurgist, Thomson Laboratory, General Electric Company, West Lynn, Mass. Manuscript received April 9, 1952.

ever, it is the purpose of this paper to present information gained from the study of other commercial alloys. Of particular interest is the titanium age-hardenable-type alloy. Considerable work was done on such an alloy (M252) developed by the Thomson Laboratory of the General Electric Company.

Since current high temperature alloys are usually based on cobalt, nickel or iron, at least one commercial alloy of each of the three base elements was studied.

EXPERIMENTAL PROCEDURE

The method of study was the complementary use of X-ray diffraction and metallography. Samples were first studied microscopically to determine the number of microconstituents present, and to estimate the number and possibly the identity of the phases present in the microstructure. The samples were then electrolytically digested to separate the microconstituents from the matrix as an insoluble residue. Drying of the collected residue resulted in a powder suitable for subsequent X-ray diffraction analysis using the Debye-Scherrer powder method. Both a photographic camera and an X-ray spectrogoniometer (G.E. XRD-1 and XRD-3, respectively) were used in obtaining the diffraction patterns.

Subsequently, correlation between the microstructure and the X-ray diffraction results was accomplished on the basis of total number of constituents observed, and a semiquantitative determination of their relative amounts present. Further correlation was obtained by the use of metallographic techniques.

Electrolytic Separation

Rosenbaum's work (2) indicates that electrolytic digestion of the matrix in 10% HCl solution was the most successful single technique to accomplish the concentration of the minor constituents. Using this technique throughout, the authors have found that those constituents which are observable in the microstructure as being insoluble in the matrix are also insoluble in the electrolyte.

The electrolytically attacked matrix is usually soluble; however, matrix particles in some specimens are often separated from the anode before dissolving, and these remain insoluble in the electrolyte. Separated residues which were known to contain a relatively large amount of matrix particles were screened through 200 mesh for further concentration of the minor constituents from the larger matrix particles. This residual undissolved matrix appeared in some of the X-ray diffraction patterns.

Each electrolytic cell consisted of 2000 ml. of 10% HCl electrolyte in a 3000-ml. beaker. The anode was the specimen alloy, and the cathode was a copper strip. The pH of the electrolyte was re-

stored at regular intervals by replacing 3 ml. of concentrated HCl per ampere-hour, this having been computed as the necessary amount, assuming that the electrolyte-to-cathode current went solely into forming H_2 .

After electrolytically digesting an alloy for 100 to 200 ampere-hours, depending on the size of the specimen, the insoluble residue was collected in three ways:

(a) The residue adhering to the anode was scraped off and washed.

(b) The upper part of the electrolyte containing fine particles in suspension was decanted through a fine-porosity fritted-glass filter crucible.

(c) The balance of the residue was separated by suction filtration through No. 41H, 11.0-cm. filter paper in a Buechner funnel.

In several cases, the particles were too small to be separated by filtration. These were separated by the use of a centrifuge.

After washing, each of these samples was dried, using alcohol followed by ether.

X-Ray Diffraction

The X-ray diffraction patterns were made on a General Electric XRD-3 Spectrogoniometer. This apparatus permits accurate measurements of interplanar spacings at low angles. It also gives direct readings of scattered X-ray intensities under simple experimental conditions, which do not require complicated and approximate corrections for absorption.

The Geiger counter is 90% efficient for $Cu K\alpha$ radiation. A nickel foil filter is placed between the detector slit and Geiger counter whenever copper radiation is used. This radiation is found to be satisfactory, and no difficulties are encountered with fluorescent radiation from the specimens.

A signal proportional to the logarithm of the counting rate is automatically recorded as the detector scans at a rate of 12 degrees per hour. The positions of the diffraction peaks can usually be determined from the recorder chart within an accuracy of a few hundredths of one degree. Whenever accurate readings of relative intensities were desired for determining structure factors, the goniometer was set at the proper angles and the scaling unit was used to time the intervals required to count 16,384 quanta.

The X-ray tube was operated on a stabilized full-wave rectified potential of 49 KVP and on a stabilized current of 16 MA.

Before each run, the X-ray tube was energized for at least 30 minutes to allow the focal spot to reach its equilibrium position, after which the main protractor of the goniometer was zeroed on the axis of the direct beam.

Powder specimens were mixed with a Zapon binder and spread flat on microscope slides over an area large enough to cover the X-ray beam completely when mounted in the specimen holder set at the lowest angle of the run.

Photographic diffraction patterns were also made on most specimens, using a powder camera with a 72-mm. radius. This was done in order to detect very weak reflections which are indistinguishable from the statistically fluctuating background counting rate in the spectrogoniometer recordings.

Interplanar spacings were computed in Ångström units ($\text{Cu K}\alpha_1 = 1.5405 \text{ Å}$). The X-ray patterns could then be compared with the 1950 issue of the ASTM X-Ray Diffraction Data Cards, including the original set and the first and second supplements.

Metallography

Samples for metallographic examination were taken directly from the sample which was ultimately electrolytically digested for X-ray diffraction analysis.

The samples were prepared using standard metallographic preparation techniques. The samples were studied in the unetched condition, then immersed in an etchant² which delineated all of the constituents present. The sample was then subjected to selective etching techniques to differentiate where possible among the constituents present. Polarized light and microhardness were also used to differentiate and identify constituents.

Chemical Analysis

Standard quantitative chemical analysis was determined on each heat of the various alloys studied in this investigation. Nitrogen analyses were made by the vacuum-fusion technique. Results of the analyses are listed in Table I.

RESULTS

X-Ray Diffraction Analysis

Specimens from the various heats of the different alloys were examined in the cast, wrought and heat treated conditions. The thermal history for each of the alloys is given in Table II, and this is then correlated with the main results listed in Table III. The results are discussed here, taking each of the five structure types found in this investigation separately. These types are: (a) spinel-type oxides, (b) the complex cubic carbides, (c) the carbonitrides isomorphous with NaCl, (d) a double nitride, (e) Laves compounds isomorphous with MgZn_2 .

²The etchants used, their chemical composition and their effect on the various microconstituents are listed in Table VIII.

Table I
Chemical Composition in Weight Per Cent

	C	Si	Mn	Cr	Co	Mo	Ti	Al	Fe	Ni	Nb	Nb + Ta	B	N ₂	W
<i>Alloy M252 (Ni Base)</i>															
Heat M477C	0.14	1.09	1.22	19.08	10.04	10.69	1.98	0.35	3.39	Bal.	*	...
Heat M253	0.19	0.67	1.06	18.73	10.17	13.94	0.52	Bal.	trace	*	...
Heat M432	0.04	0.71	0.90	18.98	9.90	10.05	2.41	1.07	3.50	Bal.	*	...
Heat M491	0.20	*	*	*	*	10.92	2.17	0.66	*	*	*	...
Heat M492	0.16	*	*	*	*	11.51	2.42	0.85	*	*	*	...
Heat K294	0.17	0.71	1.19	19.30	10.59	10.56	2.46	0.36	3.15	50.49	*	...
Heat 7382A2	0.23	0.63	0.94	18.87	10.30	9.54	2.62	0.37	4.55	50.70	*	...
Heat 31	0.22	0.85	1.17	18.78	10.51	10.24	2.23	0.69	3.90	Bal.	*	...
Heat 43186	0.19	0.97	1.14	18.71	10.32	9.60	2.26	0.56	2.58	Bal.	0.0294	...
Heat R358	0.07	0.92	1.20	18.70	9.03	9.16	5.03	0.68	1.71	Bal.	0.0343	...
Heat M660	0.25	*	*	19.00	2.50	0.60	4.0	Bal.	*	...
<i>Alloy 16-25-6 (Fe Base)</i>															
K17403	0.12	0.40	1.72	16.40	...	6.42	Bal.	26.00	0.17	...
Heat "X"	0.09	0.38	1.35	15.80	...	6.40	Bal.	25.00	0.13	...
Heat 19903	0.07	0.82	1.60	16.20	...	6.20	Bal.	25.84	0.15	...
Heat 10010	0.07	0.30	1.63	16.24	...	6.10	Bal.	26.08	0.15	...
<i>Alloy Turbalooy 13</i>															
Heat R360	0.13	0.75	1.68	17.80	...	2.48	1.37	1.37	Bal.	23.56	*	1.02
<i>Alloy I336 (Co Base)</i>															
Heat "A"	0.20	0.50	1.0	19.3	48	3.0	15.0	1.0	*	12.0
<i>Alloy I336 Nb + Ta</i>															
Heat 42858	0.20	0.21	0.54	19.08	49.46	1.29	16.74	...	1.04	...	*	11.41

*Elements present, but not determined.

Table II
Heat Treatments

Alloy	Symbol	Treatment
Alloy M252	(A)	Preheat at 1650 °F for 5 hours, 1975 °F for 3 hours. Forging at 1975 to 2050 °F to size; 3-inch, 1-inch or $\frac{3}{8}$ -inch square or round bar stock. 15-minute soaks employed throughout forging.
	(B)	Heated to 1650 °F for 1 hour, furnace-cooled.
	(C)	Heated to 2100 °F for 3 hours, air-cooled. 1500 °F for 24 hours, air-cooled. 1300 °F for 20 hours, air-cooled.
	(D)	Heated to 1950 °F for 4 hours, air-cooled. 1700 °F for 72 hours, air-cooled.
	(E)	Heated to 1950 °F for 4 hours, air-cooled. 1500 °F for 200 hours, air-cooled.
	(F)	As-received billet stock—exact treatment unknown.
Alloy 16-25-6	(G)	Preheat 1500 °F raised to 1950 °F for less than 1 hour. Forging at 1950 °F, three reheats. Cold-worked 20% at 1350 °F, strain-relieved at 1200 °F, 8 hours, air-cooled.
	(H)	1200 °F for 96.5 hours, air-cooled.
	(I)	Heated to 2300 °F for 2 hours. Charged directly into a 1500 °F furnace and held 8 hours, followed by an air cool.
Turballoy 13	(J)	2000 °F for 15 hours, air-cooled.
Alloys I336 and I336 Nb + Ta		
	(K)	Preheat at 1650 °F for 5 hours, 1975 °F for 3 hours, forging at 2000 to 2100 °F to size; 3-inch, 1-inch or $\frac{3}{8}$ -inch square or round bar stock. 15-minute soaks employed throughout forging.

(a) Although the forged and heat treated specimens had been descaled by pickling prior to electrolytic separation, the residues of several heats of M252 showed the presence of a spinel structure, presumably NiCr_2O_4 . This most probably is due to scale which was folded in during forging. None of this oxide was found in the residues of "as-cast" samples.

(b) The carbide M_6C appears to be the principal carbide for normal compositions of M252, 16-25-6, and I336. The latter two alloys may sometimes form M_{23}C_6 as a secondary carbide. These results may be seen in Table III.

Two X-ray patterns of M_6C are shown in Figs. 1a and 1b, each using a different radiation source. They show that the use of copper radiation produces patterns whose clarity is not reduced by fluorescent radiation, whose complexity is reduced by virtual elimination of $\text{K}\beta$ radiation, and whose completeness is increased by the appearance of reflections from smaller lattice spacings. Table IV lists X-ray data on both types of carbides, giving interplanar spacings (d), relative intensities (I) Miller indices (hkl) and squares of structure factors (F^2) computed from intensities. The structure factors for M_{23}C_6 were computed from intensity measurements made on a standard powder of Cr_{23}C_6 ; all other determinations were made from electrolytically separated residues.

Table III
Microconstituents

Alloy M252

Heat	Heat Treatment*	Lattice Parameters in Angström Units					Other
		Titanium Nitrogen-Rich	Carbonitride Medial	Carbon-Rich	MoC	Oxides (Spinel-Type)	
M477C	"As-Cast"	4.27
M477C	"As-Cast"	4.25	4.30	10.99
M477C	"As-Cast"	4.25	4.30	10.99
M477C	(A)	4.25	4.30	10.99
M477C	(A) plus (B)	4.25	4.30	10.99
M477C	(A) plus (C)	4.25	4.30	11.00	8.37
M253	(A)	10.99	8.43
M253	(A) plus (B)	10.99	8.43
M253	(A) plus (C)	10.99	8.43
M432	(A)	4.245	10.97	8.32
M432	(A) plus (B)	4.245	10.97	8.32
M432	(A) plus (C)	10.99	4.734, 7.696
M432	(A) plus (D) or (A) plus (E)	M ₂ Ti (MgZn ₂ Type)
M491	"As-Cast"	4.25	10.99
M492	(A)	4.25	4.30	10.99
K294	(A)	4.25	4.31	11.00
7382A2	(A)	4.25	4.31	11.00
31	Vacuum-Cast	4.311	10.99	8.08
43186	"As-Cast"	4.28	10.99
R358	(A)	4.315	10.98	4.734, 7.696
	"As-Cast"	M ₂ Ti (MgZn ₂ Type)
M660	(A)	4.25	Cr ₂₃ C ₆ Cr ₇ C ₃ , Cr ₃ C ₂

Alloy 16-25-6

Heat	Heat Treatment*	Lattice Parameters in Angström Units					Other
		MoC	M ₂₃ C ₆	Nb(C,N)	TiC	Ti(C,N)	
K17403-4	(G) plus (H)	10.98
K17403-6	(G) plus (H)	10.94
"X"	(F) plus (I)	10.68	Hex., 2.84, 4.57 CrMoN _x
19903	(F)	11.03
10010	(F)	11.02
<i>Turballoy 13</i>							
R360	"As-Cast"	4.327	4.28	4.76, 7.70
	(J)	4.327	4.28	Fe ₂ Al (MgZn ₂ Type)
<i>Alloy I336</i>							
"A"	(K)	11.00	10.64	4.448
<i>Alloy I336 Nb + Ta</i>							
42858	(K)	11.02	4.436

*See Table II for heat treatment corresponding to symbols above.

(c) From a study of the chemical compositions (Table I) and microconstituents identified (Table III) of alloys containing titanium and niobium, it will be seen that both will form their respective carbonitrides.

Special attention was given to the titanium carbonitride because of the increasing use of titanium, and the problems resulting from its use, as an age-hardening alloying constituent in high temperature alloys.

Pure synthetic powders of TiC and TiN were obtained from A. D. Mackay, Inc., and Metal Hydrides, Inc., respectively. Lattice parameters determined by the spectrogoniometer are listed below

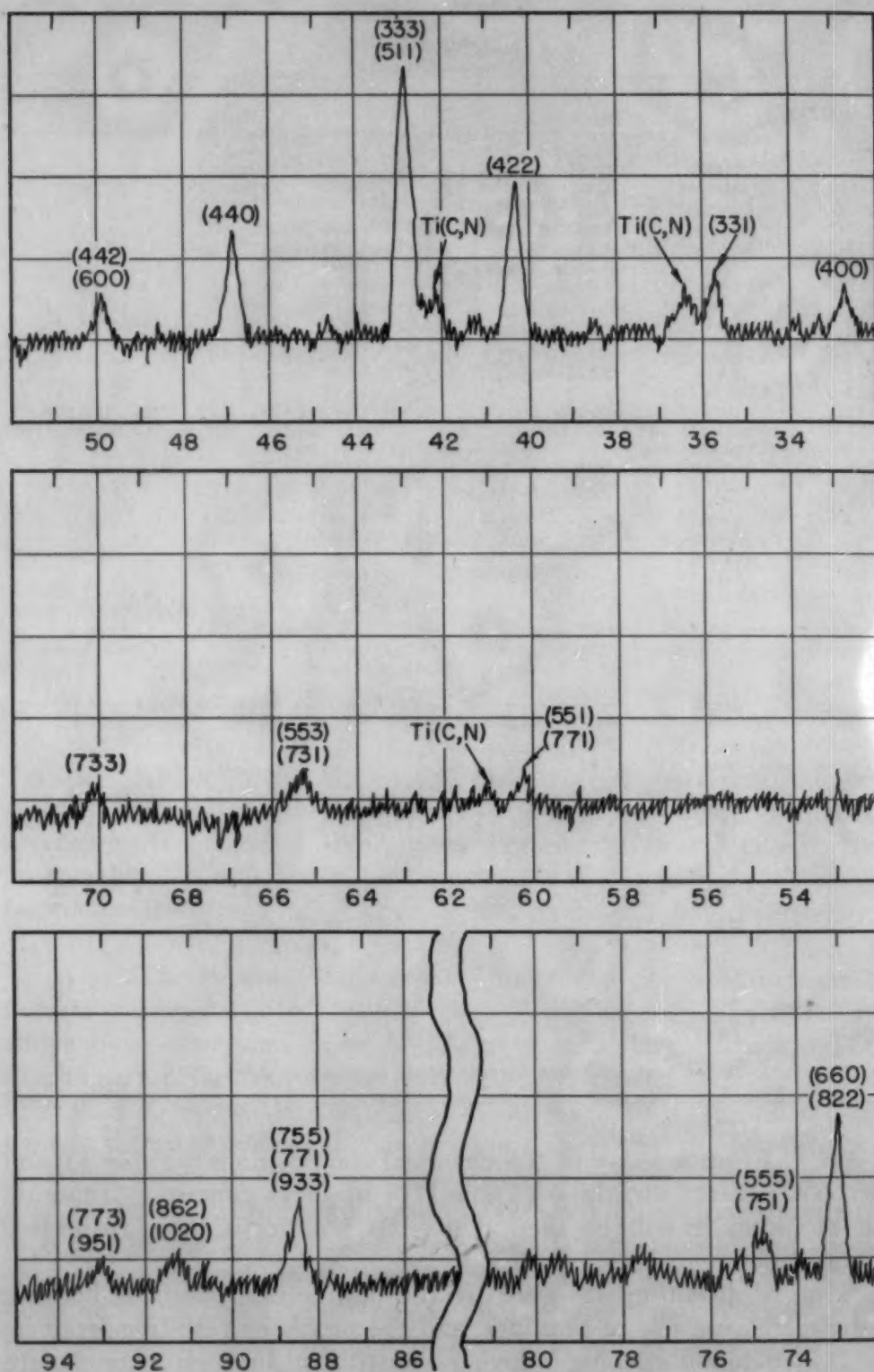


Fig. 1a—Spectrometer Recording of MoC From Alloy M252, Heat 43186, Using Nickel-Filtered Copper Radiation. Miller indices of the MoC are listed above the reflections on the chart. The angles given in the chart are two-theta.

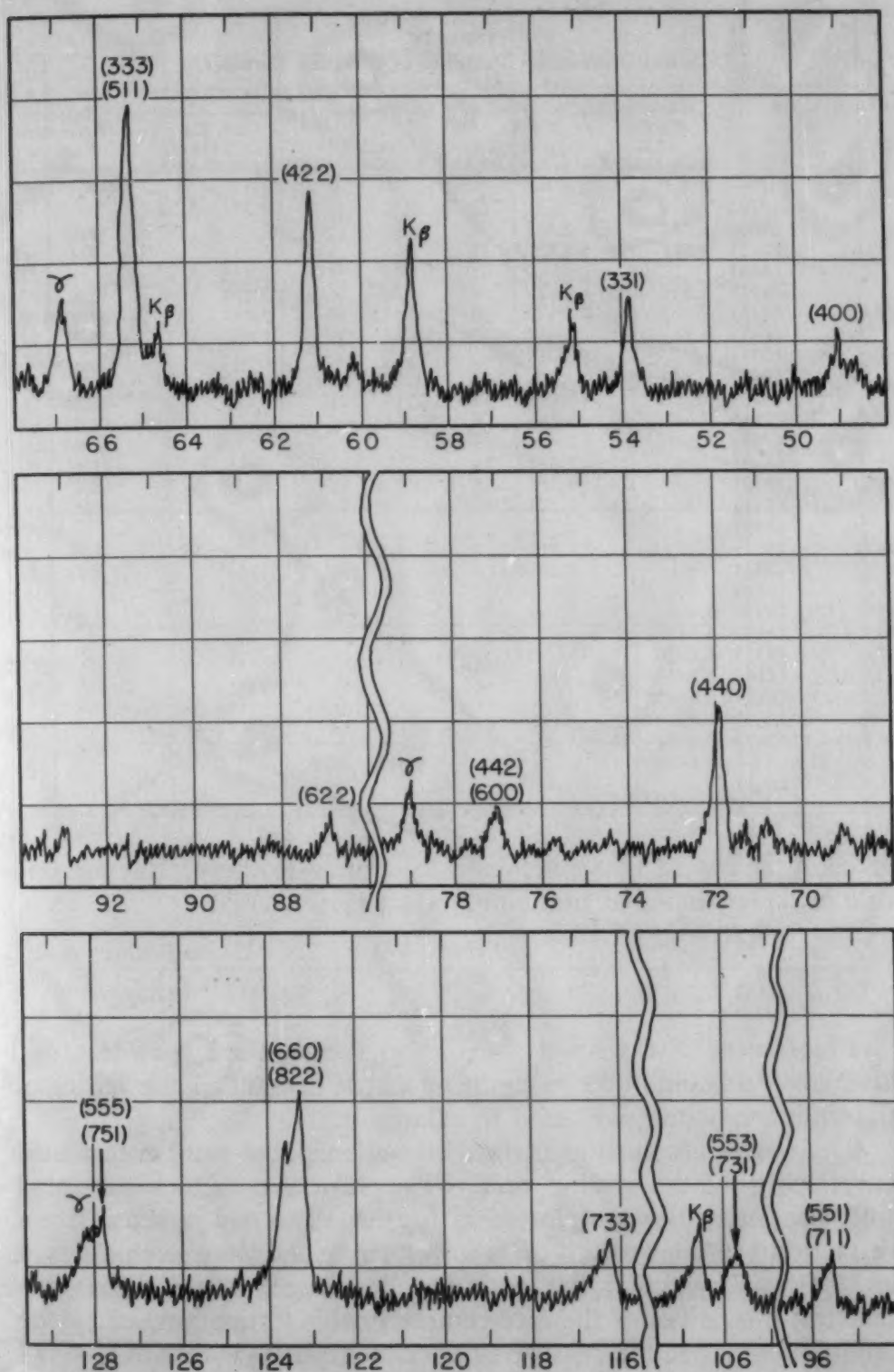


Fig. 1b—Spectrometer Recording of MaC From Alloy 16-25-6, Heat 19903, Using Unfiltered Chromium Radiation. Miller indices of the MaC are listed above the reflections on the chart. Gamma refers to the austenitic matrix found in the residue. The angles given in the chart are two-theta.

Table IV
X-Ray Diffraction Patterns of Complex Carbides

	(hkl)	MeC				M ₂₃ Co				Relative Structure Factors		
		Cu K α 1336		Cr K α Ht. 19903		Cu K α Ht. "X"		Cu K α 1336		F ²		
		a ₀ =11.00 Å		a ₀ =11.03 Å		a ₀ =10.68 Å		a ₀ =10.64 Å		MeC	M ₂₃ Co	
		d	I	d	I	d	I	d	I			
(511)	(220)	3.75	MW	
	(400)	2.744	9	2.755	7	19.5	
	(331)	2.517	18	2.526	11	9.2	
	(420)	2.39	MW	2.378	VW	21.4	
	(422)	2.241	43	2.252	46	2.18	MW	2.174	VW	53.8	27.0	
	(333)	2.113	100	2.122	100	2.053	M	2.047	W	100.0	100.0	
	(440)	1.942	25	1.950	30	1.885	W	1.883	W	97.2	52.0	
	(531)	21.0	
	(442)	(600)	1.829	5	1.839	7	11.0	14.3
	(622)	1.663	3	6.56	18.9	
	(551)	(711)	1.541	9	1.545	9	10.0
	(553)	(731)	1.432	9	1.436	9	6.94
(753)	(733)	1.343	11	1.3485	10	21.4	
	(822)	1.296	34	1.301	57	1.259	W	1.255	W	68.8	50.0	
	(555)	(751)	1.270	7	1.275	16	1.231	VW	11.1	14.9
	(840)	27.4	
	(911)	1.212	7	1.173	W	1.66	9.5	
	(842)	1.2044	6	3.23	
	(844)	1.090	VW	50.0	
	(755) (771)	(933)	1.106	13	1.108	12	3.64	12.3
	(10,2,0)	(862)	1.079	7
	(773)	(951)	1.0636	7
	(10,6,0)	(866)	0.9438	7
	(12,0,0)	(884)	0.9169	7
(777)	(11,5,1)	0.9078	7	
(10,6,4)	(12,2,2)	0.8926	13	
(993), (13,1,1)—	0.8418	7	0.817	VW	8.4	
(11,5,5)	(11,7,1)											

and compared with those obtained by Hume-Rothery, Raynor and Little in their studies of titanium steels (4).

	Present Work	Hume-Rothery et al
TiC	4.327 Å	4.325 Å
TiN	4.240 Å	4.233 Å

Fluorescent X-ray spectra made on the synthetic powders disclosed small amounts of zirconium which, if present in the lattice of a titanium compound, will tend to enlarge it.

The relative intensities of the diffraction peaks were determined accurately using the scaling unit. The structure factors computed from these intensities are plotted in Fig. 2. The odd-indexed structure factors are seen to fall on a lower curve than the even-indexed ones. This shows that the carbon and nitrogen atoms lie in the octahedral interstices of the face-centered cubic lattice formed by the titanium atoms; i.e., the structures are isomorphous with NaCl. Had they formed at the tetrahedral interstices as has been suggested as another possible structure (isomorphous with ZnS), a different group of structure factors would lie on the lower curves.

All structures identified as titanium carbonitride $\text{Ti}(\text{C}_x\text{N}_{1-x})$, or more simply $\text{Ti}(\text{C,N})$, have lattice parameters which lie between

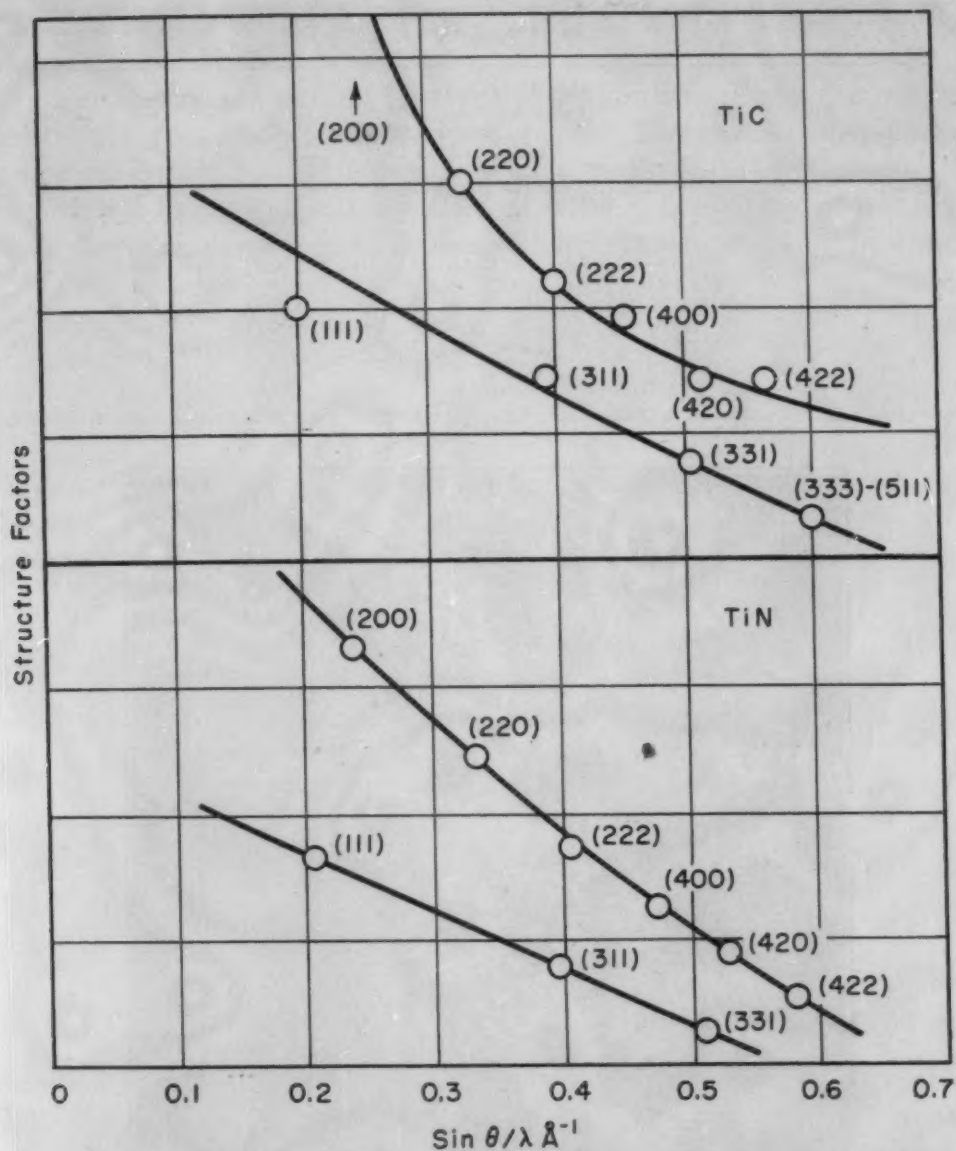


Fig. 2—Structure Factors of TiC and TiN, Showing That the Carbon and Nitrogen Atoms Occupy the Octahedral Interstices.

those of TiC and TiN, the specific value depending on the C/N ratio.

The latest references report lattice parameters for the niobium compounds as 4.470 Å for NbC and 4.379 Å for NbN (5). The structures identified as Nb(C,N) have lattice parameters lying between these values (Table III).

(d) Heat treatment (I), Table II, of Alloy 16-25-6 has been observed to produce a phase which could not be matched with any data in the literature.

Its X-ray pattern, given in Table V, shows conformity with a hexagonal lattice whose unit cell dimensions are given at the top of the table.

Table V

CrMoN_x from 16-25-6
Hexagonal; $a_0 = 2.84 \text{ \AA}$
 $c_0 = 4.57 \text{ \AA}$
 $c_0/a_0 = 1.61$

Cu K α Radiation

d	I	(hkl)
2.49 \AA	mw	(100)
2.25	m	(002)
2.18	s	(101)
1.670	w	(102)
1.522	vw	(003)
1.421	w	(110)
1.300	w	(103)
1.209	w	(112)

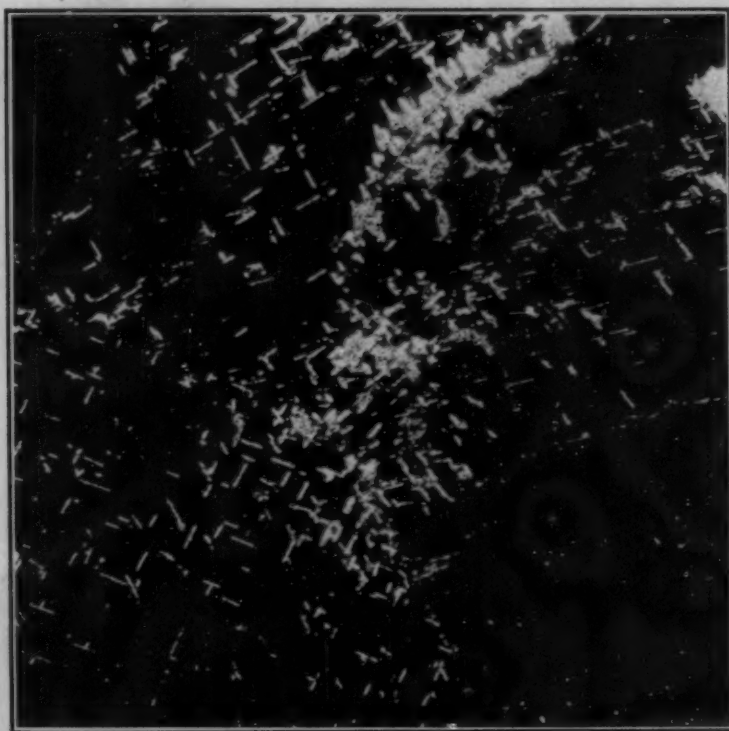


Fig. 3—Diffraction Fringes Around the CrMoN_x Needles Suggest That the Widths May Approach Optical Wave-Lengths. Polarized light. Etchant (c). $\times 500$.

This constituent occurs in the microstructure in the form of thin needles. When the microstructure is viewed under polarized light and the microscope stage is rotated, the optical anisotropy of this constituent is noted. From an examination of Fig. 3, it is to be expected that X-ray reflections from planes nearly parallel to the axes of the needles will suffer some broadening. In the X-ray pattern, the greatest line broadening was seen to occur for planes nearly parallel to the c-axis of the hexagonal lattice indicated by the X-ray pattern.

The unit cell dimensions lie between those of the similarly

shaped unit cells of Cr_2N and Mo_2C , and the a -axis is nearly equivalent to that of MoN .

The X-ray extinctions and relative intensities from the various lattice planes closely follow those of the hexagonal close-packed structure, except for the appearance of a weak (003) reflection. In an ordered hexagonal close-packed structure, consisting of alternate basal sheets of two kinds of atoms which differ appreciably in atomic

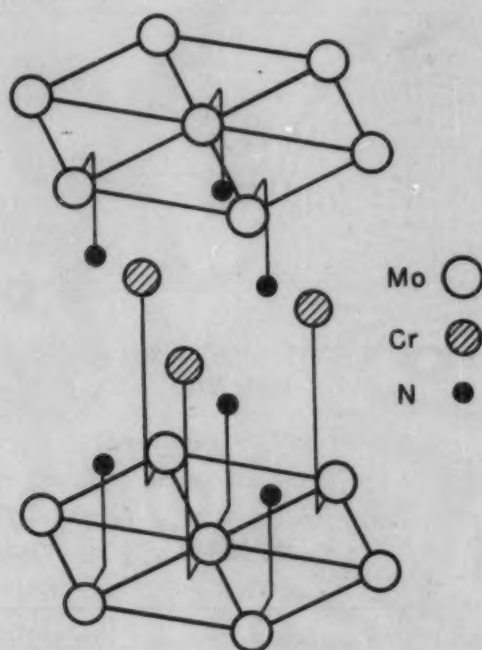


Fig. 4—Proposed Atomic Arrangement of the Saturated Double Nitride CrMoN_2 .

number, the (003) reflection would be a prominent superstructural line.

The observed lattice dimensions are just large enough to accommodate alternate basal sheets of chromium and molybdenum with nitrogen in the interstitial holes (Fig. 4). Since up to one-half of the interstitial holes may be vacant without appreciably altering the lattice parameters, the formula for this constituent should be given as CrMoN_x , with x lying between 1 and 2.

(e) Two intermetallic Laves compounds were found in this investigation, both of which are isomorphous with MgZn_2 (6). Their X-ray patterns are given in Tables VI and VII. Their lattice parameters are close to those of Fe_2W (7) and Fe_2Ti (8), which are also isomorphous with MgZn_2 .

These are hexagonal structures having 12 atoms per unit cell. The packing principle in this structure occurs for a composition having one large atom for every two small atoms, the atomic size ratio being about 1.2. The two small atoms need not be the same

Table VI

Intermetallic in M252 (M ₂ Ti)		
Hexagonal, MgZn ₂		
$a_0 = 4.734 \text{ \AA}$		
$c_0 = 7.696 \text{ \AA}$ $c_0/a_0 = 1.625$		
Cu K α Radiation		
d	I	(hkl)
2.367 \AA	45	(110)
2.174	100	(103)
2.049	22	(200)
2.017	95	(112)
1.980	73	(201)
1.924	13	(004)
1.742	7	(104)
1.527	7	(211)
1.438	9	(212)
1.367	12	(300)
1.327	27	(213)
1.284*	23*	(006)
1.231	18	(205)
1.184	17	(220)

*Interference from MoC.

Table VII

Intermetallic in Turballoy 13		
(Fe ₂ Al)		
Hexagonal, MgZn ₂		
$a_0 = 4.760 \text{ \AA}$		
$c_0 = 7.700 \text{ \AA}$ $c_0/a_0 = 1.617$		
Cu K α Radiation		
d	I	(hkl)
2.38 \AA	25	(110)
2.176	57	(103)
2.058	15	(200)
2.020	100	(112)
1.990	74	(201)
1.925	9	(004)
1.816	15	(202)
1.743	6	(104)
1.442	3	(105)
1.411	6	(204)
1.370	9	(300)
1.330	18	(213)
1.211	6	(214)
1.190	12	(220)
1.043	12	(313)
1.020	6	(401)
1.010	6	(224)

element, but must have nearly the same size.

In alloy M252, titanium and molybdenum could take the role of "large" atoms, while chromium, iron, cobalt and nickel are all nearly the same size "small" atoms. In other high temperature alloys, niobium, tantalum, wolfram and possibly aluminum could serve as large atoms.

Since the intermetallic occurs prominently in Alloy M252 when the titanium content is doubled (Heat R358), it is likely that titanium is the large atom in this phase. This is further supported by the fact that the phase forms after a prolonged aging treatment in a low

carbon heat (Heat M432), there being little opportunity for the titanium to precipitate in the form of TiC . The intermetallic in Alloy M252, therefore, is identified as M_2Ti , where the M's can be any of the small atoms.

A similar structure of slightly different lattice dimensions, identified as Fe_2Al , was observed in Turballoy 13, about which more will be said in the studies of microstructure.

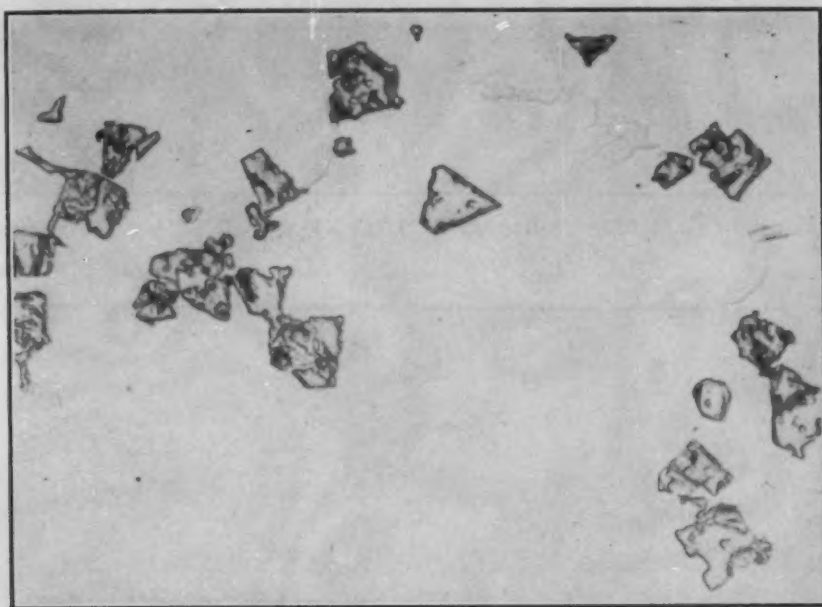


Fig. 5—Cast M252. Nitrogen-rich Ti(C, N) as found in most heats of this alloy. Unetched. $\times 500$.

Microstructure

The two minor microconstituents found in Alloy M252 by X-ray diffraction studies were titanium carbonitride and the complex carbide M_6C .

Microscopically, the titanium carbonitride constituent changes its shape and color as its lattice parameter changes. Studied in the unetched condition and using brightfield illumination, the nitrogen-rich ($a_0 = 4.25 \text{ \AA}$) particle appears as an angular idiomorphic crystal, which is golden in color. Fig. 5 shows typical particles as found in cast M252. Two crystals at high magnification (Figs. 6a and 6b) illustrate the marked tendency for this nitrogen-rich particle to occur in angular form. The carbon-rich particles ($a_0 = 4.30 \text{ \AA}$), on the other hand, are irregular in shape and lavender-gray in color when viewed under the same conditions (Fig. 7). The nitrogen-rich particles, when present in large amounts, frequently segregate to form clusters and chains (Fig. 8). Chaining of the carbon-rich Ti(C, N) may also occur and has been observed in a low carbon modification

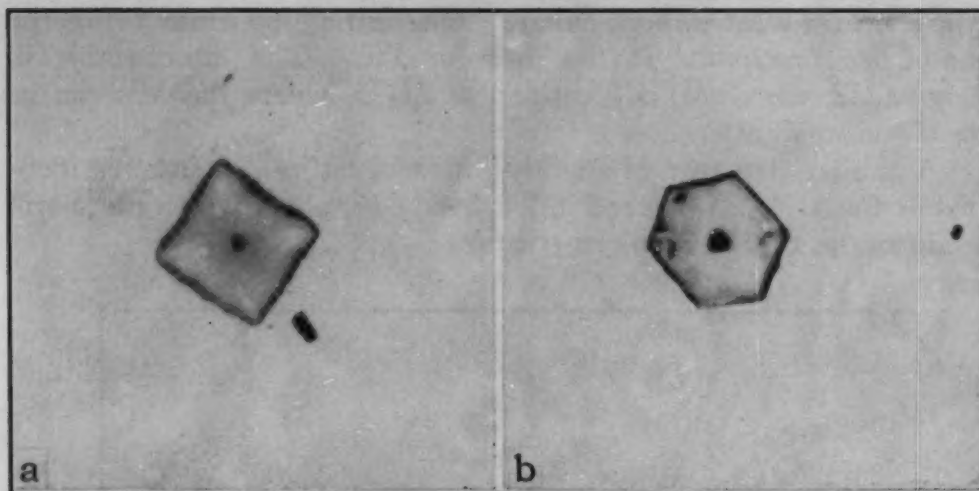


Fig. 6a-6b—Cast M252. Nitrogen-rich $Ti(C, N)$ crystals at high magnifications. Unetched. $\times 1500$.

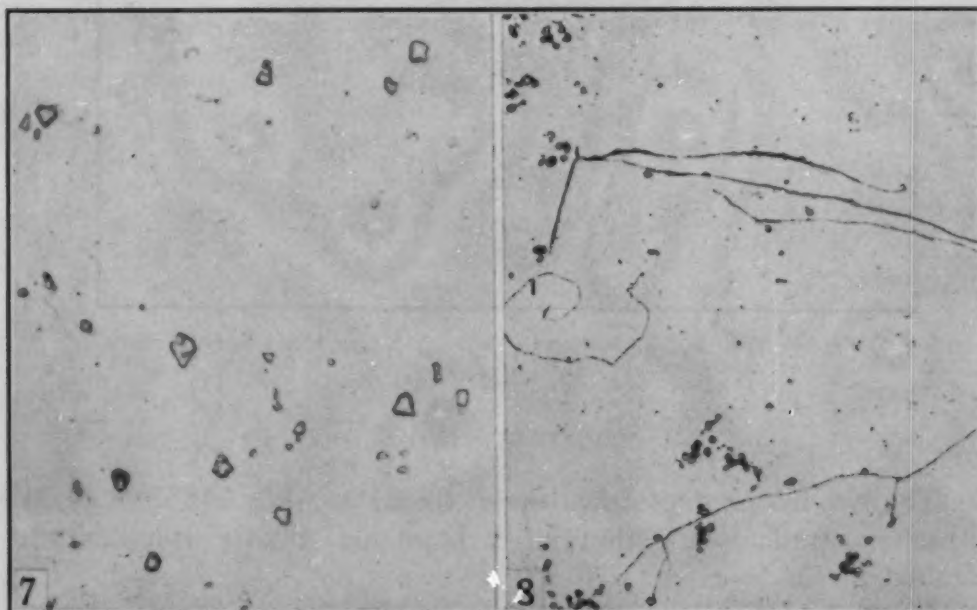


Fig. 7—Cast M252. Carbon-rich $Ti(C, N)$ as found in some heats of this alloy. Unetched. $\times 500$.

Fig. 8—Cast M252. Nitrogen-rich $Ti(C, N)$ as found in heat which was seriously contaminated with nitrogen from the air during melting and casting. Unetched. $\times 100$.

of the N155 analysis (9). Microhardness was obtained on a heat of Alloy M252 which yielded nitrogen-rich particles, whose particle size varied up to 0.002 in. The larger particles were suitable for sustaining a 100-gm. load using the Knoop microhardness tester. Five readings obtained on the larger particles varied between 2100 and 2380 Knoop hardness number. The microhardness of the carbon-rich particles was not determined but would presumably be very close to the hardness of the pure TiC .

Examination of the microstructures of M252 samples after each step of the heat treatments listed in Table II revealed no change in the size, shape, or general distribution of the N-rich $\text{Ti}(\text{C},\text{N})$. Further, a series of samples, examined after vacuum annealing for 1 hour in 100-degree steps from 1900 °F (1040 °C) to the solidus of the alloy at approximately 2300 °F (1260 °C), led to the same observation. The C-rich $\text{Ti}(\text{C},\text{N})$, on the other hand, was markedly affected, changing in both size and shape.



Fig. 9—Cast M252. Microstructural appearance of the complex carbide M_6C . Etchant (a). $\times 500$.

Examination of specimens taken from cast ingots of Alloy M252 revealed a more dense concentration of the N-rich $\text{Ti}(\text{C},\text{N})$ in the up-end of the ingot, as compared to the base or down-end.

The preceding observations suggest that the nitrogen-rich particles (4.25 Å) are solid in the liquid melt. The carbon-rich particles (4.30 Å) appear to behave much as the pure TiC would be expected to behave. Those particles which would have intermediate lattice parameters pattern their behavior as regards their N-rich or C-rich characteristics.

The complex carbide M_6C appears as a "Chinese script" constituent in the cast M252 (Fig. 9), having a slightly pink color. In wrought M252 the M_6C appears as spheroids directionally distributed in accordance with the hot working or rolling direction. Differentiation between the $\text{Ti}(\text{C},\text{N})$ and the M_6C in Alloy M252 was quite straightforward, there being the differences in color and hardness as well as etching characteristics. The M_6C was stained brown, using etchant (b), Table VIII, while the $\text{Ti}(\text{C},\text{N})$ retained its characteristic range of colors. The difference in hardness evidenced itself in the polishing of the samples, the $\text{Ti}(\text{C},\text{N})$ of all C-N ratios tending to polish in relief prominently whereas the M_6C did not.

Table VIII
Table of Etchants

Etchant	Composition	Technique	Use
(a) 92-5-3	HCl 92 ml. H ₂ SO ₄ 5 ml. HNO ₃ 3 ml.	Add H ₂ SO ₄ to HCl slowly. Use fresh solution. Etch by immersion.	General structure.
(b) Alkaline-Permanganate	4% Aqueous solution of NaOH plus saturated solution of KMnO ₄ . 1-1 ratio.	Immerse 3-4 seconds, clean with water and dry with blast of air.	Selective etch for Fe and Ni-base alloys. M ₆ C stained brown and outlined. No effect on MC M ₄ C or matrix.
(c) 10% Chromic	10% Aqueous solution of chromic acid.	Use electrolytically 5-10 seconds.	General structure.
(d) H ₂ SO ₄	20% Aqueous solution of H ₂ SO ₄ .	Immerse or swab 30 seconds at 70 °C. Quench.	Fe-Al intermetallics.
(e) Chromic-stain etch	2% Aqueous solution of chromic acid.	A light etch, electrolytically, 2-3 seconds. Follow by an immediate etch in alkaline potassium permanganate (20% KMnO ₄ , 8% NaOH) for 7 seconds.	Selective etch for Co-base alloys. M ₆ C (Cr ₄ C, or Cr ₂₃ C ₆) is etched brown. M ₆ C varies between red and green tints. Occasionally may have blue tints.

Microstructures of four variations of the composition of M252 were studied,

- (a) Heat M253, absence of titanium and aluminum.
- (b) Heat M432, low carbon.
- (c) Heat R358, low carbon, double the nominal titanium content.
- (d) Heat M660, absence of molybdenum and cobalt.

No titanium carbonitride was observed in Heat M253; however, the complex carbide M₆C was observed both in the microstructure and by X-ray diffraction analysis.

A marked reduction of the amount of M₆C present was noted in Heat M432 in the cast and wrought structures. Fig. 10 illustrates the microstructure after heat treatments (a) and (c), Table II. In addition the absence of the carbon-rich Ti(C,N) was noted, although the nitrogen-rich Ti(C,N) was present in the amount usually found in Alloy M252. Subjecting samples of this heat to heat treatment (d), Table II, resulted in agglomeration of such M₆C as was present at the grain boundaries and the appearance of an acicular constituent as seen in Fig. 11. X-ray diffraction identification reveals this constituent to be the phase M₂Ti.

The acicular phase, M₂Ti, and M₆C are both observed in the cast structure of Heat R358. The presence of M₆C is most probably due to nonequilibrium conditions. Efforts to convert this ingot to wrought stock were unsuccessful, due to its hardness and brittleness. This extreme hardness (Rockwell C-40) can well be expected from

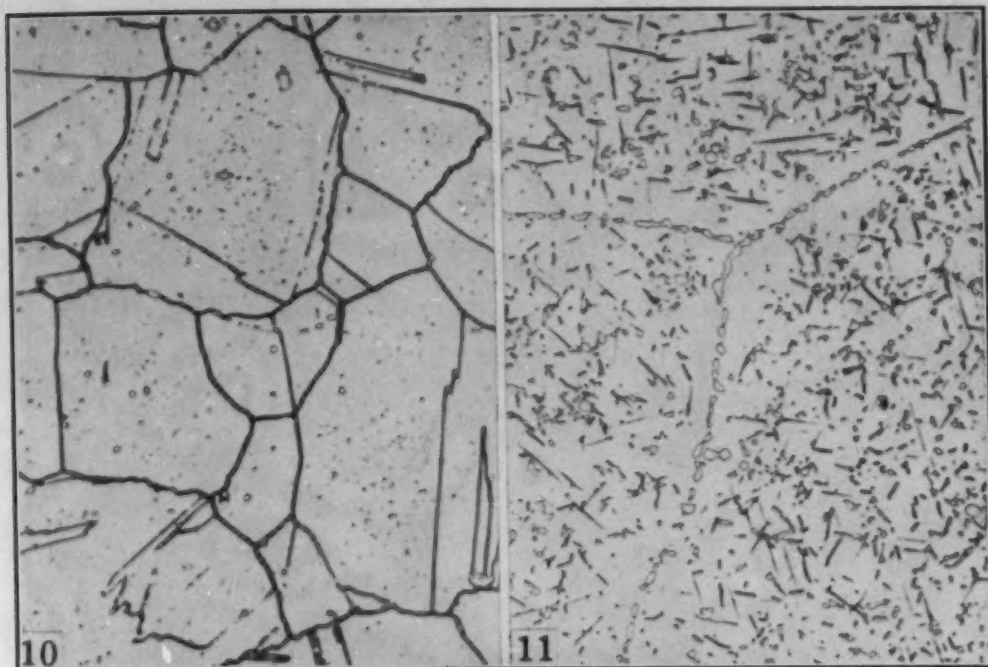


Fig. 10—Heat M432. Heat treatments (a) and (c). Etchant (a). $\times 500$.

Fig. 11—Heat M432. Heat treatments (a) and (d). Agglomeration of the M_6C at the grain boundaries; the acicular phase is M_2Ti . Etchant (a). $\times 500$.

a consideration of the fact that not only is the hard intermetallic M_2Ti present but it appears to have some coherency with the matrix (Fig. 12). Microscopically, $Ti(C,N)$ was observed in the structure.

The carbide found in Heat M660 appeared much different in color and particle size, the particle size being much smaller than that usually observed for the M_6C and the color tending more toward the red. X-ray diffraction results indicate the absence of the M_6C and the presence of chromium carbides, these results being supported by the foregoing microscopic observations. Once again the $Ti(C,N)$ was observed in the microstructure.

Alloy 16-25-6 is normally composed of two phases, austenite plus carbide, as a result of the standard commercial heat treating practices. X-ray diffraction evidence indicates that the carbide phase is the complex carbide M_6C , and studies of the microstructure using selective etchant (b) also indicate that the carbide phase is M_6C . It must be noted that this alkaline-stain etch has not been found to be too reliable in distinguishing among carbide phases. Specimens of Alloy 16-25-6 from many commercial heats, examined after various heat treatments and operating conditions, indicate that particle size plays a role in the color-staining characteristics of the etchant, even when the composition and etching time are carefully controlled from sample to sample. Notwithstanding this limitation, all of the carbide phase found in 16-25-6 stained brown in color, as prescribed, in most



Fig. 12—Heat R358, As-Cast. Islands of M_6C amidst the acicular M_2Ti . Etchant (a) $\times 500$.

Fig. 13—Heat "X", Alloy 16-25-6, Heat Treatment (I). Acicular constituent is $CrMoN_2$, the grain boundary constituent being the complex carbide $M_{23}C_6$. Etchant (c). $\times 500$.

specimens studied, so that coupled with X-ray diffraction results it seemed apparent that all of the carbide present was M_6C . The etchant, as described in Table VIII, was found to be very helpful in distinguishing grain boundary agglomeration of the carbide, in order that low magnification studies might disclose the general carbide distribution. The carbide distribution varies from random dispersion to banding of the carbide, to carbide solely at the grain boundaries and all variations between. The carbide distribution is largely determined by the cold working and thermal history of the piece, although differences were noted for samples with the same history.

In the history of the use of 16-25-6 at the Lynn River Works of the General Electric Company, only the phases austenite plus M_6C had been observed until recently when samples of 16-25-6 were subjected to thermal treatment (I). This heat treatment resulted in a three-phase condition identified by combined X-ray diffraction and metallographic techniques as austenite plus $M_{23}C_6$ plus $CrMoN_2$. The crystallography of the two minor microconstituents and their optical behavior when rotated under polarized light made the correlation of microstructure with X-ray diffraction results quite straightforward. The complex carbide $M_{23}C_6$ appears at the grain boundaries (Fig. 13).

In the austenitic Turballoy 13 three minor microconstituents were detected by X-ray diffraction analysis, TiC , $\text{Ti}(\text{C},\text{N})$ and a Laves compound identified as Fe_2Al . In an attempt to identify the grain boundary constituent (Fig. 14a), etchant (d) was employed as a selective etchant. The phase was quite strongly attacked, indicating an Fe-Al phase. This information supports the X-ray diffraction identification results of this phase as Fe_2Al . Subsequent thermal treatment (J) caused the solution of this phase, indicating that its

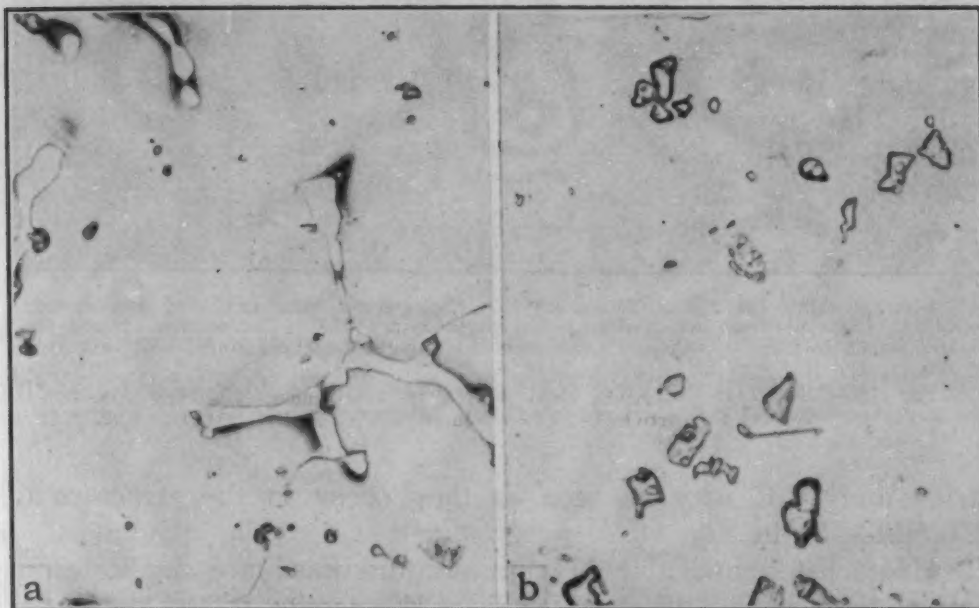


Fig. 14a—Turballoy 13, As-Cast. Irregular shaped particles, gray in color, are TiC ; the grain boundary phase is Fe_2Al . Note severe attack at edges of this phase. Etchant (d). $\times 500$.

Fig. 14b—Turballoy 13, Cast Plus Heat Treatment (J). The Fe_2Al is absent; the TiC particles have increased in size. Etchant (d). $\times 500$.

formation most probably was the result of casting inhomogeneities. Fig. 14b illustrates the microstructure after heat treatment. Note also here the growth of the TiC particles during this thermal treatment. The identification of the TiC and $\text{Ti}(\text{C},\text{N})$ was made using previously described techniques.

The cobalt-base alloys, I336 and I336 Nb + Ta, were studied and the minor microconstituents, M_6C , M_{23}C_6 and $\text{Nb}(\text{C},\text{N})$, were identified by X-ray diffraction. The carbonitride was readily recognized, due to its hardness and color, and the complex carbides M_6C and M_{23}C_6 were distinguished on the basis of acid-stain etchant (c). The limitations affecting stain etchant (b), as discussed earlier, are equally applicable to this stain etching procedure; however, with adequate care in technique and examination, a distinction can be made between carbide phases. Distinction of the two complex carbide phases in Alloy I336 may be seen in Fig. 15. Niobium carbo-

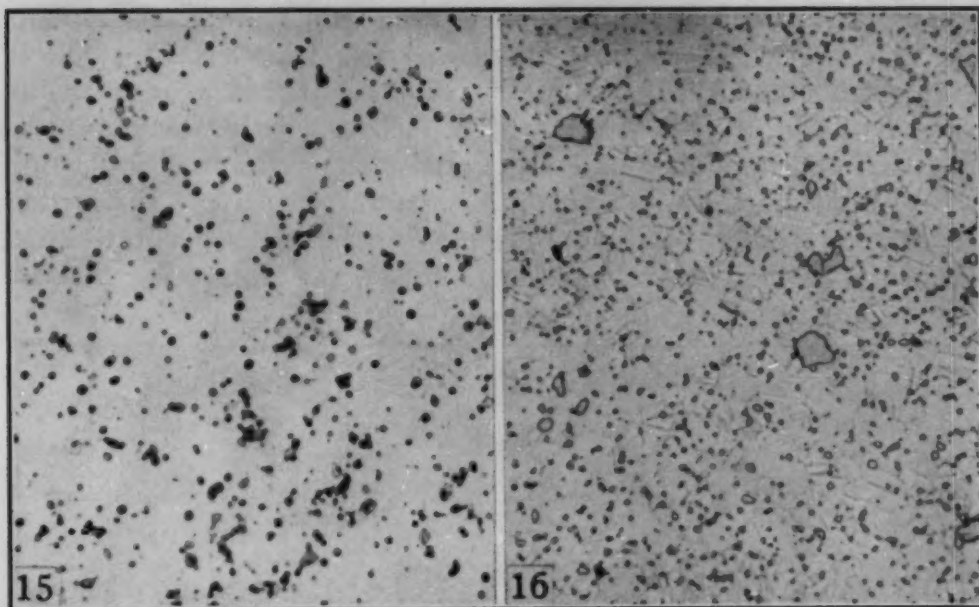


Fig. 15—Alloy I336, Heat Treatment (K). Selective etching, to distinguish between carbides. Light particles are $M_{23}C_6$, darker particles are M_6C . The etchant stained the lighter particles ($M_{23}C_6$) tan and the darker particles (M_6C) red-green. Etchant (c). $\times 500$.

Fig. 16—Alloy I336 Nb + Ta, Heat Treatment (K). Small spheroids are M_6C ; the larger particles are yellow colored Nb(C, N). Etchant (a). $\times 500$.

nitride and M_6C may be seen as they occur in the structure of I336 Nb + Ta in Fig. 16.

Heats listed in Table III but not discussed are duplicates of heats of the various alloys which were discussed. These duplicates were examined and included as supplementary confirmation of the data obtained on the original heats.

DISCUSSION OF RESULTS

The matrix phase of the high temperature alloys studied in this investigation, and indeed in most high temperature alloys, is face-centered cubic. This matrix phase is rich in some or all of the following elements: chromium, iron, cobalt and nickel, which have nearly equal atomic radii. The lattice parameter of this face-centered cubic matrix is governed not only by these elements but also by the solid solution of varying amounts of aluminum, titanium, vanadium, niobium, molybdenum, tantalum and wolfram, when any of these elements are present.

The lattice parameter of the matrix is most affected by changing atomic percentages of the latter group of elements which have comparatively large atomic radii.

This latter group of elements when dissolved in the matrix will distort the lattice in their immediate vicinity, creating high energy fields in the lattice. Other sources of high energy fields in the lattice

are the carbon and nitrogen atoms occupying interstices, which, in the undistorted lattice, are too small to accommodate them.

Therefore, it would appear that those elements found in high temperature alloys having relatively large atomic radii and conversely those having very small atomic radii would be involved in the formation of nonmatrix phases.

In the high temperature alloys studied, these large metallic atoms are involved in the formation of intermediate phases in three ways:

First, they may form intermetallic compounds, whose governing factor is atomic size.

Second, they may form hexagonal or cubic close-packed lattices whose large interstices may accommodate carbon and nitrogen atoms. These compounds may be called Hägg compounds, as it was G. Hägg (10, 11) who pointed out that their formation occurs whenever the ratio of the radii of nonmetal to metal atoms does not exceed 0.59.

Third, they may participate in the formation of the complex carbides.

The elements involved in intermediate phases which received the most attention in this investigation are molybdenum and titanium. The effects of each of these minor alloy additions are discussed here separately.

Titanium

Titanium in the high temperature alloys studied was found as a participating element in the formation of two microconstituents: (a) Hägg compounds and (b) a Laves intermetallic.

The results in Fig. 2 prove that the two Hägg compounds TiC and TiN are completely isomorphous, since carbon and nitrogen occupy the same interstices. This isomorphy favors the existence of a continuous solid solution of the TiC and TiN.

The work of Hume-Rothery, Raynor and Little (4) and Duwez and Odell (5), as well as the results of this investigation, demonstrate the existence of the binary solid solution system TiC-TiN.

Alloy M252 usually contains both a nitrogen-rich and a carbon-rich phase of this system. Metallographic evidence suggested that the nitrogen-rich Ti(C,N) is present in the liquid melt, since examination of cast billets revealed many of the near-nitrides to have segregated at the up-ends of the billets, as well as the other observations mentioned in Results. The carbon-rich Ti(C,N) appears to form after the nitrogen-rich phase in some instances, since microstructural studies reveal the carbon-rich phases often appended to or surrounding the nitrogen-rich Ti(C,N). This would indicate that the latter served as a nucleation center for the former, as would be expected from their isomorphy. Such a duplex-particle, after a sufficient time-temperature diffusion period, should become a particle

of medial composition and eventually a carbon-rich $\text{Ti}(\text{C},\text{N})$. Microstructural evidence from this investigation revealed particles having a continuous color variation from the center to the surface of the particles. Also, the residue of Heat 43186 gave broad X-ray diffraction peaks whose maxima belong to a medial lattice parameter (Table III). It is possible, therefore, that the length of time the melt is held at temperature, after the titanium addition, until it is poured or until the melt solidifies, may be sufficient time for such a process to occur.

It is suggested from these data that the nitride forms in the liquid melt either through contact with air, or contamination from the type of titanium alloying addition.

The effect on the physical characteristics of a titanium age-hardenable high temperature alloy by the presence of $\text{Ti}(\text{C},\text{N})$ inclusions is quite marked, depending on the amount and C/N ratio of the $\text{Ti}(\text{C},\text{N})$. The most undesirable effects are noted when the N-rich $\text{Ti}(\text{C},\text{N})$ is present, particularly when it is present in sufficient amounts to form "chains" or "sheets" of this hard constituent. Forgeability of the alloy is seriously impaired, the material becomes very difficult to machine, and surface defects on finished parts become plentiful.

The formation of Hägg compounds such as $\text{Ti}(\text{C},\text{N})$ and $\text{Nb}(\text{C},\text{N})$ occurs even when the amounts of the metal elements involved in the alloy are very low; e.g., 1% niobium in Alloy I336, 1.37% titanium in Turballoy 13. On the other hand, in order to form a Laves intermetallic such as M_2Ti in some of the M252-type heats, the solubility limit of the large atom in the matrix must be exceeded.

If the ratio of atomic radii does not depart too much from the ideal Laves ratio of 1.225, the Laves packing principle occurs in regions where the local composition has one large atom for every two small atoms. When the solubility limit of the large atom in the matrix is exceeded, there is a finite probability that such local regions will occur sufficiently large to start nucleation of a Laves phase. The atomic radii ratio for M_2Ti is 1.182. When there is very little carbon in the alloy, prolonged aging (1500 °F for 200 hours) effects the precipitation of M_2Ti in a heat containing 2.41% titanium. When the titanium content is increased to 5% as in Heat R338, the M_2Ti appears prominently in the cast structure. It seems likely, therefore, that in both cases the solubility of titanium in the matrix has been exceeded.

The Laves compound identified as Fe_2Al in Turballoy 13 appeared in the cast structure; however, subsequent solution treatment caused its disappearance. Its instability may arise from an unfavorable atomic radii ratio, this being 1.135, or alternatively from thermal considerations.

Molybdenum

In the high temperature alloys studied, molybdenum was found as a participating element in two types of microconstituents:

- (a) A Hägg-type double nitride.
- (b) Complex cubic carbides.

Alloy 16-25-6 has 0.15% nitrogen by weight dissolved interstitially in the matrix.

The CrMoN_x was formed as the result of treating a specimen of as-received billet stock of 16-25-6 as described by heat treatment (I), Table II. Duplication of this treatment with an intermediate air cool, after the 2300 °F (1260 °C) solution treatment, also caused the formation of the CrMoN_2 . The structure was observed and identified in a 16-25-6 part when sections were examined after a certain amount of service life. The time-temperature conditions of the part are not accurately known so that data on this heat were not included in this presentation.

Both molybdenum and chromium have favorable atomic size ratios with respect to nitrogen for the formation of Hägg compounds. Molybdenum has a favorable size with respect to carbon, but chromium does not. As a result, the nitrides of molybdenum and chromium, and the carbides of molybdenum (MoC , Mo_2C) are hexagonal Hägg compounds, while the carbides of chromium (Cr_7C_3 , Cr_{23}C_6) are more complicated structures.

Evidence indicates that the metallic framework of the CrMoN_x lattice, Fig. 4, is an ordered hexagonal close-packed structure whose interstitial holes are large enough to accommodate nitrogen atoms up to a saturated composition of CrMoN_2 . Both molybdenum and nitrogen obviously have a lower energy environment in this structure than they have in the matrix. This low energy configuration is approximated when, during diffusion, alternate molybdenum-rich (111) planes of the matrix chance to occur in the presence of much interstitial nitrogen. The (111) matrix planes then may transform into the basal planes of CrMoN_x . This is suggested by the acicular structure of this nitride seen in Fig. 13.

For the range of compositions covered by the alloys in this investigation, molybdenum also precipitates in the form of double carbides, these having complex but highly symmetrical cubic structures.

By virtue of their high degree of symmetry, Westgren and his associates were able to solve the atomic arrangements of M_{23}C_6 and M_6C (12). The resulting configurations indicate that Cr_{23}C_6 can dissolve molybdenum (or wolfram) up to a limit of $\text{Cr}_{21}\text{Mo}_2\text{C}_6$, while M_6C can range in composition from $\text{M}'_4\text{Mo}_2\text{C}$ to $\text{M}'_3\text{Mo}_3\text{C}$, where M' is a combination of chromium, iron, and cobalt. Thus, we should expect that if M_{23}C_6 forms in low molybdenum alloys, an

increase in molybdenum would result in an increasing tendency to form M_6C . This tendency has already been noted experimentally (2, 3).

Table III indicates that Alloy 16-25-6 has a composition which would ordinarily result in the formation of M_6C . There is an exception, however, in the case where the formation of the nitride $CrMoN_x$ has presumably resulted in a depletion of molybdenum from the matrix. The lattice parameter of the $M_{23}C_6$ formed in this heat suggests the composition type $Cr_{21}(Cr,Mo)_2C_6$.

As may be expected, the complex carbides were the low melting constituents in the alloys investigated.

These carbon-poor carbides may be governed by electron concentrations as well as by atomic size factors. The structure factors of these carbides (Table IV) indicate two prominent Brillouin zones. The outer one, bounded by the (660)–(822) planes, has a capacity for a total of approximately 7 electrons per metal atom. This zone has the identical shape and eight times the volume in k -space as the (330)–(411) Brillouin zone for gamma-brass, which contains 84 electrons per unit cell (13). If it be assumed that the (660)–(822) zone in M_6C is filled to the same extent, the number of electrons per unit cell is $8 \times 84 = 672$. The electrons-per-metal atom ratio for M_6C , then, is 672:96, or 7:1. This is about right for the total number of electrons in the outer d and s bands.

CONCLUSION

The results of applying the techniques involved in identification of the microconstituents in the high temperature alloys investigated, as well as studies of their behavior, have led to these conclusions:

(a) The carbonitrides of titanium and niobium will usually be found in the microstructures of alloys where these elements are used as alloying additions.

(b) The nitrogen-rich $Ti(C,N)$ is a mechanically included constituent whose formation is dependent on nitrogen contamination of the melt.

(c) One mode of formation of higher C/N ratios of the $Ti(C,N)$ is diffusion of carbon into N -rich particles resulting in medial and ultimately C -rich crystals of the $Ti(C,N)$.

(d) The N -rich $Ti(C,N)$ is relatively insensitive to heat treatments below the solidus of Alloy M252, while the C -rich $Ti(C,N)$ responds to heat treatment. Other compositions of the $Ti(C,N)$ respond as regards their C/N ratio.

(e) Increasing titanium above its nominal composition in Alloy M252, or extended thermal treatment of low carbon heats of this alloy, causes the formation of a Laves compound M_2Ti , isomorphous with $MgZn_2$.

(f) An unstable Laves compound, Fe_2Al , isomorphous with MgZn_2 , may appear in cast Turballoy.

(g) An ordered hexagonal close-packed Hägg-type double nitride, CrMoN_x , may form in Alloy 16-25-6.

(h) It is notable that molybdenum or tungsten is present in excess of 5 weight per cent in the alloys in which the complex carbide M_6C is found.

(i) The second Brillouin zone of the M_6C and M_{23}C_6 structures has a capacity for about 7 electrons per metal atom.

ACKNOWLEDGMENTS

The authors wish to express their gratitude to Messrs. W. S. Cremens, H. E. Grenoble and W. E. Jones for providing the materials for this investigation, particularly Mr. Jones for his many helpful discussions; also to the other members of the Thomson Laboratory who gave willingly and helpfully of their time and experience. We also wish to express our appreciation to Dr. N. J. Grant of M.I.T for reading and criticizing the manuscript.

References

1. F. S. Badger and W. O. Sweeney, "Metallurgy of High-Temperature Alloys Used in Current Gas Turbine Designs", Symposium on Materials for Gas Turbines, *Proceedings*, American Society for Testing Materials, 1946, p. 91-112.
2. B. M. Rosenbaum, "An X-Ray Diffraction Investigation of the Microconstituents in 20 High-Temperature Alloys", NACA Conference on High Temperature Material, June 3, 1947, p. 10-21.
3. J. R. Lane and N. J. Grant, "Carbide Reactions in High-Temperature Alloys", *TRANSACTIONS*, American Society for Metals, Vol. 44, 1952, p. 113.
4. Hume-Rothery, Raynor and Little, "On the Carbide and Nitride Particles of Titanium Steels", *Journal*, Iron and Steel Institute, Vol. 145, 1942, p. 159.
5. Duwez and Odell, "Phase Relationships in the Systems of Nitrides and Carbides of Zirconium, Columbium, Titanium and Vanadium", *Journal*, Electrochemical Society, Vol. 97, 1950, p. 299.
6. J. B. Friauf, "The Crystal Structure of Magnesium Di-Zincide", *Physical Review*, Vol. 29, 1927, p. 34-40.
7. Arnfeldt and Westgren, *Jernkontorets Annaler*, Vol. 185, 1935.
8. Witte and Wallbaum, "Thermal and X-Ray Diffraction Studies in the Iron-Titanium System", *Zeitschrift für Metallkunde*, Vol. 30, 1938, p. 221.
9. N. J. Grant, private communication.
10. G. Hägg, *Zeitschrift für physikalische Chemie*, Vol. B6, 1929, p. 221.
11. G. Hägg, *Ibid.*, Vol. 12, 1931, p. 33.
12. H. J. Goldschmidt, "Alloy Steels; The Crystal Structure of Carbides", *Iron and Steel*, Vol. 22, 1949, p. 239-246.
13. H. Jones, *Proceedings*, Royal Society, Series A, Vol. 144, 1934, p. 225-234.

DISCUSSION

Written Discussion: By Rolf Nordheim and Nicholas J. Grant, Department of Metallurgy, Massachusetts Institute of Technology, Cambridge, Mass.

The authors report precipitation of a M_2Ti phase in M432 annealed at 1500 °F and in R358 in the as-cast condition. This is in agreement with our observations on straight nickel-chromium alloys (80-20 base) with 2 to 4% titanium. With respect to the needle-like structure of the annealed alloy, Fig. 11 (electrolytically etched in an aqueous solution of 5% hydrofluoric acid and 10% glycerin), the needles grew thicker; their length, however, remained practically unchanged. Finally, the wide needles or plates almost occupied the entire surface. It thus seems that the acicular "constituents" shown in Fig. 11 may be etch-grooves rather than needles or platelets which are unattacked by the etching reagent. This view is also held by Dr. I. Servi, at Union Carbide and Carbon Research Laboratory, on the basis of electronmicroscopic examinations.

The authors did not observe, in any of their alloys, Ni-Al or Ni (Ti, Al) intermetallic compounds. We have studied the aging behavior in two alloys of the following composition:

	Cr %	Ti %	Al %	C %	Ni %
Alloy A	19.5	2.1	0.5	0.03	Balance
Alloy B	19.5	2.2	1.0	0.03	Balance

In Alloy A we found a strong aging effect at 1250 and 1350 °F, but at 1450 °F the hardness remained unchanged after aging for 90 hours. Alloy B showed strong aging effects at temperatures from 1250 to 1500 °F. It was very difficult, however, to detect any precipitate in the microstructure. For aging times up to 90 hours at the temperatures listed, the only effect of the etchant, viewed at $\times 500$, appeared to be a general attack of the grains. This effect was not observed on alloys solution-treated at 2000 °F and quenched. After 540 hours at 1450 °F, Alloy B showed a very fine precipitate at $\times 500$. Beattie and VerSnyder had subjected their Alloy M432 (2.4% Ti, 1.1% Al, and 0.04% C) to the following three individual heat treatments:

- (a) 72 hours at 1700 °F
- (b) 24 hours at 1500 °F + 20 hours at 1300 °F
- (c) 200 hours at 1500 °F

No trace of Ni-(Ti, Al) compound is reported for any of the treatments. On the basis of our results we would expect this constituent to be present, at least after heat treatment (c). The reason why Beattie and VerSnyder did not find this constituent may be due to failure of their etching reagent to develop the precipitate. Probable explanations are that cobalt and molybdenum (10% of each) increase the solubility of titanium and aluminum, or that large amounts of titanium and aluminum are tied up by nitrogen, although these explanations are less likely.

Written Discussion: By P. K. Koh, Research Laboratory, Allegheny Ludlum Steel Corp., Brackenridge, Pa.

Nickel-base titanium-bearing high temperature alloys, such as Waspaloy, and M252, have experienced troubles connected with nonmetallic in-

clusions on hot working from ingot phase to finished blade sections. Quite often a moderately severe hot cogging would cause cracking originating from segregation streaks at the center of a billet (Fig. 17). Efforts have been made at the Allegheny Ludlum Steel Corp. laboratories to identify the inclusions in the titanium-bearing high temperature alloys. Our findings check well with those of the authors except for the following points.

A transverse section from a square billet of a production heat of Waspaloy was extracted electrolytically in an FeCl_3 aqueous solution. The Debye diffraction pattern of the extract with Co-K radiations showed lines of a face-centered cubic structure, $a = 4.32 \text{ \AA}$, and another face-centered cubic structure, $a = 4.24 \text{ \AA}$. The extract was then analyzed by vacuum fusion and showed 0.827 weight % nitrogen, 9.68 weight % oxygen, and 1.12 weight % hydrogen. Considering TiO as face-centered cubic, $a = 4.235 \text{ \AA}$ ³; TiN as face-centered cubic, $a = 4.235 \text{ \AA}$ ³; TiC as face-centered cubic, $a = 4.320 \text{ \AA}$ ³; TiH_2 as cubic, $a = 4.42 \text{ \AA}$,⁴ it is very likely that besides the Ti(CN) phase in the M252 alloys which the authors investigated, there is a possibility of existence of TiO and TiH_2 , although the TiH_2 lines did not appear in the Debye pattern mentioned above.

Written Discussion: By Constance B. Craver, Research Laboratory, Allegheny Ludlum Steel Corp., Brackenridge, Pa.

The authors are to be complimented for their fine work on nickel-base alloys of the titanium age-hardenable type, and such data as presented in this paper will be of great help in their production.

For the most part, our X-ray and metallographic work on these alloys concur very well with that of the authors. A few comments are included which we think may be of interest.

In reference to the formation of Laves compound M_2Ti in low carbon M252, it is interesting to observe that prior aging treatment may affect the amount of M_2Ti precipitated at 1700 °F.

One of our experimental nickel-base alloys (Heat A509)⁵ was solution-treated at 1950 °F and aged 16 hours at 1400 °F prior to a 1700 °F, 72-hour aging treatment. In this case very few needles of M_2Ti were formed (Fig. 18). The composition of the authors' Heat M432⁵ is comparable to the

Table IX

Heat No.	C	Mn	Si	Cr	Co	Ti	Mo	Al	Fe	Ni
A509	0.04	1.19	0.57	17.71	10.13	2.57	9.40	0.92	2.26	55.21
M432	0.04	0.90	0.71	18.98	9.90	2.41	10.05	1.07	3.50	52.44
A702	0.04	0.48	0.78	17.98	2.66	10.72	1.09	0.91	65.34
A655	0.04	0.46	0.59	18.14	2.60	10.32	0.99	11.63	55.23

above-mentioned Heat A509, but M432 precipitates considerably more M_2Ti upon aging directly at 1700 °F for 72 hours after solution treating. We wonder if this has been observed or can be explained by the authors.

The acicular phase M_2Ti was observed in two experimental alloys of the M252 type in which the cobalt was replaced either with nickel (A702)⁵ or with iron (A655)⁵ (Fig. 19). Samples of both alloys which had been

³Ralph W. G. Wyckoff, *Crystal Structure*, Vol. I, Interscience Publishers, New York, 1951.

⁴ASTM Diffraction Card Index.

⁵The composition of all alloys discussed is listed in Table IX.

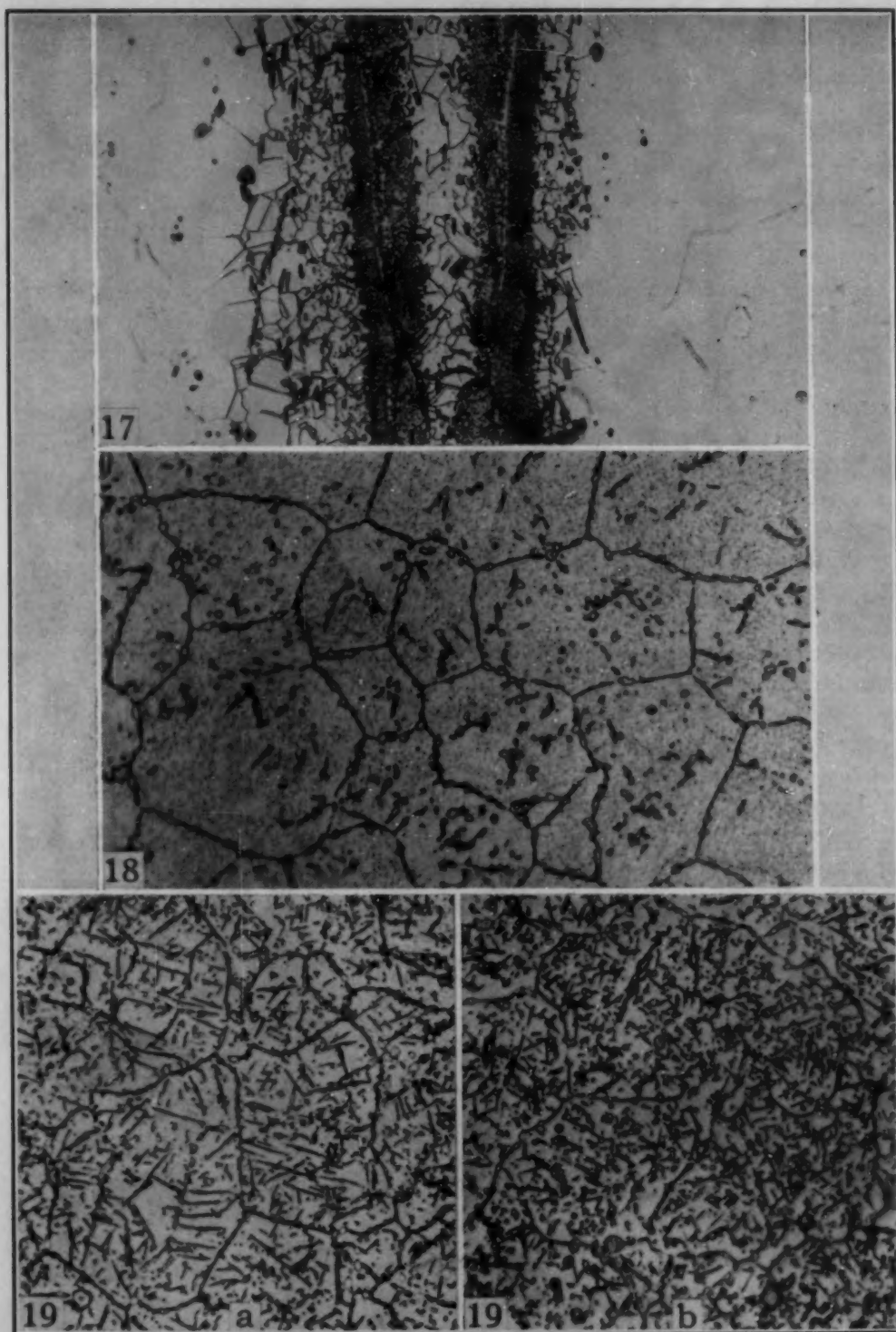


Fig. 17—Waspaloy, Bright Segregated Area in Center of a Billet. Fine grains and nonmetallics within the segregated area. Aqua regia etch. $\times 250$.

Fig. 18—Nickel-Base Alloy (Heat A509). Aging treatment: 1400°F —16 hours, plus 1700°F —48 hours. Etchant: 92 cubic centimeters HCl , 5 cubic centimeters H_2SO_4 , 3 cubic centimeters HNO_3 . $\times 500$.

Fig. 19—Aging Treatment: 1400°F —16 hours, plus 1700°F —48 hours. Etchant: 92 cubic centimeters HCl , 5 cubic centimeters H_2SO_4 , 3 cubic centimeters HNO_3 . $\times 500$. (a) Heat A702. (b) Heat A655.

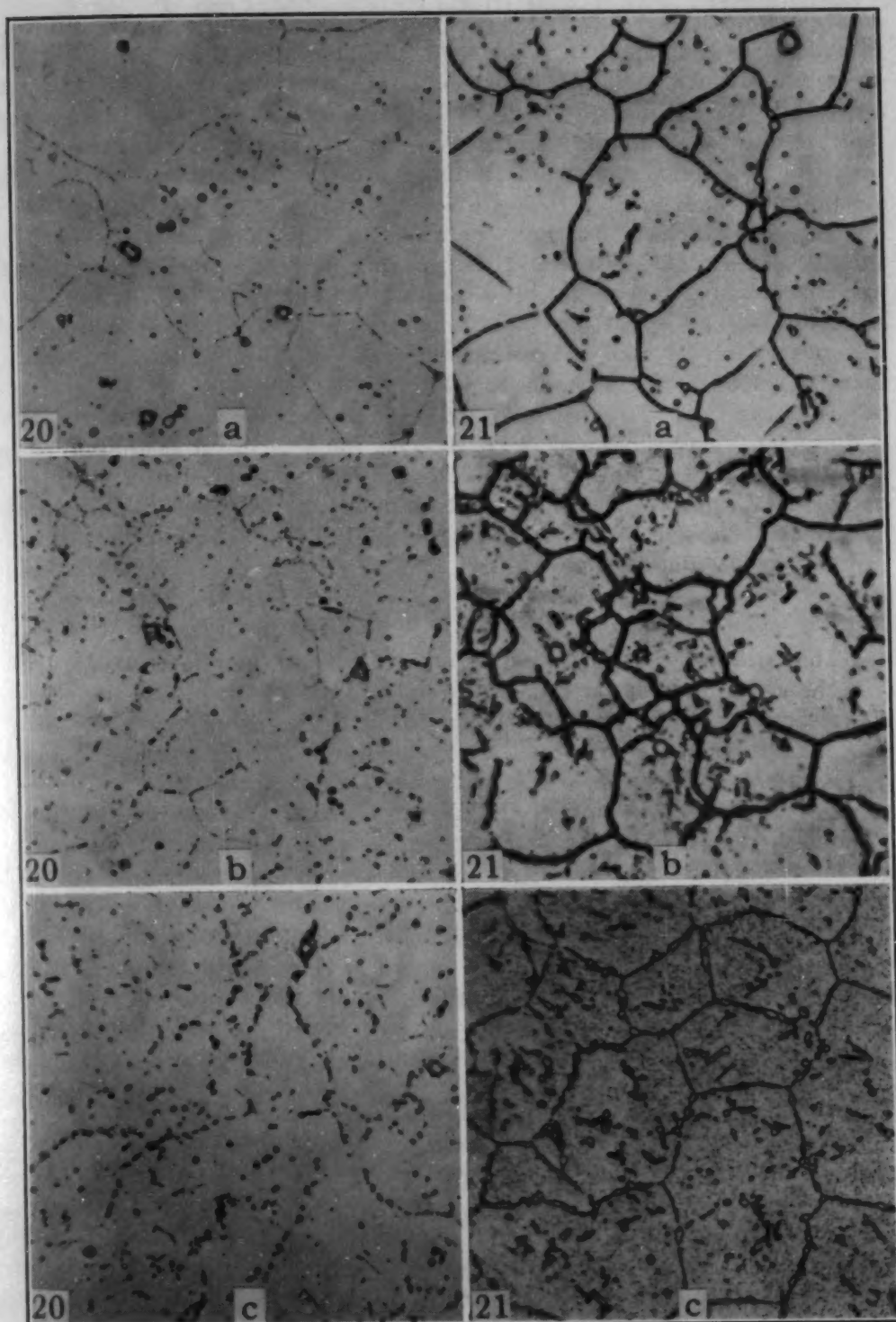


Fig. 20—Heat A509. Etchant: Alkaline permanganate. $\times 500$. (a) 1400 °F—16 hours. (b) 1500 °F—84 hours. (c) 1700 °F—72 hours.

Fig. 21—Heat A509. Etchant: 92 cubic centimeters HCl, 5 cubic centimeters H_2SO_4 , 3 cubic centimeters HNO_3 . $\times 500$. (a) 1400 °F—16 hours. (b) 1500 °F—84 hours. (c) 1700 °F—72 hours.

solution-treated and aged at 1400 °F showed a considerable amount of M_2Ti after holding at 1500 °F for 100 hours (Fig. 2). On the other hand, in Heat A509 which contains 10% cobalt, practically none of this phase is apparent after 84 hours at 1500 °F. Referring to the authors' data which indicate that the solubility of titanium in the matrix is a factor in the formation of M_2Ti , it appears that the presence of cobalt increases this solubility limit.

Fig. 20 is included to show the effect of aging on the M_6C carbide in the low carbon M252 (A509). These specimens were etched with the alkaline permanganate stain etchant which stains or outlines M_6C . A fine network of M_6C appears at the grain boundaries after 16 hours at 1400 °F and it increases in size with increasing temperature. The temperatures in this case were 1500 °F for 84 hours and 1700 °F for 72 hours.

In M252-type alloys with carbon content varying from 0.04 to 0.17%, it has been noted that a more or less continuous grain boundary phase always forms with the 1400 °F aging treatment, but apparently disappears at 1700 °F (Fig. 21). In some cases, as in Heat A509, this same continuous phase is present to a greater degree at 1500 °F. We have not identified this grain boundary phase.

Authors' Reply

The authors wish to thank the discussers for their interest and contributions. With respect to Nordheim and Grant's comments on the needle-like structure in Fig. 11, it may be said that the verity of this constituent, as a constituent in Heat M432, had been supplementarily established by examination of other specimens and other etching techniques.

In reference to the nickel-(titanium, aluminum) compound, it should be emphasized that Heat M432 contains such alloying elements as molybdenum and cobalt not present in Nordheim and Grant's Alloys A or B. The presence of these additional alloying elements is undoubtedly a first source of difference, marked enough to cause expectation of phases other than those found in the more simple nickel-titanium-aluminum ternary. It is indeed possible that the etching and electrolytic separation techniques used in this work were insensitive to the detection of order-disorder phases.

The authors agree with Dr. Koh that titanium monoxide could be in solid solution with titanium carbonitride. However, it is not present as an additional constituent, because only the titanium carbonitride was observed and well established by close correlation between metallography and diffraction.

Titanium hydride was not present as a separate constituent for the reason just mentioned. It is not likely that it could be in solution with titanium carbonitride, because it has the calcium fluoride structure rather than that of sodium chloride; that is, the hydrogen atoms occupy the tetrahedral rather than octahedral interstices.

We find the data on the titanium age-hardenable-type alloys, presented by Mrs. Craver, extremely interesting; however, the precise nature of the precipitation reactions was beyond the scope of this paper. We feel there is much to be learned in regard to this type of alloy since the phase reactions appear to be reasonably complicated.

SIGMA FORMATION AND ITS EFFECT ON THE IMPACT PROPERTIES OF IRON-NICKEL-CHROMIUM ALLOYS

BY A. M. TALBOT AND D. E. FURMAN

Abstract

The approximate sigma phase boundaries over the temperature range 1200 to 1650 °F (650 to 900 °C) have been located by metallographic means for iron-nickel-chromium alloys of relatively high alloy content and of simulated commercial quality. For conditions approaching equilibrium, the limiting sigma boundary was found to extend from about 21% chromium at 20% nickel to 24% chromium at 35% nickel. The effectiveness of silicon in moving the sigma area to lower chromium contents has been shown. Also it has been indicated that in certain compositional ranges the comparatively stable cast structure may resist the formation of sigma under the conditions that sigma would appear in a similar wrought structure.

Embrittlement as measured by room temperature impact properties increased rapidly with the first few per cent of sigma formed, regardless of the base composition.

IT has been the purpose of this investigation to locate a practical and useful sigma phase boundary in the iron-nickel-chromium alloys of simulated commercial purity and, in addition, to evaluate the embrittling effect of sigma as measured by the room temperature impact properties. The need for such information has been apparent for some time. Most of the previous investigations have been made with high purity alloys or with alloys of different quality than would be obtained with present-day alloying materials. As a result, it has often been observed in service examinations of commercial materials that sigma was present in alloys that were reputedly fully austenitic. Therefore, the approximate location of the sigma area in the iron-nickel-chromium alloys of commercial quality is of considerable interest. A related problem is the maximum amount of sigma that may be present in a particular type of alloy without causing serious embrittlement. It was with the desire of shedding some light on these two phases of the sigma problem that iron-base alloys of intermediately high alloy content were studied.

A paper presented before the Thirty-fourth Annual Convention of the Society, held in Philadelphia, October 18 to 24, 1952. The authors, A. M. Talbot and D. E. Furman, are associated with the Research Laboratory of the International Nickel Company, Inc., Bayonne, N. J. Manuscript received May 15, 1952.

REVIEW OF LITERATURE

An extensive review of the sigma literature was made by Foley (1),¹ so it is not necessary to include here more than a brief reference to a few of the more closely related investigations that have been reported. The iron-nickel-chromium equilibrium diagram as published by Schafmeister and Ergang (2) in 1939 has been the most widely used source of information as to the composition of the sigma-containing alloys. The numerous discrepancies with this diagram that have been noted from time to time have usually been attributed to variations in the minor constituents of a particular alloy. In 1949, Rees, Burns and Cook (3) published data on alloys of extraordinarily high purity. The sigma boundary as established in this work is at considerably lower chromium contents than the previously mentioned investigation placed it, and it has been observed to be in closer agreement with commercial material than might be expected. Nicholson, Samans and Shortsleeve (4) were among the first to recognize the need for making a systematic determination of the sigma boundary using alloys of simulated commercial quality. Their work published in 1951 is a practical guide for the occurrence of sigma at 1200 °F (650 °C) in alloys containing 12 to 24% chromium and up to 20% nickel. This is useful information in the range of the commercially important 18-8 type of alloys. It is also of interest that the results were in good agreement with those obtained by Rees, Burns and Cook on high purity iron-nickel-chromium alloys.

MATERIALS AND PROCEDURE

The compositional range of interest in this investigation is represented by such commercial alloys as Type 310, 20% nickel and 25% chromium; Type 330, 35% nickel and 15% chromium; and Incoloy,² 35% nickel, 20% chromium. It is the range of the relatively high alloy iron-base materials. The actual alloys used contained from 20 to 35% nickel and 15 to 30% chromium. Alloys were chosen to cover a definite area of interest and not to locate a boundary with any exacting degree of accuracy. Approximate boundaries are of more interest in considering commercial alloys that vary quite widely in composition. The incidental alloying elements were controlled to the following approximate limits: carbon less than 0.1%, manganese 1.8%, silicon 0.7%, and phosphorus, sulphur and nitrogen were taken at the levels obtained. Two of the alloys were repeated as 3% silicon variations and one of the alloys was repeated with as low a silicon content as practical to obtain. The compositions of all alloys are listed in Table I.

The alloys were made in a high frequency induction furnace

¹The figures appearing in parentheses pertain to the references appended to this paper.

²Trademark, the International Nickel Co., Inc.

Table I
Compositions of Alloys Investigated

No.	Alloy Type	Analysis							
		Ni	Cr	C	Si	Mn	S	P	N
1	20 Ni, 25 Cr	20.23	24.66	0.06	0.61	1.84	0.010	0.014	0.071
1A	20 Ni, 25 Cr, Low Si	20.24	23.79	0.07	0.20	2.04	0.007	0.016	0.094
2	25 Ni, 20 Cr	25.16	19.74	0.08	0.76	1.94	0.008	0.011	0.11
2A	25 Ni, 20 Cr, High Si	24.42	19.50	0.05	3.09	1.77	0.006	0.014	0.046
3	25 Ni, 25 Cr	25.09	25.25	0.05	0.74	1.90	0.007	0.014	0.041
4	25 Ni, 30 Cr	24.99	28.95	0.06	0.75	1.98	0.006	0.013	0.058
5	35 Ni, 15 Cr	34.25	14.15	0.05	0.60	1.76	0.007	0.019	0.028
6	35 Ni, 20 Cr	34.93	19.95	0.05	0.78	2.05	0.006	0.022	0.047
6A	35 Ni, 20 Cr, High Si	33.79	19.47	0.04	2.96	1.82	0.005	0.011	0.035
6B	35 Ni, 20 Cr, High Si	34.02	19.44	0.05	3.04	1.86	0.005	0.015	0.053
7	35 Ni, 25 Cr	34.03	23.83	0.05	0.63	1.72	0.006	0.021	0.048

using armco iron, electro nickel, and low nitrogen ferrochromium. No deoxidation was used other than the manganese and silicon additions. Ten-pound ingots were cast in 2 by 2-inch chill molds with core sand hot-tops that held about 25% of the metal. The head of the ingot was removed before forging and hot rolling to $\frac{3}{4}$ -inch rounds. The $\frac{3}{4}$ -inch bars were cold-rolled to $\frac{1}{2}$ -inch square bars with an intermediate anneal in order to obtain a final cold reduction of 23%. Half of each heat was kept in the cold-rolled condition and the rest was annealed for 1 hour and water-quenched. The annealing was carried out in the temperature range from 1900 to 1975 °F (1040 to 1080 °C) in an effort to have approximately the same grain size in all heats. The grain size was limited to a maximum ASTM value of 4.

Using the above procedure, material was available from each composition in three conditions. The cast structure was represented by the ingot head. The wrought material was in the annealed and 23% cold-worked conditions.

The presence of sigma was determined metallographically in all three conditions after exposure for various times at 1200, 1475 and 1650 °F. The exposure times were 100, 500, 1000 and 3000 hours. Charpy keyhole-notch impact values were obtained on the annealed and 23% cold-worked materials after the same periods of exposure. Rockwell "B" hardness values were obtained on the broken halves of the Charpy specimens.

Identification of sigma was based chiefly on comparative metallographic examination. While various etchants were explored, the most satisfactory one was mixed acids in glycerin of the following proportions: 3 parts glycerin, 2 parts concentrated HCl, 1 part concentrated HNO₃. In general, this etchant when freshly mixed and swabbed on the specimen will etch the sigma particles in 15 to 20 seconds while taking about a minute or more to clearly outline the carbides. If the reagent is allowed to stand for more than about an hour, it etches more rapidly and it becomes difficult to differen-

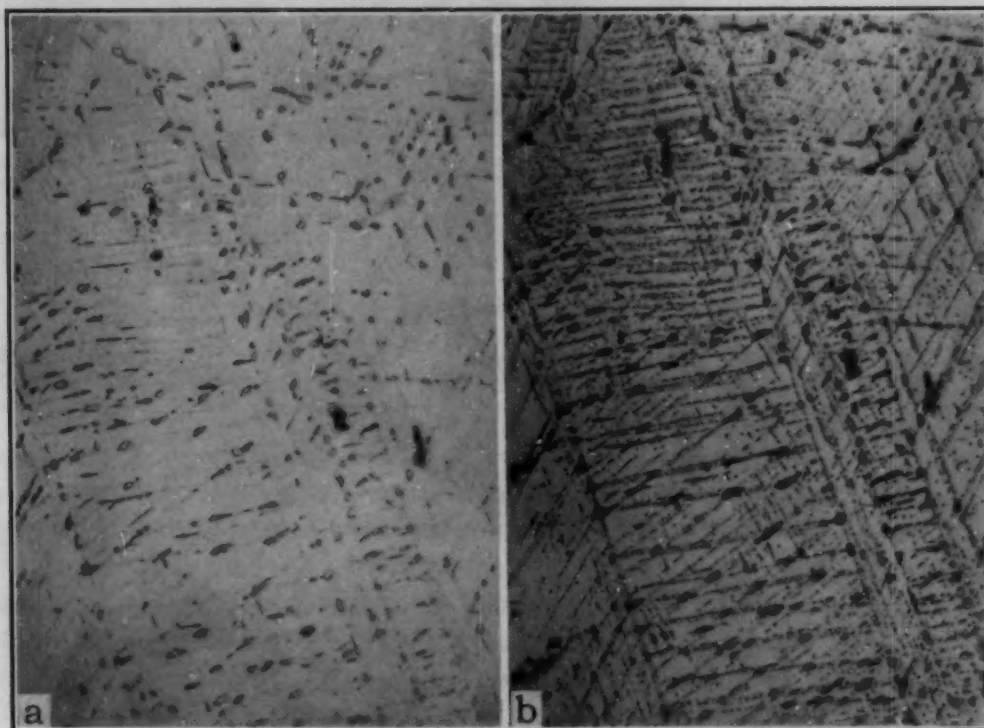


Fig. 1—Microstructure of a Moderately Cold-Worked 35% Ni, 20% Cr, 3% Si Alloy After 3000 Hours at 1200 °F (650 °C). When etched for 20 seconds with HCl and HNO₃ in glycerin, (a), sigma particles are revealed but carbides are only faintly visible. Fig. 1 (b) shows the same area etched for 90 seconds to bring out the carbides.

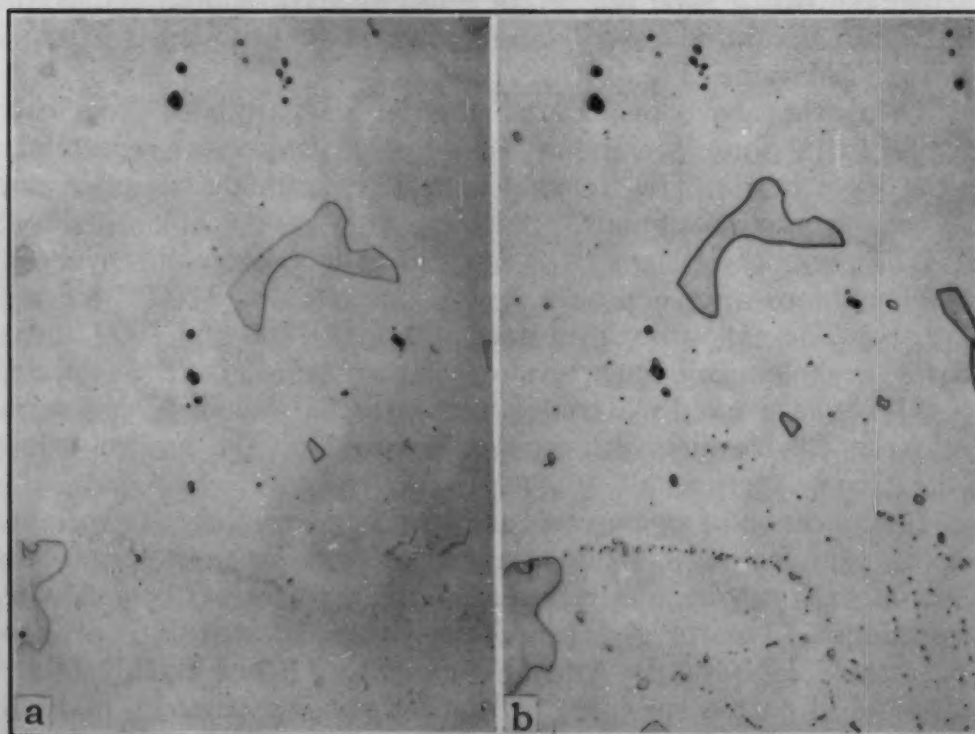


Fig. 2—Moderately Cold-Worked 25% Ni, 25% Cr Alloy After Heating for 3000 Hours at 1650 °F (900 °C). Large sigma particles (a) are visible after etching for 20 seconds with HCl and HNO₃ in glycerin. An etching time of 90 seconds (b) was required to define the smaller carbide particles.

tiate between the two phases. An illustration of this method of sigma identification is given in the two photomicrographs of each of Figs. 1 and 2. The method has proved reliable when used on the simple ternary alloys treated under known and controlled conditions. Routine service investigations have shown, however, that the method may be misleading if molybdenum is present or if the sigma was formed under fluctuating temperature conditions.

The percentage of sigma in any particular specimen was estimated by comparison with area charts drawn up for different percentages of different size particles. The location of sigma boundaries was estimated by the relative amount of sigma present in alloys within the sigma field. All boundaries are approximations, but their accuracy is sufficient when dealing with commercial quality alloys.

THE SIGMA BOUNDARIES

The specimens exposed for 3000 hours at the three temperatures were examined metallographically in determining the sigma boundaries for each of the three conditions. The results are listed in Table II and shown in Figs. 3 and 4.

From the boundaries plotted in Fig. 3, it can be seen that the sigma area extends to the lowest chromium levels in the case of the cold-worked materials, whereas the relatively more stable cast structures are indicated to have a sigma boundary located at higher chromium contents. The annealed materials were found similar to the cast materials at 1200 °F (650 °C) but almost identical to the cold-worked alloys at 1475 and 1650 °F (800 and 900 °C). At 1200 °F (650 °C) the spread of the three conditions represents the lack of equilibrium, but at the two higher temperatures there appeared to be a real difference between the cast and the wrought structures. There was no indication that any changes had taken place between 1000 and 3000 hours exposure, which would indicate a reasonable approach to equilibrium.

The fact that the cast structure is more reluctant to form sigma than the wrought structure of the same alloy composition is a little surprising. With the coring effects expected in castings, it would not be unusual to have certain areas rich in sigma-forming elements. This would result in sigma being present at lower chromium levels than in the more homogeneous wrought alloys. However, the opposite effect was observed consistently and no significant differences in chemical analysis could be found between the cast and wrought parts of any particular heat to explain it. The greater reluctance of the cast structure to form sigma with increasing chromium contents at the higher nickel levels evidently is due partially to the stability of the cast structure and partially to the increased sluggishness of the higher alloy materials.

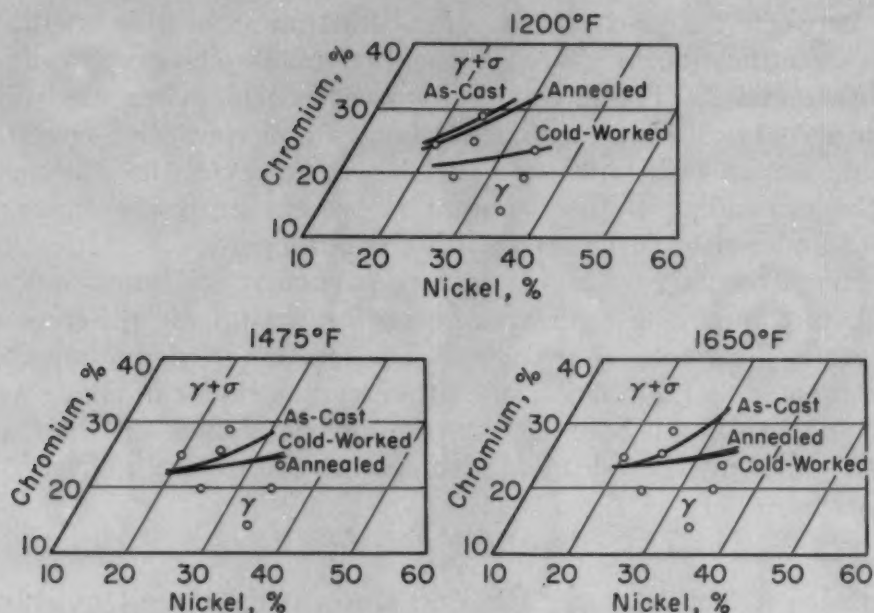


Fig. 3—Sigma Boundaries Determined at 1200, 1475 and 1650 °F (650, 800 and 900 °C) for Commercial Quality Iron-Nickel-Chromium Alloys.

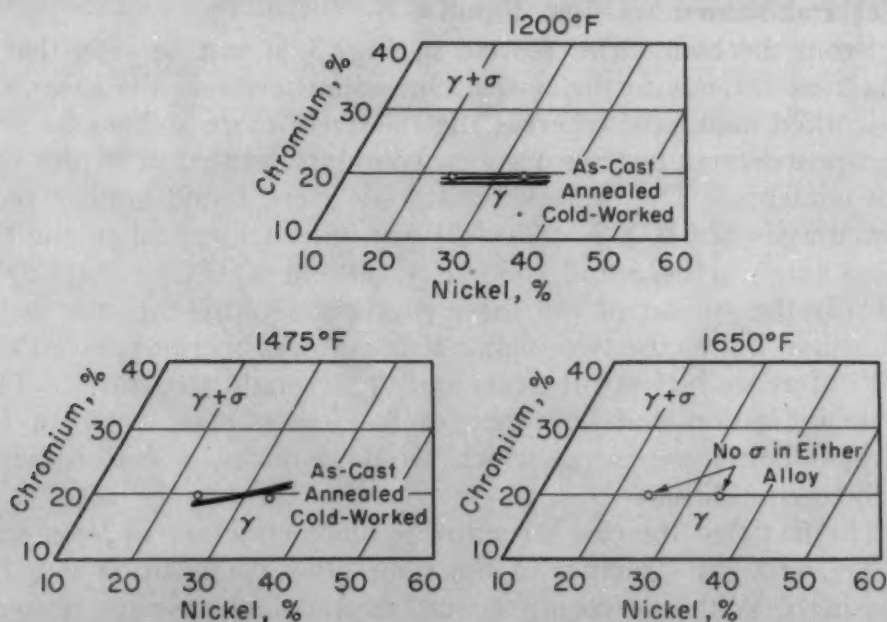


Fig. 4—Sigma Boundaries Obtained at 1200 and 1475 °F (650 and 800 °C) for Iron-Nickel-Chromium Alloys Containing 3.0% Silicon.

EFFECT OF SILICON ON THE SIGMA BOUNDARIES

Higher silicon contents are often desired for improved resistance to carburization and oxidation. The sigma-forming tendencies of silicon are well known and some measure of this effect was obtained by increasing the silicon to 3% in two of the alloys. The results obtained are shown in Fig. 4. While the differences among the three conditions were small, there were consistent differences shown. The

cold-worked material contained more sigma than the annealed, and the annealed more than the cast. At 1200 °F (650 °C) the sigma boundary with 3% silicon is at about 19% chromium, with nickel contents of 25 and 35%. At 1475 °F (800 °C) the boundary moves to slightly higher chromium contents at the 35% nickel level, and at 1650 °F (900 °C) no sigma was observed in either alloy.

Table II
Estimated Percentages of Sigma Present After 3000 Hours Exposure
at Three Temperatures of Alloys in the As-Cast, Annealed
and 23% Cold-Worked Conditions

No.	Alloy Type	1200 °F (650 °C)			1475 °F (800 °C)			1650 °F (900 °C)		
		Cast	An- nealed	Cold- Worked	Cast	An- nealed	Cold- Worked	Cast	An- nealed	Cold- Worked
1	20 Ni, 25 Cr	0	1	10	7	7	10	1	3	5
1A	20 Ni, 25 Cr, Low Si	0	0	3	<1	5	4	0	0	0
2	25 Ni, 20 Cr	0	0	0	0	0	0	0	0	0
2A	25 Ni, 20 Cr, High Si	<1	3	3	1	3	5	0	0	0
3	25 Ni, 25 Cr	0	0	10	3	10	8	<1	3	3
4	25 Ni, 30 Cr	<1	3	20	8	25	23	5	15	17
5	35 Ni, 15 Cr	0	0	0	0	0	0	0	0	0
6	35 Ni, 20 Cr	0	0	0	0	0	0	0	0	0
6A	35 Ni, 20 Cr, High Si	4	0	0
6B	35 Ni, 20 Cr, High Si	<1	3	..	0	0	..	0	0	..
7	35 Ni, 25 Cr	0	0	<1	0	0	0	0	0	0

The propensity of the 20% nickel, 25% chromium alloy, Type 310 stainless steel, to form sigma is well known. It was of interest to know whether this sigma-forming tendency could be overcome by keeping the silicon at its lowest practical limit. In Table II, the normal, 0.6% silicon alloy, No. 1, is shown to have formed sigma at all three temperatures. Alloy 1A with 0.2% silicon formed less sigma but an appreciable amount at both 1200 and 1475 °F (650 and 800 °C). The low silicon alloy has other compositional advantages such as lower chromium and higher manganese, but it may be concluded that sigma is readily formed at the 20% nickel, 25% chromium alloy level.

COMPARISON OF SIGMA BOUNDARIES BY DIFFERENT INVESTIGATORS

In Fig. 5 a comparison is made of the sigma boundaries at 1200 and 1475 °F (650 and 800 °C) as determined by various investigators. The boundaries established with the cold-worked materials were used to represent the present investigation. The line drawn in the 1200 °F (650 °C) diagram to represent the data of Nicholson, Samans and Shortsleeve was taken as the top chromium level suggested by them. It is interesting that the agreement between their work and the present work is reasonably good; one could be a continuation of the other.

The boundary is appreciably lower than that established by Schafmeister and Ergang at both 1200 and 1475 °F (650 and 800 °C). When compared with those of Rees, Burns and Cook, it is

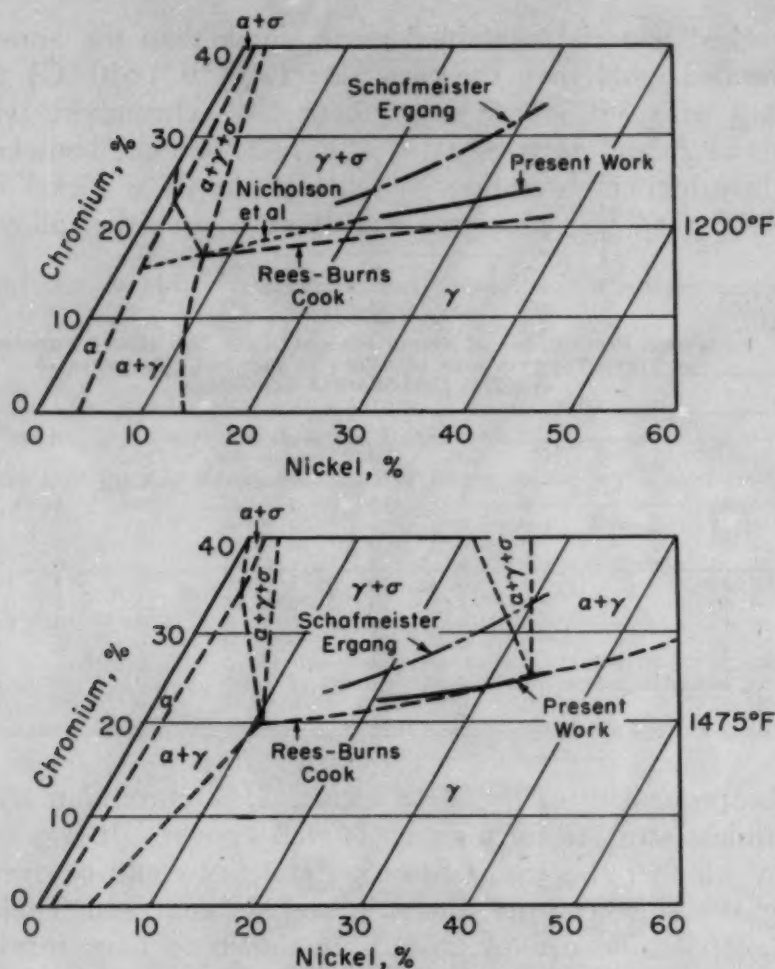


Fig. 5—A Comparison of the Sigma Boundaries Established at 1200 and 1475 °F (650 and 800 °C) for the Moderately Cold-Worked Alloys With Those of Other Investigators.

slightly higher at 1200 °F (650 °C) but identical at 1475 °F (800 °C). It would appear that the presence of carbon, manganese and nitrogen in the amounts used in the present work is counteracted by the silicon content, so the end effect is about the same as obtained with high purity alloys.

LIMITING COMPOSITIONS FREE OF SIGMA

It is of practical significance to establish the limiting boundaries for sigma-free alloys of commercial quality. The minimum chromium values obtained throughout the range from 1200 to 1650 °F (650 to 900 °C) for each condition were used to represent the limiting values given in Fig. 6. The limiting values for the cast and annealed conditions are those established at 1475 °F (800 °C), while the cold-worked values were obtained at 1200 °F (650 °C). The boundary given for the cold-worked condition is extended to lower alloy contents by using the data of Nicholson, Samans and Shortsleeve. The boundary of the 3% silicon alloys in the cold-worked condition is

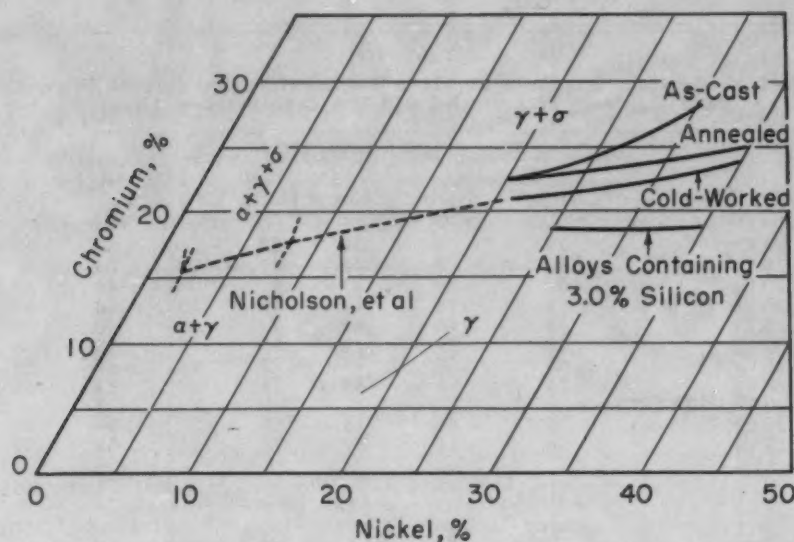


Fig. 6—Limiting Sigma Boundaries Determined Over the Temperature Range 1200 to 1650 °F (650 to 900 °C) for Commercial Quality Iron-Nickel-Chromium Alloys.

also given for comparison. These boundaries are thought to be good approximations that will vary to a certain extent, depending upon minor alloying elements, but they should serve as suitable guides.

At 20% nickel, it is indicated that with a chromium content of more than about 21%, sigma can be expected. At the 35% nickel level, freedom from sigma is indicated in the presence of as much as 24% chromium. In the case of silicon, it can be estimated that a 25% nickel, 20% chromium alloy can tolerate 1.3% silicon, and a 35% nickel, 20% chromium alloy can tolerate 2.2% silicon without forming sigma.

EFFECT OF SIGMA ON THE IMPACT PROPERTIES AND HARDNESS

Impact tests were made on the annealed and cold-worked conditions only. There was not sufficient cast material to include it in the impact tests. The keyhole-notch impact values obtained on the pieces exposed 3000 hours are given in Table III along with Rockwell "B" hardness values.

The extent of the embrittlement accompanying the formation of sigma is shown in the set of diagrams of Fig. 7. The impact value obtained for each alloy along with its position in relation to the sigma area is given for both conditions at three temperatures. Embrittlement appears substantial within the sigma field, although the closer to the boundary the less severe is the embrittling effect. At 1200 °F (650 °C) there is some apparent embrittlement within the fully austenitic field. This is due to finely precipitated carbide. The effect of nickel or chromium on the impact properties can also be obtained from the values plotted in Fig. 7.

An illustration of the embrittling effect of sigma is obtained by

Table III
Effect of 3000-Hour Exposure at Three Temperatures on Impact Properties and Hardness of Annealed and 23% Cold-Worked Alloys

No.	Alloy Type	Annealed Plus 3000 Hours at Temperature							
		As Annealed		1200°F		1475°F		1650°F	
		Charpy* Ft-Lb.	Hard. R _B	Charpy Ft-Lb.	Hard. R _B	Charpy Ft-Lb.	Hard. R _B	Charpy Ft-Lb.	Hard. R _B
1	20 Ni, 25 Cr	79	78	34	82	9	87	15	82
1A	20 Ni, 25 Cr, Low Si	82	79	45	84	20	83	51	83
2	25 Ni, 20 Cr	67	88	27	87	28	81	43	84
2A	25 Ni, 20 Cr, High Si	73	78	14	93	13	82	33	76
3	25 Ni, 25 Cr	73	74	43	78	10	80	28	75
4	25 Ni, 30 Cr	69	79	17	85	2	98	4	94
5	35 Ni, 15 Cr	65	67	43	73	45	67	59	68
6	35 Ni, 20 Cr	75	74	33	78	39	73	61	74
6A	35 Ni, 20 Cr, High Si	70	82	16	85	37	80	46	77
6B	35 Ni, 20 Cr, High Si	71	74	37	78	41	76	59	77
7	35 Ni, 25 Cr	71	74	37	78	41	76	59	77

No.	Alloy Type	Cold-Worked 23% Plus 3000 Hours at Temperature							
		As Cold-Worked		1200°F		1475°F		1650°F	
		Charpy Ft-Lb.	Hard. R _B	Charpy Ft-Lb.	Hard. R _B	Charpy Ft-Lb.	Hard. R _B	Charpy Ft-Lb.	Hard. R _B
1	20 Ni, 25 Cr	39	102	7	98	7	92	21	82
1A	20 Ni, 25 Cr, Low Si	43	102	13	100	20	86	58	80
2	25 Ni, 20 Cr	35	107	19	99	36	82	50	84
2A	25 Ni, 20 Cr, High Si	41	104	9	100	16	85	53	76
3	25 Ni, 25 Cr	36	102	12	97	9	90	26	79
4	25 Ni, 30 Cr	32	106	5	101	3	101	6	95
5	35 Ni, 15 Cr	37	101	31	92	55	70	61	70
6	35 Ni, 20 Cr	48	101	29	95	52	75	63	75
6A	35 Ni, 20 Cr, High Si	33	104	11	98	48	80	51	76
6B	35 Ni, 20 Cr, High Si	37	104	26	97	51	78	59	76
7	35 Ni, 25 Cr	37	104	26	97	51	78	59	76

*Charpy keyhole notch.

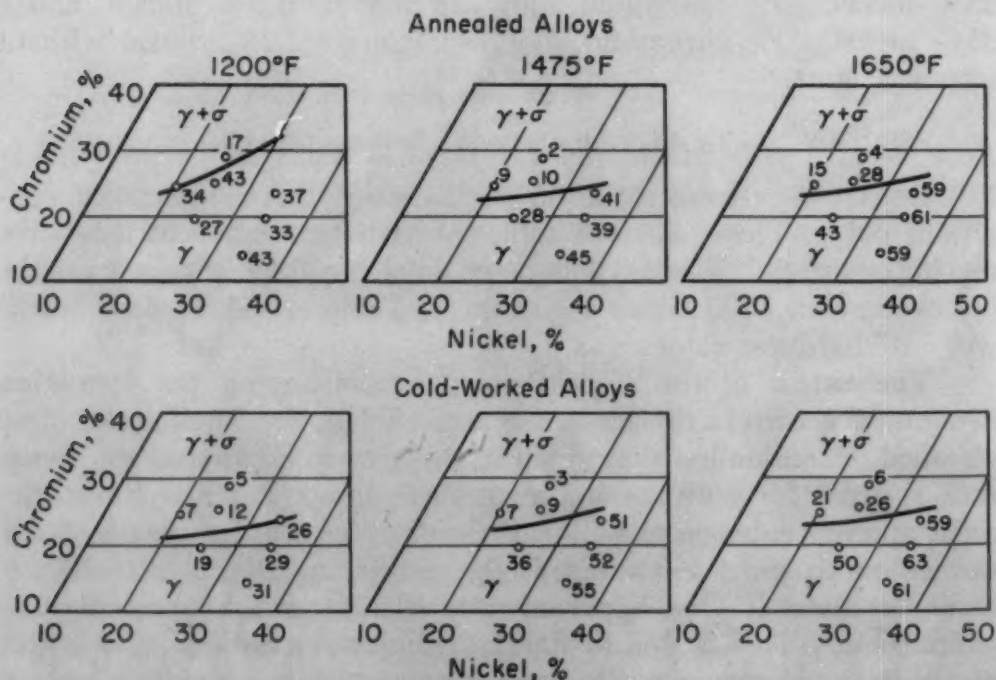


Fig. 7—Impact Values of Commercial Quality Iron-Nickel-Chromium Alloys Obtained After Heating for 3000 Hours at 1200, 1475 and 1650 °F (650, 800 and 900 °C).

plotting the percentage of sigma against the impact value. This relation is shown in Fig. 8, and it was found to hold true regardless of the base composition. It is evident that as little as 5% sigma may cause serious embrittlement and, with more than 5%, the embrittlement is certain and becomes progressively worse.

Unlike the impact results, the hardness values were rather in-

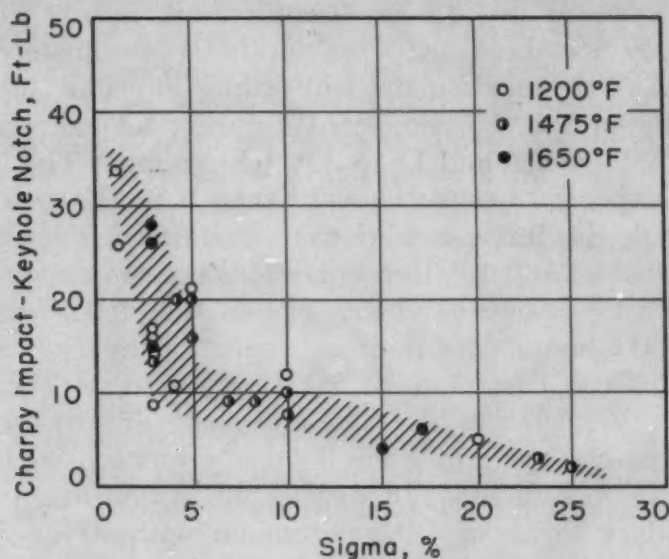


Fig. 8—Correlation of the Effect of Sigma on the Impact Resistance of Commercial Quality Iron-Nickel-Chromium Alloys.

Table IV
Effect of Exposure Time on Impact Properties of Four of the Alloys

No.	Alloy Type	Temp. °F.	Charpy Impact Values—Ft-Lbs.									
			Annealed Alloys					Cold-Worked Alloys				
			Hours at Temp.					Hours at Temp.				
			0	100	500	1000	3000	0	100	500	1000	3000
1	20 Ni, 25 Cr	1200	79	53	44	41	34	39	32	22	13	7
		1475	79	33	14	11	9	39	11	7	7	7
		1650	79	48	27	20	15	39	30	21	21	21
2	25 Ni, 20 Cr	1200	67	43	28	26	27	35	24	21	20	19
		1475	67	29	31	25	28	35	26	27	40	36
		1650	67	43	50	49	43	35	52	52	51	50
5	35 Ni, 15 Cr	1200	65	58	49	47	43	37	38	35	32	31
		1475	65	53	45	45	45	37	48	56	56	55
		1650	65	58	55	57	59	37	63	62	59	61
6	35 Ni, 20 Cr	1200	75	55	43	38	33	48	35	32	29	29
		1475	75	40	36	35	39	48	45	47	52	52
		1650	75	54	57	58	61	48	62	61	67	63

sensitive in that they gave little indication as to the extent of sigma formation. Differences in hardness were not indicative of the relative amounts of sigma, although in a given alloy there was always an increase in hardness with the appearance of sigma.

The effect of time of exposure on the impact properties of several of the alloys may be seen in Table IV. The data have been included here only for those compositions most commonly used commercially. The results were useful in estimating the approach to equilibrium

with time. In most cases, very little additional loss in impact resistance would take place after the first 500 hours of exposure. The exceptions to this behavior were usually confined to the 1200 °F (650 °C) treatments and the annealed condition.

SUMMARY

By the use of microscopic examination, impact and hardness tests, a study has been made to locate approximately the sigma boundaries and to appraise the embrittling effect of sigma in iron-nickel-chromium alloys of simulated commercial quality in the range from 20 to 35% nickel and 15 to 30% chromium. The investigation covered a temperature range from 1200 to 1650 °F (650 to 900 °C) with materials in three conditions: cast, wrought annealed and moderately cold-worked. For conditions approaching equilibrium, that is, exposing cold-worked material to the sigma-forming conditions for 3000 hours, the limiting sigma boundary was found to extend from 21% chromium at 20% nickel to 24% chromium at 35% nickel. With the more stable and sluggish structures found in annealed or as-cast materials, the boundary was moved to somewhat higher chromium contents. Increasing the silicon to 3% moved the sigma boundary to about 19% chromium with 25 or 35% nickel. The sigma boundary as determined in this investigation is a reasonable extension of the boundary as determined by Nicholson, Samans and Shortsleeve for similar materials of lower alloy content. Embrittlement as measured by room temperature impact properties increased rapidly with the first few per cent of sigma formed, regardless of the base composition. Serious embrittlement is apt to be effected by as little as 5% sigma.

ACKNOWLEDGMENTS

The authors are indebted to the International Nickel Company, Inc., for permission to publish the results of this investigation. The helpful consultation of V. N. Krivobok and the assistance of W. T. Coughlin and K. J. Walrod are gratefully acknowledged.

References

1. F. B. Foley, "The Sigma Phase", Alloy Casting Institute Bulletin No. 5, July 1945.
2. P. Schafmeister and R. Ergang, "Das Zustandschaubild Eisen-Nickel-Chrom unter besonderer Berücksichtigung des nach Dauerghühnen auftretenden sproden Gefügebestandteiles", *Archiv für das Eisenhüttenwesen*, Vol. 12, 1939, p. 459.
3. W. P. Rees, B. D. Burns and A. J. Cook, "Constitution of Iron-Nickel-Chromium Alloys at 650 to 800 °C", *Journal, Iron and Steel Institute*, Vol. 162, Pt. 3, July 1949, p. 325.
4. M. E. Nicholson, C. H. Samans and F. J. Shortsleeve, "Composition Limits of Sigma Formation in Nickel-Chromium Steels at 1200 °F (650 °C)", *TRANSACTIONS, American Society for Metals*, Vol. 44, 1952, p. 601.

DISCUSSION

Written Discussion: By P. M. Unterweiser, senior metallurgist, Heat Treat, Process Control Unit, Curtiss-Wright Corp., Wright Aeronautical Division, Woodridge, N. J.

Messrs. Talbot and Furman are to be congratulated for this very interesting study of sigma phase embrittlement and especially for the useful sigma phase boundary data which they have derived.

However, it is of interest to note their surprise that the cast structure of a given alloy composition is more reluctant to form sigma than the wrought material of similar composition. This phenomenon has been reported by a number of other investigators although, in most instances, no attempt was made to provide an explanation. The present investigators suggest one explanation for certain types of alloys, namely: "The greater reluctance of the cast structure to form sigma with increasing chromium contents at the higher nickel levels evidently is due partially to the stability of the cast structure and partially to the increased sluggishness of the higher alloy materials."

The fact that the forged specimens used in this investigation were probably forged and hot-rolled at temperatures approaching, if not actually within, the "solution treating" range seems to me to be of some significance. The authors do not indicate these temperatures, but it can be estimated that they probably exceeded 2000 °F. Subsequently, the forged specimens were cold-rolled.

Dealing with cast 25% chromium-12% nickel alloys in a recent investigation, it has been our experience that solution treating as-cast specimens in the range 2200 to 2300 °F for periods of from 1 to 4 hours proved extremely deleterious upon subsequent sensitizing. Where clearly delineated ferrite islands were observable in the material quenched from 2200 to 2300 °F, these apparently provided the nucleus for rapid carbide precipitation after a 4-hour sensitizing treatment at 1300 °F. Cold working tended to further promote the carbide-forming tendency (and resultant sigma phase). Confirming the authors' experience, this condition was especially applicable to alloys containing in excess of 1% silicon.

Written Discussion: By E. J. Dulis, Research and Development Laboratory, United States Steel Co., Kearny, N. J.

From a practical point of view, this paper serves a useful purpose in establishing sigma boundary limits for some commercial austenitic alloys not heretofore studied.

The authors compare the effect of cold working versus annealing (1900 to 1975 °F, water quench) on subsequent sigma formation at 1200 °F and attribute the sigma boundary at higher chromium contents for the annealed alloys to be due to the nonattainment of equilibrium; this difference is shown in Figs. 3 and 6 of the paper. However, it is believed that variations in annealing treatments would cause marked shifts in the non-equilibrium sigma boundary for the annealed steels heated for 3000 hours in the sigma-forming temperature range.

Retardation in the establishment of equilibrium by a suitable treatment, so that the formation of sigma is impeded, could serve as a practical means to avoid or minimize sigma occurrence. A study of the effect of prior heat treatment on precipitation of sigma phase in a 25% chromium-

20% nickel alloy was made at the U. S. Steel Research Laboratory several years ago.⁸ It was found that temperature of annealing and rate of cooling therefrom have a great effect on sigma formation. For example, specimens annealed at 1900 °F and water-quenched, air-cooled or furnace-cooled therefrom developed equilibrium amounts of sigma in 1000 hours at 1300 °F; whereas, the same steel furnace-cooled from 2100 °F showed little sigma after 3000 hours at 1300 °F. In general, higher annealing temperatures and slower rates of cooling therefrom retarded sigma formation.

Written Discussion: By Howard M. German, Driver-Harris Co., Harrison, N. J.

In the paper presented, the authors discussed iron-nickel-chromium alloys which contained a greater percentage of chromium than nickel. They did not discuss alloys having a greater percentage of nickel than chromium. We have examined many specimens of 35% nickel-16% chromium and 60% nickel-15% chromium and have not found the presence of sigma.

Authors' Reply

We wish to express our appreciation to Messrs. Unterweiser and Dulis for their comments which appear to lend further support to the idea that the sigma phase boundary is somewhat migratory in nature.

In relation to Mr. Unterweiser's remarks, it would have been more appropriate for us to have expressed our surprise as to the magnitude of the difference in sigma-forming tendencies between the wrought and cast structures at the higher alloy contents rather than about the fact that the cast structure is more reluctant to form sigma.

It is interesting that Mr. Unterweiser reports a high temperature annealing treatment to be effective in promoting the formation of sigma in cast 25% chromium-12% nickel alloys, while Mr. Dulis reports the opposite effect for wrought 25% chromium-20% nickel alloys. At first glance these might seem to be contradictory statements, but they may well be indications of the effect of segregation. The treatment used on the 25% chromium-12% nickel alloy was within the two-phase region for this alloy and, consequently, resulted in the formation of additional ferrite. The effect of forming a second phase is to cause segregation, as the composition of the second phase is different from the matrix from which it is formed. This is a segregation that would be expected to aid the formation of sigma. In the case of the 25% chromium-20% nickel alloys used by Mr. Dulis the high temperature treatment is one of homogenization, as the alloy is completely within the austenitic field at the temperatures involved. Such a treatment, therefore, retards the formation of sigma which in itself requires segregation. An optimum annealing temperature is indicated for alloys that might contain both ferrite and austenite if it is desired to retard the formation of sigma, while for alloys incapable of forming ferrite the higher the annealing temperature the greater will be the effect of retarding sigma.

It is well to recognize that mechanical and thermal treatments as well as composition affect the sigma boundary and we are indebted to the above discussions for emphasizing these points.

⁸G. V. Smith, E. J. Dulis and H. S. Link, "Effect of Prior Treatment on Precipitation of Sigma Phase", *The Welding Journal Supplement*, August 1951.

THE ELECTROLYTIC SEPARATION AND SOME PROPERTIES OF AUSTENITE AND SIGMA IN 18-8-3-1 CHROMIUM-NICKEL-MOLYBDENUM-TITANIUM STEEL

BY T. P. HOAR AND K. W. J. BOWEN

Abstract

Austenite and sigma have been extracted from 18-8-3-1 chromium-nickel-molybdenum-titanium steel, heat treated for various times at 1560 °F (850 °C), by selective anodic dissolution in 25% w/w sulphuric acid at 0.4 amp./in.² and in 50% v/v hydrochloric acid at 30 amps./in.² respectively.

The extracted austenite partially transforms to α_2 at room temperatures, the transformation being the greater the longer the previous heat treatment. There is no further transformation at -321 °F (-196 °C). This contrasts with the behavior of the austenite in the massive material, which does not transform at room temperature but does so at -321 °F (-196 °C); the easier transformation of the extracted austenite is probably due to the release of internal microstresses.

The extracted sigma is ferromagnetic at low temperatures. It is much higher in chromium and molybdenum, higher in titanium, and much lower in nickel, iron and manganese than the corresponding austenite.

Electrode potential measurements of compacted austenite and sigma residues in sodium chloride and hydrochloric acid solutions show that sigma has a greater tendency to become passive, and has a more noble passive potential than the corresponding austenite.

INTRODUCTION

PREVIOUS investigations of the constitution of 18-8-3-1 chromium-nickel-molybdenum-titanium steel (1, 2, 3)¹ have been concerned with the phases austenite, ferrite and sigma as they exist together. The present paper describes the electrolytic separation

¹The figures appearing in parentheses pertain to the references appended to this paper.

A paper presented before the Thirty-fourth Annual Convention of the Society, held in Philadelphia, October 18 to 24, 1952. Of the authors, T. P. Hoar is associated with the Department of Metallurgy, University of Cambridge, England, and K. W. J. Bowen was formerly with the Department of Metallurgy, University of Cambridge, and is now associated with the Research Department, Metals Division, Imperial Chemical Industries, Birmingham, England. Manuscript received May 15, 1952.

of austenite and sigma by selective anodic dissolution, and some of their chemical and physical properties.

Electrolytic extractions of phases have previously been made from a variety of alloys, with varying success. In the discussion of the work of Franks, Binder and Bishop (4) on chromium-nickel steels containing molybdenum, mention is made of the anodic separation of sigma from association with austenite, using hydrochloric acid as electrolyte. Kirkby and Morley (5) have described attempts at phase extraction made with a steel of similar composition to the one used in the present work, but they give no details of experimental technique or of the purity of the residues obtained. A method of electrochemical extraction was used by Raynor and Wakeman (6) for the isolation of intermetallic compounds in the aluminum-manganese system. Many techniques used to isolate carbides from steel have been reviewed by Blickwede and Cohen (7). More recently, Blickwede, Cohen and Roberts (8) have described the investigation of phases in a high speed steel, and Gilman (9) has suggested that an estimate of the partition of elements between ferrite and austenite may be obtained by preferential electrolytic dissolution, although he gives no specific results.

The electrolytic separation of austenite and sigma as residues from specimens subjected to a range of heat treatment is described below. Observations on the composition, magnetic properties and electrochemical behavior of the separated phases are also reported.

EXPERIMENTAL TECHNIQUE

Materials—The steel was in $\frac{1}{2}$ -inch and 1-inch diameter bars and had the following analysis: carbon 0.04%, manganese 0.43%, silicon 0.56%, chromium 18.4%, nickel 8.45%, molybdenum 3.40% and titanium 0.47%. Specimens were cut in the form of disks, 1 inch in diameter and 0.125 inch in height, and rods, 0.5 inch in diameter and 6 inches long.

Heat Treatment—This was carried out in an air atmosphere at a reduced pressure of one micron or better. After a standard preliminary heat treatment of 1 hour at 2100 °F (1150 °C) followed by water quenching, the specimens consisted of austenite and ferrite in approximately equal amounts together with a little titanium carbide. On reheating at 1560 °F (850 °C), ferrite transformed to sigma and austenite (3), and when the reheating time was long enough, a structure consisting solely of austenite and sigma could be retained at room temperature after quenching.

Determination of Phase Volumes—As in previous work (3), the point-counting method and "ferrometer" magnetic measurements were used to obtain the volumes of phases present.

Electrolytic Extraction of Phases—Two designs of cell were

used in the development of extraction techniques. In both, the cathodes were similar in size to the anodes and were of 18-8-3-1 steel heated at 2100 °F (1150 °C) and water-quenched.

Cells as shown in Fig. 1A were used in preliminary experiments with disk-shaped specimens, both the anodes and cathodes being half immersed in electrolyte held in 250-ml. beakers. Experience gained with this arrangement led to the adoption of the cells of the type shown in Fig. 1B, in which the anode and cathode in the form of rods fitted inside a 600-ml. beaker. The residue from the anode was

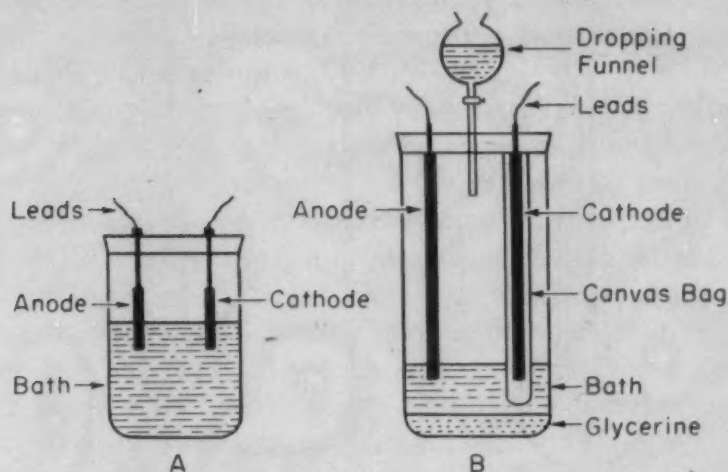


Fig. 1—Cells Used in Extraction Experiments.

collected under glycerine to protect it from attack. With the smaller cell, the whole of the electrolyte was added at the beginning of the experiment, but with the larger cell it was added gradually from a dropping funnel so that only a small portion of the anode was exposed to electrolyte at a time, and the current density on the dissolving anode could be kept steady. Several cells were held in a tank containing refrigerant to counteract the heating effect of the current.

Anodes for extraction were cleaned and weighed. At the end of an extraction, the anode was washed, dried and reweighed, so that the loss in weight could be obtained. The residue from the anode was filtered off, washed, dried and weighed.

Previous experiments had shown that a 25% w/w sulphuric acid/water electrolyte leads to preferential attack on ferrite and sigma; it was therefore used for austenite extraction. A 50% v/v hydrochloric acid/water electrolyte, which leads to preferential attack on ferrite and austenite, was used for sigma extraction.

X-Ray Examination—X-ray powder photography was used for residue identification and to indicate the presence of the α_2 body-centered cubic phase in the various "austenite" residues.

Magnetic Analysis—The ferrometer (1, 2, 3) was used to follow changes in ferromagnetism. For measurements below room temper-

ature, a specially designed vacuum flask was fitted to the instrument; this allowed specimens immersed in refrigerants to be examined.

Photomicrography and Electronmicrography—Photomicrography was used to determine and to record the structures and the varieties of selective attack that were found in specimens given different heat treatments, while electronmicrography was used to determine the shape of the residue particles and to provide additional aid in their identification.

Chemical Analysis—To determine the manner and extent of the

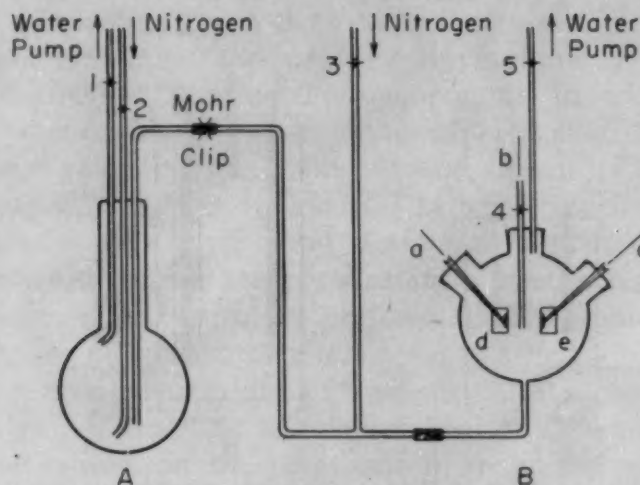


Fig. 2—Apparatus Used for Potential Measurements.

partition of elements between the phases present, some of the separated residues were analyzed by chemical methods applicable to 18-8 class steels, after preliminary spectrographic analysis.

Electrode Potential Measurements—Some measurements were made on the extracted residues of sigma and austenite from specimens heated at 1560 °F (850 °C) for 69.5 hours and water-quenched, which had consisted of these two phases only. For this purpose the residues were pressed at 112,000 psi into disks, 0.72 inch in diameter and 0.08 inch in height. Since the austenite residue contained some α_2 , after compression the disk was heated at 1560 °F (850 °C) for 20 minutes *in vacuo* and water-quenched, in which condition it was completely nonferromagnetic and consisted of austenite only.

Fig. 2 shows the apparatus used for potential measurements. Deaeration of solutions was carried out in flask A, and measurements were made in flask B. Disks of austenite and sigma were mounted separately in Perspex (Lucite) so that one flat surface was exposed in each case. Glass tubes were inserted in the back of the mounts and sealed in position. Platinum wires, a and c, passed inside the glass tubes and made contact through mercury with the rear flat surfaces of the disks. These arrangements constituted the elec-

trodes d and e, and were held in position through conical glass joints as shown. The central connection to flask B carried a reference electrode; in the diagram, the arrangement for the quinhydrone electrode is shown. The tube ended in a capillary close to the austenite and sigma electrodes; at its upper end it carried tap 4, above which quinhydrone crystals and a cleaned degreased platinum wire b were placed. For a silver/silver-chloride reference electrode a slightly modified arrangement was used. The whole apparatus was immersed in a water thermostat maintained at 77 °F (25 °C). Taps 2 and 3 were connected to a supply of nitrogen (passed over heated copper at 1110 °F (600 °C) before entering the apparatus) while taps 1 and 5 led to a water pump.

The solution to be used was placed in flask A. Initially, taps 2, 4 and 5 were closed and the Mohr clip was opened. When tap 3 was opened, admitting nitrogen to the apparatus, flask A was connected to the water pump by opening tap 1; deaeration of the solution commenced and the Mohr clip was adjusted so that maximum turbulence was produced. Deaeration was continued for 1 hour, after which tap 1 and the clip were closed and tap 5 opened. This provided deaeration of flask B, which was continued for ½ hour, during which time the three glass joints and tap 4 were opened in turn, to allow nitrogen to sweep out air pockets. Tap 3 was then closed and tap 2 and the clip opened so that sufficient solution was transferred into flask B. Tap 5 was then closed and tap 4 opened, so that some of the solution was forced up the tube of the reference electrode and around tap 4 to connect the reference electrode to the solution. Tap 4 was then closed, and finally tap 2 and the clip. The potentials of sigma and austenite against the reference electrode were measured alternately, at regular intervals, by means of a Marconi pH meter. In each experiment, after a suitable interval, air was admitted to the apparatus and further measurements were made.

RESULTS AND INTERPRETATION

Extraction of Residues

Extraction experiments were of two kinds, in which either the heat treatment of the specimens or the value of initial current densities was varied.

Austenite Extraction With 25% w/w Sulphuric Acid—In preliminary experiments with cells as shown in Fig. 1A, specimens heated at 1560 °F (850 °C) for 63 hours and water-quenched were used; they consisted of austenite and sigma only. The yield of austenite residue, which was generally low, decreased with increase in current density in the range 0.2 to 4.2 amps./in.²

In further experiments with the larger cells (Fig. 1B), the current density was held constant at 0.4 amp./in.² and specimens heated

at 1560 °F (850 °C) for 5 minutes, 2.5 hours, 69.5 hours, and 102 hours were used; a standard, nonreheated specimen was included for comparison purposes. The bath temperature varied between 68 and 77 °F (20 and 25 °C). Oxygen was evolved at the anodes in all cases. Table I gives details of these experiments.

In both series of experiments, ferrite-free anodes yielded magnetic residues, which X-ray analysis showed to be mixtures of austenite and α_2 . This is further evidence of the transformation of austenite in this steel, which we have already reported (3).

Table I
Residues Obtained by Electrolytic Extractions

All specimens first heated for 1 hour at 2100 °F (1150 °C) and water-quenched							
Extraction with 25% w/w H_2SO_4 at 0.4 amp./in. ²				Extraction with 50% v/v HCl at 30 amps./in. ²			
Time of heating at 1560 °F (850 °C)	Volume % of phases	Amount of anode dissolved g./amp.-hr.	Residue*	Yield of Residue, % of original phase	Amount of anode dissolved, g./amp.-hr.	Residue*	Yield of Residue, % of original phase
Nil	Austenite 45 Ferrite 55 (Figs. 3, 4)	0.53	Austenite (Fig. 13) and trace δ -ferrite	0.72	Nil	..
5 min.	Austenite 47 Ferrite 46 Sigma 7 (Figs. 5, 6)	Austenite, α_2 and Sigma (Fig. 14)
2.5 hr.	Austenite 71 Ferrite 14 Sigma 15 (Figs. 7, 8, 9)	0.43	Austenite and α_2 (Fig. 15)	14.2	0.39	Austenite (Fig. 17), α_2 and sigma	..
69.5 hr.	Austenite 86 Sigma 14 (Figs. 10, 11, 12)	0.40	Austenite and α_2 (Fig. 16)	10.3	0.38 (i)† 0.47 (ii)	Sigma (Fig. 18)	34 (i)† 54 (ii)
102 hr.	Austenite 86 Sigma 14	0.40	Austenite and α_2	10.3	0.48	Sigma	20

*By X-ray, magnetic measurement and electronmicrography.

†See text.

Sigma Extraction With 50% v/v Hydrochloric Acid—In preliminary experiments with the smaller cells, specimens heated at 1560 °F (850 °C) for 63 hours and water-quenched, consisting of austenite and sigma only, were again used; the current density was varied from 0.3 to 30 amps./in.²

In all hydrochloric acid extractions, the bath temperature varied from 77 °F (25 °C) for the lowest current density to 150 °F (65 °C) eventually reached for the high current densities. Oxygen was evolved at all anodes. At a current density of 0.3 amp./in.², the residue was similar to that obtained with the sulphuric acid bath under the same conditions of anode heat treatment, consisting of austenite and α_2 . With a current density of 30 amps./in.² a residue of sigma alone was obtained. At intermediate current densities, viz., 1.5, 10, 12, 16 and

30 amps./in.², the residues became decreasingly ferromagnetic as the proportion of sigma in them increased, and that of partially transformed austenite decreased.

Further extraction experiments, at a current density of 30 amps./in.² with cells of the larger type, were carried out with variously reheated specimens, with the results given in Table I. The calculation of the residue yields given therein is based on the assumption that the densities of austenite and sigma are the same, a sufficiently close approximation (10, 11, 12) in view of the other possible experimental errors. Two sets of results (i and ii) for specimens heated at 1560 °F (850 °C) for 69.5 hours are shown; results (i) were obtained under normal cell operating conditions, while results (ii) were obtained after a complete change of electrolyte had been made twice during the experiment. This alteration in technique increased the yield of sigma from 34 to 54%; evidently dissolved metal in the electrolyte reduces the efficiency of the separation process. A yield of 49% was obtained for a similar condition of heat treatment with the much smaller specimen and cell as in Fig. 1A; in that instance, the cell was operated for a much shorter time, so that dissolved metal in the electrolyte would not be expected to influence the yield obtained to the same extent.

Examination of Residues

Magnetic Examination—2.5-gram portions of the powders obtained as residues from the sulphuric acid extractions listed in Table I were placed in weighing bottles, and ferrometer readings were taken at room temperature, then in liquid nitrogen at -321 °F (-196 °C), and then again at room temperature. Similar measurements were made on the residues from the hydrochloric acid extractions listed in Table I; in this case the residues were first readily freed from any contaminating iron particles derived from the cathodes during electrolysis by means of a magnet, and were compacted at 112,000 psi into disks 0.72 inch in diameter and 0.08 inch thick.

The ferrometer results are given in Table II. Each residue from sulphuric acid extraction shows a constant degree of ferromagnetism, unaltered by low temperature; this indicates (a) the presence of α_2 formed by transformation of the austenite during or after extraction (in the first residue the ferromagnetism is probably caused by a small amount of δ -ferrite extracted with the austenite), (b) the increasing tendency of austenite to transform on extraction as the time of its formation at 1560 °F (850 °C) is increased (this is in harmony with our previous work), (c) the stability of the untransformed austenite to low temperature treatment, (d) the absence of sigma of composition that becomes ferromagnetic at low temperatures (2). The residues from hydrochloric acid extractions each

Table II
Magnetic Examination of Residues

All specimens first heated for 1 hour at 2100 °F (1150 °C) and water-quenched								
Residue From H ₂ SO ₄ Extraction					Residue From HCl Extraction			
Time of Heating at 1560 °F (850 °C)	Type	Ferrometer Reading			Type	Ferrometer Reading		
		1st at room temp.	2nd at -321 °F (-196 °C)	3rd at room temperature		1st at room temp.	2nd at -321 °F (-196 °C)	3rd at room temp.
Nil	Austenite and δ-ferrite	2	2	2	Nil
5 min.	Austenite and αs	7.5	7.5	7.5
2.5 hr.	Austenite and αs	11.5	11.5	11.5	Austenite, αs and sigma	11	14	11
69.5 hr.	Austenite and αs	13	13	13	Sigma	0	15	0
102 hr.	Austenite and αs	15	15	15	Sigma	0	15	0

show a transient increase of ferromagnetism at low temperatures, because sigma of certain compositions becomes ferromagnetic at around -171 °F (-113 °C), as we have previously shown (2, 3).

Photomicrographs and Electronmicrographs—Figs. 3 through 12 inclusive are photomicrographs of the original specimens listed in Table I, and Figs. 4, 6, 8, 9, 11 and 12 also illustrate the several kinds of selective attack found on the specimens after electrolytic extraction; they were obtained by mounting suitable pieces in bakelite and sectioning. Figs. 13 through 18 are electronmicrographs obtained from the residues listed in Table I.

Chemical Analysis—The residues listed in Table I and others similarly obtained were analyzed chemically by personnel familiar with the special techniques used for 18-8 class steels. The residues were usually slightly contaminated with titanium carbide present as particles in the steel (and containing substantially all the 0.04% of carbon), with silicon that separated from the phase or phases going into solution, and with oxygen unavoidably taken up as surface oxide film. It was not possible to estimate the elementary silicon of the residues, and consequently the distribution of the total 0.56% of silicon between the phases cannot be calculated. The amounts of the elements chromium, nickel, molybdenum, titanium, manganese and iron in each residue, as weight percentages of the total of these elements in the residues, are given in Table III. The figures for ferrite composition are calculated from the corresponding austenite analysis, the over-all steel analysis, and the volumes of the phases present, on the approximate assumption that the ferrite and austenite densities are equal. The figures for titanium are calculated from the analytical determinations of titanium and carbon, by subtraction of the amount of titanium equivalent to the carbon in titanium carbide.

Table III
Chemical Composition of Residues

All specimens initially heated for 1 hour at 2100 °F (1150 °C) and water-quenched Residues described as "Austenite" contain some α_2 ; they were all extracted with 25% w/w H_2SO_4							
Time of Heating at 1560 °F (850 °C)	Residue Analyzed	Weight of Element as					
		Percentage of Cr	Percentage of Ni	Percentage of Mo	Percentage of Ti	Percentage of Mn	Percentage of Fe
Nil	Austenite	13.2	10.0	2.5	...	0.42	73.9
	Ferrite	22.7	7.2	4.1	...	0.44	63.6
2.5 hrs.	Austenite	14.4	10.0	2.1	...	0.40	73.1
25 hrs.	Austenite	13.3	10.0	2.3	...	0.50	73.9
48 hrs.	Austenite	16.7	9.7	2.1	...	0.43	71.1
	Sigma	28.6	3.7	7.8	0.8	0.05	59.2
69.5 hrs.	Austenite	15.8	9.7	2.8	...	0.43	71.3
	Sigma	27.5	4.0	8.8	0.5	0.05	59.2

The salient features of these results are:

(a) For the nonreheated specimen containing only austenite and ferrite, the ferrite is (by calculation) higher in chromium and molybdenum, and lower in nickel and iron, than the extracted austenite, in harmony with accepted knowledge of ferrite- and austenite-forming elements.

(b) For the reheated specimens, the composition of the extracted austenite remains remarkably constant as the time of heating at 1560 °F (850 °C) is increased, except for a tendency for the chromium content to increase (mainly at the expense of the iron content). The increased tendency of the longer heated austenite to transform to α_2 may be associated with this increase of chromium.

(c) The sigma residues are much higher in chromium and molybdenum, higher in titanium, and much lower in nickel, iron and manganese than the corresponding austenite residues from the same specimens. This illustrates the known sigma-forming tendencies of chromium and molybdenum. The alteration of the chromium and molybdenum contents in the austenite caused by sigma formation is not very great, however, and indeed the chromium content of the austenite in contact with sigma is greater than that of the austenite in the nonreheated austenite-ferrite structure, since this contains 55% of ferrite while the austenite-sigma structure contains only 14% of sigma. Consequently corrosion weakness of the austenite caused by chromium impoverishment need not necessarily be expected in sigma-containing structures.

Electrode Potential Measurements—Austenite and sigma disks, prepared as described above from residues obtained from specimens containing 86% austenite and 14% sigma, were abraded with 00 emery paper and inserted in flask B (Fig. 2); the time between abrasion and immersion in electrolyte was noted. Measurements were usually first made in deaerated nitrogen-saturated solutions; then air was admitted to the system and measurements were continued.

Typical potential/time curves of sigma and austenite in 0.5 M

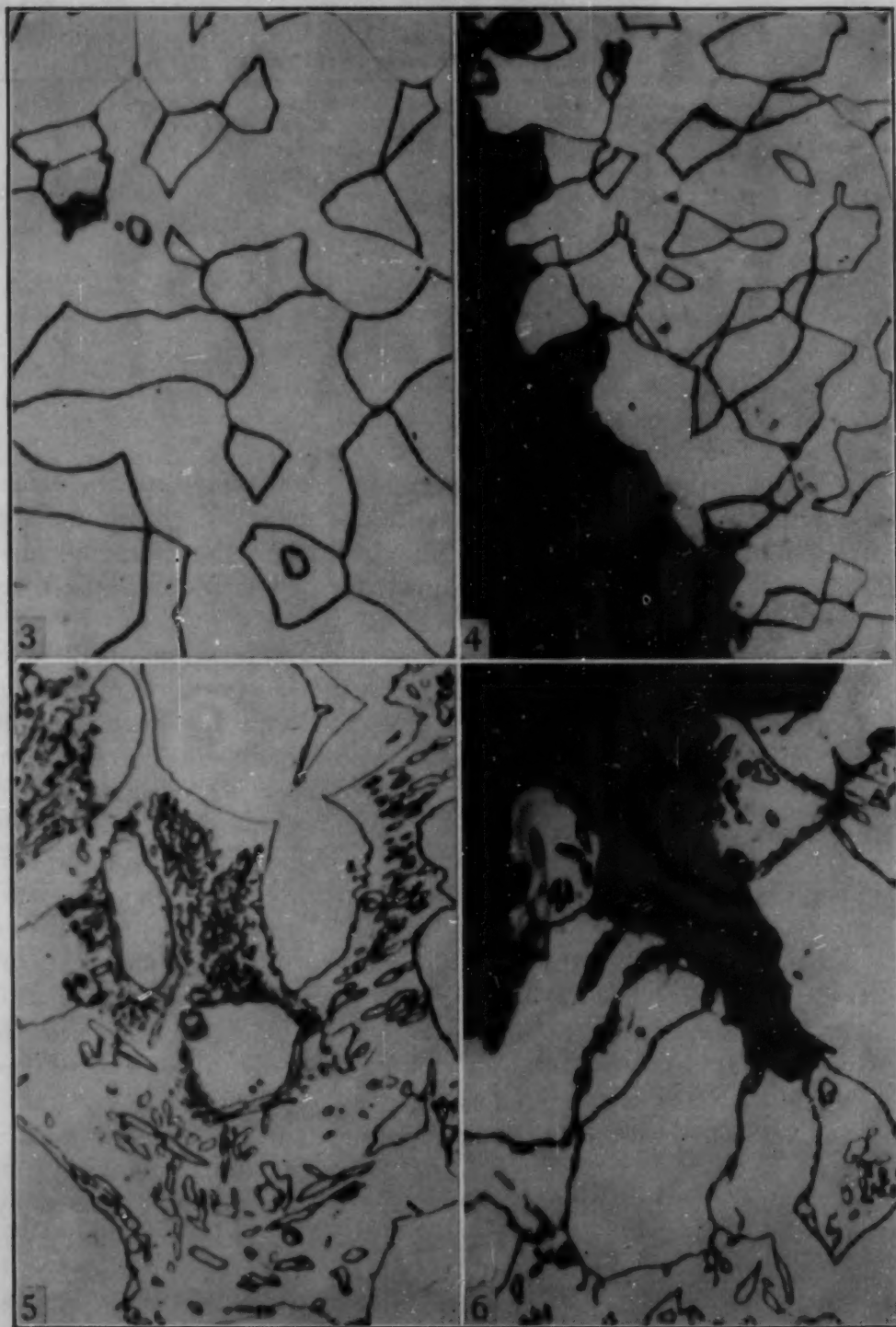


Fig. 3—1 Hour at 2100 °F (1150 °C), Water Quench. Austenite and ferrite. $\times 650$.

Fig. 4—1 Hour at 2100 °F (1150 °C), Water Quench. Selective attack on ferrite in sulphuric acid at 0.4 amp./in.² $\times 450$.

Fig. 5—1 Hour at 2100 °F (1150 °C), Water Quench, 5 Minutes at 1560 °F (850 °C), Water Quench. Austenite, ferrite and sigma. $\times 650$.

Fig. 6—1 Hour at 2100 °F (1150 °C), Water Quench, 5 Minutes at 1560 °F (850 °C), Water Quench. Selective attack on ferrite in sulphuric acid at 0.4 amp./in.² $\times 650$.

All etched in aqua regia.

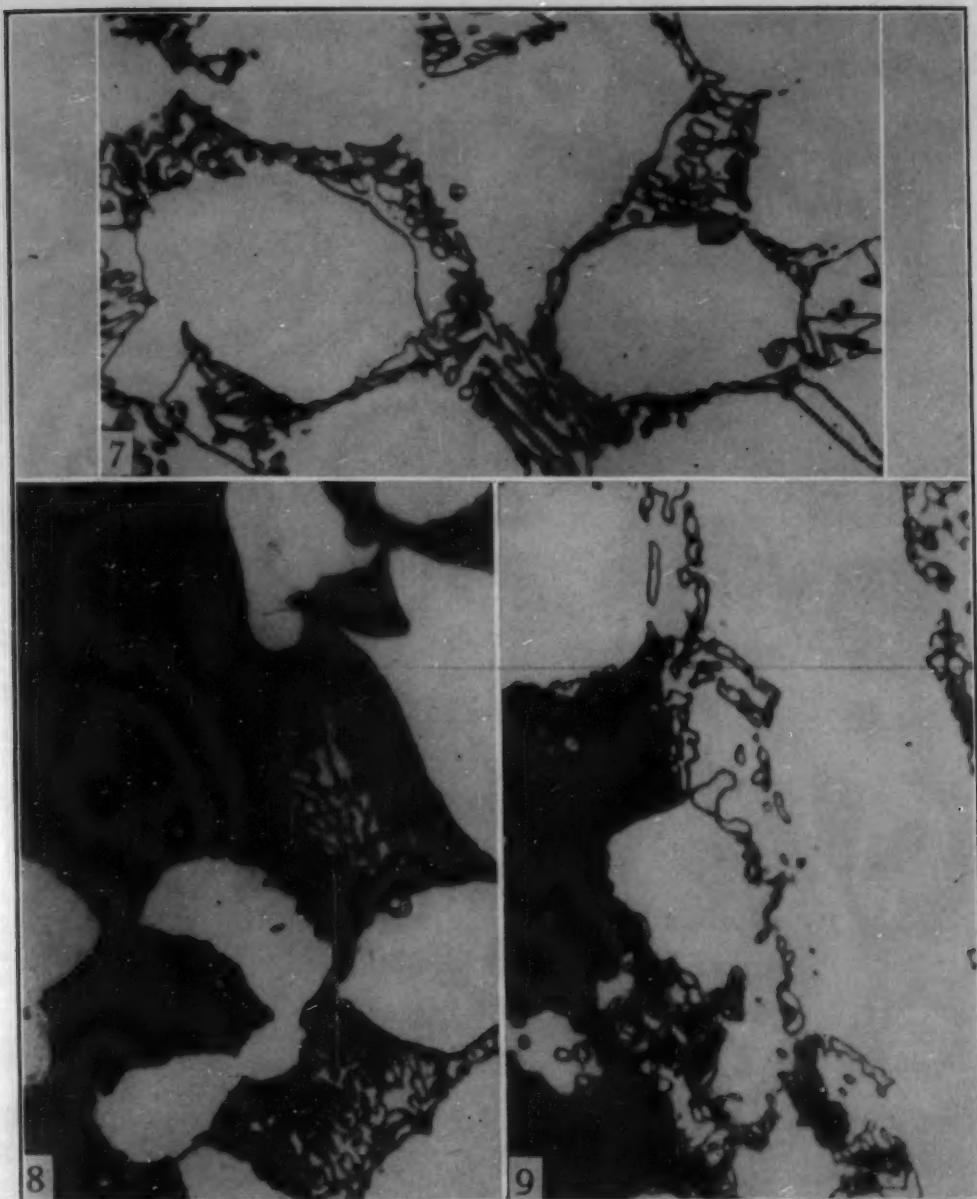


Fig. 7—1 Hour at 2100 °F (1150 °C), Water Quench, 2.5 Hours at 1560 °F (850 °C), Water Quench. Austenite, ferrite and sigma. $\times 650$.

Fig. 8—1 Hour at 2100 °F (1150 °C), Water Quench, 2.5 Hours at 1560 °F (850 °C), Water Quench. Selective attack on ferrite and sigma in sulphuric acid at 0.4 amp./in.² $\times 650$.

Fig. 9—1 Hour at 2100 °F (1150 °C), Water Quench, 2.5 Hours at 1560 °F (850 °C), Water Quench. Selective attack on ferrite in hydrochloric acid at 30 amps./in.² $\times 650$.
All etched in aqua regia.

sodium chloride solution are given in Fig. 19. Both phases showed potential values characteristic of passivity, changing little with time or with the admission of air; sigma was throughout some 0.4 to 0.6 v. more noble than austenite. Evidently both phases carried protective oxide films throughout, that on sigma being superior, as might be expected from the higher chromium and molybdenum contents of sigma.

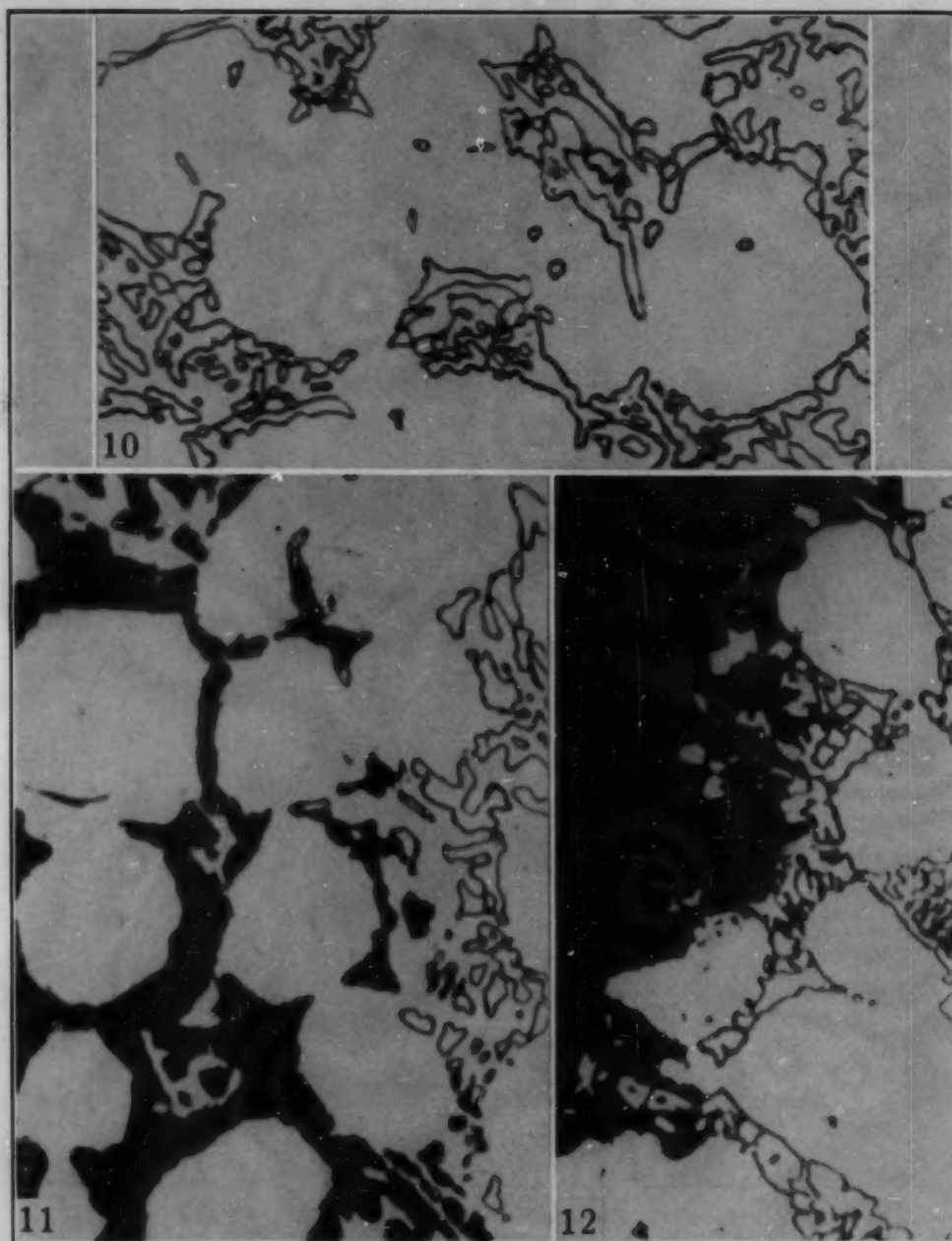


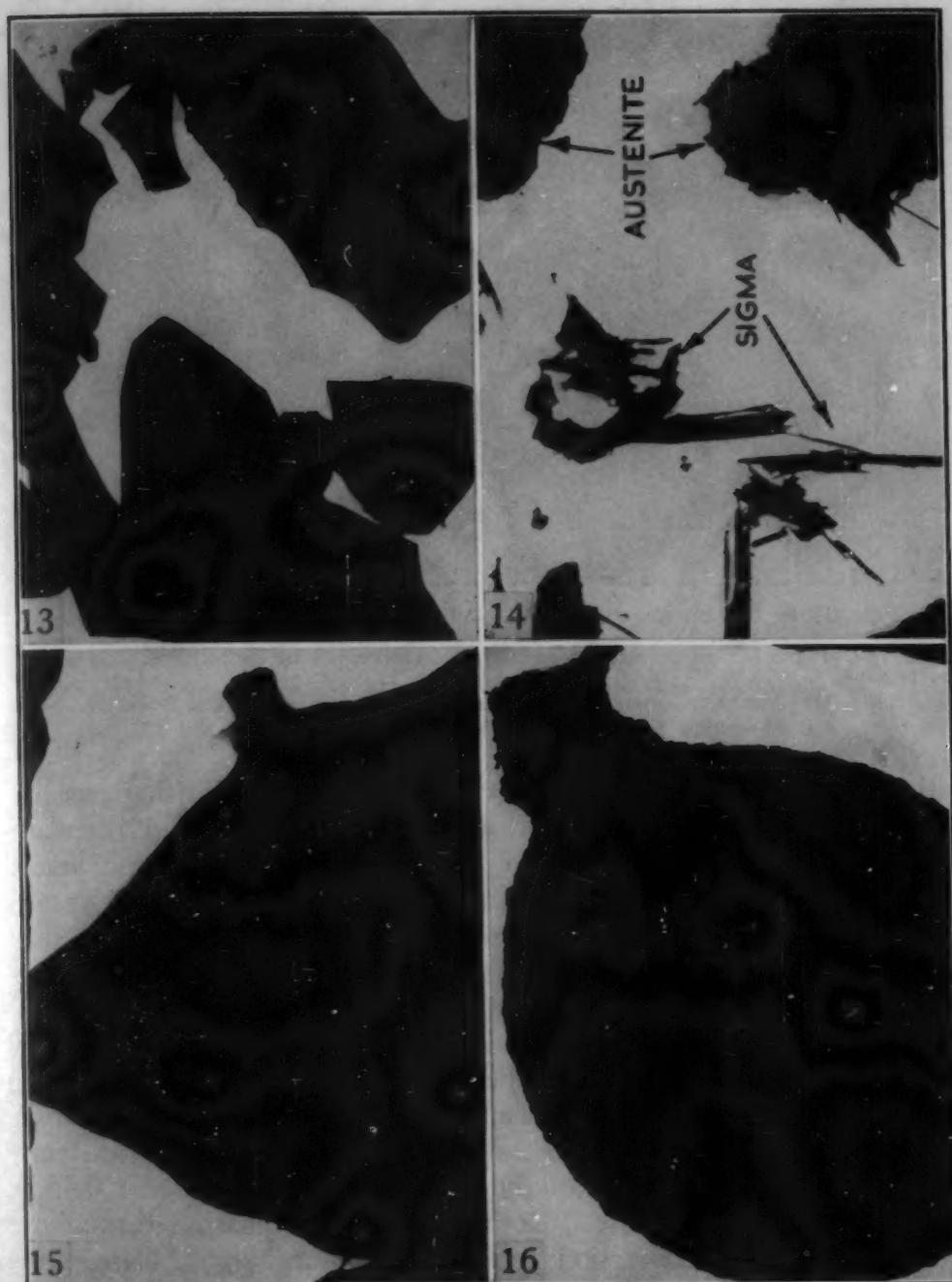
Fig. 10—1 Hour at 2100 °F (1150 °C), Water Quench, 69.5 Hours at 1560 °F (850 °C), Water Quench. Austenite and sigma. $\times 650$.

Fig. 11—1 Hour at 2100 °F (1150 °C), Water Quench, 69.5 Hours at 1560 °F (850 °C), Water Quench. Selective attack on sigma in sulphuric acid at 0.4 amp./in.² $\times 650$.

Fig. 12—1 Hour at 2100 °F (1150 °C), Water Quench, 69.5 Hours at 1560 °F (850 °C), Water Quench. Selective attack on austenite in hydrochloric acid at 30 amps./in.² $\times 650$.

All etched in aqua regia.

Fig. 20 shows a series of potential/time curves for sigma and austenite in 0.1 M hydrochloric acid, obtained in experiments in which the time of air exposure between abrasion and immersion in the deaerated solution was varied. With an abrasion-immersion period of 2 hours both sigma and austenite were active in solution



Figs. 13 to 18—Electronmicrographs of Residues Obtained in Extraction Experiments. $\times 1500$. Figs. 13 to 16 are concerned with extractions in sulphuric acid at 0.4 amp./in.² Figs. 17 and 18 are concerned with extractions in hydrochloric acid at 30 amps./in.²

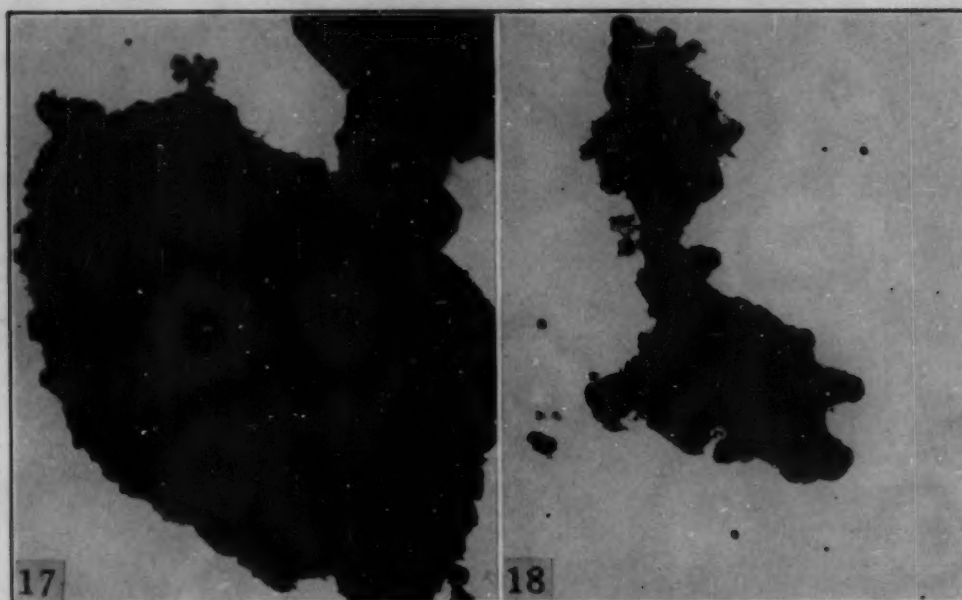
Fig. 13—Austenite From Austenite and Ferrite (See Figs. 3 and 4).

Fig. 14—Austenite and Sigma From Austenite, Ferrite and Sigma (See Figs. 5 and 6).

Fig. 15—Austenite From Austenite, Ferrite and Sigma (See Figs. 7 and 8).

Fig. 16—Austenite From Austenite and Sigma (See Figs. 10 and 11).

at potentials of approximately -0.66 and -0.72 v. (N-hydrogen scale) respectively. With abrasion-immersion periods of 4 and 6 hours, both phases showed initially high potentials, quickly became



Figs. 13 to 18—Electronmicrographs of Residues Obtained in Extraction Experiments. $\times 1500$. Figs. 13 to 16 are concerned with extractions in sulphuric acid at 0.4 amp./in.² Figs. 17 and 18 are concerned with extractions in hydrochloric acid at 30 amps./in.²

Fig. 17—Austenite From Austenite, Ferrite and Sigma (See Figs. 7 and 9).

Fig. 18—Sigma From Austenite and Sigma (See Figs. 10 and 12).

active, and then showed sudden rises in potential indicating passivation, the rises occurring sooner with specimens that had been air-exposed for the longer time. With an abrasion-immersion period of 16 hours, passive potentials were found throughout, and results in an aerated solution for an abrasion-immersion period of 24 hours were similar. In no case did the admission of air have an appreciable influence on potentials found in deaerated solutions.

Results for a series of experiments in 0.5 M hydrochloric acid are given in Fig. 21. With a period of 2 hours between abrasion and immersion, sigma was active and austenite passive in this solution. With the admission of air to the system the potential of austenite was unaltered, but sigma rapidly became passive and some 0.45 v. more noble than austenite. Both phases were passive throughout after an abrasion-immersion period of 24 hours, sigma being some 0.2 v. the more noble; corresponding measurements for deaerated and aerated solutions here showed no significant differences.

In 5 M hydrochloric acid, the potential of sigma was up to 0.4 v. more noble than that of austenite, and sigma appeared passive; however, austenite, although showing a fairly noble potential, was evidently active as shown by the colored corrosion products coming from it.

These results illustrate clearly the tendency of sigma to be considerably more noble than the corresponding austenite in sodium chloride and hydrochloric acid solutions, when both phases are in the

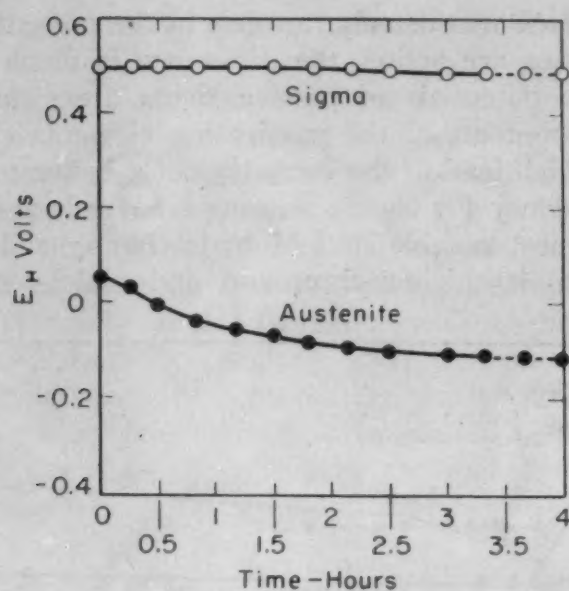


Fig. 19—Potential/Time Curves of Sigma and Austenite in 0.5 M Sodium Chloride Solution.

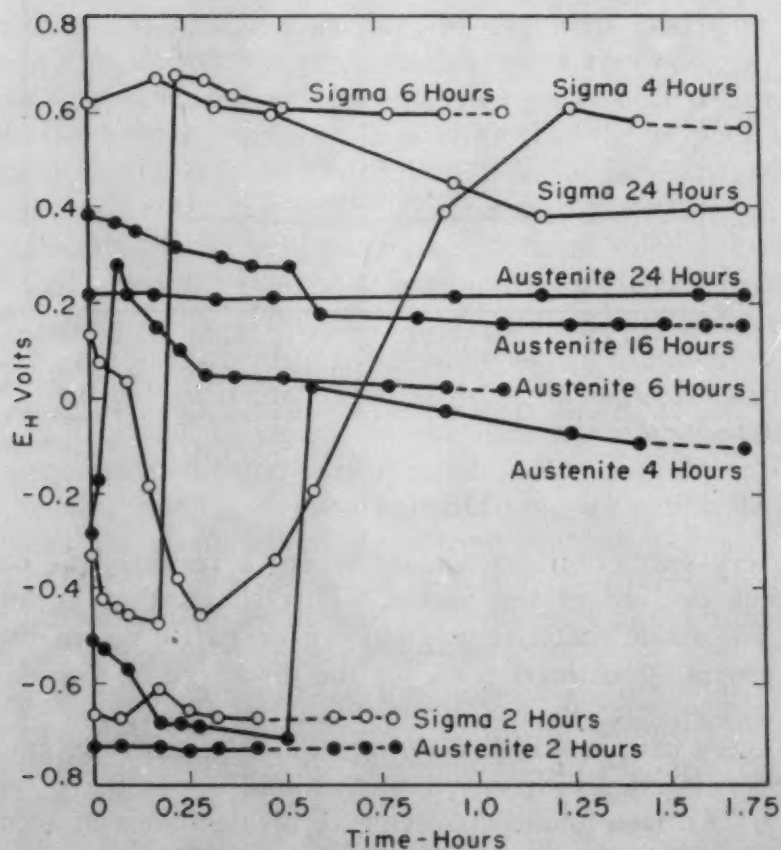


Fig. 20—Potential/Time Curves for Sigma and Austenite in 0.1 M Hydrochloric Acid.

Note: In Figs. 19, 20 and 21, experiments shown as full lines were conducted with air present throughout. Those shown with broken portions were conducted in nitrogen at first, with air admitted over the latter periods shown by the broken portions.

passive state, which was usually the case in the present experiments. When both phases are active, the difference is much less marked. The more noble potentials of passive sigma are clearly bound up with its higher contents of the passivating elements chromium and molybdenum, which lead to the formation of a better protective film. The greater tendency for sigma, as compared with austenite, to become passive (most notable in 5 M hydrochloric acid) is also undoubtedly due to its higher chromium and molybdenum contents.

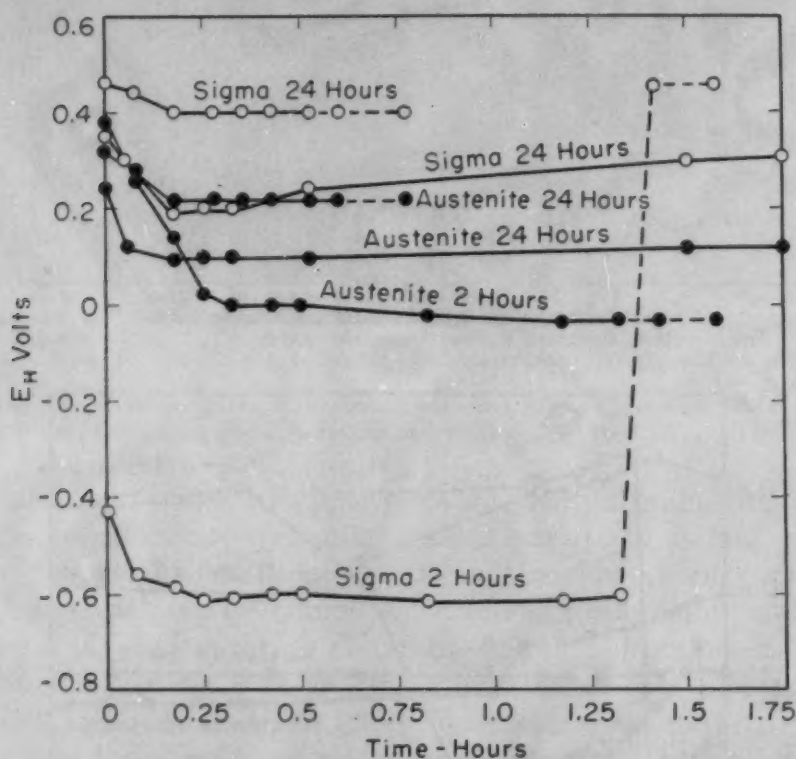


Fig. 21—Potential/Time Curves for Sigma and Austenite in 0.5 M Hydrochloric Acid.

DISCUSSION

In every extraction experiment where a residue was obtained, oxygen was evolved at the anode. This shows that at least one phase of the anode material was passive or partly so, in the usual sense of providing an inert basis for the discharge of oxygen rather than itself dissolving in accordance with Faraday's law. Furthermore, in every case in which a residue was obtained, the amount of anode material actually dissolved was around 0.4 to 0.5 g./amp.-hr. (Table I). An iron anode dissolving to bivalent ions in accordance with Faraday's law does so to the extent of 1.05 g./amp.-hr. and if dissolving to trivalent ions, of 0.70 g./amp.-hr.; and although the anode material contains substantial amounts of metals other than iron, its Faraday dissolution, in the absence of parallel oxygen discharge,

would certainly be much greater than the observed experimental amounts.

It thus appears likely that the phase found as residue is passive or partly passive under the particular extraction conditions. It is also likely, from the low figures of metal dissolved, that the other phase or phases are partly passive, either over part of their area or for part of the time, during the anodic treatment. It is significant that the yields of austenite extracted at low current density in sulphuric acid are much smaller than the yields of sigma extracted at high current density in hydrochloric acid: this general result implies that the austenite passivity is much less nearly complete than is the sigma. This greater tendency of sigma toward passivity during extraction is no doubt partly caused by the higher operating current density, but may also be an inherent tendency of sigma, associated with its higher chromium content.

The appearance of α_2 in the extracted austenite residues is of interest. We have previously shown (3) that austenite in specimens of 18-8-3-1 steel heated at 1560 °F (850 °C) does not transform at room temperature but partially transforms to α_2 on immersion in liquid nitrogen, although austenite in specimens heated at 1380 or 1470 °F (750 or 800 °C) does transform at room temperature, to an extent that increases with increase of time of heat treatment until a constant extent is reached. It is clear that the present austenite, in material heated at 1560 °F (850 °C), is intrinsically unstable; it is probably prevented from transforming at room temperature when in the massive material by the system of internal microstresses, which are released when the individual grains are extracted. Just as with the 1380 and 1470 °F (750 and 800 °C)-treated austenite in massive specimens, the transformation tendency of the 1560 °F (850 °C)-treated extracted austenite increases with increase of heating time; this effect may well be caused by the increase of chromium content in the austenite as heating is prolonged, shown in Table III.

It is also notable that no further transformation to α_2 takes place when the austenite residues from specimens heat treated at 1560 °F (850 °C) are cooled to -321 °F (-196 °C); in the absence of the microstresses present in the massive alloy, transformation has already occurred at room temperature.

The chemical analysis of the present residues has given the definite qualitative results already indicated. More refined purification techniques, especially the removal of titanium carbide and silicon particles from the residues, have recently been perfected, and future work may provide phase analyses of the present and similar alloys that can be used for a quantitative discussion of the complex phase diagrams and of the movement of elements during the attainment of equilibria.

The electrode potential experiments were not carried on for long enough times to determine what eventual breakdown of passivity, with corrosion, would occur, and further work is needed to elucidate this. They show, however, that in an initially passive austenite-sigma structure, the passive sigma will be cathodic toward the passive austenite, in sodium chloride or hydrochloric acid solutions. At first sight, this seems to suggest that the anodic austenite would be the phase first to show breakdown—which indeed may in some cases occur, with subsequent preferential austenite corrosion. But, especially under acid and/or oxygen-free conditions, the cathodic action at the passive sigma may well cause the reduction and removal of its oxide film, so that the sigma becomes active while the austenite remains passive, and if this should occur the sigma will be corroded preferentially.

The relatively small differences in electrode potential noted in cases where both phases were active suggest that, when general corrosion of an austenite-sigma structure occurs, neither phase will be corroded preferentially.

SUMMARY

1. Austenite, containing varying amounts of the transformation product α_2 , has been extracted anodically from specimens of 18-8-3-1 chromium-nickel-molybdenum-titanium steel consisting of austenite and ferrite, austenite, ferrite and sigma, and austenite and sigma, using 25% w/w sulphuric acid and a low current density (0.4 amp./in.²).

2. Sigma has been extracted anodically from specimens consisting of austenite and sigma using 50% v/v hydrochloric acid and a high current density (30 amps./in.²).

3. Magnetic analysis of the extracts has provided further evidence of the tendency of austenite to transform to α_2 , and has confirmed that sigma of certain compositions possesses a Curie point at low temperatures.

4. Chemical analysis of the extracted phases has shown that ferrite and especially sigma are richer in chromium and molybdenum, and poorer in nickel and iron, than the austenite with which they are associated. Sigma has a very low manganese content.

5. Electrode potential measurements in sodium chloride and hydrochloric acid solutions have shown that sigma is usually more noble than the corresponding austenite in these electrolytes, and shows a greater tendency to remain or to become passive.

ACKNOWLEDGMENTS

This work was carried out in the Department of Metallurgy, Cambridge University, England. We are grateful to Imperial Chem-

ical Industries Ltd. for the loan of apparatus and to Mr. W. T. Elwell of the Billingham Division of the Company for arranging the chemical analyses. We thank Mrs. A. M. B. Douglas of the Cavendish Laboratory for assistance with the X-ray examinations, and Dr. J. Nutting for assistance with the electronmicroscopy. Our thanks are also due to the Department of Scientific and Industrial Research for a grant to one of us (K. W. J. B.), during the tenure of which the work was carried out.

References

1. L. Smith and K. W. J. Bowen, "The Occurrence and Some Effects of Sigma Phase in a Molybdenum-Bearing Chromium-Nickel Austenitic Steel", *Journal, Iron and Steel Institute (British)*, Vol. 158, 1948, p. 289.
2. K. W. J. Bowen and T. P. Hoar, "Low Temperature Ferromagnetism of Sigma Phase in an Alloy Steel", *Research*, Vol. 3, 1950, p. 484.
3. K. W. J. Bowen and T. P. Hoar, "Phase Changes Associated with Sigma Formation in 18-8-3-1 Chromium-Nickel-Molybdenum-Titanium Steel", *Proceedings of the First World Metallurgical Congress, American Society for Metals*, 1951, p. 695.
4. R. Franks, W. O. Binder and C. R. Bishop, "The Effect of Molybdenum and Columbium on the Structure, Physical Properties and Corrosion Resistance of Austenitic Stainless Steels", *TRANSACTIONS, American Society for Metals*, Vol. 29, 1941, p. 35.
5. H. Kirkby and J. Morley, "The Formation of Sigma Phase in Duplex Chromium-Nickel-Molybdenum Corrosion Resisting Steels", *Journal, Iron and Steel Institute (British)*, Vol. 158, 1948, p. 289.
6. G. V. Raynor and D. W. Wakeman, "The Intermetallic Compound Phases of the System Aluminium-Manganese-Zinc", *Proceedings, Royal Society, Series A*, Vol. 190, 1947, p. 82.
7. D. J. Blickwede and M. Cohen, "The Isolation of Carbides from High Speed Steel", *Transactions, American Institute of Mining and Metallurgical Engineers*, Vol. 185, 1949, p. 578.
8. D. J. Blickwede, M. Cohen and G. A. Roberts, "The Effect of Vanadium and Carbon on the Constitution of High Speed Steel", *TRANSACTIONS, American Society for Metals*, Vol. 42, 1950, p. 1161.
9. J. J. Gilman, "Hardening of High Chromium Steels by Sigma Phase Formation", *TRANSACTIONS, American Society for Metals*, Vol. 43, 1951, p. 161.
10. P. Payson and C. H. Savage, "Changes in Austenitic Chromium-Nickel Steels During Exposures at 1100 to 1700 °F", *TRANSACTIONS, American Society for Metals*, Vol. 39, 1947, p. 404.
11. J. J. Gilman, P. K. Koh and O. Zmeskal, "Delta Ferrite Formation and its Influence on the Formation of Sigma in Wrought Heat Resisting Steel", *TRANSACTIONS, American Society for Metals*, Vol. 41, 1949, p. 1371.
12. G. V. Smith, E. J. Dulis and E. G. Houston, "Creep and Rupture of Several Chromium-Nickel Austenitic Stainless Steels", *TRANSACTIONS, American Society for Metals*, Vol. 42, 1950, p. 935.

DISCUSSION

Written Discussion: By F. L. LaQue, in charge, Corrosion Engineering Section, Development and Research Division, The International Nickel Co., Inc., New York City.

This paper is a welcome addition to the series by which these authors are contributing valuable information on the nature and occurrence of sigma phase in corrosion resisting alloys. While the alloy composition studied is not one in regular production in this country, it seems likely that some of the basic information will be applicable to the American alloys in which sigma is found—especially with respect to the probable distribution of alloys among phases and the mechanisms by which corrosion resistance may be affected.

Special significance must be attached to the observation that with 25% sulphuric acid as the electrolyte, the sigma phase is attacked in preference to austenite, while with hydrochloric acid it is the austenite that is attacked in preference to sigma. Presumably, this behavior would hold as well for normal corrosion without any impressed current, but it would be interesting if data could be provided to disclose any effects of anodic polarization on the distribution of corrosion between these phases. It would also be of interest if some data could be added with respect to behavior in the standard boiling 65% nitric acid test (ASTM Designation A-262-44T) and in the acid-copper sulphate (Strauss) test, since the presence of sigma phase has been proposed as the cause of excessive corrosion of alloys that contain molybdenum and titanium in the nitric acid without similar attack being noticed in the acid-copper sulphate solution.

The interpretation of the data in Table III would have been facilitated if the treatments used to extract the residue had been indicated definitely in the table—for example, with the specimen heated for 69.5 hours at 1560 °F it must be presumed that the austenite residue came from treatment in sulphuric acid and the sigma residue from treatment in hydrochloric acid.

It is noted that one interpretation of the data in Table III indicates that since the alloy content of the bulk austenite associated with sigma approximated the alloy content of the bulk austenite associated with ferrite in the original structure, chromium impoverishment of the surrounding phase need not necessarily be a cause of corrosion weakness in alloys that contain sigma. This apparently assumes substantial uniformity of composition of all phases without regard to distance from the phase boundaries. But, it is possible, for example, that a narrow zone of austenite in immediate contact with sigma phase might suffer a considerable depletion of alloying elements—chromium and molybdenum—which would not be reflected in the bulk analyses of these phases in the form of residues. Perhaps a chemical analysis for chromium and molybdenum of the electrolytes used for extracting the phases and of what remained of the immersed portions of the specimens would throw further light on this question.

The data from the potential measurements were interesting but, unfortunately, inconclusive, as the authors noted, in view of the possibility of reversals of potential relationships between sigma and austenite. The inference is that galvanic effects between the phases are not likely to occur in any fixed pattern and that, depending on circumstances, either phase may be attacked preferentially. However, in view of these possibilities, one could conclude that such duplex structures are not particularly desirable in corrosion resisting alloys and one might suggest that a balancing of the alloy composition to achieve and maintain a single phase would be a desirable step corrosion-wise.

We hope that the authors and their associates will continue their studies along these lines and thereby provide additional valuable information applicable to the many questions that remain.

Written Discussion: By P. K. Koh, research engineer, Allegheny Ludlum Steel Corp., Brackenridge, Pa.

The authors have made a distinct stride toward the sigma phase identification in chromium-nickel-molybdenum-titanium austenitic stainless steel by being able to isolate the sigma phase completely. During the past several years, careful observations have been made at our laboratories in attempting to achieve a complete isolation of sigma or other minor phases in various alloys. Especially in austenitic steels, matrix contamination has always been a source of trouble. Even though conditions were painstakingly duplicated with the same metallic specimen, various degrees of contamination of matrix were observed in diffraction patterns of extracts. On several occasions, due to some obscure minor differences in either experimental setup or operating conditions, results of anodic extraction from the same specimen between two of our laboratories were not congruent. We are curious to know the smallest amount of matrix contamination which can be detected by the authors' X-ray, magnetic and electro-microscopic methods. Occasionally we have obtained extracts from austenitic stainless steels, the diffraction patterns of which showed sigma lines only, but we cannot be sure of a complete isolation based upon X-ray results alone.

In the Allegheny Ludlum Research Laboratories we have adopted an electrolytic extraction procedure for minor phases in alloys with 10% NaCl aqueous solution. This electrolyte is used in place of FeCl_3 aqueous solution in extraction of sigma and chi phases from stainless steels because of its efficiency, lower resistivity and convenience in preparation. The recovery rate of sigma and carbides with the NaCl electrolyte equals or is better than with the FeCl_3 electrolyte, a higher current density can be used without excessive heating of the electrolyte, and also there is no attack on the stainless steel cathode as with the FeCl_3 electrolyte. In fact, this 10% NaCl electrolyte is also being used successfully for the extraction of minor phases in ferritic alloys and nickel-base alloys. For carbide extraction in tool steels this NaCl electrolyte eliminates the stench usually associated with the generation of hydrocarbon gases.

To compare the 50% HCl electrolyte proposed by the authors for sigma extraction with the FeCl_3 and NaCl electrolyte in use in our laboratories, a chromium-manganese-nickel steel (0.058% C, 0.47% Si, 19.85% Mn, 16.78% Cr, 0.79% Ni, 0.062% N—1 hour 2350 °F and 16 hours 1400 °F) known to contain sigma was subjected to extraction by the method described by the authors. From the Debye diffraction pattern taken on the residue extracted by the authors' procedure, only FeO and SiO_2 were observed. During the extraction by the authors' proposed procedure the following phenomena were observed:

(a) Strong chemical reaction between the metallic alloy and electrolyte during the brief interval before the current of cell was switched on.

(b) Violent effervescence of oxygen gas and acid fumes around anode, probably due to such a high current density of 30 amperes per square inch, necessitates a good ventilation system. The oxygen gas and the heat

generated by the current oxidized the alloy rapidly. This probably accounted for the FeO lines in the diffraction pattern of the extract.

It is interesting to mention that in his Doctor of Science thesis work at the Carnegie Institute of Technology, Dr. Adolph Lena, now at the Allegheny Ludlum Research Laboratories, adopted a 50% boiling HCl aqueous solution as a sigma and also general etching reagent for stainless steels with very good results.

Written Discussion: By M. T. Simnad, Metals Research Laboratory, Carnegie Institute of Technology, Pittsburgh.

The authors are to be congratulated for their interesting study of the transformation products in these alloys. They are especially to be commended for the advantage they have taken of the various techniques that are available for attacking the problem. This discussion is an attempt to appraise the aspects of the subject that are still not quite clear to me and to suggest the possibility of further developments.

1. The technique of separating the various products of phase transformations by electrolytic methods and then studying their characteristics could be applied to many alloy systems. The question arises as to what are the principles that govern the choice of electrolytes, current density, etc.? For example, what led the authors to their choice of 25% w/w sulphuric acid or to 50% v/v hydrochloric acid/water electrolytes?

2. The authors have estimated the compositions and electrode potentials of the separated constituents. However, it is important to know what are the concentration gradients at the boundary regions between these different phases and to chart the variations in electrode potentials at the depleted areas around the new phases. Similarly, the effect of the microstresses on the electrode potentials of the phases could be found by measuring the electrode potentials of the phases "in situ", and comparing with the values obtained when separated. This could perhaps be done by means of a micro-capillary technique for scanning the electrode potentials of minute areas. Also, the variations in composition and crystal structure at the phase boundaries, and of the phases when "in situ", may be measured by means of the micro-beam X-ray technique developed in the Cavendish Laboratory. Furthermore, radiotracers and autoradiography may be applied to this case.

3. The results of electrode potential measurements are most instructive. Further light may be thrown upon the properties of the surfaces if corollary experiments were carried out as follows: Stainless steels are attacked by a solution of bromine in methanol if the protective oxide films are removed; e.g., by abrading under alcohol. These steels may be abraded and then immersed in such a solution after various periods of pre-exposure to air. The time in air necessary for passivity in this solution may be compared with the time-potential curves, and would furnish useful information upon the relationship between passivity and electrode potentials. I have found, with the aid of radiochromium and the bromine-methanol technique, that oxide formation on abraded stainless steel is quite rapid at room temperature. The authors' statement, that there is a tendency for sigma to be considerably more noble than the corresponding austenite when both phases are in the passive state and that the difference is much less marked when both phases are active, does not appear to be borne out

by the figures; e.g., in 0.5 M HCl austenite is active, yet the potential difference is 0.4 v, whereas in 0.1 M HCl, and in 0.5 M HCl after 24 hours exposure to air, when both are passive, the sigma is only 0.2 v more noble than the austenite.

4. What are the authors' views on the degree of protectiveness and composition of the oxides? It seems to me that this is a field which has not been adequately studied in the past. It is a moot point as to why the relatively small increase in chromium content of the sigma should confer such a marked improvement in passivity. There does not appear to be any direct correlation between the chromium contents of the alloys and the composition of the corresponding oxide films formed on them.

5. The authors make the debatable suggestion to the effect that cathodic action at the passive sigma may cause the reduction and removal of its oxide film, so that the sigma may become active while the austenite remains passive, and that if this should occur, sigma will be corroded preferentially. I have not found it possible to reduce cathodically the oxide film present on stainless steel. This can be demonstrated by heat tinting a specimen; and upon making it cathode in acid solution, the colored oxide remains visible for very long periods of time.

It is more likely that the attack will take place in the boundary region between the phases, where depletion and favorable crystal orientation will be the factors which can lead to breakdown of passivity, as found with carbide precipitation in 18-8 stainless steels.

6. The striking effect of easier transformation of the extracted austenite that had been quenched from 850 °C is ascribed to the release of internal microstresses. The question arises: Why do microstresses not have a similar effect on specimens quenched from 800 °C or 750 °C? This relatively small difference in temperature should not cause a marked difference in the magnitudes of the internal stresses. It may be somewhat difficult to estimate the magnitude of the stresses arising in the separation of new phases, although this has been done for a 5% copper-aluminum alloy by Zakharova and Lashko (*Bull. Acad. Sci. U.R.S.S. Classe Sci. Tech.*, p. 1015, 1946). They took into account the stresses arising in diffusion processes due to the concentration gradient present around the nucleus of the new phase. The residual stress in the immediate neighborhood of the precipitate was estimated at 34 kilograms per square millimeter, while at a distance equal to ten times the radius of the nucleus it fell to 0.3 kilogram per square millimeter. Thus it is quite plausible to expect stresses of high magnitude to be present in such situations.

I think that the authors have made outstanding contributions to the subject, and their work should lead to further advances in the study of similar problems.

Written Discussion: By C. Edeleanu, Brown-Firth Research Laboratories, Princess Street, Sheffield, England.

The study of phase diagrams by analyzing the various phases of an alloy after their separation by electrochemical means is very elegant. The authors must be congratulated for having found suitable reagents, which is often one of the main difficulties. The analysis results are, however, somewhat surprising, since it is difficult to understand the very high corrosion resistance of this particular type of steel in the fully soft condition

if the chromium content of the austenite is as low as they indicate. It would be interesting to know whether a steel having the composition they suggest for austenite is in fact near the two-phase region of the diagram.

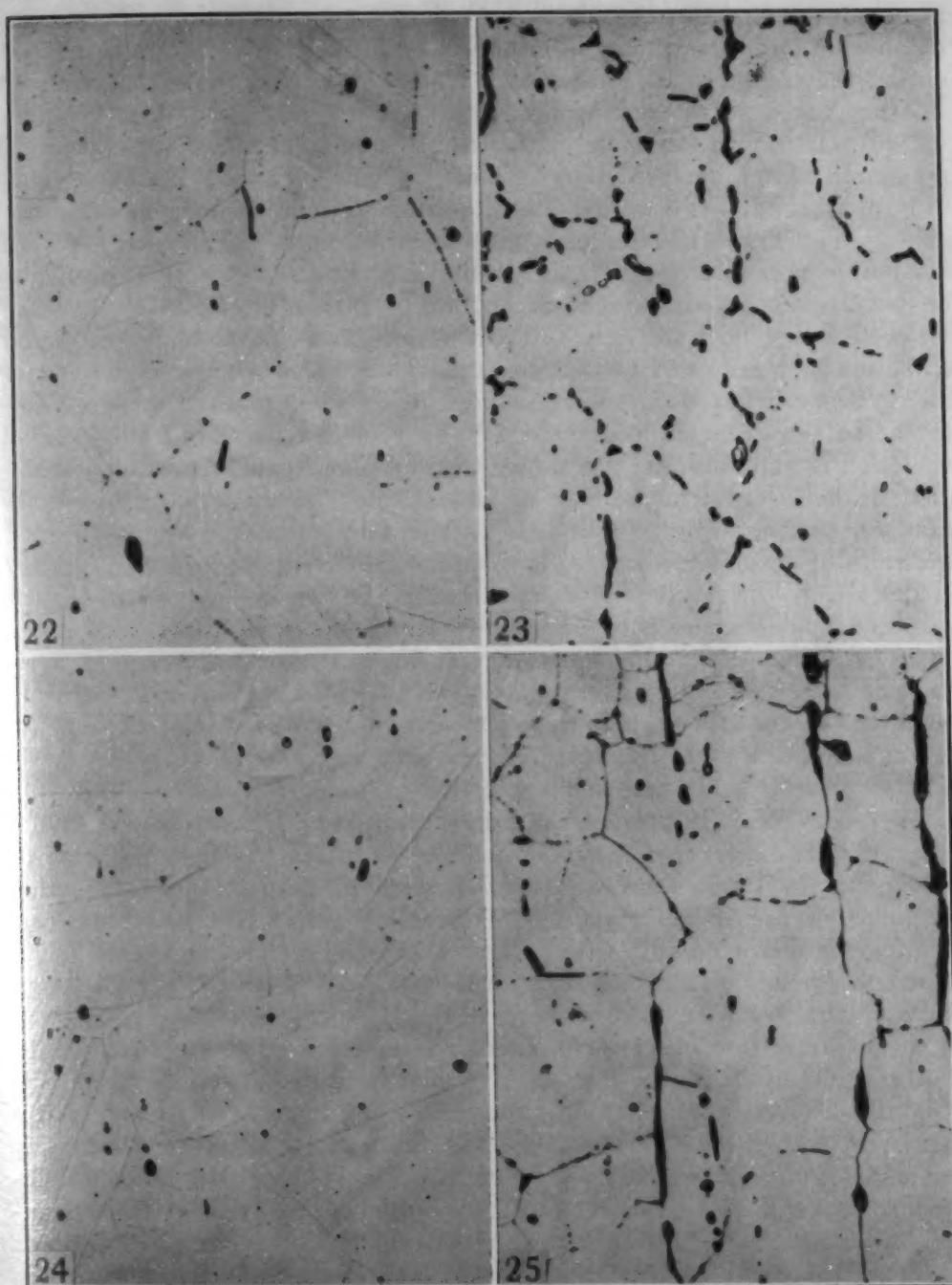
I am also uncertain that the assumption that the gas evolved from the anode is always oxygen is correct. This is certainly so in the case of sulphuric acid but in hydrochloric acid, many electrodes (e.g. aluminum, zinc) evolve hydrogen and I have found that this is so for stainless steels under conditions somewhat similar to those described in the paper. In other words, while in sulphuric acid the conditions at the anode are strongly oxidizing, they are not so in hydrochloric acid. It is, therefore, possible to explain why the two reagents act differently, since we have found that under strongly oxidizing conditions (e.g. nitric-chromic acid mixtures) the higher chromium steels are less resistant than the intermediate compositions,* while it is known from experience that the chances of passivity under somewhat reducing conditions increase with chromium content.

The efficiency of the anodic reaction in sulphuric acid is not as small as might appear, since in this case the chromium is oxidized to the hexavalent state and it was found that at somewhat lower current densities it is in fact 100% if the calculations are based on the oxidation of the nickel, iron and chromium to the di, tri and hexavalent states respectively. The inefficiency of the anodic reaction in hydrochloric acid in four of the experiments is surprising, since, if in this case the gas evolved is in fact hydrogen, more steel should have dissolved than could be predicted from Faraday's laws.

Written Discussion: By Adolph J. Lena, Research Laboratory, Allegheny Ludlum Steel Corp., Brackenridge, Pa.

The authors are to be commended on their ability to use electrolytic extraction techniques in a quantitative manner. This method of isolation of minor phases in stainless steels has been of great value for the qualitative identification of phases, but repeated attempts to apply the technique for a quantitative determination of either the amount of an individual phase or the distribution of alloying elements between phases has not been too fruitful. This can be attributed to contamination of the extracted phase, either with the matrix or with other phases that might be present in the steel. For instance, diffraction patterns of residues obtained by electrolysis in ferric chloride solutions from sigma-containing nonstabilized stainless steels will in general show the presence of chromium carbide as well as sigma. It is pertinent, therefore, that we should recognize that the quantitative application of the extraction technique used by these authors may be limited to the stabilized type of steel they employed. In this case, the carbon can be accounted for as titanium carbide and, therefore, no serious error arises in the determination of the chromium content of the austenite and sigma as long as the extraction technique adequately separates these phases, as it does in this work by Hoar and Bowen. If the titanium were not present, however, we should expect the formation of chromium carbide, and this contamination could introduce serious errors in the quantitative determination of the chromium content of sigma and possibly the austenite unless, of course, further steps were taken to separate the individual phases.

*Unpublished work by J. E. Tetiman and C. Edeleanu.



Treatment	Nitric Acid Corrosion Rate (in./mo.)
Fig. 22—Annealed	0.0012
Fig. 22—Annealed + 1 Hour at 1400 °F	0.0055
Fig. 23—Annealed + 100 Hours at 1400 °F	0.0015
Fig. 24—Annealed + 1 Hour at 1200 °F	0.0450
Fig. 25—Annealed + 100 Hours at 1200 °F	Disintegrated
All Photomicrographs × 500.	

The data in Table III on the chemical composition of residues is not definite proof that chromium impoverishment of the austenite may not be sufficiently great to cause a marked decrease in corrosion resistance, for

the analyses found in the table apply only to the gross austenite composition and tell us nothing of localized conditions adjacent to the sigma during the course of its formation. This point can be illustrated by considering the case of carbide precipitation in Types 302 (18-8) and 310 (25-20). If the carbon content of each of these steels were 0.1%, then the maximum chromium depletion assuming a Cr_7C_3 carbide would be 1.8% in both steels and this would leave the nominal chromium content of the austenite in Type 310 after precipitation at a greater value than the Type 302 before precipitation. On this basis we should not expect Type 310 to be sensitive to corrosion deficiencies due to carbide precipitation; but, as we well know, both 302 and 310 are equally susceptible to intergranular corrosion as a result of carbide precipitation. The chromium impoverishment theory is based on the assumption that the chromium depletion adjacent to the grain boundary carbides is very extensive but the over-all depletion is quite small. We should not, however, expect the impoverishment to be as great in the case of an equivalent amount of sigma formation, for this phase is an iron-rich as well as a chromium-rich phase and the ratio of chromium to iron atoms in solid solution would remain higher in the vicinity of the precipitating phase in the case of sigma than in the case of carbides where only chromium is being removed from solution.

The influence of sigma on the corrosion resistance of stainless steels has not been thoroughly investigated and many of the available data are inconclusive because of the presence of carbides. The staff of our Research Laboratory at Brackenridge has been interested for some time in the poor nitric acid corrosion resistance of extra low carbon Type 316 (18-8 Mo). We have found that the presence of sigma alone does not mean that the corrosion resistance will be impaired but that the time of holding at the sigma formation temperature and perhaps the distribution of the sigma are of importance. This conclusion may be obtained by correlating the following data with the accompanying photomicrographs (Figs. 22, 23, 24, 25) for a steel containing 0.024% C, 18.79% Cr, 11.68% Ni, 2.78% Mo and 0.045% N₂.

The precipitate observed in these photomicrographs has been identified as sigma by X-ray analysis of extracted residues. The diffraction pattern also showed weak lines of silica and strong lines of austenite. After 1 hour at 1400 °F, the corrosion rate is almost four times as great as in the annealed condition, but after 100 hours at 1400 °F the rate has decreased to a low value, regardless of the presence of a much greater quantity of sigma. A similar effect occurs in the case of carbide precipitation in higher carbon steels, and the most common explanation is that diffusion of chromium after longer times destroys the depleted areas. After 1 hour at 1200 °F, the corrosion rate is very high (although no precipitate can be observed in the microstructure) and increases with time such that disintegration occurs after either 8 or 100 hours at temperature. Even 100 hours at 1200 °F is not sufficient time to cause coalescence of the sigma. It is worth noting that none of these specimens failed to pass the Strauss test, which they most assuredly would have done had the high nitric acid rates been due to carbide precipitation.

Written Discussion: By J. I. Morley, Brown-Firth Research Laboratories, Princess Street, Sheffield, England.

The authors are to be congratulated on their efforts to obtain quantitative data regarding the partition of elements between the austenite and ferrite in 18-8-3-Ti-bearing steels.

There is, of course, no question that the delta ferrite present in this steel after quenching from 1150 °C is richer in chromium than the surrounding austenite. Our experience of the nitric acid resistance of the steel, however, does not accord with the conclusion indicated by Table III in the paper, that the equilibrium austenite at 1150 °C has a chromium content of only 13.2%. We should expect such a low chromium content to be associated with inferior nitric acid resistance.

It would be possible to estimate the composition of this austenite by taking a series of homogeneous steels of varying chromium content having 10% nickel and 2.5% molybdenum and noting the chromium content at which delta ferrite first appeared in the microstructure. Although we have not done this, we have found that for delta ferrite to be eliminated in 18-8-3-Ti-bearing steels the nickel content must be increased by 4 or 5%. The similar delta ferrite contents of one titanium-bearing steel containing 18% chromium, 8% nickel and another containing 23% chromium, 18% nickel suggest that, over this range, 2% of nickel has an equivalent ferrite-forming tendency to 1% of chromium. Therefore the chromium content at which a steel with 10% nickel and 3% molybdenum would just be free from ferrite should be approximately $(18 - 5/2)$ or $(18 - 4/2)$, i.e. 15.5 to 16.0%.

This and some other evidence of a similar kind suggests an equilibrium value of about 16% chromium for the austenite in 18-8-3-Ti-bearing steels water-quenched from 1150 °C. This would be more in keeping with its nitric acid resistance than the figure of 13.2% suggested.

Another result which appears to need further consideration before acceptance is the breakdown of the residue austenite to α_2 during electrolytic separation. It is suggested in the paper that this is due to the release of internal stresses. Are the authors satisfied that this is not the result of surface changes in the chemical composition of the finely divided residue, having in mind the oxidizing conditions of the H_2SO_4 extraction? For instance, little loss of carbon would be needed to account for such transformation, as many of these austenites owe their apparent stability at room temperature to very low carbon contents. For a given loss of carbon during extraction, the extent of transformation would be expected to increase, as it did, with the time of prior heating at 850 °C, owing to carbide precipitation. Increasing amounts of α_2 occur in solid specimens of 18% Cr-7.5% Ni-Ti-bearing steels at room temperature as the heating times and amount of carbide precipitation increase.

Written Discussion: By F. H. Keating and A. Prince, Imperial Chemical Industries Limited, Billingham, England.

The contribution of Messrs. Hoar and Bowen has advanced considerably our appreciation of the complex reactions involved in the thermal treatment of highly alloyed steels of the type which they have studied. We are led to hope that the substantial results produced by this investigation will inspire the authors to undertake, along similar lines, the even more important study of the partition of elements between the major phases in the normal duplex steels in the austenitic range.

One of the most interesting parts of the paper is that where analyses of particular residues are given. The figures quoted by the authors are in weight percentages. Equivalent figures calculated in atomic percentages are given below for the original W. Q. 1150 °C specimens ($\alpha + \gamma$) and the 69½ hours at 850 °C specimen ($\alpha + \sigma$).

		Cr	Ni	Mo	Fe	Volume %
W.Q. 1150 °C	γ	14.3	9.6	1.5	74.6	45
	α	25.0	7.0	2.5	65.5	55
69½ hours at 850 °C	γ	17.2	9.3	1.6	71.9	86
	σ	30.4	3.9	5.3	60.5	14

In every 100 atoms of each sample there would be the following number of atoms of the individual elements:

		Cr	Ni	Mo	Fe
W.Q. 1150 °C	γ	6.4	4.3	0.7	33.6
	α	13.8	3.9	1.4	36
69½ hours at 850 °C	γ	14.8	8.0	1.4	61.8
	σ	4.3	0.5	0.7	8.5

Microscopically there is seen a transformation during the 69½ hours treatment at 850 °C. The original $\alpha + \gamma$ structure is transferred to a $\gamma + \sigma$ structure, i.e. the α disappears after the 850 °C treatment.

Let us consider the α phase as W. Q. from 1150 °C.

	Cr	Ni	Mo	Fe			Cr	Ni	Mo	Fe
α	13.8	3.9	1.4	36	→	σ	4.3	0.5	0.7	8.5
						residual "a"	9.5	3.4	0.7	27.5

The figures here show that, in the transformation of α to σ , a residual "a" phase is left which resembles the original γ phase except that it has increased chromium content. This higher-chromium γ will be unstable with respect to the original γ and, if interdiffusion with equalization of concentrations is not achieved, it is suggested that it is this higher-chromium austenite which may be the unstable phase described by the authors. Microstresses have no need to be invoked then to account for the instability of a portion of the γ phase.

On the other hand, if we admit the authors' suggestion that the unstable austenite resulting from sigma formation transforms on progressive release of the local internal stresses by solution of individual grains, several interesting possibilities follow. While Messrs. Hoar and Bowen do not indicate the origin of the system of microstresses, it may be concluded that the system develops during cooling, since the duplex mass will be substantially stress-free after soaking at 850 °C for 69½ hours. The stress system will, therefore, develop from the differential contraction of the two cooling phases, γ and σ . Similarly we would expect a similar stress system to develop on the cooling of a specimen containing austenite and ferrite. Could it be that this is the origin of the stresses responsible for the puzzling cases of stress corrosion cracking in duplex austenitic steels? Can the suggestion be extended to indicate that cracking will only develop when selective solution provides an increase in the local stresses by local transformations in the austenite, or by the significant mechanical concentration of stress provided by the partial or complete removal of individual grains? These extensions of the authors' theory are purely speculative but are based on a considerable number of practical cases with which one of the writers has had to deal. One of the more interesting practical cases may be cited in support of this extension. Thick-walled tubing in 18-8

molybdenum-titanium chromium-nickel steel was used to cool an innocuous product, the cooling medium being water heavily contaminated with inorganic chlorides. The metal temperature was around 100 °C. After a few months service, savage pitting had developed on the water side. The pits were packed hard with a powder which proved to be a mixture of corrosion product and unattacked ferrite grains. In this case, it was clearly shown that the austenite was selectively attacked, but at the bottom of each pit was a family of fine cracks of the type generally observed in cases of stress corrosion cracking.

If the authors' suggestion can be followed up to throw some light on the mechanism of such failures, considerable practical benefit will result.

One rather disappointing omission from the authors' paper concerns the probable mechanism of diffusion involved in the transformation of α to σ by the 850 °C treatment. No doubt the authors would like to comment on this.

Written Discussion: By R. H. Aborn, assistant director of research, United States Steel Co. Research Laboratory, Kearny, N. J.

From long acquaintance with stainless steels I find this paper a very worthwhile contribution to our knowledge. It would be very helpful if the authors could convert the magnetic data in Table II into the approximate amount of α_2 or martensitic ferrite formed on cooling from 850 °C.

The authors show that increasing the heating period at 850 °C increases the tendency of austenite to transform on cooling, and propose an increase of chromium content as a probable cause. This seems unlikely because any increase in dissolved chromium in austenite actually increases its temperature range of stability by lowering M_s ; in fact, it is the principal cause of 18-8 made austenitic at high temperature remaining so on cooling unless cold-worked.

More probable causes of this decreased stability of austenite appear to be: (a) Longer heating time robs austenite of more carbon by formation of more titanium carbide and possibly molybdenum carbide. (b) Longer heating time agglomerates sigma, allowing larger uninterrupted austenitic regions which retain greater stresses and so induce more transformation on extraction. (c) The highest rate of sigma formation parallels the highest rate of increase of ferromagnetism, suggesting chromium depletion in austenite rather than chromium enrichment.

Authors' Reply

We are grateful to the contributors to the discussion for the many interesting points they have raised, and we shall attempt to reply comprehensively.

We agree with most of Mr. LaQue's remarks, and we have amended Table III in the sense he suggests. We do not think, however, that the selective attack on the various phases under our extraction conditions is at all likely to be paralleled under natural corrosion conditions, because in the latter case the anodic current densities are much smaller and passivation is unlikely; it is selective passivation that leads to selective attack. With regard to Mr. LaQue's third paragraph, and also in reply to Dr. Lena's second paragraph, we would emphasize that in our 18-8-3-1

chromium-nickel-molybdenum-titanium steel the high-chromium sigma is all produced within 13 minutes at 850 °C from the high-chromium ferrite originally present, as shown in our previous paper;² thus chromium impoverishment of the grain margins of the austenite cannot occur during sigma formation. Furthermore, the austenite formed from ferrite after all the sigma has formed is higher in chromium than is the original austenite. Finally, the suggestion that single-phase alloys are desirable from the corrosion point of view, although fundamentally sound, is not always practical or economical; and indeed the several well-established duplex stainless alloys appear to have the advantage over the single-phase in the matter of susceptibility to stress-corrosion cracking.

In reply to Dr. Koh, we would not of course suggest that the presence of <5% of a contaminating phase could be detected by X-rays alone. The ferrometer technique is, however, considerably more sensitive in the detection of small amounts (1% carbon) of a ferromagnetic phase. We are most interested in the alternative extraction methods outlined by Dr. Koh and hope to be able to try them. Certainly the 50% hydrochloric acid electrolyte seems quite unsuitable for the chromium-manganese-nickel steel mentioned by Dr. Koh, perhaps because of the high content of the very reactive manganese. Incidentally, we think that the diffraction pattern of Dr. Koh's residue from this steel must have been misinterpreted—it seems extremely unlikely that FeO could be present in a residue left in 50% hydrochloric acid, because both metastable wüstite and the finely divided iron + magnetite eutectoid to which it tends to decompose below 570 °C are very readily soluble in warm 50% hydrochloric acid.

Dr. Simnad's substantial contribution is most welcome. In answer to his numbered points, we would comment: (a) We chose the extraction media from previous ad hoc experiments and knowledge of the etching of these steels. We do not doubt that they could be bettered, and that, as noted above, they may not be suitable for other steels; (b) We look forward to the application of specialized techniques to the determination of phase characteristics in situ, but would warn intending experimenters of the difficulties of interpretation of electrode potential results on two-phase electrodes; (c) In the experiment that gave the results shown in our Fig. 9, the sigma electrode was passive, so that Dr. Simnad's objection does not apply; (d) We think that much more work is required before the composition of an oxide film and the degree of passivity it confers can be satisfactorily related—at present, only speculative hypotheses can be advanced; (e) Dr. Simnad may well be right that cathodic reduction of passive films on many stainless steel phases cannot be effected; (f) Heating at 800 or 750 °C produces, in our steel, austenite that partially transforms to α_2 in the bulk at room temperatures, to an extent depending on time of heating and on rate of cooling.³ We see no reason why the differences in microstresses and (presumably) austenite composition caused by the difference in heating temperature should not be sufficient to cause the somewhat greater instability of this austenite as compared with that produced at 850 °C.

Dr. Edeleanu is right in saying that hydrogen may be evolved under

²K. W. J. Bowen and T. P. Hoar, "Proceedings of the First World Metallurgical Congress", American Society for Metals, 1952, p. 695.

some conditions by local action at stainless steel anodes, but in our case of very high anodic current density the gas evolved was in fact oxygen, as stated in the paper. We did not assume oxygen evolution. Thus the inefficiency of the anodic dissolution is not surprising—on the contrary, it is confirmatory evidence of the anodic discharge of oxygen.

Concerning the nitric acid resistance of the 18-8-Mo-Ti class of steels, mentioned by Mr. LaQue and discussed by Dr. Lena, we have no data on the present material. We think that the view that sigma formation impairs nitric acid resistance may be incorrect, and that the real trouble in such steels (softened at 1050 to 1150 °C, water-quenched and then heated in the 700 to 800 °C region) may be carbide precipitation. The matter is under study by our friends at Imperial Chemical Industries, Billingham,³ and it would be premature for us to say more. Meanwhile we are interested in Dr. Lena's results for his 18-12-Mo steel, which we take to have been fully austenitic in the softened, water-quenched condition: here sigma forms from austenite, not from ferrite as in our case, and may well lead to grain margin chromium depletion in the austenite in the early stages of precipitation, the effect disappearing after long heating when diffusion equilibrium has been reached.

Mr. Morley's calculations are interesting, but we prefer our experimental figure of 13.2% chromium for the equilibrium austenite at 1150 °C for our steel. We are by no means certain that a phase with 13.2% of chromium also containing 10% of nickel and 2.5% of molybdenum would necessarily have poor nitric acid resistance or indeed that its general corrosion resistance would be poor (as suggested by Dr. Edeleanu). We agree that the matter could be settled by metallographic evidence on a series of such steels with varying chromium content. With regard to the partial transformation of residual austenite to α_2 during and after extraction, Mr. Morley's suggestion that it may be due to removal of carbon by oxidation seems to us less likely than our hypothesis of the release of microstresses, because (a) such carbon removal could be but superficial owing to the minutely small diffusion rate of carbon at room temperatures, (b) the austenite can be partially transformed while still in the bulk metal by treatment at -196 °C.²

Messrs. Keating and Prince suggest that the austenite formed from ferrite at 850 °C (after sigma formation) is, owing to its higher chromium content, the part of the austenite that transforms to α_2 on extraction. This may well be so; we should also point out that the degree of transformation to α_2 of austenite in the bulk metal cooled to -196 °C is increased with material that has been heated for longer times at 850 °C.² This may mean that some of the original (1150 °C, water-quenched) low-chromium austenite is destabilized by gain of chromium from the high-chromium austenite produced at 850 °C, on prolonged heating. We think that the microstress explanation of the α_2 transformation is in any case necessary to explain why austenite is metastable at room temperatures in the bulk metal yet transforms when extracted. The highly interesting speculations of Messrs. Keating and Prince concerning stress-corrosion cracking, which follow from the same hypothesis of internal microstresses in these duplex steels, should be followed up.

²F. H. Keating, private communication.

Concerning the diffusion mechanism of the ferrite \rightarrow sigma transformation (rapid in the present steel at 850 °C, as shown in our earlier paper³), we cannot offer Messrs. Keating and Prince much helpful comment, except to point out that the concentration changes of the component elements are not very great, so that no very large transport of matter is involved.

In reply to Dr. Aborn, we did not determine the absolute extent of the α_2 transformation in the austenite residues. With regard to the stability of austenite toward the α_2 transformation, while we agree that loss of carbon rather than gain of chromium might be a reason for the decreasing stability of the austenite with increase of time of heating, we are not at all convinced that increase of chromium content tends to stabilize austenite of the present composition. Even in the straight chromium-nickel steels, increase of chromium beyond about 17% tends to destabilize austenite, an increase of nickel being simultaneously required if the softened, water-quenched material is to remain fully austenitic;⁴ and in a steel also containing 3% of molybdenum and 1% of titanium (both ferrite formers) it is probable that increase of chromium above about 13% tends to destabilize austenite. We believe that the whole question of the relative stability and ease of transformation of the austenitic and ferritic phases in complex high chromium-nickel steels needs re-examination, quite apart from the matter of sigma formation.

⁴J. G. H. Monypenny, "Stainless Iron and Steel", Chapman and Hall, London, 3rd edition, 1951, Vol. 1, p. 69.

EFFECT OF CARBON CONTENT ON 18-4-1 HIGH SPEED STEEL

BY ARTHUR H. GROBE AND GEORGE A. ROBERTS

Abstract

Complete hardness data, for hardening and tempering, are reported for five 18-4-1 high speed steels with carbon contents varying from 0.52 to 0.78% and one steel with 0.57% carbon and 1.21% vanadium. The steels were austenitized for 0.1 to 300 minutes at temperatures of 1800 to 2350 °F (980 to 1290 °C). For four austenitizing conditions of 30 seconds at 2200, 2300, 2350 and 2400 °F (1205, 1260, 1290 and 1315 °C), followed by oil quenching, tempering studies were conducted for times of 0.1 to 100 hours at temperatures of 200 to 1300 °F (95 to 705 °C).

The data on the effect of austenitizing time and temperature on the oil-quenched hardness are presented as iso-hardness lines on time-temperature plots for each steel. The tempering data are recorded as master tempering curves where hardness is plotted against the tempering parameter $T(c + \log t)$ for each austenitizing temperature for every steel.

Unnotched Izod impact tests were made using five steels oil-quenched from 2200 °F (1205 °C) and three steels from 2350 °F (1290 °C). These specimens were double tempered at 950 to 1200 °F (510 to 650 °C). The relative increases in toughness obtained by lowering the austenitizing temperature or by decreasing the carbon content are discussed.

INTRODUCTION

FOR many years 18-4-1 tungsten high speed steels have been produced with a variety of carbon contents, ranging from 0.50 to 0.80%. Thirty years ago cutting tools were normally produced from steel with 0.60 to 0.70% carbon, but have been in more recent years made with 0.68 to 0.80% carbon. The increase in carbon content of consumer and producer specifications has been accompanied by a companion increase in vanadium content from the range 0.75 to 1.00% to the range 0.90 to 1.25%.

A paper presented before the Thirty-fourth Annual Convention of the Society, held in Philadelphia, October 18 to 24, 1952. Of the authors, Arthur H. Grobe is research metallurgist, and George A. Roberts is chief metallurgist, Vanadium-Alloys Steel Co., Latrobe, Pa. Manuscript received March 28, 1952.

At the same time lower carbon 18-4-1 high speed steels continue to be produced for special purposes. These steels now contain 0.90 to 1.25% vanadium. For hot working dies of maximum hot hardness, 18-4-1 high speed steels with 0.50 to 0.55% carbon have proved popular. Steels with 0.55 to 0.70% carbon are employed for cutting tools requiring high resistance to breakage. This carbon range is also often chosen when high speed steel, because of its high wear resistance and good edge strength, is desired for cold work applications, such as blanking, trimming and forming dies. The majority of cutting tools made from 18-4-1 steel have in recent years contained 0.70 to 0.75% carbon, and a limited amount of this steel in a carbon range of 0.75 to 0.80% has been used for broaches and single-point cutting tools where higher hardness and wear resistance are desired.

Recent publications have outlined in detail the metallurgical characteristics and mechanical properties of 18-4-1 high speed steel in the standard 0.70 to 0.75% carbon range (1, 2, 3).¹ The hardening and tempering reactions have been accurately followed by hardness measurements and these have been related to the mechanical properties obtained with bend tests and unnotched Izod impact tests. Basically it is desired to evaluate the differences in mechanical properties, particularly in ductility, that will cause or permit differences in performance on actual applications. That high speed steel of varying carbon content has been selected for different applications attests to the somewhat improved ductility of lower carbon grades, but there has always been debated the question of whether the same benefits with respect to toughness could not have been obtained by the use of standard high speed steels treated from lower austenitizing temperatures. It has been shown, for instance, that the impact strength (roughly proportional to ductility at the same hardness, i.e., at the same yield strength) can be raised at least fourfold in 0.72% carbon 18-4-1 by a decrease of 300 °F (150 °C) in the hardening temperature. Does lowering the carbon content by 0.20% provide a greater improvement?

Since, as the carbon content is lowered, the maximum obtainable hardness is limited in 18-4-1 high speed steel, it becomes necessary to first study the hardening and tempering characteristics of the series of steels in question. Comparisons of properties should only be made at equivalent hardness levels and between equivalent metallurgical structures. Therefore, the hardening and tempering reactions in six high speed steels with carbon contents from 0.52 to 0.78% were investigated and metallographic comparisons were made prior to the impact strength determinations.

¹The figures appearing in parentheses pertain to the references appended to this paper.

MATERIALS

Five 18 (% W) - 4 (% Cr) - 1 (% V) high speed steels were selected from regular production lots of arc-melted steel to be as closely similar in all important elements, except carbon, as possible. These steels, Table I, had carbon contents of 0.52, 0.58, 0.67, 0.72 and 0.78%. An additional steel (Steel D, Table I) was chosen with 0.57% carbon but with higher than normal vanadium to show the influence of vanadium content itself upon the hardening and tempering reactions. All steels were rolled to approximately 1/2-inch square bar stock and annealed.

Table I
Composition of Steels

Steel	C	Si	Mn	S	Per Cent		W	Cr	V	Mo
					P					
A	0.78	0.27	0.23	0.009	0.016		18.12	4.02	1.00	0.39
B	0.72	0.34	0.25	0.008	0.015		18.08	4.04	1.05	0.33
C	0.67	0.25	0.23	0.009	0.015		17.55	4.02	1.04	0.40
D	0.57	0.32	0.23	0.012	0.014		18.00	4.06	1.21	0.37
E	0.58	0.28	0.24	0.008	0.016		18.26	4.04	0.99	0.36
F	0.52	0.31	0.25	0.008	0.018		17.60	3.89	1.06	0.38

EFFECT OF AUSTENITIZING TEMPERATURE

Samples 1/2 inch long from each steel were austenitized in a barium chloride internal electrode salt bath at temperatures of 1800, 1900, 2000, 2100, 2200, 2250, 2300 and 2350 °F (985, 1040, 1095, 1150, 1205, 1230, 1260 and 1290 °C). Individual austenitizing times used were 0.1, 1, 5, 15, 30, 60, 150 and 300 minutes at temperature. Samples were quenched in oil to room temperature, and after grinding to remove all traces of decarburization, the Rockwell C hardnesses were determined.

The results of the quenched hardness studies are presented in a series of six iso-hardness charts (Figs. 1 to 6 inclusive), in which points of equivalent hardness are connected as a function of austenitizing temperature and time. For instance, Steel E, hardened from 2200 °F (1205 °C), has as-quenched hardnesses as follows:

Hardness Rockwell C	Austenitizing Time Minutes
58-59	0.1 - 0.4
59-60	0.4 - 1
60-61	1 - 2
61-62	2 - 10
62-61	10 - 70
61-60	70 - 150
60-59	150 - 300

It should be noted that as the austenitizing time exceeds a certain value, the hardness decreases, an indication that retained austenite is

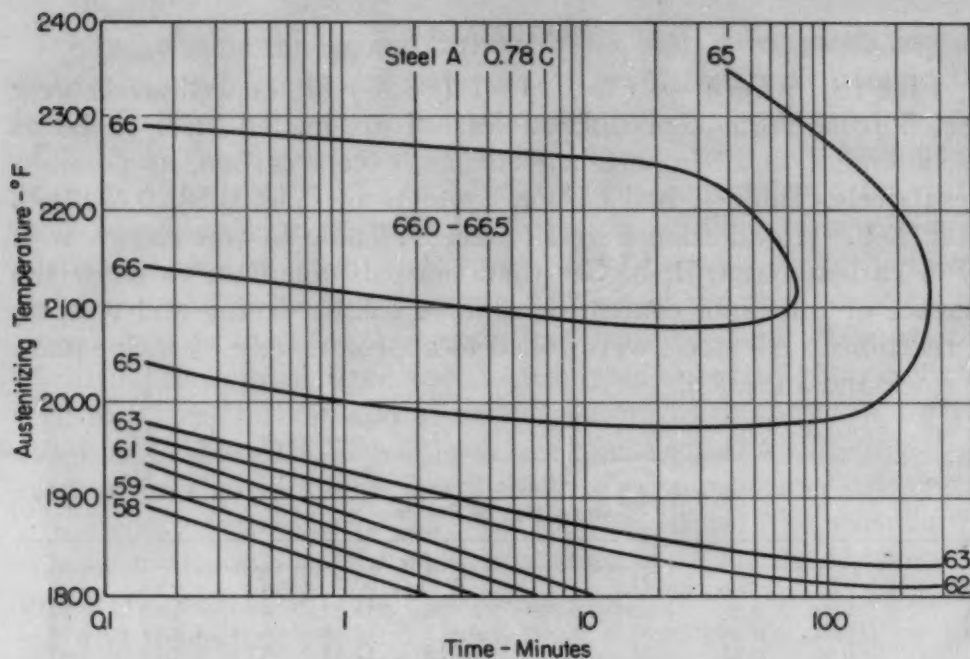


Fig. 1—Oil-Quenched Hardness of Steel A (0.78% Carbon) as a Function of Austenitizing Time and Temperature.

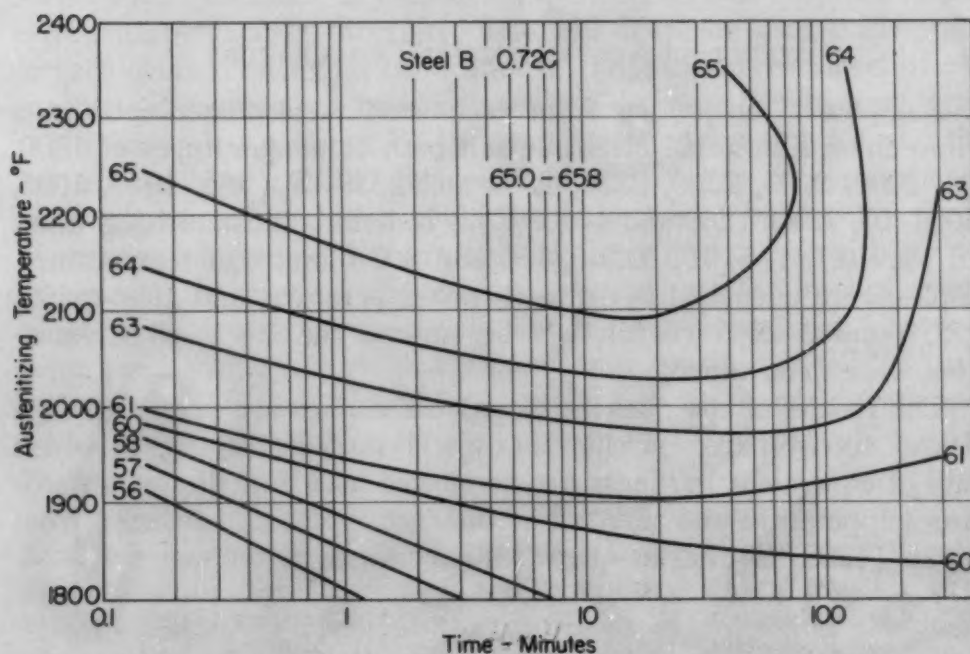


Fig. 2—Oil-Quenched Hardness of Steel B (0.72% Carbon) as a Function of Austenitizing Time and Temperature.

now present in sufficient volume to counter the effect of increased martensite hardness caused by added carbide solution. This effect, surprisingly, can occur at hardnesses as low as Rockwell C-49 (see Steel F, hardened from 1900 °F or 1040 °C). It should not be inferred that this decrease in hardness with austenitizing time and

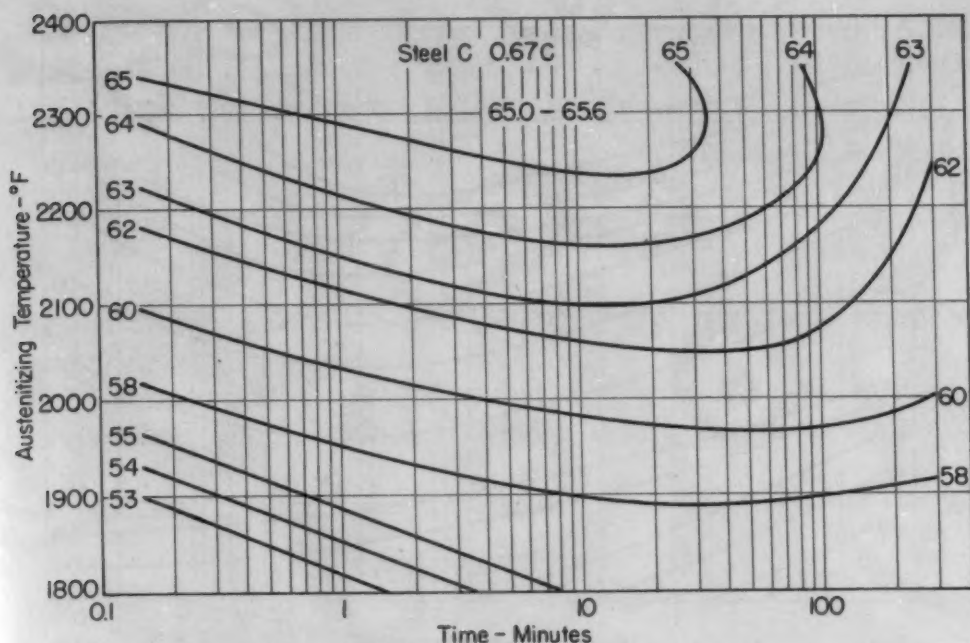


Fig. 3—Oil-Quenched Hardness of Steel C (0.67% Carbon) as a Function of Austenitizing Time and Temperature.

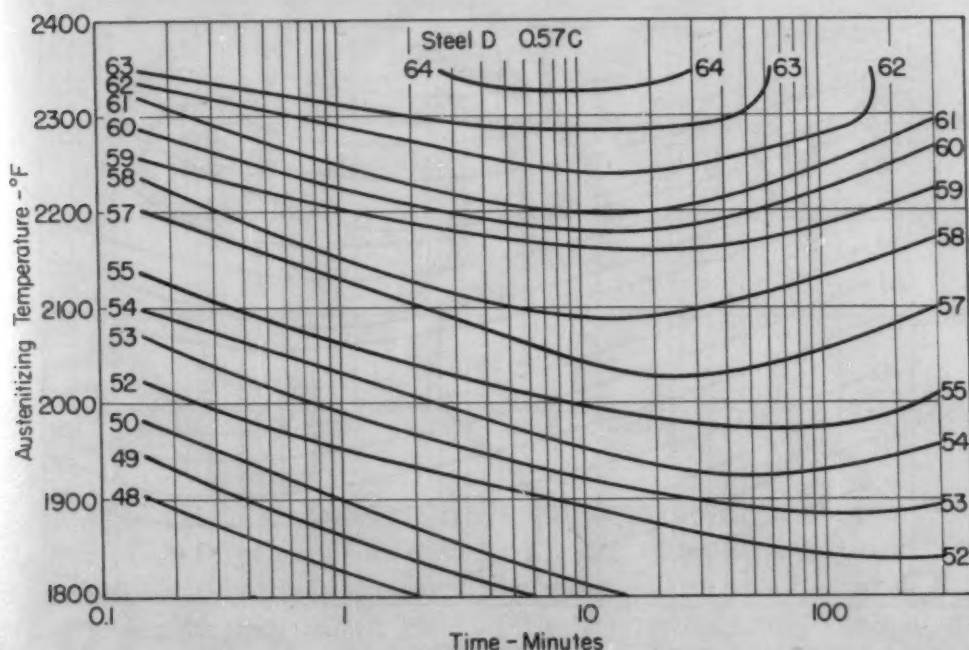


Fig. 4—Oil-Quenched Hardness of Steel D (0.57% Carbon - 1.21% Vanadium) as a Function of Austenitizing Time and Temperature.

the attendant turning up of the iso-hardness curves is related to a fixed quantity of retained austenite. The amount of austenite required will depend upon the carbon content and hardness of the martensite and thus will vary with the carbon content of the steel and the austenitizing temperature. This becomes so intense at higher carbon contents and higher temperatures that a limited field of time

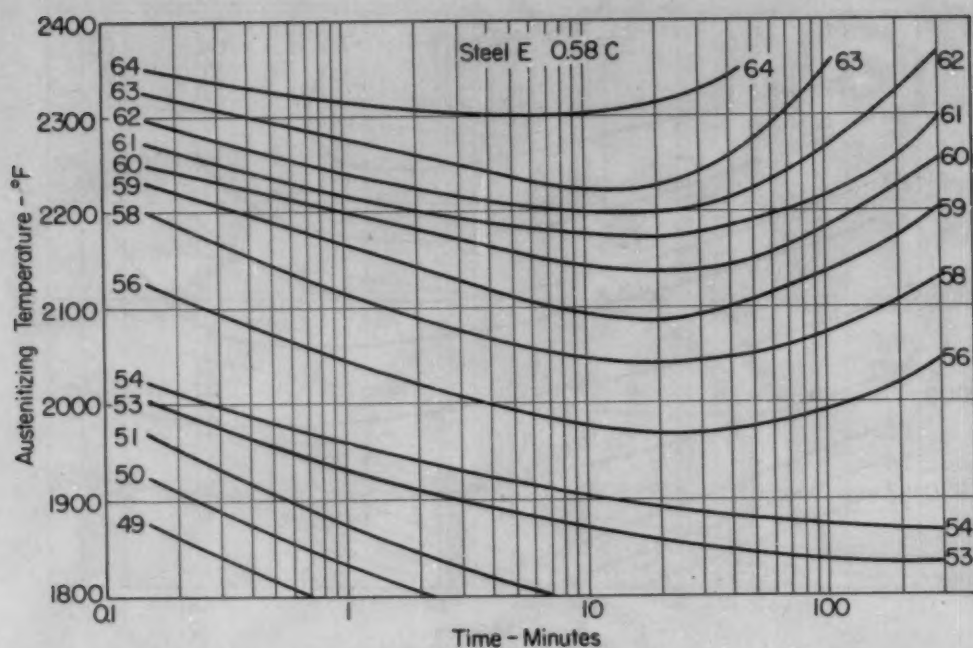


Fig. 5—Oil-Quenched Hardness of Steel E (0.58% Carbon - 0.99% Vanadium) as a Function of Austenitizing Time and Temperature.

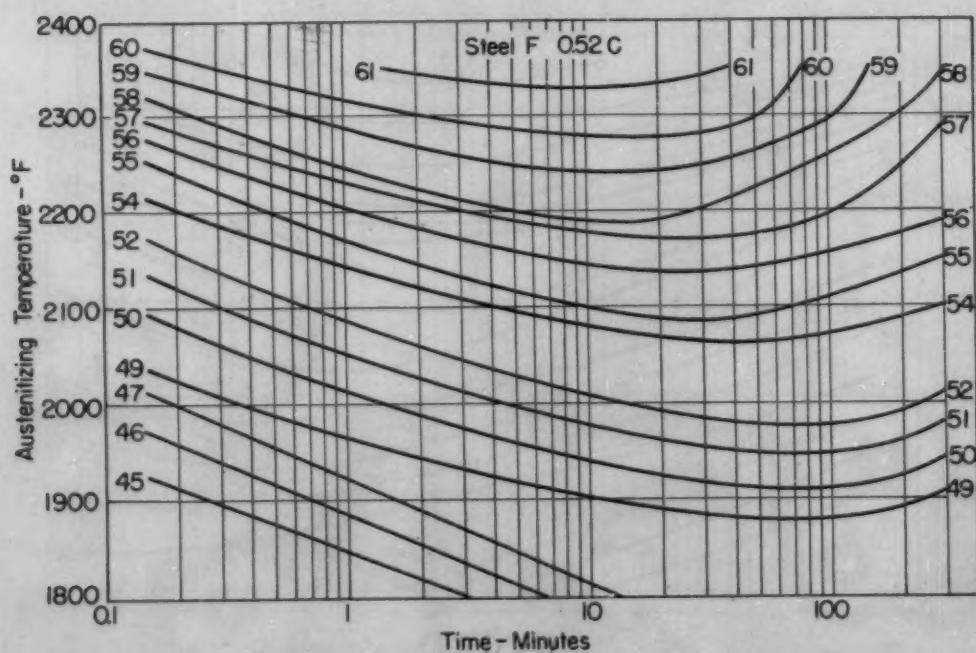


Fig. 6—Oil-Quenched Hardness of Steel F (0.52% Carbon) as a Function of Austenitizing Time and Temperature.

and temperature completely encloses the maximum hardness for the steel, as in Steel A (0.78% carbon) at hardness between Rockwell C-66.0 and 66.5.

A comparison of Steels D and E permits an evaluation of the effect of higher vanadium contents at constant carbon content on the carbide solubility or response to hardening in these steels. Steel E,

with 0.58% carbon and 0.99% vanadium, is approximately 1 to 1.5 Rockwell C points harder than Steel D, with 0.57% carbon and 1.21% vanadium, as shown in the tabulation below:

Austenitizing Temp., °F	Austenitizing Time, Min.	Quenched Hardness—Rockwell C	
		Steel E	Steel D
2300	1	63-64	62-63
2100	10	59	58
1900	3	53	51-52

As described later, these differences are not maintained after tempering.

Intercept grain size determinations were made on each of the as-quenched samples which showed a definite grain size after nital

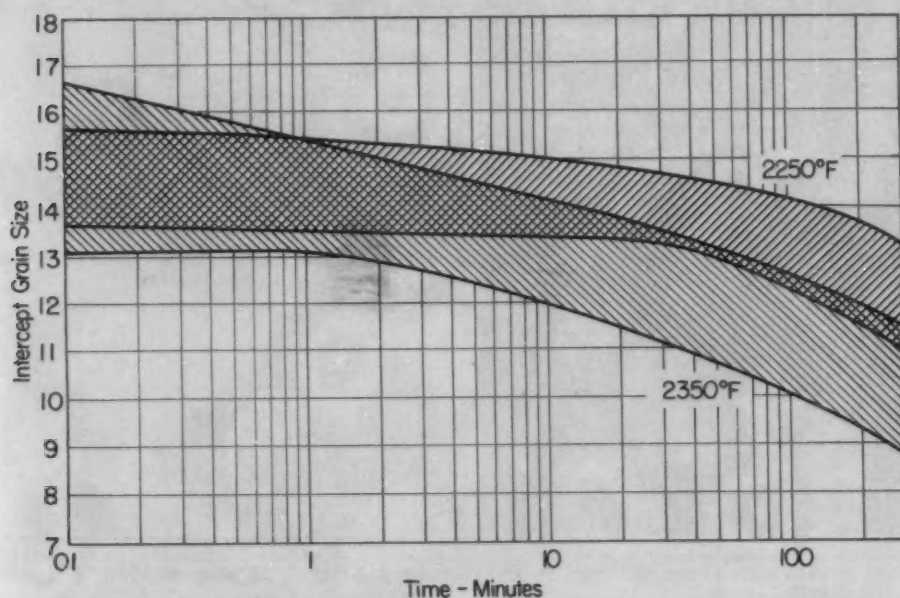


Fig. 7—Range of Intercept Grain Size for All Steels Hardened From 2250 and 2350 °F (1230 and 1290 °C) as a Function of Austenitizing Time.

etching. Grain growth occurred as expected with time and temperature of austenitizing but did not appear to be affected in a regular or consistent manner by carbon content. The results for all steels have been plotted in two bands (Fig. 7) representing the growth as a function of time when austenitized at 2250 and 2350 °F (1230 and 1290 °C), respectively. At short times the curves for both temperatures overlap. Samples held at 2350 °F (1290 °C) start to coarsen after 1 minute, while those held at 2250 °F (1230 °C) do not coarsen until after about 20 minutes.

During the course of metallographic examination, two distinctly different and interesting as-quenched structures were observed in addition to the usual structure of excess carbides in a light-etching matrix. One of these occurs in all steels after quenching from low

austenitizing temperatures and the other occurs in the lower carbon steels quenched from high temperatures.

Fig. 8 is a photomicrograph of the former structure in Steel A after quenching from 1900 °F (1040 °C) (1 minute at temperature). Under these conditions the chromium carbides, $M_{23}C_6$ (4), are not completely dissolved and at high magnification appear as small black dots throughout the structure. Larger black areas evident in Fig. 8

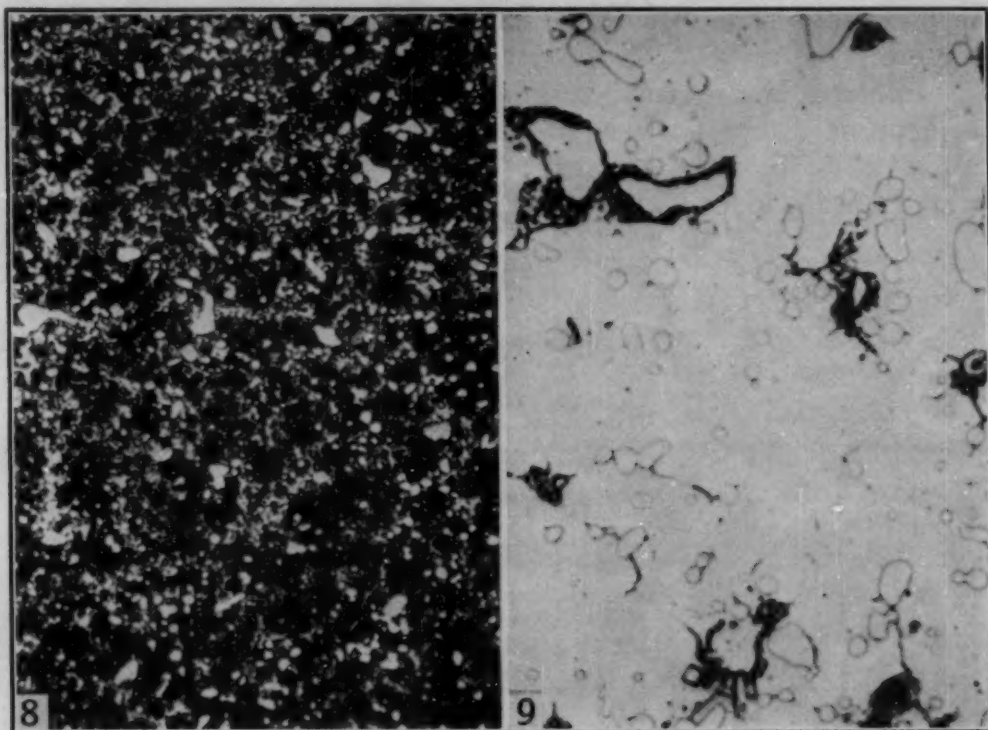


Fig. 8—Microstructure of Steel A Oil-Quenched After 1 Minute at 1900 °F (1040 °C). Nital etch. $\times 500$.

Fig. 9—Microstructure of Steel F Oil-Quenched After 1 Minute at 2350 °F (1290 °C). Nital etch. $\times 1500$.

are presumed to be a high temperature transformation product formed on quenching the inhomogeneous austenite. This product is probably analogous to the fine pearlite often formed at the knee of the "S-curve" when plain carbon steels are quenched. It appears in all steels of the 18-4-1 type, regardless of carbon content, within the range of this investigation, and disappears at higher austenitizing temperatures and times.

Fig. 9 depicts the structure of Steel F austenitized at 2350 °F (1290 °C) for 1 minute. This 0.52% carbon 18-4-1 steel on heating at temperatures of about 2100 to 2300 °F (1150 to 1260 °C) has a normal austenite plus carbide structure. Existing phase diagrams of the Fe-C-W system would indicate that ferrite might exist in such steels at all temperatures up to the melting point. Metallographic evidence fails to reveal any ferrite at this intermediate temperature

range. On further heating, however, delta-iron (ferrite) is formed from the austenite and, on quenching, such areas will either transform completely to a dark-etching transformation product or, if large, will so transform only at their interfaces with the austenite. Such ferrite areas and transformed zones are clearly seen in Fig. 9. These structures are typically apparent in decarburized high speed steel of normal carbon content and have been discussed in the literature in connection with such a phenomenon. Their formation is not, however, a sufficient criterion for decarburization, since they will occur only if the decarburization has been conducted at a sufficiently high temperature, or if previously decarburized steel is so heated.

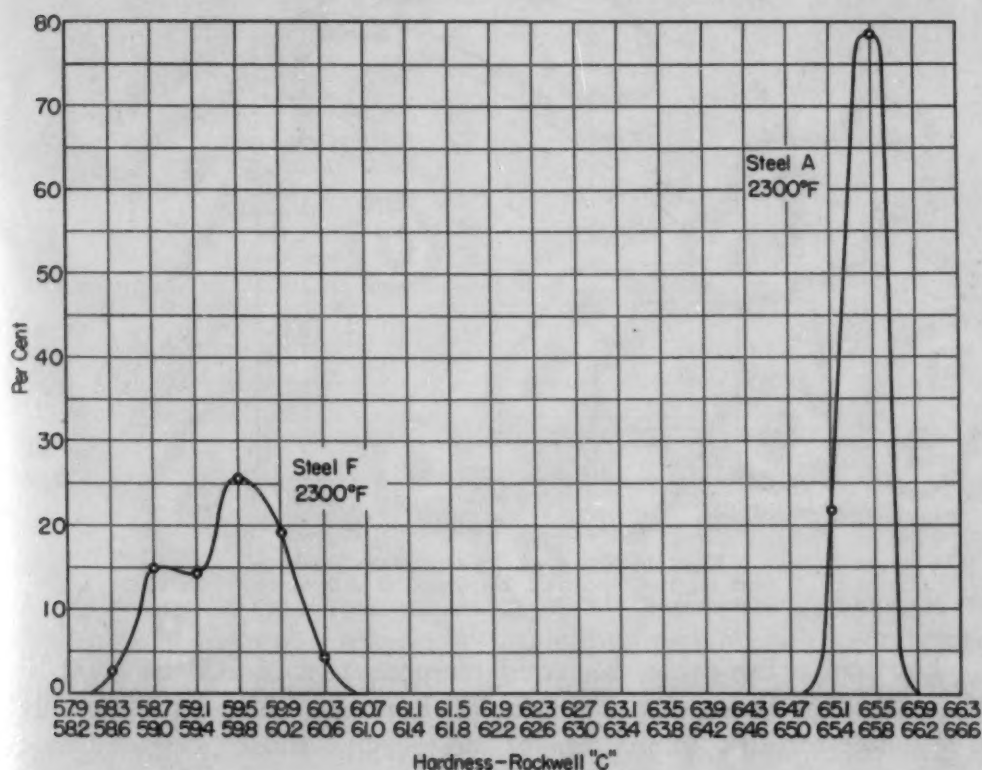


Fig. 10—Distribution Curves of Quenched Hardness for Steels A and F Oil-Quenched After 30 Seconds at 2300 °F (1260 °C).

EFFECT OF TEMPERING

The experimental technique employed to investigate the effect of tempering on this series of steels was identical with that previously recorded. It should be noted that the specimens were treated in a semimuffle gas-fired furnace and held at the austenitizing temperature 30 seconds. The as-quenched hardness was determined on each of the 120 specimens per steel for each austenitizing temperature. The distribution of the hardnesses so obtained for Steels A and F austenitized at 2300 °F (1260 °C) is plotted in Fig. 10. The constancy of the quenched hardness readings is less for the lower carbon

material (Steel F). Causes for this are probably the greater sensitivity of low carbon martensite to slight changes of carbon content and the inherent lack of sensitivity of the Rockwell C hardness scale at higher hardness values.

The as-quenched hardness for each steel from the four austenitizing temperatures is shown in Fig. 11. Here again the difference between Steels D and E with varying vanadium contents at constant carbon content is apparent.

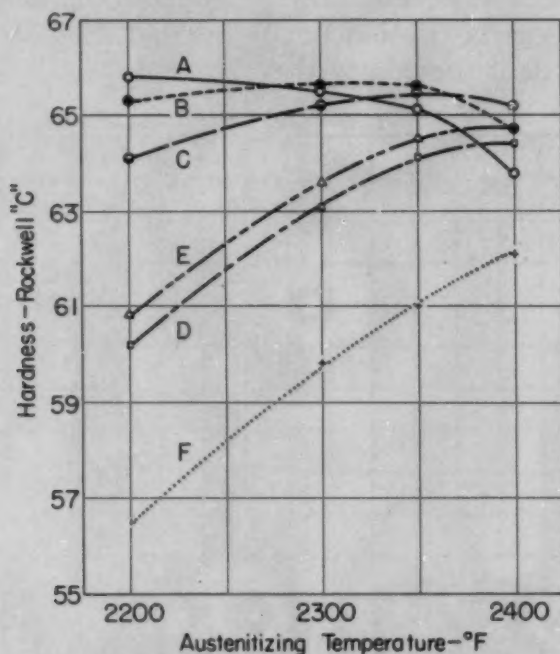


Fig. 11—Effect of Austenitizing Temperature on the Quenched Hardness of All Steels Investigated.

The tempering cycles included temperatures of 200 to 1300 °F (95 to 705 °C) and times of 0.1 to 100 hours. While complete data are available for all combinations of these cycles, those presented here are primarily limited to the practical range of commercial heat treating on high speed steel. Thus, all data for tempering temperatures below 600 °F (315 °C) and for final hardnesses lower than Rockwell C-45 achieved by high temperature tempering are eliminated. Four sets of master tempering curves, one for each of the austenitizing temperatures 2200, 2300, 2350 and 2400 °F (1205, 1260, 1290 and 1315 °C), are shown in Figs. 12 to 15 inclusive. On each of these charts, curves for all six steels of varying carbon content are included.

Master tempering curves relate hardness to the tempering parameter

$$T(c + \log t)$$

where T is the absolute temperature of tempering in °R
 c is a constant arbitrarily assigned a value of 20, and
 t is the tempering time in hours.

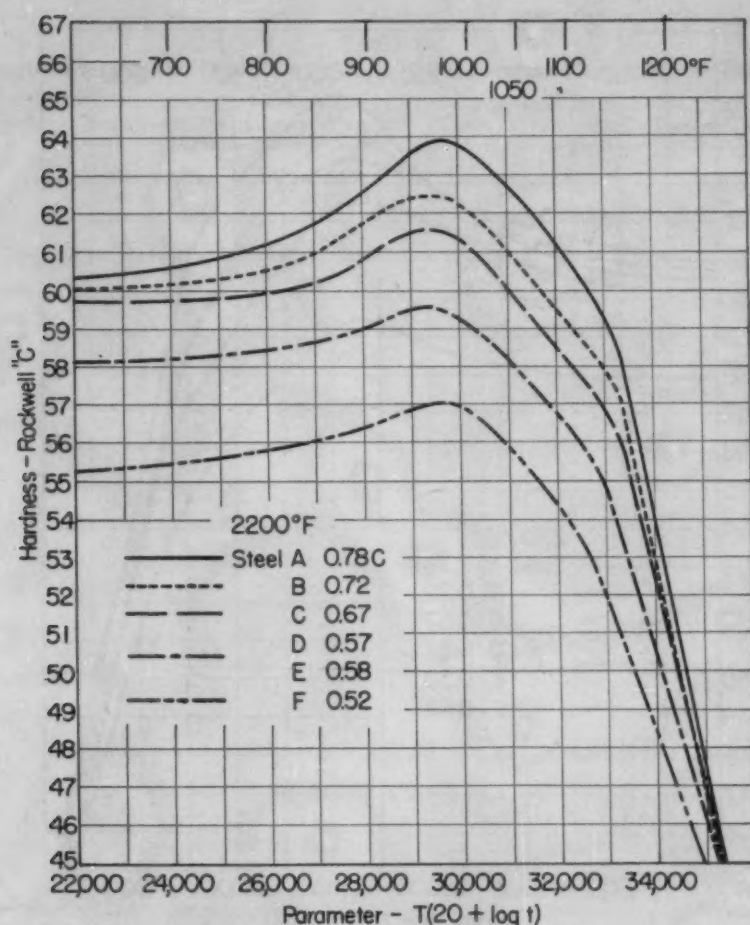


Fig. 12—Master Tempering Curves for All Steels Oil-Quenched After 30 Seconds at 2200 °F (1205 °C).

From previous data on tempering of high alloy tool steels, it was determined that the constant "c" varied appreciably with composition and hardening temperature (1). In the discussion of (1), it was suggested independently by both Jaffe and Cohen that, because of the inexplicable variation of "c", an average value be calculated and used so that all master tempering curves would be directly comparable and so that the effect of changes in composition, heat treatment or other variables could be studied from such curves. To this end a constant of 20 has been assigned to the data of this paper, following the practice previously established (5).

The curves of Figs. 12 to 15 are plotted for tempering cycles giving a parameter between 22,000 and 36,000. Also shown at the top of each curve are tempering temperatures for a cycle in which the total tempering time is 5 hours. With respect to hardness, the time of tempering during multiple tempering is additive, so that the 5-hour period is equivalent to double tempering for 2½ hours plus 2½ hours, and represents average commercial practice. For ease in converting to other tempering cycles providing equivalent hardness,

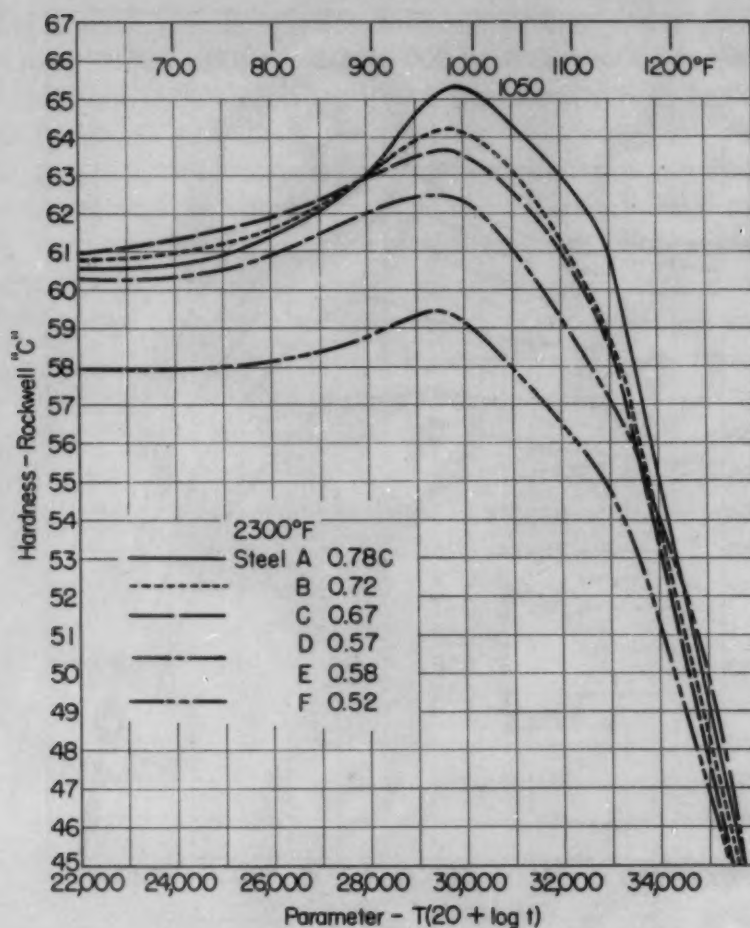


Fig. 13—Master Tempering Curves for All Steels Oil-Quenched After 30 Seconds at 2300 °F (1260 °C).

Fig. 16 has been prepared relating tempering temperature to the tempering parameter for a variety of tempering times. The actual data in this paper include times of tempering of 0.1 to 100 hours, and an extrapolation to the longer times of 1000 or 10,000 hours is feasible. Such extrapolations of short-time data are valuable in studies of steels exposed to elevated temperatures for long times, as in hot work tooling. Such curves again apply only to data based on a constant "c" equal to 20.

Despite the fact that Steels D and E have quenched hardnesses which differ by 1 to 1.5 points Rockwell C, they are equally hard when tempered above 600 °F (315 °C). One master tempering curve has been drawn for both.

IMPACT STRENGTH

Experimental procedure for the unnotched Izod impact tests was identical with that previously reported (3). Steels A, B, C, E and F were hardened from 2200 °F (1205 °C), and Steels A, B and E

Table II
Impact Strength for Five 18-4-1 Steels Oil-Quenched From 2200 °F (1205 °C)

Samples Tempered 2½ Hours Plus 2½ Hours at Indicated Temperatures Impact Strength Average of 10 Samples					
Steel	Intercept Grain Size	Tempering Temp. °F	Impact Strength Foot-Pounds	3 $\sigma_{\bar{x}}$ Foot-Pounds	Rockwell C Hardness
A	14.7	950	35.5	2.8	64.0
		1000	39.4	2.9	63.1
		1050	40.8	2.2	61.1
		1100	41.8	2.9	59.6
		1150	47.6	2.8	55.3
		1200	48.7	4.5	48.5
B	13.8	950	42.1	2.4	62.6
		1000	44.2	2.6	62.0
		1050	48.5	5.1	60.5
		1100	47.2	3.5	58.6
		1150	52.1	3.5	54.7
		1200	53.9	2.8	47.8
C	15.0	950	56.0	6.9	61.4
		1000	64.3	7.7	60.9
		1050	67.5	8.4	59.6
		1100	70.4	8.8	58.1
		1150	66.6	4.8	53.2
E	16.4	950	66.3	7.2	59.7
		1000	66.4	10.7	59.4
		1050	61.1	8.2	57.9
		1100	68.0	11.3	56.7
		1150	58.4	14.1	51.2
		1200	59.6	6.2	47.5
F	16.2	950	70.4	15.7	57.4
		1000	78.3	11.8	57.2
		1050	60.1	14.6	56.0
		1100	73.4	11.6	54.2
		1150	66.6	6.9	50.2

Table III
Impact Strength for Five 18-4-1 Steels Oil-Quenched From 2350 °F (1290 °C)

Samples Tempered 2½ Hours Plus 2½ Hours at Indicated Temperatures Impact Strength Average of 10 Samples					
Steel	Intercept Grain Size	Tempering Temp. °F	Impact Strength Foot-Pounds	3 $\sigma_{\bar{x}}$ Foot-Pounds	Rockwell C Hardness
A	11.9	950	27.6	2.1	65.0
		1000	20.6	4.8	65.9
		1050	20.7	2.7	64.8
		1100	20.1	2.0	63.0
		1150	23.1	2.8	58.6
		1200	37.2	3.4	50.4
B	10.9	950	29.8	1.8	65.0
		1000	27.8	2.3	65.0
		1050	28.7	1.3	64.2
		1100	28.2	1.4	61.8
		1150	30.2	1.8	57.7
		1200	45.7	1.9	49.7
E	11.2	950	51.8	3.8	63.6
		1000	52.2	6.6	63.4
		1050	52.0	3.2	61.4
		1100	57.8	7.3	60.0
		1150	53.4	8.2	55.2
		1200	45.9	3.3	51.4

from 2350 °F (1290 °C). Samples were tempered for 2½ hours plus 2½ hours at 950 to 1200 °F (510 to 650 °C) in 50 °F intervals. Ten specimens were treated for each treating cycle, and the results

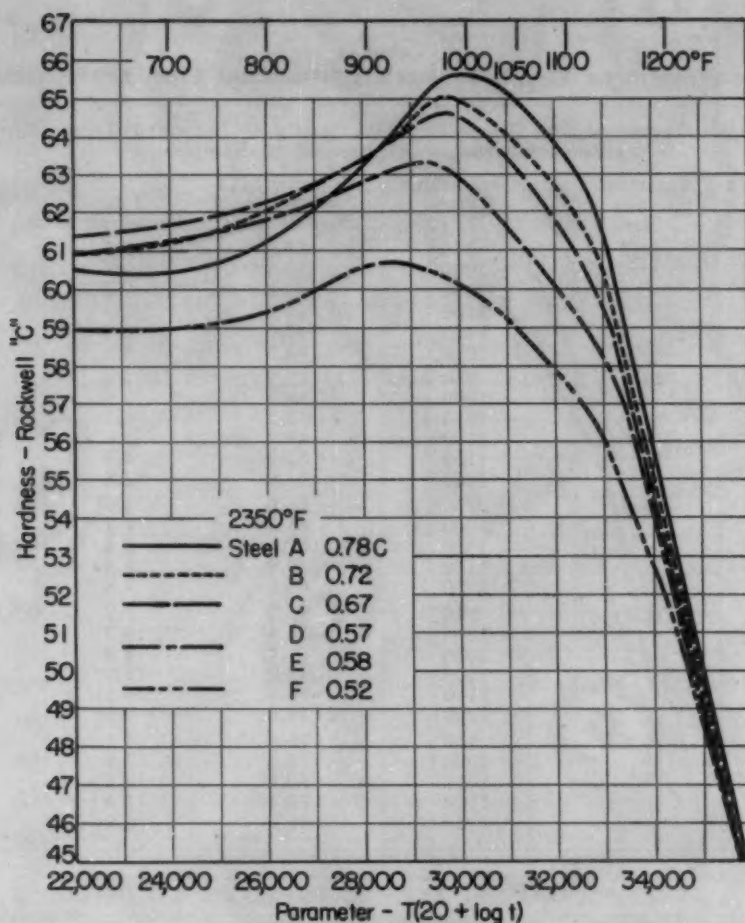


Fig. 14—Master Tempering Curves for All Steels Oil-Quenched After 30 Seconds at 2350 °F (1290 °C).

in Tables II and III are the average of each group with the calculated $3\sigma_x$ values.

Fig. 17 illustrates the effect of hardness on the impact strength of the three steels quenched from 2350 °F (1290 °C). As shown previously (3), there is little effect of hardness on the impact strength at hardness levels over Rockwell C-60 for Steel B with 0.72% carbon. Steel A at 0.78% carbon is less ductile and Steel E (0.58% carbon) is considerably more ductile. At hardnesses below Rockwell C-60 both Steels A and B exhibit a significant improvement in ductility similar to the behavior of the 8.00% molybdenum high speed steels (3), but the lower carbon type, E, suffers a loss in impact strength. At approximately Rockwell C-50, when hardened from 2350 °F (1290 °C), therefore, there is little difference in the impact strength of 18-4-1 high speed steel with 0.72 and 0.58% carbon.

No curves are presented for the steels hardened from 2200 °F (1205 °C) because there is no statistically significant difference in impact strength at equivalent hardnesses between Steels C, E and F. It will be noted from Table II that the spread of data is great (high

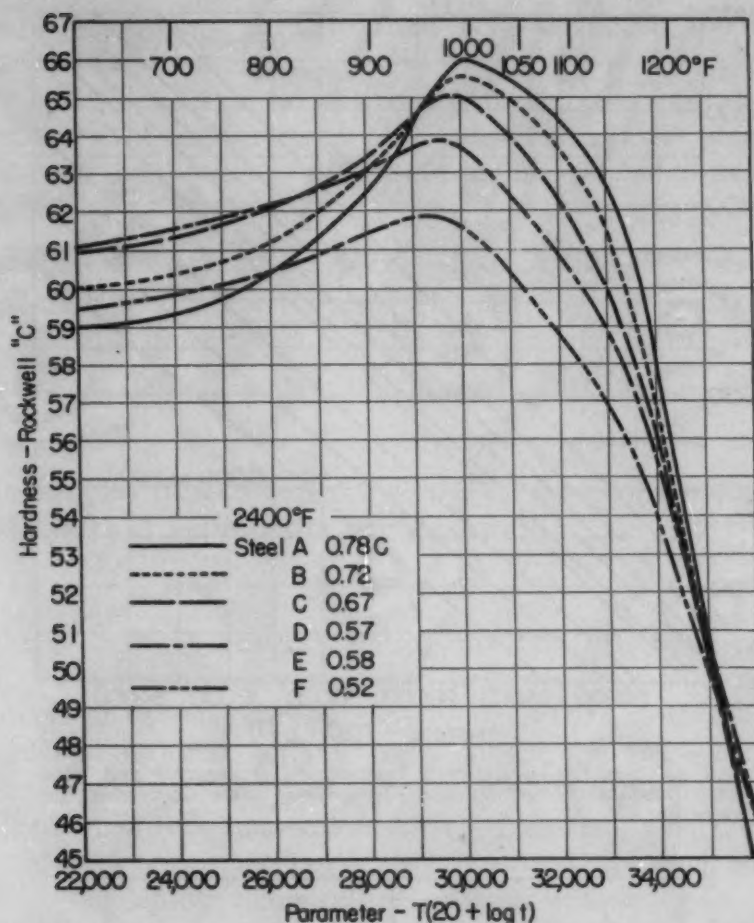


Fig. 15—Master Tempering Curves for All Steels Oil-Quenched After 30 Seconds at 2400 °F (1315 °C).

values of $3\sigma_{\bar{z}}$) for these three steels. This is a result of the fact that with energy absorption values greater than 60 foot-pounds on un-notched Izod tests, the indicated impact strength depends upon the exact physical nature of the break and its relation to the holding fixture. Although it is impossible to state with assurance that one of these steels is equal in ductility to another at a given hardness, it is believed that they are not essentially different. If plotted against hardness, the two steels between 0.50 and 0.60% carbon (E and F) show dips in impact strength between Rockwell C-55 and 60 that are similar to those previously noted for the tungsten-molybdenum high speed steels between Rockwell C-60 and 65. The reasons for these changes are not clear but they may well be associated with a precipitation phenomenon during the tempering process.

The following conclusions are evident:

1. When hardened from the same hardening temperature and compared at the same hardness level, a decrease in carbon content increases the impact strength.
2. In general, lowering of carbon content is more effective in

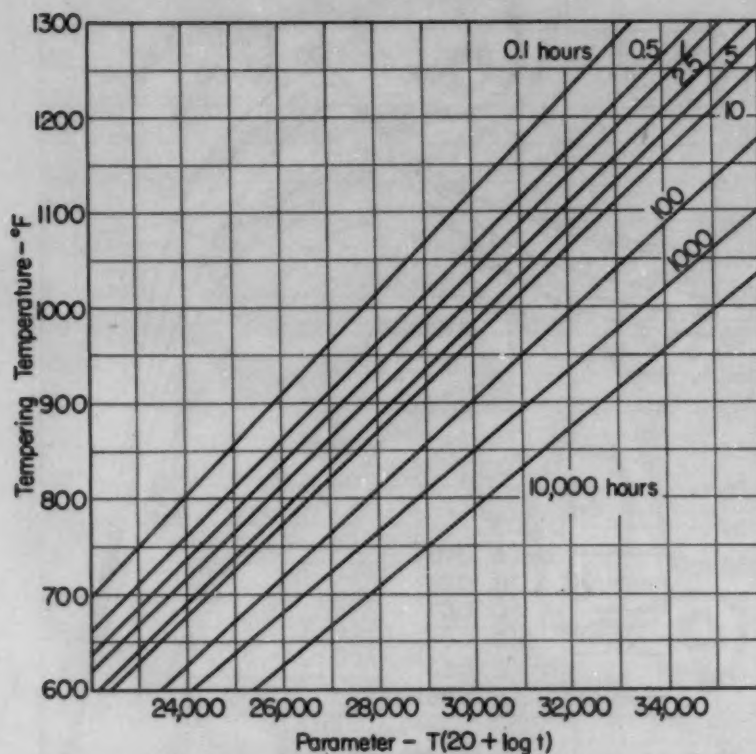


Fig. 16—Relation Between Tempering Temperature and Tempering Parameter for Various Tempering Time Assuming the Tempering $c = 20$.

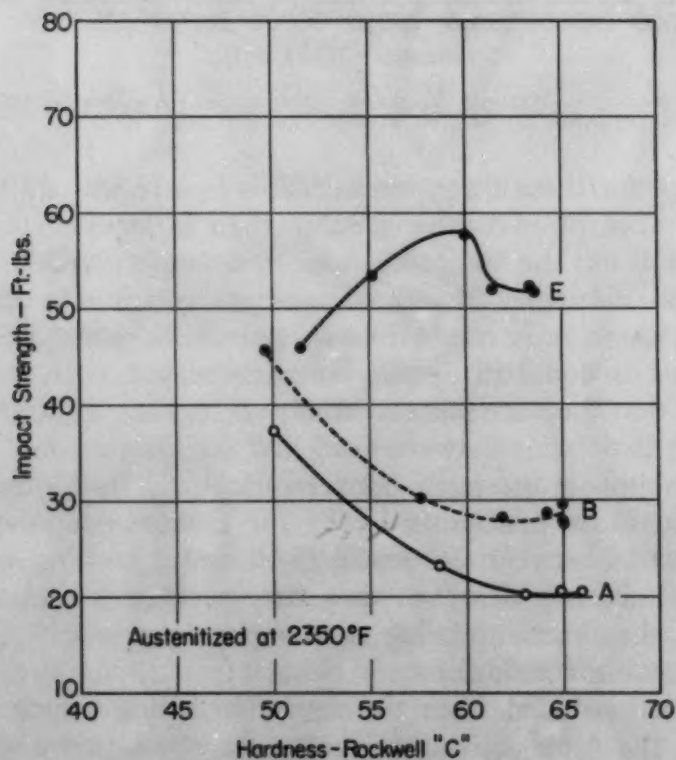


Fig. 17—Impact Strength of Steels A, B and E After Austenitizing for 30 Seconds at 2350 °F (1290 °C) and Double Tempering at 950 to 1200 °F (510 to 650 °C).

obtaining high impact strength than is lowering of the hardening temperatures in any one steel.

For example, let it be desired to produce a tool at Rockwell C-60 because of considerations of wear. The impact strength data obtained from the foregoing and from previous publications are shown in the following tabulation:

Carbon Content of 18-4-1 Steel	IMPACT STRENGTH—UNNOTCHED IZOD—FOOT-POUNDS—ROCKWELL C-60			
	Hardened From			
	2350 °F	2300 °F	2200 °F	2100 °F
0.78	20-25	40-45
0.72	28-33	38-43	43-48	55-60
0.67	60-70
0.58	50-60	60-70

All samples treated to Rockwell C-60 by double tempering 2½ plus 2½ hours at appropriate temperature.

SUMMARY

1. Iso-hardness curves relating austenitizing temperature and time to the quenched hardness are presented for six 18-4-1 high speed steels of varying carbon content from 0.52 to 0.78%.

2. Metallographic studies have shown the presence of ferrite (delta-iron) at high austenitizing temperatures in the lower carbon steels. Such ferrite is not evident at lower austenitizing temperatures.

3. Master tempering curves are presented for each of the steels from four hardening temperatures, along with a chart permitting utilization of these data to determine equivalent tempering cycles to produce any desired hardness above Rockwell C-45.

4. The effect of carbon content, austenitizing temperature and hardness on the impact strength of 18-4-1 high speed steel has been investigated.

References

1. G. A. Roberts, A. H. Grobe and C. F. Moersch, Jr., "The Tempering of High Alloy Tool Steels", *TRANSACTIONS, American Society for Metals*, Vol. 39, 1947, p. 521.
2. A. H. Grobe and G. A. Roberts, "The Bend Test for Hardened High Speed Steel", *TRANSACTIONS, American Society for Metals*, Vol. 40, 1948, p. 435.
3. A. H. Grobe and G. A. Roberts, "Unnotched Impact Strength of High Speed Steels", *TRANSACTIONS, American Society for Metals*, Vol. 42, 1950, p. 686.
4. D. J. Blickwede, M. Cohen and G. A. Roberts, "The Effect of Vanadium and Carbon on the Constitution of High Speed Steel", *TRANSACTIONS, American Society for Metals*, Vol. 42, 1950, p. 1161.
5. A. E. Nehrenberg, "Master Curves Simplify Stainless Tempering", *Steel*, Vol. 127, Oct. 23, 1950, p. 72-76, 88.

DISCUSSION

Written Discussion: By A. E. Nehrenberg and J. G. Y. Chow, Research Laboratory, Crucible Steel Company of America, Harrison, N. J.

The present paper should be welcomed by both manufacturers and users of high speed steels, for it clarifies questions which constantly arise concerning the relative merits of low carbon 18-4-1 high speed steel versus the standard analysis austenitized at lower temperatures. The data have been so concisely presented that it is easy to lose sight of the fact that the paper is the result of the heat treatment and examination of a tremendous number of specimens. We should like to congratulate the authors on the excellence of their comprehensive paper.

Our comments will pertain to the dark-etching structure illustrated by Fig. 9 of the paper. This structure is commonly observed not only in the decarburized zone of standard 18-4-1 high speed steel, but in certain other high alloy steels as well. The authors commented in general that this structure is the result of the transformation during the quench of the delta ferrite formed during heating of the low carbon 18-4-1 to temperatures above about 2300° F. The authors did not discuss this transformation in any detail and since work which we recently have completed in our laboratory has suggested that this transformation is an unusual one not heretofore clearly interpreted in the literature, we have prepared several photomicrographs to illustrate some of our observations concerning the nature of the transformation.

The material used for our photomicrographs happens to be a 0.40% carbon, 11.5% tungsten, 2.0% chromium, 0.4% vanadium commercial hot work steel, but our work has indicated that the transformation is the same as the one observed by the authors in their low carbon high speed steel. It will be noted that tungsten is present both in the low carbon high speed steels studied by the authors and in the steel selected for our photomicrographs, but it should not be inferred that the transformation depends upon the presence of tungsten. We have found that the same transformation occurs in straight chromium steels such as Types 430 and 446, for example.

Fig. 18 is comparable to the authors' Fig. 9 and illustrates the microstructure resulting from a water quench of the 0.40% carbon, 11.5% tungsten, 2% chromium steel from 2400 °F. The sample was tempered so that the martensite would be readily distinguishable from the delta ferrite. The large white structure in the center of the photomicrograph is delta ferrite which has been retained by the rapid quench from 2400 °F. The dark-etching structure appears in areas which were delta ferrite at 2400 °F.

The dark-etching structure forms only during a quench from this high temperature. If a sample of this steel is heated to 2400 °F, furnace-cooled to 2250 °F and water-quenched from this lower temperature, the dark-etching structure is absent and there is no evidence that delta ferrite had existed at the high temperature.

The effect of cooling from 2400 to 2250 °F at a rate considerably faster than that of a furnace cool is shown in Fig. 19. The sample photographed was heated at 2400 °F for 5 minutes, transferred to a furnace at 2250 °F, held 2 minutes, water-quenched, and tempered to darken the martensite. The area at the center of the micrograph outlined with grain boundary

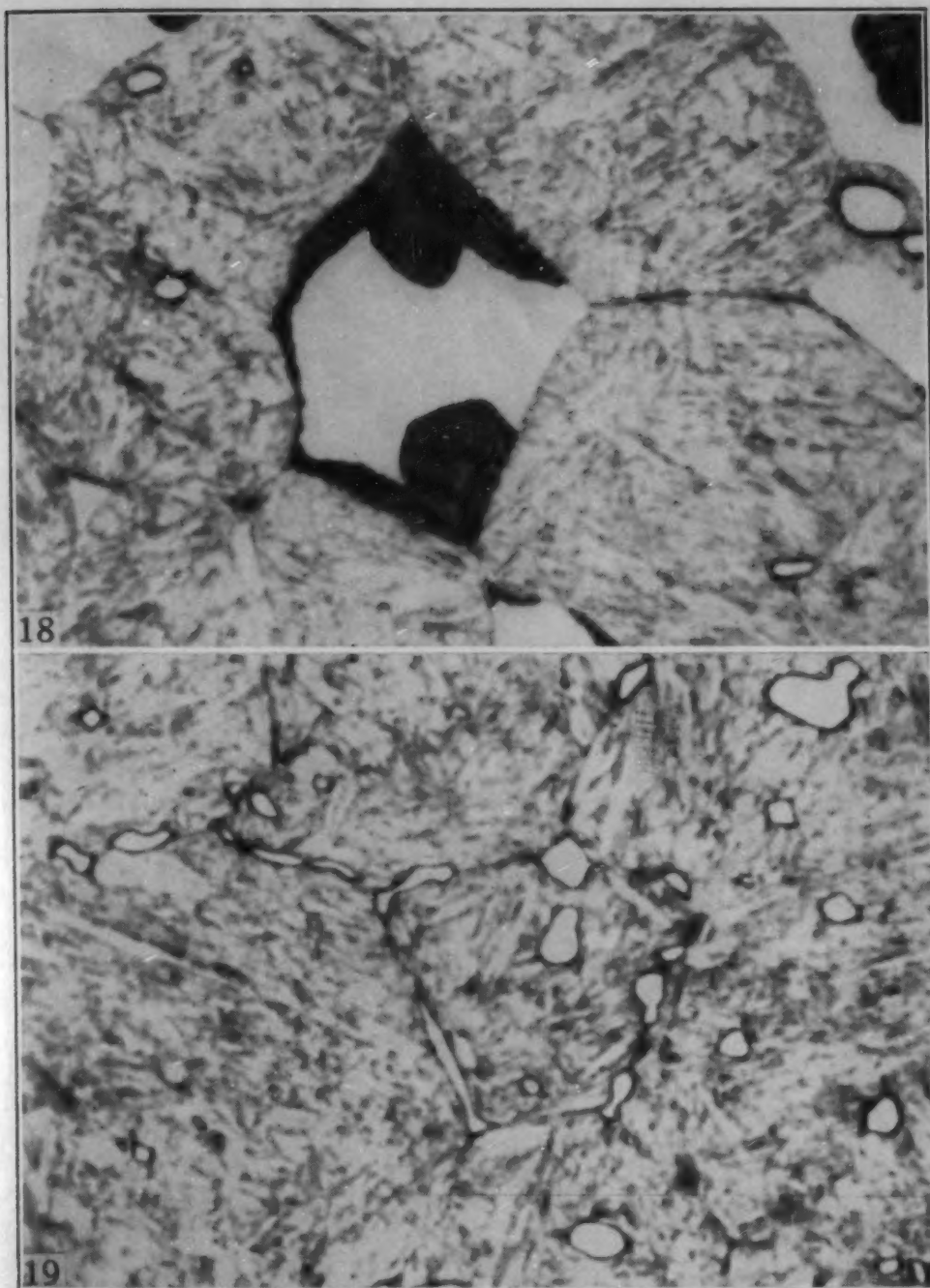


Fig. 18—Dark-Etching Transformation Product in 11.5% Tungsten-2% Chromium Steel Heated 5 Minutes at 2400 °F, Water-Quenched, and Tempered 2 Minutes at 1300 °F. Etched in 5% picral plus 0.01% HCl. $\times 2500$.

Fig. 19—Carbides in Former Delta Ferrite-Austenite Grain Boundaries Resulting From Retarded Cool From 2400 to 2250 °F. Sample was heated 5 minutes at 2400 °F, transferred to furnace at 2250 °F, held 2 minutes, water-quenched, and tempered 2 minutes at 1300 °F. Etched in 5% picral plus 0.01% HCl. $\times 2500$.

carbides was presumably delta ferrite at 2400 °F and transformed to austenite during the retarded cool to 2250 °F. Associated with this transformation there has been a precipitation of carbides predominantly at the old delta ferrite-austenite grain boundaries.

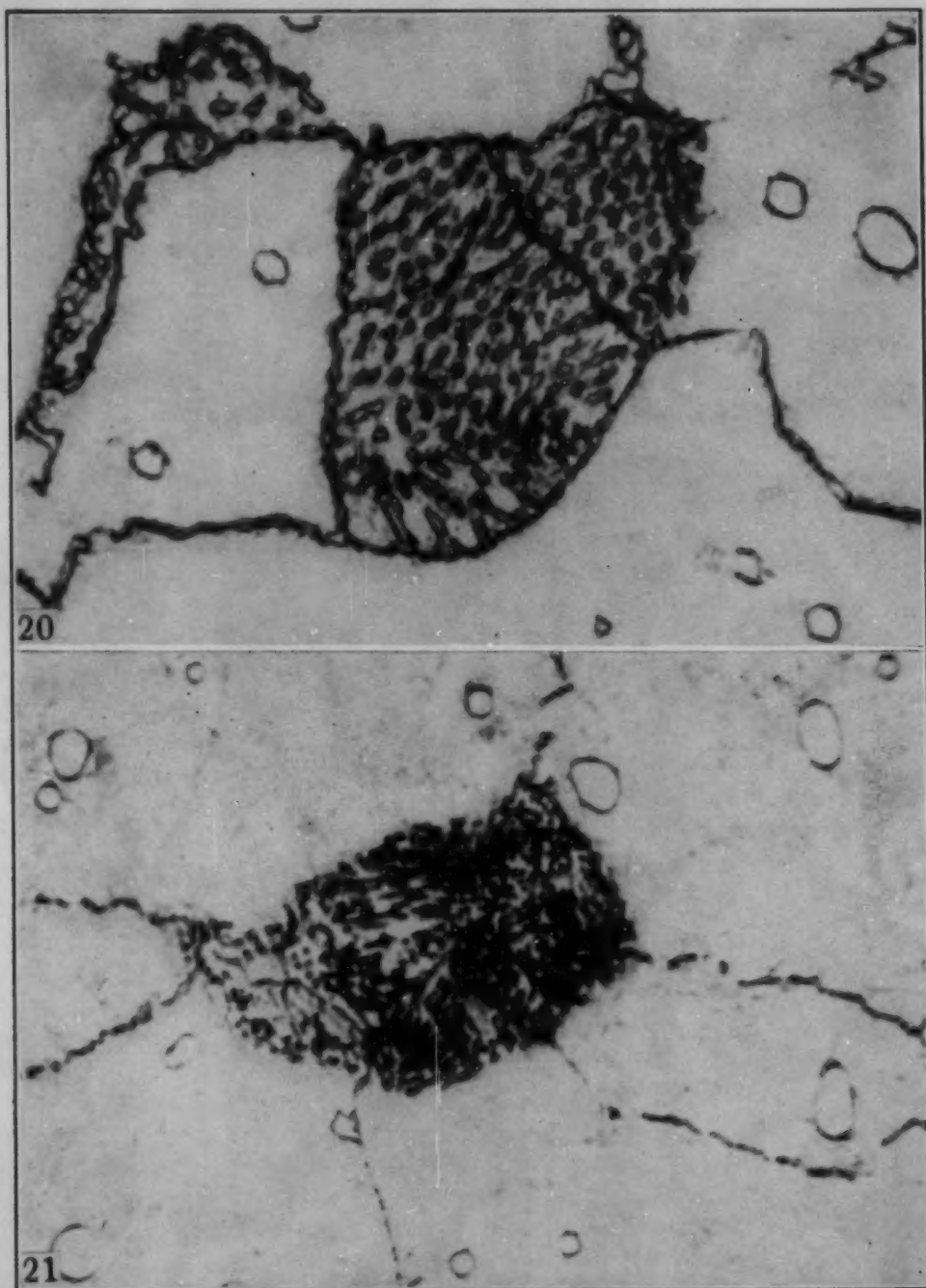


Fig. 20—Effect of Faster Cooling Rate at Very High Temperatures Than That Employed for Fig. 19. Sample was heated 5 minutes at 2400 °F, transferred to a furnace at 1800 °F, held 2 minutes, water-quenched, and tempered 2 minutes at 1100 °F. Tempered martensite is underetched and appears light-etching. Etched in 5% picral plus 0.01% HCl. $\times 2500$.

Fig. 21—Effect of Faster Cooling Rate Between 2400 and 1800 °F Than That Used for Fig. 20. Sample was heated 5 minutes at 2400 °F, transferred to lead bath at 1800 °F, held 2 minutes, water-quenched, and tempered 2 minutes at 1300 °F. Tempered martensite is underetched and appears light-etching. Etched in 5% picral plus 0.01% HCl. $\times 2500$.

A sample heated 5 minutes at 2400 °F, transferred to a furnace at 1800 °F for 2 minutes, water-quenched and tempered was found to have the microstructure illustrated by Fig. 20. In this photomicrograph, and

in the one to follow, the martensite areas are light-etching, though tempered, because we were unable to develop darkened areas without over-etching the areas containing mixed lamellar and spheroidal carbides. These carbides occupy areas which were delta ferrite at 2400 °F. The matrix structure is martensite. Thus, at the time of quenching, the delta ferrite areas had transformed to an aggregate of austenite and precipitated carbides. The martensite in the final structure formed during the quench from 1800 °F to room temperature.

Finally, a sample heated at 2400 °F and transferred to a lead bath at 1800 °F instead of a furnace, in order to get a faster cooling rate down to 1800 °F, held 2 minutes and water-quenched, was found to have the fine, lamellar structure shown in Fig. 21. The finer structure is the result of the increase in cooling rate in the temperature range 2400 to 1800 °F.

These and many other observations we have made in a variety of high alloy steels indicate that in certain steels, in which delta ferrite reverts to austenite during cooling, the areas of delta ferrite may transform at very high temperatures to an aggregate of austenite and carbides in the manner illustrated by our photomicrographs. As far as we have been able to ascertain, the precipitation of the carbide and the transformation of the delta ferrite to austenite occur practically simultaneously. Thus, the transformation appears to be one involving the formation of an aggregate of austenite plus carbides from delta ferrite. The transformation occurs at high temperature, in this case above about 1800 °F. At these temperatures austenite is an equilibrium phase. The effect of increased rates of cooling in the temperature range down to about 1800 °F is to produce finer aggregates of carbide in the austenite.

We would be interested in the authors' comments concerning our interpretation of the transformation responsible for the dark-etching structure observed in their low carbon high speed steel.

Written Discussion: By W. E. Bancroft, chief metallurgist, Pratt and Whitney Division, Niles-Bement-Pond Co., West Hartford, Conn.

The authors are to be commended on one of their usual laborious and painstaking investigations. The information presented in this paper with reference to hardening characteristics and the effect of tempering as portrayed by the master tempering curves is very valuable and will be helpful in the production heat treating and applications of the tungsten-type high speed steels. The curves shown in Fig. 16, relating tempering temperature and time to the tempering parameter, are especially helpful in making use of the master tempering curves.

We feel somewhat disappointed, however, in the meagerness of the data presented on impact strength of the various steels studied in this paper. For example, while the authors first studied the effect of eight different austenitizing temperatures, together with a variety of time cycles, on the as-quenched hardness, then selected four hardening temperatures, together with an extensive series of tempering temperatures, to study the effect of tempering on steels of various carbon contents, they used only two hardening temperatures for their study of impact strength and only included three steels for one of these hardening temperatures (2350 °F).

In the authors' introduction it was stated that one of the objects of this investigation was to determine whether lowering the carbon content

in 18-4-1 high speed steel would provide greater improvement in impact strength than would lowering the austenitizing temperature some 200 to 300 degrees. We would question whether the amount of impact data shown in the paper is sufficient to support the authors' conclusion that lowering the carbon content is more effective than lowering the hardening temperature in improving toughness.

Analyzing the tabulation of impact values given on the seventeenth page of the paper, we would point out the following: First, when Steel B is hardened from 2350 °F and tempered to Rockwell C-60, an impact value of approximately 30 foot-pounds is shown, and when this same steel is hardened from 2100 °F and tempered to Rockwell C-60, an impact value of approximately 57 foot-pounds is developed, an increase of 27 foot-pounds. Now to compare Steel B, hardened from 2350 °F, with a lower carbon steel, hardened from the same temperature, we find Steel E showing an impact strength of approximately 55 foot-pounds, which is an increase of only 25. Or if we were to take the extreme condition shown in this tabulation, we might compare Steel B, hardened from 2350 °F, with Steel E, hardened from 2200 °F. Here we find an increase of 35 foot-pounds, but this is partly brought about by lowering the austenitizing temperature 150 °F, so is only partly due to the lower carbon content of Steel E.

Another point which merits consideration is the effect of the lower carbon content on such properties as wear resistance and red hardness. If we should produce two tools having the same hardness and approximately the same high impact strength, one made from a 0.72% carbon steel and the other from a 0.58% carbon steel, might it not be found that the tool having the lower carbon content would have lower wear resistance and red hardness?

We would also like to ask why the authors used salt-bath hardening for the series of specimens on which they reported the as-quenched hardness and then changed to a muffle furnace for the specimens used for tempering and impact studies.

There is a well-known differential in effective temperature between these two methods of hardening which does not seem to be taken into account in this paper.

Authors' Reply

The authors are indebted to Messrs. Nehrenberg and Chow for their comments on the existence of delta ferrite in a low carbon, high tungsten hot work die steel and its transformation on cooling. Particularly do we wish to compliment them on the excellent photomicrographs which accompany their comments and form a valuable supplement to this paper.

We did not discuss this transformation in great detail because we were unable to decide which of the several possible theories were best. In low carbon high speed steels the limited amount of ferrite and the fine structure make resolution difficult. We feel that additional evidence is required to prove that the transformation involves a change of delta ferrite to austenite plus carbide at high temperatures.

More likely the transformation is complex and its nature depends on both the cooling rate and the temperature of holding. Thus, Nehrenberg and Chow prove by Fig. 19 that the gamma-to-delta transformation is

reversible between temperatures of 2250 and 2400 °F. Figs. 20 and 21, however, do not clearly prove that the delta-to-austenite plus carbide reaction is a reality. A zone of minimum ferrite stability between 1800 and 2300 °F is probable (of the gamma-loop type). Time is required to completely reverse the ferrite-to-austenite transformation and this is only possible in a limited temperature zone. One can preserve delta ferrite by fast cooling through this zone to a temperature where ferrite is again stable — though now capable of holding less carbon in solution.

In answer to Mr. Bancroft's comments, while we appreciate the fact that more impact data would be desirable, the object was to determine if the lower carbon high speed steels would provide higher impact strengths than had been obtained in past investigations with standard carbon material hardened from low temperatures. In this light the data show that values of 60 to 80 foot-pounds are possible with the lower carbon steels, while the maximum obtained with 0.72% carbon 18-4-1 was 55 to 60 foot-pounds. The increase is not great and would, naturally, be accompanied by some sacrifice of wear resistance and hot hardness.

With regard to the type of heating equipment used in these tests, we would prefer to use salt baths for all experiments, since a more accurate knowledge of bath temperature is possible. However, where large numbers of samples are to be treated together, it is more convenient for us to use semi-muffle furnaces. Samples can be readily observed at all times during the heating, and furnace capacity is greater. It is not expected that the austenitizing conditions indicated by the nominal temperatures are exactly reproducible by others. For this reason we generally employ a series of austenitizing temperatures by means of which other investigators may interpret their results.

THE EFFECT OF SILICON ON THE TEMPERING OF MARTENSITE

BY A. G. ALLTEN AND P. PAYSON

Abstract

Evidence that silicon affects hardness during the tempering of steels led to an investigation of the tempering of 0.6% carbon-base and 0.4% carbon, 3% nickel-base steels which contained up to 2.2% silicon. Hardness, dilatometric, specific volume, electrical resistivity, and X-ray diffraction measurements were used.

The results demonstrate that the temperature at which cementite forms, on heating of the martensite of steels at a definite rate, is raised in relation to the silicon contents of the steels. The temperature at which cementite formed in the 3% nickel-base steels was raised about 250 °F (140 °C) by an increase of silicon from 0.5 to 2.2%. Epsilon iron carbide was detected in the 0.6% carbon steels after tempers at lower temperatures than those required to produce cementite.

The softening of the 2.2% silicon steels was retarded in the tempering range of 400 to 600 °F (205 to 315 °C). The hardness after a given temper in the 400 to 600 °F (205 to 315 °C) range was found to depend only on the silicon and carbon contents of the steels. A mechanism which involves coherency hardening is postulated as the cause of the retarded softening of the high silicon steels.

The notch impact properties of the tempered steels were affected by the presence of silicon. The transformation of retained austenite was retarded as a result of the presence of silicon in the 2.2% silicon steels. Silicon did not precipitate as a compound or in the carbides during the various stages of tempering.

INTRODUCTION

IN the study of the properties of HY-Tuf (1)¹ it was found that this medium alloy steel when hardened by an oil quench, and subsequently tempered, did not soften during tempering over the range 300 to 700 °F (150 to 370 °C) as other medium alloy steels did. For some time the reason for the anomalous behavior remained elu-

¹The figures appearing in parentheses pertain to the references appended to this paper.

A paper presented before the Thirty-fourth Annual Convention of the Society, held in Philadelphia, October 18 to 24, 1952. The authors, A. G. Allten and P. Payson, are both associated with the Research Laboratory, Crucible Steel Company of America, Harrison, N. J. Mr. Allten is senior metallurgist and Mr. Payson is assistant director of research. Manuscript received April 10, 1952.

sive, but eventually it was established that the high silicon content of the steel, namely about 1.5%, was responsible for the unexpected resistance of the hardened steel to tempering.

A review of the literature gave little indication that silicon retarded softening in the tempering of martensite. Bain's curves (2), which have been referred to repeatedly, show the higher silicon steels to be harder over the whole range of tempering temperature, but they do not show any discontinuous effect in the tempering range 300 to 700 °F (150 to 370 °C). Furthermore, Bain states, "One may assume, since silicon is not present in any large proportion in the carbide, that its effect is to strengthen the ferrite in which the gradually coarsening carbides are dispersed."

On the other hand, the well-known silico-manganese steels, AISI 9260 and its modifications, have been used for at least 50 years, and their tempering curves which are not simple straight lines have long been reported in the data sheets published by steel manufacturers. Gill and his associates (3), however, dismiss the unusual behavior of the silicon steels with the statement, "These (silicon) steels resist tempering to a somewhat better degree than do plain carbon steels."

The present authors believe that this long-neglected phenomenon has considerable academic interest, and some practical value as well. Accordingly, some work was done to try to establish the mechanism by which silicon retards the softening of martensite during tempering.

MATERIALS

It has been established in the laboratory with which the authors are associated, by the study of a wide variety of compositions in which silicon has been consistently varied from low to high amounts, that the effect of silicon on the tempering of martensite is the same in all steels. Most of the work to be reported here was done on only 4 steels—a 0.6% carbon, 0.8% manganese-base composition with 0.4 and 2.2% silicon; and a 0.4% carbon, 3.0% nickel-base composition with 0.5 and 2.2% silicon. However, for the sake of completeness, data on a few other steels have been included.

All of the steels were made in small induction furnace melts, and were forged to 5/8-inch square bars which were annealed by a furnace cool from 1450 °F (790 °C). The analyses of these bars are given in Table I. In the discussion, the steels will hereafter be referred to by the "type designation" shown in Table I.

EXPERIMENTAL METHODS

All the steels, except for the 3.0% silicon, and 3.7% silicon, 3% nickel steels, were austenitized at 1600 °F (870 °C) for 1 hour, for hardening. This treatment was sufficient to produce a homogeneous austenite in the lower silicon steels. The two highest silicon steels

Table I
Analyses of Experimental Steels With Varied Silicon

Steel No.	Type Designation*	C	Mn	Si	Ni	Atomic % Si
1	0.4% Silicon, 0.6% Carbon	0.60	0.79	0.38	0.7
2	0.63	0.85	0.87	1.7
3	0.61	0.86	1.53	2.9
4	2.2% Silicon, 0.6% Carbon	0.62	0.87	2.25	4.2
5	0.5% Silicon, 3% Nickel	0.40	0.82	0.46	3.44	0.9
6	0.8% Silicon, 3% Nickel	0.40	0.81	0.80	3.41	1.5
7	1.5% Silicon, 3% Nickel	0.40	0.83	1.47	3.30	2.8
8	2.2% Silicon, 3% Nickel	0.38	0.86	2.18	3.41	4.1
9	3.0% Silicon, 3% Nickel	0.34	0.74	3.01	3.07	5.7
10	3.7% Silicon, 3% Nickel	0.36	0.73	3.67	3.07	6.8

*Steels are referred to by this designation in the text of the paper.

were austenitized at 1675 °F (915 °C), but even after this treatment these steels contained a small amount of residual ferrite.

In the preliminary work, the steels were quenched in water from the austenitizing temperatures, but, because some cracking was encountered, subsequent hardening was done in oil. It was found that the 0.6% carbon steels, as well as the higher alloyed steels, could be hardened through uniformly in 1/2-inch sections in an oil quench. When it was desired to minimize the amount of retained austenite which would otherwise have been present in the steels, the test pieces, after they had been cooled to about 300 °F (150 °C) in the quench, were transferred immediately to liquid nitrogen and allowed to cool to the temperature of the refrigerant, about -320 °F (-195 °C).

Tempering was generally carried out in liquid baths held to ± 5 °F. For the hardness surveys, separate samples were used for each temperature. In the study of the effect of time in tempering, the same sample was heated repeatedly, being cooled to room temperature periodically for measurements of hardness.

Hardness measurements were made on a calibrated Rockwell hardness tester. Most of the measurements were made by the same skilled operator. The measurements are believed to be good within ± 0.5 Rockwell C hardness point.

Specific volume was determined by a method previously described (4) which is accurate to ± 0.00002 cubic centimeter per gram.

Length changes in 1/4-inch diameter by 4-inch samples of the hardened steels were observed in a dilatometer during heating of the samples at carefully controlled rates. The samples were heated to 1000 °F (540 °C), cooled to room temperature, and reheated in the dilatometer to 1000 °F (540 °C) to check the cooling curves obtained during the initial run. A dilatometer of the type described in ASTM Designation B95-39 (5) was used. Measurements are believed accurate to ± 0.0001 inch per inch.

A set of 1/4-inch diameter samples of the hardened 0.5 and 2.2% silicon, 3% nickel steels were given cumulative 2-hour tempers at

100 °F intervals in the range of room temperature to 1000 °F (540 °C), and were measured for resistivity after each temper.

Several X-ray diffraction techniques were employed, viz.:

a. Qualitative determinations for retained austenite were made on hardness test pieces of the 0.6% carbon silicon steels. A series of successive etches and grindings was used to eliminate errors due to surface preparation. Samples were exposed in a 20-centimeter diameter asymmetric-type focusing camera. The presence, or absence, of the (111) austenite line was noted. Chromium radiation with a vanadic oxide "beta" filter in front of the film was used. No quantitative determinations of retained austenite were made.

b. The broadness of the (211) ferrite line as a function of tempering temperature was observed on samples of the 0.4 and 2.2% silicon, 0.6% carbon steels which had been tempered for 2-hour periods at 100 °F intervals in the range 300 to 700 °F (150 to 370 °C). The samples were ground to the radius of a 10-centimeter diameter cylindrical back-reflection focusing camera. Chromium radiation, without a filter, was employed. The line width at half intensity was determined by means of a microphotometer.

c. Residues were obtained by electrolytic extraction of $\frac{3}{8}$ by $\frac{3}{8}$ by 4-inch samples of quenched and tempered 0.5 and 2.2% silicon, 3% nickel steels. A special electrolyte (6) designed for quantitative carbide extraction was used. This electrolyte consists of 160 grams of citric acid and 60 grams of ammonium chloride dissolved in water to make a liter of solution. The residues were washed in water, alcohol, and ether, and were mixed with collodion, while still wet, and formed into 0.5-millimeter diameter rods. The rod-shaped samples were exposed in a 114.6-millimeter diameter Debye camera. Chromium radiation with a suitable beta filter in front of the film was used.

d. The nature of the carbides in solid samples of the 0.6% carbon silicon steels was determined after various tempering treatments. Flat samples were mounted at a grazing angle of 60 degrees to the incident radiation in the 114.6-millimeter Debye camera, and radiation from the slit of a pentaerythritol monochromator was permitted to enter the camera. Both chromium and iron radiations were employed.

RESULTS

Figs. 1 and 2 show that in the tempering of two steels of different base compositions to which silicon has been added, the following facts may be observed:

1. There is an almost parallel drop in hardness from the as-quenched value to that after a 2-hour temper at 300 °F (150 °C), in the steels of the same base composition, regardless of silicon content.

2. The effect of silicon becomes apparent after tempers between 300 and 400 °F (150 and 205 °C). The rate of softening with tempering temperature decreases in the steels between 300 and 500 °F (150 and 260 °C), and the magnitude of this decrease in softening rate is related to the silicon contents of the steels. In fact, the rate of softening becomes nil at about 500 °F (260 °C) in the steels which contain 1.5 and higher percentages of silicon.

3. The rate of softening begins to increase again at about 600 °F (315 °C) in the 0.6% carbon steels, and at 550 °F in the 3% nickel steels.

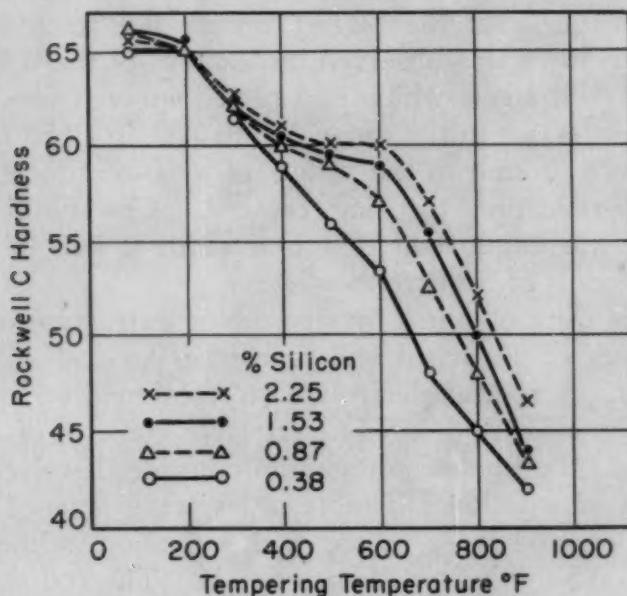


Fig. 1—Effect of Silicon on the Tempered Hardness of 0.6% Carbon Steels—Hardened 1600 °F (870 °C), Water-Quenched, Cooled to -320 °F (-195 °C); Tempered for 2-Hour Periods at Indicated Temperatures.

4. Finally, the rate of softening at about 800 °F (425 °C) is actually greater in the highest silicon steels of each series than in the lower silicon steels. The latter phenomenon is most readily seen in Fig. 1. However, the hardnesses of the steels of each series after a 900 °F (480 °C) temper are greater with increasing silicon content.

Hardness is a complex mechanical property in that it can be a resultant of several processes which affect the resistance to flow of a metal. Jack (7) has recently described three recognized hardening processes and three softening reactions as applied to the tempering of martensite. Data, such as those of Figs. 1 and 2, suggest that some hardening process occurs in high silicon steels to decrease the rate of softening at tempering temperatures between 400 and 600 °F (205 and 315 °C).

It is well known that silicon produces solid solution hardening

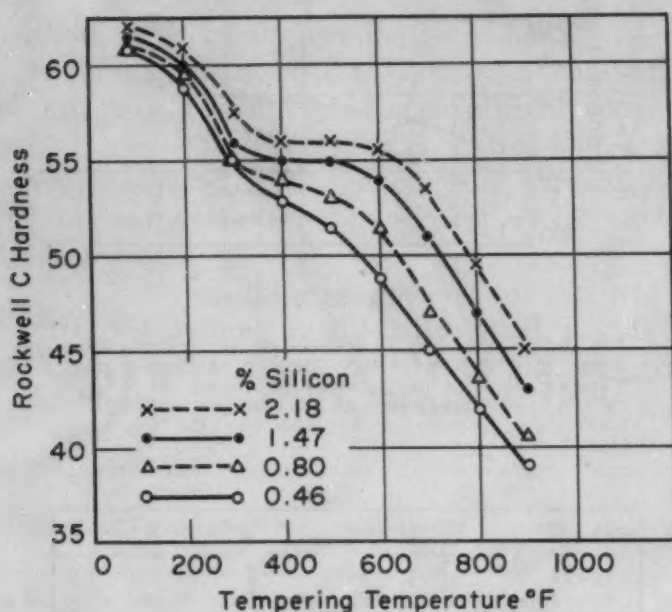


Fig. 2—Effect of Silicon on the Tempered Hardness of 3% Nickel Steels—Hardened 1550 °F (845 °C), Water-Quenched, Cooled to -320 °F (-195 °C); Tempered for 2-Hour Periods at the Indicated Temperatures.

of ferrite. However, it seemed obvious that such solid solution hardening was not the only cause of the hardness differences between the low and high silicon steels of Figs. 1 and 2. The solid solution hardening of ferrite by dissolved silicon might be a major cause of the hardness differences shown for the 900 °F (480 °C) temper. The hardness differences attributable to silicon content after a 600 °F (315 °C) temper are greater than those after a 900 °F (480 °C) temper, and therefore the solid solution hardening effect cannot be the sole cause of the hardness differences after the 600 °F (315 °C) temper.

Dispersion hardening by precipitation of a compound of silicon seemed, from the first, to be unlikely. The structural compositions of nickel steels containing up to 5% of silicon were investigated long ago by Guillet (8) and no structural inhomogeneity due to silicon was found. Also, silicon in the quantities present in the steels of Figs. 1 and 2 should be completely soluble in iron, even in the presence of the other alloying elements in the steels.

Recent work (9) has shown that silicon does not enter into cementite in combination with carbon and iron, and therefore such a relationship cannot be the cause of the above-mentioned retarded softening.

A plot of hardness after a 600 °F (315 °C), 2-hour temper versus atomic per cent of silicon was made for the steels of Figs. 1 and 2. The curves are shown in Fig. 3, and it is evident that equal additions of silicon produce equal increases in the hardness after the 600 °F

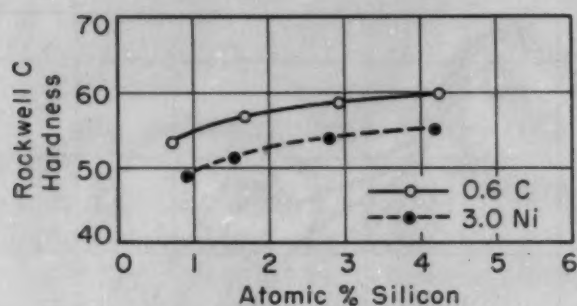


Fig. 3—Effect of Silicon on the Hardness After a 600 °F (315 °C) Temper of Steels of Varying Base Compositions—Hardened 1600 °F (870 °C). Water-Quenched, Cooled to -320 °F (-195 °C); Tempered at 600 °F (315 °C), 2 Hours.

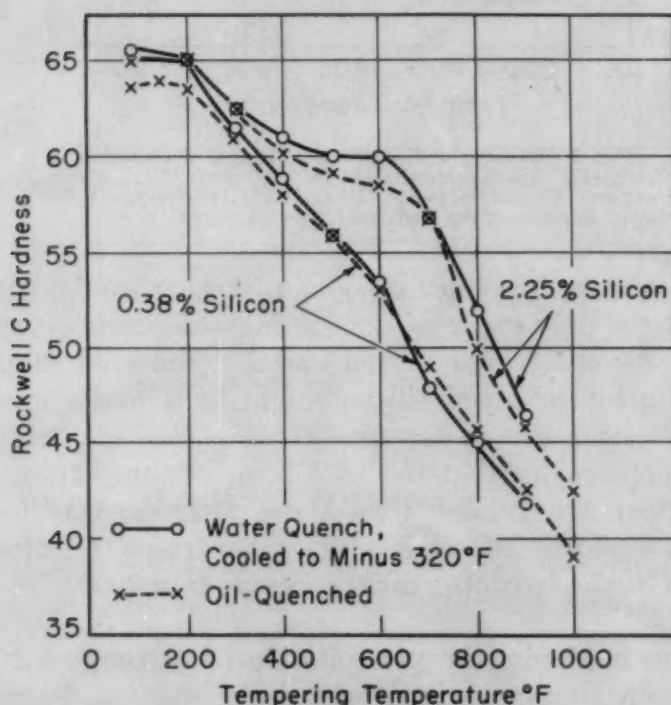


Fig. 4—Effect of Retained Austenite on the Tempered Hardness of 0.6% Carbon-Base Silicon Steels—Hardened From 1600 °F (870 °C); Tempered 2 Hours at the Indicated Temperatures.

(315 °C) temper in steels of the 0.6% carbon-base composition of Fig. 1 and the 3% nickel-base composition of Fig. 2.

The curves of Fig. 3 also indicate that the hardnesses after a 600 °F (315 °C), 2-hour temper cannot be increased appreciably by silicon additions of over 4 atomic per cent.

The effect of retained austenite is shown in Fig. 4 in which are plotted the hardnesses obtained on tempering of the 0.4 and 2.2% silicon, 0.6% carbon steels as refrigerated, and as quenched to room temperature. All of the retained austenite was not eliminated from

the 0.6% carbon steels by the cooling to -320°F (-195°C), and it is probable that only about 30% (10) was so removed, as compared with the amount which would have been present on a water quench to room temperature. However, the curves of Fig. 4 show that the retained austenite is effective in reducing the hardnesses in the 2.2% silicon, 0.6% carbon steel after 2-hour tempers in the 400 to 600 $^{\circ}\text{F}$ (205 to 315 $^{\circ}\text{C}$) range.

Also Fig. 4 indicates that the presence of retained austenite decreases the rate of softening in the latter steel at 700 $^{\circ}\text{F}$ (370 $^{\circ}\text{C}$). X-ray tests indicated that the retained austenite was partially transformed in the latter steel after a 700 $^{\circ}\text{F}$ (370 $^{\circ}\text{C}$), 2-hour temper.

Table II
Effect of Tempering Temperature and Time on the Hardness of 0.60% Carbon-Base Silicon Steels

$\frac{1}{4}$ by $\frac{1}{2}$ by $\frac{3}{8}$ -inch disks of the following steels were heated to 1600 $^{\circ}\text{F}$ for 1 hour, oil-quenched and tempered cumulatively as indicated.

Steel No.	Tempering Temp., $^{\circ}\text{F}$	Si		Rockwell C Hardness As Quenched		
		1	2.2	63.5	64.5	
Steel No.	Tempering Temp., $^{\circ}\text{F}$	Rockwell C Hardness As Tempered				
		5 Minutes	10 Minutes	30 Minutes	1 Hour	2 Hours
1	150	63.5	63.5	63.5	63.5	64
4	150	64.5	65	65	65	65
1	200	63.5	63.5	63.5	63.5	63.5
4	200	65	65	65	65	65
1	300	63	62.5	61.5	61	61
4	300	64	64	63	62.5	62.5
1	400	60.5	60	58.5	58	58
4	400	61.5	61.5	61	60	60
1	500	58	58	57	56	56
4	500	60	60	59.5	59	59
1	600	55	54	53	53	53
4	600	59	58.5	58.5	58.5	58.5
1	700	51.5	51	50	49	49
4	700	58	58	57	57	57
1	800	48	47.5	46.5	46	45.5
4	800	55.5	55.5	53.5	51.5	50
1	900	44	44	43.5	43	43
4	900	49.5	48.5	47	45.5	46
1	1000	42.5	42	40	39	39
4	1000	47	45.5	43.5	42.5	42.5

The changes in hardness with tempering time are shown in Tables II and III for the 0.6% carbon silicon steels and the 3% nickel-base, silicon steels. The former steels contained retained austenite, but no retained austenite could be found in the 3% nickel steels after refrigeration.

Tables II and III show that most of the change in hardness at tempering temperatures in the range 80 to 600 $^{\circ}\text{F}$ (25 to 315 $^{\circ}\text{C}$) takes place in the first hour of tempering, in both high and low silicon steels. Some of the data of Table III have been plotted in Fig. 5. Fig. 5 shows that 88-hour tempers of the 2.2% silicon, 3% nickel

Table III
Effect of Tempering Temperature and Time on the Hardness of 3% Nickel Silicon Steels

$\frac{1}{2}$ by $\frac{1}{2}$ by 1-inch samples of the following steels were hardened 1600 °F for 1 hour, oil-quenched, cooled to -320 °F and tempered cumulatively with respect to time as indicated.

Steel No.	Tempering Temp., °F	Steel No.	Rockwell C Hardness As Tempered									
		Si	5 Min.	10 Min.	30 Min.	1 Hr.	2 Hrs.	5 Hrs.	10 Hrs.	20 Hrs.	40 Hrs.	88 Hrs.
5	200	0.5	60.5	58.5	59.5	58.5	58.5	59	58	58	58	57.5
8	200	2.2	61.5	60.5	61	61	61	60.5	60	60	59.5	59
5	300	0.5	57.5	56.5	57	56.5	56	56	55	54.5	54.5	54.5
8	300	0.5	59	58.5	58.5	58	58	58	57.5	57.5	57	57
5	400	0.5	56	53.5	54.5	53	53	53	52	52	52.5	52
8	400	0.5	58	57	57	56.5	57	57.5	57.5	57.5	57	57
5	500	0.5	53	52.5	53	52	52	52	51	50.5	50.5	50
8	500	0.5	56.5	55.5	57	56	56.5	56.5	57	57	56.5	56.5
5	600	0.5	51	50	49	48.5	49	48	47.5	46.5	45.5
8	600	0.5	57	56.5	56	56	56.5	56	56	56	55.5
5	700	0.5	48	47.5	46	45	45	42
8	700	0.5	55	55	55	54.5	54.5	52.5
5	800	0.5	44	43.5	43	42	42	42	41	41	40	38
8	800	0.5	53	52.5	51	49.5	49.5	49.5	48.5	48.5	48	47
5	1000	0.5	39	38	37	36	35.5	34	33	32	29
8	1000	0.5	44.5	43	41.5	41.5	41	39.5	39	38	36

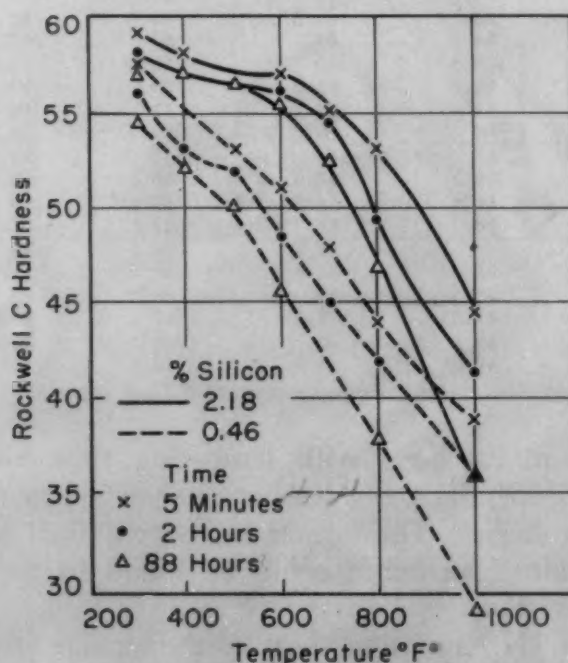
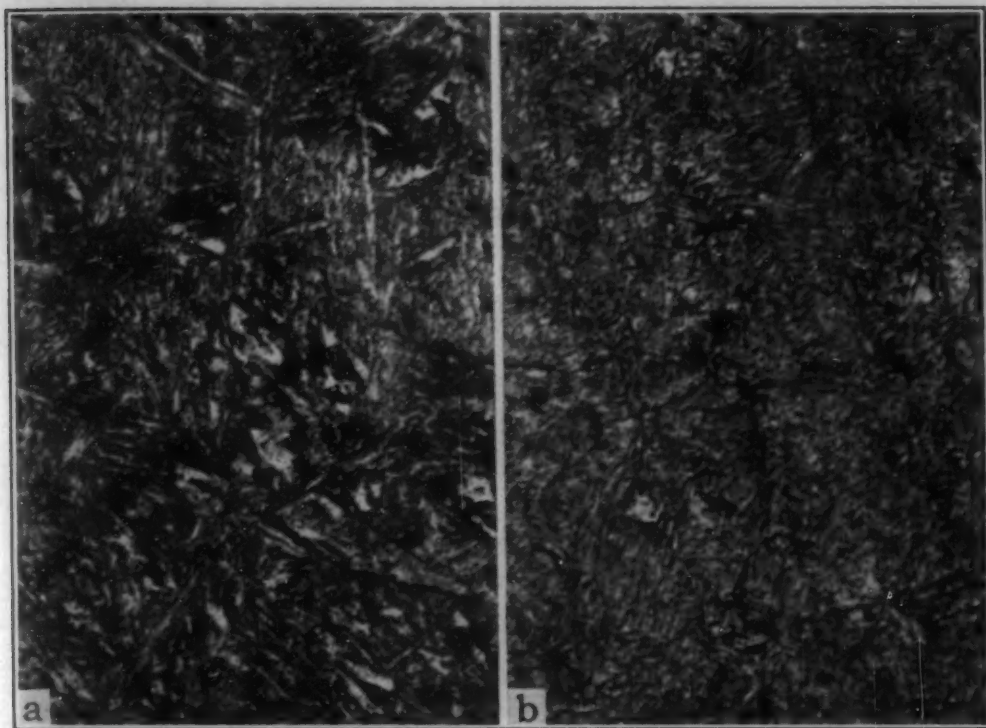


Fig. 5—Effect of Tempering Time on the Hardness of 3% Nickel Steels of 0.5 and 2.2% Silicon Contents—Hardened 1600 °F (870 °C), Oil-Quenched and Cooled to -320 °F (-195 °C); Tempered as Indicated.

steel at temperatures of 400, 500 and 600 °F (205, 260 and 315 °C) produce relatively little change from the hardnesses of 2-hour tempers at the corresponding temperatures. A slightly greater hardness decrease was found after an 88-hour temper at 300 °F (150 °C) than after similar tempers in the 400 to 600 °F (205 to 315 °C) range. It seems evident from Fig. 5 that some process occurred to maintain hardness during the 400 to 600 °F (205 to 315 °C) tempers in the 2.2% silicon, 3% nickel steel since, with the same tempering conditions, the hardnesses of the 0.5% silicon, 3% nickel steel decreased to a greater degree.



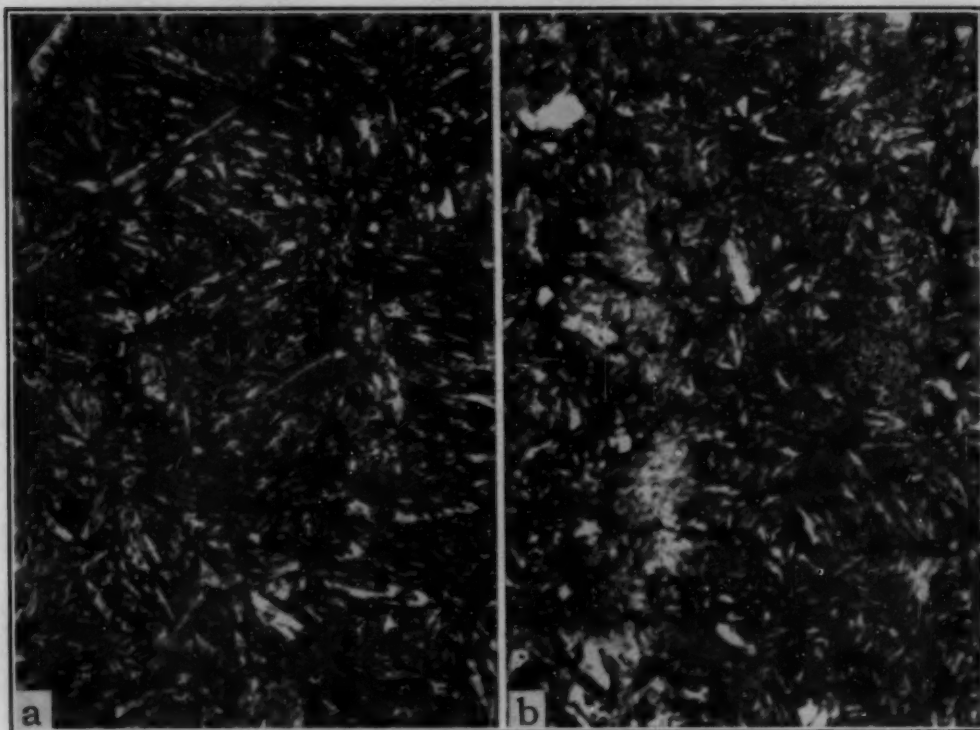
Microstructure in 3% Nickel Steels Containing 0.5 and 2.2% Silicon

Fig. 6a—0.5% Silicon Steel Tempered 2 Hours at 600 °F (315 °C). Hardness Rockwell C-48.5. Fig. 6b—2.2% Silicon Steel Tempered 2 Hours at 600 °F (315 °C). Hardness Rockwell C-56. Steels were oil-quenched from 1600 °F (870 °C) and cooled to minus 320 °F. Etched 45 seconds in picral plus 0.04% HCl. $\times 1000$.

Examination of the microstructures of the 0.6% carbon and 3% nickel-base silicon steels revealed that the development of the usual tempered structures in the 2% silicon steels was, like the hardness decrease, "retarded" in the tempering temperature range between 400 and 600 °F (205 and 315 °C). Figs. 6a and 6b illustrate the differences in microstructure in the 3% nickel-base steels caused by silicon content. The fact that the microstructures in the 2% silicon steels were much lighter etching than those in the 0.4% silicon steels of 0.6% carbon and 3% nickel-base compositions, after tempers at

400, 500 and 600 °F (205, 260 and 315 °C), is an argument against dispersion hardening by precipitation in the higher silicon steels. If particles of an iron-silicon compound or an iron-silicon carbide precipitated in the 400 to 600 °F (205 to 315 °C) tempering temperature range, one would expect the higher silicon steels to etch at least as rapidly as the lower silicon steels after tempers in the latter range.

The austenitic grain size in the higher silicon steels was considerably smaller for a given austenitizing temperature than in the



Microstructure in 3% Nickel Steels Containing 0.5 and 2.2% Silicon

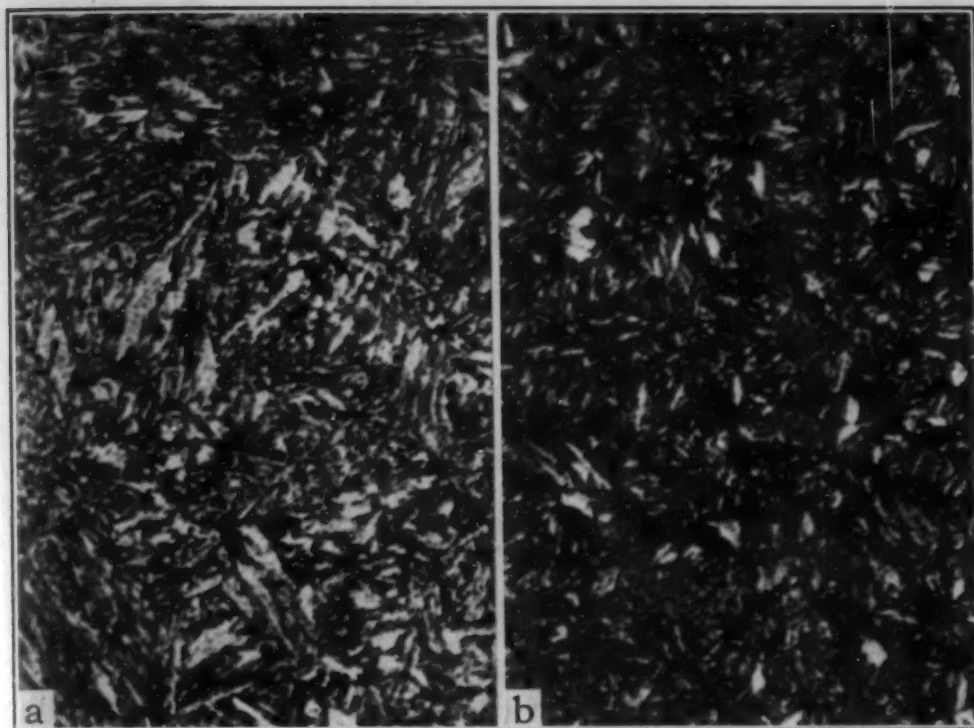
Fig. 7a—0.5% Silicon Steel Tempered 2 Hours at 800 °F (425 °C). Hardness Rockwell C-42. Fig. 7b—2.2% Silicon Steel Tempered 2 Hours at 800 °F (425 °C). Hardness Rockwell C-49.5. Etched 45 seconds in picral plus 0.04% HCl. $\times 1000$. Steels were oil-quenched from 1600 °F (870 °C) and cooled to minus 320 °F.

low silicon steels. The martensite needles were smaller in the high silicon steels than in the low silicon steels, probably in consequence of the smaller austenitic grain size of the former steels.

The microstructures of the 0.5 and 2.2% silicon, 3% nickel steels as tempered at 800 °F (425 °C), showed outlining of the prior austenite grain boundaries (Fig. 7a and 7b). The grain boundary outline was more pronounced in the latter steel, which also showed traces of a discontinuous grain boundary network after a 700 °F (370 °C), 2-hour temper. It is interesting to note that the minimum value of notch impact strength, as given in Fig. 14, occurred in the 2.2% silicon, 3% nickel steel after an 800 °F (425 °C) 2-hour temper, coincident with the above-noted grain boundary condition. However,

a grain boundary condition is also present in the 0.5% silicon, 3% nickel steel after the 800 °F (425 °C) temper, and none is present after the 600 °F (315 °C), 2-hour temper which produces the lowest impact strength in the low silicon steel (see Fig. 6a).

The structures produced in the low silicon steels, after 2-hour tempers at temperatures over 800 °F (425 °C), showed coarser carbides and more light-etching, acicular patches of ferrite than seen in



Microstructures in 3% Nickel Steels Containing 0.5 and 2.2% Silicon

Fig. 8a—0.5% Silicon Steel Tempered 2 Hours at 1000 °F. Hardness Rockwell C-36. Fig. 8b—2.2% Silicon Steel Tempered 2 Hours at 1000 °F. Hardness Rockwell C-41.5. Etched 45 seconds in picral plus 0.04% HCl. $\times 1000$. Steels were oil-quenched from 1600 °F (870 °C) and cooled to minus 320 °F.

the high silicon steels. The net effect is a “darker etching” structure in the high silicon, as compared with the low silicon steels. This etching effect is illustrated by Figs. 8a and 8b for the 0.5 and 2.2% silicon, 3% nickel steels after tempers of 1000 °F (540 °C), 2 hours.

Examination of the 2.2% silicon, 3% nickel steel and the 2.2% silicon, 0.6% carbon steel after tempers of 88 hours at 1000 °F (540 °C) showed no evidence that graphitization had taken place in these steels.

The data obtained from dilatometer runs on the 0.6% carbon steels of 0.4 and 2.2% silicon contents are shown in Fig. 9. The length changes during the first stage of tempering (up to 400 °F) were the same in all samples. There was a slight expansion starting at about 425 °F (220 °C) in the 0.4% silicon steel which is attrib-

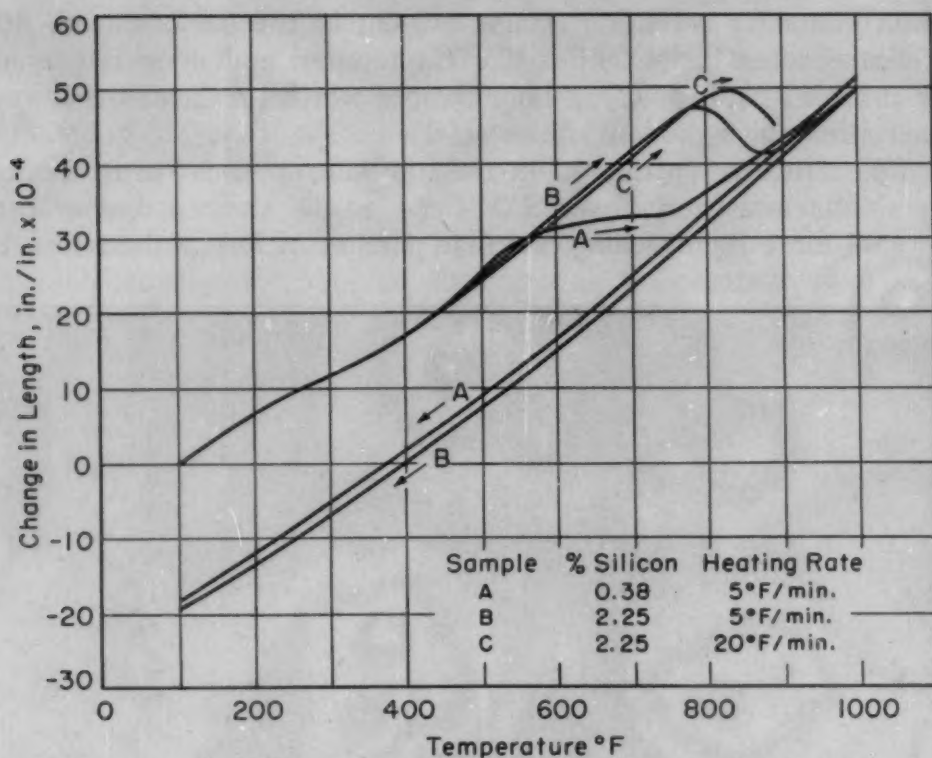


Fig. 9—Dilation on Tempering of 0.6% Carbon Steels Containing Silicon—Hardened 1600 °F (870 °C), Oil-Quenched and Tempered in the Dilatometer.

utable to the transformation of retained austenite. There was no corresponding expansion in the samples of the 2.2% silicon steel.

There was a marked contraction which started at about 550 °F (290 °C) in the 0.4% silicon steel, and at 750 °F (400 °C) in the 2.2% silicon steel, as shown by the curves for the 5-degree-per-minute heating rates. A 20-degree-per-minute heating rate caused the contraction to be noticeable only after a temperature of 775 °F (415 °C) had been reached in the 2.2% silicon steel. The temperature range over which the contractions occurred was greater in the 0.4% silicon steel than in the 2.2% silicon steel.

The contractions described above are mainly associated with the formation of cementite during the third stage of tempering, as demonstrated by the studies of Antia, Fletcher and Cohen (11).

It is interesting to note that the high silicon steel of Fig. 9 had a slightly greater coefficient of contraction on cooling from 1000 °F (540 °C) than the low silicon steel. These slight differences in contraction coefficients are thought to be attributable to a slightly greater degree of completion of the third stage of tempering in the low silicon steel.

Fig. 9 indicates that the high silicon steel underwent a greater degree of contraction during tempering than the low silicon steel.

There is no expansion indicated in the curve for the 2.2% silicon

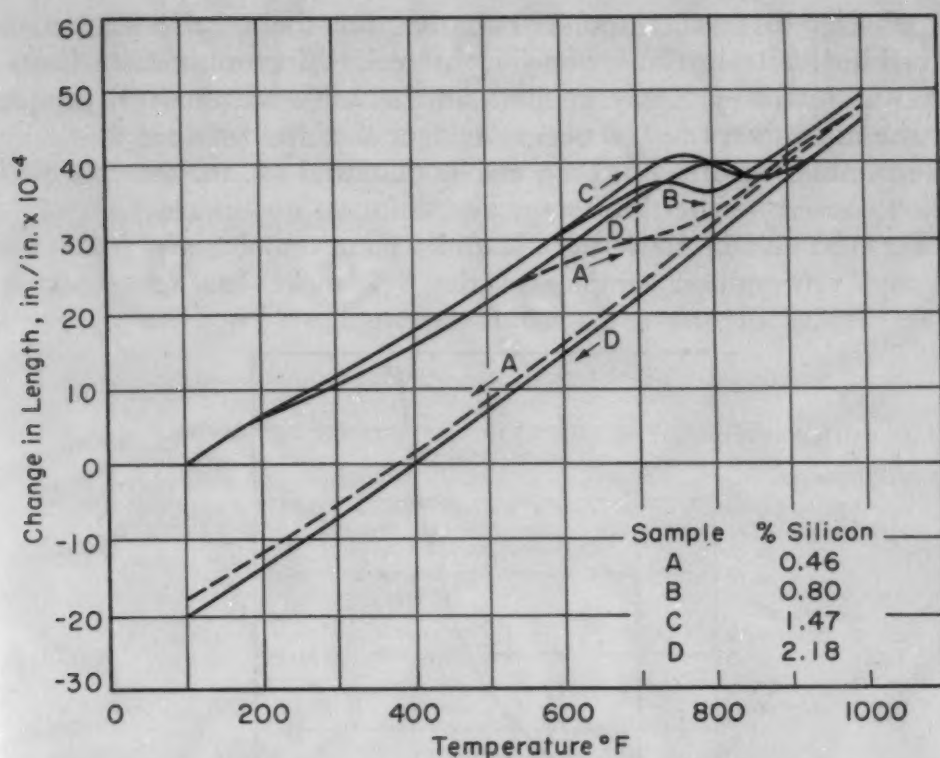


Fig. 10—Effect of Silicon on the Dilation on Tempering of 3% Nickel Steels —Hardened 1600 °F (870 °C), Oil-Quenched, Cooled to -320 °F (-195 °C); Heated and Cooled in Dilatometer at Rate of 5 °F per Minute.

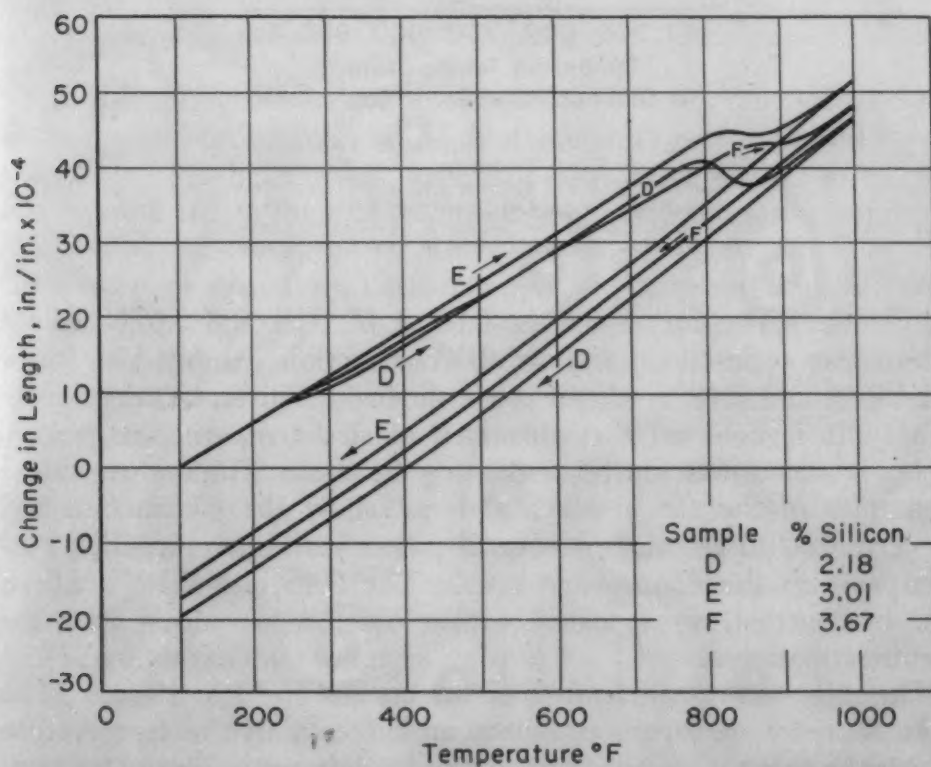


Fig. 11—Effect of Silicon on the Dilation on Tempering of 3% Nickel Steels —Hardened From 1600 °F (870 °C) for the 2.2% Silicon Steel, 1675 °F (915 °C) for the 3.0 and 3.7% Silicon Steels, Cooled to -320 °F (-195 °C); Heated and Cooled in the Dilatometer at 5 °F per Minute.

steel of Fig. 9, to correspond with that for the transformation of retained austenite in the lower silicon steel. Since no retained austenite was found by X-ray methods in the 2.2% silicon steel sample after the dilatometer test, it seems evident that the retained austenite transformation occurred during, and is obscured by, the general contraction caused by the third-stage reactions.

Figs. 10 and 11 show the dilatometer curves obtained for hardened and refrigerated samples of the 3% nickel-base composition

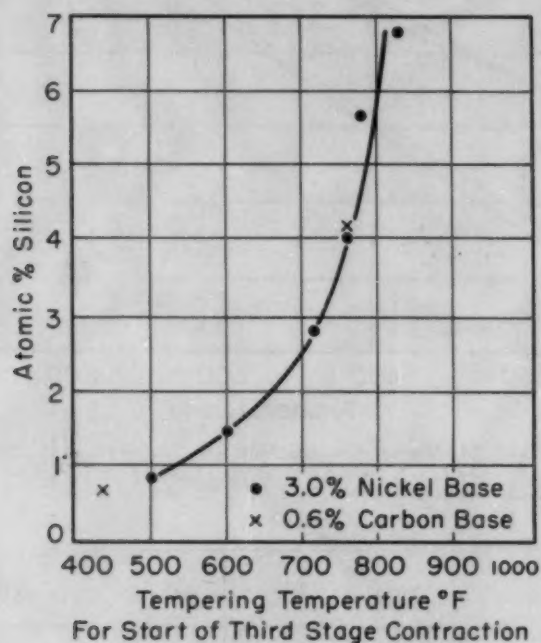


Fig. 12—Effect of Silicon on Temperature for Start of Third Tempering-Stage Contraction—Samples of 0.6% Carbon and 3% Nickel-Base Compositions Were Oil-Quenched From 1600 °F (870 °C), Cooled to -320 °F (-195 °C) and Heated at 5 °F per Minute in the Dilatometer.

silicon steels. The curves for the 0.80, 1.47, 3.01 and 3.67% silicon steels of this series do not show the contraction exhibited by those for the 0.46 and 2.18% silicon steels during the first 400 degrees of heating. It is believed that this lack of first-tempering-stage contraction is accounted for by tempering at room temperature, since the samples of the steels which did not show the contraction had been permitted to remain for several weeks in the as-quenched condition prior to the dilatometer tests. The 0.46 and 2.18% silicon steels, in contrast, were tested within one or two days after the hardening treatment.

The most important feature of the curves of Figs. 10 and 11 is that an increase of silicon produces an increase in the temperature at which the third-stage contraction can be detected. The latter temperatures are plotted in Fig. 12 as a function of atomic per cent of

silicon. Also tabulated and plotted are data obtained from dilatometer curves (not shown) of the hardened and refrigerated 0.4 and 2.2% silicon, 0.6% carbon steels. The samples of the 3.01 and 3.67% silicon, 3% nickel steels contained streaks of ferrite after the hardening treatment. The latter condition was due to segregation as well as to the high silicon contents of the steels. However, the presence of ferrite in the latter steels did not affect their third-stage reaction temperatures.

Fig. 12 shows a definite relationship between silicon content and

Table IV
Effect of Tempering on the Electrical Resistivity of Silicon Modifications of 3% Nickel Steel

Samples $\frac{1}{4}$ inch diameter by 4 inches long were tested for resistivity at 80°F; as hardened 1600°F for 1 hour, oil-quenched and cooled to -320°F; and after the indicated tempers.

Tempering Temp., °F	Electrical Resistivity, Microhm Cm. As Cumulatively Tempered in 2-Hour Periods		Difference Between Resistivity —As Hardened and As Tempered—	
	Steel 5 0.5% Si	Steel 8 2.2% Si	Steel 5 0.5% Si	Steel 8 2.2% Si
As Hardened	37.5	54.8	0.0	0.0
200	36.6	54.1	0.9	0.7
300	35.2	53.1	2.3	1.7
400	34.1	52.4	3.4	2.4
500	33.0	51.7	4.5	3.1
600	32.2	50.9	5.3	3.9
700	31.2	49.8	6.3	5.0
800	31.1	48.7	6.4	6.1
900	30.7	48.1	6.8	6.7
1000	30.1	47.6	7.4	7.2

the temperature at which the contraction due to the third stage of tempering can be detected in the dilatometer at a definite heating rate. Also, Fig. 12 indicates that there is a limit, with respect to temperature, beyond which the third stage of tempering cannot be suppressed by additions of silicon.

Electrical resistivity data obtained on tempered samples of the 0.5 and 2.2% silicon, 3% nickel steels are given in Table IV. If silicon had left its condition of solid solution in the matrix of the steel, either as an iron-silicon compound, or a carbide, some disproportionate decrease in the resistance would be expected. On the contrary, it was found that the decrease in resistance with tempering up to about 800°F (425°C) was greater in the low silicon steel than in the high silicon steel. Thus the data indicate that there is no decrease in the amount of silicon in solid solution in the steel at any tempering temperature.

The dimensional changes caused by tempering of the 0.5 and 2.2% silicon, 3% nickel steels were studied by means of specific volume measurements. The results are given in Table V, which shows that the contractions that accompany the first stage of tempering of both low and high silicon nickel steels take place largely within

the first 5 minutes of tempering in the range 200 to 500 °F (95 to 260 °C).

There are inconsistent variations, beyond the usual limits of error for specific volume determinations, in the data of Table V. These variations occur, for the most part, in the measurements representing the tempers in the range 200 to 500 °F (95 to 260 °C). Also, it is curious that the contractions in the low silicon, 3% nickel steel are not greater with increasing time at 400 and 500 °F (205 and

Table V
Effect of Tempering Temperature and Time on the Specific Volume of 3% Nickel-Base Silicon Steels

$\frac{1}{2}$ by $\frac{1}{2}$ by 1-inch annealed samples of the following steels were hardened 1600 °F for 1 hour, oil-quenched, cooled to -320 °F and tempered cumulatively with respect to time, as indicated.					
Steel No.	Si	Annealed Sp. Vol.			
5	0.5	0.12768 Cubic Centimeter per Gram			
8	2.2	0.12941 Cubic Centimeter per Gram			
Steel No.	Tempering Temp., °F	Specific Volume cc. per Gram as Hardened	Decrease From As-Hardened Specific Volume Caused by Tempering cc. per Gram		
			5 Minutes	2 Hours	10 Hours
5	200	0.12839	0.00009	0.00011	0.00004
8	200	0.13026	0.00011	0.00018	0.00010
5	300	0.12839	0.00019	0.00020	0.00021
8	300	0.13024	0.00020	0.00022	0.00022
5	400	0.12838	0.00019	0.00020	0.00024
8	400	0.13024	0.00015	0.00025	0.00023
5	500	0.12839	0.00023	0.00031	0.00026
8	500	0.13024	0.00026	0.00020	0.00020
5	600	0.12835	0.00031	0.00041	0.00052
8	600	0.13020	0.00024	0.00022	0.00028
5	700	0.12839	0.00062
8	700	0.13024	0.00031
5	800	0.12833	0.00058	0.00069	0.00065
8	800	0.13021	0.00039	0.00068	0.00073
5	1000	0.12833	0.00068	0.00066	0.00068
8	1000	0.13021	0.00080	0.00083	0.00085

260 °C), for X-ray diffraction results show that a considerable contraction should occur because of cementite formation at these temperatures.

However, the fact that the specific volume of the high silicon steel of Table V does not decrease appreciably with 2-hour tempers at increasing tempering temperatures between 300 and 600 °F (150 and 315 °C) is significant. The contraction from the as-hardened specific volume with time at 600 °F (315 °C) between 5 minutes and 10 hours is practically constant. These data indicate that the composition of the martensite which is in equilibrium with the first-stage precipitate does not change much either with tempering temperatures in the range 200 to 600 °F (95 to 315 °C), or with tempering times of 5 minutes to 10 hours at these temperatures. If the composition of the martensite does change in this tempering range,

some process which can cause volume changes must take place to offset any contraction.

It is interesting to note that the 2.2% silicon, 3% nickel steel undergoes a greater contraction from the as-hardened specific volume when tempered at 1000 °F (540 °C) than does the 0.5% silicon, 3% nickel steel. As indicated in Table V, both steels have contracted about the same amount from the as-hardened condition after 2-hour

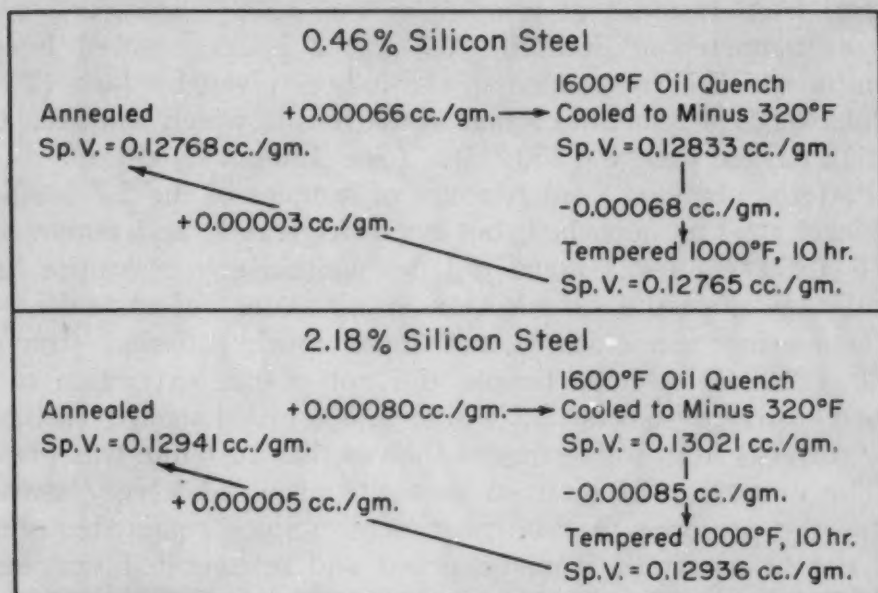


Fig. 13—Specific Volume Changes Due to Hardening and Tempering of 3% Nickel Steels of 0.5 and 2.2% Silicon Contents.

tempers at 800 °F (425 °C). Additional contraction, therefore, takes place in the high silicon steel during the temper at 1000 °F (540 °C), while the low silicon steel is seen, from Table V, to have retained the specific volume of the 800 °F (425 °C) temper.

Examination of the specific volume changes caused by martensite formation in both high and low silicon, 3% nickel steels showed that the high silicon steel expanded more than the low silicon steel on hardening. This was also found to be true of the 0.4 and 2.2% silicon, 0.6% carbon steels.

The diagram of Fig. 13 shows the relative volume changes occurring in hardening and tempering of the high and low silicon, 3% nickel steels. The difference between specific volumes for the as-annealed and tempered high silicon steel of 0.00005 cubic centimeter per gram may have no significance, since a deviation from the mean of ± 0.00002 cubic centimeter per gram may be associated with each measurement. The reason for the greater expansion of the high silicon steels on hardening is not clear. It is hardly possible that retained austenite differences can account for the anomaly. It is

possible that the presence of considerable numbers of silicon atoms in the steel may produce strains in the martensite which are not relieved until after the 800 °F temper.

Much time was spent in an attempt to obtain electrolytic extractions of the carbides from the tempered 3% nickel-base silicon steels for identification by means of X-ray techniques.

Initially, the extraction samples were not refrigerated to -320 °F (-195 °C) after a quench from 1600 °F (870 °C). Patterns obtained from residues of samples of the 0.5% silicon, 3% nickel steel, as tempered at 500 °F (260 °C), 2 hours, showed lines of cementite which corresponded to the indices given by Jack (7) for the "platelets" of cementite found in martensite which had been tempered 12 days at 480 °F (250 °C). (See Table VI.)

Patterns obtained from residues of samples of the 2.2% silicon, 3% nickel steel as quenched, but not refrigerated, and tempered at 500 °F (260 °C) for 2 hours did not contain any cementite lines; instead, they showed a surprisingly strong pattern of austenite.

Tempering temperatures and times much different from the 500 °F (260 °C), 2-hour temper did not permit extraction of the retained austenite from the 2.2% silicon, 3% nickel steel, even though X-ray patterns from solid samples showed that austenite was present.

The extraction of retained austenite provided a very sensitive test for the presence of this constituent. Since retained austenite could not be extracted from quenched and refrigerated samples of the 2.2% silicon, 3% nickel steel as tempered at 500 °F (260 °C), 2 hours, it was concluded that the refrigeration had transformed practically all of the austenite in the nickel steels.

A few lines of cementite were detected in the residues obtained from the quenched and refrigerated 0.5% silicon, 3% nickel steel after a temper at 400 °F (205 °C) for 2 hours, but the pattern obtained after a 500 °F (260 °C), 2-hour temper of a sample of this steel showed all of the lines characteristic of the "two-dimensional" or plate-like cementite referred to above. A similar pattern to that obtained from residues of the 500 °F (260 °C), 2-hour temper of the 0.5% silicon, 3% nickel steel was obtained from the residues of the 2.2% silicon, 3% nickel steel as tempered at 800 °F (425 °C), 2 hours. No pattern of a carbide was obtained from the residues of the low silicon nickel steel obtained after 2-hour tempers at 300 °F (150 °C), or below, or from residues of the high silicon nickel steel obtained after 2-hour tempers at 700 °F (370 °C), or below. However, some lines were detected which were attributable to manganese sulphide and probably other inclusions.

The results of the X-ray diffraction work on phases present in the solid samples of the 0.6% carbon silicon steels are given in Table VI. The carbide-phase diffraction lines which were obtained with

Table VI
X-Ray Reflections Obtained From Tempered 0.60% Carbon Silicon Steels Compared With Those From Cementite and Epsilon Iron Carbide*

The interplanar spacings (d) in kX units and the observed intensities† (I) are given for $\frac{1}{4}$ by $\frac{1}{2}$ by $\frac{1}{8}$ -inch samples of Steels 1 (0.4% Si) and 4 (2.2% Si) as oil-quenched from 1600°F and tempered as shown.

Crystalline Cementite		Two-Dimensional Cementite*		Epsilon* Iron Carbide		Ferrite		Austenite		0.4% Silicon (Steel 1)				2.2% Silicon (Steel 4)			
										Tempered 250°F, 5 Days	Tempered 600°F, 2 Hours	Tempered 700°F, 2 Hours	Tempered 700°F, 2 Hours	Tempered 600°F, 2 Hours	Tempered 600°F, 85 Hours	Tempered 700°F, 2 Hours	Tempered 800°F, 2 Hours
I	d	I	d	I	d	I	d	I	d	I	d	I	d	I	d	I	d
VW	3.36
VW	3.02
W	2.54	M	2.51
MS	2.37	MB	2.38	M	2.36	W	2.39	VW	2.36	...
MW	2.25	M	2.26
MW	2.21	M	2.20	VW	2.12	VW	2.20	VW 2.17
...
MS	2.10	W	2.10
MS	2.06	MS	2.06	†	...	S	2.08	MW	2.08	MW	2.08	W	2.08
M	2.02	V	2.02	VS	2.02	VS	2.02	VS	2.02	VS	2.02
VS	2.00	S	2.02
MS	1.97	WB	1.97
M	1.86
MS	1.85	MB	1.83	M	1.80	MW	1.79	VW	1.83	W	1.83	W	1.81
...
M	1.76	WB	1.76
M	1.68	VW	1.68	VW	1.68
W	1.63
...
M	1.582	S	1.57	MS	1.60	VW	1.60	VW	1.60	VW	1.61
W	1.539	VWB	1.53	W	1.57	W	1.57	W	1.57	W	1.57
MW	1.506	S	1.44	S	1.43	S	1.43	SB	1.43	MS	1.44
VW	1.409	MS	1.430	S	1.43
W	1.403
VW	1.346	W	1.36	VW	1.36	VW	1.36

the 0.6% carbon steels were very faint, and the contrast between lines and background in the films was low. Therefore, it was not possible to obtain good reproductions of the patterns by photographic printing. Differences between films, accountable to differences in the nature of the carbides present, were, however, unmistakable, although the lines were often so faint that reliable estimates of relative intensities could not be made.

Table VI shows that the same X-ray reflections were found in both the 0.4 and the 2.2% silicon, carbon steels after tempers of 5 days at 250 °F (120 °C). The same reflections were found in the 2.2% silicon steel after 2-hour tempers at temperatures up to 700 °F (370 °C), and after an 85-hour temper at 600 °F (315 °C). The latter X-ray reflections, as shown by Table VI, correspond to those observed by Jack (7) in the martensite of 1.3% carbon steels after long tempers at 250 °F (120 °C). Jack demonstrated by X-ray methods that the carbide responsible for the above reflections was a coherent precipitate of close-packed hexagonal structure. He called the carbide epsilon iron carbide and believed that it was a transition structure of composition Fe_3C which could decompose by structural changes into orthorhombic Fe_3C (cementite). There is controversy (12) as to whether the epsilon carbide dissolves in favor of cementite when the latter is nucleated, or whether the epsilon carbide decomposes as postulated by Jack.

The properties and nature of coherent precipitates have been described by Geisler (13).

The X-ray reflections from the silicon steel samples, which correspond to the indices given by Jack for the epsilon carbide reflections, are probably attributable to a coherent transition precipitate of a carbonitride (7) similar in structure to the epsilon carbide. This is suggested because of the fact that the steels which were studied contained small amounts of nitrogen, up to about 0.02%. For all practical purposes the precipitate may be considered as the epsilon carbide. The reflections referred to cannot be attributable only to nitrides since, as indicated in Table VI, they vanish in the low silicon steel on the formation of cementite at 500 °F (260 °C) but persist to 700 °F (370 °C) in the high silicon steel.

Cementite lines were found in samples of the 2.2% silicon, 0.6% carbon steel, as indicated in Table VI. The cementite produced at 800 °F in the high silicon carbon and 3% nickel steels, and at 500 °F (260 °C) in the low silicon steels, was imperfect as to crystalline form. Other investigators (7) have noted such imperfections in the structure of the cementite first formed on tempering. All of the reflections given for crystalline cementite in Table VI were found in a pattern from a solid sample of the annealed 0.4% silicon, 0.6% carbon steel.

Table VI shows that retained austenite lines were present in the 2.2% silicon, 0.6% carbon steel after a temper of 85 hours at 600 °F (315 °C). The diffraction pattern of the 0.4% silicon, 0.6% carbon steel, as tempered at 600 °F (315 °C), 5 minutes, contained no retained austenite lines. Further investigation showed that retained austenite was present in the latter steel after a 400 °F (205 °C), 2-hour temper, but not after a 500 °F (260 °C), 2-hour temper. The 2.2% silicon, 0.6% carbon steel, as tempered at 700 °F (370 °C), 2 hours, gave a diffraction pattern which contained austenite lines (albeit of diminished intensity from those observed after a 600 °F (315 °C) temper). A temper of 2 hours at 800 °F (425 °C) was

Table VII
Width of (211) Ferrite Line After 2-Hour Tempers of 0.6% Carbon-Base Silicon Steels

Tempering Temp., °F	Line Width at Half Intensity, mm.	
	0.4% Silicon	2.2% Silicon
300	10.2
400	10.0	11.5
500	8.4	10.0
600	8.0	10.1
700	6.4	8.3

required to produce a pattern containing no evidence of austenite lines.

Further study is required before more can be said about the transformation of retained austenite in the silicon steels.

The results of the X-ray line width measurements are shown in Table VII for the 0.4 and 2.2% silicon, 0.6% carbon steels as tempered 2 hours at temperatures in the range of 300 and 700 °F (150 and 370 °C). Measurements of the very broad lines present after tempers at below 300 °F (150 °C) could not be made, but these lines were wider than those present after the 300 °F (150 °C) temper.

The line widths given in Table VII probably represent primarily the degrees of tetragonality of the martensite remaining in the steels after the various tempers. The microphotometer tracings, however, showed little evidence of a double peak in intensity which would indicate tetragonality.

DISCUSSION

The above results show that silicon, in the steels which were studied, retards the processes involved in the formation of cementite, which constitutes the third stage of tempering. How silicon effects this retardation is a question which was not answered by the experiments described. The data presented in Fig. 12 suggest that greater amounts of energy, in the form of increased tempering temperature,

must be supplied to initiate the nucleation of cementite as the silicon contents of the steels are increased.

The resistance of the retained austenite to transformation on tempering in the high silicon steels may be directly related to the formation of cementite.

While silicon may reduce the activity of carbon in martensite and thus retard the entire tempering process, the first-stage processes which occurred on heating between 80 and 300 °F (25 and 150 °C), do not appear from the above results to have been much affected by the presence of silicon. The formation of the coherent epsilon carbide apparently does not require large-scale movement of carbon atoms in contrast to the formation of cementite (7).

Whatever the mechanism by which silicon retards the tempering processes, it remains of interest to examine the tempering of the 3% nickel-base silicon steels of 0.5 and 2.2% silicon contents with respect to several properties as measured at room temperature.

Fig. 14 shows the effect of 2-hour tempers in the range 80 to 1000 °F (25 to 540 °C) on certain properties of the latter steels. Both high and low silicon steels decrease in hardness and specific volume at about the same rate with tempers up to 300 °F (150 °C). Epsilon carbide or carbonitride probably forms in both steels over this temperature range, and the hardness of the martensite decreases due to partial loss of tetragonality and stress relief. Cementite forms in the low silicon steel, as determined by X-ray methods, at about 400 °F (205 °C), and the hardness and specific volume of this steel decrease steadily with increasing tempering temperature. The formation of cementite appears to be nearly complete in the low silicon steel after a 2-hour temper at 700 °F (370 °C), as indicated by electrical resistivity and specific volume tests. The hardness declines steadily, however, probably because of changes in the size and degree of dispersion of the cementite.

It is reasonable to assume, from the X-ray work on the 0.6% carbon silicon steels, that the coherent transition precipitate persists in metastable equilibrium with carbon dissolved in martensite, to temperatures as high as 700 °F (370 °C) in the high silicon steel.

The electrical resistivity curves of Fig. 14 show that there is a decrease in resistivity in both high and low silicon steels throughout the 400 to 600 °F (205 to 315 °C) tempering range. The rate of resistivity decrease is less in the high silicon steel than in the low silicon steel, but the decrease indicates a loss of carbon from solid solution in both steels. Furthermore, it is probable that there is a slight stress relief of the martensite in the high silicon steel on tempering at 400 °F (205 °C), and above, which might produce changes in resistivity.

Since cementite does not form with 2-hour tempers of the high

silicon steel until a temperature over 700 °F (370 °C) is reached, carbon lost by the tetragonal martensite must produce further growth of the coherent epsilon phase. The growth of the coherent precipitate, as outlined above, would tend to strain the matrix and harden the

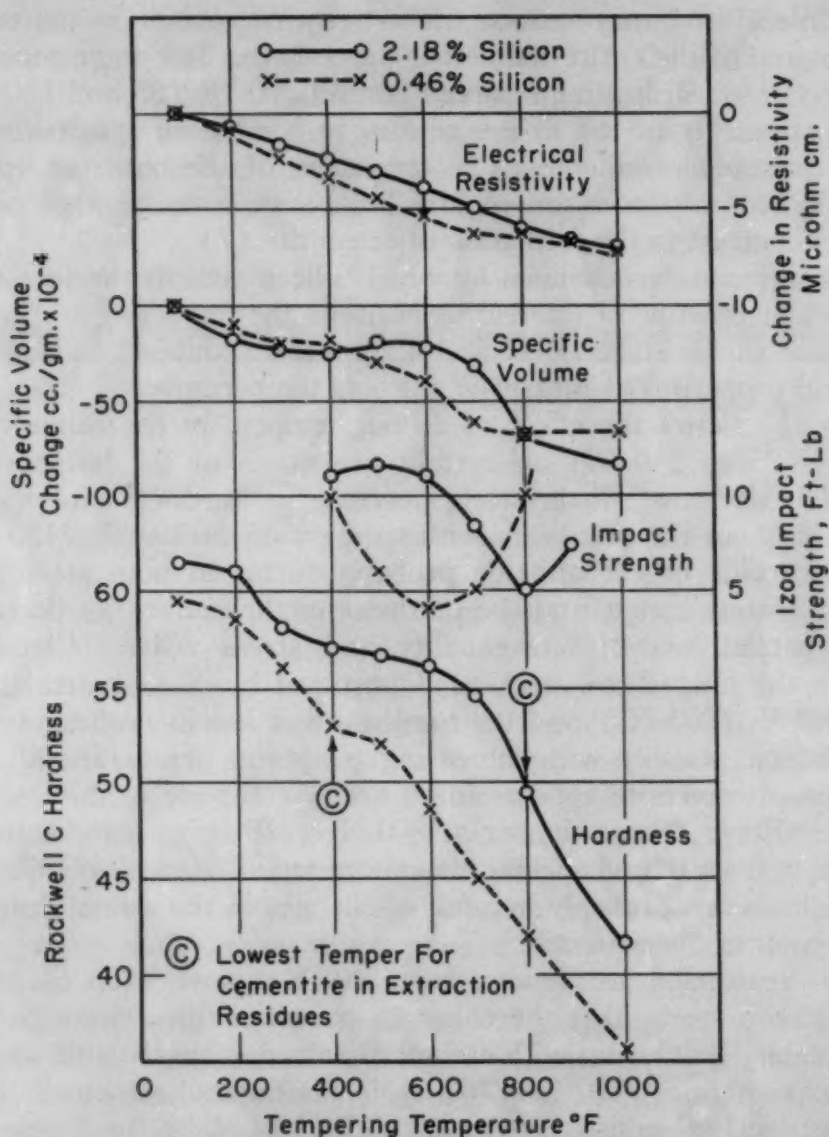


Fig. 14—Effect of Tempering Temperature on the Room Temperature Properties of 3% Nickel Steels Containing 0.5 and 2.2% Silicon—Hardened 1600 °F (870 °C), Oil-Quenched, Cooled to -320 °F (-195 °C); Tempered for 2-Hour Periods at the Indicated Temperatures.

steel against the softening processes involving loss of carbon and stress relief. Such a hardening process would be intensified, according to the ideas of Geisler (13), by the presence of an element such as silicon which normally produces solid solution hardening of ferrite.

The specific volume changes are somewhat difficult to account

for by the latter hardening mechanism. It is well known that a marked contraction takes place when the epsilon carbide forms from freshly quenched martensite with tempers at about 200 °F (95 °C). Whether expansion or contraction would accompany the growth of the coherent precipitate would probably depend on the nature of the strains set up by precipitation. The lack of change of specific volume after 2-hour tempers at 400, 500 and 600 °F (205, 260 and 315 °C) in the high silicon steel of Fig. 14 does not prove that coherency hardening is absent.

The decrease in hardness on long tempering at 700 °F (370 °C) may be attributable to loss of coherency caused by rapid growth of the transition precipitate.

Fig. 5 showed that the hardness of the 2.2% silicon, 3% nickel steel decreases slightly with time at tempering temperatures of 300 and 400 °F (150 and 205 °C). The decrease in hardness may be attributable to formation of the transition precipitate with time, but without sufficient growth to promote much coherency hardening.

Fig. 4 showed that the presence of a small amount of retained austenite decreased the hardness of the 2.2% silicon, 0.6% carbon steel, as tempered in the range of 400 to 600 °F (205 to 315 °C). The decrease in hardness may be interpreted by the above coherency hardening hypothesis as due to partial relief of the coherency strains by the deformation of austenite.

In summation, the above results indicate that the differences in hardness between high and low silicon steels, as shown in Figs. 1 and 2, are attributable to the following three effects of the silicon dissolved in the steels:

- a. The solid solution hardening effect of silicon in the ferrite, or martensite of the steel.
- b. The effect of silicon in retarding cementite formation and thereby maintaining a larger amount of carbon in the martensite.
- c. The coherency hardening due to growth of the epsilon transition precipitate in the higher silicon steels.

Izod impact tests were made on tempered samples of the 0.5 and 2.2% silicon, 3% nickel steels in an attempt to relate changes in impact strength to the other property changes described above. The impact test results of Fig. 14 show that both high and low silicon steels decreased in impact strength in a manner which has been generally associated with the tempering of the martensites of medium carbon steels. Increased silicon content, however, resulted in an increase in the tempering temperature required to produce the minimum impact strength. The impact minima appear, from Fig. 14, to be associated with a condition of the steel which occurred during the third stage of tempering, since cementite was present in both high and low silicon steels after the tempers which produced the minima.

However, the relation of cementite formation to the initial embrittlement, at tempering temperatures below those which produced the impact minima, is not yet clear. Fig. 14 shows that both high and low silicon steels have nearly the same impact strengths after a 400 °F (205 °C), 2-hour temper. Cementite is detectable in the low silicon steel after this temper, but not in the high silicon steel. The former decreases in impact as the tempering temperature increases to 600 °F (315 °C), whereas the latter remains fairly constant up to about a 700 °F (370 °C) temper. Cementite is not evident, even after this temper in the high silicon steel, yet the impact value begins to decrease and at the same time there is a decrease in hardness and specific volume. Loss of coherency of the epsilon carbide may account for the loss of impact strength, as well as for the loss of hardness. It is conceivable that discrete particles of the incoherent epsilon carbide could be as effective for nucleating fracture as discrete particles of cementite.

SUMMARY

The effect of silicon on the tempering of 3% nickel and 0.6% carbon-base steels was investigated by means of hardness, electrical resistivity, dilatometric, specific volume, and X-ray diffraction methods. Most attention was given to steels of these base compositions containing about 0.4 and 2.2% of silicon.

Some of the results of the investigation are as follows:

1. Retarded softening of the 2.2% silicon steels in the tempering range of 400 to 600 °F (205 to 315 °C) was found. There was no evidence that this retardation was attributable to precipitation of an iron-silicon compound or an iron-silicon carbide.
2. The temperature at which cementite forms, on heating silicon steels at a definite rate, is raised in a definite relation to the atomic per cent of silicon present.
3. The 2.2% silicon, 3% nickel steels underwent a greater expansion on hardening and a greater contraction on tempering than did the 0.4% silicon steels of similar base composition.
4. The transformation of retained austenite occurs at temperatures, in the 2.2% silicon steels, which are about 200 °F (95 °C) higher than for the 0.4% silicon steels.
5. What is believed to be a coherent transition carbide, or carbonitride, was found, by X-ray means, to persist on tempers of 600 °F (315 °C), 85 hours, and 700 °F (370 °C), 2 hours, in the 2.2% silicon, 0.6% carbon steel. The same phase was found after a temper at 250 °F (120 °C) of the 0.4% silicon, 0.6% carbon steel. The high silicon steels of 2.2% silicon content contained cementite only after tempers of 2 hours, at above 700 °F (370 °C), whereas cemen-

tite was found in the 0.4% silicon steels after 2-hour tempers at 500 °F (260 °C).

A mechanism which involves coherency hardening of the high silicon steels in the temperature range of 400 to 600 °F (205 to 315 °C) is suggested to account for the retarded softening of these steels.

ACKNOWLEDGMENT

The authors are grateful to the management of the Crucible Steel Company of America for permission to present the data given in this paper, and to their colleagues in the Research Laboratory, G. A. Stefanelli, A. Simon, R. Gross, F. Baureis, and Miss A. Herenchak, for assistance in the heat treatment and testing of specimens and in the preparation of the paper.

References

1. P. Payson and A. E. Nehrenberg, "New Steel Features High Strength and High Toughness", *The Iron Age*, Oct. 21, Oct. 28, 1948.
2. E. C. Bain, FUNCTIONS OF THE ALLOYING ELEMENTS IN STEEL, American Society for Metals, Cleveland, 1939, p. 239.
3. J. P. Gill and Associates, TOOL STEELS, American Society for Metals, 1944, Fig. 146, p. 338.
4. Discussion of paper by S. G. Fletcher and M. Cohen, "The Effect of Carbon on the Tempering of Steel", TRANSACTIONS, American Society for Metals, Vol. 32, 1944, p. 359.
5. ASTM Standards, 1949, Pt. 2, p. 712.
6. Report to Crucible Steel Company of America, "Identification of the Carbides in Complex Steels", Battelle Memorial Institute, 1944, p. 95.
7. K. H. Jack, "Structural Transformations in the Tempering of High-Carbon Martensitic Steels", *Journal, Iron and Steel Institute*, Vol. 169, 1951, p. 26.
8. L. Guillet, "Quaternary Steels", *Journal, Iron and Steel Institute*, 1906, No. II, p. 1.
9. W. S. Owen, "The Carbide Phase in Iron-Carbon-Silicon Alloys", *Journal, Iron and Steel Institute*, Vol. 167, Pt. 2, February 1951, p. 117-120.
10. B. L. Averbach, L. S. Castleman and M. Cohen, "Measurement of Retained Austenite in Carbon Steels", TRANSACTIONS, American Society for Metals, Vol. 42, 1950, p. 112.
11. D. P. Antia, S. G. Fletcher and M. Cohen, "Structural Changes During the Tempering of High Carbon Steel", TRANSACTIONS, American Society for Metals, Vol. 32, 1944, p. 290.
12. M. Cohen and E. C. Roberts, "Martensite Decomposition", Lecture at Ninth Annual Pittsburgh Conference on X-Ray and Electron Diffraction, November 1951.
13. A. H. Geisler, "Property Changes During Aging", *Metals Technology*, August 1948, T.P. 2436.

DISCUSSION

Written Discussion: By F. W. Boswell and R. L. Cunningham, physical metallurgists, Department of Mines and Technical Surveys, Ottawa, Ont., Canada.

The authors state that there is a controversy as to whether the epsilon carbide dissolves in favor of cementite, when the latter is nucleated, or whether the epsilon carbide itself decomposes to cementite.

We have carried out the following experiment in an attempt to shed some light on this question.

A sample of commercial grade steel containing 0.90% carbon was austenitized at 1550 °F, quenched in brine and immediately cooled in liquid air to minimize retained austenite. The specimen was tempered at 390 °F for 1 hour to produce epsilon carbide without the production of cementite. Next, the sample was etched rather heavily in nital, carefully rinsed, and dried. This treatment left the carbide phase in relief, and a reflection electron diffraction pattern from this surface showed only the lines of epsilon carbide. The specimen was then tempered at 840 °F for 1 hour under very high vacuum so that the surface was not appreciably altered by reaction with the atmosphere. After this heat treatment, cementite is the only carbide present. Without any further surface treatment, a diffraction pattern was again obtained. The film showed strong lines due to ferrite and a few very faint lines which were probably due to oxides.

We interpret these results to mean that epsilon carbide has redissolved in the matrix, thereby converting the projections to ferrite. The possibility that the observed results were due to the decarburization of the carbide to produce ferrite was considered to be extremely unlikely. We would expect that if the carbon were lost from the carbide by oxidation, then the resultant ferrite itself would have been oxidized. Therefore we conclude that epsilon carbide particles do not transform to cementite.

Written Discussion: By B. S. Lement, Department of Metallurgy, Massachusetts Institute of Technology, Cambridge, Mass.

The authors are to be commended for their comprehensive investigation of the tempering of silicon steels. However, I would like to point out some alternatives with respect to interpretation of their experimental results.

On their eleventh page the authors state that the microstructures in Figs. 7a and 7b show an outlining of the prior austenitic grain boundaries. Comparing Fig. 7b, in which the outlining is clearest, with ASTM grain size standards and correcting for the high magnification used, $\times 1000$, yields a value of about ASTM No. 12 for the grain size of the 2.2% silicon, 3% nickel steel. It seems surprising that such a small grain size could be due to prior austenitic grains. Perhaps the observed outlining is actually associated with martensite plate boundaries. In certain areas martensite plates can appear as essentially equiaxed grains which are, of course, smaller than the prior austenitic grains.

This possibility is supported by the electron micrograph of a 0.6% carbon, 1.5% silicon steel quenched from 1600 °F and tempered at 1000 °F. As shown in Fig. 15 the structure consists of cementite mainly in the form of spheroidal particles situated at the boundaries of ferrite grains.

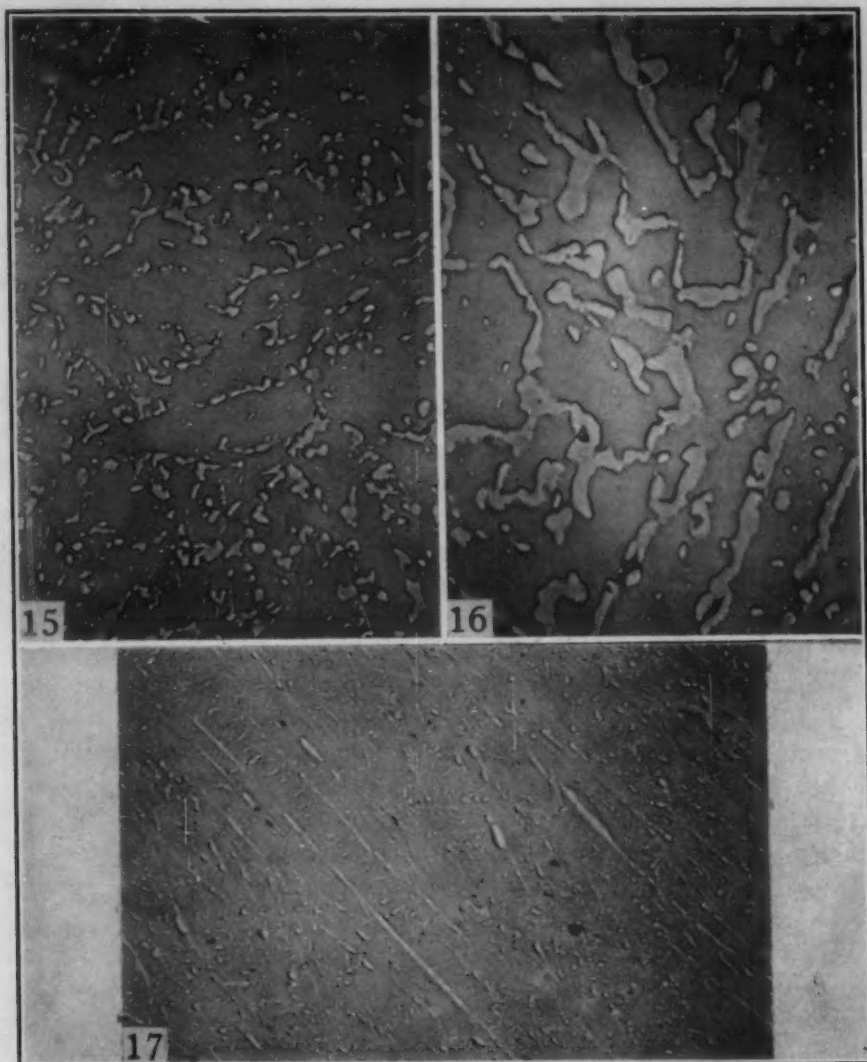


Fig. 15—Electron Micrograph of 0.6% Carbon, 1.5% Silicon Steel Tempered at 1000 °F. Spheroidized cementite present at ferrite grain boundaries. Picral-HCl etch. Negative parlodion replica rotary shadowed with chromium. $\times 5000$.

Fig. 16—Electron Micrograph of 1.4% Carbon Steel Tempered at 1000 °F. Discontinuous cementite network present at ferrite grain boundaries. Picral-HCl etch. Negative parlodion replica rotary shadowed with chromium. $\times 5000$.

Fig. 17—Electron Micrograph of 0.4% Carbon Steel Tempered at 500 °F. Elongated cementite present at martensite plate boundaries. Picral-HCl etch. Negative parlodion replica rotary shadowed with chromium. $\times 5000$.

The ferrite grain size of Fig. 15 is about ASTM No. 14; whereas the austenitic grain size as determined by slack quenching, which allowed proeutectoid ferrite to form along austenitic grain boundaries, was found to be ASTM No. 4-5. The occurrence of spheroidal cementite shown in Fig. 15 was predicted by Owen² on the basis of his analysis of the kinetics of the third-stage reaction in this steel as determined by precision length measurements.

It has not been generally realized that even in plain carbon steels

²W. S. Owen, "The Effect of Silicon on the Kinetics of Tempering", to be submitted to the American Society for Metals.

there is a pronounced tendency for cementite to form as a network at what are at first martensite plate boundaries but eventually become ferrite grain boundaries as the tempering temperature is increased and carbon is drained from the martensitic matrix. The culmination of this process is shown in Fig. 16 which is an electron micrograph of a 1.4% carbon, high purity iron-carbon alloy quenched from 2200 °F and tempered 1 hour at 1000 °F. Here we see an almost continuous cementite network at the grain boundaries of what is essentially ferrite. This network has formed at the expense of (a) carbide particles which dissolve within the grains and (b) carbon which precipitates from the martensitic matrix. This tendency for grain boundary carbide formation was found to occur in high purity iron-carbon alloys ranging from 0.15 to 1.4% carbon and is believed to be a contributing cause of the so-called "irreversible temper brittleness" reported by Libsch³ to occur in plain carbon steels tempered above about 800 °F.

On their twelfth page the statement is made that no "grain boundary condition" is present in the microstructure of the 0.5% silicon, 3% nickel steel after a 600 °F, 2-hour temper which produces the lowest impact strength. Although Fig. 6a of the paper shows only very slight indications of possible grain boundary outlining, it is believed that a "grain boundary carbide condition" would be revealed by examination in an electron microscope. This contention is based on the results of a recent investigation⁴ of the tempering of high purity iron-carbon alloys. For example, it was found that tempering a 0.40% carbon alloy at only 450 °F, after quenching from 1550 °F, results in the initial formation of elongated carbide films at martensite plate boundaries. The formation of such carbide films coincides with the initiation of the third stage of tempering and it is therefore believed that the carbide is a form of cementite.

Tempering the 0.40% carbon alloy 1 hour at 500 °F results in more pronounced carbide films at martensite plate boundaries, as shown in the electron micrograph of Fig. 17, and thus a correlation with the so-called "500 °F embrittlement" is evident. The embrittlement due to formation of carbide films is opposed by the softening effect due to depletion of the martensite matrix in carbon content as tempering is continued above 500 °F, which explains the fact that the room temperature impact strength eventually increases. It seems reasonable to assume that the presence of 0.5% silicon and 3% nickel could displace the impact minimum from, say, 500 to 600 °F; therefore, it is believed that this 600 °F impact minimum is due to essentially the same type of embrittlement found in plain carbon and low alloy steels of medium carbon content.

There are also differences with respect to the authors' interpretation of the hardness changes in the 2.2% silicon, 3% nickel steel. Alternative explanations for these hardness changes are summarized in the following tabulation:

³J. F. Libsch, A. E. Powers and G. Bhat, "Temper Embrittlement in Plain Carbon Steels", *TRANSACTIONS, American Society for Metals*, Vol. 44, 1952, p. 1058.

⁴B. S. Lement, B. L. Averbach and M. Cohen, "Microstructural Changes on Tempering Iron-Carbon Alloys—Part I", to be submitted to the American Society for Metals.

Temper °F	Hardness Change	Authors' Interpretation	Discusser's Interpretation
70 to 400	Decreases appreciably (Re 62 to 57)	Formation of ϵ -carbide without sufficient growth to promote much coherency hardening.	Loss of coherency between martensite and ϵ -carbide plus lowering of carbon content of matrix.
400 to 700	Decreases slowly (Re 57 to 56)	Growth of ϵ -carbide and resultant coherency hardening slightly counterbalanced by softening due to both lowering of carbon content of matrix and stress relief.	Hardening due to solution of ϵ -carbide in martensitic matrix overbalanced by softening due to coagulation and decrease in amount of ϵ -carbide.
700 to 800	Decreases rapidly (Re 56 to 49)	Loss of coherency of ϵ -carbide.	Formation of cementite and lowering of carbon content of martensite. Solution of ϵ -carbide essentially completed.
800 to 1000	Decreases rapidly (Re 49 to 42)	Formation of cementite.	Continued formation of cementite and lowering of carbon content of martensite matrix which tends to become ferrite.

The alternative explanations of hardness changes are based on a current electron microscopic investigation of the same 0.6% carbon, 1.5% silicon steel referred to in Fig. 15. Initial evidence of solution of ϵ -carbide was found after tempering at about 500 °F and virtually complete solution was found to occur at about 800 °F. Solution of ϵ -carbide and its simultaneous coagulation could account for the retarded softening which occurs in the range of about 400 to 700 °F in the 2.2% silicon, 3% nickel steel. This would also account for the observed increase in specific volume from 400 to 600 °F; however, the decrease in specific volume beyond 600 °F suggests the third stage actually starts earlier than indicated by the X-ray work. Precipitation, coherency hardening, and loss of coherency of ϵ -carbide is believed to take place below about 400 °F, similar to what occurs in plain carbon steel.

Finally, it is stated on the twenty-sixth page that a small amount of retained austenite decreased the hardness of the 2.2% silicon, 0.6% carbon steel because of "partial relief of the coherency strains by the deformation of austenite". Would the authors please amplify this statement and tell why the hardness decrease cannot be attributed to the very presence of retained austenite?

Written Discussion: By W. J. Barnett, R. P. Frohmberg and A. R. Troiano, Department of Metallurgy, Case Institute of Technology, Cleveland.

The marked retardation effect of silicon on the third-stage tempering reaction, as clearly demonstrated by the authors, is interesting. Do the authors have any information as to the effect of silicon on the carbon content of the martensite existing in metastable equilibrium with the epsilon iron carbide at the end of the first-stage reaction? Conceivably, this may constitute an additional factor in the explanation of the resistance to softening exhibited by the high silicon steels.

In attempting to correlate changes in mechanical properties with the martensite decomposition mechanism, we believe that the role of coherency should be emphasized as purely speculative. While it may seem logical to presuppose coherency, no definite experimental evidence has been presented to support its existence. Experiments directed toward clarification of this point are in progress at Case.

In the course of an investigation of the high strength characteristics

of alloy steels sponsored by the U. S. Department of the Air Force (Wright Air Development Center)* the tempering of SAE 2340 was studied. In view of the similarity of SAE 2340 and the authors' 3.5% nickel-0.5% silicon steel, a portion of our results which may be relevant to the present investigation is presented.

Carbides were electrolytically extracted in a cell similar to that used by Blickwede and Cohen.⁵ The anolyte was an aqueous solution of 15% sodium citrate, 1% potassium bromide, and 0.1% potassium iodide. The catholyte was an aqueous solution of 10% copper sulphate. Debye X-ray patterns of the residues were taken with cobalt K α monochromatic radiation. Residues extracted from specimens of SAE 2340 tempered at 400 °F for 1 and 4 hours consisted principally of epsilon iron carbide together with a trace of plate-like cementite. Specimens of SAE 2340 tempered at 500 °F for 1 hour yielded residues consisting primarily of plate-like cementite with only a trace of epsilon iron carbide. Tempering for 1 hour at temperatures above 500 °F gave residues consisting of cementite, as was observed by the authors.

In a similar manner, the carbide products of martensite decomposition have been observed for SAE 2340, as a function of tempering time as well as temperature. A correlation of carbide type and room temperature impact strength exhibited a marked parallel between the time or temperature of the transition of epsilon iron carbide to cementite, and the time or temperature of the decrease in room temperature impact. More specifically, it appears that the embrittled state is associated with the third stage of tempering. A more complete analysis of these observations together with results on SAE 4330 and SAE 4340 will be presented in the near future.

Written Discussion: By A. H. Geisler, General Electric Research Laboratory, The Knolls, Schenectady, N. Y.

The authors are to be commended for attempting the difficult operation of correlating structure with properties in order to understand the behavior of a complex material. Unfortunately, there are several pieces of information yet to be desired. Perhaps the most important is the detection of a truly coherent form of the carbide precipitate. It should be pointed out that some of the favorite techniques which are currently being used to prepare samples for diffraction studies would be expected to be wholly inadequate for detecting coherent precipitates. Since coherency depends upon the constraining effect of the matrix surrounding a precipitate particle, then any technique in which the matrix is removed wholly or in part would alter the state of strain in the precipitate. Thus extraction techniques for X-ray diffraction studies and relief etching techniques for electron diffraction studies cannot be regarded as reliable in revealing the character and behavior of coherent precipitates. This conclusion is not intended to be a specific criticism of the authors' paper but more as a caution concerning the general use of these techniques, which has been pointed out in other discussions. A more reliable practice for obtaining maximum intensity in X-ray diffraction consists of studying the reaction products formed in single matrix crystals.

*Contract No. AF33 (038)-22371.

⁵D. J. Blickwede and M. Cohen, "Isolation of Carbides From High Speed Steel", *Transactions, American Institute of Mining and Metallurgical Engineers*, Vol. 185, 1949, p. 578.

Authors' Reply

We wish to thank the discussers for their comments.

Dr. Lement has estimated the grain size of the outlined areas in the photomicrograph of Fig. 7b to be about ASTM No. 12. A sample of the 2.2% silicon, 3% nickel steel was quenched from 1600 to 1200 °F, held 10 minutes to produce proeutectoid ferrite in the austenite grain boundaries and water-quenched. The size of the outlined grains ranged from ASTM No. 8 to 12. We, therefore, believe that the outlines shown in Fig. 7b are in the prior austenite grain boundaries. The austenitic grain size, as determined in a similar manner for the 0.5% silicon, 3% nickel steel of Fig. 7a, was found to be ASTM No. 6 when the steel was austenitized at 1600 °F. The "ferrite grain size" or the size of tempered martensite plates was, on the average, much smaller in the 2.2% silicon than in the 0.5% silicon, nickel steel.

We agree with Dr. Lement that a grain boundary condition may exist in the 0.5% silicon, 3% nickel steel as tempered at 600 °F, and our statement in the paper should be modified in this respect.

The 600 and 800 °F tempers produced maximum loss of room temperature notch impact strength in the 0.5 and 2.2% silicon, 3% nickel steels, respectively. We regard this embrittlement, in both steels, to be the same as the "500 °F embrittlement" referred to by Dr. Lement. Fractures produced by the latter type of embrittlement are frequently coarse and have been termed "intergranular". This coarseness of fracture suggests some relation of the fracture to the prior austenite grains after tempers which produce maximum embrittlement.

The correlation of mechanical properties with the structural changes which occurred during the various tempering stages in the high silicon steels was intended to be purely speculative. We have been unable to find any evidence, by magnetic or other means, of coherent precipitation or hardening in the high silicon steels after tempers in the range 400 to 600° F.

As Dr. Geisler has indicated, all speculation must be qualified by the lack of proof of a coherent condition in the epsilon carbide. In fact, the original postulation of Jack, concerning the coherent nature of the epsilon carbide, was based on deductions from X-ray patterns obtained from polycrystalline samples. Further evidence that the epsilon carbide is in reality a coherent precipitate would be desirable.

We believe that Dr. Lement's interpretation of the hardness changes in the high silicon steels is more nearly correct than ours. Our idea concerning the effect of retained austenite on the hardness of the high silicon steels would, of course, be wrong according to Dr. Lement's interpretation of the hardness data.

Unfortunately, we do not have any information as to the carbon content of the martensite which is in metastable equilibrium with the epsilon carbide at the end of the first stage of tempering, as requested by Messrs. Barnett, Frohberg and Troiano. Such information for the high silicon steels as tempered in the 400 to 600 °F range would be desirable, since it seems likely that considerable solution of the epsilon carbide may occur in these steels prior to the formation of cementite.

The electron diffraction technique described by Messrs. Boswell and Cunningham might be of further value in the study of the solution of epsilon carbide in the 2% silicon steels. Thus, samples of these steels as tempered in vacuo in the 400 to 600 °F range should indicate epsilon carbide and ferrite in relief when studied by the latter technique.

Messrs. Barnett, Frohberg and Troiano report that they were able to extract the epsilon carbide from samples of SAE 2340. We find this to be interesting, since we were unable to isolate the epsilon carbide by our electrolytic extraction procedure.

MICROSTRUCTURE

(1952 Edward deMille Campbell Memorial Lecture)

BY CYRIL STANLEY SMITH

INTRODUCTION

I REGRET that I did not personally know the man to whose honor this lecture is dedicated. In 1924, as a young immigrant of only a few days' standing, I attended a meeting in Boston of the American Society for Metals (then the American Society for Steel Treating) and I have only one recollection of the entire proceedings—the personality of Professor Edward deMille Campbell, who discussed some of the papers. At that time metallography was at the apex of its growth. Despite the fact that in the intervening years structure on an atomic scale has been of greater novelty and scientific interest, it is perhaps not inappropriate for a Campbell lecturer to re-examine the basis of structure as it exists on a scale adapted to the optical microscope.

Although modern metallography stems from Sorby's work in the 1860's, a consideration of microstructure permeates the writings and thinking of most metallurgists, engineers, and physicists in earlier times, albeit with some uncertainty as to the nature of the structural units. As we discuss in modern terms the structure of metals, it is well to remember that we do this against a background including the preoccupation of the ancient Greeks with the form of things in general, the alchemist's mystic excitement on obtaining the star of antimony, the artisan's age-old use of the appearance of fracture as a test for the uniform quality of his materials, and particularly the experience of the biologist and geologist whose sciences have been built around a sensitivity to the relation between genesis, form, and function.

The tendency of the modern metallurgist to regard the term "structure" as synonymous with "crystal structure" is justified only because in the last twenty years the greatest advances in the science of metals have been in that field. The precise symmetries of the ideal lattice, though of basic importance, are actually less interesting scientifically, less responsible for engineering properties, and certainly less appealing aesthetically than are departures from regularity. It is the study of imperfections—and particularly the patterns of their interaction—that is the most promising field for advance in scientific metal-

This is the Twenty-seventh Edward deMille Campbell Memorial Lecture, presented by Cyril Stanley Smith, director, Institute for the Study of Metals, University of Chicago, Chicago. The lecture was presented October 22, 1952, during the Thirty-fourth Annual Convention of the Society, held in Philadelphia.

lurgy. This lecture will deal with some aspects of their interaction as observable with the microscope.

The very term structure implies interrelation between parts with reference to the whole. Some awareness of the interaction of the varied aspects of structure generally is necessary in order fully to understand any particular structure. I propose, therefore, to discuss briefly the topological, the geometric, and the metric aspects of structure, and finally to show how most of the principal forms of metallic microstructures can be seen to result from the characteristic properties of the various kinds of interface that can be formed between different crystals, and on the very different ways in which these interfaces respond to forces tending to displace them. Some of what follows has appeared elsewhere in more detail, but partial repetition is necessary to present a balanced picture.

MICROSTRUCTURE AND THE REQUIREMENTS OF SPACE-FILLING

An isolated object in space can clearly have any shape whatsoever. If it shares any features with neighboring objects it is less free. The mere fact that a grain boundary in a metal must belong to both of the grains that it separates has some interesting consequences, for it limits the shapes of grains in an aggregate. The general relation in two dimensions between grains, grain boundaries, and grain corners can conveniently be described in terms of the basic topological relation (a form of Euler's Law)

$$C - E + P = 1 \quad \text{Equation 1}$$

where C, E, and P represent, respectively, the number of corners, edges, and polygons in an isolated connected array. The polygons are not necessarily straight-sided figures but may be any two-dimensional features defined by a closed connected set of lines: the relations are unaffected by any continuous distortion, as can be seen in Figs. 1a and 1b which are topologically identical though geometrically different. As discussed in a paper before the 1951 ASM symposium on Interfaces (1),¹ certain special relations come about if consideration is limited to arrays of polygons in which three edges meet at every corner, as is generally the case for metal grains because of grain boundary tension effects. Under these conditions $E = 3/2 C$. Also, since in any two-dimensional net an n -sided polygon contributes $n/2$ edges, except for those forming the periphery of the area under consideration where the edge is unshared by another polygon

$$E = \frac{\sum nP_n}{2} + \frac{E_b}{2} \quad \text{Equation 2}$$

¹The figures appearing in parentheses pertain to the references appended to this lecture.

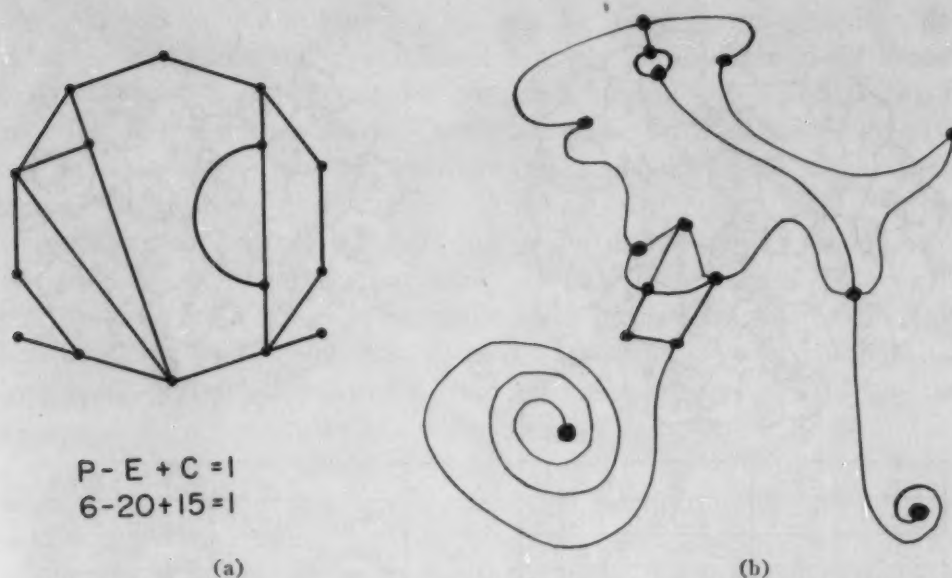


Fig. 1—Two Networks of Lines and Polygons That Are Topologically Identical, Showing That Relations Are Unaffected by Distortion. (Sketch of cyclist at right by Rainey Bennet.)

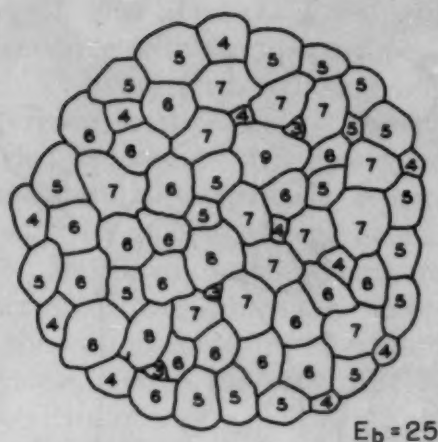
where E_b is the number of unshared edges at the boundary. By combining these relations with Equation 1 it results that

$$\sum (6 - n) P_n = E_b + 6 \quad \text{Equation 3}$$

This is illustrated by Fig. 2, which is a group of grains excised from ASTM grain size standard No. 3 with the "severed" grain boundaries at the periphery artificially reconnected to give only three-ray corners. The complication introduced by the treatment of the periphery can be minimized by considering an infinite array of cells or by selecting a sample of such a nature that it could by duplication continuously fill space, which is equivalent to saying that its severed boundaries must conform topologically to those of a hole cut in a net of hexagons. Such groups will have a peripheral structure such that those corners from which a severed edge originates outnumber by exactly six those peripheral corners that remain normally connected (see Fig. 3, taken from Reference 1, which should be consulted for further information). Within such an extended or properly selected sample not only is the average grain exactly a hexagon but also the number of grains with three, four, five, six, seven, or any number of sides must conform exactly to the relation that

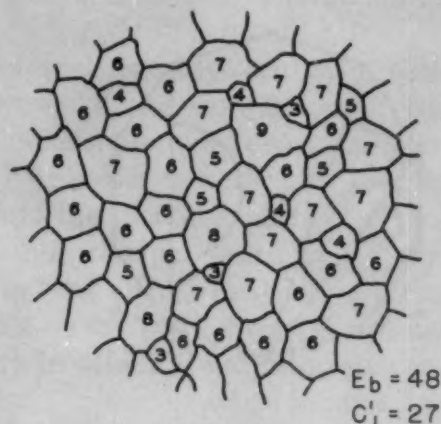
$$4P_3 + 3P_4 + 2P_5 + 1P_6 + 0P_7 - 1P_7 - 2P_8 \dots - (n - 6) P_n = 0 \quad \text{Equation 4}$$

If there is a single seven-sided grain somewhere in the array there must be a five-sided one. A nine-sided grain must be accompanied by a triangular one or by three pentagons or by some other assortment of grains with less than six sides in conformity with the rule.



n	3	4	5	6	7	8	9
(6-n)	3	2	1	0	-1	-2	-3
P_n	3	11	20	20	13	2	1
$(6-n)P_n$	9	22	20	0	-13	-4	-3
$\Sigma(6-n)P_n = E_b + 6$							
$31 = 25 + 6$							

Fig. 2—Microstructure of Polycrystalline Metal Considered as an Isolated Array of Polygons With Only Three-Ray Corners. (From Reference 1.)



n	3	4	5	6	7	8	9
P_n	3	4	5	19	13	3	1
(6-n)	3	2	1	0	-1	-2	-3
$P_n(6-n)$	9	8	5	0	-13	-6	-3
$\Sigma(6-n)P_n = E_b - 2C_i + 6$							
$0 = 48 - 54 + 6$							

Fig. 3—Connected Array of Grains Cut From an Extended Net. (From Reference 1.)

Plane and Curved Grain Boundaries: Grain Shape and Grain Growth

This relation is of interest to metallurgists not only because it so beautifully expresses the basis of grain shape, but also because it immediately shows the reason for grain growth under the influence of the surface tension associated with grain boundaries. Grain growth would not occur if all grain boundaries were straight, for there would be no gain in energy resulting from their motion. The topological relations, of course, are independent of straightness and hold for any amount of distortion, regular or irregular. When, however, they are combined with the geometric requirements of minimum surface energy some interesting facts result. If the boundaries are of equal energy (which to a first approximation is the most likely condition²) then the angles at which they meet at a three-grain corner must, under simple surface tension equilibrium, all be 120° . The corner angle of a regular straight-sided polygon of n sides is $\pi(1 - 2/n)$. If grains were all hexagons, the desired 120° angle could be achieved with plane interfaces. However, the grains in the usual random array are not all hexagons, but there are some with less and some with more than six

²The reader must not overlook the fact that this is a simplification. Many important structural details stem from the fact that grain boundary energy is a factor of orientation, becoming low at small orientation differences and at critical orientations corresponding to twins. Statistically, however, most boundaries in a random polycrystal will be of approximately the same energy.

sides. If the corner angles are to be 120° then those with less than six sides will have to have convex boundaries and those with more than six sides will be concave boundaries, and the stage is set for growth. If the temperature is sufficiently high for diffusion to occur each boundary will move toward its center of curvature to produce a decrease in its area and energy. An isolated circular grain, entirely surrounded by another of different orientation, would shrink at an ever-increasing rate and disappear. Grains in a normal polycrystalline material have boundaries continually intersecting each other and the shrinkage of one boundary means an extension of some others, though, of course, there must be a net decrease in area if growth is to occur. As a triangular grain shrinks and disappears the boundaries of all of the adjacent three grains extend gradually until they join in stable configuration at a single apex. A shrinking four-sided grain, on the other hand, must pass through a point of instability at one of its corners where it joins momentarily with three other grains, providing a four-ray corner which will be followed by rapid readjustment to produce two stable three-ray corners, one of which will belong to a three-sided grain which now can slowly disappear without further instability. These movements are vividly demonstrated by a froth of soap bubbles which is geometrically and topologically almost identical with an aggregate of metal grains (Fig. 4).

In three dimensions the situation is more complicated though the principles are the same. Except for a sphere completely embedded in another grain, the only grain that can shrink and disappear without disarranging its neighbors is the tetrahedron which, as it disappears, leaves the four adjacent grains meeting at a point with the grain edges at the tetrahedral angle of $109\frac{1}{2}^\circ$, each edge being formed by the meeting of three faces at 120° . No plane-faced polyhedron can be made with corners conforming to this arrangement (2). The minimum-area tetrakaidecahedron of Lord Kelvin (3) is apparently the best solution to the problem of space-filling under these conditions, and an array of grains all of this shape would be completely stable, provided the boundary conditions did not introduce instability. In practice, of course, such regularity of shape is rarely achieved and the Kelvin body is known in nature only in biological tissues of unusual regularity (4). It has never been observed in metal grains or soap bubbles.

The basic topological characteristic of a connected aggregate of three-dimensional cells is

$$C - E + P - B = 1$$

Equation 5

where B represents the number of three-dimensional cells and P the number of two-dimensional cells (septa) separating them. It is easily shown that if we limit ourselves to junctions of cells in three dimen-

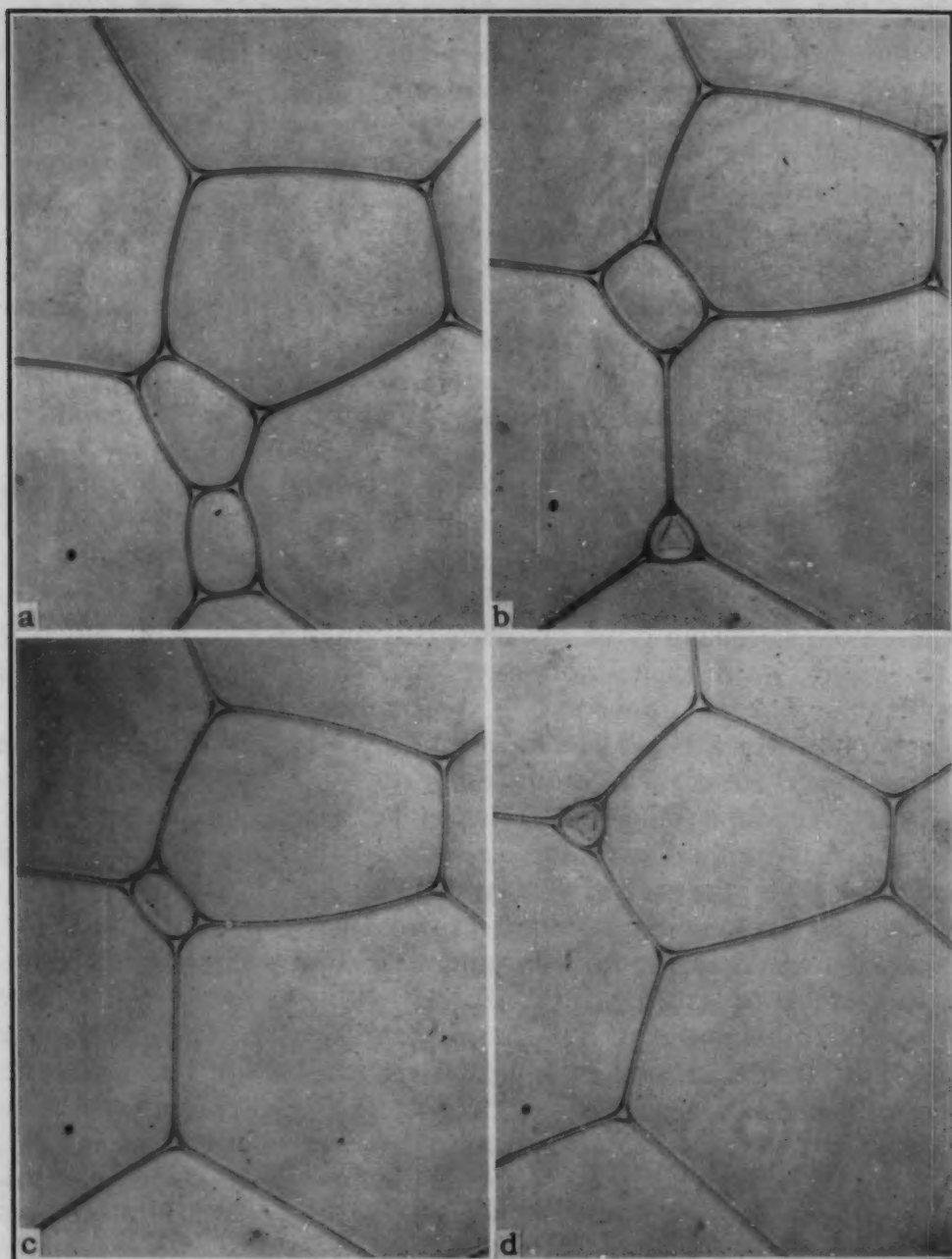


Fig. 4—Successive Stages in the Disappearance of Bubbles by Diffusion. $\times 2.5$.
(Reduced $\frac{1}{3}$ in reproduction.)

sions such that four meet at each and every point (corresponding to the requirements of local surface tension equilibrium) then

$$\sum (6 - n) P_n = 6 (B + 1) \quad \text{Equation 6}$$

Other interesting relations (derived in detail in Reference 1) are that the number of polygons per three-dimensional cell must outnumber the corners by exactly one, and that the average number of edges per polygon tends toward $5\frac{1}{2}$ as the number of corners per

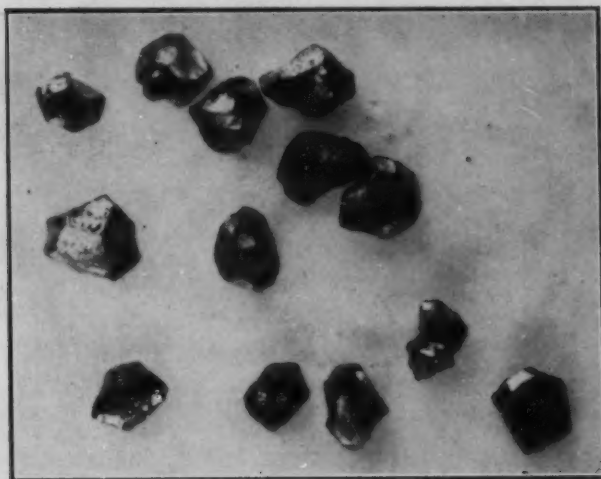


Fig. 5—Grains of β Brass Isolated by Fracture in the Hot-Short Range. $\times 20$.

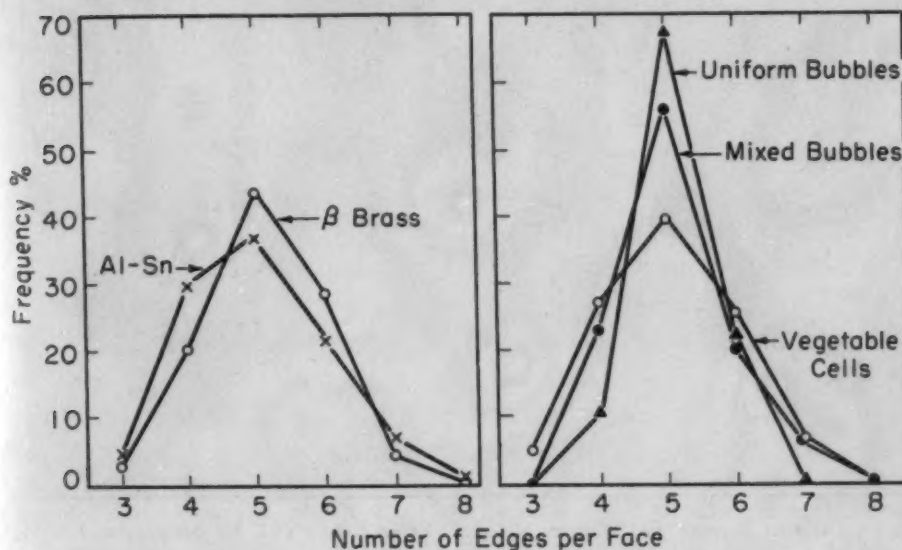


Fig. 5a—Observed Frequencies of Occurrence of Various Polygonal Faces on Grains of Two Alloys, Compared With Those in Soap Froth (8) and Vegetable Cells (7).

cell approaches six, the number corresponding to the configuration of minimum interface area. This queer number—the three-dimensional equivalent of the hexagon in two dimensions—accounts for the prevalence of pentagonal faces in bubbles and grains. This is clearly shown in the appearance of β brass grains (Fig. 5), and by the actual measurements of grains plotted in Fig. 5a which shows the results of Desch (5) (1919) and Williams³ (6) (1952) together with the studies of bubbles and vegetable cells made by Matzke and Nestler

³Williams's studies were made by the use of the important new technique of stereoscopic radiomicrography, which permits one to see clearly the arrangement in space of phases which differ in density or X-ray absorption. It is no longer necessary for the metallographer to limit his thinking to two dimensions, for two X-ray photographs taken at slightly differing angles show the complete spatial disposition of phases with startling clarity. The method awaits only the development of better resolving power with short exposure times to be competitive with or even superior to visual microscopy on anything but single phase systems.

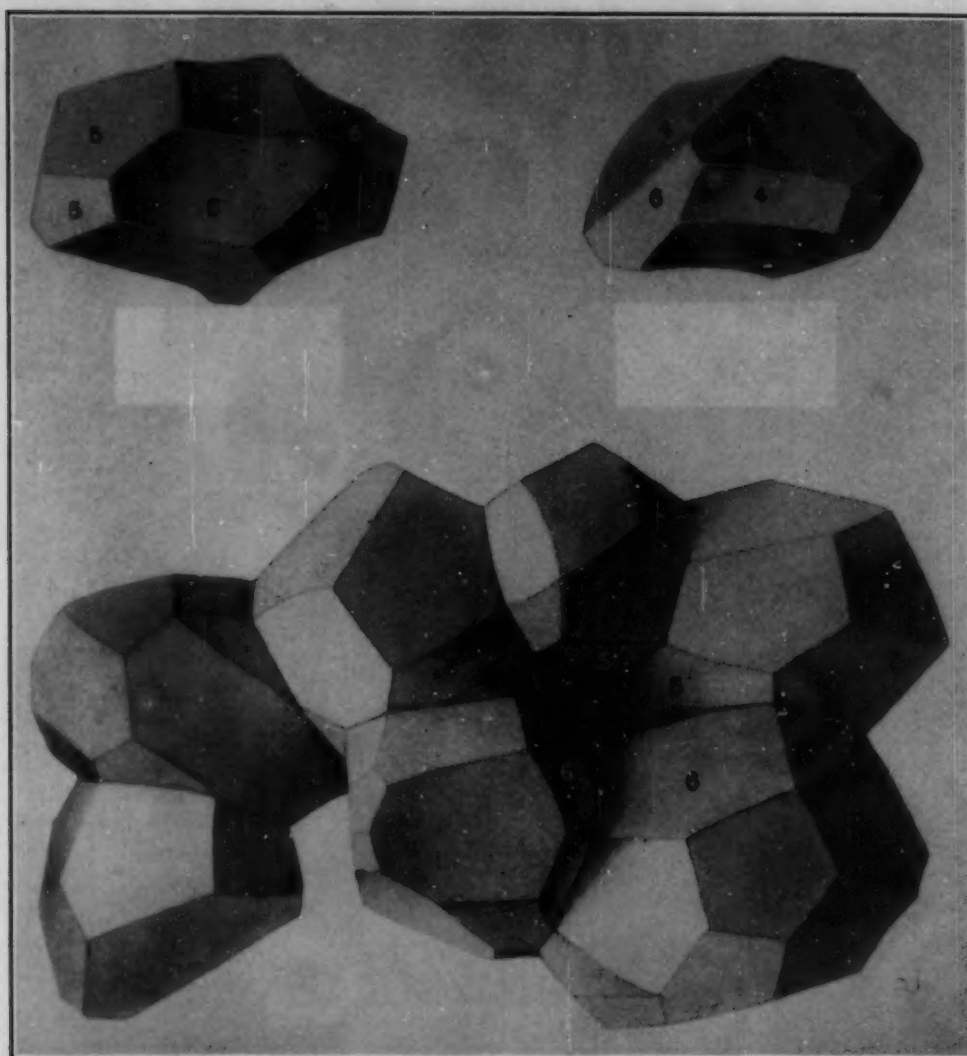


Fig. 6—Cells in Human Fat Tissue, $\times 400$. (From Lewis (9), by permission.)

(7, 8). The human fat cells shown in Fig. 6 [taken from Lewis (9)] would be accepted by any metallurgist as drawings of typical grains. This similarity in shape between such diverse materials serves to emphasize the nature of the basic principles involved. The shape of a metal grain is not primarily a result of the fact that it is crystalline but comes about from the requirement of an approximately minimum area of the interface. It is not the billions of atoms in the crystal body neatly arranged upon their uniform lattice that count; it is the very small number in the disorganized junction between two crystals. Even more important than the matter itself is the necessary interrelation between its one-, two-, and three-dimensional aspects.

A soap froth will continue to grow in average cell size by diffusion of gas from the high pressure bubbles to their neighboring low pressure ones until only plane films or none at all are left. It has been well established that normal grain growth in metals ceases (even

for very long annealing treatments) at a certain maximum grain size which depends on the particular material but is generally about 0.1 to 1 mm. This slowing and cessation of growth is partially due to the presence of inclusions, partially to the fact that grain boundary energy does vary significantly with orientation, and perhaps partially to the fact that as a boundary moves more slowly because of smaller curvature it has a greater opportunity to achieve a structure of lower energy and disorder, hence of still lower mobility.

The effect of orientation differences shows up not only in the possibility of a torque opposing grain boundary rotation but also in that it makes possible stable corners with more than six surfaces meeting at a point. Nine surfaces or more can meet at a point and remain in equilibrium if the new surfaces that would be formed by their rearrangement in a configuration of lower *area* have a higher *energy* than the resultant of the others in its direction. Williams (6) has shown that as many as 4% of the grain corners in a very large-grained aluminum-tin alloy deviate from the surface tension ideal.

Inclusion restraint is independent of energy and depends only on geometry. Though a spherical inclusion will hold back a grain boundary, the maximum force that it can exert is equal to the surface tension acting on a ring at a latitude of 45°, beyond which the boundary will pull away. In essentially two-dimensional grains with one-dimensional boundaries the situation is quite different, for the boundary can become perfectly straight between any pair of inclusions and thereafter its migration must stop. It is unlikely, however, that such action is responsible for the cessation of grain growth in ordinary thin-strip materials (11), for inclusions must be small compared with the thickness, and some other factor must be sought.

SURFACE-TENSION EQUILIBRIUM IN POLYPHASE ALLOYS

In the above discussion of grain growth it was assumed for simplicity that all interfaces in a single-phase alloy are identical in energy and hence that they reach equilibrium at 120°. The writer has elsewhere (12) shown that if there are three different interfaces meeting in a randomly oriented polyphase alloy, they also will establish positions in accordance with simple surface tension equilibrium, in which case the ratio of the sines of the angles between any two interfaces are in the ratio of the energies of the opposite interfaces. In the case of a two-phase alloy there will be grain corners where two crystals of the same phase will meet one of a difference phase: there are two interphase interfaces (identical if we neglect orientation effects) and one single-phase grain boundary meeting at a point (Fig. 7). In this case the equilibrium angle of the included phase is as follows:

$$\theta = 2 \cos^{-1} \frac{\gamma_{11}}{2 \gamma_{12}}$$

Equation 7

where γ_{11} and γ_{12} are the interface free energies of the monophase and duplex boundaries, respectively. Depending on the relative value of these energies the second phase will meet a grain boundary in the first at an angle that can be anything from 0 up to nearly 180°. The angle, called the *dihedral angle*, definitely characterizes a given alloy and can be changed only by influencing the ratio of interface energies. Measurements of these angles in several systems are summarized elsewhere (13, 14).

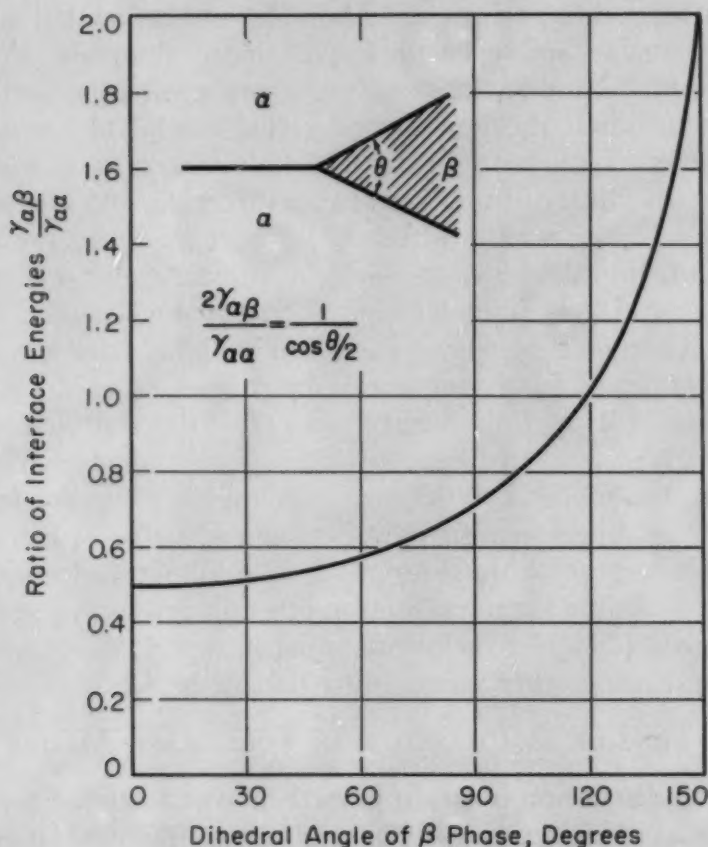


Fig. 7—Curve Showing Variation of Dihedral Angle With Ratio of Interface Energies.

The most interesting structures and resulting mechanical properties occur in the range where the dihedral angle is 60° or less; unless this angle exceeds 60° the second phase must spread continuously along all grain edges forming a single network throughout the entire sample and providing a continuous channel for flow or diffusion. If θ is zero, the second phase will penetrate entirely between the grains. If it is weak, the alloy will be exceedingly brittle, and if it is chemically reactive, the alloy will have wretched corrosion resistance. It is generally a liquid phase that behaves in this way, for the interface between two crystals (except in certain highly critical orienta-

tions) generally has too high an energy. The complete loss of strength that occurs when an alloy is heated to its solidus temperature is well known, though it is not always recognized as being due purely to surface forces. The rapid failure of stressed metal when in contact with a molten one (e.g. stainless steel with brazing solder, or brass with mercury) is another well-known manifestation of the same effect.

To summarize, the structure of an idealized (two-dimensional) two-phase alloy consists of space subdivided into cells according to topological principles, the cells meeting each other at points (averaging six per cell) at each of which three cells meet, the angles at the corners corresponding to surface-tension equilibrium. The junction points are of three kinds, namely those corners formed of grains of the same kind (in which case the angles are 120° regardless of which phase is concerned), those corners formed by two grains of the first kind and one of the second, and lastly, those formed by two grains of the second phase and one of the first. Although the mixed phase corners both involve two two-phase boundaries of identical character, the dihedral angle will be different if the third boundary, the monophase grain boundary, differs in energy. These factors are clearly seen in the microstructure of the alpha-beta bronze (Fig. 8). (The rather conspicuous twin boundaries are not involved in this discussion: These are low energy boundaries, immobile under surface-tension forces.) If the second phase is liquid, there will obviously be only one kind of two-phase corner, while if $\theta \leq 60^\circ$ there will be no single-phase (120°) corners, and there will be no grain contacts whatever if θ is zero. If particles of one phase are not in contact with grain boundaries of another but are entirely embedded within a single grain, the interface in seeking the lowest energy configuration will seek minimum area and the particle will become circular even though it be solid.

The details of the actual shape will depend partly on the historical accidents determining the number of neighbors that a given grain possesses; curvatures must arise to reconcile the necessary corner angles with the number of corners on any grain. As the relative amounts of the two phases change, or their relative grain sizes, the general appearance of the microstructure will change because of the *number* of contacts of different kinds; nevertheless, the *angles* will stay constant and the structure must always be built up by connecting only three kinds of corners.

The typical metallographer's section of a piece of metal, though two-dimensional, does not represent a two-dimensional equilibrium structure but rather is an approximately random section through a three-dimensional network of surfaces meeting at the correct angles. The corner angles that can be measured under the microscope are, therefore, not all identical with the true dihedral angle as it exists in



Fig. 8—Microstructure of Two-Phase Alloy Showing Different Types of Grain Junction ($\alpha\beta$ Copper-Tin Alloy, 16% Sn, Annealed 16 Hours 650 °C and Quenched). $\times 250$.

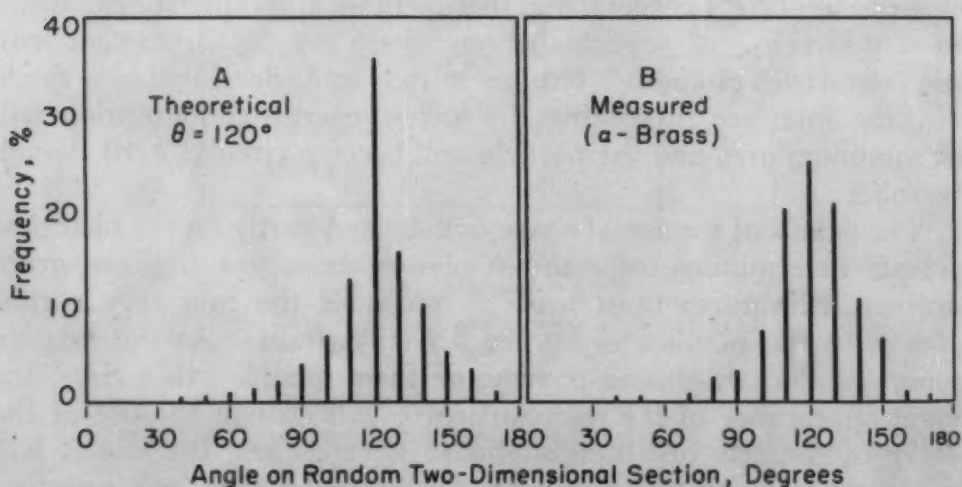


Fig. 9—Distribution of Dihedral Angles Resulting From Random Sectioning. (a) Theoretical; (b) Observed.

three dimensions but actually may vary from 0 to nearly 180°, depending on the orientation of the sectioning plane with respect to the true dihedral angle. This is capable of statistical analysis, and it turns out that actually the true angle is also the most probable one (12). Actual measurements of grain corner angles in a typical single-

phase alloy (α brass) are shown in Fig. 9, compared with the theoretical distribution resulting from random sectioning for a single dihedral angle of 120° . The wider distribution of the experimental data in the vicinity of 120° shows that the picture advanced above is somewhat idealized, and suggests that either there is an appreciable variation of interface energy with orientation, or that there is failure to achieve equilibrium. The latter is not a factor in ordinary well-annealed samples (15), but the orientation effect is important. The measurements of Chalmers (16) and Dunn *et al* (17), as well as the theoretical treatment of Read and Shockley (18), show why this

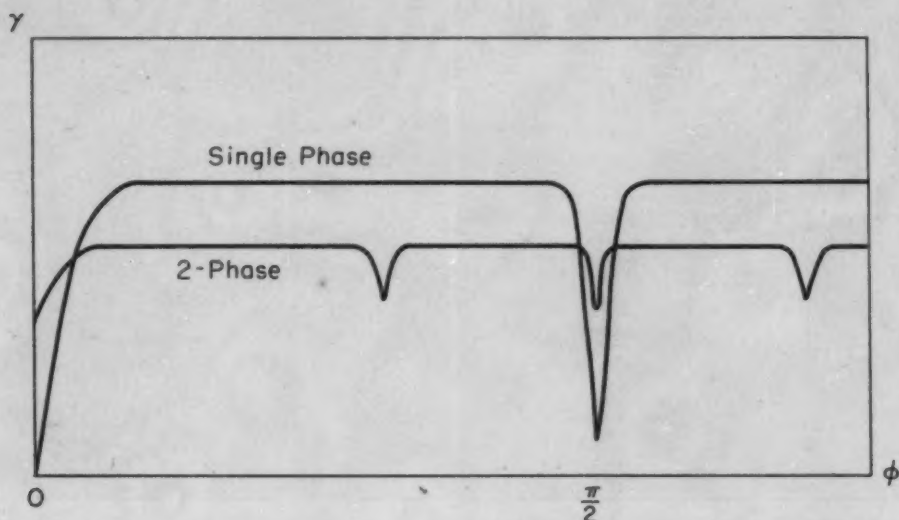


Fig. 10—Hypothetical Curves Illustrating Variation of Grain Boundary Energy With Orientation Between Crystals.

should be so. Nevertheless, to a good first approximation the simple fluid interface theory is applicable in structures of normally worked and recrystallized material, for in such randomly oriented structures there is only a small probability that two grains will meet each other at an angle that gives a boundary of low energy.

Structures With Anisotropic Interfaces

Although there is no experimental evidence, the variation of energy of a grain boundary symmetrically oriented between two crystals as they rotate around one axis from identity to a twinning position must be somewhat as shown in Fig. 10. Structures strikingly different from the simple foam structures result in polycrystalline structures if the grains are not randomly oriented but meet each other at those angles that critically correspond to low interface energies. The straight lines of annealing twins are perhaps the most familiar manifestation of this. These boundaries have only a small fraction of the energy of normal grain boundaries and hence have very little

effect on the latter where they intersect them, but this low energy pertains only to boundaries exactly oriented (both as to the plane of the boundary itself as well as the orientation of the two crystals it separates) so that a high "torque" resists any attempt to move it,

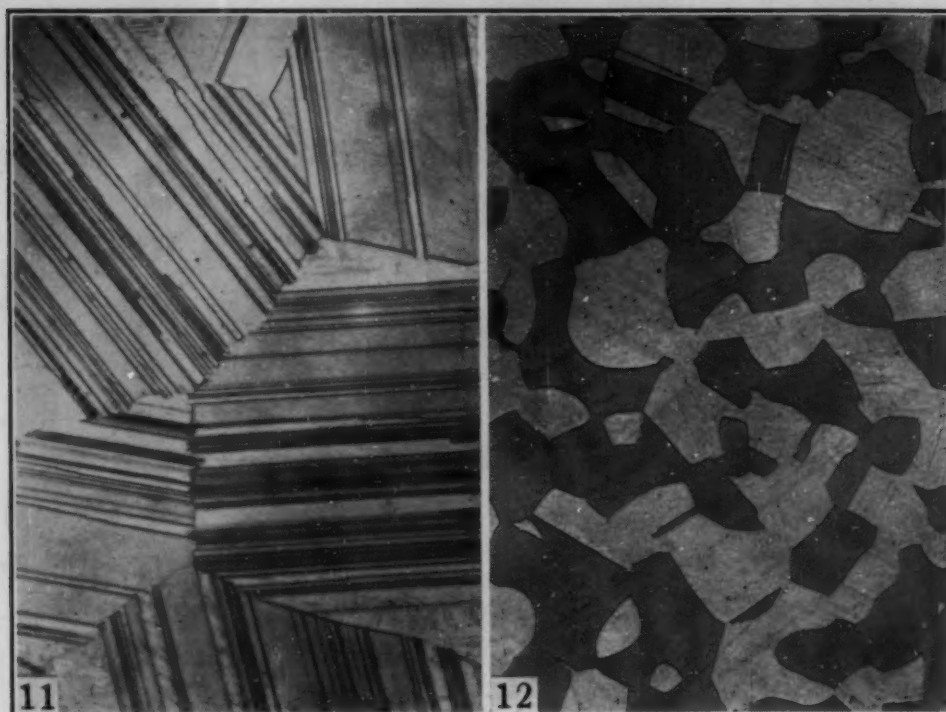


Fig. 11—Oriented Two-Phase Structure in $\alpha\kappa$ Copper-Silicon Alloy (5.54% Silicon, Annealed 750 °C, Then 5 Hours 793 °C and Quenched). $\times 500$.

Fig. 12—Random Two-Phase Structure in Same Alloy as Fig. 11. (Produced from random $\alpha\beta$ structure at 845 °C, cooled to 826 °C and quenched.) $\times 100$.

(Figs. 11 and 12 from *Transactions*, American Institute of Mining and Metallurgical Engineers, Vol. 137, by permission.)

and the structure must be highly geometric. Annealing twins in face-centered cubic metals form planes that cannot be displaced either by surface or mechanical forces. Mechanical twin boundaries in hexagonal and tetragonal metals are of higher energy, more easily moved and less critically dependent upon exact orientation.

In two-phase alloys, when the requirement of randomness is not met, strikingly different structures result. If, in precipitation or transformation, a nucleus of new phase is free to select its orientation within a parent crystal, it will generally appear in one of the critical orientations in which the interface has a low energy, and it will generally grow in a more or less geometrical shape which cannot change without a considerable increase in interface free energy. The sharp concentration gradients at edges favor lateral extension, to produce the plate-like Widmanstätten structures first studied in detail by Mehl and his collaborators (19). The common occurrence of such struc-

tures undoubtedly served to blind metallographers to the simplicity of the fluid-like surface tension rules which apply to randomly oriented structures. The striking difference between micrographs of the same α/κ copper-silicon alloy as shown in Figs. 11 and 12 is solely due to the precise orientation relations across the α/κ interface in the first and its random orientation in the second structure. If an alloy with a Widmanstätten structure is annealed, there is generally little change in shape, confirming the fact that despite its high interface area it is of low interface energy, which is only possible for certain exactly specified orientations. If the orientation relation between the two phases is upset, the boundary will no longer be in a critical orientation, its energy will not vary much as it rotates, and it will seek the low area forms corresponding to the equilibrium of simple fluid interfaces, with smoothly rounded surfaces meeting each other at the appropriate dihedral angles.

That a very slight orientation change will produce this effect is shown in Figs. 13 to 16 which represent an α/β brass after various treatments. Fig. 13 shows a microstructure after cooling from the β phase field to 700 °C to cause precipitation of α phase in a typical Widmanstätten form. Fig. 14 shows that even after annealing for 48 hours at 700 °C the α grains, though larger, maintain their anisotropic shape. However, the alloy of Fig. 15, which was cold-worked only 5% and annealed 2 hours at 700 °C, shows a totally different arrangement of α because the orientation has been slightly changed and the interface is now free to adjust without regard to exact spatial directions. Since this slight working has not caused extensive recrystallization of the β phase, many α particles find themselves completely isolated and approach a spherical shape under surface tension forces. Others have dihedral angles where grain boundaries in either α or β are involved. Fig. 16 shows the same alloy cold-worked more extensively—33%—before reannealing, producing more extensive recrystallization in the β phase. The contrast between Figs. 14 and 15 is most striking and results from presumably small orientation changes.

Distribution of a Minor Liquid Phase in a Polycrystalline Matrix

The case where the second phase is liquid is particularly interesting. The dihedral angle in various systems can be anywhere from 0 to very nearly 180°; in general, the more similar in composition the liquid is to the solid the lower the energy of the liquid/solid interface and hence the lower the dihedral angle. In a liquid there can be no grain boundaries, so there is one less type of corner possible than in an alloy with two solid phases. The structure, as seen on two-dimensional sections, is composed of arcs of solid/liquid interface smoothly connecting points where they join each other in pairs, meeting a grain boundary at the proper dihedral angle. If θ is greater

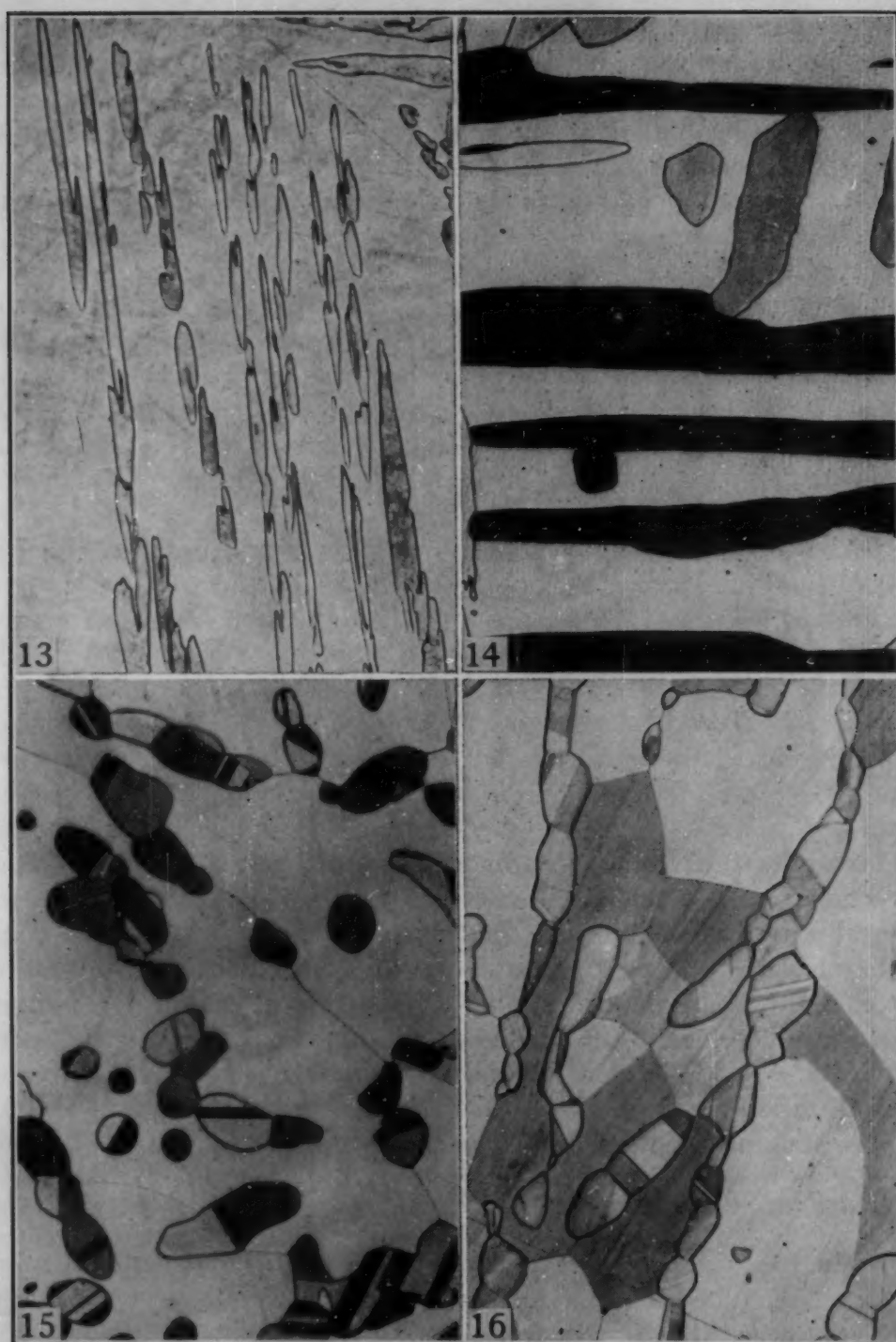


Fig. 13—Microstructure of 60-40 Brass Slowly Cooled From 850 to 700 °C and Quenched to Give Widmanstätten Precipitation of α . Etched $\text{NH}_4\text{OH} + \text{H}_2\text{O}_2$. $\times 100$.

Fig. 14—Same Sample as Fig. 13, Held 48 Hours at 700 °C Before Quenching. $\times 100$.

Fig. 15—Microstructure of $\alpha\beta$ Brass Treated as in Fig. 13, Subsequently Cold-Rolled 5% Reduction and Reannealed 4 Hours at 700 °C. $\times 100$.

Fig. 16—Microstructure of $\alpha\beta$ Brass Treated Same as Fig. 15, Except for 33% Reduction Before Last Anneal. $\times 100$.

than 60° there will be some corners with three grains meeting each other at 120° ; if θ is less than 60° there can only be $\alpha\alpha\text{L}$ -type junctions, while if θ is 0, grain boundaries must entirely disappear and the structure consists of individual crystals entirely isolated from each other by rounded liquid films. If the volume of liquid is sufficiently great the grains will become spherical or as nearly so as the variation of liquid/solid interface energy with orientation will allow. When the liquid content is limited it will, provided the dihedral angle is 0, spread first over the grain boundary to form a two-dimensional film no thicker than that necessary to give low surface energy, and the excess will collect at grain corners, rounding them off to a degree permitted by the volume of liquid present. As with other simple metallurgical structures, soap bubbles serve as an illustration. Figs. 17 a-d show a two-dimensional array of soap bubbles in a cell with an increasing amount of liquid: this can be seen to fill out the three-bubble corners, decreasing their curvature while the thickness of one-dimensional contact between the grains away from the corners remains more or less unaffected.

In most close-packed metals the equilibrium shape of the crystal in a liquid not greatly differing in composition and at high temperatures is nearly spherical, although at low temperatures in liquids of greatly different composition the forms may become strongly angular. In crystals with strong homopolar or ionic binding the interface energy may be strongly anisotropic and the equilibrium shape hence far from spherical.⁴ The great difference in shape between titanium carbide and tungsten carbide in the usual cobalt binder is almost certainly due to such anisotropy in the latter, but not the former case.

If the liquid/solid energy is only slightly less than half the average grain boundary energy, very slight changes in the latter will have a large effect on liquid continuity. For example, in copper-bismuth alloys although the highest grain boundary energy gives a zero dihedral angle, there is a fair fraction of boundaries—about 45% in a typical randomly oriented recrystallized alloy—that do not have liquid films and hence correspond to positive dihedral angles. In a truly random alloy the fraction is just the probability that two grains will meet at an angle less than that at which the curve of boundary energy versus orientation exceeds twice the solid/liquid interface energy. This depends both on the boundary and on the composition of the liquid and different alloys differ greatly. For example, a zinc-rich zinc-cadmium alloy, annealed at 338°C to contain a small amount of eutectic (Fig. 18), has about 70% of boundaries free from liquid, while a cadmium-rich alloy under the same conditions has only about 30%.

⁴For an excellent discussion of equilibrium shape of crystals under anisotropic surface energy, see Conyers Herring (20).

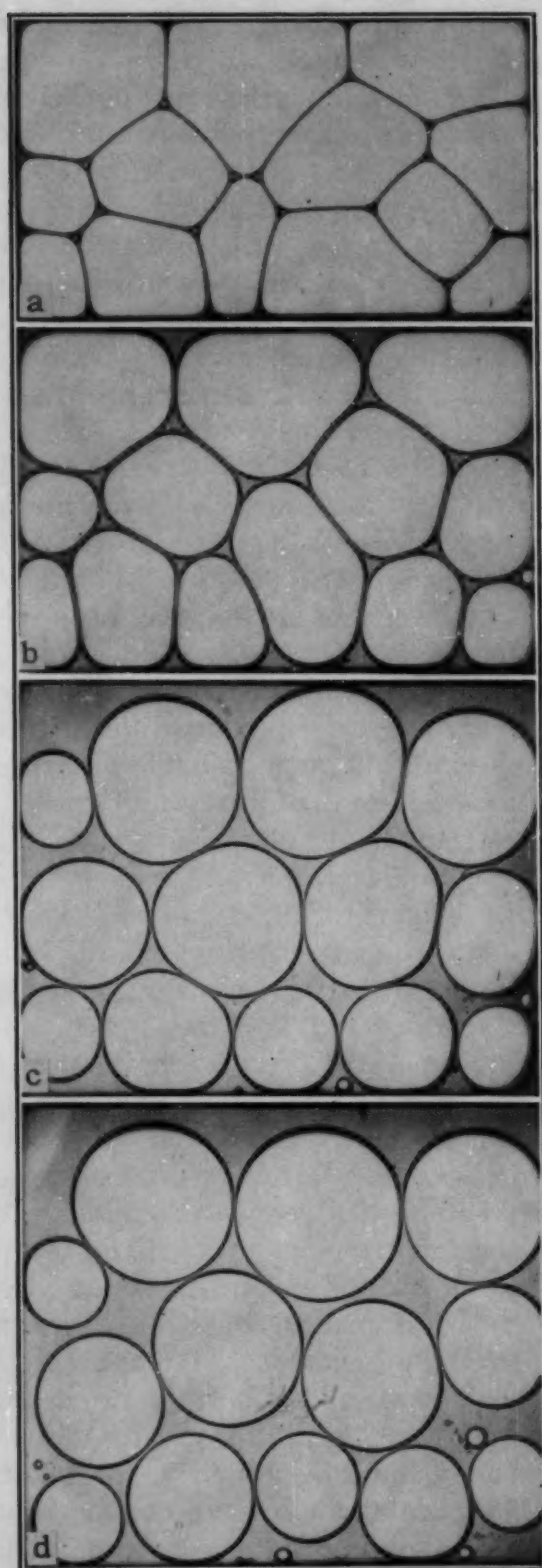


Fig. 17—Appearance of Soap Bubbles in Two-Dimensional Cell With Increasing Fraction of Liquid Phase.

Grain Boundary Melting

Although the idea of a thick amorphous metal boundary is generally untenable, it seems highly probable that high energy boundaries (those beyond the range where the simple dislocation model applies) have a structure not greatly different from that of a layer of liquid approximately one or two atoms thick, and that it can pass continuously into normal three-dimensional liquid as the solidus temperature is approached.

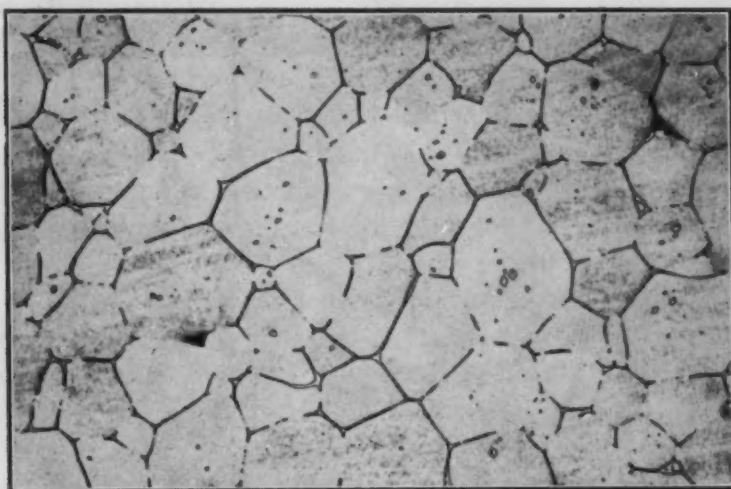


Fig. 18—Microstructure of Zn-Cd Alloy (5% Cd) Cold-Rolled and Annealed 20 Minutes at 338 °C. Nital etch, $\times 100$.

In pure metals and in alloys where solid and liquid do not greatly differ in composition the solid/liquid interface energy is always less than half the grain boundary energy, and at the melting point, the total interface free energy of the system is less if liquid replaces the boundary and separates the grains. At temperatures below the true melting point of a large single crystal it is possible to use some grain boundary free energy to provide the free energy needed to melt a small volume of liquid.

The free energy needed to produce a mole of liquid is zero at the normal melting point and at other temperatures it can be obtained from the thermodynamic relation (with pressure constant)

$$\frac{\partial \left(\frac{\Delta F}{T} \right)}{\partial \left(\frac{1}{T} \right)} = \Delta H \quad \text{Equation 8}$$

where ΔH is the heat of fusion. Assuming ΔH to be constant over a short temperature interval (i.e. assuming $\Delta C_p = 0$), and integrating

$$\frac{\Delta F}{T} = \Delta H \left(\frac{1}{T} - \frac{1}{T_m} \right) \quad \text{Equation 9}$$

or

$$\Delta F = \Delta H_m \frac{T_m - T}{T_m} = \Delta H \frac{\Delta T}{T_m} \quad \text{Equation 9a}$$

This is free energy needed per molar volume of liquid.

Consider first the surface free energy that can be obtained by replacing the portion of the boundaries where three grains meet along an edge with small arcs of solid/liquid interface,⁵ as in Fig. 19, the

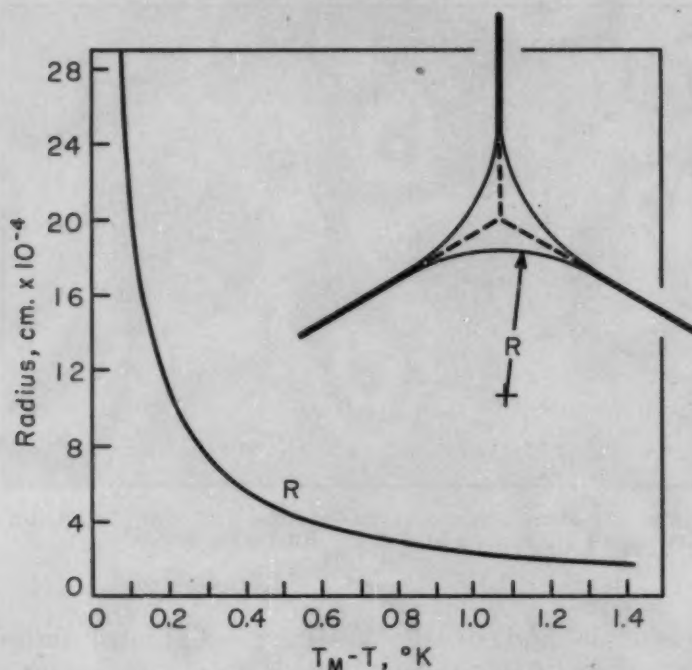


Fig. 19—Replacement of Grain Corners by Liquid at Temperatures Below the Melting Point.

volume between them being filled with liquid. The available free energy from this change of interfaces is, per centimeter of grain edge

$$\Delta F = R (\sqrt{3}\gamma_{ss} - \pi\gamma_{sl}) \quad \text{Equation 10}$$

By equating this to the free energy needed to form the liquid in the intervening space and which has a volume of $R^2 \left(\sqrt{3} - \frac{\pi}{2} \right)$ per cm. length of grain edge, we get

$$R (\sqrt{3}\gamma_{ss} - \pi\gamma_{sl}) = R^2 \left(\sqrt{3} - \frac{\pi}{2} \right) \cdot \frac{\Delta H_m \Delta T}{T_m} \frac{\rho}{M} \quad \text{Equation 11}$$

⁵The author wishes to thank Dr. Harvey Brooks of Harvard University and Dr. John Fisher of the General Electric Company who independently called the author's attention to the correct manner of this calculation, which he had previously given erroneously. Discussions with L. Guttman and J. W. Stout of Chicago have also been most helpful.

or

$$R\Delta T = \frac{(\sqrt{3}\gamma_{ss} - \pi\gamma_{sl})}{\left(\sqrt{3} - \frac{\pi}{2}\right)} \frac{T_m M}{\Delta H_m \rho} \quad \text{Equation 12}$$

It should be noticed that no liquid will appear at the grain edges unless $\frac{\gamma_{sl}}{\gamma_{ss}} < \frac{\sqrt{3}}{\pi}$ or 0.5513, which corresponds to a dihedral angle of 50°.

If appropriate values for copper,* are substituted in Equation 12, $R\Delta T = 2.23 \times 10^{-4}$ cm., which is plotted as a function of ΔT in Fig. 19. The radii are far from negligible.

By similar arguments one could deduce the extent to which the apices of four grains are rounded and replaced by liquid where they meet. The calculation is difficult because of the complicated shape of the nearly spherical surfaces involved, and is of trivial value.

The two-dimensional boundary is more difficult to treat than the grain corner because volume adjustments are possible through lateral displacement. As Chalmers (21) has so clearly pointed out, it is energetically costly to have, at temperatures below the equilibrium melting point, a thickness of liquid between two crystals that exceeds the distance over which the effect of lattice forces is felt through the liquid. The simple analysis of Speiser and Spretnak (22) is erroneous in that it assumes that the whole free energy resulting from the replacement of a high energy grain boundary with two other interfaces of lower energy is available for producing a second phase. Actually, although no second phase can appear unless such free energy is available from the change in interfaces, the system can always find a solution of still lower energy at the point of balance between increasing volume free energy and decreasing interface energy as the crystals separate.

Consider the transition from a grain boundary to three-dimensional liquid as the temperature increases to the melting point. As a simple model the energy may be divided into volume and surface terms, although in reality the two must be interdependent and inseparable, for both terms will depend upon the distance between the opposing crystals, i.e., on the effective thickness of the boundary material. The volume term, representing the change of free energy on passing from solid to liquid, is zero at the melting point and increases at lower temperatures in accordance with Equation 10. At a given temperature the energy required to produce liquid will increase linearly with volume, or with thickness if we consider its relation to unit projected area. Values appropriate for copper at various temperatures below the melting point are plotted in Fig. 20. The surface term can be regarded as passing from slightly less than the normal low-temperature

* $\gamma_{ss} = 575$ erg/cm², $\Delta H_m = 1.7 \times 10^{10}$ erg/cc
 $\gamma_{sl} = 177$ erg/cm², $M = 63.6$ gm, $\rho = 8.4$ gm/cc
 $T_m = 1356$ °K

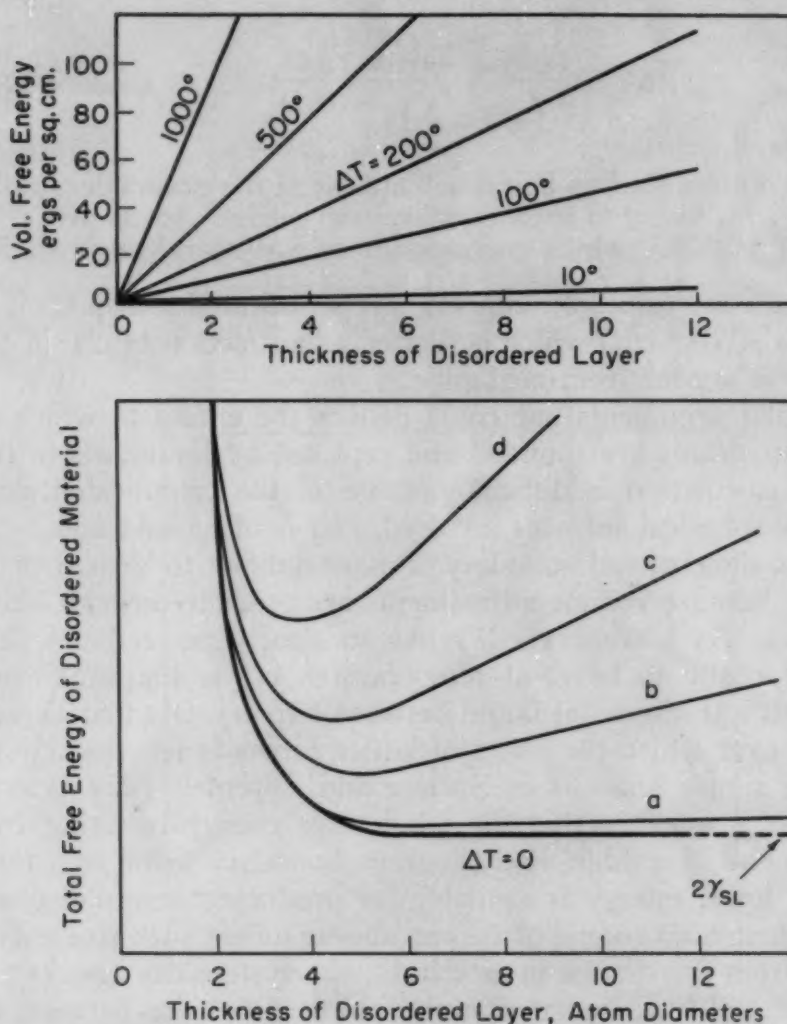


Fig. 20 (Upper)—Volume Free Energy Required to Produce Liquid as a Function of Thickness and Temperature.

Fig. 21 (Lower)—Schematic Variation of Grain Boundary Energy With Thickness at Various Temperatures Below Melting Point.

grain boundary energy at the appropriate small spacing to twice the solid/liquid interface energy at large spacings. To the extent that it exceeds the latter figure it is a measure of the interaction between the opposing lattice forces, and is in essence a microscopic strain energy. Though nothing is known of this, it seems reasonable to suppose that it increases exponentially as distances decrease below one or two atom diameters, and that it becomes negligible at spacings beyond about ten atoms. The heavy curve in Fig. 21 represents schematically such behavior. The total free energy of the system is equal to this surface term plus the volumetric term of Fig. 20, giving the total free energy of the boundary as shown for the curves at various values of ΔT , as in Fig. 21. The system will adjust itself to the minimum free energy at any temperature which, it will be seen, progres-

sively increases as ΔT decreases. At temperatures only slightly below the melting point where the slope of the volume free energy term is very small, the minimum free energy must correspond to thicknesses only slightly less than twice the maximum range of lattice forces in the liquid.

On this highly qualitative model one would expect a decrease in grain boundary energy and an increase in effective thickness at a rate reciprocally dependent on the difference between the temperature and the true melting point of the material. The effective viscosity of the grain boundary in shear would vary with temperature almost precipitously near the melting point, and could easily account for the pre-melting grain boundary weakness studied by Chalmers (23).

In alloy systems the composition of the liquid will differ from that of the solid. If the solid/liquid interface has a high energy and the dihedral angle consequently is not zero, the presence of liquid will have little effect upon the grain boundary of the higher melting phase. If, however, the solid/liquid interface has less than half the grain boundary energy, then a lower free energy will accompany the production of appreciable volumes of liquid at crystal compositions below the single-crystal saturation. In effect, one is balancing available surface free energy against the free energy required for a composition change. Though the latter is not as easily computable as in the pre-melting of a pure substance, as discussed above, nevertheless qualitatively it is known that if the solubility is small the percentage change of concentration resulting from a slight change of free energy is quite large. In most cases a small solubility usually means a liquid differing greatly in composition and a solid/liquid interface energy that is higher than grain boundary energy. Almost invariably when this is not so, peculiar grain boundary effects are observed. Many of the curious cases of grain boundary embrittlement known to metallurgists seem to involve some such factor—the embrittlement of copper containing traces of bismuth, the hot-shortness of iron with sulphur, the concentration of oxygen in copper grain boundaries which renders it so susceptible to hydrogen embrittlement, and perhaps also the influence of boron on the hardenability of steel. It should be noted that the effect will be insignificant if large solubilities exist and will be nonexistent if the solid/liquid interface does not have an energy of less than half of the normal grain boundary energy.

THE MEASUREMENT OF MICROSTRUCTURES

A third feature of any microstructure is its metric aspect, the actual areas and volumes of various constituents and the boundaries between them. Though quantitative microscopic methods were used by petrographers over a century ago and they were applied to metallurgical problems early in the twentieth century, they seem to have

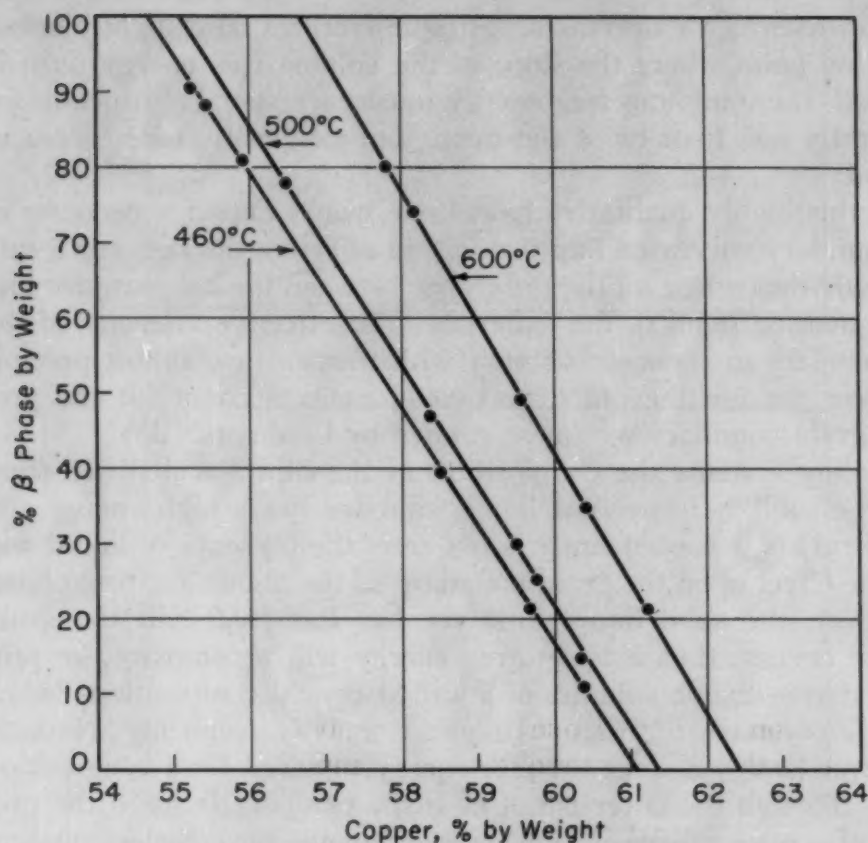


Fig. 22—Results of Metallographic Measurement of β Phase Fractions in Annealed $\alpha\beta$ Brasses as a Function of Composition. (From *Transactions*, American Institute of Mining and Metallurgical Engineers, Vol. 194, with permission.)

been forgotten by metallurgists until their resurrection only five years ago by Morris Cohen (24).

The simplest methods of measurement depend on the probability of intersection of a line randomly traversing the various two- and three-dimensional features of a structure. The volume fractions of various phases are directly in the ratio of the average lengths of traverse across them of a randomly applied line, subject only to statistical errors, which can be made as small as desired. In most metallurgical samples the structure itself is sufficiently random to permit measurements on a single extended two-dimensional cross section. Fig. 22 [from a paper by Beck and Smith (25)] shows how closely the measurements on a series of alloys in a two-phase field conform, as they should, to the well-known lever rule. The amount of a phase varies linearly with composition, and the limits of a two-phase field in a constitution diagram can be determined by linear extrapolation to 100% of each phase. A three-phase field can, in principle, be defined by means of volume measurements on only three alloys. Because there is no nucleation problem and diffusion paths are far shorter, equilibrium is much easier to obtain than in alloys

annealed for the usual bracketing method of establishing phase boundaries.

It is often desirable to know the area of an internal interface, for example, the total area of grain boundaries in a given sample. In the past this has been calculated approximately from the average grain diameter by assuming a certain shape of grain. Guttman and the writer have recently shown (26), however, that the randomness of the metallographer's section provides him with the basis of an easy statistical method for measuring grain boundary areas with no assumptions whatsoever as to shape. The average number of times that

$$\frac{N}{L} = \frac{2}{\pi} \frac{l}{A} = \frac{1}{2} \frac{S}{V}$$

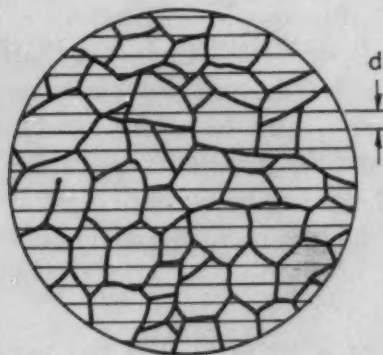


Fig. 23—A Grid Superimposed on a Microstructure for Grain Boundary Area Measurement by Intercept Counting. (From *Transactions, American Institute of Mining and Metallurgical Engineers*, 1952, with permission.)

grain boundaries are intersected by unit length of a line traversing a structure in all directions at random is exactly one-half the ratio of grain boundary area to volume. The average grain volume or average maximum grain diameter can be computed from this ratio only by assuming that all grains are identical in shape and size, which is never actually the case.

In practice, a grid of known length and area can be applied to the structure, as in Fig. 23, at many different angles and the number of intersections recorded. It is also a useful fact that the intercept count (the reciprocal of the average linear traverse across the grain) is exactly $2/\pi$ times the ratio of length of grain boundary as seen on a two-dimensional section to the area studied.

A CLASSIFICATION OF MICROSTRUCTURES

We have discussed above the spatial arrangement, the geometry, and the measurement of microstructures. In what follows an attempt will be made to show how the classical structures of the metallographer

depend primarily on the interfaces involved. Any microstructure is a result of the past history of the system, and structures depend almost entirely on the properties of the nearly two-dimensional interfaces between phases, the manner of their motion, and the diffusion that may or may not occur along them.

The chief characteristics of an interface include its effective thickness, the degree of disorder (i.e. its coherence or lack of it) and the nature of the composition gradient associated with it. There can be a compositional gradient alone, with only minor structural discontinuities, as in the case of coring in a single crystal of a solid solution, and there can be crystallographic continuity or coherence with or without compositional discontinuity and either sharply or diffusely located in space. A coherent or semi-coherent boundary is likely to be strongly anisotropic in structure and behavior, and to have strain associated with it which may affect large volumes of adjacent crystals. An incoherent interface, conversely, tends to be isotropic, of high energy, and to allow ready relaxation along it of both strain or composition gradients. Tables I and II show how structures can be rather simply classified in such terms. There are intermediate cases of all degrees of partial coherence, and examples can usually be found of high, low, and negligible coherence in any type of transformation or alloy.

The photograph of a two-dimensional array of soap bubbles in the Bragg model, Fig. 24, illustrates the structural differences between the two types of interface. The partially coherent boundary (lower

Table I
Types of Interfaces Between Crystals

	Incoherent	Partially Coherent	Coherent
Probable structure of interface	Disordered; essentially a nearly two-dimensional liquid layer.	Largely coherent but with dislocations nearly uniformly spaced and forming nearly two-dimensional array.	No dislocations; gradual strain transition from one lattice to the other.
Nucleation	At grain boundary or by migration together of imperfections in strained lattices. Rarely forms spontaneously.	Fluctuation within crystal.	Fluctuation within crystal.
Manner of motion	Easy movement of atoms, both laterally and across interface.	Movement of dislocations <i>normal</i> to interface (requires diffusion).	Movement of coherent zone of strain normal to interface. (No diffusion involved.)
Restraints to motion	Inclusions and other geometric restraints.	Volume strain energy.	Volume strain energy.
Typical shape of constituent bounded by interface	Isolated crystals are spherical, otherwise polycrystalline foam structure.	Anisotropic; typically plate-like.	Anisotropic, usually lenticulate; rarely plate-like.
In real structures there will exist all intermediate degrees of partial coherence.			

Table II
Classification of Common Structures in Terms of Interface Type

Change Occurring at Interface	Incoherent	Partially Coherent	Coherent
Orientation change only.	Normal (high energy) grain boundary network.	Low energy boundary (polygonization) network.	Twin boundary.
Change in structure only.	Transformation products of pure metals near transformation point.	Transformation products of pure metals at temperatures somewhat below transformation temperature (e.g. acicular ferrite or α titanium).	Transformation far below T_c , martensite.
Change in both composition and structure.	Interphase boundary in randomly oriented (worked and annealed) polyphase, polycrystalline alloys.	Widmanstätten structures. Oriented metastable intermediate phases in precipitating systems (e.g. θ' in CuAl).	Widmanstätten structures. (Perfect coherence rare.) Preprecipitation zones in aged supersaturated alloys.
Laterally duplex.	Eutectoid structures. Discontinuous precipitation.	Bainite (?)	Existence highly improbable.
Gradual gradient in composition.	—	Coring.	—

left) is composed of imperfections (dislocations) clearly interacting with each other through their strain fields, but separated by many "atom" rows of normal structure. The incoherent boundary (top) continues very few atom rows across it, for the majority of atoms in it are of abnormal coordination. Some such structures must exist in the boundaries between three-dimensional metal crystals, for they depend more on geometry and topology than on the precise nature of interatomic forces. The bubble model cannot depict either twins or boundaries between crystals that differ in structure or composition.

The simplest incoherent interface is the high energy grain boundary. Since it is highly disordered it can move easily at high temperatures by individual transfer of atoms to one or the other adjacent crystal lattice. Diffusion along it can easily relax gradients of either strain or composition. If it moves into a strained or supersaturated crystal, the crystal growing behind it will be unstrained and of nearly equilibrium composition. The nucleation of a new crystal surrounded by such an interface can be properly described by conventional nucleation theory, for the volume and surface energy terms are essentially independent, and strain energy is negligible.

A coherent interface involves little interface energy, and it is easily nucleated, but (except in the rare cases of no change in volume or shape) its migration involves an accumulation of elastic strain, and it cannot move indefinitely unless the driving free energy is large. Partially coherent interfaces (most commonly represented by small angle, low energy grain boundaries or by the highly oriented two-phase interfaces that appear in Widmanstätten structures) are intermediate. They have some localized imperfection and can partially

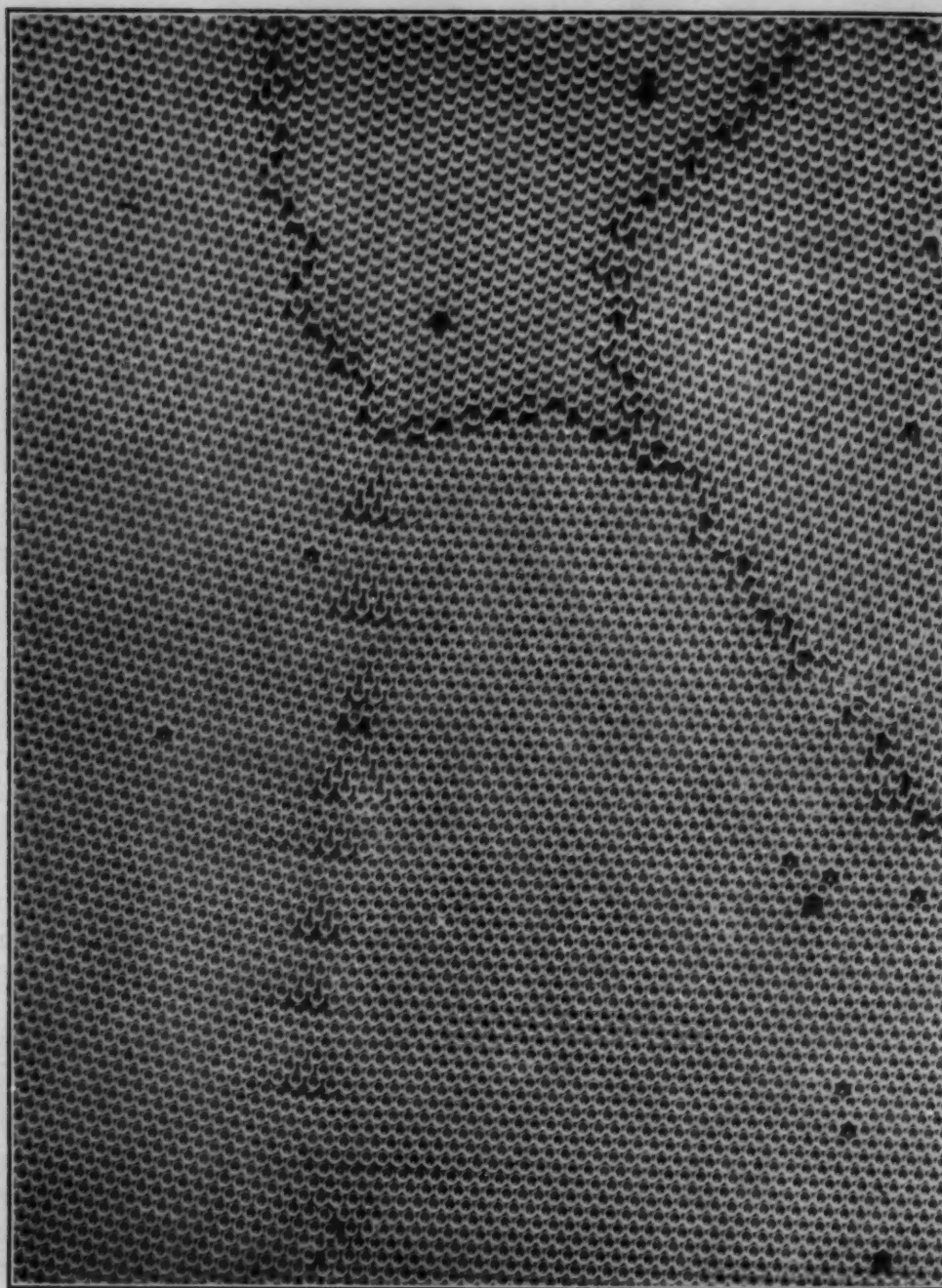


Fig. 24—Coherent and Incoherent Boundaries Between Two-Dimensional Crystals in a Bragg Model. (Reproduced from *METAL PROGRESS*, October 1950.)

relax strain and because of low interface energy they are easily nucleated at temperatures where diffusion is possible.

It is characteristic of the incoherent interface that it is difficultly nucleated; it can be formed by the collection together of many imperfections, as in recrystallization, where many subboundaries join to form a normal high energy boundary. Once such an interface exists, it can move readily. The simplest case of this kind is the grain

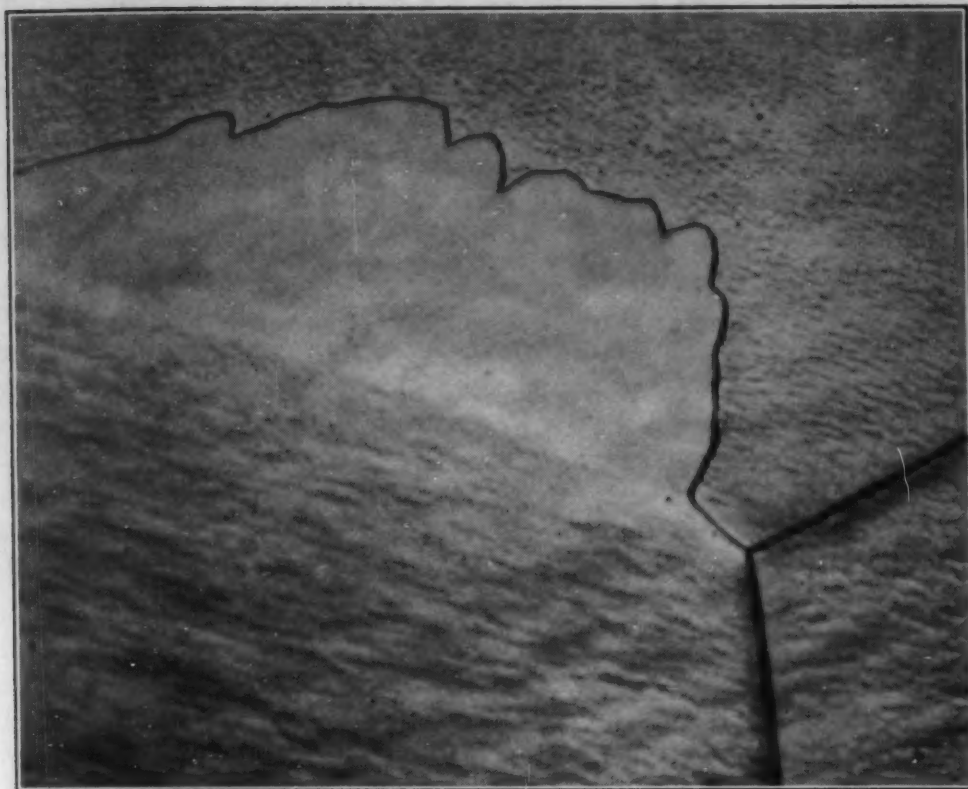


Fig. 25—Grain Boundary Migration in Annealed Slightly Strained Aluminum. $\times 75$. (From *Journal of Applied Physics*, Vol. 21.)

boundary migration that occurs on annealing slightly cold-worked material, as so beautifully depicted by Beck (27, 28). Fig. 25 is taken from one of his papers and shows one slightly strained grain growing into its neighbor. Though there is an increase of normal grain boundary area, there is a much larger decrease of invisible low angle boundaries (the interacting networks of dislocations resulting from "recovery" of plastic and elastic strain) and a net decrease of free energy. As the disordered boundary sweeps along it allows complete reconstitution to occur. All strain is relieved and the atoms are deposited on the crystal behind the advancing boundary in equilibrium lattice positions. It is important to realize that this must happen entirely in the almost two-dimensional disordered zone and is possible only because of the existence of extreme disorder there. The movement of a partially coherent interface cannot accomplish reconstruction.

Interface Motions During Transformation

If a transformation is to occur giving rise to a new phase separated from its matrix by an incoherent interface, this will appear most easily at a grain boundary. Though it is probably nucleated by a coherent fluctuation in a crystal, its continued coherent growth would involve increasing strain and require considerable free energy for its

propagation to significant size. However, if such a fluctuation occurs near a grain boundary it can grow into the *adjacent* grain with which it is not coherent with only the small amount of energy that is necessary to change the curvature of a nearly flat interface.

Consider Fig. 26 which shows schematically a grain boundary between two triangular close-packed lattices with an area of square lattice formed mostly coherently within the left grain. If the square lattice represented a nucleus of a stable new phase in the vicinity of the grain boundary, it could grow into the grain in which it had formed only if the change of free energy resulting from the transformation was sufficient to overcome the increasingly high elastic strain energy that opposes its growth. It could, however, grow into the right grain by the movement of the disordered interface, which would leave behind it an increasing area of equilibrium square material without increasing strain. The rate would depend on diffusion along the interface, and have little relation to volume diffusion. There would be no orientation relation between the new phase and the matrix grain in which it is growing, except for the *avoidance* of coherent orientations. At temperatures increasingly below the transformation temperature, diffusion will become slower, but the free energy change is higher and strain becomes less of a barrier, and coherent forms are thereby increasingly favored. The various configurations of proeutectoid ferrite in steels discussed by Mehl (29) agree with this viewpoint: Widmanstätten forms appear only at large undercooling. Similarly, it would be anticipated that Widmanstätten structures would be less common in transformations that occur on heating, for increasing ΔF is then accompanied by increasing diffusion which favors the incoherent boundary.

The above relates to changes of structure alone, but the same principles apply when there is also a change of composition.

Interfaces and Precipitation

In most solid solutions it is possible to have small zones differing in composition from the average but maintaining complete continuity of all lattice planes, i.e., with completely coherent interfaces. This is usually the first stage in precipitation from a supersaturated solid solution. The requirement of coherence generally necessitates a gradual gradient in strain and composition, and there will be no crystallographic imperfections. Lattice strain increases with the size of these zones, and it will often happen that beyond a certain size the aggregations will be able to maintain nearly perfect coherence only on one plane and will break it on others either by the generation of dislocations or by their migration to the appropriate place in the lattice. Such is the nature of the θ' phase in aged copper-aluminum alloys: it can form only when the interface has become partially

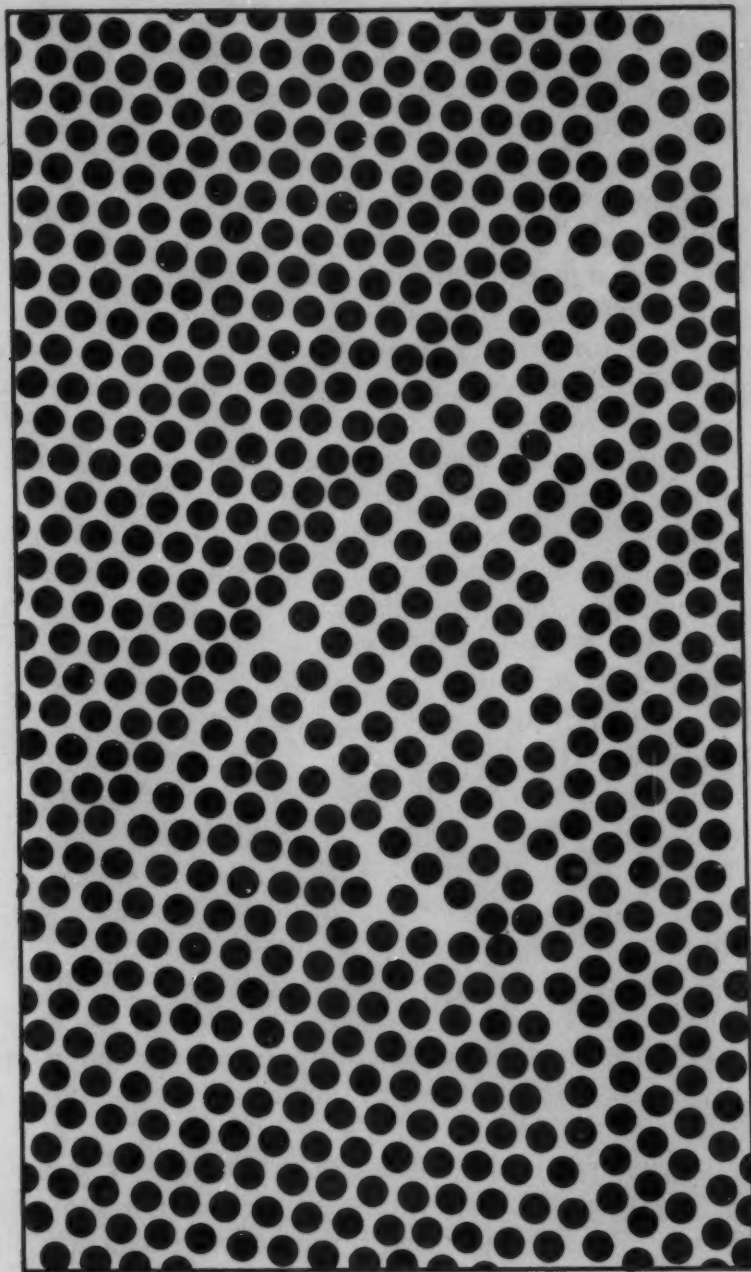


Fig. 26—Formation of a Nucleus by Coherent Fluctuation in the Vicinity of a Disordered Grain Boundary. (Drawing is based on a grain boundary in array of bubbles, as in Fig. 24.)

incoherent, for only then is it possible to have the necessary lower symmetry of the precipitating particle. The fact that coherence can remain high in the major plane of contact enables this phase of non-equilibrium structure to be effectively stable as long as its orientation is not changed by some external agency. Ideal compositional equilibrium cannot exist in crystals of different phases when they are joined by a crystallographically coherent boundary. The θ phase that represents true equilibrium results only when coherence is completely

broken, which can happen only at a grain boundary or at some other highly strained location where a nucleus can appear of an orientation which does not permit a coherent interface. Particles of such an equilibrium constituent, since they must have a disordered interface, will be approximately spherical in shape if they appear in the middle of a grain and lens-shaped at a grain boundary. Their formation will be vastly accelerated by deformation, for this provides the imperfections that by their aggregation form the interface.

Discontinuous precipitation is a most interesting case. As is well known, this form of precipitation occurs only on aging alloys with a high degree of supersaturation. It commences always at grain boundaries and advances into the adjacent grains, often unsymmetrically. Both structure and composition change abruptly at the interface, and no visible gradient is apparent ahead of this. It appears that as the interface advances, lateral diffusion along it transforms the strained inhomogeneous supersaturated crystal into unstrained equilibrium parent and precipitate phases, arranged in a more or less lamellar structure extending behind the interface. Such complete reorganization can occur only at a disordered, incoherent interface and is quite distinct from the mechanism that gives rise to coherent precipitation within the grains. The disordered interface that is necessary requires considerable free energy for its nucleation, and it does not readily form by an internal fluctuation; however, the proper structure already exists at a grain boundary, and at its simplest discontinuous precipitation is nothing more than the growth of one grain into its neighbor. It is closely analogous to recrystallization, as in Fig. 25, except that composition, as well as strain, is relaxed. The equilibrium second phase collects in a more or less pearlitic structure and once nucleated will continue to grow edgewise as the interface advances, with repeated branching if necessary to maintain the proper spacing.

If this mechanism is the correct one, then the orientation of the major phase in a zone of discontinuous precipitation should *not* bear an exact orientation relationship with the grain in which it is growing but, on the contrary, should be nearly identical with the orientation of the neighboring grain. That this is the case is clearly seen in Figs. 27 and 28 which show the microstructure of an alloy of zinc with 2% of copper, annealed at 200 °C to produce discontinuous precipitation. Both micrographs show the same area, but Fig. 28 was taken with polarized light to show orientation relations. There can be no doubt that the major phase in the discontinuously precipitated areas has an orientation identical with the grain adjacent to that into which it is advancing. This grain was indeed the nucleus for it. The similarity to Fig. 25 is striking, and leaves no doubt that the change in structure has resulted from the migration of the grain boundary.

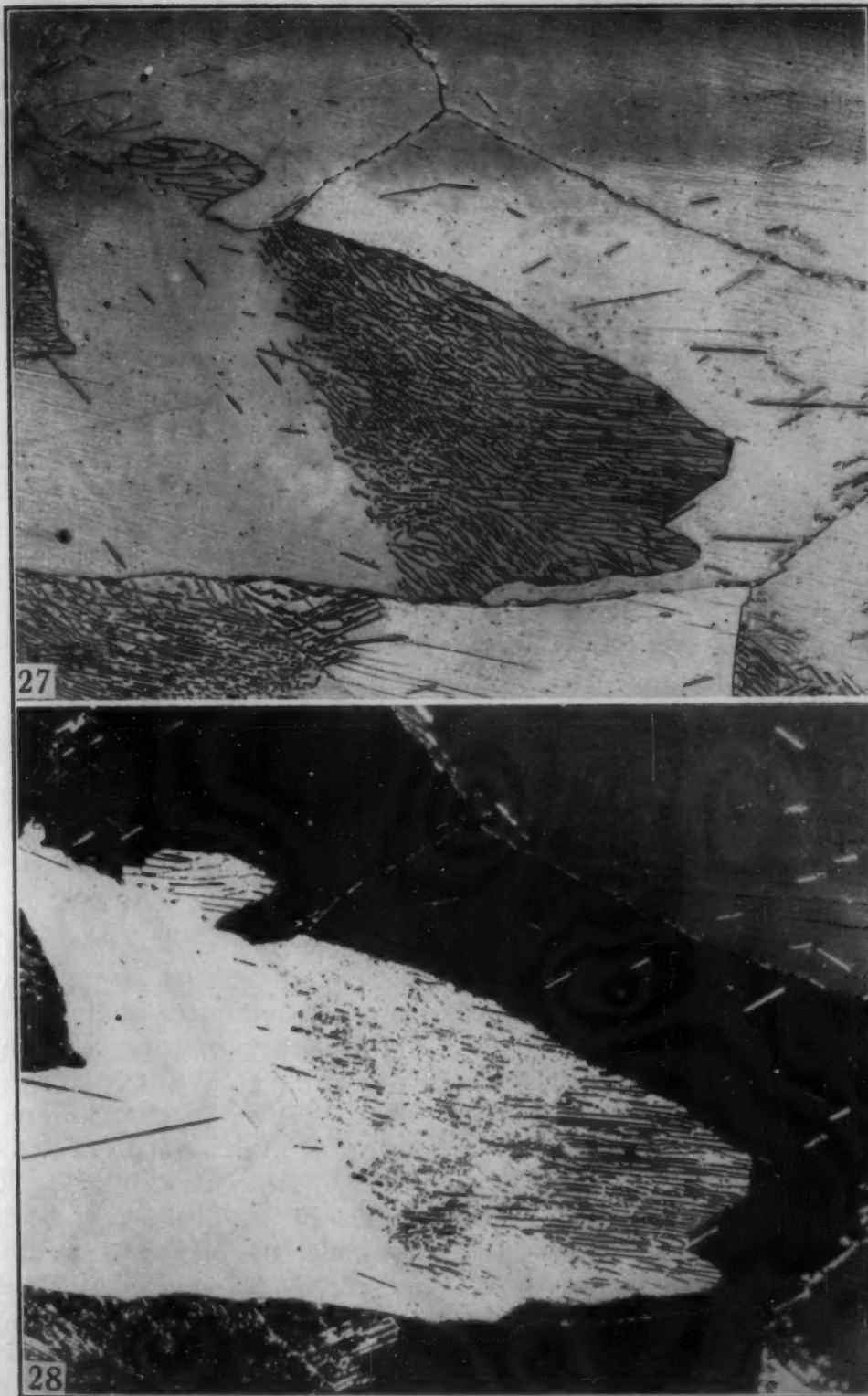


Fig. 27—Microstructure of Zinc-Copper Alloy (2% Cu). Annealed 12 hours 400 °C; cooled to and annealed 36 hours at 200 °C. Shows area of discontinuous precipitation. $\times 200$.

Fig. 28—Same Field as Fig. 27, Under Polarized Illumination.



Fig. 29—Microstructure of Copper-Silver Alloy (3.75% Ag). Quenched 700 °C; reannealed 16 hours at 400 °C to develop discontinuous precipitation. Etched $\text{NH}_4\text{OH} + \text{NH}_4(\text{SO}_4)_2$. $\times 100$.

The photomicrograph, Fig. 29, is of an alloy of copper with 3.75% silver annealed at 400 °C to develop discontinuous precipitation. It is immediately apparent that the areas of discontinuous precipitation originate solely at grain boundaries, and that they grow only into one grain, not both. Moreover, if the portion of the grain that is growing is twinned, the twin boundary can be traced in the precipitated area, while if the precipitated area is advancing into a twinned grain, the twin is obliterated. Confirmation of the predicted identity of orientation was obtained on a similar sample by C. S. Barrett, using X-rays. Fig. 30 shows the appearance under the microscope of two adjacent grains, into one of which discontinuous precipitation has advanced. The circles indicate the areas irradiated by the small X-ray beam used for the back-reflection Laue photographs reproduced in Figs. 31a and 31b, respectively. The pattern from the precipitated area clearly has spots corresponding in position with those from the adjacent grain (though more sharply defined), and there is no apparent simple orientation relationship with the grain into which it is growing.

Discontinuous precipitation is sometimes not as simple as in the samples given. The simple lamellar structure, so reminiscent of pearlite, will not appear if the advancing interface frequently encounters minute already-precipitated particles that can grow at the interface. If one of these should appear between two edgewise-advancing lamellae it will compete for material and may grow in their stead, resulting in a series of short disconnected particles of the second phase instead of the long plates that result from continued branching growth from the first nucleus. Moreover, just as extensive recrystallization occurs

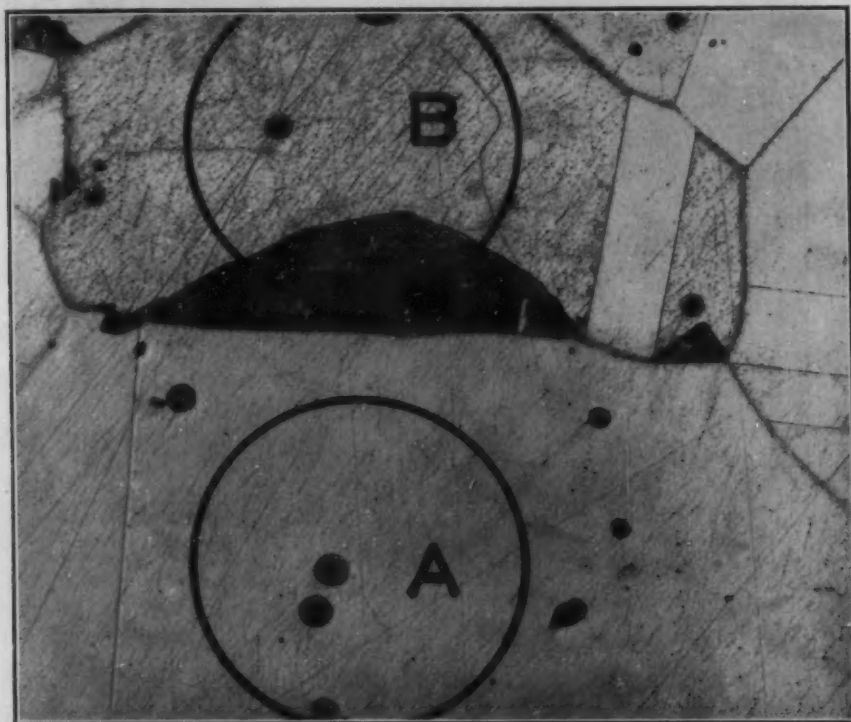
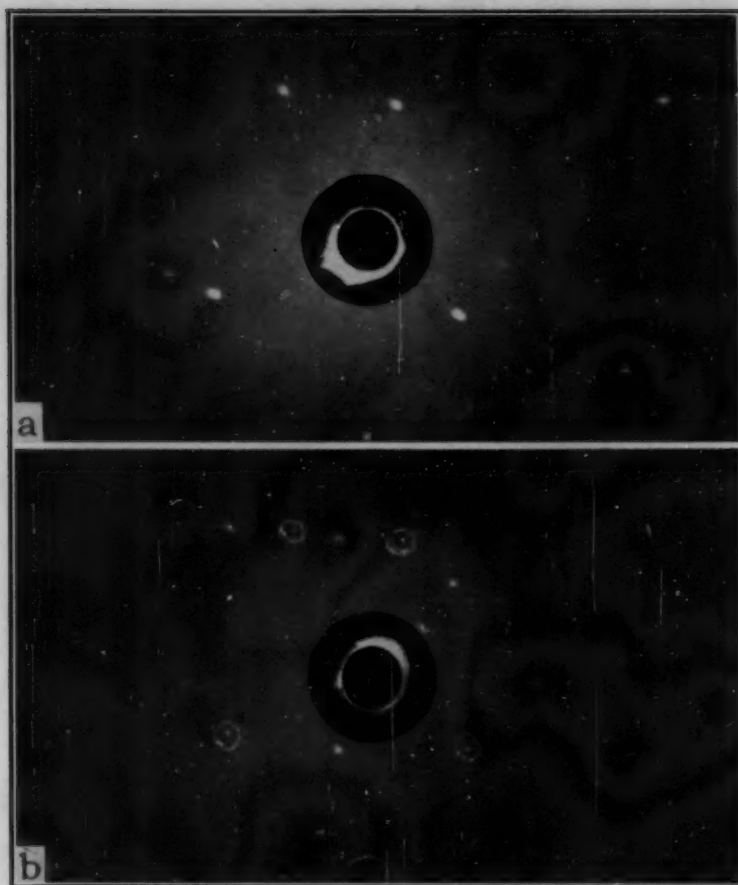


Fig. 30—Another Area of Specimen Shown in Fig. 29, With Location of X-Ray Beams Marked. $\times 100$.

when heavily cold-worked metal is annealed (contrasting with the simple extension of one grain into its neighbor, as in Fig. 25), so in precipitating systems, if there is a high degree of strain, many small grains widely differing in orientation may appear. These have actually been observed in beryllium-copper where the precipitated areas grow both ways from the boundaries at which they form and possess extremely small grain size (30). Discontinuous precipitation involves an increase in area of a high energy interface, and it can only proceed when the change of free energy accompanying the reaction is sufficient to supply the necessary surface free energy. In alloys such as beryllium-copper where many new grains are formed, the interface energy is extremely high, and the precipitated zones can advance only as long as a high degree of supersaturation exists in the neighboring



Figs. 31a and 31b—Back-Reflection Laue Patterns of Areas Marked in Fig. 30. The circles in Fig. 31b designate spots corresponding to the adjacent crystal.

crystals. If continuous precipitation is simultaneously proceeding within the crystals, it may reach such a stage that discontinuous growth can no longer advance into it with any gain of energy.

Although a disordered, disoriented interface must divide a supersaturated crystal from the precipitated area growing into it, the interface between the two phases in the latter is not so limited. Indeed, the interface energy between them will be less, and the driving force for the reaction greater, if they are mutually oriented. Thus, one sees in the transformed areas of Fig. 27 plates of the ϵ phase of a habit identical with the few that formed by a Widmanstätten mechanism within the crystal behind. There will be competition between the continuation of an oriented plate and the maintenance of approximately equal spacing, which necessitates frequent branching at the time the advancing interface is of small, increasing radius.

An essentially analogous situation exists in eutectoid transformations. The best known case is that of pearlite in steel, which forms most frequently at grain boundaries and often grows into only one grain. In the writer's opinion its nucleation is the result of a fluc-



Fig. 32—Orientation of $\{110\}$ Axes of Pearlitic Ferrite, as Related to Austenite Crystal in Which it Is Growing. (From Smith and Mehl (32), *Transactions, American Institute of Mining and Metallurgical Engineers*, Vol. 150, with permission.)

tuation near the grain boundary which produces a small zone of ferrite, coherent in one grain but incoherent with the neighboring grain across the boundary. If this occurs in the vicinity of a carbide particle or if a carbide particle is nucleated nearby following the rejection of carbon from the ferrite, the two constituents can simultaneously grow by the advance of the incoherent boundary into the neighboring grain. Repeated lateral branching of both ferrite and cementite can maintain the critical spacing for maximum growth rate without renucleation and without destroying the continuity of the disordered interface as it advances through the austenite. The orientation relationship between the ferrite in the pearlite and the austenite grain into which it is growing is, therefore, just the *avoidance* of those orientations where a coherent interface is possible. In simple cases the ferrite may be in a coherent orientation to the austenite in the grain across the grain boundary from the one into which it is growing. No data are available on the latter point, but the similarity with discontinuous precipitation makes a confident prediction possible.

Excellent studies of the orientation relationships in pearlite were made by Mehl and Smith (31) and by Smith and Mehl (32), respec-

tively. The results of the latter are reproduced in Fig. 32 and seem to provide corroboration of the "avoidance" hypothesis.

It is a reasonable prediction that in a polycrystal, the orientations not represented in plots such as Fig. 32 would be found if the ferrite orientations were referred to the appropriate adjacent austenite crystals. Although Smith and Mehl proposed certain orientations as the center of their scattered results, it is at least equally satisfactory to re-

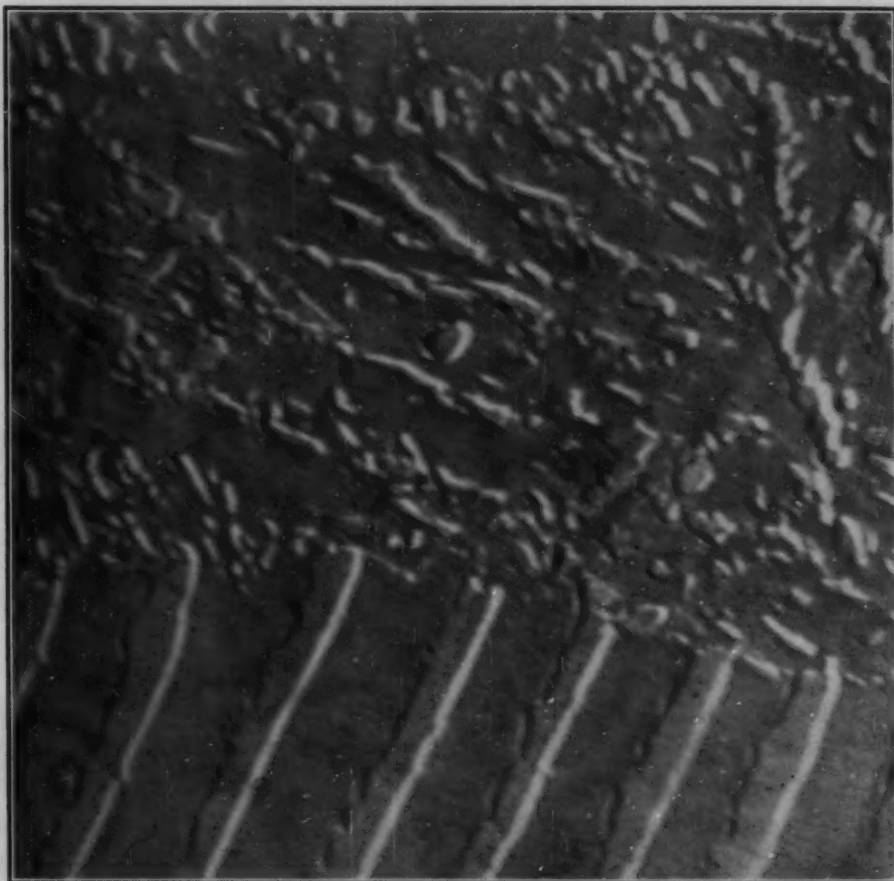


Fig. 33—Electron Micrograph of Interface Between Pearlite and Tempered Martensite, Commercial Tool Steel Containing 0.9% Carbon, 1.6% Manganese. Pearlite grown at 697 °C, then quenched and tempered 5 minutes at 500 °C.

gard the orientations as being distributed at random except for the avoidance of certain areas. They say: "It was found that ferrite in pearlite assumes a discrete number of determinate orientations rather than an infinite number of random orientations." They also point out that the orientation relationships observed are quite different from those that exist between proeutectoid ferrite and austenite in hyper-eutectoid steels, and the mechanism of formation is therefore different.

Essentially the pearlitic growth mechanism can only proceed with interfaces between ferrite and austenite at orientations near the high horizontal plateau of the curve relating surface energy to orientation

(Fig. 10). Fluctuations will most readily occur at the low energy cusps, but these cannot grow except with enough free energy to overcome strain restraint. Though the disordered interface must always be present for pearlite to grow, the nature of nucleation may not always be as suggested, and certainty is not so when pearlite is nucleated away from a grain boundary or when it is observed to grow into both grains from a boundary.

It is an inherent characteristic of the highly disordered boundary that lateral diffusion along it should be extremely high. If this is considerably higher than volume diffusion, then the entire transformation could occur in this two-dimensional interface, and three-dimensional gradients of carbon concentration ahead of it might be very small. Mr. Richard Grace has attempted to investigate this point by quantitative metallography on a partially transformed quenched and tempered steel (Fig. 33).⁶ Preliminary measurements do indicate some enrichment of carbon ahead of the ferrite. No after-growth has ever been observed in either pearlite or discontinuous precipitation, and complete equilibrium seems to be established by the passage of the interface.

If this general viewpoint is correct, then the incoherent interface becomes the point of most interest in considering factors affecting the hardenability of steel. The bulk free energy changes are important, of course, but the major effect of alloying elements on transformation kinetics would now seem to result from their effect on the structure and properties of the interface between ferrite and austenite. Any alloying element will make possible the construction of a lower energy boundary and a generally more compact structure through which diffusion would be less easy, simply because a selection is possible between atoms of various sizes and coordination numbers in bridging the gap between perfect lattices.

SUMMARY

In order to understand microstructure it is desirable to consider the interaction of all three aspects—the topological, the geometric, and the metric. In two dimensions the average grain must be a hexagon with certain definite relations between the number of grains with other than six sides. Local surface tension equilibrium requires grain junctions to be at 120° , which necessitates curved grain boundaries in random arrays of grains and hence makes grain growth inevitable. The faces of three-dimensional grains must approximate $5\frac{1}{2}$ edges on the average. Their similarity to bubbles and cells in biological tissue emphasizes the importance of mathematical rather than physical factors in their shape. In two-phase alloys the 120° grain corner angle is replaced by some other angle, which depends on the energy of the

⁶Thanks are due to Messrs. Ellis and Thourson of the International Harvester Company for making the replica and electron micrographs of these samples.

interfaces involved and can be considered to be a result of simple surface-tension equilibrium of fluid interfaces. If the angle is 60° or less, a second phase (even in minor amount) will be completely continuous along grain edges, and if 0° , it will spread over the faces. Anisotropic structures, such as Widmanstätten structures, occur only when there is a precise orientation relationship between the two phases, and slight disturbance of the orientation produces structures with curved interfaces as in a typical foam structure. If grain boundary energy is a higher fraction than 0.55 of the solid/liquid interface, grain corners will be appreciably rounded and the intervening space filled with equilibrium liquid at temperatures below but near to the melting point. A simple model is discussed suggesting that even a plane grain boundary should change its properties rapidly at temperatures close to the melting point and at compositions near to the solid solubility limit if the solubility is small and if the liquid, when it appears, has a low interface energy against the crystals. Some such factor is involved in many of the mysterious cases of brittleness known to metallurgists, such as the embrittlement of bismuth copper and the hot-shortness of steels.

An attempt is made to classify metallographic structures in terms of the characteristics of the interface between the phases involved. The nucleation of a new phase on transformation is more simply regarded as the formation of a stable interface than the formation of a stable crystal. A high energy, disordered, incoherent, interface is rarely formed but easily moved if it is present. Transformations requiring disordered interfaces occur chiefly at grain boundaries and often proceed merely by the moving of the boundary, as in the cases of recrystallization, discontinuous precipitation and eutectoid transformations. A coherent interface is more easily nucleated by spontaneous fluctuation, but since its migration involves increasing elastic strains, it will not proceed indefinitely unless the driving free energy change is very large. The various stages of precipitation from solid solution correspond to complete coherence, partial coherence, or incoherence. Only if an incoherent boundary separates phases can the two attain the ideal equilibrium composition, and it is only when partial coherence is maintained that metastable phases can persist. The analogy between discontinuous precipitation and recrystallization is a close one. Both occur by the motion of an incoherent interface. It is shown that the major phases in discontinuously-precipitated areas in both zinc-copper and copper-silver alloys are identical in orientation with the adjacent grains, and the reaction is nothing more than the migration of the grain boundary with complete relaxation of strain and composition along it. Similarly, it is postulated that in the growth of pearlite in eutectoid steels the ferrite nucleus results from spontaneous fluctuation near to an austenite grain boundary and that it grows by migra-

tion of the boundary into the adjacent crystal. Unlike martensite, there is not a specifiable exact relationship in orientation between the austenite grain and the ferrite in pearlite growing into it, but rather the *avoidance* of the few orientations that could be coherent. It is suggested that two-dimensional diffusion along the interface is dominant, and that the structure, energy, and mobility of interfaces are not a unique function of their orientation and composition alone, but depend also on the rate at which they are moving.

ACKNOWLEDGMENTS

The author has been greatly helped by discussions on various aspects of microstructure with Messrs. Nicholson, Guttman, Barrett, Stout and others of the Institute for the Study of Metals. K. K. Ikeuye made and heat treated most of the alloys, and he and Mrs. Betty Nielsen are responsible for the photomicrographs.

The research would have been impossible without the generous unrestricted support of the Institute by its industrial sponsors, or the support of the U. S. Army Ordnance Department (Contract No. DA-11-022-ORD-834) and the Office of Naval Research (Contract No. N-6ori-IV, NR 019 302).

References

1. C. S. Smith, "Grain Shapes and Other Metallurgical Applications of Topology", in *Metal Interfaces*, American Society for Metals, Cleveland, 1952, p. 65-113.
2. C. S. Smith, "Further Notes on the Shape of Metal Grains", to be published in *Acta Metallurgica*.
3. Lord Kelvin, "On the Division of Space With Minimum Partitional Area", *Philosophical Magazine*, Vol. 24, 1887, p. 503-514; *Collected Papers*, Vol. 5, p. 333.
4. W. A. Macior and E. B. Matzke, "An Experimental Analysis of Cell-Wall Curvatures . . .", *American Journal of Botany*, Vol. 38, 1951, p. 783-793.
5. C. H. Desch, "The Solidification of Metals From the Liquid State", *Journal*, Institute of Metals, Vol. 22, 1919, p. 241-263.
6. W. M. Williams and C. S. Smith, "A Study of Grain Shape in an Aluminum Alloy . . .", *Transactions*, American Institute of Mining and Metallurgical Engineers, Vol. 194, 1952, p. 755-765.
7. E. B. Matzke, "The Three-Dimensional Shape of Bubbles in Foam . . .", *American Journal of Botany*, Vol. 33, 1946, p. 58-80.
8. E. B. Matzke and J. Nestler, "Volume Shape Relationships in Variant Foams . . .", *American Journal of Botany*, Vol. 33, 1946, p. 130-144.
9. F. T. Lewis, "A Further Study of the Polyhedral Shapes of Cells", *Proceedings*, American Academy of Arts and Sciences, Vol. 61, 1925, p. 1-34.
11. P. A. Beck et al, "Grain Growth in High-Purity Aluminum and in an Aluminum-Magnesium Alloy", *Transactions*, American Institute of Mining and Metallurgical Engineers, Vol. 175, 1948, p. 372-394.
12. C. S. Smith, "Grains, Phases, and Interfaces: An Interpretation of Microstructure", *Transactions*, American Institute of Mining and Metallurgical Engineers, Vol. 175, 1948, p. 15-51.

13. C. S. Smith, "Interphase Interfaces", in *Imperfections in Nearly Perfect Crystals*, National Research Council Conference (1950), New York, John Wiley, 1952, p. 377-401.
14. C. S. Smith, "Interfaces Between Crystals", in *L'Etat Solide*, Report of Nineteenth Conference on Physics of the Solvay Institute, Brussels, 1952, p. 11-53.
15. K. K. Ikeuye and C. S. Smith, "Studies of Interface Energies in Some Aluminum and Copper Alloys", *Transactions*, American Institute of Mining and Metallurgical Engineers, Vol. 185, 1949, p. 762-768.
16. K. T. Aust and B. Chalmers, "The Specific Energy of Crystal Boundaries in Tin", *Proceedings of the Royal Society*, Vol. 201A, 1950, p. 210-215; "Surface Energy and Structure of Crystal Boundaries in Metals", *Proceedings of the Royal Society*, Vol. 204A, 1950, p. 359-366.
17. C. G. Dunn et al, "The Effect of Orientation Difference on Grain Boundary Energies", *Transactions*, American Institute of Mining and Metallurgical Engineers, Vol. 185, 1949, p. 125-132. Also, "Relative Energies of Grain Boundaries in Silicon Iron", *Transactions*, American Institute of Mining and Metallurgical Engineers, Vol. 188, 1950, p. 1245-1248.
18. W. T. Read and W. Shockley, "Dislocation Models of Crystal Grain Boundaries", *Physical Review*, Vol. 78, 1950, p. 275-289. Also, W. Shockley, "Dislocation Models of Grain Boundaries", Report of Nineteenth Conference on Physics of the Solvay Institute, Brussels, 1952, p. 431-485.
19. R. F. Mehl and C. S. Barrett, "Studies Upon the Widmanstätten Structure", *Transactions*, American Institute of Mining and Metallurgical Engineers, Vol. 93, 1931, p. 78-110. Also, many subsequent papers by these authors in *Transactions*, American Institute of Mining and Metallurgical Engineers.
20. Conyers Herring, "Use of Classical Macroscopic Concepts in Surface Energy Problems", Symposium on the Structure and Properties of Surfaces, National Research Council, 1952. To be published in book form.
21. R. King and B. Chalmers, "Crystal Boundaries", in *Progress in Metal Physics*, ed. B. Chalmers, Vol. I, 1949, p. 127-162.
22. J. W. Spretnak and R. Speiser, "Grain and Grain Boundary Compositions", *TRANSACTIONS*, American Society for Metals, Vol. 43, 1951, p. 734-748.
23. B. Chalmers, "Crystal Boundaries in Tin", *Proceedings of the Royal Society*, Vol. 175A, 1940, p. 100-110.
24. R. T. Howard and Morris Cohen, "Quantitative Metallography by Point Counting and Lineal Analysis", *Transactions*, American Institute of Mining and Metallurgical Engineers, Vol. 172, 1947, p. 413-426.
25. L. H. Beck and C. S. Smith, "Copper-Zinc Constitution Diagram, Redetermined . . . by Means of Quantitative Metallography", *Transactions*, American Institute of Mining and Metallurgical Engineers, Vol. 194, 1952, p. 1079-1083.
26. C. S. Smith and L. Guttman, "Measurement of Internal Boundaries in Three-Dimensional Structures by Random Sectioning", paper to be published in *Transactions*, American Institute of Mining and Metallurgical Engineers.
27. P. A. Beck and P. R. Sperry, "Strain Induced Grain Boundary Migration in High Purity Aluminum", *Journal of Applied Physics*, Vol. 21, 1950, p. 150-152.
28. P. A. Beck, "Interface Migration in Recrystallization", in *Metal Interfaces*, American Society for Metals, Cleveland, 1952, p. 208-247.
29. R. F. Mehl and A. Dubé, "The Eutectoid Reaction", in *Phase Transformations in Solids*, National Research Council Conference (1948), New York, John Wiley, 1951, p. 545-587.

30. C. S. Smith, "Discussion—Theory of Age Hardening", in *Age Hardening of Metals*, American Society for Metals, Cleveland, 1940, p. 425-426.
31. R. F. Mehl and D. W. Smith, "Orientation of Ferrite in Pearlite", *Transactions*, American Institute of Mining and Metallurgical Engineers, Vol. 116, 1935, p. 330-341.
32. G. V. Smith and R. F. Mehl, "Lattice Relationships in Decomposition of Austenite . . .", *Transactions*, American Institute of Mining and Metallurgical Engineers, Vol. 150, 1942, p. 211-226.

It is unfortunate that the name most deserving of perpetuation in the metallographic field, that of Henry Clifton Sorby, was applied by the early metallographers to a structure that has since come to be regarded as merely a modification of another, and the name Sorbite has passed into oblivion. It would cause no confusion in scientific literature and would be a fitting memorial to a great man if the name were resurrected and applied to all those structures of a lamellar nature that are now called pearlite.

THE MECHANISM AND KINETICS OF THE FIRST STAGE OF TEMPERING

BY C. S. ROBERTS, B. L. AVERBACH AND MORRIS COHEN

Abstract

The mechanism and kinetics of martensite decomposition in the first stage of tempering were studied by means of X-ray and length measurements in a series of high purity iron-carbon alloys and commercial steels. In particular, a single-crystal X-ray technique was employed to ascertain the changes in the martensitic matrix attending the rejection of carbon.

The first stage of tempering proceeds by the growth of an aggregate, consisting of low carbon martensite and a hexagonal close-packed carbide, at the expense of the primary martensite. The low carbon martensite is tetragonal, with an axial ratio corresponding to a carbon content of about 0.25%, and appears to be in metastable equilibrium with the hexagonal carbide. The latter has the approximate composition $Fe_{2.4}C$. The third stage of tempering, involving the formation of cementite, generally begins before the completion of the first stage.

The kinetics of the retained austenite transformation in the second stage of tempering were obtained as a by-product of this work, and are reported in an appendix. The magnitude of the activation energy for the second-stage reaction, and its dependence on carbon content, both suggest that carbon diffusion in austenite is the controlling process.

IN the tempering of hardened steel, the first stage (in order of increasing tempering time and temperature) is recognized as the decomposition of the martensite into a low carbon solid solution and a carbide other than cementite. The second stage of tempering overlaps the first, and comprises the transformation of the retained austenite.¹ However, considerable uncertainty exists concerning the

¹The third stage of tempering involving the ultimate formation of cementite is not treated in this paper, although it was invariably encountered in attaining the end of the first stage.

This paper is based on a portion of a thesis submitted by C. S. Roberts in partial fulfillment of the requirements for the degree of Sc.D. in Metallurgy at the Massachusetts Institute of Technology, October 1951.

A paper presented before the Thirty-fourth Annual Convention of the Society, held in Philadelphia, October 18 to 24, 1952. Of the authors, C. S. Roberts is associated with the Metallurgical Laboratories, Dow Chemical Co., Midland, Mich., and B. L. Averbach and Morris Cohen are associated with the Department of Metallurgy, Massachusetts Institute of Technology, Cambridge, Mass. Manuscript received April 10, 1952.

Table I
Composition and Metallography of Alloys

Alloy or Steel No.	% C	% Mn	% Si	Austenitizing Temp., °F	Quenching Medium	Fracture Grain Size	% Retained Austenite, Quenched to 72 °F	% Retained Austenite, Refrigerated
122	0.29	*	*	1600	10% Brine	6	1.2	0.4
123	0.39	*	*	1550	10% Brine	5	1.6	0.1
124	0.62	*	*	1500	10% Brine	4½	4.1	2.0
103 Steel	0.68	0.78	0.21	1500	Water	6	7.6	2.5
125	0.78	*	*	1500	10% Brine	5½	7.0	3.0
105 Steel	0.93	0.42	0.19	1550	Water	6	11.0	3.3
126	0.96	*	*	1550	10% Brine	4½	10.0	4.1
127	1.16	*	*	1650	Water	70% 1, 30% > 1	19.9	6.4
128	1.43	*	*	1850	Water	> 1	32.3	12.9

*For the high purity alloys, silicon and oxygen <0.01%, all other elements <0.001%.

nature of the decomposition products and their mechanism of formation.

The present paper describes a quantitative study of the first stage of tempering in which a single-crystal X-ray diffraction technique was used to investigate the products and mechanism of martensite decomposition, while precision length measurements were employed to establish the kinetics of this decomposition. Suitable corrections were made for the accompanying effects of the retained austenite transformation. The studies were carried out as a function of carbon content both in high purity iron-carbon alloys and in commercial steels.

EXPERIMENTAL MATERIALS

Seven high purity iron-carbon alloys² and two commercial plain carbon steels³ were chosen for investigation. The chemical analyses are listed in Table I. The high purity alloys were cast as 30-pound, 3-inch diameter ingots, which were subsequently hot-forged and hot-swaged to 5/8-inch diameter rods. The commercial steels were received as 5/8-inch diameter hot-rolled rods.

The hypoeutectoid materials were then normalized and the hyper-eutectoid materials were put into the spheroidized condition. Following such pre-treatments, all decarburization was removed by machining. Hardening temperatures were selected to give complete carbide solution, and the absence of carbides and proeutectoid constituents was verified metallographically. The hardening details and the fracture grain size are summarized in Table I.

²Vacuum-melted and cast ingots prepared by National Research Corporation, Cambridge, Mass.

³These two steels were selected from a series kindly furnished by the Carnegie-Illinois Steel Corporation.

The retained austenite contents were determined after the hardening quench and after subsequent refrigeration in liquid nitrogen. A lineal analysis technique (1)⁴ was used for the 1.16% carbon and the 1.43% carbon alloys, and the other determinations were made by integrated X-ray intensities (2). The probable error was about $\pm 0.5\%$ for the lineal analysis and about $\pm 0.3\%$ for the X-ray results.

FIRST-STAGE PRODUCTS OF DECOMPOSITION

Kurdjumov (3) showed in an early X-ray diffraction study that a transition carbide is precipitated during tempering. More recently Jack (4) found that the first-stage precipitate is a hexagonal close-packed carbide with the following parameters:

$$a = 2.73 \text{ kX}, \quad c = 4.33 \text{ kX}, \quad c/a = 1.58$$

This phase was named ϵ -iron carbide, since it is isomorphous with ϵ -iron nitride. Although the nominal composition of the ϵ -carbide is sometimes regarded as Fe_2C , Jack had evidence to suggest a composition between Fe_2C and Fe_3C .

In a similar diffraction study, Nygren (5) also identified the ϵ -carbide during the first stage of tempering, and reported the following lattice parameters:

$$a = 2.74 \text{ kX}, \quad c = 4.36 \text{ kX}, \quad c/a = 1.59$$

These parameters were obtained on tempering the high purity alloy containing 0.62% carbon in Table I. On the basis of the similarity of lattice spacings of ferrite and the ϵ -carbide in certain directions, Jack postulated that the precipitate was coherent with the matrix. This coherency could account for the increase in hardness found during the first stage of tempering.

The conversion of tetragonal martensite to cubic martensite of the same carbon content, as proposed by some of the early investigators (6, 7, 8) is refuted by the observed precipitation of ϵ -carbide from the martensite. On the other hand, such precipitation is consistent with the work of others (3, 9, 10, 11) who reported a gradual rejection of carbon during the first stage, accompanied by a decrease in the tetragonality of the martensite. At the end of the first stage, it was presumed that a matrix of cubic ferrite remains with the precipitated carbide. All of the aforementioned X-ray data were obtained from powder patterns. It may be noted that the tetragonality of the martensite varies linearly with the carbon content, but because of the broadness of the diffraction lines and the merging of the doublets, there are no reliable data on the tetragonality of martensites with less than about 0.60% carbon.

Averbach and Cohen (12) studied the kinetics of the first stage

⁴The figures appearing in parentheses₄ pertain to the references appended to this paper.

in a 1% carbon steel and calculated that approximately 0.6% carbon⁵ remained in solution in the ferrite at the end of the first stage. Kurdjumov and Lyssak (13, 14) used a single-crystal X-ray technique to trace the decomposition of the martensite. They reported a carbon content of about 0.3% at the end of the first stage in an iron-carbon alloy containing 1.4% carbon (13), and 0.25% carbon at the end of the first stage in a 1% carbon steel (14). Moreover, their X-ray evidence showed clearly that martensite decomposes by a heterogeneous process. The martensite does not lose its tetragonality gradually; instead a new martensite is formed, with a tetragonality corresponding to about 0.25% carbon. Both martensites exist together, with more of the low tetragonality martensite forming at the expense of the primary martensite as the tempering proceeds. At the end of the first stage, the remaining phases are the low tetragonality martensite and the transition carbide.

This direct evidence of a discontinuous decrease in tetragonality, based on single-crystal studies, is in sharp contradiction to the generally accepted gradual decrease in tetragonality, as indicated by the powder pattern work. Kurdjumov and Lyssak reconciled the discrepancy by showing how the overlapping of the broad lines from the two martensites could produce an apparently gradual decrease of tetragonality in powder patterns due to the progressive change in the relative amounts of the two martensites.

In the experiments described here, the single-crystal X-ray diffraction method was used to observe the crystallographic changes in the martensitic solid solution during the first stage. Since the austenite and martensite have the Kurdjumov-Sachs⁶ orientation relationship in iron-carbon alloys, a single crystal of austenite will transform on quenching to a myriad of martensite plates which are oriented in one of eight unique positions. Accordingly the X-ray reflections (002) and (200) (020), which comprise one martensite doublet, may be diffracted separately and recorded on individual films, as described below. With this technique it is possible to measure the changes in tetragonality of the martensitic solid solution without the interference of overlapping doublets, thus avoiding the limitation inherent in the polycrystalline methods.

Four high purity iron-carbon alloys containing 0.78%, 0.96%, 1.16% and 1.43% carbon were adopted for these X-ray investigations. Single crystals were obtained by coarsening specimens about $\frac{1}{4}$ inch square by 2 inches long for 24 hours at a temperature about 100 °F (55 °C) below the solidus. This treatment produced austenite grains about $\frac{1}{16}$ to $\frac{3}{16}$ inch diameter, and these usually cracked in an intercrystalline fashion on quenching. After such hardening, the speci-

⁵This value was based on rough assumptions for the specific volume and composition of the carbide phase. The latter had not been identified at the time.

⁶(111)_A || (101)_M; $[\bar{1}\bar{1}0]_A$ || $[1\bar{1}\bar{1}]_M$ (15).

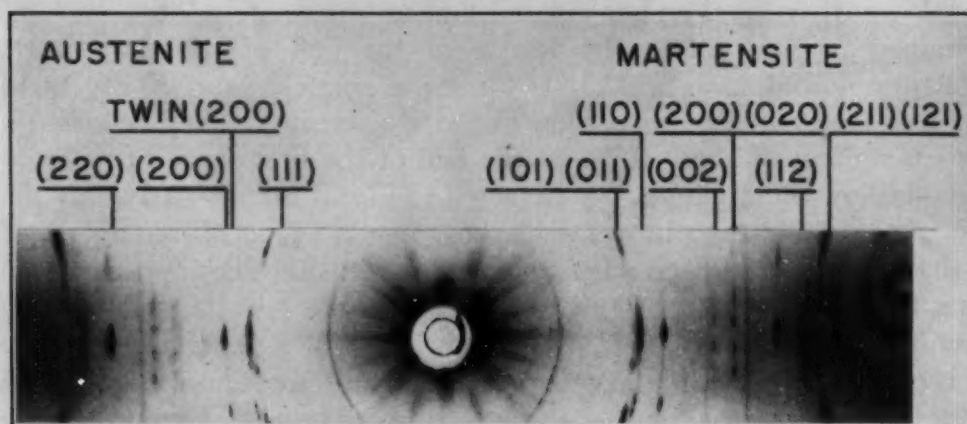


Fig. 1—Rotation Patterns From Iron-Carbon Alloy 128 (1.43% Carbon) Single Crystal. Smooth lines are from porcelain cement.

mens were etched in dilute HCl and the grains separated by a light hammer tap. The individual crystals were then etched in dilute HNO_3 to remove any plastic deformation, and were used directly in the diffraction studies with negligible difficulties from their slight asymmetry.

All diffraction patterns were made in a Unicam single-crystal goniometer camera of 6-centimeter diameter which allowed both complete rotation and oscillation over small angular ranges. Filtered iron $\text{K}\alpha$ radiation was employed and precise calibration of the camera was accomplished by means of well-annealed powder specimens of pure platinum.

Each specimen was carefully mounted with porcelain cement on the conically ground end of a short length of 2-millimeter glass rod. Reference lines were cut with a diamond on the rods parallel to their axes. The crystals were oriented so that an austenite cube axis was coincident with the axis of rotation and perpendicular to the X-ray beam. The rod and crystal could be removed periodically from the camera for tempering treatments, and the original orientation could be duplicated from the reference scratches.

The optimum crystal size was found to be between 0.5 and 1 millimeter. Larger crystals caused a sacrifice in resolution by spot enlargement, while smaller ones caused undue complications of the patterns by increasing the relative volume of the omnipresent twins.

Fig. 1 shows the complete rotation pattern produced from a single crystal of the 1.43% carbon alloy. Located on the equator are both the (200) and the (220) austenite spots. Between them and appearing slightly above and below the equator are the 16 (200) (020) and the 8 (002) reflections from the martensite superimposed in four spots. This positioning is a manifestation of the Kurdjumov-Sachs orientation relationship⁽¹⁵⁾. The (200) (020) spots occur

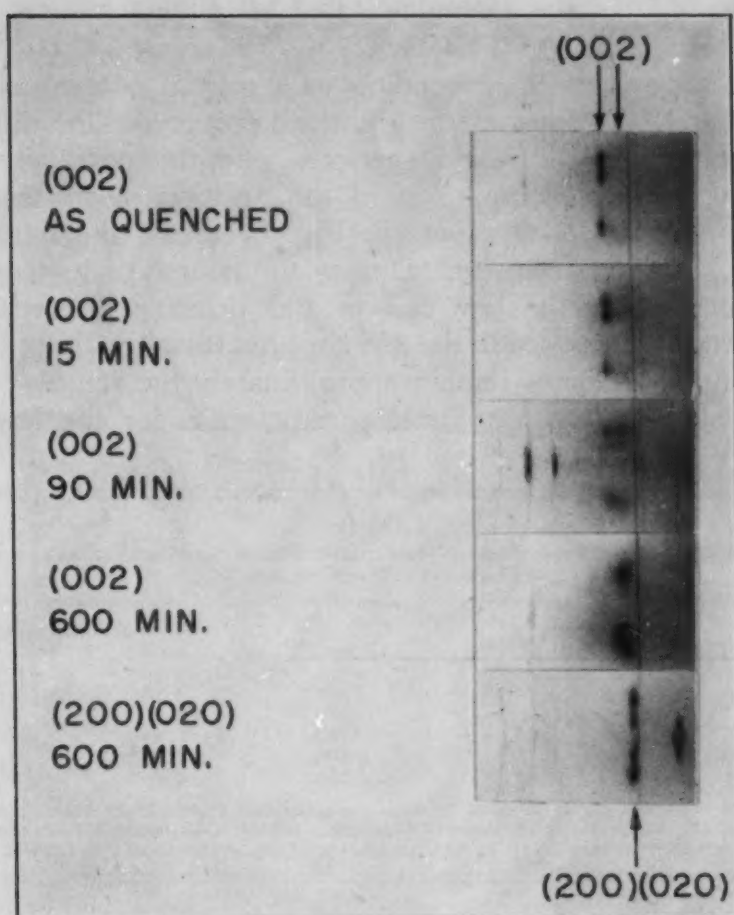


Fig. 2—Oscillation Patterns Showing (002) and (200)(020) Martensite Spots From Alloy 128 (1.43% Carbon) Tempered at 200 °F (93 °C).

at the higher angle and are approximately twice as intense as those from the (002) plane.

In order to study the first-stage tempering behavior, the (200)(020) and the (002) components must be recorded on separate films. This requires oscillation patterns over a range of 15 and 25 degrees, respectively, in order to include all planes of each group. Exposure times were 15 to 30 minutes for the rotation patterns and 5 to 10 minutes for the oscillation patterns. Intensities were measured from traces obtained with a Kipp and Zonen microphotometer.

The first-stage mechanism reported by Kurdjumov and Lyssak (14) was confirmed. The oscillation patterns showing only the (002) martensite reflections gave consistent evidence that the decomposition proceeds by the formation of a low carbon martensite at the expense of the primary martensite. The ϵ -carbide is also formed at the same time, but its diffraction lines are too weak to appear in these patterns.

In Fig. 2, the (002) spots are reproduced from oscillation

patterns made from the 128 alloy (1.43% carbon) after a series of tempering times at 200 °F (93 °C). A new set of (002) spots appears at a position corresponding to a carbon content of 0.25%. The sharp and faint lines at the right are polycrystalline diffractions from the platinum calibration specimen and the porcelain cement, respectively. Visual comparison of the position of the spots with that of the (200) (020) spots in Fig. 2 reveals the tetragonality of the low carbon martensite. During the course of tempering, the relative intensity of the low carbon and primary martensite lines changes progressively until the primary martensite disappears, but the positions of the lines remain approximately the same.

The values of the tetragonal parameter, c , for the low carbon

Table II
Carbon Content of Low Carbon Martensitic Phase for Various Alloys and Tempering Temperatures

Alloy No.	Initial % C	Temp., °F	Final Martensite	
			$c(kX)$	% C*
125	0.78	250	2.893	0.28
126	0.96	250	2.893	0.28
127	1.16	250	2.890	0.25
128	1.43	250	2.890	0.25
128	1.43	200	2.888	0.23
128	1.43	150	2.880	0.17

*The carbon content corresponding to each value of the c parameter was obtained by an extrapolation of the available parameters for primary tetragonal martensite of known carbon contents. These values extrapolated to the parameter of cubic ferrite at 0% carbon.

phase and the corresponding carbon contents are summarized in Table II. The precision of these measurements is about 0.05% carbon. It is evident that the carbon content of the low carbon martensite does not vary materially with the carbon content of the primary martensite. This finding suggests that the low carbon martensite may be in metastable equilibrium with the ϵ -carbide, as both form simultaneously out of the primary martensite. The slight increase in carbon content of the low carbon martensite with temperature may be significant, and is in the proper direction to support the concept of metastable equilibrium with the ϵ -carbide.

FIRST-STAGE KINETICS

The kinetics of the first and second stages of tempering were observed by measurements of unit length changes (16) after a series of tempering treatments. Specimens 4 inches long by $\frac{3}{8}$ -inch diameter were austenitized for 30 minutes in lead or salt baths controlled to ± 5 °F (± 3 °C). After the quench, a 45-minute delay for cleaning and temperature equalization occurred prior to the initial length measurement. Tempering was conducted at eight temperatures, ranging from 68 °F ± 1 °F (20 °C ± 0.5 °C) to 500 °F ± 5 °F

($260^{\circ}\text{C} \pm 3^{\circ}\text{C}$) and extending up to 5000 hours. The occasional cracked specimens were rejected, and repeat runs were made. Usually consistent results were obtained from the duplicate specimens in each case.

The presence of retained austenite was taken into account by measuring length changes on two sets of specimens with different, but known, quantities of retained austenite produced with and without refrigeration (see Table I). With the aid of simultaneous

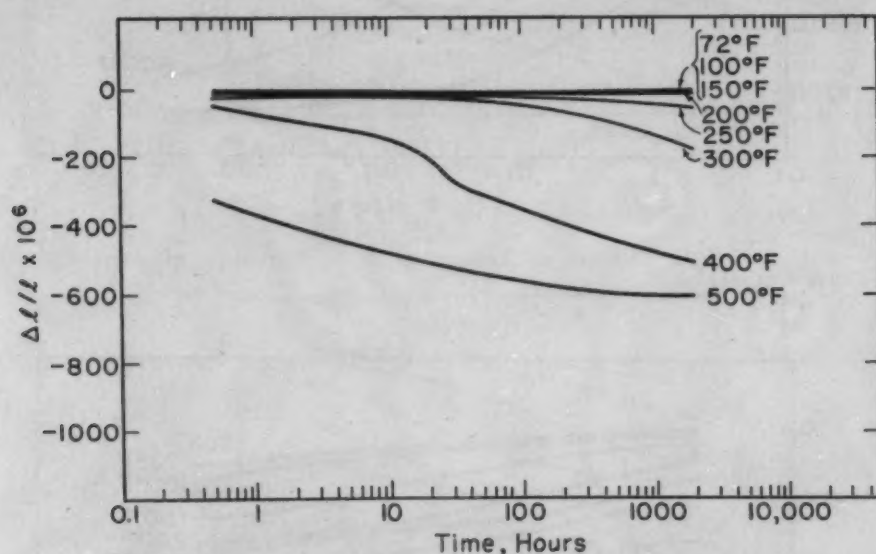


Fig. 3—Length Changes on Tempering 100% Martensite of Alloy 122 (0.29% Carbon).

equations (16), it was possible to evaluate separately the unit length changes attributable to the martensite and to the retained austenite. Although an individual length measurement was accurate to within ± 2 microinches per inch, the final accuracy of each length change was probably no better than $\pm 5\%$.

There has been some question about the use of length changes for kinetic measurements since the relief of macrostresses can also produce a change in length. This possibility was investigated by determinations of specific volume and length on the same specimen. It was shown that, even for the alloy with the highest carbon content at the highest tempering temperature, the differences between the specific volume and corresponding unit length changes were within 5%, which is the experimental error. Furthermore, even on tempering to produce a spheroidized structure, the contribution of stress relief to the total observed length change was less than 10%.

The unit length changes for 100% martensite (i.e., corrected for the presence of the retained austenite⁷) in each of the steels listed

⁷The unit length changes for 100% austenite (i.e., corrected for the presence of martensite) are discussed in Appendix A.

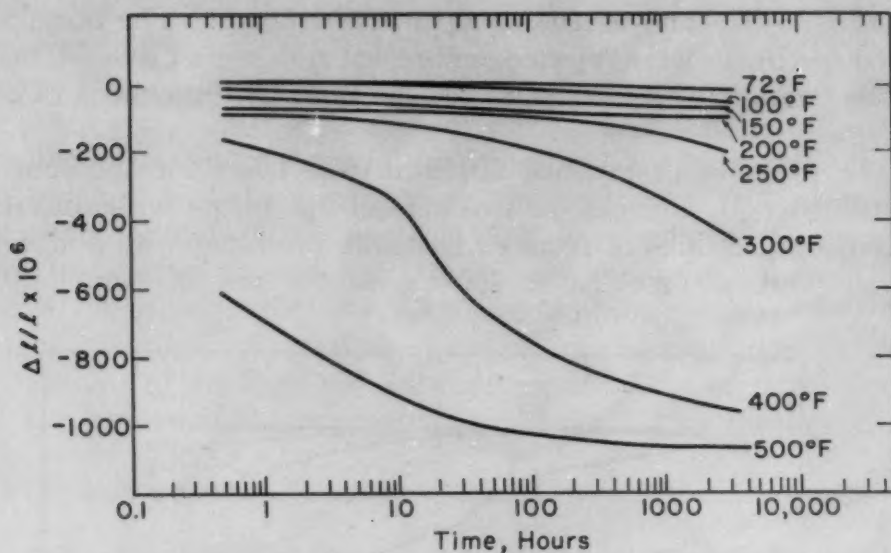


Fig. 4—Length Changes on Tempering 100% Martensite of Alloy 123 (0.39% Carbon).

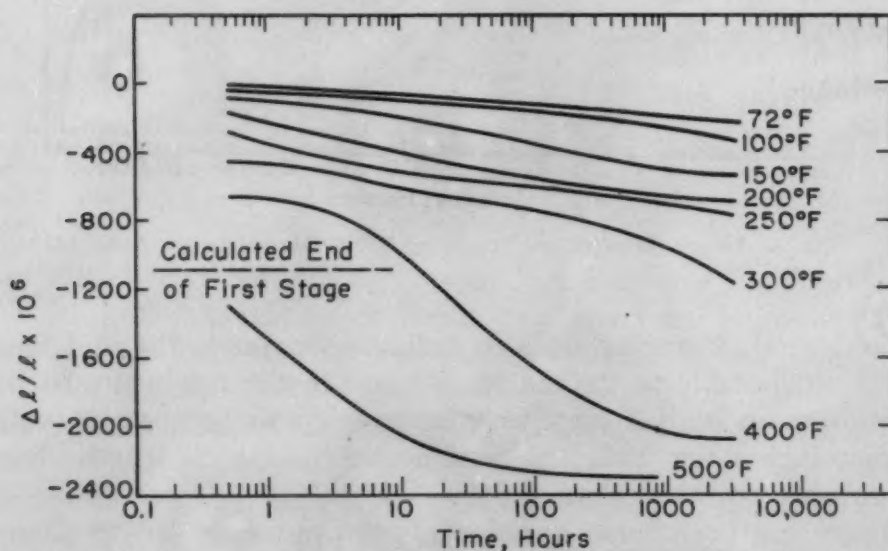


Fig. 5—Length Changes on Tempering 100% Martensite of Alloy 124 (0.62% Carbon).

in Table I are shown in Figs. 3 to 11. The kinetic behavior shows a consistent trend as a function of carbon content, with slight differences in detail between the high purity alloys and the commercial steels. For example, in Fig. 6, a plateau denoting the end of the first stage is clearly seen. In the high purity alloys, this plateau is much less evident and overlapping of the first and third stages is involved. Irrespective of the overlapping, it is evident from Figs. 3 to 11 that the third stage of tempering is definitely underway on tempering for 1 hour above 400°F (205°C). This early formation

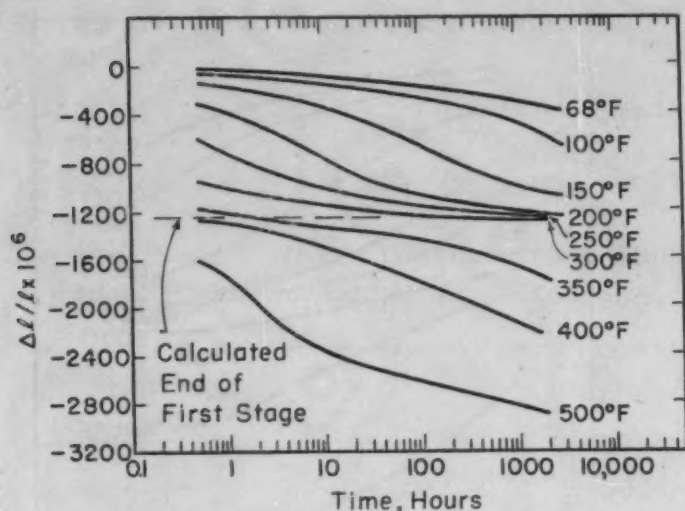


Fig. 6—Length Changes on Tempering 100% Martensite of Steel 103 (0.68% Carbon).

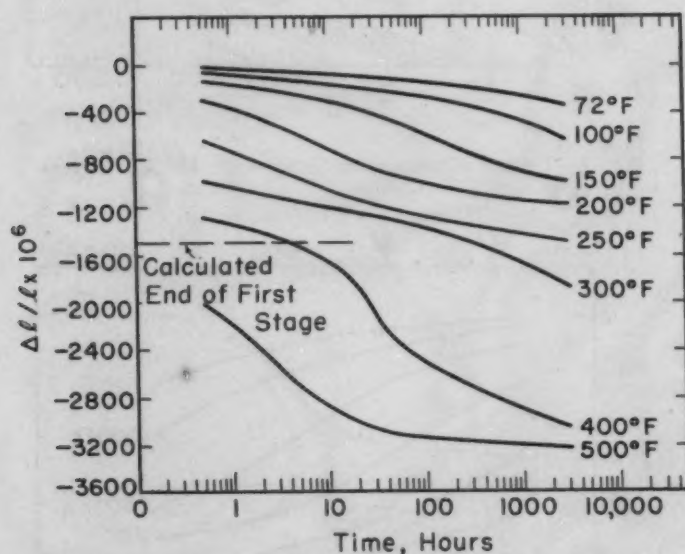


Fig. 7—Length Changes on Tempering 100% Martensite of Iron-Carbon Alloy 125 (0.78% Carbon).

of cementite at the expense of the ϵ -carbide may well account for the 500 °F (260 °C) embrittlement phenomenon.

The observed data are well represented by a rate equation of the form (12):

$$\frac{df}{dt} = K(1-f)t^m \quad \text{Equation 1}$$

f = fraction transformed

t = time

K = rate constant (temperature dependent)

m = constant

If y is the observed unit length change and a the total unit length

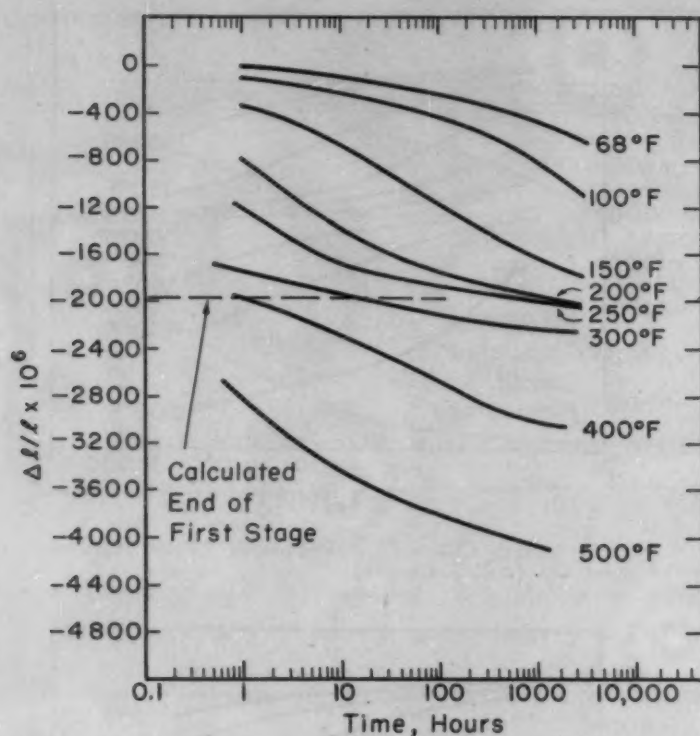


Fig. 8—Length Changes on Tempering 100% Martensite of Steel 105 (0.93% Carbon).

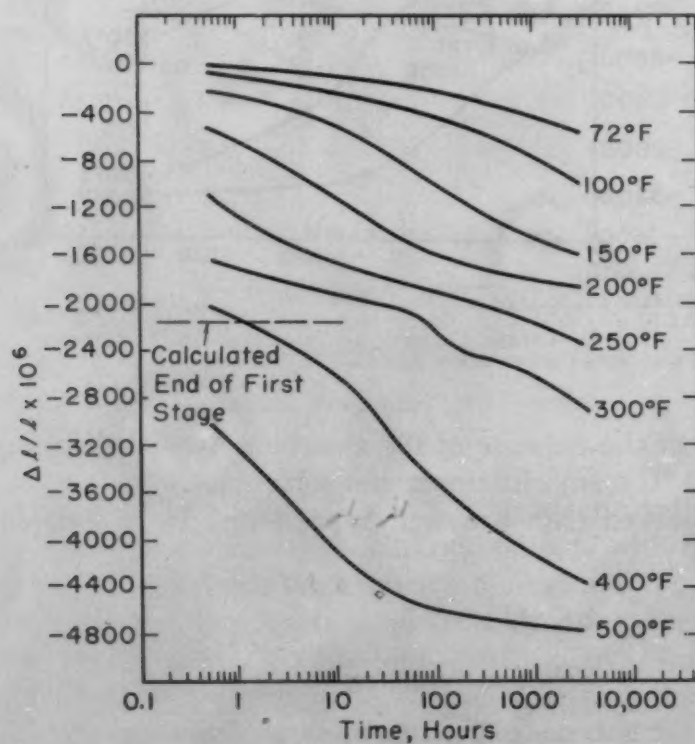


Fig. 9—Length Changes on Tempering 100% Martensite of Alloy 126 (0.96% Carbon).

change at the end of the first stage, the above equation can be integrated to the form:*

$$\log \log \left(\frac{a}{a-y} \right) = (m+1) \log t + \log \left(\frac{K}{2.3(m+1)} \right) \quad \text{Equation 2}$$

A plot of $\log \log [a/(a-y)]$ versus $\log t$ should yield a straight line from which m and K may be evaluated.

The X-ray data were used to compute values for a . In Fig. 6, a plateau at $y = 1260$ microinches per inch is observed for the 0.68%

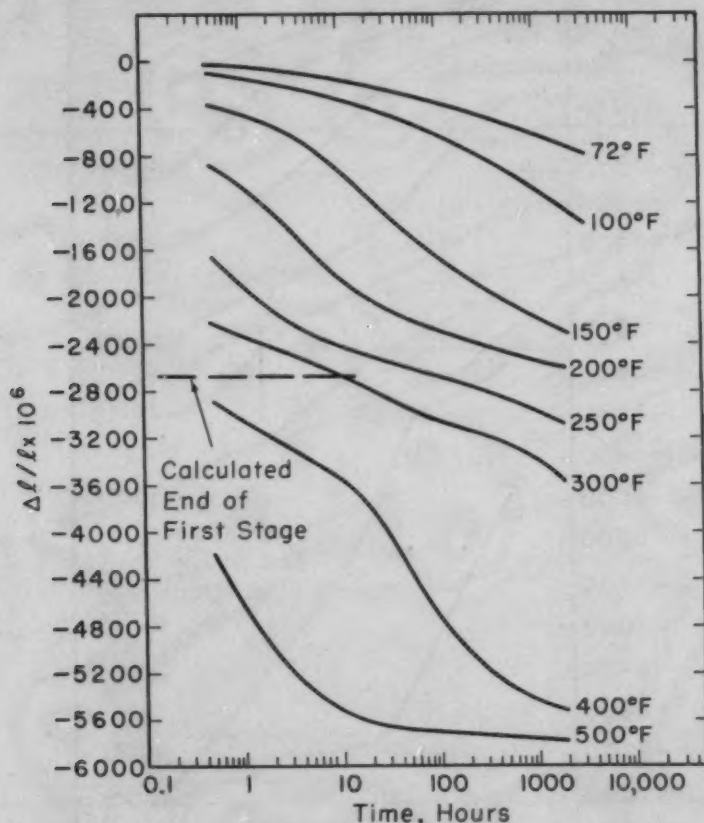


Fig. 10—Length Changes on Tempering 100% Martensite of Alloy 127 (1.16% Carbon).

carbon steel at the end of the first stage. This can be combined with the parameters of the ϵ -carbide reported by Nygren and the lattice parameters of the 0.25% carbon martensite (see previous section) to calculate the composition of the carbide.⁸ The ϵ -carbide is thus found to correspond to the formula $\text{Fe}_{2.4}\text{C}$. Since it has been shown that the composition of the low tetragonal martensite produced by

*In previous papers the last term of Equation 2 has been written

$$\log \left(\frac{K}{2.3} \right)$$

In this form the term $m+1$ is included in the constant K , but the rate constant then has a different value than that defined above. For clarity the rate constant is now defined by Equation 1 and the identity of the constant is maintained in the integrated form. The authors are grateful to L. J. E. Hofer and E. M. Cohn for pointing out this discrepancy.

⁸This point was brought out by Dr. B. S. Lement, whose calculations are summarized in Appendix B.

the first stage of tempering does not vary with the carbon content of the primary martensite (see Table II), it was assumed that the composition of the ϵ -carbide is also invariant, and to a close approximation the value of a can then be represented by:

$$a = 2930 \times 10^{-6} (C_p - 0.25) \quad \text{Equation 3}$$

where C_p is the carbon content of the primary martensite.

A typical check on the validity of the rate equation is illustrated

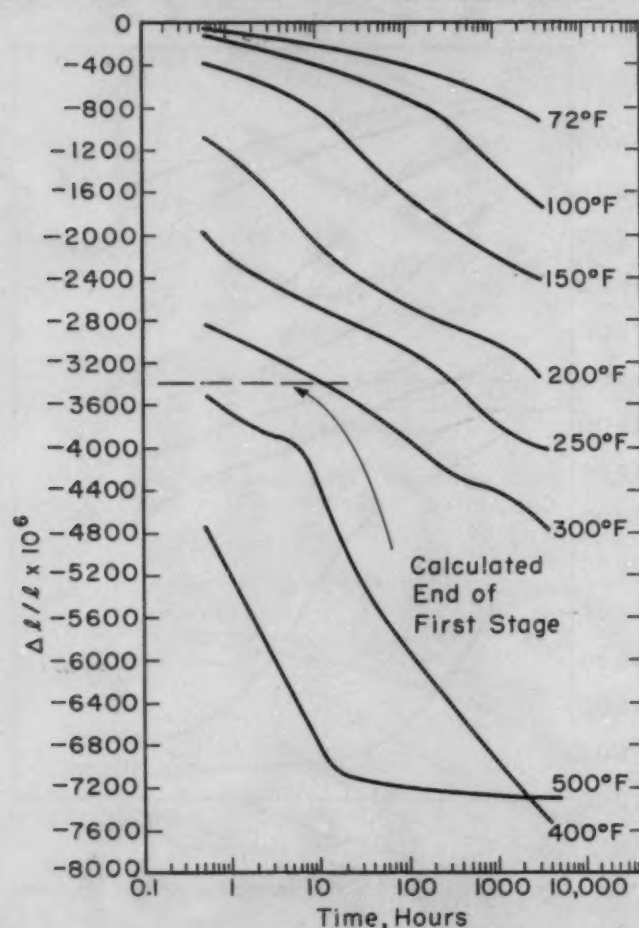


Fig. 11—Length Changes on Tempering 100% Martensite of Alloy 128 (1.43% Carbon).

in Fig. 12 in the case of the 1.43% carbon high purity alloy. The low carbon alloys (0.29% and 0.39% carbon could not be analyzed in this way because of the high relative error in the data obtained at the low tempering temperatures, but all of the other alloys exhibited a kinetic behavior similar to that of Fig. 12. Most of the data conform to straight lines when plotted according to Equation 2, and when the values of a are taken from Equation 3. There is some deviation near the end of the first-stage transformation caused by overlapping of the third stage. There is also some deviation during the early times at low tempering temperatures. This is attributable

Table III
Values of m for First Stage of Tempering

Alloy or Steel No.	% C	$a \times 10^6$	m					Average
			72°F	100°F	150°F	200°F	250°F	
103 Steel	0.68	1260	-0.70	-0.70	-0.66	-0.71	-0.69	-0.69
125	0.78	1550	-0.73	-0.71	-0.69	-0.71	-0.74	-0.72
105 Steel	0.93	1990	-0.70	-0.68	-0.69	-0.71	-0.72	-0.70
126	0.96	2080	-0.72	-0.70	-0.66	-0.69	-0.73	-0.70
127	1.16	2660	-0.71	-0.69	-0.68	-0.65	-0.67	-0.68
128	1.43	3460	-0.70	-0.70	-0.70	-0.69	-0.72	-0.70
Average	-0.71	-0.70	-0.68	-0.69	-0.71	-0.70

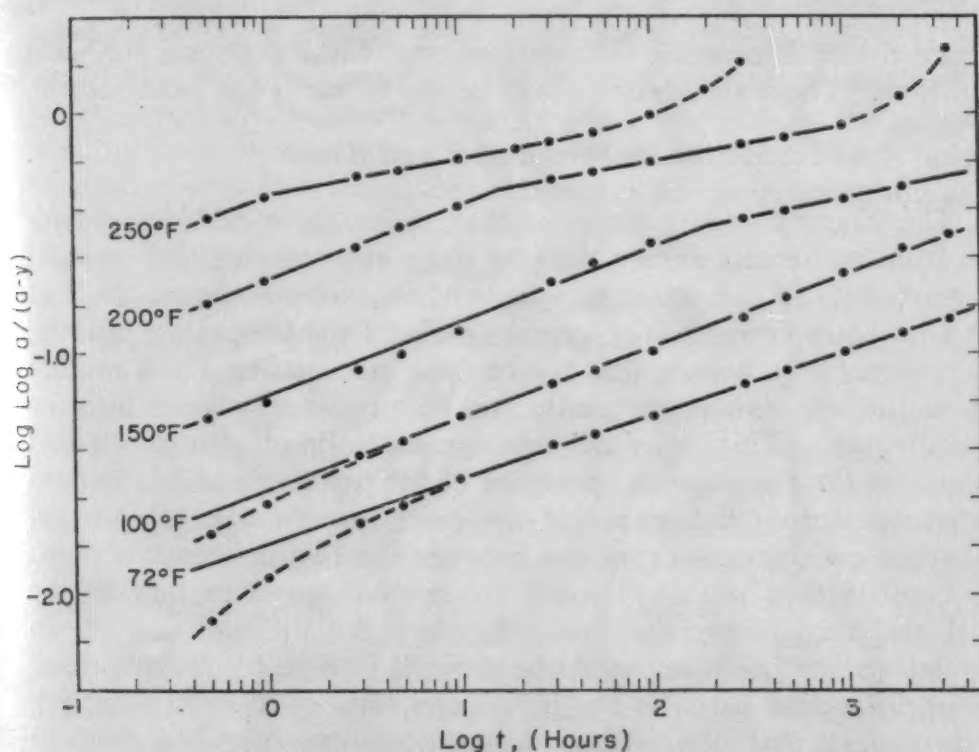


Fig. 12—Rate Equation for First Stage of Tempering 1.43% Carbon.

to the length changes which occur during the 45-minute period prior to the initial reading, and which are ignored in these considerations.

The values of m are listed in Table III. It is evident that this parameter (averaging -0.7) is independent of temperature and carbon content. Furthermore, there seems to be no significant difference in this respect between the high purity alloys and the steels. The remarkable constancy of the quantity m , notwithstanding the many variables at play, lends further credence to Equations 2 and 3 as well as to the length and X-ray measurements on which the calculations are based.

The values of K are listed in Table IV. Unlike the m parameter,

Table IV
Values of Rate Constant, K, First Stage of Tempering

Alloy or Steel No.	Carbon Content (Wt., %)	K					
		Temperature (°F)					
		68	72	100	150	200	250
124	0.62	0.0121	0.0164	0.0321	0.0717	0.113
103 Steel	0.68	0.00777	0.0186	0.0429	0.110	0.248
125	0.78	0.00885	0.0156	0.0345	0.0885	0.188
105 Steel	0.93	0.0102	0.0184	0.0585	0.171	0.354
126	0.96	0.00972	0.0183	0.0411	0.116	0.275
127	1.16	0.0112	0.0194	0.0615	0.153	0.369
128	1.43	0.0111	0.0187	0.0365	0.139	0.309

the rate constant increases with temperature, carbon content and steel impurities. These relationships will be discussed in the next section.

MECHANISM OF THE FIRST STAGE

The X-ray evidence indicates that, when the ϵ -carbide precipitates from martensite during the first stage of tempering, the remaining martensite is not uniformly depleted in carbon. From the fact that a low carbon martensite appears early in the tempering process, it is reasonable to believe that the regions surrounding the ϵ -carbide become the low carbon martensite and that two new phases form as an aggregate. This type of heterogeneous decomposition would account for the simultaneous presence of the primary and low carbon martensites during the course of the reaction. At any given time, the carbon concentration gradient between the two martensites probably constitutes a relatively small volume compared to that of the initial and final martensites, and therefore the diffraction spots in the intermediate positions would be difficult to detect. Nevertheless, diffuse diffraction between the initial and final spots was observed, which suggests that intermediate compositions may exist as a gradient between the primary and low carbon martensites. The further growth of the ϵ -carbide particles would then depend upon carbon diffusion through this gradient.

The persistence of the low carbon martensite is noteworthy, considering the rapid decomposition of the primary martensite. This persistence (as well as the fixed carbon level) is readily explained on the basis of a metastable equilibrium between the low carbon martensite and the ϵ -carbide. According to this concept, there is no tendency for the low carbon martensite to lose carbon until the ϵ -carbide begins to disappear in favor of cementite during the third stage of tempering. Another consequence of the postulated metastable equilibrium is that primary martensites containing about 0.25% should precipitate little, if any, ϵ -carbide during tempering. This is

probably the reason for the anomalous tempering characteristics of the 0.29 and 0.39% carbon alloys (Figs. 3 and 4) in which the first-stage length changes are so small that the experimental error becomes too large for accurate rate analysis.

It now remains to account for the general kinetic behavior reported in the previous section. The slope of the linear plot derived from Equation 2 is $(m + 1) = n = +0.3$ (Table III). Zener (19) has shown that a precipitation reaction takes the form:

$$f = \text{const. } t^n \quad \text{Equation 4}$$

$$\frac{df}{dt} = \text{const. } t^{n-1} = \text{const. } t^m \quad \text{Equation 5}$$

where $n = 5/2$ for disks, 2 for rods, and $3/2$ for spheres. In these equations, it is assumed that the process is growth-controlled; in other words the nuclei are already present at $t = 0$ or are generated very early in the reaction. If nucleation should occur as a function of time, n would be increased. Thus, neither progressive nucleation nor the particle shapes listed above can explain the low value of n (or m) found in the tempering process.

When the impingement of reacted or depleted regions is taken into account, a factor $(1 - f)$ is introduced in Equation 5, which then becomes identical with the empirical Equation 1, but this correction does not lower n or m . For a pearlitic-type of two-phase growth in one direction, n is reduced to 1 because the diffusion distance remains constant, being of the order of one-half the interlamellar spacing. However, the transformation rate (df/dt) should then be independent of time ($m = 0$), contrary to the tempering results.

A growth model that would lower n to about the level that has been observed for first-stage tempering is illustrated in Fig. 13. Here the low carbon martensite advances into the primary martensite on a plane front, with the ϵ -carbide precipitating or growing behind the front, and carbon diffusion being required from progressively greater distances ahead of the front as the reaction proceeds. It will be demonstrated later that in this case, $n = 1/2$ and $m = -1/2$, which is in reasonable agreement with the experimental values of 0.3 and -0.7 respectively.

It is conceivable, for example, that the second strain of the original martensitic transformation (17) divides each plate into a large number of lamellar regions, and that the boundaries of these regions provide the nucleation sites for the ϵ -carbide. Such nucleation may occur during hardening quench or very quickly on tempering with the accompanying formation of low carbon martensite in the immediate surroundings. The main decomposition process can then be described in terms of the proposed model.

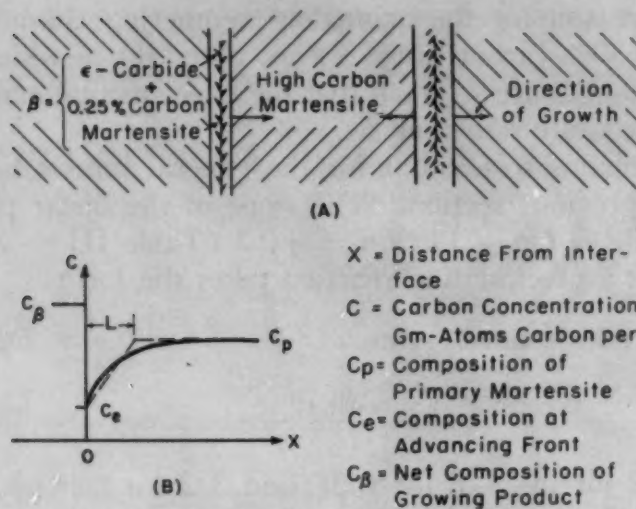


Fig. 13—(A)—Plane—Front Growth of Aggregate at Expense of Primary Martensite. (B)—Carbon Concentration Gradients at Advancing Front.

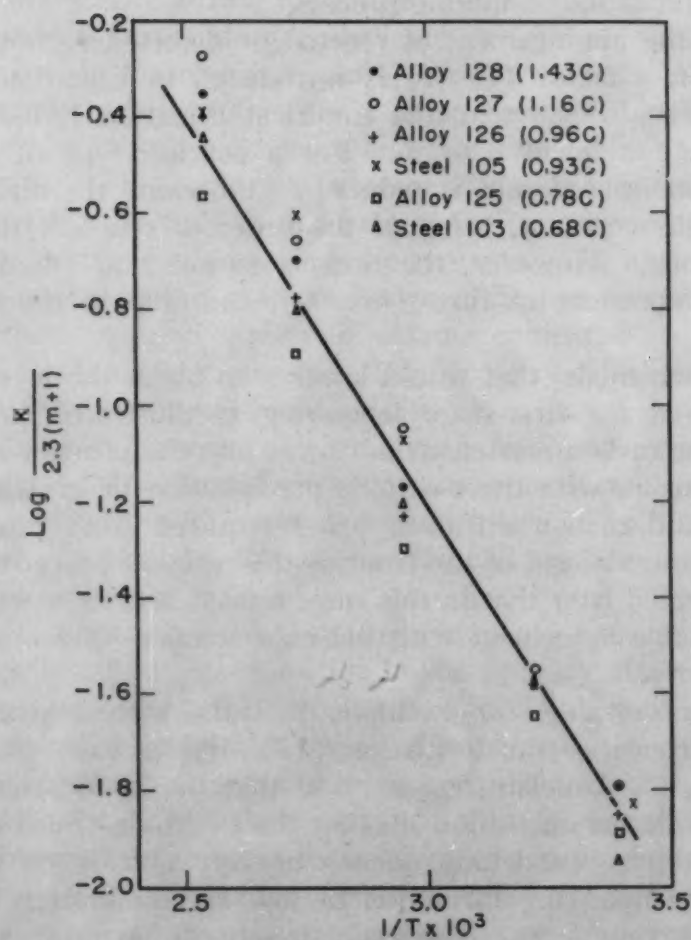


Fig. 14—Temperature Dependence of Rate Constant, K .

The carbon concentration gradient at the advancing front is depicted in Fig. 13B. As the front moves, a carbon balance requires that

$$C_p A \frac{dr}{dt} = C_e A \frac{dr}{dt} + JA \quad \text{Equation 6}$$

where C_p = carbon concentration in the aggregate of ϵ -carbide and low carbon martensite

C_e = carbon concentration in the low carbon martensite

A = constant area of advancing front

$\frac{dr}{dt}$ = rate of advance of front

J = flux of carbon atoms down the concentration gradient toward the advancing front.

From Fick's law, $J = D(\partial c / \partial x)$, where D is the diffusion coefficient of carbon in martensite and $(\partial c / \partial x)$ is the concentration gradient. As a first approximation, the gradient may be assumed linear, or

$$\frac{\partial c}{\partial x} = \frac{C_p - C_e}{L} \quad \text{Equation 7}$$

where C_p = carbon concentration in primary martensite

L = maximum diffusion distance = $B(Dt)^{1/2}$

B = a geometric constant. D is taken to be independent of carbon concentration.

Then Equation 6 becomes

$$\frac{dr}{dt} = \frac{D^{1/2}}{Bt^{1/2}} \cdot \frac{C_p - C_e}{C_p - C_e} \quad \text{Equation 8}$$

On the basis of the model under consideration,

$$\frac{df}{dt} = \frac{NA}{V_0} \cdot \frac{dr}{dt} \cdot (1-f) = \frac{NAD^{1/2}}{BV_0} \frac{(C_p - C_e)}{(C_p - C_e)} \cdot (1-f) t^{-1/2} \quad \text{Equation 9}$$

where N = number of advancing fronts, which is taken to be independent of time

A = area of fronts (independent of time)

V_0 = volume of primary martensite at $t = 0$

$(1-f)$ = impingement correction.

Comparing Equations 9 and 1, it is now seen that $m = -1/2$ (or $n = +1/2$) and

$$K = \frac{NAD^{1/2}}{BV_0} \frac{(C_p - C_e)}{(C_p - C_e)} \quad \text{Equation 10}$$

Not only do the theoretical values of m and n come out to be reasonably close to the observed quantities, but two predictions become possible with regard to the rate constant K . Because K varies as $D^{1/2}$, the activation energy for K should be one-half that of carbon diffusion in martensite. The plot in Fig. 14 indicates that Q_K is about 8000 cal/mol, and that it does not vary significantly with carbon content. This suggests an activation energy of 16,000 cal/mol for carbon diffusion in martensite, which seems reasonable considering the value of 20,000 cal/mol for the diffusion of carbon in alpha iron (2)).

According to Equation 10, K should be a linear function of the carbon content (C_p) of the primary martensite, at any given tempering temperature. As shown in Fig. 15, the K values for the high purity alloys (taken from Table IV) conform to this prediction, ex-

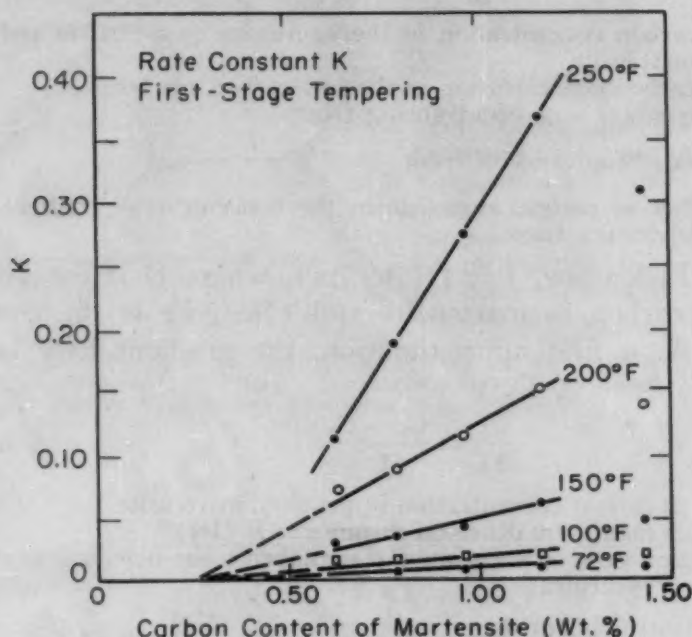


Fig. 15—Composition Dependence of Rate Constant, K .

cept for the highest carbon content. Moreover, the straight-line relationships seem to extrapolate $K = 0$ in the vicinity of $C_p = 0.25\%$, as should be the case for the proposed model.

CONCLUSIONS

The following conclusions may be drawn from these experiments:

1. The first stage of tempering does not consist of the progressive rejection of carbon and decrease in tetragonality of the primary martensite. Rather, it is comprised of the growth of a low carbon tetragonal martensite and a hexagonal close-packed ϵ -carbide at the expense of the primary martensite.
2. The low carbon martensite has an axial ratio corresponding to about 0.25% carbon and the ϵ -carbide has the approximate composition $Fe_{2.4}C$. The two phases appear to be in metastable equilibrium at the end of the first stage.
3. The first stage of tempering obeys kinetics which suggest that:
 - a. The ϵ -carbide and low carbon martensite grow as an aggregate with an advancing plane front.
 - b. Favored sites for the nucleation of the aggregate are present initially and, to a first approximation, the transformation proceeds by growth.

- c. The reaction rate is controlled by the diffusion rate of carbon in martensite through the gradient between the advancing low carbon martensite and the retreating primary martensite.
4. The incidental elements in plain carbon steel do not alter the general kinetics and mechanism of the first stage of tempering. However, they do increase the tempering rate.
5. The transformation rate of retained austenite in the second stage of tempering is controlled by the rate of carbon diffusion in the austenite (Appendix A).

ACKNOWLEDGMENTS

The authors wish to express their thanks for the effective assistance of Leonard Sudenfield, Harold Ludwig, and Walter Fitzgerald, and for the financial support of the Instrumentation Laboratory of the Massachusetts Institute of Technology. The commercial steels were supplied through the courtesy of the Carnegie-Illinois Steel Company.

Dr. B. S. Lement kindly contributed the calculations in Appendix B.

Appendix A

THE SECOND STAGE OF TEMPERING

The unit length changes resulting from the decomposition of the retained austenite in the steels and in the iron-carbon alloys were calculated (16). Useful data were obtained for the steels 103 (0.68% carbon) and 105 (0.93% carbon) and the two high carbon alloys 127 (1.16% carbon) and 128 (1.43% carbon). Because of the large ratio of martensite-to-austenite in all of these alloys, errors in the original data and in the retained austenite determinations are considerably magnified in separating the austenite components, and the resultant probable error is estimated to be about $\pm 10\%$.

The unit length changes produced by the decomposition of the austenite component in alloy 128 (1.43% carbon) are shown in Fig. 16. The data are only given for temperatures of 200 °F (93 °C) and above, where the characteristic transformation to bainite occurs. For lower temperatures, the data confirmed the observations by Averbach and Cohen (12) of a small isothermal transformation to martensite immediately after the quench at a rate nearly independent of the temperature. These results are omitted from Fig. 16 in order to avoid complication.

The activation energies for the second stage were determined by plotting the logarithm of time required for a given amount of transformation versus the reciprocal of the absolute temperature.

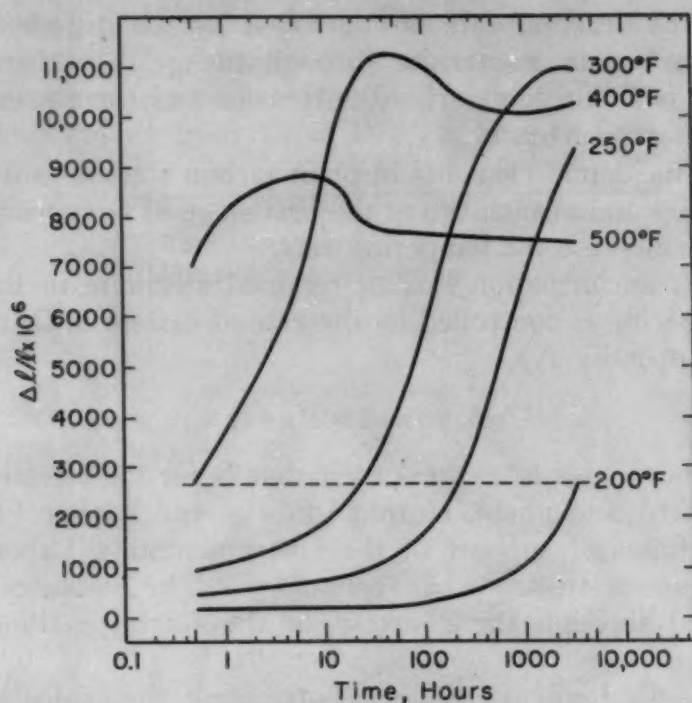


Fig. 16—Length Changes Resulting From Decomposition of 100% Austenite of Iron-Carbon Alloy 128 (1.43% Carbon).

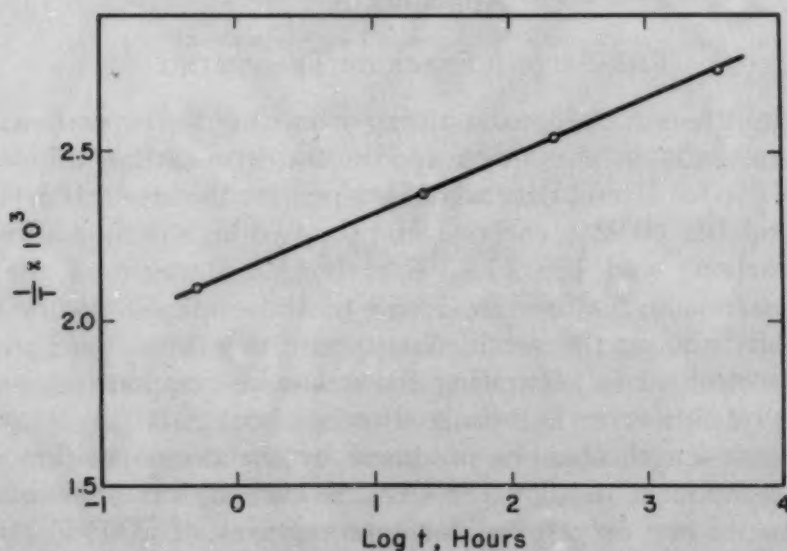


Fig. 17—Second-Stage Activation Energy Plot for Alloy 128 (1.43% Carbon).

Fig. 17 illustrates this plot for alloy 128 (1.43% carbon) using the transformation level indicated by the dashed line in Fig. 16.

The second-stage activation energies are given as a function of carbon content in Fig. 18. On the same plot is shown the activation energies obtained by Wells, Batz and Mehl (18) in their study of carbon diffusion in austenite. Considering the fact that the diffusion

measurements were made at temperatures well up in the austenitic range, the similarity in magnitude of the carbon-diffusion and austenite-decomposition activation energies is most striking. Even the dependence on carbon content is approximately the same; the difference between the two lines in Fig. 18 exceeds the experimental error of ± 2000 cal/mol (in the present work) only at the lowest

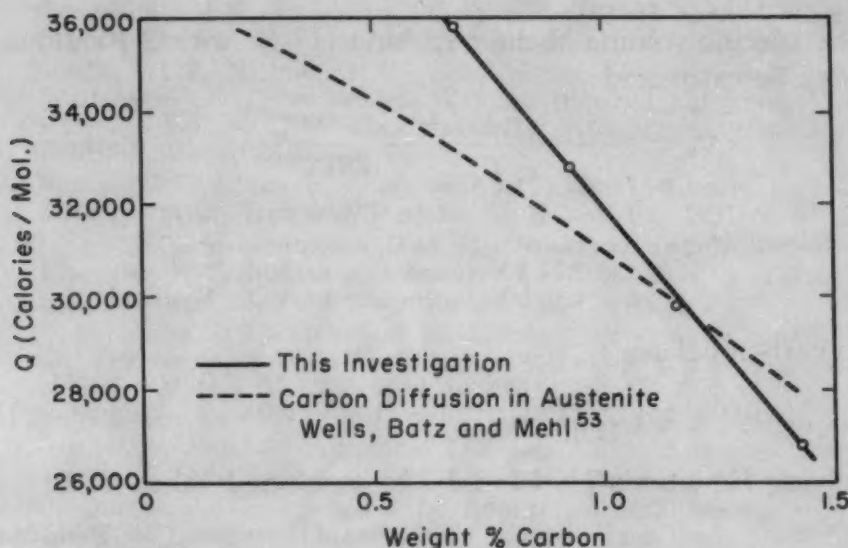


Fig. 18—Variation of Second-Stage Activation Energy With Carbon Content.

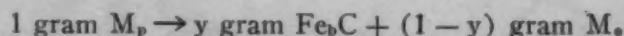
carbon level. Thus, the indications are that the transformation of retained austenite to bainite during the second stage of tempering is controlled by the rate of carbon diffusion in the austenite.

Appendix B

CALCULATION OF CHEMICAL COMPOSITION OF EPSILON CARBIDE

By B. S. LEMENT^o

For Steel No. 103 (0.68% carbon) the unit length change, $\Delta L/L$, corresponding to the end of the first stage was found to equal 1260×10^{-6} . At the end of the first stage the tempering reaction may be written as follows:



$$\frac{\Delta L}{L} = \frac{1}{3} \left[\frac{y \bar{V}_e + (1 - y) \bar{V}_{M_s} - \bar{V}_{M_p}}{\bar{V}_{M_p}} \right] \quad \text{Equation 11}$$

^oDepartment of Metallurgy, Massachusetts Institute of Technology, Cambridge, Mass.

where:

$$\begin{aligned} y &= \text{wt. \% } \epsilon\text{-carbide (Fe}_3\text{C)} \\ 1 - y &= \text{wt. \% martensite (M}_s\text{) containing 0.25\% carbon} \\ \bar{V}_{M_s} &= \text{specific volume of martensite containing 0.25\% carbon} \\ \bar{V}_{M_p} &= \text{specific volume of martensite containing 0.68\% carbon} \\ \bar{V}_\epsilon &= \text{specific volume of } \epsilon\text{-carbide} \end{aligned}$$

From the known parameters of the body-centered tetragonal martensite as a function of carbon content, $\bar{V}_{M_p} = 0.1288$ cc/gm, and $\bar{V}_{M_s} = 0.1277$ cc/gm.

The specific volume of the ϵ -carbide (HCP with 2 Fe atoms per cell) may be calculated:

$$\bar{V}_\epsilon = \frac{0.866 a^2 c}{1.6502 (2) \left(55.85 + \frac{12.01}{b} \right)} \quad \text{Equation 12}$$

$$\begin{aligned} \text{where: } b &= \text{ratio of Fe to C atoms in } \epsilon\text{-carbide} \\ a &= 2.74 \text{ kX (according to A. E. Nygren)} \\ c &= 4.36 \text{ kX (according to A. E. Nygren)} \end{aligned}$$

From a carbon balance:

$$0.0068 = y \frac{12.01}{12.01 + 55.85b} + (1 - y) 0.0025 \quad \text{Equation 13}$$

Solving Equations 11, 12 and 13 for selected values of b :

b	Formula of ϵ -Carbide	Atomic % Carbon	Weight % Carbon	Calculated $\Delta L/L$	Ratio of Calculated to Observed $\Delta L/L$
3	$\epsilon\text{-Fe}_3\text{C}$	25.0	6.68	-470×10^{-6}	0.37
2.4	$\epsilon\text{-Fe}_{2.4}\text{C}$	29.4	8.22	-1270×10^{-6}	1.01
2.2	$\epsilon\text{-Fe}_{2.0}\text{C}_0$	31.0	8.9	-1500×10^{-6}	1.19
2	$\epsilon\text{-Fe}_2\text{C}$	33.3	9.7	-1810×10^{-6}	1.43

It is thus believed that ϵ -carbide has formula corresponding to $\text{Fe}_{2.4}\text{C}$, since the calculated contraction is then equivalent to the observed contraction at the end of the first stage.

As an approximation:

$$\begin{aligned} \frac{\Delta L}{L} \text{ per \% C precipitated in form of } \epsilon\text{-Fe}_{2.4}\text{C} \text{ during first stage} &= \\ \frac{-1260 \times 10^{-6}}{0.68 - 0.25} &= -2930 \times 10^{-6} \end{aligned}$$

This may be written in the form of Equation 3

$$a = 2930 \times 10^{-6} (C_p - 0.25) \quad \text{Equation 3}$$

References

1. R. T. Howard and M. Cohen, "Quantitative Metallography by Point-Counting and Lineal Analysis", *Transactions, American Institute of Mining and Metallurgical Engineers*, Vol. 172, 1947, p. 413.
2. B. L. Averbach, L. S. Castleman and M. Cohen, "Measurement of Retained Austenite in Carbon Steels", *TRANSACTIONS, American Society for Metals*, Vol. 42, 1950, p. 112.

3. G. Kurdjumov, "X-Ray Investigation of the Structure of Tempered Carbon Steels", *Zeitschrift für Physik*, Vol. 55, 1929, p. 187.
4. K. H. Jack, "Structural Transformations in the Tempering of High-Carbon Martensitic Steels", *Journal, Iron and Steel Institute*, Vol. 169, 1951, p. 26.
5. A. E. Nygren, unpublished research, Massachusetts Institute of Technology, 1951.
6. H. Hanemann and L. Traeger, "The Transformations of Hardened Steel on Tempering", *Stahl und Eisen*, Vol. 46, 1926, p. 1508.
7. T. Matsushita and K. Nagasawa, "On the Mechanism of the Tempering of Steels", *Journal, Iron and Steel Institute*, Vol. 116, 1927, p. 311.
8. K. Honda and Z. Nishujama, "On the Nature of Tetragonal and Cubic Martensites", *Science Reports, Tohoku Imperial University, Series I*, Vol. 21, 1932, p. 299; *TRANSACTIONS, American Society for Steel Treating*, Vol. 20, 1932, p. 464.
9. E. Ohman, "X-Ray Investigations on the Crystal Structure of Hardened Steel", *Journal, Iron and Steel Institute*, Vol. 123, 1931, p. 445.
10. G. Hägg, "X-Ray Investigation on the Structure and Decomposition of Martensite", *Jernkontorets Annaler*, Vol. 118, 1934, p. 173; *Journal, Iron and Steel Institute*, Vol. 130, 1934, p. 439.
11. D. P. Antia, S. G. Fletcher and M. Cohen, "Structural Changes During the Tempering of High Carbon Steel", *TRANSACTIONS, American Society for Metals*, Vol. 32, 1944, p. 290.
12. B. L. Averbach and M. Cohen, "The Isothermal Decomposition of Martensite and Retained Austenite", *TRANSACTIONS, American Society for Metals*, Vol. 41, 1949, p. 1024.
13. G. Kurdjumov and L. Lyssak, "The Application of Single Crystals to the Study of Tempered Martensite", *Journal, Iron and Steel Institute*, Vol. 156, 1947, p. 29.
14. G. Kurdjumov and L. Lyssak, "Kinetics of the Primary Stage of Martensite Decomposition", *Journal of Technical Physics*, Vol. 19, 1949, p. 525.
15. G. Kurdjumov and G. Sachs, "Concerning the Mechanism of Steel Hardening", *Zeitschrift für Physik*, Vol. 64, 1930, p. 325.
16. B. L. Averbach, M. Cohen and S. G. Fletcher, "The Dimensional Stability of Steel. Part III—Decomposition of Martensite and Austenite at Room Temperature", *TRANSACTIONS, American Society for Metals*, Vol. 40, 1948, p. 728.
17. E. S. Machlin and M. Cohen, "Habit Phenomenon in the Martensitic Transformation", *Transactions, American Institute of Mining and Metallurgical Engineers; Journal of Metals*, Vol. 3, November 1951, p. 1019.
18. C. Wells, W. Batz and R. F. Mehl, "Diffusion Coefficient of Carbon in Austenite", *Transactions, American Institute of Mining and Metallurgical Engineers*, Vol. 188, 1950, p. 553.
19. C. Zener, "Theory of Growth of Spherical Precipitates From Solid Solution", *Journal of Applied Physics*, Vol. 20, 1949, p. 950.
20. C. A. Wert, "Diffusion Coefficient of C in α Iron", *Physical Review*, Vol. 79, 1950, p. 601.

DISCUSSION

Written Discussion: By W. J. Wrazej, Physical Metallurgy Division, Department of Mines and Technical Surveys, Ottawa, Ont., Canada.

It is of great importance for a practical metallurgist to learn what is the cause of the changes of so many mechanical properties (hardness,

stresses, cracking, etc.) connected with the first stage of tempering. Any information in that field is of great value.

Have the authors confirmed the actual analysis of the austenite by parameter determination in 0.39 and 0.29% carbon alloys?

The authors have confirmed the lattice parameter for ϵ -carbide, using a sample with 0.62% carbon. I have found that bainite is an unavoidable structure component seen at higher magnification in all quenched hypoeutectoid iron-carbon alloys regardless of the rate of quenching and also the temperature and the time of heating. Would any carbide, that might have been associated with bainite, have been taken into consideration?

The existence of stresses in ferrite in tempered steels has been indicated by me (*Journal, Iron and Steel Institute*, 1946, No. II, p. 147P). The distortion of ferrite appears to be obvious because the iron atoms in the interfaces are shared between ferrite and the newly-formed iron-carbon compound. Is the broadening of the diffraction lines (200, 020) seen in Fig. 2 at the final stage (600 minutes at 200 °F) of tempering really connected with the existence of tetragonal newly-formed martensite (roughly 0.25% carbon) or with the distorted ferrite resulting from tempering? What are the other parameters of this newly-formed martensite (0.25% carbon), as they are not quoted in Table II?

How is it that the sample containing 1.43% carbon when tempered at 150 °F shows a smaller c -axis and correspondingly lower carbon content of the newly-produced martensite than the samples tempered at higher temperatures? Would it not be that the lesser distortion of ferrite as pointed out in 1946 is responsible?

The authors say (on the seventh page): "It is evident that carbon content of the low carbon martensite does not vary materially with the carbon content of the primary martensite." There are two conclusions to be drawn from that statement. Either the untempered martensite needles (plates, domains) are all of the same carbon content in all samples, which to me is very probable, or the same temperature of tempering applied to martensites with varying carbon contents results in the same quantity of retained carbon in the newly-formed martensitic needles.

In conclusion, one must commend the authors for broadening our knowledge of iron-carbon alloys because we all realize that the "well-known" iron-carbon alloy system has many puzzling features to be explained.

Written Discussion: By A. G. Allten, Research Laboratory, Crucible Steel Company of America, Harrison, N. J.

The authors are to be complimented on the excellent work done for this interesting paper.

Perhaps it is not appropriate, at this time, to introduce data which involve alloy steels, or such vaguely understood phenomena as hardness changes. However, several observations were made during our investigation of tempering in high silicon steels, which seem to be related to two statements made by the authors.

The authors show that epsilon carbide is in metastable equilibrium with 0.25% carbon martensite after the end of the first stage of tempering, regardless of the carbon content of the primary martensite. The upper two curves of Fig. 19 show the hardnesses of two high silicon alloy steels

of nearly the same base compositions, but of different carbon contents, as-quenched, refrigerated, and tempered at the indicated temperatures. Cementite was not found in either steel, because of the high silicon contents, after 2-hour tempers at 600 °F. Therefore, it seems reasonable to assume that epsilon carbide is in equilibrium with the same low carbon martensite in both steels after the 600 °F temper. However, appreciable differences in hardness exist between the high and low carbon steels, even though the carbon content of the martensite in both steels may be nearly

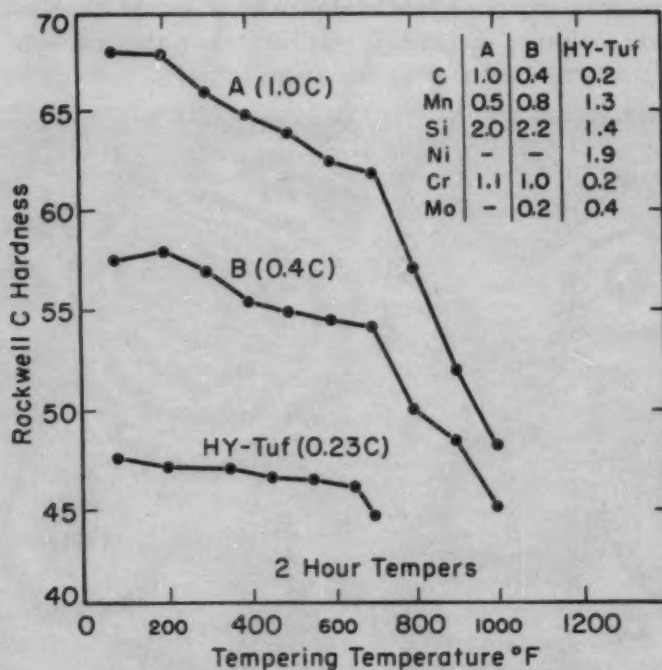


Fig. 19—Hardness Curves of Silicon Alloys As-Quenched, Refrigerated and Tempered at Indicated Temperatures.

the same. This introduces a question: Are these hardness differences, between high and low carbon steels at or near the end of the first stage of tempering, attributable to differences in the amount of epsilon carbide in the steels?

Data presented by Fletcher and Cohen¹⁰ indicate that such hardness differences after the first stage of tempering also exist, between steels of various carbon contents, when the alloy and silicon contents are low.

Note, also, that the decrement from as-quenched hardness to the hardness after a 2-hour temper at 600 °F becomes smaller with decrease in carbon content.

The corresponding decrement in hardness is relatively small in the 0.2% carbon, 1.4% silicon, alloy steel, HY-Tuf.

This observation seems to be in accord with the deduction, made by the authors, that little, if any, change would occur in the composition of primary martensites of 0.25% carbon content during the first stage of tempering.

¹⁰S. G. Fletcher and M. Cohen, "The Effect of Carbon on the Tempering of Steel", *TRANSACTIONS, American Society for Metals*, Vol. 32, 1944, p. 333, Fig. 2.

Written Discussion: By B. S. Lement, research staff, Department of Metallurgy, Massachusetts Institute of Technology, Cambridge, Mass.

From a recent study¹¹ of the tempering of the same high purity iron-carbon alloys used by the authors, I have obtained some electron microscopic evidence with respect to the sites at which ϵ -carbide precipitates during the first stage of tempering. The authors assume that the second strain of the original martensitic transformation divides each plate into a large number of lamellar regions, the boundaries of which provide the nucleation sites for the ϵ -carbide. From the results of my examination using the electron microscope, no evidence was found that ϵ -carbide precipitates in such fashion; instead, it appears that this carbide forms as a

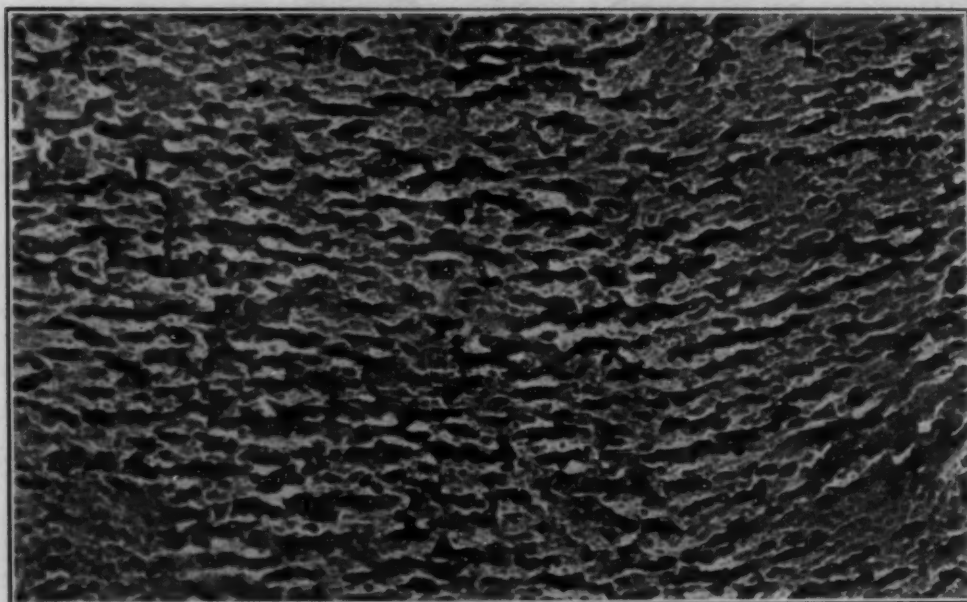


Fig. 20—Electron Micrograph of 1.43% Carbon, High Purity Iron-Carbon Alloy Austenitized at 2200 °F, Brine-Quenched to Room Temperature and Tempered 1 Hour at 400 °F. Structure consists of subgrains of tempered martensite with epsilon carbide present at subboundaries. Metallographic specimen was etched in modified picral. Negative parlodion replica rotary shadowed with chromium. $\times 20,000$.

discontinuous network along the boundaries of subgrains in the martensite. Since subgrains of about the same size were also found in retained austenite, it is believed that the subgrains in austenite are inherited by the martensite as a result of the hardening transformation. The subboundaries in martensite provide convenient nucleation sites both from the standpoint of their availability and the relatively short distance required for carbon diffusion.

The presence of subgrains about 1000 Å in diameter is shown in Fig. 20, which is an electron micrograph of the authors' 1.43% carbon alloy tempered at 400 °F. There appears to be a subboundary network of ϵ -carbide present in tempered martensite. The thickness of this carbide network is apparently nonuniform, reaching a maximum value of about 200 Å in some locations.

¹¹B. S. Lement, B. L. Averbach and M. Cohen, "Microstructural Changes on Tempering Iron-Carbon Alloys", to be submitted to the American Society for Metals.

A departure from the conventional method of shadowing replicas was utilized in obtaining the electron micrograph of Fig. 20. Instead of the replica remaining in a fixed position, it was rotated during chromium evaporation. This results in delineation of the microconstituents by a dark border and the obscuring effect of "white shadows" is eliminated. Rotary shadowing was first utilized by Heinmets¹² for studying biological specimens; however, it should prove quite useful for determining fine structures in metals.

Authors' Reply

Mr. Wrazej has brought up several interesting points. The lattice parameters of the austenite were not determined in this investigation, but these measurements will be included in future work. No bainite was observed in the specimens used for the calculations. An effort was made to maintain uniformly rapid quenching conditions and since the specimens were quite small, it is not likely that any appreciable quantity of bainite was formed in the alloys containing more than 0.6% carbon, on which the calculations were based.

The appearance of the 0.25% carbon martensite line should not be confused with the broadening of a ferrite line by internal stresses. In the single crystal technique the (002) line of tetragonal martensite is completely separated from the other line in the doublet, and it is quite clear from Fig. 2 that a new and separate (002) line corresponding to the 0.25% carbon martensite is formed. Broadening due to internal stresses would simply diffuse the original (002) line without changing its position materially.

An increase in the c parameter of the low carbon martensite as the tempering temperature is increased is attributed to an increase in the solubility of carbon in the martensite in metastable equilibrium with the ϵ -carbide. This is shown for the 1.43% carbon alloy in Table II. On tempering at 250 °F, all four alloys arrive at the same carbon content (within experimental error) in the martensitic matrix at the end of the first stage.

The authors are grateful to Mr. Allten for including his hardness data on silicon alloy steels. Plain carbon steels also show some of the features exhibited by Fig. 19. The hardness differences between high and medium carbon steels at the end of the first stage may be attributed to differences in the amount of precipitated ϵ -carbide. The ϵ -carbide, as shown in the electron micrograph of Dr. Lement in Fig. 20, is quite finely distributed and the hardness might well increase with the amount of this carbide. The hardness level of the 0.23% carbon steel shown in Fig. 19 does not change much on tempering in the first stage. This is confirmed by some recent results of Dr. Lement on 0.15% carbon steel which remains essentially constant in hardness on tempering during the first stage. According to the present investigation, ϵ -carbide would not be expected to precipitate in these low carbon steels.

The authors thank Dr. Lement for the inclusion of his electron micro-

¹²F. Heinmets, "Modification of Silica Replica Technique for Study of Biological Membranes and Application of Rotary Condensation in Electron Microscopy", *Journal of Applied Physics*, Vol. 20, 1949, p. 385.

graph showing the distribution of ϵ -carbide at subboundaries in the martensite. This is a new finding, and will have to be considered in theories of tempering. However, the kinetic treatment presented in this paper is still applicable; the plane-front growth of the ϵ -carbide merely starts from a network of subgrain boundaries rather than from an array of parallel zones, as depicted in the hypothetical model of Fig. 13.

THE EFFECT OF QUENCHING AND TEMPERING ON RESIDUAL STRESSES IN MANGANESE OIL HARDENING TOOL STEEL

BY HAROLD JACK SNYDER

Abstract

The effect of quenching and tempering on the distribution of residual stresses in a manganese oil hardening tool steel is discussed. The data presented indicate that the principal quenching stresses in a fully hardened flat specimen are tensile, equal in all surface directions, and concentrated within a surface layer 0.025 inch in thickness. A tempering treatment progressively decreases these surface stresses until they become negligible or slightly compressive, but the tempering treatment does not affect the depth of penetration. The maximum drop in residual surface stress occurs with tempering between 425 and 650 °F (220 and 345 °C).

The effects of etching, lapping and grinding on residual stresses in the same steel have also been investigated. Tests indicated that etching in a 5% solution of nital introduces no residual stresses; lapping induces compressive stresses to a depth of 0.0003 inch; grinding induces unequal biaxial stresses which penetrate to a greater depth in hardened than in tempered or annealed manganese oil hardening steel.

INTRODUCTION

QUENCHED metals contain residual stresses which can be either beneficial or detrimental to their service applications. The residual stresses induced by heat treatment as well as other operations greatly affect the behaviors of the metals in service (1, 2, 3).¹ In the case of steels, the problem of controlling residual stresses is made complex by the phase transformations which occur during hardening or upon tempering. Phase transformations are known to alter the normal thermal stress pattern induced in a metal (4, 5). Conse-

¹The figures appearing in parentheses pertain to the references appended to this paper.

From a thesis submitted by Mr. Snyder to the Department of Metallurgical Engineering, University of Pittsburgh, in partial fulfillment of the requirements for the degree of Master of Science.

A paper presented before the Thirty-fourth Annual Convention of the Society, held in Philadelphia, October 18 to 24, 1952. The author, Harold Jack Snyder, is a research associate, Mellon Institute of Industrial Research, Pittsburgh. Manuscript received May 16, 1952.

quently, the prediction of the most favorable heat treatment for a particular steel is almost impossible unless the effects of quenching and tempering on the stress pattern of that steel are actually known. While information on the residual stress pattern in several quenched steels is available in the literature (5-8), the effects of tempering on such a pattern has never been completely illustrated in the references surveyed. Early investigators (6, 9) in the field of quenching stresses generally state that tempering either eliminated or progressively decreased residual stresses. This generalization was valid until recently, when Boegehold (4) showed that a tempering treatment on steels containing retained austenite did not necessarily decrease or eliminate internal stresses, but could also increase the magnitude of the residual quenching stress. The early investigators (4, 9) presented little or no quantitative information on the actual distribution of stresses in quenched and tempered steels. The work described in this paper deals solely with the distribution of quenching and tempering stresses in a manganese oil hardening steel.

EXPERIMENTAL PROCEDURE

Residual stresses were induced in steel specimens by quenching and tempering to different hardness levels. The magnitude and distribution of these stresses were determined with an adaptation of the Bauer and Heyn (10) technique. The procedure consisted of removing thin surface layers from the heat treated specimens, while observing the resultant curvature changes by Letner's (11) optical interference method. The stress values for the distributions were subsequently calculated from a mathematical relationship that exists between stress and curvature previously introduced by Treuting and Read (12).

Specimen Preparation

Manganese oil hardening tool steel was used in this investigation and had the following chemical composition: carbon 0.90%, manganese 1.30%, chromium 0.42%, tungsten 0.42%, phosphorus 0.025%, sulphur 0.017%, silicon 0.32%. Six specimens were milled from flat stock to provide 2 by 2 by $\frac{1}{2}$ -inch test blocks. These pieces were surface ground to remove decarburization and then placed in a neutral salt bath (20% NaCl, 25% KCl, and 55% BaCl₂ by weight) for hardening. Five of the six test pieces were hardened by quenching in oil, after they had been subjected to the following treatments: 15-minute preheat at 1250 °F (675 °C); salt bath temperature was raised to 1475 °F (800 °C); 10-minute soak at 1475 °F (800 °C). After quenching, four of the five hardened test pieces were individually tempered in a low temperature salt bath for 1 hour before air cooling from the tempering temperature.

The one test sample which had not been hardened was subjected to the following so-called stress relieving treatment: 24 hours at 1100 °F (595 °C), furnace cool to 500 °F (270 °C), air cool to room temperature. The quenching, tempering and annealing treatments gave residual stress specimens having average hardness values shown in Table I.

Table I
Rockwell "C" Hardness Values of Heat Treated Residual Stress Specimens

Specimen No.	Treatment	Average Rockwell "C" Hardness
1	As-Quenched, 1475 °F (800 °C)	64
2	Tempered 1 hr., 425 °F (220 °C)	58
3	Tempered 1 hr., 650 °F (345 °C)	53
4	Tempered 1 hr., 800 °F (425 °C)	48
5	Tempered 1 hr., 1150 °F (620 °C)	35
6	Stress Relieved, 1100 °F (595 °C)	10

Optical Interference Method for Determining Residual Stresses

A highly polished reflectent reference surface was obtained by lapping and subsequently polishing by several strokes on 4/0 emery paper in accordance with Letner's (11) method.

The method for measuring internal stresses consisted of the following steps: (a) Metal was removed from the surface opposite the polished reference side of the test piece. (b) Curvature was measured before any metal was removed and after each metal removal. (c) Stresses were calculated with the data obtainable from a graph showing curvature as a function of metal thickness removed.

Metal Layer Removal Techniques—Chemical etching, lapping, and surface grinding provided three ways of removing surface layers from the quenched and tempered specimens. The samples were weighed and measured with a micrometer before removing any surface material. Thereafter the amount of metal removed was calculated from the weight loss.

Since the method of removing metal generally influences the results of residual stress determinations, it was necessary to investigate the effects of etching, lapping, and grinding on the curvature of the steel, for these methods have been the target of criticisms on previous investigations (13).

The surface opposite the polished side on three 2 by 2 by 1/4-inch pieces of annealed manganese oil hardening tool steel, which had been given a stress relief anneal for 24 hours at 1100 °F (595 °C), was subjected to two successive surface removals by etching in a 5% solution of nital, while the remainder of the specimen was protected from etching with Gulfwax. Curvature measurements were made before etching and after each etch. The results shown in Fig. 1

indicate that etching manganese oil hardening tool steel in a 5% solution of nital did not introduce any noticeable curvature or stress and could be safely used for removing surface layers.

The same steel pieces were subjected to lapping. Lapping was done on a Lapmaster (cast iron plate) with 500 cm³ of cutting oil containing 19 grams of 800-grit Al₂O₃ abrasive as the lapping vehicle. Once lapping was begun, the specimens were removed intermittently for curvature examinations. Lapping of the test blocks was continued

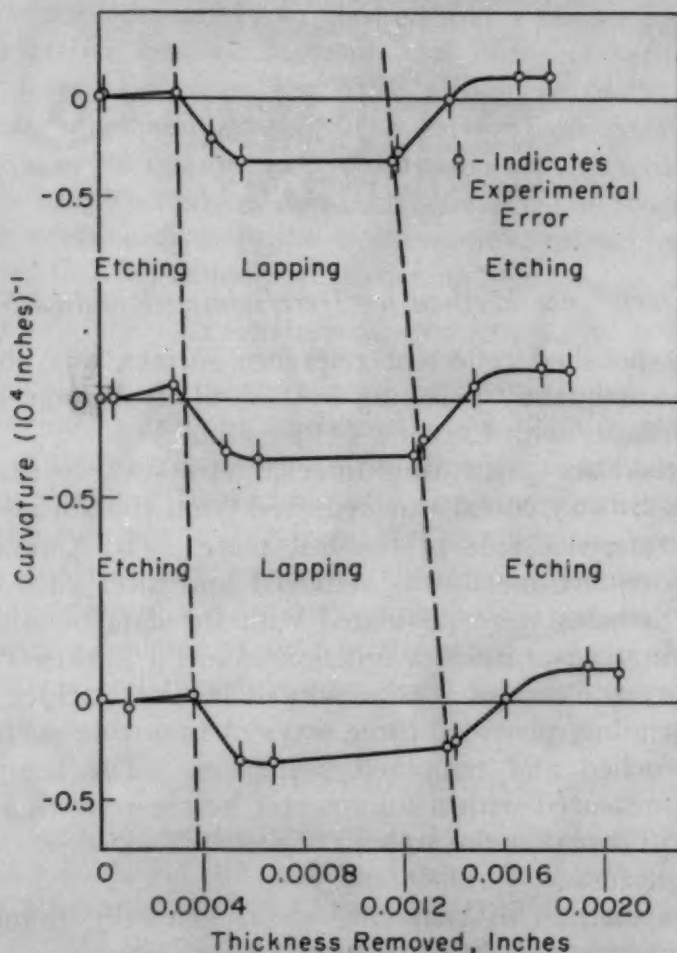


Fig. 1—Curvatures Induced in Annealed Manganese Oil Hardening Tool Steel by Etching and Lapping.

until the curvature became practically constant as illustrated in the central portion of Fig. 1. At this point, lapping was terminated and etching was again used for dissolving surface layers. Etching was carried on until the curvatures ceased to change appreciably.

Conclusions drawn from the lapping effects, illustrated in Fig. 1, were that lapping under the conditions employed introduced negative curvature (-0.35×10^{-4} /inch approximately) or a nominally compressive stress. This compressive stress extends to a depth of ap-

proximately 0.0003 inch and can be thoroughly removed by etching a similar amount away in a 5% solution of nital. This indicated that lapping was a safe means for removing surface layers if its effects were etched away afterwards.

An investigation of the effect of grinding on manganese oil hardening tool steel was not necessary, since information on this subject was already available in literature. Letner (11) presented the fact that grinding with a white fused alumina wheel (8 by $\frac{1}{2}$ by $1\frac{1}{4}$ inches) of 46 grit and "J" hardness under the following conditions would induce stresses which affected this steel to a depth of 0.0045 inch.

Wheel speed (idling)	6000 feet per minute
Traverse speed	50 feet per minute
Crossfeed	0.050 inch
Downfeed	0.0007 inch
Grinding fluid	none (air)

Knowledge of this fact made grinding a suitable tool for removing surface material. Layers were stripped without affecting the remaining metal by first grinding and then taking off an additional 0.0045 inch by lapping and etching.

Once the effects of etching, lapping, and grinding on curvature were established, the arrangement of a test procedure was readily accomplished. Since etching was the best means for separating metal, it alone was used for removals until approximately 0.005 inch was removed from the surface of each experimental block. Lapping in conjunction with etching was the technique employed for detaching material until slightly more than 0.020 inch was stripped from one side of the test pieces. In all instances where lapping was used, it preceded the etching. This allowed the effects of lapping to be continuously offset by the etching away of 0.0003 inch. The material discarding procedure from 0.020 inch to the center of the specimen was threefold in nature. First, the experimental blocks were ground on the side under investigation; secondly, they were lapped until an additional 0.005 inch was taken off; and thirdly, all were etched in nital. In this way it was possible throughout the entire investigation to separate metal layers from the test piece with a minimum amount of after-effects.

Curvature Measurement—The optical interference method introduced by Letner (11) was used for measuring curvatures and consisted briefly of the following procedure. First, an interference pattern was established by placing an optical flat on the polished surface of the test piece and passing monochromatic (sodium) light through the flat. Secondly, the interference pattern thus set up between the bottom surface of the optical flat and the polished surface of the specimen was photographed at unit magnification. Thirdly, the pho-

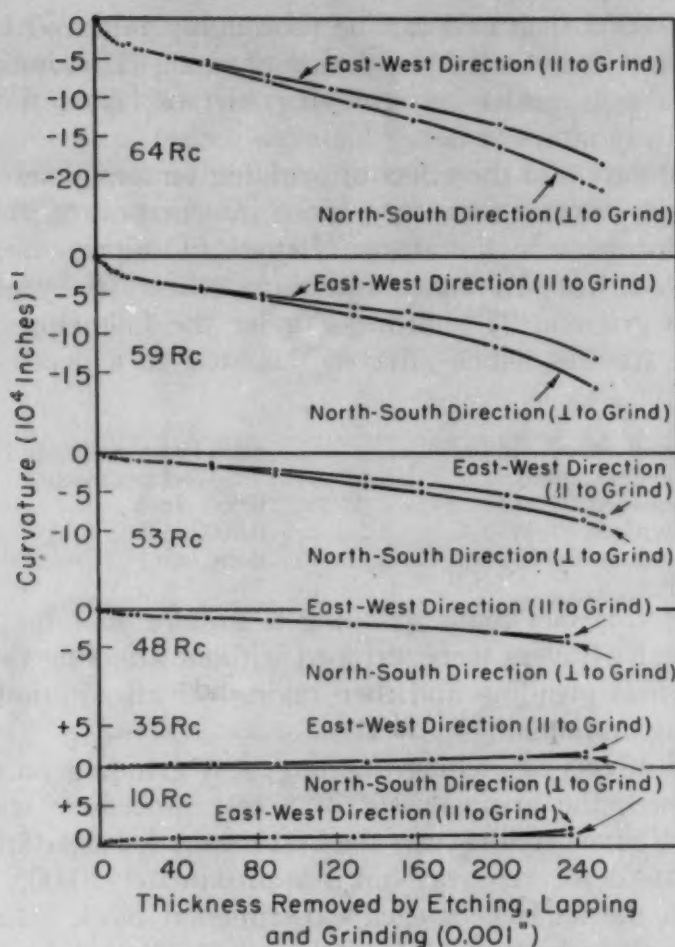


Fig. 2—Curvature Variation With Metal Removal From Heat Treated Specimens of Manganese Oil Hardening Tool Steel.

tographic negative of the interference pattern was used to graphically plot the profile of the surface.

Once the profile of the test piece was plotted, the curvature was then determined from the following geometrical relationship between the reciprocal of the arc radius $1/R$, the arc height h , and the gage length L .

$$\text{Curvature} = \frac{1}{R} = \frac{8h}{(4h^2 + L^2)}$$

or since $h \ll L$

$$\frac{1}{R} = \frac{8h}{L^2}$$

Every specimen was subjected to twenty-two alternate surface removals and curvature measurements. One curvature measurement constituted the plotting of two individual profiles, since profiles were

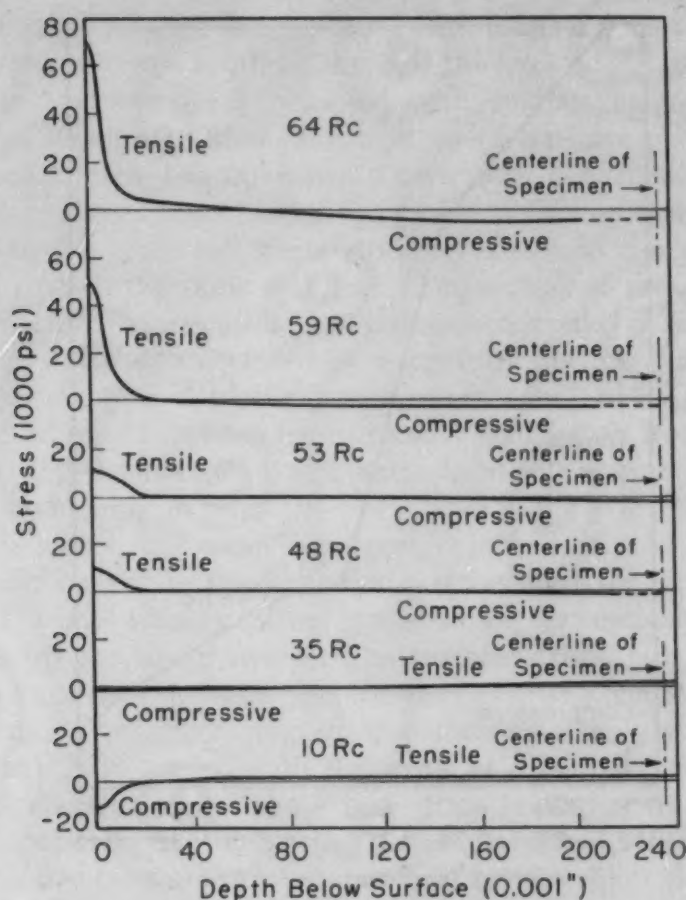


Fig. 3—Residual Stress Distribution in Heat Treated Specimens of Manganese Oil Hardening Tool Steel.

made at right angles in an effort to observe any directional effects. A graph of curvature versus thickness removed was plotted for the test blocks and is shown in Fig. 2.

Stress Calculation—The mathematical relationship existing between curvature and stress has been presented in different forms by many investigators (11, 14, 15, 16). For the case of biaxial stress in beams where the principal stresses σ_x and σ_y are equal, Treuting and Read (12) derived the following expression in terms of curvature c , distance from initial centerline to original surface Z_0 , and distance from initial centerline to instantaneous surface Z_1 , using the modulus of elasticity E of the material and Poisson's ratio ν .

$$\sigma(Z_1) = \frac{E}{6(1-\nu)} \left[(Z_0 + Z_1)^2 \frac{dc}{dZ_1} + 4(Z_0 + Z_1)c - 2 \int_{Z_1}^{Z_0} c dZ \right]$$

Equation 1

In order to apply this equation to determine residual stress, it was necessary to make expanded plots of Fig. 2. From these ex-

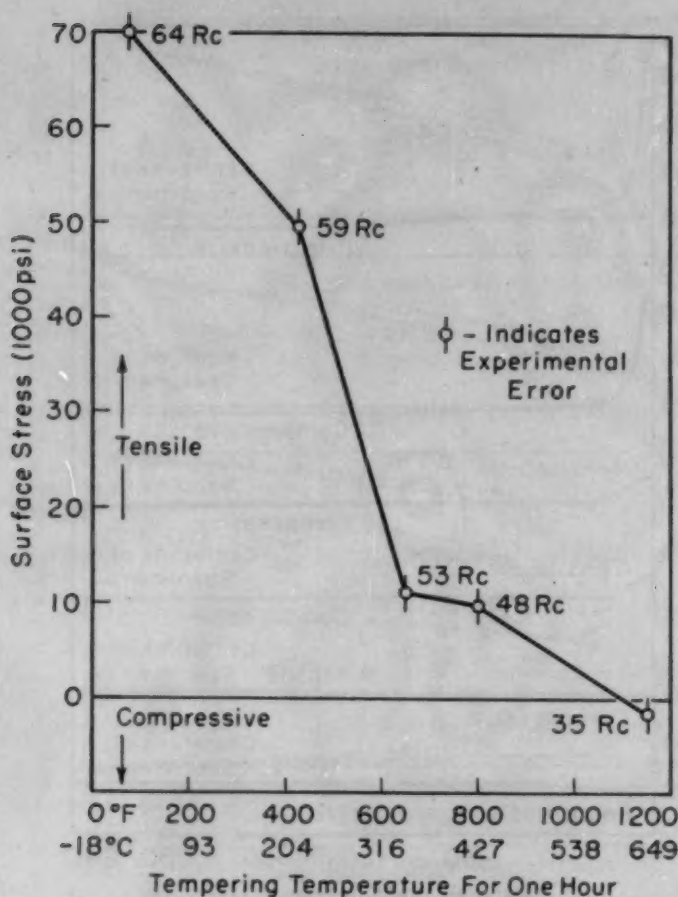


Fig. 4—Effect of Tempering on Surface Stress in Quenched Manganese Oil Hardening Tool Steel.

panded working curves the essential values (slope, dc/dZ_1 , curvature, c , thickness removed, and area under the curve) for calculating stress were either read or measured. This equation was used to calculate the stress distributions shown in Fig. 3.

The accuracy in measuring stress depends both on curvature and on the slope as determined from the curvature versus thickness removed curve. Because of this, the stress error varies within a specimen and between different specimens. Naturally, the error is greatest where slope determinations are most difficult. Therefore, the maximum error for each specimen was calculated by comparing the results obtainable when using the extremes in slope measurements at the surface. The results of the individual specimens are indicated by a vertical line in Fig. 4.

DISCUSSION OF RESULTS

The unique feature of the residual stress distribution curves shown in Fig. 3 is the narrow range of thickness in which the larger residual heat treating stresses are concentrated. In each specimen

the larger stresses were concentrated within 0.025 inch of the surface or approximately one tenth of the half-thickness. All the remaining half of the specimen was occupied with smaller balancing stresses of the opposite sign. Other investigators (5-8) have presented stress distribution curves, but none has shown such a narrow band (0.025 inch) of large stress concentration. Some of this unlikeness no doubt arises from the different steels studied, except in the case of Scott (5) who studied the same material. Regardless of the reason for its difference from others, the result obtained could prove important, particularly to those interested in using fully hardened sections without the presence of a tensile stress on the surface. To accomplish this it would only be necessary to remove 0.025 inch from the surface of the hardened pieces in a non stress-inducing manner, i.e., lapping followed by etching in nital.

To industry, the most important result illustrated by the stress distribution curves is the quenching stress and the way tempering affects it. Fig. 4 illustrates that tempering at successively higher temperatures progressively reduced the surface stress, but Fig. 3 shows that it did not appreciably affect the depth to which the main stresses penetrated. The decreasing of the surface stress with increasing temperature is in accord with the work of others (4, 6, 9), particularly Boegehold (4).

The possibility of tempering a fully hardened steel surface from tension to compression appeared rather remote upon first glance, so the last point on the tempering temperature versus residual surface stress curve in Fig. 4 drew particular attention. The introduction of an entirely new residual stress in that particular specimen, during its cooling from the tempering temperature, was believed to be the reason for the compressive stress. This explanation is substantiated by reference to Sachs (7). Sachs determined residual stresses in steel pieces cooled from below the upper critical and showed that such action creates compressive surface stress. In other words, if the phase transformation is eliminated, it is impossible to obtain a tensile stress on the surface.

The same explanation fits the behavior of the Rockwell C-10 specimen in Fig. 3. The noticeable difference in the magnitude of compressive surface stress between the Rockwell C-10 test piece and the Rockwell C-35 is attributed to dissimilar heat treatment. The Rockwell C-10 test piece was never hardened, but was taken in the annealed condition and given a 24-hour stress relief anneal at 1100 °F (595 °C), whereas the Rockwell C-35 specimen was fully hardened and then tempered at 1150 °F (620 °C) for 1 hour. Consequently, the Rockwell C-10 specimen did not have any tensile quenching stresses to overcome and as a result possibly was more susceptible to the introduction of compressive stress than the Rockwell C-35 piece.

Another feature of industrial importance illustrated by the curve in Fig. 4 is the abrupt drop in residual surface stress between the temperature 425 and 650 °F (220 and 345 °C). This is an interesting result because after quenching, manganese oil hardening tool steel is ordinarily tempered in the 300 to 500 °F (150 to 270 °C) range. Tempering in this range is considered adequate enough for causing any retained austenite to transform and severe residual stress to disappear without appreciably decreasing hardness. Regarding residual stress magnitude, however, the experimental information indicates it may be beneficial to increase the tempering temperature range limit to possibly 650 °F (345 °C) on occasions where the hardness loss is inconsequential and low residual stress is of prime importance.

The curvature curves shown in Fig. 2 display several interesting phenomena. Although the curvature of each experimental block was simultaneously measured in two different directions (at right angles), only one curve for each piece resulted during the early removals. Since in this case equality of curvature represents equality of stress, it was decisively concluded that residual heat treating stresses are equal and uniform in all surface directions. This conclusion is a logical assumption of thermal stress theory which is seldom proved.

The dividing in the later portion of the curvature curves shown in Fig. 2 was caused by grinding. The curvature measurements on each specimen remained equal in both measured directions as long as etching alone or lapping in conjunction with etching was employed for surface removals. Once grinding was used for stripping material, curvatures measured in the east-west direction (parallel to grind) were always algebraically greater than the curvatures measured in the north-south direction (perpendicular to grind). These findings were conclusive evidence that grinding stresses are of an unequal biaxial nature which agrees with the data presented by Letner (11). At the same time the Rockwell C-64, C-58, and C-53 curves were dividing, the Rockwell C-10, C-35, and C-48 curves were continuing in a smooth fashion. Such a behavior made it appear evident that the effects of grinding were essentially eliminated in the Rockwell C-10, C-35, and C-48 samples by lapping and etching. This was no doubt true, since the depth to which grinding stresses penetrated in a specimen similar to the Rockwell C-10 was effectively removed from all the test pieces after grinding. These happenings were fruitful, since they showed that the penetrating effect of grinding was influenced by hardness, the grinding stresses penetrating deeper with increasing hardness.

Although the information obtained on etching and lapping from the preliminary experiment is not complete and will be dealt with

more thoroughly in a later publication, it is worthwhile mentioning here for the purpose of summation.

Fig. 1 illustrates that etching does not introduce any significant curvature (stress). Nevertheless, the curvature observed was slightly positive and could mean one of two things. Either the curvature was caused by the release of compressive stresses present in the specimen surface, which is the meaning preferred by the author, or the introduction of tensile stresses by the etching. Regardless of how it is interpreted, the evidence is still contradictory to the work of Lihl (17). Lihl contends that all acid etching introduces compressive stress. The difference between Lihl's results and those of the author no doubt stems from the methods used by each. Lihl used X-ray diffraction and determined microstresses whereas the author conducted a macroscopic investigation, so they cannot be entirely likened to each other.

CONCLUSIONS

The following conclusions were based on the behavior of 2 by 2 by 1/2-inch specimens of manganese oil hardening tool steel, quenched in oil from 1475 °F (800 °C).

1. Residual surface stress is approximately 70,000 psi tension.
2. Primary residual quenching stresses extend to a depth below the surface of approximately 0.025 inch.
3. Residual stresses are progressively reduced by tempering at successively higher temperatures.
4. Residual stresses are eliminated by tempering for 1 hour at 1150 °F (620 °C).
5. The residual surface stress in a fully annealed piece, after it has been stress relief annealed for 24 hours at 1100 °F (595 °C), is approximately 12,000 psi compressive.

As a result of this investigation the following conclusions should also be applicable to other steels.

6. Residual heat treating stresses in flat beams are equal and uniform in all surface directions, neglecting edge effects.
7. The effects of grinding penetrate deeper in hardened than in annealed or tempered steel.
8. Surface grinding induces unequal biaxial stresses.

The following facts regarding the effects of etching and lapping on manganese oil hardening tool steel are mentioned for the purpose of summation and should be considered only as indications of behavior.

9. Etching in a 5% solution of nital does not induce any stress.
10. Lapping induces compressive stresses which extend to a depth of 0.0003 inch.

ACKNOWLEDGMENT

The facilities for this research were provided by the Grinding Wheel Institute. Acknowledgment is extended to Dr. Harold R. Letner of the Mellon Institute for his generous council and to Dr. J. Alfred Berger of the University of Pittsburgh for his helpful suggestions.

References

1. J. O. Almen, "Fatigue Failures Are Tensile Failures", *Product Engineering*, March 1951, p. 102-123.
2. K. Heindlhofer, *Evaluation of Residual Stresses*, McGraw-Hill Book Company, Inc., New York, Toronto, London, 1948, p. 6, 7, 28.
3. C. A. Zapffe, "Boiler Embrittlement", *Transactions*, American Society of Mechanical Engineers, Vol. 66, 1944, p. 81-126.
4. A. L. Boegehold, "Some Effects of Quenching and Tempering on Residual Stresses in Steel", *METAL PROGRESS*, February 1950, p. 183-188.
5. H. Scott, "Origin of Quenching Cracks", *Scientific Papers of the Bureau of Standards*, Vol. 20, 1924-26, p. 399-444.
6. V. H. Bühler, H. Buckholtz and E. H. Schulz, "Eigenspannungen bei der Wärmebehandlung von Stahl", *Archiv für das Eisenhüttenwesen*, Vol. 5, 1931-1932, p. 413.
7. G. Sachs, "Residual Stresses in Metals", *Akademische Verlagsgesellschaft m.b.H.*, 1937, p. 216-217.
8. V. H. Bühler and E. Scheil, "Zusammenwirken von Wärme- und Umwandlungs Spannungen in abgeschreckten Stählen", *Archiv für das Eisenhüttenwesen*, Vol. 6, 1932-1933, p. 283; "Einfluss der Abschreckbedingungen auf die Eigenspannungen von Stählen", *Archiv für das Eisenhüttenwesen*, Vol. 7, 1933-1934, p. 359.
9. T. McL. Jasper, "Calculation of Quenching Stresses in Hardened Steel", *Engineer*, Vol. 118, 1924, p. 343.
10. E. Heyn and O. Bauer, "On Stresses in Cold Drawn Metals", *Internationale Zeitschrift für Metallographie*, Vol. 1, 1911, p. 16-50.
11. H. R. Letner, "Application of Optical Interference to the Study of Residual Surface Stresses", to be published in *Proceedings*, Society for Experimental Stress Analysis.
12. R. G. Treuting and W. T. Read, Jr., "A Mechanical Determination of Biaxial Residual Stress in Sheet Materials", *Journal of Applied Physics*, Vol. 22, February 1950, No. 2, p. 130-134.
13. D. J. Demorest and D. O. Leeser, "A Study of Residual Stresses in Flat Beams by Electropolishing Methods", presented at the annual meeting of the Society for Experimental Stress Analysis, Philadelphia, Nov. 28-30, 1951.
14. D. G. Richards, "A Study of Certain Mechanically-Induced Residual Stresses", *Proceedings*, Society for Experimental Stress Analysis, Vol. 3, No. 1, 1945, p. 40-61.
15. N. N. Davidenkov and E. M. Shevandin, "The Study of Residual Stresses Due to Bending", *Journal of Technical Physics*, Vol. 9, No. 12, 1939, p. 1112-1124.
16. F. Stäblein, "Spannungsmessungen an einseitig abgeloschten Knuppeln", *Kruppsche Monatshefte*, Vol. 12, 1931, p. 93-98.
17. F. Lihl, "Anderung des Spannungszustandes der Werkstoffoberfläche durch Atzen", *Archiv für Metallkunde*, Vol. 1, October 1946, p. 16-25.

DISCUSSION

Written Discussion: By S. R. Maloof, H. R. Erard and R. K. Steele, metallurgists, Springfield Armory, Springfield, Mass.

The author's Fig. 4 is of particular interest to us, since we have been using an X-ray method developed in our laboratory to study the relief of the surface residual stress on tempering. At the present time, we have information on an FS 1050 steel oil-quenched from 1550 °F and tempered in the range 200 to 1200 °F. All specimens were air-cooled from the tempering temperature. The specimens used were approximately $\frac{1}{4}$ by $\frac{5}{8}$ by 6 inches. The X-ray measurements were made with unfiltered CrK α radiation on the unresolved (211) K α -doublet of ferrite with a Norelco high-

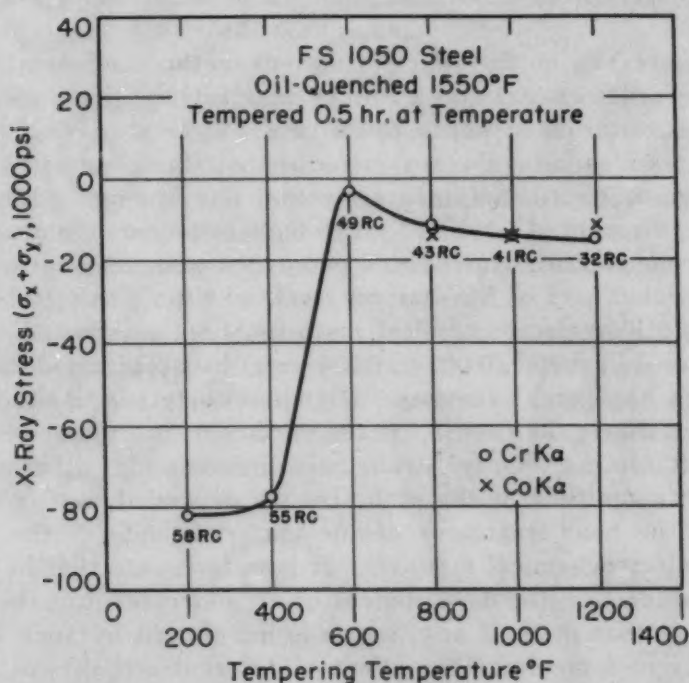


Fig. 5—Reduction in the Surface Stress of FS 1050 Steel on Tempering $\frac{1}{2}$ Hour at the Temperatures Indicated.

angle X-ray spectrometer. At the higher tempering temperatures, it was possible to check the results with CoK α radiation reflected from the (310) planes of ferrite. Following the temper, the specimens were given a light polish on 3/0 emery paper and etched with 10% nital to remove about 0.002 inch.

The results of our investigation are shown in Fig. 5 in which it is seen that the surface stress is markedly reduced on tempering above 400 °F, confirming the findings of the author. The X-ray stresses determined with CoK α radiation are in excellent agreement with those determined with CrK α radiation. Although the author's specimens contained tensile stresses and ours compressive stresses, Boegehold² has pointed out that the formation of tensile or compressive stresses in the surface layers would depend

²See Reference 4 of paper.

on several factors, principally the hardenability of the steel. For that reason, we plan to extend our investigation to steels of greater hardenability to determine if, in some steels, a reversal of stress actually occurs on tempering as stated by Boegehold.² The desirability of tempering above 400 °F in practice, therefore, will depend not only on the loss in hardness tolerable but also on the sign of the stress in the "as-quenched" condition. Our results also confirm the findings of the author that additional compressive stresses may develop on air cooling from the higher tempering temperatures. It might be mentioned in passing that we have found in several instances that it is possible to produce very high compressive stresses in the surface by air cooling the piece from the austenitizing temperature to below the A_1 temperature, and then quenching to room temperature. The pieces heat treated as such had a hardness of only Rockwell C-20.

The author's results on the effect of various methods of metal removal on residual stress determinations are very interesting, since we plan to study the stress variation in depth by X-rays. It is gratifying to know that weak solutions of nital do not introduce additional stresses of any appreciable magnitude into the surface layers. The finding of Lihl,³ however, cannot be discounted entirely. Although he showed unequivocally that strongly acidic solutions introduced compressive stresses into the surface of well-annealed bars of low carbon steel, whether the metal was removed by chemical or electrochemical methods, he also showed that the electrolytic removal of metal (0.002 to 0.004 inch) in weakly acidified water did not introduce any "etch" stresses. His chief objection to the removal of metal in this manner was that it left the surface of the metal in a rough condition, unsuitable for X-ray strain measurements. Furthermore, he showed that the magnitude of the etch stresses depended on (a) the material used, (b) the heat treatment of the material, and (c) the current density used in electrochemical methods. It is unfortunate that he did not use nital in his studies on the development of etch stresses, but the author has clearly shown that little, if any, stress is introduced by such etching. We plan to study in some detail the effect of different etchants of varying concentration on the lattice parameter of a number of well-annealed and stressed steels, removing the metal chemically and by electrochemical methods. Such information is absolutely necessary whether X-ray or mechanical methods are used in such stress studies.

The author's statement, on the eleventh page, that Lihl determined microstresses is questionable on two accounts. First, microstresses are reflected in the broadening of the X-ray diffraction maxima. Macro-stresses, on the other hand, are manifested by a displacement of the diffraction maxima (change in lattice spacing). Lihl reported changes as large as 8×10^{-4} Å in the lattice parameter of ferrite, and this value is far greater than the experimental error of lattice parameter determination by the X-ray back-reflection method, viz., 1×10^{-4} Å. While a microstress gradient within the volume irradiated by the X-ray beam would give rise to a macrostress, it does not follow that such a stress gradient is essential to the development of macrostresses.⁴ Further confirmation of the fact

²See Reference 17 of paper.

⁴G. B. Greenough, "Macroscopic Surfaces Produced by Plastic Deformation", *Journal Iron and Steel Institute*, Vol. 169, 1951, p. 235.

that such a microstress gradient could not account entirely for the observed changes may be had by a closer examination of Lihl's results. He found that the stress sum as determined from a single measurement of strain normal to the surface agreed quite well with the sum of the individual stress components determined by the two-exposure X-ray method. This would not be true if a microstress gradient existed. Greenough⁴ also found that etching annealed steel developed compressive stresses.

It is hoped to present to this Society at some future date our X-ray stress determinations on quenched and tempered steels.

Author's Reply

It is reassuring indeed to find that other investigators of the same subject are obtaining results similar to those of the author, particularly while employing a different technique.

The discussers were thoughtful to point out the reason for their results being opposite in sign to those presented in the paper. As they implied, their steel, FS 1050, did not have sufficient hardenability to become hardened throughout the entire cross section when quenched from the austenitizing temperature, hence their steel had a resultant surface stress which was compressive instead of tensile. Nevertheless, the effect of tempering was the same in both cases—namely, decreasing surface stress with progressively increasing tempering temperature.

The discussor's comments on the X-ray work of Lihl and Greenough as to whether or not they measured macro- or microstresses are enlightening. However, since the validity of the results presented in this work does not depend on either the findings of Lihl or Greenough, no further comments on their work need be made.

A STUDY OF THE MECHANISM OF THE DELAYED YIELD PHENOMENON

BY T. VREELAND, JR., D. S. WOOD AND D. S. CLARK

Abstract

This paper presents the results of an experimental investigation of the behavior of an annealed low carbon steel subjected to a rapidly applied constant stress and to repeated short-duration stress-pulses. The test stresses were greater than the upper yield stress. The material was aged at various temperatures between stress-pulses, and the effect of the time of aging on the number of stress-pulses to induce yielding was determined.

Plastic and anelastic microstrain of the order of 30×10^{-6} in./in. is observed prior to the onset of yielding in rapidly applied constant stress tests and in repeated stress-pulse tests. Aging of the specimens for a sufficient length of time at a given temperature between stress-pulses induces recovery in the material such that yielding does not occur in repeated stress-pulse and aging cycles. The activation energy of the recovery process corresponds, within the limits of the experimental accuracy, to the activation energies of carbon and nitrogen diffusion in iron.

These effects are discussed in terms of the dislocation theory of yielding. The delayed yield and the microstrain are attributed to the action of dislocations within the crystals of the material. The recovery process is attributed to the diffusion of carbon and nitrogen to the dislocations which have been displaced, thus stabilizing the array of dislocations for the particular stress condition.

THE DEPENDENCE of yield point and strain aging phenomenon on carbon and nitrogen in steel has been studied by other investigators. Muir (1)¹ and Davenport and Bain (2) have demonstrated that the activation energy of strain aging (return of the yield point) is almost exactly that for the diffusion of carbon in alpha iron. Several other investigators have demonstrated that the presence of the upper yield point in low carbon steel is intimately related to the presence of carbon and nitrogen (3-5). The upper yield point and strain aging phenomenon are theoretically described

¹The figures appearing in parentheses pertain to the references appended to this paper.

A paper presented before the Eighth Western Metal Congress of the Society, held in Los Angeles, March 23 to 27, 1953. Of the authors, T. Vreeland, Jr., is research assistant, D. S. Wood is assistant professor of mechanical engineering, and D. S. Clark is professor of mechanical engineering, California Institute of Technology, Pasadena, Calif. Manuscript received January 2, 1952.

by the concept of dislocations and their interaction with interstitial solute atoms, such as carbon and nitrogen in the steel. Such descriptions have been given by Cottrell (6, 7), Nabarro (8), and Cottrell and Bilby (9).

Previous investigations at the California Institute of Technology (10-12) have shown that a definite period of time is required for the initiation of yielding in annealed low carbon steel subjected to rapidly applied constant stress exceeding the static upper yield stress. In those investigations, the tests were continued at constant stress until yielding occurred. By considering the concepts of the dislocation theory, one may suspect that if the material is subjected to a stress greater than the static upper yield stress and that stress is released before yielding can take place, some conditioning action occurs that may have a permanent effect on the delay characteristics of the material.

The purpose of the investigation discussed in this paper is to determine whether or not the cumulative time at stress for a series of stress-pulses is the same as the delay time required for the initiation of yielding in a single rapid-loading test. The influence of aging at different temperatures for different intervals of time between the stress-pulses is considered in this study. Sensitive strain measurements are made during the stress-pulses and during rapidly applied constant stress tests in an attempt to detect any plastic or anelastic microstrain that may occur.

MATERIAL, TEST SPECIMENS, AND TREATMENTS

The specimens used in this investigation were machined from $\frac{5}{8}$ -inch diameter hot-rolled bars from a single billet. Three check analyses made by the mill on random bars all gave the following results:

	%
Carbon	0.12
Manganese	0.43
Phosphorus	0.019
Sulphur	0.042
Silicon	0.27
Copper	0.23
Tin	0.037

A drawing of the test specimen used in this investigation is shown in Fig. 1. The gage section was finished by grinding. A thin, flat gage section was employed to facilitate the application of SR-4 strain gages.

Two groups of specimens were employed in this investigation. The first group consisted of specimens which had been annealed for 1 hour in pure dry hydrogen at a temperature of 1700 °F (930 °C). These were used for a study of plastic and anelastic microstrain prior to yielding.

The results of a previous investigation (12) indicate that a homogenizing treatment at 1300 °F (700 °C) for a long period following the annealing treatment brings the material closer to a state of perfect equilibrium and considerably reduces the scatter in the rapid-load test data. Such a treatment was given to the second group of specimens, which were used for the static tests, rapid-load tests,

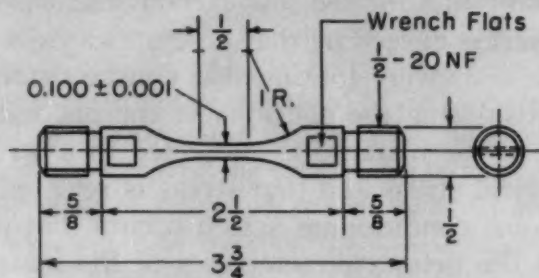


Fig. 1—Test Specimen.

and stress-pulse and aging tests. The hydrogen atmosphere was purified, and a pure hydrocarbon was introduced to prevent specimen decarburization. The heat treatment was as follows:

- (a) Annealed at 1680 °F (915 °C) for 2½ hours.
- (b) Homogenized at 1300 °F (705 °C) for 22 hours.

The homogenization treatment did not change the grain size or hardness of the material. The ASTM grain size was observed to be 6.7, and the average of 20 hardness determinations was 54 on the Rockwell B scale. Microscopic examination of the material showed that no detectable change occurred in the amount of pearlite present in the surface of the specimen as a result of the homogenizing treatment. The fact that the hardness of the material was not changed by this treatment also indicates that the carbon content was not changed appreciably.

EQUIPMENT

The tests were made with the rapid-load testing machine described in a previous paper (10). Suitable alteration of a part of the actuating mechanism permits the application of a stress-pulse to the test specimen.

The extensometers described in a previous paper (11) were used for tests in which only the initiation of yield strain was to be detected. Tensile and bending strains were measured by means of SR-4 resistance-sensitive wire strain gages. One Type A-5 gage was bonded to each side of the gage section of the test specimen.

Plastic and anelastic microstrain was measured by employing a strain bar which was attached to one end of the specimen. The nominal dimensions of the gage section of the specimen and the strain bar are the same; hence, the elastic strains in the specimen and the bar are nearly equal. The strain bar is made of X4130 steel, heat-

treated so that it remains elastic under the loads used in this investigation. Two Type A-5 gages are bonded to the gage section of the strain bar and electrically connected to the two gages bonded to the gage section of the specimen in such a manner that the elastic strain in the strain bar is subtracted from the total strain in the specimen. This arrangement permits the use of the maximum possible sensitivity of the recording system without exceeding the total strain-recording capacity of the system.

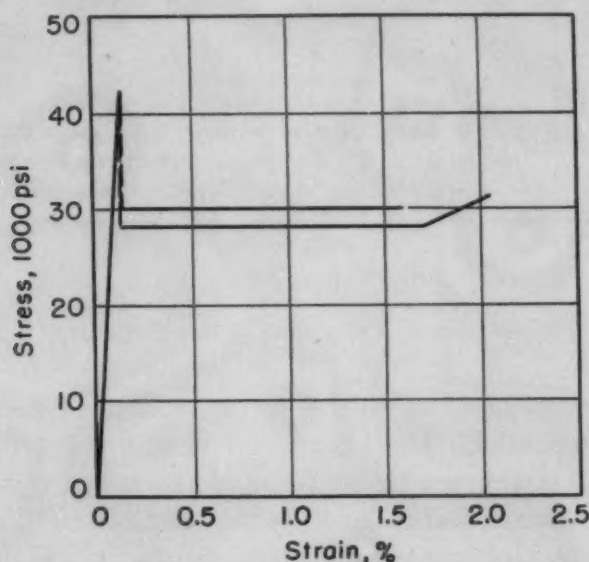


Fig. 2—Static Stress Versus Strain-Annealed and Homogenized Material.

The load acting on the specimen was measured by means of a dynamometer employing Type AB-14, SR-4 strain gages with suitable temperature compensation.

The signals from the strain gage bridge circuits were recorded on photographic paper by a galvanometer-type recording oscillograph. A 3000-cycle-per-second carrier bridge amplification system was used.

TEST PROCEDURE AND EXPERIMENTAL RESULTS

Static Tension Tests—The static tension tests were performed in the rapid-load testing machine by manual operation of the pressure system. The load was applied to the specimen in increments, and each increment was held for 3 minutes before recording values of load and tensile strain. When the specimen yielded, the load was removed and then reapplied in increments to determine the lower yield stress. The test was discontinued when the bonded strain gages came loose from the specimen at a strain of approximately 2%. Static stress-strain curves for the annealed and homogenized material are presented in Fig. 2.

Rapid-Load Tension Tests—The rapid-load tension tests which were made to determine the stress–delay time characteristics of the material were performed in the manner described in a previous paper (10). The test results are plotted in Fig. 3.

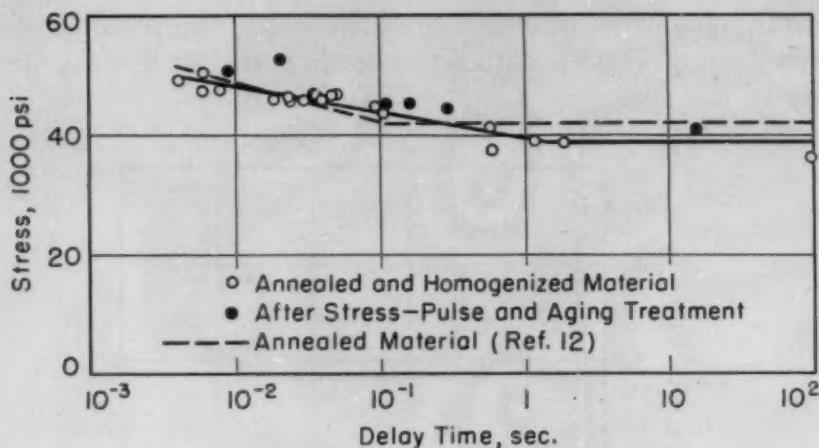


Fig. 3—Delay Time Versus Stress.

The extent of bending in the specimen during rapid-load tension tests was investigated. The maximum bending strain found in nine tests was 6.2% of the tensile strain, and the mean was 2.9%.

Repeated Stress-Pulse Tests—The tests which were employed to study the effect of stress-pulses and aging on the delay time were made by imposing a stress-pulse of essentially constant magnitude and duration on the specimen. The pulse was as follows:

- (a) Stress of $45,000 \pm 800$ psi applied in approximately 0.007 second.
- (b) Stress held essentially constant for 0.029 ± 0.001 seconds.
- (c) Stress removed in approximately 0.003 second.

The delay time for the material when subjected to a stress of 45,000 psi is approximately 0.050 second, which is greater than the duration of one stress-pulse and less than the duration of two stress-pulses. Thus, the material might be expected to yield during the second stress-pulse if there is no recovery between pulses. This procedure provides a method of detecting any recovery that may occur between stress-pulses.

The specimens were aged for various intervals of time between stress-pulses at temperatures of 70, 150 and 200 °F (21, 66 and 93 °C). The procedure of aging the specimen at 150 and 200 °F (66 and 93 °C) after a stress-pulse was as follows:

- (a) Specimen removed from rapid-load machine and placed in an oil bath at desired temperature within 5 minutes after stress-pulse (temperature controlled to ± 1 °F).
- (b) Specimen removed from oil bath after desired aging period and immediately cooled in powdered dry ice (-109 °F or -78 °C).
- (c) Specimen brought to approximately 70 °F in an alcohol bath 5 minutes prior to next stress-pulse.

- (d) Stress-pulse applied when specimen reached 70 °F; specimen temperature determined by thermocouple and recording potentiometer.

The initiation of yielding was determined with the extensometers in the majority of the stress-pulse tests. A typical record of a stress-pulse is shown in Fig. 4.

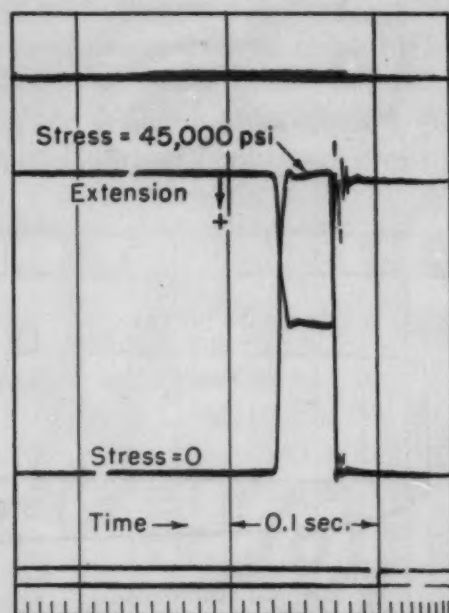


Fig. 4—Typical Record of a Stress-Pulse.

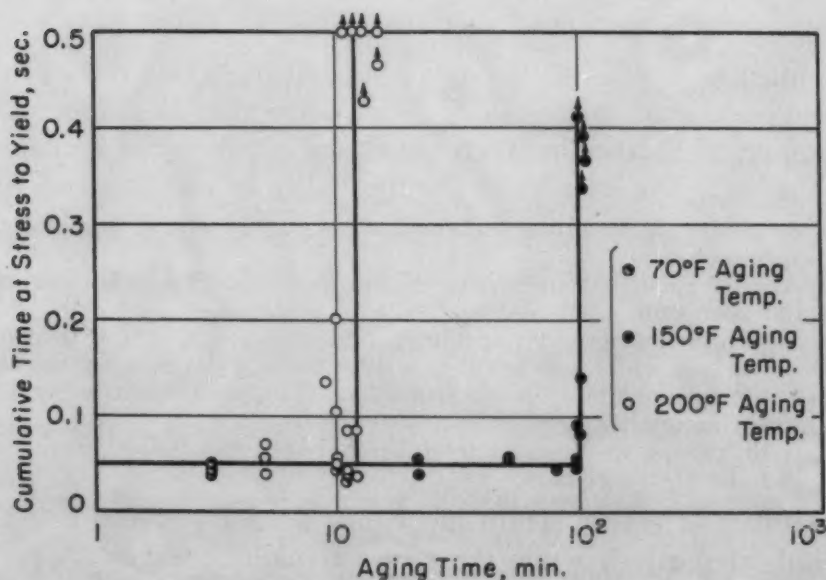


Fig. 5—Cumulative Time at Stress to Yield Versus Aging Time.

The cumulative time at stress before yielding is plotted in Fig. 5 as a function of aging time between stress-pulses for the three aging temperatures. The specimens which were aged at 70 °F for 3 minutes

yielded during the second stress-pulse, and the cumulative time at stress before yielding was approximately equal to the normal delay time at the same stress. Aging at 150 °F and 200 °F for periods equal to or greater than a certain critical value induced recovery from the effects of the previous stress-pulse. This is shown by the fact that yielding did not take place in successive stress-pulse and aging cycles. The data show that recovery is accomplished by aging for a minimum of approximately 12 minutes at a temperature of 200 °F and 100 minutes at 150 °F.

Measurement of Plastic and Anelastic Microstrain—A typical record of microstrain in a rapid-load test is shown in Fig. 6. A cor-

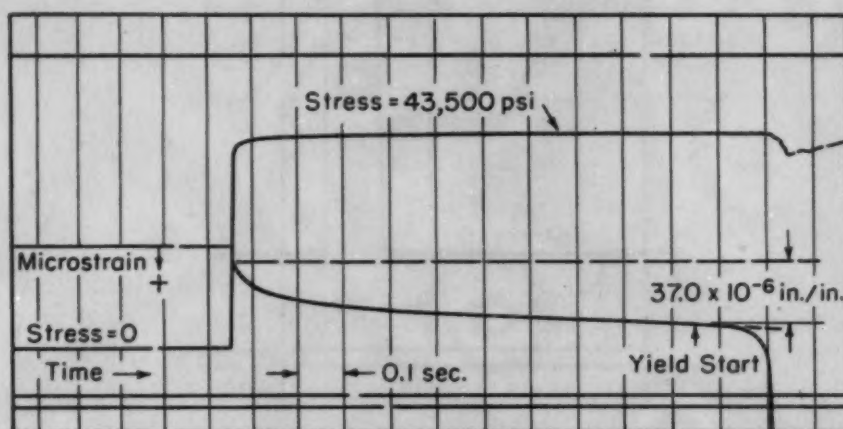


Fig. 6—Typical Record of Microstrain Under Constant Stress.

rection must be applied to the data obtained from this record in order to obtain values of microstrain. This correction is made necessary by an imperfect balance between the elastic strain in the specimen and the strain bar. The sources of the inequality of elastic strain are:

- (a) A difference in cross sectional areas of the strain bar and the specimen.
- (b) A difference in sensitivities of the gages on the strain bar and the specimen.
- (c) Misalignment between specimen and strain bar at the threaded connection which can result in a difference of the bending moment in the specimen and in the strain bar. This will result in bending strain inequality.
- (d) A difference in Young's modulus between the X4130 strain bar and the test specimen.

These sources of elastic strain inequality do not produce any change in the indicated strain while the stress remains constant. Therefore, the changes of indicated strain which occur during the period of substantially constant stress may be attributed to plastic and anelastic microstrain in the specimen. The microstrain shown in the records is indicated by a downward deflection of the trace, whereas an unbalanced elastic strain may deflect the trace in either direction. The

strain which is indicated on the record during the period of stress rise is subtracted from the total indicated strain; thus, any microstrain occurring during the period of stress rise is neglected.

Anelastic and plastic strains which may occur in the strain bar also introduce a subtractive error. Hence, the measured microstrain is always less than the true plastic and anelastic microstrain in the specimen. Although it is difficult to make a reliable estimate of the total error due to these effects, there is some justification for believing that it is small. First, the strain correction for elastic unbalance is normally a small portion of the indicated microstrain during the entire record. Hence, the microstrain which may occur during the period of stress rise is small compared to the total microstrain. Second, the stress in the strain bar is approximately one-fourth the value of the yield stress for this material; therefore, the anelastic and plastic strain in it should be negligible.

A mean value of microstrain of 30×10^{-6} in./in. was found to take place prior to yielding in ten tests at various stresses. Although the microstrain varied from 20×10^{-6} in./in. to 37×10^{-6} in./in. in these tests, there is no systematic correlation with the magnitude of the stress. The microstrain rate during each test decreases with time until yielding starts. A recovery of approximately 50% of the microstrain was observed when the stress was removed. Successive stress-pulse and aging cycles showed decreasing amounts of microstrain in each stress-pulse cycle. When the aging conditions induced recovery, the decrease in microstrain for successive stress-pulse aging cycles was greater.

The distribution of the microstrain over the specimen gage length was investigated. The difference in strain between two regions of the gage section was measured by means of four Type A-8, SR-4 strain gages. Two gages were bonded to each region, one on each side of the gage section, and the four gages were electrically connected so as to measure the strain difference between the two regions. These strain gages have a gage length of $\frac{1}{8}$ inch, and the specimen gage length is $\frac{1}{2}$ inch. The specimen was subjected to a rapid load, and the resulting test record indicates no inhomogeneity in strain prior to the initiation of yielding. A second indication of the distribution of the microstrain was obtained in the following manner: The surface of a test specimen was mechanically polished, etched, and examined microscopically at magnifications of 100 and 600 diameters between successive stress-pulses in an attempt to detect the formation of slip lines. No slip lines were observed until yielding took place during the third stress-pulse. Slip lines were then observed within the single Luders' band which had formed.

Tests on Material Previously Subjected to Stress-Pulse and Aging Cycles—The influence of stress-pulse and aging cycles on the

static stress-strain relationship and on the stress – delay time relationship was investigated. Tests were conducted on specimens which had been previously subjected to stress-pulses followed by sufficient aging to produce recovery. Hence, none of these specimens had previously yielded.

The static upper and lower yield stress and the yield strain are not changed significantly by the stress-pulse and aging treatment. The results of the stress – delay time determinations are plotted in Fig. 3. These tests show that the delay times are greater by a factor of approximately 4 than the delay times for the original material for corresponding stresses.

DISCUSSION OF RESULTS

The relations between delay time and stress for the annealed and annealed and homogenized material are given in Fig. 3. The scatter in the data was found to be reduced by the homogenizing treatment. This treatment also produced changes in the stress – delay time relationship which was previously reported for the original annealed material (12). The reduced scatter and the changes in the stress – delay time relationship can be attributed to a closer approach to the equilibrium state in the annealed and homogenized material. The amount of bending found in the rapid-load tensile tests is sufficient to introduce the scatter found in the stress – delay time determinations of the annealed and homogenized material.

The results of the repeated stress-pulse tests, presented in Fig. 5, show that a definite recovery from the effects of the previous stress-pulse takes place when the time and temperature between stress-pulses is sufficient. An activation energy for the recovery process can be found by assuming that the recovery follows a law of the form

$$t \sim e^{Q/RT},$$

where t is the critical aging time for recovery,

Q is the activation energy of the recovery process,

R is the gas constant, and

T is the absolute aging temperature.

The recovery times of 12 minutes at 200 °F and 100 minutes at 150 °F give an activation energy of 18,800 cal/mole for the recovery process. There is an uncertainty of 10% in this value due to scatter in the critical aging time and the fluctuation of the aging temperature. This activation energy corresponds to the activation energy of strain aging (1, 2, 8), (18,100 cal/mole), and to the activation energy of the diffusion of carbon and nitrogen in alpha iron [carbon: 18,100 cal/mole (13), 19,800 cal/mole (14); nitrogen: 17,700 cal/mole (14)]. Thus, it is reasonable to assume that the mechanism of recovery from previous stress-pulses is related to the mechanism of the

return of the yield point and to the diffusion of carbon and nitrogen in the steel.

A microstrain of approximately 30×10^{-6} in./in. was measured prior to yielding for both rapid loading and repeated stress-pulses. The microstrain appears to be independent of the applied stress within the range of stress covered in this investigation. This value of microstrain agrees in order of magnitude with that found by Averbach (15) (50 to 60×10^{-6} in./in.) in static tests on polycrystalline samples of iron and steel.

Cottrell (7) has recently presented some promising additions to the previous concept of the mechanism for the initiation of yielding in polycrystalline low carbon steel. He extends the previous theory of dislocations anchored by interstitial solute atoms to include the following concepts:

- (a) Releasing a dislocation from a grain boundary requires a larger force than releasing an anchored dislocation within a crystal.
- (b) A few dislocations are released prior to yielding, and their movement is obstructed by interaction with other nearby anchored dislocations or grain boundaries. Yielding is not initiated until the resistance offered by obstructions to the movement of dislocations is overcome.

An anchored dislocation within a crystal may move when its total energy is greater than the potential energy of the anchoring barrier. The potential energy of the barriers changes with the applied stress. For a given stress, the number of dislocations which can move in a given time is determined by the statistics of the fluctuations in thermal energy of the dislocations. Therefore, a definite period of time would be required for a particular stress to release a given number of dislocations. When a sufficient number of dislocations are released and move to an opposing obstruction, they may overcome the restraint offered by the obstruction and initiate an avalanche of dislocations which results in yielding. The delayed yield phenomenon may be explained by this mechanism. Furthermore, the relatively constant value of microstrain observed before yielding in this investigation can also be qualitatively explained by these concepts.

No inhomogeneity in microstrain was found prior to yielding. This indicates that the microstrain does not result from the progressive formation of the Luders' band which appears on yielding. For a quantitative treatment of the dislocation theory of the observed microstrain, the number of dislocations which can be moved or the distance which these dislocations can move before being stopped by obstructions must be assumed. If the density of dislocations which are moved is ρ per unit area and if the mean distance which the dislocations move is L , the movement of the dislocations causes a tensile strain of about $\rho L \lambda_0 / 2$, where λ_0 is the magnitude of the dislocation slip vector. If the obstacles which stop the movement of a dislocation within the

crystal are assumed to be the mosaic boundaries with a spacing of about $L = 10^{-4}$ cm (18), and taking $\lambda_0 = 2.5 \times 10^{-8}$ cm for alpha iron, then by the above formula, between 10^7 and 10^8 dislocations per cm^2 must be moved to produce a tensile strain of 30×10^{-6} in./in.

When the stress is rapidly removed before the initiation of yielding, approximately 50% of the microstrain is recovered. This indicates that some of the dislocations which were displaced by the applied stress return toward their original positions when the stress is removed, as might be expected.

The microstrain rate, prior to the initiation of yielding, decreases with time. This might be accounted for by a depletion of the reservoir of dislocations which may be moved by the applied stress. This may also account for the decreasing amount of microstrain induced by successive stress-pulses when recovery does not take place. When the aging treatment between stress-pulses induces recovery, a greater decrease in the microstrain in successive stress-pulses is found. The recovery mechanism may be explained by the diffusion of carbon and nitrogen to the dislocations which have been displaced. The resulting array of dislocations, anchored by atmospheres of carbon and nitrogen, may be expected to be more stable than the original array under the particular stress condition. Successive stress-pulse and aging cycles then produce less microstrain, and yielding does not take place. The more stable configuration of dislocations for the particular stress condition is also indicated by the results of the rapid-load tensile tests on the material which had previously been subjected to stress-pulse and aging cycles in which recovery took place. The delay times for the initiation of yielding are increased by a factor of approximately four over the delay times for the original material for corresponding stresses.

SUMMARY AND CONCLUSIONS

The results of the repeated stress-pulse tests on annealed low carbon steel show that a definite recovery from the effects of the previous stress-pulse takes place when the combination of time and temperature between stress-pulses is sufficient. For aging periods longer than the critical recovery time at a given aging temperature, repeated stress-pulse and aging cycles do not produce yielding. For aging periods shorter than the critical recovery time, the specimen yields when the cumulative time at stress is approximately equal to the normal delay time. This recovery process is found to be associated with an activation energy corresponding to the activation energy of strain aging and diffusion of carbon and nitrogen in the steel. The repeated stress-pulse and aging treatment stabilizes the material such that the delay times are increased for the same stress.

Sensitive strain measurements under conditions of rapid loading

and stress-pulses indicate that a plastic and anelastic microstrain of approximately 30×10^{-6} in./in. precedes the yield strain. The delayed yield and the microstrain may be attributed to the action of dislocations within the crystals.

The recovery phenomenon and the increase in delay times for the previously stressed and aged material may be attributed to the diffusion of carbon and nitrogen to the dislocations which have been displaced, thus stabilizing the array of dislocations for the particular stress condition.

ACKNOWLEDGMENTS

This investigation was conducted under the sponsorship of the Office of Naval Research. The rapid-load testing machine used in this investigation was constructed by the California Institute of Technology under a contract with the United States Air Force. Appreciation is expressed to the U. S. Air Force for permission to use the machine.

References

1. J. Muir, "On the Recovery of Iron From Overstrain", *Philosophical Transactions*, Royal Society of London, Series A, Vol. 193, Pt. 1, 1900, p. 1.
2. E. S. Davenport and E. C. Bain, "The Aging of Steel", *TRANSACTIONS*, American Society for Metals, Vol. 23, 1935, p. 1047.
3. J. R. Low, Jr., and M. Gensamer, "Aging and the Yield Point in Steel", *Transactions*, American Institute of Mining and Metallurgical Engineers, Vol. 158, 1944, p. 207.
4. A. N. Holden and J. H. Hollomon, "Homogeneous Yielding of Carburized and Nitrided Single Iron Crystals", *Journal of Metals*, February 1949, *Metals Transactions*, American Institute of Mining and Metallurgical Engineers, Vol. 185, p. 179.
5. H. Schwartzbart and J. R. Low, Jr., "The Yielding and Strain-Aging of Carburized and Nitrided Single Crystals of Iron", *Journal of Metals*, September 1949, *Metals Transactions*, American Institute of Mining and Metallurgical Engineers, Vol. 185, p. 637.
6. A. H. Cottrell, "Effect of Solute Atoms on the Behavior of Dislocations", Report of a Conference on Strength of Solids, Physical Society of London, 1948.
7. A. H. Cottrell, "The Yield Point in Single-Crystal and Polycrystalline Metals", Symposium on the Plastic Deformation of Crystalline Solids, Mellon Institute, 1950.
8. F. R. N. Nabarro, "Mechanical Effects of Carbon in Iron", Report of a Conference on Strength of Solids, Physical Society, London, 1948.
9. A. H. Cottrell and B. A. Bilby, "Dislocation Theory of Yielding and Strain Aging of Iron", *Proceedings*, Physical Society of London, Sec. A, Vol. 62, Pt. 1, 1949, p. 49.
10. D. S. Clark and D. S. Wood, "The Time Delay for the Initiation of Plastic Deformation at Rapidly Applied Constant Stress", *Proceedings*, American Society for Testing Materials, Vol. 49, 1949, p. 717.
11. D. S. Wood and D. S. Clark, "The Influence of Temperature Upon the Time Delay for Yielding in Annealed Mild Steel", *TRANSACTIONS*, American Society for Metals, Vol. 43, 1951, p. 571.

12. D. S. Wood and D. S. Clark, "Delayed Yield in Annealed Steels of Very Low Carbon and Nitrogen Content", *TRANSACTIONS, American Society for Metals*, Vol. 44, 1952, p. 726.
13. J. K. Stanley, "The Diffusion and Solubility of Carbon in Alpha Iron", *Transactions, American Institute of Mining and Metallurgical Engineers*, Vol. 185, 1949, p. 752.
14. C. Wert and C. Zener, "Interstitial Atomic Diffusion Coefficients", *Physical Review*, Vol. 76, Ser. 2, 1949, p. 1169.
15. B. L. Averbach, Discussion of paper by A. H. Cottrell, Symposium on the Plastic Deformation of Crystalline Solids, Mellon Institute, 1950.
16. F. Seitz, "The Theory of Plastic Flow in Single Crystals", Symposium on the Plastic Deformation of Crystalline Solids, Mellon Institute, 1950.

DISCUSSION

Written Discussion: By William C. Leslie, Research Laboratory, United States Steel Co., Kearny, N. J.

The authors found that relations between delay time and stress were not the same for material held at 1700 °F for 1 hour and slowly cooled and material annealed at 1680 °F, then held for 22 hours at 1300 °F and slowly cooled (Fig. 3). The scatter in the data was also reduced by the homogenization treatment at 1300 °F. The authors attributed these effects to a closer approach to equilibrium in the homogenized material.

It is suggested that the change in delay time and reduced scatter of the data may be due to removal of nitrogen from solution in ferrite by formation of silicon nitride during the homogenization treatment. An examination of the literature^{2, 3} indicates that a period of 22 hours at 1300 °F, followed by slow cooling, will cause silicon nitride to form in the silicon-killed steel used by the authors. If the steel contains aluminum, aluminum nitride may be formed. Is information on the aluminum content available to the authors? For these reasons, results obtained with a silicon-killed steel may not correspond with results which might be obtained with aluminum-killed or rimmed steels.

Written Discussion: By B. L. Averbach and H. Muir, Department of Metallurgy, Massachusetts Institute of Technology, Cambridge, Mass.

The authors have found anelastic and plastic microstrains of the order of 30×10^{-6} prior to yielding in annealed 1020 steel. The relaxation of the anelastic component is quite rapid, and a dynamic test such as that used by the authors is necessary to observe it. It should be pointed out, however, that the plastic microstrain prior to the upper yield point can be observed at normal testing speeds.

Roberts, Carruthers and Averbach⁴ measured the changes in length of a specimen which had been loaded to a given stress level and then unloaded. Their method employed a mechanical-optical comparator and was sensitive to changes of the order of 5×10^{-6} inch per inch. They observed

²W. C. Leslie, K. G. Carroll and R. M. Fisher, "Diffraction Patterns and Crystal Structure of Si_3N_4 and Ge_3N_4 ", *Journal of Metals*, February 1952, p. 204.

³H. F. Beeghly, "Behavior of Nitrogen and Some of Its Compounds in Steel", *Analytical Chemistry*, July 1952, p. 1095.

⁴C. S. Roberts, R. C. Carruthers and B. L. Averbach, "The Initiation of Plastic Strain in Plain Carbon Steels", *TRANSACTIONS, American Society for Metals*, Vol. 44, 1952, p. 1150.

plastic strains of 30 to 50×10^{-6} prior to the upper yield and they showed that this figure did not include anelastic strain. They were thus able to establish an elastic limit and a region of plastic flow prior to the upper yield.

In the course of further work now in progress at Massachusetts Institute of Technology, we have been able to observe pre-yield strains more conveniently by the use of electrical strain gages (Baldwin SR-4, Type A-3) mounted on tensile specimens. This technique requires careful attention to temperature compensation, and requires the elimination of bending effects in order to minimize the zero shift which would obscure the microstrain. A specimen is loaded to a given stress level, unloaded, and the residual strain measured. In each case sufficient time is allowed for the anelastic component to relax. The strain gage technique appears to give the same results as the previous method.

At present we are investigating the effects of tempering temperature and carbon content on the elastic limit and pre-yield phenomena of quenched plain carbon steels. A preliminary survey has already shown that steels with carbon contents from 0.08 to 0.8% and with tempering temperatures between 800 and 1300°F exhibit a pre-yield strain and this may be apparently regarded as the normal behavior. In addition, the magnitude of this pre-yield strain may vary considerably and appears to be a function of the carbon content and heat treatment.

Table I
Stress-Strain Readings for Three Specimens of 0.08% Carbon Steel

Brine-Quenched From 1675°F , Tempered 1 Hour at 1300°F and Air-Cooled		Brine-Quenched From 1675°F , Tempered 1 Hour at 1200°F and Air-Cooled		Brine-Quenched From 1675°F , Tempered 1 Hour at 1100°F and Air-Cooled	
Stress psi \times 10^{-3}	Strain After Unloading 10^6	Stress psi \times 10^{-3}	Strain After Unloading 10^6	Stress psi \times 10^{-3}	Strain After Unloading 10^6
0	0	0	0	0	0
2	0	2	0	2	0
4	0	4	0	4	0
6	0	6	0	6	0
8	0	8	0	8	0
10	0	10	0	10	0
12	0	12	0	12	0
14	0	14	0	14	0
16	0	16	0	16	0
18	0	18	0	18	0
20	0	20	0	20	0
22	0	22	0	22	0
24	0	24	0	24	0
26	1	26	0	26	0
28	2	28	0	28	0
30	4	30	0	30	0
32	4	32	1	32	0
34	4	34	2	34	0
36	6	36	3	36	0
38	8	38	5	38	0
40	12	40	13	40	0
42	21*	42	60	44	<1
40	Drop of Load >14,000	42.2	Drop of Load >14,000	48	>1
		41.5		50	3
				52	8
				54	18
				54.7	Drop of Load >13,000
				51.8	

*Values marked are estimated by extrapolation.

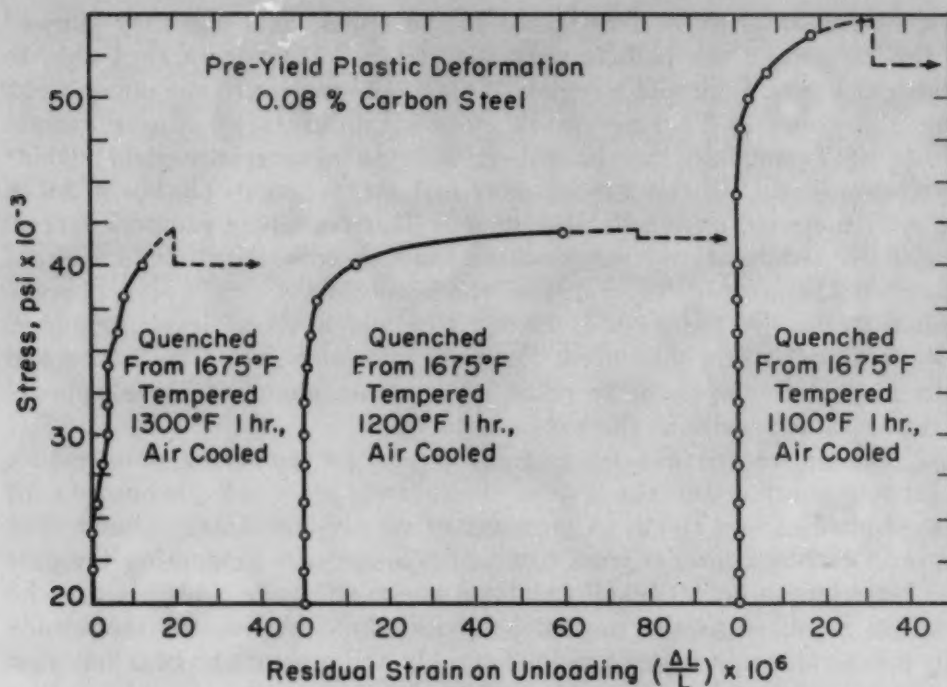


Fig. 7—Pre-Yield Plastic Deformation, 0.08% Carbon Steel.

Table II
Summary of Results for Three Specimens of 0.08% Carbon Steel

	Brine-Quenched From 1675° F, Tempered 1 Hour at 1300 °F and Air-Cooled	Brine-Quenched From 1675° F, Tempered 1 Hour at 1200 °F and Air-Cooled	Brine-Quenched From 1675° F, Tempered 1 Hour at 1100 °F and Air-Cooled
Elastic limit, psi	36,000	32,000	44,000
Upper yield, psi	42,000	42,200	54,700
Lower yield, psi	40,000	41,500	51,800
Total pre-yield microstrain	21×10^{-6}	76×10^{-6}	33×10^{-6}

Three examples of pre-yield phenomena are given in Fig. 7. These curves refer to three specimens of the following composition: 0.08% carbon, 0.39% manganese, 0.029% sulphur, 0.011% phosphorus and a trace of silicon. These specimens were brine-quenched from 1675 °F, tempered at 1100, 1200 and 1300 °F respectively, and air-cooled. In each case the specimen was loaded to the indicated stress level and the residual strain measured on unloading. Actual stress and strain readings are shown in Table I, and it can be seen from these values that a definite drop of the load corresponding to the upper yield point occurs in each case. It is quite evident, however, that a measurable plastic strain has occurred prior to yielding and these are summarized in Table II.

The existence of a plastic pre-yield deformation in steels which show a delay time would seem to be of considerable theoretical significance with reference to the mechanism of plastic deformation. The pre-yield phenomenon may also be of significance in embrittlement and it would be

very interesting to see what effects variations in heat treatment might have on the microstrain and delay time phenomena.

Written Discussion: By A. N. Holden and J. R. Low, Jr., Knolls Atomic Power Laboratory, General Electric Co., Schenectady, N. Y.

There are a few instances where an interpretation can be placed on the experimental work that differs from the views presented in the paper.

First of all, it seems contradictory to suggest that the effect of a succession of stress-pulses is strictly cumulative (in the absence of sufficient aging) and also report that the microstrain observed during a stress-pulse is relaxed by 50% upon release of that stress. At least some fractional increase in time at stress ought to be observed for the pulsing technique over the single stress technique; perhaps if the pulse time were a smaller fraction of the delay time observed for single stress tests, the sensitivity to any effect would be increased.

The second point concerns the interpretation of the microstrain before yielding. Cottrell's notion that small amounts of plastic strain occur before the yielding cataclysm is verified for polycrystals both by this work and the previous work of Roberts, Carruthers and Averbach.⁴ We dislike, however, to consider the microstrain to result from the movement of 10^8 dislocations in any square centimeter for distances corresponding to 10^{-4} cm (the mosaic block size) and then becoming hung up on a subboundary. We prefer the simpler concept that some smaller number of dislocations move the grain diameter before becoming hung up. In the case at hand, an ASTM No. 6.7 grain size would allow a movement 4×10^{-3} cm to the grain boundaries and require the strain contribution of less than 10^6 dislocations on any square centimeter to produce the observed microstrain.

The reasoning behind this preference is as follows: If we are considering crystals formed during transformation or during recrystallization, these crystals are in the annealed condition and probably contain little more than 10^8 cm⁻² dislocations. These may be considered randomly distributed or packed in mosaic subboundaries, according to preference, but in either situation they constitute a negligible barrier to the motion of any dislocation.

A simple and unoriginal calculation will show that a network of mosaic boundaries 10^{-4} cm apart on any square centimeter would contain 2×10^4 cm of boundary that could be packed with 10^8 dislocations at an average spacing of 2×10^{-4} cm or 8000 atoms. This dilute spacing is quite consistent with a dislocation model of the boundary between mosaic blocks with angular discrepancies of less than 1 minute. However, this dilute spacing is inconsistent with the notion that subboundaries impede the motion of dislocations. It is apparent that much higher dislocation densities ($\sim 10^{11}$ cm⁻²) would be necessary to pack boundaries close enough to impede moving dislocations.

There is a simple test we would like to see the authors perform that should distinguish between subboundary and grain boundary restraint. This test would involve measuring the microstrain before yielding for the same material in the same annealed condition but with a range of grain sizes. Obviously, if the microstrain is a consequence of the movement of dislocations to subboundaries, no grain size effect will be found. If the dislocations are free to move to grain boundaries, a single Frank-Read

source will throw off more loops and contribute more to the microstrain in a coarse-grained specimen than in a fine-grained specimen. We should expect to detect greater microstrain in coarse-grained specimens if grain boundaries are the barriers of importance.

Authors' Reply

Mr. Leslie has suggested that the formation of nitrides during the long homogenization treatment may have an effect upon the delay time for yielding. This is certainly possible. However, it may be pointed out that according to the Cottrell mechanism of yielding, that portion of the nitrogen (and carbon) which is responsible for the yield phenomenon is not in solid solution in the usual sense. That is, it is bound to dislocations and grain boundaries. This binding may be strong enough to prevent that portion of the nitrogen from forming silicon or aluminum nitrides, even though the nitrogen which is in simple solid solution does form such nitrides.

The authors do not have information on the aluminum content of the steel.

The previous measurements of pre-yield plastic microstrain made by Roberts, Carruthers and Averbach and the more recent work by Averbach and Muir given in the discussion are most interesting. The authors regret that they had not seen the complete paper describing the former work before their present paper was written. It is gratifying that the order of magnitude of the microstrains found by the two groups is the same. The authors feel that it may be rather difficult to secure closely reproducible measurements of the total plastic microstrain prior to yielding. A large part of that strain may occur at a stress very slightly below the upper yield stress, as shown in one of the curves given in the discussion. Thus, slight variations between specimens, small load variations, etc., may alter the value of microstrain at which final yielding begins.

The authors thoroughly agree with Holden and Low that it is preferable to consider the microstrain as the result of the motion of dislocations to grain boundaries or other obstacles having a much larger spacing than mosaic boundaries. Furthermore, the dislocations which have moved toward grain boundaries may be arranged in discrete groups on individual slip planes, since a single Frank-Read source may generate a whole family of dislocations all lying in the same slip plane. The dislocations in any one of these groups would be spaced in a definite pattern on the slip plane which is determined by their interactions with each other and with the grain boundary and the externally applied stress.

The authors intend to study the effect of grain size on the microstrain before yielding. However, the steel employed in the present investigation does not seem to be suitable for this purpose for two reasons: first, the presence of carbides would complicate the interpretation of the results, since they constitute obstacles to dislocation motion of a somewhat different nature than grain boundaries; second, attempts to alter the grain size systematically and uniformly by the strain-anneal method have not been successful with this particular steel. For these reasons, the authors intend to study the grain size effect, using a high-purity iron containing an amount

of carbon sufficient to cause a definite yield point without the presence of precipitated carbides.

Regarding the cumulative effect of successive stress-pulses, the authors realize that their data are certainly inconclusive, since it was possible to apply only two stress-pulses before yielding when no aging was used between pulses. However, it seems possible that the effect of successive stress-pulses is very nearly cumulative in spite of the strain relaxation accompanying unloading. The strain relaxation may be attributed to the reverse motion of the dislocations in the individual groups caused by their mutual repulsive interactions when the applied stress is removed. This takes place very rapidly (in zero time on the millisecond time scale indicated in the paper) since these dislocations have no Cottrell atmospheres. If none of these dislocations forms a Cottrell atmosphere or is obliterated by a dislocation of the opposite sign during the period between stress-pulses, they can all move back to their previous positions in a very short time when the next stress-pulse is applied. In this case, the effect of repeated stress-pulses would be cumulative unless the pulses were far shorter than the normal delay time, such that the time to move these free dislocations would be appreciable compared to the stress-pulse duration. On the other hand, if some of the dislocations formed Cottrell atmospheres during the unloaded period or were obliterated on removal of the load, the effect of repeated stress-pulses would not be cumulative. In this case, new dislocations would have to be generated, or other dislocations moved before the previous configuration of dislocations was attained, and this would require an appreciable length of time.

X-RAY MEASUREMENT OF RESIDUAL STRESS IN HARDENED HIGH CARBON STEEL

BY A. L. CHRISTENSON AND E. S. ROWLAND

Abstract

An X-ray method is described for the measurement of macro or engineering stress in hardened high carbon steel. The method is described in detail and applied to the measurement of O.D. surface stress in carburized and hardened rings of SAE 4620 steel with heat treated, ground and electrolytically polished surfaces. Comparisons of elastic strain, obtained by externally loading the rings and measured by X-ray and SR-4 strain gage techniques, indicated a precision of the X-ray method of ± 3000 to 4000 psi.

RESIDUAL stress in steel as well as other metals has been of paramount concern to the metallurgist for many years. Its unquestioned relationship with distortion and failure during processing; its possible effect on both the static and the dynamic mechanical properties of the finished part; and the suspicion that steel quality and microstructure are not the sole criteria for judging metallurgical excellence have led to the development of many techniques for measuring residual stress and studying its sources and influence. With the exception of the X-ray method, these techniques in general are destructive to the part under study and thereby prohibit any normal service test on that part after the stresses have been evaluated. Another serious limitation to their use is the likelihood of introducing spurious stress during the necessary stock removal if the hardness of the sample is above very moderate levels. On the other hand, the X-ray method is commonly considered valueless at approximately the same degree of steel hardness, but for other reasons.

These experimental obstacles have led to a paucity of information concerning the cause and effect of residual stress under conditions of heat treatment, processing, and service where its effect, if of any consequence, is undoubtedly the greatest. With the hope of alleviating this situation somewhat and with the belief that of all the avenues available to the metallurgist for steel product improvement, the control of residual stress conceivably offers the most significant gain in metallurgical design, a re-examination of the various techniques for measuring stress was undertaken in the hope of extending

A paper presented before the Thirty-fourth Annual Convention of the Society, held in Philadelphia, October 18 to 24, 1952. The authors are, respectively, research metallurgist and chief metallurgical engineer, The Timken Roller Bearing Company, Canton, Ohio. Manuscript received May 21, 1952.

residual stress measurement to a more desirable range of hardness and structures. For the reasons given above, the X-ray method offered the most attractive possibilities and this work to date has been wholly confined to this approach. Of course, it is recognized that the usual X-ray technique, in common with all others, yields only an average stress value on a macro scale and provides no indication of the micro or tessellated stresses. Furthermore, the micro rather than macro stress present in a given steel in the final analysis may predetermine its load-carrying capacity or service life. However, the repeatedly demonstrated erratic correlation of steel quality with steel performance certainly suggests that a favorable macro residual stress may minimize the influence of the discontinuities in steel structure that give rise to micro stress.

Our studies have not yet provided any clue to the importance of residual stress, but the adaptation of the X-ray method to hard steels has been sufficiently successful that it is believed adequate to answer the question. The development of this method is not complete from any standpoint and at best is awkward and time consuming. However, the results are believed to warrant a progress report at this time for the primary purpose of enlisting the aid of other investigators who have perhaps temporarily abandoned this approach. It is believed that such additional aid will result in a rapid improvement of the technique in both speed and accuracy of measurement.

DISCUSSION OF PRINCIPLES

The principles of stress measurement by X-ray are fundamentally simple. It is actually, as in other techniques, a measurement of strain and not stress, and in this respect is superior to the other schemes in that only the elastic strain, which is the sole source of stress, is measured. The interplanar distance of a given family of atomic planes in the phase under study is used as the indicator of elastic strain present. This interplanar distance is determined at two or more angular orientations of those planes to the direction in which it is desired to measure the stress. The common procedure, known as the two-exposure method, is to determine the "d" value of the planes parallel with the direction of stress and again at some angle ψ , usually 45 degrees oblique to this direction as shown in Fig. 1. The "d" values are then substituted in a theoretically derived expression that relates them to the stress, one form of which is as follows (1)¹:

$$S = \frac{d_\psi - d_i}{d_o} \cdot \frac{E}{1 + \nu} \cdot \frac{1}{\sin^2 \psi}$$

where E = Young's modulus

ν = Poisson's constant

d_o = the stress-free interplanar distance for which one may substitute either d_ψ or d_i with negligible error

S = stress

¹The figures appearing in parentheses pertain to the references appended to this paper.

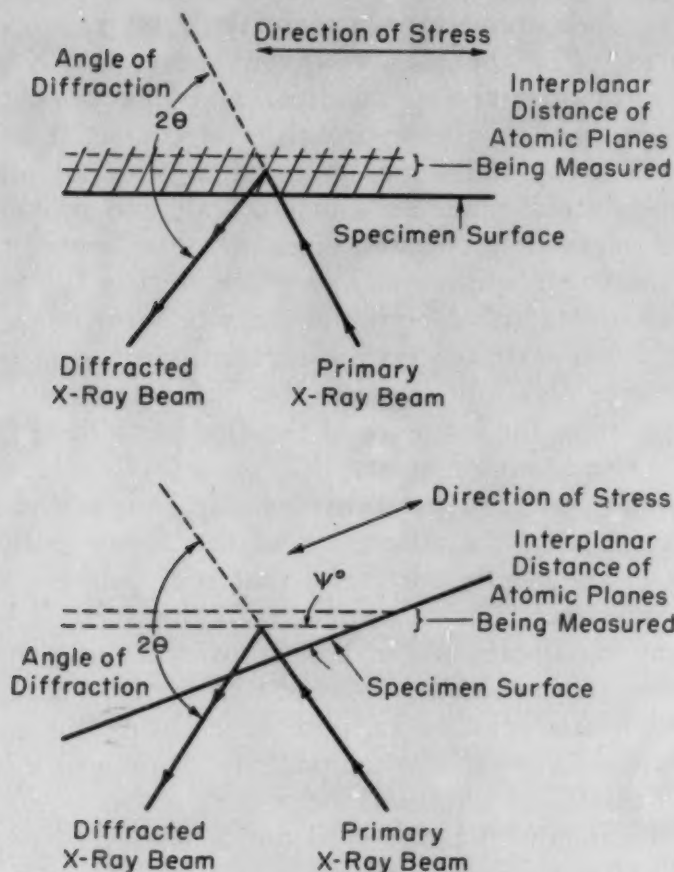


Fig. 1—Orientation of Lattice Planes Measured to Direction of Stress.

This particular form of the equation is interesting since a simple rearrangement indicates that d_ψ is a straight-line function of $\sin^2 \psi$, wherein the slope of the line is $[(1 + \nu)/E]d_0S$ and the y intercept $d_0 [1 - (\nu S/E)]$ and in the absence of stress, d_ψ becomes constant and equal to d_0 .

$$d_\psi = \left[\frac{(1 + \nu)}{E} d_0 S \right] \sin^2 \psi + d_0 \left(1 - \frac{\nu S}{E} \right)^*$$

This relationship is graphically illustrated in Fig. 2 where it is noted that all lines have a common intersection whose coordinates and d_0 ($S = 0$) and $\sin^2 \psi = [\nu/(1 + \nu)]$ thereby enabling, at least in principle if not actually, direct and separate experimental determination of the physical constants E and ν by the simple expedient of stressing the specimen to two different levels of stress in a suitable fixture (2). Furthermore, it is possible, again in principle, to extrapolate the lines to $\sin^2 \psi = 1$, at which point the planes are perpendicular to the stress in question and the difference in the "d" value at this point and the d_ψ at $\sin^2 \psi = [\nu/(1 + \nu)]$, divided by

*This expression is only valid for a unidirectional surface stress and in event of bi-directional stress, it is necessary to substitute the quantity $d_0 [1 - (\nu S'/E)]$, where S' is the stress at right angle to S , for d_0 in the equation.

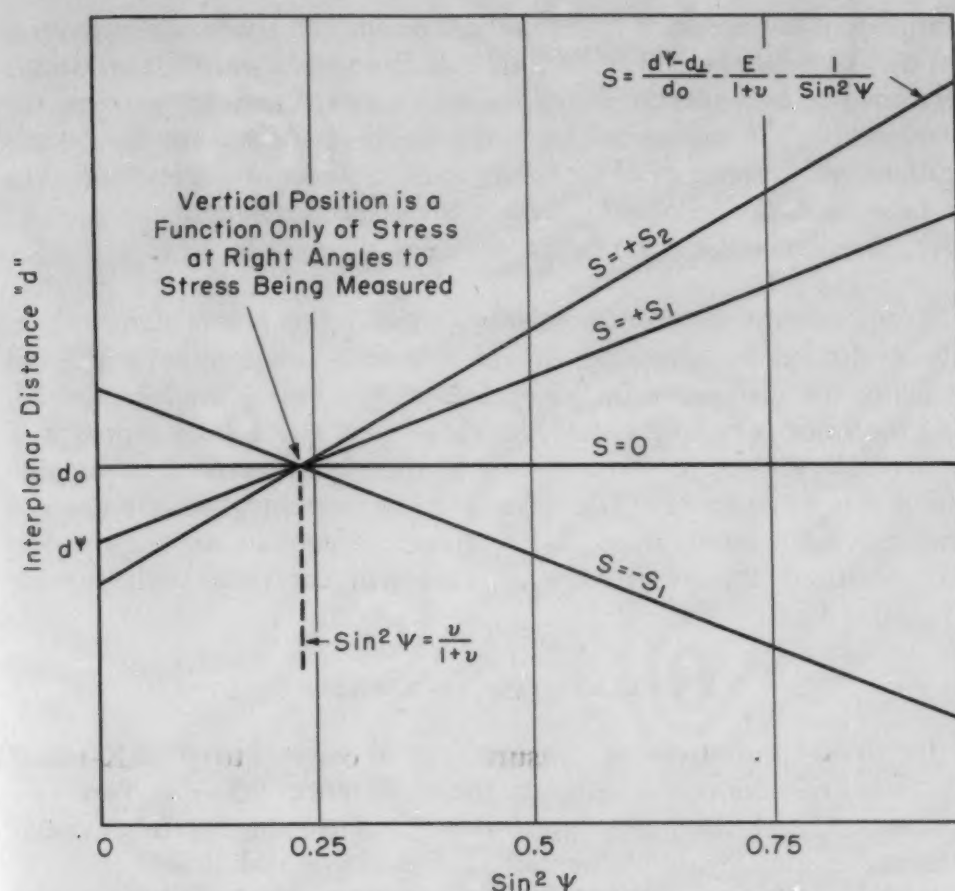


Fig. 2—Theoretical Relation of Interplanar Distance "d" and Specimen Orientation ψ at any Given Stress Level.

d_ψ at $\sin^2 \psi = [\nu/(1 + \nu)]$ will be a direct measure of the unit elastic strain in the direction of stress under consideration.

These principles are rigorous and will apply in the experimental determination of stress if E remains independent of the ψ angular orientation of the crystalline planes with the direction of stress, or the material is isotropic. It is known, however, that iron is anisotropic in nature, but little is known of the behavior of an anisotropic crystal surrounded and confined by other crystals of random orientation. Will such a crystal or grain stress to the mass average or strain to the mass average when a stress is imposed upon the mass? Thus, the possibility yet exists that individual grains within a polycrystalline material composed of anisotropic crystals may behave in an isotropic manner in the absence of preferred orientation, and the value of E , the bulk modulus that obtains from other routine mechanical tests, will apply to the determination of stress in steel.

It would be an experimental nicety if the X-ray modulus of elasticity proved constant and equal to the bulk modulus over all orientations of the crystal to the direction of stress, but this cannot always be expected. However, from the practical point of view it

is completely unnecessary that this be true for the successful measurement of stress by the X-ray method. If the values of "d" are always determined at two specific ψ angles, such as zero and 45 degrees, the difference in "d" values will always be proportional to the stress despite any difference in E that may exist at those ψ angles, and thus may be equated as follows by a constant of proportionality.

$$S = K(d_{\psi_2} - d_{\psi_1})$$

The constant of proportionality, termed the stress constant, is easily evaluated by stressing the sample in known increments and measuring the difference in "d" values at the two ψ angles selected. This procedure is indeed highly desirable even though the value of E remains independent of orientation and thereby directly determinable in the stress measurement itself because, as metallurgists, we are not particularly interested in an X-ray stress value, but an engineering stress, fictitious though it may be, that will correlate with regular strain gage data.

EXPERIMENTAL NECESSITIES

In stress measurement, in contrast to most X-ray diffraction work, we are concerned only in the difference between two "d" distances and not their absolute values. Consequently, the experimental necessities are fundamentally few and are as follows:

1. We must obtain lines of sufficient intensity above the level of general background radiation at two ψ orientations of the sample that their absolute positions may be accurately determined or their relative positions precisely fixed.

2. The line positions must be identical at zero stress or differ by an amount that remains constant from sample to sample, thereby permitting an arithmetical correction.

3. The difference in "d" values derived from the line positions must be equated to engineering stress by a suitable calibration process.

For the purpose of procuring maximum sensitivity of stress measurement, the following is also desirable.

4. The line being measured be diffracted at a very high 2θ angle; and the two ψ angles selected be as far apart as possible in the range of 0 to 90 degrees.

Failure to meet the first requirement listed has been the prime obstacle to the use of X-rays for the determination of stress in hardened steel. The nature of this material is such that the diffracted lines are very broad and diffuse with ill-defined peaks. Therefore, when a high level of general background radiation is superimposed on the lines, the precise measurement of their position becomes difficult if not impossible.

One can do nothing about the line breadth since it is a character-

istic of martensite. It is possible, however, to reduce the background considerably by a correct choice of radiation and filter. The background mainly arises from two sources, the continuous radiation from the X-ray tube and the fluorescent radiation from the sample. If these two undesired components of the diffracted beam are essentially of shorter wave lengths than the desired monochromatic component from the tube, it may be possible to select a filter material whose

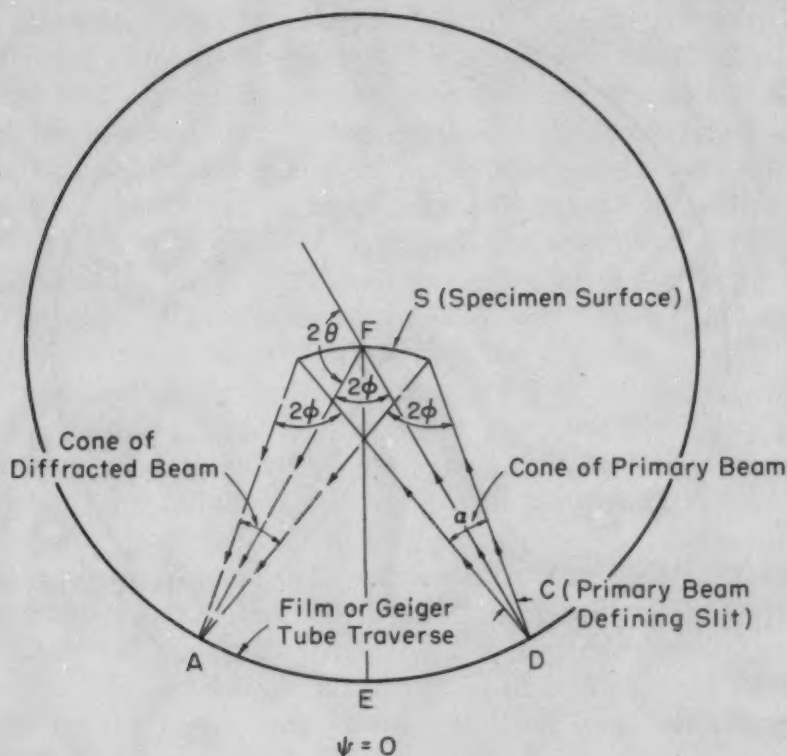


Fig. 3—X-Ray Focussing Conditions With Sample in Normal $\psi = 0$ Position.

absorption edge lies between and effectively reduce the background. To take advantage of this filtering principle, it is axiomatic that a radiation be used that is of longer wave length than the characteristic radiation of the material being examined.

Requirement No. 2 stems from the fact that rotation of the specimen from a position of $\psi = 0$ to an oblique angle may result in a 2θ shift in the position of the diffracted line although no stress be present in the sample. This is a geometrical error arising from the use of a primary beam that is not infinitely thin, the magnitude of this error depending on the particular camera or goniometer design used. Its source is illustrated in Figs. 3 and 4² where the condition arising in a circular camera, chosen for reasons that will be apparent

²A concave specimen surface has been used in the illustrations but these principles apply equally well to flat or convex surfaces when the angle of divergence of the primary X-ray beam is small and no implication that the stress sample need possess a concave surface is intended.

later, has been greatly magnified. We observe in Fig. 3 where the ψ angle is zero, that all diffracted rays arising within the specimen area impinged upon by the primary beam converge to the point A on the film or goniometer circle. However, in Fig. 4 where all conditions are the same except that the specimen has been rotated to an angle of ψ , the diffracted rays converge on the point B instead of A; and are not only well dispersed upon their arrival at the film,

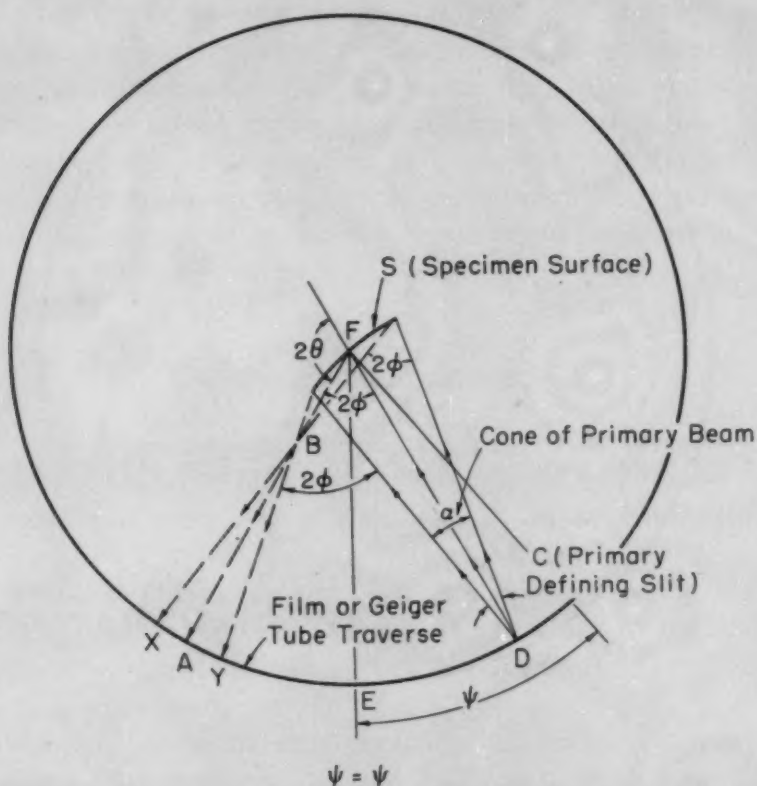


Fig. 4—X-Ray Focussing Conditions With Sample Rotated ψ Degrees From Normal Position.

thus broadening the line, but their mean position is no longer at A. It is further noted that the deviation of the mean position from point A is a function of the three angles ψ of the sample, 2ϕ of the line, and α of the primary beam. The introduction of a defining slit at or near the focal point B will aid in minimizing this deviation and increase line resolution but complete elimination of it can be accomplished only by moving the film or Geiger tube forward to point B.

TECHNIQUE

A General Electric X-Ray Corporation XRD-3 X-ray spectrometer was used in this investigation. The physical layout of the goniometer arrangement may be visualized from the diagram in Fig. 4 and photograph in Fig. 16. For the purpose of gaining

intensity, all Soller baffles were removed from the path of the primary and diffracted beams. This procedure contributes toward line skewness and some loss of resolution, but the lines obtained from hard steel are already so diffuse that little is lost. A slit 0.010 inch wide and normally fixed at A was then moved forward 2.57 inches along the path AF toward F. This puts the slit nearer the point B of convergence of the rays diffracted from the sample surface when the sample is rotated to the angle ψ and thereby increases line contrast and resolution (Fig. 4). As has been mentioned previously, the position of point B along the path AF is a function of the particular ψ angle used and computations indicated that the distance AB was 2.08 inches for a ψ angle of 45 degrees and 3.18 inches when ψ was 60 degrees. Since measurements at both these angles were contemplated and it was believed that repetitious relocation of the slit would be undesirable, the distance of 2.57 inches was selected for AB since it is the focal point for ψ of 52.5 degrees, the arithmetical mean of 45 and 60 degrees. The slit formerly at A was replaced by another slit 0.020 inch wide at point A to reduce the angular spread of the diffracted rays passing through the slit at point B and thereby reduce the line broadening and line displacement resulting from rotation of the sample to ψ . It is apparent from Fig. 4 that the same result can be accomplished by reducing the angle α of the primary beam, but experimentation proved that, for a given line displacement and broadening, greater intensity is obtained by the above procedure. These computations are based on the 211 martensitic line diffracting at 155 degrees (2θ) and obviously do not approach optimum conditions for the 220 austenite line diffracting at 128 degrees (2θ), but for convenience the above slit system was used in all measurements herein reported.

In the past, many investigators have used cobalt or iron radiation in their studies of stress in steel. Both of these radiations furnish a ferrite or martensite line in the desirable 2θ range of 140 to 165 degrees and are excellent selections when the steel hardness is sufficiently low that sharp lines are obtained. When the lines become very diffuse as at high hardness levels, however, and it is imperative that the background radiation be grossly reduced, one finds the proper filter material to be pretty much a Hobson's choice wherein the line intensity is reduced at about the same rate as the background. This situation is avoided by the use of chromium radiation since it has a longer wave length than the secondary iron radiation and a 0.001-inch thick vanadium foil will reduce the background and line intensities in the ratio of 20 to 1. The improvement that accrues with this technique is shown in Fig. 5 where the lines used for stress measurement are indicated by arrows. The pattern from chromium radiation in this figure was obtained by operation of the chromium tube at 35 KV

and 22 milliamperes tube current and with the use of 0.001-inch thick vanadium filter, the procedure followed in all stress measurements. Using this radiation, the martensite 211 planes diffract at about 155 degrees (2θ) and the 220 austenite line is available at 128 degrees, which is a little lower 2θ angle than desired for sensitivity of measurement but is adequate for the purpose. The softness of the chromium radiation possibly contributes further gain in line sharpness in the instance of a sharp gradient of stress in depth since it will diffract only from the extreme surface of the sample. In the absence

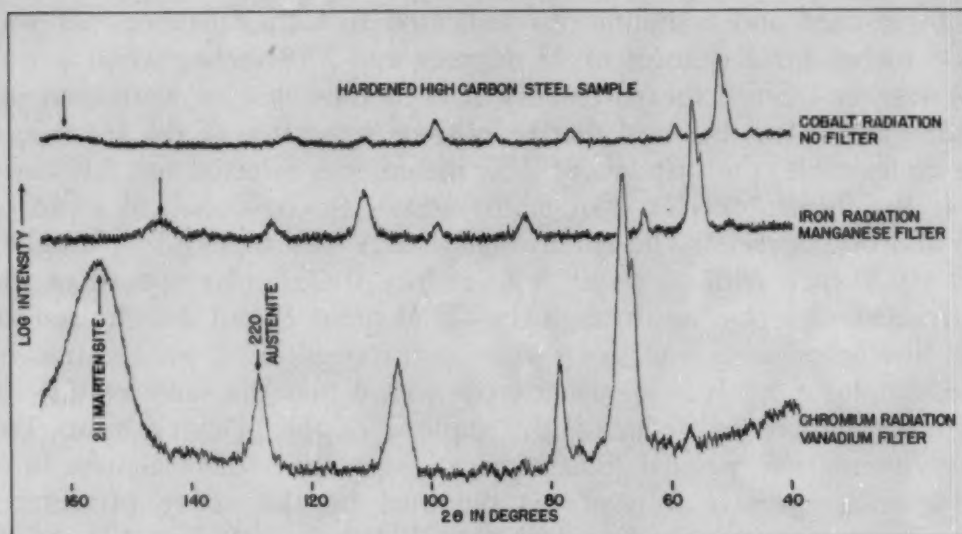


Fig. 5—Diffraction Pattern Obtained from Hardened Steel Using Various Radiations. All traces are plotted to the same intensity scale.

of austenite, and using the above technique, it is possible to attain a ratio of line intensity to background of 10 to 1 instead of the more commonly encountered ratios of 1.2 or 1.5 to 1. Perhaps some of this improvement is indirectly achieved from the Geiger tube since it is itself a fair monochromator, being a little more sensitive to softer radiations. The decided advantage of using chromium radiation was first demonstrated to us by the work of C. M. Schwartz and D. Vaughn of the Battelle Memorial Institute on a sponsored project for the development of an X-ray method for the determination of stress by film technique.

Once the necessary diffraction lines are obtained, the problem of how to measure them remains. It is noted in Fig. 6 that, whereas the lines are well defined as a whole, they are very wide and possess broad peaks that do not lend themselves to precise positioning. It is obvious that the true line positions are in the neighborhood of the center of the inverted peaks, but it is equally apparent that there is no way of precisely determining the true positions in view of the lack of symmetry of the lines. In most routine X-ray diffraction

work this line broadness would simply prevent the successful use of X-rays; however, in stress measurement it is only necessary to determine the angular 2θ shift in the lines produced by the angular ψ rotation of the specimen. Thus, if relative positions can be assigned to the lines, these relative, albeit fictitious, positions may be used successfully for stress measurement. Accordingly, it is noted in Fig. 6 that over a considerable range of 2θ , the sides of the lines are linear.

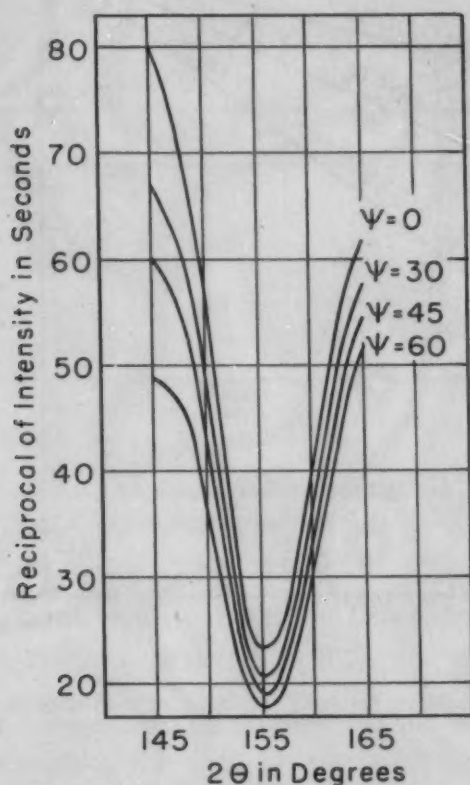


Fig. 6—The Effect of ψ Orientation of Specimen on Line Symmetry.

Thus, advantage of this fact may be taken to fix a relative position for a line by extrapolating the linear portions of the sides to their intersection and arbitrarily designating the angle 2θ at the point of intersection to be the line position. Unfortunately, there is a factor that must be considered in using this simple procedure. Further inspection of Fig. 6 discloses a change in line symmetry with the angle ψ of the specimen, an apparent rotation of the line about the center point of its base.

Computation and experimentation subsequently revealed that the change in line symmetry was the result of a variation in intensity with 2θ that appears to all practical purposes to be a linear function of 2θ and caused by a variation in the cone of radiation subtended at the target by the area of the sample from which the Geiger tube receives its diffracted energy. This variation with 2θ in the region

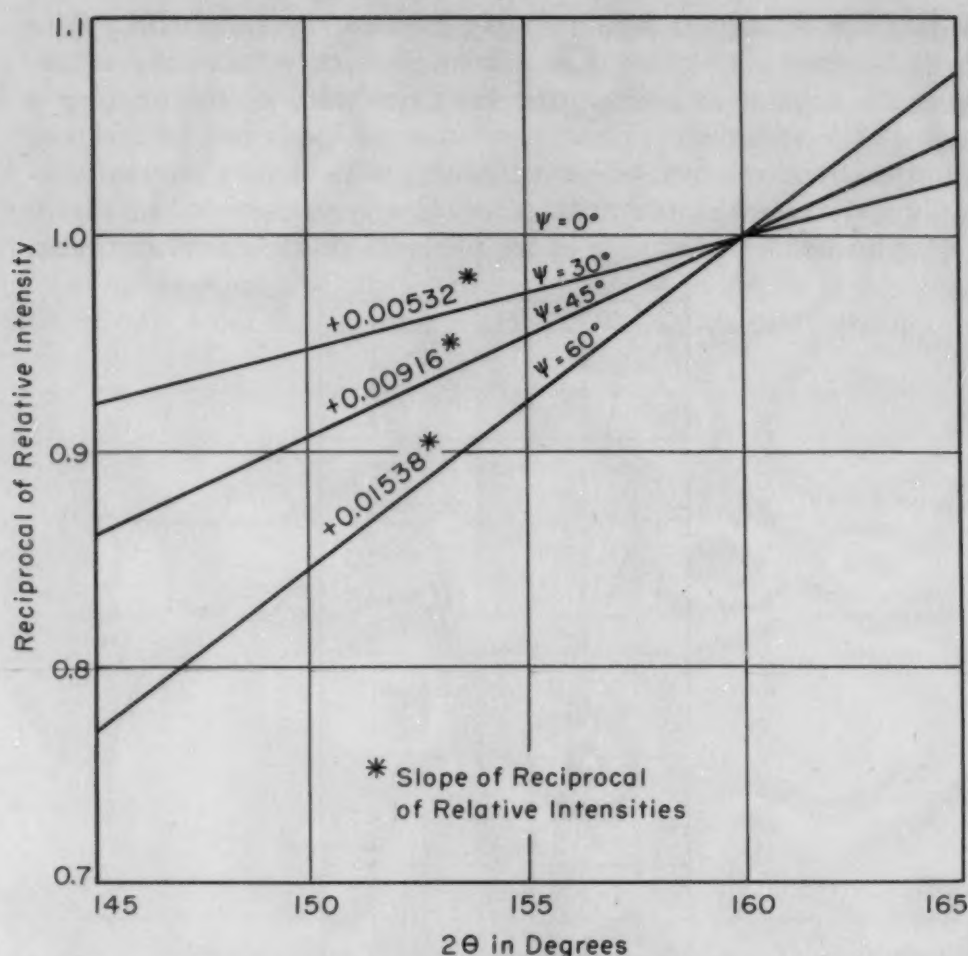


Fig. 7—Variation in Relative Intensity With 2θ at ψ Angles of 0, 30, 45 and 60 Degrees in the Region 145 to 165 Degrees (2θ).

of 145 to 165 degrees (2θ) obtained on a sample of copper is shown in Fig. 7. Similar measurements taken on ferritic iron established the relationship from 120 to 130 degrees (2θ) shown in Fig. 8. One might assume from inspection of these figures that the relative intensities of the various ψ angles are equal at 160 and 126 degrees (2θ), respectively, but these values have been proportionately adjusted to be equal to one at 160 and 126 degrees (2θ) and thus indicate only the relative variation in intensity with 2θ obtained at each ψ angle and not the true intensity relationship of one line to another. Thus, each sloping line in these figures is displaced vertically for convenience until they do coincide at the two 2θ values given. It must be emphasized that this variation in intensity is not merely a background problem and, therefore, capable of correction by linear subtraction, but a proportional variation of the line intensity as well as the background. Of particular importance is the fact that a linear relation (actually a very slight departure from linearity) between 2θ and the X-ray intensity was established at all ψ angles

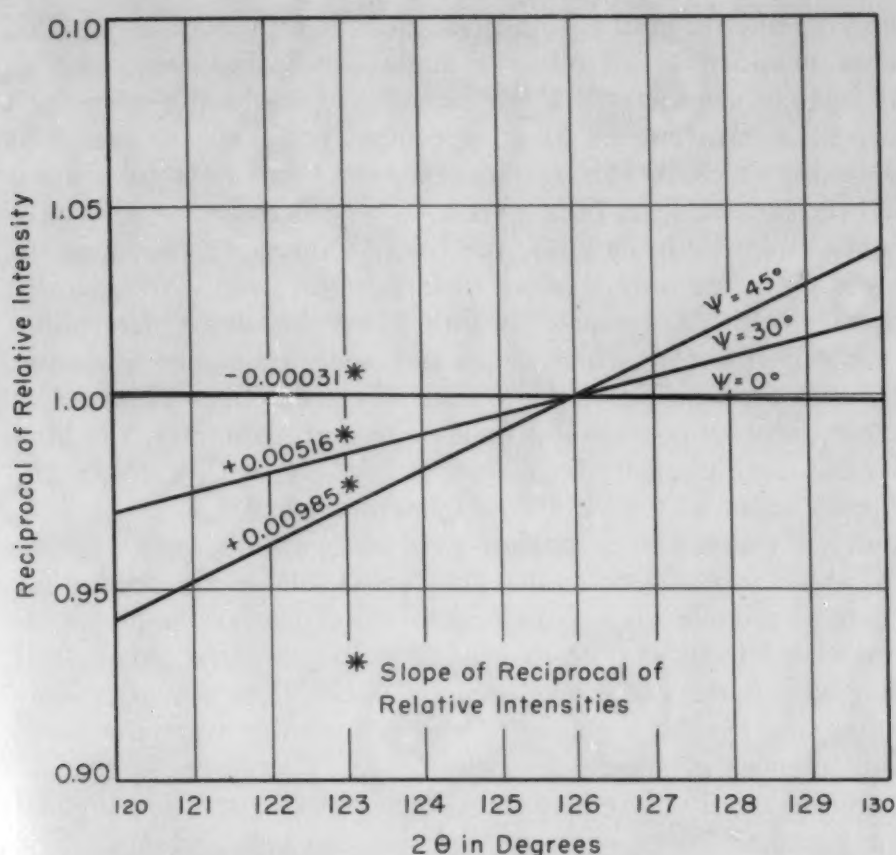


Fig. 8—Variation in Relative Intensity With 2θ at ψ Angles of 0, 30 and 45 Degrees in the Region 120 to 130 Degrees (2θ).

desired for the stress measurements. This suggests two alternate means of compensating the data for the intensity variation.

First, one may divide the intensity values obtained during the line measurements at the various 2θ angles at each ψ angle by the relative intensities at these 2θ angles indicated by the appropriate ordinate values of Figs. 7 and 8. This procedure will place all line measurements on a constant intensity basis and is rigorous if precise relative intensity factors can be determined. An alternate procedure is derived from the change in symmetry of the line itself. It is observed in Fig. 6 that the slope of the left side of the line obtained at $\psi = 0$ is considerably greater than that of the right side. As the ψ angle is increased to 60 degrees, the effect of the linear intensity variation is to gradually equalize the slopes, until the line is nearly symmetrical. Thus, if one were to apply a very slight correction to the data at $\psi = 60$ degrees it is possible to cause the line to be completely symmetrical. A series of multiplication factors that vary linearly with 2θ will suffice for this correction. It is recognized that such a series will introduce a small error because a straight line altered in this manner will no longer be linear, but the error is

negligible. Likewise, similar multiplication factors may be applied to the data obtained at all other ψ angles, including zero, and so adjust all lines to symmetry. The effect of this method of correction is to place all measurements at all specimen positions on the same intensity basis, which in this instance is now equivalent to some ψ angle slightly greater than 60 degrees. The advantage of this procedure is that one need not know the relative intensity values at the various ψ angles, but only that at each ψ angle used, the intensity varies linearly with 2θ , because the line symmetry itself determines its own correction factors which are found easily by algebraic means. Of course, the assumption is made that when the lines obtained at the different ψ angles possess the same degree of symmetry, the lines will be on the same intensity basis and, conversely, if they are on the same intensity basis they will be equally symmetrical.

Initially, it was hoped that relative intensity values, such as those in Figs. 7 and 8, could be obtained that were sufficiently precise for construction of a table of intensity factors. However, small variations were found from sample to sample that prevented this. It is not known why these variations occurred since it is a matter only of slit system and specimen geometry, but conceivably were the result of small differences in specimen positioning. Therefore, in the absence of precise relative intensity data, the second correction method was adopted and as later events proved was the better choice. The complete procedure is then as follows. The line position and shape is first determined by rapidly scaling with a low degree of precision. Two points, spaced as far apart as possible with reference to 2θ , are then selected on the linear portion of each side of the line. Eight readings, each to a precision of $\frac{1}{2}\%$ probable error, the time required for 16,384 counts, are taken at each of these four points and averaged. The relative slopes of the two sides of the line are thus determined and a series of multiplication factors that vary linearly with 2θ and equal to one at 160 degrees (2θ) are applied to the four values obtained to produce equal slopes of the two sides of the line. The four "corrected" values of inverse intensity are then extrapolated algebraically to their intersection and the relative value of 2θ for the line from whence "d" is derived, is established by the point of intersection.

Table I shows the data, and correction factors applied to these data, obtained on a specimen of hardened steel at the ψ angles of 0, 45, and 60 degrees. The method of obtaining these correction factors is indicated in the appendix. The values of 2θ and d resulting from extrapolation of the uncorrected inverse intensities have also been tabulated in Table I for the sake of a later discussion. It is of interest to note that, while the method used in obtaining the proper correction factors for these data is derived directly from the lack of symmetry

Table I

2 θ	Time in Seconds (Inverse Intensity)	Correction Factor	Corrected Time in Seconds	
$\psi = 0$				
150.0	192.10	0.7589	145.75	Corrected 2 $\theta = 155.242^\circ$
151.5	133.60	0.795065	106.22	Corrected d = 1.172714 Å
159.0	109.25	0.97589	106.62	Uncorrected 2 $\theta = 154.688^\circ$
161.0	155.62	1.02411	159.37	Uncorrected d = 1.173973 Å
$\psi = 45^\circ$				
150.0	155.03	0.85725	132.899	Corrected 2 $\theta = 155.204^\circ$
151.5	110.27	0.878662	96.890	Corrected d = 1.172799 Å
159.0	100.53	0.985725	99.095	Uncorrected 2 $\theta = 154.812^\circ$
161.0	145.03	1.014275	147.100	Uncorrected d = 1.173689 Å
$\psi = 60^\circ$				
150.0	141.42	0.9318	131.78	Corrected 2 $\theta = 155.196^\circ$
151.5	108.02	0.94203	101.76	Corrected d = 1.172817 Å
159.0	104.60	0.99318	103.89	Uncorrected 2 $\theta = 155.053^\circ$
161.0	142.95	1.00682	143.93	Uncorrected d = 1.173140 Å
Increase in Correction Factor per Degree				
ψ				Corrected
0	0.02411		$d_{\psi=60^\circ} - d_{\psi=0^\circ} = 1.03 \times 10^{-4}$ Å	
45	0.014275		$d_{\psi=45^\circ} - d_{\psi=0^\circ} = 0.85 \times 10^{-4}$ Å	
60	0.00682		Uncorrected	
			$d_{\psi=60^\circ} - d_{\psi=0^\circ} = 8.33 \times 10^{-4}$ Å	
			$d_{\psi=45^\circ} - d_{\psi=0^\circ} = -2.84 \times 10^{-4}$ Å	

of these lines, the differences in the increase in correction factor per degree found necessary to restore the lines to symmetry at the ψ angles of 0, 45, and 60 degrees are at least approximately equal to the differences in slopes of the relative intensities obtained from a specimen of copper and indicated in Fig. 7. The correction factors per degree for these data are tabulated at the end of Table I and are now compared to those from copper.

DIFFERENCE IN CORRECTION FACTOR PER DEGREE

	Stress Sample	Copper Sample
$\psi = 0 - \psi = 45$ degrees	0.00983	0.00916
$\psi = 0 - \psi = 60$ degrees	0.01729	0.01538

The agreement is seen to be fairly good but not exact and continued experience indicated an unexplained sample-to-sample variation in the differences of correction factor per degree required between the various ψ angles of sufficient magnitude that a fixed set of factors were useless. As a word of caution, it must be mentioned that the four 2 θ points selected on the sides of the lines for line position determination will not necessarily remain unchanged when the ψ angle is changed. They remained constant in the illustration (Table I) because the stress level in this particular sample was very low.

One experimental necessity remains yet to be considered. It is essential that the line positions obtained at the different ψ angles of the sample be identical at zero stress, or their differences must be

evaluated for determination of absolute stress. For reasons already discussed, it is expected that some angular shift will occur though no stress be present. To accomplish this evaluation, it is necessary that a specimen possessing a known stress be used. At the suggestion of Dr. John Norton of the Massachusetts Institute of Technology, metallic powders were employed for this purpose, since they possess no

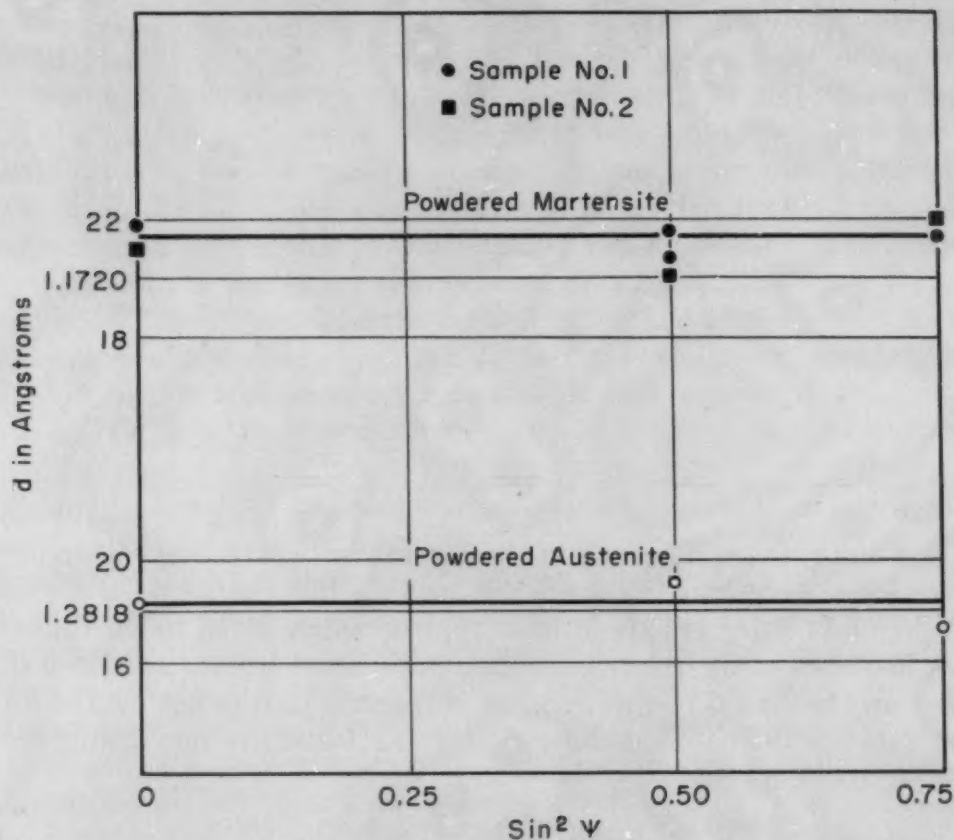


Fig. 9—Variation of "d" Value With ψ Orientation of Specimens of Powdered Martensitic and Austenitic Steel.

macro stress. Samples of powdered martensite and austenite of the same chemical composition as the solid stress samples to be studied (except for carbon content) were prepared from the dust that resulted from dry grinding hardened bars of these compositions after the dust had been magnetically cleansed of wheel debris. It was found necessary to adjust the carbon content to reduce the proportionate amount of austenite in the martensite sample and vice versa. The austenitic powder was prepared from a steel containing 1.5% carbon and the martensite powder from a steel of 0.60% carbon.

A thin film of each of the two powders was adhered to a form of the same contour as the solid stress specimens to be examined and, as anticipated, a displacement of line position with rotation of the sample was observed. However, it was also noted that displacing

the specimen slightly off the goniometer center to a position slightly beyond F along a continuation of the line EF in Fig. 3 affected the line displacement. Trial and error quickly established the fact that no shift of the martensite line resulted throughout the range of ψ from 0 to 60 degrees if the sample surface were about 0.023 inch off goniometer center or of the austenite line in the range 0 to 45 degrees (ψ) if the specimen were displaced 0.017 inch. Since this technique eliminated the necessity of correcting the final stress value, the above sample positioning was used for all measurements. Off centering of the specimen unquestionably prevents a true determination of line position, but this is of no concern since we are already using fictitious values for the line positions. The "d" values obtained from two martensitic powders and a single austenitic powder, using the above technique, are shown in Fig. 9.

DATA

Representative data are presented in Figs. 10 to 15 and Tables II and III from measurements of stress in the circumferential direction of four tubular specimens, 4 inches O.D., 3 inches I.D. and 1½ inches high, of SAE 4620 carburized on the O.D. and I.D. surfaces and hardened. All specimens exceeded Rockwell C-60 in hardness and possessed varying amounts of austenite. Specimen No. 2 was oil-quenched from cyanide salt, and Nos. 1, 3 and 4 were oil-quenched from a standard hardening furnace with no atmospheric protection. All samples were tempered at 350 °F (175 °C) and slit longitudinally at one point along the circumference to facilitate external loading. Evidence that little surface decarburization was present in all samples was established by subsequent X-ray examination. The measurements on specimens 1 and 2 were taken on the as-heat treated

Table II

Specimen Condition	X-Ray Stress in		X-Ray Stress Difference		Stress Difference From Original Condition SR-4 Strain Gage (psi)
	Martensite (psi)	Austenite (psi)	(From Original Condition) (Martensite) (psi)	(Austenite) (psi)	
Specimen No. 3—Electropolished Surface					
Original	-14,400	-2,100	0	0	0
Loaded in tension 1st time	+37,800	+53,000	+54,600	+55,100	+52,200
Loaded in tension 2nd time	+92,000	+105,000	+106,400	+107,100	+119,100*
Second load released†	-5,500	+6,900	+8,900	+9,000	+13,100

*The austenite yielded and the strain gage summed the elastic and plastic strain, whereas the X-ray measurements indicated only the elastic strain, or strain gage was in error.

†The specimen would have returned to the original stress condition had it not yielded plastically during the second loading.

Table III

Specimen Condition	X-Ray Stress in		X-Ray Stress Difference		Stress Difference From Original Condition SR-4 Strain Gage (psi)
	Martensite (psi)	Austenite (psi)	(From Original Condition) (Martensite) (psi)	(Austenite) (psi)	
Specimen No. 4—Ground Surface					
Original	-40,000	-21,000	0	0	0
Loaded in tension 1st time	+1,600	+22,000	+41,600	+43,000	+41,300

surfaces whereas No. 3 was electropolished and No. 4 ground before determination of stress.

X-ray measurements made at four ψ angles on the martensite line

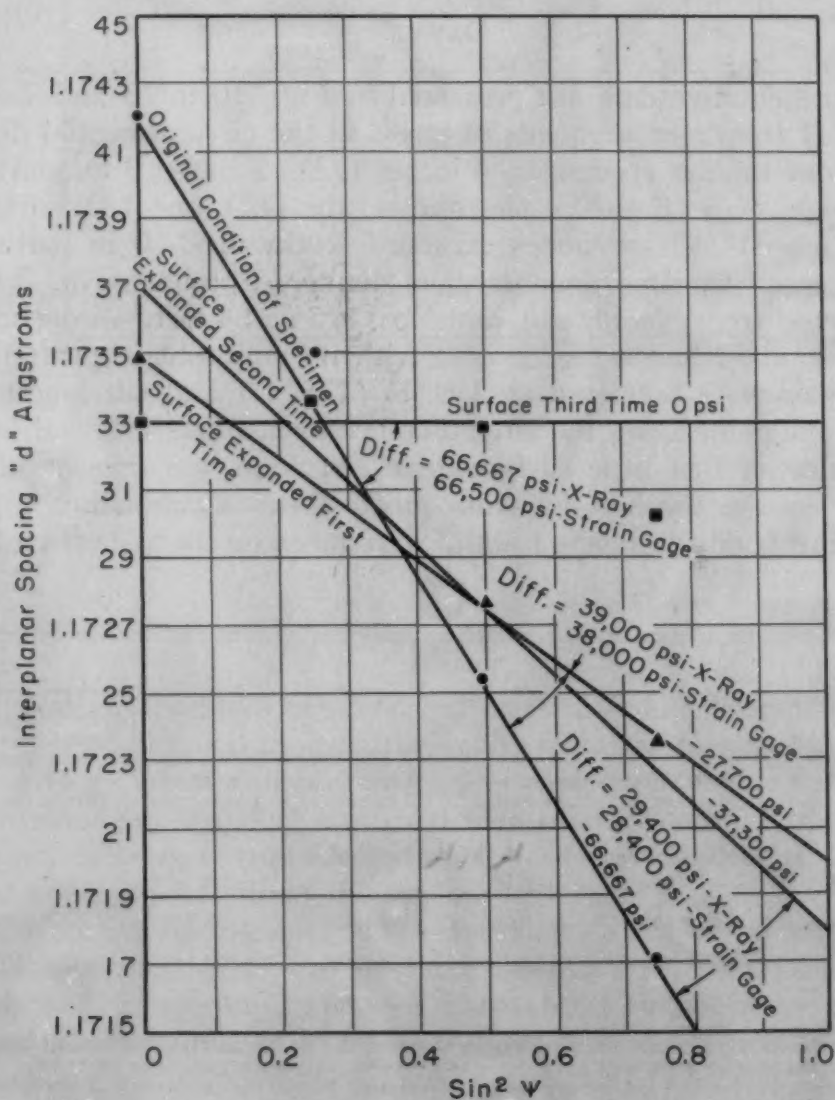


Fig. 10—Stress Measurements of Martensitic Phase in Specimen No. 1.

of specimen No. 1 as the sample was received resulted in the straight-line relationship between "d" and $\sin^2 \psi$ that theory prescribes if E remains constant with change in orientation of the lattice planes with the direction of stress (Fig. 10). Assuming the bulk modulus of 30×10^6 psi and Poisson's constant of 0.28 that obtains from routine mechanical tests on this material, the slope of the line indicated the stress to be 66,667 psi in compression. SR-4 strain gages (see Fig. 16) were thereupon mounted 180 degrees from the slit and adjacent to the area in which the stress had been measured. The ring was compressed on a diameter perpendicular to this area until the strain gages indicated the area had been expanded equivalent to a reduction in strain of 28,400 psi. Then additional X-ray measurements were taken at $\psi = 0$ and $\psi = 60$ degrees which signified a stress level of 37,300 psi in compression and difference from the original condition of 29,400 psi. The agreement between X-ray and strain gage measurements proved remarkable. Two additional expansions of the specimen, the second of sufficient magnitude to reduce the surface stress to zero, provided equally good correlation between X-ray and strain gage data. Among all these data, only the "d" value measured at $\psi = 60$ degrees with the specimen in the third expanded condition appears seriously in error, and this point is so obviously out of line that it is believed that it may be safely disregarded. It is noted, however, that all the lines in Fig. 10 do not intersect in the region of $\sin^2 \psi = 0.22$ to 0.23 as theory demands if Poisson's constant be 0.28. This is believed to have resulted from a change in the longitudinal stress of the specimen by the compression exerted to change the circumferential stress. In other words, although the attempt was made to "load" the ring circumferentially only, some longitudinal straining also resulted.

Better corroboration of theory in this one respect was obtained from the measurements on specimen No. 2 (Fig. 11) where the lines do cross at the theoretical point. However, the agreement between strain gage measurements and X-ray measurements of the difference in stress before and after bending is not as good as previously obtained using the other sample. This was later discovered to be a result of the sample base, which served to position the sample, being somewhat off perpendicular to the O.D., thereby causing a small error in sample positioning. This error was subsequently corrected; but prior to re-examining the sample, the strain gages were replaced with new ones and the sample surface was mistakenly abraded gently by hand with fine emery cloth for better gage adhesion. Stress measurements were then taken on the O.D., the results of which are indicated by the dashed line in Fig. 11. The "d" values, as plotted, form a curve instead of a straight line, and the surface stress is considerably greater in compression than before sanding, the specimen

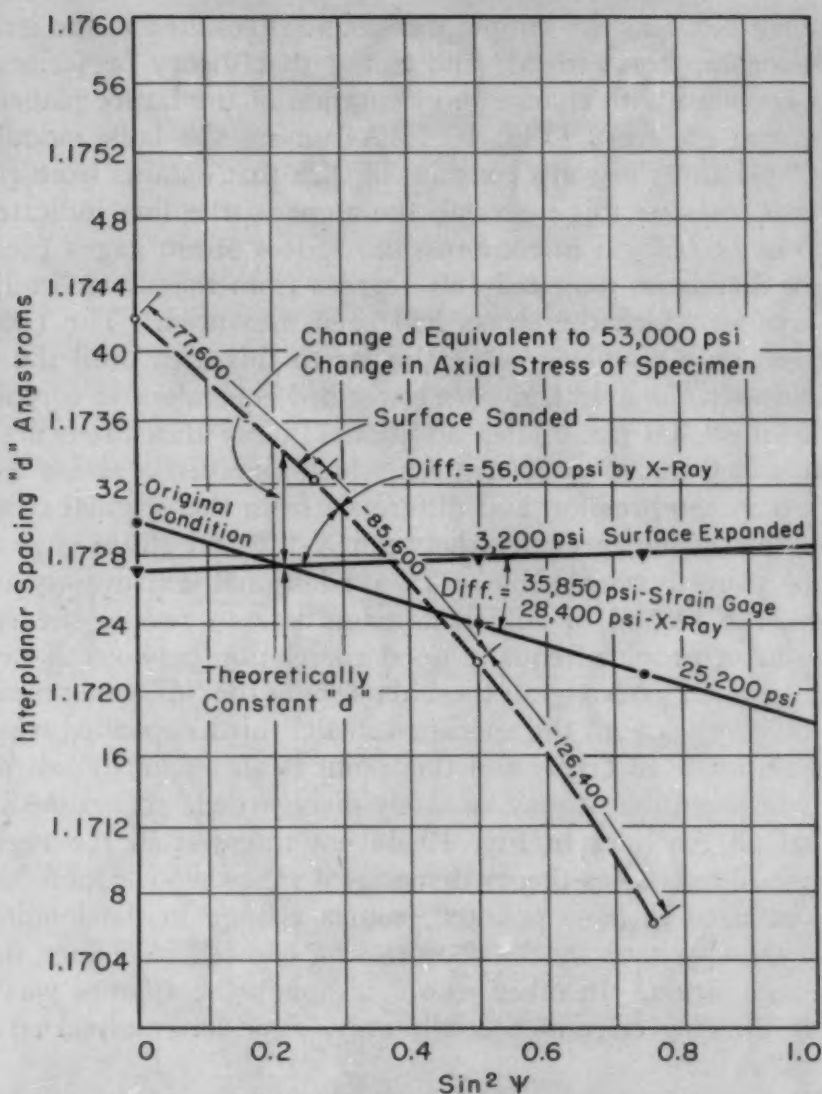


Fig. 11—Stress Measurements of Martensitic Phase in Specimen No. 2.

remaining unloaded. This experiment was repeated on other samples for verification and the phenomenon was confirmed. The increase in compressive stress is likely the result of cold work induced by the sanding, and the curved relation obtained between "d" and $\sin^2 \psi$ suggests that the effect of the cold work is superficial and the stress quickly reduces below the extreme surface. Since the mean depth of the X-ray penetration probably decreases as the angle ψ is increased because the angle of emergence of the diffracted beam from the specimen surface is considerably reduced, the effect is to obtain a stress measurement closer to the surface. If the stress gradient is sharp, the curved line would result. Some evidence that the cold work hypothesis is correct is obtained from the assumption that a random sanding of the specimen surface should induce an equal stress change in the axial direction as the circumferential direction. With this

assumption it is expected that the difference in circumferential stress, before and after sanding, as denoted by the difference in slopes of the respective "d" versus $\sin^2 \psi$ lines would be equivalent to the stress change in the axial direction as indicated by the vertical displacement of the "d" value at $\sin^2 \psi$ equal to 0.22 or 0.23. The average circumferential stress after sanding proved to be 81,600 psi in compression as compared to 25,000 psi originally present. The cold work was, therefore, responsible for 56,400 psi change circumferentially. This value compares quite well with the 53,000 psi change in the axial stress as computed from the upward displacement in "d" value at $\sin^2 \psi = 0.225$.

The stress measurements on specimens 3 and 4 were extended to both the austenite and martensite phases, and while the previous measurements were made on specimens whose surfaces were unaltered following heat treatment, the two samples with which we are now concerned had stock removed in the one case by electrolytic polishing and the other by grinding. This departure from the former procedure was prompted not by curiosity of their relative effects on surface stress, but the necessity of determining if stress in such surfaces could be measured. Ground surfaces must yield to examination if the surface residual stress is to be measured in many finished parts and stock must be removed to measure stress in depth. Grinding is known to induce stress where none exists before and is, therefore, not suited to stock removal for determination of stress in depth. Electrolytic polishing is believed reasonably safe from this standpoint although there is the possibility of stress arising from hydrogen impregnation and it is commonly believed that a stress relief may arise through intergranular attack.

The data obtained on the electrolytic polished specimen (No. 3) are presented in Figs. 12 and 13 and Table II. In the original unloaded condition, the measurements indicated a stress level of 14,400 psi in compression in the martensitic phase and 2100 psi compression in the austenite. After the superimposition of 52,200 psi in tension (by SR-4 strain gages) on these prior stress levels by bending the specimen, the X-ray technique using the same value of E and ν for both phases indicated 37,800 and 53,000 psi tension in the two phases, respectively. The increase in tensile stress from the loading proved to be 54,600 psi in the martensite and 55,100 psi in the austenite, which compare very well with the value of 52,200 psi obtained from the strain gages. From the excellent agreement of these data, it appears evident that electrolytic polishing does not render the surface insensible to examination and that electrolytic polishing need not seriously relieve surface stress by intergranular attack, else the increase in surface stress from the loading would have been much less than the strain gage signified it should be. On the other hand, the

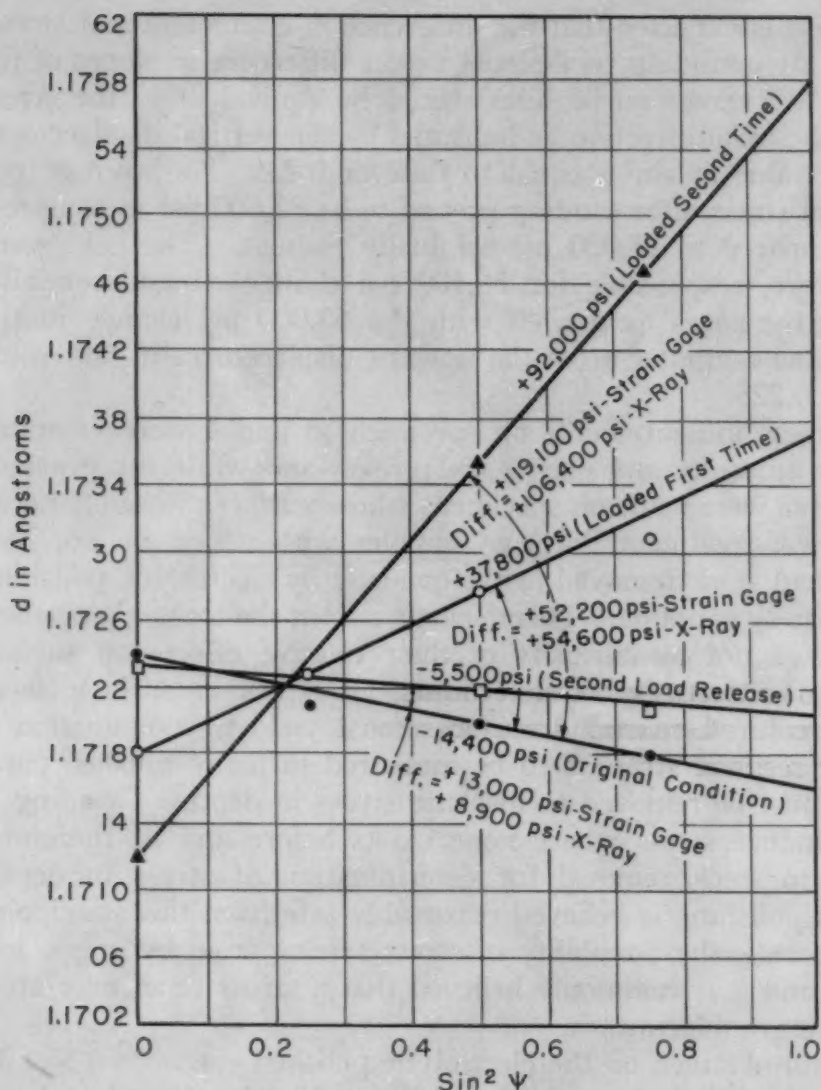


Fig. 12—Stress Measurements of Martensitic Phase in Specimen No. 3.

difference in initial stress poses the question of whether this difference may be altered or reversed in direction if the material is stressed beyond the yield strength of the weaker austenitic phase.

In an attempt to answer this question, the surface of the specimen was once more raised in tension until the strain gages indicated an increase of 119,100 psi over the unloaded condition. Because of the previous stress condition of the sample, this value was thought sufficient to cause yielding in the austenite. Stress measurements were thereupon made while the sample remained under this load and a value of 92,000 psi tension stress in the martensite was obtained and 105,000 psi in the austenite. The stress increases agreed quite well, 106,400 psi and 107,100, respectively, but the increase was considerably less than the 119,100 psi shown by the strain gages. Disregarding for a moment the possibility that the strain gages may have been

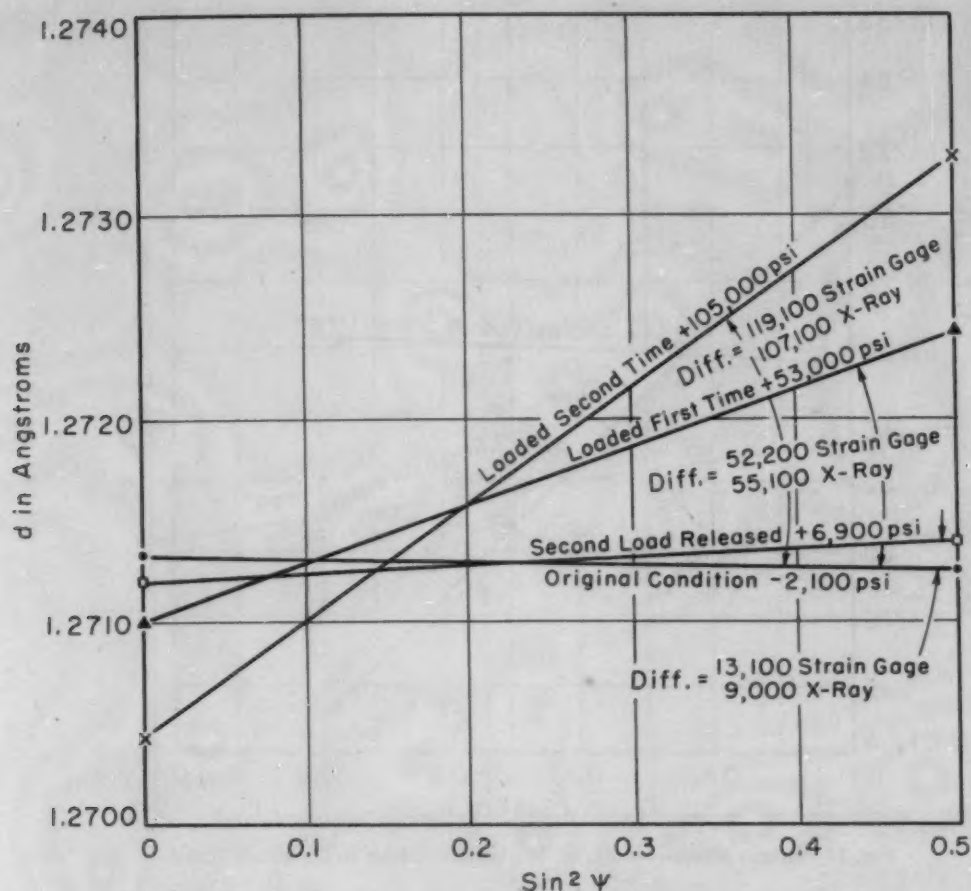


Fig. 13—Stress Measurements of Austenitic Phase in Specimen No. 3.

in error from exceeding their capacities, one must in this instance conclude that the proportional limit in tension of the austenite was exceeded, inducing plastic flow in the austenite, and the creep in the austenite prevented the development of additional elastic stress in the martensite. From this standpoint, then, the yield strength of the austenite confined within the martensite in this sample is about 105,000 psi.

Upon completion of the above measurements, the specimen was released from load and the stress in the two phases again measured. A stress of 5500 psi in compression was found in the martensite and 6900 psi in tension in the austenite. These results are significant in that they depart from the previous values obtained in the unloaded condition by plus 8900 psi in the martensite and plus 9000 psi in the austenite. The magnitudes of the departure are believed beyond the realm of experimental error and prove that yielding of the austenite occurred during the prior loading. Of further interest is the fact that this magnitude is reasonably close to the stress difference of 13,000 psi that one might compute from the plastic strain indicated by the strain gages as having taken place during this prior loading.

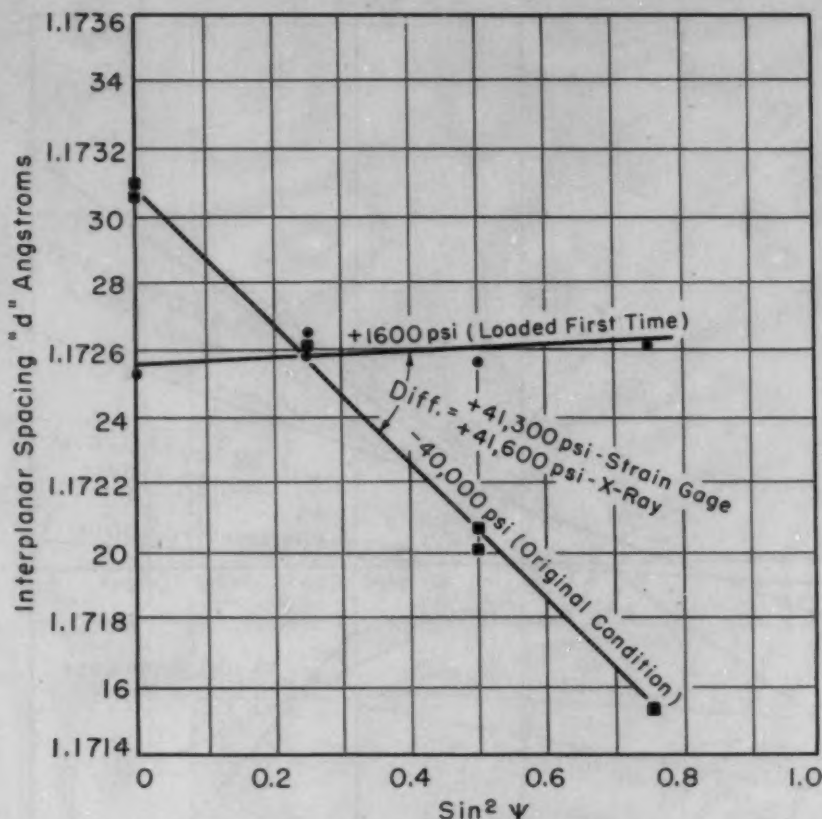


Fig. 14—Stress Measurements of Martensitic Phase in Specimen No. 4.

The results from the fourth specimen are shown in Figs. 14 and 15 and Table III. Here we observe stresses in the unloaded state of 40,000 psi in the martensite and 21,000 psi in the austenite, both compressive. An increase of 43,000 psi in surface stress in the tensile direction by bending eliminated the former surface compressive stress and created a tensile condition of 1600 psi in the martensite and 22,000 psi in the austenite. The increases in tensile stress of the two phases were 41,600 and 43,000 psi, respectively, which agree very well with each other and the value of stress imposed. Once again we note a difference in stress in the two phases; and, more importantly, ground surfaces are amenable to stress examination.

DISCUSSION OF RESULTS

It appears that residual stress may be determined in both the martensitic and austenitic phases of hardened high carbon steel with a precision of ± 3000 or 4000 psi. Furthermore, the bulk modulus value of 30 million psi and Poisson's constant of 0.28 used together in the term $E/(1 + \nu)$ are valid for chromium radiation for both the austenite and martensite phase at all ψ orientations to the direction of stress. Separate verification of the individual value of 0.28 for Poisson's constant for martensite also obtains from the data, but the

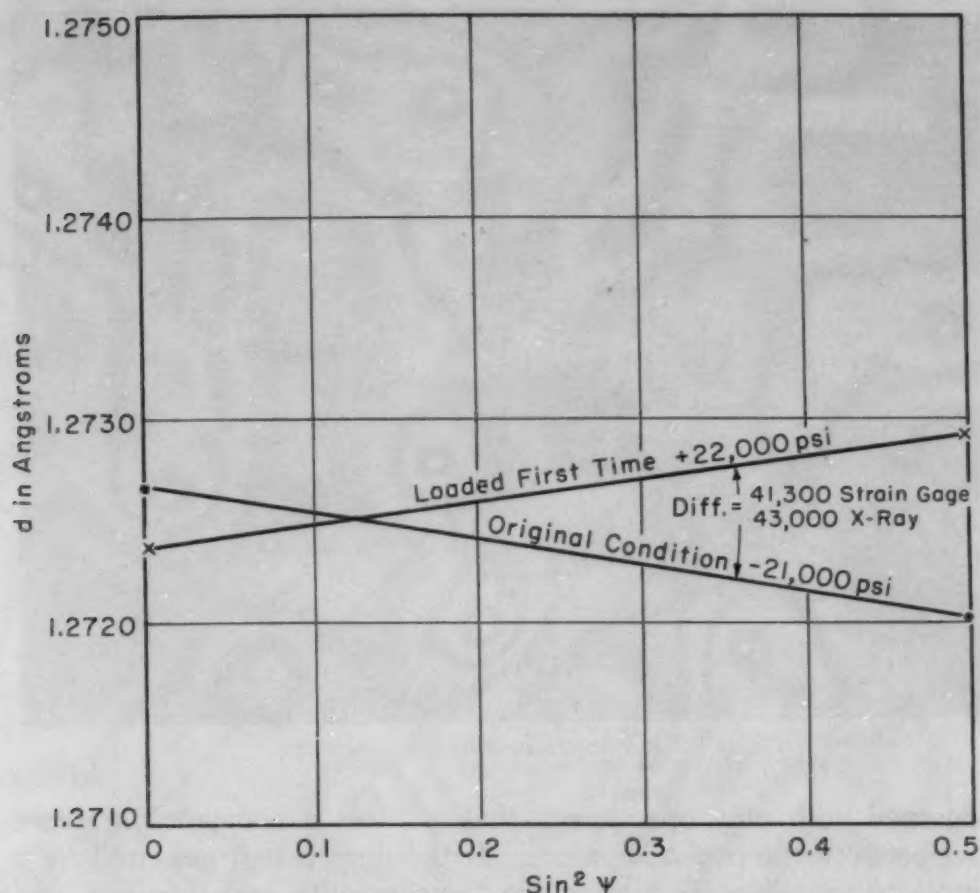


Fig. 15—Stress Measurements of Austenitic Phase in Specimen No. 4.

scatter in the austenite measurements precludes establishing any definite value for Poisson's constant for austenite. A better means of attaining unidirectional loading of the sample will be necessary for positive evaluation of this constant and it is only possible to state that the ratio $E/(1 + \nu)$, wherein E is 30 million psi and ν is 0.28, also holds for austenite. In comparing the X-ray stress measurements to strain gage measurements it must also be mentioned that the average reading of two strain gages were taken as the strain gage measurement and in most instances the X-ray data correlated about as well with the strain gage averages as the strain gages checked each other.

Having established the adequacy of the particular technique used, the question arises whether it is really necessary to use any correction factors to put the lines at all ψ angles used on the same intensity basis. To answer this question we must look to the relationship of $\Delta 2\theta = 2\theta_{\psi=\psi} - 2\theta_{\psi=0}$ obtained by merely extrapolating the uncorrected inverse intensity readings taken on the sides of the lines to their points of intersection, to the corresponding $\Delta 2\theta$ derived from the corrected intensity data. In considering this relationship we are

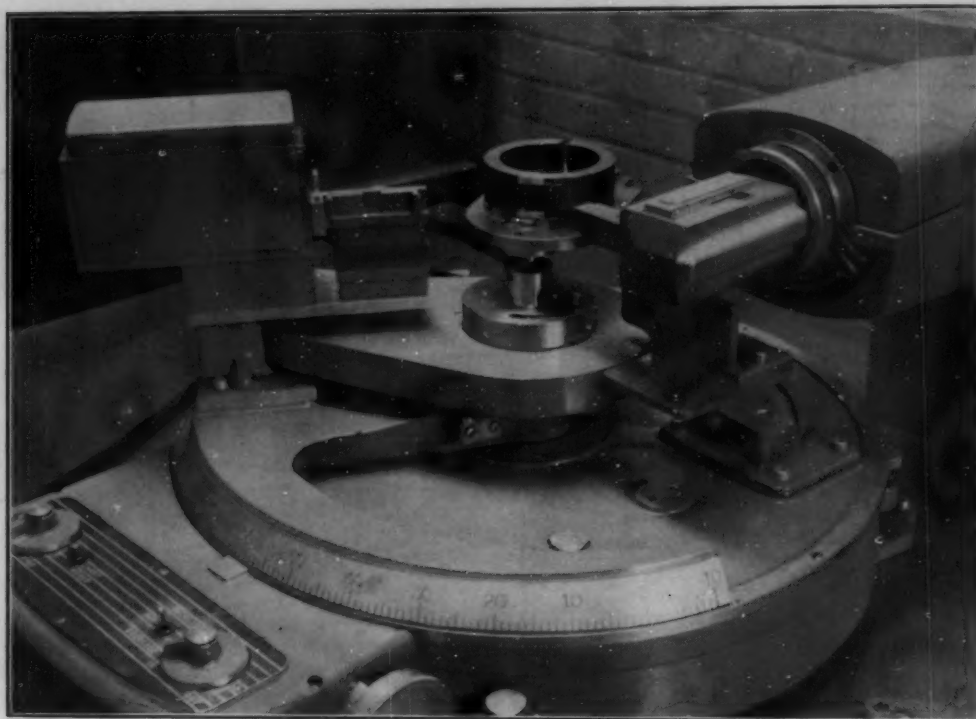


Fig. 16—X-Ray Spectrogoniometer Arrangement.

concerned with only one aspect, that is, does a constant difference exist between the two $\Delta 2\theta$ values. If the lines being measured from sample to sample were always the same breadth and intensity, one assumes a constant error, capable of elimination by arithmetic means, would be introduced by extrapolation of the uncorrected data. But with variation in relative line intensity and sharpness it is conceivable that there would also be a variation in line skewness and a sample to sample difference in $\Delta 2\theta$ would be obtained at any given stress level if the uncorrected intensity data were used.

The relation of $\Delta 2\theta$ (uncorrected) to $\Delta 2\theta$ (corrected) obtained on the martensite line of five specimens is shown in Fig. 17. It is noted that a reasonably constant difference between the two does obtain in these samples and the possibility of using the uncorrected intensities does exist. The differences are noted to be approximately -0.19 degree when the two ψ angles used are 0 and 45 degrees, and -0.40 degree when they are 0 and 60 degrees, which values must be added to the respective uncorrected $\Delta 2\theta$'s when the stress is computed or the stress equivalent to these values must be added. The data shown in Table I affords a means of comparing stress values computed from both uncorrected and corrected intensity data.

CORRECTED DATA				
$\Delta "d"$		Stress Factor	Stress, Psi	ψ Angles Used
1.03×10^{-4}	\times	2,667	= 2,747	0, 60
0.85×10^{-4}	\times	4,000	= 3,400	0, 45

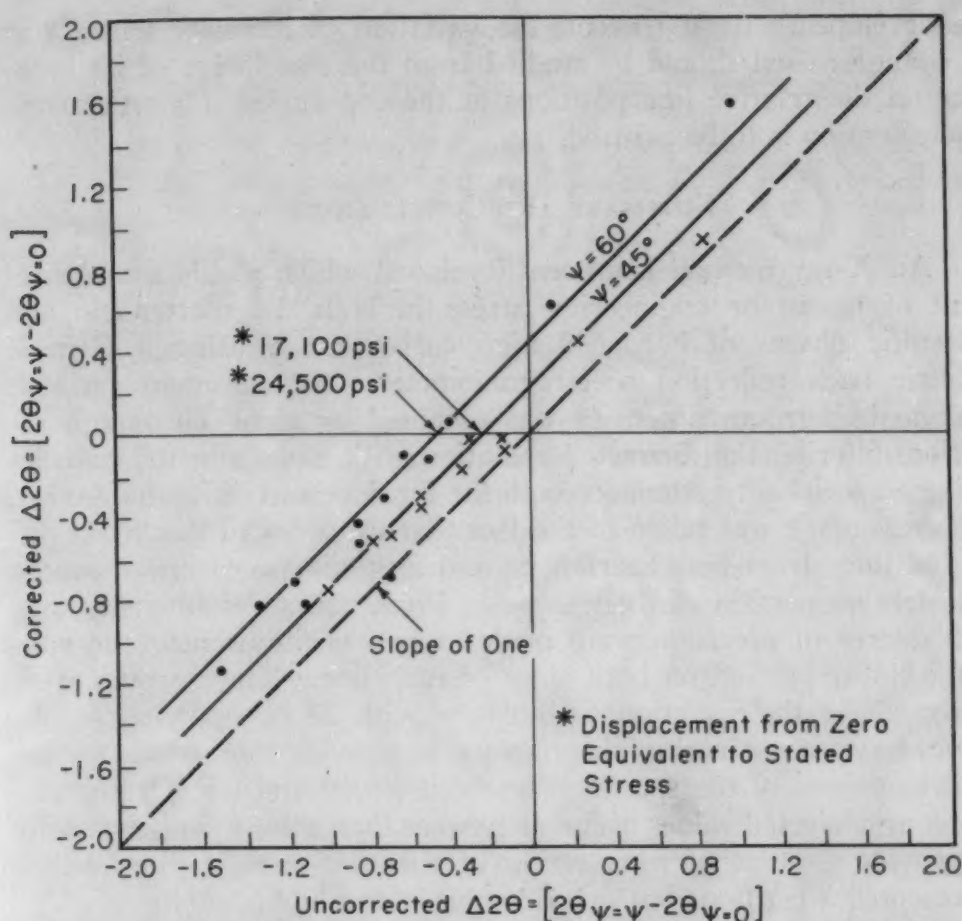


Fig. 17—Relation of Uncorrected $\Delta 2\theta$ and Corrected $\Delta 2\theta$ Obtained on Five Samples.

UNCORRECTED DATA					ψ Angles Used
Δ "d"		Stress Factor	=	Stress, Psi	
-8.23	×	2,667	=	-22,216	0, 60
				+24,500	
		Total		2,284	
-2.84	×	4,000	=	-11,360	0, 45
				+17,100	
		Total		5,740	

The practical agreement of these values is believed to suggest further study of the possibility of eliminating the correction procedure. However, until considerably more data are acquired, the use of measurements of the line sides for fixing relative line positions without correcting the measurements for variation of intensity with 2θ is considered inadvisable.

It must be emphasized that the intensity correction procedure adopted was necessitated by the particular means of establishing line position—the sides of the lines—and the slit system used. Therefore, this procedure may be rendered unnecessary or less important if other methods for fixing line positions and different slit arrangements

are developed. In any event, the variation of intensity with 2θ at all ψ angles used should be studied from the standpoint of its influence on the relative line positions at these ψ angles if a true stress determination is to be assured.

SUMMARY AND CONCLUSIONS

An X-ray method has been developed which yields a measurement of macro or engineering stress in both the martensitic and austenitic phases of hardened high carbon steel, using a General Electric back reflection spectrogoniometer. A maximum ratio of peak to background intensity was obtained by using chromium radiation, filtering the diffracted radiation with vanadium foil and devising a special slit system for both the incident and diffracted beams.

Advantage was taken of the fact that the sides of the broad diffracted lines from both martensite and austenite were linear over a considerable portion of their slopes. Point counts of intensity to a high degree of precision were made at two positions near the ends of the linear portion on both sides of each line. These values were corrected for the variation of intensity with 2θ by applying a self-induced system of multiplying factors to provide line symmetry for all orientations of the specimen between $\psi = 0$ and $\psi = 60$ degrees. The four corrected values of intensity were then solved mathematically to provide a point of intersection of the two straight lines which represented a fictitious but precise value of the line position.

Both martensitic and austenitic powders, necessarily containing zero macro stress, were used to calibrate the method. The position of the specimen relative to the goniometer center was adjusted until the line positions for both austenite and martensite were unchanged as ψ was varied from 0 to 60 degrees.

The method was finally applied to the measurement of surface stress on the O.D. of 4-inch diameter rings of carburized and hardened SAE 4620 steel in the as-heat treated, ground and electrolytically polished conditions. External loading was applied to these rings after slitting and the resulting elastic strain measured simultaneously with SR-4 strain gages and by the above X-ray technique. The agreement between the two methods of measurement indicated a probable precision of the X-ray method of ± 3000 to 4000 psi.

ACKNOWLEDGMENT

The authors wish to acknowledge indebtedness to Miss Pauline Scheerer and Mr. John Birtalan who carried out much of the experimental work. They also wish to express their appreciation to Professors John Norton and Bertram Warren and Mr. Robert Ogilvie of the Massachusetts Institute of Technology for several stimulating discussions.

Appendix

METHOD OF COMPUTING CORRECTION FACTORS

The slopes of the two line sides are determined from the uncorrected data, for example, from the data at $\psi = 45$ degrees shown on Table I.

$$\frac{155.03 - 110.27}{151.5 - 150.0} = 29.84 \text{ seconds per degree}$$

$$\frac{145.03 - 100.53}{161.0 - 159.0} = 22.25 \text{ seconds per degree}$$

It is immediately evident from these values that if the slopes are to be equalized the set of factors linearly proportional to 2θ that are to be applied to the inverse intensity values must increase with 2θ . This increase is then arbitrarily taken to be 0.02 per degree and the factors that derive from this value of 0.02 and assumed to be 1 at 160 degrees (2θ) are applied to the uncorrected inverse intensity data.

2θ	$(160 - 2\theta) 0.02$	Correction Factor at 2θ
150.0	$(160 - 150.0) 0.02 = 0.200$	$1 - 0.200 = 0.80$
151.5	$(160 - 151.5) 0.02 = 0.170$	$1 - 0.170 = 0.83$
159.0	$(160 - 159.0) 0.02 = 0.020$	$1 - 0.020 = 0.98$
161.0	$(160 - 161.0) 0.02 = -0.020$	$1 + 0.020 = 1.02$

2θ	Inverse Intensity Time in Seconds		Correction Factor		Corrected Intensity
150.0	155.03	\times	0.80	=	124.0240
151.5	110.27	\times	0.83	=	91.5241
159.0	100.53	\times	0.98	=	98.5194
161.0	145.03	\times	1.02	=	147.9306

The relative slopes from these "corrected" intensities are again determined and found to be 21.6666 and 24.7056 seconds per degree, respectively.

It is now observed that we have over-corrected in the sense that the ratio of the slopes is less than one instead of greater than one as formerly. However, computation will demonstrate that the change in slope of each side induced by the correction is essentially a linear function of the increase per degree of the correction applied. Thus, we may establish two linear equations from the change in slopes of the line sides caused by use of the arbitrarily chosen increase of 0.02 in the correction factors and solve them simultaneously for the increase per degree of correction factors necessary to equalize the slopes of the line sides.

$$29.8400 - \left[\frac{29.8400 - 21.6666}{0.02} \right] x = S$$

$$22.2500 - \left[\frac{24.7056 - 22.2500}{0.02} \right] x = S$$

Solving for x , the increase per degree in correction factor that

will result in each line side possessing slope S , we find the value of 0.1428, from which the correction factors shown in Table I have been computed.

References

1. C. S. Barrett, "Structure of Metals", McGraw-Hill Publishing Company, 1943, p. 273.
2. R. F. Hanstook and E. H. Lloyd, "An X-Ray Method of Measuring Poisson's Ratio", The Institute of Mechanical Engineers (British), *Applied Mechanics*, War Emergency Issue No. 26, Vol. 157; *Proceedings*, 1947.

DISCUSSION

Written Discussion: By J. A. Bennett and H. C. Vacher, National Bureau of Standards, Washington, D. C.

The authors have performed a valuable piece of work in developing this method of attack on the difficult problem of stress measurement in hardened steel. However, I believe that their method of treating the data has made it difficult to evaluate the possible accuracy of the method.

It is pointed out on the fifth page that the stress is proportional to the difference in "d" values at two ψ angles. This proportionality is independent of stress normal to the plane in which the measurements are taken and does not require any assumption regarding the value of E or ν . However, the authors have attempted to determine the stress without evaluation of this proportionality constant by assuming values of elastic modulus and Poisson's ratio. In doing so they have introduced some uncertainties and have not utilized the data to best advantage. For example, since the uncertainty of the "d" values appears to be independent of ψ , the best determination of stress can obviously be obtained from the "d" values at $\psi = 0$ and $\psi = 60^\circ$, and actually little loss in accuracy would be expected to result from neglecting the intermediate values. However, the authors have neglected one of the 60-degree values in Fig. 10 in favor of values which appeared to give a stress more in agreement with the strain gage readings.

It is difficult to understand the reason for making these time-consuming measurements at intermediate ψ angles. They would increase the precision of the determination of elastic modulus and Poisson's ratio for the individual crystals, but these determinations require a knowledge of the longitudinal stress in the specimen. Lacking this knowledge it is impossible to say whether the failure of the curves to intersect at $\sin^2 \psi = 0.22$ is due to biaxial stress or an error in the assumed value of Poisson's ratio.

In discussing Figs. 12 and 13, the authors attribute the increase in tensile stress after unloading to the plastic deformation during the second loading, and point out that the change in X-ray stress agrees with the change in strain gage reading. This would not be expected; if plastic deformation in tension had occurred on the surface, then on release of load the X-ray stress would have shifted in the compression direction, while the change in strain gage reading would be positive, as observed. Is it possible that the plastic deformation occurred some distance below the

surface, due to the higher strength of the carburized layer, resulting in a residual stress change in the tension direction on the surface?

Written Discussion: By E. I. Blount and A. L. Ellis, International Harvester Manufacturing Research, Chicago.

We want to congratulate Messrs. Christenson and Rowland on their fine work, which seems to provide a solution, at least in principle, to the problem of measuring stresses in hardened steel parts by means of X-rays. We have also been interested in this subject and are very grateful to the authors for the opportunity to discuss their work before publication.

Clearly, the use of filtered chromium radiation is the key to success in this work. With cobalt and iron radiation, the peak-to-background intensity ratios have been hopelessly low. With chromium, however, the lines are so much better as to make measurement practicable with the goniometer, and possibly even with film techniques.

The next problem is a method for measuring the lines. To our knowledge, two procedures have been suggested—namely, Rowland and Christenson's, and the parabolic method of Ogilvie.^a The latter consists of fitting a parabola to the peak of the line by the method of least squares. Both methods involve fictions and assumptions. In the case of the authors' method, some of these are as follows: First, that there is a linear portion on the sides of the lines. We are not able to verify this in all cases, and, indeed, it would be fortuitous if it turned out to be true. The next assumption is that "when the lines obtained at the different ψ angles possess the same degree of symmetry, the lines will be on the same intensity basis". This assumption is unnecessary if the calibrating specimen lines are sufficiently similar to those of the unknown.

The assumptions made in the parabolic method seem to play a less important part. Here, since the parabola is automatically symmetrical, there is an error involved in fitting an unsymmetrical curve to it; but since the asymmetry is not marked at the peak, and is due to a function which varies more slowly with 2θ than the intensity of the line, this effect will be small and to a sufficient degree correctible mathematically. This would appear to lead to less dependence on the line shape of the calibrating specimen. This method also gives a result which is closer to the actual peak of the line than the result formed by the authors' method. This is not important for stress measurements, but would be desirable, for instance, in determining the carbon content of martensite or austenite by the variation of lattice parameter. Finally this method appears more convenient, involving less calculation, and also allowing, after a few points have been measured, selection of the rest to obtain maximum precision. (In both methods the precision decreases if the peak is far away from the middle of the range of points measured.) For these reasons we have selected the parabolic method, but have not verified Ogilvie's claims of precision. On one specimen we made 10 determinations of line position, taking 5 counts of 12,800 (each accurate to 0.6%) for each determination, and found a probable error of 0.06 degree, which is exactly what we calculated the probable error to be. Ogilvie reported reproducibility to 0.01 degree with measurements individually accurate to 3%. We do not under-

^aR. E. Ogilvie, "Stress Measurement With the X-Ray Spectrometer". Thesis, Massachusetts Institute of Technology, 1952.

stand the reason for this disagreement but, since it is of some importance, we hope it can be resolved in the future.

As yet, because our specimen-positioning device has only very recently been completed, we have made only a few determinations of change in stress, and have not had a chance to calibrate with a stress-free powder. So far, however, we have found an encouraging correlation between X-ray and strain-gage measurements, with a probable error from the best straight line of about 4000 psi for determinations requiring 1,300,000 counts which took us about 2 hours. We expect improvements in this to result from modification in the slit system and improvements in the strain-gage methods. This work was done on a 6-inch O.D. ring of carburized and hardened AISI 4720 steel (Rockwell C-62).

So far, this is all very encouraging, but there remains a disturbing note. Rowland and Christenson have found that they get good results using the bulk elastic moduli in their calculations. Ogilvie, on the other hand, found values of the stress constant K which were larger than the calculated value based on the bulk moduli. The difference was 22% for a spheroidized specimen and 32% for a hardened one. Our results so far indicate a constant about 20% larger than calculated. An investigation of this matter indicates to us that there is no reason to expect the bulk moduli to be usable in this work, and also that any theoretical prediction would be extremely difficult and tenuous. Thus, the stress constant can only be determined by experience. It is somewhat disturbing to find this disagreement, and it is something that will have to be clarified before residual stress measurements can be made with confidence. However, the present work has removed some of the most serious obstacles in the application of X-ray techniques to the measurement of residual stresses and it is very probable that this problem of determining the stress constant will be resolved without too much difficulty.

Written Discussion: By C. M. Schwartz, assistant supervisor, Battelle Memorial Institute, Columbus, Ohio.

The authors are to be congratulated on their significant contribution to the measurement of stress in hardened steel. It would appear that the X-ray spectrometer is a most valuable tool for this application, providing advantages over film techniques in the form of accurate measurement of diffraction-line shape and of reduction of background intensity.

In the course of a preliminary investigation of this problem at Battelle (supported by Timken Roller Bearing Company), D. A. Vaughan⁴ and I examined the feasibility of stress measurement in hardened steel using film techniques. The samples were the same as those described in the paper—namely, carburized and hardened rings of SAE 4620 steel. Co radiation is unsatisfactory for hardened steel. Since these samples usually contain appreciable amounts of retained austenite, Fe radiation cannot be used because of superposition of 220 martensite and 400 austenite reflections. This difficulty led to consideration of other radiations. It was found that Cr radiation provided measurable back-reflection lines of the martensite phase resolved from those of austenite. Mn radiation was used to obtain the 311 reflection from austenite at 150 degrees 2θ .

In order to test the precision of the film techniques using these three

⁴Research physicist, Battelle Memorial Institute, Columbus.

radiations, known stresses, mechanically induced, were compared with X-ray measured stresses. Agreement was obtained between the two sets of measurements which indicated an over-all precision of ± 5000 psi in the X-ray data. As an example of these tests, Table IV shows the results of X-ray measurements of stress in the austenite phase, compared with the corresponding induced loads. The agreement is within the precision stated, except when loaded above 40,000 psi. Since the initial surface stress was 27,000 psi in compression (by X-rays), and since the ring did not return to its original curvature upon release of these higher loads, it was concluded that the austenite phase deformed plastically. Under the same load conditions, the martensite showed no evidence of yielding.

This suggests yield in the austenite somewhat below 72,000 psi in compression, a lower value than that appearing in this paper for yield of austenite in tension. However, because of the carbon gradient in these rings, this difference in yield may represent only sample variation.

Table IV
Comparative Measurements of Induced Stress in the Austenite Phase of a Carburized and Hardened SAE 4620 Steel by X-Ray and Mechanical Methods

Mechanically Induced Stress, 1000 psi*	X-Ray Measurement of Induced Stress, 1000 psi†
Loaded -10	-9
Unloaded 0	0
Loaded -20	-18
Unloaded 0	0
Loaded -15	-9
Unloaded 0	0
Loaded -30	-27
Unloaded 0	-9
Loaded -35	-35
Unloaded -2	0
Loaded -40	-36
Unloaded -3	-9
Loaded -45	-36
Unloaded -4	-9

*The induced stresses were produced by spreading the ring and the stress values computed from the measured change in curvature.

†The specimen was a 4-inch O.D. ring slit longitudinally. The initial circumferential stress, measured by X-rays, was 27,000 psi in compression.

The laborious correction procedure involved in the authors' method of obtaining the necessary precision raises the question whether another choice of X-ray beam geometry would not reduce line asymmetry and thus reduce the amount of correction required.

I believe that some of the difficulty lies in the use of vertical line focus without Soller baffles. Since this type of sample produces a broad line, irrespective of beam geometry, and since focusing conditions are far from fulfilled, it would appear that parallel-beam geometry would offer greater reduction of line asymmetry. This might be accomplished without excessive loss of intensity by changing to horizontal line focus and collimating to limit both horizontal and vertical divergence.

Written Discussion: By S. R. Maloof and H. R. Erard, metallurgists, Springfield Armory, Springfield, Mass.

Renewed interest in the development of an X-ray method for the determination of residual stress in hardened steel was anticipated with the

development of a Geiger-counter X-ray spectrometer. At the Springfield Armory for the past several months, we have investigated the possibility of using a Norelco high-angle X-ray spectrometer for measuring residual strains in quenched and tempered medium carbon steels. Whereas the authors have tested their method on the martensitic and austenitic phases of high carbon steel, we have performed our measurements on the broadened 211 $K\alpha$ -doublet of ferrite. Nevertheless, whether the diffracting phase be that of ferrite, martensite, or austenite, one is still confronted with the same experimental problems as outlined by the authors. It might be mentioned that the superiority of chromium radiation over cobalt radiation for strain measurements on hardened steels was shown some 13 years ago by F. Gisen.⁵

We have given the problem of measuring the apparent peak position of broadened doublets considerable study. When the diffraction maxima of a resolved doublet are broadened by irregular lattice strains or by small crystallite size, they merge together in such a fashion that the apparent peak position of the sum curve approaches as a limit its center of gravity. Because of the greater degree of broadening on the high-angle side of the doublet, the apparent peak position of the sum curve lies at a lower angle than the calculated center of gravity. This is tantamount to saying that the sum curve is never symmetrical, but is skewed toward the low-angle side. Reference to Fig. 6 of this paper confirms this observation. For this reason, the intersection of the extrapolated linear portions of the sides of such a skewed curve would give a value for the peak position lower than its true value. However, the lack of symmetry of the intensity distribution about the apparent maximum of any broadened doublet, we believe, does not prevent a true determination of the peak position. In Fig. 18 is shown a portion of a plot of the intensity distribution about the apparent maximum of the broadened 211 $K\alpha$ -doublet of ferrite.⁶ This particular plot is for a bar ($\frac{1}{4}$ by $\frac{5}{8}$ by 6 inches) of FS 1050 steel oil-quenched from 1550 °F and tempered $\frac{1}{2}$ hour at 400 °F. Intensity readings were taken every 0.1 degree 2θ . The skewness of the curve is readily apparent. The value of the peak position as determined by the method of least squares is in excellent agreement with the value determined graphically as indicated in the plot. Where the peaks are extremely broad and no other feature of the sum curve is desired, we have found the method of least squares to be quite rapid and to give reliable results. As the tempering temperature is raised, the peak sharpens considerably and we prefer to use the graphical method to fix its position. Whichever of the methods was used to locate the peak, and we have made comparisons on a considerable number of peaks of varying breadths, the agreement between the two methods was found to be excellent and the total time elapsed in obtaining a value for the residual stress was not more than 2 hours.

In order to confirm the reliability of the measurements, the bar was placed in a bending fixture designed for use with our goniometer.^{5, 6} The biaxial stress sum as determined from a measurement of the strain normal

⁵F. Gisen, "Applicability of the X-Ray Back-Reflection Method to Stress Determinations in Quenched and Tempered Alloyed Steels", *Technische Mitteilungen Krupp-Forschungsberichte*, Supplement, 1939, p. 35-40.

⁶S. R. Maloof and H. R. Erard, "A Critical Evaluation of a Norelco High-Angle X-Ray Spectrometer for Elastic Strain Measurements", accepted for publication in the *Review of Scientific Instruments*.

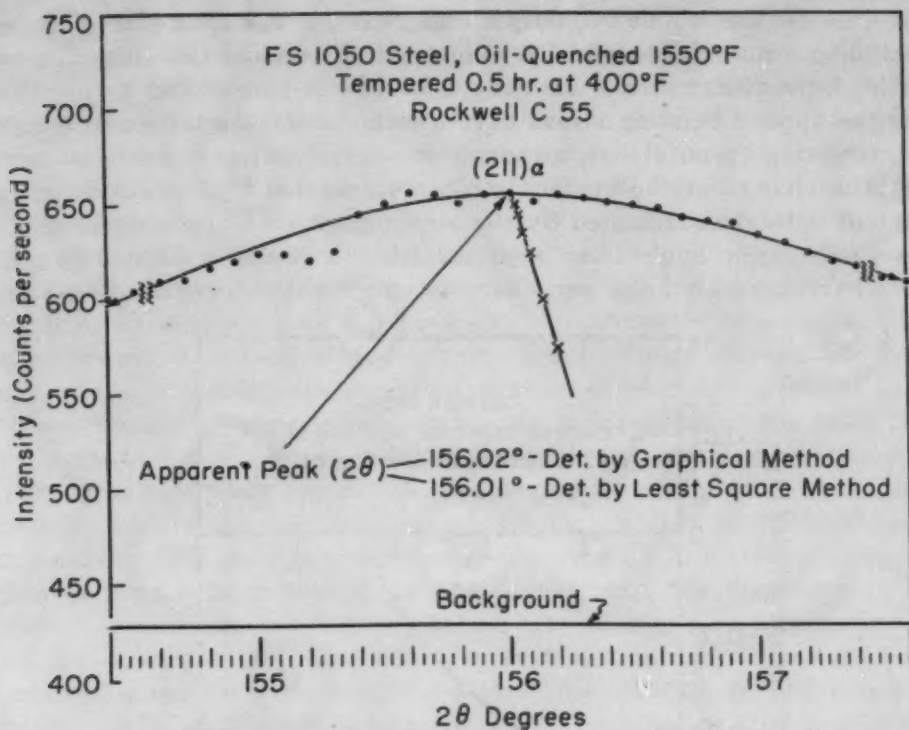


Fig. 18—Intensity Distribution About the Apparent Maximum of the Broadened 211 $K\alpha$ -Doublet of Ferrite in Quenched and Tempered FS 1050 Steel. (Maloof and Erard.⁵)

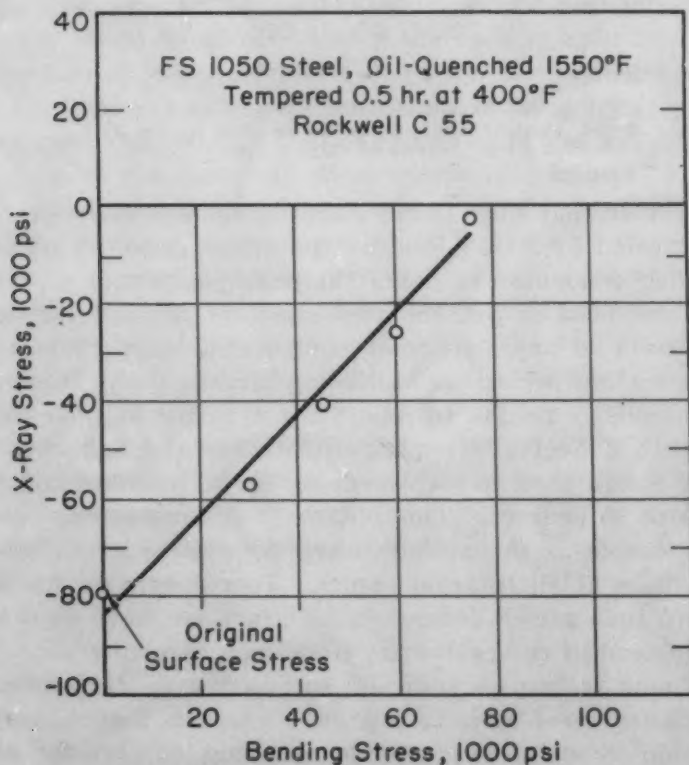


Fig. 19—Decrease in the Biaxial Stress Sum as Determined by X-Rays for a Quenched and Tempered FS 1050 Steel as a Function of the Applied Bending Stress.

to the surface was about 79,000 psi compression. The surface was then subjected to a uniaxial tensile stress in bending. While the specimen was under load, the X-ray stress was redetermined. A plot of the X-ray stress versus the applied bending stress gave a straight line as shown in Fig. 19. It is interesting to note that, although the surface stress sum was determined, the change in the surface stress as revealed by X-rays is in fair agreement with that indicated by the strain gage. Also, the experimental points deviate not more than 4000 psi from a linear relationship. The authors have used a similar procedure to check their X-ray findings; and,

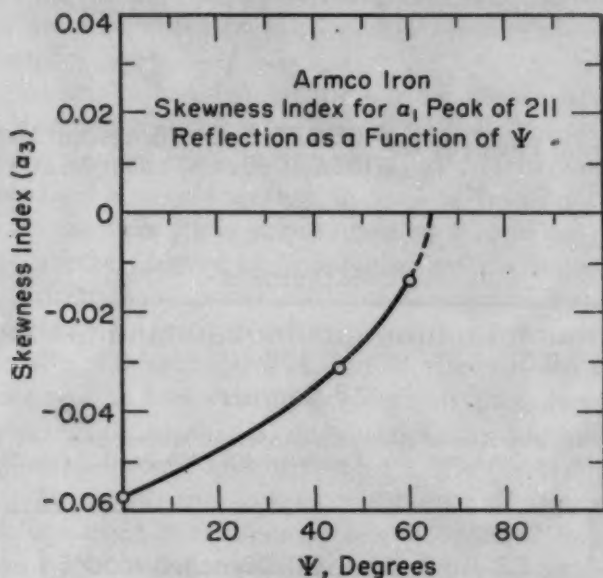


Fig. 20—Skewness Index Plotted as a Function of the Rotation Angle ψ for the a_1 Peak of the 211 Reflection From Ferrite of Armco Iron.

in view of the fact that they found good agreement between the change in stress as revealed by X-rays and by the strain gage, we obviously cannot criticize their procedure of fixing the peak position.

We have not used as yet the two-exposure method for determining the residual stress in any particular component, since there are several features of the method which are still being investigated. However, we do have some preliminary results to report which might be of interest to the authors. With a 1-degree diverging slit rather than the customary 4-degree slit, we found that no displacement of the peak occurred for rotation angles up to 60 degrees. This obviously eliminates the need for off-centering the sample as the authors have done in order to maintain the same peak position at all rotation angles. To compensate for the loss in intensity due to such a well-defined initial beam, we have used a 1-degree receiving slit instead of the customary 0.006-inch receiving slit. This combination was found to furnish sufficient intensity even for strain measurements on hardened steel bars. At large diffraction angles, very little is lost in resolution by employing a wide receiving slit; at the same time, there is considerable gain in intensity. As the specimen was rotated from $\psi = 0^\circ$ to $\psi = 60^\circ$, it was noted that the intensity distribution about the apparent peak became more symmetrical and increased in breadth. To

determine the rotation angle at which the distribution would be perfectly symmetrical, the skewness index as defined in statistics was computed and plotted as a function of the rotation angle ψ . The results shown in Fig. 20 are for the intensity distribution about the α_1 peak of the 211 reflection from ferrite of a stress-free bar of armco iron. It is seen that the skewness index drops to zero at an angle of about 65 degrees, thus confirming the observations of the authors. It would appear, therefore, that the α_1 component of a resolved doublet can be used to detect peak displacement and change in line symmetry as the rotation angle is increased.

It is possible with a Norelco X-ray spectrometer to move the Geiger tube forward a considerable distance. Our findings may be briefly summarized. For $\psi = 0^\circ$, the apparent peak is displaced downward in angle 2θ and broadens out; there is some gain in intensity of the peak relative to the background. For $\psi = 45^\circ$ and 60° , the peak is displaced downward at a faster rate than for $\psi = 0^\circ$, but begins to taper off as the point of convergence for the diffracted rays for both angles is approached; there is also considerable gain in sharpness and some gain in intensity of the peak. However, for a fixed position of the Geiger tube, the displacement of the peak relative to its position before the Geiger tube was moved forward is not the same for the three rotation angles. Indications are that a convenient position of the Geiger tube would be somewhere between 2 and 3 inches, which is in good agreement with the value of 2.57 inches chosen by the authors to place an additional slit.

We would like to comment briefly on some of the theoretical aspects of this paper. A plot of "d" versus $\sin^2 \psi$ should be a straight line, provided that the strain is uniform within the volume irradiated by the X-ray beam. The curved line shown in Fig. 11 for the sanded surface could be explained by the presence of microstresses induced by the cold working. It is indeed surprising to find that the plots shown in Figs. 10 to 15 are all linear, in spite of the fact that microstresses are known to exist in hardened steel. Although microstresses are generally detected by the broadening of the diffraction maxima and macrostresses by the displacement of the maxima, a residual microstress gradient would contribute to the residual macrostress as determined by X-rays. This would have the effect of changing the slope of the line representing the original condition of the specimen prior to loading, and might even cause the line to be curved. On loading, therefore, the crossover point for the various lines would be different from that predicted by theory. Also, as pointed out by the authors, the application of a biaxial stress to the specimen would change the theoretical crossover point for the various lines. It is easily shown that for biaxial loading the intersection of the lines is given by the following expression:

$$\sin^2 \psi = \frac{v \left(1 + \frac{\sigma_l}{\sigma_t} \right)}{1 + v}$$

where v is Poisson's ratio and σ_l and σ_t are the longitudinal and circumferential stresses, respectively. If $\sigma_t = 0$, then the foregoing expression degenerates to that given by the authors for uniaxial loading. An improper choice of the value for Poisson's ratio cannot explain the large difference

noted in Figs. 10, 13, and 15 between the theoretical crossover point and that actually observed.

Written Discussion: By John T. Norton and Robert E. Ogilvie, Department of Metallurgy, Massachusetts Institute of Technology, Cambridge, Mass.

In this paper the authors have made an important contribution to the problem of measuring surface stresses in steels of high hardness. There are two salient points which should be emphasized. The first is the successful selection of the wavelength of incident radiation, thickness of filter and operating voltage of the X-ray tube which has permitted them to obtain a high ratio of the intensities of line to background. Without this, precise measurement of line position would be impossible. Secondly, they have observed that the diffraction lines have linear portions on the sides of considerable extent, which permit them to make an accurate extrapolation to a point corresponding to the line peak. That this point may not be the true intensity maximum is of no particular consequence, since it is merely a reference point used to measure the small line shift due to the residual stress.

The reasons for the existence of the linear sides of the diffraction lines is not clear at present but it has been confirmed in our own laboratory under similar conditions. Whether or not it would be true in other cases of broad diffraction lines still remains to be seen.

Another method of determining the position of the maximum of a broad line has been used recently in our laboratory on problems very similar to those described by the authors. This procedure involves making accurate measurements of the intensity by counting at several known angles in the vicinity of the broad diffraction peak. About five or more points are needed, ranged on both sides of the actual maximum. Using the method of least squares, a parabola with a vertical axis is calculated which makes the best fit to the measured points. The angle at which the vertical axis lies results from the calculation and represents the angle of the intensity maximum. The results have been surprisingly good and lines which have a width of about 8 degrees at half maximum have consistently shown a reproducibility of better than 0.02 degree. Using this procedure, excellent results have been obtained in determining the experimental stress constant for the steels of high hardness. Once the procedure has been set up, the necessary calculation can be made very rapidly.

Authors' Reply

The authors greatly appreciate the interest of the various discussers and wish to thank them for their contributions to this paper.

Messrs. Bennett and Vacher rightfully point out that the determination of stress only requires measurements to be taken at two ψ angles and additional measurements at intermediate values of ψ merely increase the time for the determination. In the routine determination of stress, of course, one would use only two ψ angles, but some flexibility in choice of two ψ angles to be used is from the practical standpoint also necessary and it is, therefore, desirable to have some knowledge of the variation of the constant of proportionality with the angle ψ . This consideration led to the measurements at the intermediate ψ angles of 30 and 45 degrees

and to the particular graphical method employed in presenting these data. On the other hand, it must be emphasized that the stress constant of proportionality was not arbitrarily computed by the assumption of values for E and ν , without experimental evaluation, but these measurements actually comprise an experimental evaluation of this constant, which, fortuitously or otherwise, proved to be equal to the theoretical constant one would compute by using the values of E and ν that obtain from mechanical tests.

One might conclude from the agreement of the experimentally derived stress constant with the computed constant that the small anisotropic crystals comprising the steel mass are behaving isotropically within the mass with mechanical properties similar to the mass as a whole; however, all measurements were made on the 211 martensite and 220 austenite planes and, therefore, may not be indicative of results that may be obtained from other lines. Furthermore, the somewhat higher stress constant obtained by Messrs. Blount and Ellis, and by Mr. Ogilvie whose work is cited by them, also using the 211 line but fixing its relative positions by the parabolic method described by Dr. Norton, suggests that the experimental X-ray stress constant may vary somewhat from the true constant by an experimental artifact introduced by the particular technique used. Thus, until more information is accumulated, the remarks in the text of this paper concerning the validity of the bulk modulus in computing the stress constant must be considered to apply only under the particular experimental conditions present in this work.

Work underway in our laboratory at the present time indicates that a little higher stress constant indeed is obtained using the parabolic method described by Dr. Norton, though our own preliminary results show the constant to be less than 10% greater than computed using the bulk modulus instead of 20% as obtained by Messrs. Blount and Ellis and 32% by Mr. Ogilvie. It may be significant that Mr. Ogilvie used a flat sample, Messrs. Blount and Ellis a 6-inch round, and we a 4-inch round for the determinations. However, whatever the source of these apparent discrepancies in stress constant may be, they need not interfere with useful stress measurement by X-ray technique if the specimen geometry and slit system used is properly calibrated, but only make imperative a calibration process until more is known. Our own experience with the parabolic method shows it to be very reproducible and it should be mentioned that its very real advantage is in the fact that measurements are made only at the peak of the line where the intensities are high.

Dr. Schwartz suggests consideration of parallel beam geometry and Dr. Maloof and Mr. Erard of a third method for fixing line position. We welcome these suggestions and recognize that many technique possibilities are yet unexplored. The particular technique selected for this work resulted from many compromises imposed by specimen contour and certain inflexibilities of equipment design, which could have been overcome but was not believed justified until some evidence was secured that the X-ray method itself was practical. For example, the convex surface of the round samples in combination with the off-focus slit system used for convenience in many instances caused severe flattening of the peak of the diffraction lines and necessitated use of the line sides instead

of the peaks for fixing relative line positions. Also, it is highly desirable that a means be provided for relocating the Geiger tube to proper focusing conditions for any ψ angle. We believe the real value of this work lays not in the development of a particular experimental technique but in the presentment of evidence that the X-ray method itself can with success be applied to the determination of stress in hardened steel despite the fact it has been rather thoroughly discredited in the past for this particular application. It is hoped and expected that the combined efforts of all interested in the study of stress in these hard materials giving diffuse lines will soon furnish the necessary techniques to put this measurement on a routine laboratory basis.

Messrs. Bennett, Vacher, Maloof and Erard concur in emphasizing that the determination of Poisson's constant, and thus the elastic modulus, separately from the stress constant, by the cross-over point of the "d" versus $\sin^2 \psi$ lines requires the application of a unidirectional stress only. This was also stated in the text but Messrs. Maloof and Erard were kind enough to show the relation between the cross-over point and the increase in bidirectional stress imposed. Messrs. Maloof and Erard express surprise that the "d" versus $\sin^2 \psi$ lines are linear in view of the fact that this requires a uniform stress in the sample volumes inspected at each ψ angle, which volume, from the absorption standpoint, perforce must be different at each ψ angle. We believe this to result from the relatively low penetration of the chromium radiation into the sample which would tend toward uniformity of stress in the sample volume examined. Where a sharp stress gradient at the surface exists, such as when the second sample was sanded, a curved line would be expected and was obtained. More surprising is that the modulus must remain constant for the lines to be linear and linearity was obtained though the crystallites are anisotropic and somewhat different modulus is expected at each ψ angle.

It was gratifying to learn that Messrs. Maloof and Erard observed about the same change in line symmetry with change in ψ angle as we encountered. As a word of caution, however, it must be mentioned that this change in symmetry is to a large extent a function of the slit system used and use of a single detector slit will tend to make the line more symmetrical at ψ equal to zero instead of 60 degrees. Computation will easily demonstrate that this phenomenon results from a change in absorption with 2θ at ψ angles other than zero. Therefore, it is not expected that true line symmetry will always be obtained at a ψ angle approximately 65 degrees.

Messrs. Bennett and Vacher are correct in stating that the change in stress noted in Figs. 12 and 13 after all loads were released and attributed to plastic deformation of the austenite is in the wrong direction for the deformation to have occurred at the specimen surface. In the absence of more experience and knowledge it is inadvisable to speculate further as to the reason for these results.

THE INDIUM-ARSENIC SYSTEM

BY T. S. LIU AND E. A. PERETTI

Abstract

The binary system indium-arsenic has been investigated by thermal, X-ray and metallographic methods of analysis. The existence of an intermediate phase corresponding closely to the composition InAs was confirmed. It melts at 942 °C (1730 °F) and forms a eutectic with indium and with arsenic (under pressure). The In-InAs eutectic occurs at 0.02% arsenic and melts at 155.2 °C (312 °F), and the InAs-As eutectic contains 82% arsenic and melts at 731 °C (1348 °F). The single-phase regions in the solid state are quite restricted.

UP to the present time there is no published report of experimental work on indium-arsenic alloys, except that Iandelli (1)¹ prepared the intermediate phase InAs. Using X-ray diffraction methods, Iandelli concluded that InAs has a face-centered cubic, zinc blende-type structure, with a lattice parameter of 6.036 Å. He used indium with 2% germanium for preparing his alloys; the purity of the arsenic is not stated. In this investigation, systematic study of the phase diagram has been made using thermal analysis, X-ray diffraction and metallographic techniques.

EXPERIMENTAL PROCEDURE

High purity indium² obtained from the Indium Corporation of America and purified lump arsenic obtained from the J. T. Baker Chemical Company, and resublimed in our laboratories, were used to prepare the alloys.

Due to the sublimation of arsenic, every alloy in this system was prepared in an evacuated and sealed capsule. It was found that a 30-gram melt was the maximum amount that could be conveniently handled in a single capsule. For alloys containing more than 50 weight per cent arsenic, even less alloy could be handled in a capsule because of the bulkiness of the element. For these alloys, therefore, 20-gram melts were made.

¹The figures appearing in parentheses pertain to the references appended to this paper.

²The indium had a guaranteed purity of 99.97% with the following analysis: Cu, 0.002%; Pb, 0.006%; Sn, 0.01%; Zn, 0.01%. The resublimed and crystallized arsenic was spectrographically analyzed, and showed the following impurities: Cu, 0.000X; Pb, 0.00X (low); Sb, 0.0X (high); Fe, 0.000X; Bi, 0.0X.

A paper presented before the Thirty-fourth Annual Convention of the Society, held in Philadelphia, October 18 to 24, 1952. Of the authors, T. S. Liu is research metallurgist, Horizons, Inc., Cleveland, Ohio, and E. A. Peretti is acting head, Department of Metallurgy, University of Notre Dame, Notre Dame, Ind. Manuscript received April 3, 1952.

Fifty-two alloys were prepared by weighing the pure constituents on an analytical balance. To minimize the change of intended composition due to loss of arsenic, no alloy was used more than once—every alloy was prepared from fresh indium and fresh arsenic.

Due to the relatively high melting point of InAs and the great tendency for indium and arsenic to form this phase, in preparing the alloys, constant shaking of the capsule was necessary, at a temperature where the arsenic vapor pressure is not too high and the indium entirely molten, to avoid the formation of an InAs surface layer on the metals. Holding at just above the sublimation point of arsenic promotes the formation of InAs, thus reducing pressure inside the capsule. For these reasons, in the preparation of the alloys, the temperature was first raised to about 290 °C (550 °F), the capsule was well shaken at this temperature, then raised to 616 °C (1140 °F) and well shaken again. The final step in heating was to bring the melt to around 950 °C (1740 °F) to insure complete melting of the InAs. Frequent shaking of the capsule at this temperature insured uniformity of composition. It was found that cooling in an upright position with the bottom solidifying first would minimize explosions and give relatively sound ingots. Because there is no way of losing metal in an evacuated sealed capsule, the intended composition could be safely used without chemical analysis, as long as the alloy was uniform in its composition.

Cooling and heating curves were obtained with controlled rates that ranged from $\frac{1}{2}$ to 2 °C per minute. For controlled rates, a Variac coupled to a gear-reduction box driven by a Telechron synchronous clock motor was connected in series with the furnace power line. This gave fairly constant heating and cooling rates. For alloys with less than 39.5 weight per cent arsenic (InAs composition) Vycor crucibles with argon protecting atmosphere and a constant stirring device previously described (2) could be successfully applied. This method, however, could not be used where alloys contained more than 39.5% arsenic, as the excessive volatilization would change the composition continuously during analysis. For these alloys, there were used evacuated capsules with the thermocouple protecting tube sealed in at the bottom. Temperatures were measured with calibrated platinum versus Pt-10% Rh or chromel versus alumel thermocouples.

For metallographic examination of the alloys, the technique described by Carapella and Peretti (3) was used, with slight modifications. Flat surfaces were prepared from specimens containing less than 20% arsenic by cutting with a razor blade, but when the arsenic content exceeded 20%, sections were prepared by slicing with an abrasive wheel. Vilella's reagent was used as etchant for alloys up to 39.5% arsenic. For alloys with more than 39.5% arsenic, an

Table I
Thermal Data of the System Indium-Arsenic

Weight % Arsenic	Atomic % Arsenic	Liquidus °C	Solidus °C
0	0	156.4	156.4
5.00	7.46	624.8	155.2
9.87	14.36	721.2	155.0
14.81	21.03	793.2	155.0
19.75	27.38	851.2	154.5
24.69	33.43	889.0	153.7
35.52	45.76	927.6	153.2
39.50	50.00	942.0	942.0
44.10	54.72	941.0
50.00	58.28	939.2
55.01	65.19	911.1	731.2
60.01	69.68	892.3	743.0*
69.99	78.12	856.7	742.1*
80.00	85.69	777.3	743.0*
84.99	89.66	747.2	{732.5*
90.01	93.24	764.8	{730.8
100.00	100.00	731.2
		

*Heating curve values.

alkaline etchant was used (1 part 30% H_2O_2 + 5 parts H_2O + 10 parts NH_4OH).

X-ray diffraction patterns were taken of many of the alloys to check the results of thermal and metallographic studies. Chromium and cobalt radiations were used. At 30 KVP and 10 ma, exposure times ranged from $1\frac{1}{4}$ to 3 hours. Debye and symmetrical back-reflection focusing cameras were used.

RESULTS

The arrest points obtained by thermal analysis are listed in Table I. In the high-arsenic alloys, where both heating and cooling curve values are listed, more weight is given to the latter because of the experimental procedure. In cases where supercooling was noted, extrapolation of the direct-rate curve yielded a range of values. It is therefore believed that the liquidus temperatures are probably not more accurate than $\pm 2^\circ\text{C}$. Due to the consistent temperature readings obtained for the indium-rich eutectic reaction, it is considered that these results are probably accurate to $\pm 0.5^\circ\text{C}$.

For alloys with more than 39.5% arsenic, the use of a capsule limited the amount of alloy used to eight grams, and the analyses were performed without stirring. It is also obvious that there is a pressure factor involved. It is, therefore, believed that the liquidus temperatures are not more accurate than $\pm 3^\circ\text{C}$ and the arsenic-rich eutectic temperature not more accurate than $\pm 1^\circ\text{C}$.

The phase diagram of the system indium-arsenic is shown in Fig. 1. Six specimens of InAs composition were used to determine the melting point of InAs using both Vycor crucible with argon and constant stirring and evacuated capsules. The results checked to within 0.5°C .

No satisfactory etchant was found to attack the InAs phase, although our tests were not exhaustive. Fig. 7 shows InAs with its characteristic pittings. As X-ray photographs of alloys near the InAs composition showed no detectable change in the lattice spacing with change in composition, it is believed that this one-phase region must be very small. Precision lattice constant determinations of this phase gave a value of 6.058_4 \AA . Debye pattern results are given in Table II.

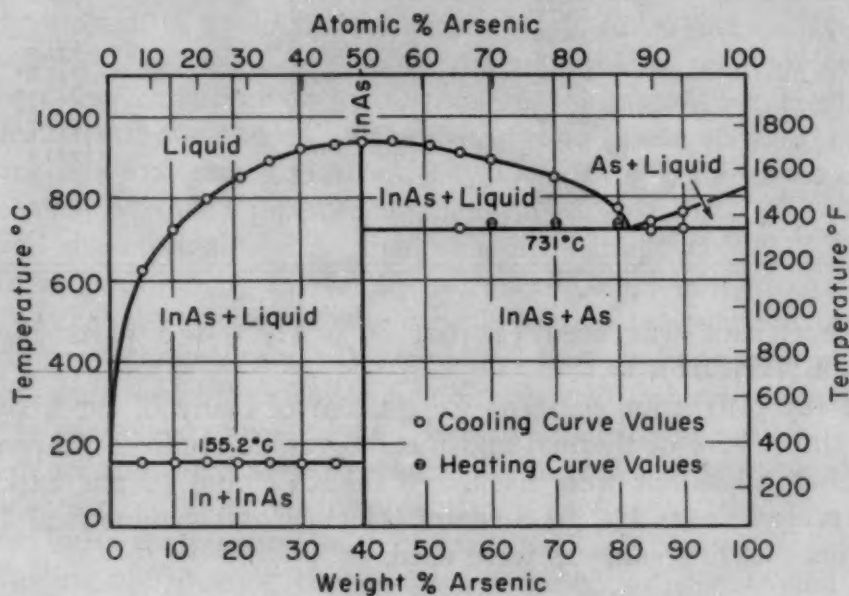


Fig. 1—The Indium-Arsenic Phase Diagram.

Table II
Debye Pattern of InAs*

θ°	$\sin \theta$	d	Observed Int.	hkl	λ
78.75	0.98079	0.914	W	622	a_2
78.35	0.97940	0.913	W	622	a_1
76.05	0.97051	0.924	M	533	a_2
75.58	0.96848	0.924	S	533	a_1
69.59	0.93720	0.956	S	620	a_2
69.20	0.93483	0.957	VS	620	a_1
62.65	0.88822	1.008	VW	600 } 442 }	a
61.31	0.87725	1.022	S	531	a_2
61.08	0.87525	1.022	VS	531	a_1
56.95	0.83819	1.068	M	440	a
50.45	0.77107	1.161	S	511 } 333 }	a
46.68	0.72507	1.235	VS	422	a
41.78	0.66621	1.344	VW	420	a
40.48	0.64912	1.379	S	331	a
36.68	0.59728	1.491	M	400	a
31.13	0.51690	1.732	VW	222	a
29.80	0.49697	1.801	S	311	a
26.76	0.45028	1.800	VW	311	β
25.20	0.42578	2.102	S	220	a
22.73	0.38630	2.098	VW	220	β
17.68	0.30362	2.948	VW	200	a
15.36	0.26492	3.379	M	111	a

*Cobalt radiation with iron filter.

VS, very strong; S, strong; M, medium; W, weak; VW, very weak.

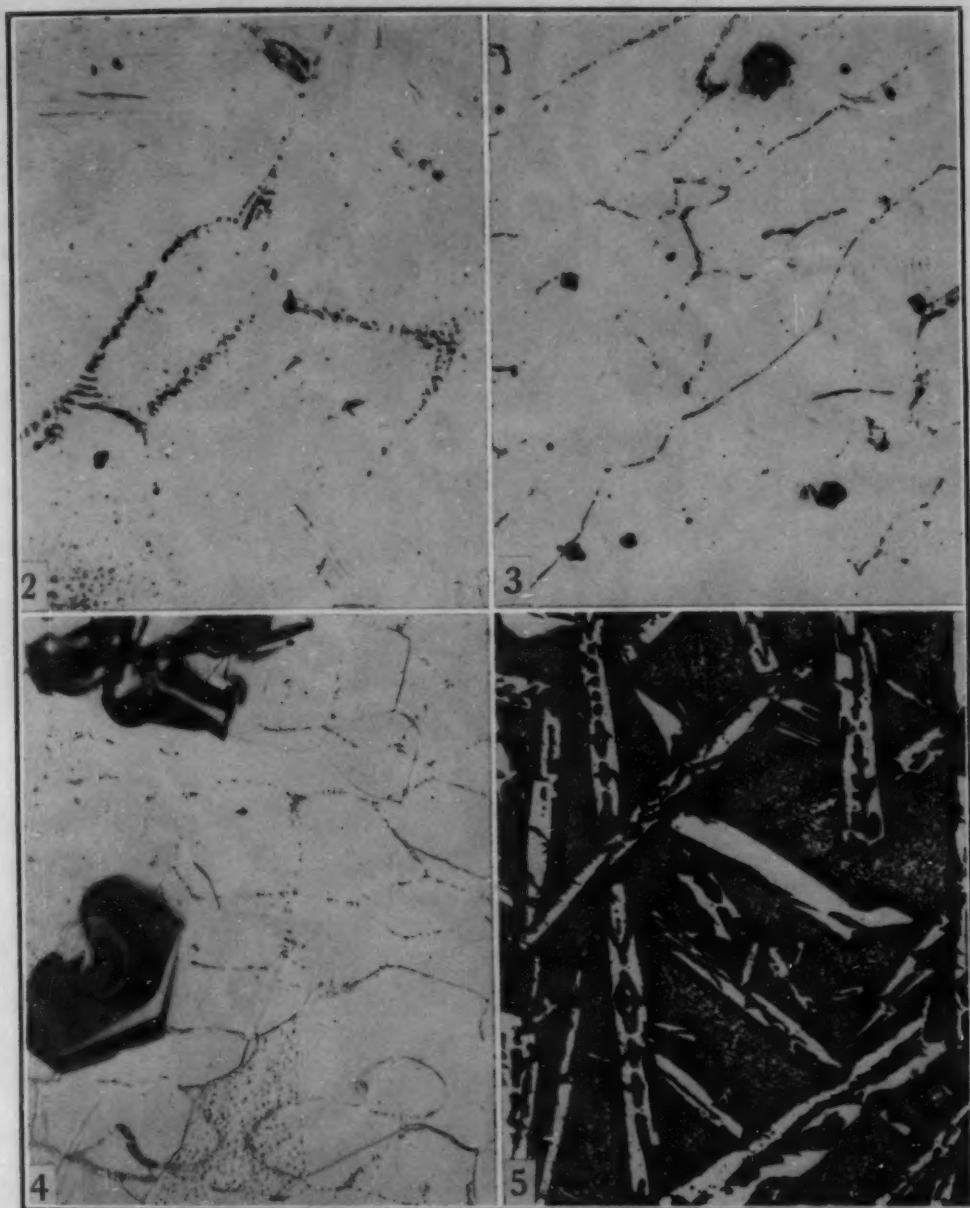


Fig. 2—0.02% Arsenic, 99.98% Indium, As-Cast, Eutectic Composition. Etchant—Vilella's Reagent. $\times 250$.

Fig. 3—0.5% Arsenic, 99.5% Indium, As-Cast, Primary InAs Plus Eutectic. Etchant—Vilella's Reagent. $\times 250$.

Fig. 4—2% Arsenic, 98% Indium, As-Cast, Primary InAs Plus Eutectic. Etchant—Vilella's Reagent. $\times 250$.

Fig. 5—15.8% Arsenic, 84.2% Indium, Furnace-Cooled, Primary InAs Plus Eutectic. Etchant—Vilella's Reagent. $\times 50$.

The InAs phase forms a eutectic with indium at 0.02% arsenic, Fig. 2. This eutectic reaction occurs at 155.2°C (315°F). The composition of this eutectic was determined entirely by metallographic examination of specimens whose arsenic content varied from 0.02 to 9.9%. When the specimen contained primary InAs, it could be clearly differentiated from the eutectic, as shown in Figs. 3, 4, 5

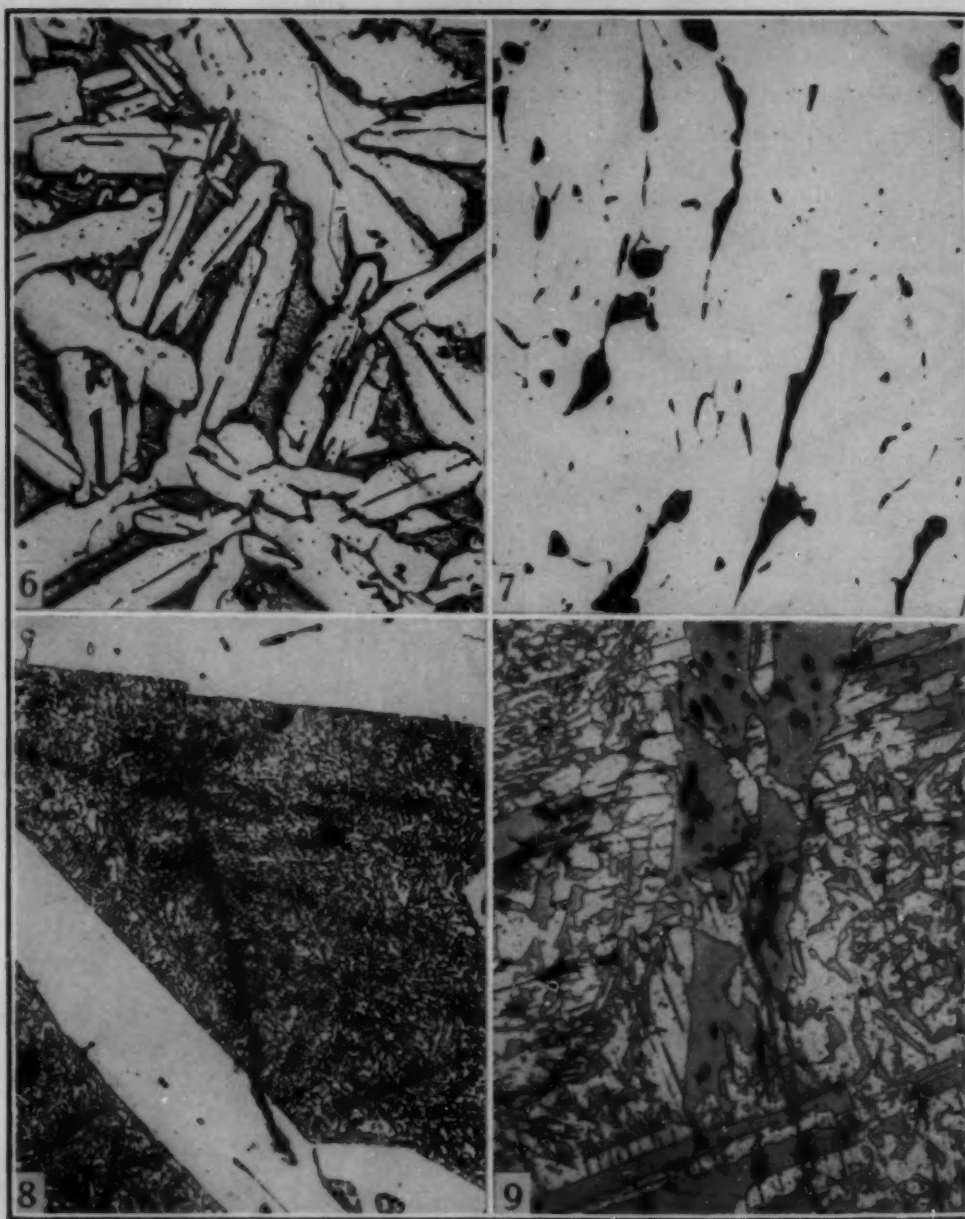


Fig. 6—35.5% Arsenic, 64.5% Indium, Furnace-Cooled, Primary InAs Plus Eutectic. Unetched. $\times 50$.

Fig. 7—39.5% Arsenic, 60.5% Indium, Furnace-Cooled, Pitted Intermediate Phase InAs. Unetched. $\times 75$.

Fig. 8—55% Arsenic, 45% Indium, As-Cast, Primary InAs Plus InAs-As Eutectic. Etchant—1 part 30% H_2O_2 + 5 parts H_2O + 10 parts NH_4OH . $\times 300$.

Fig. 9—80% Arsenic, 20% Indium, Furnace-Cooled, Primary InAs Plus InAs-As Eutectic. Etchant—1 part 30% H_2O_2 + 5 parts H_2O + 10 parts NH_4OH . $\times 75$.

and 6. However, due to eutectic divorcement, it was difficult to determine when primary indium existed. Therefore, the eutectic composition was determined by preparing alloys containing a diminishing percentage of arsenic and noting the point of disappearance of the primary InAs phase.

As can be seen from Fig. 2, the solubility of arsenic in indium

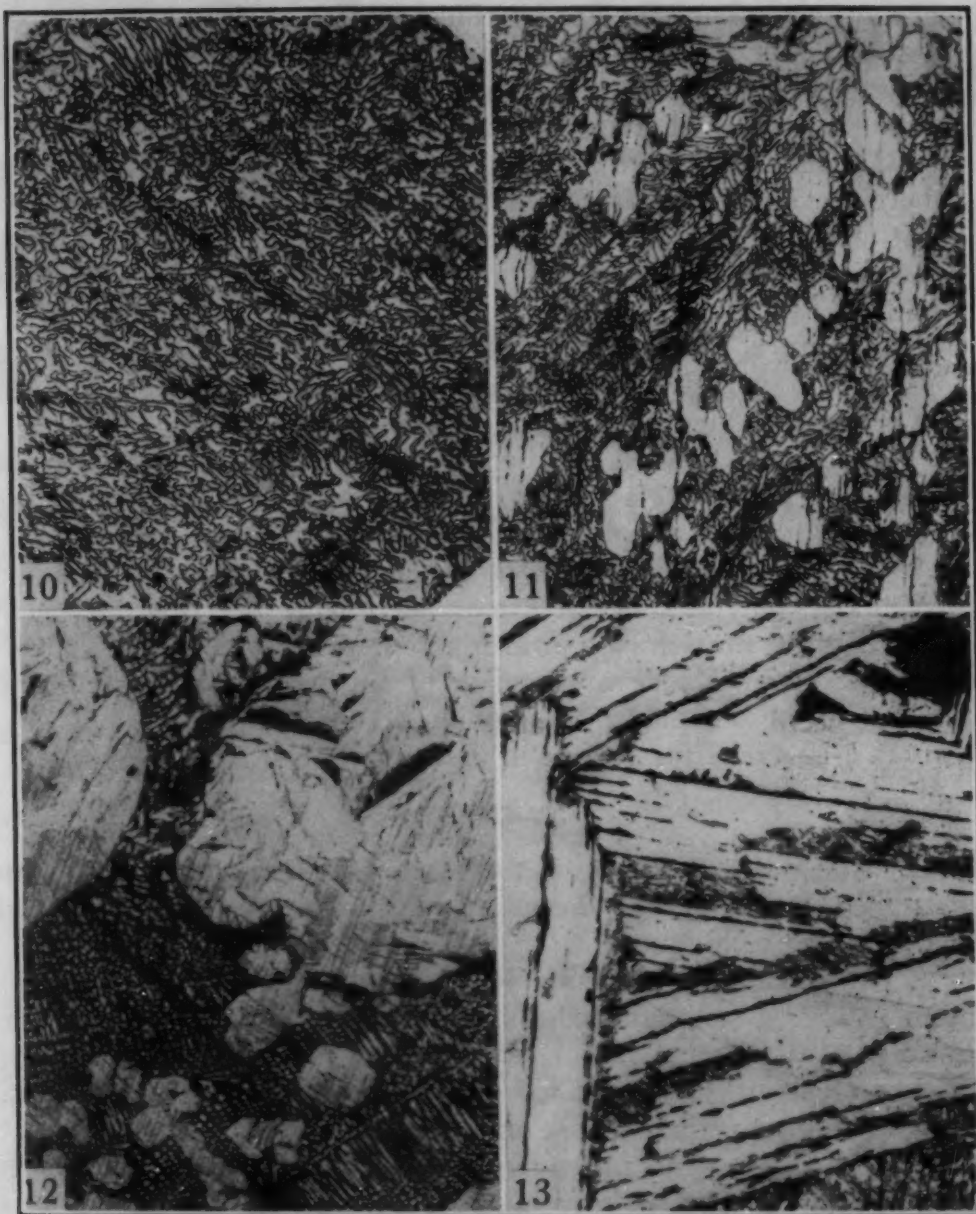


Fig. 10—82% Arsenic, 18% Indium, As-Cast, Eutectic of InAs and Arsenic. Etchant—1 part 30% H_2O_2 + 5 parts H_2O + 10 parts NH_4OH . $\times 300$.

Fig. 11—86% Arsenic, 14% Indium, As-Cast, Primary Arsenic Plus Eutectic. Etchant—1 part 30% H_2O_2 + 5 parts H_2O + 10 parts NH_4OH . $\times 250$.

Fig. 12—87.5% Arsenic, 12.5% Indium, As-Cast, Primary Arsenic Plus Eutectic. Etchant—1 part 30% H_2O_2 + 5 parts H_2O + 10 parts NH_4OH . $\times 75$.

Fig. 13—95% Arsenic, 5% Indium, As-Cast, Primary Arsenic Plus Eutectic. Etchant—1 part 30% H_2O_2 + 5 parts H_2O + 10 parts NH_4OH . $\times 250$.

must be less than 0.02%. No measurable difference in the lattice spacings of pure indium and indium in the two-phase alloys can be found in the X-ray photograms.

The InAs also forms a eutectic (under pressure) with arsenic. It contains 82% arsenic and melts at 731°C (1350°F). Figs. 8 to 13 show typical microstructures encountered in this portion of the

binary system. The shape and etching characteristics of the primary phases on either side of the eutectic are entirely different. However, because of the difficulty of preparing arsenic-rich alloys due to the pressure factor and the explosion hazard involved, alloys near the eutectic composition were not made at closer than 2% intervals. It is therefore believed that this eutectic occurs at $82 \pm 2\%$ arsenic.

It was concluded that the solubility of indium in arsenic is small for the same reasons advanced for the low solubility of arsenic in indium.

Satisfactory hardness tests could not be made on high-arsenic alloys due to porosity in the specimens. The intermediate phase InAs gives a hardness of about 210 Brinell.

It should be pointed out here that the phase diagram for the InAs-As portion of this system, as seen in Fig. 1, is not a true equilibrium diagram at a pressure of one atmosphere. It is obvious that no liquid arsenic exists at atmospheric pressure. Since liquid arsenic exists only at above 36 atmospheres (4), the InAs-As region of the diagram thus drawn probably represents a condition at this pressure. The probable appearance of this region at atmospheric pressure can be obtained by sectioning at one atmosphere a Roozeboom P-T-X model for InAs and arsenic.

SUMMARY

1. The phase diagram of the system indium-arsenic has been determined by means of thermal analysis, X-ray diffraction and metallographic techniques.

2. Two eutectic reactions occur, one at $155.2 \pm 0.2^\circ\text{C}$ containing 0.02% arsenic and consisting of indium and InAs, and the second one at $731 \pm 1^\circ\text{C}$ (1350°F) with $82 \pm 2\%$ arsenic at a pressure of about 36 atmospheres, consisting of InAs and arsenic.

3. An intermediate phase exists corresponding closely to the composition InAs. This phase melts at $942 \pm 0.5^\circ\text{C}$. It has a face-centered cubic, zinc blende-type structure with a lattice parameter of 6.058_4 \AA .

4. The single-phase regions in the solid state were found to be quite small.

ACKNOWLEDGMENT

The authors wish to express their indebtedness to the Indium Corporation of America for the generous loan of the indium used in the investigation.

References

1. Aldo Iandelli, "Sulla Struttura Dei Composti InP, InAs e InSb", *Gazzetta Chimica Italiana*, Vol. 71, No. 1, 1941, p. 58.
2. T. S. Liu and E. A. Peretti, "The Indium-Antimony System", *TRANSACTIONS, American Society for Metals*, Vol. 44, 1952, p. 539.

3. S. C. Carapella, Jr., and E. A. Peretti, "Metallography of Indium and Indium-Rich Alloys", *METAL PROGRESS*, Vol. 56, No. 5, November 1949, p. 666.
4. S. Horiba, "Stoichimetrie und Verwandtschaftslehre", *Zeitschrift für physikalische Chemie*, Vol. 106, 1923, p. 295.

DISCUSSION

Written Discussion: By Alvin J. Thompson, head, Department of Mining and Metallurgy, New Mexico Institute of Mining and Technology, Socorro, N. M.

At the New Mexico Institute of Mining and Technology we have done considerable work on the indium-sulphur and indium-oxygen systems, including thermal analysis, X-ray, and free energy studies.

I would like to compliment the authors on the excellent photographic studies accompanying this paper. The photographs seem to confirm quite well the presence of a single indium-arsenic compound, and the location of the eutectic points.

The insolubility of arsenic in indium and of indium in arsenic is perhaps to be expected, considering the difference in the atomic radii and crystalline structure. The same solid insolubility was found to exist in the indium-sulphur system, in which there is also an appreciable difference in crystal structure and atomic radii. In the indium-rich alloy of the indium-sulphur system the insolubility extended into the liquid range as well.

I note the statement by the authors that "InAs . . . has a face-centered cubic, zinc blende-type structure . . .". While it is true that when considered separately zinc and sulphur in sphalerite each have face-centered cubic structure, I believe that together they form an interpenetrating cubic lattice which would more accurately be described as a complex cubic structure.

It would perhaps have been illuminating to have been able to show pressure readings above the melt in this work. I am wondering if the authors do have any data to indicate the volatility of the InAs or the stability of this compound. In the study of the indium-sulphur system at the New Mexico Institute of Mining and Technology, we made entropy and free-energy studies by determining the equilibrium constants in the reduction of the various sulphides with hydrogen. We gave some thought to obtaining compound stability figures by vapor pressure measurements above the melts, but never decided on the proper techniques to employ.

Authors' Reply

We wish to thank Professor Thompson for his kind comments.

We prefer the "zinc blende type" structure designation because it specifies the atom positions to be (000) plus face-centered cubic translation and ($\frac{1}{4}$, $\frac{1}{4}$, $\frac{1}{4}$) plus face-centered cubic translation, while "complex cubic structure" is less definite.

No measurements were made of the stability of InAs. However, as its melting point (942 °C) would indicate, it is fairly stable. While all of the alloys were made in sealed tubes, those containing arsenic in percentages up to the InAs composition could be heated in the open, under a protective atmosphere (once they had been formed), without undue volatilization losses.

PLASTIC STRESS-STRAIN RELATIONS OF ALCOA 14S-T6 FOR VARIABLE BIAXIAL STRESS RATIOS

BY JOSEPH MARIN, L. W. HU AND J. F. HAMBURG

Abstract

The plastic stress-strain relations in this investigation were obtained for an aluminum alloy designated as Alcoa 14S-T6. These stress-strain relations were found for bi-axial tensile stresses produced by subjecting a thin-walled tubular specimen to axial tension and internal pressure.

Three types of biaxial stress tests were conducted in this study—constant stress ratio tests and two types of variable stress ratio tests. In the constant stress ratio tests, plastic stress-strain relations were obtained for conditions where the ratio of the axial to the lateral stress was maintained essentially constant for each test. These constant stress ratio tests were made to provide control data and to determine the influence of the biaxial stresses on the ductility, yield strength, and fracture strength. The constant stress ratio tests showed that the biaxial yield strength values are in approximate agreement with the distortion energy theory. The biaxial fracture strength, however, is in best agreement with the maximum stress theory. A comparison of the true biaxial plastic stress-strain relations for various principal stress ratios with values predicted by either the flow or deformation-type theory shows an approximate agreement between test results and theory. The ductility under biaxial stress conditions was found to decrease with increase in the biaxiality of the stresses. The theoretical values of ductility based upon the significant strain and the deformation theory agree approximately with the actual ductility values.

The main object of this study is not to report on the foregoing constant stress ratio tests but rather to determine the validity of the flow-type theory in predicting plastic stress-strain relations under combined stresses. For this purpose, two types of variable stress ratio tests were conducted. In one type of variable stress ratio test, a stress was applied in the axial or lateral direction to a selected plastic strain value, followed by a stress in the other direction perpendicular to the first direction of stressing. In a second type of variable stress ratio test, a stress in one di-

A paper presented before the Thirty-fourth Annual Convention of the Society, held in Philadelphia, October 18 to 24, 1952. The authors, Joseph Marin, L. W. Hu and J. F. Hamburg, are associated with the Department of Engineering Mechanics, The Pennsylvania State College, State College, Pa. Manuscript received March 25, 1952.

rection was followed by a stress in the right-angled direction and then by a stress in the first direction. The results of these tests indicate that the flow theory gives a good approximation to the experimental results. Both types of variable stress ratio tests show that the path of loading has little effect on the true fracture strength and that the fracture strength is approximately defined by the maximum stress theory. The variable stress ratio tests, using different paths of loading to arrive at the same state of stress, give widely different values of strains. This lends support to the flow rather than the deformation or slip type of theories since the latter theories require these strains to be the same.¹

THERE are a number of engineering problems where it is important to know the plastic stress-strain relations in metals subjected to combined stresses. These problems include (a) design of structural and machine members where small plastic strains are permissible, (b) determination of factors of safety in constructions based on ultimate strength rather than the yield strength of the material, (c) design of members in which residual stresses are initially produced to improve the subsequent load-carrying capacity of the construction as used, for example, in the design of some pressure vessels and guns, and (d) the improvement of various metal-forming operations where permanent plastic strains are produced.

To solve the foregoing problems, many engineering theories have been proposed in recent years (1-4).² The purpose of these theories is to define mathematical equations for the stress-strain relations in the plastic range in the case of combined stresses. In these theories, the object is to determine the stress-strain relations for all states of combined stresses based on a plastic true stress-strain relation in simple tension. In order to determine which of the engineering theories is most suitable, it is necessary to investigate many states of combined stresses and numerous materials. Constant stress ratio tests cannot distinguish between the various theories, and it is for this reason that the emphasis in this paper is on variable stress ratio tests. Constant stress ratio tests were made, however, to provide basic information on the influence of the biaxial stress ratio upon the plastic stress-strain relations and upon the mechanical properties.

TEST PROCEDURE

Material Tested and Specimen—The material tested in this

¹In this paper, when reference is made to the flow and deformations theories, the simple types of theories based on the effective, significant or octahedral shear stress and strain are intended.

²The figures appearing in parentheses pertain to the references appended to this paper.

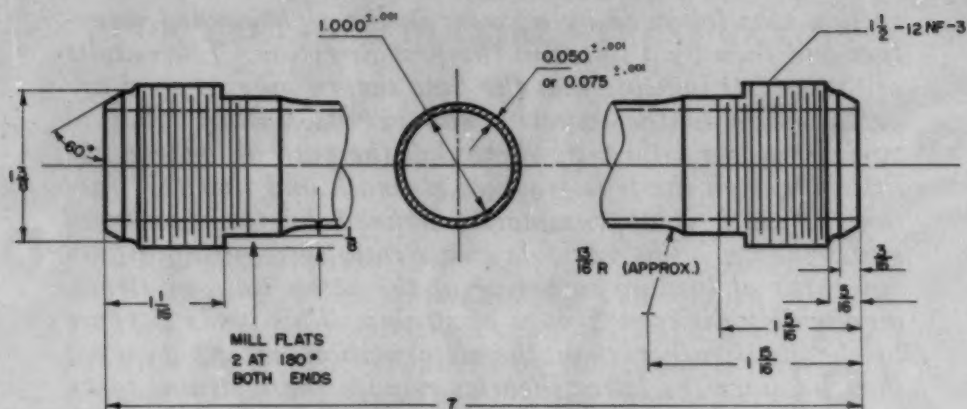


Fig. 1—Tubular Specimen.

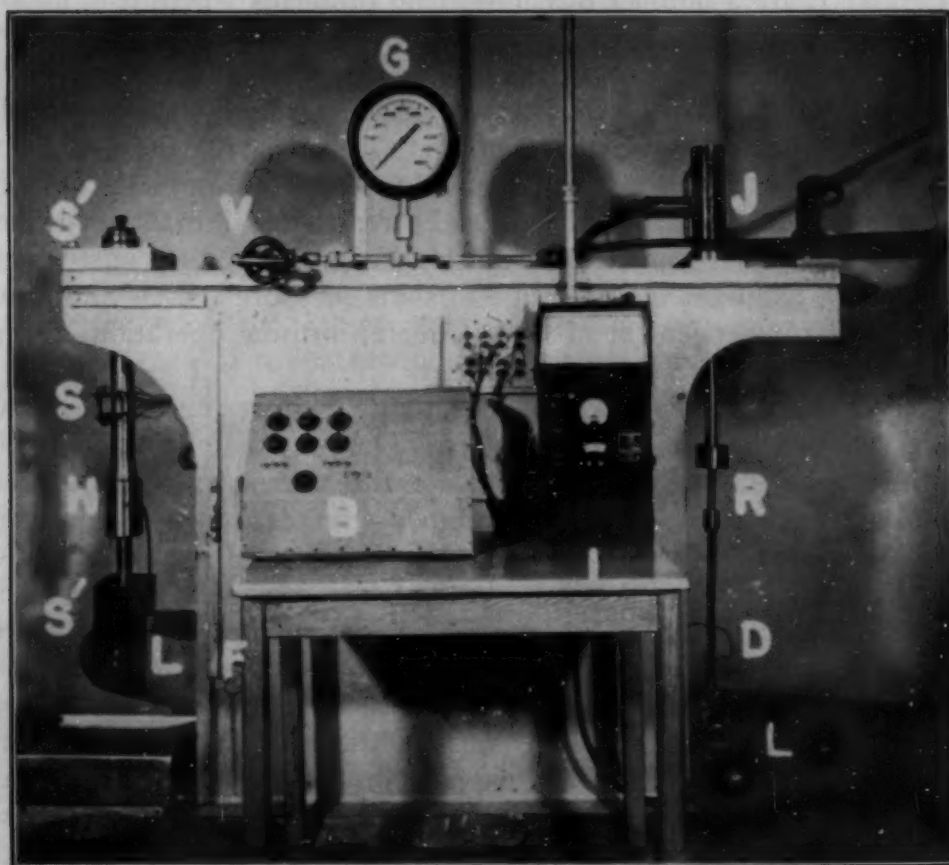


Fig. 2—Testing Machine.

investigation was an aluminum alloy designated as 14S-T6. The material was supplied in the form of hot-rolled machine cylinders, $7\frac{1}{4}$ inches long with a $1\frac{5}{8}$ -inch O.D. and $\frac{1}{16}$ -inch bore. The nominal composition, in addition to aluminum and normal impurities, consists of 4.4% copper, 0.8% silicon, 0.8% manganese and 0.4% magnesium. The Research Laboratories of the Aluminum Company of America

supplied control test data on the yield strength, tensile strength and ductility. These data were obtained primarily to determine the anisotropy of the material. To do this, specimens were taken from the cylinders in the axial, lateral and diagonal directions.³ The average values of the properties were: yield strength—62,400 psi $\pm 3\%$; tensile strength—69,100 psi $\pm 4\%$; elongation in 4 diameters—6.5 to 12%. The test data supplied showed about 8% variation in tensile strength due to anisotropy, and about 8% variation due to normal variations in the material.

The dimensions of the machined specimen for the combined stress tests are shown in Fig. 1. The specimens were machined on both the inside and outside, and the wall thickness was measured by an apparatus as described in Reference 5.

Testing Machine—Fig. 2 shows the testing machine used to apply internal pressure and axial load to the specimen S. The axial load is applied to the specimen S by a lever L, vertical rod R and hydraulic jack J. The magnitude of the axial load is determined by the dynamometer D. The internal pressure is applied to the specimen through a valve V and a pump unit not shown. This pressure is measured by a pressure gage G.

Method of Measuring Strains—The strains in the elastic range of loading were measured by SR-4 electric strain gages placed both in the axial and lateral directions. A clip-type gage, as described in Reference 6, was used to measure both the axial and lateral plastic strains. The strain readings were observed on an indicator I, using a switch box B so that all strains could be read on the indicator I.

Method of Testing—In testing, the specimen is first assembled in the testing machine with the elastic strain gages and clip gages attached as shown in Fig. 2. The manner of loading used will then depend upon the type of test being conducted. In all cases, predetermined values of the load are applied, with value of loads and strain being recorded at suitable load or strain intervals.

Constant Stress Ratio Tests

The influence of combined stresses on the plastic stress-strain relations and mechanical properties was first determined by a series of constant stress ratio tests. In these tests the ratio of the principal stresses was maintained essentially constant by maintaining a constant ratio of the internal pressure to the axial load.

The nominal or conventional stress-strain relations for various values of the principal stress ratios are given for the axial and tangential stresses in Figs. 3 and 4. At least two specimens were tested for each stress ratio. The equations used for calculating the

³The diagonal direction is 45 degrees to the axial or lateral directions.

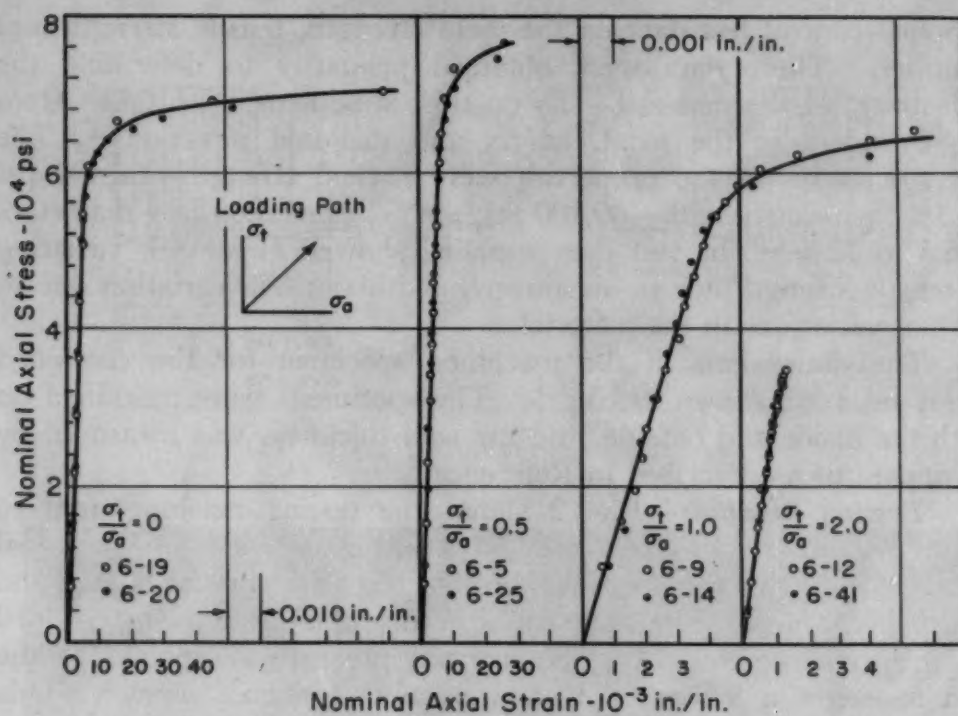


Fig. 3—Nominal Axial Stress-Strain Relations for Constant Stress Ratio Test.

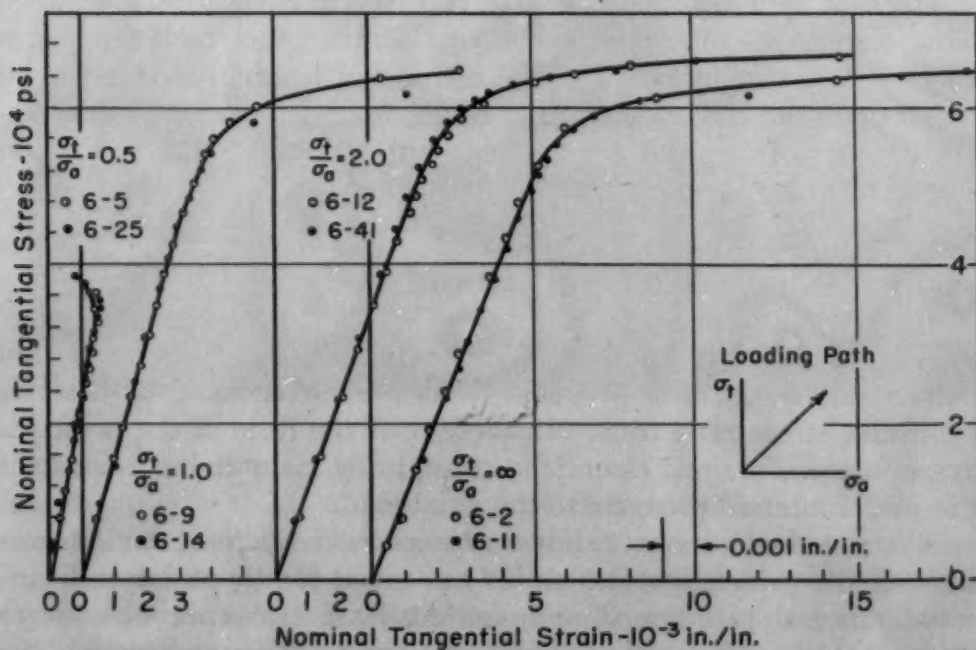


Fig. 4—Nominal Tangential Stress-Strain Relations for Constant Stress Ratio Test.

nominal axial and tangential stresses are, respectively,

$$\sigma_a = \frac{pd^2 + 4P/\pi}{4t(d+t)} \quad \text{Equation 1}$$

$$\sigma_t = \frac{pd}{2t} \left[\frac{1 + 2(t/d) + 2(t/d)^2}{1 + (t/d)} \right] \quad \text{Equation 2}$$

where d = internal diameter, t = wall thickness, P = axial load, and

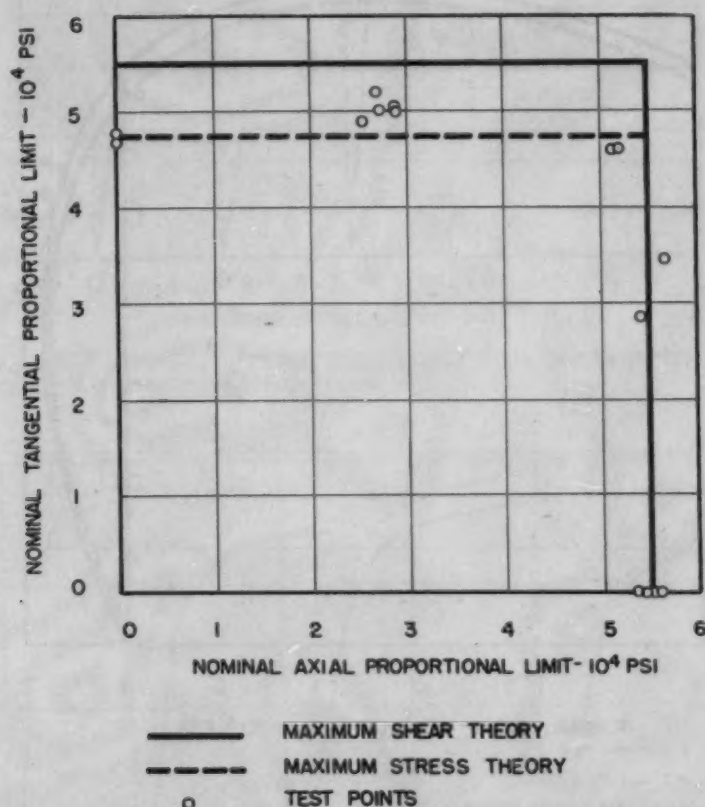


Fig. 5—Comparison of Proportional Limits With Theories of Failure for Constant Stress Ratio Tests.

p = internal pressure. Equation 2 gives the maximum tangential stress based on the Lamé theory for a thick-walled cylinder.

The nominal strain values plotted in Figs. 3 and 4 were determined by the SR-4 indicator readings. These readings were corrected for lateral sensitivity and the "combined stress effect", since the manufacturer's calibration constant supplied with the strain gages applies to uniaxial stress and materials with Poisson's ratio = 0.285. From Figs. 3 and 4 the values of the proportional limits and yield strengths were determined for the various principal stress ratios. The yield stresses were determined, based upon an equivalent offset strain as defined in Reference 6 and using a value of 0.002 inch per inch offset strain for defining the yield stress in simple tension. A comparison is given in Figs. 5 and 6 between the actual proportional

limit values and yield stresses with the values predicted by the theories of failure. Fig. 5 shows that the proportional limit values are in approximate agreement with the maximum stress theory. Fig. 6 shows that the distortion energy theory is in approximate agreement with test results if the radial stress is either neglected or considered.

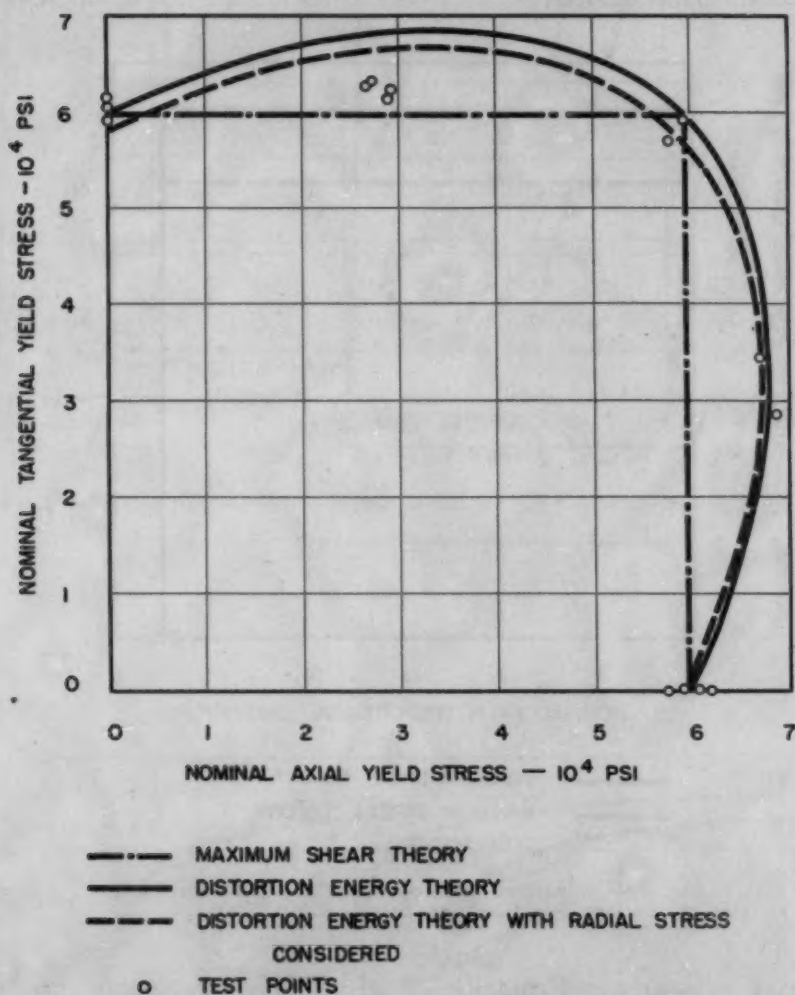


Fig. 6—Comparison of Yield Strengths With Theories of Failure for Constant Stress Ratio Tests.

The actual relations between the true stresses and strain in the axial and tangential directions are shown in Figs. 7 and 8 respectively. These true stress-strain relations differ from the nominal stress-strain relations of Figs. 3 and 4, since they consider the change in gage length and change in cross sectional dimensions with increase in load. The experimental curves in Figs. 7 and 8 represent the average curves based upon at least two specimens.

The determination of the true stress and true strain equations used for determining the values plotted in Figs. 7 and 8 is explained

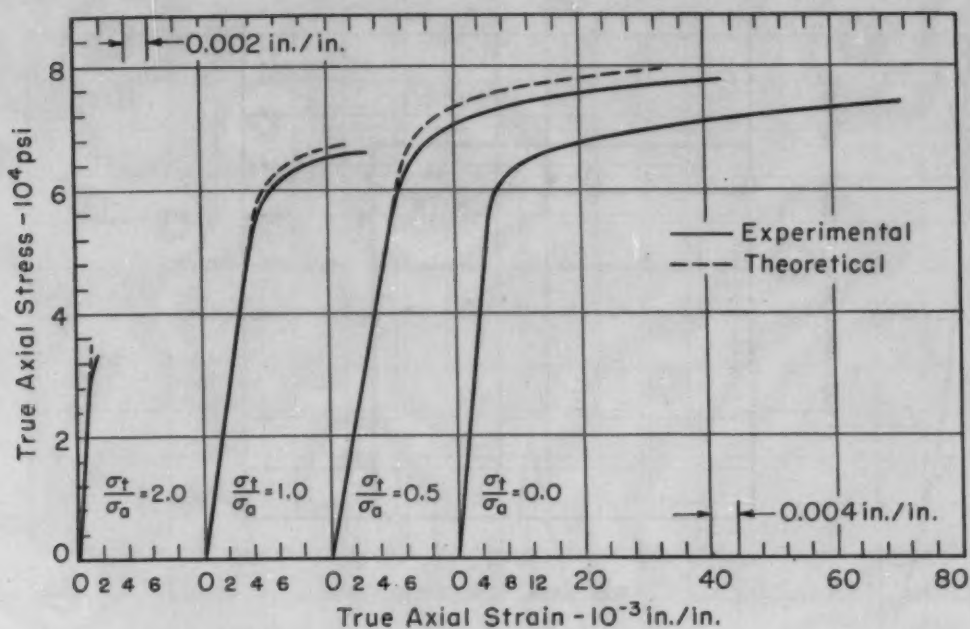


Fig. 7—Comparison of True Axial Stress-Strain Relations With Plasticity Theory for Constant Stress Ratio Tests.

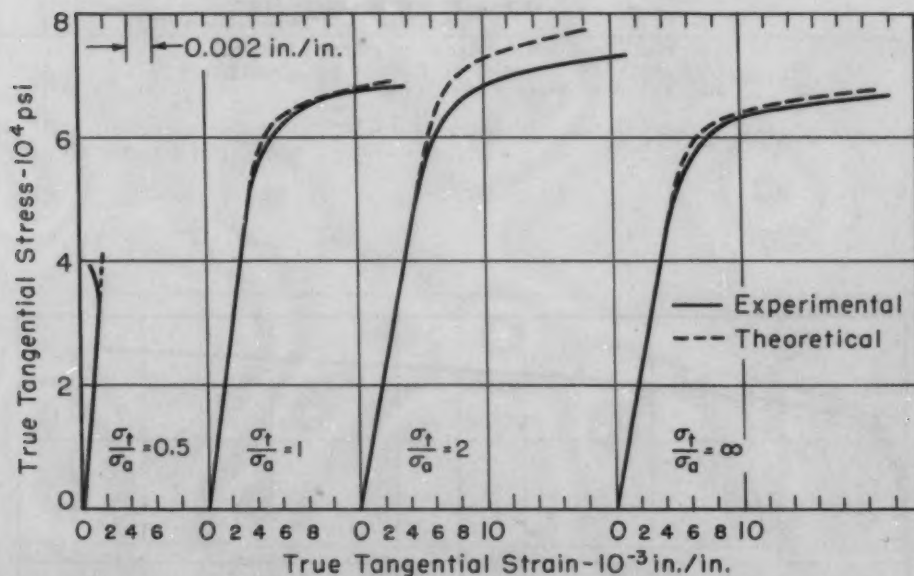
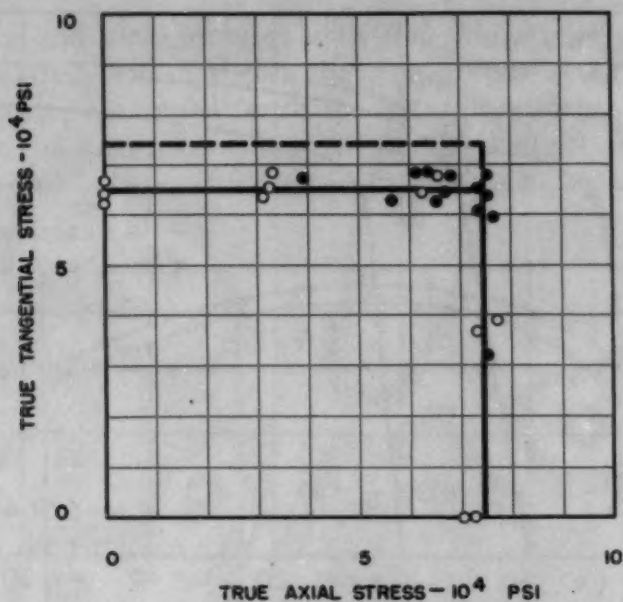


Fig. 8—Comparison of True Tangential Stress-Strain Relations With Plasticity Theory for Constant Stress Ratio Tests.

in detail in References 5 and 6. It is shown in these references that the true axial and tangential strains in terms of the nominal axial and tangential strains are, respectively,

$$\begin{aligned} \epsilon_a &= \ln(1 + e_a) \\ \epsilon_t &= \ln(1 + e_t) \end{aligned} \quad \text{Equation 3}$$

where e_a is the axial nominal strain and e_t is the average of the tan-



- MAXIMUM STRESS THEORY
 - - - MAXIMUM SHEAR THEORY
 ○ CONSTANT STRESS RATIO TEST
 ● VARIABLE STRESS RATIO TEST

Fig. 9—Comparison of True Fracture Stresses With Theories of Failure for Constant and Variable Stress Ratio Tests.

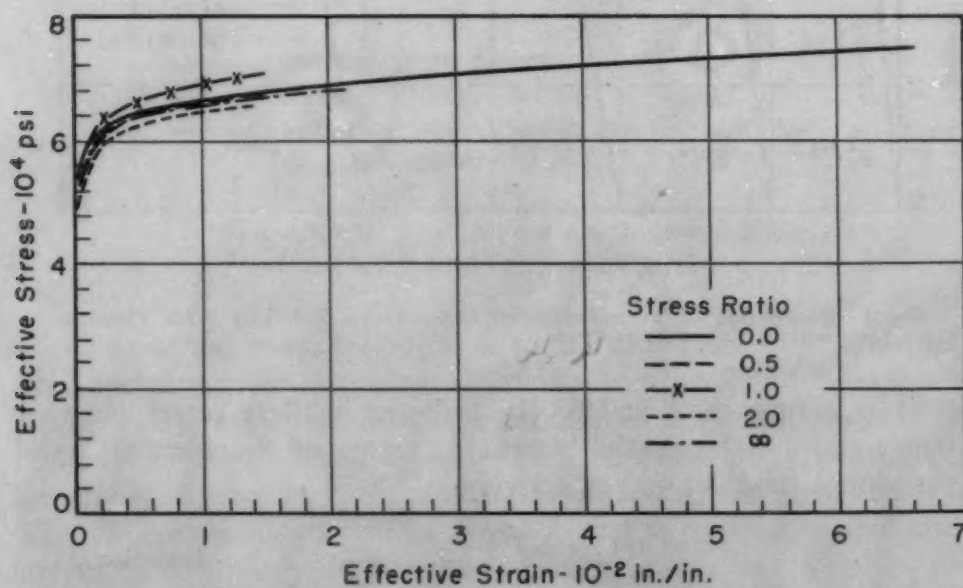


Fig. 10—Effective Stress-Strain Relations for Constant Stress Ratio Tests.

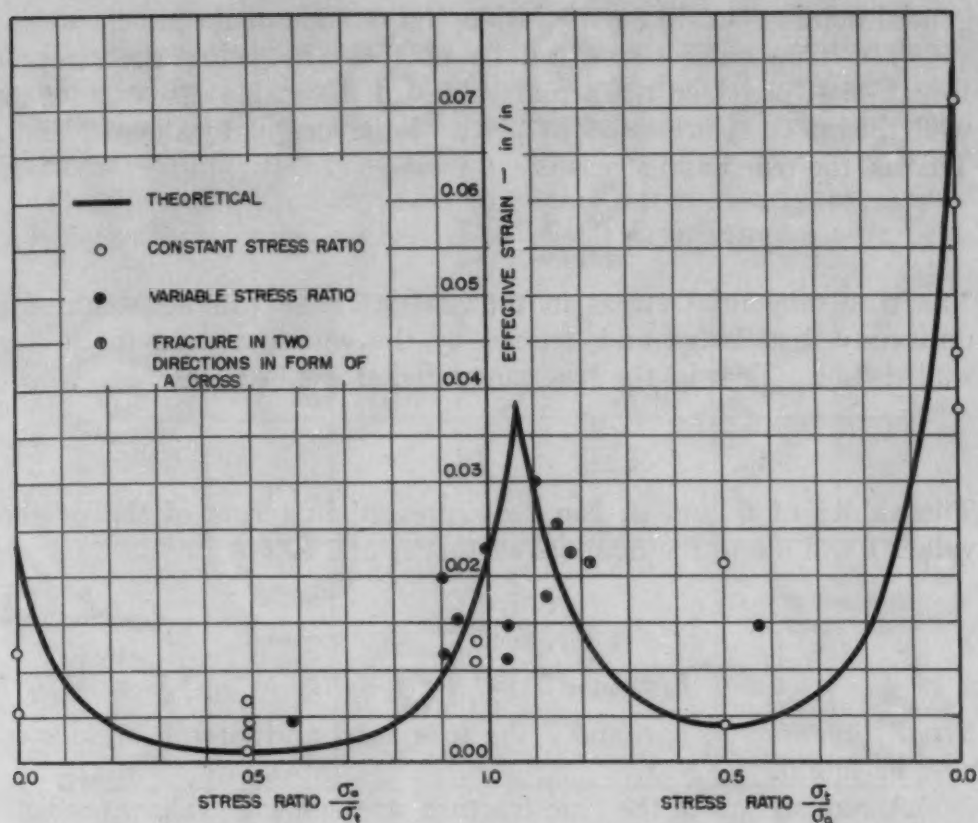


Fig. 11—Comparison of Ductility With Theoretical Values for Constant and Variable Stress Ratio Tests.

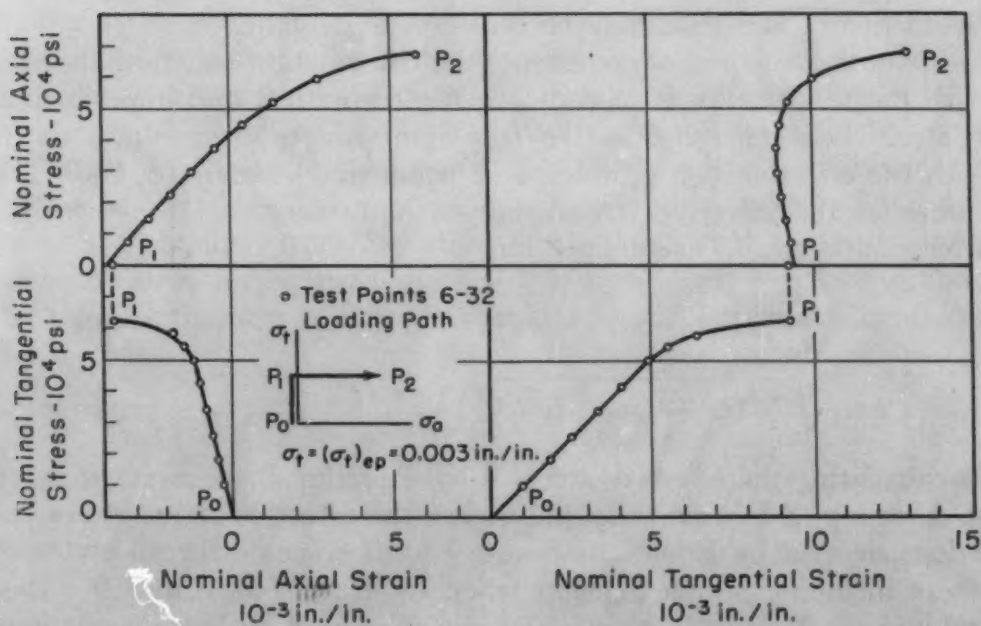


Fig. 12—Nominal Stress-Strain Relation for Variable Stress Ratio Test—Set A, No. 4.

gential nominal strain on the inside and outside of the tube.

The true axial stress can be obtained by using the stress of Equation 1, provided the actual values of the inside diameter d_p and wall thickness t_p are used in place of the original values d and t . That is, the true axial stress is

$$\sigma_a = \frac{pd_p^2 + 4P/\pi}{4t_p(d_p + t_p)} \quad \text{Equation 4}$$

The true tangential stress in the plastic range can be assumed as uniformly distributed and defined by the equation used for a thin-walled tube. That is, the true tangential stress becomes

$$\sigma_t = \frac{pd_p}{2t_p} \quad \text{Equation 5}$$

The values of t_p and d_p can be expressed in terms of the original values t and d and the nominal strains e_a and e_t (6) or

$$t_p = \frac{t}{1 + e_a + e_t} \quad \text{Equation 6}$$

$$d_p = (d + 2t)(1 + e_t) - 2t_p \quad \text{Equation 7}$$

From Equations 4, 5, 6 and 7 the true axial and lateral stresses can now be found.

A comparison of the true fracture stresses with values predicted by the theories of failure is shown in Fig. 9. These results show that the maximum stress theory is a good approximation to the test values.

In Figs. 7 and 8 the theoretical plastic stress-strain relations are shown, based upon either the deformation or flow theory. Considering discrepancies due to experimental errors, the agreement between theory and tests may be considered adequate.

Another method of comparing the deformation and flow theories with the test results is to compare the theoretical and experimental relations between the effective (or significant or octahedral) stress with the effective (or significant or octahedral) strain (5, 6). The values of the effective stress and strain in terms of the principal stresses and strains are defined by

$$\bar{\sigma} = \sqrt{\frac{1}{2} [(\sigma_a - \sigma_t)^2 + (\sigma_t - \sigma_r)^2 + (\sigma_r - \sigma_a)^2]} \quad \text{Equation 8}$$

$$\bar{\epsilon} = \sqrt{\frac{4}{3} (\epsilon_a^2 + \epsilon_a \epsilon_b + \epsilon_b^2)} \quad \text{Equation 9}$$

In calculating the effective stress $\bar{\sigma}$ by Equation 8 the average value of $\sigma_r = -p/2$ is used. By the theory the effective stress-strain relations defined by Equations 8 and 9 must coincide for all states of stress including simple tension when by Equations 8 and 9 $\bar{\sigma} = \sigma$ and $\bar{\epsilon} = \epsilon$. That is, by the theory, the effective stress-strain relations for various states of combined stress should coincide with the simple

tension stress-strain relation. Fig. 10 shows that the experimental effective stress-strain relations do agree approximately with the simple tension stress-strain relation. In other words, for the foregoing constant stress ratio tests the deformation or flow theory is in good agreement with the test results.

Ductility of materials under combined stresses may be defined in various ways. One method is to select the maximum true prin-

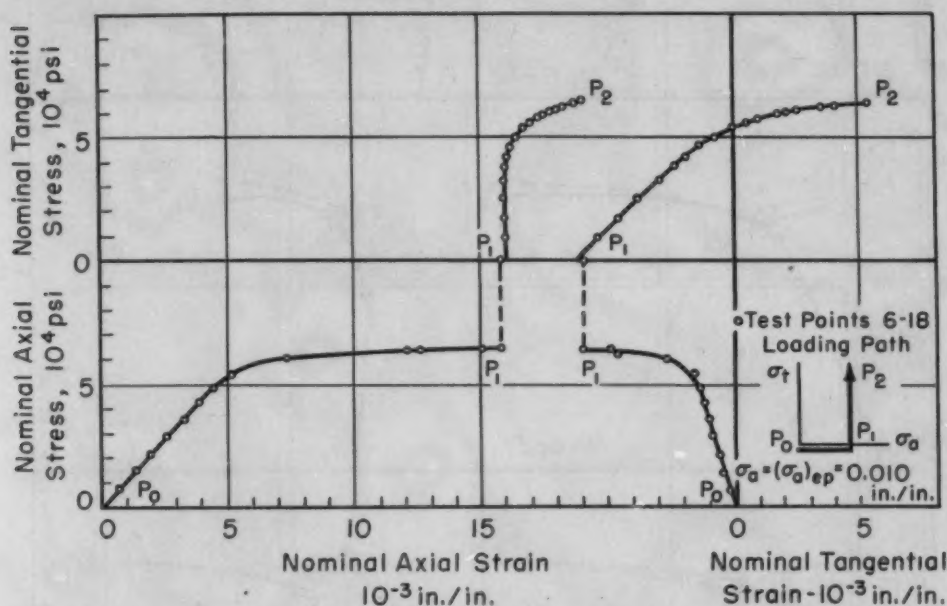


Fig. 13—Nominal Stress-Strain Relation for Variable Stress Ratio Test—Set B, No. 4.

icipal strain as the measure of ductility. An examination of these values as shown in Figs. 7 and 8 shows that the ductility decreases with increase in biaxiality of the stresses.

Another measure of ductility for combined stresses may be taken as the value of the effective strain $\bar{\epsilon}$ at fracture as calculated from Equation 9. These test values of ductility based on Equation 9 are shown in Fig. 11. The corresponding theoretical values of the ductility are obtained from Equation 8, assuming that the true stress-strain relation for simple tension is $\bar{\epsilon} = \epsilon$ and then replacing σ and ϵ by the effective stress $\bar{\sigma}$ and strain $\bar{\epsilon}$, $\bar{\sigma} = k\bar{\epsilon}^n$ or using Equation 8 for $\sigma_r = 0$,

$$\bar{\epsilon} = \left(\frac{\bar{\sigma}}{k}\right)^{1/n} = \left(\frac{\sqrt{\sigma_a^2 - \sigma_a\sigma_t + \sigma_t^2}}{k}\right)^{1/n}$$

$$\text{That is, for } \sigma_t = (\sigma_t)_F, \bar{\epsilon} = \left(\frac{\sigma_t}{k}\right)^{1/n} \left(1 - \frac{1}{R} + \frac{1}{R^2}\right)^{1/2n} \quad \text{Equation 10a}$$

$$\text{and for } \sigma_a = (\sigma_a)_F, \bar{\epsilon} = \left(\frac{\sigma_a}{k}\right)^{1/n} (1 - R + R^2)^{1/2n} \quad \text{Equation 10b}$$

where $R =$ the principal stress ratio, σ_t/σ_a ,

and $(\sigma)_F =$ stress at fracture.

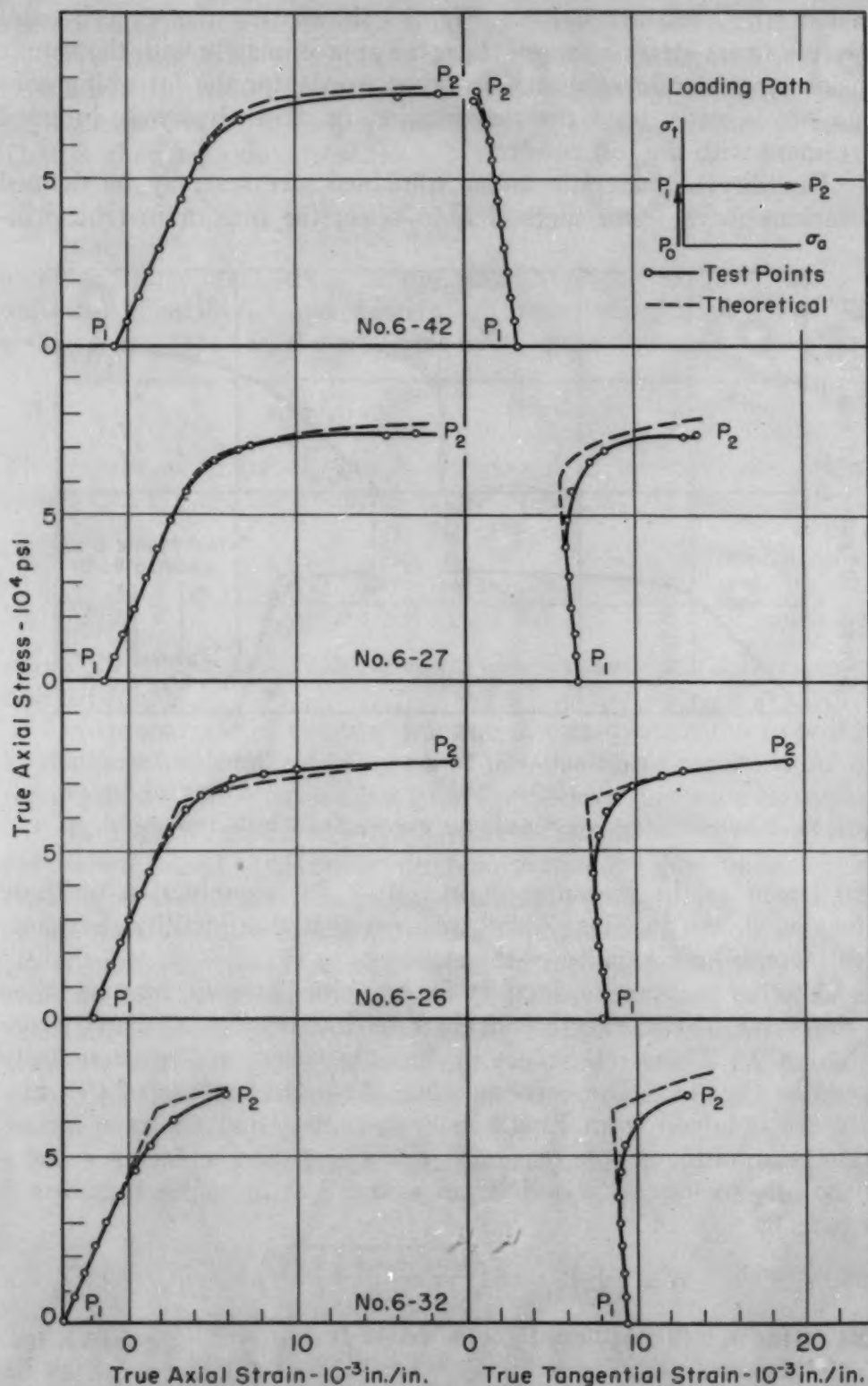


Fig. 14—Comparison of True Stress-Strain Relations With Flow Theory of Plasticity for Variable Stress Ratio Tests—Set A.

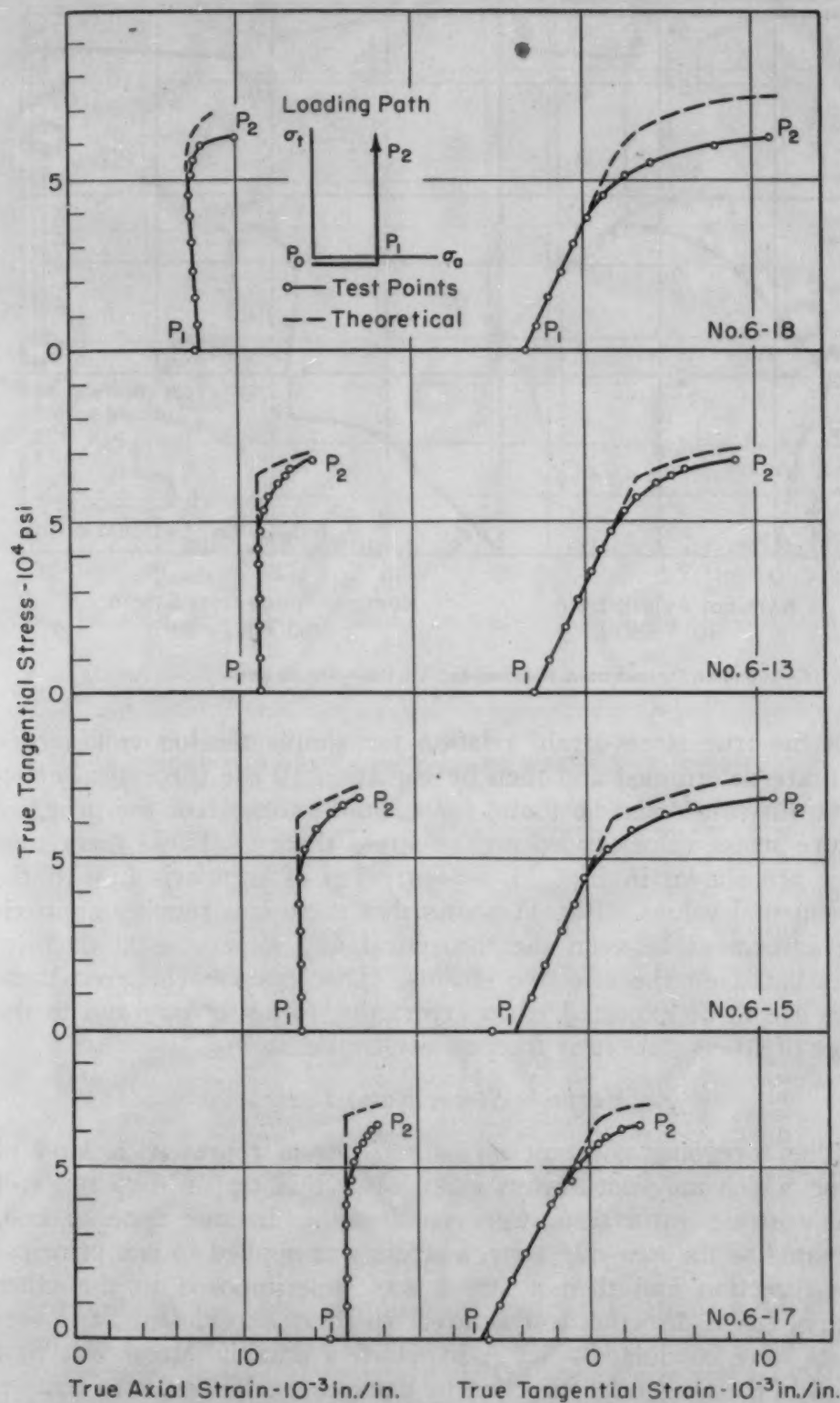


Fig. 15—Comparison of True Stress-Strain Relations With Flow Theory of Plasticity for Variable Stress Ratio Tests—Set B.

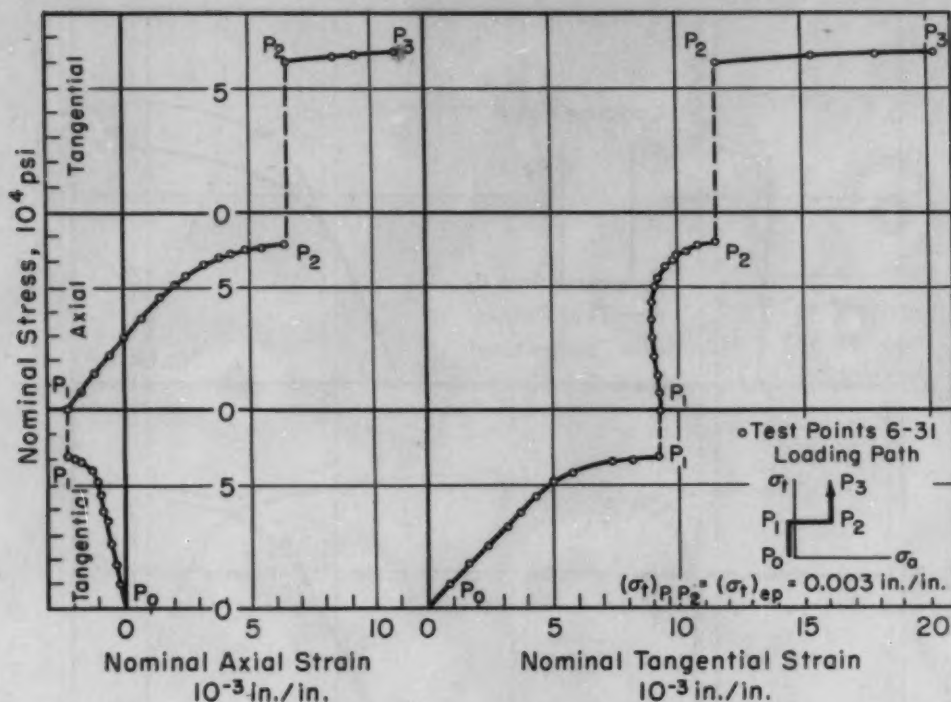


Fig. 16—Nominal Stress-Strain Relation for Variable Stress Ratio Test—Set C, No. 4.

From the true stress-strain relation for simple tension values of k and n are determined and then by Equation 10 the theoretical effective strain values can be found for various ratios R of the principal fracture stress values based on the stress theory. These theoretical values are shown in Fig. 11 for purposes of comparison with the experimental values. Fig. 11 shows that there is a roughly approximate agreement between the theoretical and experimental ductility values based on the effective strains. Discrepancies between these values are to be expected when errors due to anisotropy and to the change of stress state near fracture are considered.

Variable Stress Ratio Tests

The foregoing constant stress ratio tests represent a kind of loading which may not always exist. For this reason, two types of variable stress ratio tests were conducted. In one type of test, designated as the *two-step tests*, a stress was applied in one principal stress direction and then a stress was superimposed in the other principal stress direction to fracture. In these experiments, two sets of tests were conducted—Set A in which a uniaxial stress was first applied in the tangential direction by using a special device to remove the axial loading produced by the internal pressure, and Set B in which the axial stress was first applied. In both sets of tests, the specimens were initially subjected to various magnitudes of uniaxial stresses in one direction before subsequent loading in the other

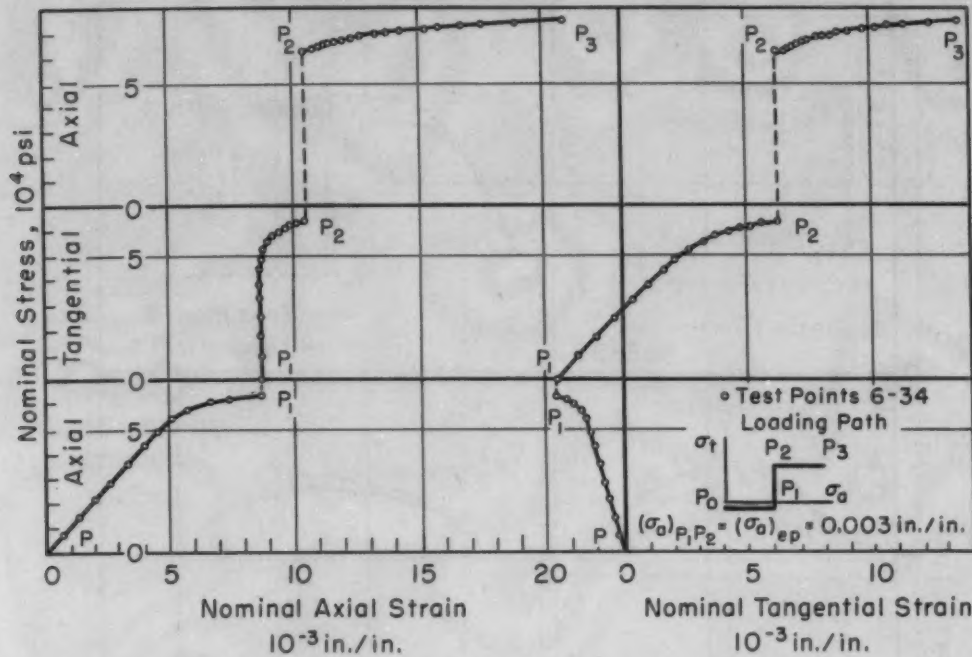


Fig. 17—Nominal Stress-Strain Relation for Variable Stress Ratio Test—Set D, No. 4.

Table I
Comparison of Strain Components for Loading Path Dependency

Point	Total Nominal Axial Strain in./in.				Total Nominal Tangential Strain in./in.			
	Set A	Set B	Δ (A-B)	$\frac{\Delta}{A}$ (A-B) %	Set A	Set B	Δ (A-B)	$\frac{\Delta}{A}$ (A-B) %
1	0.00260	0.00800
2	0.00330	0.01585	-0.01255	-380.3	0.00840	0.00630	0.00210	25.0
3	0.00370	0.01310	-0.00940	-254.1	0.00860	0.00605	0.00255	29.6
4	0.00400	0.01855	-0.01455	-363.8	0.00880	0.00360	0.00520	59.1
5	0.00215	0.00965
6	0.00305	0.01545	-0.01240	-406.6	0.01035	0.00550	0.00485	46.9
7	0.00355	0.01280	-0.00925	-260.6	0.01085	0.00545	0.00540	49.8
8	0.00405	0.01825	-0.01420	-350.6	0.00140	0.00300	0.00840	73.7
9	0.00340	0.00770	-0.00430	-126.5	0.00620	0.00615	0.00005	0.80
10	0.00410	0.01445	-0.01035	-252.4	0.00650	0.00310	0.00340	52.3
11	0.00450	0.01190	-0.00740	-164.4	0.00670	0.00370	0.00300	44.8
12	0.00495	0.01725	-0.01230	-248.5	0.00695	0.00100	0.00595	85.6
13	0.00450	0.00730	-0.00280	-62.2	0.00165	-0.00050	0.00215	76.7
14	0.00515	0.01330	-0.00815	-158.3	0.00155	-0.00120	0.00275	177.4
15	0.00547	0.01110	-0.00563	-102.9	0.00150	-0.00005	0.00155	103.3
16	0.00580	0.01595	-0.01015	-175.0	0.00145	-0.00315	0.00460	317.3

direction. Some of the nominal stress-strain relations for both Set A and Set B tests for these two-step tests are shown in Figs. 12 and 13. To compare these test results with the values predicted by the flow theory, true stress-strain relations for both the axial and tangential direction were determined as shown in Figs. 14 and 15. In Figs. 14 and 15, the theoretical stress-strain relations based on the flow theory are also plotted. An examination of Figs. 14 and 15 shows that in

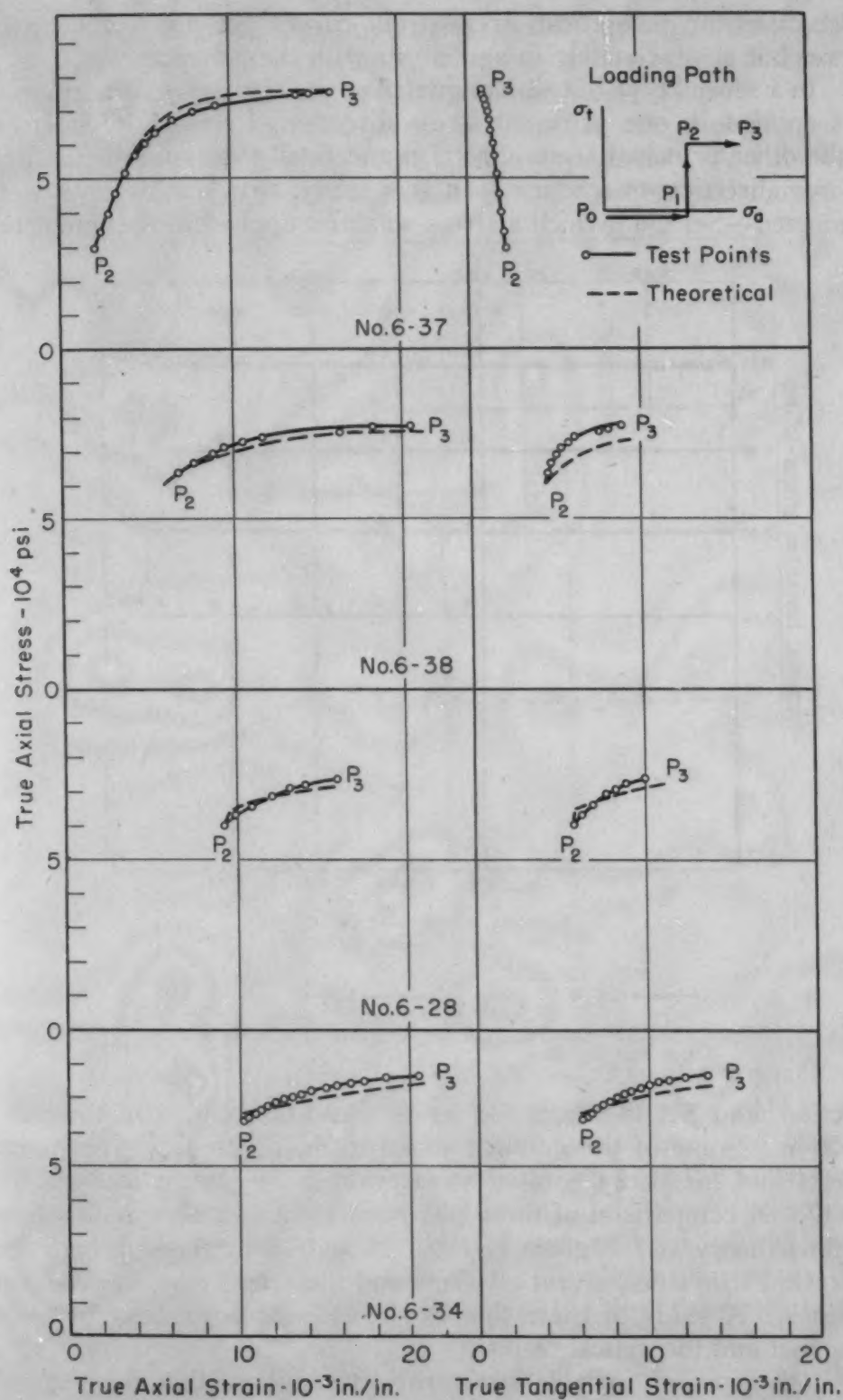


Fig. 19—Comparison of True Stress-Strain Relations With Flow Theory of Plasticity for Variable Stress Ratio Tests—Set D.

most cases the theoretical stress-strain curves are above the actual curves but approximately in agreement with the actual curves.

In a second type of test, designated as the *three-step tests*, a stress was applied in one principal stress direction, followed by a stress in the other principal stress direction and finally stressing in the first loading direction to fracture. In this study, two sets of tests were conducted—Set C in which a stress was first applied in the tangential

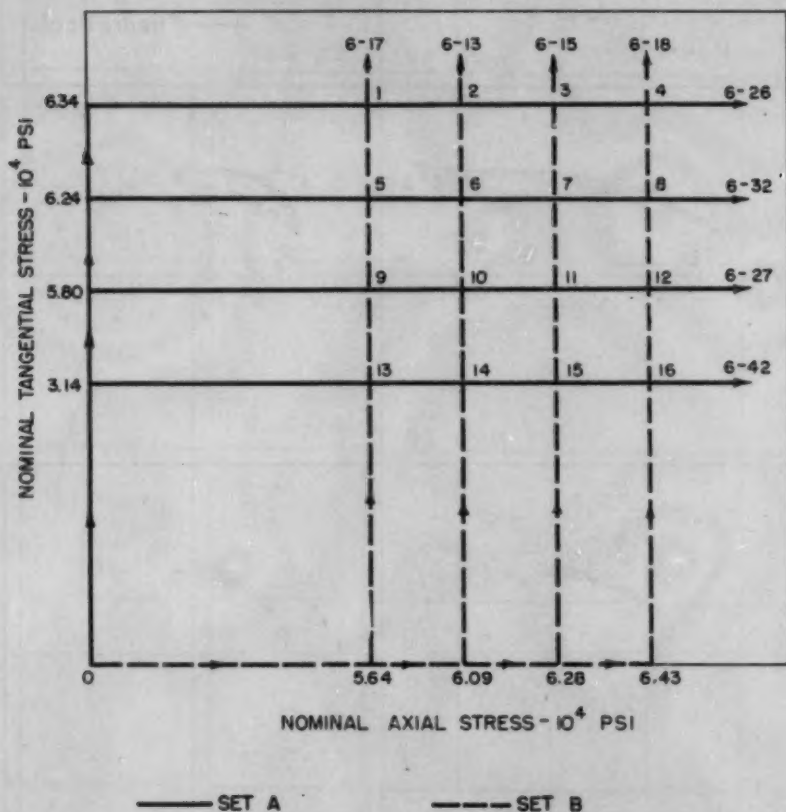


Fig. 20a—Loading Path for Variable Stress Ratio Tests
—Set A and Set B.

direction, and Set D where the stress was first applied in the axial direction. Some of the nominal stress-strain relations for both sets of tests and for various initial stress values are shown in Figs. 16 and 17. A comparison of these test results with values predicted by the flow theory (8) is given in Figs. 18 and 19 by plotting both the theoretical true stress-strain relations and the actual true stress-strain relations. A study of these figures shows good agreement between the actual and theoretical results.

Both types of variable stress ratio tests show that the path of loading has little effect upon the true fracture strength and that the fracture strength is approximately defined by the maximum stress theory. Fig. 9 shows the fracture strength values and values given by the maximum stress theory. Fig. 11 also shows that the path of

loading has no great effect upon the ductility and that the ductility may be approximately predicted by the effective strain at fracture using stress values defined by the maximum stress theory.

The foregoing variable stress test results can also be used to distinguish between the slip (7) and flow-type theory. To show the distinction between these two theories, the loading paths used are

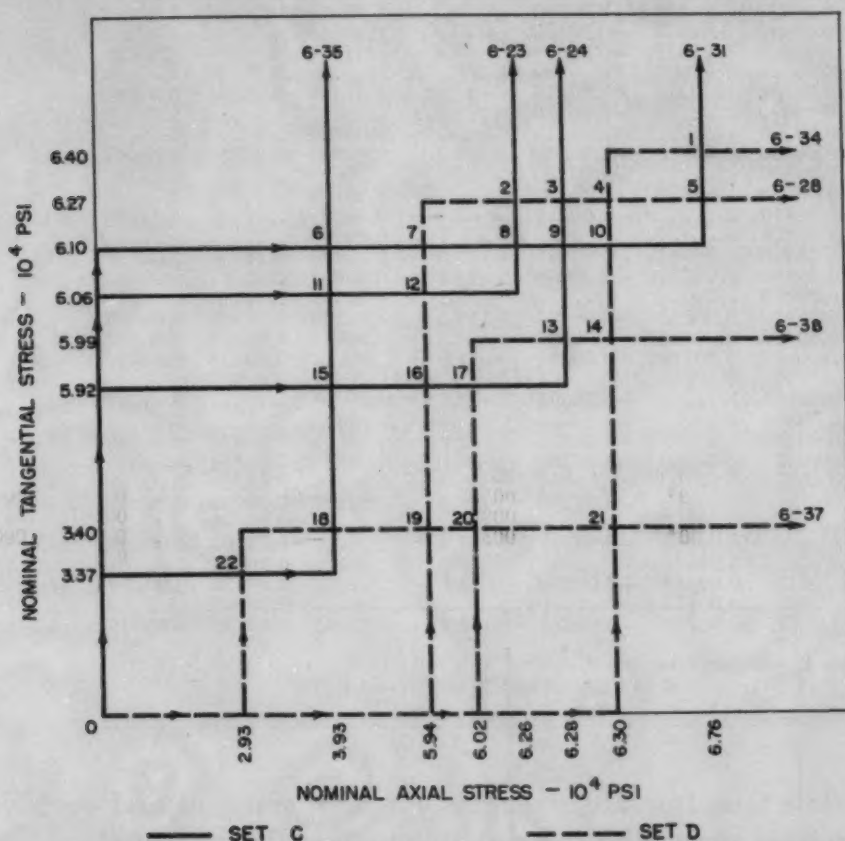


Fig. 20b—Loading Path for Variable Stress Ratio Tests—Set C and Set D.

first summarized as shown in Figs. 20a and 20b. In Figs. 20a and 20b, the two paths of loading used to arrive at the same state of stress are indicated. According to the slip theory the axial and tangential strains corresponding to each final loading point are the same, regardless of the loading path used. Tables I and II show the strains in the axial and tangential directions for each path of loading and the percentage difference in these strains. The large percentage differences in Tables I and II give support to the flow theory rather than the slip theory.

CONCLUSIONS

For the 14S-T aluminum alloy tested in this investigation and for biaxial tensile stresses the following conclusions can be made:

(a) The yield strength is in approximate agreement with the distortion energy theory.

Table II
Comparison of Strain Components for Loading Path Dependency

Point	Total Nominal Axial Strain				Total Nominal Tangential Strain			
	in./in.		% (C-D)		in./in.		% (C-D)	
	Set C	Set D	Δ (C-D)	C	Set C	Set D	Δ (C-D)	C
1	0.00950	0.01210	-0.00260	-27.4	0.01680	0.00745	0.00935	55.7
2	0.00530	0.01020	-0.00490	-9.2	0.00880	0.00640	0.00240	27.3
3	0.00445	0.01025	-0.00580	-130.3	0.00660	0.00640	0.00020	3.0
4*	0.01035	-0.00035	-3.4	0.00650	0.00120	18.5
		0.01000		0.00530
5	0.00790	0.01205	-0.00415	-52.5	0.01400	0.00755	0.00645	46.1
6*	0.00090	-0.00170	-188.9	0.00890	0.00330	37.1
	0.00260	0.00560
7	0.00330	0.00910	-0.00580	-175.7	0.00960	0.00515	0.00445	46.4
8*	0.00400	-0.00120	-30.0	0.00995	0.00285	28.6
	0.00520	0.00710
9*	0.00410	-0.00015	-2.9	0.00995	0.00400	40.2
	0.00425	0.00595
10	0.00420	0.00965	-0.00545	-129.8	0.01000	0.00450	0.00550	55.0
11*	0.00190	-0.00070	-36.8	0.00665	0.00120	18.0
	0.00260	0.00545
12	0.00410	0.00090	-0.00490	-119.5	0.00700	0.00500	0.00200	28.6
13	0.00420	0.00700	-0.00280	-66.7	0.00565	0.00455	0.00120	21.2
14*	0.00710	-0.00240	-33.8	0.00455	0.00030	6.6
	0.00950	0.00425
15*	0.00165	-0.00095	-57.6	0.00555	0.00040	7.2
	0.00260	0.00515
16	0.00360	0.00875	-0.00575	-143.0	0.00535	0.00455	0.00080	15.0
17	0.00375	0.00660	-0.00285	-76.0	0.00535	0.00435	0.00100	18.7
18	0.00275	0.00300	-0.00025	-9.1	0.00230	0.00210	0.00020	8.7
19*	0.00500	-0.00300	-60.0	0.00165	0.00075	45.5
	0.00800	0.00090
20*	0.00515	-0.00115	-22.3	0.00160	0.00030	18.8
	0.00630	0.00130
21*	0.00865	+0.00290	+33.5	0.00155	0.00095	61.3
	0.00575	0.00060
22	0.00185	0.00220	-0.00035	-18.9	0.00265	0.00230	0.00035	13.2

*Two tests in one set intersected.

$$\Delta = C_1 - C_2 \text{ and } \% = (C_1 - C_2)/C_1$$

(b) The true fracture strengths for both constant and variable stress ratio tests agree with the maximum stress theory. It should be noted that these tests are restricted to biaxial tension.

(c) The true ductility may be approximately determined by the effective strain at fracture.

(d) The flow theory gives a good approximation for the plastic stress-strain relations for numerous variable stress ratio tests conducted.

(e) The variable stress ratio test results support the flow theory rather than the slip theory.

ACKNOWLEDGMENTS

The authors sincerely appreciate the help offered by the Office of Army Ordnance under whose sponsorship this project was performed.

References

1. A. Nadai, "Theory of Flow and Fracture of Solids", McGraw-Hill Book Company, Vol. 1, 1951.

2. R. Hill, "The Mathematical Theory of Plasticity", Oxford University Press, 1950.
3. A. M. Freudenthal, "The Inelastic Behavior of Engineering Materials and Structures", John Wiley & Sons, Inc., 1950.
4. D. C. Drucker, "Stress-Strain Relations in the Plastic Range", Publication A11S1 for Office of Naval Research. Published by Brown University, 1950.
5. J. Marin, J. H. Faupel, V. L. Dutton and M. W. Brossman, "Biaxial Plastic Stress-Strain Relations for 24S-T Aluminum Alloy", N.A.C.A. Technical Note 1536, May 1948, 96 pages.
6. J. Marin, B. H. Ulrich and W. P. Hughes, "Plastic Stress-Strain Relations for 75 S-T Aluminum Alloy Subjected to Biaxial Tensile Stresses", N.A.C.A. Technical Note 2425, 1951.
7. S. B. Batdorf and B. Budiansky, "A Mathematical Theory of Plasticity Based on the Concept of Slip", N.A.C.A. Technical Note 1871, 1949.
8. L. W. Hu and J. Marin, "Determination of Theoretical Plastic Stress-Strain Relations for Variable Combined Stress Ratios", American Society of Mechanical Engineers, Paper 52-APM-29.

DISCUSSION

Written Discussion: By M. H. Lee Wu, research group leader, Department of Aeronautical Engineering and Applied Mechanics, Polytechnic Institute of Brooklyn, Brooklyn, N. Y.

The authors have performed a very useful experiment. It is indeed

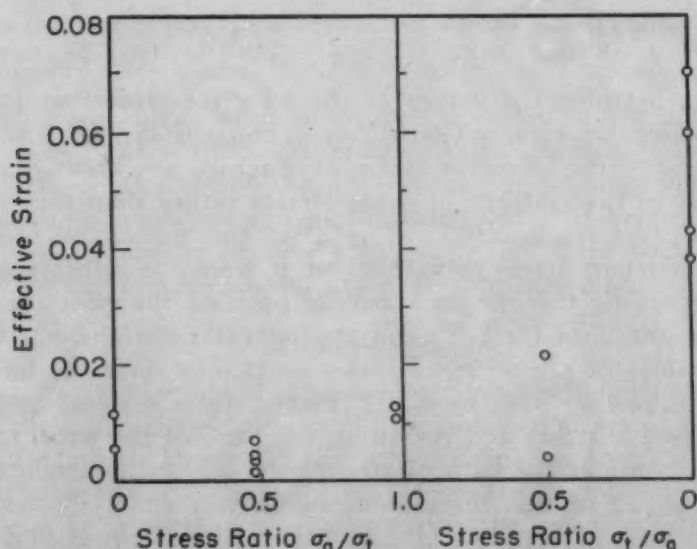


Fig. 21—Effective Strain at Fracture for Constant Stress Ratio Tests. (From Fig. 11.)

very important to know the validity of current theories of plasticity for complex loading paths (variable stress ratios). However, the writer feels that the experimental data reported may be interpreted differently.

First, consider the data given in Fig. 11 of the paper. The values of the effective strains at fracture for the constant stress ratio are taken from this figure and replotted in Fig. 21 of this discussion. It can be seen that

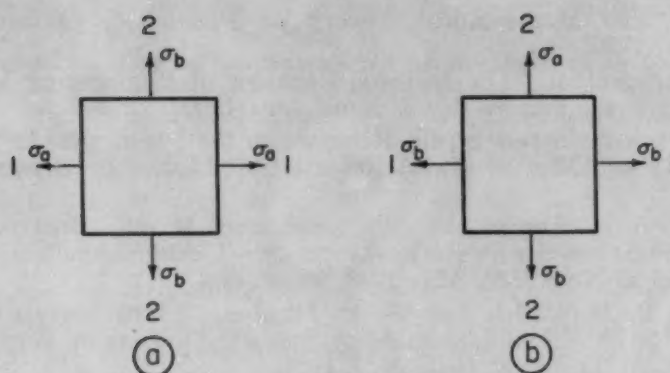


Fig. 22—Elements Subjected to Biaxial Stress.

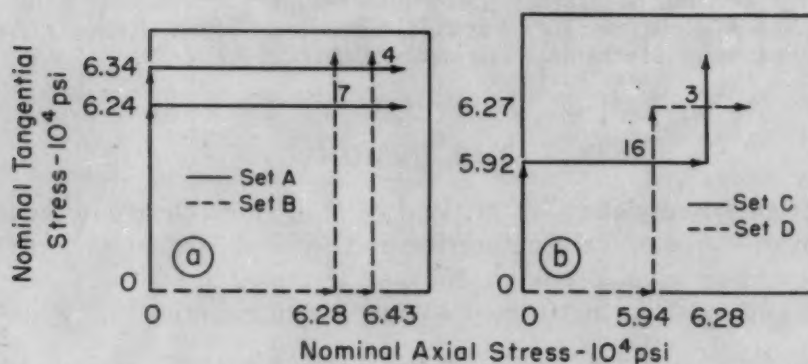


Fig. 23—Loading Path for Variable Stress Ratio Tests. (From Figs. 20a and 20b.)

the difference between the values of the effective strains at fracture for constant stress ratio $\sigma_a/\sigma_t = 0.0$ and $\sigma_t/\sigma_a = 0.0$ is large. This indicates that the values of the effective strain at fracture are greatly affected by the anisotropy of the material or other effects rather than the stress ratio, because both cases are uniaxial. (Fig. 21 of this discussion includes only the data for constant stress ratio, because it would be difficult to obtain a conclusion regarding the effect of loading path on the effective strains at fracture from the data for both constant stress ratio and variable stress ratio if the values of plastic strains at a particular state of stress depend greatly on the loading path by which that state is reached as mentioned in the paper (see abstract and the twentieth page of the paper).

Secondly, consider the data of strain components for loading path dependency. Fig. 22 of this discussion shows two small elements having principal axes 1-1 and 2-2. In Fig. 22a, the small element is first subjected to a principal stress of magnitude σ_a along direction 1-1, and then subjected to a principal stress along direction 2-2 whose magnitude increases gradually from 0 to σ_b . The resulting plastic strains are e_1 and e_2 , respectively. In Fig. 22b, a small element of the same material is first subjected to a principal stress σ_a along direction 2-2 and then a principal stress along 1-1 increasing from 0 to σ_b . The resulting plastic strains in the two directions are respectively e_2 and e_1 . Now, if the material under consideration is isotropic before loading, the strains along the directions 1-1 and 2-2 in Fig. 22a are equal to the strains along the directions 2-2 and 1-1 in Fig.

22b, respectively. If these values of strains do not agree, it means the material is anisotropic, and the difference is an indication of the degree of effect of anisotropy on the strains. Tables I and II of the paper compared the strain components for loading path dependency. The corresponding loading paths were shown in Figs. 20a and 20b of the paper. It would be important to examine the effect of anisotropy on the strain components. A few paths taken from Figs. 20 of the paper are shown in Figs. 23a and 23b of this discussion. These paths are similar to the paths shown in Fig. 22 of this discussion. At points 7 and 4 of Fig. 23a of this discussion, the differences between the axial strains e_a of Set A and the tangential strains e_t of Set B, and the differences between the tangential strains e_t of Set A and the axial strains e_a of Set B indicate approximately the effect of anisotropy. Similarly, at points 16 and 3 in Fig. 23b of this discussion, the differences between e_a of Set C and e_t of Set D and the differences between e_t of Set C and e_a of Set D indicate approximately the effect of anisotropy of the material on the strains. The values of the strains at these points taken from Tables I and II of the paper are listed in the following tabulation:

COMPARISON OF STRAIN COMPONENTS FOR EFFECT OF ANISOTROPY

Point	e_a	e_t	Δ	$\frac{\%}{A}$	e_t	e_a	Δ	$\frac{\%}{A}$
	Set A	Set B	(A - B)	A	Set A	Set B	(A - B)	A
4	0.00400	0.00360	0.00040	10	0.00880	0.01855	-0.00975	-111
7	0.00355	0.00545	-0.00190	-54	0.01085	0.01280	-0.00195	-18
	e_a	e_t	Δ	$\frac{\%}{C}$	e_t	e_a	Δ	$\frac{\%}{C}$
	Set C	Set D	(C - D)	C	Set C	Set D	(C - D)	C
3	0.00445	0.00640	-0.00195	-44	0.00660	0.01025	-0.00365	-55
16	0.00360	0.00455	-0.00095	-26	0.00535	0.00875	-0.00340	-63

The values of percentage differences are calculated in a similar manner to those in Tables I and II of the paper in order to compare their magnitudes. It is seen that the values of the differences due to anisotropy calculated in the preceding tabulation are of the same order of magnitude as those given in Tables I and II of the paper. This indicates that the effect of anisotropy on the strain components is very pronounced.

Authors' Reply

The authors appreciate the comments made by the discussor and agree with her fully when she points out the pronounced effect of the anisotropy of material tested. However, the authors believe that the discrepancy may be attributed to the anisotropy of materials, provided the loading processes can be proved to be commutative for anisotropic materials.

THE ENDURANCE LIMIT OF TEMPER-BRITTLE STEEL

BY R. D. CHAPMAN AND W. E. JOMINY

Abstract

This paper gives an account of an investigation of the effect of temper brittleness of an SAE 5140 steel on the endurance limit at both room temperature and at minus 35 °F. Three different heat treatments were given the material, one to make the material brittle at room temperature, the second, the standard temper brittle treatment of furnace cooling from the tempering temperature and the third, to make the steel as ductile as possible. All these treatments were selected to produce the same hardness in the steel.

Both polished and notched bars were tested in fatigue at room and subzero temperatures. In addition, tensile and standard V-notch Charpy impact specimens were tested at the same temperatures. Although the hardnesses were the same and the Charpy impact values varied considerably, no substantial change in endurance limit could be found between the embrittled and nonembrittled material at the two temperatures studied. The results also indicate no change in the notch sensitivity factor of endurance specimens between the embrittled and nonembrittled steel.

THE PURPOSE of the investigation reported here was to determine what, if any, was the effect of temper brittleness as measured by the loss of notch toughness based on the Charpy impact test, as compared with the endurance limit in bending of steel at room temperature as well as at subzero temperatures. So often in the design of parts the endurance limit is of prime importance rather than the impact resistance as indicated by the Charpy test.

Several authorities have studied the relationship between impact values and fatigue properties. Greaves (1-4),¹ Gough (5), Hollomon (6), Wishart and Lyon (7) and Morris (8) have each investigated certain phases of this subject. According to Gillett (9), however, there is no evidence to prove that when temperature sensitivity is shown by notched impact it also exists in notched fatigue.

To obtain the evidence which Gillett said was lacking and also to

¹The figures appearing in parentheses pertain to the references appended to this paper.

A paper presented before the Thirty-fourth Annual Convention of the Society, held in Philadelphia, October 18 to 24, 1952. Of the authors, R. D. Chapman is research metallurgist, and W. E. Jominy is chief metallurgist—Research, Chrysler Corp., Engineering Division, Detroit. Manuscript received April 9, 1952.

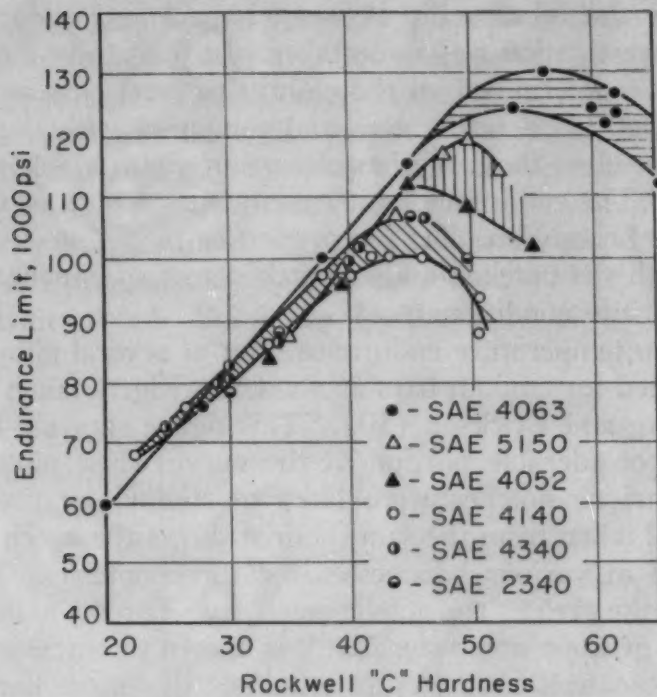


Fig. 1—Fatigue Strength of Several Alloy Steels.

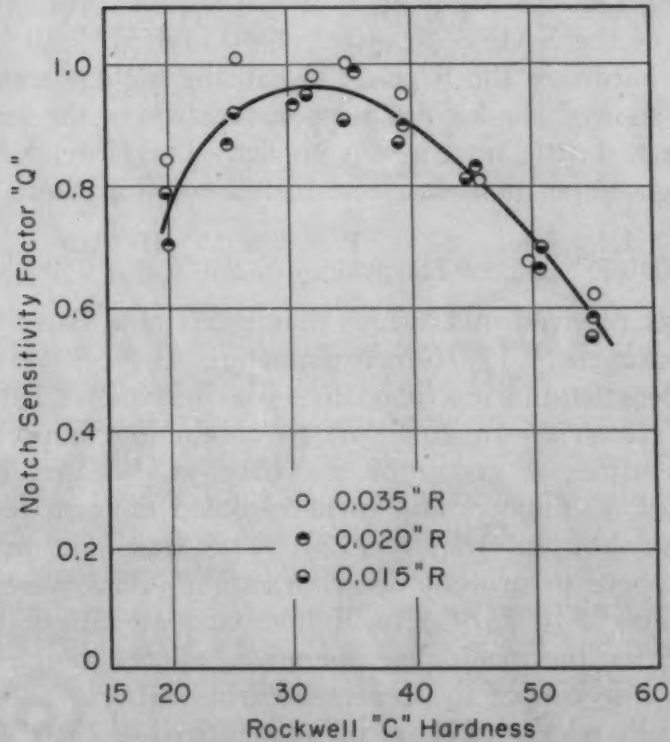


Fig. 2—Notch Sensitivity—SAE 4063.

further study the relationship between impact and endurance properties, this investigation was undertaken. In this study the endurance limit was to be determined on the embrittled steel both at room temperature and at 35 °F below zero and compared with the endurance of the same steel in the same hardness range but which was treated to be ductile. The endurance limit was measured both in the notched and unnotched condition. Tensile properties of the steel were measured both with the notched and unnotched test specimens and in the ductile and brittle conditions.

The room temperature endurance limit of several alloy steels has been established for smooth bars as shown in Fig. 1 taken from Garwood, Zurburg and Erickson (10). This figure shows a linear relation over a considerable portion of the curve when plotted against hardness. Various notches were likewise studied by these investigators. Fig. 2 taken from the same source shows the notch sensitivity of SAE 4063 at various hardnesses for three notches. The higher the "q" value the greater the notch sensitivity. For the material tested in Fig. 2, the greatest notch sensitivity is shown to correspond with a hardness of Rockwell C-30. Approximately this same hardness was used in all the test bars studied in this investigation.

EXPERIMENTAL PROCEDURE

Material Tested—Studying four SAE steels, Jominy (11) has shown that of the SAE 8640, 4042, 1340 and 5135 all heat treated to the same hardness, the SAE 5135 had the highest transition temperature or showed the highest temperature where the steel changed from ductile to brittle fracture on impact. Therefore, SAE 5135 of the following composition was used in this investigation:

	C	Mn	Si	P	S	Ni	Cr	Mo	Cu
SAE 5135	0.37	0.75	0.22	0.016	0.025	0.05	0.98	0.02	0.08

The steel was received in 1 $\frac{7}{8}$ -inch diameter round bars, which were forged and swaged to 1 $\frac{1}{16}$ -inch diameter. These were in turn cut into 8-inch lengths and machined to $\frac{5}{8}$ -inch diameter bars.

Heat Treatment—In an effort to obtain low impact values at room temperature, a group of the bars was heated to 2500 °F (1370 °C) for 30 minutes and furnace-cooled to form facets as described by Strohm and Jominy (12). This was done in a purified argon atmosphere to prevent decarburization. Bars were next normalized at 1700 °F (925 °C) for 1 hour and all fatigue bars rough machined. After the machining operation, all the rough bars were plated with dense copper to prevent decarburization. The bars were then individually packed in charcoal, austenitized at 1550 °F (845 °C) for $\frac{1}{2}$ hour and oil-quenched in a fixture (Fig. 3) on revolving cylinders to maintain symmetry.

The fatigue bars are individually placed on these chain-driven rolls and oil is pumped over the hot specimen at the rate of about 60 gallons per minute. The oil enters at the top of this fixture through narrow slots which run the entire length of the fixture. In quenching, the sample is placed on the rolls which are turning and by means of a quick-opening valve the oil is shot directly on the piece. This quenching procedure has produced very uniform and reproducible results. The bars were immediately stress-relieved at 400 °F (205 °C) for 1 hour and air-cooled. Subsequently, the material was tempered at

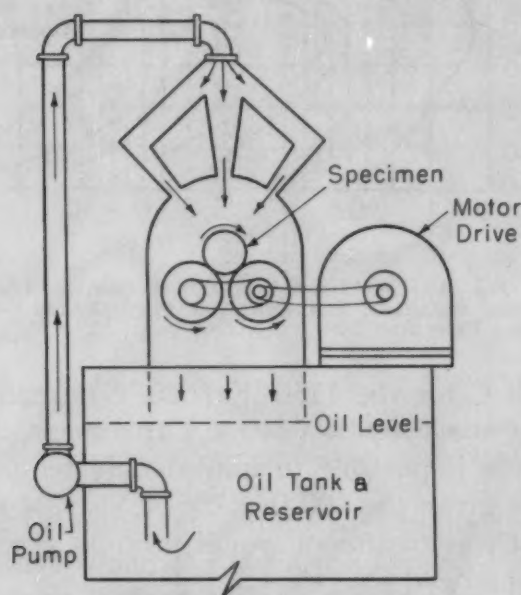


Fig. 3—Schematic Drawing of Chrysler Quenching Tower for Fatigue Specimen.

1050 °F (540 °C) for 2 hours and furnace-cooled. As discussed under the impact property section of this paper it will be seen that this high temperature treatment definitely lowered the room temperature impact properties of the steel. (See Table II.)

The heat treatment for the remaining bars was as follows: All material was normalized at 1700 °F (925 °C), copper-plated, austenitized at 1550 °F (845 °C) for ½ hour at heat and oil-quenched, followed by an immediate stress relief at 400 °F (205 °C). The embrittled bars were tempered at 1050 °F (540 °C) for 2 hours and furnace-cooled, whereas the bars considered as nonembrittled were tempered at 1150 °F (620 °C) for 20 minutes in salt and oil-quenched.

The main difference in these last two treatments is the tempering temperature and the tempering times. The 1050 °F (540 °C) temperature was first selected because it had been found to give the maximum embrittlement for this particular steel. Fig. 4 from Hollomon's (13) paper shows the familiar "C" curves for temper brittleness and

after 2 hours considerable decrease in impact values has occurred at 1000°F (540°C). Since it was desirable to maintain the same hardness from both heat treatments, a higher temperature for a shorter time without loss of impact was necessary. It was found that 1150°F (620°C) temperature for 20 minutes in salt gave this result. The resulting hardness from these treatments gave a spread of from 27

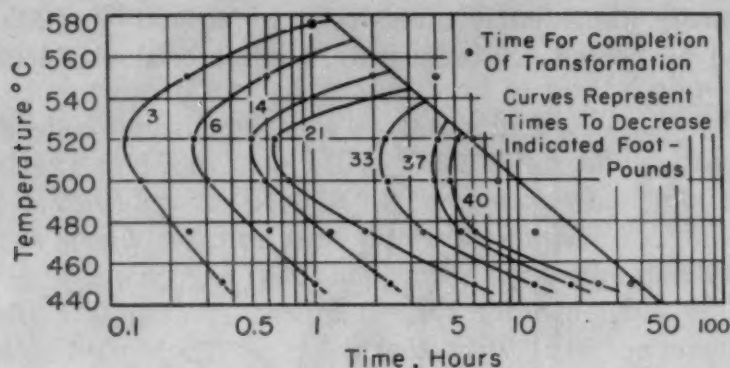


Fig. 4—Time-Temperature-Transformation Diagram for Temper Brittleness Transformation (From Data of Greaves and Jones; Their Steel D).

to 30 Rockwell C for the 1150°F (620°C) treatment and 28 to 30 Rockwell C for the 1050°F (540°C) treatment.

Since it was impossible to immediately temper the as-quenched bars, they were given the 400°F (205°C) stress relieving treatment. It was felt that this treatment would prohibit cracking. These treatments are summarized in Table I.

Impact Properties—Standard V-notch Charpy impact bars were machined according to ASTM E23-47T Type A specification and given the same heat treatments as outlined for the fatigue bars. These were broken at room temperature (75°F) and at minus 30°F with the results shown in Table II. Although the complete transition curve

Table I
Heat Treatments for Test Specimens

Heat Treatment No. 1	Heat Treatment No. 2	Heat Treatment No. 3
Normalize at 1700°F—1 hr.	Normalize at 1700°F—1 hr.	Heated to 2500°F in Argon for 30 min.—furnace cooled
Rough machined	Rough machined	Normalize at 1700°F—1 hr.
Copper plated	Copper plated	Rough machined
Austenitize at 1550°F—1 hr.	Austenitize at 1550°F—½ hr.	Copper plated
at heat	at heat	Austenitize at 1550°F for ½ hr.
Oil quench	Oil quench	at heat
Stress relieve at 400°F—1 hr.	Stress relieve at 400°F—1 hr.	Oil quench
Temper 1150°F for 20 min.	Temper 1050°F for 2 hrs.	Stress relieve at 400°F—1 hr.
in salt		
Oil quench	Furnace cooled	Temper 1050°F for 2 hrs.,
		furnace cool
Hardness range	Hardness range	Hardness range
Rockwell C—27-30	Rockwell C—28-30	Rockwell C—28-30

was not determined from a ductile to brittle fracture, it can be seen from Table II that the transition temperature for the first heat treatment was below minus 30°F, for the second it was between 75°F and minus 30°F, while for the third it appears to be near room temperature.

Table II
Charpy Impact Values of SAE 5135 Steel

Treatment	Room Temp. Impact—75°F	Impact at Minus 30°F
Normalized,	100	75.8
Austenitized and	92.7	76.2
Tempered at 1150°F	90.0	82.9
Oil quench	91.3	78.0
Average	93.6	78.2
Heat Treat No. 1	Average Hardness—Rockwell C—29.9	
Normalized,	79.0	22.9
Austenitized and	77.8	26.3
Tempered at 1050°F	73.0	22.7
Furnace cool	72.3	20.5
Average	75.5	23.1
Heat Treat No. 2	Average Hardness—Rockwell C—30.0	
Heated 2500°F		
Normalized,	39.7	19.0
Austenitized and	43.3	16.4
Tempered at 1050°F	43.7	16.8
Furnace cool	43.5	17.8
Average	42.5	17.5
Heat Treat No. 3	Average Hardness—Rockwell C—30.0	

Metallographic examination of these bars in the as-quenched condition showed the percentage of martensite present to be 98%.

Test Bars—After rough machining and heat treating, the fatigue bars were finished to the dimensions shown in Fig. 5. The polished bars were next ground in a longitudinal direction followed by a super-finishing operation likewise moving in a longitudinal direction with the axis of the sample. These finishing operations produced a surface of 0 to 2.0 microinches.

Notches are very difficult to reproduce and must not have circumferential scratches. The technique found most reproducible has been to first grind the sides of the notches by using a wheel dressed to 60 degrees and relieved so that the root of the notch is not touched by the wheel. Next the root of the notch was finished by using a copper wire lapping procedure. The specimen is centered in a lathe and rotated while the copper wire impregnated with abrasive is held in a frame normal to the specimen's major axis. The wire is driven by means of an electric motor and moved across the notch. Such a procedure produced notches which vary from 7/12 microinches and concentricity at the minimum section within 0.0002 inch.

Two sets of 10 each polished fatigue specimens were finished from heat treatment No. 1, along with two sets of 10 each of the

tion were the Moore-type rotating beam operating in the vicinity of 8000 rpm. The endurance limit for both the polished and notched bars was determined at room temperature and is shown in Table III. Subsequent to these tests the machines were moved into the cold testing laboratory at minus 35°F. Several mechanical changes had to be incorporated in the machines such as using lighter oil, reducing the speed to about 3000 rpm and other minor changes. Polished and notched bars were run at this temperature with results shown in Table III.

Table III
Endurance Limits for Embrittled and Nonembrittled SAE 5135 Steel

Treatment	Endurance Limit psi—Room Temp.			Rockwell C
	Smooth Bar	Rockwell C	Notched Bar	
Nonembrittled (heat treat No. 1)	77,000	28	44,000	28
Embrittled (heat treat No. 3)	75,000	29	43,000	28
Cold Temperature—Minus 35				
Nonembrittled (heat treat No. 1)	81,000	27	44,000	29
Embrittled (heat treat No. 2)	83,000	29	49,000	29

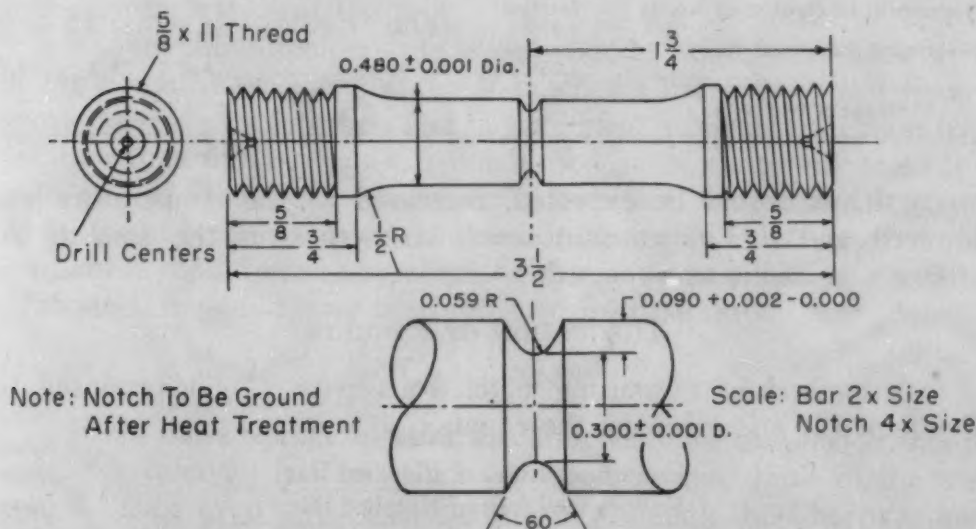


Fig. 6—Notched Tensile Bar With Same Stress Concentration Factor as 0.035-Inch R Notched Endurance Bar.

The smooth and notched tensile bars were pulled at both room temperature and at minus 35°F. For the cold-treated results, an insulated box was placed between the cross heads of the tensile machine. The box was cooled by circulating acetone, which had been sprayed over dry ice, through a coil within the box. Temperature within the box was controlled by means of a differential thermocouple operating a motor-driven fan. With this arrangement, the temperature could be maintained within $\pm 2^\circ\text{F}$. To measure the temperature

of the work, a dummy sample was made and a thermocouple percussion welded at the center. Time was measured to bring the piece to -35°F and when the bars were tested another $\frac{1}{2}$ hour was allowed as a safety precaution before the bar was pulled. Tensile properties are shown in Table IV. In order to measure the reduction of area in the notched bars, the diameters were measured before and after testing on an optical comparator. It will be noted that the tensile

Table IV
Polished and Notched Tensile Properties of SAE 5135 Steels*

Treatment	Bar Type	Ultimate Strength psi	Yield Strength psi	Elongation %	Reduction of Area %	Rockwell C
Room Temp. (75°F)						
Nonembrittled (heat treat No. 1)	Smooth	134,600	120,600	30.7	63.6	28
Embrittled (heat treat No. 3)	Smooth	135,700	120,900	29.0	58.2	28.5
Nonembrittled (heat treat No. 1)	Notched (.059")	203,500	185,300	4.0	34.9	28
Embrittled (heat treat No. 3)	Notched (.059")	208,800	192,600	3.0	26.4	28.8
Subzero Temp. (Minus 35°F)						
Nonembrittled (heat treat No. 1)	Smooth	143,000	127,200	29.4	62.2	28.5
Embrittled (heat treat No. 2)	Smooth	144,700	130,800	31.0	60.8	29.5
Nonembrittled (heat treat No. 1)	Notched (.059")	215,300	2.8	32.5	27.5
Embrittled (heat treat No. 2)	Notched (.059")	220,500	3.2	28.8	29.5

*Average of two tests.

strength, as would be expected, increased as the temperature was lowered and the increase in notch strength over the smooth bar strength is about as expected.

DISCUSSION OF RESULTS

A method of measuring notch sensitivity ("q") proposed by Peterson (15) is given by the equation:

$$q = \frac{\frac{\text{Endurance Limit of Polished Bar}}{\text{Endurance Limit of Notched Bar}} - 1}{K_t - 1}$$

where K_t is the stress concentration predicted from theory. From such a relationship the notch sensitivity factor was found for these materials as shown below in Table V.

Table V
Notch Sensitivity Factors

Treatment	Temp., °F	q
Nonembrittled (Heat Treat No. 1)	75	0.9
Embrittled (Heat Treat No. 3)	75	0.9
Nonembrittled (Heat Treat No. 1)	-35	1.0
Embrittled (Heat Treat No. 2)	-35	0.9

From these values it can be seen that at room temperature there is no difference in notch sensitivity resulting from the two heat treatments. At cold temperatures the values are reversed from what might be expected. In other words, the notch sensitivity factor "q" shows no effect on the embrittled and nonembrittled material. However, comparing these values with those in Fig. 2 they appear to be quite consistent in magnitude.

In comparing endurance limit to tensile strength the normal relationship is to use 50% of the ultimate strength as the endurance limit for the polished bar. It will be noted from these tests that the values vary from 55 to 57%. However, when the notched-bar endurance limit is compared to the notched-bar tensile strength, this percentage drops to 20-22%. This comparison should be made only with discretion. Although the stress concentration factor was calculated to be the same for both tensile and fatigue bars, the fatigue failure is one which takes place in the elastic range, while the tensile failure is plastic. It will be recalled that the shear forces are greatest at the very root of the notch in a tensile bar [Neuber (14)] and during pulling, this notch will deform plastically, thereby changing the stress concentration at the root.

The transition temperature is known to be raised with the severity of the notch. For example, the V-notched Charpy bars will have a greater stress concentration and in turn yield a higher transition temperature than the 0.035-inch R notch used in the endurance test. It is quite possible that although the endurance bars were tested at minus 35 °F the material was not in the all-brittle range. However, if temper brittleness should have any effect on the endurance limit of the SAE 5135 steel, it should have been reflected in these tests.

CONCLUSIONS

From these tests it appears that the metallurgical phenomenon of temper brittleness has no effect on the endurance limit of the steel tested. Thus even at cold temperatures, although the Charpy impact value decreased, the endurance limit remained unchanged. Therefore, in engineering applications where a temper-embrittled steel is used, we believe the endurance limit of the part will be unaffected, even at temperatures below the transition temperature.

Appendix

From work done at Chrysler the stress concentration factor " K_t " for the 0.035-inch R notch has been calculated to be 1.82 in the fatigue bar. This notch is 0.090 inch deep and the bar radius under the notch is 0.150 inch. However, the notch in the fatigue bar is in bending and has a stress distribution different than in tension.

Therefore, a new notch had to be used in the tensile tests. The calculations used for this new notch are shown below.

Keeping the same bar radius under the notch ("a") of 0.150 inch and the same depth of notch ("t") of 0.090 inch a value now must be assumed for the radius of the notch ("ρ") or 0.059 inch. For the "Theory of Notch Stresses" by H. Neuber the constant "N" must first be calculated where

$$N = \frac{a}{\rho} + \frac{2}{m} \sqrt{\frac{a}{\rho} + 1} + 2$$

and where "1"/m is Poisson's Ratio = 0.26.

Now—

$$\begin{aligned} N &= \frac{0.150}{0.059} + 0.52 \sqrt{\frac{0.150}{0.059} + 1} + 2 \\ &= 5.52 \end{aligned}$$

Next the ratio of maximum stress to normal stress is determined from the equation

$$\begin{aligned} \alpha_{tk} &= \frac{1}{N} \left[\frac{a}{\rho} \sqrt{\frac{a}{\rho} + 1} + \left(0.5 + \frac{1}{m}\right) \frac{a}{\rho} + \left(1 + \frac{1}{m}\right) \left(\sqrt{\frac{a}{\rho} + 1} + 1 \right) \right] \\ &= 1.87 \end{aligned}$$

Using the correction (K_t) for the stress concentration factor developed by Neuber in which

$$K_t = 1 + \frac{(\alpha_{fk} - 1)(\alpha_{tk} - 1)}{[(\alpha_{fk} - 1)^2 + (\alpha_{tk} - 1)^2]^{\frac{1}{2}}}$$

Where " α_{fk} " is the "form factor for surface notches" and " α_{tk} " is the "form factor for deep notches" with

$$\alpha_{tk} = 1.87 \text{ and}$$

$$\begin{aligned} \alpha_{fk} &= 1 + 2 \left(\frac{t}{\rho} \right)^{\frac{1}{2}} \\ &= 1 + 2 \left(\frac{0.090}{0.059} \right)^{\frac{1}{2}} = 3.48 \end{aligned}$$

Then

$$K_t = 1 + \frac{(3.48 - 1)(1.87 - 1)}{[(3.48 - 1)^2 + (1.87 - 1)^2]^{\frac{1}{2}}}$$

$$= 1.82 \text{ or the same } K_t \text{ value as for the endurance bar.}$$

However, several values of ("ρ") were assumed before the value

used in this explanation was found to give the correct value of K_t .

The average stress concentration factor of the tensile bars was 1.85. The variation from this figure, due to small differences in machining the notch, ranged 1.84 to 1.86.

ACKNOWLEDGMENT

The steel used in this project was furnished by the Laboratories of the Climax Molybdenum Company of Michigan. The tempering of all bars and the testing of the Charpy impact specimens were also carried on in their Laboratories. All fatigue testing was done by the Metallurgical Department of the Chrysler Corporation.

References

1. R. H. Greaves, "Temper Brittleness of Nickel-Chrome Steel", *Journal, Iron and Steel Institute*, Vol. 100, 1919, p. 329.
2. R. H. Greaves, M. Fell and Sir R. Hadfield, "Further Communication of Temper Brittleness of Nickel-Chrome Steel", *Journal, Iron and Steel Institute*, Vol. 100, 1919, p. 340.
3. R. H. Greaves and J. J. A. Jones, "Temper Brittleness of Nickel Chromium Steels", *Journal, Iron and Steel Institute*, Vol. 102, 1920, p. 171.
4. R. H. Greaves and J. J. A. Jones, "Temper Brittleness of Steel; Susceptibility to Temper Brittleness in Relation to Chemical Composition", *Journal, Iron and Steel Institute*, Vol. 111, 1925, p. 231.
5. H. J. Gough, *Staffordshire Iron and Steel Institute*, 1934-35, Vol. 50, p. 97.
6. J. H. Hollomon and L. D. Jaffe, "Ferrous Metallurgical Design", John Wiley, 1947, p. 166.
7. H. B. Wishart and S. W. Lyon, "Effect of Overload on the Fatigue Properties of Several Steels at Low Temperature", *TRANSACTIONS, American Society for Metals*, Vol. 25, 1937, p. 640.
8. D. O. Morris, "Composition and Physical Properties of Steel in Relation to Fatigue", *The Failure of Metals by Fatigue*, Melbourne University Press, 1946.
9. H. W. Gillett, "Impact Resistance and Tensile Properties of Metals at Sub-Atmospheric Temperatures", Special Technical Publication No. 47, American Society for Testing Materials, August 1941.
10. M. F. Garwood, H. H. Zurburg and M. A. Erickson, "Correlation of Laboratory Tests and Service Performance", *Interpretation of Tests and Correlation With Service*, published by American Society for Metals, 1951, p. 1.
11. W. E. Jominy, "Present Day Approach to the Choice and Application of Automotive Steels", Society of Automotive Engineers, Preprint 101, January 1948.
12. J. R. Strohm and W. E. Jominy, "High Forging Temperatures Revealed by Facets in Fracture Tests", *TRANSACTIONS, American Society for Metals*, Vol. 36, 1946, p. 543.
13. J. H. Hollomon, "Temper Brittleness", *TRANSACTIONS, American Society for Metals*, Vol. 36, 1946, p. 473.
14. H. Neuber, "Theory of Notch Stresses", J. W. Edwards, Ann Arbor, Michigan, 1946.
15. R. E. Peterson, "Methods of Correlating Data From Fatigue Tests of Stress Concentration Specimens", Stephen Timoshenko 60th Anniversary Volume, Macmillan Company, 1938.

DISCUSSION

Written Discussion: By H. B. Knowlton, chief engineer, Materials Engineering, International Harvester Co., Chicago.

We are very glad that the authors of this paper have made an investigation of the effect of temper brittleness upon fatigue failures of both notched and unnotched specimens. And we are glad that their research investigation has confirmed our rather hazy field experience that steels, which show a considerable degree of temper brittleness, may not cause any trouble with parts which fail only in fatigue in a ductile manner. There is undoubtedly a minimum toughness which is necessary to prevent brittle failure of any given production part. However, this minimum toughness may be considerably lower than is frequently expected. For example, it is found that the cold notch toughness of certain automotive spring steels may be quite low, and yet these steels have stood up very satisfactorily in subzero service for many years before we started making the cold notch toughness test.

In this connection, it has been noted that Boegehold and Dolan working independently have found that slack quenching may reduce fatigue strength slightly, but not nearly so much as will be indicated from the results of notch toughness tests. Some work currently going on with cold drawn steels also indicates that the notch toughness test is not a good criterion for fatigue strength of even parts containing small fillets.

There seems to be very little definitely known about the mechanism of the origin of fatigue failures at the present time. We are tempted to hazard a guess that it will sometimes be found that fatigue failures of any parts containing commercial fillets do not originate within a single crystal irrespective of the strength and other properties of adjacent crystals. It seems quite probable that a considerable deformation of the weak crystal must take place before the fatigue rupture occurs. If the adjacent crystals are considerably stronger than the weakest crystal, is it not possible that they may strengthen the entire area beneath the fillet, and prevent sufficient deformations to cause origin of fatigue? The tendency of the notch impact test, and of ballistic tests, is to concentrate the stress on a single crystal and consequently may account for the differences obtained with notch impact, and notch fatigue tests.

Written Discussion: By Harry Majors, Jr., lead engineer, California Research and Development Co., Livermore, Calif.

Upon reading this paper carefully several questions have arisen which are not apparent from the text but which could be handled best by discussion. In any event it is gratifying to note in this paper on properties of SAE 5140 steel an attempt to give several properties so that in future discussion of general behavior of materials all assertions will be compatible with carefully performed experiments. It is worth noting that Neuber's work on notches is a theoretical analysis based upon well-known assumptions in the theory of elasticity. In the reference list, mechanical engineers, theoretical men and metallurgists have contributed to our sum total of knowledge on temper brittleness.

Is there any indication from observations of the microstructure that

would show the difference between an embrittled and unembrittled steel as related to the mechanical properties?

Although it was not pertinent to the authors' objective, it would have been valuable to have shown the curves of impact energy versus temperature and percentage of fibrous fracture.

Is it possible for the authors to present the endurance curves in order that the amount of "scatter" can be compared with the very great care used in preparing the fatigue specimens? What care was used in preparing the impact specimens?

When the Moore-type machine is placed in a cold room it was inferred that no difficulty was experienced. Any further details on this procedure would be enlightening.

Would the authors hazard a guess as to the amount of residual stress in the embrittled and unembrittled material?

Authors' Reply

The authors wish to thank Messrs. Knowlton and Majors for their discussion of this paper. Mr. Knowlton brings out a very excellent point in his discussion as to just how ductility is needed in a part that is in fatigue. This question needs considerable metallurgical investigation to add to our knowledge of ductility. We believe that there is a certain threshold value for ductility but are unable to give limits. As our knowledge on this subject increases we are able to come closer to actual limitations and our thinking is that this value is lower than we had generally believed. From our data it is apparently below 20 foot-pounds of impact.

We have been told of a crankshaft for an aircraft engine which performed satisfactorily although the steel from which it was made had an Izod impact strength of 4 foot-pounds. Service and stress is involved in this consideration, for we know that some diesel engines successfully use high strength cast iron whose impact strength is less than 1 foot-pound. As for his description of the mechanism of fatigue, such a condition could very well exist.

It has been observed, as Mr. Knowlton says, that slack quenching reduces the endurance limit for a given hardness level. This reduction we believe is due to the presence of weaker pearlite grains among the tempered martensite grains. We agree with Mr. Knowlton that the stronger martensite grains, if in sufficient quantity, help to produce an endurance limit that is higher than would have been obtained with all pearlite grains.

In reply to Mr. Majors' questions, no differences were noted in the microstructure of the embrittled and nonembrittled samples under the optical microscope and using known etching reagents including zephiran chloride for temper brittleness. Some work was likewise done on the electron microscope but no conclusive results were reached. We agree with Mr. Majors that it would have been desirable to present the complete curve of temperature versus impact. Two of the curves involved, however, may be found in Ref. 11. To save space in the paper, the S-N curves were not presented. However, very good curves were obtained with our endurance specimens, resulting in very little scatter. More scatter resulted when

the specimens were tested in the cold room. As for the preparation of the Moore machines for the cold room, several modifications had to be made as indicated on the eighth page of our paper. Further details which might be of interest were that the ball-bearing housings and felt packing were washed and degreased and then saturated with special sub-zero oil. Likewise, the gaps on the microswitches were enlarged to prevent stopping the machines as a result of a frost buildup. The R. R. Moore machines were also re-wired to prevent shorting.

A tungsten carbide milling cutter of proper radius was used in machining impact specimens. In developing this method, it was found that further honing and polishing with emery gave no improvement.

It is exceedingly difficult to give anything worthwhile on the residual stresses of our test specimens without a rather comprehensive examination. Whatever the residual stress pattern, the results of endurance tests seem to be consistent in showing no relationship with notched impact.

THE EFFECT OF VARIOUS HEAT TREATING CYCLES UPON TEMPER BRITTLINESS

BY L. D. JAFFE, D. C. BUFFUM AND F. L. CARR

Abstract

Material from one heat of SAE 3140 steel was quenched and tempered. Portions were subjected to twenty different temper embrittlement cycles involving slow and rapid heating and cooling, with and without isothermal holding at one temperature. The temperature of transition from tough to brittle fracture in the V-notch Charpy test was determined after each treatment. The increase in transition temperature produced by a treatment was considered a measure of the degree of embrittlement caused by the treatment. Cooling to room temperature between tempering and isothermal embrittlement treatments did not affect the resulting embrittlement. Embrittlement developed more rapidly on continuous cooling than during isothermal holding at any temperature. When several embrittlement treatments were applied to the same specimens, each contributed to the embrittlement, but the combined effect was often less than the sum of the effects of the individual treatments applied separately.

MUCH WORK has been done on the effect of isothermal embrittling treatments and of furnace-cool embrittling treatments upon the temperature of transition from tough to brittle fracture of steels susceptible to temper brittleness. There has been little study of the degree of embrittlement, as indicated by transition temperature, developed by other heating and cooling cycles.

The purpose of this investigation was to study the effect of various heating, holding, and cooling cycles, in the ferrite range, upon the transition temperature of a susceptible steel.

EXPERIMENTAL WORK

Previous work at this laboratory (1-7)¹ indicated that SAE 3140 steel was well suited for the study of temper brittleness. A heat of SAE 3140 steel studied in the previous investigations was used in this one. This material was in the form of hot-rolled barstock

¹The figures appearing in parentheses pertain to the references appended to this paper.

A paper presented before the Thirty-fourth Annual Convention of the Society, held in Philadelphia, October 18 to 24, 1952. Of the authors, L. D. Jaffe and D. C. Buffum are associated with the Watertown Arsenal Laboratory, Watertown, Mass., and F. L. Carr is associated with National Research Corp., Cambridge, Mass. Manuscript received April 10, 1952.

5/8 inch in diameter and had the following composition (in per cent):

C	Mn	Si	S	P	Ni	Cr	Mo	V	N
0.39	0.79	0.30	0.028	0.015	1.26	0.77	0.02	<0.01	0.006

The barstock was cut into specimen blanks 2-3/16 inches long. These blanks were austenitized at 900 °C (1650 °F) for 1 hour and water-quenched, then tempered 1 hour at 675 °C (1245 °F). [This tempering temperature was the highest which could be safely used without exceeding the A_{e1} temperature (3).] The blanks were then divided into 20 groups of 12 blanks each. These were further heat treated as indicated in Table I. The isothermal embrittling temperature of 500 °C

Table I
Summary of Heat Treatment and Results
All Specimens Austenitized 1 Hour at 900 °C (1650 °F), Water-Quenched,
and Tempered 1 Hour at 675 °C (1245 °F)

Group	Cooling From Temper	Heating Method	Embrittling Treatment			Hardness Rockwell C	Transition Temp. °C
			Temp. °C	Time Hours	Cooling		
1	Water-quenched	24	-80
2	17°C/hr to RT*	22	-10
3	Water-quenched	Salt at	500	1	Water-quenched	22	-65
4	Water-quenched	Salt at	500	1	17°/hr to RT	22½	-55
5	Water-quenched	Salt at	500	48	Water-quenched	23½	0
6	Water-quenched	Salt at	500	48	17°/hr to RT	23½	+20
7	Water-quenched	17°/hr to	500	1	Water-quenched	24	-65
8	Water-quenched	17°/hr to	500	1	17°/hr to RT	23	-40
9	Water-quenched	17°/hr to	500	48	Water-quenched	23	+15
10	Water-quenched	17°/hr to	500	48	17°/hr to RT	23	+25
11	Salt at 500°C	0	17°/hr to RT	23	-55
12	Salt at 500°C	500	1	Water-quenched	22½	-65
13	Salt at 500°C	500	1	17°/hr to RT	23½	-50
14	Salt at 500°C	500	48	Water-quenched	24	+5
15	Salt at 500°C	500	48	17°/hr to RT	24	+25
16	17°/hr to 500°C	0	Water-quenched	20½	-20
17	17°/hr to 500°C	500	1	Water-quenched	22	-25
18	17°/hr to 500°C	500	1	17°/hr to RT	21½	-5
19	17°/hr to 500°C	500	48	Water-quenched	22	+20
20	17°/hr to 500°C	500	48	17°/hr to RT	22½	+35

*Room temperature.

(930 °F) is the temperature at which embrittlement would most rapidly develop, as previously determined (3). The microstructure produced by these treatments was tempered martensite. Metallographic examination of specimens in the quenched condition showed no visible undissolved carbide and an ASTM austenitic grain size of 8.

After heat treating, each group of blanks was machined into standard V-notched Charpy specimens. Four Rockwell C hardness readings were taken on each specimen. The groups were then broken over a range of temperatures on a 217 foot-pound Charpy machine with a striking velocity of 16.8 feet per second. The impact energy and per cent fibrous fracture² are presented graphically as functions

²The per cent fibrous was estimated by examining the fractured surface with the unaided eye or at a magnification of not more than 24 times.

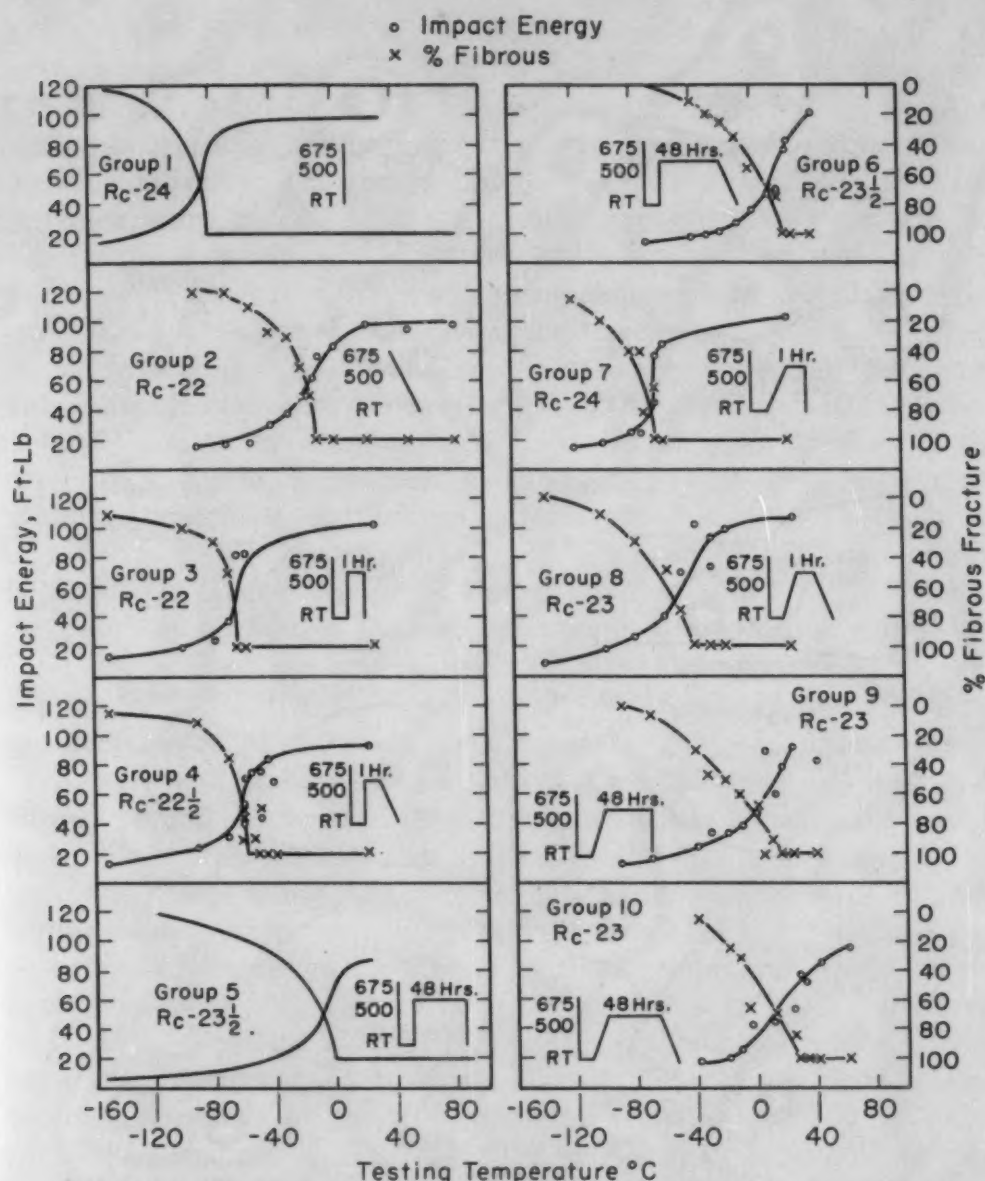


Fig. 1—Transition Curves for SAE 3140 Cooled to Room Temperature After Tempering. Groups held 1 hour at 900 °C (1650 °F), water-quenched, tempered 1 hour at 675 °C (1245 °F) then treated as indicated schematically above. Curves for Groups 1 and 5 based on large number of data points from this and previous work (3-7).

of testing temperature in Figs. 1 and 2.

In Table I are tabulated, for each group, the average Rockwell C hardness and the transition temperature, taken as the lowest temperature at which the fracture is 100% fibrous on the per cent fibrous fracture versus testing temperature curve.

DISCUSSION

Comparing the results of treatments involving quenching directly from the temper to the embrittling temperature, with those of the corresponding treatments involving quenching to room temperature and reheating rapidly, the transition temperatures are in all cases the

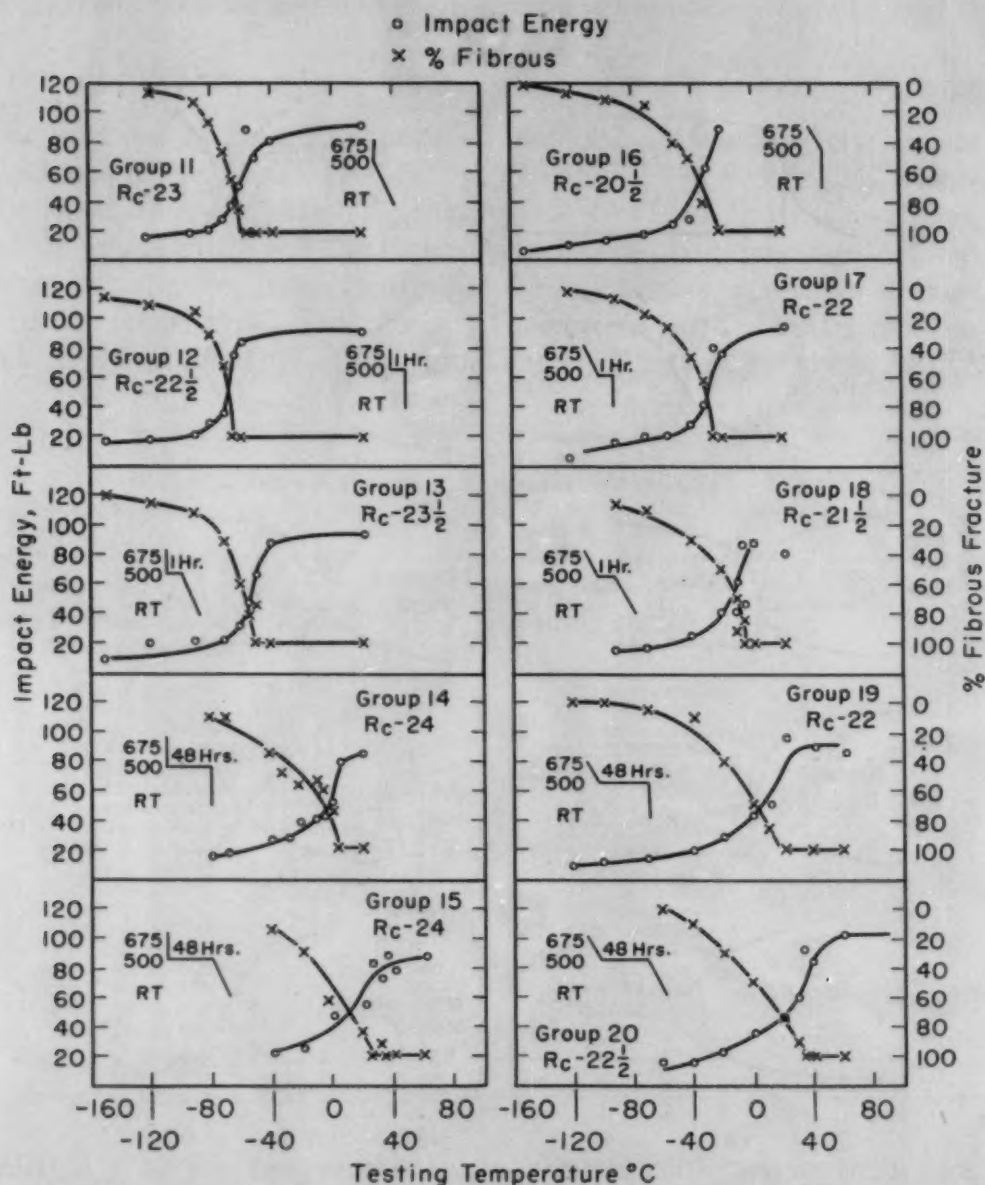


Fig. 2—Transition Curves for SAE 3140 Not Cooled to Room Temperature After Tempering. Groups held 1 hour at 900 °C (1650 °F), water-quenched, tempered 1 hour at 675 °C (1245 °F) then treated as indicated schematically above.

same within 5 °C (groups 12-15 versus groups 3-6 respectively). As the precision of the transition temperature determinations is about ± 5 °C, the cooling to room temperature between temper and embrittling treatment had no significant effect.

For convenience, the increase in transition temperature produced by a given treatment will be referred to as the "transition temperature increase" or "T. T. I." for the treatment, and used as a measure of embrittlement. Slow heating at 17 °C per hour from room temperature to 500 °C (930 °F) introduced a T.T.I. averaging 10 °C (groups 7-10 compared with groups 3-6). Slow cooling at the same rate from

500 °C (930 °F) to room temperature produced a T. T. I. of 15 °C, on the average (groups 4, 6, 8, 10, 11, 13, 15, 2, 18, 20, versus groups 3, 5, 7, 9, 1, 12, 14, 16, 17, 19 respectively). The effects of slow heating and of slow cooling over this range are thus the same within experimental error. It should not be assumed that this is true for all temperature ranges, however. Pellini and Queneau's results (8) indicate the contrary, and it would hardly be expected, for example, that slow heating to a high tempering temperature would give the same T. T. I. as slow cooling from the temper.

Slow cooling at 17 °C per hour from the temper to the isothermal embrittling temperature produced a T. T. I. averaging 50 °C, when the transition temperature without the slow cool was -50 °C or lower (groups 1, 12, 11, 13 compared to groups 16, 17, 2, 18 respectively). When the transition temperature without this slow cool was +5 °C or higher, the T. T. I. averaged only 15 °C (groups 14, 15 vs. groups 19 and 20). There was some suggestion that the T. T. I. became progressively smaller as the transition temperature (without the slow cool) rose. Thus, for transition temperatures of -80, -65, -55, -50, +5 and +25 °C, the T. T. I. was 60, 40, 45, 45, 15 and 10 °C respectively (groups in order given above). It would appear that a fixed treatment induces less additional embrittlement in specimens already severely embrittled than in specimens not embrittled. This is in line with the finding that during isothermal embrittlement the transition temperature varies, roughly, as the logarithm of the embrittling time, rather than linearly with time (3-5).

Slow cooling from the temper to room temperature at 17 °C per hour introduced a T. T. I. of 70 °C (group 2 vs. group 1), in agreement with previous work (3-4). This value also equals, within experimental error, the sum of the T. T. I. (50 °C) produced by slow cooling previously unembrittled material from 675 to 500 °C (1245 to 930 °F) and the T. T. I. (15 °C) produced by slow cooling from 500 °C (930 °F) to room temperature. Most of the embrittlement on the slow cool from the temper to room temperature evidently developed above 500 °C (930 °F). Apparently this is not due to the steel already being severely embrittled by the time it is cooled to 500 °C (930 °F), as a slow cool from 500 °C (930 °F) to room temperature never gave a T. T. I. of more than 25 °C. The data of Pellini and Queneau (8) also indicate that most of the embrittlement on continuous cooling from the tempering temperature arises above 500 °C (930 °F); Hultgren and Chang (9) reported all the embrittlement developed above 500 °C (930 °F).

An isothermal hold of 1 hour at 500 °C (930 °F) produced a T. T. I. of 15 °C, for material with a previous transition temperature of -80 °C (group 12 vs. group 1). This agrees with previous work (3). For material with a prior transition temperature of -55 °C or

higher, the T. T. I. was zero, within experimental error (groups 13, 17, 18 compared to groups 11, 16, 2 respectively).

A 48-hour hold at 500 °C (930 °F) introduced a T. T. I. of 80 °C, when the prior transition temperature was -55 °C or lower (groups 14, 15 versus groups 1, 11). This too agrees with previous work (3, 5, 6). When the prior transition temperature was -20 °C or higher, the T. T. I. was only about 40 °C (groups 19, 20 versus groups 16, 2 respectively). For three treatments, therefore, material otherwise having a transition temperature above about -50 °C showed less T. T. I. than steel whose transition temperature (without these treatments) was below about -50 °C.

For some treatments, data are available for 1-hour and for 48-hour holds at 500 °C, but no comparable data are available for zero hold. Between 1 hour and 48 hours the T. T. I. averaged 70 °C (groups 9, 10 versus groups 7, 8). This checks both with the previous results (3) and with the values cited above for 1- and 48-hour holds, starting with low transition temperatures.

The maximum embrittlement of any group was that of group 20, which had a transition temperature of +35 °C. This group was cooled at 17 °C per hour from 675 °C to 500 °C (1245 to 930 °F), held 48 hours at 500 °C (930 °F), and cooled at 17 °C per hour to room temperature, making the total time of treatment about 86 hours. For comparison, the highest transition temperature developed by isothermal holding up to 240 hours was +25 °C (produced by a 240-hour hold at 500 °C) (3). Embrittlement thus takes place more rapidly in treatments involving continuous cooling than it does isothermally at any temperature. This strengthens a conclusion reached earlier for the same heat of steel (3). Pellini and Queneau reported a similar finding for a different heat, but on a third heat they state "the times and temperatures required to develop temper brittleness were approximately the same whether embrittlement was induced isothermally or on continuous cooling" (8).

Transition temperatures in all cases agreed with previously published results for the same heat treatment within 5 °C (groups 1, 2, 3, 5) (3-6).

CONCLUSIONS

1. Quenching to room temperature between tempering and isothermal temper embrittlement treatments had no significant effect upon the resulting embrittlement.
2. Slow heating to the isothermal embrittlement temperature of 500 °C (930 °F) introduced the same amount of embrittlement as slow cooling from this temperature, within experimental error. This conclusion may not apply to other temperatures.
3. Most of the embrittlement produced by slow cooling from the

tempering temperature of 675 °C (1245 °F) developed above 500 °C (930 °F).

4. For the heat investigated, embrittlement developed more rapidly in treatments involving continuous cooling than during isothermal holding at any temperature.

5. When several embrittlement treatments were applied successively to the same specimens, each contributed to the embrittlement. When the transition temperature was high, the introduction of an additional embrittlement treatment often did not produce as large an increase in transition temperature as when the prior transition temperature was low.

References

1. D. C. Buffum, "The Effect of Dimensional Changes on Square V-notched Charpy Bars", ASTM Bulletin No. 160, September 1949, p. 45-47.
2. L. D. Jaffe and D. C. Buffum, "Temper Brittleness of Plain Carbon Steels", *Transactions, American Institute of Mining and Metallurgical Engineers*, Vol. 180, 1949, p. 513-518.
3. L. D. Jaffe and D. C. Buffum, "Isothermal Temper Embrittlement", *TRANSACTIONS, American Society for Metals*, Vol. 42, 1950, p. 604-618.
4. D. C. Buffum and L. D. Jaffe, "Effect of Strain Rate on Toughness of Temper-Brittle Steel", *TRANSACTIONS, American Society for Metals*, Vol. 43, 1951, p. 644-650.
5. L. D. Jaffe and D. C. Buffum, "Retrogression of Temper Brittleness", *Revue de Metallurgie*, Vol. 48, 1951, p. 609-612.
6. D. C. Buffum and L. D. Jaffe, "Effect of Hardness on Temper Brittleness", *Transactions, American Institute of Mining and Metallurgical Engineers*, Vol. 191, 1951, p. 540.
7. F. L. Carr, M. Goldman, L. D. Jaffe and D. C. Buffum, "Effect of Hardness on the Level of the Impact Energy Curve for Temper-Brittle and Unembrittled Steel", *American Society for Metals*, Preprint No. 26, 1952.
8. W. S. Pellini and B. R. Queneau, "Development of Temper Brittleness in Alloy Steels", *TRANSACTIONS, American Society for Metals*, Vol. 39, 1947, p. 139-161.
9. R. R. Hultgren and C. Chang, "Investigation on the Temper Brittleness of Steels. Final Report. Effect of Chemical Composition". University of California, Institute of Engineering Research, Report to Office of Naval Research, 15 February 1951.

EFFECT OF HARDNESS ON THE LEVEL OF THE IMPACT ENERGY CURVE FOR TEMPER BRITTLE AND UNEMBRITTLED STEEL

BY FRANK L. CARR, MANUEL GOLDMAN, LEONARD D. JAFFE
AND DONALD C. BUFFUM

Abstract

Specimen blanks of martensitic SAE 3140 steel were tempered for short times at several temperatures between 500 and 675 °C (930 and 1245 °F) to give various hardnesses ranging from Rockwell C-20½ to C-38. Comparisons of energy levels in the V-notched Charpy test were made at 200 °C (390 °F) above the temperature of transition from ductile to brittle failure. The impact energy level, within the hardness range investigated, is approximately 10 ft-lbs higher for the unembrittled than for the embrittled steel. A linear relationship between impact energy level and hardness exists in the hardness range of Rockwell C-27 to at least C-38.

INTRODUCTION

IN THE EARLY research on temper brittleness of steel, measurements were made in terms of energy required to fracture specimens at a fixed temperature of test. In 1943, Jolivet and Vidal (1)¹ pointed out that results so obtained are very difficult to interpret, because they depend upon the relation of the testing temperature to the temperature of transition from tough to brittle fracture. This transition temperature in general was variable and unknown. Since then, investigations have been primarily concerned with the transition temperature as a measure of temper brittleness, rather than with the energy required for fracture.

In the course of work upon transition temperatures (2), it was noted that the energy for fracture of embrittled steel approached a different level than that for unembrittled steel, as the testing temperature was increased above the transition zone. The present work investigates the effects of hardness and temper brittleness upon the level of the energy versus testing temperature curve above the transition.

¹The figures appearing in parentheses pertain to the references appended to this paper.

A paper presented before the Thirty-fourth Annual Convention of the Society, held in Philadelphia, October 18 to 24, 1952. Of the authors, Frank L. Carr is associated with the National Research Corp., Cambridge, Mass., Manuel Goldman with Battelle Memorial Institute, Columbus, Ohio, and Leonard D. Jaffe and Donald C. Buffum with the Watertown Arsenal Laboratory, Watertown, Mass. Manuscript received April 8, 1952.

EXPERIMENTAL

The material used in this investigation was commercial SAE 3140 steel,² hot-rolled 5/8-inch round of the following composition:

C	Mn	Si	S	P	Ni	Cr	Mo	V	N
0.39	0.79	0.30	0.028	0.015	1.26	0.77	0.02	<0.01	0.006

A time-temperature-transformation diagram was available to indicate

- Impact Energy
- Impact Energy, Previous Work²
- ◻ % Fibrous Fracture
- ◻ % Fibrous Fracture, Previous Work²

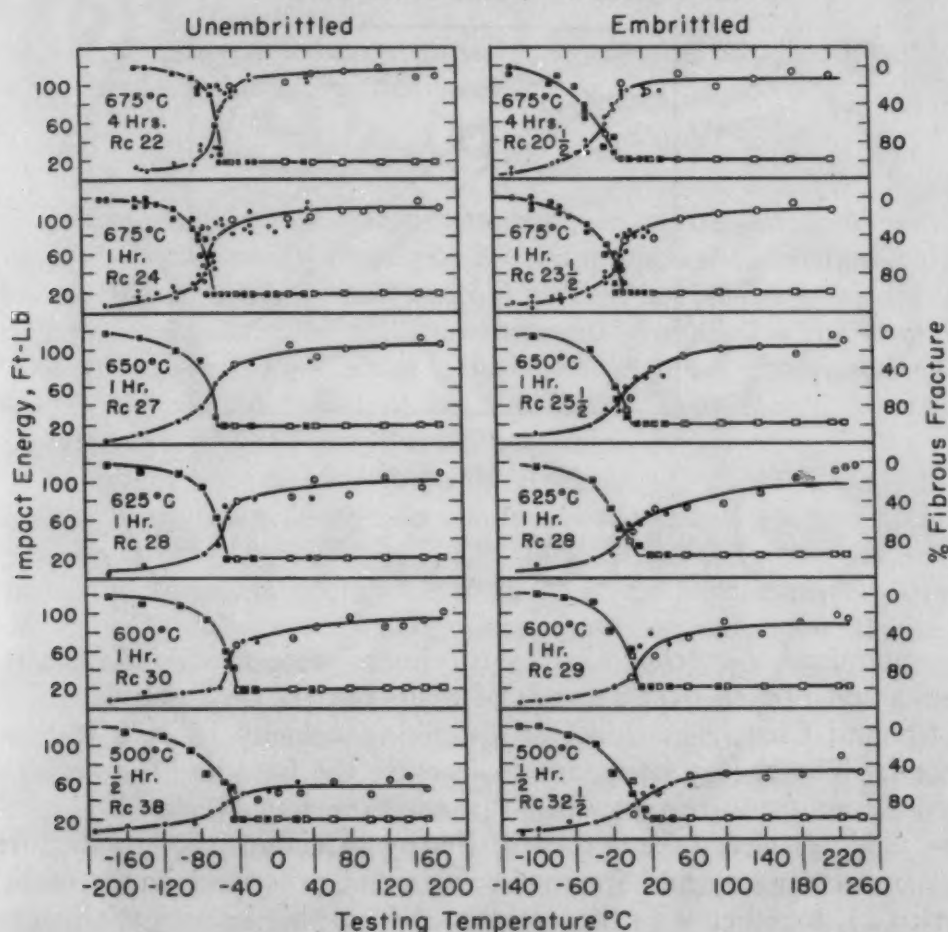


Fig. 1—Impact Energy and Fracture Curves for Tempered Martensitic SAE 3140 Steel of Various Hardnesses.

the extent of temper embrittlement to be expected following a fixed austenitizing and tempering treatment (3). This diagram was used to select tempering treatments that would give variations in hardness and a minimum degree of embrittlement. The A_{e1} temperature for this stock had been determined previously to be approximately 690 °C (1275 °F).

²Other experiments on the same heat have been reported (see References 2, 3, 4, 5 and 6).

Rounds $2\frac{3}{16}$ inches long were cut from the bar stock. They were austenitized 1 hour at 900 °C (1650 °F), and water-quenched to give a microstructure of 100% martensite. Groups of specimens were tempered 4 hours at 675 °C (1245 °F), 1 hour at 675, 650, 625, 600 °C (1245, 1200, 1155, 1110 °F) and 0.5 hour at 500 °C (930 °F). All blanks were quenched in water from the temper. Half of each group was left "unembrittled", the other half was given an embrittling treatment of 48 hours at 500 °C (930 °F) and water-quenched. These treatments were the same as those used in a previous investigation (2).

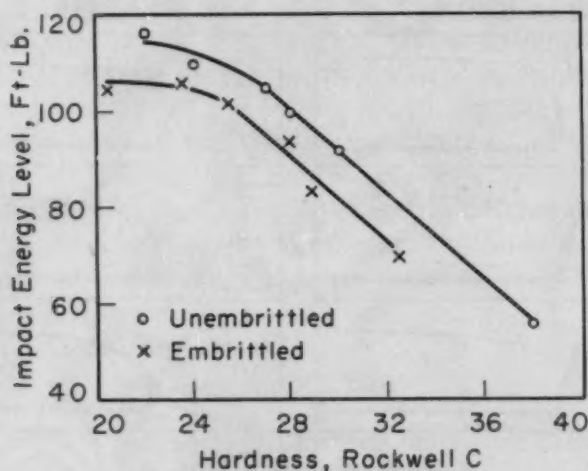


Fig. 2—Impact Energy Level Versus Rockwell C Hardness for Tempered Martensitic SAE 3140 Steel (Energy Level Taken at 200 °C (390 °F) Above the Transition Temperature).

Standard V-notched Charpy specimens were machined from the blanks and broken over a range of temperatures on a standard 217-foot-pound Charpy machine, at a striking velocity of 16.8 feet per second. The energy necessary to fracture the bars and the per cent fibrous fracture were recorded.³ In addition, four Rockwell C hardness readings were taken on each Charpy specimen prior to fracture.

Impact energy and fracture curves, not presented in the earlier work (2), together with those obtained from this investigation, form the composite impact energy and fracture diagram shown in Fig. 1. For the groups of different hardnesses, a comparison of impact energy levels is made at 200 °C (390 °F) above the transition temperature⁴ of each group. This comparison of energy levels is at a temperature well above that at which the impact energy has reached a constant value. Evaluation of the composite impact energy and fracture diagram provides the data listed in Table I. Fig. 2 shows the

³The percentage of fibrous fracture was determined by examining the fractured surface with the unaided eye or at magnification up to 24 diameters.

⁴The transition temperature is taken as the lowest temperature at which the fracture curve is 100% fibrous.

Table I
Impact Energy Level for SAE 3140 Steel of Different Hardness
at 200 °C (390 °F) Above the Transition Temperature

Tempering Treatment	Unembrittled		Embrittled	
	Hardness Rockwell C	Impact Energy Level, Ft-Lbs	Hardness Rockwell C	Impact Energy Level, Ft-Lbs
675 4 Hrs.	22	116	20½	105
675 1 Hr.	24	110	23½	106
650 1 Hr.	27	105	25½	102
625 1 Hr.	28	100	28	94
600 1 Hr.	30	92	29	84
500 ½ Hr.	38	56	32½	70

relationship existing between impact energy level and hardness for temper brittle and unembrittled steel.

RESULTS

Examination of the impact energy versus temperature curves reveals that the energy level generally approaches a constant value upon increasing testing temperature. The lowest temperature at which this constant value appears seems to depend upon the location of the transition from ductile to brittle fracture. Thus, whenever possible, any consideration of impact energy level should be made with reference to this transition temperature.

Within the hardness range of Rockwell C-22 to C-32½ the impact energy level of the temper embrittled steel is consistently below that of the unembrittled SAE 3140 steel of the same hardness, generally differing in energy by 10 ft-lbs. For hardnesses Rockwell C-27 to C-38 the impact energy level is dependent upon hardness and decreases in a linear manner as the hardness is increased. There is a decrease of impact energy of 4½ ft-lbs for an increase of one Rockwell C unit of hardness within this range.

The maximum impact energy versus hardness curves apparently level off above the linear region. This is in all probability due to the limiting (nonlinear) nature of the Rockwell hardness scale, the capacity of the testing machine, and the limit of maximum toughness that may be obtained with SAE 3140 steel.

CONCLUSIONS

1. For steels of the same hardness the impact energy level is higher for the unembrittled than for the temper embrittled material.
2. For the material used in this investigation the difference between energy levels is approximately 10 ft-lbs over the hardness range investigated.
3. A linear relationship between impact energy level and hardness exists in the hardness range of Rockwell C-27 to at least C-38.

ACKNOWLEDGMENT

The authors wish to thank Mr. Irving Preble for the heat treatment of specimens used in this investigation.

References

1. H. Jolivet and G. Vidal, "The Temper Brittleness of Steel", *Comptes Rendus*, Vol. 216, 1943, p. 664.
2. D. C. Buffum and L. D. Jaffe, "Effect of Hardness on Temper Brittleness", *Transactions*, American Institute of Mining and Metallurgical Engineers, Vol. 191, 1951, p. 540.
3. L. D. Jaffe and D. C. Buffum, "Isothermal Temper Embrittlement", *TRANSACTIONS*, American Society for Metals, Vol. 42, 1950, p. 604.
4. L. D. Jaffe and D. C. Buffum, "Temper Brittleness of Plain Carbon Steels", *Transactions*, American Institute of Mining and Metallurgical Engineers, Vol. 180, 1949, p. 513.
5. L. D. Jaffe and D. C. Buffum, "Retrogression of Temper Brittleness", *Revue de Metallurgie*, Vol. 48, 1951, p. 609.
6. D. C. Buffum and L. D. Jaffe, "Effect of Strain Rate on Toughness of Temper Brittle Steel", *TRANSACTIONS*, American Society for Metals, Vol. 43, 1951, p. 644.

DISCUSSION

Written Discussion: By Francis W. Boulger, supervising metallurgist, Battelle Memorial Institute, Columbus, Ohio.

There has been considerable interest recently in the problem of securing consistent Charpy values. The authors are to be congratulated on showing that reproducible results can be obtained on different specimens of the same steel made and tested at different times over a period of several years.

The decrease of 10 foot-pounds in Charpy level, at 200 °C above the transition temperature, resulting from temper brittleness, seems less marked than the difference of 75 °C in transition temperature previously reported as resulting from the same cause. Which method of evaluating the effect of temper brittleness do the authors recommend?

Perhaps the conclusion that a linear relationship exists between hardness and energy values should be restricted to the samples tested, especially since the figure of 4½ foot-pounds per Rockwell C unit is mentioned in the text. Data obtained in our laboratory indicate that this incremental value holds for relatively tough steels. However, steel composition and specimen orientation influence the decrease in energy value corresponding to an increase in hardness level of one Rockwell C unit.

Written Discussion: By E. F. Bailey and J. A. Kies, Naval Research Laboratory, Washington, D. C.

This paper calls attention to an effect of temper brittleness usually disregarded and reminds us that the common definition and the usual standard by which it is measured are highly arbitrary and not intended primarily to provide an understanding of the effects. It would seem that the authors are presently concerned not so much with establishing an empirical guide in which the Charpy test is to be used, for example in pre-

dicting armor performance, as they are in suggesting ways of obtaining insight into causes of brittleness and relations between temper embrittlement and flow and fracture. We would like to ask the authors if they have found relationships for other steels to be as shown in their Fig. 2 for SAE 3140. Charpy tests at the Naval Research Laboratory on SAE 3330 have shown no detectable difference between the energy absorbed in embrittled and unembrittled specimens at equal hardness when broken at temperatures well above the transition. If such a difference is peculiar to certain steels, that fact should be useful in a study of causes associated with composition.

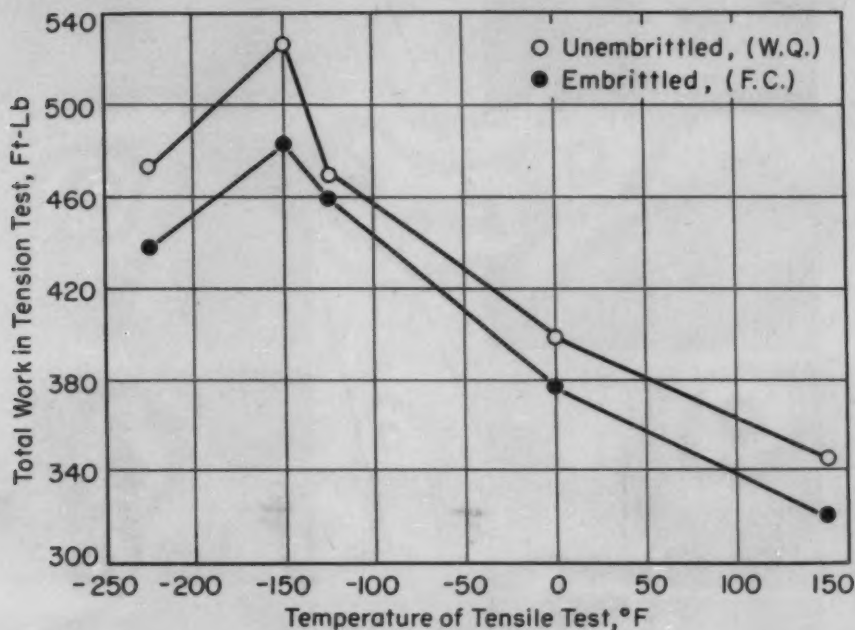


Fig. 3—Effect of Testing Temperature and Degree of Embrittlement on Work to Fracture in Tension.

There is an interesting parallelism between the results of the authors' Fig. 2 and some tensile test results obtained in our laboratory on SAE 3330. In our case all fractures were accompanied by at least 55% reduction of area and therefore could be classed as well above the brittle transition, if such can be said to exist for tensile tests of this material. The hardness at test temperature was not measured, but the yield strength at 0.2% elongation was a linear function of temperature and was the same for embrittled and unembrittled specimens so that the temperature scale shown in Fig. 3 could just as well be replaced by a linear scale of yield strength decreasing from left to right. The yield strength was 116,000 psi at 225 °F and 97,000 psi at +150 °F. The energy absorbed as indicated by the area under the load-extension curves is plotted, therefore, essentially as a function of hardness at the test temperature. The shape of the curves is about the same as in Fig. 2 of the paper, and the energy difference is about constant for the embrittled and nonembrittled specimens. The important difference is that the energy goes just opposite to the Charpy results; that is, it increases at increasing yield strength over most of the range instead of decreasing as in the Charpy tests. This is mentioned

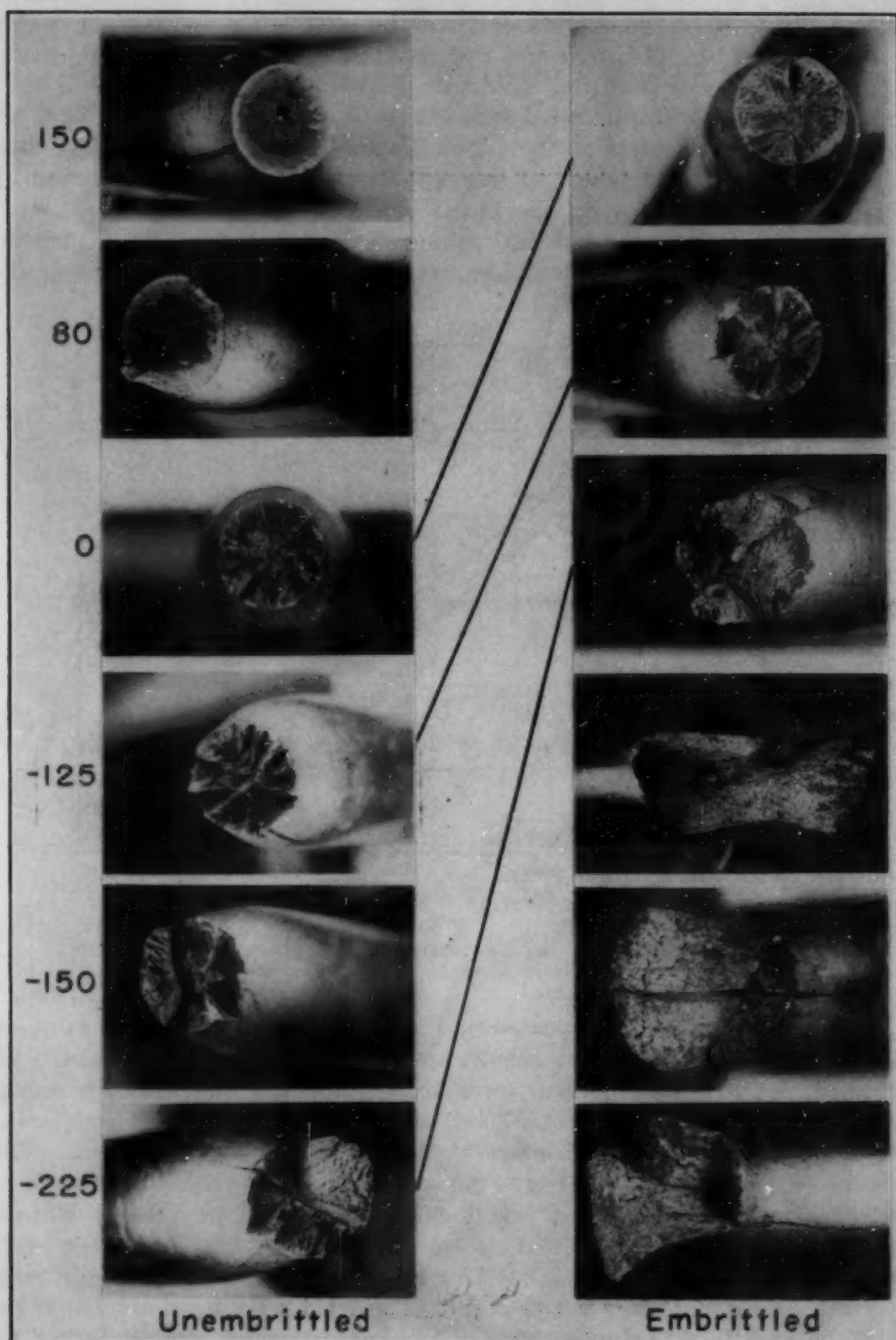


Fig. 4—Tensile Fracture Appearance as a Function of Degree of Embrittlement and Testing Temperature. Connecting lines indicate similar fracture appearance.

because it is thereby obvious that even the practical significance, much less the physical interpretation of energy absorption figures for either the Charpy or the tensile tests, is highly questionable. The energy absorption differences found here and attributed to temper brittleness seem slight in

either case as compared with differences accompanying hardness changes or temperature-imposed yield strength changes. One must conclude from this and other evidence that the reason why spectacular differences, as revealed by shifts in Charpy transition temperature, exist is not that corresponding spectacular differences in the structure or plasticity are produced but that such small changes can markedly shift the point of mechanical instability when the situation is such that extremely fast fracture propagation can feed on the elastic energy of the specimen. Strong evidence for this seems to lie in the observation that the magnitude of the shift in brittle transition temperature and the transition temperature itself are neither one unique, but depend on the mechanical arrangement of the test. The use of a criterion of mechanical instability for the collapse of a specimen or structure by fast fracturing is under investigation at the Naval Research Laboratory and several publications have resulted. The material-dependent aspects of the instability are by no means understood beyond the knowledge that both energy absorption and fracture appearance are dependent on crack velocity in such a way that brittle fracture is ordinarily high speed, and high fracture speed itself restricts plastic flow so that a self-triggering action can result. The physical aspects of fracture will not be understood until effects of crack velocity, strain rate, and loading speed on dW/dA , the work per unit fracture area, are understood.

The striking effect of temper embrittlement on the fracture appearance of tensile bars of SAE 3330 is illustrated in Fig. 4. There is a remarkable similarity or rather equality between the fracture appearance in embrittled and unembrittled specimens, provided bars associated with the right temperature difference are compared. This temperature shift to obtain equal fracture appearance is quite large, amounting to 150 °F at one end of the scale and becoming 225 °F for the embrittled bar broken at 0 °F. It is not known whether it is possible to obtain equality in appearance for all of the specimens of the series. Referring back to Fig. 3 one can see that a given fracture appearance is not associated with a definite energy absorption; for example, the furnace-cooled specimen broken at 150 °F looked just like the water-quenched specimen broken at 0 °F, whereas the respective work values were 320 and 395 foot-pounds. Similarly the furnace-cooled specimen broken at 0 °F looked just like the water-quenched specimen broken at -225 °F; however, the work values were quite different, 375 and 475 foot-pounds respectively. Thus spectacular differences due to temper embrittlement can be found in the tensile test as well as in the Charpy test.

Another feature of the fracture appearance not visible in these photographs was the presence of fine ball-and-socket type of shiny surface elements like those prominently and abundantly found on cast steel and on aluminum alloy castings. These may be intergranular or along dendritic boundaries or lineages wherein brittle constituents are concentrated. The interesting point here is that such surfaces in our SAE 3330 steel fractures are not exclusively associated with temper brittleness but like the gross features can be made to correspond in the embrittled and unembrittled samples by matching up specimens tested at sufficiently different temperatures.

One must conclude from these tensile results that a slight energy

difference does exist between embrittled and unembrittled steels which oddly enough is not dependent on the temperature of the test. Fracture appearance greatly magnifies the differences between the embrittled and unembrittled conditions, along with the density of micro-fracture sources. The similarity of fracture appearances suggests that a lesser degree of temper embrittlement occurred in the "unembrittled" condition.

Authors' Reply

In reply to the question raised by Mr. Boulger, we believe that the transition temperature is still the best criterion for comparing Charpy impact data. It should be added, however, that there is great need for a criterion that will make a more quantitative comparison possible.

Messrs. Bailey and Kies ask if the relationship discussed in the paper has been noted on other steels. In a study made by the authors on plain carbon steel it also appeared that the energy level above the transition was higher in the unembrittled condition (4).

With regard to the work on SAE 3330, it would be worthwhile for the Messrs. Bailey and Kies to publish further details regarding the heat treatment and design of the test specimen, so that their work can be properly evaluated. It should be explained that the hardness values in Fig. 2 of the paper were all measured at room temperature; accordingly, Fig. 3 cannot be readily compared to Fig. 2.

In general, we concur with the remaining comments of the discussers.

CORRELATION OF MACHINABILITY WITH INCLUSION CHARACTERISTICS IN RESULPHURIZED BESSEMER STEELS

By LAWRENCE H. VAN VLACK

Abstract

Some of the factors affecting shapes and sizes of inclusions in rolled resulphurized steels are examined. These inclusion characteristics are governed by (a) the silicon content of the steel, (b) the sulphur content of the steel, (c) the mechanical working which the steel receives, and (d) possibly by the oxygen content of the sulphide phase.

These characteristics, in turn, influence the machinability of the steels when other metallurgical factors are equal.

IN DISCUSSING the effects of sulphur upon the machinability of wrought metals in 1938, Knowlton (1)¹ observed that it is more desirable to have the sulphide phase in a "lumpy" form. More recent studies at Battelle and within the United States Steel Company (2) have reinforced that observation. It was noted (2) that steels of higher silicon contents, which possessed lower machinability index ratings, had more "plastic"-type inclusions. Conversely, steels with high machinability indices had "globular"-type inclusions. In summarizing a large number of machinability data from commercial blows of B-1113 steel, it was concluded that optimum machinability was obtained when the inclusions were predominantly globular in shape. The inclusion shapes were rated as "plastic" or "globular" by making a comparison of those observed in a microsection with standardized charts. Where necessary, the shapes were further divided as "mostly globular, some plastic" or "mostly plastic, some globular".

An effort is made in this study to more firmly establish the relationship between the inclusion's characteristics and machinability of resulphurized steels. A more quantitative measure of shape, the length/width ratio, was used. Preliminary work also indicated that not only the shape but also the number of the inclusions was related to the silicon content and to the machinability. The number of inclusions was more easily determined than the shape, and was subject to fewer statistical errors. Therefore, that variable was also investigated.

¹The figures appearing in parentheses pertain to the references appended to this paper.

A paper presented before the Thirty-fourth Annual Convention of the Society, held in Philadelphia, October 18 to 24, 1952. The author, Lawrence H. Van Vlack, is process metallurgist, United States Steel Company, Pittsburgh. Manuscript received April 10, 1952.

EXPERIMENTAL PROCEDURE

Samples—Samples used for inclusion determinations were those previously used for machinability studies. The steels in one series were B-1112 steels which had had varying amounts of oxygen and silicon added (2). The ingot and billet identifications were maintained during rolling. A second series was from bars selected randomly from B-1113 heats for machinability tests.

The metal analyses used were the check analyses on the bars obtained for the machinability index ratings. Oxygen was determined by vacuum fusion analyses on samples from the same bars or from the samples used for microscopic examination. The data are summarized in Table I.

Table I
Machinability Data—B-1112 Controlled Heat

Ingot-Billet	Chemical Analyses—%						Incl/mm ²	L/W	Mach. Index	Remarks
	C	Mn	P	S	Si	O				
1- 5	0.06	0.94	0.10	0.20	0.009	0.011	82	3.7	185	O ₂ added
1-10	0.05	0.99	0.09	0.19	0.025	0.028	112	4.1	138	O ₂ added
2- 5	0.05	0.91	0.09	0.20	0.007	0.014	96	3.2	181	Roll scale
2-10	0.06	0.95	0.09	0.19	0.018	0.025	147	3.5	135	added
3- 4	0.06	0.95	0.10	0.20	0.009	0.010	96	2.7	184	No additions
3-10	0.07	0.96	0.09	0.19	0.018	0.027	112	3.9	157	No additions
4- 3	0.06	0.95	0.09	0.20	0.013	0.018	143	8.9	182	Si added
4-10	0.06	0.95	0.09	0.18	0.025	0.019	153	5.1	121	Si added
5- 5	0.06	0.94	0.10	0.20	0.018	0.017	151	5.5	173	Si added
6- 5	0.06	0.95	0.09	0.20	0.025	n.d.	190	7.2	161	Si added
7- 5	0.06	0.94	0.09	0.20	0.029	0.015	190	5.8	145	Si added
8- 5	0.06	0.94	0.09	0.20	0.037	n.d.	200	10.2	143	Si added
9- 5	0.07	0.94	0.09	0.20	0.044	0.017	258	13.4	132	Si added
10- 5	0.07	0.94	0.09	0.20	0.009	0.012	118	5.6	185	No additions

Machinability Index Ratings—The machinability index was measured by the constant-pressure lathe test described by Boulger (3). The ratings for the steels indicate the relative cutting speeds when a constant pressure was applied to the tool. They are to be compared with an index of 100 for a standard B-1111 steel. The ratings for the controlled series were made at Battelle Memorial Institute. Those on the randomly selected samples were made at the Duquesne Works and the Research and Development Laboratory of the United States Steel Company.

Shape of Inclusions—The length/width ratios were determined with the aid of an ocular micrometer on the microscope. The maximum width and length of each inclusion were used (Fig. 1). The L/W value for each steel sample is the average of the L/W ratios of at least 25 inclusions selected randomly across the microsection of the steel. To insure randomness in the selection of inclusions for shape measurements, the microscope stage was moved ahead a pre-determined distance *without* observation. Then with observation, the

sample was moved forward to the *next* following inclusion. That inclusion was measured and the process repeated. The increment of distance was chosen so that the full width of the microsection was traversed. It was felt that the above procedure satisfactorily eliminated the human error of selection, and permitted only errors of a statistical origin.

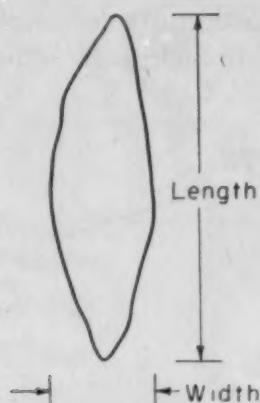


Fig. 1—The Shapes of the Inclusions Were Measured as the Ratio of Their Lengths to Their Widths.

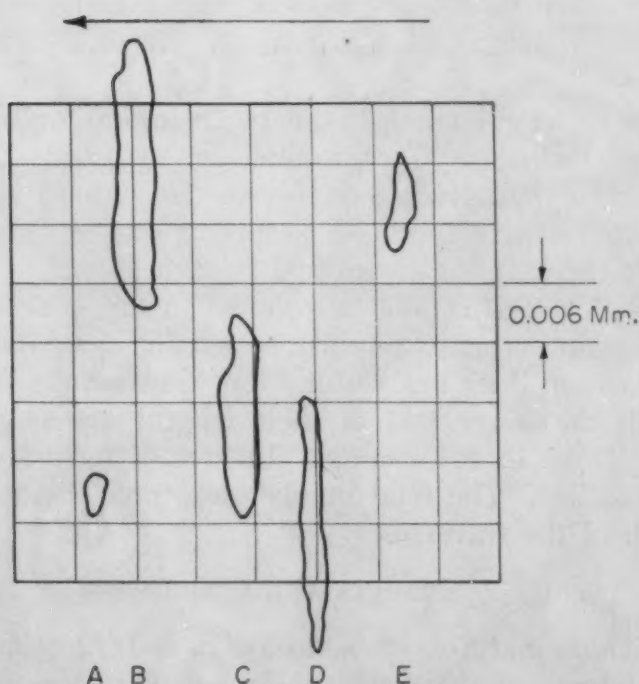


Fig. 2—Diagram of the Technique Used for Counting Inclusions. (See the Text for Explanation.)

Size of Inclusions—The number of inclusions is related to the size of the inclusions for a steel of any given sulphur content, pro-

viding that there is not a change in inclusion volume resulting from major changes in inclusion composition. The number was determined by counting the inclusions observed microscopically in traverses across the full width of the microsection. The total number counted was then converted to "inclusions per square millimeter" for an index of inclusion size.

Fig. 2 illustrates the procedure followed in making the inclusion counts. Since those sulphide inclusions which are greater than 0.005

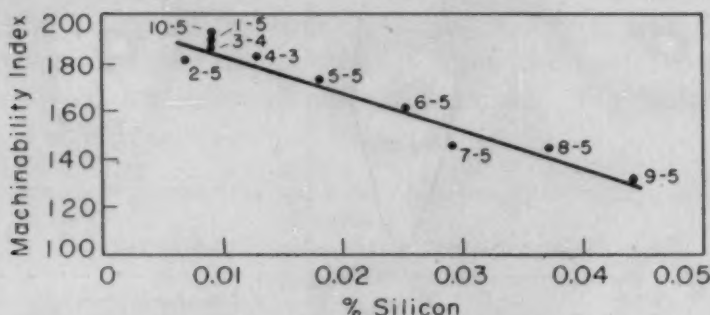


Fig. 3—The Variation of Machinability With Silicon Content (2).

Ingot 1—No silicon added; Ingot 2—No silicon added; Ingot 3—No silicon added; Ingot 4—0.006% silicon added; Ingot 5—0.010% silicon added; Ingot 6—0.013% silicon added; Ingot 7—0.021% silicon added; Ingot 8—0.031% silicon added; Ingot 9—0.042% silicon added; Ingot 10—No silicon added.

(Ingot and billet number indicated. Ten billets per ingot.)

millimeter in length are believed to be important for machinability, only those inclusions 0.006 millimeter or greater in length were counted. The appropriate grid (grain size ocular) and magnification were selected so that the lower size limit was easily measured.

From the samples shown in Fig. 2, it should be noted that both inclusions B and D cannot be counted in the same traverse without introducing an error. One must be left for the adjacent traverse so that duplication does not result. For consistency, only those inclusions with the lower end of their lengths crossing the grid were counted. Thus, in the example illustrated, inclusions B, C and E would be tallied. The total number was then divided by the length and width of the traverse.

RESULTS AND DISCUSSION

The Shape and Size of Inclusions in B-1112 and B-1113 Steels— The dependence of the machinability upon silicon content is shown in Fig. 3. All of these data are from middle positions in successive ingots in one heat. Thus, they represent a series of controlled tests in which all of the variables except silicon have been held essentially constant. Fig. 4 shows the relationship of inclusion shape to the machinability index. As pointed out earlier, the inclusions of smaller

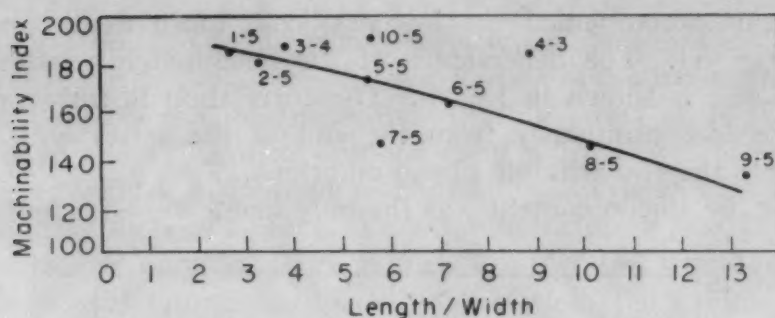


Fig. 4—The Variation of Machinability With Inclusion Shape. (Same steels as in Fig. 3.)

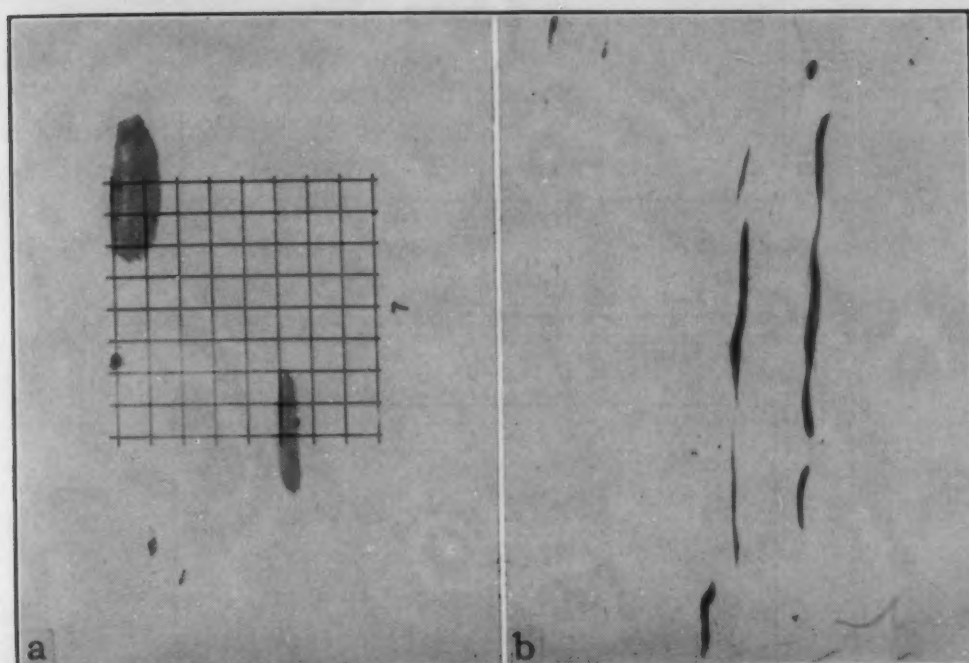


Fig. 5—Sulphide Inclusions in Mid-Ingot Billets.
(a) Ingot 3—Billet 4. No silicon added. (Grid used for inclusion counting.)
(b) Ingot 9—Billet 5. 0.042% silicon added. $\times 600$.

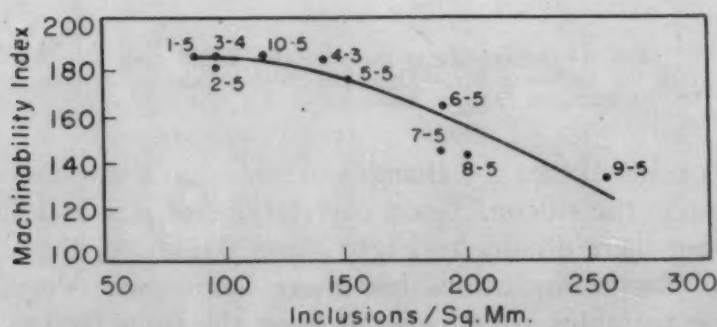


Fig. 6—The Variation of Machinability With Inclusion Count. All of the steels had 0.20% sulphur (Table I). Thus the inclusion count is an inverse index of the inclusion size. (Same steels as in Fig. 3.)

L/W ratios accompanied the lower silicon, more easily machined steels (Fig. 5). The dependence of the machinability index upon inclusion size is shown in Fig. 6. The correlation is rather marked and proceeds continuously from the end of the series with silicon additions to the end without silicon additions.

Since the silicon content was the only factor varied intentionally,

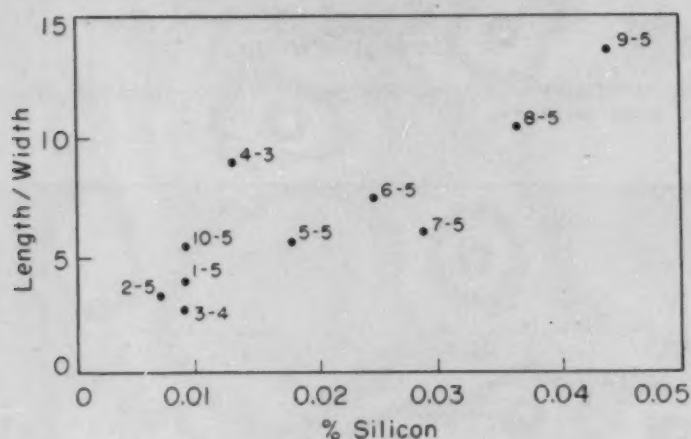


Fig. 7—Dependence of Inclusion Shape Upon the Silicon Content in Controlled Samples. (Same steels as in Fig. 3.)

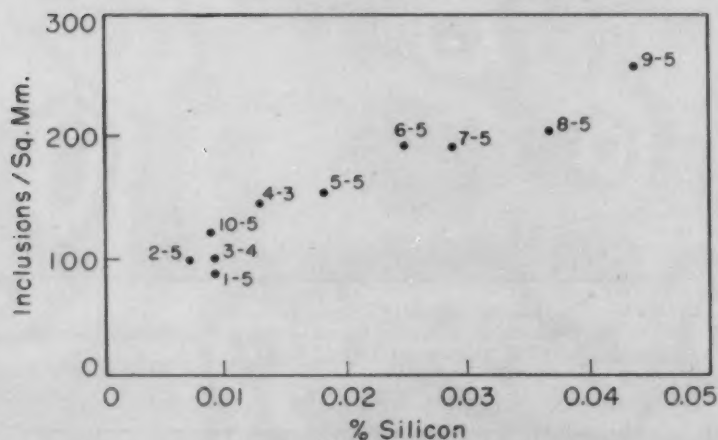


Fig. 8—Dependence of the Inclusion Count (and Therefore the Inclusion Size) Upon the Silicon Content in Controlled Samples. (Same steels as in Fig. 3.)

it must be concluded that the changes in inclusion shape and size were dependent upon the silicon. Good correlations of size and shape with silicon content were obtained (Figs. 7 and 8). Also, the steels with the longer, "plastic" inclusions had more inclusions. Very probably both of these variables are dependent upon the same factors.

The silicon content probably does not affect the machinability index directly. Otherwise, the machinability of other steels would be as sensitive to small variations in the silicon content as the free-

machining steels. The foregoing data would substantiate the suggestion that the silicon affects the distribution of the inclusions, which, in turn, controls the machinability. In this series of B-1112 steels which have almost identical sulphur contents, the presence of fewer, *but larger*, inclusions favored machinability. It would be expected, however, that there is a practical maximum inclusion size, because the extreme case of only one large inclusion in the steel would, of course, produce unsatisfactory machinability results. Some evidence of this expected maximum is indicated by the change in slope of the curve in Fig. 6.

The results described above were obtained from a series of samples which were essentially identical except for their silicon contents. All were from the same heat, and from approximately the same relative positions in successive ingots. Each received the same rolling and cooling treatments. In commercial steels, the above factors are not identical. Consequently, the relationships which have been described will probably show a greater degree of variance in commercial practice. Figs. 9, 10 and 11 show the spread which was observed in twenty-five commercial steels (Table II).

Table II
Machinability Data—Random Samples of B-1113 Steel

Heat	Chemical Analyses—%					Incl/mm ³	L/W	Mach. Index	Remarks
	C	Mn	S	Si	O				
0137	0.08	0.86	0.33	0.004	0.024	102	6.4	189	
0138	0.07	0.95	0.33	0.004	0.018	96	3.7	190	
0243	0.07	0.77	0.28	0.004	0.025	61	3.2	167	
0454	0.08	0.77	0.28	0.005	0.030	56	3.4	198	
0836	0.08	0.95	0.26	0.007	0.023	78	2.7	197	
0847	0.07	0.85	0.29	0.010	0.026	87	5.2	192	
0987	0.10	0.95	0.37	0.004	0.0093	194	7.7	144	Oxygen check 0.0105
01046	0.09	0.77	0.39	0.004	n.d.	n.d.	4.5	217	
01124	0.06	0.74	0.31	0.006	0.033	70	3.3	209	
01481	0.08	0.83	0.29	0.017	0.044	97	4.2	181	
01492	0.08	0.91	0.34	0.005	0.026	124	3.4	195	
03260	0.08	0.85	0.37	0.004	0.014	135	5.7	171	
03604	0.08	0.90	0.30	0.005	0.017	110	4.8	158	
03609	0.09	0.84	0.35	0.004	0.022	104	3.4	169	
03701	0.08	0.81	0.29	0.005	0.033	92	8.0	160	
03872	0.08	0.83	0.33	0.004	0.020	94	5.6	177	
03985	0.08	0.81	0.27	0.004	0.027	65	4.1	186	
04414	0.07	0.86	0.30	0.004	0.026	74	4.8	188	
04482	0.07	0.88	0.32	0.009	0.021	82	4.5	169	
04486	0.08	0.79	0.30	0.029	0.022	300	7.7	134	
04494	0.08	0.90	0.30	0.007	0.048	90	6.4	166	
04840	0.09	0.96	0.26	0.010	0.016	118	4.6	190	
04847	0.09	0.82	0.34	0.008	0.018	157	9.6	160	
04848	0.10	0.89	0.34	0.005	0.013	106	3.7	189	
04849	0.09	0.85	0.31	0.010	0.016	125	2.6	183	
05291	0.08	0.93	0.26	0.010	0.036	n.d.	3.7	171	
05419	0.12	0.92	0.37	0.006	0.024	120	4.7	160	

The machinability showed the closest relationship to the inclusion count (Table III). Because of that fact, it seemed advisable to examine further the various factors, other than silicon, which affect the inclusion count.

Table III
Significance of Factors Affecting Machinability of B-1113 Steel

Correlation	Line of Central Tendency		Stand. Dev. Mach. Index	Coef. of Correlation <i>r</i>
	MI = 150	MI = 190		
Mach. Index vs. Incl/mm ²	Incl/mm ² = 205	Incl/mm ² = 60	± 13	-0.65
Mach. Index vs. L/W	L/W = 9.2	L/W = 2.8	15	-0.60
Mach. Index vs. Si	Si = 0.026	Si = 0	17	-0.40

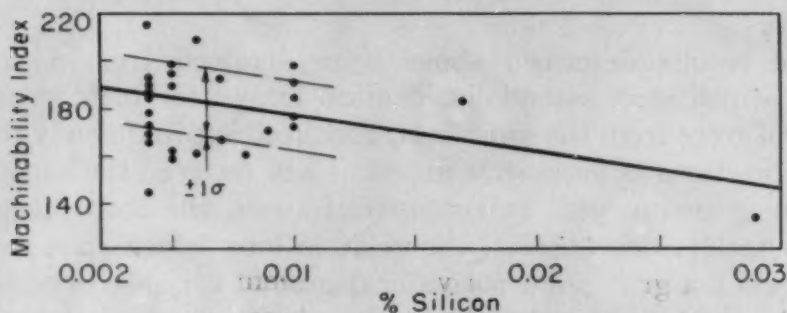


Fig. 9—The Variation of Machinability With Silicon Content for Twenty-Seven Randomly Selected Samples of B-1113 Steel From Commercial Lots. (See Table II.)

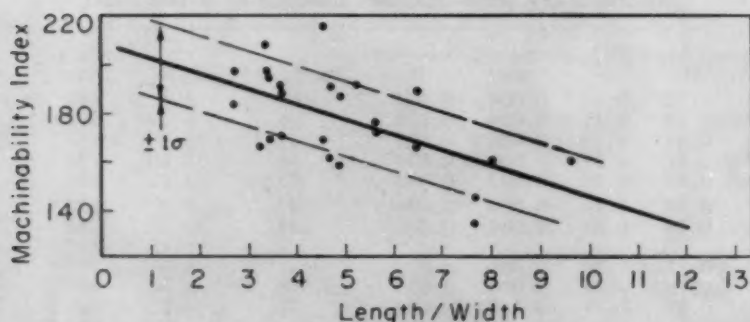


Fig. 10—The Variation of Machinability With Inclusion Shape. (Same samples as in Fig. 9.)

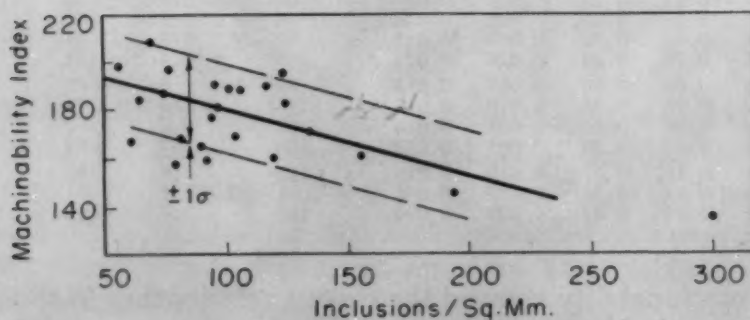


Fig. 11—The Variation of Machinability With Inclusion Count. (Same samples as in Fig. 9. They varied from 0.26 to 0.37% sulphur.)

As might be expected, the number of inclusions observed depends upon the sulphur content. Fig. 12 shows this relationship for twenty-three B-1113 steels. Increased sulphur increases the machinability (2); therefore, it is indicated that a larger number of inclusions resulting from an increased sulphur content improve the machinability, although an increase in the number of inclusions in a steel of a given

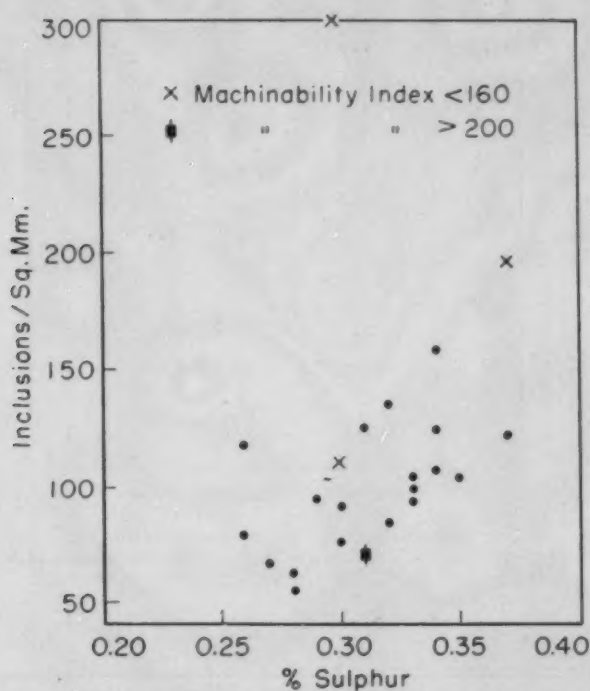


Fig. 12—The Relationship of Inclusion Count to Sulphur Content in Twenty-Three B-1113 Steels.

sulphur content is not to be desired. Fig. 13 shows a schematic representation of this relationship.

An effect of mechanical working upon the size of inclusions in free-machining steels might also be anticipated. Estimates of the size of inclusions, which may be calculated from the inclusion count and length/width ratio, show a reduction as large as 6 to 1 during the hot rolling of $7\frac{7}{8}$ -inch square blooms to $2\frac{1}{2}$ -inch square billets. At high rolling temperatures, the sulphide inclusions are plastically deformed and pinched off. At lower hot rolling temperatures, they are observed to be fractured.

The fracturing and diminution in size of the sulphide inclusions become pronounced in cold working (Fig. 14). The inclusion count in a hot-rolled $\frac{7}{8}$ -inch round was determined to be 85 per square millimeter. When the same steel was further cold drawn to a $\frac{3}{4}$ -inch round, the inclusion count increased to 120 per square millimeter. Since cold working also changed other metallurgical factors, the effect

of the diminution of inclusion size upon machinability was not separately evaluated.

Inclusion Composition—While the bottom tests from the ingots (Table I) contained more silicon, more elongated inclusions, and a larger number of inclusions, the lowering of the machinability index was greater than might be expected from those factors alone. The

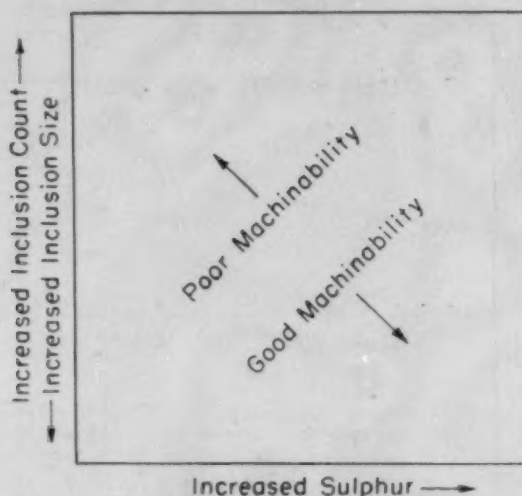


Fig. 13—Schematic Representation of the Dependence of Machinability Upon Sulphur Content and Inclusion Count, or Size. (Other factors equal.)

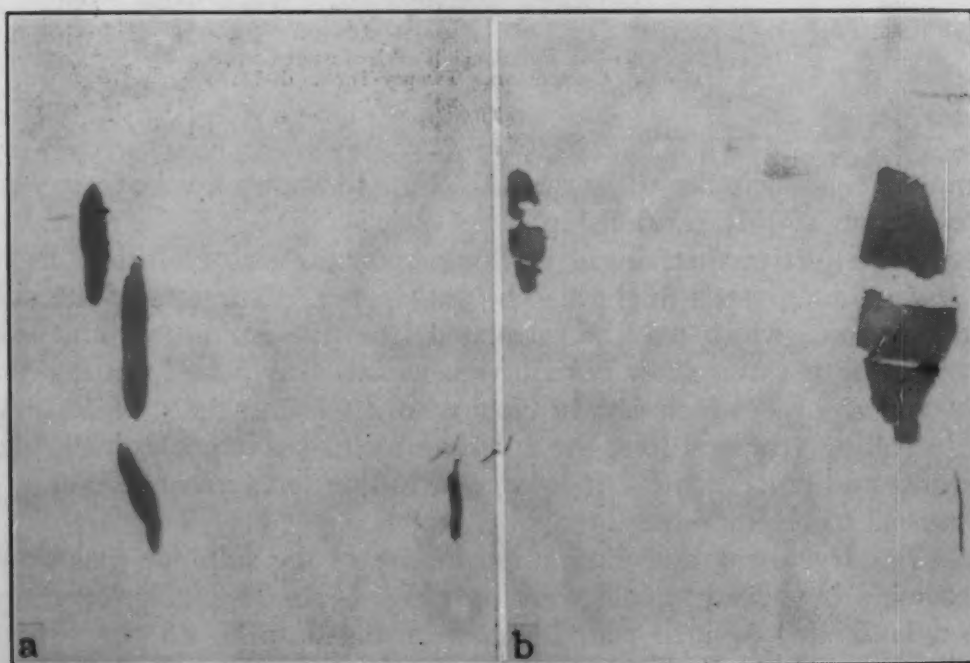


Fig. 14—B-1113 Steel (C—0.09%, Mn—0.77%, S—0.31%, Si—0.005%). $\times 400$. (a)—Hot-rolled to $\frac{3}{8}$ -inch rounds. The sulphide inclusions in this steel were not fractured. (b)—Same steel as above but with subsequent cold drawing to $\frac{3}{8}$ -inch rounds. Fractured inclusions were common.

microscopic examination of the mid-ingot samples showed that essentially all of the inclusions were of the manganese sulphide type² (Fig. 5). The inclusions in the bottom cuts of comparable ingots contained a glassy phase as well as the sulphide phase (Fig. 15). The suspicion that the bottom cuts contained higher oxygen contents was verified

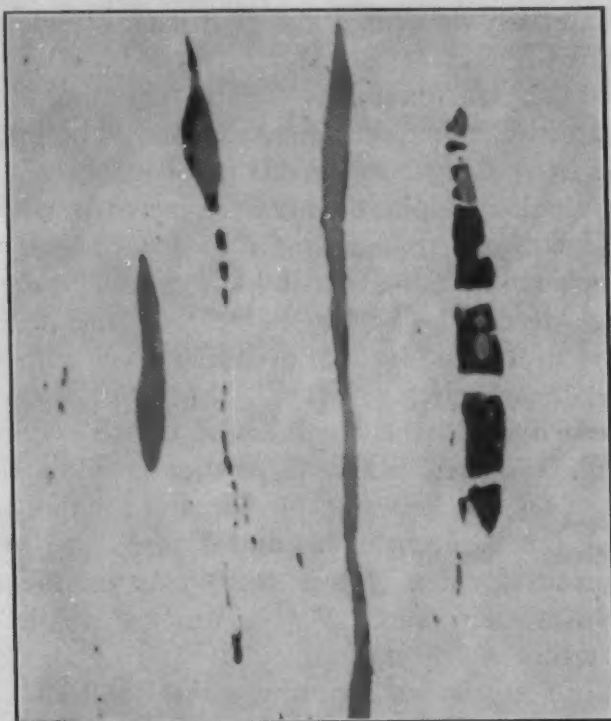


Fig. 15—Inclusions in Bottom Cuts. Ingot 3—Billet 10. Lighter gray—sulphide; Darker gray—Mn-SiO₂ glass. $\times 600$.

by vacuum fusion analyses (Table I). It might be concluded that the additional decrease in the machinability for the bottom-cut samples is attributable to these glassy oxide inclusions.

The higher oxide content of the bottoms must be attributed to segregation of a MnO-SiO₂ glass³ during solidification. The mechanism of this segregation in the bottom of the ingots is not understood. It may be noted that neither the oxygen content nor the amount of segregation is markedly affected by oxygen additions in Ingots 1 and 2. (Compare with Ingot 3 in Table I.)

The change in inclusion plasticity with the variation in silicon content of the steel indicates that there is also a change in the composition of the sulphide phase. To date, no method of inclusion analysis in free-machining steels is entirely satisfactory. While it is

²MnS will dissolve up to about 50% FeS in solid solution. The exact amount is dependent upon the Mn and S content of the steel. Likewise, the sulphide phase will dissolve an undetermined amount of oxygen.

³The etching characteristics indicate that the siliceous glass is comparatively rich in MnO.

possible that there might be some silicon dissolved in the sulphide phase with the higher silicon contents, the suggestion that silicon reduces the solubility of oxygen in the sulphide phase appears more plausible. To support this latter viewpoint is the fact that steel with a low oxygen analysis (Heat MX-0987, Table II) had plastic inclusions, even with a low silicon content. Furthermore, a deoxidizer, such as aluminum, materially increases the plasticity of sulphide inclusions during rolling (4).

Inclusions and Machinability—In the foregoing discussion, it was concluded that the machinability index is affected by inclusions in three different ways: (a) Larger inclusions favor machinability. (b) More inclusions (by higher sulphide contents) increase machinability. (c) Glassy oxide inclusions reduce machinability. These conclusions are in line with previous investigations by others concerning the mechanics of machining. Merchant (5) had noted that steel with coarse inclusions machined more readily than a similar steel with fine inclusions. He found the "machining constant", the mean shear strength, the strain hardenability, and the hardness of the two steels were essentially identical. The only major difference between the two was in the coefficient of friction between the chip and the tool face. He therefore concluded, on the basis of his and Zlatin's (6) work, that large sulphide inclusions form a (lubricating) coat on the tool face more effectively than smaller ones. As yet, we have made no further attempt to verify this interpretation.

Armour (7) concluded that the main effect of abrasive phases upon machinability is the reduction in tool life. The presence of the glassy oxide inclusions was observed to reduce tool life in his tests. In addition, the speed of cutting is also reduced by some additional mechanism. This is observed to be so because the standards are "sandwiched" in with the test bars in the fixed-pressure lathe tests, and any effect on the tool would change the cutting rates on the standards as well as the test bar. It is postulated that the more abrasive phases, such as glass, may adversely affect the coefficient of friction across the tool face.

SUMMARY

In the way of summary, it was observed that the shape and size of inclusions in B-1112 and B-1113 steels are affected by (a) the silicon content of the steel, (b) the sulphur content of the steel, (c) the mechanical working which the steel receives, and (d) possibly by the oxygen content of the sulphide phase.

The machinability, in turn, is dependent upon the size (or number) of inclusions in the steel to a considerable extent when other metallurgical factors are comparable (Fig. 11).

ACKNOWLEDGMENTS

The completion of this investigation has been dependent on many others. The microscopic examination of these resulphurized bessemer steels was originally suggested by E. W. Pierce and T. M. Garvey. The samples of steel were received from Gary Works, Duquesne Works, and the Pittsburgh Laboratories of United States Steel Company and from Battelle Memorial Institute where the machinability ratings had been made. Most of the tedious microscopic work was performed by Winnifred Oakes and Clara Novak of the South Works' Research Laboratory.

References

1. H. B. Knowlton, "Machinability of Wrought Metals", *Machining of Steels*, American Society for Metals, 1938, p. 50.
2. F. W. Boulger, H. A. Moorhead and T. M. Garvey, "Superior Machinability of MX Explained", *Iron Age*, Vol. 167, May 17, 1951, p. 90-95.
3. F. W. Boulger, H. L. Shaw and H. E. Johnson, "Constant Pressure Lathe Test for Measuring the Machinability of Free-Cutting Steels", *Transactions*, American Society of Mechanical Engineers, Vol. 71, No. 5, July 1949, p. 431.
4. C. E. Sims, "Non-Metallic Inclusions", *Basic Open Hearth Steelmaking*, 2nd Ed., American Institute of Mining and Metallurgical Engineers, 1951, p. 480.
5. M. E. Merchant, "Metal Cutting Research", *Machining—Theory and Practice*, American Society for Metals, 1950, p. 25.
6. M. E. Merchant and N. Zlatin, "Basic Reasons for Good Machinability of 'Free Machining' Steels", *TRANSACTIONS*, American Society for Metals, Vol. 41, 1949, p. 647-672.
7. J. D. Armour, "Metallurgy and Machinability", *Machining—Theory and Practice*, American Society for Metals, 1950, p. 142.

DISCUSSION

Written Discussion: By Edward A. Loria, senior engineer, Metallurgy, The Carborundum Company, Niagara Falls, N. Y.

Two questions come to mind when reading this interesting paper. The first pertains to the limits within which data can be reproduced in tests on the same steel, and the second pertains to a calculation of the quantity of inclusions to weight percentages.

With reference to Table I, giving the constant-pressure machinability ratings for several steels, would the author include the data on coefficients of variation so that one may know the reproducibility of the data, for example, for Steel 1-5 with an average index of 185 compared to Steel 4-10 with an average index of 121? The same question can be asked in regard to the data in Table II. Also, would the author furnish the ingot dimensions and state the position (location) of each billet with respect to the ingot so that perhaps some conclusion on the amount of inclusions with ingot position may be determined?

Would the author calculate, from the inclusion counts, the weight percentages of the inclusions in the steels, using specific gravity values of

7.9 for steel and 3.7 for the inclusions? The writer⁴ made some measurements on the amount of inclusions in acid electric cast steels by a point-count method, in an effort to determine its relation to tensile ductility, and came out with calculated weight percentages that were on the high side of what would be expected. The point that silicon may reduce the solubility of oxygen in the sulphide phase is well taken. It is believed that aluminum does the same thing to an even greater degree and hence changes sulphide inclusion types and methods of distribution in steel.

It may be of interest to know that now the Battelle constant-pressure lathe has been adapted for the machinability testing of gray cast iron.^{5, 6} Small variations in the cutting characteristics produced by variations in chemistry and microstructure can be detected.⁷ The predominant effect of total carbon and silicon in promoting graphitization results in higher indices for irons possessing greater quantities of these elements. The amount of graphitic carbon is a potent factor in controlling the machinability. The mechanism of cutting, peculiar to gray iron, appears to be produced by the discontinuity of the metal caused by the graphite flakes and the lubricating action of the graphite in lowering friction between tool and chip. The low zero elongation values for cast iron may also influence its machining characteristics.

Written Discussion: By H. L. Shaw, research metallurgist, and F. W. Boulger, supervising metallurgist, Battelle Memorial Institute, Columbus, Ohio.

We at Battelle were very pleased with the findings presented by the author. The quantitative data support the previous results (Ref. 2 of the paper) obtained on some of the same steels in showing that the constant-pressure machinability index of Bessemer free-cutting steel appears to be affected by the size, shape, and number of sulphide inclusions. These factors appear to be controlled by the silicon content of the steel and processing practice as well as the sulphur content.

The author chose to eliminate from consideration all inclusions with lengths less than 0.006 millimeter. This means that inclusions with small cross sectional areas or volumes were not counted if equiaxed, but were counted if the length-width ratios were large. Thus the inclusion counts used for Fig. 6 are probably influenced by inclusion shape. This bias would be expected to be more noticeable for steels at the left end of the trend line, which are shown in Fig. 4 to have small length-width ratios. The approach to a constant machinability level, in Fig. 6, may result from neglecting the effect of small equiaxed sulphides rather than from approaching an optimum inclusion size. If the cross sectional area of inclusions is important, a straighter trend line should result from counting inclusions smaller than 0.006 millimeter in length.

It should be noted that the machinability ratings for Fig. 4 were obtained in turning tests on bars. If the length-width ratio of inclusions

⁴E. A. Loria, "Rating Inclusion Structures in Cast Steels and Their Effects on Tensile Properties", *Electric Furnace Steel Proceedings*, American Institute of Mining and Metallurgical Engineers, Vol. 8, 1950, p. 191-209.

⁵E. A. Loria, "New Methods for Testing Machinability of Gray Iron", *Foundry*, Vol. 80, 1952.

⁶E. A. Loria, "Machinability of Gray Iron by Constant-Pressure Lathe Tests", *Foundry*, Vol. 80, 1952, p. 194-200.

⁷E. A. Loria, F. W. Boulger and H. L. Shaw, "What Constituents Affect Machinability of Gray Irons", *American Machinist*, October 1952, p. 122.

Ther 65 ml
July 49 P 431
2004 was
July

is as important as it seems to be, the relationship with machinability should vary for machining in other directions.

The author quotes Merchant and Zlatin as stating that "large sulphide inclusions form a lubricating coat on the tool face more effectively than smaller ones". This may not be the intrinsic result of inclusion size; it may reflect a difference in the compositions of large and small sulphide inclusions. The large sulphides may have a composition with better lubricating properties than the composition of the smaller sulphides.

The author concluded that glassy oxide inclusions have a harmful effect on machinability as measured by the constant-pressure test. This agrees with Armour's conclusion that glassy oxides shorten tool life, but the suggested mechanism is different. Armour attributes the shortened tool life to abrasiveness of the oxides. Ref. 3 of the paper shows that constant-pressure test ratings agree with tool life, even though no tool wear occurs in the fixed-pressure lathe test. It appears, therefore, that glassy oxides also signal poorer lubricating properties of sulphides. With two variables involved, it is impossible to decide whether abrasive oxides or sulphides with poor lubricating properties are more responsible for poor tool life in commercial operations.

Written Discussion: By Edsel E. Bishop, metallurgical engineer, Wycoff Steel Co., Ambridge, Pa.

The reference pertaining to the effect of cold working upon the fracturing of sulphide inclusions and other metallurgical factors as well as machinability indicates the need for a detailed investigation of this phase. It is logical for one to predict the fracturing of inclusions in severe percentages of cold work, since it is a known fact that hot working in lower rolling temperature ranges will cause brittle sulphide inclusions to break up into fragments. C. E. Sims, Battelle Memorial Institute, also referred to the fracturing of inclusions due to cold working, but he also did not qualify the statement any further (Basic Open-Hearth Steelmaking, American Institute of Mining and Metallurgical Engineers, 1944).

Whether the fracturing of inclusions has a direct bearing upon the machinability rating of a steel has not been definitely established. However, it is believed that other metallurgical factors such as strengthening the ferrite, decreasing the ductility, and stress pattern, overshadow possible effects of fractured inclusions.

In regards to possible effects of cold drawing upon the fracturing of sulphide inclusions, it has been our experience that one must qualify such a statement by including many factors, such as chemical composition, prior hot mill conditions, and percentage of cold work. To be practical and consider normal drafts is a very important consideration. Fig. 14 of the paper refers to a condition which has been known to be impractical on a commercial basis. It is not a normal condition to take a $\frac{1}{8}$ -inch draft on a 1-inch round bar of B-1113 analysis.

Many tests taken on our cold drawn free-machining bars reveal that under certain conditions a heavy draft may not cause sulphide inclusions to fracture, whereas under other conditions, a very light draft will cause the sulphide inclusions to be severely fractured.

A detailed investigation is now being conducted at our plant to learn how to control sulphide inclusion fracturing attributable to the cold draw-

ing operation and to determine the effect of fractured inclusions and other metallurgical changes occurring during cold working on the machining characteristics of several grades of steel.

Written Discussion: By R. G. Wells, petrographer, United States Steel Co., Pittsburgh.

The photomicrographs shown in Fig. 16 support the author's conclusion that the shape and size of the inclusions in free-machining steels are affected by the silicon content of the steel.

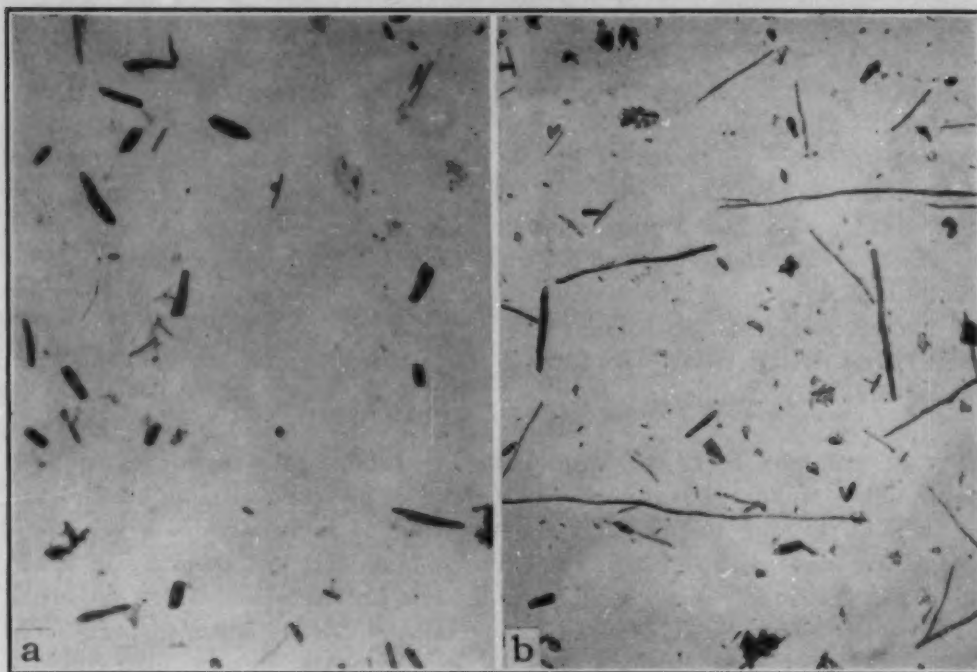


Fig. 16—Inclusions Extracted Electrolytically. Transmitted light. $\times 100$. (a) From a $\frac{7}{8}$ -inch hot-rolled bar of B-1112 steel analyzing: carbon 0.07%, manganese 0.94%, phosphorus 0.09%, sulphur 0.20%, silicon 0.009% and oxygen to 0.012%. (b) From a $\frac{7}{8}$ -inch hot-rolled bar of B-1112 steel—same heat as (a)—analyzing: carbon 0.07%, manganese 0.94%, phosphorus 0.09%, sulphur 0.20%, silicon 0.044% and oxygen to 0.017%.

Photomicrographs a and b are of sulphide inclusions extracted electrolytically from two similarly processed B-1112 steel rods. The extracted inclusions were mounted in an immersion oil and photographed in transmitted light. The hot-rolled rods were from two ingots of the same heat of steel: one ingot was untreated and contained 0.009% silicon, and the other was treated so as to contain 0.044% silicon. The sulphide inclusions from the untreated steel (photomicrograph a) are of the short, globular type, whereas those from the treated steel (photomicrograph b) are of the stringer type.

Author's Reply

I have appreciated the comments which have been offered. I feel they have added to the value of the paper.

In answer to the specific questions of Mr. Loria, it may be stated that the standard deviation of Samples 1-5 and 4-10 were plus or minus 1.2% and plus or minus 1.7%, respectively (3). A more general statement of the reproducibility of the machinability tests may be had by

pointing out that the control limits set in our Research Laboratory on the standard B-1111 steel are 95% within plus or minus 3 out of 42, i.e., a standard deviation of plus or minus 3.6%.

The first series of steels was poured as 21-by-21-inch ingot (6425#). The commercial steels in the second series were made as 23-by-35-inch ingots (13,325#). There were ten billets from each ingot of the controlled heat. These were numbered from top to bottom so that the fifth billet represents a middle position.

Inclusion volumes had been determined for the 9-5 and 10-5 test positions by the point-counting technique. For each of these locations, the volume of inclusions was found to be close to 1.00% (within the limit of statistical accuracy). Using the figures supplied by Mr. Loria and making the assumption that all sulphur is present in inclusions large enough to be counted, the "sulphur" content may be calculated to be 0.18%. It must be realized that the densities chosen and the assumptions made are such as to make the results out of line on the low side. An independent check on the inclusion volume may be made from the inclusion shape and count figure if it is assumed that the inclusions approximate, on the average, a prolate spheroid in shape. On that basis, the "sulphur" content was calculated to be about 0.25%. While this calculation would agree with Mr. Loria's findings and would suggest that some oxygen may be present in the inclusion to increase the inclusion volume, we would hesitate to place any quantitative significance on the difference realized. Rather, it is expected that the oxygen content of the inclusion may be determined more directly by an extraction method, such as Mr. Wells has described.

It is true that the lower limitations placed upon the inclusion size in tallying the number of inclusions could place a bias upon the data, as pointed out by Shaw, if there were no fracturing of the inclusions during their elongation. Actually, experience indicated that with the diminution in inclusion size the average length was not sufficiently changed to markedly affect the proportion of inclusions below the minimum size limit. Consequently, it is felt that any possible bias cannot account for all of the inflection noted in Fig. 6.

Shaw and Boulger suggest that the inclusion composition, rather than the inclusion size (and shape), may be the factor which affects the machinability properties of the steel. If that be true, the machinability properties of a homogeneous steel should be isotropic with respect to inclusion orientation; i.e., machinability should be the same for each cutting direction because the inclusion composition would be identical. Work is now in progress which would supply this information.

We certainly do agree with Mr. Bishop that other metallurgical factors probably overshadow the possible effects of fractured inclusions in cold drawn steels. It was because cold working also changed other metallurgical factors that we made no attempt to evaluate the effect of the diminution of inclusion size during cold working upon machinability. We look forward to the findings of the investigation which he is now conducting concerning the control of sulphide inclusion fracturing during cold working, as well as the effect of the metallurgical changes during cold working upon machinability.

DETERMINATION OF OXYGEN IN METALS AND METAL OXIDES BY THE ISOTOPIC METHOD

BY A. D. KIRSHENBAUM AND A. V. GROSSE

Abstract

The quantitative methods for determining the oxygen content of metals used at present are long, tedious and at times not too accurate, requiring complete removal and recovery of oxygen in the metals or oxides. The Isotopic Method, as described in this paper, uses O^{18} and does not require quantitative separation or recovery of the oxygen, thus giving fast results accurately. The only requirement of this method is exchange of all oxygen atoms in the system, which is accomplished at the temperatures used. Good, accurate oxygen values were obtained with this method for several copper-oxygen and iron-oxygen alloys and for copper and iron oxides.

THE OXYGEN content of metals such as copper and steels has in the past been determined by several different methods, namely, the vacuum-fusion, aluminum reduction, carbon reduction, hydrogen reduction, etc., the vacuum-fusion method being the most popular. In the aluminum reduction method the steel is reduced with aluminum at 1100 to 1150 °C (2010 to 2100 °F) in either a hydrogen atmosphere (5, 6)¹ or at reduced pressure (20) with subsequent solution of the iron-aluminum melt in 4N-HNO₃ (17) and the oxygen chemically determined from the Al₂O₃ formed and assumes that all of the oxygen will appear as Al₂O₃. According to Pigott (20) a single analysis may require several days. This method is not accurate when SiO₂ is present (17).

In the carbon reduction method, the metal sample is reduced at elevated temperatures by carbon with or without tin in a nitrogen atmosphere (23), a reducing atmosphere or in vacuum (14, 18). This method requires complete reduction of all the metal oxides present to carbon monoxide. In the hydrogen reduction method the sample is reduced with hydrogen; the amount of oxygen present is

¹The figures appearing in parentheses pertain to the references appended to this paper.

This work was sponsored by Flight Research Laboratory, Wright Air Development Center, Wright-Patterson Air Force Base, Dayton, Ohio.

A paper presented before the Thirty-fourth Annual Convention of the Society, held in Philadelphia, October 18 to 24, 1952. The authors, A. D. Kirshenbaum and A. V. Grosse, are associated with the Research Institute of Temple University, Philadelphia. Manuscript received April 30, 1952.

determined either from the amount of hydrogen consumed or from the amount of water collected (2, 26). In this method, as in the carbon reduction method, *all* of the oxide has to be reduced to water and *all* of the water collected quantitatively.

In the other chemical methods, the metals are removed by chemical action, such as reaction with hydrogen chloride, chlorine, bromine or iodine (3, 4, 15, 19), leaving unattacked oxides, carbides and nitrides, which have to be analyzed further and the oxygen estimated. These methods generally require long periods of time to make a single analysis, are tedious, and in many cases the results are open to various criticisms.

The vacuum-fusion method depends upon the reduction of metal oxides by carbon to carbon monoxide in the liquid metal. In this method the metal is reacted with powdered graphite, in vacuum, with or without tin, to form stable carbides, while the oxides are reduced at elevated temperatures (11, 18-22, 24, 25). The oxygen-containing gases formed should be reduced to CO. The method requires *complete removal and recovery of all of the oxygen in the metal*. This, at times, makes the method long and tedious. It was observed by Alexander (1) and Mallett (16) that the presence of silicon in steels prevents complete reduction of the oxides. Ziegler (27), Thompson and Holm (26) and Alexander (1) found that Al_2O_3 inclusions in steels, if present, will not be reduced in any reasonable time.

The method used by the authors to determine the oxygen content of metals and metal oxides is an extension of the Elementary Isotopic Method developed in recent years by the writers for organic compounds (7, 8, 9 and 13) and for fluorocarbons (12).

Principle of the Isotopic Method

The principle of the Isotopic Method is an adaptation of the isotopic dilution principle originally introduced by Hevesy and Paneth (10). A known weight of substance to be analyzed together with a known weight of metal or metal oxide containing a given amount of oxygen of known O^{18} concentration is heated for 30 to 60 minutes at the vicinity of their melting points in a platinum, molybdenum or other oxygen-free metal tube. At this temperature all the oxygen atoms exchange statistically with the various oxygen-containing compounds (metal oxides, CO and CO_2). The ratio of the oxygen isotopes ($\text{O}^{18}/\text{O}^{16}$) in all these oxygen-containing compounds at equilibrium is identical.

The ratio $\text{O}^{18}/\text{O}^{16}$ can be determined with a high degree of precision by means of modern isotopic mass spectrometers. Only an aliquot sample of the equilibrated mixture need be taken for mass analysis. Usually a fraction of a cc. is sufficient. *Therefore quantitative removal of all the oxygen is not only unnecessary but even*

undesirable. Knowing the ratio, it is easy to calculate the original oxygen content from the simple mixture rule, namely

$$X \% = \frac{b(m - n)}{a \cdot n} \cdot 100$$

In this equation a is the known weight of the sample, containing X weight % of the oxygen to be analyzed, and is equilibrated with a known weight, b , of O^{18} labeled oxygen containing m atom % of oxygen-18 in excess of the normal isotopic concentration ($\sim 0.21\%$) and n atom % is the excess oxygen-18 concentration after equilibration. The exact normal isotopic concentration is determined before each analysis.

Because the isotopes are mixed and measured on an atom per atom basis, b should be expressed either in gram-atoms or, more simply, in weight units using the same atomic weight of the element as in a . Thus b is not expressed in actual milligrams of the heavy isotope, but in equivalent milligrams of the normal isotopic mixture.

In the analysis of metals and oxides for oxygen, it is important to insure complete exchange of the O^{16} and O^{18} atoms. With organic and fluorocarbon compounds complete exchange is obtained by heating them with molecular O^{18} enriched oxygen. But with metals and oxides this is most readily accomplished by preparing master alloys or oxides containing known weights of oxygen and O^{18} concentrations, mixing them with the samples to be analyzed and finally heating the mixtures at their melting points.

Since iron and copper are the two most important metals of our technology, we have chosen these metals and their oxides to demonstrate the practicability and the advantages of the Isotopic Method in determining the oxygen content of metals and oxides. In the near future this method of analysis will also be used on other metals such as chromium, titanium and zirconium.

The precision of the Isotopic Method is independent of the oxygen concentration in the metal. If small quantities of oxygen are expected, the amount of oxygen-18 added (as O^{18} Master Alloy) to the sample can be adjusted accordingly. Thus results of high precision may be obtained even if traces of oxygen are present.

APPARATUS

The apparatus consists essentially of (a) a 6-kilowatt converter and high-frequency induction furnace and (b) a vacuum system for separating and sampling gases.

High-Frequency Induction Furnace—The furnace used is an Ajax-Northrup 6-kilowatt converter-type high-frequency induction furnace manufactured by the Ajax Electrothermic Corporation of Trenton, N. J.

Glass-Vacuum System—The apparatus as shown in Fig. 1 consists essentially of a platinum or molybdenum reaction vessel and a pyrex glass vacuum system. The reaction vessel consists of a $\frac{1}{2}$ -inch O.D. platinum tube with 0.015-inch wall or molybdenum test tube (A) with 0.09-inch wall inserted into a $1\frac{5}{8}$ -inch O.D. quartz test tube (B) and held in place by a rubber stopper. The dead space between the platinum or molybdenum and quartz tubes is filled with

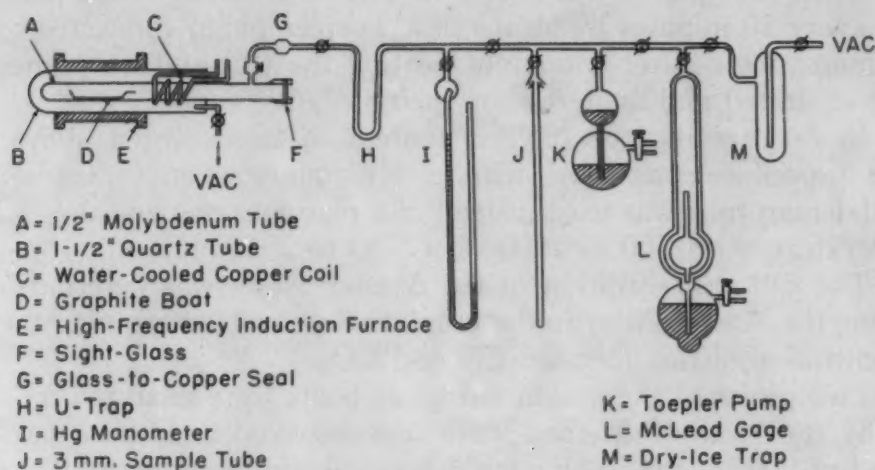


Fig. 1—Apparatus for Separating and Sampling Gases.

zirconium oxide. The part of the platinum or molybdenum tube near the rubber stopper is cooled by means of a water-cooled copper coil (C). A graphite boat (D) containing the metal and Master Alloy is inserted into the platinum or molybdenum tube and carefully centered within the coil of the high-frequency induction furnace (E). The temperature of the melt is read through the sight glass (F).

The platinum or molybdenum tube is connected to the pyrex vacuum and gas sampling system by means of a glass-to-copper seal (G). The pyrex vacuum and gas sampling system consists of U-trap (H), mercury manometer (I), 3 mm. O.D. sample tube (J), Toepler pump (K), McLeod gage (L) and dry ice trap (M).

EXPERIMENTAL PROCEDURE

In determining the oxygen content of the copper-oxygen alloys, a known weight of the copper-oxygen alloy sample to be analyzed (~ 100 to 500 mg) was mixed with a known weight (~ 100 to 200 mg) of O^{18} labeled copper-oxygen Master Alloy containing a given amount of oxygen of known O^{18} concentration. The mixture was put into a baked graphite boat (baked at 1000°C or 1830°F for 3 hours while pumping at $<10^{-4}$ mm. pressure), the graphite boat surrounded by a platinum sheet and then inserted into a platinum tube ($\frac{1}{2}$ -inch O.D.). The platinum tube, centered in an evacuated quartz tube (32 mm. O.D.), in the high frequency induction furnace (4 inches

long, 32 mm. I.D.), was connected to the vacuum system and evacuated to 10^{-4} mm. Hg pressure or lower. The platinum tube was then closed off from the vacuum system and heated to between 1000 to 1100 °C (1830 to 2010 °F), by means of the induction furnace. Upon heating at about 1000 °C (1830 °F), CO and CO₂ containing the *equilibrated concentration* was liberated. The copper alloy was heated for 1 hour. To insure equilibrium conditions, the gases liberated were circulated from the cold to the hot zone of the platinum tube every 10 minutes by means of a Toepler pump connected to the platinum tube. After 1 hour of heating the CO and CO₂ liberated were separated and analyzed for their O¹⁸/O¹⁶ ratios.

In determining the oxygen content of iron-oxygen alloys, the same procedure was used with a few minor changes, namely, a molybdenum tube was used instead of a platinum one and the heating temperature was 1500 to 1600 °C (2730 to 2910 °F).

The O¹⁸ concentration of the Master Alloy was determined by heating the Master Alloy in the graphite boat and determining the O¹⁸ concentration of the liberated CO and CO₂.

Two pieces of the graphite used as boats were analyzed for oxygen by the Isotopic Method; one was unbaked and the other was heated at 900 °C (1650 °F) for 3 hours while pumping at 10^{-5} mm. Hg. The oxygen content was determined by heating in a platinum tube for 1 hour at 900 °C (1650 °F), a known weight of graphite with a known amount of oxygen containing a given concentration of O¹⁸. The CO₂ formed was analyzed for O¹⁸ concentration. The per cent oxygen in the graphite was calculated from the dilution of the O¹⁸ concentration.

Preparation of O¹⁸ Metal Master Alloys

Copper-Oxygen-18 Master Alloy—The copper-oxygen-18 Master Alloy was prepared by heating a platinum boat containing copper powder with O¹⁸ labeled oxygen, the optimum reaction temperature being about 400 °C (750 °F). After all the required oxygen had been consumed, the copper-copper oxide mixtures were heated at 450 to 500 °C (840 to 930 °F) for 24 hours in order to distribute the O uniformly throughout the copper powder. After cooling, the copper-copper oxide alloy was ground in an agate mortar and pestle. The weight per cent oxygen in the Master Alloy was 5.373% and the O¹⁸ concentration was 14.8655 atom %.

Iron-Oxygen-18 Master Alloy—The preparation of the iron-oxygen-18 Master Alloy was essentially the same as the copper-oxygen-18 Master Alloy except for the reaction temperature being higher (550 to 600 °C). The weight per cent oxygen in the Master Alloy was 6.950% and the O¹⁸ concentration was 11.5011 atom %.

Table I
Samples of Copper, Iron and Their Oxides by the Isotopic Method

Sample	% O in Original Metal*	% Gain in Weight	Total % O	Remarks
Copper powder	0.812	J. T. Baker Chemical Co. 99.29% Cu
Copper powder heated in O ₂	0.812	0.075	0.887	
Copper powder heated in O ₂	0.812	0.134	0.946	
Copper powder heated in O ₂	0.812	2.193	3.005	
Copper powder heated in O ₂	0.812	8.73	9.54	
Cupric oxide	20.12 (Theor. 100% CuO)	Baker & Adamson, reagent grade powder
Iron powder	2.072	Mallinckrodt, analytical reagent reduced iron powder; 97.66% Fe
Iron powder heated in O ₂	2.072	9.406	11.478	
Ferric oxide	30.00 (Theor. 99.81% pure Fe ₂ O ₃)	J. T. Baker's C.P. analyzed powder. 99.81% Fe ₂ O ₃ , 0.00% FeO

*As analyzed by the Isotopic Method.

Samples Analyzed

The copper-oxygen samples analyzed were copper powder, cupric oxide, and several samples of copper powder heated in oxygen. The iron-oxygen samples analyzed were iron powder, ferric oxide and iron powder heated in oxygen. These samples are shown in Table I.

Method of Calculation

As stated previously, the per cent oxygen is calculated from the formula

$$\text{O \%} = \frac{b(m - n)}{a \cdot n} \cdot 100$$

The per cent oxygen obtained is then corrected for the oxygen content of the graphite boat used. This correction is obtained from the difference in weight of the graphite boat used to calculate the O¹⁸ concentration of the Master Alloy and the weight of the boat used in the analysis. This difference in weight multiplied by the per cent oxygen in the graphite is either added or subtracted, as the case may be, from the oxygen values obtained from the formula above.

Example:

$$\begin{aligned} \text{Let } a &= 100.00 \text{ mg} \\ b &= 7.00 \text{ mg}^* \end{aligned}$$

$$\begin{aligned} m &= 10.0000 \\ n &= 5.0000 \\ m - n &= 5.0000 \end{aligned}$$

$$\text{then uncorrected \% O} = \frac{7.00 (5.0000)}{100.00 (5.0000)} \cdot 100 = 7.00\% \text{ or } 7.00 \text{ mg.}$$

*Obtained by multiplying % O in Master Alloy by weight of Master Alloy used.

Table II
Determination of Oxygen in Copper and Copper-Oxygen Alloys

Substance	1 Copper Powder	2 Copper Powder Heated in O ₂	3 Copper Powder Heated in O ₂	4 Copper Powder Heated in O ₂	5 Copper Powder Heated in O ₂	6 —Cupric Oxide— a b	
a, mg. weight of substance	141.70	505.58	409.72	158.51	60.11	43.24	43.04
Weight of Cu-O ¹⁸ added, mg.	174.86	119.95	108.60	100.61	266.25	105.45	89.52
b, mg. of O added	7.98	6.32	5.84	5.41	19.31	5.67	4.81
Atom % O ¹⁸ in b above	14.8655	14.8655	14.8655	14.8655	14.8655	14.6986	14.4937
—normal concentration	0.2264	0.2264	0.2264	0.2264	0.2264	0.2167	0.2287
=m	14.6391	14.6391	14.6391	14.6391	14.6391	14.4819	14.2650
Atom % O ¹⁸ in equilibrated mixture	13.0271 13.0134	8.9061	9.5954	7.9639	10.9267 10.8460	5.6578	5.0937
Average =	13.0203				10.8864		
—normal concentration	0.2268	0.2149	0.2122	0.2292	0.2442	0.2167	0.2287
=n	12.7935	8.6912	9.3832	7.7347	10.6422	5.4411	4.8650
m - n	1.8456	5.9479	5.2559	6.9044	3.9969	9.0408	9.4000
% oxygen in substance, experi- mental (uncorrected)	0.812	0.855	0.798	3.051	8.94	21.79	21.59
Difference in weight of graphite boats, mg. Cu-O ¹⁸ —sample	-0.05	+111.4	+321.8	-33.9	+21.1	-356.5	-362.0
% O in graphite	0.185	0.185	0.185	0.185	0.185	0.185	0.185
% oxygen in substance, experi- mental (corrected)	0.812	0.896	0.942	3.015	9.58	20.26	20.05
% oxygen in substance, theoretical or calculated from gain in weight	0.887	0.946	3.005	9.54	20.12	20.12
Difference (E-T)	+0.009	-0.004	+0.010	+0.04	+0.14	-0.07

Now if 2.0000 g. = weight of boat used to determine O¹⁸ concentration
in Master Alloy

1.98500 g. = weight of boat used to determine % O above
and 0.100% = % oxygen in graphite

then 0.0100×15.00 mg. = 0.015 or 0.02 mg.

now % O in copper corrected for oxygen in graphite

$$= \frac{\text{uncorrected wt. of O in Cu} - \text{wt. of O in graphite}}{\text{weight of sample, a}} \times 100$$

$$= \frac{7.00 - 0.02}{100.0} \times 100 = 6.98\%$$

Experimental Results

The results obtained upon analyzing the various copper, copper-oxygen, cupric oxide, iron, iron-oxygen, ferric oxide and graphite samples are shown in Tables II, IV, VI, and are summarized in Tables III, V, VII.

A study of these tables shows that good, accurate results are obtainable by the Isotopic Method of analysis, the average deviation from true values being 4 parts per thousand. The *b* values in Tables II and IV were obtained by multiplying the weight of the O¹⁸ Master Alloys by the per cent oxygen in these alloys (5.373 wt. % and 6.950 wt. % in the copper and iron Master Alloys, respectively), while *m* values are the O¹⁸ concentration of the oxygen above normal in the Master Alloys used.

Table III
Determination of Oxygen in Copper and Copper-Oxygen Alloys

Sample No.	Weight Mg.	Calculated % O in Copper			Observed % Oxygen	Difference
		In Original Copper	% Gain in Wt.	Total %		
1	141.70	0.812
2	505.58	0.812	0.075	0.887	0.896	+0.009
3	409.72	0.812	0.134	0.946	0.942	-0.004
4	158.51	0.812	2.193	3.005	3.015	+0.010
5	60.11	0.812	8.73	9.54	9.58	+0.04
6 (a)	43.24	20.12	20.26	+0.14
(b)	43.04	20.12	20.05	-0.07
(Cupric oxide)				(Theor. 100% CuO)		

Table IV
Determination of Oxygen in Iron and Iron-Oxygen Alloys

	1 Iron Powder	2 Iron Powder Heated in O ₂	3 Ferric Oxide Fe ₂ O ₃
a. weight of substance, mg.	320.54	77.69	51.79
Weight of Fe-O ¹⁸ added, mg.	106.76	100.57	100.13
b. weight of O added, mg.	7.38	6.99	6.96
Atom % O ¹⁸ in b above	11.5011	11.5011	11.5011
—normal concentration	0.2292	0.2292	0.2292
m =	11.2719	11.2719	11.2719
Atom % O ¹⁸ in equilibrated mixture	6.3094	5.2706	3.7106
	5.2086	3.7522
	3.7599
Average =	5.2396	3.7409
—normal concentration	0.2298	0.2122	0.2294
n =	5.0796	5.0274	3.5115
m - n	5.1923	6.2445	7.7604
% oxygen in substance (uncorrected)	1.960	11.175	29.700
Difference in weights of graphite boats (Fe-O ¹⁸ -sample), mg.	+195.1	+14.1	+32.3
% O in graphite	0.185	0.185	0.185
% oxygen in substance, experimental (corrected)	2.072	11.507	29.81
% oxygen in substance, theoretical or calculated from gain in weight	11.478	30.00
			Theor. on pure Fe ₂ O ₃
Difference (E-T)	+0.029	-0.19

Table V
Determination of Oxygen in Iron and Iron-Oxygen Alloys

Sample No.	Weight	Calculated or Theoretical % O in Fe			% O	Difference
		In Original Fe	% Gain in Wt.	Total %		
1	320.54	2.072
2	259.63	2.072	0.303	2.375	2.315	-0.060
3	306.35	2.072	0.459	2.531	2.496	-0.035
4	202.32	2.072	1.322	3.394	3.401	+0.007
5	77.69	2.072	9.406	11.478	11.507	+0.029
6	51.79	30.00	29.81	-0.19
(Fe ₂ O ₃)				(Theor. 99.81% pure Fe ₂ O ₃)		

Table VI
Determination of Oxygen in Graphite

Substance	Unbaked Graphite Boat	Baked Graphite Boat	Graphite Powder
a, weight of sample, mg.	499.65	565.41	481.27
b, weight of O ₂ added, mg.	3.24	2.64	2.41
Atom % O ¹⁸ in b above	5.2977	5.2977	5.2977
—normal concentration	0.2182	0.2182	0.2182
=m	5.0795	5.0795	5.0795
Atom % O ¹⁸ in equilibrated mixture	3.6398	3.8662	4.1358
—normal concentration	0.2287	0.2287	0.2287
=n	3.4111	3.6375	3.9071
m-n	1.6684	1.4420	1.1724
% O in graphite	0.317	0.185	0.150

Table VII
Determination of Oxygen in Graphite

Sample	Sample Mg.	Weight of O ¹⁸ , Mg.	Analysis % O
Unbaked graphite boat	499.65	3.24	0.317
Baked graphite boat	565.41	2.64	0.185
Graphite powder	481.27	2.41	0.150

DISCUSSION OF RESULTS

A study of the principle behind the Isotopic Method, the procedure used and results obtained shows that the Isotopic Method has a great advantage over the methods used at present in the industry, since accurate results are obtained in a very short time (2 hours). The reason for the fast accurate results lies in the principle of the method, namely, that complete removal and recovery of all the oxygen in the metal is not necessary. The only requirement of this method is complete statistical exchange between all the oxygen atoms of the various oxygen-containing compounds (metal oxides, CO and CO₂). At the elevated temperatures used, complete exchange is obtained within 30 minutes.

This method of analysis is now being extended to the determination of oxygen in various other metals, particularly to titanium and zirconium.

ACKNOWLEDGMENT

The financial support of the Wright Air Development Center is gratefully acknowledged.

References

1. L. Alexander, W. M. Murray and S. E. Q. Ashley, "Determination of Oxygen in Steel by the Vacuum Fusion Method", *Analytical Chemistry*, Vol. 19, June 1947, p. 417.
2. W. A. Baker, "The Estimation of Oxygen in Metals", *Journal, Institute of Metals*, Vol. 65, No. 2, 1939, p. 345.

3. H. F. Beeghly, "Ferrous Metallurgy", *Analytical Chemistry*, Vol. 23, February 1951, p. 228.
4. E. W. Colbeck, S. W. Craven and W. Murray, "Description of the Procedure Now Adopted for the Chlorine Method", *Journal, Iron and Steel Institute*, Vol. 143, 1941, p. 332.
E. W. Colbeck, S. W. Craven and W. Murray, "General Summary Showing the Applicability and Utility of the Chlorine Method", *Journal, Iron and Steel Institute*, Vol. 143, 1941, p. 339.
5. N. Gray and M. C. Sanders, "Aluminium-Reduction Method for the Gravitimetric Determination of Total Oxygen in Plain Carbon Steels", *Iron and Steel Institute, Special Report*, No. 25, 1939, p. 103.
6. N. Gray and M. C. Sanders, "The Development and Comparison of Two Procedures for the Aluminium Reduction Method for Determining Oxygen in Steel. General Summary Showing Applicability of the Aluminium-Reduction Method", *Journal, Iron and Steel Institute*, Vol. 143, 1941, p. 321.
7. A. V. Grosse, S. G. Hindin and A. D. Kirshenbaum, "Elementary Isotopic Analysis. Determination of Oxygen", *Journal, American Chemical Society*, Vol. 68, Oct. 17, 1946, p. 2119.
8. A. V. Grosse, S. G. Hindin and A. D. Kirshenbaum, "Elementary Isotopic Analysis", *Analytical Chemistry*, Vol. 21, March 1949, p. 386.
9. A. V. Grosse and A. D. Kirshenbaum, "Direct Determination of Oxygen in Organic Compounds by Elementary Isotopic Analysis", *Analytical Chemistry*, Vol. 24, March 1952, p. 584.
10. G. von Hevesy and F. Paneth, "Lehrbuch der Radioaktivität", 2nd Edition, 1931, p. 164-171. Johan Ambrosius Barth, Leipzig, Germany.
11. L. Jordan and J. R. Eckman, "Gases in Metals", *Scientific Papers*, U. S. Bureau of Standards, Vol. 20, No. 514, 1925, p. 445.
12. A. D. Kirshenbaum, A. G. Streng and A. V. Grosse, "A Direct Method for Determining Oxygen in Fluorocarbon Derivatives". Submitted to *Analytical Chemistry* for publication, Dec. 12, 1951.
13. A. D. Kirshenbaum and A. G. Streng, "Direct Determination of Oxygen in Rubber. A Comparison between the Isotopic and the Schütze-Unterzaucher Methods". Submitted to *Analytical Chemistry* for publication, Dec. 27, 1951.
14. W. T. Kroll and A. W. Schlechton, "Reactions of Carbon and Metal Oxides in a Vacuum", *Transactions, Electrochemical Society*, Vol. 93, 1948, p. 247.
15. W. C. Lilliendahl, D. M. Wroughton and E. D. Gregory, "The Quantitative Evaluation of Oxygen in Zirconium", *Transactions, Electrochemical Society*, Vol. 93, 1948, p. 235.
16. M. W. Mallett, "A Versatile Vacuum-Fusion Apparatus", *Transactions, American Society for Metals*, Vol. 41, 1949, p. 870.
17. J. Massinon, "Le Dosage de l'Oxygène dans les Aciers par Diffusion de l'Aluminium", *Revue de Métallurgie*, Vol. 44, May-June 1947, p. 174.
18. I. Musatti and G. Ziliani, "Il Metodo di Riduzione con Carbonio nel Vuoto nella Determinazione dell'Ossigeno Totale nel Rame", *Metallurgia Italiana*, Vol. 29, November 1937, p. 589.
19. P. Oberhoffer, R. Scherer, J. Keutmann and H. Strauch, "Die Bestimmung des Sauerstoffs im Eisen", *Stahl und Eisen*, Vol. 45, Sept. 10, 1925, p. 1555.
20. E. C. Pigott, "Hydrogen, Nitrogen and Oxygen in Ferrous Metals. Their Properties and Their Determination—Part V", *Metallurgia*, Vol. 37, March 1948, p. 263.
21. L. Reeve, "Improvements in the Vacuum Fusion Method for Determination of Gases in Metals", *Transactions, American Institute of Mining and Metallurgical Engineers*, Vol. 113, 1934, p. 82.

22. C. N. Rice, "Determination of Oxygen by the Vacuum Fusion Method", *U. S. Atomic Energy Commission*, MDDC-356, Oct. 5, 1944. 6 pages.
23. L. Singer, "Rapid Determination of Oxygen in Steel", *Industrial and Engineering Chemistry (Analytical Edition)*, Vol. 12, March 15, 1940, p. 127.
24. H. A. Sloman, "The Vacuum Fusion Method for the Determination of Oxygen, Nitrogen and Hydrogen in Steel. The Determination of the Oxygen Content of Surface Oxide Films", *Iron and Steel Institute, Special Report*, No. 25, 1939, p. 43.
25. H. A. Sloman, "The Application of the Vacuum-Fusion Method to the Determination of the Oxygen, Hydrogen and Nitrogen Contents of Non-Ferrous Metals, Alloys and Powders", *Metallurgia*, Vol. 32, September 1945, p. 223.
26. J. G. Thompson and V. C. F. Holm, "Hydrogen-Reduction Method for the Determination of Oxygen in Steel", *Journal of Research*, U. S. Bureau of Standards, Vol. 21, July 1938, p. 79.
27. N. A. Ziegler, "Reduction of Oxides in Graphic Vacuum Fusion Method of Analysis for Oxygen", *Mining and Metallurgy*, Vol. 14, June 1933, p. 260.

DISCUSSION

Written Discussion: By Manley W. Mallett, assistant supervisor, Thermal Chemistry Group, Battelle Memorial Institute, Columbus, Ohio.

I am pleased to see the authors have demonstrated that the isotopic dilution method can be applied to the determination of oxygen in metal oxides and in oxidized metal powders. The title of the paper is somewhat misleading in that no analyses of "oxygen in metals", that is, internally contained oxygen, are reported. In 1949, some exploratory work was done at Battelle Memorial Institute on applying the isotopic method to the analysis of oxygen in titanium. However, the pressure of other work prevented us from bringing this study to a satisfactory conclusion. We, therefore, are looking forward with great interest to the results the authors obtain in applying the method to titanium and zirconium.

I would like to ask the authors if they observed any interference from the use of the molybdenum reaction vessel. Gulbransen and Andrew² have reported oxidation of molybdenum to occur at oxygen pressures as low as 10^{-6} mm Hg. It has been our experience that at 1500°C and 10^{-4} mm Hg pressure, molybdenum oxidizes rapidly, forming volatile oxides which sublime to cooler parts of the system. If this occurs, at least part of the gas is being constantly removed from the reaction in the form of molybdenum oxide sublimate, and true equilibrium of the extracted gases cannot be achieved. The effect of this reaction on the analyses may not be detected at the high oxygen levels of the present work but would probably be quite bothersome at oxygen levels of most interest in vacuum-fusion analysis, that is, at 0.01% or lower.

In extending the isotopic method to low-oxygen metals, a number of modifications will be required. The use of samples in powder form would invalidate results because of the large surface area. In spite of elaborate cleaning precautions, some oxidation product is always found on the surface. Therefore, analytical samples should have a minimum surface area. A spherical sample would be ideal.

²"Pittsburgh International Conference on Surface Reactions", Corrosion Publishing Company, Pittsburgh, 1948, p. 222.

The authors state that the great advantage of the isotopic method is the short time required for an analysis. I believe they will find that, in working in a more precise range, many of the time-consuming factors of the vacuum-fusion method will come into play. The furnace parts and crucible will have to be degassed to a high degree so blanks can be reduced to a minimum. The principal saving of time would then seem to be in the analysis of the gas after extraction. Would it be feasible to make the mass spectrometer an integral part of the vacuum-extraction train?

Written Discussion: By W. C. Lilliendahl, advisory engineer, Metals Section, Research Department, Westinghouse Electric Corp., Bloomfield, New Jersey.

The work reported in this paper is an important contribution in this field as it represents a relatively new approach to the determination of oxygen in metals. There are several points, however, in connection with the use of this method which are not dealt with in detail and could be clarified.

It is implied that in the equilibration of O^{18} the mixture of powders is heated to a range including the melting point. It would seem that if the melting point were not reached, equilibration in a statistical sense would be related to particle size of the powder mix of which no mention is made.

Referring to the heating furnace, did the authors note deterioration and increased porosity of the platinum or molybdenum tubes as a result of carburization in the heating cycle?

The relative precision and accuracy of this method in the range of oxygen concentrations studied would suggest further investigation on the transition metals as planned by the authors.

Working in the low range of oxygen concentrations found in these metals, it would seem that difficulties in mass spectrometry might arise that would not materially affect the data in the work reported.

The masses which predominate are presumably CO^{28} , CO^{30} , CO_2^{44} , CO_2^{46} , and CO_2^{48} . Interfering masses could be N^{28} , NO^{30} , NO_2^{46} , $C_2H_4^{28}$, $C_2H_6^{44}$ and N_2O^{44} . Of these masses N^{28} would be most likely to be present. The authors do not state whether nitrogen was liberated from their samples but it is certainly present in the gases liberated from the usual vacuum-fusion melt.

Oxygen analysis as applied to MO, U, Ti, and Zr must yield accurate data in the range of 0.03% oxygen or less, with an absolute precision of approximately $\pm 0.0002\%$. This would mean that in the isotopic method the total amount of gas would be of the order of a few liter microns for (0.1 to 0.5 gm.) samples. While this pressure would be increased by the addition of material containing O^{18} enriched oxygen, there would probably be a limit to the ratio of O^{18}/O^{16} for maximum precision in the mass spectrometer. As the oxygen to be determined decreases, the presence of interfering masses would be expected to exert an increasing effect on the accuracy and precision of the method.

Authors' Reply

Replying to W. C. Lilliendahl's discussion, no difficulties are expected in the mass spectrometry of samples in the low range of oxygen concentration. Nitrogen is liberated from our samples; but it is standard practice

to determine the N_2 content of $CO-N_2$ mixtures from the N or mass 14 peak with no corresponding interference from the CO peaks.

For samples expected to contain small amounts of oxygen larger samples (5 to 10 grams) can be used if desired; however, the precision of the Nier-Consolidated Isotopic Mass-Spectrograph permits the determination of the O^{18}/O^{16} ratio to the sixth decimal place which is substantially beyond our presently used accuracy.

No deterioration or increased porosity of the platinum or molybdenum tubes was observed, since there was no direct contact of the tubes with the graphite boat. A thin sheet of expendable platinum or molybdenum was wrapped around the graphite boat, thus preventing deterioration of the tubes.

In response to M. W. Mallett's discussion, we are pleased to learn that Battelle was interested in the isotopic method.

By the term "oxygen" we mean the element and are determining it in all forms present in the sample, not necessarily meaning only molecular oxygen (O_2).

Regarding subliming molybdenum oxides, a closed platinum extension can be added to the molybdenum tube and complete isotopic exchange achieved by heating the platinum tube periodically to the sublimation temperature.

The method is not limited to metals in powder form. If large areas should be troublesome, suitable changes can be made. The master alloy and sample can be added in chunks or lumps of desired size. The fundamental advantage of the isotopic method is that quantitative results are obtained without quantitative isolation or separation of any oxygen compound. The mass spectrometer could certainly be made part of the apparatus and the samples mass analyzed at desired intervals during degassing. The analysis could be stopped whenever sufficient mass data were obtained; a considerable saving in time and effort could thus be achieved.

THE INFLUENCE OF BORON ON CASE HARDENABILITY IN ALLOY CARBURIZING STEELS

BY C. F. JATCZAK AND E. S. ROWLAND

Abstract

The carburized end-quenched test was used to evaluate the effect of boron on the case hardenability of 80B20, 94BV20, 94B20 and 47B20 steels over the range of carbon contents between 0.60 and 1.0% for several heat treating conditions. Boron-free steels of substantially the same base analyses were procured and processed through all treatments with their boron-treated counterparts. Double quench treatments were simulated by gas carburizing the end-quench bars at 1700 °F (925 °C), air cooling, reheating to quenching temperatures of 1475, 1525, 1600 and 1700 °F (800, 830, 870, 925 °C) and end-quenching. Two popular single quench treatments were performed by pack carburizing the end-quench bars at 1700 °F (925 °C), direct end-quenching one group and pot cooling the other to 1525 °F (830 °C) before end-quenching.

THE RAPID increase in the use of boron-treated steels in the last two years has focussed a great deal of attention on the properties and characteristics of these types. The experience thus gained by manufacturer and user alike has resolved many of the problems inherent in the making, fabricating and heat treating of boron steels. One of the important questions about which controversy still exists is that of the influence of boron in the higher carbon levels of the case of carburized parts.

Our interest in this particular problem lies in the need to assess the possibilities of wartime use of boron-treated alloy steels in tapered roller bearing races. Our production heat treating equipment is designed for double quench practice on SAE 4620 steels and utilizes a fairly low hardening temperature. Furthermore, most of the races are hardened on a serrated plug which produces metallic contact between the race and the lands of the plug during the quenching cycle. Both of these conditions cause us to pay more attention to case hardenability in prospective steels for bearing application than if a single treat, drop hardening practice were used.

A paper presented before the Thirty-fourth Annual Convention of the Society, held in Philadelphia, October 18 to 24, 1952. Of the authors, C. F. Jatczak is research metallurgist and E. S. Rowland is chief metallurgical engineer with The Timken Roller Bearing Company, Steel and Tube Division, Canton, Ohio. Manuscript received April 11, 1952.

REVIEW OF THE LITERATURE

Rahrer and Armstrong (1)¹ were the first to establish the fact that the effect of boron on the hardenability of steel was influenced by the carbon content. Using the recommended hardening temperatures for each carbon range from below 0.20 to about 1.0% carbon on ladle and mold-treated carbon and alloy steels, they showed a linear decrease in the average hardenability factor for boron from about 2.0 at 0.20% to 1.0 (no effect) at about 0.90% carbon.

These results effectively stopped further experimental work on boron in high carbon steels until the present shortage of some alloying elements made imperative the substitution of lower alloyed boron treated for standard carburizing steels on the basis of equivalent core hardenability. Doubts were immediately raised regarding the ability of the boron-treated steels to harden in the case. However, scattered data published in the last year by Wray (2), Knowlton (3) and McBride (4) and obtained from carburized end-quenched bars indicate that a significant hardenability effect of boron is obtained in the higher carbon levels of the case, provided that single quench practice is used and/or the maximum carbon concentration in the case is restricted to about 0.90%. No systematic investigation of the effects of all commercial carburizing and hardening treatments on a single boron-treated carburizing steel has heretofore been published.

PROCEDURE

Four grades of boron treated carburizing steels were selected for study, namely, 80B20, 94B20, 94BV20 and 47B20, the base analysis of the last type being a low nickel modification of SAE 4620 used extensively during World War II by the bearing industry. These steels were procured in the form of 1¼-inch diameter hot-rolled bars from commercial, ladle-treated open-hearth and electric furnace heats. Untreated steels of the same compositions were obtained, when necessary, in the form of 30-pound induction heats forged to the same size. The analyses and other essential data are shown in Table I. Standard end-quenched hardenability curves for these steels in the uncarburized condition, quenched from 1700 °F (925 °C), are given in Fig. 1.

End-quench bars machined from these steels were heat treated in two ways. The bars destined for double quench treatments were gas carburized in a small Hevi-Duty fan driven retort carburizer for 16 hours at 1700 °F (925 °C) using a 10:1 ratio of RX to natural gas. Dummy bars, 1-inch diameter by 6-inch long, carefully machined on centers were inserted alternately with the end quench bars in such numbers that a dummy bar for carbon gradient determina-

¹The figures appearing in parentheses pertain to the references appended to this paper.

Table I
Compositions of Steels Tested

Type	Heat No.	Boron Addition	Chemical Analysis										Grain Size	
			C	Mn	Si	Cr	Ni	Mo	Cu	V	Ti	B		Al
8020	2653 Ind.	0.21	0.72	0.28	0.26	0.40	0.09	0.10	5/7
80B20	10541 E.F.	Gr. #79	0.19	0.78	0.32	0.21	0.37	0.10	0.13	0.038	0.0007	0.055	5/7
9420	57222 O.H.	0.18	0.97	0.23	0.40	0.51	0.13	0.09	5/7
94B20	68775 O.H.	Gr. #79	0.22	0.83	0.24	0.40	0.36	0.12	0.09	0.020	0.0007	0.017	5/8
9420	68696 O.H.	0.22	0.80	0.20	0.40	0.33	0.12	0.11	5/8
94BV20	40189 O.H.	Gr. #1	0.18	0.90	0.27	0.45	0.46	0.12	0.08	0.045	0.0003	0.043	5/7
4720	2654 Ind.	0.20	0.55	0.27	0.66	1.24	0.22	0.07	6/8
47B20	02324 E.F.	Gr. #79	0.23	0.65	0.20	0.60	1.24	0.29	0.12	0.040	0.0008	0.036	6/8

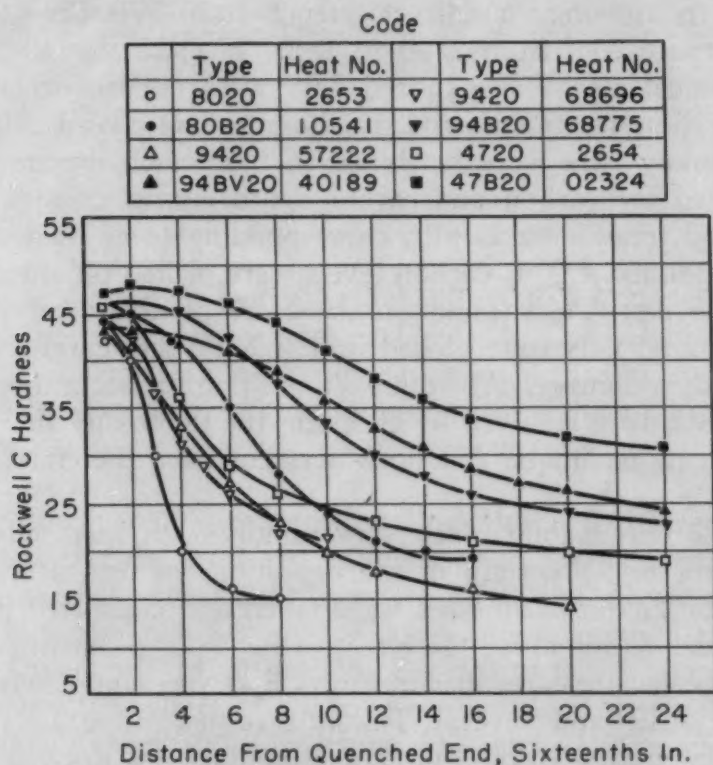


Fig. 1—Standard Hardenability Curves of All Steels in Uncarburized Condition, End-Quenched From 1700 °F (925 °C).

tion was present for each hardening temperature of each steel. After carburizing, all bars were removed from the retort and air-cooled. Preliminary experiments showed clearly that the error in prior structure due to air cooling from the carburizer rather than oil quenching was negligible compared to the errors in subsequently grinding flats on distorted bars. Both the standard and dummy bars were reheated in a salt bath for 45 minutes at temperatures of 1475, 1525, 1600 and 1700 °F (800, 830, 870, 925 °C), the standard bars end-quenched and the dummy bars cooled in Silocel. Thirty-minute tempering at 1200 °F (650 °C) was found necessary in a few cases to facilitate machining of the dummy bars. The precaution of putting the dummy

bar through the same hardening austenitizing treatment as the end-quenched bar was shown by preliminary experiments to be vitally necessary since the carbon diffusion encountered at the higher hardening temperatures caused discrepancies of as much as 0.07% carbon between as-carburized and reheated bars.

The end-quench bars destined for single quench treatments were pack carburized at 1700 °F (925 °C) in a low energized compound to produce the same carbon gradient as the gas carburizing cycle, approximately 0.01% carbon drop per 0.001-inch depth between 1.0 and 0.50% carbon. Dummy bars were included for each steel and each of the two treatments, (a) direct quench from 1700 °F (925 °C), and (b) furnace cool from 1700 to 1525 °F (925 to 830 °C), followed by quenching. The standard bars were end-quenched as the final step in these treatments and the dummy bars cooled in Silocel.

The dummy bars were machined in 0.005-inch increments, the chips analyzed for carbon and carbon-depth curves constructed for each steel and treatment. Depths corresponding to at least the 0.60, 0.70, 0.80, 0.90 and 1.00% carbon levels were picked off these curves and duplicate flats wet ground on the corresponding end-quenched bars. All ground flats were etched in 4% Nital and carefully examined for grinding damage. Any doubts regarding the accurate positioning of the flats were resolved by checking the depths by the M_s case depth measuring technique (5) on wafers cut from the end-quenched bars.

Since the hardenability may vary rapidly with small changes in carbon content under certain of the conditions of test, Rockwell A and 500-gram Tukon hardnesses were taken and converted to Rockwell C in order to minimize the effect of depth of penetration of the indenter. The hardness-depth curve was first run completely on the Rockwell A scale and several Tukon readings taken to precisely determine the hardness position corresponding to Rockwell C-60. Conversion curves were obtained directly by using all three measuring methods on a single polished flat of an end-quenched bar of 4700 steel melted to 1.0% carbon which covered the full range of microstructures encountered.

The distance on the end-quenched bar to the Rockwell C-60 position was taken as the hardenability criterion in all cases. This value approximates closely the 90% martensite level but, more importantly, is only slightly above the generally conceded minimum acceptable hardness for carburized parts.

RESULTS AND DISCUSSION

The carburized end-quench data for the four temperatures plotted as distance to the Rockwell C-60 versus carbon content for the 8020 and 80B20 steels are shown in Fig. 2. The untreated steel exhibits

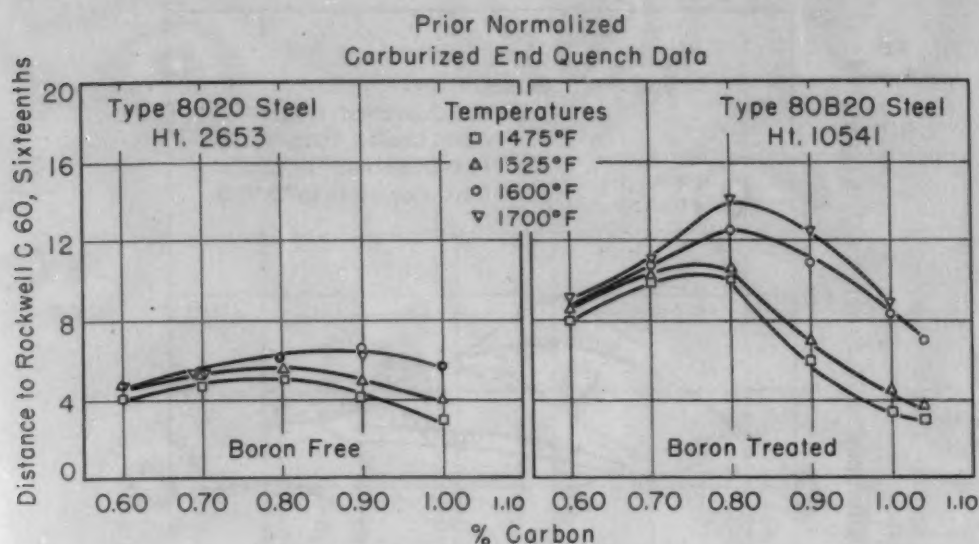


Fig. 2—Case Hardenability of 8020 and 80B20 Steels After Air Cooling From Carburizing and Reheating to Four Hardening Temperatures.

the familiar maximum in the hardenability-carbon curve corresponding to the point at which excess carbide is retained in the austenite to nucleate the transformation during quenching and to deplete the austenite in alloy content. This maximum shifts to higher hardenability values and higher carbon contents as the hardening temperature is raised.

The boron-treated counterpart shows the usual large increase in hardenability at the 0.60 and 0.70% carbon levels, thus maintaining the advantage shown at 0.20% carbon (Fig. 1). Above about 0.80% carbon, however, the boron steel loses this advantage rapidly when quenched from the 1475 to 1525 °F (800 to 830 °C) range until at 1.0% carbon, the effect of boron is negligible. This checks well with the original Rahrer and Armstrong (1) data. When quenched from 1600 and 1700 °F (870 and 925 °C), however, the boron steel retains a significant advantage at all carbon contents, although the increment due to boron is much less at 1.0% than at 0.60% carbon.

Plotted together in Fig. 3 are the results on both steels after the single quench treatments. On the plain steel, the results are not essentially different from the reheating treatment at 1700 °F (925 °C). The results at the 0.70% carbon level are low by an amount about equal to the probable experimental error, about $1\frac{1}{2}$ sixteenths in this hardenability range. The 80B20 steel, however, shows a distinct loss in hardenability at all carbon levels as a result of either direct quenching from 1700°F (925 °C) or pot cooling to 1525 °F (830 °C) followed by quenching when compared with the 1700 °F (925 °C) reheat. Wray (2) reported a loss in core hardenability in 86B20 steel on quenching direct from the carburizer when compared to a reheat to approximately the same temperature. His

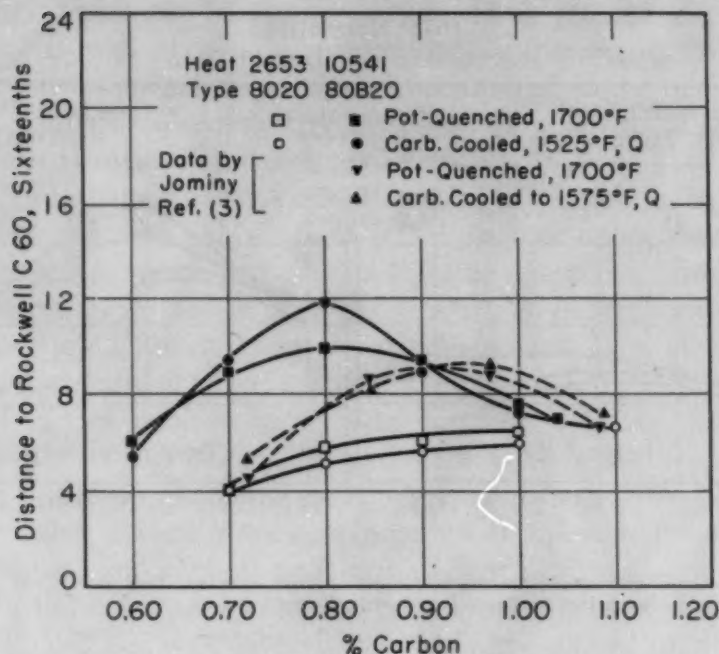


Fig. 3—Effect of Single Quench Treatments on the Case Hardenability of 8020 and 80B20 Steels.

results showed that pot cooling to 1575 °F (855 °C) before quenching restored the core hardenability to the level obtained on reheating. Only at the 0.80% carbon level did we get a hardenability improvement of the pot cool to 1525 °F (830 °C) treatment over the direct quench and neither reached the level of the 1700 °F (925 °C) reheat although they are probably within the experimental error at 1.0% carbon. The two dotted curves in Fig. 3 represent data by Jominy taken from an SAE Division VIII report edited by Knowlton (3) on an 80B20 heat of lower alloy content which confirms the lack of effect of pot cooling prior to quenching in this carbon range. The large case hardenability advantage of single over double quench treatments at normal hardening temperatures is, of course, obvious.

The effect of boron on the hardenability through the case of steel of somewhat higher alloy content (94BV20) is shown in Fig. 4. Some important differences from the previous pair of steels are immediately apparent. At the 1475 °F (800 °C) hardening temperature, the plain and boron-treated steels are an exact match over the entire carbon range shown, while at 1525 °F (830 °C) the plain 9420 has slightly higher hardenability in the 0.80 to 0.90% carbon range. Only at the higher reheating temperatures of 1600 and 1700 °F (870 and 925 °C) does the boron-treated material show to real advantage. Even here, the hardenability difference is reduced to near zero at 1600 °F (870 °C) before the 1.0% carbon level is reached while at 1700 °F (925 °C) the effect is quite small at this carbon level. When proper allowance is accorded to the alloy difference between the two steels,

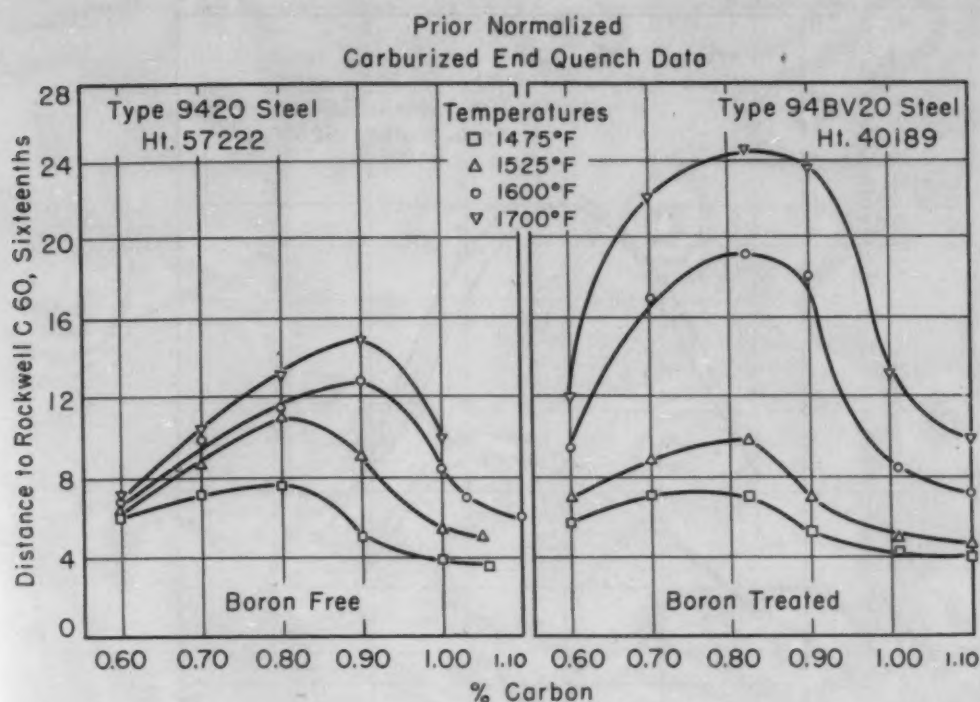


Fig. 4—Case Hardenability of 9420 (Heat 57222) and 94BV20 Steels After Air Cooling From Carburizer and Reheating to Four Hardening Temperatures.

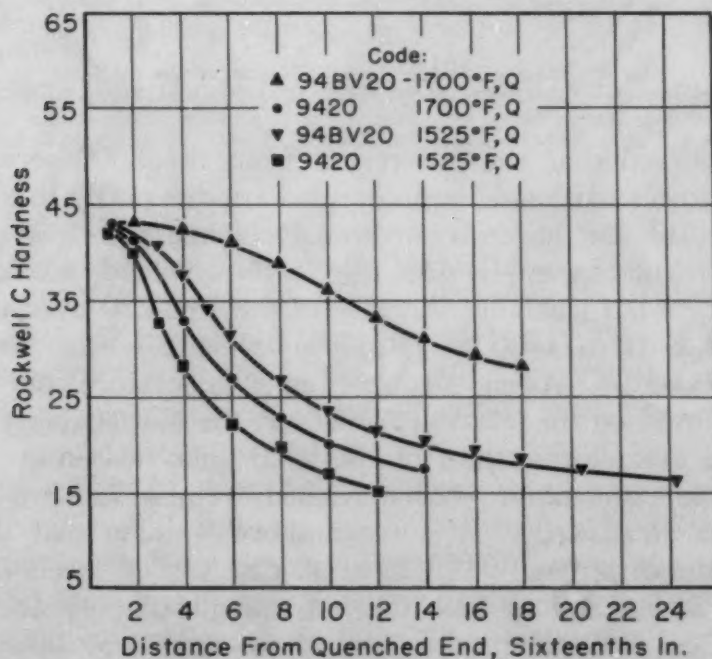


Fig. 5—Standard Core Hardenability Curves of 9420 (Heat 57222) and 94BV20 End-Quenched From 1525 and 1700 °F (830 and 925°C).

the boron-treated heat appears to better advantage and, at these high hardening temperatures, the boron effect is about the same as in the 80B20 steel.

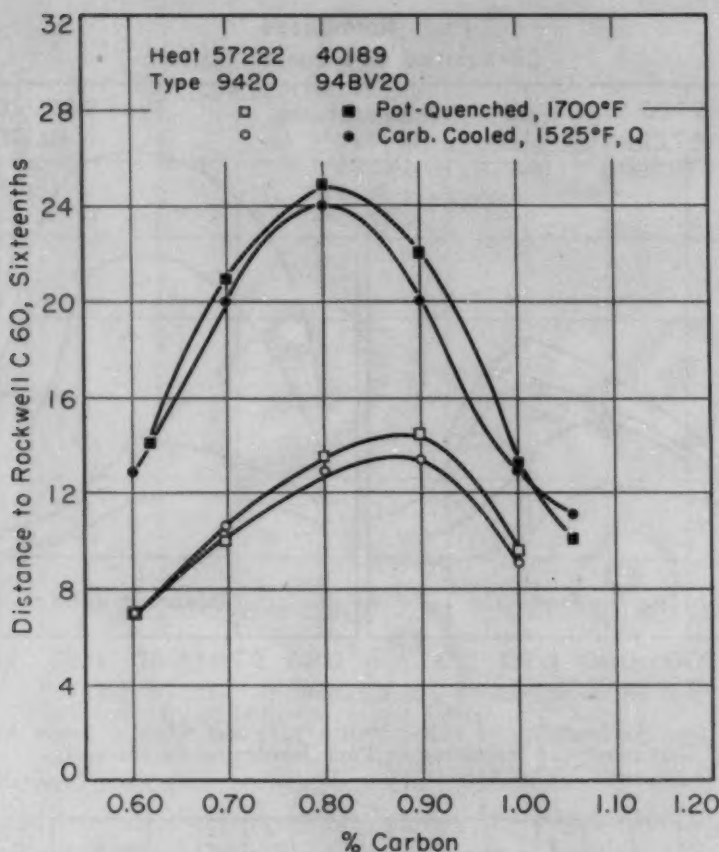


Fig. 6—Effect of Single Quench Treatments on the Case Hardenability of 9420 (Heat 57222) and 94BV20 Steels.

It is believed that the differences from the 8000 series steels noted at the lower hardening temperatures are due partly to the lower alloy content of the boron-treated analysis but principally to the vanadium content of the 94BV20. Fig. 5 shows clearly the usual increment in core hardenability increase of the 94BV20 over the 9420 when quenched from 1700 °F (925 °C) in spite of the low boron value of 0.0003%. When a quenching temperature of 1525 °F (830 °C) is used on the 94BV20, however, the hardenability falls to a value little greater than that of the 9420 quenched from 1700 °F (925 °C), while the plain 9420 quenched from 1525 °F (830 °C) shows only a small drop. It is the authors' opinion that the poor response of the carburized 94BV20 at all case carbon levels from the 1475 to 1525 °F (800 to 830 °C) hardening range is due to the nucleating effect of the undissolved vanadium carbide in the austenite.

A glance at Fig. 6 is sufficient to reveal that the single quenching treatments on the 9400 steels show nothing startling. The results on the plain heat are in good agreement with the 1700 °F (925 °C) quench of Fig. 4 and the same may be said of the boron-treated analysis. The small loss in hardenability on cooling to 1525 °F (830 °C) before quenching may not be real. Of course, a great ad-

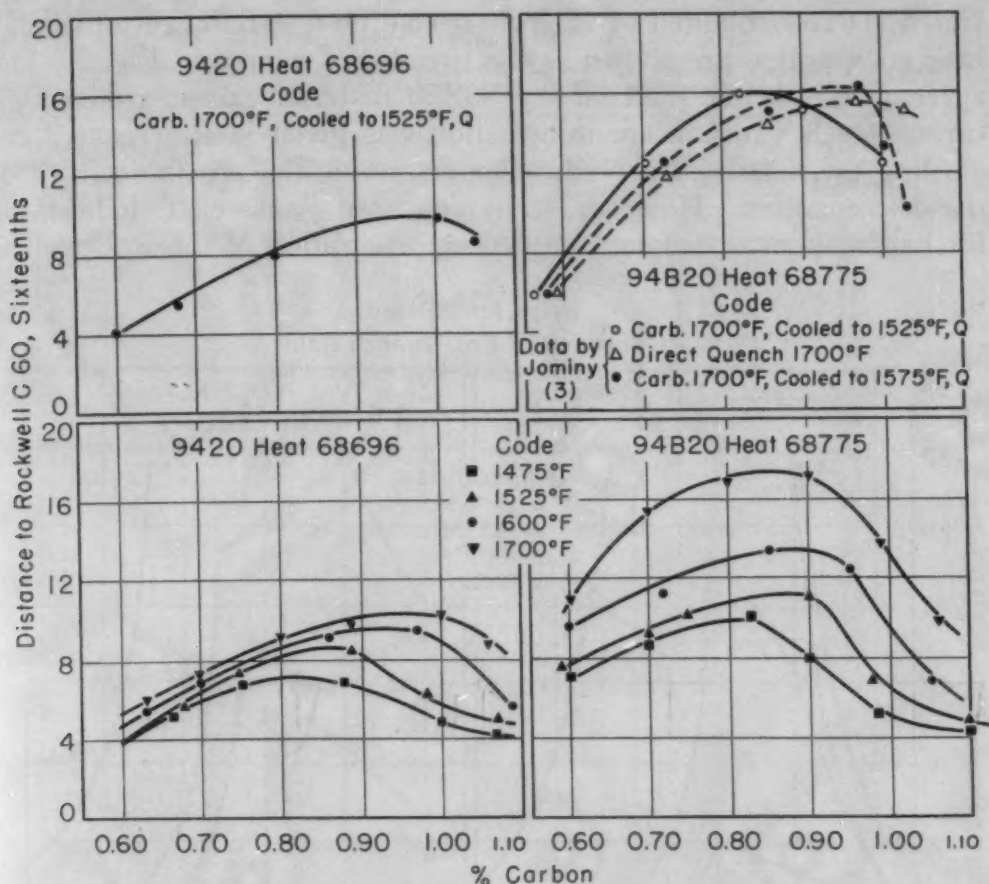


Fig. 7—Case Hardenability of 9420 (Heat 68696) and 94B20 Steels. Bottom, after air cooling from carburizer and reheating to four hardening temperatures, and Top, after carburizing at 1700 °F (925 °C), cooling to 1525 °F (830 °C) and quenching.

vantage in case hardenability exists in favor of single quenching over a double quench treatment at a normal hardening temperature of 1525 °F (830 °C).

In view of the results obtained on 94BV20, a heat of 94B20 (Heat No. 68775 of Table I), treated with Grainal No. 79, was chosen as representative of this type. Since the alloy content of this heat was considerably lower than the original 9420 heat (No. 57222), an additional 9420 heat (No. 68696) was chosen as companion material to test with it. The double quench treatments on both heats at the four quenching temperatures are shown in the lower part of Fig. 7 and exhibit the same behavior as the 8020 and 80B20 types of Fig. 2, also Grainal No. 79 treated. There is little effect of the boron above 0.90% carbon until the quenching temperature is raised to 1600 °F (870 °C).

Of the single quench treatments, only the one involving cooling from the carburizer to 1525 °F (830 °C) before quenching was used. The results are a good match for the respective 1700 °F (925 °C) reheating treatments. Jominy's data, taken from the same SAE Divi-

sion VIII report edited by Knowlton (3), on a 94B20 heat of similar base composition are shown as the two dotted curves in Fig. 7. The agreement is better than on the 80B20 material except at the high carbon levels. Insufficient information was given in Reference 3 regarding the details of procedure to determine the possible causes of the discrepancies. However, if Jominy used Rockwell C indications for hardness measurement, the deeper penetration of the Rockwell C

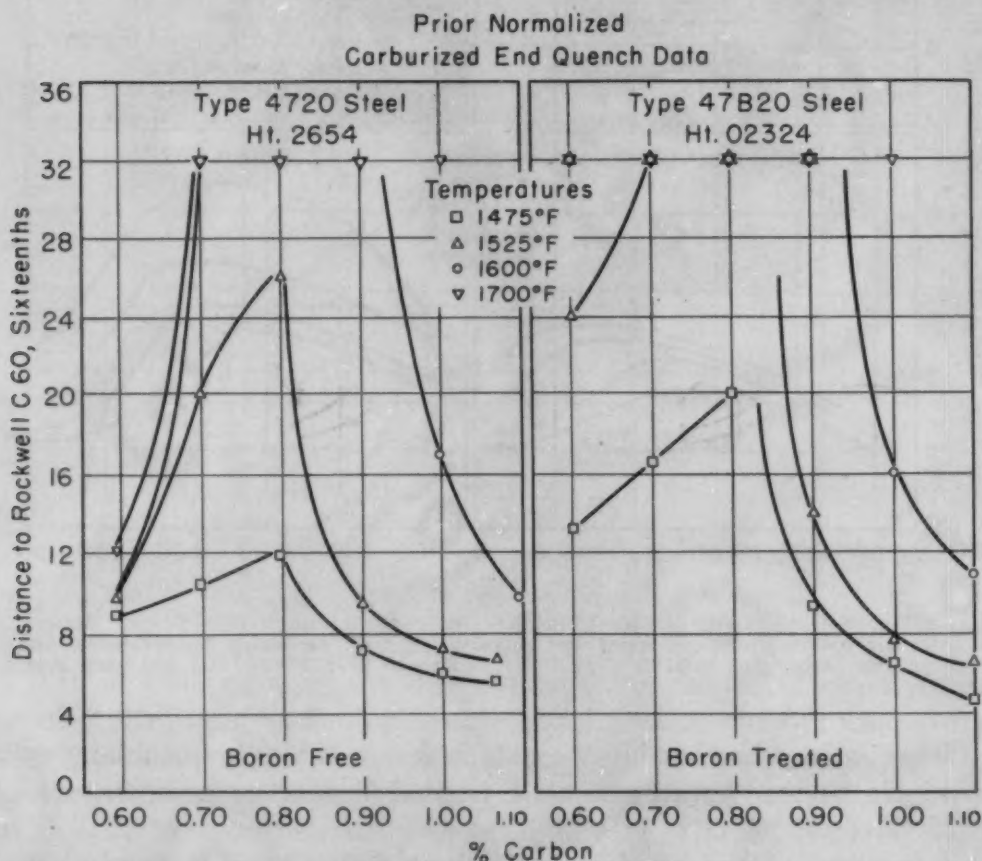


Fig. 8—Case Hardenability of 4720 and 47B20 Steels After Air Cooling From Carburizer and Reheating to Four Hardening Temperatures.

indenter into the harder underlying structure would affect the hardness results, and the shape of the final curve obtained would be altered accordingly and in the direction indicated.

Finally, in order to show the behavior of boron in a base composition of higher alloy content, the same series of tests were run on a 4720 and 47B20 heat. The results for the double treatments, shown in Fig. 8, are quite fragmentary because at many of the testing conditions the hardenability of the intermediate carbon levels is too high for the end-quench test to measure. The behavior of boron at this alloy level is quite similar to the previous types tested. There is no effect of boron at the 1.0% carbon level for quenching temperatures as high as 1600 °F (870 °C), while a significant improvement due to

Table II
Boron Multiplying Factors for All Carbon Levels and Treatments
Corrected to Base Analysis of Boron-Free Steel

Quench Temperature °F	Carbon Level					
	0.60	0.70	0.80	0.90	1.00	1.05
80B20 (Heat 10541) Corrected to Heat 2653						
1475	1.52	1.47	1.40	1.21	1.08
1525	1.52	1.47	1.36	1.15	1.05
1600	1.57	1.54	1.53	1.37	1.21
1700	1.57	1.54	1.53	1.44	1.25
1525D	1.68	1.68	1.32	1.06
1700D	1.65	1.43	1.33	1.06
94BV20 (Heat 40189) Corrected to Heat 57222						
1475	1.07	1.10	1.10	1.07	1.07	1.06
1525	1.13	1.12	1.00	1.00	1.00	1.04
1600	1.62	1.47	1.45	1.30	1.17	1.06
1700	1.70	1.62	1.50	1.38	1.28
1525D	1.65	1.55	1.50	1.33	1.32
1700D	1.65	1.62	1.43	1.33	1.33
94B20 (Heat 68775) Corrected to Heat 68696						
1475	1.50	1.28	1.20	1.09	1.02	1.03
1525	1.45	1.30	1.24	1.15	1.04	1.00
1600	1.54	1.35	1.31	1.15	1.10	1.03
1700	1.57	1.53	1.44	1.38	1.20	1.05
1525D	1.50	1.62	1.55	1.28	1.18
1700D
47B20 (Heat 02324) Corrected to Heat 2654						
1475	1.20	1.20	1.25	1.15	1.00	0.97
1525	1.50	1.19	1.00	0.97
1600	1.67	0.97
1700	1.50
1525D	1.50
1700D	1.44

boron was noted at the 0.90% carbon level. The single quench treatments, though run, are not included because only the 0.60% carbon levels were measurable.

The data of Table II are an attempt to summarize the effect of boron on the case hardenability of all steels for all treatments covered in the investigation. In Table II are listed the multiplying factors for boron at each carbon level and treatment computed by the same procedure as was used by Rahrer and Armstrong (1). Briefly, the distances to Rockwell C-60 (approximately 90% martensite) on the hardenability curves were converted to DI values for both the plain and boron-treated steels. The DI values for the boron-treated steels were then corrected to the base analysis of the appropriate boron-free steel. The ratio of these DI values is the multiplying factor for boron at each carbon level and treatment. It is recognized that this is a synthetic multiplying factor in some respects since solution is far from complete in many treatments. It is assumed that the degree of solution in the boron-treated and boron-free steel at a given carbon level and treatment are the same and hence the multiplying factor is a true relative value of the boron effect.

The increase in boron effect with increase in quenching temperature and decrease in carbon level is clearly apparent. It is equally

clear that, as far as the carburized end-quenched bar is able to follow, the boron effect from the Grainal No. 79 additions is very close to the same value at all three levels of alloy content.

SUMMARY

The carburized end-quenched test was used to evaluate the effect of boron on the case hardenability of 80B20, 94BV20, 94B20 and 47B20 over the range of carbon contents between 0.60 and 1.0% for several heat treating conditions. Boron-free steels of substantially the same base analyses were procured and processed through all treatments with their boron-treated counterparts. Double quench treatments were simulated by gas carburizing the end-quench bars at 1700 °F (925 °C), air-cooling, reheating to quenching temperatures of 1475, 1525, 1600 and 1700 °F (800, 830, 870 and 925 °C) and end-quenching. Two popular single quench treatments were performed by pack carburizing the end-quench bars at 1700 °F (925 °C) direct end-quenching one group and pot cooling the other to 1525 °F (830 °C) before end-quenching. Dummy specimens destined for carbon gradient determinations were included for each steel and treatment and carried through the entire heat treating cycle except for cooling in Silocel instead of end-quenching. Duplicate flats were wet ground at approximately 0.010-inch carbon level increments from 1.0 to 0.60% carbon, the longitudinal hardness determinations made by Rockwell A and 500-gram Tukon methods and converted to Rockwell C. The results are presented as a series of plots of the distance from the quenched end to the Rockwell C-60 position on the end-quench bar for each hardening treatment on each steel. Multiplying factors for boron were computed and are presented in tabular form for each carbon level and treatment for the boron-treated steels with the analyses of these steels corrected in DI value to the base composition of the boron-free counterparts.

CONCLUSIONS

1. For all heat treatments used, the effect of boron on the case hardenability of all four boron-treated steels investigated decreased with increase in carbon content.
2. In double quench practice, the effect of boron is low to negligible at high carbon levels with a normal hardening temperature in the 1475 to 1525 °F (800 to 830 °C) range. In general, the boron effect increased with quenching temperature at a given carbon level.
3. Both single quench treatments employed yielded much higher boron effects at the higher carbon levels than double quench treatments at normal hardening temperatures. Both treatments yielded results about equal to that obtained on reheating and quenching from 1700 °F (925 °C). No evidence of serious fading of the boron effect

as a result of direct quenching was noted in the carbon range investigated and pot cooling to 1525 °F (830 °C) before quenching did not increase the boron effect.

4. In the normal hardening range of 1475 to 1525 °F (800 to 830 °C) with double quench practice, the single heat of 94BV20 (treated with Grainal No. 1) tested exhibited negligible boron hardenability effect at all carbon levels investigated. Higher hardening temperatures and single quench treatments yielded as large boron effects as any obtained. It is believed that this behavior is due to the nucleating effects of undissolved vanadium carbide on austenite transformation at low solution temperatures. In contrast, a heat of 94B20 (Grainal No. 79 treated) showed much higher boron effects at low hardening temperatures and underwent only the normal small increase in boron effect with increase in quenching temperature.

5. Within the limits of hardenability measurement, the steels treated with Grainal No. 79 appeared to show the same behavior over the full range of alloy content from 80B20 to 47B20.

References

1. G. D. Rahrer and C. D. Armstrong, "The Effect of Carbon Content on the Hardenability of Boron Steel", *TRANSACTIONS, American Society for Metals*, Vol. 40, 1948, p. 1099.
2. P. R. Wray, "Boron Steels for Constructional Parts and for Carburizing", *METAL PROGRESS*, Vol. 60, 1951, p. 59.
3. H. B. Knowlton, "Reports on Boron Steels", *SAE Journal*, Vol. 59, 1951, p. 17.
4. B. L. McBride, "Review of Boron Steel Development", *SAE Journal*, Vol. 60, 1952, p. 26.
5. E. S. Rowland and S. R. Lyle, "The Application of M_s Points to Case Depth Measurement", *TRANSACTIONS, American Society for Metals*, Vol. 37, 1946, p. 27.

DISCUSSION

Written Discussion: By E. J. Dofter and W. E. Jominy, Engineering Department, Chrysler Corp., Detroit.

The authors should be commended on their excellent paper in which due recognition was given to precautions necessary in running carburized end-quench hardenability test bars. Based on work done in our laboratories on carburized steels of similar composition, we generally agree with the results presented in this paper. Perhaps because of the renewed interest in carburized hardenability test bars, there has been less agreement between laboratories on techniques to be used in running such tests as well as in how data should be reported.

In their paper the authors mentioned that carburized and direct quenched bars were reheated in a salt bath to successingly higher temperatures. Since no mention was made of the type of salt used or what measures were taken to protect the surface of the carburized bars, we wondered

if the authors experienced any difficulty from surface disturbances such as carburization or decarburization on the test bars.

The authors also mention that the 500-gram Tukon load was used to determine exactly the hardness position corresponding to Rockwell C-60 after the bar had been run using the Rockwell A. In this connection, it has been our experience that light loads, such as are frequently used with the Tukon, tend to give more scatter due to inhomogeneities and banding in steel, so that it is generally more difficult to determine exactly the hardenability to a given hardness. As the authors mention, tests made on carburized bars using heavy loads yield erroneous results because of the penetration effect. As a compromise between these two conditions we have employed the Rockwell N-15 scale with very satisfactory results.

It has also been our experience that on carburized bars at 1.00% carbon and above, the maximum hardness is seldom attained near the water-cooled end on direct-quenched test bars due to the presence of retained austenite. It thus becomes very difficult to determine hardenability at high carbon contents using hardness methods. Metallographic examination of test bars can overcome this. It has been our practice to sub-cool bars where the presence of retained austenite is suspected. Would the authors care to comment on their experience with retained austenite in carburizing hardenability studies?

Written Discussion: By Harry B. Knowlton, chief engineer, Materials Engineering, International Harvester Co., Chicago.

The authors are to be congratulated on presenting some very timely and valuable data upon the effect of boron on the case hardenability of various alloy steels. We are certainly much concerned with developing all possible information with regard to the effect of various alloying elements upon the hardenability of the case portion of case-hardened steel parts. We have been fairly successful in calculating the expected hardenability of 0.90 carbon layers of some of the alloy steels, although we have been told that the same multiplying factors, which are given for hardenability effect of different elements at 0.40 carbon, cannot always be used at carbon contents of 0.70 to 0.90. It has been stated that high nickel content has a much greater effect upon the hardenability of high carbon steels than it does with 0.40 carbon steels. We believe that there is need for a great deal more data on this subject.

We feel very much encouraged over the results presented by the authors of this paper, as they would indicate that while the hardenability effect of boron decreases with increase of carbon content, it seems to remain fairly constant for different alloy steels when given a direct quench from 1700 °F. We are particularly interested in this subject because we feel that we must determine the minimum hardenability which may be expected with the lowest hardenability heat of any proposed steel. Certainly we must guarantee that any production part under consideration can be hardened to the specified minimum (Rockwell C-57 or 60) on the surface with a production quench.

Similarly it may be necessary that different depth below the surface shall attain the minimum necessary hardness to meet the stress at that depth. The authors of this paper are concerned primarily with hardness of Rockwell 60 and above, which is logical for their products. The writer

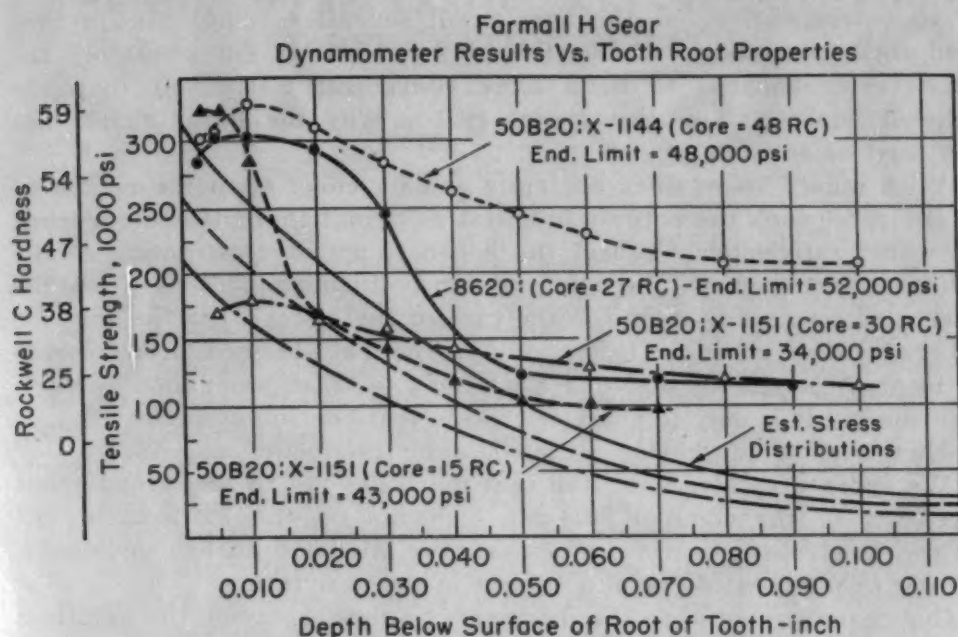


Fig. 9—Farmall H Gear Dynamometer Results Versus Tooth Root Properties.

believes, however, that those concerned with heavy-duty case-hardened gears and pinions should take into consideration the minimum hardness which will be obtained by a production heat treatment of various steels, at various depths below the surface.

In some cases the boron steels have shown an advantage over previous steels in that they have produced a hardness of Rockwell C-50 for a greater depth. (See Fig. 9.) In another case, we found a tendency for the hardness at a depth of about 0.015 to 0.020 inch below the surface, determining the difference between success and failure. We would urge everyone concerned with case-hardened alloy steel parts to make an extensive study of the effect of hardness, at different levels in the case, upon actual performance in service.

Authors' Reply

We are happy that some interest has been shown in this subject of carburized hardenability, since it has such real importance on the performance of heavy-duty gears and roller-bearing components.

Messrs. Dofter and Jominy's question regarding surface protection during reheating of the bars in salt is well taken. A 50% KCl-50% NaCl bath was used at the lower temperatures and a 90% BaCl₂-10% NaCl bath at 1700 °F. These baths were deoxidized at regular intervals and the carbon cuts taken on the dummy bars never showed carbon loss to a depth greater than 0.005 inch. Since the dummy bars had a greater opportunity for carbon loss than the end-quench bars (due to Silocel cooling) and no hardness readings were taken at depths below the surface of less than 0.015 inch, we did not feel that decarburization affected the results in any way.

The 500-gram Tukon test does produce significant scatter of readings

due to heterogeneity but the average of several readings always produced good correlation with the Rockwell A test. In our laboratory the Tukon tester happens to be a more convenient instrument than the Rockwell Superficial but we see no reason why the latter should not be at least as satisfactory.

With regard to retained austenite and its effect upon the results of this study, we took the entirely practical viewpoint that the end-quenched bars would satisfactorily reflect the hardness and microstructure of the production part quenched after the same austenitizing conditions. While the presence of retained austenite in the case of these steels (particularly the 4720 grade) does lower the hardenability over that obtained after sub-zero treatment, it is seldom that one can afford to treat production parts in this manner. It is only in those few cases that the sub-zero treated end-quenched bar should provide useful data for production control.

We agree with Mr. Knowlton that much has yet to be learned about the effects of the common alloying elements on the hardenability of high carbon steels and carburized cases. We intend to publish some work from our own laboratory on this subject in the near future.

Our thanks are due to the discussers of this paper for the additions they have made to its value.

THE ROLE OF ANELASTICITY IN CREEP, TENSION, AND RELAXATION BEHAVIOR

By J. D. LUBAHN

Abstract

The gradual shortening that follows the removal of the load in a creep test is called creep recovery. The experiments described in this paper show that creep recovery exhibits the same behavior characteristics as anelastic deformation. Both can be described in terms of a mechanical model composed of springs and dashpots.

In a Cr-Mo-V steel, the amount of creep recovery as a function of time is related to (a) the deviations from linearity of a stress-strain curve at small stress, (b) the temporary shortening and eventual lengthening following partial unloading, and (c) the stress relaxation behavior (at constant length) following partial unloading. The observations are explained quantitatively by identifying creep recovery with anelastic deformation.

There is a limiting stress for the Cr-Mo-V steel, below which creep is essentially all anelastic. This limiting stress depends somewhat on the duration of the creep test; it is about 20,000 psi at 800 °F (425 °C) and can be raised to at least 40,000 psi by as little as one per cent plastic strain at 800 °F (425 °C).

THE INFLUENCE OF STRESS AND TIME ON CREEP RECOVERY—PART I

TORSION pendulum experiments (1)¹ on metal wires have shown that a sufficiently small constant stress will produce non-instantaneous strain (creep) that is completely recoverable isothermally in a sufficiently long time. This noninstantaneous strain has been called anelastic strain (or anelastic creep), and is to be distinguished from elastic strain, which occurs instantaneously. Anelastic strain exhibits the following characteristics in isothermal tests:

(a) The amount of strain introduced in a given time is proportional to the stress;

(b) The curve of shortening versus time after unloading is identical with the prior curve of lengthening versus time under constant load, for times that are considerably shorter than the duration of prior load;

¹The figures appearing in parentheses pertain to the references appended to this paper.

The author, J. D. Lubahn, is associated with the Metallurgy Research Department, The Knolls, General Electric Co., Schenectady, N. Y. Manuscript received July 3, 1952.

(c) When the time after unloading is comparable with or exceeds the loading time, the curve of shortening versus time is related to the prior lengthening curve in a more complex manner. The relationship is also more complicated when the prior load is not constant or when only part of it is removed. However, the mechanical behavior under any conditions can be described in terms of a mechanical analogy (2) in which springs and dashpots are arranged in the manner shown in Fig. 1.

The anelastic characteristics described above have been determined at very low stress levels—so low that plastic strain (permanent,

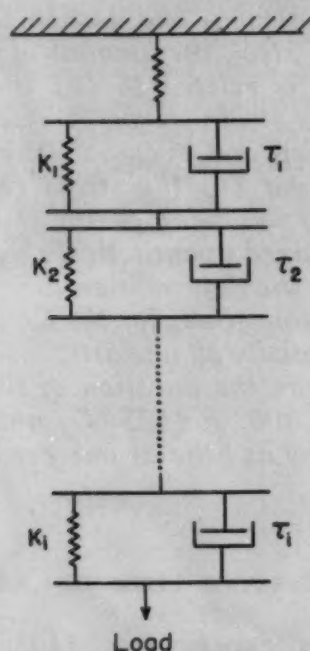


Fig. 1—Schematic Diagram Showing a Spring-Dashpot Analogue to Anelastic Strain.

or nonrecoverable strain) does not occur and the specimen will return to its original configuration if allowed to remain at zero applied stress for a sufficiently long time. It has been found (3-6) that gradual shortening also will occur isothermally following unloading from much higher stresses, particularly stresses so high that plastic creep has occurred, that is, the specimen will not return subsequently to its original length. Under these conditions the gradual shortening observed after unloading may be of a different nature from what has been called anelastic behavior, and so it has become customary to refer to it as "creep recovery" rather than anelasticity. It will be the purpose of this paper to examine in detail the nature of creep recovery at comparatively high stresses both in the presence and absence of plastic strain, to show that creep recovery conforms to the same set

of laws as does anelastic shortening, and thus actually is anelastic shortening, and to inquire into the effects of this anelastic strain on various deformation behaviors.

Test Procedure and Equipment

The tests were made in a four-bar horizontal creep furnace, the temperature of which could be controlled to within 3 °F with time and along the gage length. The furnace winding was a spiral with a tap and resistor approximately 12 inches from each end to adjust temperature distribution manually. A movable platinum-platinum-rhodium thermocouple in a tube parallel to the specimens and equidistant from all of them provided a convenient and accurate means of checking the temperature distribution.

Load was applied through a 100:1 lever combination. The bar from which the weight pan was hung was maintained in a horizontal position by means of a threaded rod and nut at the opposite end of the furnace, which facilitated moving the entire specimen assembly either forward or backward under load, thus raising or lowering the lever arm as its angular position changed with the creep.

When a load was to be applied, the lever arm was first raised to the top of its stroke so that when the load was applied the lever arm would come to a horizontal position rather than to the bottom of its stroke. The load was applied in a second or two.

The specimen was one-half inch in diameter and had a 10-inch gage length. The change in distance between split clamps at the ends of the gage length was transferred to the outside of the furnace by means of two pairs of rods, each pair consisting of a rod from each end of the gage length. The relative motion for the two rods of each pair was measured by a 1/10,000-inch dial gage. The two pairs of rods were symmetrically disposed so that the two dial gages measured extension on diametrically opposite sides of the bar. The changes in reading on the two gages were averaged and divided by ten to obtain centerline strain.

Strain-Time Relations for Creep Recovery

Fig. 2 shows strain-time data for a Cr-Mo-V² steel at 800 °F following unloading from 46,000 psi. The prior load of 46,000 psi caused about 0.0002 plastic strain in its 100-hour duration. Curve b in Fig. 2 is a magnification in time of curve a. The rate of shortening is very large at first, but it diminishes rapidly and becomes very small in a length of time comparable with the load duration. Further shortening cannot be measured with the present gage in a time that is reasonable to wait. The curve has the general form of

²Main constituents: 0.41% carbon, 0.99% chromium, 0.58% molybdenum, 0.31% vanadium; oil-quenched from 1650 °F as a 3-inch round, tempered 12 hours at 1240 °F, then 5 hours at 1100 °F.

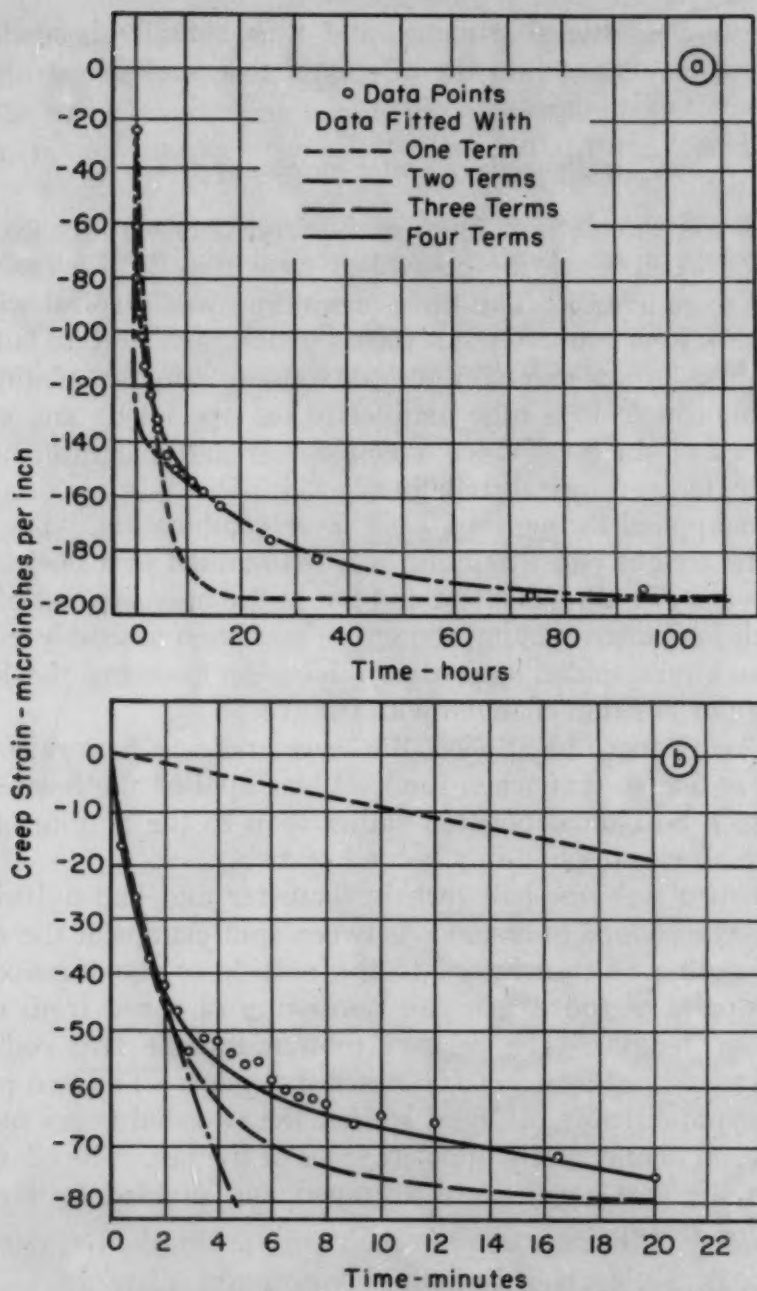


Fig. 2—(a) Strain-Time Curve at 800 °F After Unloading From Approximately a 100-Hour Period at 46,000 Psi and 800 °F; (b) Magnification in Time of (a).

the exponential decay curves that are characteristic of anelastic shortening. Fig. 2 shows that the curve cannot be fitted with a single term of the form

$$\epsilon = a(1 - e^{-t/\tau}), \quad \text{Equation 1}$$

where ϵ is the shortening per unit length, t is time beginning at the instant of unloading, and a and τ are constants. In other words, it is necessary that there be several spring-dashpot combinations with

different relaxation times τ in the mechanical analogue of Fig. 1. A method of successive approximations, using more and more terms as required (see Fig. 2), shows that four terms, with relaxation times a factor of ten apart in successive terms, are required to fit the data. Thus, the equation for the curve is

$$10^6 \epsilon = 63.4 (1 - e^{-t/1500}) + 63.4 (1 - e^{-t/150}) + 17.8 (1 - e^{-t/15}) + 54.0 (1 - e^{-t/1.5}).$$

Equation 2

The concept of a relaxation spectrum provides a more direct method of finding the exponential series that fits the creep recovery

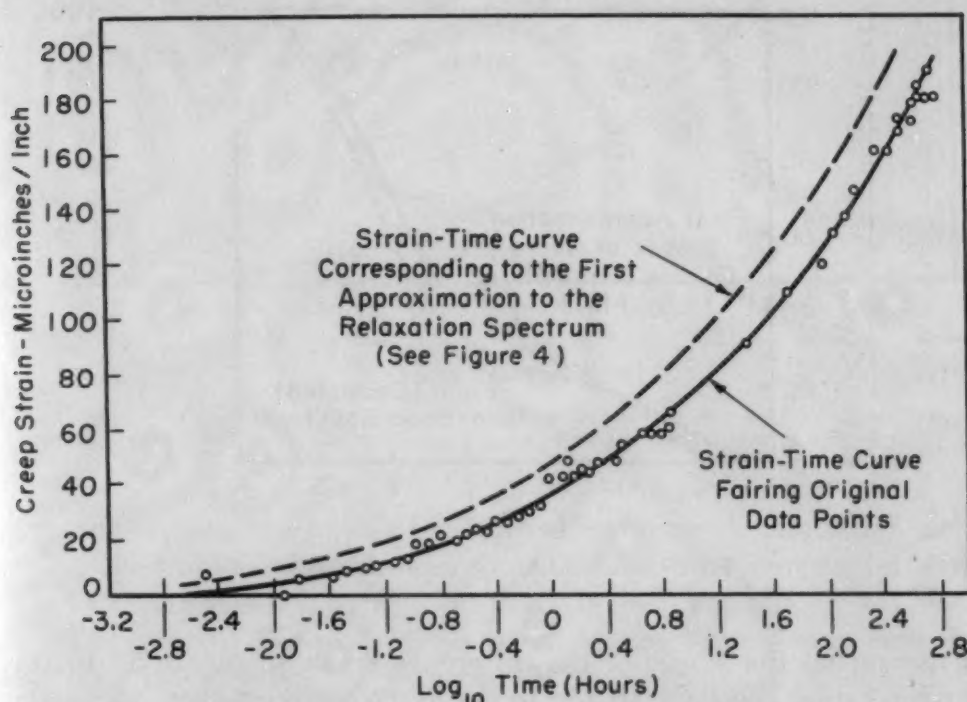


Fig. 3—Creep Curve for Cr-Mo-V Steel at 40,000 Psi and 800 °F After Pre-straining by 0.007 at 68,000 to 72,000 Psi and Resting 1000 Hours at 4000 Psi.

data. Consider an infinite series of terms, each like that in Equation 1, each having an infinitesimal as its coefficient, and each having a relaxation time greater by an infinitesimal than that of the preceding term. Then the series can be represented by a graph, with ordinate $\psi(\tau)$, which is called a relaxation spectrum. Dividing the area under the curve into infinitesimally narrow vertical rectangles, the area of each rectangle is the coefficient "a" of one of the terms of the infinite series, and the abscissa to the center of the rectangle is the logarithm of the relaxation time τ for that term. Such a relaxation spectrum can be approximated by finite series similar to Equation 2 when the elements of area have finite width.

The relaxation spectrum can be determined to a close approximation (7) by plotting the creep recovery versus log time and meas-

uring the slopes. The slopes are nearly the correct ordinates for the relaxation spectrum if the log time values are taken as the corresponding abscissa values. It was found for the material and conditions of the present investigation that this first approximation to the relaxation spectrum usually corresponds to a slightly higher strain versus log time curve than the measured one; but if the difference is small, the first approximation relaxation spectrum can be adjusted to the correct curve. The adjustment is made by subtracting the strain versus log time curve calculated from the approximate relaxation spectrum from the measured strain versus log time curve,

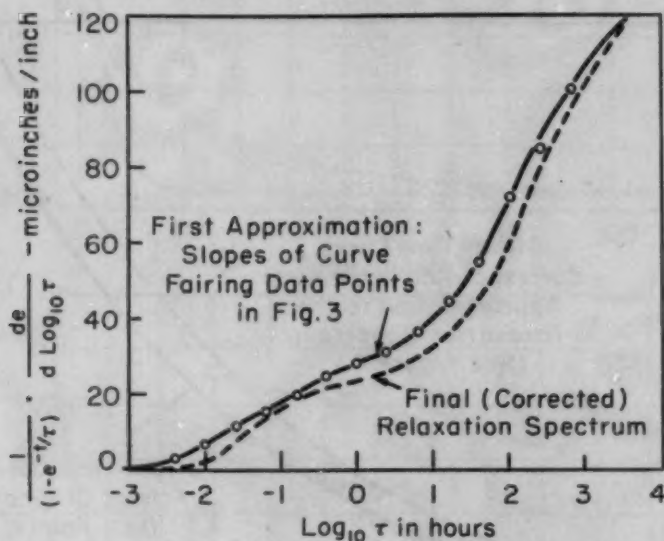


Fig. 4—Relaxation Spectrum Corresponding to the Creep Data of Fig. 3.

and measuring the slopes of the difference curve to obtain an increment relaxation spectrum to add to the first approximation. A single correction often is sufficient.

Figs. 3, 4, and 5 illustrate the calculation of the relaxation spectrum from creep recovery data. Fig. 3 shows creep data, expressed as creep strain versus log time obtained under conditions (see Part III) where the specimen eventually returned to its original length following removal of the load. By the definition given in the introduction, the creep strain for the test of Fig. 3 was anelastic strain. The solid line in Fig. 3 fair the data points, and the measured slopes of this line are plotted in Fig. 4 as a first approximation to the relaxation spectrum. The strain-time curve corresponding to this approximate relaxation spectrum is shown dashed in Fig. 3. From the difference between the solid and dashed curves in Fig. 3, the approximate relaxation spectrum in Fig. 4 was corrected to the final one. Fig. 5 shows that the strain-time curve corresponding to the final relaxation spectrum compares favorably with the original data. For

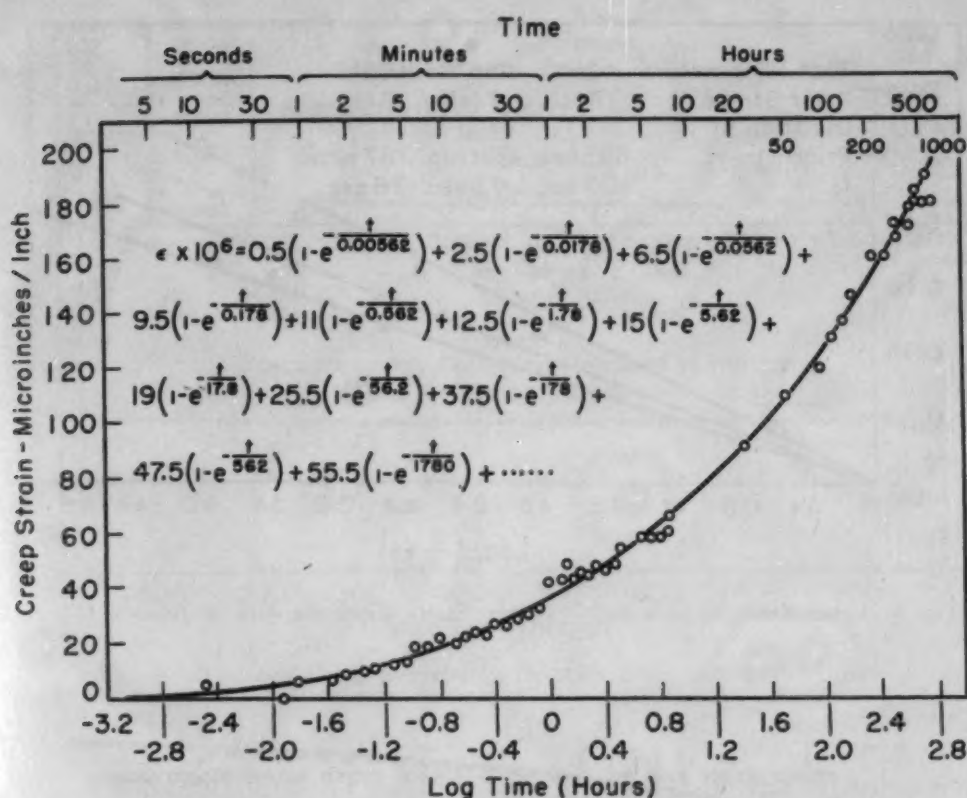


Fig. 5—Creep Curve for Cr-Mo-V Steel at 40,000 Psi and 800 °F After Pre-straining by 0.007 at 68,000 to 72,000 Psi and Resting 1000 Hours at 4000 Psi.

purposes of accuracy in this example, the successive relaxation times were taken only a factor of three apart, but for most purposes a factor of ten in the successive relaxation times is good enough.

The general form of curves of creep recovery versus time has also been investigated by Johnson (3), who proposed a logarithmic relation

$$\epsilon \sim \log \left(\frac{t}{t_0} + 1 \right) \quad \text{Equation 3}$$

up to a certain time, after which the length remains constant. Fig. 6 depicts Johnson's creep recovery data following the longest duration of loading at each temperature. Equation 3 fits quite well provided that t_0 is suitably chosen. Johnson's data exhibit the same general characteristics as those described above. The rate of shortening is very large at first, although it soon becomes very small. The spread of relaxation times necessary to represent his data by an exponential series is very broad, as is illustrated in Fig. 7 where Equation 3 has been approximated by an exponential series over a range of times slightly greater than that of Johnson's data. The figure illustrates a fact that is generally true for the conditions of this investigation, namely, that if an exponential series is to fit a set of creep recovery

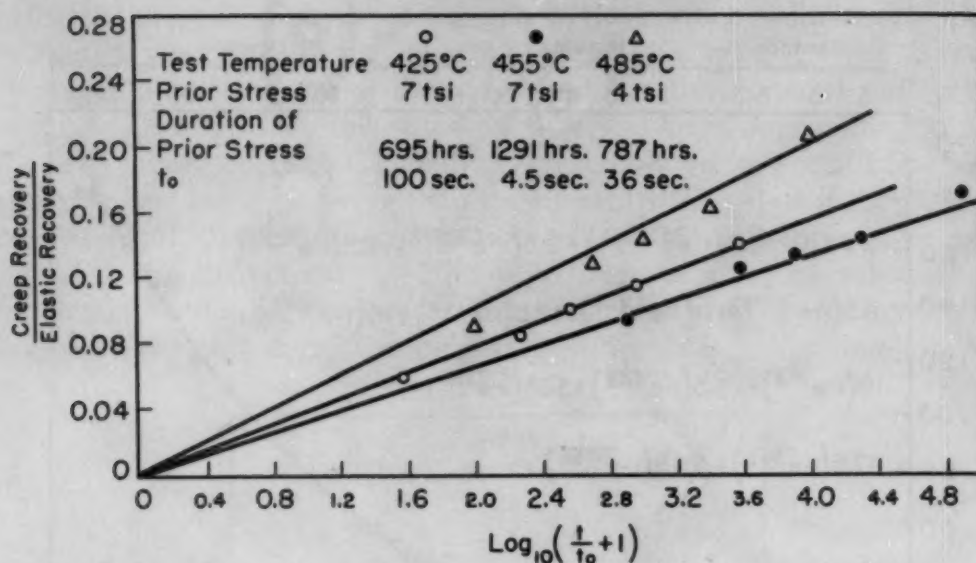


Fig. 6—Creep Recovery of a 0.17% Carbon Steel. From the data of Johnson (3).

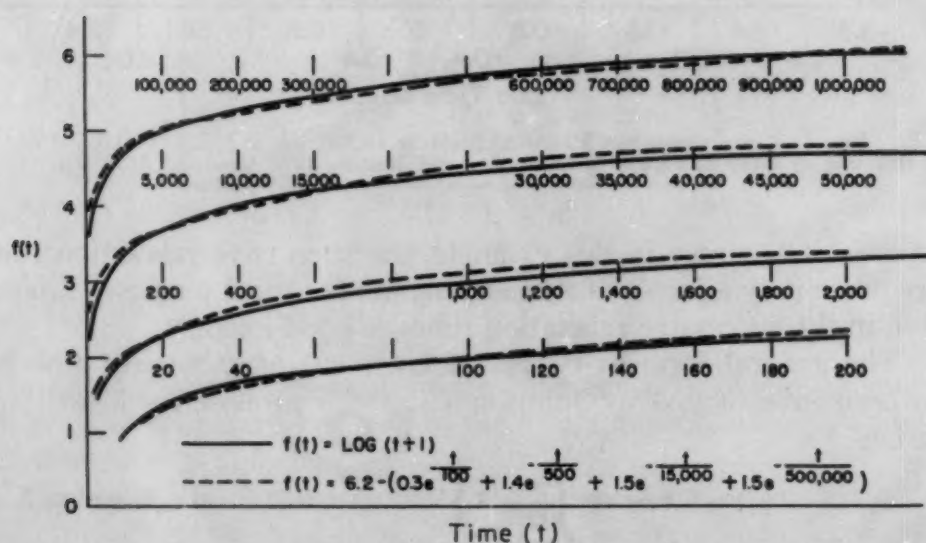


Fig. 7—Approximation to $\text{Log}(t+1)$ by an Exponential Series.

data, the spread of relaxation times will have to be approximately the same as the spread of time values covered by the data.

Although Equation 3 fits Johnson's data fairly well prior to the point of leveling off, it is not entirely satisfactory because there is nothing about the relation to indicate when or in what manner leveling off will occur, or how the proportionality constant depends on the prior load duration. It will be shown that an equation of the form of Equation 2 fits his data just as well, and that it does make specific predictions as to the way in which the rate of creep recovery changes and the time and manner of leveling off.

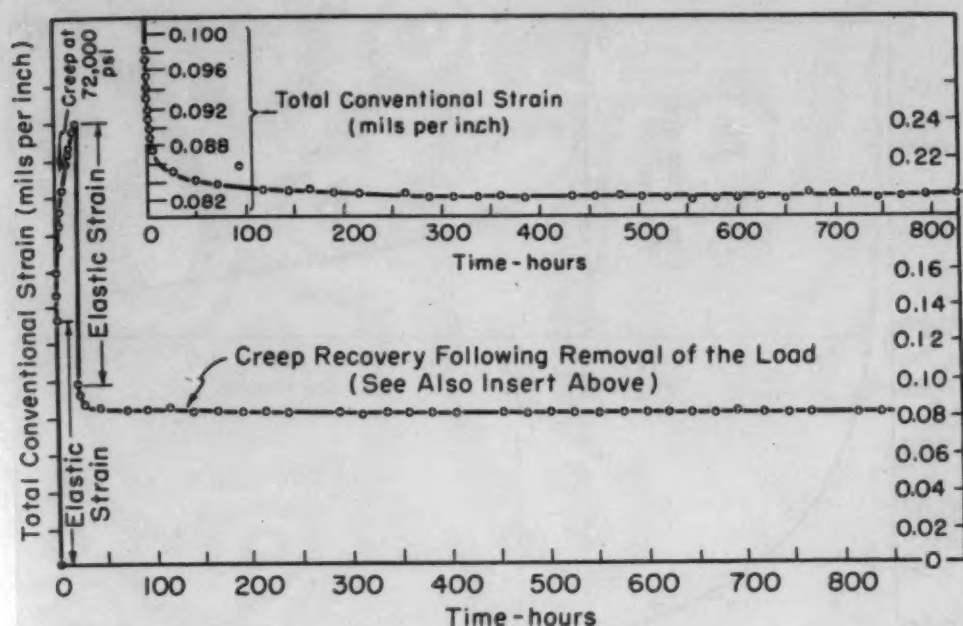


Fig. 8—Creep and Creep Recovery in Cr-Mo-V Steel at 800 °F. 72,000 psi was applied for 22.96 hours and then removed.

Although Johnson's data (3) seem to indicate that creep recovery eventually ceases, the possibility still remains that the rate of shortening becomes increasingly smaller, but does not vanish. Consequently, the question of whether or not creep recovery eventually ceases was re-examined in some detail. Of course, it is to be expected that creep recovery would cease when the specimen had returned to its annealed length, for it seems unlikely that more strain would be regained by creep recovery after unloading than the creep caused by the original load. On the other hand, the small magnitude of the creep recovery effects compared with the very large values of prior creep under load suggests that the specimen might stop shortening at a length considerably longer than the initial length. Whether or not the specimen will stop shortening at a length longer than the annealed length is a fundamental matter; for if it does not, the term "plastic strain" to denote the part of the creep that is not recoverable, even in very long times, is meaningless.

When creep recovery data are represented directly as strain versus time, there is sometimes the appearance of an equilibrium length having been reached, while at other times it appears that shortening will always continue, though at an ever-decreasing rate. Fig. 8 shows data where an equilibrium length appears to have been reached. Within the limit of the scattering, the length has not changed during an interval of time that is as long as the period during which shortening occurred. Fig. 9 shows data where there is no clear indication that an equilibrium length will be reached. The whole curve has

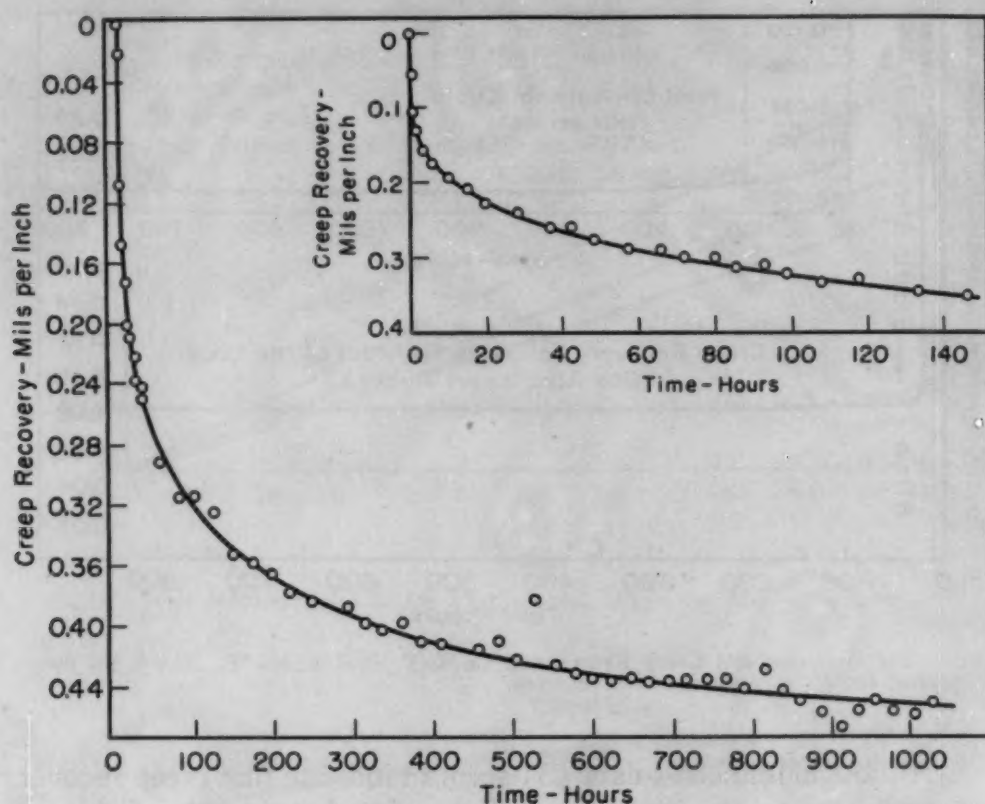


Fig. 9—Creep Recovery at 4000 Psi Following About 1200 Hours at 68,000 to 72,000 Psi. 800 °F. Cr-Mo-V steel.

about the same shape as a magnification in time of its early portion, suggesting that creep recovery may be no more complete after 1000 hours than it was after 140 hours.

For the purpose of making a better estimate of whether or not an equilibrium length is reached during creep recovery, the long-time data for the various tests are represented in Fig. 10 as strain versus $t/(t+5)$ (t in hours). The reduction in, and duration of, prior load and the resulting plastic strain are also shown in the legend of Fig. 10. The time function of Fig. 10 has the advantage that $t=0$ and $t=\infty$ are at finite positions on the abscissa scale: at $t/(t+5)=0$ and $t/(t+5)=1$. The curves for tests 1, 5, 6, and 9 definitely approach a finite value. For test 9, the definiteness of approach to a limit is indicated more clearly in Fig. 11, which shows more of the earlier part of the curve. This curve, as well as the curve for test 5 in Fig. 10, becomes concave downward near the end of the test, thus showing a particularly clear approach to a finite limiting strain.

Although four of the nine curves in Fig. 10 appear to approach a limiting strain, three of the others (2, 7, and 8) are so steep at long times that it is impossible to say whether a limit is approached or not, even by expanding the abscissa scale to reduce the steepness (Fig. 12). Also, there is some doubt about the existence of a limiting strain for

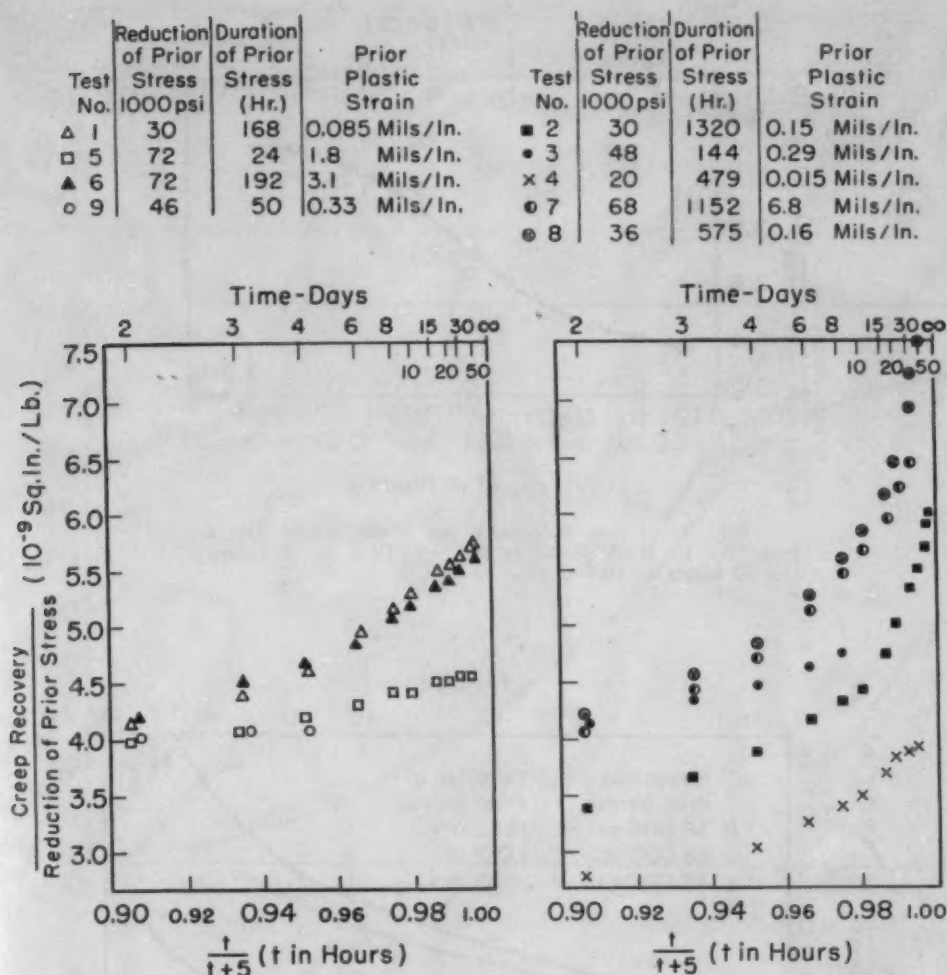


Fig. 10—Creep Recovery per Unit Stress Decrement for Cr-Mo-V Steel at 800 °F.

tests 3 and 4. It is significant that the three curves not having an obvious limiting strain correspond to the longest durations of prior loading. One might suspect that the length of time for leveling off might increase with the duration of prior load, so that the failure of tests 2, 7, and 8 to level off might be due solely to the fact that the creep recovery measurements were not extended far enough in comparison to the duration of prior load.

The possible influence of prior load duration on the "leveling-off" time was investigated for those curves that definitely "leveled off". Of course, the leveling-off time is a somewhat indefinite quantity that will have to be determined in accordance with a more or less arbitrary definition. The leveling-off time was taken as the time when the strain first fell short of the extrapolated limiting strain by less than the spread of scattering of the data points with respect to strain. Fig. 13 shows that the typical scattering at long times is about 5×10^{-6} for a stress change of 30,000 psi, and Fig. 14 shows that the worst scattering is about 1×10^{-5} to 2×10^{-5} for a stress change of

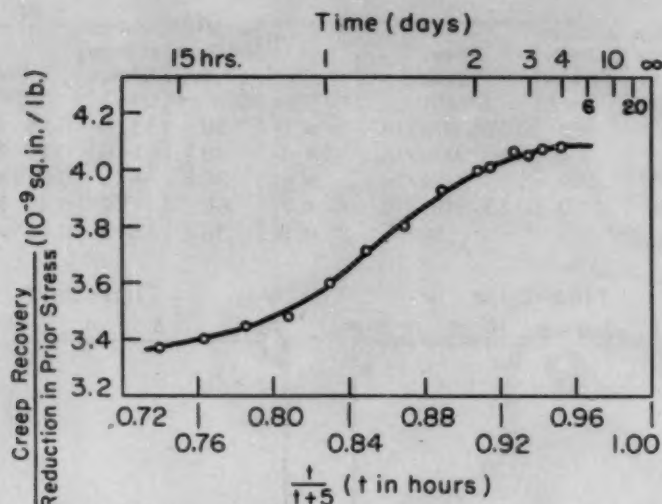


Fig. 11—Creep Recovery per Unit Stress Decrement for Cr-Mo-V Steel at 800 °F. Test No. 9 following 50 hours at 46,000 psi.

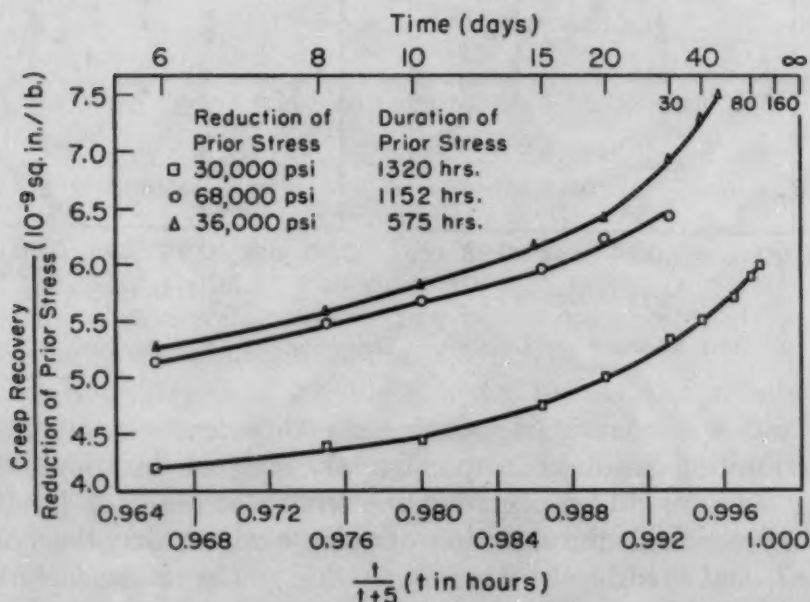


Fig. 12—Creep Recovery per Unit Stress Decrement for Cr-Mo-V Steel at 800 °F. Magnification of last part of curve of Fig. 10.

20,000 psi. Taking 3×10^{-10} per unit stress change as a rough value of the scattering in Fig. 10, the leveling-off times as shown in Table I are obtained. These values have been plotted against the duration of prior load in Fig. 15, which shows that leveling off occurs in about 2.5 times the duration of prior load for the material and conditions of the present investigation.³ Consequently one would expect to see

³Johnson (3) found for a given temperature that the leveling-off time for creep recovery was between $\frac{1}{2}$ and 15 times the load duration depending on the absolute magnitude of load duration.

Table 1

Test No.	Duration Prior Load (Hours)	Leveling-Off Time (Hours)
1	168	About 400
5	24	About 150
6	192	About 400
9	50	About 50

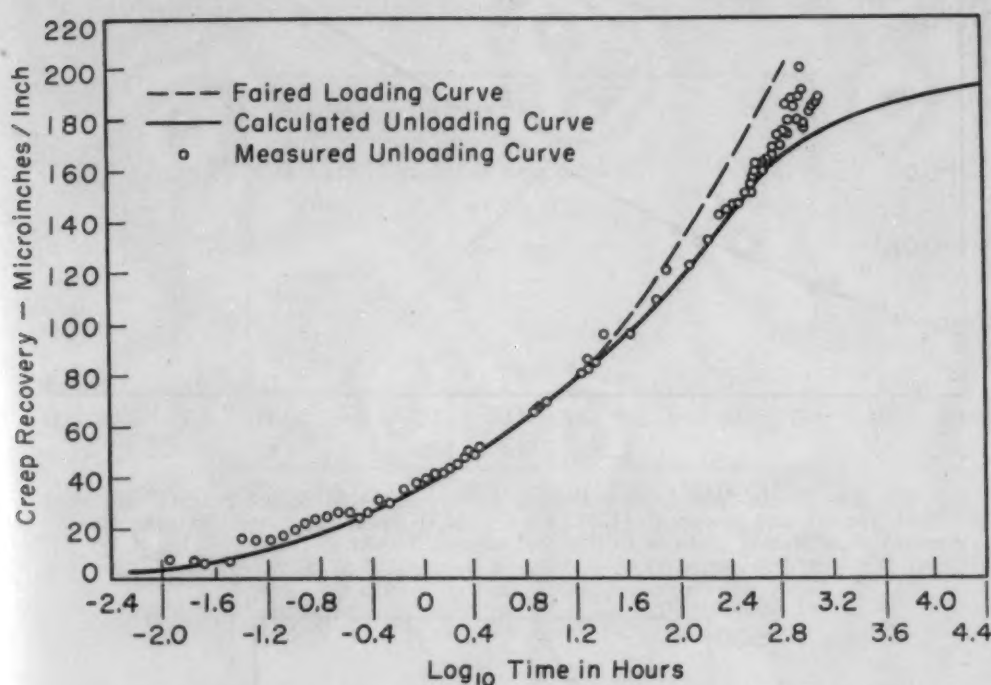


Fig. 13—Creep Recovery at 4000 Psi Following a Creep Test of 580 Hours Duration at 40,000 Psi and 800 °F (see Fig. 5).

a definite limiting length being approached, if not already reached, when the creep recovery data extend to times at least 2.5 times the duration of prior load. On the other hand, it would not be surprising to find that the limiting strain, if any, was not apparent from creep recovery data extending to times considerably less than 2.5 times the duration of prior load. Fig. 16 shows that the definiteness of the limiting strain bears the expected relationship to the creep recovery time and to the duration of prior load.

It seems reasonable to conclude from the foregoing that creep recovery eventually ceases after unloading a creep specimen, and therefore that part of the original creep is really plastic (nonrecoverable). Eventual cessation of shortening after unloading is one characteristic of anelasticity. Consequently, the conclusion that creep recovery also ceases eventually supports the hypothesis that creep recovery is in reality anelastic shortening, conforming to the spring-dashpot analogy.

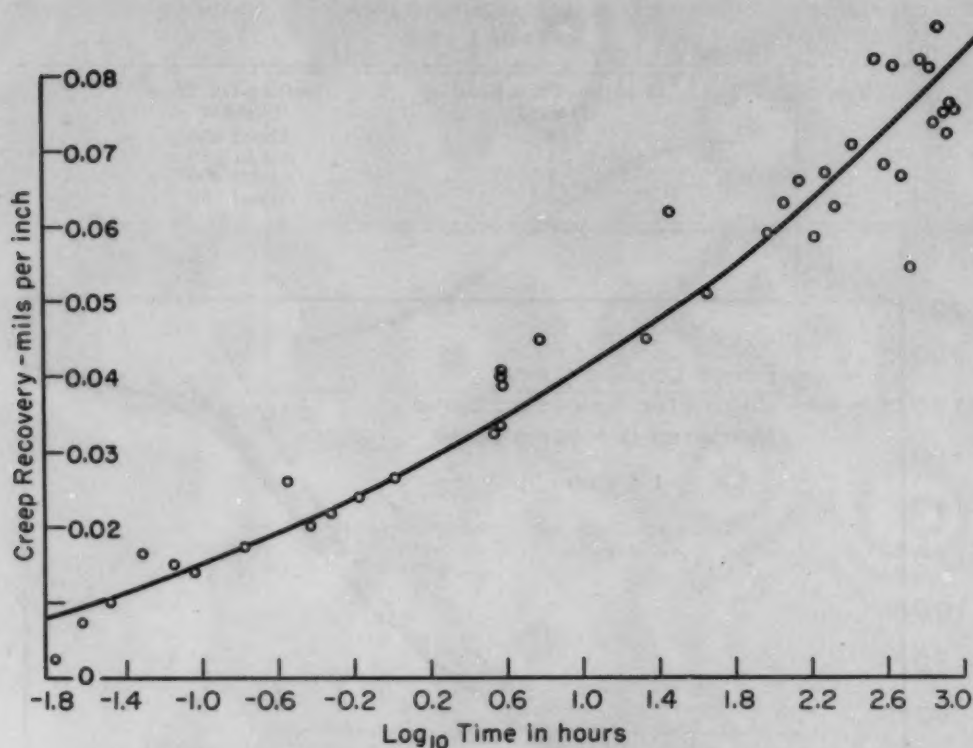


Fig. 14—Strain-Time Data Following Unloading From 20,000 Psi. Oil-quenched (3-inch round) and tempered (1250 °F) Cr-Mo-V steel. Test temperature: 800 °F. Amount of scattering peculiar to this test only of 9 tests.

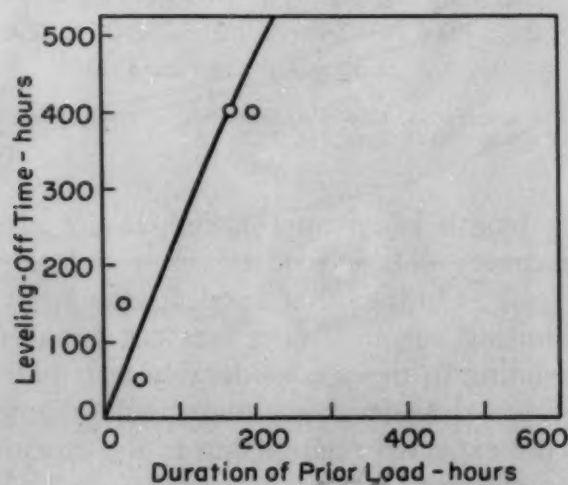


Fig. 15—Effect of Prior Load Duration on What Length of Subsequent Time at Zero Load Is Required to Reach Equilibrium Length. Test temperature: 800 °F. Points are for tests 1, 5, 6, and 9 in Fig. 10.

Relations Between Creep and Creep Recovery

When a load is removed only after stretching has ceased, and where all the strain eventually is recovered following removal of the load, the spring-dashpot analogy predicts that the strain-time curves

under load (creep) and following removal of the load (creep recovery) will be congruent. This congruency has been observed for very small stresses and under other suitable conditions in torsion pendulum experiments (1).

For the material and temperatures used in the present investigation, it was found possible under certain conditions to suppress plastic flow entirely during the application of the load (see Part III). Yet in no instance, whether plastic flow was suppressed or not, did

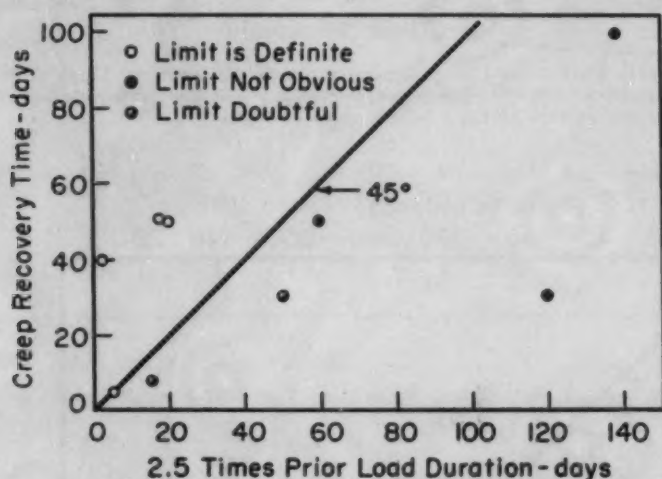


Fig. 16—Relationship Between the Definiteness With Which an Equilibrium Length Is Reached During Creep Recovery and the Ratio of Prior Load Duration to Extent of Creep Recovery Measurements.

there appear to be a limiting creep strain, or strain that would never be exceeded under load. Fig. 3 illustrates, for example, that a limiting anelastic strain had not been reached in 580 hours. In the present investigation, therefore, the load was always removed before stretching had ceased. Under these conditions the spring-dashpot analogy predicts that the loading and unloading strain-time curves will be congruent at short times but will deviate at times comparable to the duration of the prior load.

The observation that the recoverable part of the creep strain increases indefinitely with time at load is in contradiction to Johnson's observations on 0.17% carbon steel that the recoverable part of the creep strain reaches a limit in 200 hours. In his tests this limit was not exceeded, even for times of 1000 hours.

The fact that anelastic creep apparently does not approach a limit under load can be expressed also in terms of the relaxation spectrum. It means that the relaxation spectrum does not fall to zero, even for relaxation times that are considerably longer than the longest values of load duration used in the tests. On the contrary, the relaxation spectrum apparently falls to zero for relaxation times that are of the

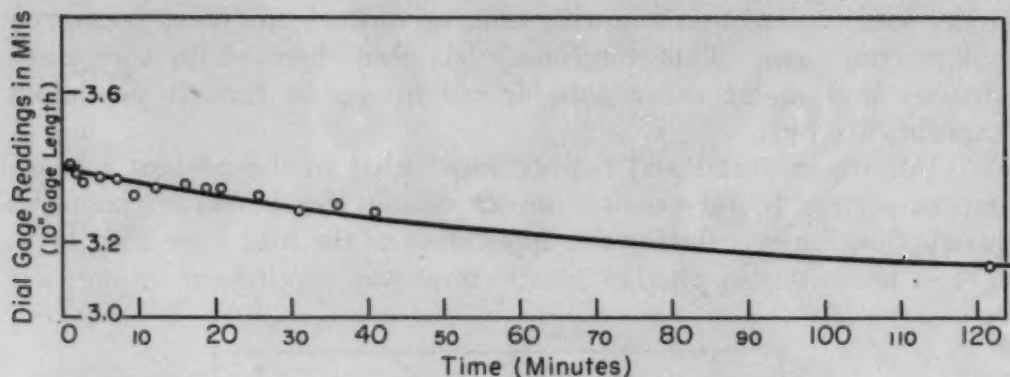


Fig. 17—Early Portion of Creep Recovery Curve Following 7 Days at 20,000 Psi. Cr-Mo-V steel tested at 800 °F. Specimen previously has been subjected to 45,000 psi for 96 hours but had rested 23 days before reloading.

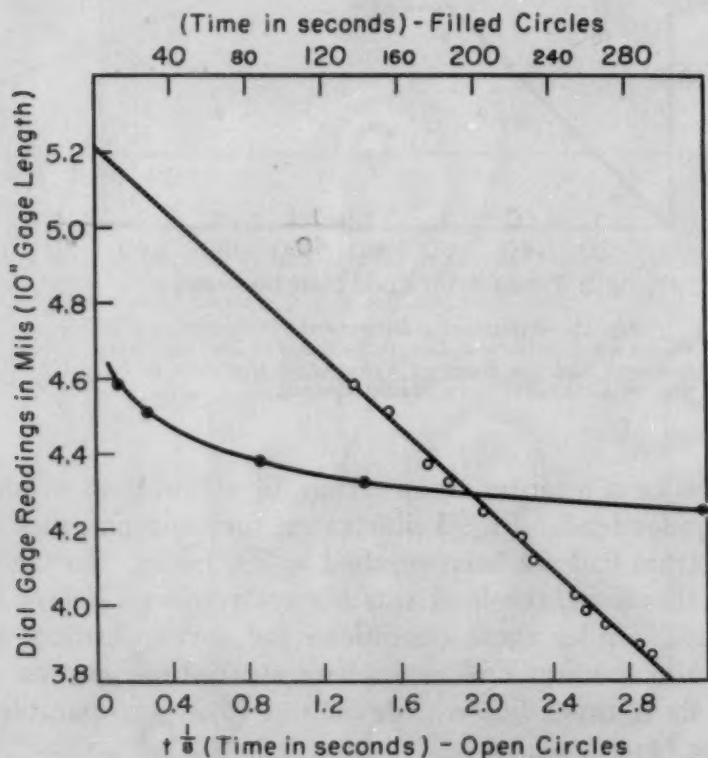


Fig. 18—Early Portion of Creep Recovery Curve Following 96 Hours at 45,000 Psi. Cr-Mo-V steel. 800 °F.

same order as the shortest times of measurement, as shown in Fig. 4. If the relaxation spectrum had exhibited a finite height for relaxation times considerably shorter than the shortest time of measurement, then considerable strain would have appeared between the change in load and the first reading, and extrapolation of the data to the length at the instant of load change would have been impossible. Under these conditions no clear separation of elastic and nonelastic deformation can be made by this method. This is the case for copper and for the

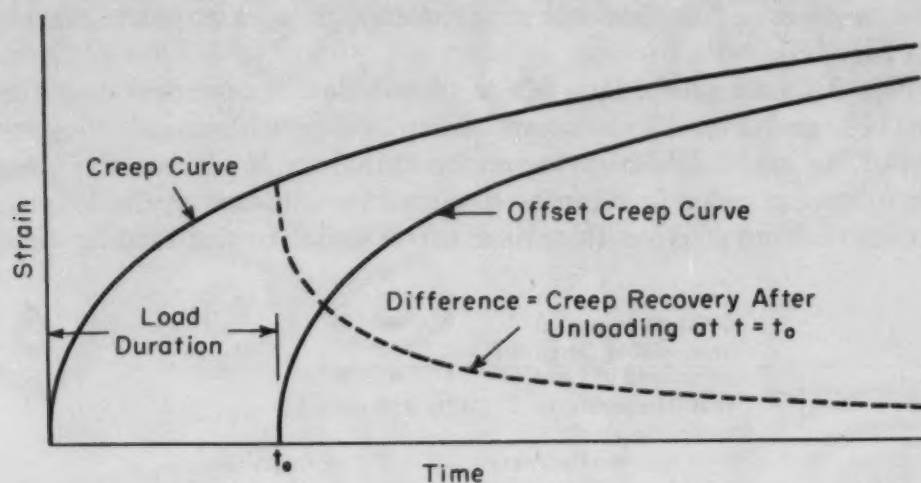


Fig. 19—Schematic Diagram Illustrating Method of Determining Anelastic Shortening After Unloading From Data on Anelastic Lengthening Prior to Unloading.

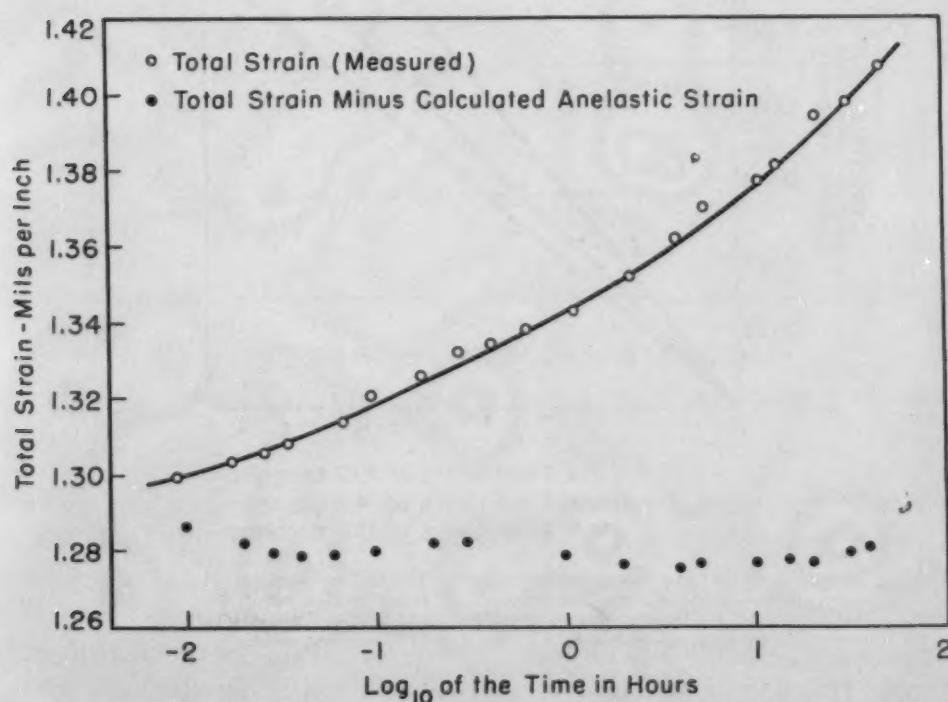


Fig. 20—Creep Curve for 30,000 Psi Applied Following About 100 Hours of Creep at 46,000 Psi and Subsequent Resting for 100 Hours. Also shown is the calculated plastic creep taking account of the anelasticity (see Fig. 2) exhibited during the resting period.

aluminum alloy 61ST at room temperature (8), except for exceedingly small load changes. For the conditions of the present experiments, however, extrapolation to the strain or length value immediately following a load change was usually feasible using a straight time scale (Fig. 17), but in a few cases the use of a t^n scale was re-

quired to obtain a line that was straight enough to extrapolate reasonably (Fig. 18).

Fig. 5 shows creep data where plastic flow was suppressed (see Part III), and Fig. 13 shows the creep recovery data following removal of the load. If the spring-dashpot analogy is correct, the creep curve following unloading can be obtained by subtracting the original creep curve from itself with a time offset equal to the loading time,

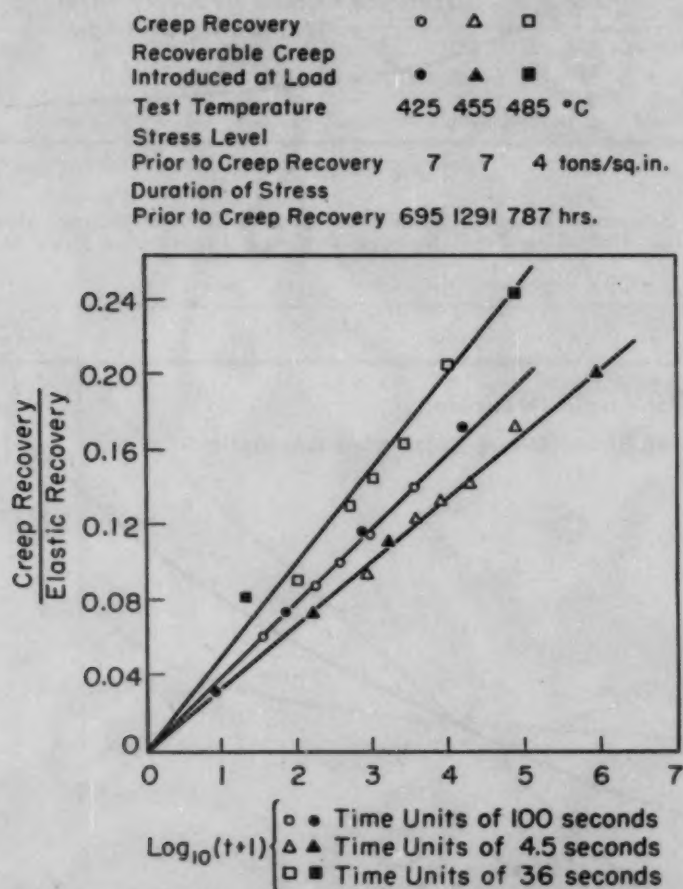


Fig. 21—Comparison of the Time Dependence of Recoverable Creep Introduced at Load and Creep Recovery Following Removal of a Load of Long Duration. From data of Johnson (3) on a 0.17% carbon steel.

as shown in Fig. 19. In this manner one obtains the calculated unloading curve shown in Fig. 13. This curve conforms very closely to the data at all values of time except the very longest times, where the specimen appears to be shortening somewhat more rapidly than predicted by the spring-dashpot analogy. In this experiment the creep strain is essentially all recoverable, and it is recovered in a manner conforming closely to the spring-dashpot analogy.

According to the spring-dashpot analogy, one should be able to calculate anelastic creep at any stress from the creep recovery data

following removal of a different stress, if all the strain values (creep recovery) are multiplied by the ratio of the two stresses. An illustration of this type of calculation is shown in Fig. 20. This figure shows a creep curve at 30,000 psi following a 100-hour period of resting from a period (about 100 hours) of previous loading at 46,000 psi. Fig. 2 shows the creep recovery obtained during the resting period. The anelastic creep at 30,000 psi was calculated from the creep re-

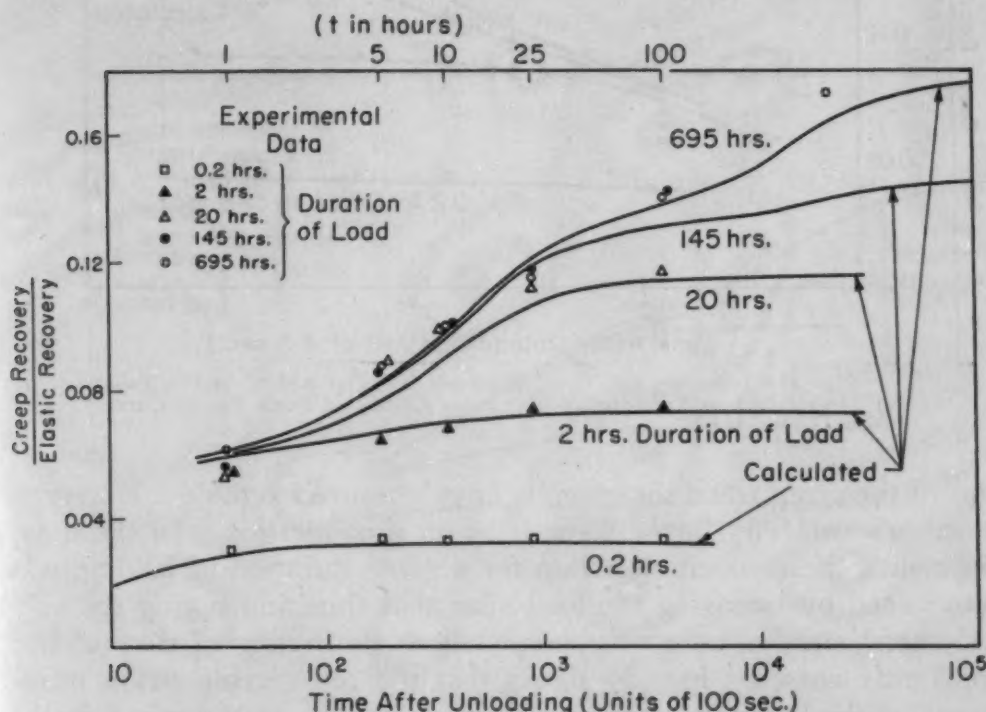


Fig. 22—Johnson's (3) Creep Recovery Data at 425 °C and 7 Tons per Square Inch as Compared With Curves Calculated From the Faired Curve in Fig. 21 for 425 °C.

covery data in Fig. 2 by multiplying the creep recovery values by 30,000/46,000. The resulting values then were subtracted from the creep curve in Fig. 20, which shows both the creep curve and the difference between observed creep and calculated anelastic creep. This difference would be the plastic part of the creep; and since the difference plots as a horizontal line, it must be concluded that the plastic part of the creep is negligible and that the data are consistent with the assumptions of the calculations—namely that the anelastic effects are linear in stress, identical on loading and unloading for times much shorter than the load duration, and, in general, conform to the spring-dashpot analogy.

The experiments just described were carried out at stresses much higher than those of the torsion pendulum experiments, but still under conditions such that plastic flow was suppressed. It is more difficult to establish that the spring-dashpot analogy is valid for the anelastic

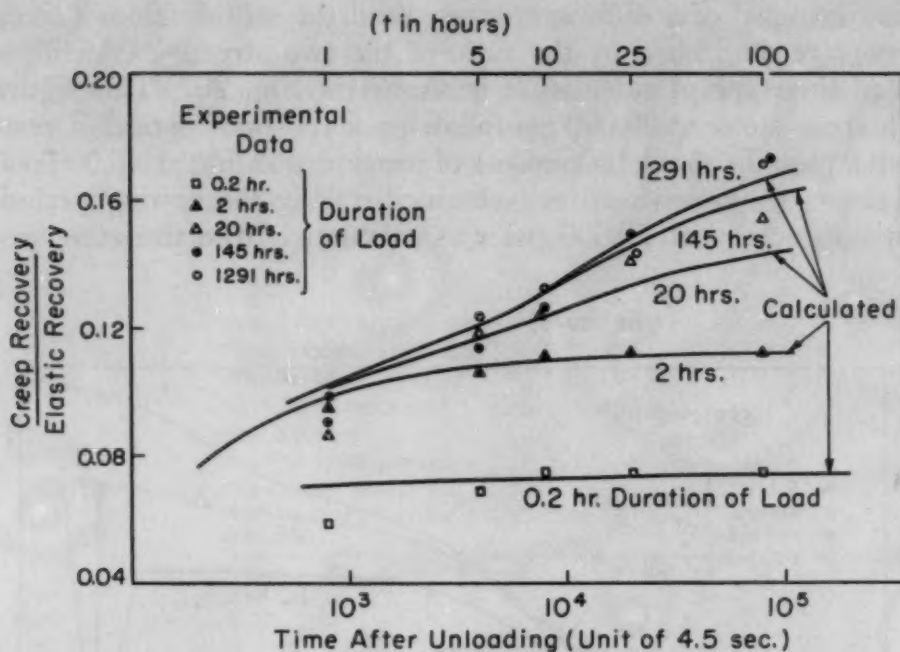


Fig. 23—Johnson's (3) Creep Recovery Data at 455 °C and 7 Tons per Square Inch as Compared With Curves Calculated From Faired Curve in Fig. 21 for 455 °C.

part of the creep when the creep is largely nonrecoverable. However, Johnson's data (3) throw some light on this question. In these experiments, the recoverable strain for a given duration of loading was determined by removing the load after that time and noting the subsequent shortening up to the point where shortening of the bar had apparently ceased. Fig. 21 shows that the recoverable strain introduced under load and determined by unloading as described is the same function of time at load as is the creep recovery upon unloading from a loading period of long duration. The agreement is best for the lowest temperature.

The connection between the recoverable part of the creep strain and the creep recovery can be further investigated using Johnson's data (3) by considering how prior load duration should affect the shape of creep recovery curves for the shorter durations of loading, when only part of the possible recoverable strain has been introduced. The exponential series

$$\epsilon = 0.039 [6.2 - (0.3e^{-t/100} + 1.4e^{-t/1000} + 1.5e^{-t/15,000} + 1.5e^{-t/300,000})]$$

(see also Fig. 7) expresses the variation of anelastic strain with time for Johnson's data at the lowest temperature (see Fig. 21). Using the method of Fig. 19, one can calculate creep recovery curves for each of the load durations that Johnson used. These calculated creep recovery curves have been plotted in Fig. 22 together with Johnson's data points. The experimental data correspond to the calculated curves within the limit of scattering about a calculated curve con-

sidered as a trend curve. Of course, the nature of the calculations insures that the calculated curves will fit the data points at the extreme right (within the scattering of Fig. 21), but the good fit elsewhere in Fig. 22 lends support to the concept that the spring-dashpot analogy expresses the relation between creep recovery and the recoverable part of the original creep, even when most of the creep is nonrecoverable and when the duration of loading has been so short

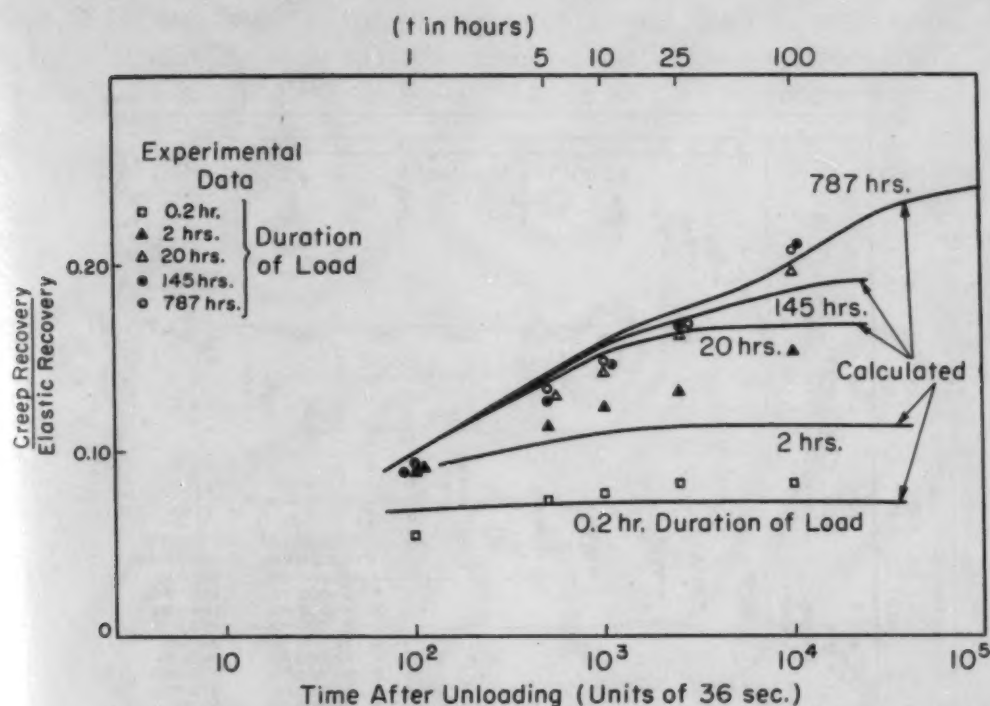


Fig. 24—Johnson's (3) Creep Recovery Data at 485 °C and 4 Tons per Square Inch as Compared With Curves Calculated From the Faired Curve in Fig. 21 for 485 °C.

that only part of the possible recoverable creep was introduced. An analysis similar to that in Fig. 22 was carried out for the other two temperatures that Johnson used. The results, as shown in Figs. 23 and 24, in general confirm the conclusion from Fig. 22. The evidence available from Figs. 23 and 24 must be considered as having much less weight than that of Fig. 22, however, because of the sparser data and the larger scattering.

Effect of Stress Decrement

According to the spring-dashpot analogy, the creep recovery at a certain time following a load decrement should be proportional to the magnitude of the load decrement.

The data (9) supporting the idea that anelastic effects are linear with stress are very meager, the range of stress covering only a factor of four. There are even less data relating to the linearity of creep

recovery with stress following creep that is partially plastic (3, 5), the range of stress being no greater than a factor of 1.5. In fact, one investigation (10) on tin at room temperature suggested that creep recovery was not linear with stress. To investigate further the linearity with stress, each of several bars was subjected to a different stress between 20,000 and 72,000 psi for a considerable length of time, and then the amount of shortening after unloading was observed as a

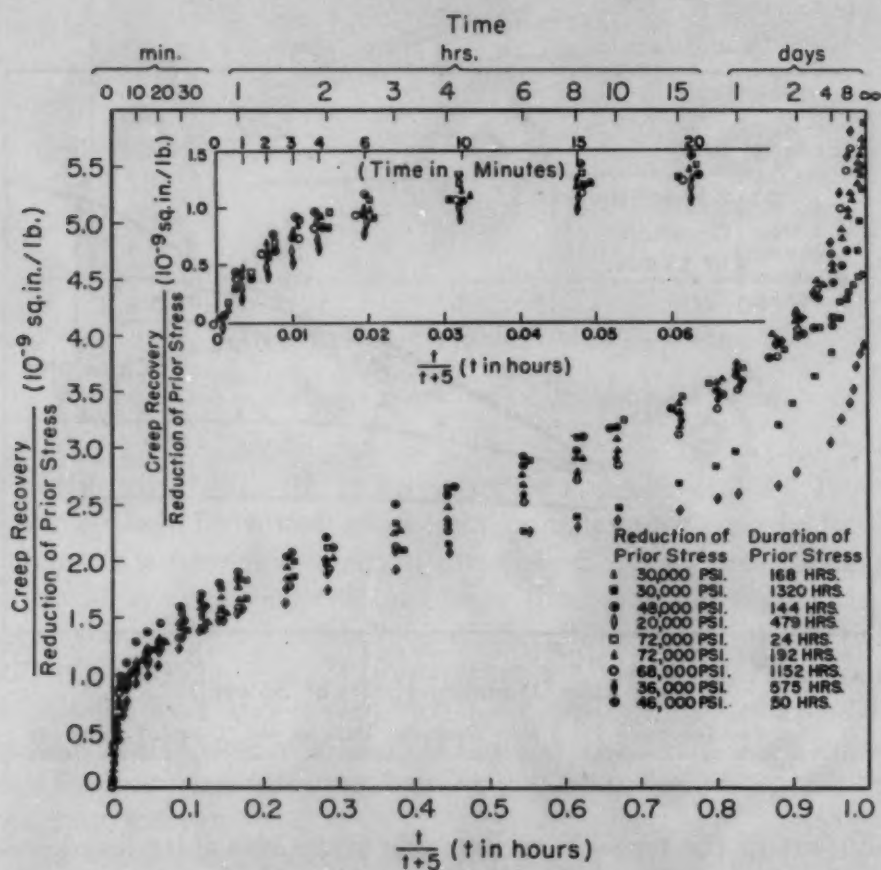


Fig. 25—Creep Recovery per Unit Stress Decrement as a Function of Time for Cr-Mo-V Steel Tested at 800 °F.

function of time. Fig. 13 shows a set of data whose scattering was typical of all the tests except that at the lowest stress (20,000 psi). At 20,000 psi, the scattering was unaccountably greater than for the other tests (see Fig. 14). The data following unloading from different stresses, expressed as the ratio of gradual shortening to the preceding stress decrement, are summarized in Fig. 25. The steep portion at the right is magnified in Figs. 10 and 12.

Fig. 25 shows that for times less than about 3 hours, the creep recovery is proportional to the stress. The same fact is represented in Fig. 26 in a more lucid manner in the three lowest curves. Fig. 26 also illustrates that the scattering for the longer times in Fig.

25 is not the result of a definite tendency toward a nonlinearity with stress, for the points show random scattering about horizontal trend lines. The magnitude of the scattering in comparison with the magnitude of the effect can be viewed more readily in Fig. 27, where the absolute magnitude of the creep recovery is plotted against stress. Here again, for times up to 3 hours, a comparatively high degree of linearity with stress is apparent. At 20 hours the scattering is still small except for the two tests which fall considerably off the curve at small stresses. (One of these represents the test with unusually large scattering shown in Fig. 14.) At still longer times there is a

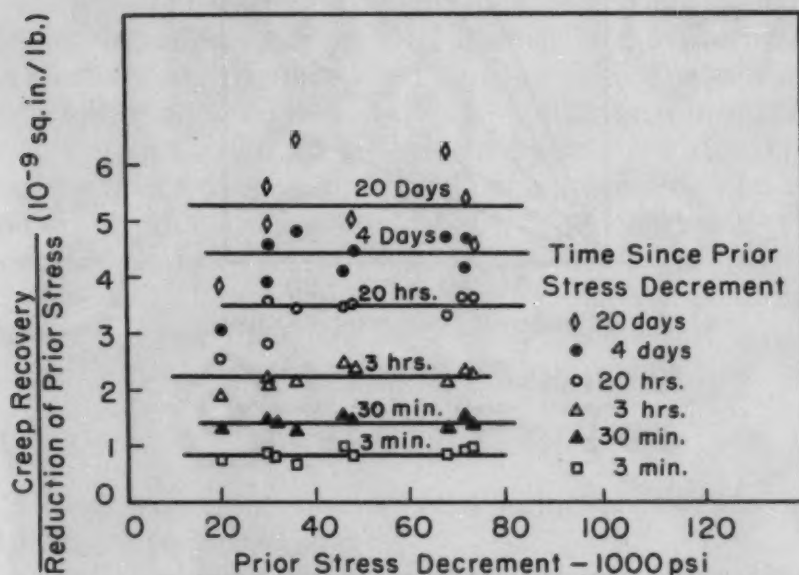


Fig. 26—Creep Recovery Behavior of Cr-Mo-V Steel at 800 °F—a Crossplot of Fig. 25.

considerable increase in scattering, which is readily apparent when Fig. 10 is compared with the insert in Fig. 25. It is especially noticeable in Fig. 26, which shows a tenfold increase in scattering at 20 days over that at 3 or 30 minutes although a tendency toward nonlinearity with stress still does not appear, as shown by a lack of trend of the curve for 20 days.

Since the greatly increased scattering at longer times in Fig. 26 cannot be accounted for as a failure to conform to a condition of linearity with stress, a different explanation might be sought. The reason for the increased scattering becomes obvious from Fig. 28, where creep recovery divided by stress is plotted against the duration of the prior load—a variable not considered in the preceding figures. At long times following the prior load decrement, Fig. 28 shows a trend toward greater creep recovery per unit stress with increasing duration of prior load. In fact, the scattering about the sloping

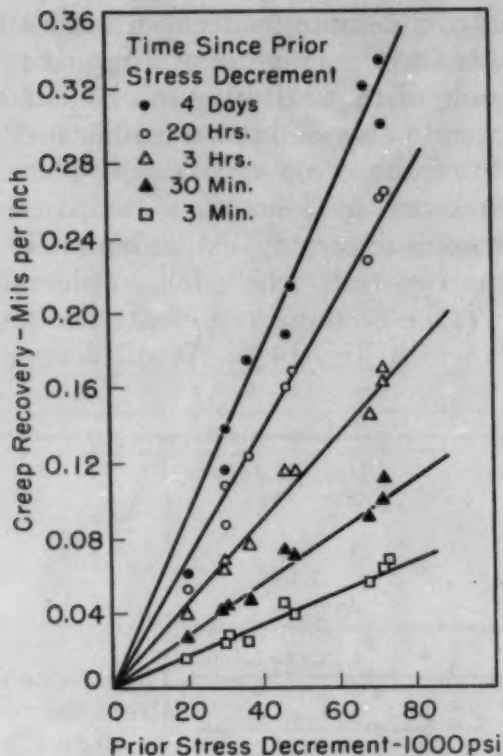


Fig. 27—Creep Recovery as a Function of Prior Stress Decrement for Various Constant Values of Time Since the Stress Decrement. Co-Mo-V steel tested at 800 °F.

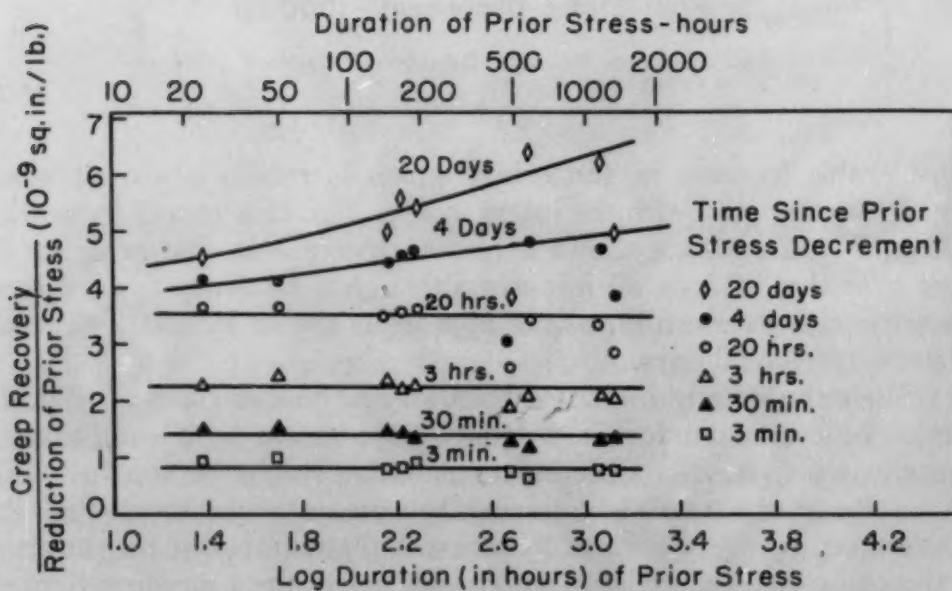


Fig. 28—Effect of Duration of Prior Stress on the Creep Recovery per Unit Stress Decrement for Various Constant Values of Time Since the Stress Decrement. Cr-Mo-V steel tested at 800 °F.

trend curves for 4 days and 20 days in Fig. 28 is hardly greater than that for short times, and certainly it is much less than that in the upper curves of Fig. 26, where duration of prior load is not taken into account.⁴ The effects of prior load duration shown by Fig. 28 also account for much of the scattering for the longer times in Fig. 27.

In Fig. 28 the increase in creep recovery with increasing load duration for long times (but not short times) following the prior load decrement is to be expected from the spring-dashpot analogy, since more recoverable deformation is introduced in a longer period of loading. The spring-dashpot analogy accounts equally well for the lack of effect of load duration for short times following the load decrement. The excess strain introduced during extended loading over that introduced during brief loading is characterized by a long time constant and is introduced slowly. This strain also reappears slowly following a decrease in load, so that in short times it would not be apparent as an excess over that recovered after brief loading. From the above discussion, it would be expected that an effect of the duration of prior loading would begin to be noticeable at a time following the load decrement that roughly equals the shortest duration of prior load. Examination of Fig. 28 shows that these times are comparable, since the curve for 20 hours is the last to be horizontal and the shortest duration of load is 24 hours (log time = 1.38).

SUMMARY AND CONCLUSIONS

Creep recovery conforms to the spring-dashpot analogy under all conditions investigated so far.

The shortening following unloading varies with time in a way that can be expressed by the equation

$$\text{creep recovery} = \int_{\tau=0}^{\infty} (1 - e^{-t/\tau}) \psi(\tau) d \log \tau,$$

which can be closely approximated by the series

$$\text{creep recovery} = \sum_i a_i (1 - e^{-t/\tau_i}).$$

Each term in this series represents the behavior of a spring and dashpot in parallel.

The shape of the creep recovery curve can be described in terms of three portions. In the first part, the creep recovery varies with

⁴The two sets of points in Fig. 28 that are considerably lower than the curves for four days and 20 days probably should not be considered as detracting from the definiteness of the trend, for two reasons: (a) one of them is a far more questionable test from the standpoint of scattering than any of the other eight tests; and (b) these two tests have proven their nonconformity at 20 hours, where the horizontal trend is well established from data at still shorter times and where a downward trend (to take account of the two low points) seems unlikely.

time after unloading in the same way that the recoverable part of the measured creep strain varies with time at load. Deviations occur at a time that is some fraction of the duration of prior load. This fraction depends on what is considered to be a significant "deviation". For practical purposes it may be taken as one-tenth. The last part of the curve is flat, the limiting value of creep recovery being equal to the recoverable part of the creep introduced during the prior load period. The time at which the creep recovery curve becomes flat is some multiple of the prior load duration. This multiple depends on what one means by "flat", but it may be taken as three for practical purposes. The limiting length for creep recovery may be the annealed length or a considerably longer length, depending on the magnitude and duration of prior load and the conditions of strain hardening before applying this load. The middle part of the creep recovery curve is related to the curve of the recoverable part of the creep versus time at load in a complex manner that conforms to the spring-dashpot analogy.

Also as predicted by the spring-dashpot analogy, the amount of creep recovery is proportional to the prior stress decrement for any value of the time after unloading that is substantially shorter than the prior load duration.

The conformity of both creep recovery and anelasticity to the spring-dashpot analogy suggests that creep recovery actually is anelastic shortening, and that the terms "creep recovery" and "anelastic shortening" may be used interchangeably. Identifying creep recovery with anelastic strain, one may envision creep as the sum of two different kinds of strain, anelastic and plastic, occurring simultaneously but independently and according to different laws. This viewpoint is supported by an analysis of certain types of creep behavior that otherwise would be difficult to explain, but which are easily understood in terms of this viewpoint (see Part II).

INFLUENCE OF ANELASTICITY ON TENSION, CREEP, AND RELAXATION—PART II

The coexistence of elastic behavior with either anelastic or plastic behavior in a single test has been widely recognized. The possibility that plastic and anelastic behaviors may coexist has received much less attention. It has been shown in Part I that creep recovery conforms to the spring-dashpot analogy, as does anelasticity. From this fact it has been suggested that creep recovery is anelasticity, and that anelastic and plastic strains can appear simultaneously, but independently and according to different laws. We shall now inquire further into this suggestion, and investigate in detail, and at significant stresses, a variety of experimental conditions for which two or more kinds of strain occur in the same test.

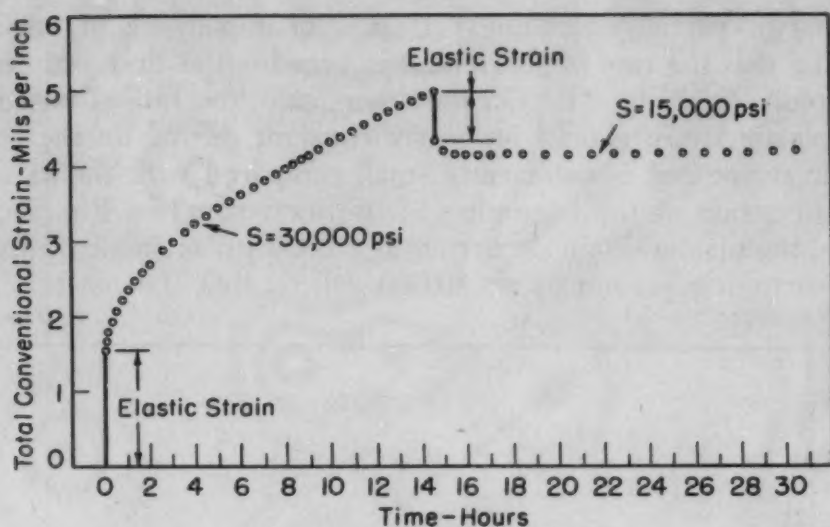


Fig. 29—Behavior of Cr-Mo-V Steel at 1000 °F Upon Partial Unloading.

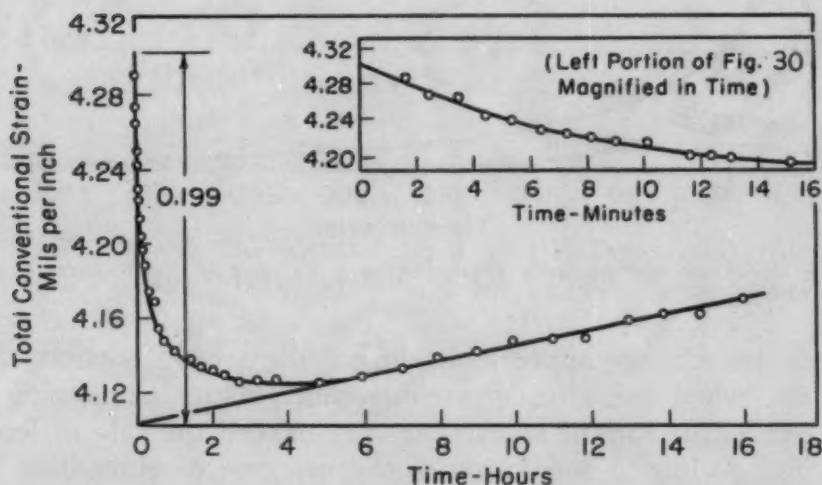


Fig. 30—Same as Fig. 29—Curve Segment for $S = 15,000$ Psi Greatly Magnified.

Partial Unloading

The simplest example of a test in which both anelastic and plastic strain occur is one in which a high load causes combined anelastic and plastic creep, and the anelastic strains are recovered upon subsequent unloading. This type of test has been discussed in detail in Part I.

If part of the load is removed during a creep test, the conditions are suitable for the occurrence of all three types of strain. Because of the reduction in load, elastic strain occurs immediately and anelastic shortening occurs gradually thereafter; because of the remaining load, plastic strain continues gradually thereafter.

Figs. 29 and 30 illustrate the behavior that is observed under

conditions of partial unloading. It is a characteristic of anelastic shortening that the rate of shortening is very high at first and diminishes rapidly (see Fig. 2). On the other hand, the rate of extension due to plastic strain should be nearly constant during an increment of plastic strain that is sufficiently small compared with the value of the plastic strain at the beginning of the increment; in Fig. 29, for example, the plastic strain occurring at 15,000 psi is small compared to that occurring previously at 30,000 psi, so that the plastic creep

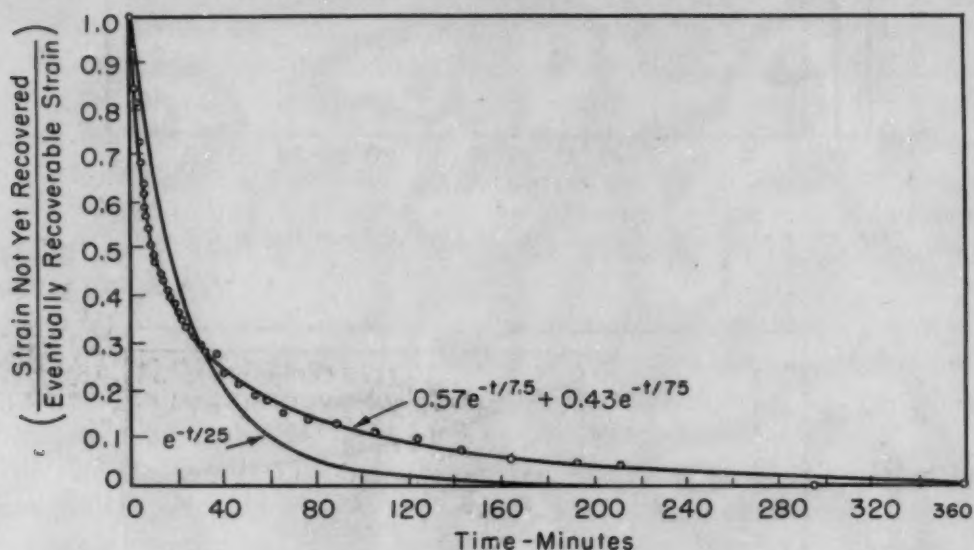


Fig. 31—Fractional Anelastic Shortening as a Function of Time—Same Conditions as Fig. 29.

rate should not change appreciably during the second portion of the test. Thus, when anelastic shortening and plastic lengthening can occur together, the rate of shortening may exceed the rate of lengthening at first, while at longer times the net rate of elongation may become zero and then positive. This behavior is illustrated by Fig. 30, which also shows that the plastic creep rate (after dying out of the anelastic effects) is nearly constant.

By taking advantage of the constancy of plastic creep rate, the anelastic effects can be roughly determined. Thus, as shown in Fig. 30, the anelastic shortening not yet obtained is the vertical distance between the experimental curve and the extrapolation of the linear portion at the right. Since anelastic behavior is usually expressed in terms of the fraction of the whole effect, the values of anelastic shortening determined from Fig. 30 were divided by the total shortening of 0.199 mils per inch shown in Fig. 30. The upper value was determined by means of a short extrapolation, as shown in the inset in Fig. 30. The resulting function can be fitted quite closely (see Fig. 31) by the exponential expression

$$a = 0.57e^{-t/7.5} + 0.43e^{-t/75}$$

Equation 4

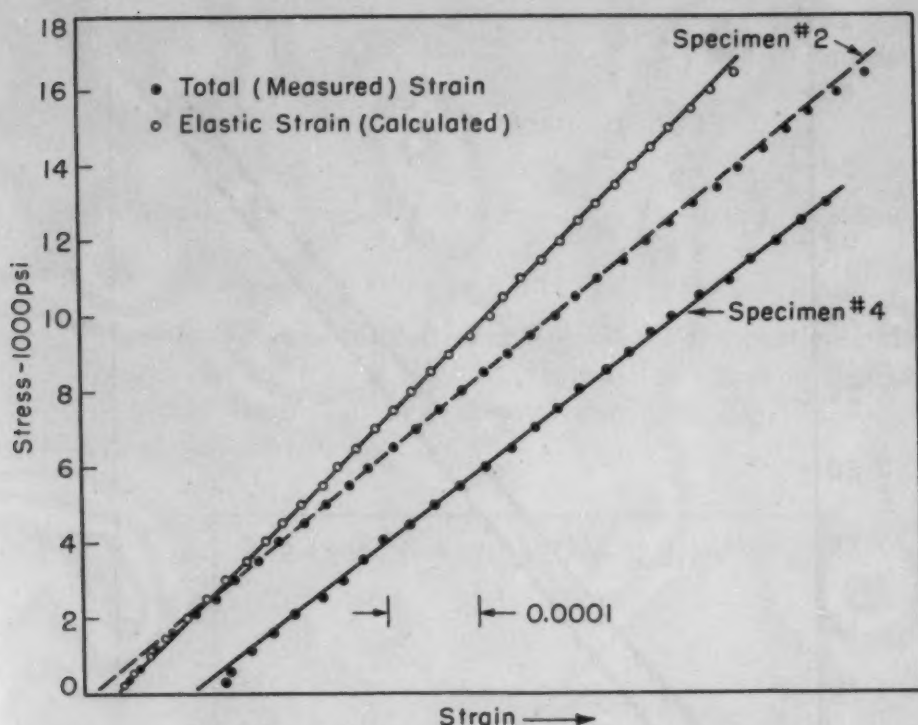


Fig. 32—Stress-Strain Curves of Cr-Mo-V Steel at 1000 °F and a Stressing Rate of 18,000 Psi per Hour. Also corrected stress-strain curve obtained by subtracting the anelastic strains as shown in Fig. 34.

although a single exponential term will not represent the function (see also Fig. 2). In other words, the behavior cannot be described in terms of a single relaxation time.

Modulus Effects

The effect of anelastic behavior on the determination of modulus of elasticity is well known at very small stresses (1). The tests described below will illustrate the effects at large stress.

In four identical tests on Cr-Mo-V steel at 1000 °F, the stress-strain curve always showed a convexly-downward tail preceding the straight portion (see Fig. 32), whereas the room temperature curve was straight throughout to a high degree of accuracy (see Fig. 33). When the anelastic strains were subtracted from the total strains, the resultant stress-strain curve was linear (Fig. 32). Apparently the phenomenon of anelasticity is responsible for the tail on the as-measured stress-strain curve at elevated temperature.

The anelastic strains were determined from Fig. 31, which is derived from the results (Figs. 29 and 30) of an experiment performed later on the same specimen as that giving the left-hand modulus curve in Fig. 32. Equation 4 gives the relative anelastic strain as a function of time for constant load. For a constant loading rate

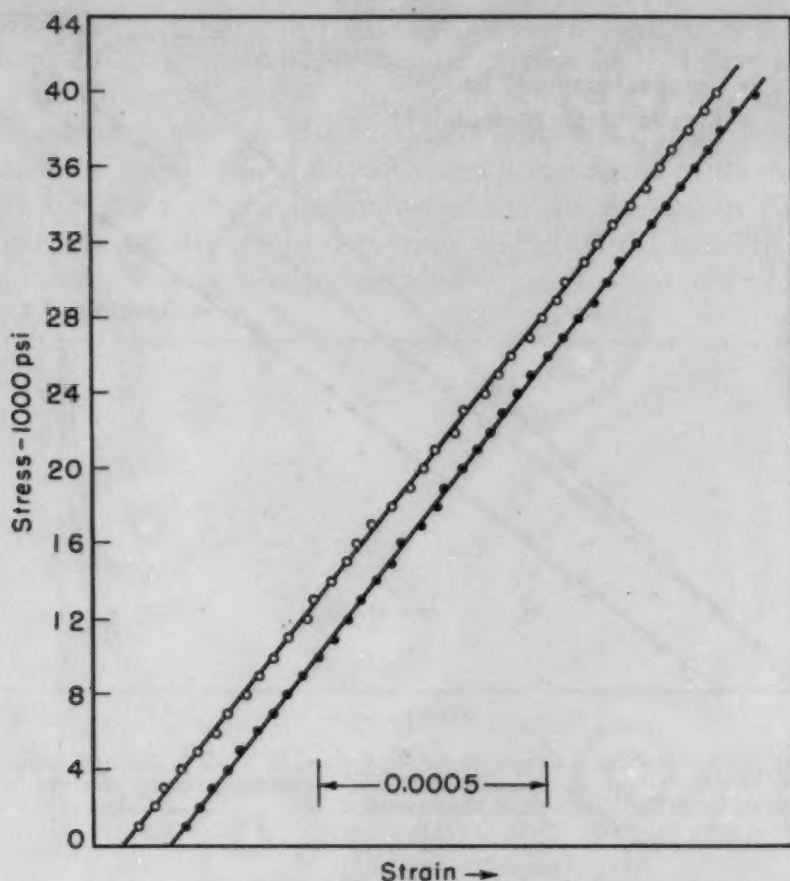


Fig. 33—Stress-Strain Curves for Two Specimens of Cr-Mo-V Steel Tested at Room Temperature.

($\dot{S} = dS/dt$) test beginning at $t = 0$, the stress at time t will be

$$S = \dot{S}t \quad \text{Equation 5}$$

and

$$dS = \dot{S}dt \quad \text{Equation 6}$$

If the anelastic effects are linear with stress, the strain after time t at a stress S that is constant up to the instant considered can be found from Equation 4 as

$$\epsilon(t) = KS(1 - 0.57e^{-t/7.5} - 0.43e^{-t/75}) \quad \text{Equation 7}$$

where K is 0.199×10^{-3} per 15,000 psi according to Fig. 30 or 1.33×10^{-8} per unit stress. At time t' , there will be an anelastic strain $d\epsilon$ due to an increment of stress dS applied at time t . This strain is

$$d\epsilon = KdS \left(1 - ae^{-\frac{-t'+t}{\tau_1}} - be^{-\frac{-t'+t}{\tau_2}} \right) \quad \text{Equation 8}$$

where $a = 0.57$, $b = 0.43$, $\tau_1 = 7.5$ and $\tau_2 = 75$. Substituting Equation 6 into Equation 8 and rearranging,

$$d\varepsilon = K\dot{S} \left(1 - \frac{ae^{t/\tau_1}}{e^{t'/\tau_1}} - \frac{be^{t/\tau_2}}{e^{t'/\tau_2}} \right) dt \quad \text{Equation 9}$$

Integrating over the range of times from zero to t' ,

$$\int_0^{\varepsilon} d\varepsilon = K\dot{S} \left(t' - \frac{a}{e^{t'/\tau_1}} \int_0^{t'} e^{t/\tau_1} dt - \frac{b}{e^{t'/\tau_2}} \int_0^{t'} e^{t/\tau_2} dt \right) \quad \text{Equation 10}$$

$$\varepsilon = K\dot{S} [t' - a\tau_1(1 - e^{-t'/\tau_1}) - b\tau_2(1 - e^{-t'/\tau_2})] \quad \text{Equation 11}$$

Equation 11 has been plotted in Fig. 34 for the particular loading rate employed in the test of Fig. 32. It was the curve of Fig. 34 that was subtracted from the experimental curve in Fig. 32 to get the truly elastic line shown.

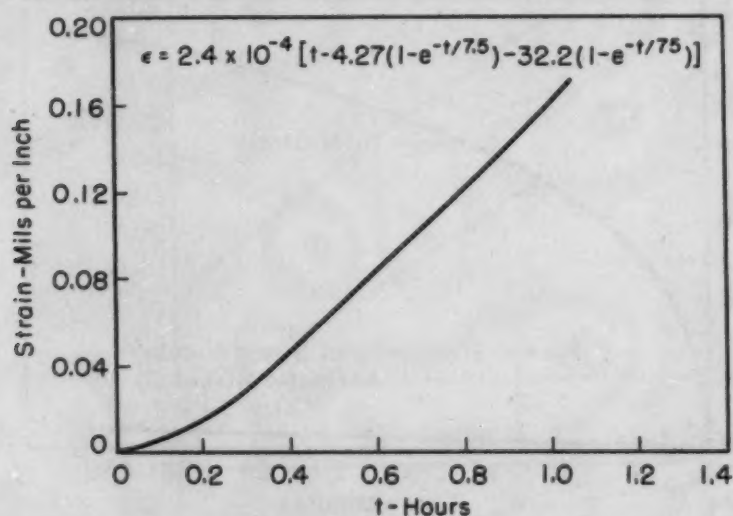


Fig. 34—Anelastic Strains Developed During Loading for a Constant Stressing Rate of 18,000 Psi per Hour. Calculated from the equation shown.

The anelastic behavior affects not only the shape of the modulus curve, but also the value of modulus of elasticity, as shown in Fig. 32. The curve of stress versus *elastic* strain has a slope of 24.2×10^6 , whereas a straight line through the observed points (neglecting the tail) has a slope of 19.6×10^6 . If the test were made sufficiently slowly, all the anelastic strain of Fig. 31 would occur at each stress, the stress-strain curve would be linear (since both elastic and eventual anelastic effects are linear with stress) and the modulus would be 18.3×10^6 psi.⁵

Combinations of Anelastic and Plastic Behaviors

As discussed in Part I, creep recovery behavior is such that the rate of shortening is high at first and is eventually very much smaller

⁵Fig. 30 shows the ultimate anelastic strain for $S = 15,000$ psi as 0.199 mils per inch. The elastic strain would be $15,000 / (24.2 \times 10^6) = 0.620$ mils per inch. This gives a total strain of 0.819 mils per inch for $S = 15,000$ psi, or an apparent modulus of 18.3×10^6 psi.

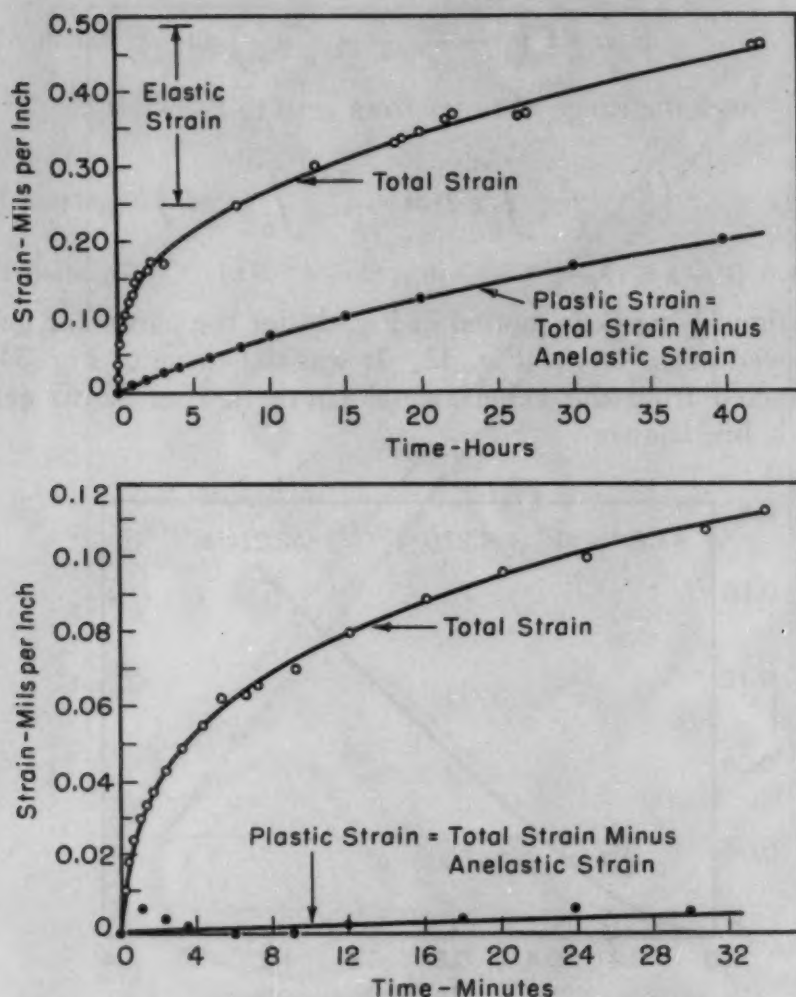


Fig. 35—Variation of Total Strain and Plastic Strain With Time Following Application of an Initial Stress of 5000 Psi for Quenched and Tempered (1250 °F) Cr-Mo-V Steel, Tested at 1100 °F.

—say 10^{-6} times the initial rate. This behavior is in sharp contrast to “plastic” behavior at elevated temperatures, where the strain rate at constant stress changes only gradually with time. The widely different relation between strain and time for anelastic and plastic deformation furnishes a basis for distinguishing them when they occur simultaneously. It is observed that the measured strain-time curve changes slope very rapidly following either an increase (Fig. 35) or a decrease (Fig. 36) in load. On increasing the load the bar lengthens rapidly at first and much more slowly later. Following a decrease in load (but not to zero) the bar shortens very rapidly at first, much less rapidly after awhile, and finally lengthens at a rate that approaches a constant value or perhaps that decreases very slowly. These two widely different measured strain-time behaviors following loading and unloading respectively can be corrected for the anelastic behavior.

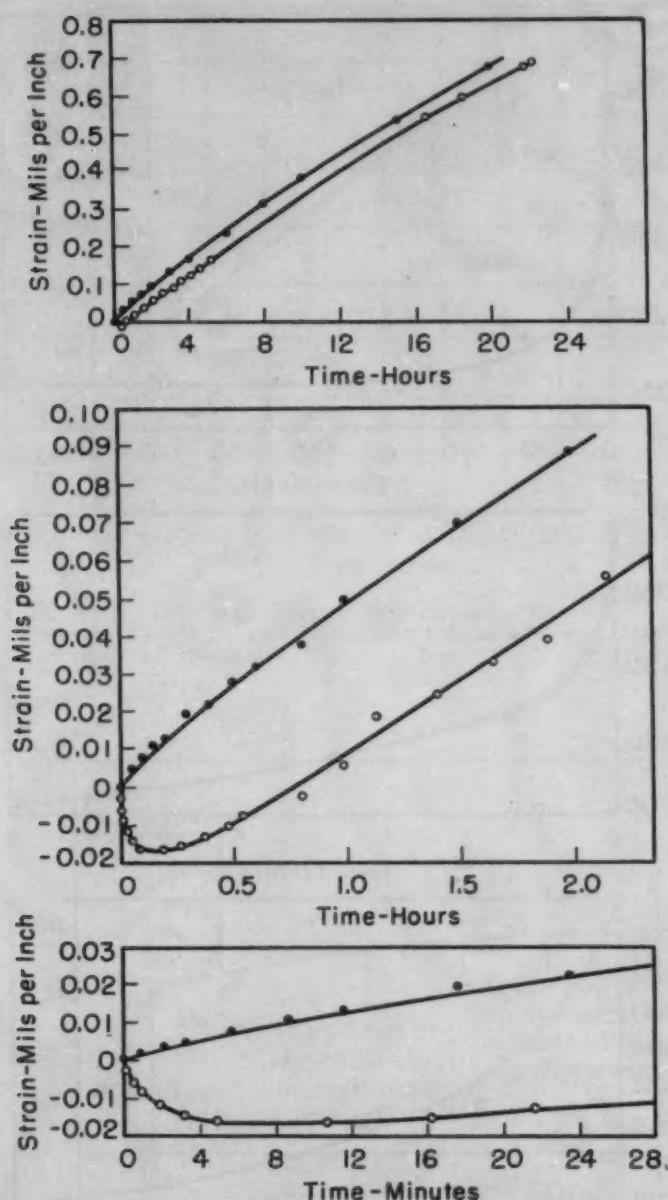


Fig. 36—Variation of Total Strain and Plastic Strain With Time After Reducing the (Conventional) Stress From 14,000 to 12,000 Psi. Quenched and tempered (1250 °F) Cr-Mo-V steel, tested at 1100 °F.

The basis for the correction is the measured strain-time curve following unloading to zero stress from some stress that has been maintained constant for a long time (see Fig. 37). This curve gives the anelastic strain as a function of time for a particular stress change. The anelastic strain for some other stress change can be determined by multiplying by the ratio of the two stresses, since the anelastic effects are proportional to² stress (see Part I). Then for creep following an increase in load, the anelastic strain (as a function of time) corresponding to the load change can be subtracted from the total

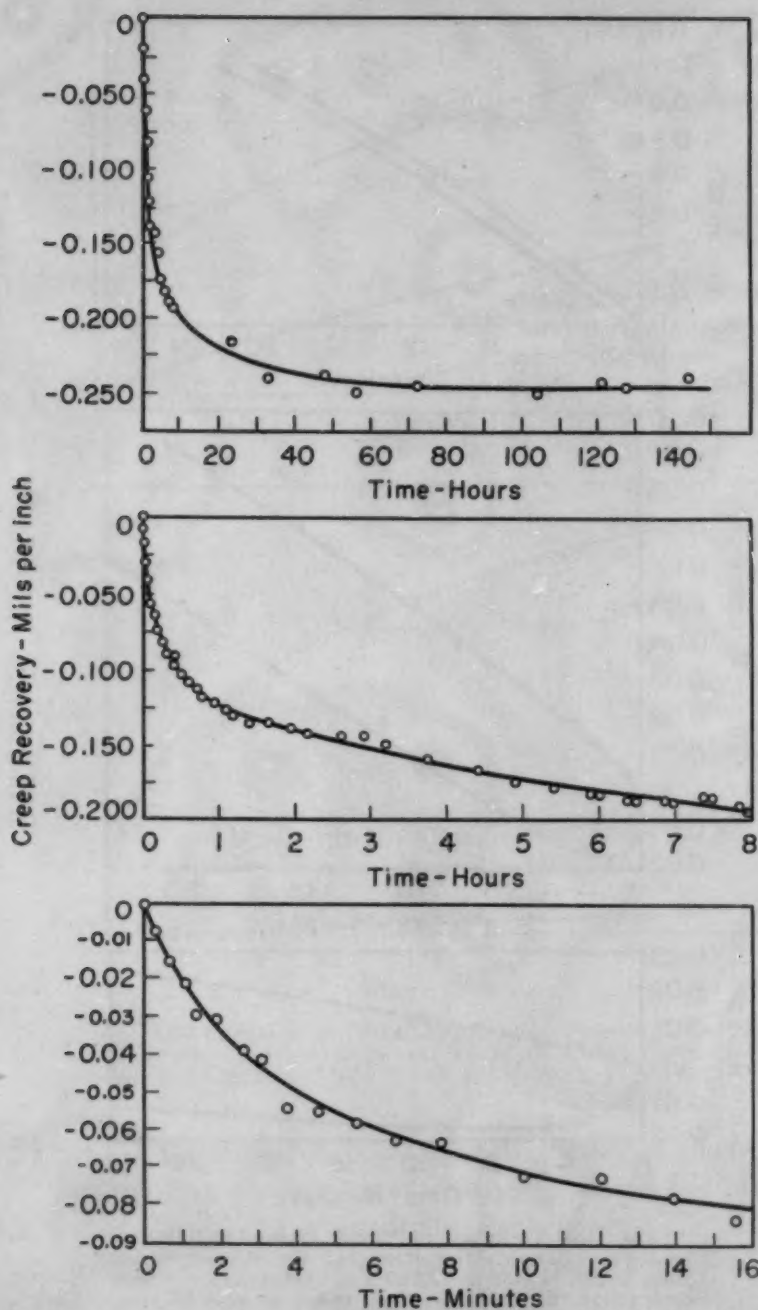


Fig. 37—Creep Recovery at Zero Stress After Removal of 5000 Psi. Oil-quenched (3-inch round) and tempered (1250 °F) Cr-Mo-V steel, tested at 1100 °F.

strain (as a function of time), leaving the plastic strain (as a function of time). When this is done, the remaining curve (Fig. 35) is nearly straight with a slightly decreasing slope. In a similar manner, for creep following a decrease in load, the anelastic strain corresponding to the load change can be added to the total strain to give the plastic strain. Again the result is nearly a straight line with a positive and

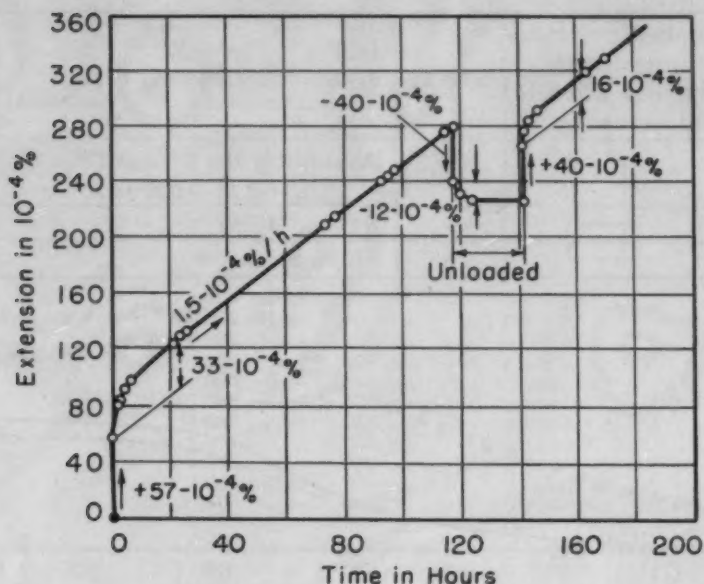


Fig. 38—Creep Data on Lead Showing Effect of Temporary Unloading and Subsequent Reloading. From Hanffstengel and Hanemann (6).

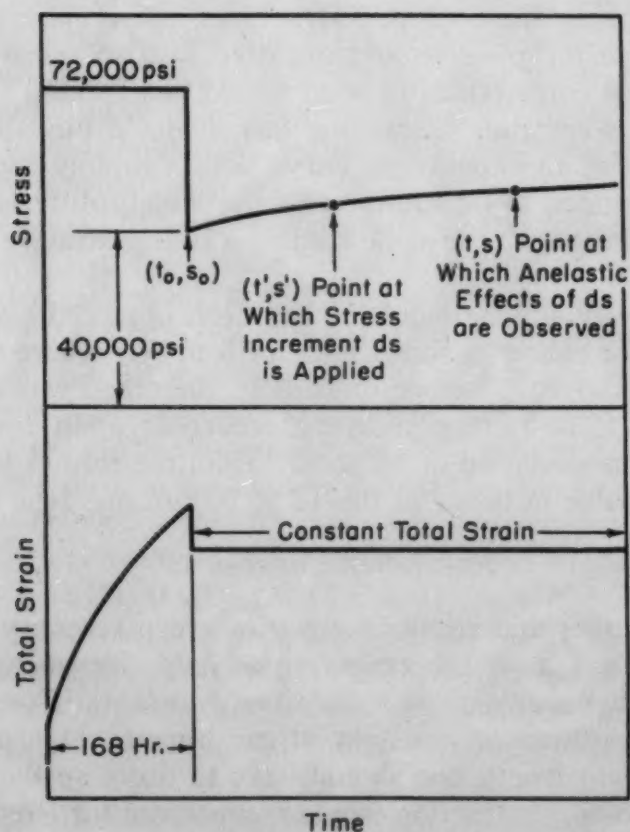


Fig. 39—Schematic Diagram Showing the Conditions Under Which the Stress Would Be Expected to Increase During Relaxation.

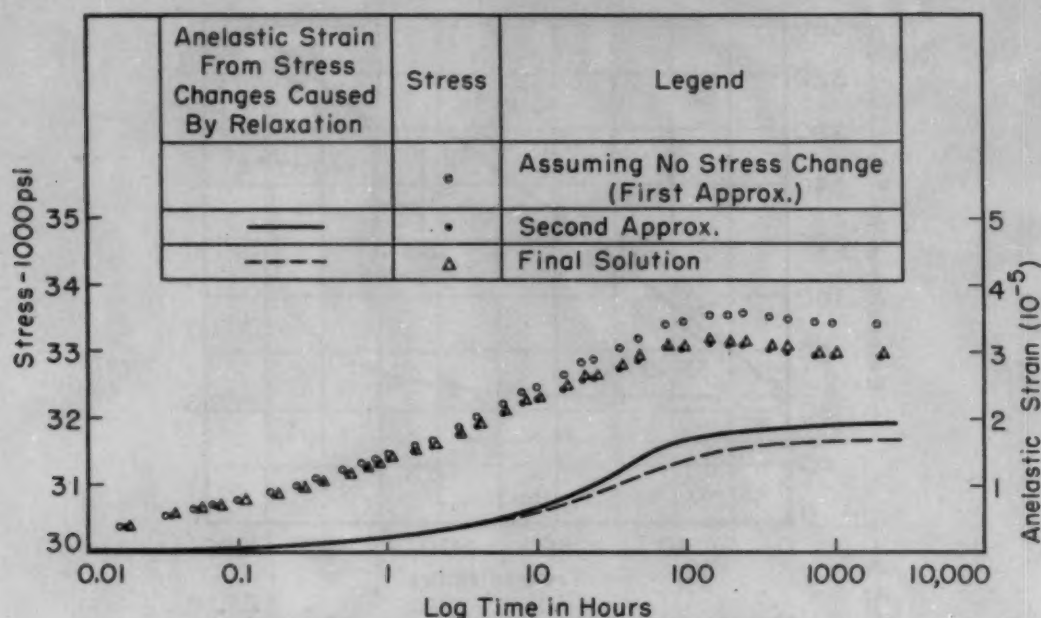


Fig. 40—Calculated Relaxation Curve for Cr-Mo-V Steel at 800 °F Following 168 Hours at 72,000 Psi and Reduction to 40,000 Psi.

slightly decreasing slope (Fig. 36). Thus, the remaining curve has the same shape for positive and negative load increments; furthermore, the shape corresponds to what would be expected as the plastic behavior. It is certainly a startling fact, if not a fundamentally significant one, that an exponential curve with a rapidly changing slope can be either added to or subtracted from widely different measured strain-time curves with the same result—a nearly straight line in both cases.

Qualitatively similar behavior has been observed previously (4, 6). Fig. 38, for example, shows data for lead (6) where the load was temporarily removed. Before unloading, the creep was linear; after unloading, 12×10^{-6} creep recovery occurred; upon reapplying the former load, the deviation of 16×10^{-6} from the former linearity was mostly explainable in terms of the 12×10^{-6} of anelastic strain.

Relaxation Phenomena

The processes that result in creep or creep recovery at constant load should also cause relaxation (gradually decreasing stress) if the length of the specimen is maintained constant. For example, if a specimen lengthens at constant stress because of creep, then to maintain constant length one should have to decrease the stress with time so that elastic contraction would compensate for lengthening due to creep. It is found experimentally that the stress does have to be decreased continuously to maintain constant length following a sudden change from zero load to some tensile load. This effect is relaxation,

Table II
Length Changes Accompanying Sudden Load Decrements

Temperature	Stress Changed From	Strain Change	Modulus
800 °F	46,000 psi to zero	0.00174	26.4×10^6
	30,000 psi to zero	0.00112	26.8×10^6
	30,000 psi to zero	0.00114	26.4×10^6
	48,000 psi to zero	0.00182	26.3×10^6
	20,000 psi to zero	0.00074	27.0×10^6
	72,000 psi to zero	0.00296	24.3×10^6
	72,000 psi to zero	0.00277	26.0×10^6
	72,000 psi to 4,000 psi	0.00272	25.0×10^6
	40,000 psi to 4,000 psi	0.00139	25.9×10^6
1000 °F	20,000 psi to 16,000 psi	0.00017 ¹	23.4×10^6
	16,000 psi to 12,000 psi	0.00017 ²	22.3×10^6
	12,000 psi to 8,000 psi	0.00018 ³	21.8×10^6
	8,000 psi to 4,000 psi	0.00018 ⁴	21.8×10^6
	15,000 psi to 8,000 psi	0.00032 ⁵	21.5×10^6
	4,000 psi to 2,000 psi	0.00009 ²	21.8×10^6
	2,000 psi to 1,000 psi	0.00005 ⁶	20.0×10^6
	30,000 psi to 16,000 psi	0.00070 ⁸	21.2×10^6
	8,000 psi to 4,000 psi	0.00018 ⁸	21.3×10^6
1100 °F	5,000 psi to zero	0.00026 ⁵	19.6×10^6
	14,000 psi to 12,000 psi	0.00010 ⁵	19.0×10^6
	12,000 psi to 10,000 psi	0.00009 ⁶	22.2×10^6
	14,000 psi to 12,000 psi	0.00010 ⁵	19.0×10^6
	12,000 psi to 10,000 psi	0.00008 ⁵	23.5×10^6

in the usual sense of the word. However, if the stress is applied and then reduced in such a way that creep recovery would have occurred at the reduced stress, then to maintain constant length at the reduced stress one should have to increase the stress gradually so that elastic lengthening would compensate for the shortening due to creep recovery, as shown schematically in Fig. 39.

Fig. 40 shows the stress variation that would be expected at constant length if the anelastic behavior of Fig. 41 were to prevail following a decrease to 40,000 psi from a 168-hour sojourn at 72,000 psi and 800 °F (425 °C) and if no plastic strain occurred. The relaxation curve in Fig. 40 was calculated by a series of approximations. First the anelastic shortening at constant length was calculated assuming no stress change following the change from 72,000 to 40,000 psi, that is, due only to the zero \rightarrow 72,000 psi change and the 72,000 \rightarrow 40,000 psi change. Then the stress increments that cause elastic lengthening just compensating for the anelastic shortening were determined using $E = 26,000,000$ psi (Table II); and this curve of stress versus time constitutes a first approximation to the relaxation curve. For succeeding approximations the anelastic shortening was recalculated assuming the relaxation (stress versus time) curve of the preceding approximation. Fig. 40 shows that the procedure converges quickly.

The calculation of the anelastic strains resulting from the stress changes during relaxation requires an integration of the strain changes caused by all the infinitesimal stress changes due to the relaxation, according to the equation

$$\epsilon = \int_{S_0}^S dS' \sum a_i \left(1 - e^{-\frac{t-t'}{\tau_i}} \right) \quad \text{Equation 12}$$

in which

$$\epsilon = \sum a_i (1 - e^{-t/\tau_i}) \quad \text{Equation 13}$$

is the anelastic strain at time t caused by unit stress change, and the other symbols are defined by Fig. 39. Since the graphical strain-time relation of Fig. 41 was used instead of an algebraic relation such as

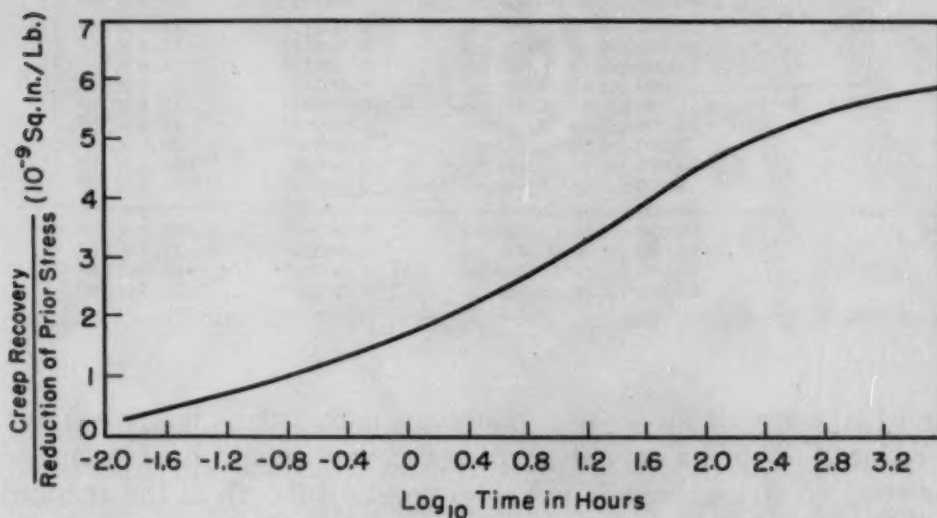


Fig. 41—Creep Recovery Per Unit Stress Decrement as a Function of Time Following Unloading. Cr-Mo-V steel tested at 800 °F. Averaged from tests in Figs. 10, 12 and 25 with long prior load durations.

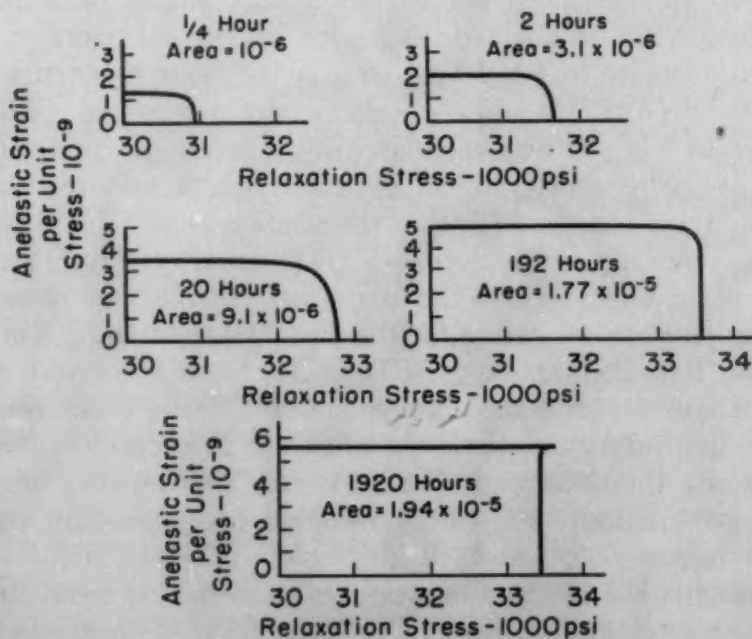


Fig. 42—Determination of Anelastic Strains Due to Stress Changes During Relaxation for the Conditions of Fig. 39. Second approximation.

Equation 13, the integration of Equation 12 was performed graphically. Several convenient times were chosen, the integrations for which are exemplified by Fig. 42.

Fig. 43 shows the results of a test under conditions similar to those in Fig. 39. The results are as expected in so far as the initial increase of stress at constant length is concerned; but the eventual

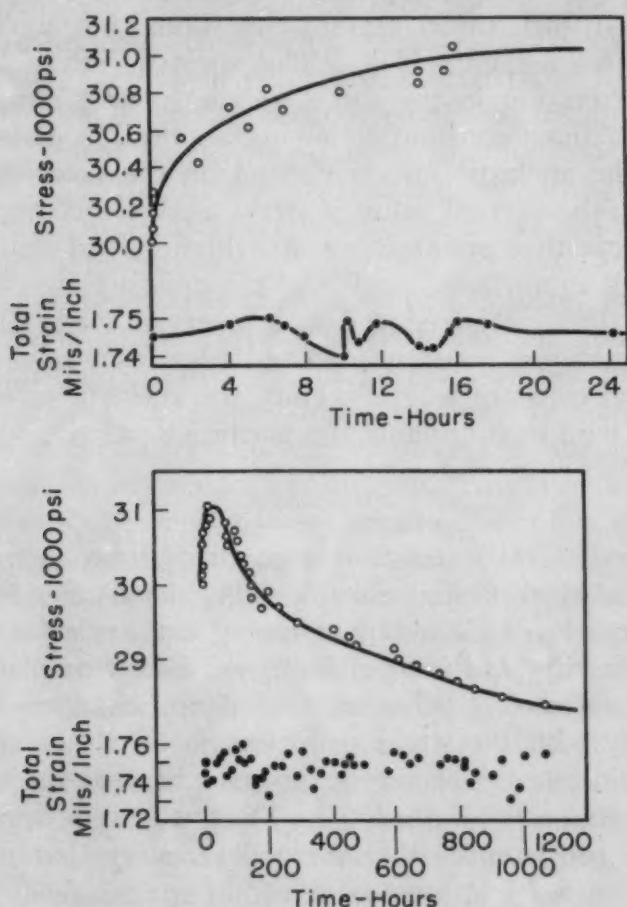


Fig. 43—Relaxation Test on Cr-Mo-V Steel at 800°F in Which the Total Strain After Unloading From 45,000 to 30,000 Psi Is Maintained Constant. Upper figure is a magnification of the early portion of the lower figure. Creep strain at 45,000 psi was 0.00047.

decrease in stress to values even lower than the initial stress indicates the occurrence of plastic creep, an effect that was not expected from the results of an earlier experiment in which no plastic creep occurred at 30,000 psi after preloading about 100 hours at 46,000 psi and then resting 100 hours (Fig. 20). In the test of Fig. 43 there was more plastic prestrain (0.00047) than in the earlier experiment (0.00033), so that more subsequent resistance to plastic deformation would be expected in the test of Fig. 43; but on the other hand, there was opportunity for additional strengthening by strain aging during the no-

load period following the prestrain in the earlier test, in a manner observed previously (11).

Applications

Under ordinary conditions, anelastic strain is just as detrimental to the service life of a metal part as plastic strain. It contributes to the creep strain that occurs under constant load, just as the plastic strain does. In fact, under certain conditions, the creep may all be anelastic strain (see Part III). The anelastic strain likewise contributes to relaxation in the same way as plastic strain, when the length is maintained constant following application of load. On the other hand, the anelastic effects depend on the prior stress change, rather than on the current value of stress as does plastic creep. Figs. 30 and 43 show that prestraining at a higher load than the service load will result in anelastic strains of the opposite sign to the plastic strains when the load is reduced to the service load. They cause a tendency to shorten at constant load and a tendency toward increasing tensile stress at constant length. Thus, the anelastic effects following overstressing tend to counteract the plastic effects.

SUMMARY

Many mechanical tests show departures from a combination of ideal elastic and ideal plastic behavior. The departures studied in this investigation can be explained by assuming that anelastic strain occurs simultaneously with, and independently of, elastic or plastic strain.

For purely elastic behavior the strain changes linearly and instantaneously with the stress; when anelastic strain also occurred, the stress-strain curve was no longer straight, and its average slope depended on the rate of loading. The measured deviations from linearity were consistent with the creep recovery that was observed following unloading.

For purely plastic behavior the length of a specimen never decreases as long as the load is a tensile load; when anelastic strain also occurred, however, shortening was observed whenever the load was decreased. Also, since the anelastic strain rate may change much more than the plastic strain rate, the creep curves sometimes had a much different shape when most of the strain was anelastic than when most of it was plastic.

Anelastic strain affects the relaxation behavior in the same way that it affects creep behavior. If the length is held constant after applying an initial load, the stress decreases with time due to anelastic strain as well as to plastic strain. If the length is held constant after decreasing the load, however, the stress increases at first and then may decrease (due to plastic flow) or may not decrease if the remaining stress is not large enough to cause a significant plastic creep rate.

Thus, in either creep or relaxation, the anelastic effects tend to counteract the plastic effects if the specimen is prestrained at a higher load and then partly unloaded.

THE BOUNDARY BETWEEN ANELASTIC AND PLASTIC BEHAVIOR— PART III

Early room temperature tension tests showed the existence of a rather definite limiting stress below which a metal remained elastic and above which permanent deformation occurred. Both above and below this limit the deformation occurred almost instantaneously, and very little additional extension occurred in long periods of time at constant load. The rate of deformation had very little influence upon the stress-strain curve; in other words, the metal was not "rate sensitive" at room temperature.

Later it was found that at elevated temperatures the deformation behavior of metals differed from that first observed at room temperature. At high temperatures metals "crept", or deformed with time at constant load. In addition, they were very rate-sensitive. Contrary to low temperature experience, there did not appear to be a limiting stress below which plastic deformation would not occur, although the rate of creep was very small at very low stresses.

Experiments using a torsion pendulum (1) have shown that creep at sufficiently low stresses is eventually recoverable. A twisted bar eventually returns to its original untwisted configuration. This behavior has been called "anelastic", and the eventually recoverable creep has been called anelastic strain. There is gradual recovery of part but not all of the creep introduced at higher stresses. This gradual and partial shortening has been called "creep recovery". The evidence contained in Parts I and II suggests that creep recovery is anelastic shortening, and that creep is due to simultaneous and independent anelastic and plastic deformation.

If creep is indeed a superposition of anelastic and plastic strains, there may be a limiting stress, below which creep is essentially anelastic and above which it is partly plastic. Exceedingly small stresses generally have been used in the torsion pendulum tests (1) in order to avoid any measurable plastic strain. In these tests the stress level was too small to be of engineering interest as a working stress value. On the other hand, the stress to which one could go before causing a measurable plastic strain might be considerably higher than that generally used in the torsion pendulum experiments. Furthermore, the amount of plastic strain that could be considered negligible in comparison with the anelastic strain would be much larger for engineering purposes than for research. We shall now investigate the behavior of metal when the plastic strain is comparable with or smaller than the anelastic strain.

It has been shown in Part I that the anelastic strain obtained in a given time is proportional to the stress (Fig. 27).⁶ The plastic strain obtained in a given time, on the other hand, varies much more rapidly with stress. Fig. 44 shows creep curves for a Cr-Mo-V steel plotted as log creep strain versus log time. At 800 °F (425 °C) the curves are parallel lines for the four stresses shown. Fig. 45 is a crossplot of Fig. 44 at $\frac{1}{2}$ hour and 100 hours showing how the creep

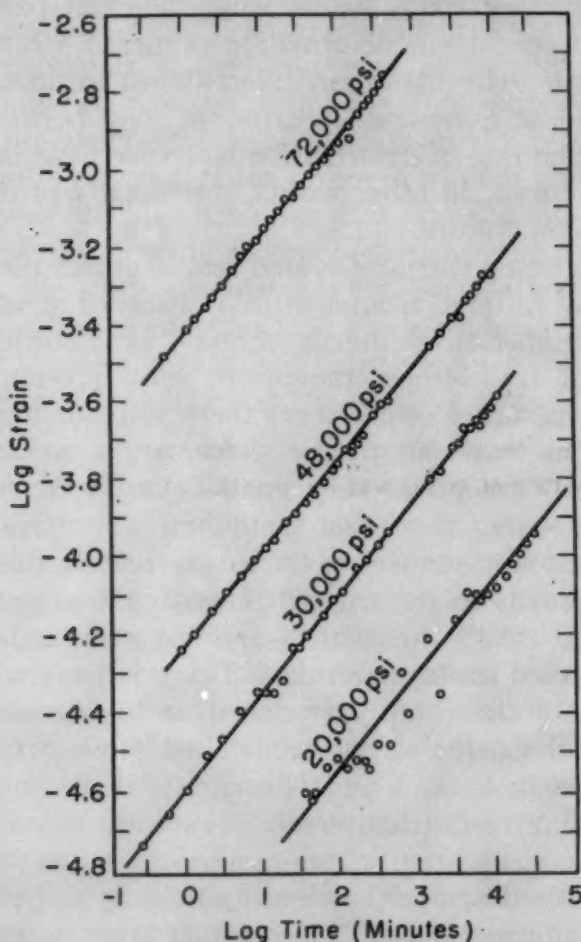


Fig. 44—Creep Curves at 800 °F for a Low-Alloy Steel. Three-inch round heated 1650 °F for 5 hours, oil-quenched; tempered 12 hours at 1240 °F, 5 hours at 1100 °F. Elastic strain not included.

strain varies with stress. The creep strain increases rapidly with stress—approximately as the second or third power. At some other time than $\frac{1}{2}$ hour or 100 hours the stress-strain relation for creep would be similar, because the log-log plots in Fig. 44 are parallel.

⁶Fig. 27 shows creep recovery data. The creep recovery equals the anelastic creep only if the duration of prior load is several times the creep recovery time. This condition is fulfilled for creep recovery times in Fig. 27 up to 20 hours. The anelastic creep might be 5 or 10% higher than the creep recovery for a time of 4 days (see Fig. 28).

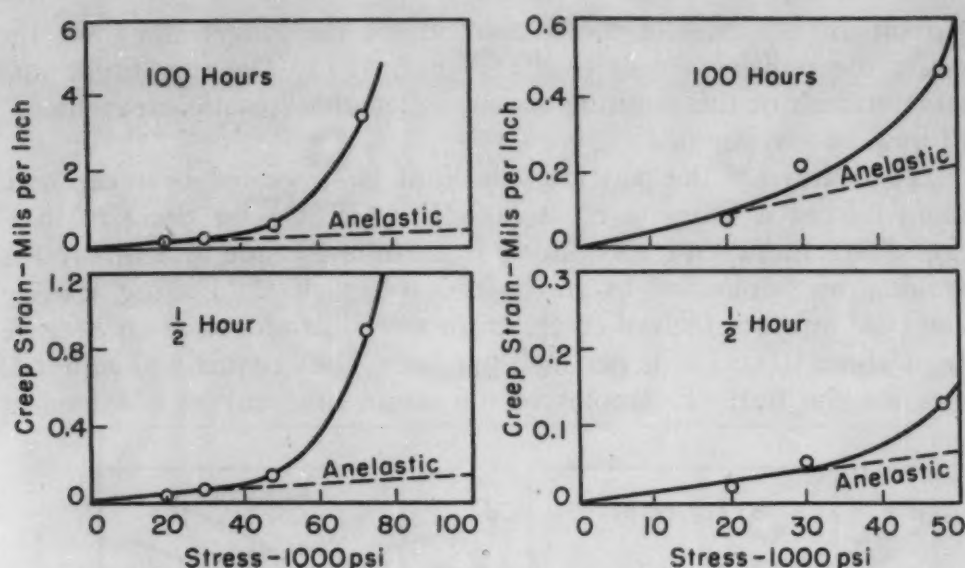


Fig. 45—Effect of Stress Level on Anelastic Strain and Creep Strain for Two Durations of Loading. Curves at right are magnifications of early part of curves at left. Anelastic values are from Fig. 27 and creep values are obtained by cross plotting Fig. 44.

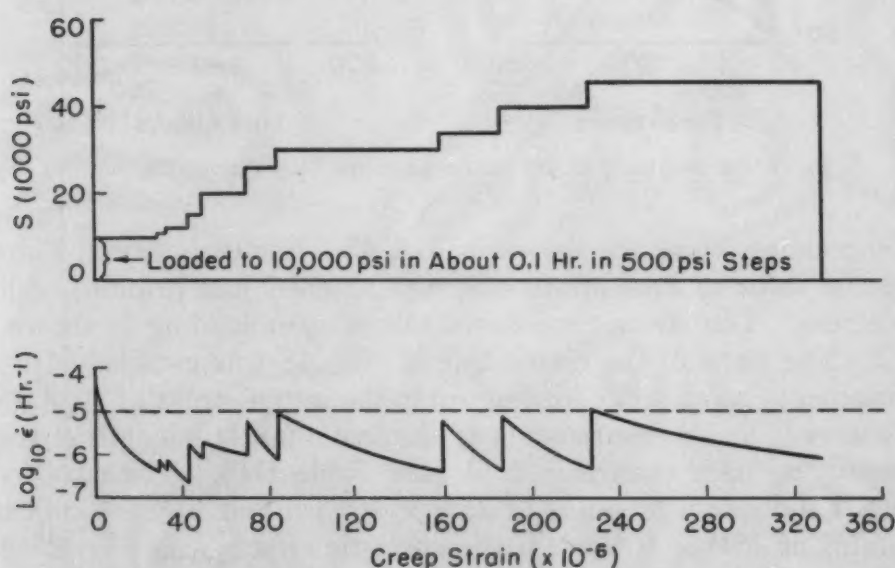


Fig. 46—Step Test on Cr-Mo-V Steel at 800 °F.

Fig. 45 shows also the anelastic data for $\frac{1}{2}$ hour and 100 hours as reproduced from Fig. 27. Fig. 45 shows that the creep strain decreases rapidly as the stress decreases, and becomes equal to the anelastic strain at a stress of 20,000 to 30,000 psi. Because of the scattering caused by inherent differences between different specimens, there is considerable uncertainty as to the stress below which all the creep is anelastic; but it is clear from the figure that such a limiting stress does exist. Of course this limiting stress will depend some-

what on the duration of the measurement; the longer the time, the smaller the limiting stress (see also Fig. 45). The magnitude and characteristics of this limiting stress, called the "plastic creep limit", will now be investigated.

The nature of the plastic creep limit is suggested by creep data obtained from a "step test" at 800 °F (425 °C) on the Cr-Mo-V steel, where more load was added from time to time and finally the specimen was unloaded to zero stress (Fig. 46). During loading about 0.33 mils per inch of creep strain were introduced at an average rate of about 0.0033 mils per inch per hour, thus requiring about 100 hours for the test. Examples of the strain-time curves obtained at

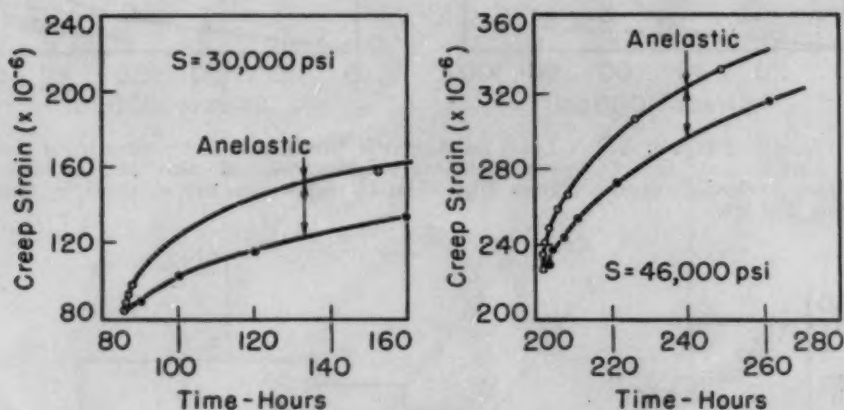


Fig. 47—Examples of Creep Curves From the Step Test of Fig. 46.

each successive stress are shown in Fig. 47. For each stress, Fig. 48 shows the value of total strain that was reached just prior to adding more stress. The strain-time curve following unloading is shown in Fig. 2. The slope of the elastic line in Fig. 48 was established from measurements taken while loading up to the initial stress of 10,000 psi (see Fig. 49) and measurements of the instantaneous length changes accompanying each change in load (see Table III). The data from Table III indicate a modulus of 25.9×10^6 psi and Fig. 49 indicates a modulus of 26.0×10^6 psi; if the anelastic effects (see Fig. 2) due to a loading time in Fig. 49 of 0.1 hour were taken into account, the true modulus would be about 26.5×10^6 psi, agreeing favorably with the average from Table III when the scattering is considered.

It is evident from Fig. 48 that the nonelastic strains are quite small compared to the elastic strains, and from Fig. 2 that more than half the nonelastic strain is recoverable. To evaluate the nature of the strain obtained in the step test of Fig. 46, it was assumed that the creep recovery in Fig. 2 is anelastic strain, which conforms to the spring-dashpot analogy. According to this assumption, the anelastic strain introduced is the sum of the anelastic strains due to all preceding stress increments. The anelastic strain due to any one stress

Table III
Length Changes Accompanying the Sudden Load Changes of Fig. 46 — 800 °F

Stress Changed From	Strain Change	Modulus
12,000 to 16,000 psi	156×10^{-6}	25.7×10^6 psi
16,000 to 20,000 psi	155	25.8
20,000 to 26,000 psi	234	25.6
26,000 to 30,000 psi	152	26.2
30,000 to 34,000 psi	162	24.7
34,000 to 40,000 psi	228	26.4
40,000 to 46,000 psi	228	26.4
46,000 to zero	1735	26.5
		25.9×10^6 average

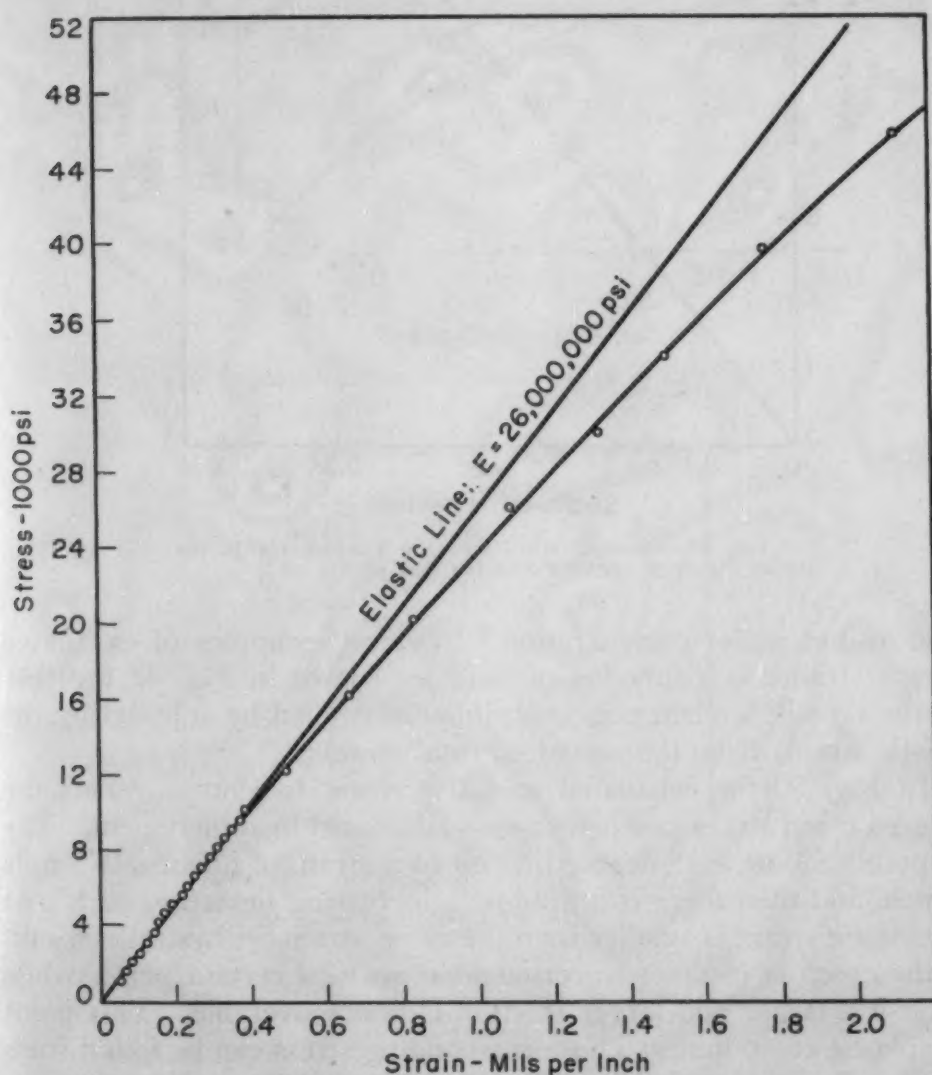


Fig. 48—Total Strain Reached at Each Successively Higher Stress in the Test of Fig. 46.

increment will be the appropriate value from Fig. 2 multiplied by the ratio of the stress increment to 46,000 psi, the time value used in Fig. 2 being the interval from the application of the load increment

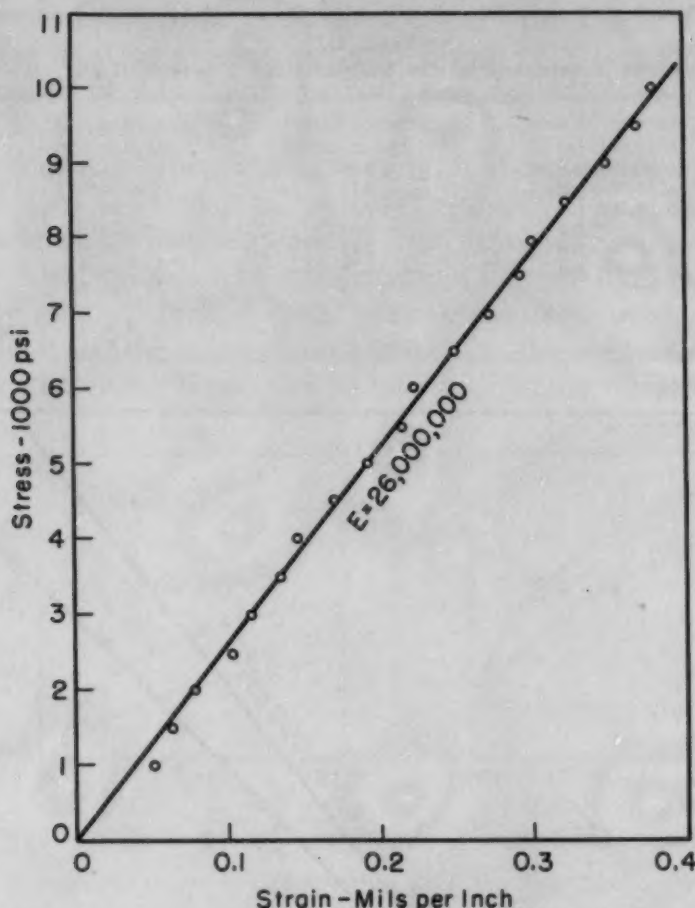


Fig. 49—Stress-Strain Curve for Loading Up to the Initial Stress of 10,000 Psi in the Test of Fig. 46.

to the instant under consideration.⁷ Typical examples of calculated anelastic strains as a function of time are shown in Fig. 47 together with the time-dependent plastic strains determined by subtracting the anelastic strains from the measured total strains.

In Fig. 50 the calculated anelastic strain is plotted versus the measured creep strain just before each additional load increment. The data points follow a 45-degree line up to a strain of about 0.075 mils per inch, and then there is a gradually increasing deviation such that the anelastic strain is smaller than the creep strain. Physically speaking, the creep is completely recoverable up to a certain point, while beyond it a larger and larger fraction is nonrecoverable. This point is the plastic creep limit. The corresponding stress can be found from Fig. 51, where stress is plotted versus the plastic part of the creep strain. The plastic strain was obtained by subtracting the calculated anelastic strain from the creep strain for each point in Fig. 50. Fig. 51 shows that there is a definite plastic creep limit at about 20,000 psi.

⁷Taking the creep recovery values in Fig. 2 as equal to the anelastic strain suffered during load results in slightly too little anelastic strain at long times (see Part I).

Of course this limit would be somewhat smaller if each load increment were maintained longer (see also discussion pertaining to Fig. 45). By contrast, Fig. 52, which shows the stress versus total creep, illustrates the absence of a dividing line at finite stress between the two behaviors usually represented, namely elastic behavior and creep behavior. According to Fig. 52 the "elastic limit" that is so familiar and important in low temperature behavior is zero at 800 °F (425 °C).

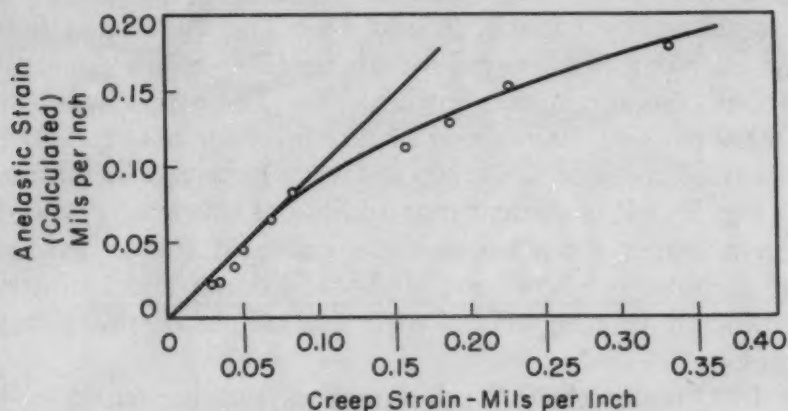


Fig. 50—Calculated Anelastic Strains Reached in the Test of Fig. 46.

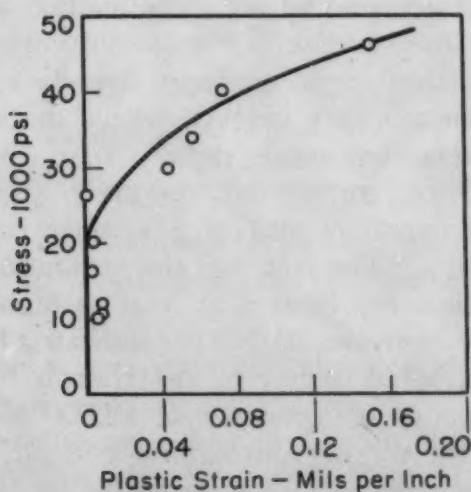


Fig. 51—Stress Versus Plastic Strain Introduced at That Stress and All Preceding (Lower) Stresses for Test of Fig. 46.

The fact that there is no region of purely elastic behavior at elevated temperatures has been widely recognized. However, the prevalent conclusion drawn from this fact, namely, that there is no region where plastic behavior is absent, must now be reconsidered in the light of Fig. 51, which indicated a definite boundary below which plastic deformation is negligible.

Following the no-load resting period at the end of the test of Fig. 46, a stress of 30,000 psi was applied for a period of 48 hours. When the anelastic strain, calculated as before, was subtracted off, a practically horizontal line was obtained (Fig. 20), indicating that all the creep introduced at 30,000 psi was recoverable. Fig. 20 shows that the plastic creep limit can be raised by plastic strain. This limit is about 20,000 psi for no plastic strain (Fig. 51), whereas it is raised to something higher than 30,000 by 0.00033 plastic strain.

Another example of increasing the plastic creep limit by plastic prestrain is shown by Figs. 3, 9, and 13. The metal was first prestrained at 68,000 to 72,000 psi for about 1200 hours during which about 0.007 plastic strain was introduced. The stress was then reduced to 4000 psi and maintained at this level for about 1000 hours. During this time, most of the creep recovery expected in infinite time occurred (Fig. 9). It is evident that additional shortening would have occurred in a longer time, because the curve in Fig. 9 has not yet leveled off completely; however, slight additional shortening would not be significant in comparison with the effects of the subsequent load changes.

After 1000 hours at 4000 psi the stress was increased to 40,000 psi and maintained at this value for 580 hours. The resulting creep curve is shown in Fig. 3. Using the faired curve, the expected creep recovery curve was calculated by the same method as used in Part I. The calculated and measured creep recovery curves are shown in Fig. 13. The calculated curve conforms closely to the data at all values of time except the very longest, where the specimen appears to be shortening somewhat more rapidly than the spring-dashpot analogy predicts. Thus, we see that the creep strain introduced at 40,000 psi is all recoverable, and in a manner conforming to the spring-dashpot analogy. The fact that the strain was all recoverable shows that the plastic creep limit is at least as high as 40,000 psi, a considerable increase over the 20,000 psi indicated by Fig. 51. The increase must be attributed largely to the strain hardening caused by the 0.007 strain introduced previously at 68,000 to 72,000 psi, and possibly partly to strain aging during the no-load period following the prestraining, as suggested in Reference 11.

A few general remarks should be made about the magnitude of the creep-recovery effects and their engineering importance. The creep recovery at 800 °F (425 °C) per unit stress e_a/S is about 6×10^{-9} for rather long times (Fig. 10). If the elastic modulus S/e_e is 25×10^6 psi (Table II), the ratio of eventual anelastic strain to elastic strain is

$$\frac{e_a}{e_e} = \frac{e_a}{S} \frac{S}{e_e} = (6 \times 10^{-9}) (25 \times 10^6) = 0.15$$

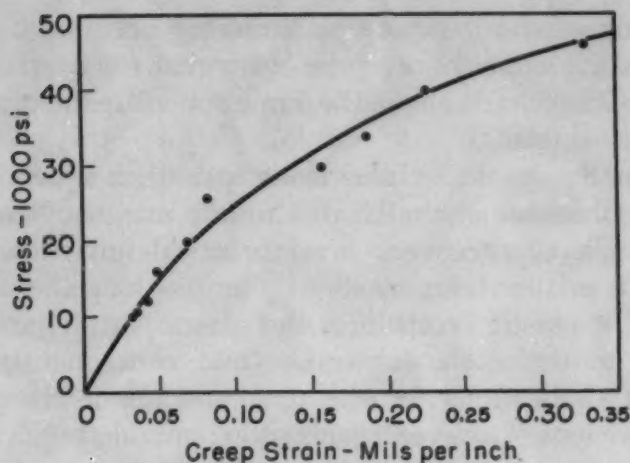


Fig. 52—Cumulative Nonelastic Strain Reached at Each Successively Higher Stress in the Test of Fig. 46.

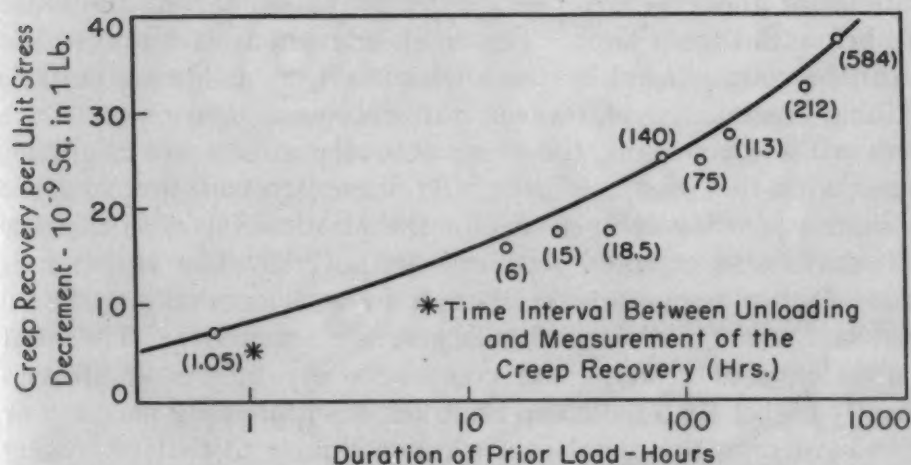


Fig. 53—Creep Recovery of Cr-Mo-V Steel at 1000 °F.

Fig. 53 shows the creep recovery obtained at 1000 °F (540 °C). The value of creep recovery for the longest load duration and the longest time following unloading is 37×10^{-9} per unit stress decrement. For a modulus of 21.6×10^6 (Table II), the ratio of creep recovery to elastic strain is 0.80. The data at 1100 °F (595 °C) is meager, but one test (Fig. 37) shows that creep recovery for a stress decrement of 5000 psi is 0.250 mils per inch. This is essentially equal to the elastic strain of 0.243 inch per inch ($E = 20.6 \times 10^6$ from Table II).

The above data show that the creep recovery becomes an increasingly large fraction of the elastic strain, and therefore increasingly important, as the temperature increases. On the other hand, the largest stress, and thus also the largest elastic strain, that is of engineering interest decreases with increasing temperature, because

of the increasing ease with which plastic creep occurs. Consequently the largest absolute values of creep recovery that are practically attainable in Cr-Mo-V steel are about the same for all temperatures, let us say of the order of 0.0003.

Because of the way that plastic creep and creep recovery vary with stress, and because of the small absolute magnitude of the creep recovery effects, creep recovery is of practical importance only for stresses that are smaller than, or slightly larger than, the plastic creep limit. Below the plastic creep limit the plastic strains are negligible in comparison to the anelastic strains, and consequently there are many practical applications for the phenomenon of creep recovery. Creep can be prevented or even reversed by suitable prestraining, and stress relaxation can be prevented or reversed by prestraining at a stress higher than the service stress, as shown in Part II. For stresses slightly exceeding the creep limit—that is, when the plastic strains are significant, but smaller than the anelastic strains—the engineering applications of the creep recovery effects are similar to those for stresses below the creep limit. The creep or relaxation due to plastic strain can be counteracted by the anelastic effects following suitable prestraining treatments. However, for stresses that are very much larger than the creep limit, the creep recovery effects are negligible compared with the plastic effects. At these stresses the anelastic effects cannot possibly compensate for the plastic effects, so that the practical usefulness of creep recovery disappears. The situation is similar at higher temperatures, though in a manner not quite so startling, because of the somewhat larger rate sensitivity. The most likely possibility of utilizing the creep recovery effects at stresses significantly higher than the creep limit lies in suppressing plastic flow by strain hardening the metal in a manner similar to that producing the results of Figs. 13 and 20.

SUMMARY

At elevated temperatures, the anelastic strain for a given time increases linearly with stress. The plastic strain for a given time varies with stress approximately as the square or cube, with the effect that the strain rate for small stresses is exceedingly small, while the strain rate at stresses not too much higher is enormous. Consequently, there is a “plastic creep limit” below which the rate of plastic straining is negligibly small compared with the rate of anelastic straining. In other words, there is a finite limiting stress below which plastic strain does not occur, although this fact has been obscured in the past by observations that the limiting stress is zero for the total nonelastic deformation.

The plastic creep limit is at a practically significant stress. It is about 20,000 psi at 800 °F (425 °C) for a Cr-Mo-V steel quenched

as a 3-inch round and tempered. What is perhaps of more significance is that it can be raised by deforming the metal plastically at the elevated temperature. One experiment at 800 °F (425 °C) has shown that as little as 0.7% plastic strain produces enough strain hardening to raise the plastic limit from 20,000 to at least 40,000 psi.

The existence of a plastic creep limit, as described above, does not mean that there is creep above a certain stress and none below it. It only means that creep is all anelastic below the stress, while at higher stresses the creep is partly anelastic and partly plastic. In fact, without a rigorous analysis using data obtained following unloading from the creep load, it is generally impossible to observe any discontinuity in the creep behavior at the plastic limit.

Then what is the practical significance of the plastic creep limit? The significance lies in inherent differences between anelastic and plastic behavior. A bar will either shorten anelastically if there has been a decrease in the tensile load or lengthen anelastically following a load increase, whereas plastic shortening never occurs under tensile load regardless of prior load changes. This means that the dimensional changes due to plastic deformation are always undesirable in structural applications, whereas the dimensional changes due to anelastic deformation can be arranged to be desirable. If the stress is below the plastic creep limit, the plastic effects are negligible compared to the anelastic effects, and wholly desirable dimensional changes are attainable by suitable prestraining. In addition, within a restricted range of stress above the plastic creep limit, the anelastic effects can be made to counteract the undesirable plastic effects.

ACKNOWLEDGMENT

The author is indebted to E. J. Faught, R. G. Feustel, H. A. Lequear and G. R. Cornell for assistance in conducting the tests and making the calculations.

References

1. T. S. Kê, "Experimental Evidence of the Viscous Behavior of Grain Boundaries in Metals", *Physical Review*, Vol. 71, 1947, p. 533.
2. C. M. Zener, "Elasticity and Anelasticity of Metals", Chicago Press, 1948.
3. A. E. Johnson, "The Creep Recovery of a 0.17% Carbon Steel", *Journal, Institute of Mechanical Engineers*, Vol. 145, 1941, p. 210.
4. H. Zschokke, "Creeping Results and Recovery at High Temperature—Influences and Evaluation", *Brown Boveri Review*, Vol. 25, 1938, p. 247.
5. H. J. Tapsell, "The Phenomenon of Creep Recovery", London Congress of the International Association for Testing Materials, held April 19-24, 1937, London.
6. K. V. Hanffstengel and H. Hanemann, "Creep in Lead Under Stress", *Zeitschrift für Metallkunde*, Vol. 30, 1938, p. 41.
7. C. M. Zener, "Anelasticity of Metals", *Transactions*, American Institute of

Mining and Metallurgical Engineers, Vol. 167, 1946, p. 155.

8. J. D. Lubahn, "Creep-Tensile Relations at Low Temperatures", General Electric Research Laboratory Report No. RL-558, July 1951.
9. T. S. Kê, unpublished research.
10. B. Chalmers, "Precision Extensometer Measurements on Tin", *Journal, Institute of Metals*, Vol. 61, 1937, p. 103.
11. H. A. Lequear and J. D. Lubahn, "Recovery and Creep in an Alloy Steel", American Society for Testing Materials (to be published).

THE DETERMINATION OF THE ELASTIC CONSTANTS OF METALS BY THE ULTRASONIC PULSE TECHNIQUE

BY MYRON B. REYNOLDS

Abstract

The ultrasonic pulse technique has been used to determine the Young's modulus, shear modulus, and Poisson ratio of the following polycrystalline metals: beryllium, columbium, zirconium, titanium, vanadium, thorium, uranium, alpha brass, and Type 347 stainless steel.

The relationships between elastic wave velocities and elastic constants are given for the case of an isotropic solid. Elastic wave propagation and reflection are treated briefly. The ultrasonic pulse technique is described, including the internal reflection method of Hughes for determination of the shear wave velocity in cylindrical specimens.

The ultrasonic pulse apparatus is described and the computation of wave velocities illustrated.

The elastic moduli obtained are tabulated and discussed. A comparison is made with data from the literature where such data exist. For the metals columbium, titanium, thorium, and vanadium, it is believed that all three elastic constants have not been previously reported.

INTRODUCTION

THE ultrasonic pulse technique offers a convenient means for the measurement of the elastic constants of solid materials. The measurements are nondestructive. In addition, only one small sample of material suffices for the determination of Young's modulus, the shear modulus, and Poisson's ratio. The use of ultrasonic techniques for nondestructive inspection of metals is well known throughout industry. The use of ultrasonic techniques for measurement of elastic constants of metals is probably not so well known and will be discussed in some detail for the benefit of those practicing metallurgists unfamiliar with the method.

Propagation of Elastic Waves in Solids

Before describing the ultrasonic pulse technique for elastic constant measurement, it would be well to consider the types of elastic disturbances (or waves) which may be propagated through a solid.

A paper presented before the Thirty-fourth Annual Convention of the Society, held in Philadelphia, October 18 to 24, 1952. The author, Myron B. Reynolds, is associated with the Knolls Atomic Power Laboratory, Fuel Systems Unit, General Electric Co., Schenectady, N. Y. Manuscript received February 21, 1952.

In general, these waves are of two kinds: those which are propagated on the surface of a solid in a manner analogous to the propagation of ocean waves and those which travel inside the material. Only the latter kind will be considered here. Internal elastic waves are of two types: longitudinal waves in which the particle displacement is parallel to the direction of propagation and shear waves in which the particle displacement is perpendicular to the direction of propagation. Shear waves in solids exhibit polarization phenomena of the type observed in the propagation of light.

In general, the velocities of propagation of elastic waves in a solid are dependent upon the density of the solid, its elastic constants, the direction of propagation, and the ratio of the wave length* of the elastic disturbance to the physical dimensions of the solid. In isotropic solids the elastic constants are independent of direction, and, therefore, so are the wave velocities. The following relations hold for the velocities of elastic waves in an isotropic solid of physical dimensions large in comparison with a wave length:

$$V_s = \sqrt{\frac{\mu}{\rho}} \quad \text{Equation 1}$$

$$V_L = \sqrt{\frac{Y}{\rho} \frac{1 - \sigma}{(1 + \sigma)(1 - 2\sigma)}} \quad \text{Equation 2}$$

in which V_s = shear wave velocity
 V_L = longitudinal wave velocity
 μ = shear modulus of elasticity
 Y = Young's modulus
 σ = Poisson's ratio
 ρ = density of the solid

The velocity of propagation of a longitudinal wave in a rod, in a direction parallel to the axis of the rod, is dependent upon the ratio of the transverse dimension of the rod to the wave length of the disturbance. If the transverse dimension of the rod is large in comparison with the wave length, the velocity is that given by Equation 2. However, as the wave length increases or the rod cross section decreases, the wave velocity decreases until the limiting velocity

$$V_0 = \sqrt{\frac{Y}{\rho}} \quad \text{Equation 3}$$

is reached. This is the so-called "thin rod" velocity as compared with the "bulk" velocity given by Equation 2.

Elastic Wave Reflection at Boundaries

Elastic waves are reflected and refracted at boundaries between media of different elastic properties in the same manner as light

*Wave length here is defined as the wave velocity divided by the predominant vibration frequency. For the derivation of Equations 1 and 2 the reader is referred to any standard text on elasticity or classical mechanics.

waves are reflected and refracted at boundaries between media of different refractive indices (1).¹ As in the optical case, the angle of incidence is equal to the angle of reflection in the simple reflection of an elastic wave. However, at a "free surface", that is, at the boundary between a solid and either air or vacuum, reflection of a different type occurs. In Fig. 1 let arrow A indicate the direction

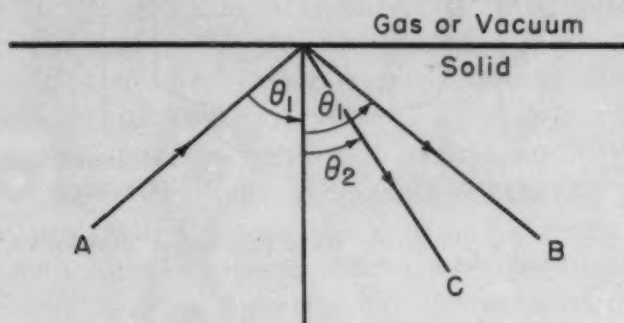


Fig. 1—Elastic Wave Reflection at a Free Surface.

of the propagation of a longitudinal wave in a solid so that its angle of incidence upon the free surface is θ_1 . Then the condition of stress equilibrium at the boundary requires a shear wave C reflected at angle θ_2 in addition to the longitudinal wave B reflected at angle θ_1 . Angles θ_1 and θ_2 are related as follows:

$$\frac{\sin \theta_1}{\sin \theta_2} = \frac{V_L}{V_s} \quad \text{Equation 4}$$

Likewise, a shear wave incident upon a free surface results in both a reflected shear wave and a reflected longitudinal wave at angles which satisfy a relation of the same type as Equation 4.

Elastic Wave Propagation Between Parallel Boundaries of a Solid

Let us consider a section of a solid which has two opposite surfaces accurately plane and parallel with two piezoelectric crystal transducers attached directly opposite each other on these surfaces. (See Fig. 2.) If one of the transducers (which shall be called the "transmitter") is properly excited, an elastic wave pulse will be generated with its propagation direction normal to the surface. This pulse will travel through the solid along path \overline{ab} , as in Fig. 2. Not all the energy in the wave pulse will be transferred to the "receiver" transducer, however; a wave will be reflected back along path \overline{ba} . Upon reaching the first surface this wave then will be reflected back along path \overline{ab} . These reverberations will continue until all the energy of the original wave pulse has been dissipated. The type of wave encountered will depend upon the transducer producing it: either a longitudinal or a shear wave reverberating in the same

¹The figures appearing in parentheses pertain to the references appended to this paper.

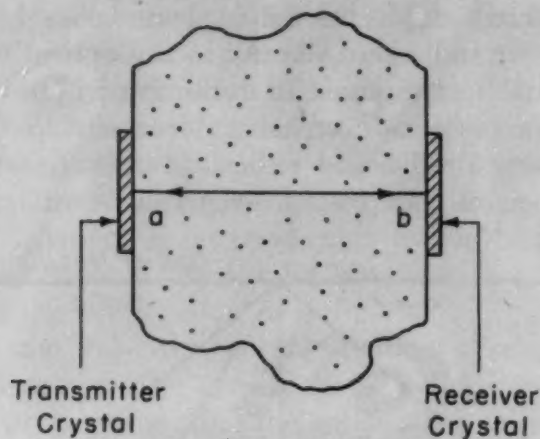


Fig. 2—Elastic Wave Propagation Between Boundaries in a Solid.

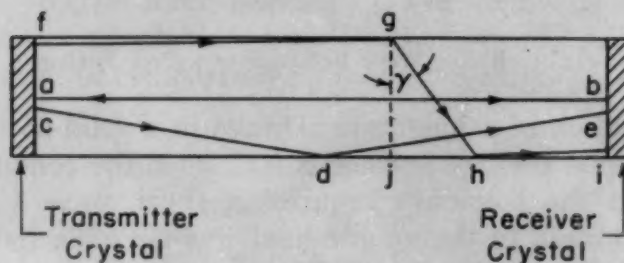


Fig. 3—Elastic Wave Propagation in a Cylindrical Rod.

fashion. The successive reverberations may be detected by either transducer as a series of electrical signals separated by time intervals proportional to the total path length for a complete reverberation which is twice the perpendicular distance between the parallel surfaces.

Wave Propagation in a Cylindrical Rod

Let us consider a cylindrical rod with a diameter which is large in comparison with a wave length and with ends accurately perpendicular to its axis (2). Let appropriate piezoelectric transmitter and receiver transducers be cemented to the ends, as in Fig. 3, with the cross sectional area of the transducers approximately equal to the cross sectional area of the rod.

Now let a short, longitudinal elastic wave pulse be generated by exciting the transmitter crystal. (It is assumed that the transducer generates only a longitudinal wave.) The simplest paths by which this wave pulse may reach the receiver crystal are as follows:

a. *Direct transmission along path \overline{ab} .* If the pulses appearing at the receiver are considered in chronological order, the first pulse received must correspond to this direct mode of transmission, since the highest possible velocity of propagation is the bulk velocity given by Equation 2.

b. *Simple reflection at cylinder wall as in path \overline{cde} .* This mode results from the fact that the transmitter generates a divergent wave rather than a pure plane wave. The effect of this is to delay the arrival of the pulse at the receiver by a time which is proportional to the increase in path length over the direct path length \overline{ab} . Inspection of Fig. 3 will show that the increase in path length is small and has no fixed value. Its only observable effect, therefore, is to lengthen and distort the received pulse.

c. *Conversion to shear mode by reflection at the surface with reconversion to longitudinal mode on the opposite surface as in path \overline{fghi} .* As a result of the cylinder wall reflections mentioned above, reflected shear waves originate at various points along the cylinder wall and are propagated across the rod at the angle predicted by Equation 4 for the case of grazing incidence. The effect of this mode of transmission is to delay the arrival of the pulse at the receiver by a fixed length of time which is equal to the difference between the pulse transit time along path \overline{gh} at the shear wave velocity and the transit time along path \overline{jh} at the longitudinal velocity. Referring to Fig. 3, it is apparent that

$$\sin \gamma = \frac{V_s}{V_L} \quad \text{Equation 5}$$

If the rod diameter is D ,

$$\overline{gh} = \frac{D}{\cos \gamma} \quad \text{Equation 6}$$

and

$$\overline{jh} = D \tan \gamma \quad \text{Equation 7}$$

Then the time delay resulting from this mode of transmission is

$$\Delta t = D \left(\frac{1}{V_s \cos \gamma} - \frac{\tan \gamma}{V_L} \right) \quad \text{Equation 8}$$

or

$$\Delta t = \frac{D}{V_s V_L} \left(V_L^2 - V_s^2 \right)^{1/2} \quad \text{Equation 9}$$

For a given rod Δt is a constant, since the exact point at which reflection and conversion to the shear mode takes place has no appreciable effect on the total path length.

d. *Multiple simple reflections at the cylinder ends to give paths such as \overline{abab} , \overline{ababab} , etc.* This is a simple case of internal reverberation between the cylinder ends and requires no comment since it was discussed in a previous paragraph. (See under Elastic Wave Propagation Between Parallel Boundaries of a Solid.)

e. *Any combination of the paths mentioned above.*

Measurement of Wave Velocities in Cylindrical Rods

The pulses arriving at the receiver end of the rod previously described may be amplified electrically and presented on an oscilloscope as functions of time. The relative times of arrival of various received pulses may be measured with the appropriate electronic equipment, and wave velocities can be computed from these time data and from the rod dimensions if the pulses can properly be identified as to their path type. Due to the unlimited number of paths where-

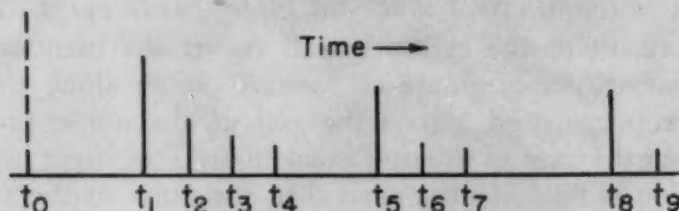


Fig. 4—Chronological Presentation of Received Pulses.

by a pulse may be propagated through a cylindrical rod, a single pulse applied to the transmitter end of such a rod could, in principle, give rise to an infinity of received pulses. Fortunately, the number of received pulses is limited due to absorption and scattering, and, therefore, the number of received pulses to be identified is reasonable.

The times of arrival of typical received pulses resulting from a single pulse are presented on a linear scale in Fig. 4 where the lines which represent pulse arrivals are designated in chronological order as t_0 , t_1 , t_2 , t_3 , etc. The time of the application of the pulse to the transmitter end of the rod is represented on the scale at t_0 , although in practice a pulse corresponding to this time rarely appears on the oscilloscope, and t_0 is not measured directly. Time t_1 is that of a pulse arriving by the direct path corresponding to \overline{ab} shown in Fig. 3. Time t_2 corresponds to arrival by path \overline{fghi} ; t_3 to arrival by a path in which two conversions to the shear mode take place along the way; t_4 to arrival by a path involving three such conversions; t_5 to arrival by path \overline{abab} shown in Fig. 2; and t_8 to arrival by the path \overline{ababab} . A brief study of Figs. 3 and 4 shows that if the rod length is L and the longitudinal wave velocity is V_L , the time of arrival of any pulse at the receiver end of the rod is given by

$$t_1 = t_0 + (2n_1 + 1) \frac{L}{V_L} + m_1 \Delta t \quad \text{Equation 10}$$

in which Δt is defined by Equation 9 and in Fig. 4 has the values $(t_2 - t_1)$, $(t_3 - t_2)$, $(t_4 - t_3)$, $(t_6 - t_5)$, $(t_9 - t_8)$, etc., and m_1 and n_1 are integers or zero.

It is evident from the above that for a cylindrical rod a single experiment can give sufficient data to permit the computation of both

V_L and V_s . In terms of rod diameter D and the delay time Δt , V_s is computed simply:

$$V_s = \frac{V_L}{\sqrt{1 + \left(\frac{V_L \cdot \Delta t}{D}\right)^2}} \quad \text{Equation 11}$$

The longitudinal wave velocity V_L may be determined from Equation 10 after eliminating t_0 in either of two ways: by measuring t_1 as a function of L for $m_1 = 0$ and $n_1 = 0$, or by measuring t_1 as a function of n_1 at constant L and $m_1 = 0$.

Although the method outlined above is very convenient for wave velocity determinations in the case of cylindrical specimens, it is apparent that wave velocity determinations can be made on any specimen of reasonable size which has two opposite surfaces accurately plane and parallel. If the longitudinal wave velocity is sought, transducers generating or receiving longitudinal waves are used; if the shear wave velocity is sought, transducers generating or receiving shear waves are used. Care must be taken that the shear transducers are attached to the specimen with their vibration axes parallel. In either case the wave velocity sought is computed from the simple time-of-arrival formula

$$t_1 = t_0 + (2n_1 + 1) \frac{L}{V} \quad \text{Equation 12}$$

in which V is the appropriate wave velocity, and the other quantities are the same as in Equation 10.

Given the density of a solid and the velocities of waves in the solid, the elastic constants of the solid are computed as follows:*

$$\text{Shear modulus: } \mu = V_s^2 \rho \quad \text{Equation 13}$$

$$\text{Poisson's ratio: } \sigma = \frac{1 - 1/2 \left(\frac{V_L}{V_s}\right)^2}{1 - \left(\frac{V_L}{V_s}\right)^2} \quad \text{Equation 14}$$

$$\text{Young's modulus: } Y = 2V_s^2 \rho \left[1 + \frac{1 - 1/2 \left(\frac{V_L}{V_s}\right)^2}{1 - \left(\frac{V_L}{V_s}\right)^2} \right] \quad \text{Equation 15}$$

Apparatus and Experimental Technique

The ultrasonic pulse apparatus is shown schematically in Fig. 5. In the present work the transmitter crystal was excited either with an R. F. pulse from a pulse generator similar to that described by Beers and Durand (3), or with a rectangular pulse from a Hewlett-Packard Model 212A pulse generator. The signal from the receiver

*For an isotropic solid $Y = 2\mu(1 + \sigma)$. Using this relation, Equations 13, 14 and 15 follow directly from Equations 1 and 2.

crystal was fed directly into a preamplifier of the Jordan and Bell type (4). The output from this preamplifier was rectified, amplified by a video amplifier of approximately 100-db gain, and fed into the oscilloscope. A Du Mont Model 256-D oscilloscope was used to observe and time the received pulses and to trigger the pulse generator. The variable calibrated sweep delays of this oscilloscope permit time measurements to be made with an error of not more than $0.1 \mu \text{ sec}$ under ideal conditions.

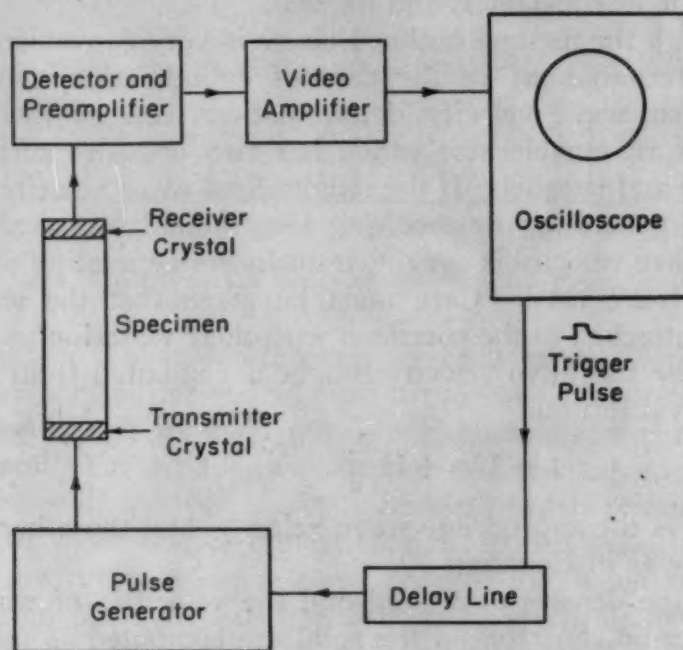


Fig. 5—Ultrasonic Pulse Apparatus for Elastic Wave Velocity Measurements.

The physical arrangement of the specimen holder and the accompanying preamplifier is shown in Fig. 6. Electrical contact with the crystals was made by means of small strips of bronze spring stock. The block holding the transmitter crystal contact and the V-block holding the specimen were movable so that specimens of different size could be accommodated.

For the generation of longitudinal wave pulses either barium titanate or X-cut quartz crystals were used. Barium titanate crystals were found to be more effective than quartz as transmitters, since they can be connected directly to the coaxial cable from the output of a pulse generator with less impedance mismatch than is the case for quartz. They were inferior to quartz as receivers, however, due to the high input impedance of the preamplifier. Longitudinal wave transducers, whether quartz or barium titanate, were coupled to specimens by means of a thin film of light oil.

Shear wave pulses were generated and received by means of AC-

cut quartz crystals. These crystals were attached to specimens by a thin film of salol, care being taken to keep the X-axes of the two crystals parallel.

All the crystal transducers, as furnished by the manufacturers, were silvered on both sides in order to eliminate the need for separate electrodes. Crystals with resonant frequencies of 1, 2, 5, and 10 mc/sec were available; the pulse vibration frequency which was used depended upon the specimen size, absorption, etc.

The time zero, t_0 , was found to be reasonably constant on the oscilloscope delay scale for any given pair of transmitter and receiver

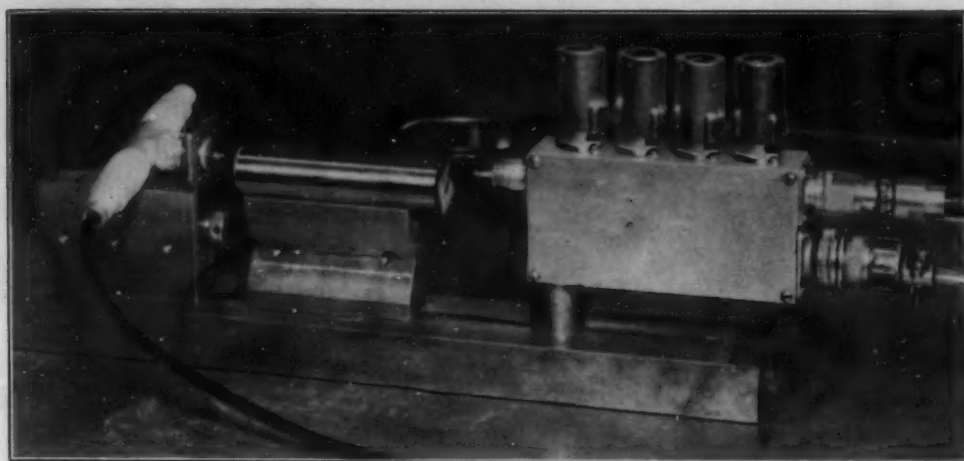


Fig. 6—Specimen Holder and Preamplifier, Showing a Specimen and Piezoelectric Crystals in Place.

crystals, but it was dependent upon crystal thickness and also area to a slight extent. This zero was determined for each series of measurements either by measuring t_1 (see Fig. 4) for a standard rod or by measuring t_1 for two or more rods of identical diameter and material but of different lengths. The values obtained were fitted to the equation

$$t_1 = t_0 + aL$$

Equation 16

by the least square or an equivalent method.

In order to check the technique of determining both wave velocities by the use of longitudinal pulses only, a number of brass cylinders were prepared from the same piece of stock. All the cylinders of one series had the same diameter but different lengths, while all the cylinders of the other series had the same length but different diameters. Measurements were made using crystals having 1, 2, and 5 mc/sec resonant frequencies which were excited in each case with pulses of the appropriate vibration frequency. At each frequency t_1 and t_2 first were measured for each of the rods of the same diameter. Then t_0 and a of Equation 16 were determined by the least square method. Having determined t_0 , t_1 and t_2 were measured for each of the speci-

mens of the same length but different diameters. The results of these wave velocity measurements are given in Table I.

Table I
Elastic Wave Velocities in Brass Rod

Rod Diameter	Frequency	$V_L \times 10^{-5}$	$V_s \times 10^{-5}$	$\frac{\lambda}{D}$
1 in.	1 mc	4.26 ₁ cm/sec	1.98 ₃ cm/sec	0.17
1	2	4.28 ₈	2.01 ₈	0.08
1	5	4.28 ₃	2.01 ₀	0.03
0.75	1	4.29	0.22
0.75	2	4.30	0.11
0.75	5	4.29	0.04
0.5	1	4.05	0.34
0.5	2	4.31	0.17
0.5	5	4.31	0.07
0.375	1	*3.10	0.45
0.375	2	4.22	0.22
0.375	5	4.25	0.09
0.25	1	*2.05	0.67
0.25	2	4.03	0.33
0.25	5	0.13

As the rod diameter decreased, the sharpness of received pulses decreased until resolution finally became so poor that the measurements were meaningless. The starred values of V_L are questionable in view of the fact that the thin rod velocity for brass is 3.22×10^5 cm/sec. The ratio of wave length (longitudinal wave) to rod diameter is tabulated for comparison purposes, since velocity should depend upon this ratio rather than either diameter or wave length alone. The table shows that for values of λ/D greater than approximately 0.2 the wave velocity tends to decrease, but that the longitudinal wave velocities measured under conditions where $\lambda/D < 0.2$ either are equal to true bulk velocities or are in error by a very small amount.

The time delay, Δt , due to mode-conversion reflections in the 1-inch diameter rods, was determined for each of the three frequencies. The shear wave velocities computed from these values are in close agreement.

To illustrate the method for the computation of both wave velocities from the results of a single set of measurements, data for a series of Type 347 stainless steel rods are given in Table II. The rod diameter was 2.49₄ cm. and the pulse vibration frequency was 5 mc/sec.

The values of t_1 and rod length L in the above table were used to compute t_0 and a in Equation 16 by the least square method. Using the value obtained for t_0 , V_L was computed for each rod. The average value for V_L was computed from the least square value of a , since

$$\frac{1}{a} = V_L \quad \text{Equation 17}$$

The average value of Δt was found to be 6.79₂ μ sec for this

Table II
Wave Velocity Data, Stainless Steel Rods

Rod Length	t_0	t_1	t_2	Δt	$V_L^* \times 10^{-5}$
4.600 cm	22.41 μ sec	30.42 μ sec	37.19 μ sec	6.77 μ sec	5.74 ₃ cm/sec
6.194	22.41	33.19	39.98	6.79	5.74 ₆
9.244	22.41	38.50	45.28	6.78	5.73 ₆
12.856	22.41	44.82	51.62	6.80	5.73 ₇
16.87	22.41	51.78	58.60	6.82	5.74 ₄

*Computed values.

$1/a = 5.741 \times 10^5$
 $t_0 = 22.41 \mu \text{ sec}$ } Least square values

series of measurements. From this value, and from the value 2.49₄ centimeters for D , V_s was computed from Equation 11 and found to be $3.09_2 \times 10^5$ cm/sec.

The oscilloscope presentation of pulses transmitted through one

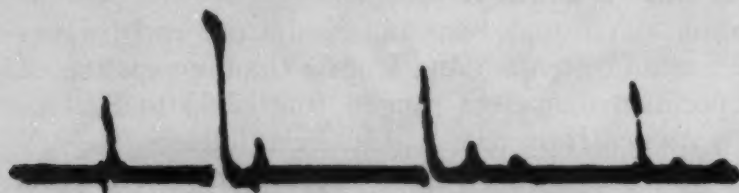


Fig. 7—Oscilloscope Presentation of Pulses Transmitted Through a Cylindrical Rod of Stainless Steel.

of the stainless steel cylinders is shown in Fig. 7. The individual pulses may be identified by reference to Fig. 4. A pulse corresponding roughly to t_0 appears in this case because of electrostatic leakage between the contact springs of the two crystals.

MATERIALS

Propagation velocities for both longitudinal and shear waves were measured in the following polycrystalline metals:

Brass. A series of seven rods ranging from 4.87 to 9.54 centimeters in length was cut from a piece of alpha brass 1-inch diameter round stock. Four additional rods, 5.39 centimeters in length and ranging from 0.639 to 1.91 centimeters in diameter, also were cut from the same piece of stock. In each case the ends of the rod were faced off accurately perpendicular to the rod axis. The brass was found by chemical analysis to contain 1.5% lead and 39.0% zinc.

Beryllium. A piece of Brush BPQM beryllium in the form of a rectangular parallelepiped, 3.73 by 5.89 by 7.30 centimeters, was ground to secure accurately parallel faces. A similar parallelepiped of extruded beryllium was available as well as a specimen of hot-pressed material prepared in this laboratory.

Columbium. Four pieces were cut from a piece of $\frac{1}{2}$ -inch diameter Fansteel columbium rod. After vacuum annealing these pieces for one hour at 1050 °C (1920 °F), ends were ground so that they would

be perpendicular to the cylinder axes. Lengths of the rods ranged from 3.03 to 13.74 centimeters.

Zirconium. Three cylinders were cut from a piece of 1.507-centimeter diameter rod of Bureau of Mines zirconium. This rod was vacuum-annealed for one hour at 800 °C (1470 °F) before machining off the ends of the cylinders. The lengths of the cylinders ranged from 5.52 to 11.27 centimeters. Wave velocities also were measured in a cylinder of crystal bar metal 1.25 centimeters diameter by 10.42 centimeters long.

Thorium. A cylinder, 8.786 centimeters long by 10.20 centimeters diameter, was machined from a piece of thorium obtained from the Ames Laboratory.

Vanadium. A cylinder, 4.84 centimeters long by 0.914 centimeter diameter, was machined from a piece of ductile vanadium prepared at this Laboratory.

Titanium. A sample was obtained from each of two heats of Allegheny Ludlum titanium and from a titanium casting of unknown origin. Specimen diameters ranged from 2.53 to 8.54 centimeters, and lengths ranged from 3.08 to 11.02 centimeters.

Uranium. A number of cubes, approximately 3 centimeters per side, were cut from uranium metal. Anisotropy resulting from fabrication was destroyed by heat treatment.

Stainless Steel. A piece of Type 347 stainless steel round was annealed at 1070 °C (1960 °F), followed by a water quench. The rod then was centerless ground to 2.49 centimeters diameter and cut into cylinders ranging in length from 4.60 to 16.87 centimeters.

RESULTS

The results of wave velocity measurements are listed in Table III which also includes the computed elastic constants. Where more than one specimen was measured, the velocities given are mean velocities. The densities given are measured values except in the cases of uranium and thorium where literature values are used. The quantities tabulated are the following:

V_L	Longitudinal wave velocity in cm/sec
V_s	Shear wave velocity in cm/sec
σ	Poisson's ratio
ρ	Density in grams/cm ³
μ	Shear modulus in dynes/cm ²
Y	Young's modulus in dynes/cm ²
f	Wave vibration frequency in megacycles/sec

The elastic constants given in Table III are estimated to be in error by not more than $\pm 1\%$ except in the cases of columbium, titanium, and vanadium. For these three, the error may be as high as 3 or 4% due to variations among individual specimens for columbium and titanium and to the small cross section of the one available vanadium specimen.

The values obtained for the elastic constants were converted into English units and in Table IV are compared with the values obtained by other workers. Sufficient information is not available to justify detailed comment in the case of most of the metals listed, but it is

Table III
Elastic Wave Velocities and Elastic Constants for Some Metals*

Metal	$V_L \times 10^{-5}$	$V_s \times 10^{-5}$	σ	ρ	$\mu \times 10^{-11}$	$Y \times 10^{-11}$	f
Alpha Brass	4.28	2.02	0.36	8.45	3.45	9.35	5
Beryllium	12.89	8.88	0.05	1.87	14.7	30.9	10
Zirconium:							
Bu. Mines	4.62	2.34	0.33	6.57	3.61	9.57	5
Crystal bar	4.65	2.25	0.35	6.48	3.28	8.84	5, 10
Columbium	4.92	2.10	0.38	8.56	3.75	10.4	5
Titanium	5.99	2.96	0.34	4.54	3.98	10.6	2
Uranium	3.37	1.94	0.25	18.6	7.03	17.6	2
Thorium	2.94	1.56	0.30	11.5	2.80	7.28	1, 2
347 Stainless Steel	5.74 ₀	3.09 ₂	0.30	7.91	7.57	19.6	5
Vanadium	6.00	2.78	0.36	6.03	4.66	12.7	10

*All quantities given in cgs units.

1 dyne/cm² = 1.4504×10^{-5} psi

evident that the elastic constants obtained by the ultrasonic pulse technique generally are lower than those obtained by the conventional tensile test methods. The reason for this is not clear, since the essentially adiabatic values obtained by the ultrasonic pulse method should be greater than those obtained under the more nearly isothermal conditions of the conventional test. It should be noted that there is close agreement between the values obtained for beryllium here and those obtained by Gold (6) who also used the ultrasonic pulse technique.

Schwope and co-workers (7) have measured the Young's modulus of sheet Bureau of Mines zirconium as a function of direction relative to the rolling direction. They obtained the value 13.9×10^6 psi for the modulus parallel to the rolling direction which was in agreement with the value computed in this report from wave velocities in the axial direction in rod specimens of this material. These rods have not been examined for evidence of rolling texture, but there is little doubt that they were not entirely isotropic. The crystal bar metal exhibited lower elastic moduli than the Bureau of Mines metal. Since texture information was not available for either metal, it is difficult to say whether the difference in moduli was due to texture difference or simply to difference in purity.

The values obtained for uranium in this work differ from those reported by Laquer (8), who used the vibrating-rod technique to determine wave velocities. This difference is not unexpected, since Laquer's uranium had not received special treatment to ensure random grain orientation. In the present work, longitudinal wave velocities were

Table IV
Comparison of Results of the Present Work With Literature Values

Metal	$Y \times 10^{-6}$	$\mu \times 10^{-6}$	σ	Source
Alpha Brass	13.6 psi 15	5.00 psi	0.36	Present work Metals Handbook (5)
Beryllium	44.8 43.0	21.3 21.2	0.05 0.01	Present work Gold (6)
Zirconium	12.8 - 13.9 13.6 - 14.2 11.35	4.76 - 5.24	0.33 - 0.35 0.32 - 0.35	Present work Schwope, Stockett (7) Metals Handbook
Columbium	15.1	5.44	0.38	Present work
Titanium	15.4 16.8	5.77	0.34	Present work Metals Handbook
Uranium	25.5 29.8	10.2 12.1	0.25 0.23	Present work Laquer (8)
Thorium	10.6	4.06	0.30	Present work
347 Stainless Steel	28.4 28	11.0	0.30	Present work Metals Handbook
Vanadium	18.4 21.0 - 22.5	6.76	0.36	Present work Kinzel (9)

measured in three mutually perpendicular directions in each of more than a dozen different specimens of uranium, some of which were in the as-worked condition. Although these specimens differed markedly in their degree of anisotropy, the geometric mean of the longitudinal wave velocities in the three directions for any given specimen was never found to deviate from the value of 3.37×10^5 cm/sec by as much as 1%. Specimens were selected for shear wave velocity measurements only after isotropy had been assured by longitudinal wave velocity measurements for each of the three directions.

SUMMARY

The principles of elastic wave propagation have been outlined with particular reference to the relation of the elastic wave velocities in an isotropic solid to the elastic moduli of that solid. The elastic pulse technique for wave velocity measurements has been described, including the technique outlined by Hughes for determining shear wave velocities in cylindrical rods using the same longitudinal wave-type crystal transducers as are used for the longitudinal wave velocity determination.

The utility as well as the limitations of the ultrasonic pulse technique for elastic constant determinations has been demonstrated by measurements on two well-known metals: alpha brass and stainless steel. The technique has been applied to the determination of both elastic moduli and the Poisson ratio of each of a number of less common metals: columbium, titanium, thorium, and vanadium. In addition, the elastic moduli and Poisson ratio of beryllium, uranium, and zirconium have been redetermined. The results of these measurements have been tabulated and are briefly discussed.

References

1. J. Prescott, "Elastic Waves and Vibrations of Thin Rods", *Philosophical Magazine*, Vol. 33, 1942, p. 703-754.
2. D. S. Hughes, W. L. Pondrom and R. L. Mims, "Transmission of Elastic Pulses in Metal Rods", *Physical Review*, Vol. 75, 1949, p. 1552-1556.
3. *MIT Radiation Laboratory Series*, Vol. 18 (Vacuum Tube Amplifiers). McGraw-Hill Book Co., Inc., New York City, p. 306-313.
4. W. H. Jordan and P. R. Bell, "A General Purpose Linear Amplifier", *Review of Scientific Instruments*, Vol. 18, 1947, p. 703-705.
5. METALS HANDBOOK, American Society for Metals, Cleveland, 1948.
6. L. Gold, "Evaluation of the Stiffness Coefficients for Beryllium From Ultrasonic Measurements in Polycrystalline and Single Crystal Specimens", Report AECD-2644, United States Atomic Energy Commission, Technical Information Division, Oak Ridge, Tenn., 1949.
7. A. D. Schwoppe and S. J. Stockett, "Directional Tensile Properties of Sheet Zirconium", Report BMI-T-32, Battelle Memorial Institute, Columbus, Ohio, 1950.
8. H. L. Laquer, "Elastic Constants and Sound Velocities; III. The Elastic Constants of Uranium", Report AECD-2606, United States Atomic Energy Commission, Technical Information Division, Oak Ridge, Tenn., 1949.
9. A. B. Kinzel, "Properties of Vanadium Metal", *METAL PROGRESS*, Vol. 58, 1950, p. 344-B.

DISCUSSION

Written Discussion: By Darrell S. Hughes, professor of physics, The University of Texas, Austin, Texas.

Ultrasonic pulse methods offer a quick and accurate method of determining elastic constants. For isotropic materials, the method of utilizing the dilatational-rotational conversion to derive the longitudinal and rotational velocities from a single experimental setup is particularly convenient, as driver and detector need be coupled only for dilatational energy transmission to the sample. This is so much simpler than shear coupling that a considerable saving is effected.

In work with separate driver and detector crystals, we have found a modulated pulse to offer no detectable advantage and indeed to entail some disadvantages. If a single crystal is used as driver and detector, the modulated pulse is apparently highly advantageous. The velocity is computed from the time of arrival of the pulse. The precise time that will be read depends upon the amplifications, the judgment of the observer, and various other factors. It can usually be safely assumed that the arrival is read late, i.e. the computed velocities are low. Actually, if wide-band amplifiers are used and care taken in the readings, this error can be made very small, of the order of 0.03μ seconds. A very sharp rising pulse is desirable. We use a rise time of about 0.05μ seconds. The measurements can be repeated with high precision. Thus our measurements on brass agree precisely with the value of V_L of Table III and are less than 0.5% different for V_s .

There is of course some question of whether the simple geometrical theory outlined on the fourth and fifth pages is adequate. Dr. W. L. Pondrom in some unpublished work* has investigated rigorously the propa-

*Propagation of Elastic Pulses in Rocks, W. L. Pondrom, Technical Report No. 7, N6onr-266 T. O. VII.

gation of pulses in cylindrical rods and flat plates. This investigation showed that energy is transmitted by the paths shown in Fig. 3. Actually, the line **fg** should be drawn along the boundary. These arrivals are observed because all possible paths of this type have the same transmission time. Paths such as **cde** have varying transmission times and hence show no detectable first arrival. We have measured the shear velocity in fused quartz both by this method and by means of Y-cut crystals and found the two methods to agree within about 0.05%.

A more serious error can perhaps arise from the fact that inevitably the measured velocity is the velocity of high frequency waves of an unknown frequency and band width. The possibility of the velocity and particularly the shear velocity being a function of frequency cannot a priori be ruled out.

Thus in Table IV, Laquer's and Reynolds' values for uranium differ by about 17%. If Reynolds' shear velocity is about 8% high, this discrepancy would disappear. Assuming that uranium may display anelasticity as formulated by Zener, a strain relaxation time of about 0.06μ seconds with an assumed signal frequency of 2 mc. would give just this change in shear velocity. A method of determining the velocity of waves of definite frequency is certainly desirable, but appears to be unobtainable at the present time.

On the other hand, the resonant frequency of a bar is a complex function of the rod shape, dimension, and elastic constants. It is difficult to allot an error to measurements made by this method, but 8% seems excessive. Until the same sample of uranium can be measured by both methods, it is probably useless to undertake an elaborate explanation of the discrepancy.

Probably a check with published values should not in general be expected. First, it is difficult to be certain that the materials are the same. Second, different methods will almost certainly give somewhat different results. In the usual static testing machine it is doubtful that sufficient time for temperature equilibrium is allowed. Static testing usually involves rather large deformations, and strain hardening may ensue. The past history of the material also may have a decided effect. Thus we have found that in hardened 4340 steel the elastic constants increase by 3% as the drawing temperature is raised from 300 to 1200 °F.

Apparently unexplainable discrepancies remain. Our measurement of the adiabatic constants of Armco iron is about 3% low compared to Bridgman's isothermal values. We have measured the isothermal moduli of fused quartz and Carboloy and the adiabatic moduli by pulse methods. For these materials, the adiabatic values appear some 1 to 2% too high.

Written Discussion: By Henry L. Laquer, staff member, University of California, Los Alamos Scientific Laboratory, Los Alamos, N. M.

Dr. Reynolds has reported an interesting set of measurements of the sound velocities and elastic constants for some of the metals which are of special interest to the atomic energy program. He has used the ultrasonic pulse technique which by now is well known but certainly not standardized in detail, i.e., different laboratories use quite different mechanical and electronic assemblies to achieve the same results.

We have made similar and as yet unpublished measurements at Los

Alamos using both the previously described resonance or vibrating rod technique,² operating at frequencies between 5 and 150 Kc, and a modification of the ultrasonic pulse technique, operating at frequencies between 0.5 and 5 Mc. In the pulse technique work, we have used only quartz crystals. We have also used Y-cut shear crystals for the direct determination of V_s , rather than relying on the conversion to the shear mode which dispenses with the shear crystals and the difficulties involved in attaching them to the specimen but which does require that all sample surfaces be machined accurately and smoothly. Another difference in techniques is that, since we do not "detect" the signal, we observe the individual cycles in each pulse rather than the pulse envelope. This avoids some of the difficulties sometimes encountered in locating the "foot" of the echo, and it certainly simplifies the differential measurements which are involved in the determination of the pressure and temperature coefficients of the velocities.

The directly determined experimental quantities are frequencies with the resonance technique and times with the pulse technique. With a knowledge of the length of the specimen one then readily calculates the velocities V_o and V_s , in the former case, and V_L and V_s in the latter. The moduli are derived quantities in any dynamic measurement and involve the square of the velocities and the densities. For this reason we prefer to make all comparisons in terms of the velocities rather than of the moduli, a presentation which also, incidentally, halves the percentage discrepancies.

Table V lists our measurements on single samples of miscellaneous materials together with the results of Reynolds and of other workers. Quantities in brackets represent derived values, and measurements indicated as made at "low" frequency were made with the resonance technique. None of our samples received any special heat treatments. Our work does by no means represent a complete study but was done in a rather haphazard manner, usually at the request of other people from our laboratory. The only reason for presenting the data is to show that they are in general agreement with those of the other workers.

Our beryllium sample was a disk pressed from powder and had a density of only 1.59, or 85% of that of Reynolds. Unpublished work on other powder compacts of less than theoretical density has indicated that there is an approximate proportionality between V_L and ρ , so that one might expect velocities about 15% below those for the full density material.

Our first zirconium sample was swaged Bureau of Mines material, and the agreement is excellent. Our second sample was a very coarse-grained Foote Mineral Company crystal bar which had been machined into a cylinder. This material appeared to have pronounced directional properties and was investigated for that very reason. The measured shear velocity, V_s , is 2% above that of Reynolds but about 3.5% below the value for the swaged material. The rod velocity, V_o , is 5% higher than that calculated from Reynolds' data; on the other hand, it is within 1% of the value calculated for the swaged material. Finally, the longitudinal wave velocity, V_L , derived in this case, since the measurements were made by the resonance technique, is very high and obviously incorrect, whereas Reynolds' directly measured V_L is in very close agreement with the results on the

²H. L. Laquer, W. E. McGee and M. F. Kilpatrick, "The Elastic Constants of Uranium", *TRANSACTIONS, American Society for Metals*, Vol. 42, 1950, p. 771.

Bureau of Mines samples. This shows that with anisotropic materials relatively small differences in the measured quantities can lead to large discrepancies in the derived quantities.

Our titanium sample was a 10-pound Du Pont ingot and did not transmit sound equally well at different points, indicating some porosity or blow-holes. Nevertheless, the agreement is quite close for V_L ; however, our V_s is 7% high. Fufeld* used the resonance technique on commercial rods which he subjected to a 66% reduction in area and then annealed.

Our molybdenum sample was taken from stock and is probably Fan-steel rod. It had a density of 9.96 ± 0.04 gms/cc, or about 98% of the X-ray value.

The results compared in Table V thus indicate that whenever there is no question as to preferred orientation or soundness of material, different observers using different techniques at different frequencies readily agree on sound velocities within 2% and hence should agree in the elastic moduli to within 4 or 5%. This general agreement then excludes appreciable systematic errors and makes the pronounced disagreement in the case of uranium most disturbing. In Table VI we have compared Reynolds' uranium data with our previous averages² and have added some recent results on samples of different thermal and mechanical treatment. On the basis of the information available to Reynolds at the time his report was written, one could have suggested at least three possible explanations for the 5 to 8% discrepancies between the velocities shown in the first two lines of Table VI. We shall now discuss the following three possibilities:

- (a) a frequency dispersion of the velocities,
- (b) preferred orientation in our samples,
- (c) different materials, due to the very different heat treatments employed.

A variation of the velocity of sound in any metallic material as a function of the frequency has, to the best of my knowledge, not been reported for the frequency range of 1 Kc to 10 Mc. The pulse technique measurements on the as-cast specimen No. 6a indicate that the measured V_L agrees with our previously calculated value. On the other hand, we did not succeed in transmitting shear waves through this or any other sample of coarse-grained uranium. However, the pulse technique results obtained with two samples containing sufficient impurities to obstruct grain growth (Nos. 63, 64) fall between our previous data and those of Reynolds. After one makes a correction for the slight density difference, the velocities in these "impure" samples are less than our previous averages by 2%, which is not much more than the combined experimental errors. However, the fact that the shear velocity measured by the pulse technique on these samples is less than our previous average by only 3% makes most unlikely the explanation that the 8% discrepancy with Reynolds' data is caused by frequency dispersion.

The second possible explanation of the discrepancies and the one suggested by Reynolds is that our previous samples might have had appreciable preferred orientation. Now it is true that uranium is notoriously prone to the development of directional properties and that the resonance technique does not permit the detection and elimination of these directional

*See footnote 5 in Table V.

Table V

	Fre- quency (Mc)	V_L (cm/sec) $\times 10^5$	Diff.	V_s (cm/sec) $\times 10^5$	Diff.	V_o (cm/sec) $\times 10^5$	Diff.	σ
<i>Beryllium:</i>								
REV	10	12.89 ± 0.06	8.88 ± 0.04	(12.86)	0.05
Gold ³	10	12.65	- 2%	8.88	0%	(12.65)	- 2%	0.01 ₁
Overton ⁴	10	12.55 ± 0.02	- 3%	8.83 ± 0.03	-0.6%	(12.55)	- 2%	0.01 ₁
LA	2 1/4, 5	11.57 ± 0.03	-10%	7.74 ± 0.04	-13%	(11.45)	-11%	0.09 ₁
<i>Zirconium, Bureau of Mines:</i>								
REV	5	4.62 ± 0.02	2.34 ± 0.01	(3.82)	0.33
LA	2 1/4, 5	4.69 ± 0.01	+1.5%	2.36 ± 0.01	+1%	(3.84)	+0.5%	0.33
<i>Zirconium, Crystal Bar:</i>								
REV	5, 10	4.65 ± 0.02	2.25 ± 0.01	(3.69)	0.35
LA	Low (6.14)		+32%	2.29	+2%	3.86	+5%	0.42
<i>Titanium:</i>								
REV	2	5.99 ± 0.12	2.96 ± 0.06	(4.85)	0.34
Fusfeld ⁵	Low	4.97 ± 0.01	+2%
LA	1, 2 1/4, 5	6.02 ± 0.03	$\pm 0.5\%$	3.17 ± 0.01	+7%	(5.13)	+6%	0.31
<i>Molybdenum:</i>								
LA	2 1/4	6.37 ± 0.02	3.41 ± 0.06	(5.50)	0.30

³Louis Gold, "Evaluation of the Stiffness Coefficients for Beryllium From Ultrasonic Measurements in Polycrystalline and Single Crystal Specimens", *Physical Review*, Ser. 2, Vol. 77, 1950, p. 390.

⁴W. C. Overton, Jr., "Ultrasonic Measurements in Metallic Beryllium at Low Temperatures", *Journal of Chemical Physics*, Vol. 18, 1950, p. 113.

⁵H. I. Fusfeld and J. T. Gilbert, "Some Physical Properties of Titanium", *Physical Review*, Ser. 2, Vol. 77, 1950, p. 302.

properties in as elegant a way as Reynolds did with his measurements along the three perpendicular directions of his cubes. (By the way, it would be interesting to see the three different values whose geometric mean is 3.37, say for the best and worst sample.) Our approach then was to eliminate or at least minimize orientation effects by studying samples of different thermal and mechanical history. The previously studied samples had been swaged and annealed, γ -extruded, and as-cast. Of the new samples No. 6a was cast and then furnace-cooled. Sample No. 9 was cast by induction heating into a 1-inch diameter crucible and cooled much more rapidly. Samples Nos. 21 and 23 were hot drawn and then annealed. All these samples, with the exception of No. 23, gave results in substantial agreement with our previous data, and it would appear most unlikely that all these samples should be subject to the same kind of preferred orientation. Another check on whether any sample has preferred orientation can be had by comparing Poisson's ratio, σ , as calculated from two of the velocities and also σ_{Dip} as obtained from the velocity dispersion for higher harmonic resonances.² Thus the cold-swaged and only slightly annealed samples Nos. 22 and 24 show exactly this kind of anisotropy, and it is interesting to note that their V_o values are within a per cent of the value calculated from Reynolds' data, but the V_s values are higher by 9%. Thus we have shown that one can produce one kind of preferred orientation which does make V_s too large in terms of Reynolds' results, but at the same time introduces an effect opposite to the observed one in V_o , and also an abnormal σ value, which did not occur in our earlier work.

We are then left with the last possibility, namely, that there were inherent structural differences in the samples studied. This explanation does appear rather far-fetched at first glance, and I certainly do not know of any other material in which heat treatment can produce such large effects

Table VI

	ρ gms/cc	Fre- quency Mc	V_L (cm/sec) $\times 10^5$	Diff.	V_s (cm/sec) $\times 10^5$	Diff.	V_o (cm/sec) $\times 10^5$	Diff.	σ	σ_{Dip}
Reynolds, Special Heat Treatment Previous Average (Swaged Annealed 4 Hours at 600°C), γ -Extruded, Cast)	18.6 (?)	2	3.37 \pm 0.02	1.94 \pm 0.01	(3.07 \pm 0.02)	0.25
No. 6a, As Cast, Furnace-Cooled	18.96 \pm 0.03	Low	(3.54 \pm 0.07)	+5 \pm 3%	2.09 \pm 0.01	+8 \pm 1%	3.29 \pm 0.04	+7 \pm 2%	0.23 \pm 0.02
No. 9, As Cast, Crucible-Cooled	1, 2 $\frac{1}{4}$, 5	3.52 \pm 0.04	+4 \pm 2%	No. Transm.
No. 16', Water-Quenched from 725°C	Low	3.25 \pm 0.00 ₄	+6 \pm 1%	0.21 \pm 0.02
No. 21, Hot Drawn (500°C), Annealed ($\frac{1}{2}$ Hour at 550°C)	2 $\frac{1}{4}$	3.18 \pm 0.03	-5 \pm 2%	1.77 \pm 0.04	-9 \pm 2%	(2.83)	-8%	0.27 ₄
No. 23, Same as No. 21, Higher Purity Material	18.87 \pm 0.02	Low	(3.51)	+4%	2.06 ₄ \pm 0.00 ₁	+6 \pm 1%	3.24 ₇ \pm 0.00 ₄	+6 \pm 1%	0.23	0.20 \pm 0.01
No. 22, Hot Drawn (500°C), Cold- Swaged Annealed ($\frac{1}{2}$ Hour at 550°C)	18.99 \pm 0.01	Low	(3.25)	-4%	2.06 ₄ \pm 0.00 ₃	+6 \pm 1%	3.14 ₄ \pm 0.00 ₃	+3 \pm 1%	0.16	0.23 \pm 0.02
No. 24, Same as No. 22, Higher Purity Material	18.95 \pm 0.03	Low	(3.05)	-9%	2.12 ₁ \pm 0.00 ₁	+9 \pm 1%	3.05 ₄ \pm 0.00 ₁	-1 \pm 1%	0.03 ₄	0.23 \pm 0.01
No. 63, 64 "Impure" Fine-Grained Material, As Cast, Furnace-Cooled	18.99 \pm 0.01	Low	(3.12)	-7%	2.11 ₄ \pm 0.00 ₁	+9 \pm 1%	3.10 ₃ \pm 0.00 ₂	+1 \pm 1%	0.07 ₂	0.23 \pm 0.01
No. 64a, b, 65a, b, Ditto	18.8 \pm 0.1	2 $\frac{1}{4}$, 5	3.43 \pm 0.02	+2 \pm 1%	2.04 \pm 0.01	+5 \pm 1%	(3.20)	+4%	0.22
	18.85 \pm 0.05	Low	3.21 \pm 0.01	+5 \pm 1%	0.21 \pm 0.01	0.21 \pm 0.02

without being evident in the microstructure. It seems likely that Reynolds subjected his samples to a very drastic quench so as to secure random orientation. Our one water-quenched sample No. 16' gave values even lower than those of Reynolds, and appreciably so. How the quenched material differs from slowly-cooled annealed material I do not know. In quenching from the β -range, the transformation probably proceeds in a diffusionless martensitic fashion. Also, a rapid quench could produce microcracks. If the effect is real, then it might be possible to produce even larger differences by quenching thinner pieces.

We can only conclude that it is obviously difficult for different investigators to obtain concordant results on a metal as anisotropic and capricious as uranium, and that it will require further investigation before this specific problem can be solved.

Written Discussion: By Harry Majors, Jr., lead engineer, California Research and Development Co., Livermore, Calif.

Here is discussed a very timely paper on a convenient method which is of interest to all who make stress calculations, especially where thermal stresses are predominant. The ultrasonic pulse technique has many advantages.

The trend in engineering design is to calculate for elevated temperature conditions; hence, one would like the elastic constants as a function of temperature. What is the upper temperature limit at which the ultrasonic apparatus can be used? What modifications are needed to permit the determination of the elastic constants at various temperatures?

Table IV presents some results for the Poisson ratio of beryllium in which a value of 0.05 appears to be exceptionally low. Would the author comment whether or not a variation of Poisson's ratio was detected with the direction of working?

It would have been of great interest if the conventional, isothermal moduli were available for comparison with the adiabatic moduli of Table IV.

Further comments are made. First, a search was made for reported values of Poisson's ratio which are tabulated in Table VII.

Table VII
Poisson's Ratio of Materials That Rupture With a Brittle Fracture
at Room Temperature in a Uniaxial Stress Field

Material	Poisson's Ratio
Cast iron, no alloying element	0.211
Multicomponent glass, Type 496/644	0.197
Multicomponent glass, Type 506/602	0.221
Thermometer glass, 16III	0.228
Range of values for other types of multicomponent glass	0.197 to 0.319

Even though glass and cast iron are considered brittle generally, the discussor cannot say that they are anisotropic.

Secondly, Table VIII was produced from Equation 18.

$$\mu = \left[\frac{E}{2G} - 1 \right] \quad \text{Equation 18}$$

This equation is derived from well-known relationships in the theory

of elasticity and is valid for these assumptions:

- (a) Material is homogeneous
- (b) Material is isotropic
- (c) Forces acting cause small deformations
- (d) No effect of past history
- (e) Laws of Newtonian Mechanics are valid

As indicated in Table VIII, small changes in ratio of E/G produce large changes in μ .

Beryllium is anisotropic, but Poisson's ratio was computed from an equation assuming isotropic conditions.

Maybe the low value recorded here is due to the fact that beryllium is not isotropic and that the equation used is very sensitive to small changes in the variables. On the other hand, when Poisson's ratio is reported for known brittle materials the values hover around 0.20.

Table VIII
Poisson's Ratio Versus the Ratio of E/G
(using Equation 1)

E/G	μ
2.0	0.00
2.1	0.05
2.2	0.10
2.3	0.15
2.5	0.25
2.7	0.35
3.0	0.50
E = modulus of elasticity in tension	
G = modulus of elasticity in torsion	
μ = Poisson's ratio	

Value of Poisson's ratio for cast iron was obtained from a Master of Science Thesis by R. W. Vose, Massachusetts Institute of Technology, 1936, while the values for glass were obtained from the International Critical Tables, Volume II, p. 93, Table II.

Author's Reply

The author wishes to express his thanks to the reviewers for the interest indicated by their comments.

Professor Hughes' comment concerning the geometry of Fig. 3 is indeed justified, although the author intended in the text to convey the fact that paths fg and hi were actually parallel to the cylinder wall.

The author has observed no dependence of wave velocity upon pulse vibration frequency which could not be attributed to variation in the ratio of wavelength to specimen cross section, although admittedly no detailed investigation of this phenomenon has been attempted.

The author has discussed the question of wave velocities in uranium with Dr. Laquer in person. It is quite possible that his explanation for the difference in our wave velocity values is correct. When time permits, this matter will be investigated in somewhat more detail, using new samples of uranium.

The low Poisson ratio for beryllium was a topic of considerable discussion when it was first brought to the attention of metallurgists at this

Laboratory several years ago. As Mr. Majors points out, the sensitivity of the Poisson ratio to variations in the ratio of the two elastic moduli makes a precise determination of this constant somewhat difficult. However, the Poisson ratio for beryllium turns out to be roughly an order of magnitude less than that for more common metals. An error of approximately 20% in the ratio of the two elastic moduli would be required to produce an order of magnitude error in the value of the Poisson ratio. Commercially available polycrystalline beryllium is indeed textured, but the author has found that the variation in wave velocity with direction in this material does not exceed a few per cent. This applies to both wave velocities and is based on measurement of both wave velocities in each of the three mutually perpendicular directions, in each of a number of beryllium specimens. Since the wave velocities reported are mean velocities, it would be rather difficult to explain the low value of the Poisson ratio for beryllium on the basis of experimental error in the wave velocity determinations. Also, a determination of the shear modulus of beryllium by the torsion pendulum technique gave a result in good agreement with that obtained by the ultrasonic pulse method. Consequently, there is good reason to believe that the Poisson ratio of beryllium is unusually low in value.

The temperature limitations of the ultrasonic pulse technique are determined by the properties of the piezoelectric transducers and of the coupling fluid or cement. Because of its rather low Curie temperature, barium titanate is useful only at temperatures below about 70 °C. Quartz, however, with a couplant such as solder, or a high melting point cement, may be used at temperatures up to within perhaps 100 °C of its alpha-beta transformation point (573 °C). The vibrating rod technique is probably much more suitable for high temperature measurements than is the ultrasonic pulse technique, particularly if the rod is driven by the electrostatic method.

Since the above paper was written, the elastic wave velocities in vanadium have been redetermined, using a larger (and purer) specimen of vanadium than was originally available. The elastic constants obtained from the new measurements differ from the previously determined values by less than 1%.

CONSUMABLE-ELECTRODE ARC MELTING OF ZIRCONIUM METAL

BY W. W. STEPHENS, H. L. GILBERT AND R. A. BEALL

Abstract

A production-model, consumable-electrode arc melting furnace for zirconium and its alloys has proved successful.

Contamination experienced in other methods of melting is avoided by using a pressed electrode of zirconium metal.

Metal recovery from 8-inch diameter, 200-pound rough ingots varies from 75 to 85%. Scalpings are re-used in later runs.

INTRODUCTION

AS A CONTINUATION of the zirconium-melting development work by the Bureau of Mines at Albany, Oregon, a production-model inert-atmosphere arc melting furnace has been developed in which consumable electrodes are employed to produce ingots of zirconium and its alloys.

Earlier work (1)¹ showed that consumable-electrode melting has advantages over tungsten-electrode (2, 3) or graphite-crucible melting (4, 5), in that no tungsten or carbon is picked up and the spattering commonly encountered when sponge is melted poses no problems.

The prototype furnace for consumable-electrode melting employed in this work utilized electrodes formed by hot forging and rolling iron-sheathed sponge briquettes (1). These electrodes were not only expensive to produce but, owing to their physical condition and shape, required a threaded electrical connection. An ingot was made up, using many electrodes, and cold shuts often occurred in the finished ingot at the locations where electrodes were changed. As the formed electrodes had an irregular cross section, they were not amenable to the system of feed rolls and sliding contacts employed by Parke and Ham (6) and later by Kessler and Hansen (7) in the experimental melting of molybdenum and alloys.

¹The figures appearing in parentheses pertain to the references appended to this paper.

A paper presented before the Eighth Western Metal Congress of the Society, held in Los Angeles, March 23 to 27, 1953. Of the authors, W. W. Stephens was formerly metallurgist, H. L. Gilbert is chemical engineer, and R. A. Beall is physicist, all of the Bureau of Mines, Albany, Ore. Manuscript received June 26, 1952.

EXPERIMENTS

The principal problem encountered in forming pressed or sintered bars of zirconium lay in the massive form of the sponge metal produced by the Kroll process. This sponge was hand-cut to pass 1-inch mesh size, and bars compacted from such lumps had poor cohesion.

Later, use of a large gyratory crusher made it possible to produce a fairly uniform material that would pass a $\frac{1}{4}$ -inch mesh size.

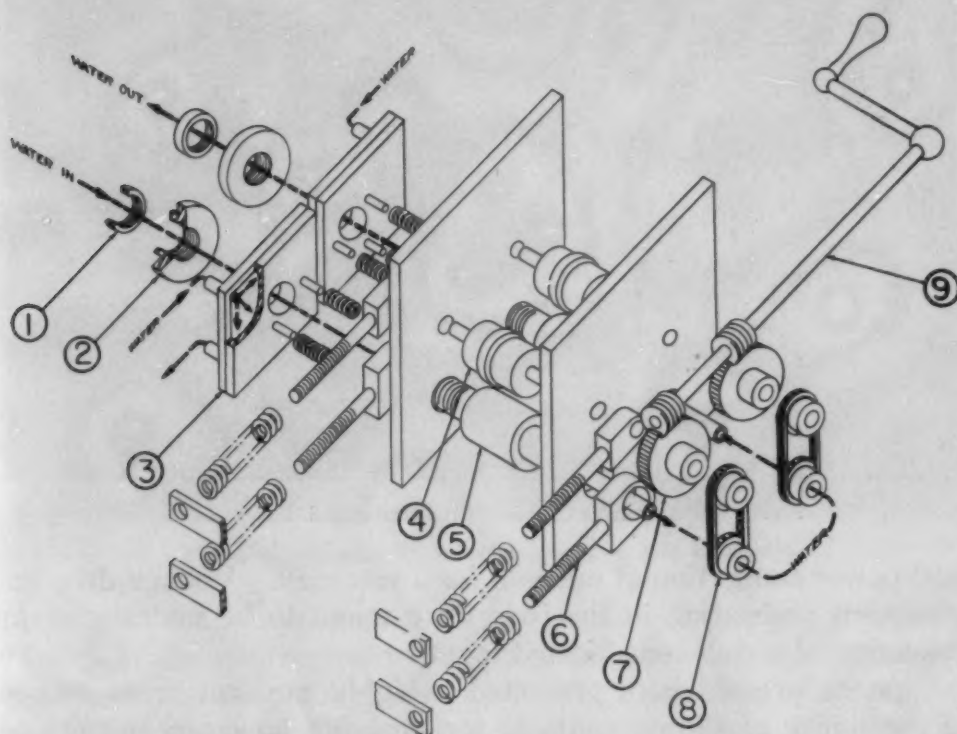


Fig. 1—Sketch of Power Application and Drive Rolls. 1) Lock nut for rotor, 2) Rotary contact, 3) Stationary contact, 4) Mechanical-drive roll, 5) Power-application roll, 6) Spring-loaded roll bearings, 7) Worm gears for feed rolls, 8) Interlock chains, 9) Drive crank.

It was found that 50 tons per square inch die pressure would consolidate such sponge into a usable electrode. Use was made of a dual-action powder metallurgy press at the Bureau of Mines Boulder City, Nevada, station to produce 2 by 2 by 20-inch electrodes. A lateral die-holding pressure of 1500 tons and a vertical-compaction pressure of 2000 tons were employed. Bars made by this method were strong and dense. Electrical resistivity of the pressed bars was found to vary from 125 to 155×10^{-6} ohms/cm./cm.²

When two bars were beveled slightly at the ends and joined by inert atmosphere tungsten-arc welding, the electrical resistivity of the joint section was found to be lower than that of an equivalent length of normal bar. Several bars were joined and provided with an elec-

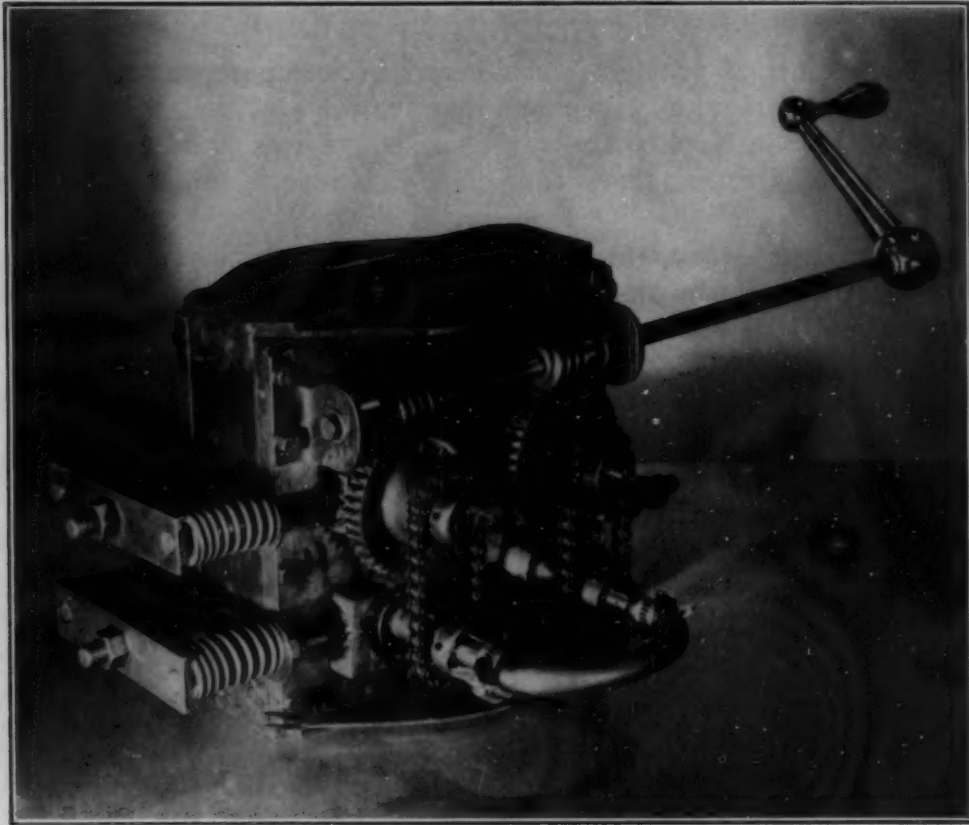


Fig. 2—Photograph of Power Application and Drive Rolls.

trical power connection at one end for a test melt. Voltage drop and subsequent preheating in the bars were found to be undesirable for production of a well-consolidated ingot.

As the pressed bars presented a highly uniform cross section, the possibility of sliding contacts for applying power near the pool level was considered, but abandoned in favor of water-cooled copper rollers that would have less tendency to seize or gall. A sketch of these power application and drive rolls and photographs of the assembly are shown in Figs. 1, 2, 3. As a practical limit to the length of prewelded electrodes was evident, the welding step was incorporated into the melting furnace. The general design of the furnace is shown in Fig. 4.

The supply of pressed electrodes, 1, is contained in the bar-joining tank, 2. Bars are entered in the guide, 3, and, by use of the view port, 4, and a pair of sealed-in rubber gloves, 5, the bars are joined by a small tungsten electrode powered through a separate direct-current circuit, 6. The drive box, 7, contains the drive rolls, 8, powered by a hand crank, 9. Power is applied by water-cooled cables and copper tube, 10, to the water-cooled copper power rolls, 11. Electrical insulation is provided by a phenolic resin washer, 12, vacuum-sealed by rubber "O" rings, as are all other joints in the

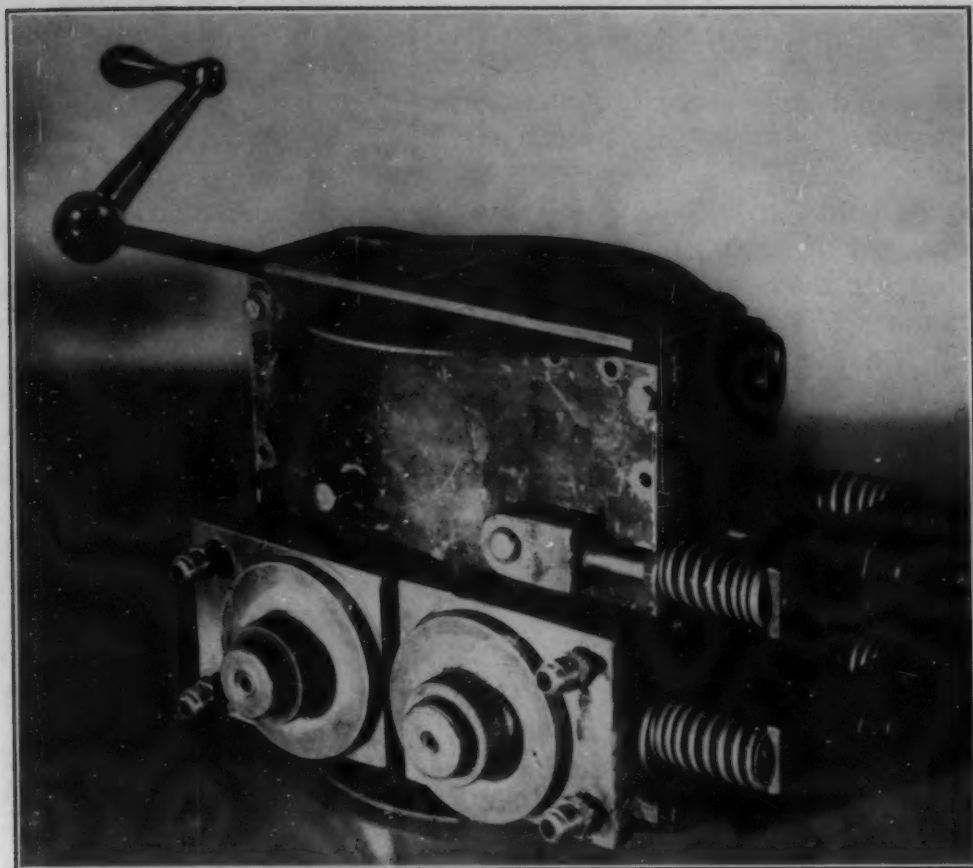


Fig. 3—Photograph of Power Application and Drive Rolls.

furnace. The water jacket, 13, is machined inside to provide a $\frac{1}{8}$ -inch water gap between the jacket and the $\frac{1}{4}$ -inch thick copper-melting crucible containing the ingot, 14. About 20 gallons per minute of cooling water at 45 pounds pressure flows from bottom, 15, to top, 16. Power is applied to the copper-melting crucible by a bus-bar connection, 17. The eyepiece, 18, permits observation of the molten pool of metal. Attachment and removal of the melting-crucible assembly are facilitated by a small cart, 19. Two vacuum lines are provided for quick evacuation.

OPERATION

In operation, a supply of pressed bars is placed in the bar-joining tank and the furnace evacuated to a pressure of less than 50 microns. The gloved entrances are protected by internal mechanical locks. After evacuation, the furnace is filled with mixed inert gas consisting of 80% helium and 20% repurified argon. This mixture permits a higher-voltage arc than pure argon and a steadier arc than pure helium. The glove-port locks are then opened, and the bar joining is begun. The $\frac{1}{8}$ -inch tungsten electrode is employed, with a power input of 25 volts and 100 amperes direct current (straight

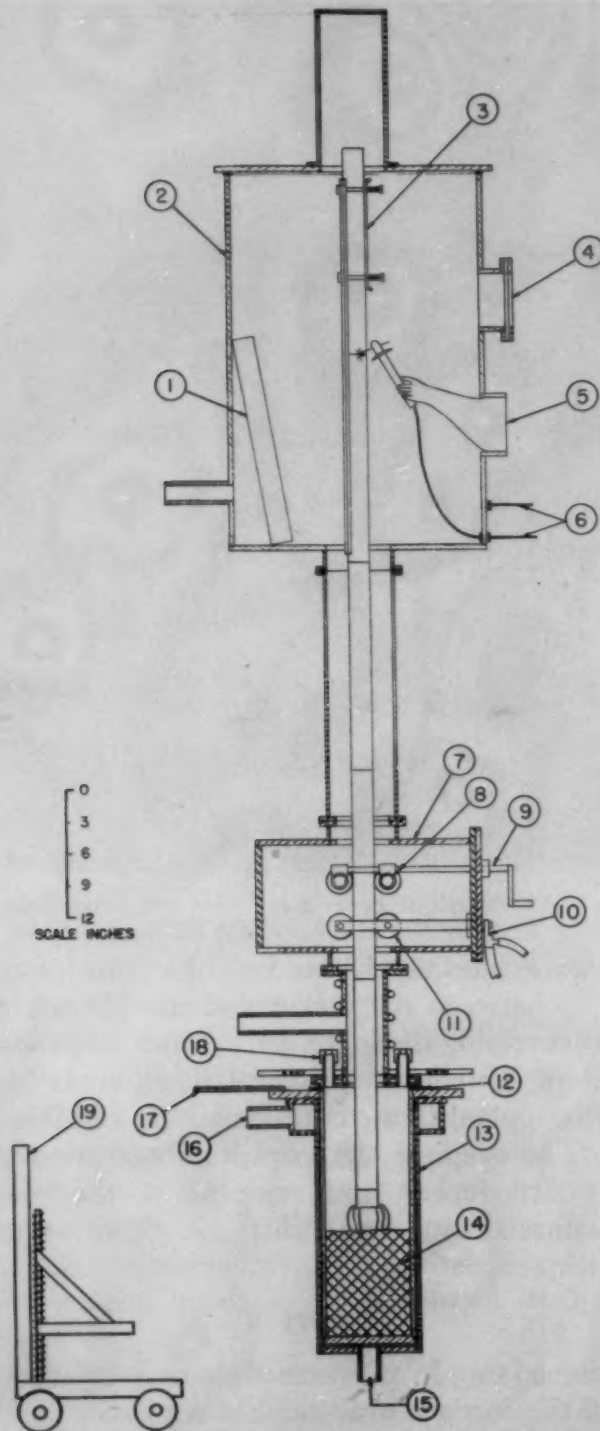


Fig. 4—General Design of Furnace. 1) Electrode supply, 2) Vacuum-tight tank, 3) Aligning guides, 4) Viewing port, 5) Rubber glove for bar joining, 6) Welding power leads, 7) Drive box, 8) Mechanical-drive rolls, 9) Crank for electrode drive, 10) Main power to electrode, 11) Power application rolls, 12) Electrical insulation ring, 13) Water jacket, 14) Zirconium ingot in melting cup, 15) Water inlet, 16) Water outlet, 17) Main power to melting cup, 18) Eyepiece, 19) Cart for removing melting-cup assembly.

polarity). Bars are welded on the two opposed sides not in contact later with the drive and power rolls. When enough bar is made up to reach to a zirconium starter pad in the bottom of the melting crucible, the power generators are started and melting is initiated.

For routine work, three men are employed. The bar joiner places bars in the guide, and welds the joints as they pass his position. The generator tender controls the welding generators, checks water temperature and pressure, and relieves the melter on a 10-minute schedule. Observation through the eyepieces permits the generator tender to adjust the power to give optimum melting conditions. The melter operates the feed crank to advance the electrode at such a rate as to maintain a predetermined voltage across the arc. Fig. 5 shows the equipment and two of the operators during a run.

Power requirements do not vary widely for a given metal or alloy. An input of 3500 to 3700 amperes at 40 to 45 volts direct current (straight polarity) assures a wall-to-wall melt of zirconium in an 8-inch diameter crucible. In all cases the power input has to be reduced during the last few minutes of melting, or serious shrink pipes result.

Actual rate of melting or kilowatt-hour requirement per pound of electrode consumed varies with the amount of magnesium, residual or added for purposes of arc stabilization (1). Normal variation is 0.39 to 1.15 kilowatt-hour per pound of electrode consumed, the higher inputs being employed in questionable cases to assure adequate consolidation of the ingot. Usual addition of magnesium for this purpose is 0.02 to 0.04% as wire placed in the sponge during pressing.

Ingots of 200 pounds rough weight have been produced without difficulty. Recovery of finished metal after the ingots are machined to cylinder is 75 to 85%, depending upon the residual magnesium and magnesium chloride in the sponge metal from which the bars are pressed. All metal removed in dressing the ingots is recovered and added to the sponge employed in making further electrode bars. The appearance of a pressed bar and of rough and finished ingots is shown in Fig. 6.

Production of alloys in this furnace was again complicated by the relatively coarse particle size of the sponge zirconium. Divided metal additives or master alloys may be added during pressing, but segregation was so serious as to require that individual bar charges be mixed separately. Wires or rods of the additive may be prepared to calculated diameter, so that a 20-inch length constitutes the exact amount desired per bar. This wire or rod may then be placed in the center of the electrode bar during pressing.

A series of alloy ingots was prepared in this manner, with addition of 2.5% of a given metal as wire. The usual distribution range in the finished ingots was 2.2 to 2.8%.

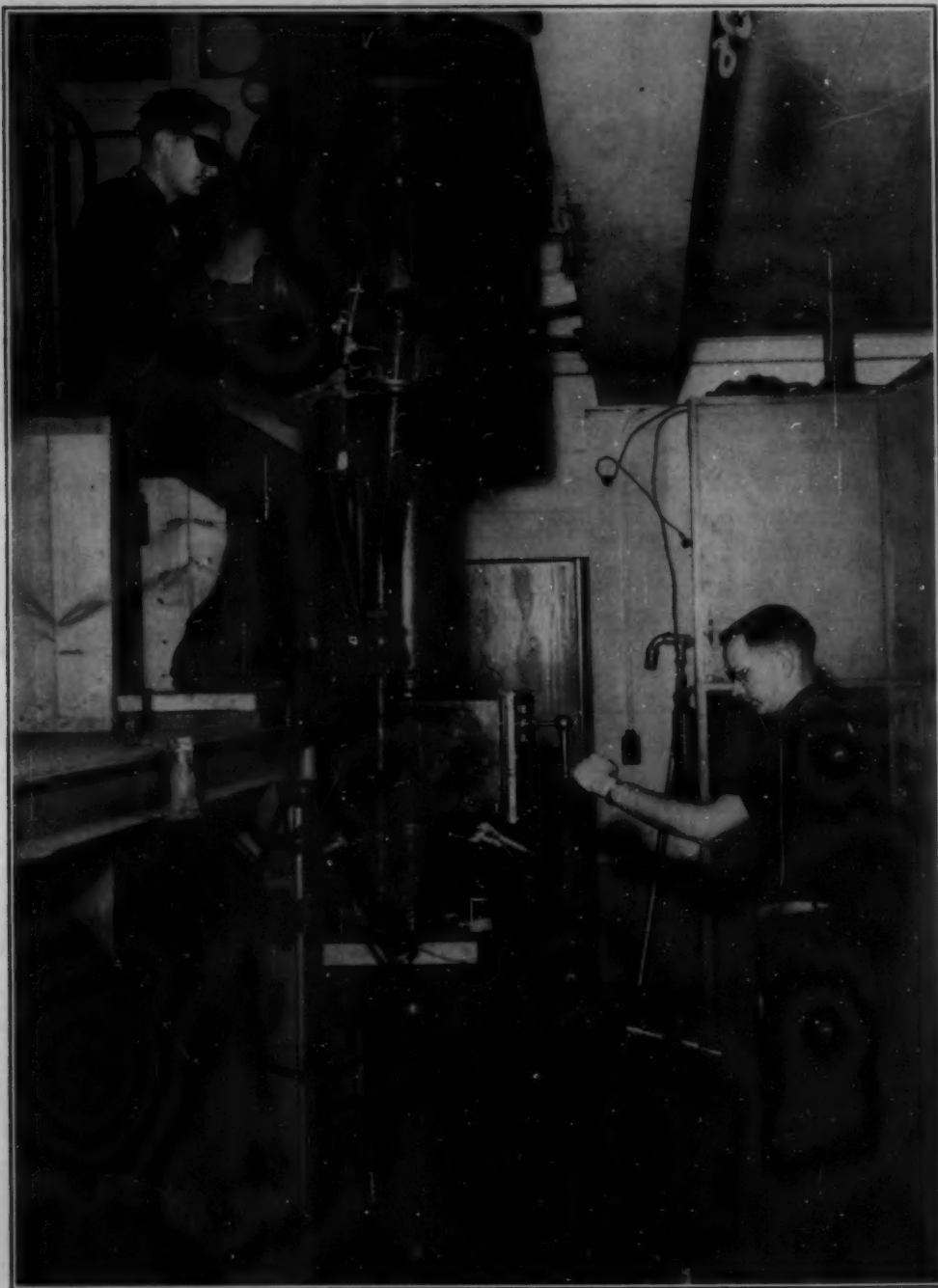


Fig. 5—Photograph of the Equipment and Operators During a Run.

A mechanical feeder geared to the electrode-feeding crank was found satisfactory for adding metal shot or wire to the molten pool, with homogeneity equal to or better than that obtained by making the addition to the bars during pressing.

If greater homogeneity were required for research purposes, the initial ingot was press-forged and form-rolled to a 2-inch square rod and remelted in the same furnace. Several such "double-melted"



Fig. 6—Showing Appearance of Pressed Bar and of Rough and Finished Ingots.

ingots varied only slightly from the desired alloy concentration. Metal recovery on remelting was 95%, as no magnesium chloride was present to form intrusions at the crucible wall.

It must be noted that the press employed in making up the electrode bars for this furnace is of unusual capacity. To eliminate use of this press, one may utilize a small automatic press to turn out round, rectangular, or hexagonal compacts approximately 1 inch thick. These forms can be continuously machine-welded up the sides to give the effect obtained with the present bars. Tests also indicate the feasibility of continuously pressure-welding a stack of such compacts during the melting operation by use of a very heavy secondary current applied by auxiliary contact shoes or rollers.

The present furnace may be employed with equal success in

melting tantalum, niobium, hafnium, titanium, thorium, uranium, molybdenum, and other refractory metals and alloys. While it offers no outstanding advantages over the auto-extrusion electrode furnace developed by Parke and Ham (6) in the case of powdered metals, it does provide for use of more massive lumps of metal and permits remelting alloys without modification of equipment.

This furnace design also permits retraction of the electrode at any time, which is impossible with the auto-extrusion furnace.

No size limitation of this equipment is seen in producing ingots through 16- or 18-inch diameter. The use of direct current is desirable from the standpoint of high recovery of ingot, but tests have shown that alternating current may be employed in most cases. Use of three-phase alternating current with three electrodes might prove useful in producing ingots larger than 18 inches in diameter should the need for such ingots arise.

Combination of the furnace described herein with the extraction principle of earlier furnaces employed by the Bureau of Mines (1) and Parke and Ham (6) would greatly increase the practical length of ingots and offer the further advantage of a fixed length of electrode from contact rolls to molten pool.

CONCLUSIONS

It is felt that the furnace described offers a practical means for producing large ingots of refractory metals and alloys with a power requirement of less than 0.5 kilowatt-hour per pound. Initial recovery of machined ingot ranges from 75 to 85% of input metal. Recovered scalplings are remelted.

Alloy ingots may be remelted for improved distribution of additives in the same furnace without modification.

The process and equipment are simple, effective, and economical.

ACKNOWLEDGMENTS

The authors wish to acknowledge the unstinting efforts of John O. Borg, chemical engineer, and Franklie Wagy and Lambert Woudenburg, technicians, of the Melting Development Section at the Albany, Oregon, Station, in developing the consumable-electrode furnace.

Special mention must also be made of the cooperation and assistance of R. R. Lloyd and F. S. Wartman of the Bureau of Mines station at Boulder City, Nevada, who made it possible to obtain the pressed bars required for the experiments.

References

1. H. L. Gilbert, W. A. Aschoff and W. E. Brennan, II, "Arc Melting of Zirconium Metal", *Journal, Electrochemical Society*, Vol. 99, 1952, p. 191.

2. W. J. Kroll, A. W. Schlechten and L. A. Yerkes, "Ductile Zirconium From Zircon Sand", *Transactions, Electrochemical Society*, Vol. 89, 1946, p. 263.
3. W. E. Kuhn, "Production of Titanium Ingots by Melting Sponge Metal in Small Inert-Atmosphere Arc Furnaces", *Journal, Electrochemical Society*, Vol. 99, 1952, p. 89.
4. W. J. Kroll, C. T. Anderson and H. L. Gilbert, "A New Graphite Resistor Vacuum Furnace and Its Application in Melting Zirconium", *Transactions, American Institute of Mining and Metallurgical Engineers*, Vol. 175, 1948, p. 766.
5. W. J. Kroll and H. L. Gilbert, "Melting and Casting Zirconium Metal", *Journal, Electrochemical Society*, Vol. 96, 1949, p. 158.
6. R. M. Parke and J. L. Ham, "The Melting of Molybdenum in the Vacuum Arc", *Transactions, American Institute of Mining and Metallurgical Engineers*, Vol. 171, 1947, p. 416.
7. H. D. Kessler and M. Hansen, "A Study of Arc-Melted Molybdenum-Rich Chromium-Molybdenum Alloys", *TRANSACTIONS, American Society for Metals*, Vol. 42, 1950, p. 1008.

SOME PROPERTIES OF HIGH PURITY ZIRCONIUM AND DILUTE ALLOYS WITH OXYGEN

R. M. TRECO

Abstract

A systematic investigation has been made of the physical and mechanical properties of dilute alloys of oxygen in high purity iodide-refined zirconium. A marked strengthening effect was observed as a result of oxygen additions. Results of tensile tests at elevated temperatures up to 400 °C (750 °F) are also presented. Preparation of alloys is discussed in detail.

INTRODUCTION

THE development of zirconium as an important metal for atomic energy applications has been considerably slowed because of the effect of very small amounts of impurities on the otherwise excellent corrosion resistance of this metal. On the other hand, very pure crystal bar, though not lacking in corrosion resistance, is soft and ductile with consequent deficiency in hardness and tensile strength. Attempts to prepare zirconium alloys having greater strength have been limited by several factors. Chief of these has been the difficulty involved in melting such alloys in a suitable crucible and atmosphere so as to preserve the original corrosion resistance of the iodide crystal bar. In view of these difficulties, the use of gaseous elements, such as oxygen and hydrogen, appears attractive in view of the high affinity of the metal for these gases.

Earlier work on the zirconium-gas systems arose as a natural consequence of the van Arkel hot-wire method of preparing iodide crystal bar as outlined in the classical work of J. H. de Boer and J. D. Fast (1, 2).¹ Later investigations by J. D. Fast (3), Sieverts and Roell (4), Ehrke and Slack (5), Hall, Martin and Rees (6) have been concerned with the sorption and desorption of gases in zirconium used as a "getter" in vacuum tubes. The results of these investigations vary considerably because of differences in the purity of the zirconium available. A recent paper by Gulbransen and Andrew (7) discusses the kinetics of the reactions of several gases with zirconium at relatively low temperatures. However, the effect of dissolved gases on

¹The figures appearing in parentheses pertain to the references appended to this paper.

This work was carried out at the M. I. T. Metallurgical Project under Contract No. AT(30-1)-981 with the U. S. Atomic Energy Commission.

A paper presented before the Eighth Western Metal Congress of the Society, held in Los Angeles, March 23 to 27, 1953. The author, R. M. Treco, is research metallurgist, Bridgeport Brass Co., Bridgeport, Conn. Manuscript received May 1, 1952.

the properties of the metal itself does not appear to have been previously investigated.

The use of hydrogen as a strengthening agent was considered to be of secondary importance and the present work outlines detailed results for oxygen additions only.

MATERIALS

The zirconium used for this work was supplied by the Foote Mineral Co. and consisted of a number of iodide crystal bars of low hafnium content, having excellent corrosion resistance. Results of chemical and spectrographic analyses of the bars are given in Table I

Table I
Analyses of Zirconium Crystal Bars

Bar No.	Z62-1	Z62-2	Z62-3	Z62-4	Z62-5	Z62-6	Z62-7	Z62-8
Element (ppm)								
C	650	340	260	330	310	420	250	230
O ₂	260	360	...	210	...	220	220	...
Na	10	8	36	14	16	6	16	10
Fe	280	160	350	500	235	290	280	640
Ni	< 50	110	480	410	< 25	< 25	< 50	70
Al	30	30	30	20	< 25	< 25	25	< 25
Ca	15	15	10	15	12	< 10	10	< 10
Cr	15	20	65	< 10	< 10	< 10	< 10	< 20
Cu	10	45	< 10	< 10	10	10	10	< 10
Mg	8	< 5	< 5	5	< 5	< 5	< 5	< 5
Mn	< 5	< 5	< 5	< 5	< 5	< 5	< 5	< 5
Pb	< 20	< 20	< 20	< 20	< 20	< 20	< 20	< 20
Si	40	25	< 25	35	< 25	60	25	45
Sn	< 20	< 20	< 20	< 20	< 20	< 20	< 20	< 20
Ti	45	35	< 25	20	< 25	< 25	60	< 25
V	< 100	< 100	< 100	< 100	< 100	< 100	< 100	< 100
Hf	280	290	...	180	240	...

< = less than.

and it will be noted that the initial oxygen content was about 0.025% by weight with approximately 0.001% nitrogen in most of the bars. Degassing indicated an average initial hydrogen content of 0.01% by weight. Principal impurities were carbon, iron and nickel.

Linde tank oxygen of 99.5% purity was used for the gas additions. Gas of this purity was sufficient since the addition of one weight per cent of oxygen could only increase the nitrogen content by about 44 ppm.² The gas was dried by passing it over evacuated, sieved Drierite through an alcohol - dry ice cold trap into a mercury-sealed storage flask.

PREPARATION OF METAL

The individual crystal bars were prepared by machining small flats on opposite sides of each bar for the entire length (about 18

²Chemical analyses indicate that considerably less nitrogen than this is actually added to the metal with experimental technique outlined due to its much slower sorption in the metal. Nitrogen increases of about 5 ppm or less were actually obtained. Hence, the gas is in effect "purified".

inches). In order to bring the bars to size, they were reduced 20% in thickness by cold rolling followed by annealing for one hour at 650 °C (1200 °F) in a vacuum furnace. After this treatment, the bars were recrystallized and could be cold-reduced another 20%. This treatment was repeated until all bars were reduced to the same thickness of 0.170 inch. Cold working and annealing had the effect

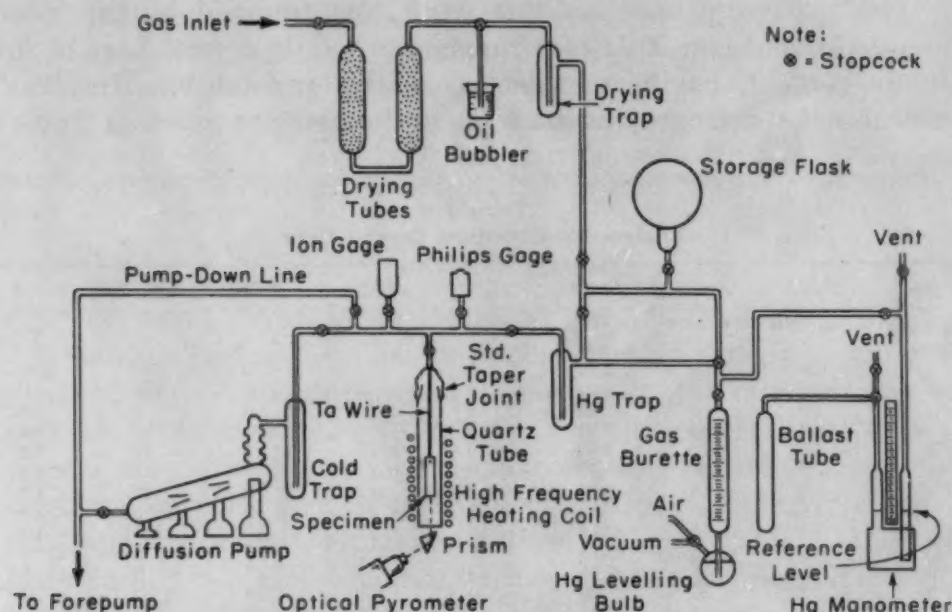


Fig. 1—Schematic Diagram of a High Vacuum System for Controlled Additions of Gases to Metals.

of breaking up the original coarse grains into a fine-grained homogeneous structure, while retaining the original hardness level of the bars.

The annealed strips were then cut into specimens 3 inches long by $\frac{1}{8}$ inch thick, the widths varying from $\frac{1}{4}$ to $\frac{3}{8}$ inch, and a small hole drilled in one end.

In order to remove tool contamination from machining, the metal was etched for 2 to 4 minutes in a solution of 50% nitric acid by volume to each 100 cc of which 10 to 15 drops of hydrofluoric acid were added. The solution was prepared fresh for each use. The metal was also degreased in acetone and then stored in a vacuum desiccator.

EXPERIMENTAL PROCEDURE

The preparation of gas alloys of zirconium requires a high vacuum system and some method of introducing the desired gas under known and reproducible conditions. For this work a glass system consisting of three parts was especially designed to satisfy these requirements.

A schematic diagram is shown in Fig. 1. The first part consisted of an oil diffusion pump and a high vacuum manifold to which was attached a movable quartz tube approximately 30 by 3.5 cm. A high-frequency induction coil for heating the specimens was closely fitted to the quartz tube. The second part of the system consisted of a water-jacketed, calibrated gas burette, of the type used for gas analyses, connected to the vacuum manifold and a mercury manom-

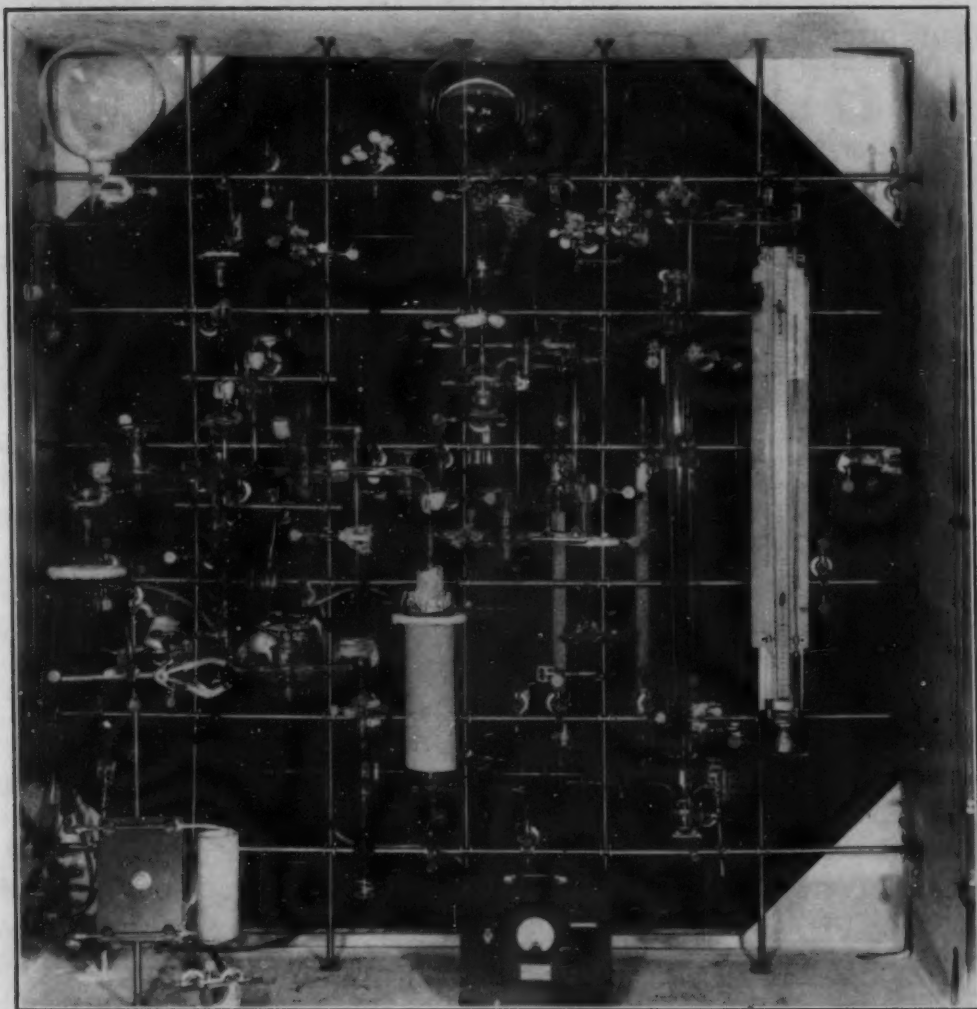


Fig. 2—View of High Vacuum System and Gas Measurement Apparatus Showing Arrangement of Parts.

eter for pressure measurements. A cold-trap separated the first and second parts of the system for the isolation of mercury vapor. The third part of the system consisted of a large mercury-sealed gas storage flask which could be connected to either the gas measuring system or to a drying train and cold-trap through which gas was supplied to the system. A view of the entire assembly is shown in Fig. 2.

DEGASSING OF METAL

In order to put all the metal in a similar condition and to prevent weight losses during diffusion, a degassing operation was required. Weighed samples were hung from a tantalum rod in the evacuated quartz reaction tube and the system evacuated to 5×10^{-5} mm. Hg or better. The metal was at first heated to 1055°C (1930°F) and a large volume of gas removed. Heating was continued until a pressure less than 0.02 to 0.04 micron was attained at temperature. This required 30 to 60 minutes for 10 to 12 grams of metal. Further heating to 1280°C (2335°F) produced little increase in pressure.

Later experiments on 150-gram and larger bars required only 90 to 120 minutes for complete degassing, indicating that the degassing rate depends more on the geometry of the bar (hence the effective diffusion distance) than the weight of metal in the bar. These last figures were for large-diameter ($\frac{1}{8}$ inch) crystal bars.

On cooling there was a distinct evolution of gas at 865°C (1590°F), indicating that the solubility of the gas is considerably greater in the beta than in the alpha phase, as is well known. The gas is apparently hydrogen since no condensate was formed on the glass and neither oxygen nor nitrogen appears to be removable in this way. T. T. Magel (8) has also shown previously that the gas evolved from crystal bar is hydrogen.

At temperatures in excess of 1500°C (2730°F) there is an evolution of other metal impurities (particularly iron, manganese and magnesium). At these temperatures zirconium may also distill onto the quartz tube.

A number of important phenomena accompany the degassing operation. There is, of course, an appreciable weight loss as shown in Table II, which also shows the equivalent hydrogen content of the original metal. In addition there is a considerable surface roughening and a definite volume change (usually contraction) amounting to as much as 10%. The volume change did not correlate with the hydrogen content. It appears that the dimensional changes and surface roughening during degassing are the product of two separate reactions. In the first case, a decrease in volume occurs as hydrogen is removed and the density is increased. However, during degassing, heat was applied until the evolved gas choked the vacuum pumps at which time the metal was allowed to cool until the pressure dropped again. This heating and cooling through the transformation apparently caused the surface roughening and warping noted, although stress relief may also contribute to warping. The number of thermal cycles varied for each specimen, but no account was taken of the number of cycles.

Considerable warping of some specimens along the longitudinal

Table II
Degassing Data

Specimen No.	Degassing Temp. (°C)	Weight Loss (%)	Equivalent at % H ₂
1-A	1055	0.0113	1.01
1-B	1055	0.0078	0.70
2-A	1055	0.0080	0.72
2-B	1280	0.0069	0.62
2-C	1280	0.0088	0.79
3-A	1280	0.0060	0.54
3-B	1280	0.0096	0.86
3-C	1055	0.0083	0.74
3-D	1055	0.0065	0.58
4-A	1280	0.0057	0.51
4-B	1280	0.0120	1.08
5-A	1055	0.0149	1.33
5-B	1055	0.0124	1.08
5-C	1055	0.0101	0.90
5-D	1055	0.0111	1.00
6-C	1280	0.0140	1.25
6-D	1280	0.0120	1.08
7-A	1280	0.0087	0.78
7-B	1280	0.0086	0.77
7-C	1280	0.0079	0.71
8-A	1280	0.0085	0.76
8-B	1280	0.0051	0.46
8-C	1280	0.0058	0.52
8-D	1280	0.0059	0.53
8-E	1280	0.0146	1.30

axis, occasionally accompanied by twisting about this axis, also occurred. After straightening, warping sometimes occurred on reheating, but a number of specimens showed no further tendency to warp. Round specimens used in later work showed no warping tendency even after severe cold working.

PREPARATION OF OXYGEN ALLOYS

The preparation of oxygen alloys depends on the well-known "gettering" activity of zirconium metal for gases and the rapid diffusion of these gases in the metal so as to leave a fresh surface exposed for further absorption. Various data have been reported in the literature (see Ref. 9 for a convenient summary) indicating that oxygen is rapidly absorbed at temperatures ranging from 200 to 1600 °C (390 to 2910 °F). Since it was desired to keep the grain size as small as possible while minimizing diffusion time, first attempts were made at 1055 °C (1930 °F).

The method of adding oxygen was as follows: A degassed sample was hung from a tantalum rod (both sample and rod having been previously weighed) in a quartz reaction tube with a flat bottom. The reaction tube, manifold and gas burette were all evacuated to a pressure less than 10^{-5} mm. Hg. The burette, gas storage flask and manometer were then closed off from the rest of the system and a known amount of oxygen measured out and sealed into the burette. Excess oxygen was then pumped out and after a good vacuum was

again attained the reaction tube was closed off from the diffusion pump. Oxygen in the burette was then released into the system and the manometer pressure noted. The zirconium specimen was heated to 1055 °C (1930 °F) and held at temperature until the pressure in the system dropped to about 1 mm. Hg at which point a brilliant corona discharge appeared in the tube. Further heating was then useless since the vacuum would not improve and a considerable amount of zirconium can be sputtered from the specimen at this pressure. The system was then opened to the diffusion pump and rapidly evacuated, after which the specimen was held at the diffusion temperature for the necessary time to produce a homogeneous alloy. At 1055 °C (1930 °F), 45 minutes was required to absorb all the oxygen, but when the temperature is raised to 1280 °C (2335 °F) (corrected true temperature³) the time is reduced to 2 to 5 minutes for a 0.4 weight per cent alloy. At this temperature one hour is ample to produce a completely homogeneous alloy by diffusion.

After diffusion, specimen and hanger were removed from the vacuum system, weighed again and the increase compared with the calculated quantity of gas added to the system. Recoveries of about 99% of the added gas can usually be attained.

PREPARATION OF TEST PIECES

Specimens after oxygen diffusion were ground on all sides into small slabs approximately 3 by 0.250 by 0.110 inches. Grinding provided a good surface for resistivity measurements and also sufficed to straighten any pieces which had warped slightly. Straightening by bending was not successful for the higher concentration alloys which proved to be quite brittle.

Following the resistivity test, specimens were ground to form tensile blanks with a 1-inch gage length, 0.150 inch wide by 0.110 inch thick, with suitable radii at the ends of the gage length.

RESULTS AND DISCUSSION

The results of the physical and mechanical tests to which these alloys were subjected are most conveniently summarized in the data of Table III in which experimental properties are tabulated in order of increasing atom per cent of oxygen. Specimens having the same numeral were cut from the same bar and designated A, B, C, etc. Whenever possible, average figures have been noted. Exact values are shown in the following curves for the individual properties discussed.

³Stated temperatures were obtained by means of a recently calibrated Leeds and Northrup Optical pyrometer sighted on bright metal surface through a silvered prism and the bottom of the quartz tube. A calibration curve for each quartz tube was determined with a tantalum ribbon filament lamp for the absorption correction. Finally, the temperature was corrected for a spectral emissivity value of 0.32.

OXYGEN ANALYSES

Representative samples were taken after final grinding from each bar to which oxygen had been added as well as from suitable control bars. Oxygen analyses were made on these bars by the hydrogen chloride method (10) and the results compared with the amount of added oxygen. It must be remembered that the analytical results show the *total* oxygen present which includes the initial oxygen present in the bars (a variable quantity) as well as the added

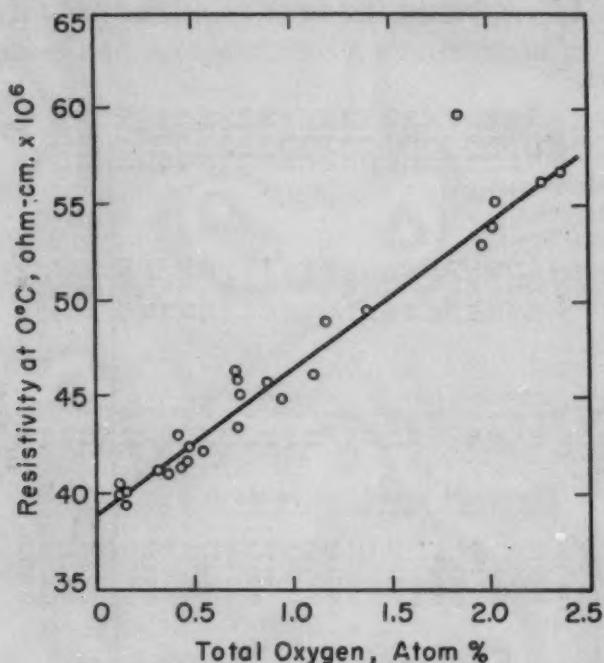


Fig. 3—Effect of Oxygen on Electrical Resistivity of Iodide Zirconium.

oxygen. All results of tests described below are based on the corrected total amount of oxygen. Comparison of added and corrected oxygen content may be obtained by reference to columns 2 and 3 of Table III.

Resistivity—Resistivity measurements were made with the specimens clamped between knife edges in a constant temperature oil bath near room temperature. Resistivities thus obtained were corrected to 0 °C for comparison purposes using a temperature coefficient of $4.4 \times 10^{-3}/^{\circ}\text{C}$ (11). The average resistivity value for pure, degassed, annealed metal was found to be 39.84×10^{-6} ohm-cm. at 0 °C. This is slightly lower than the value of 41.0×10^{-6} ohm-cm. for the same temperature given by van Arkel (11). The difference is considered to be significant in view of the higher purity of metal used in this work.

Fig. 3 is a plot of the resistivity data showing a linear relation between this property and atomic per cent oxygen. Extrapolation

Table III
Properties of Zirconium-Oxygen Alloys

Specimen No.	Wt. % Added O ₂	Wt. % Total O ₂	At. % Total O ₂	ρ_o^* (ohm-cm) ($\times 10^6$)	k _o [†] (cal/deg/ cm/sec)	Average Hardness (R _A)	0.1% Yield (psi)	0.2% Yield (psi)	Ultimate Tensile (psi)	Elong. in 1 in. (%)	Young's Modulus (psi) ($\times 10^6$)
4-C	0	0.0210	0.120	40.31	0.0396	30.0	10,740	11,200	31,450	24.9
6-B	0	0.0220	0.125	39.96	0.0400	21.0	9,250	11,180	21,750	16.2
1-A	0	0.0260	0.148	39.32	0.0407	26.5	12,860	14,850	32,200	43.1
1-B	0	0.0260	0.148	40.00	0.0400	26.0	10,800	14,250	32,400	35.1
7-C	0.0390	0.0550	0.313	41.11	0.0388	16,100	18,675	33,950	> 15.1
8-C	0.0292	0.0640	0.364	41.11	0.0388	30.5	16,900	19,100	33,200	18.8
7-A	0.0539	0.0725	0.412	42.89	0.0372	34.0	23,600	27,900	40,900	14.5
8-A	0.0390	0.0740	0.420	41.29	0.0386	32.5	16,780	19,820	32,900	> 22.4
8-E	0.0472	0.0800	0.455	41.65	0.0384	31.5	19,750	22,350	34,350	16.0
7-B	0.0661	0.0830	0.471	42.36	0.0377	36.0	16,800	20,950	33,000	> 11.6
6-D	0.0670	0.0950	0.539	42.24	0.0378	30.5	19,200	22,450	31,000	> 10.9
6-C	0.0936	0.125	0.708	43.41	0.0368	41.5	25,000	28,400	44,200	14.4
8-B	0.0945	0.125	0.708	46.18	0.0346	42.0	27,700	30,800	44,150	12.8
5-A	0.131	0.127	0.720	45.87	0.0348	42.5	29,500	31,450	58,100	13.3	10.7
5-D	0.134	0.128	0.725	45.10	0.0354	40.0	29,450	33,150	45,800	11.3
8-D	0.125	0.153	0.866	45.72	0.0349	42.5	22,850	27,400	37,200	> 8.7
6-A	0.131	0.166	0.939	44.97	0.0355	44.0	28,000	31,400	36,900	> 7.5
5-C	0.197	0.195	1.102	46.17	0.0346	48.0	37,300	41,500	51,800	4.9	9.8
5-B	0.213	0.208	1.172	48.98	0.0326	48.0	44,100	48,100	66,500	5.2
2-A	0.226	0.244	1.375	49.62	0.0322	53.5	30,200	37,000	57,500	8.6	12.2
3-B	0.338	0.327	1.836	59.69	0.0268	54.0	45,200	50,600	74,600	3.7
2-C	0.350	0.350	1.963	53.01	0.0302	56.0	59,730	4.7
3-A	0.376	0.361	2.024	53.84	0.0297	57.5	39,400	44,700	59,400	2.6
4-B	0.370	0.363	2.035	55.22	0.0289	54.0	32,500	44,300	73,000	3.6
4-A	0.411	0.405	2.266	56.24	0.0284	58.0	73,800	4.2
2-B	0.415	0.422	2.359	56.74	0.0282	59.0	45,400	53,500	73,100	2.6

* ρ_o = Resistivity at 0 °C.
 $\dagger k_o$ = Equivalent Thermal Conductivity.
 > = Greater than.

of this curve to zero oxygen indicates a resistivity of 38.8×10^{-6} ohm-cm. for virtually gas-free zirconium.

Thermal Conductivity—Thermal conductivities were calculated from the Wiedemann-Franz ratio which appears to be consistent with experimental values of electrical resistivity and thermal conductivity (12) obtained for zirconium. The equivalent thermal conductivity for a measured resistivity of 39.84×10^{-6} ohm-cm. is 0.040 cal/°C/cm/sec. Thermal conductivity on this basis is decreased about 10% for each atomic per cent of oxygen added.

Hardness—A great many hardness tests were made both on longitudinal surfaces and across transverse sections in order to ascertain

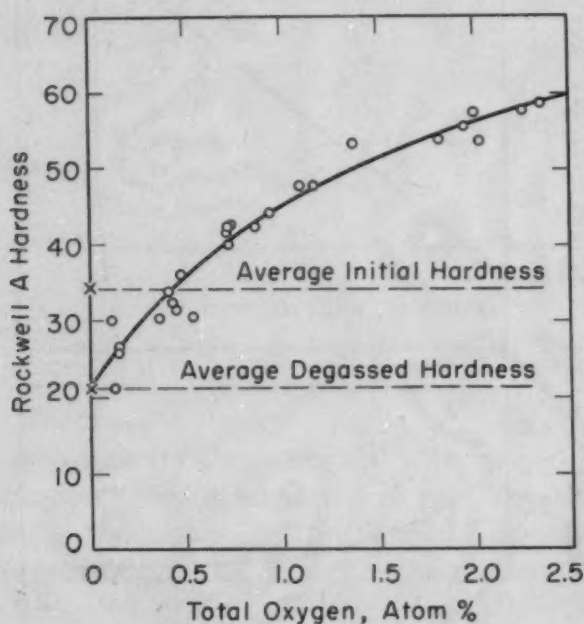


Fig. 4—Effect of Oxygen on Hardness of Iodide Zirconium. Comparison of initial and degassed hardness as shown by the dotted lines.

the uniformity, hence homogeneity, of the diffused alloys. For this latter purpose, the 15N scale was selected and a total variation of 1.0 point edge-to-edge existed, for example, in sample Z62-2C. This is a very small variation for practical purposes.

The hardness test is very sensitive to structural variations so that even average results must be interpreted with care. This is particularly true of the pure metal samples which were very soft and coarse-grained. The effects of degassing and annealing were to lower the hardness about 13 points Rockwell A, an average value for pure metal after hydrogen removal being A-21. However, one or two samples showed soft spots somewhat below this value. It is noteworthy that the softest specimen (Z62-6B) did not have the greatest

elongation since orientation also has a large influence on this property.

The average results of a great many hardness tests are shown in Fig. 4, and it appears that the first small additions of oxygen have the greatest hardening effect, though hardness continues to increase with greater amounts of oxygen.

It is apparent that hardness does not increase linearly with added oxygen although forming an extensive solid solution with zirconium. J. H. de Boer and J. D. Fast (13) have shown that the oxygen atoms

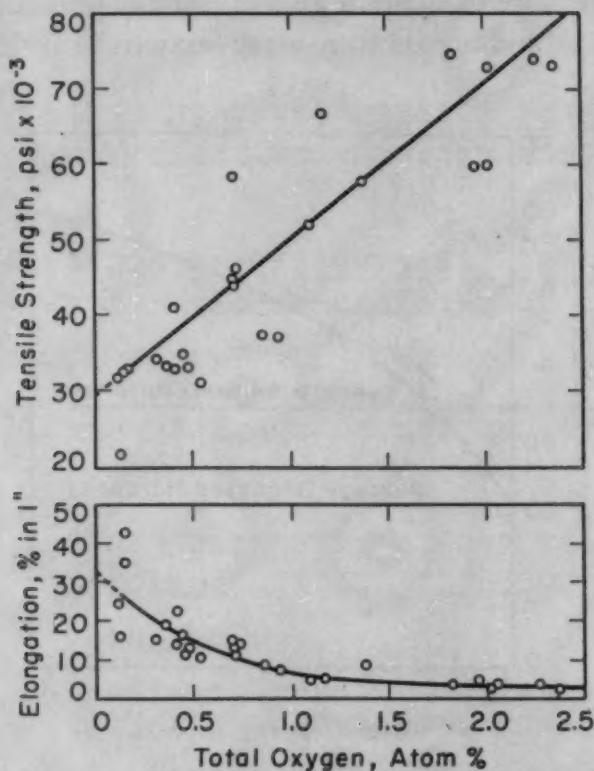


Fig. 5—Effect of Oxygen on Ultimate Tensile Strength and Elongation of Rectangular Test Specimens of Iodide Zirconium.

occupy an interstitial position. One explanation of the rapid embrittling effect of oxygen may be the distribution of these atoms in preferred positions which inhibit the normal slip processes of the hexagonal lattice during plastic deformation. This blocking of the lattice movements is reflected in higher yield strengths.

It is believed that hydrogen has a similar though smaller effect on hardness and ductility. Substantial cold reduction of crystal bar is usually impossible without prior degassing.

Tensile Properties—It will be seen from Table III that the 0.2% yield strength is increased by a factor of nearly three for the first 0.7 atomic per cent of oxygen added, but increases less rapidly with further additions, while the ultimate strength is increased about 60%

for each atomic per cent of added oxygen with a corresponding decrease in ductility.

A few values obtained for the modulus of elasticity indicate that no change was evident in this property.

The tensile properties as a function of oxygen content are summarized in Figs. 5 and 6. An unsuccessful attempt was made to cor-

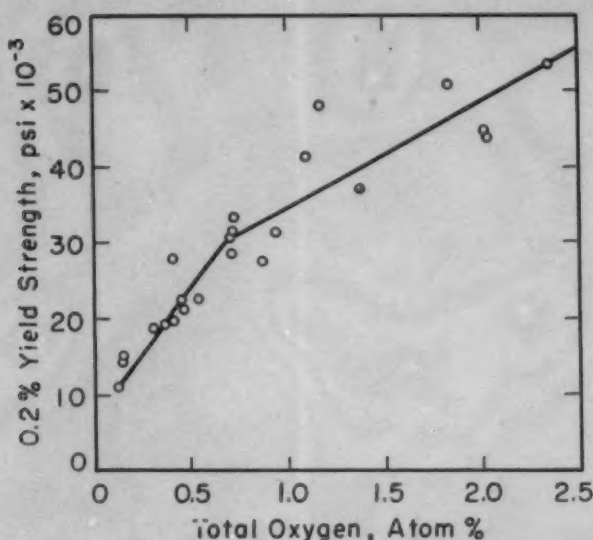


Fig. 6—Effect of Oxygen on 0.2% Yield Strength of Iodide Zirconium Determined by Double Dial Gages Attached to the Specimens.

relate scattered points on these curves with minor impurities; e.g., carbon, iron, etc. The wide variation in per cent elongation for the control samples is thought to be the result of orientation differences in individual grains since these samples were comparatively coarse-grained.

Metallography—The microstructure of these alloys and also the pure metal are very similar to crystal bar as received. No structural features related to the added oxygen were detected or expected in view of the high solubility of oxygen in zirconium.

Fig. 7 shows a typical microstructure after the addition of 0.13 weight per cent O_2 . The mixed structure is typical of metal which has been cycled through the alpha-beta transformation.

In some cases the coarse-grained structure was undoubtedly responsible for some of the erratic results. For the work at elevated temperatures, the alloys were cold-worked and annealed to produce a recrystallized structure. A typical recrystallized structure for a 0.14% alloy is shown in Fig. 8 after a 6% cold reduction followed by 2 hours at 800 °C (1470 °F).

Workability—An alloy of 0.25 weight per cent O_2 was cold-rolled bare from a thickness of 0.196 to 0.056 inch, a total reduction of 72%. During this reduction the hardness increased from A-50 to

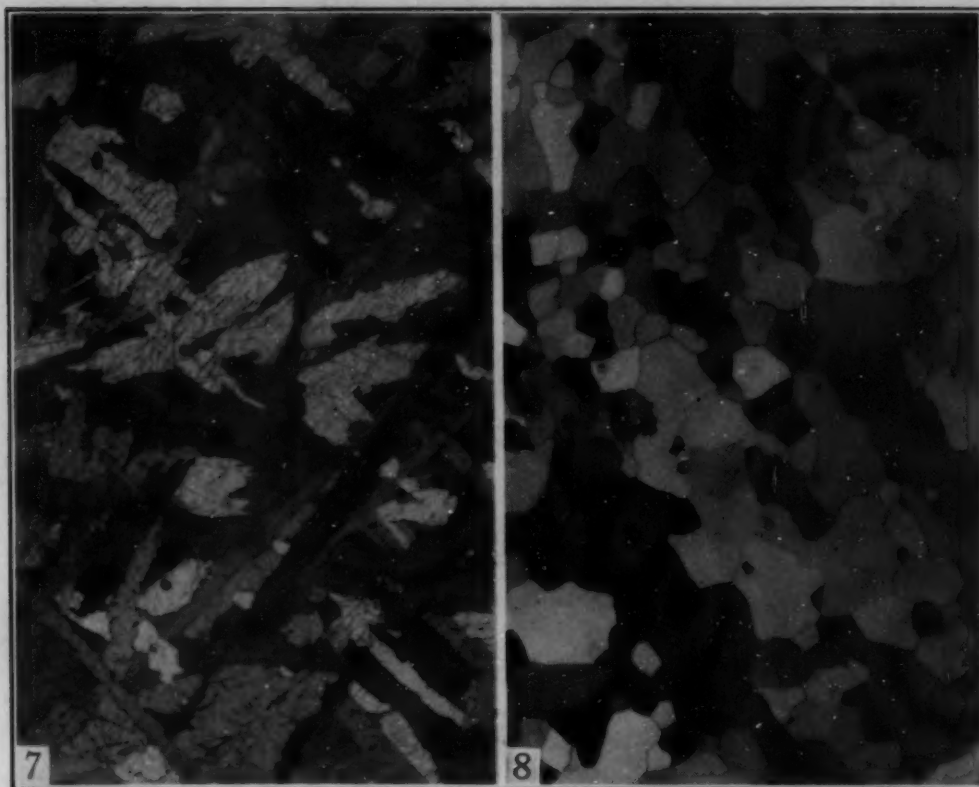


Fig. 7—Typical Microstructure of Iodide Zirconium After Degassing and Addition of 0.13 Weight Per Cent Oxygen. Electropolished. Polarized light. $\times 50$.

Fig. 8—Recrystallized Structure of 0.14 Weight Per Cent Oxygen Alloy After Cold Reduction of 6% Followed by 2 Hours at 800 °C in Vacuum. Electropolished. Polarized light. $\times 100$.

A-61. Further rolling was possible, although edge cracking appeared. The alloy, as has been shown, could also be annealed for further rolling. In general, oxygen alloys may be readily cold-worked if the oxygen does not exceed about 0.25 weight per cent. If the alloy exceeds this amount, the ductility suffers and hot working is preferable.

Annealing—Oxygen does not appear to effect the recrystallization of zirconium after cold working followed by vacuum or purified inert-gas annealing treatments. However, the hardness level of recrystallized oxygen alloys cannot be lowered by any treatment to values less than those shown in the hardness composition curve of Fig. 4.

Diffusion Rate—The diffusion of oxygen in zirconium at temperatures exceeding 1000 °C (1830 °F) is remarkably fast. Time was not available for a detailed analysis of diffusion rates. However, an approximate diffusion constant at 1280 °C (2335 °F) was obtained by determining the homogeneity of an alloy sample to which a known amount of oxygen was added and the time noted for complete diffusion through a known volume. The relation between these quantities is as follows (14):

$$c = \frac{Q}{\sqrt{\pi Dt}}$$

where D = diffusion constant, cm^2/sec

c = concentration, $\text{cc O}_2/\text{cc Zr}$

t = time, second

Q = ratio of diffused oxygen to surface area, cc/cm^2

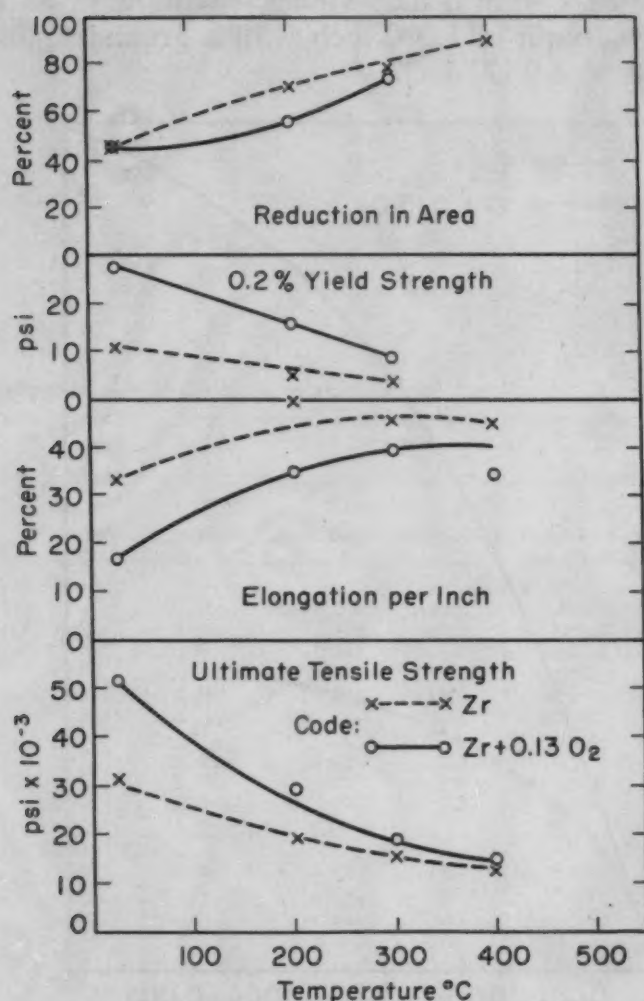


Fig. 9—Elevated Temperature Tensile Properties.

The diffusion constant thus obtained is equal to $5.25 \times 10^{-6} \text{ cm}^2/\text{sec}$ and represents a minimum value since a homogeneous condition may have been present before the elapsed time of 60 minutes. This value when applied to metal sections of entirely different geometry gave values for the diffusion time in accord with those actually observed.

Elevated Temperature Tensile Tests—The tensile properties of the zirconium-oxygen alloys at elevated temperature are of interest, particularly as compared with the properties of pure zirconium.

For comparison purposes, two large crystal bars from the same lot of material described above were made into a number of round tensile bars. Sample preparation included: degassing of bars;

machining to cylinders; cold swaging and annealing to bring the bars down to the correct diameter; addition of 0.13 weight per cent O_2 to the samples from one of the bars; cold reduction and annealing to recrystallize the coarse-grained structures; and, finally, machining and precision grinding to final test bar shape and size.

The tensile bars were 3 inches long, having a $\frac{1}{4}$ -32 thread on each end, a gage length of 1.000 inch with a ground radius at each end and a diameter of 0.171 inch.

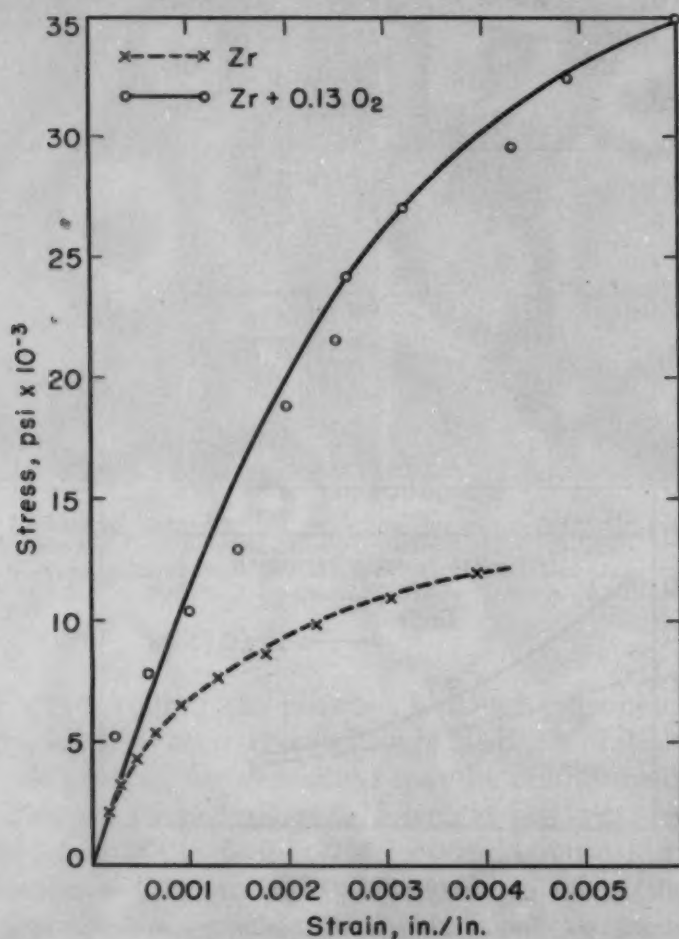


Fig. 10—Stress-Strain Curve 22 °C.

The tensile specimens were screwed into stainless steel adapters made long enough to fit into a split-type resistance furnace. An atmosphere of heated purified argon surrounded the specimens during the test, and temperature was maintained quite accurately by means of two thermocouples attached at either end of the specimen gage length. Extension of the specimens was measured by the bridge travel as indicated by 0.0001 and 0.001 inch dial gages. For the room temperature tests an Olsen extensometer reading to 0.0001 inch was clamped directly on the specimen. It was found that a correction factor was necessary to compensate for the stretch of the linkages

Table IV
Elevated Temperature Tensile Tests—0.13% Oxygen Alloy

Specimen* No.	Wt. % Added O ₂	Temp. (°C)	0.1% Yield (psi)	0.2% Yield (psi)	Young's Modulus (psi) ($\times 10^{-6}$)	Ultimate Tensile (psi)	Elong. in 1 In. (%)	Red. in Area (%)
9A-3	0.135	22	24,200	31,600	12.0	48,500	10.9	57.1
9B-2	0.136	22	25,650	30,700	11.7	55,380	22.5	40.7
9D-1	0.134	22	16,000	21,100	11.25	48,860	13.4	42.8
9D-4	0.131	22	53,460	20.4	40.3
9A-2	0.136	200	29,140	28.2	62.8
9B-1	0.138	200	13,300	16,000	7.0	29,120	37.9	53.9
9C-1	0.122	200	13,200	16,000	11.8	28,770	28.3
9D-2	0.136	200	12,700	15,400	11.8	29,030	44.6	56.2
9A-1	0.124	300	8,000	9,300	12.0	19,990	40.4	79.9
9B-4	0.132	300	6,000	8,500	19,620	44.0
9C-2	0.126	300	8,200	9,500	11.3	19,560	34.1	73.3
9D-3	0.133	300	16,230	38.7
9A-4	0.126	400	15,700	37.1
9B-3	0.117	400	14,300	32.5
9C-3	0.124	400	14,490	34.8
9C-4	0.126	400	14,630	33.4

*All tensile specimens from same original crystal bar.

Table V
Pure Zirconium Elevated Temperature Tensile Tests

Specimen* No.	Temp. (°C)	0.1% Yield (psi)	0.2% Yield (psi)	Young's Modulus (psi) ($\times 10^{-6}$)	Ultimate Tensile (psi)	Elong. in 1 In. (1%)	Red. in Area (%)
10C-4	22	31,900	30.5	42.5
10B-4	22	8,750	10,600	12.0	29,600	33.8
10D-3	22	32,000	35.5	46.6
10C-3	200	19,200	61.0	94.4
10D-4	200	2,800	4,800	9.3	19,000	44.9	64.8
10E-4	200	3,550	5,700	17.5	18,500	69.3	72.7
10B-3	200	3,300	4,890	9.8	19,600	28.3	56.2
10D-2	300	16,250	54.4	86.4
10E-3	300	14,550	43.1	62.6
10C-2	300	2,850	3,900	14.3	15,475	48.9	84.5
10B-2	300	16,000	37.1	80.0
10B-1	400	13,150	46.3	87.8
10C-1	400	13,020	51.9	94.8
10D-1	400	13,800	52.6
10E-1	400	12,600	28.7

*All tensile specimens from same original crystal bar.

attached to the specimen. This was obtained by direct calibration using all three gages. Despite the above care, it was very difficult to get good results for the yield strength and modulus of elasticity. This is due in part to the small size of the specimens, the requirement of a correction factor and the nature of the stress-strain curves for these materials.

After testing, the tensile specimens were sectioned through the gage length and the threaded portion. These sections were analyzed for oxygen and it was found that the bars were quite homogeneous in composition.

Table IV gives the tensile properties for the oxygen alloys.

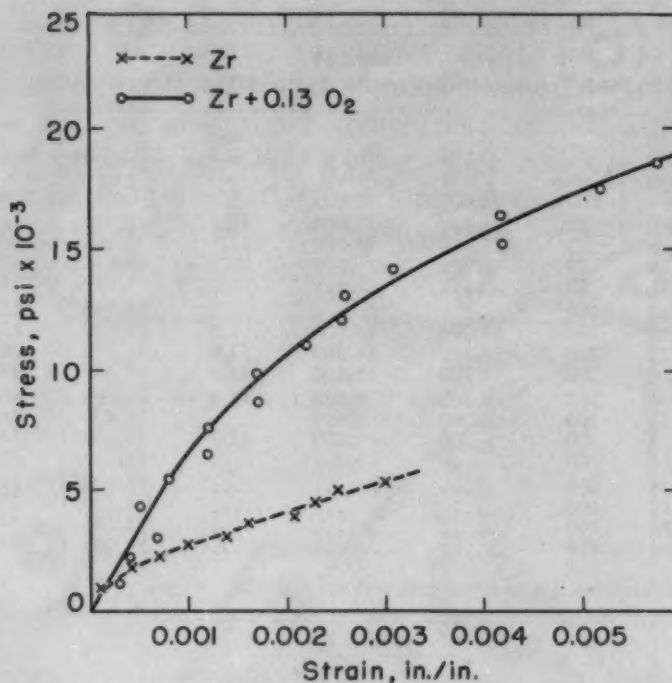


Fig. 11—Stress-Strain Curve 200 °C.

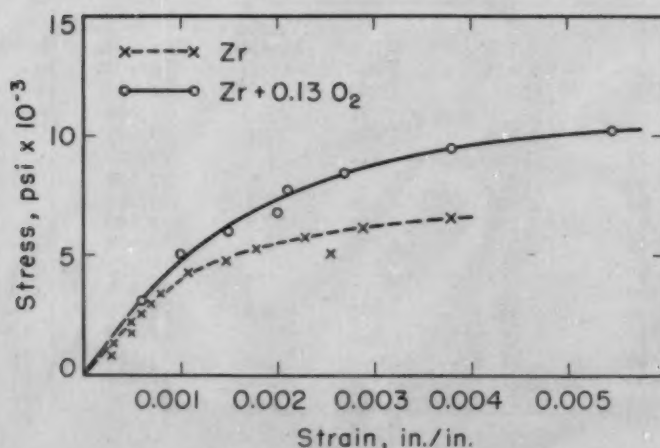


Fig. 12—Stress-Strain Curve 300 °C.

while Table V shows the results for the pure zirconium. These results indicate that the very pure, degassed zirconium is much softer and more ductile than previous values in the literature have shown. As a result, the values for the oxygen alloys must be considered only in relation to the control samples.

Fig. 9 summarizes the elevated temperature properties of the two sets of samples, alloy and pure metal. It will be seen that the ultimate strength of the alloy is greater at all temperatures, but that the difference is greatest at room temperature, while at 400 °C (750 °F) the difference is small, indicating that the 0.13% alloy loses strength more rapidly than pure zirconium as the temperature

is increased. In the case of the 0.2% yield strength, the picture is not quite so bad, since the alloy has about double the strength of the pure metal at 300 °C (570 °F).

In ductility, of course, the alloy, being harder, lags behind the pure metal. However, the picture is still encouraging since ductility of both is ample at elevated temperatures.

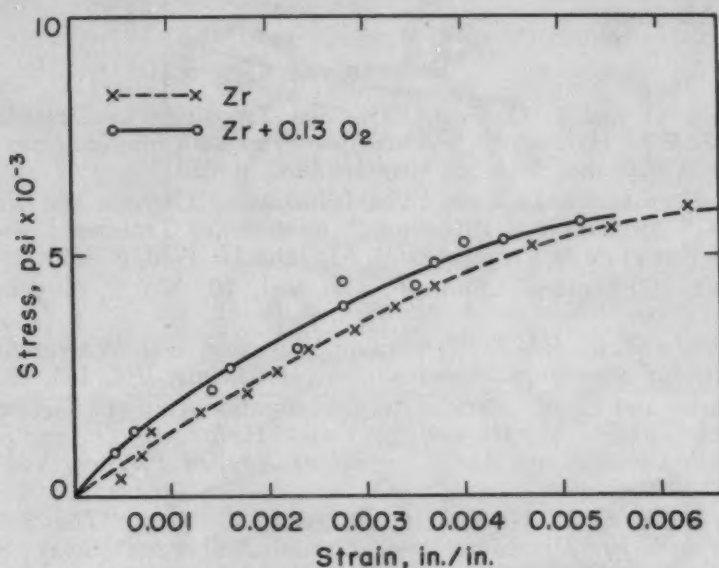


Fig. 13—Stress-Strain Curve 400 °C.

These curves also show the advantages of hot working the alloys above 300 °C (570 °F) where the yield strength is low and ductility great.

Figs. 10, 11, 12 and 13 show relative stress-strain curves of pure zirconium and the 0.13% O₂ alloy at each of the testing temperatures employed. It is apparent that there can be no definite yield point for the higher temperature tests.

SUMMARY

It has been shown that the strength properties of pure crystal bar zirconium are enhanced by the addition of small amounts of oxygen with resistivity and ductility only slightly impaired, while larger amounts produce brittleness.

The oxygen alloys were found to have good working properties and are comparable to pure zirconium in this respect.

Tensile properties at elevated temperature have been compared for the 0.13 weight per cent alloy and pure zirconium. It is shown that strength at elevated temperatures is increased by the addition of oxygen.

In addition, the techniques for producing these alloys are discussed in some detail.

ACKNOWLEDGMENT

The author wishes to express his appreciation to Dr. Albert R. Kaufmann for his inspiring guidance in the development of zirconium metallurgy and to the following men who played a large part in the preparation and testing of these alloys: C. E. Latham-Brown, P. J. Femino, A. Giordano, D. Centauro, Dr. T. T. Magel, E. B. Read and L. R. Allen.

References

1. J. H. de Boer and J. D. Fast, "The α - β Transition in Zirconium in the Presence of Hydrogen", *Recueil des Travaux Chimiques des Pays-Bas et de la Belgique*, Vol. 55, May 15, 1936, p. 350.
2. J. H. de Boer and J. D. Fast, "The Influence of Oxygen and Nitrogen on the α - β Transition of Zirconium", *Recueil des Travaux Chimiques des Pays-Bas et de la Belgique*, Vol. 55, June 15, 1936, p. 459.
3. J. D. Fast, "Zirconium", *Foot-Prints*, Vol. 10, No. 2, December 1937, p. 1.
4. A. Sieverts and E. Roell, "Zirkonium, Thorium und Wasserstoff", *Zeitschrift für anorganische und allgemeine Chemie*, Vol. 153, 1926, p. 289.
5. L. F. Ehrke and C. M. Slack, "An Investigation Into the Gettering Powers of Various Metals for the Gases Hydrogen, Oxygen, Nitrogen, Carbon Dioxide and Air", *Journal of Applied Physics*, Vol. 11, February 1940, p. 129.
6. M. N. A. Hall, S. L. H. Martin and A. L. G. Rees, "The Solubility of Hydrogen in Zirconium and Zirconium-Oxygen Solid Solutions", *Transactions*, Faraday Society, Vol. 41, 1945, p. 306.
7. E. A. Gulbransen and K. F. Andrew, "Kinetics of the Reactions of Zirconium With O_2 , N_2 and H_2 ", *Transactions*, American Institute of Mining and Metallurgical Engineers, Vol. 185, August 1949, p. 515.
8. T. T. Magel. Private communication to the author.
9. S. Dushman, "Scientific Foundations of Vacuum Technique", 1949, p. 583-584 and 670-673. John Wiley & Sons, Inc., New York.
10. E. B. Read and L. P. Zepatti, "Determination of Oxygen in Zirconium Metal", *U. S. Atomic Energy Commission Document*, AECD-2798, no publication date, declassified Feb. 14, 1950. 10 pages.
11. A. E. van Arkel, editor, "Reine Metalle", 1939, 574 pages. Julius Springer, Berlin, Germany.
12. F. W. Boulger, "The Properties of Zirconium", *U. S. Atomic Energy Commission Document*, AECD-2726, March 15, 1949, p. 13 and 15.
13. J. H. de Boer and J. D. Fast, "Electrolysis of Solid Solutions of Oxygen in Metallic Zirconium", *Recueil des Travaux Chimiques des Pays-Bas et de la Belgique*, Vol. 59, February 1940, p. 161.
14. R. M. Barrer, "Diffusion in and Through Solids", 1941, Cambridge University Press, Cambridge, England.

DISCUSSION

Written Discussion: By J. H. Keeler, Metallurgy Research Department, General Electric Company, The Knolls, Schenectady, N. Y.

There is a great need for information concerning the influence of oxygen on the properties of zirconium, and the author has made a worth-while contribution to the literature.

It should be pointed out that all crystal-bar zirconium does not have

to be degassed before substantial cold reduction. A number of investigators have reported considerable reduction without prior degassing, and at the General Electric Research Laboratory we have cold-rolled crystal-bar zirconium about 99.8% to a thickness of slightly less than 0.001 inch without degassing or any intermediate anneals.

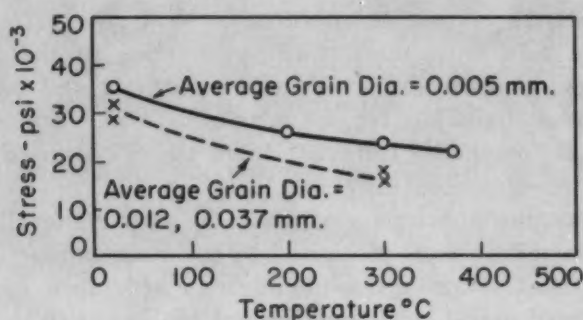


Fig. 14—Higher Ultimate Strength Exhibited by Specimens Having Larger Grain Size.

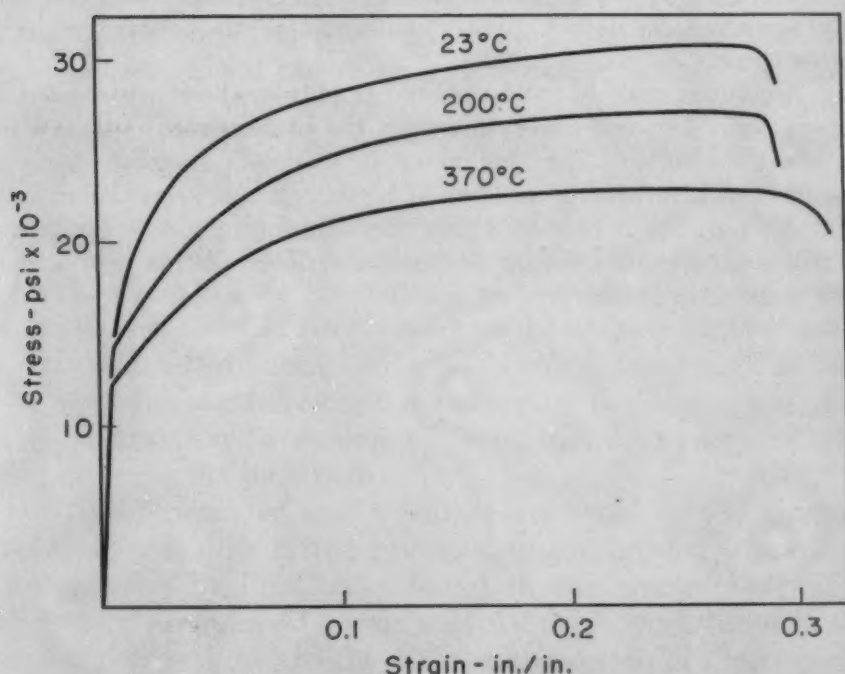


Fig. 15—Yield Point Effect, as Shown by Sudden Drop in Stress-Strain Curve, Occurs With Fine-Grained Specimens.

Could the author tell us the grain size of his crystal-bar tensile specimens? We have found that large-grained material exhibits lower strength values in the 25 to 300 °C temperature range than does fine-grained material as shown in Fig. 14.

In our tests between 200 and 370 °C, we observed in fine-grained specimens a more or less sudden change in slope of the stress-strain curve (Fig. 15) which was interpreted as a yield point effect. This yield point effect was not observed at room temperature or in the coarse-grained

specimens. Perhaps the specimens in the tests reported by Mr. Treco were coarse-grained and thus did not exhibit a yield point.

Author's Reply

It is interesting to note that Mr. Keeler has observed a grain-size effect in zirconium on both ultimate strength and the yield point phenomena, which varies with testing temperature. While no attempt was made to correlate grain size with mechanical properties in the present work, there did not appear to be any grain size effect for the oxygen alloy of Table IV. Specimens from bar No. 9A which were fine-grained (0.050 mm) do not appear to be markedly different from those obtained from bar No. 9D which was coarse-grained (0.200 mm).

The pure zirconium specimens of Table V were generally fine-grained since the heat treatments were designed to produce similar structures. It is true, however, that strain-aging phenomena are more likely to be observed in fine-grained metal, and some recent high sensitivity tensile work⁴ on pure titanium has shown a similar yield point phenomena on very fine-grained metal at temperatures greater than about 120 °C. The method of strain measurement in the zirconium-oxygen alloys may not have been sufficiently sensitive to detect such phenomena if they occurred above room temperature.

Iodide zirconium may be cold-reduced readily without a previous degassing operation. In some cases, however, the presence of hydrogen may seriously affect ductility. For this work it was necessary to degas for other reasons, and a surprising amount of hydrogen was removed from the original crystal bar. It is probable that the amount of gas depends upon the equilibrium conditions existing during reduction and this may account for variable quality in iodide process metal.

⁴F. D. Rosi, F. C. Perkins and B. H. Alexander, "Mechanical Properties of Titanium", Report No. YE52-0451, Sylvania Electric Products Inc., Bayside, N. Y.

THE ZIRCONIUM-NICKEL PHASE DIAGRAM

BY E. T. HAYES, A. H. ROBERSON AND O. G. PAASCHE

Abstract

A diagram for the zirconium-rich portion of the zirconium-nickel system has been developed which shows a very limited solubility of nickel in alpha zirconium at room temperature. The maximum solubility of nickel in beta zirconium is 1.9% at 961 °C (1762 °F). Two intermediate phases are recognized and tentatively identified as Zr_2Ni (24.4% Ni) and $ZrNi$ (39.2% Ni). Eutectic reactions occur at 17% nickel and 961 °C (1762 °F) and 27% nickel and 985 °C (1805 °F).

RESEARCH to enhance the physical properties of ductile zirconium by alloy additions is receiving ever-increasing attention as it becomes evident that zirconium, like its sister metal titanium, is destined to become available for everyday engineering use. However, before any new metal can reach its ultimate effective use, data regarding basic fundamental properties and relationships with other metals must be established. The paucity of information on zirconium phase diagrams led the Bureau of Mines, U. S. Department of the Interior, and the Air Matériel Command into a cooperative program designed to provide a firm base for alloy development and further study of mechanical properties. Previously published reports on a portion of this work include the zirconium-iron (1),¹ zirconium-titanium (2), and zirconium-chromium (3) equilibrium diagrams. The zirconium-nickel series presented herein was studied because it was hoped that nickel, in addition to raising the mechanical strength of zirconium, might improve the heat resistance.

In the absence of any literature reference to the zirconium-rich portions of the system, the preliminary assumption was made that it resembled the Fe-Fe₃C type found in the zirconium-iron (1) and zirconium-chromium (3) systems. All prior work listed in the literature was directed toward the nickel-rich portion of the system.

Wallbaum (4) made a few cursory studies of the nickel-rich area and noted the presence of $ZrNi_3$. Likewise, Allibone and Sykes (5) surveyed the same portion of the diagram. The validity of their work is questionable, since their melting crucibles were made of alundum,

¹The figures appearing in parentheses pertain to the references appended to this paper.

A paper presented before the Eighth Western Metal Congress of the Society, held in Los Angeles, March 23 to 27, 1953. Of the authors, E. T. Hayes and A. H. Roberson are metallurgists, Federal Bureau of Mines, Albany, Ore.; O. G. Paasche is a metallurgist, W.A.E., Bureau of Mines, and associate professor of mechanical engineering, Oregon State College, Corvallis, Ore. Manuscript received July 10, 1952.

which undoubtedly introduced appreciable amounts of aluminum and oxygen into their alloys.

The diagram shown by Hansen (6) indicates the presence of a eutectic at about 45% nickel. However, this is outside the range of the present investigation and was not verified.

PREPARATION OF ALLOYS

The alloys used in this investigation were prepared from high-grade zirconium sponge produced by magnesium reduction of zirconium tetrachloride. A typical analysis of this material showed the following values: O₂, 0.08%; Fe, 0.06%; N₂, 0.01%; C, 0.02%; and other impurities, such as Pb, Ti, Si, Ni, and Al, less than 0.01% each. Nickel was added in the form of foil normally used as plate caps in radio-transmission tubes.

All alloys were prepared by melting 50-gram compacts in a Kroll-type (7) arc furnace in an inert atmosphere. The furnace was evacuated twice and back-filled with helium, which was gettered by melting a center zirconium button immediately before the alloys were melted. Each alloy was remelted at least once to promote homogeneity.

Specimens containing up to 4% nickel could be rolled at 850 °C (1560 °F). After a soaking period of 120 hours at 950 °C (1740 °F), they were encased in an iron sheath and rolled to 0.080-inch sheet. The rolled sheet was cut into convenient-size specimens, which were again sealed in quartz tubing, heated for 120 hours, and water-quenched. The quenched specimens were reheated to selected temperatures and cooled at various rates.

Above 4% nickel the as-cast buttons were sealed in quartz, homogenized for 120 hours at 950 °C (1740 °F), and water-quenched. Suitable specimens were cut from the ingots, resealed in quartz, and given the same heat treatments as the rolled samples.

A total of over 200 alloys was prepared during the investigation. The more pertinent compositions are shown in Table I.

Table I
Alloy Composition

Alloy No.	% Ni	Alloy No.	% Ni
1739	0.43	3429	2.50
3408	0.52	3430	3.00
3409	0.80	3431	3.9
1745	1.0	1783	4.7
3411	1.06	1779	7.2
3410	1.32	1787	7.8
3412	1.40	1789	9.6
3426	1.45	1793	14.9
3427	1.73	1794	20.0
1741	1.90	1795	29.7
3413	1.95	1797	39.6
3428	2.00	1800	49.9
3414	2.15	1802	59.3

Differential thermal analysis was used to determine the eutectoid temperature. A Leeds & Northrup X-Y recorder simultaneously plotted specimen temperature versus temperature differential between the specimen and a nickel neutral body. A temperature difference of 2.5°C produced a deflection of 1 inch on the Y axis of the recorder. All chromel-alumel couples were checked against a Bureau of Standards secondary standard thermocouple. Uniform heating and cooling rates of 5°C per minute were obtained by using a Wheelco program controller. All measurements were made in vacuum (less than 1 micron) or in purified helium.

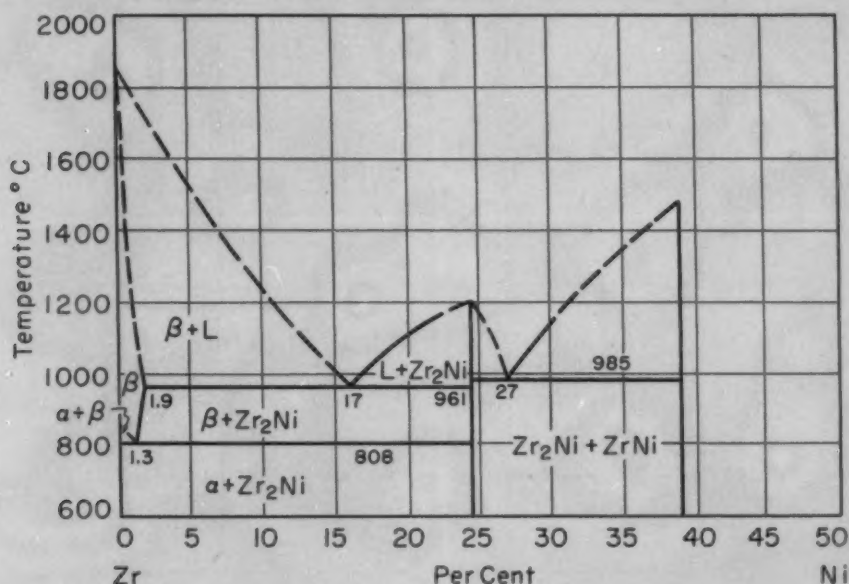


Fig. 1—Zirconium-Nickel Equilibrium Diagram.

Melting points of the eutectics and the compounds were measured in a high-vacuum induction furnace, using an optical pyrometer. Pyrometer readings were taken on the bottom of a hole drilled in the sample to determine the onset of melting. When the material could not be drilled, wedge-shaped openings about $\frac{3}{8}$ inch deep were filed in the specimens. A marked decrease in the heating rate at the instant of melting was detected readily by this method, and data could be reproduced with an accuracy of plus or minus 10°C .

X-ray diffraction patterns were obtained with a North American Philips recording Geiger spectrometer. Both powdered and bakelite-mounted specimens were used in this work.

CONSTITUTION DIAGRAM

The diagram developed by this research is shown in Fig. 1. The solubility of nickel in alpha zirconium was not determined precisely, since it was believed to be very small. The presence of small amounts of iron in the starting materials obviated the possibility of

using metallographic techniques, since the presence of the Zr-Fe eutectoid masked any effects of small nickel additions. X-ray diffraction patterns of 0.43% nickel alloys showed no detectable change from that of pure zirconium, indicating a very low solubility of nickel.

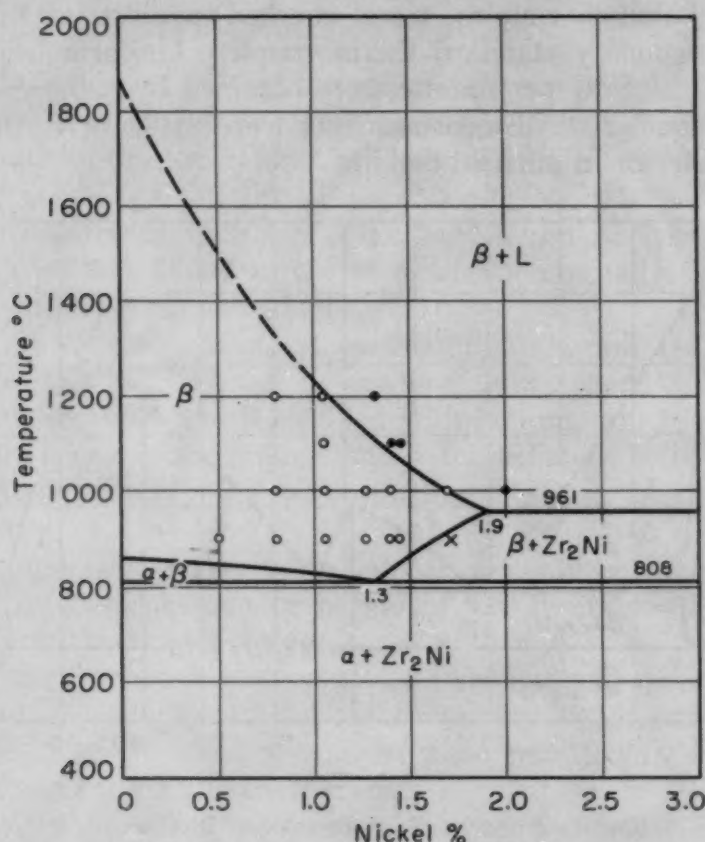


Fig. 2—Beta Field of the Zirconium-Nickel Equilibrium Diagram.

Outlining the beta field depended entirely on metallographic techniques, since the beta phase could not be retained by any of the quenching methods used, thus eliminating any possible use of X-ray diffraction studies. Specimens were heated at varying temperature levels and water-quenched. All specimens exhibiting a 100% transformed beta structure were considered to have been beta at the temperature from which the specimen was quenched. The acicular structure of transformed beta is similar to that of martensite in steel and results from the polymorphic transformation at high temperatures. The typical Widmanstätten pattern of the acicular alpha grains (transformed beta) is shown in Fig. 3.

The results of quenching and slow cooling selected alloys from various temperature levels are depicted in the detailed diagram of the beta field shown in Fig. 2.

The presence of a second phase, which occurred as a finely

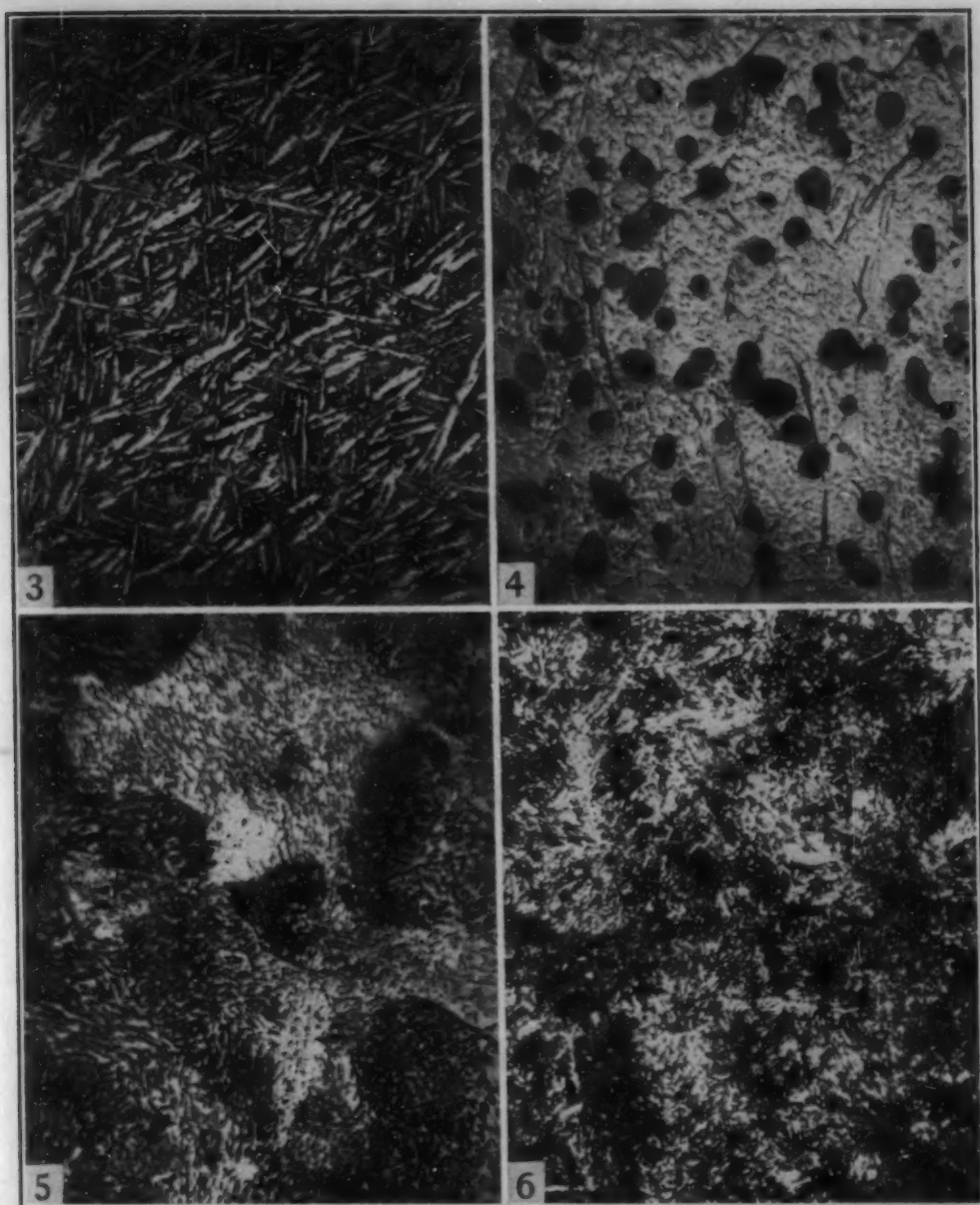


Fig. 3—Acicular Alpha Grains (Decomposed Beta), 1.3% Nickel, Quenched From 950 °C. $\times 500$.

Fig. 4—Alpha (Beta at Temperature) With Zr_2Ni , 1.95% Nickel, Quenched From 850 °C. $\times 500$.

Fig. 5—Eutectoid 1.3% Nickel, Rapidly Cooled From 950 °C. $\times 500$.

Fig. 6—First Eutectic (Beta Plus Zr_2Ni) As-Cast. $\times 500$.

All specimens etched with Vilella's reagent.

divided random precipitate, was first observed in the 1.9% nickel alloy quenched from 950 °C (1740 °F) and indicated that the solubility of nickel in beta zirconium probably did not exceed 1.9% at the eutectic temperature (961 °C). Fig. 4 shows a typical area of the quenched 1.95% alloy, with the Zr_2Ni precipitated in a beta matrix.

Furnace cooling the alloys showed that the beta phase decom-

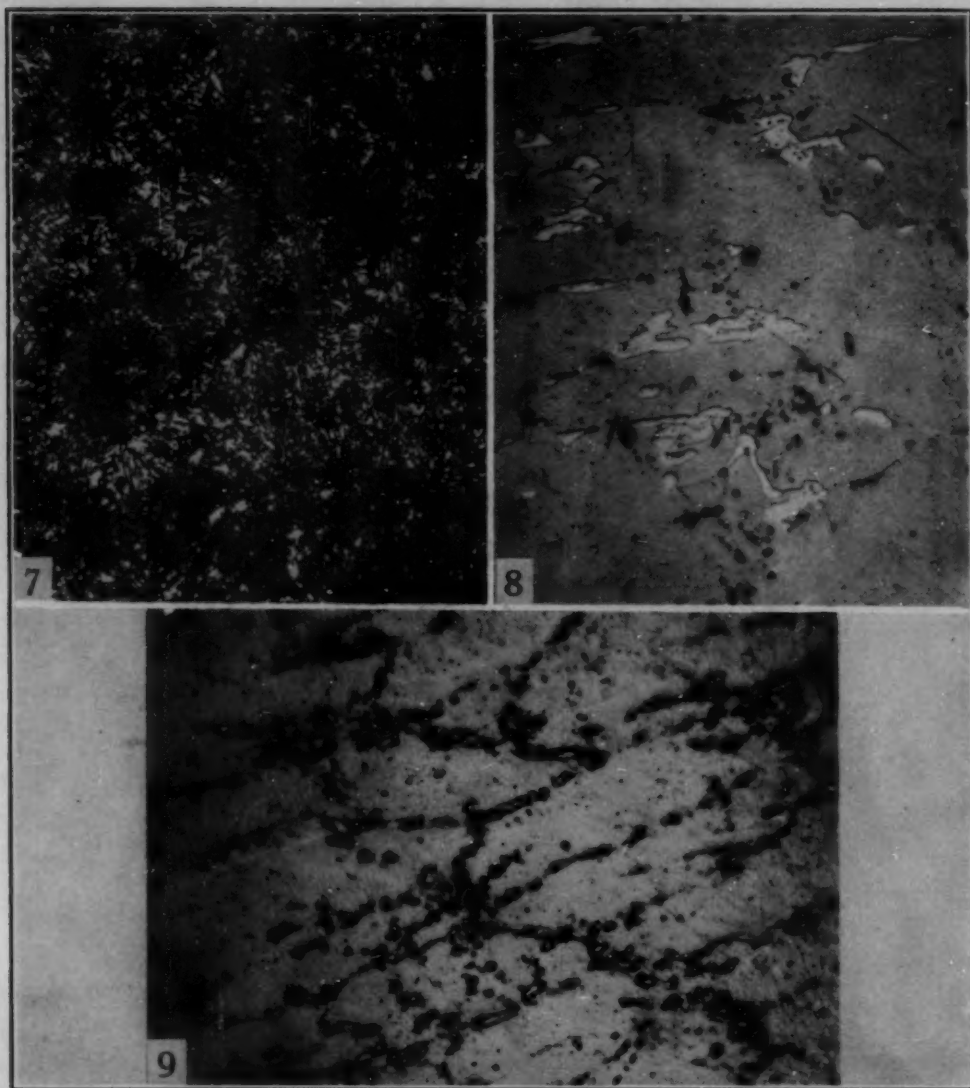


Fig. 7—Second Eutectic ($Zr_2Ni + ZrNi$) As-Cast. $\times 500$.

Fig. 8—Intermediate Phase Zr_2Ni As-Cast. $\times 500$.

Fig. 9—Intermediate Phase $ZrNi$ As-Cast. $\times 500$.

All specimens etched with Vilella's reagent.

posed eutectoidally. The eutectoid composition was shown to be 1.3% nickel.

The eutectoid structure was best developed in rapidly cooled specimens, the optimum structure development being produced by removing the specimens from the furnace while they were still encased in quartz and placing them in front of a blower.

Fig. 5 shows the typical structure of the 1.3% alloy, which was cooled as described above.

Thermal analysis studies placed the eutectoid temperature at $808 \pm 5^\circ C$. The alpha plus beta field was tentatively established by extrapolating from the transformation temperature of zirconium ($862^\circ C$) to the eutectoid composition and temperature (1.3% nickel

and 808 °C). This tentative establishment was made necessary by the known presence of about 0.08% oxygen in the zirconium. De Boer and Fast (8) showed that even small amounts of oxygen might cause significant shifts in the transformation range, and data obtained by thermal analysis indicated that the transition temperature was as much as 50 °C above the accepted values.

Metallographic examination of homogenized as-cast structures placed the eutectic of beta zirconium, Zr_2Ni , at 17% nickel. Fig. 6 is typical of the appearance of a representative homogenized 17% alloy. Melting point studies established the eutectic temperature at 961 °C (1762 °F). Unlike its Zr-Fe and Zr-Cr predecessors, which showed only one intermediate phase ZrX_2 , the zirconium-nickel system instead shows two compounds, Zr_2Ni and $ZrNi$. Zr_2Ni , containing 24.4 weight % nickel, has a melting point in the vicinity of 1200 °C (2190 °F). This compound forms a eutectic with the next intermediate phase, $ZrNi$ (39.2% nickel), at 27% nickel and 985 °C (1805 °F). The typical structure of this second eutectic is illustrated in Fig. 7. The melting point of Zr-Ni is about 1470 °C (2680 °F). Diagram studies were not carried beyond this point. The microstructures of the two intermediate phases are shown in Figs. 8 and 9, respectively. The presence of minor constituents is the result of small variations from the theoretical compositions. The location of both eutectics and compounds was accomplished by metallographic examination of homogenized cast specimens.

Numerous heat treated samples were examined by X-ray diffraction but neither phase was positively identified as to actual structure. The fact that the two zirconium-rich eutectics have melting points within 25 °C of one another can be classed only as a coincidence, since the metallographic evidence and melting points of the two compounds preclude the extended solubility-type system encountered in titanium-chromium or a peritectic-type reaction.

SUMMARY

An investigation of the zirconium-nickel system covering composition ranges up to 40% nickel was accomplished, and the following salient features were established:

1. Negligible solubility of nickel in zirconium at room temperature.
2. Eutectoidal decomposition of the beta solid solution at 1.3% nickel and 808 °C (1486 °F).
3. The maximum solubility of nickel in beta zirconium is about 1.9% at the eutectic temperature (961 °C).
4. Presence of an intermediate phase at 24.4% nickel. This phase, believed to be Zr_2Ni , has a melting point near 1200 °C (2190 °F).

5. A eutectic reaction occurs between beta zirconium and the intermediate phase Zr_2Ni at 17% nickel and 961 °C (1762 °F).

6. A second intermediate phase was located at 39.2% nickel and tentatively identified as $ZrNi$. This compound melted at approximately 1470 °C (2680 °F).

7. Between the two intermediate compounds a eutectic was located at 27% nickel and 985 °C (1805 °F).

ACKNOWLEDGMENTS

The authors wish to express their appreciation to the Air Matériel Command, Wright-Patterson Air Force Base, which sponsored this work and granted permission for its publication. The assistance of the following co-workers likewise is gratefully acknowledged: W. L. O'Brien and H. G. Anderson, metallography; R. L. Carpenter, thermal analysis; D. M. Deardorff, melting point studies; and P. F. Francoeur, alloy preparation.

References

1. E. T. Hayes, A. H. Roberson and W. L. O'Brien, "Constitution and Mechanical Properties of Zirconium-Iron Alloys", *TRANSACTIONS, American Society for Metals*, Vol. 43, 1951, p. 888-904.
2. E. T. Hayes, A. H. Roberson and O. G. Paasche, "Zirconium-Titanium System—Constitution and Properties", Bureau of Mines, Report of Investigation 4826, 1951.
3. E. T. Hayes, A. H. Roberson and M. H. Davies, "Zirconium-Chromium Phase Diagram", *Journal of Metals*, March 1952, p. 304-306.
4. H. J. Wallbaum, "The Systems of the Iron Metals With Titanium, Zirconium, Columbium and Tantalum", *Archiv für das Eisenhüttenwesen*, Vol. 14, 1941, p. 521-526.
5. T. E. Allibone and C. Sykes, *Journal, Institute of Metals*, Vol. 39, 1928, p. 179-182.
6. Max Hansen, "Aufbau der Zweistofflegierungen", Edwards Brothers, Inc., Ann Arbor, Mich., 1943, p. 969.
7. W. J. Kroll, "The Production of Ductile Titanium", *Transactions, Electrochemical Society*, Vol. 78, 1941, p. 35-47.
8. J. H. De Boer and J. D. Fast, "The Influence of Oxygen on the Alpha-Beta Transition of Zirconium", *Recueil des Travaux Chimiques des Pays-bas*, Vol. 59, 1940, p. 161-167.

THE SYSTEM ZIRCONIUM-SILICON

BY C. E. LUNDIN, D. J. MCPHERSON AND M. HANSEN

Abstract

The phase diagram of the zirconium-silicon system was determined, with particular emphasis on the zirconium-rich portion. The principal methods used were metallography of cast and heat treated specimens, detection of incipient melting, thermal analysis, and X-ray diffraction analysis. The alloys were prepared under protective helium atmospheres in a nonconsumable electrode arc furnace.

THE zirconium-silicon phase diagram was developed in conjunction with the study of seven other zirconium binary systems under the sponsorship of the Atomic Energy Commission. No previous diagram exists. Limited information (1)¹ exists concerning the intermetallic compound ZrSi_2 (38.09 weight per cent silicon). The structure is reported to be orthorhombic, with lattice constants: $a = 3.72 \text{ \AA}$, $b = 14.61 \text{ \AA}$, $c = 3.67 \text{ \AA}$.

EXPERIMENTAL PROCEDURE

Materials

Westinghouse "Grade 3" iodide zirconium crystal bar (nominally 99.8% pure) was sand-blasted and pickled in HF-HNO_3 solution to remove the surface film of corrosion product, resulting from grade designation tests. The crystal bar was cold-rolled to strip, pickled again for iron removal, and cut into squares approximately $\frac{1}{32}$ inch thick and $\frac{1}{4}$ inch square. These platelets were then cleaned in acetone, dried, and stored for furnace charging.

High purity silicon, 99.99%, in the form of pyrolytic crystals, was obtained from duPont and Johnson Matthey and Company. The crystals were of appropriate size for arc furnace charging and required no further preparation. Another grade of silicon, used in alloys

¹The figures appearing in parentheses pertain to the references appended to this paper.

This paper is based on a portion of the work carried out at Armour Research Foundation for the Atomic Energy Commission under Contract No. AT(11-1)-149, "Phase Diagrams of Zirconium-Base Binary Alloys". Final Report No. (C00-89).

A paper presented before the Eighth Western Metal Congress of the Society, held in Los Angeles, March 23 to 27, 1953. Of the authors, C. E. Lundin is metallurgical engineer, Dow Chemical Company, Rocky Flats Plant, Denver, Colo.; D. J. McPherson is supervisor of physical metallurgy research, and M. Hansen is chairman, Metals Research Department, Armour Research Foundation of Illinois Institute of Technology, Chicago. Manuscript received April 9, 1952.

containing more than 50 atomic per cent of this element, was 80-mesh Electro Metallurgical Corporation silicon powder of 99.9% purity. This material was not suitable for the arc furnace, so it was consolidated by premelting in an atomic hydrogen arc and then crushed to $-\frac{1}{4}$ -inch granules for charging stock.

Equipment and Procedures

The element zirconium is closely related to titanium in physical properties and, accordingly, the same precautions for melting and heat treating zirconium binary alloys and special techniques for phase diagram determination are required. Equipment for melting and annealing such alloys and for the determination of melting points and solidus curves under highly protective conditions has been described in an investigation of the titanium-silicon system (2) and in a concurrent paper dealing with zirconium-tin alloys (3).

Twenty-gram ingots of the alloys were prepared by arc melting with a tungsten electrode in a water-cooled copper block under a

Table I
Pretreatment* and Annealing Data for Zirconium-Silicon Alloys

Annealing Temperature, °C	Alloys, % Silicon	Hours at Temperature
1467	0-0.4, 1, 5, 10, 15, 20, 35	$\frac{1}{2}$
1400	0-0.4, 1, 5, 10, 12, 24	$\frac{1}{2}$
1300	0-0.4, 1, 5, 10, 15	1
1200	0-13, 15, 17	6
1100	0-13	16
1000	0-13, 15, 17, 21, 24, 30, 35	24
900	0-13, 15, 17, 20, 24	50
875	0-13	100
850	0-13	100
825	0-13	100
800	0-13, 15, 20, 24, 30, 35	100
700	0-0.4, 0.6, 0.8, 1, 5, 7, 10, 13	250

*Prior to the tabulated isothermal anneals, specimens were cold-pressed 0 to 55%, homogenized 50 hours at 1150 °C, then reduced by cold rolling 0 to 89%. The largest cold reductions were obtained with the most dilute alloys. Alloys with more than 7% silicon were not amenable to any cold reduction.

protective atmosphere of high purity helium. The alloys were inverted and melted four times without opening the furnace.

Alloy ingots were homogenized and cold-worked to the maximum extent possible prior to isothermal annealing.

Specimens were annealed in Vycor or quartz bulbs sealed in vacuo or under argon, depending upon the temperature of treatment. Molybdenum liners were used for some high temperature anneals. Quenching was accomplished by breaking the annealing bulbs under water. Temperature control was within ± 3 °C of the reported temperatures. A schedule of pretreatment and annealing data for zirconium-silicon alloys is presented in Table I.

The melting points of the metals and intermetallic compounds,

and eutectic and peritectic temperatures were determined by the metallographic detection of incipient melting in specimens quenched in a high temperature vacuum induction furnace, and, independently, by thermal analysis for temperatures under 1650 °C (3000 °F). Furnaces and techniques for both methods have been described in detail (2).

RESULTS AND DISCUSSION

The Phase Diagram

The addition of a small increment of silicon by weight to zirconium causes a rather large shift in the atomic per cent silicon. This

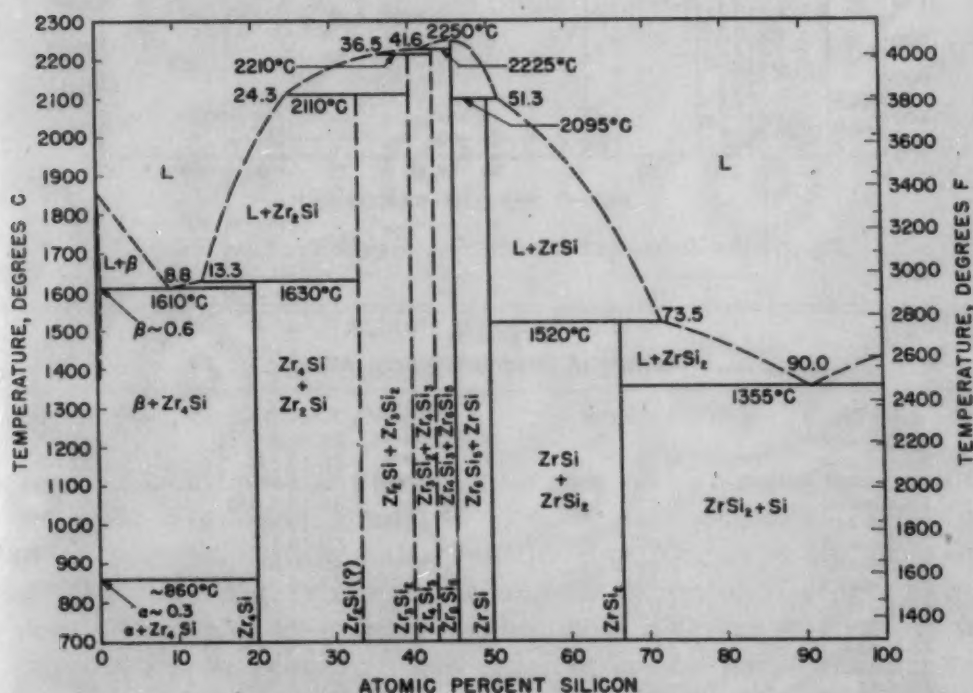


Fig. 1—The Zirconium-Silicon System, Atomic Per Cent Silicon.

is more prominent in the zirconium-rich portion of the diagram, and manifests itself by a crowding of phase fields on a weight per cent diagram toward the zirconium end. Accordingly, it was necessary to prepare many alloys in small increments of silicon by weight to completely survey the phase fields. The contracted scope of work for this system was to determine the phase diagram from 0 to 50 atomic per cent (23.53 weight per cent) silicon. However, a sufficient number of alloys were cast to survey the entire binary system.

Figs. 1 and 2 represent the phase diagram on an atomic and weight per cent basis, respectively. Analyses of the zirconium-silicon alloys are presented in Table II.

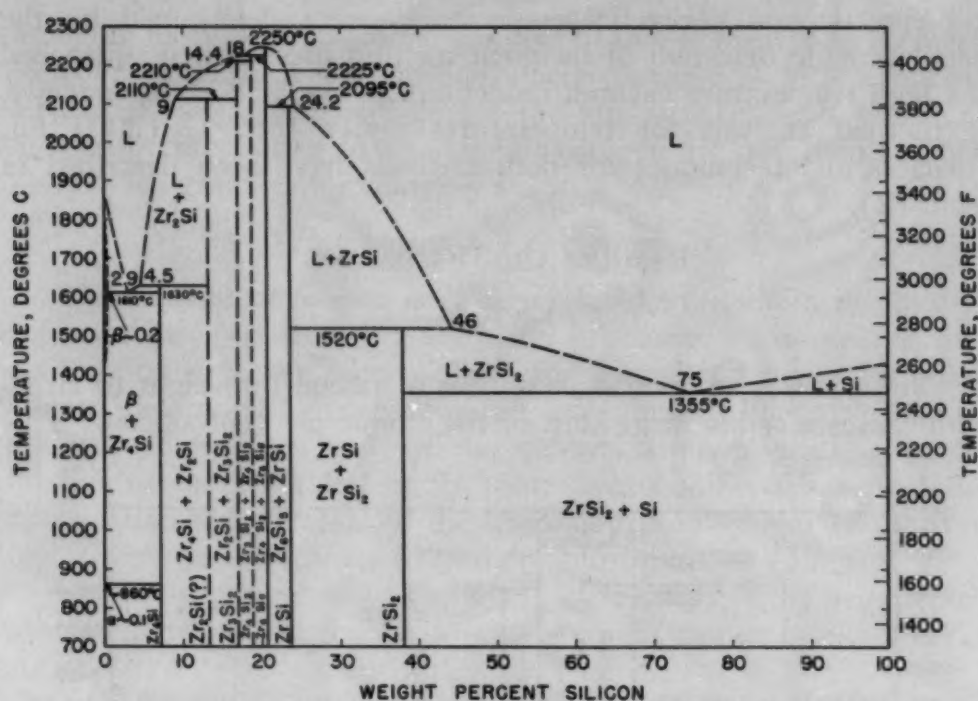


Fig. 2—The Zirconium-Silicon System, Weight Per Cent Silicon.

Table II
Analyses of Zirconium-Silicon Alloys

Alloy No.	Wt. % Silicon	Alloy No.	Wt. % Silicon
ZS-0.1-463	0.02	ZS-16-853	15.5
ZS-0.2-464	0.18	ZS-17-549	17.7
ZS-0.3-465	0.29	ZS-18-854	17.6
ZS-0.4-466	0.42	ZS-18.5-856	18.7
ZS-0.5-467	0.47	ZS-19-855	19.1
ZS-0.6-439	0.60	ZS-19.5-857	19.3
ZS-0.7-468	0.65	ZS-20-413	19.5
ZS-0.8-440	0.78	ZS-20.5-862	20.1
ZS-1-441	1.0	ZS-21-548	20.5
ZS-2-450	2.1	ZS-21.5-859	21.0
ZS-3-451	2.9	ZS-22-547	22.3
ZS-4-452	4.1	ZS-22.5-860	22.8
ZS-5-453	4.9	ZS-23-595	22.4
ZS-5-409	4.7	ZS-23.5-861	23.5
ZS-6-454	5.9	ZS-24-545	24.4
ZS-7-455	7.2	ZS-24.5-863	24.3
ZS-7-555	7.4	ZS-25-414	24.6
ZS-8-456	7.7	ZS-26-544	25.5
ZS-8-554	8.4	ZS-28-543	27.4
ZS-9-457	9.2	ZS-30-415	29.1
ZS-10-458	10.3	ZS-35-416	36.1
ZS-10-410	10.4	ZS-45-417	45.6
ZS-10-412	10.7	ZS-55-418	54.9
ZS-11-553	11.7	ZS-65-419	65.2
ZS-12-552	11.3	ZS-75-420	76.1
ZS-13-594	13.3	ZS-85-422	84.5
ZS-14-550	14.3	ZS-95-423	95.6
ZS-15-411	14.5

Alloys Dilute in Silicon

Fig. 3, containing the results of the isothermal anneals, shows the zirconium-rich region of the diagram on an expanded scale.

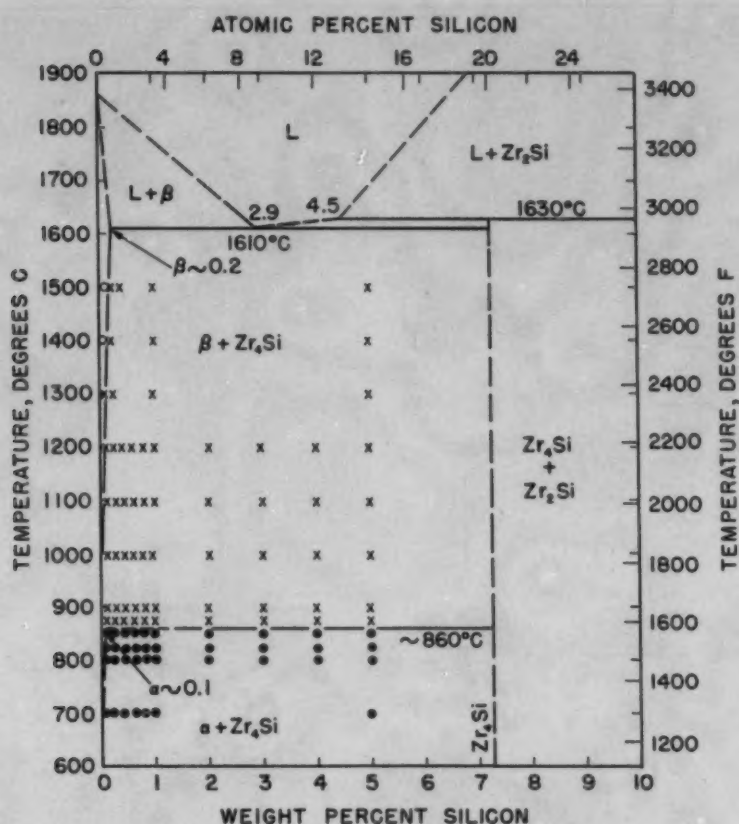


Fig. 3—The Constitution of Zirconium-Rich Zirconium-Silicon Alloys.

The allotropic transformation, $\alpha \rightleftharpoons \beta$, in zirconium has been reported by Vogel and Tonn (4) to occur at $862 \pm 5^\circ\text{C}$ (1585°F), and is accepted by the authors in the construction of the diagrams. Investigations were made on the transformation of "Grade 3" zirconium crystal bar preliminary to the phase diagram studies. It was found that specimens from five different crystal bars exhibited two-phase ($\alpha + \beta$) structures after annealing in the temperature range between 851 and 868°C (1560 and 1595°F). Because of impurity content, this grade zirconium appears to transform over a temperature range close to the ideal transition point.

Consequently, the effect of silicon additions on the allotropic transformation of zirconium could not be precisely determined because this element displays extremely limited solubility in both zirconium modifications. Three-phase structures, stemming from the above-mentioned two-phase field in unalloyed zirconium, were observed in the very dilute alloys.

The maximum solubility of silicon in beta zirconium is illustrated by a 0.18% silicon alloy quenched from 1467°C (2670°F) (Fig. 4). Crystals of Zr_4Si are present in a matrix of decomposed beta. Silicon solubility in alpha zirconium is less than 0.1%. This

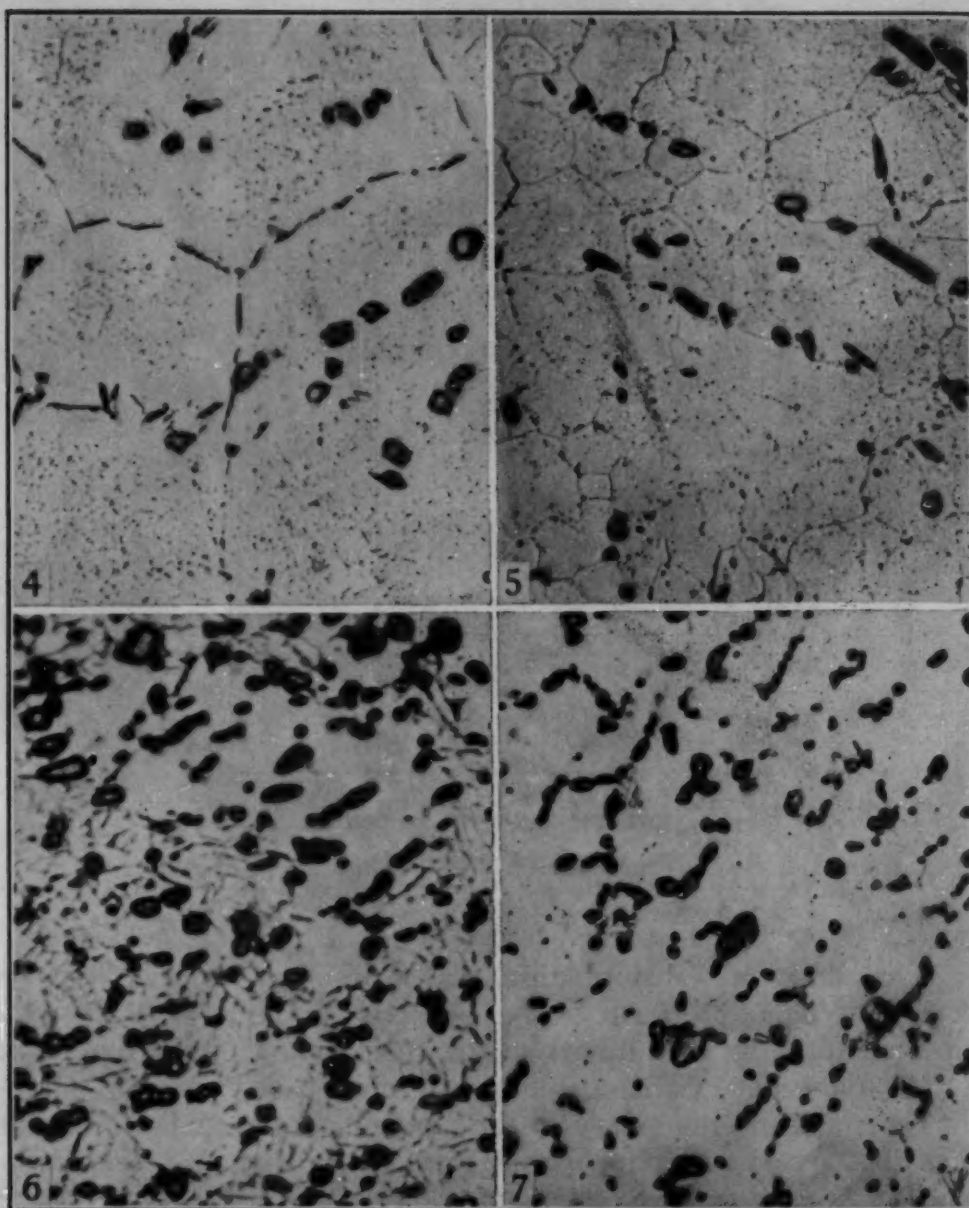


Fig. 4—0.18% Silicon Alloy, Water-Quenched After Annealing $\frac{1}{2}$ Hour at 1467 °C (2675 °F). Crystals of Zr_4Si in a matrix of decomposed beta. Limited solubility of silicon in beta zirconium evident. Etchant: 20% HNO_3 , 20% HF in glycerin. $\times 250$.

Fig. 5—0.10% Silicon Alloy, Water-Quenched After Annealing 100 Hours at 825 °C (1515 °F). Crystals of Zr_4Si in a matrix of equiaxed alpha zirconium. Limited solubility of silicon in alpha zirconium evident. Etchant: 20% HNO_3 , 20% HF in glycerin. $\times 250$.

Fig. 6—0.60% Silicon Alloy, Water-Quenched After Annealing 100 Hours at 875 °C (1605 °F). Zr_4Si crystals in a matrix of beta zirconium. Some nonequilibrium alpha also present. Etchant: 20% HNO_3 , 20% HF in glycerin. $\times 500$.

Fig. 7—0.60% Silicon Alloy, Water-Quenched After Annealing 100 Hours at 850 °C (1560 °F). Zr_4Si crystals in a matrix of isothermal alpha. Etchant: 20% HNO_3 , 20% HF in glycerin. $\times 500$.

is shown in Fig. 5; Zr_4Si crystals are present in a matrix of isothermal alpha after an anneal at 825 °C (1515 °F). The transformation level for silicon alloys lies between 875 and 850 °C (1605 and

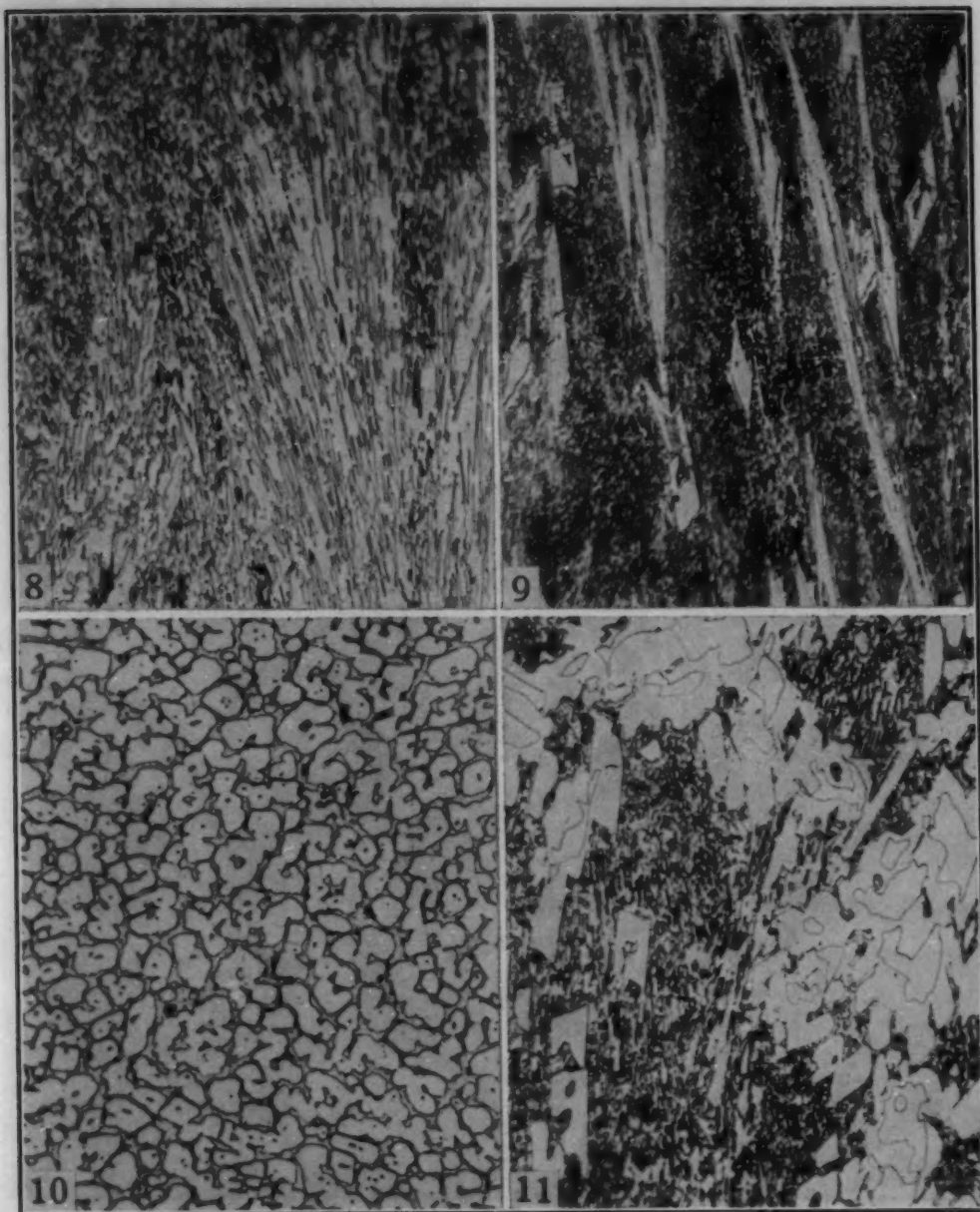


Fig. 8—2.9% Silicon Alloy, As-Cast. Structure of the eutectic, $Zr-Zr_4Si$. Etchant: 20% HNO_3 , 20% HF in glycerin. $\times 250$.

Fig. 9—4.1% Silicon Alloy, As-Cast. Primary crystals of Zr_4Si in a matrix of eutectic $Zr-Zr_4Si$. Etchant: 20% HNO_3 , 20% HF in glycerin. $\times 250$.

Fig. 10—4.9% Silicon Alloy, Water-Quenched After Annealing 6 Hours at $1200^\circ C$ ($2190^\circ F$). Predominantly Zr_4Si in a network of beta agglomerated from the annealed eutectic. Etchant: 20% HNO_3 , 20% HF in glycerin. $\times 250$.

Fig. 11—4.9% Silicon Alloy, As-Cast. Primary Zr_2Si crystals, peritectic rims of Zr_4Si in a matrix of eutectic. Etchant: 20% HNO_3 , 20% HF in glycerin. $\times 250$.

$1560^\circ F$), as shown by Figs. 6 and 7. Both are 0.60% silicon alloys; the former, quenched from $875^\circ C$ ($1605^\circ F$), contains transformed beta plus Zr_4Si , while the latter, quenched from $850^\circ C$ ($1560^\circ F$), shows equiaxed $\alpha + Zr_4Si$.

These data indicate that silicon additions to zirconium may re-

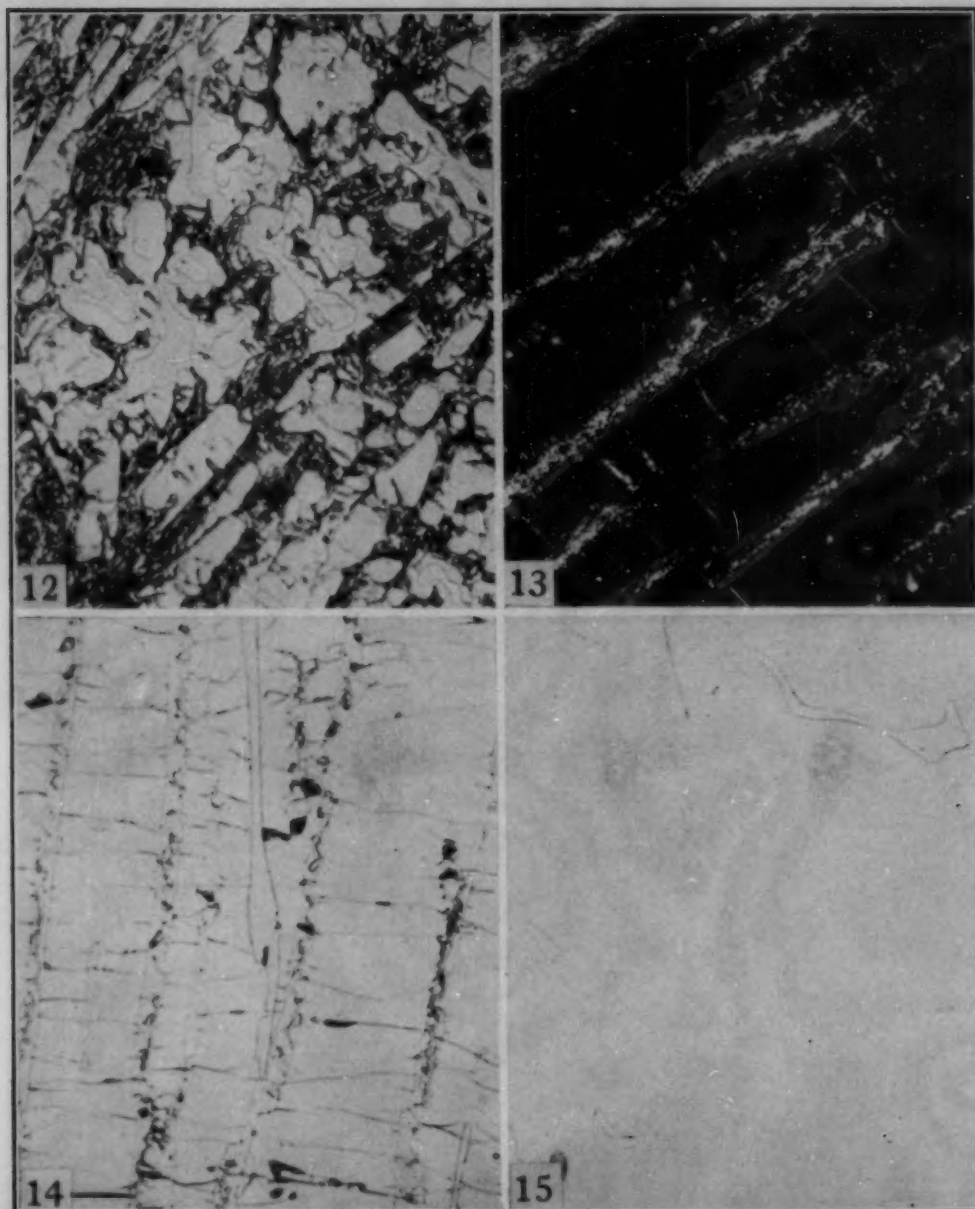


Fig. 12—9.2% Silicon Alloy, As-Cast. Primary Zr_3Si_2 crystals and peritectic rims of Zr_5Si_3 . No detectable Zr_4Si_3 rims, but appreciable residual eutectic. Etchant: 20% HNO_3 , 20% HF in glycerin. $\times 500$.

Fig. 13—14.3% Silicon Alloy, As-Cast. Cracked primary crystals of Zr_3Si_2 , peritectic rims of Zr_5Si_3 , and a small amount of residual eutectic. Unetched, polarized light. $\times 200$.

Fig. 14—14.5% Silicon Alloy, As-Cast. First appearance of Zr_4Si_3 primary crystals, cracked peritectic walls of Zr_3Si_2 , secondary rims of Zr_5Si_3 , and some eutectic. Etchant: 20% HNO_3 , 20% HF in glycerin. $\times 250$.

Fig. 15—17.6% Silicon Alloy, As-Cast. Nearly single-phase Zr_4Si_3 . Some residual Zr_3Si_2 at boundaries. Etchant: 20% HNO_3 , 20% HF in glycerin. $\times 250$.

sult in either a eutectoid or a peritectoid reaction at less than 0.1% silicon and between 850 and 875 °C (1560 and 1605 °F).

Intermediate Phases

Due to the large number of intermediate phases within a limited range of composition, the interpretation of structures and the micro-

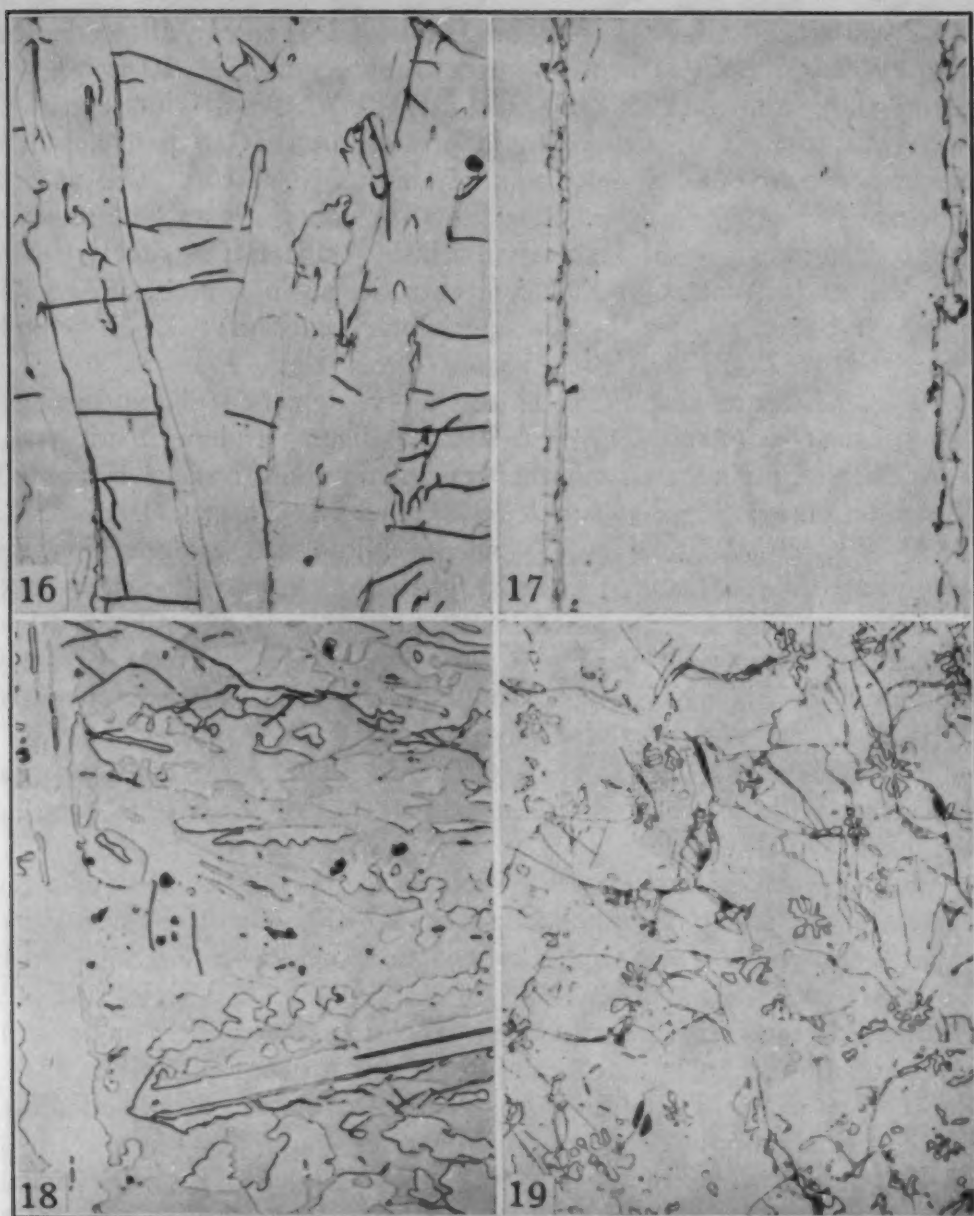


Fig. 16—18.7% Silicon Alloy, As-Cast. Primary crystals of $ZrSi_2$, rosette peritectic rims of Zr_4Si_3 , and matrix of Zr_3Si_2 . Etchant: 20% HNO_3 , 20% HF in glycerin. $\times 250$.

Fig. 17—20.1% Silicon Alloy, As-Cast. Nearly single-phase $ZrSi_2$ and peritectic rims of Zr_4Si_3 and Zr_3Si_2 . Etchant: 20% HNO_3 , 20% HF in glycerin. $\times 250$.

Fig. 18—22.3% Silicon Alloy, As-Cast. Primary $ZrSi_2$ surrounded by peritectically formed $ZrSi$. Etchant: 20% HNO_3 , 20% HF in glycerin. $\times 250$.

Fig. 19—23.5% Silicon Alloy, As-Cast. Small primary rosettes of $ZrSi_2$ in a matrix of the peritectically formed $ZrSi$. Etchant: 20% HNO_3 , 20% HF in glycerine. $\times 150$.

scopic identification of phases were exceedingly difficult under bright-field illumination. The use of polarized light proved to be exceptionally helpful in this respect because all of the intermediate phases yielded striking contrasts in color.

The eutectic between zirconium and Zr_4Si (7.14% silicon) at $1610 \pm 15^\circ C$ ($2930^\circ F$) is shown in Fig. 8, the as-cast structure

of a 2.9% silicon alloy. Fig. 9, an as-cast 4.1% silicon alloy, depicts primary crystals of Zr_4Si in a matrix of eutectic. Fig. 10 is a 4.9% silicon alloy, annealed at 1200 °C (2190 °F). Approximately 75% Zr_4Si in a matrix of zirconium is present in this structure, which indicates a compound composition of about 7% silicon. The as-cast structure of a 4.9% silicon alloy shows primary crystals of another phase, designated Zr_2Si (tentative, 13.33% silicon), peritectic walls of Zr_4Si , and a matrix of Zr - Zr_4Si eutectic, as in Fig. 11. Accordingly, Zr_4Si is formed by the peritectic reaction: $Zr_2Si + \text{melt (4.5\% Si)} \rightleftharpoons Zr_4Si$ at 1630 ± 15 °C (2965 °F).

Fig. 12, an as-cast 9.2% silicon alloy, depicts still another primary phase, designated Zr_3Si_2 (17.02% silicon) and peritectic walls of Zr_2Si , indicating that another peritectic melt has been passed. This reaction is: $Zr_3Si_2 + \text{melt (9\% Si)} \rightleftharpoons Zr_2Si$, at 2110 ± 25 °C (3830 °F). Fig. 13, a 14.3% silicon alloy, as-cast, contains the same phases, but a decided increase in the amount of Zr_3Si_2 present. However, in Fig. 14, the as-cast structure of a 14.5% silicon alloy, another peritectic melt has been passed, and new primary crystals, designated Zr_4Si_3 (18.74% silicon) appear, with peritectic rims of Zr_3Si_2 . Zr_3Si_2 is formed by the reaction: $Zr_4Si_3 + \text{melt (14.4\% Si)} \rightleftharpoons Zr_3Si_2$ at 2210 ± 25 °C (4010 °F). This same configuration of phases, with an increase to nearly 100% of Zr_4Si_3 , is seen in Fig. 15, a 17.6% silicon alloy.

Fig. 16, an as-cast 18.7% silicon alloy, discloses new primary crystals of the phase designated Zr_6Si_5 (20.40% silicon), surrounded by peritectic walls of Zr_4Si_3 . This reaction involves: $Zr_6Si_5 + \text{melt (18\% Si)} \rightleftharpoons Zr_4Si_3$ at 2225 ± 25 °C (4035 °F). Zr_6Si_5 is the only intermediate phase in the zirconium-silicon system which melts with an open maximum. The melting temperature is 2250 ± 25 °C (4080 °F). Fig. 17, the as-cast structure of a 20.1% silicon alloy, shows a nearly single-phase Zr_6Si_5 structure.

In an alloy containing 22.3% silicon, Fig. 18, Zr_6Si_5 remains the primary phase, but is surrounded by new peritectic rims of a phase designated $ZrSi$ (23.53% silicon). Rosette-shaped primaries of Zr_6Si_5 are still seen in an alloy containing about 24% silicon, Fig. 19. However, in the as-cast structure of a 24.3% silicon alloy, Fig. 20, Zr_6Si_5 has disappeared; $ZrSi$ is the primary phase (nearly 100%) with a peritectic network of the phase designated $ZrSi_2$ (38.09% silicon). Accordingly, $ZrSi$ is formed at 2095 ± 25 °C (3805 °F) by the reaction: $Zr_6Si_5 + \text{melt (24.2\% Si)} \rightleftharpoons ZrSi$.

Fig. 21, the as-cast structure of a 36.1% silicon alloy, depicts primary $ZrSi$ crystals, peritectic walls of $ZrSi_2$, and a matrix of $ZrSi_2$ -Si eutectic. The composition of the peritectic liquid which reacts with $ZrSi$ to form $ZrSi_2$ is very nearly approached in Fig. 22, an as-cast alloy containing 45.6% silicon. Very small amounts of

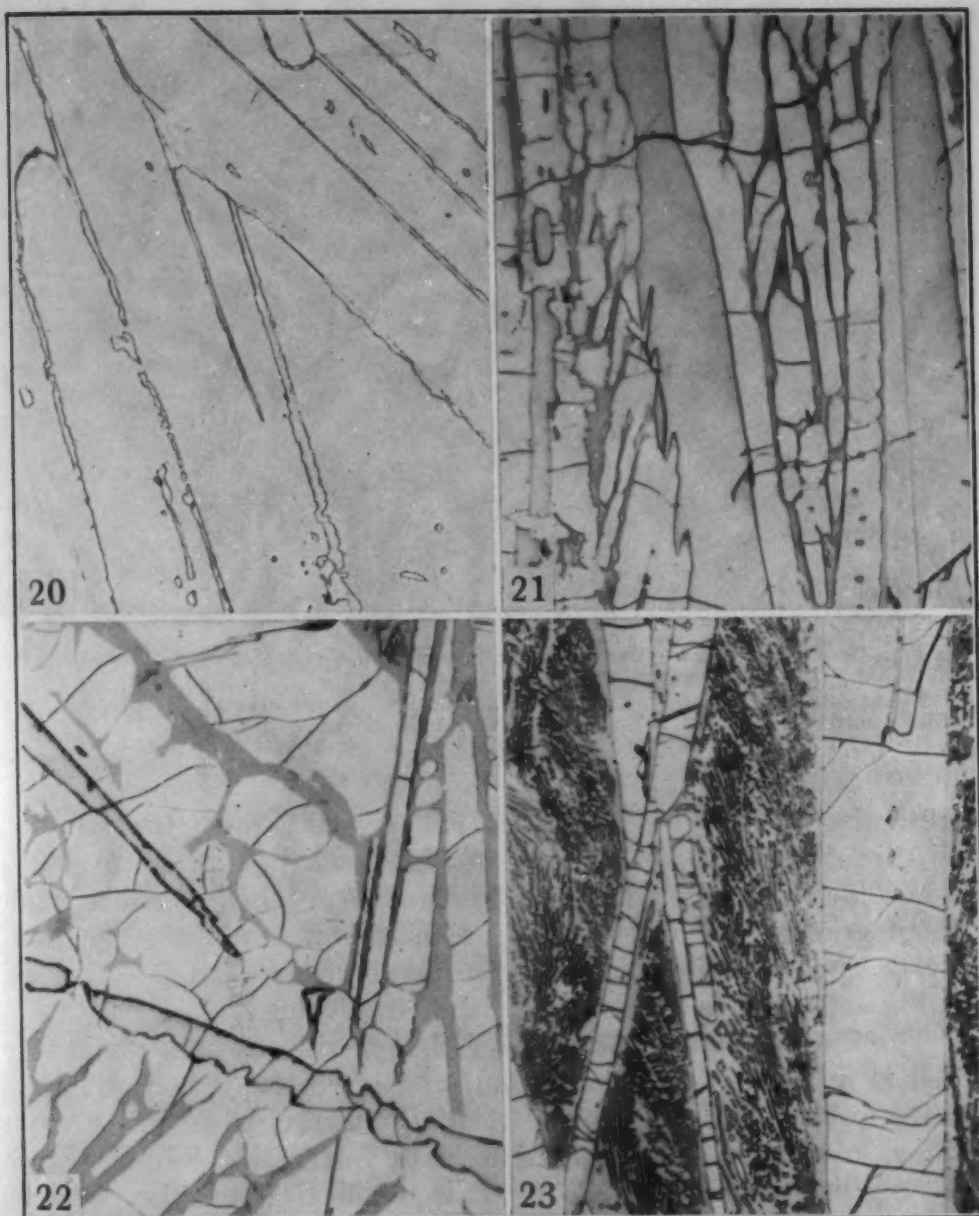


Fig. 20—24.3% Silicon Alloy, As-Cast. Nearly single-phase primary crystals of ZrSi in a matrix of peritectically formed ZrSi₂. Etchant: 20% HNO₃, 20% HF in glycerin. $\times 250$.

Fig. 21—36.1% Silicon Alloy, As-Cast. Gray primary crystals of ZrSi, peritectic walls of ZrSi₂, and divorced eutectic ZrSi₂-Si. Etchant: 20% HNO₃, 20% HF in glycerin. $\times 250$.

Fig. 22—45.6% Silicon Alloy, As-Cast. Small amount of gray primary ZrSi crystals surrounded by peritectic walls of ZrSi₂ in a matrix of eutectic ZrSi₂-Si. Etchant: 20% HNO₃, 20% HF in glycerin. $\times 250$.

Fig. 23—54.9% Silicon Alloy, As-Cast. Primary crystals of ZrSi₂ in a matrix of eutectic ZrSi₂-Si. Etchant: 20% HNO₃, 20% HF in glycerin. $\times 200$.

ZrSi primary crystals remain, surrounded by ZrSi₂ peritectic walls and a matrix of eutectic. The reaction involves: $\text{ZrSi} + \text{melt (46\% Si)} \rightleftharpoons \text{ZrSi}_2$ at $1520 \pm 15^\circ \text{C}$ (2770°F).

ZrSi₂ is the primary phase in a eutectic matrix in Fig. 23,

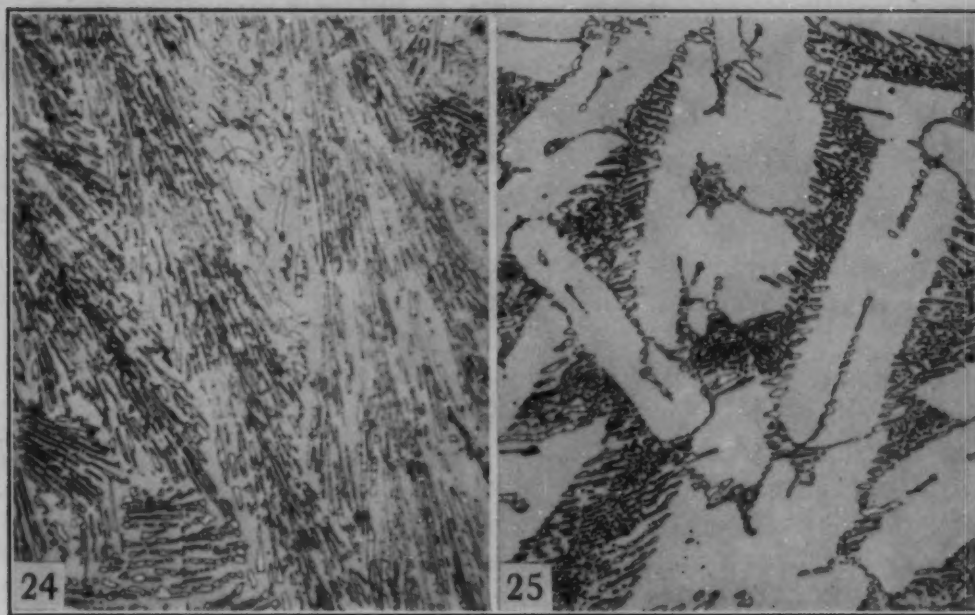


Fig. 24—76.2% Silicon Alloy, As-Cast. Structure of the ZrSi_2 -Si eutectic. Etchant: 20% HNO_3 , 20% HF in glycerin. $\times 200$.

Fig. 25—84.5% Silicon Alloy, As-Cast. Primary silicon crystals in a matrix of ZrSi_2 -Si eutectic. Etchant: 20% HNO_3 , 20% HF in glycerin. $\times 250$.

representing a 54.9% silicon alloy. The structure of the eutectic, ZrSi_2 -Si at $1355 \pm 15^\circ\text{C}$ (2470°F), is shown in Fig. 24, a 76.2% silicon alloy. Fig. 25, an as-cast 84.5% silicon alloy, contains about 50% of primary silicon crystals in a matrix of eutectic. The solubility of zirconium in silicon is considerably less than 5%, but no attempt was made to precisely determine the value.

The intermediate phase Zr_2Si (13.33% silicon) was tentatively placed at its theoretical composition, in view of work done by Paul Pietrokowsky (5) and from the relative amounts of phases present in alloys made in this investigation. The alternative formula Zr_3Si (9.30% silicon) is a possibility, but is not likely from the previous considerations.

The formulas Zr_3Si_2 and Zr_4Si_3 were the most likely for the two peritectically formed intermediate phases between 14.5 and 20.1% silicon. Two nearly single-phase structures were observed at about 20.1 and 24.3% silicon, and conform to the ideal compositions Zr_6Si_5 and ZrSi , respectively. The intermediate phase ZrSi_2 was previously identified by Naray-Szabo (1).

X-ray structure determination was limited in the present work, because all except one of the intermediate phases are peritectically formed. Annealing to obtain nearly single-phase structures was virtually impossible because of very low rates of diffusion. A Debye-Scherrer photogram of a 24.4% silicon alloy representing nearly 100% ZrSi was successfully indexed. A hexagonal lattice was

Table III
Melting-Range Determinations

Alloy Wt. % Silicon	Thermal Analysis Arrests, °C	Incipient Melting	
		Melting Observed, °C	No Melting, °C
Pure Zirconium	1852
1.8	1585
3.0	1610
2.9	1615	1580
4.9	1630
4.9	1630	1600
9.4	1630
14.3	2130	2090
14.5	2225	2195
19.5	2225
20.1	2250
22.3	2095
44.2	1520, 1365
45.6	1520
74.5	1350
Pure Silicon	1410

indicated, with lattice constants: $c = 12.772 \text{ \AA}$, $a = 7.005 \text{ \AA}$, $c/a = 1.823$.

Melting Determinations

Thermal analysis of a large portion of the diagram was impossible, due to the high temperatures involved. Incipient melting techniques were relied upon to supply information concerning the high temperature features. This method, too, was more difficult to apply than is normally the case because of the complexity of structures resulting from the many peritectic reactions. Whereas the normal accuracy of determinations at 2200°C (3990°F) has proved to be about $\pm 15^\circ\text{C}$ (if quenching increments are kept small enough), detection of incipient melting in the complicated structures observed for this system was at times uncertain and exterior signs of melting had to be used. This would place the values in error on the high side and the order of accuracy perhaps -50°C .

In general, the thermal results obtained correlated well with as-cast structural relationships. Table III presents the thermal analysis and incipient melting data.

SUMMARY

Zirconium-silicon alloys, systematically prepared throughout the range of compositions, were examined metallographically in the as-cast and heat treated state. In conjunction with thermal analysis and incipient melting data, the diagrams of Figs. 1, 2 and 3 were determined. The system is characterized by seven intermediate phases, Zr_4Si (7.14% silicon), Zr_2Si (13.33% silicon), Zr_3Si_2 (17.02% silicon), Zr_4Si_3 (18.74% silicon), Zr_6Si_5 (20.40% silicon), ZrSi (23.53% silicon), and ZrSi_2 (38.09% silicon). Only one, Zr_6Si_5 , displays an open maximum melting temperature (2250°C). The

remainder are formed peritectically. The peritectic temperatures and compositions of the reacting melts are as follows: for Zr_4Si , 1630 °C (2965 °F) and 4.5% silicon; for Zr_2Si , 2110 °C (3830 °F) and 9% silicon; for Zr_3Si_2 , 2210 °C (4010 °F) and 14.4% silicon; for Zr_4Si_3 , 2225 °C (4035 °F) and 18% silicon; for ZrSi , 2095 °C (3805 °F) and 24.2% silicon; and for ZrSi_2 , 1520 °C (2770 °F) and 46% silicon. There are two eutectics, one between zirconium and Zr_4Si at 2.9% silicon and 1610 °C (2930 °F), and the other between silicon and ZrSi_2 at 75% silicon and 1355 °C (2470 °F). The solubility of silicon in zirconium is very limited in both alpha ($<0.1\%$) and beta ($<0.2\%$) zirconium. The effect of silicon on the allotropic transformation of zirconium is undetermined, but shown to be very small.

ACKNOWLEDGMENT

The authors are grateful to the Atomic Energy Commission, the sponsors of this work, for permission to publish this paper. Thanks are due R. F. Domagala for the heat treatment of alloys, C.A. Johnson for metallographic work, and W. Rostoker for the interpretation of X-ray diffraction patterns.

References

1. Naray-Szabo, "The Structure of Zirconium-Silicide, ZrSi_2 ", *Zeitschrift für Kristallographie*, Vol. 97A, 1937, p. 223.
2. M. Hansen, H. D. Kessler and D. J. McPherson, "The Titanium-Silicon System", *TRANSACTIONS, American Society for Metals*, Vol. 44, 1951, p. 518.
3. D. J. McPherson and M. Hansen, "The System Zirconium-Tin", Preprint No. 34, American Society for Metals, Philadelphia Convention, 1952.
4. R. Vogel and W. Tonn, "A Transition Point for Zirconium", *Zeitschrift für anorganische und allgemeine Chemie*, Vol. 202, 1931, p. 293.
5. P. Pietrokowsky, "Crystal Structure of Zirconium-Rich Compounds With Silicon and Tin", submitted for publication to *Acta Crystallographica*, 1952.

THE SYSTEM ZIRCONIUM-TIN

By D. J. McPHERSON AND M. HANSEN

Abstract

The highly reactive zirconium-tin alloys were prepared and heat treated under protective conditions. The phase diagram was established, based on micrographic and X-ray diffraction analysis, metallographic detection of incipient melting, and thermal analysis.

THE zirconium-tin system was investigated as a part of an Atomic Energy Commission program on the equilibrium diagrams of binary zirconium alloys. No previous unclassified work has been done on this diagram. Micrographic analysis of as-cast and heat treated specimens was the principal tool in the present work. Thermal analysis and X-ray diffraction served as auxiliary techniques.

EXPERIMENTAL PROCEDURES

Materials

A "low-hafnium" zirconium crystal bar, produced by the decomposition of a volatile iodide onto a hot filament, was employed for these studies. Westinghouse "Grade 3" crystal bar was used for the majority of alloys. A limited number of alloys were prepared with the higher purity Westinghouse "Grade 1" zirconium for final refinement of certain phase boundaries. The zirconium crystal bar, as-received, was coated with corrosion product from a standard autoclave test by which its Grade designation is determined. This was cleaned by a sand-blasting and HF-HNO₃ pickling technique developed by the Atomic Energy Commission. The bars were then cold-rolled to approximately $\frac{1}{32}$ -inch sheet, pickled for iron removal, sheared to $\frac{1}{4}$ -inch squares, cleaned in acetone, and stored for arc furnace charge.

High purity tin was received in the form of hemispherical ingots from Vulcan Detinning Company. Spectrographic analysis provided by the manufacturer showed this tin to be 99.99% pure. These ingots were rolled to sheet, sheared, and cleaned as above.

This paper is based on a portion of the work carried out at Armour Research Foundation for the Atomic Energy Commission under Contract No. AT(11-1)-149, "Phase Diagrams of Zirconium-Base Binary Alloys". Final Report, No. (COO-89).

A paper presented before the Eighth Western Metal Congress of the Society, held in Los Angeles, March 23 to 27, 1953. Of the authors, D. J. McPherson is supervisor, Physical Metallurgy Research, and M. Hansen is chairman, Metals Research Department, Armour Research Foundation of Illinois Institute of Technology, Chicago. Manuscript received April 9, 1952.

Melting Practice

Zirconium-tin alloys were prepared by arc melting in a water-cooled copper crucible, employing a tungsten-tipped electrode and an atmosphere of high purity helium. A drawing of the furnace and description of general melting techniques have been presented by the authors in previous publications (1, 2).¹ Alloys containing 0 to 35% tin were melted in the cavity of a copper block inserted into a spun copper crucible. The arc was struck on a tungsten stud in the copper block, obviating initial contact between the tungsten electrode and alloy charge. Alloys containing more than 35% tin were characterized by high tin losses when melted in this manner. This difficulty was overcome in large measure by pre-compacting the alloy charge and melting directly in a conical-bottomed copper crucible. All alloys were inverted and remelted three to five times without opening the furnace. Most of the alloys employed weighed 20 to 30 grams. Control melts of unalloyed zirconium were prepared and checked for hardness and microstructure throughout the melting program. Tungsten analyses on a number of random alloys averaged less than 0.05%.

Annealing Treatments

Alloy ingots were cold-compressed, homogenized, then cold-rolled to the maximum possible reduction as a pretreatment prior to isothermal annealing. Those compositions too brittle for cold work were only homogenized before the equilibrium anneals. In order to avoid contamination of these highly reactive alloys, no hot working steps were employed.

Annealing treatments were carried out with specimens sealed in Vycor (up to 1100 °C) or quartz bulbs. For treatments up to 950 °C (1740 °F), the bulbs were evacuated. Above this temperature, a reduced pressure of argon, necessary to balance one atmosphere of external pressure at the annealing temperature, was admitted to prevent collapse of the bulbs. Liners of 0.003-inch molybdenum sheet were placed in bulbs scheduled for treatment above 1200 °C (2190 °F), serving the dual purpose of specimen protection and physical support for the bulb walls. An unalloyed zirconium control specimen was included with every heat treatment. Specimens were quenched from the furnace into tanks provided with hinged paddles. The specimen bulbs were broken under water, thus insuring a rapid quench.

Both vertical and horizontal tube furnaces were available for heat treatments up to 1500 °C (2730 °F). Temperature control within ± 3 °C was accomplished with Wheelco Model 252P Capaciline in-

¹The figures appearing in parentheses pertain to the references appended to this paper.

struments or Leeds and Northrup Micromax controllers, operated in conjunction with Claud S. Gordon Xactlines.

Melting-Range Determinations

For the determination of solidus curves and eutectic and peritectic horizontals occurring at high temperatures above the useful range of thermocouples, the micrographic detection of incipient melting in heated and quenched samples is an expedient technique. A high temperature vacuum induction furnace and quenching technique to accomplish this have been described (1). Specimens are supported by a tungsten wire within a tantalum heating chamber. Temperatures are determined with an optical pyrometer calibrated against the melting points of several pure metals. Specimens are quenched from a series of temperatures by allowing the wire and sample to drop onto a cold bottom plate, and are examined microscopically for signs of incipient melting.

A thermal analysis technique, employing doubly-protected platinum/platinum - 10% rhodium thermocouples and high purity graphite crucibles in a hermetically sealed induction furnace has also been described (1). This equipment was useful in detecting melting temperatures below about 1650 °C (3000 °F). Cooling and heating curves were automatically plotted on a Brown Electronik Recorder, wired to plot a point every second. Generally, two cooling and two heating curves, employing a rate of 1 to 2 °C per second, were obtained for each alloy.

RESULTS AND DISCUSSION

The Phase Diagram

The phase diagram of the zirconium-tin system is presented in Fig. 1. An expanded diagram of the zirconium-rich region, including most of the data points, is given in Fig. 2. Some data points were omitted for the sake of clarity. The diagrams are based on the analyzed compositions listed in Table I. A large number of unanalyzed alloys gave supporting evidence to the phase relationships shown.

Zirconium-Rich Alloys

A preliminary investigation was undertaken in order to check the temperature of the allotropic transformation, $\alpha \rightleftharpoons \beta$, in "Grade 3" zirconium crystal bar. Five random bars were pretreated by cold pressing, homogenization and cold rolling, then annealed at five temperatures between 850 and 890 °C (1560 and 1635 °F) and water-quenched. The production of two-phase ($\alpha + \beta$) structures gave evidence that this material transforms over a range of temperatures (because of impurities) near the ideal transformation point. The apparent range of transformation, from this limited study, extended

Table I
Analyses of Zirconium-Tin Alloys*

Alloy No.	Wt. % Tin	Alloy No.	Wt. % Tin
ZT 0.5-161	0.49	ZT 21-189	22.3
ZT 1-162	0.85	ZT 22-191	23.5
ZT 2-168	1.9	ZT 23-192	23.1
ZT 2-803	2.1	ZT 24-196	24.2
ZT 3-169	3.1	ZT 25-123	25.9
ZT 4-170	3.9	ZT 30-124	29.4
ZT 4-804	4.3	ZT 35-125	30.6
ZT 5-171	4.7	ZT 40-126	37.0
ZT 6-172	5.8	ZT 45-128	40.2
ZT 6-805	6.3	ZT 50-129	40.7
ZT 7-173	7.3	ZT 43-208	42.1
ZT 8-806	7.9	ZT 45-157	44.1
ZT 8-174	8.5	ZT 47-202	46.7
ZT 9-449	9.0	ZT 50-158	48.5
ZT 10-807	9.8	ZT 52-207	50.5
ZT 10-177	10.5	ZT 55-152	52.6
ZT 11-178	11.3	ZT 56-209	55.5
ZT 12-808	11.8	ZT 58-210	57.2
ZT 12-179	12.2	ZT 60-153	58.5
ZT 13-180	12.9	ZT 65-148	64.9
ZT 14-182	14.1	ZT 70-154	65.6
ZT 15-183	15.5	ZT 75-155	73.3
ZT 16-184	15.9	ZT 80-156	79.5
ZT 17-185	17.5	ZT 85-147	87.1
ZT 18-194	20.2	ZT 90-149	92.6
ZT 19-187	20.7	ZT 95-151	95.5
ZT 20-122	21.2		

*Method of analysis: Specimens dissolved in fluoboric and dilute sulphuric acids. Acidity adjusted to 20% HCl. Tin reduced with iron powder and titrated with N/10 iodine.

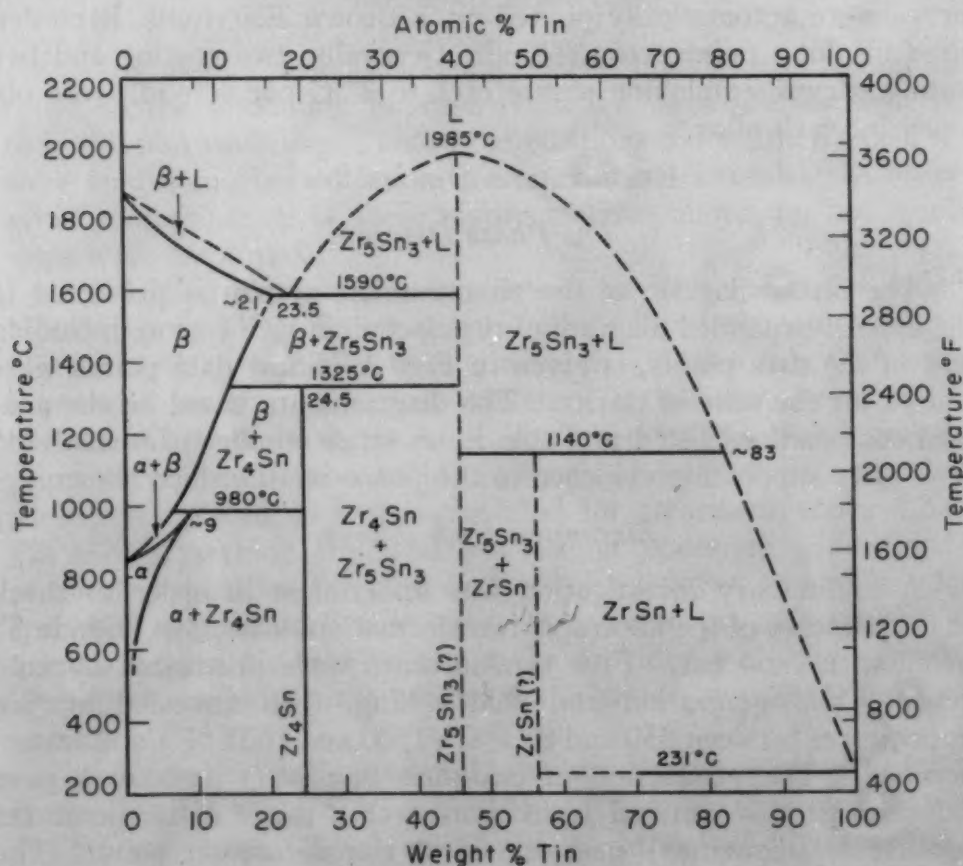


Fig. 1—The Zirconium-Tin System

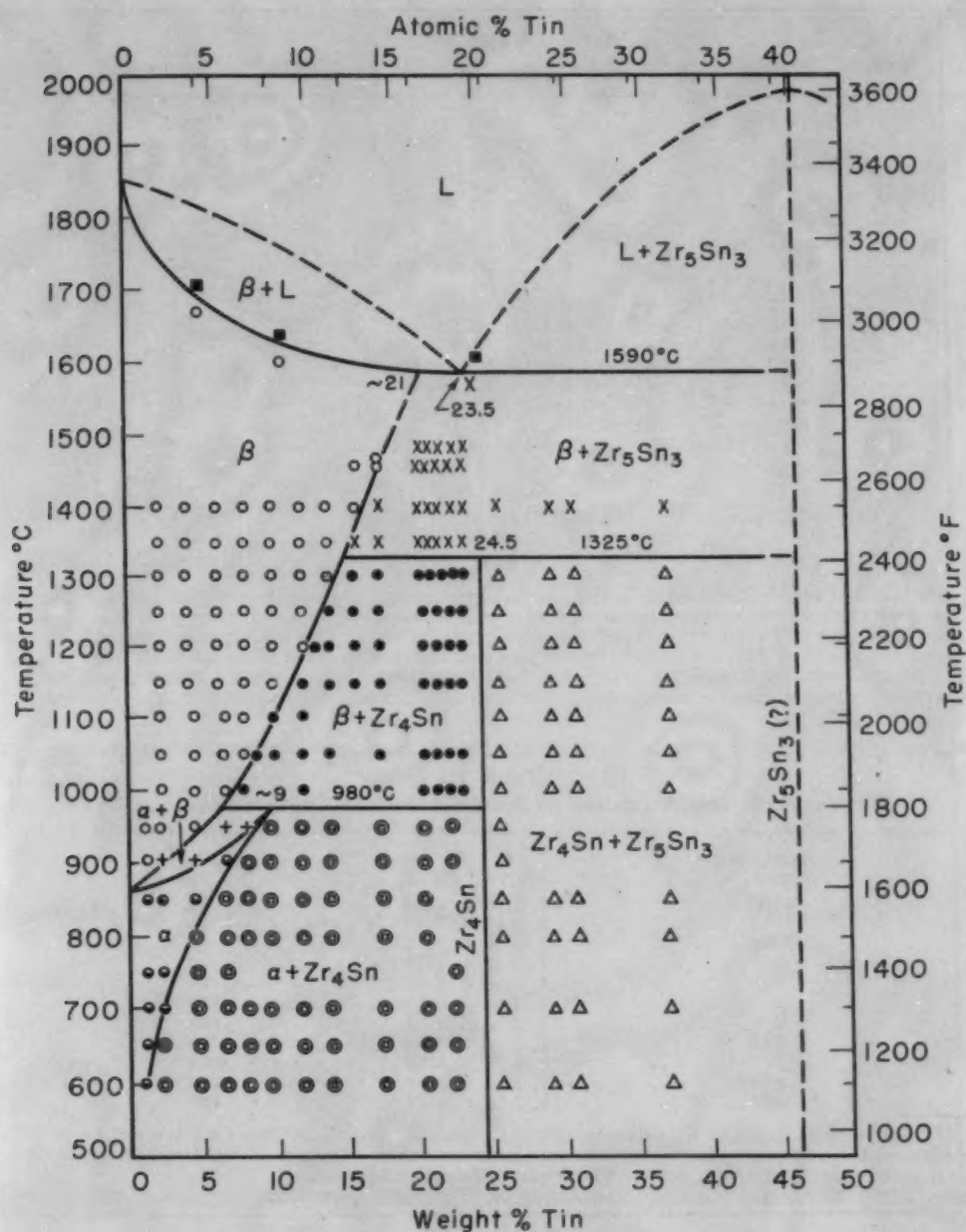


Fig. 2—The Constitution of Zirconium-Rich Zirconium-Tin Alloys

from 851 to 868 °C (1565 to 1595 °F). This is, at least, quite close to the value of 862 ± 5 °C reported by Vogel and Tonn (3), so this figure was adopted for construction of the diagram.

On a basis of preliminary time versus temperature studies for equilibrium states, the heat treatments in Tables II and III were scheduled. In addition to these isothermal anneals followed by water quenching, the examination of as-cast alloys and alloys slowly cooled through certain regions was also instrumental in determining the phase relationships.

The position of the eutectic at 23.5% tin is bracketed quite

Table II
Pretreatment* and Annealing Data for Zirconium-Tin Alloys

Annealing Temp., °C	Alloys, % Tin	Hours at Temp.
1472	17-23	1/4
1460	16-22	1/2
1400	0.5-25, 30, 35, 40	2
1350	0.5-25, 30, 35, 40	2
1300	0.5-25, 30, 35, 40	5
1247	0.5-25, 30, 35, 40	5
1200	0.5-25, 30, 35, 40	7
1153	0.5-25, 30, 35, 40	16
1098	0.5-25, 30, 35, 40	20
1048	0.5-25, 30, 35, 40	20
997	0.5-25, 30, 35, 40	20
947	0.5-25, 30, 35, 40	28
902	0.5-25, 30, 35, 40	30
851	0.5-15, 17, 19, 21, 23, 25, 30, 35, 40	50
750	2, 4, 6-10, 12, 14, 16, 18, 20, 22, 24, 30, 35, 40	150
652	2, 4-10, 12, 14, 16, 18, 20, 22, 24, 30, 35, 40	247
548	2, 4, 6, 8, 10, 12	400

*Prior to the tabulated equilibrium anneals, specimens were cold-pressed, then homogenized 5 hours at 1100°C and water-quenched, and finally cold-rolled to the maximum reductions possible. The degree of cold work depended upon composition. The 2% tin alloy was cold-pressed 31% and cold-rolled 82%, whereas these respective reductions for a 20% tin alloy were 2% and 0%. Alloys containing more than 24% tin were not amenable to any cold reduction.

Table III
Pretreatment* and Annealing of Special "Grade 1" Zirconium-Tin Alloys

Annealing Temp., °C	Alloys, % Tin	Hours at Temp.
1100	1, 2, 4, 6, 8-14	20
1054	1, 2, 4, 6, 8-14	16
1006	1, 2, 4, 6, 8-14	45
957	1, 2, 4, 6, 8-14	70
905	1, 2, 4, 6, 8-14	74
853	1, 2, 4, 6, 8-14	120
801	1, 2, 4, 6, 8-14	145
748	1, 2, 4, 6, 8-14	280
702	1, 2, 4, 6, 8-14	355
656	1, 2, 4, 6, 8-14	400
604	1, 2, 4, 6, 8-14	445

*Prior to the tabulated equilibrium anneals, these compositions were cold-pressed 14 to 33%, homogenized 5 hours at 1100°C and water-quenched, then reduced by cold rolling 19 to 79%. The degree of cold reduction decreased with increasing tin content.

accurately by the alloys of Figs. 3 and 4. The eutectic temperature was confirmed independently by the microscopic evaluation of specimens quenched in the incipient melting furnace and by thermal analysis. Fig. 5, an as-cast 30.6% tin alloy, is typical of the Zr_5Sn_3 plus eutectic structures obtained in the 24 to 46% tin composition range.

The highest temperature at which the $\beta/\beta + Zr_5Sn_3$ phase boundary was experimentally located was 1472°C (2680°F). Figs. 6 and 7 show 17.5 and 20.2% tin alloys, respectively, quenched after an anneal at this temperature. The extrapolation of this phase boundary to the eutectic temperature indicates a maximum solubility of tin in beta zirconium of approximately 21%.

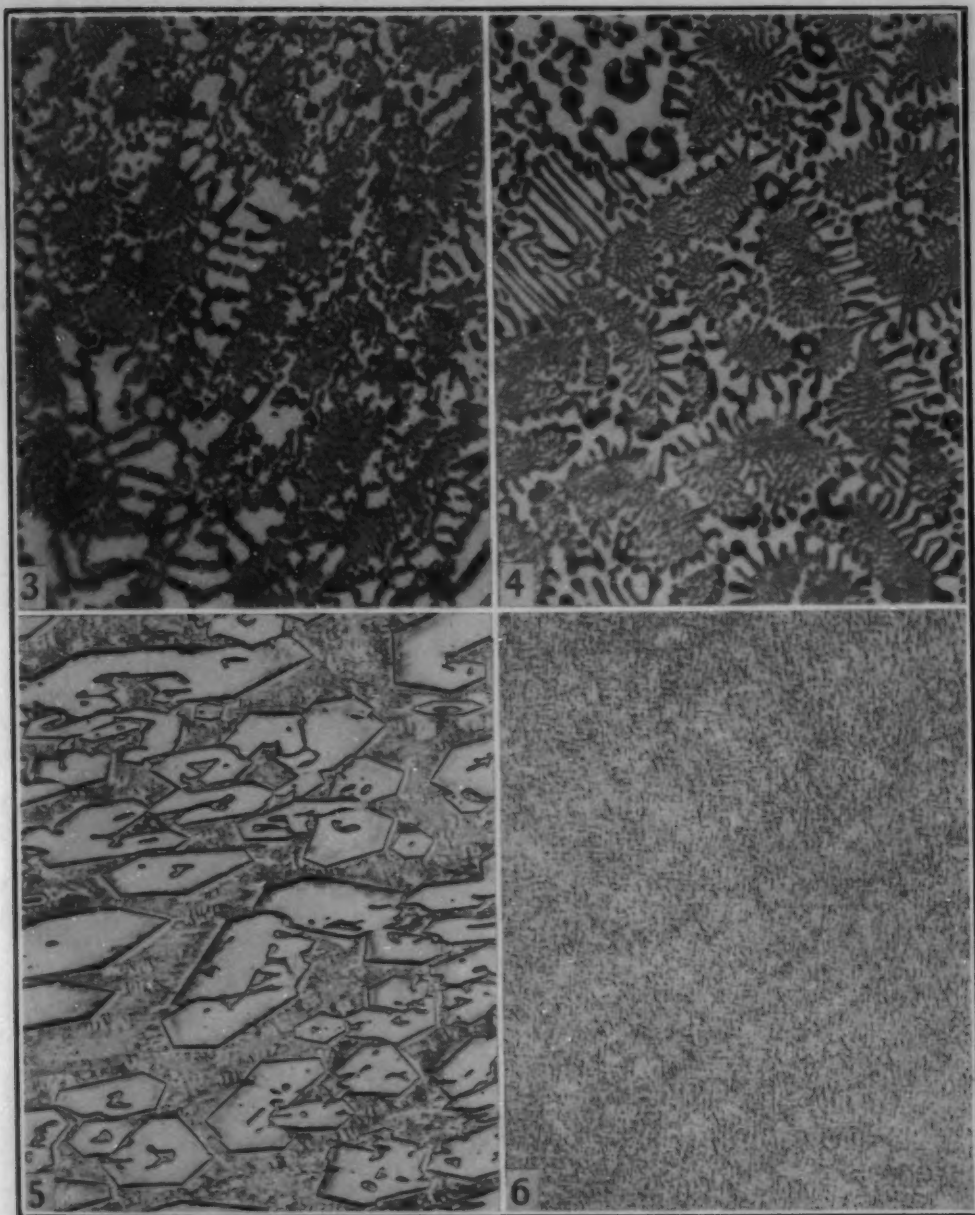


Fig. 3—23.1% Tin Alloy, As-Cast. Predominantly eutectic, with some residual primaries of beta zirconium. Etchant: 20% HF, 20% HNO₃ in glycerine. $\times 750$.

Fig. 4—24.2% Tin Alloy, As-Cast. Predominantly eutectic with a few primary crystals of Zr₅Sn₃. Etchant: 20% HF, 20% HNO₃ in glycerine. $\times 750$.

Fig. 5—30.6% Tin Alloy, As-Cast. Primary crystals of Zr₅Sn₃ in a matrix of Zr-Zr₅Sn₃ eutectic. Unetched. $\times 100$.

Fig. 6—17.5% Tin Alloy, Water-Quenched After Annealing $\frac{1}{4}$ Hour at 1472°C. Transformed beta structure. Etchant: 20% HF, 20% HNO₃ in glycerine. $\times 150$.

The sequence of as-cast zirconium-tin microstructures gave no clue as to the existence of a zirconium-rich intermediate phase; however, anneals in the solid state clearly proved that Zr₄Sn, having a singular composition at 24.55% tin, is formed by the peritectoid reaction: $\beta + \text{Zr}_5\text{Sn}_3 \rightleftharpoons \text{Zr}_4\text{Sn}$ at about 1325°C (2415°F). Figs. 8 and 9 are the microstructures of a 23.5% tin alloy, quenched after

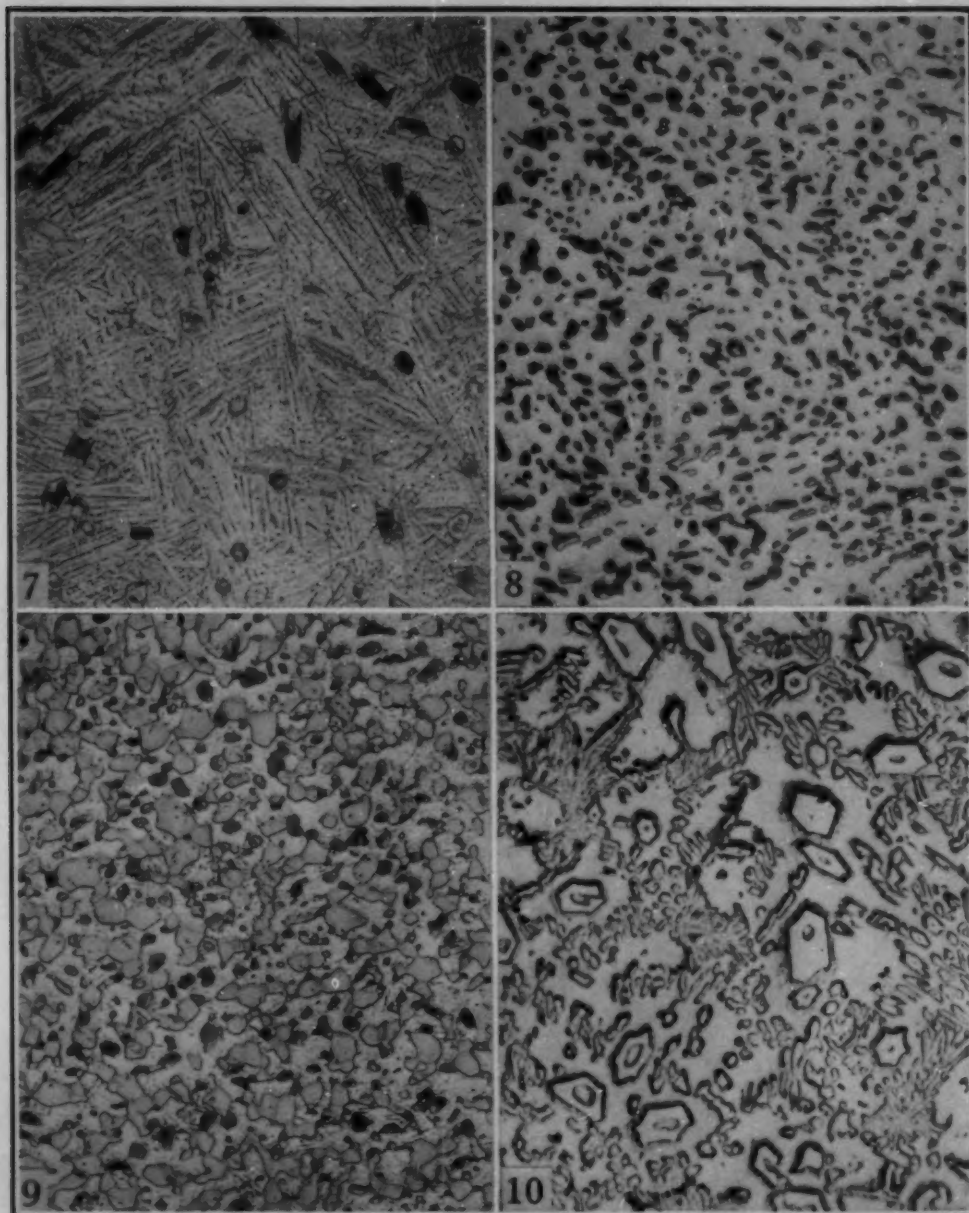


Fig. 7—20.2% Tin Alloy, Water-Quenched After Annealing $\frac{1}{2}$ Hour at 1472°C. Transformed beta plus Zr_5Sn_3 crystals. Etchant: 20% HF, 20% HNO_3 in glycerine. $\times 150$.

Fig. 8—23.5% Tin Alloy, Water-Quenched After Annealing 2 Hours at 1350°C. Transformed beta plus Zr_5Sn_3 crystals. Etchant: 20% HF, 20% HNO_3 in glycerine. $\times 150$.

Fig. 9—23.5% Tin Alloy, Water-Quenched After Annealing 5 Hours at 1300°C. Original structure of transformed beta and Zr_5Sn_3 (small dark crystals) reacting peritectoidally to form $ZrSn$ phase (gray). Etchant: 20% HF, 20% HNO_3 in glycerine. $\times 150$.

Fig. 10—24% Nominal Tin Alloy, Induction-Melted in Graphite. Some primary Zr_5Sn_3 in a matrix of divorced Zr - Zr_5Sn_3 eutectic. Unetched. $\times 150$.

annealing at 1350 and 1300 °C (2460 and 2370 °F), respectively. The peritectoid nature of the compound formation is better illustrated in the sequence of structures in Figs. 10 and 11. This alloy, containing, nominally, 24% tin, was induction-melted in a graphite crucible. Fig. 10 represents the as-cast structure and Fig. 11 is the same alloy

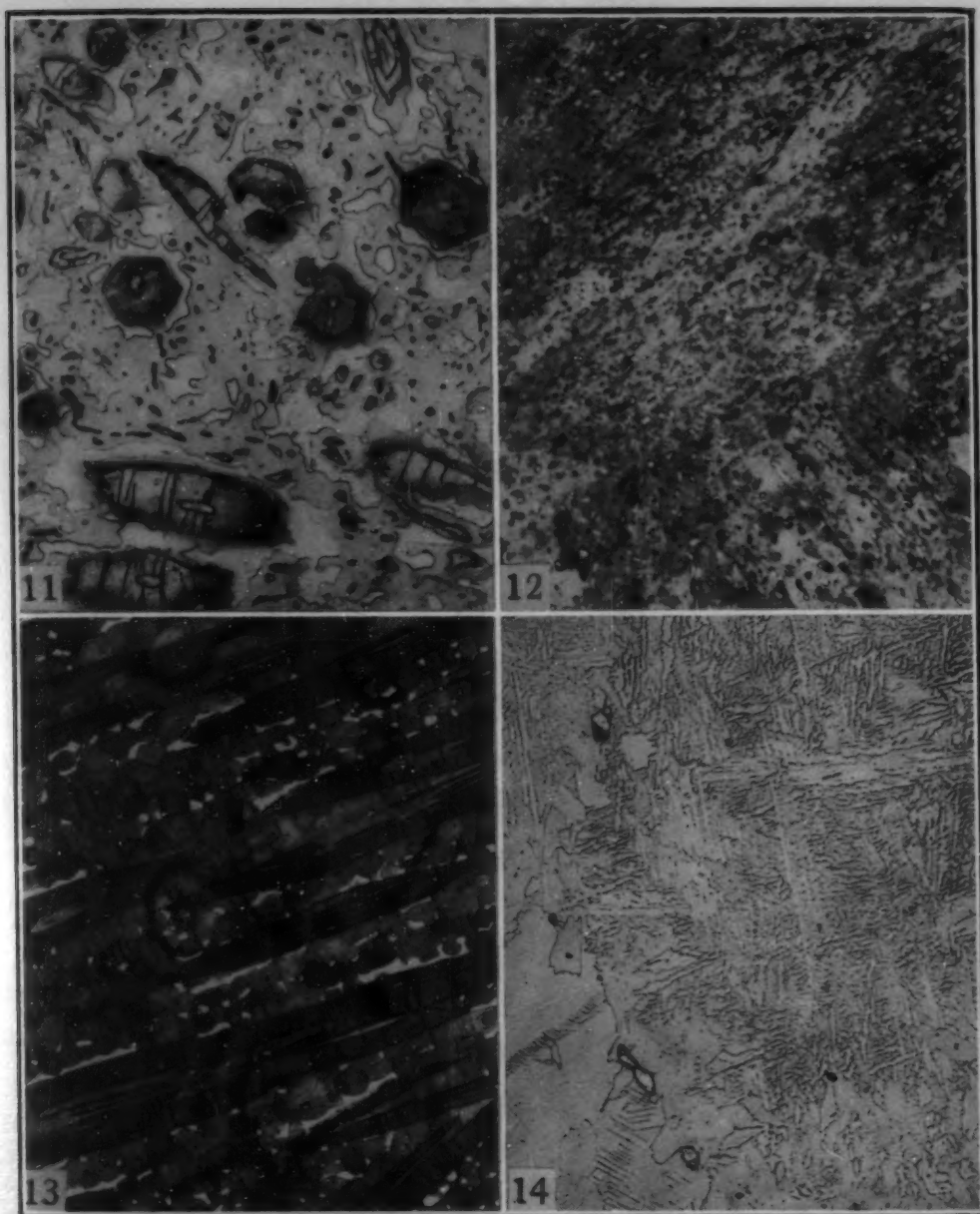


Fig. 11—24% Nominal Tin Alloy (Induction-Melted). Water-Quenched After Annealing 20 Hours at 1051°C. Peritectoid formation of Zr_4Sn from the reaction between beta zirconium and Zr_5Sn_3 . Etchant: 20% HF, 20% HNO_3 in glycerine. $\times 150$.

Fig. 12—24.2% Tin Alloy. Water-Quenched After Annealing 45 Hours at 951°C. Nearly single-phase Zr_4Sn . Small amounts of unreacted beta and Zr_5Sn_3 remain. Etchant: 20% HF, 20% HNO_3 in glycerine. $\times 150$.

Fig. 13—29.4% Tin Alloy. Water-Quenched After Annealing 5 Hours at 1247°C. Annealed in the $Zr_4Sn + Zr_5Sn_3$ field. Small amounts of unresorbed beta phase remain. Etchant: 20% HF, 20% HNO_3 in glycerine. $\times 150$.

Fig. 14—7.9% Tin Alloy. Water-Quenched After Annealing 45 Hours at 1006°C. Transformed beta and Zr_4Sn phases are in equilibrium. Etchant: 20% HF, 20% HNO_3 in glycerine. $\times 150$.

after an anneal at 1051°C (1925°F). Since the reaction is not complete, the three-phase peritectoid arrangement is clear. The optimum amounts of Zr_4Sn were obtained by annealing a 24.2% tin arc-melted alloy at various temperatures below 1300°C (2370°F).

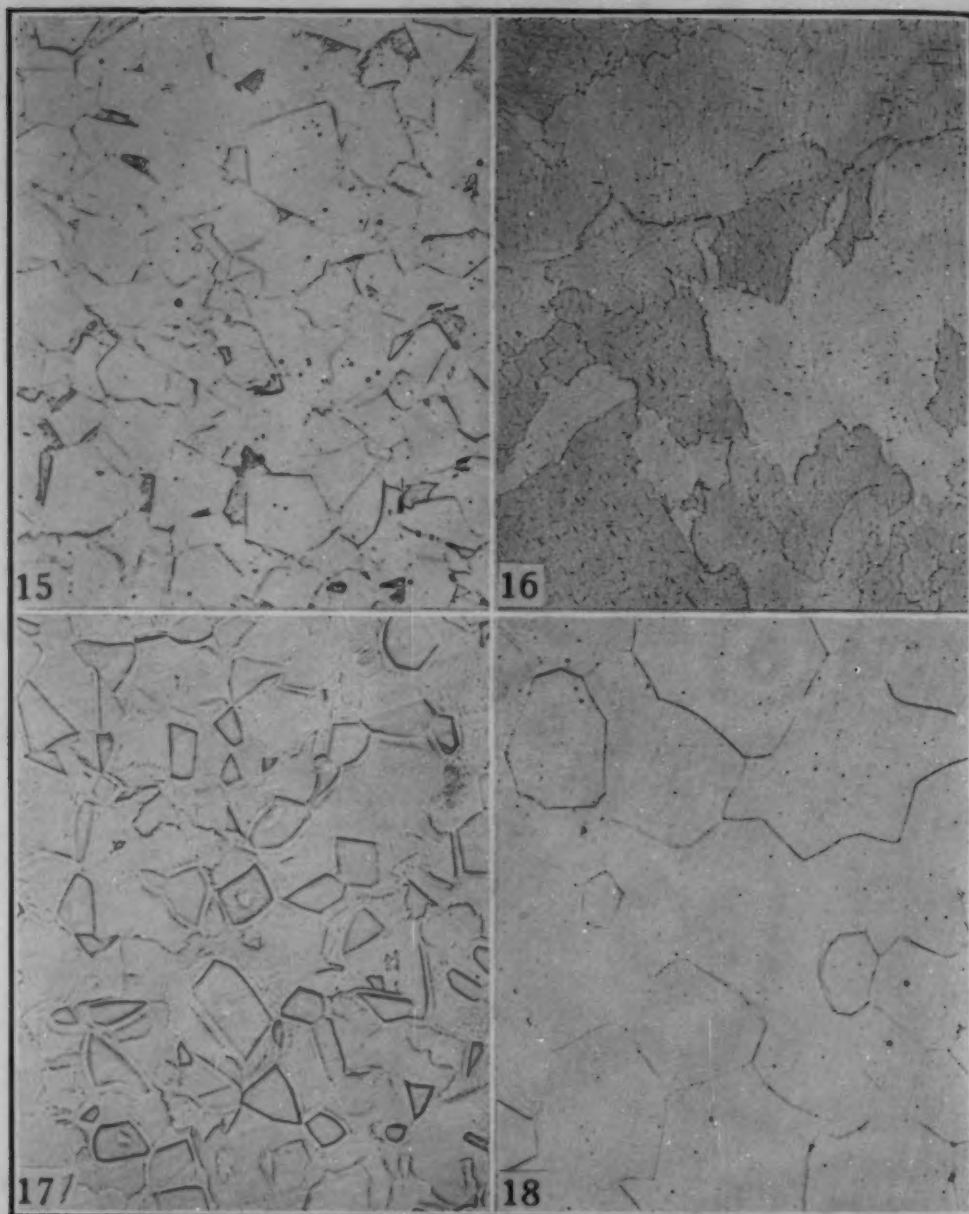


Fig. 15—7.9% Tin Alloy, Water-Quenched After Annealing 70 Hours at 957°C. Isothermal alpha and transformed beta are present. Etchant: 20% HF, 20% HNO₃ in glycerine. $\times 150$.

Fig. 16—1.0% Tin Alloy, Water-Quenched After Annealing 74 Hours at 905°C. "Serrated" alpha transformation product, indicating that the alloy was annealed in the beta field. Etchant: 20% HF, 20% HNO₃ in glycerine. $\times 150$.

Fig. 17—2.1% Tin Alloy, Water-Quenched After Annealing 74 Hours at 905°C. Equiaxed isothermal alpha plus serrated alpha transformation product formed on quenching. This alloy was annealed in the $\alpha + \beta$ field. Etchant: 20% HF, 20% HNO₃ in glycerine. $\times 150$.

Fig. 18—6.3% Tin Alloy, Water-Quenched After Annealing 74 Hours at 905°C. 100% equiaxed alpha, formed isothermally. Etchant: 20% HF, 20% HNO₃ in glycerine. $\times 150$.

Fig. 12 shows the structure of this alloy after a 45-hour anneal at 951°C (1745°F). Only small residual amounts of beta and Zr₅Sn₃ remain. The peritectoid temperature level was checked by reannealing specimens of the nearly 100% Zr₄Sn alloy at 1100, 1200, 1300,

and 1350 °C (2010, 2190, 2370, and 2460 °F) in order to reverse the reaction. Only the specimen annealed at 1350 °C (2460 °F) decomposed into beta and Zr_5Sn_3 phases.

Fig. 13 represents the structure of a 29.4% tin alloy annealed at 1247 °C (2280 °F), in the $Zr_4Sn + Zr_5Sn_3$ field. The reaction is nearly complete, but some unresorbed beta phase remains.

A sample of the 24.2% tin alloy containing nearly 100% Zr_4Sn was subjected to X-ray analysis. The specimen was prepared by filing. Iron particles were removed magnetically and the powders were exposed to filtered, characteristic copper $K\alpha$ radiation. The resulting pattern was indexed on a face-centered tetragonal Hull-Davey chart. The lattice parameters were: $a = 7.645 \text{ \AA}$, $c = 12.461 \text{ \AA}$; $c/a = 1.63$.

The alpha solid solution enters into the peritectoid reaction: $\beta + Zr_4Sn \rightleftharpoons \alpha$ at approximately 980 °C (1795 °F) and 9% tin in this system. The photomicrographs of Figs. 14 and 15 show the best evidence for the peritectoid temperature level. Both figures represent a 7.9% tin alloy; the former, annealed at 1006 °C (1845 °F), consists of $\beta + Zr_4Sn$, while the latter, annealed at 957 °C (1785 °F), contains $\alpha + \beta$. This peritectoid level was placed by the examination of several series of annealed alloys prepared with extremely clean Westinghouse "Grade 1" zirconium crystal bar. Considerable difficulty had been experienced earlier in interpreting the structures obtained in "Grade 3" zirconium alloys.

The sequence of structures in Figs. 16 through 19 presents excellent evidence of the phase relationships in this region of the diagram. This series of alloys was annealed at 905 °C (1660 °F); Fig. 16, 1.0% tin alloy, is transformed beta, Fig. 17, a 2.1% tin alloy, contains $\alpha + \beta$. Fig. 18, a 6.3% tin alloy, falls in the alpha solid solution field, and Fig. 19, a 7.9% tin alloy, represents an $\alpha + Zr_4Sn$ structure.

The alpha solid solution field extends to about 9% at the peritectoid temperature, 980 °C (1795 °F). The solid solubility of tin in alpha decreases rather sharply with falling temperature as indicated by Figs. 20 and 21, representing alloys annealed at 801 °C (1475 °F). In this case, again, alloy structures based on "Grade 3" zirconium crystal bar were exceedingly difficult to interpret. The relatively large number of impurity particles always present in this grade zirconium made it nearly impossible to detect the initial appearance of the Zr_4Sn phase, which also precipitates as a very fine dispersion of particles in the lower temperature ranges. Use of the special "Grade 1" zirconium-base alloys, which yielded alpha structures relatively free of impurities, made it possible to locate the $\alpha/\alpha + Zr_4Sn$ phase boundary with considerable accuracy.

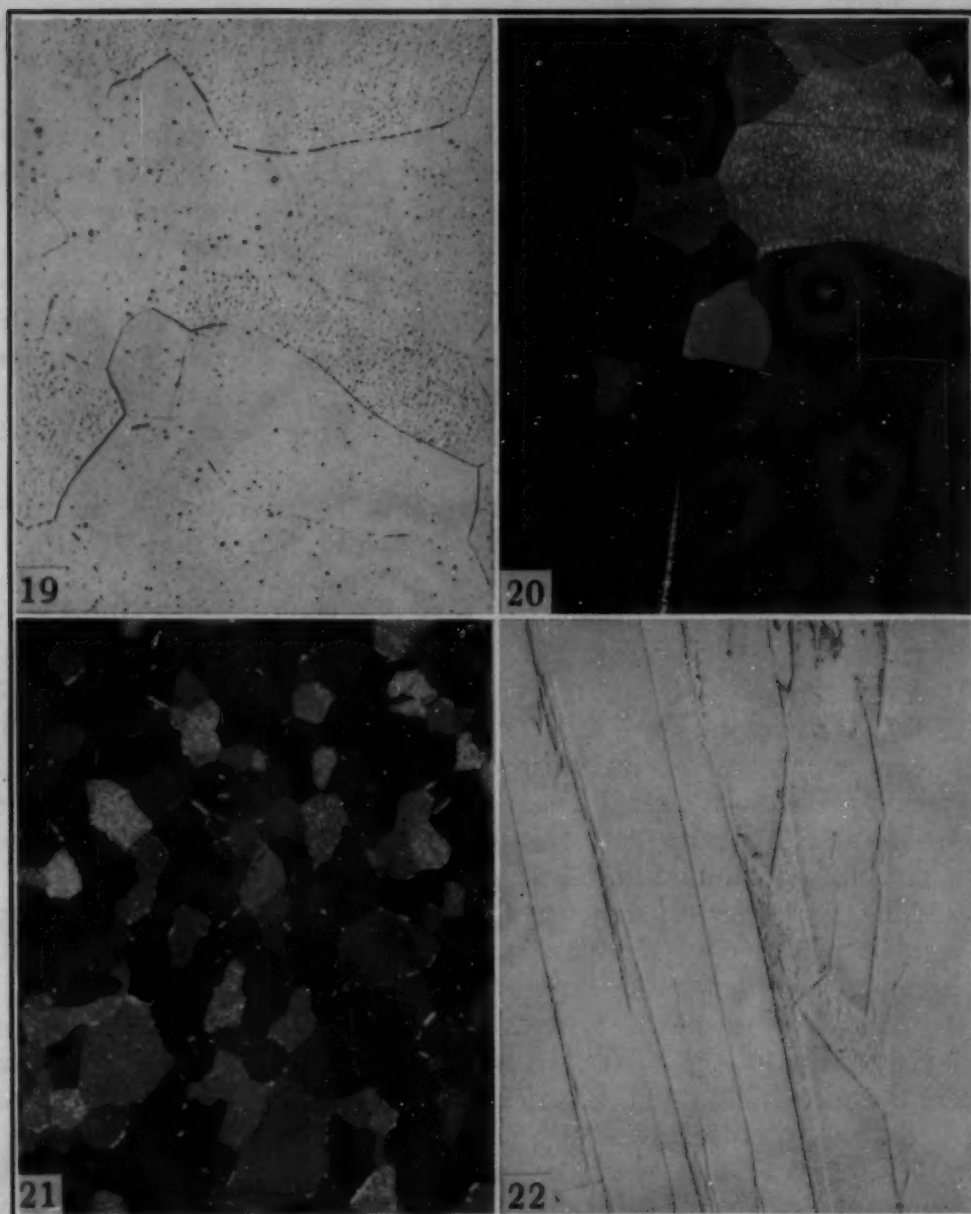


Fig. 19—7.9% Tin Alloy, Water-Quenched After Annealing 74 Hours at 905°C. Alpha plus fine precipitation of Zr_3Sn particles. Etchant: 20% HF, 20% HNO_3 in glycerine. $\times 150$.

Fig. 20—2.1% Tin Alloy, Water-Quenched After Annealing 145 Hours at 801°C. 100% equiaxed alpha. Unetched, polarized light. $\times 150$.

Fig. 21—4.3% Tin Alloy, Water-Quenched After Annealing 145 Hours at 801°C. Alpha plus Zr_3Sn particles, principally in the grain boundaries. Note the decrease in grain size upon crossing the $\alpha/\alpha + Zr_3Sn$ boundary (compared with Fig. 20). Unetched, polarized light. $\times 150$.

Fig. 22—40.2% Tin Alloy, As-Cast. Primary crystals of Zr_3Sn in matrix of Zr-Zr $_3$ Sn $_3$ eutectic. Unetched. $\times 150$.

The Intermediate Phase at 47% Tin

The intermediate phase which enters into a eutectic reaction with zirconium presented unusual experimental difficulties. Figs. 22 through 24 represent as-cast 40.2, 44.1 and 46.7% tin alloys,

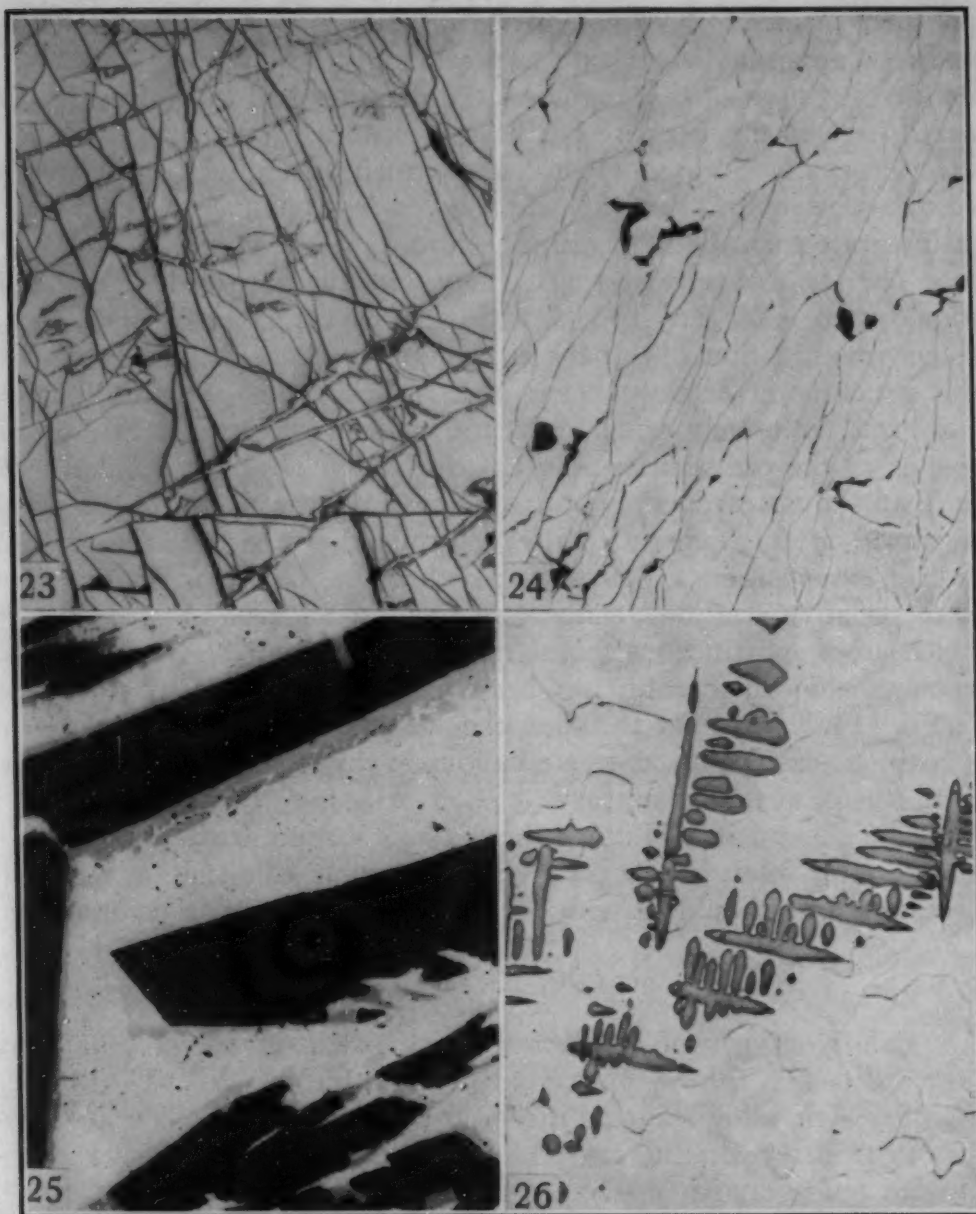


Fig. 23—44.1% Tin Alloy, As-Cast. Cracked Zr_3Sn_3 primaries and small amount of residual eutectic. Unetched. $\times 150$.

Fig. 24—46.7% Tin Alloy, As-Cast. Nearly 100% primary Zr_3Sn_3 crystals. Unetched. $\times 150$.

Fig. 25—65.6% Tin Alloy, As-Cast. Primary crystals of Zr_3Sn_3 , peritectic rims of $ZrSn$, and a matrix of tin. This specimen was allowed to stand 15 minutes after polishing before photographing. The Zr_3Sn_3 darkens rapidly in air and contrasts sharply with the peritectic phase. Unetched. $\times 250$.

Fig. 26—95% Nominal Tin Alloy, Melted in Porcelain Crucible for Thermal Analysis. Primary $ZrSn$ crystals in a matrix of tin. Etchant: 20% HF, 20% HNO_3 in glycerine. $\times 150$.

respectively. Some residual eutectic is present in both the former alloys, whereas the last represents nearly 100% of this phase. Melting point determinations on the 46.7% alloy showed that this phase melts with an open maximum at $1985 \pm 25^\circ C$ ($3605^\circ F$). The phase is exceedingly unstable toward air and/or moisture; a freshly

polished surface will commence to discolor in a matter of minutes, and whole ingots disintegrate to powder in a few weeks. Alloys for the investigation of this region of the diagram had to be freshly prepared periodically, because of this fact. Storage of melted specimens in a vacuum desiccator prolonged their usefulness appreciably. Alloys containing 30 to 45% tin showed less tendency to completely disintegrate than the alloys in the 45 to 75% tin range.

The formula in closest agreement with the observed single-phase composition is Zr_3Sn_2 (46.45% tin); however, Pietrokowsky, in a recent investigation (4) of the zirconium-tin phase, has reported that the structure is Zr_5Sn_3 (hexagonal, Mn_5Si_3 type), so this formula has been tentatively adopted in the present work. Zr_5Sn_3 corresponds to the composition 43.84% tin, which is about 3% lower in tin than the observed single-phase alloys. In the diagram, the phase is placed at the experimentally determined, rather than the ideal, Zr_5Sn_3 composition. This shift may not be too surprising in view of the relative size independence of the Mn_5Si_3 type of structure, in which atom substitutions might rather easily occur. A similar shift from stoichiometric ratio has been noted in the case of the phase Ti_5Si_3 (1). Attempts to index the Debye-Scherrer X-ray patterns of many as-cast and heat treated alloys in this composition area were unsuccessful at this laboratory.

The general instability of these alloys made efforts to determine whether this intermediate phase has a variable composition fruitless. Tentatively, it should be considered to have a singular composition.

Tin-Rich Alloys

The two types of structures which occur in alloys containing more than 47% tin are illustrated in Figs. 25 and 26. The former is a 65.6% tin alloy showing a typical three-phase peritectic arrangement: primary Zr_5Sn_3 crystals, a peritectic wall of a new intermediate phase, and a matrix of tin. The latter is a nominal 95% tin alloy which contains only primary dendrites of the new phase in a matrix of tin. Only the tin-rich alloys which were nearly free of Zr_5Sn_3 showed any stability in normal atmospheres; others tended to decompose rapidly after preparation. This fact, and the coexistence in the alloys of phases melting at 1985 and 232 °C (3605 and 450 °F), made heat treatments to develop the peritectically formed intermediate phase virtually impossible. A series of thermal analyses indicated that the peritectic temperature was located at 1140 ± 15 °C (2085 °F). The only other heating and cooling arrest was obtained at 231 ± 1 °C. The position of the peritectic melt, deduced from the disappearance of Zr_5Sn_3 as a primary phase in arc-cast alloys, was roughly located between 80 and 87% tin. A special series of alloys in the composition range 75 to 95% tin was prepared to check

this more accurately. These alloys were placed in carbon cups inside sealed quartz capsules and held for 20 hours at 1152 °C (2105 °F), just above the peritectic temperature. Alloys containing 85% or more tin were completely molten; while alloys containing less than 80% tin contained liquid plus solid phases at this temperature. Accordingly, the peritectic melt must be at $83 \pm 3\%$ tin.

Identification of the intermediate phase formed by the peritectic reaction at 1140 °C (2085 °F) between Zr_5Sn_3 and the melt containing 83% tin required rather special techniques. Several two-phase alloys containing primary crystals of this intermediate phase were subjected to anodic dissolution in a 10% NaOH electrolytic bath, stainless steel plates serving as cathodes. The tin matrix was taken into solution and small deposits of the primary phase were collected. Two samples from separate alloys were adequate for semimicro analyses. The tin contents proved to be 53.3 and 51.2% in the two tests. The most likely stoichiometric composition in this vicinity is $ZrSn$ (56.55% tin). Since the analytical accuracy on such samples cannot be considered too high, this formula is tentatively adopted for the intermediate phase, although the evidence is not entirely satisfactory. Certainly, the analytical evidence seems to refute the existence of a phase located nearer the end of the peritectic horizontal, such as $ZrSn_2$ (72.33% tin).

Some of the material collected from the electrolytic baths was subjected to X-ray analysis. A Debye-Scherrer pattern was taken, using filtered, characteristic copper $K\alpha$ radiation. A complex pattern was obtained which has tentatively been indexed as orthorhombic, with the following parameters: $a = 7.43 \text{ \AA}$, $b = 5.82 \text{ \AA}$, $c = 5.16 \text{ \AA}$; $a:b:c = 1.28:1:0.885$.

By the rules of phase equilibria, tin must enter into either a eutectic or a peritectic with $ZrSn$. In order to check this point, alloys with 95, 97, 99, and 99.5 nominal % tin were examined metallographically and subjected to accurate thermal analysis. The arrests in these alloys were not distinguishable from that of pure tin within $\pm 1^\circ\text{C}$. The alloy most dilute in zirconium (99.5% tin) still showed primary $ZrSn$ crystals in a tin matrix. Accordingly, the eutectic or peritectic must occur between 99.5 and 100% tin, and at $231 \pm 1^\circ\text{C}$.

Melting-Range Determinations

A preliminary investigation was undertaken to determine the melting point of the "Grade 3" Westinghouse zirconium crystal bar used as melting stock. An average value of 1852 °C (3365 °F) was obtained in about a dozen checks in the incipient melting furnace. The maximum variation between individual runs was $\pm 10^\circ\text{C}$. The figure compares favorably with 1857 °C (3375 °F) obtained by Zwicker, quoted by de Boer (5), and 1865 °C (3390 °F) reported

by Cubicciotti (6), and was accordingly used in construction of the diagrams.

The incipient melting techniques described earlier were employed for solidus, eutectic, and intermetallic compound melting determinations in the 0 to 47% tin alloy range, but were inapplicable at higher tin contents because of the presence of free tin in all of these alloys. Thermal analysis was employed for zirconium-rich alloys melting within the useful temperature range of platinum/platinum-10% rhodium thermocouples and in all tin-rich alloys. The data are summarized in Table IV.

Table IV
Melting-Range Determinations

Alloy, Wt. % Tin	Thermal Analysis		Incipient Melting	
	Arrests, °C	Comments	Melting Observed, °C	No Melting, °C
4.7	1710	1675
10.5	1635	1600
20*	1592 > 1604	Sloping
21.2	1610	1575
24.2	1575	1555
24*	1590
30.6	1585
37.0	1905
46.7	1985
50.5	1875
60*	1121
62*	1144	Sharp, level
70*	1140...230	Sharp, level
75*	1165
85*	1173...230
95*	231	Iron-Constantan
97*	231	Iron-Constantan
99*	231 +	Iron-Constantan
99.5*	231	Iron-Constantan
100	231 +	Iron-Constantan

*Nominal composition.

GENERAL COMMENTS ON ZIRCONIUM-TIN ALLOYS

Some safety precautions have been found necessary in the handling and storage of zirconium-tin alloys, particularly those containing 45 to 65% tin. On one occasion a freshly prepared alloy within this composition range burst into flames spontaneously in a sample envelope, causing a small fire among similarly stored specimens. Alloys in the vicinity of the eutectic composition (24% tin) tend to spark brilliantly on cutting and burn if in finely divided form, although there is no danger of spontaneous combustion in this composition range.

In view of the general phase relationships, as well as the instability of tin-rich zirconium-tin alloys, they are considered to be devoid of possible utility, and of academic interest only.

SUMMARY

Techniques for the production and heat treatment of high purity zirconium-tin alloys free from contamination are described.

The phase diagram of this system has the following features:

1. Three intermediate phases exist; these are Zr_4Sn (24.55% tin), which is formed by the peritectoid reaction: $\beta + Zr_5Sn_3 \rightleftharpoons Zr_4Sn$ at $1325 \pm 20^\circ C$ ($2415^\circ F$); Zr_5Sn_3 (tentative; 43.84% tin) which melts with an open maximum at $1985 \pm 25^\circ C$ ($3605^\circ F$); and $ZrSn$ (tentative; 56.55% tin) formed by a peritectic reaction between Zr_5Sn_3 and a melt containing about 83% tin at $1140 \pm 15^\circ C$ ($2085^\circ F$).
2. Zirconium and Zr_5Sn_3 give rise to a eutectic at 23.5% tin and $1590 \pm 15^\circ C$ ($2895^\circ F$).
3. The solubility of tin in beta zirconium is approximately 21% at the eutectic temperature, 15% at $1325^\circ C$ ($2415^\circ F$), and 6.5% at $980^\circ C$ ($1795^\circ F$).
4. Tin raises the $\alpha \rightleftharpoons \beta$ transformation temperature of zirconium, which results in the peritectoid reaction: $\beta + Zr_4Sn \rightleftharpoons \alpha$ at $980 \pm 20^\circ C$.
5. The solubility of tin in alpha zirconium decreases from 9% at $980^\circ C$ ($1795^\circ F$) to about 1.5% at $600^\circ C$ ($1110^\circ F$).
6. Tin displays no appreciable solid solubility for zirconium. The eutectic or peritectic (undetermined) between tin and $ZrSn$ must exist at higher tin content than 99.5%, and not more than $1^\circ C$ above or below the melting point of tin.

ACKNOWLEDGMENTS

The authors are grateful to the Atomic Energy Commission, sponsor of the work, for permission to publish this paper. Thanks are due to Messrs. C. E. Lundin and R. F. Domagala for supervising the melting and heat treatment of the many alloys; C. A. Johnson for the metallographic work; and Dr. W. Rostoker for interpretation of the X-ray diffraction patterns.

References

1. M. Hansen, H. D. Kessler and D. J. McPherson, "The Titanium-Silicon System", *TRANSACTIONS, American Society for Metals*, Vol. 44, 1952, p. 518.
2. M. Hansen, E. L. Kamen, H. D. Kessler and D. J. McPherson, "Systems Titanium-Molybdenum and Titanium-Columbium", *Transactions, American Institute of Mining and Metallurgical Engineers*, Vol. 190, 1952, p. 881.
3. R. Vogel and W. Tonn, "A Transition Point for Zirconium", *Zeitschrift für anorganische und allgemeine Chemie*, Vol. 202, 1931, p. 293.
4. P. Pietrokowsky, "Crystal Structure of Zirconium-Rich Compounds With Silicon and Tin", to be published in *Acta Crystallographica*, 1952.
5. J. H. de Boer, "Zirconium", *Industrial and Engineering Chemistry*, Vol. 19, 1927, p. 1256.
6. D. Cubicciotti, Technical Report No. 6, "The Melting Point-Composition Diagram of the Zirconium-Oxygen System". U. S. Navy, Office of Naval Research, Research Contract N7-onr-329, Task Order II, May 1950.

DISCUSSION

Written Discussion: By H. A. Wilhelm, associate director, Ames Laboratory, U. S. Atomic Energy Commission, Iowa State College, Ames, Iowa.

Previous to the writing of this paper, the authors and I were together in a conference on this system, and data from my laboratory were compared with data of the authors. Although we differ slightly in observations on two or three minor points, the material as the authors have presented it is entirely acceptable at this time. The authors are to be commended on the high quality of their experimental investigation leading to this outstanding contribution.

Written Discussion: By H. A. Saller, supervisor, and F. A. Rough, assistant supervisor, Battelle Memorial Institute, Columbus, Ohio.

The authors are to be congratulated for having done an excellent job in working out the zirconium-tin system. This alloy system was also studied at Battelle Memorial Institute, and the resulting data are in close agreement with those of the authors. In the work which was done at Battelle, considerable emphasis was placed upon the determination of the solubility of tin in alpha zirconium and the possible effects of various base material compositions upon this solubility.

The study of the solubility of tin in alpha zirconium is complicated by the difficulty in obtaining equilibrium. Hence, a first appraisal might lead one to think that considerably more tin is soluble in alpha zirconium than has been reported. However, when the alloys are suitably heat treated for long periods of time, a decreasing and generally lower solubility curve is detected similar to that presented in the paper under discussion.

The solubility of tin in alpha zirconium was first determined using arc-melted alloys prepared from Grade I Foote Mineral Company crystal bar zirconium. Subsequently, arc-melted alloys were prepared and studied using Grade III Westinghouse crystal-bar zirconium and Bureau of Mines AB Grade sponge zirconium. AB Grade sponge-base alloys were also induction-melted in graphite crucibles for similar studies. For those who are not familiar with zirconium, the spectrographic purity of these three base materials is generally good, with small variations in the amounts of the various elements which are present. One exception to this is the presence of perhaps 1500 ppm of magnesium in the AB sponge zirconium. In addition, the oxygen and nitrogen contents vary roughly as follows:

	Oxygen	Nitrogen
Crystal-bar zirconium	100 to 200 ppm	10 to 30 ppm
AB sponge zirconium	1000 ppm	20 to 50 ppm

The vacuum-induction-melted AB sponge-base alloys also contained from 0.2 to 0.3 weight per cent carbon while the magnesium content was reduced to perhaps 200 ppm by vacuum melting.

The solubility of tin in alpha zirconium in all of the above-described alloys was found to be similar, indicating that the base material composition variations had no appreciable effect upon this feature of the system.

Authors' Reply

The authors are grateful for the corroborating comments and addenda of Messrs. Wilhelm, Saller and Rough. The characteristic analyses of the

various zirconium grades supplied by Messrs. Saller and Rough are particularly appreciated. Regarding the effect of inherent contaminants on the solute solubility in alpha zirconium, we have not studied the solubilities in magnesium-reduced zirconium. We have, however, studied this feature in several "sister" systems with titanium, using both magnesium-reduced and iodide titanium-based alloys, and have found, in agreement with Saller and Rough, that the alpha solid solubility is not measurably affected when these solubilities are low. In connection with the phase boundaries originating from, and in the immediate vicinity of, the $\alpha \rightleftharpoons \beta$ transition point, however, such impurities have an exceedingly detrimental effect on the placement of boundaries. Since most zirconium actually does not transform at a singular temperature (i.e., possesses a two-phase $\alpha + \beta$ field near the transition temperature due to impurities), limited ternary fields will result in this area of any binary system, and affect the placement of the apparent binary phase boundaries. The greater the oxygen and nitrogen content of the zirconium or titanium used, the more severe is this problem.

The authors were aware of the concurrent work on the zirconium-tin system by both the Iowa State and Battelle groups and had most informative discussions with them during the course of the work presented. No reference to this was made in the paper because of the classification status of their work at that time.

THE MARTENSITE TRANSFORMATION TEMPERATURE IN TITANIUM BINARY ALLOYS

BY POL DUWEZ

Abstract

The temperature at which the martensite transformation from beta solid solution to alpha prime supersaturated solid solution takes place has been measured in binary alloys of titanium with columbium, tantalum, tungsten, iron, chromium, and manganese. In all cases, the M_s curve decreases with increasing amount of all elements. The critical concentration above which the beta structure is retained after quenching in the above-mentioned binary alloys is discussed in connection with results published by other investigators.

INTRODUCTION

PREVIOUS studies have shown that in titanium binary alloys the beta solid solution is not retained by quenching, unless the concentration of the alloying element is above a certain critical value. For lower concentrations, the beta solid solution decomposes, at least partially, into a supersaturated alpha solid solution, generally referred to as alpha prime. The temperature at which this reaction takes place has been shown to be independent of the rate of cooling in the case of titanium-molybdenum (1)¹ and titanium-vanadium (2) alloys; it is therefore believed to be of the martensitic type. The present work is concerned with the determination of the temperature at which the martensite-like reaction, beta to alpha prime, takes place in binary alloys of titanium with columbium, tantalum, tungsten, iron, chromium, and manganese.

PREPARATION OF ALLOYS AND METHODS OF MEASURING

The alloys of titanium with manganese, tungsten, and tantalum were obtained from Battelle Memorial Institute through the courtesy of Dr. R. I. Jaffee, and some of the titanium-columbium alloys were kindly furnished by Dr. Max Hansen of Armour Research Foundation. All these alloys were made with pure titanium produced by the iodide process and were melted in a water-cooled copper crucible in an arc under helium or argon. The alloys of titanium with iron and

¹The figures appearing in parentheses pertain to the references appended to this paper.

A paper presented before the Eighth Western Metal Congress of the Society, held in Los Angeles, March 23 to 27, 1953. The author, Pol Duwez, is professor of mechanical engineering, California Institute of Technology, Pasadena, Calif. Manuscript received April 10, 1952.

chromium and some of those with columbium were prepared in this laboratory in an arc furnace previously described (1).

The technique used for the determination of the transformation temperature during rapid cooling was that described by Greninger in his study of martensite in carbon steels (3). The same technique has been used more recently for the study of some titanium binary systems (1, 2, 4). The specimens were about 0.020 inch thick and 1/16 inch square. Chromel-alumel wires, 0.005 inch in diameter, were placed between the two pieces and the assembly spot-welded. The specimens were heated by means of a molybdenum coil in vacuum and rapidly cooled by a helium jet. The temperature was recorded on a rotating drum-type oscillograph. The break in the cooling curve due to the heat released by the transformation was quite easy to locate with an accuracy of $\pm 5^\circ\text{C}$. However, the scatter between results obtained on different samples of the same alloy was generally greater than $\pm 5^\circ\text{C}$.

RESULTS

The results of measurements of transformation temperature versus concentration are shown in Figs. 1 and 2. In Fig. 1, the curves previously published for titanium-molybdenum (1) and titanium-vanadium (2) alloys have been reproduced. For each alloy, at least 10, and in some cases as many as 25, tests were made with cooling rates in the range of 100 to 10,000 $^\circ\text{C}$ per second. In all cases, no appreciable effect of rate was found and the length of the vertical bar on the diagrams of Figs. 1 and 2 indicates the temperature interval corresponding to the random scatter in experimental results.

The results of this study indicate that as the amount of alloying element soluble in beta titanium is increased, the beta-to-alpha-prime transformation temperature decreases steadily. In addition, it has been shown (1, 2) that the relative amount of beta transforming into alpha prime decreases also with increasing concentration, and hence the thermal arrest becomes weaker and difficult to observe. It is therefore not possible, with the sensitivity of the present method of measurement, to establish the M_s curves below approximately 300 $^\circ\text{C}$ (570 $^\circ\text{F}$). These curves, however, could be extrapolated, providing the concentration above which the beta phase is retained by quenching is determined by other methods. Microscopic observation is probably the most reliable method for determining the concentration at which the change occurs from a beta-plus-alpha-prime needle structure into a pure beta structure. The results of previous studies (5-12) on this subject are summarized in Table I.

When the various critical concentrations given in Table I are plotted on the graphs of Figs. 1 and 2 on the horizontal axis, it becomes apparent that, with the exception of iron, the M_s curves may be extrapolated to these concentrations, although in some cases a rather

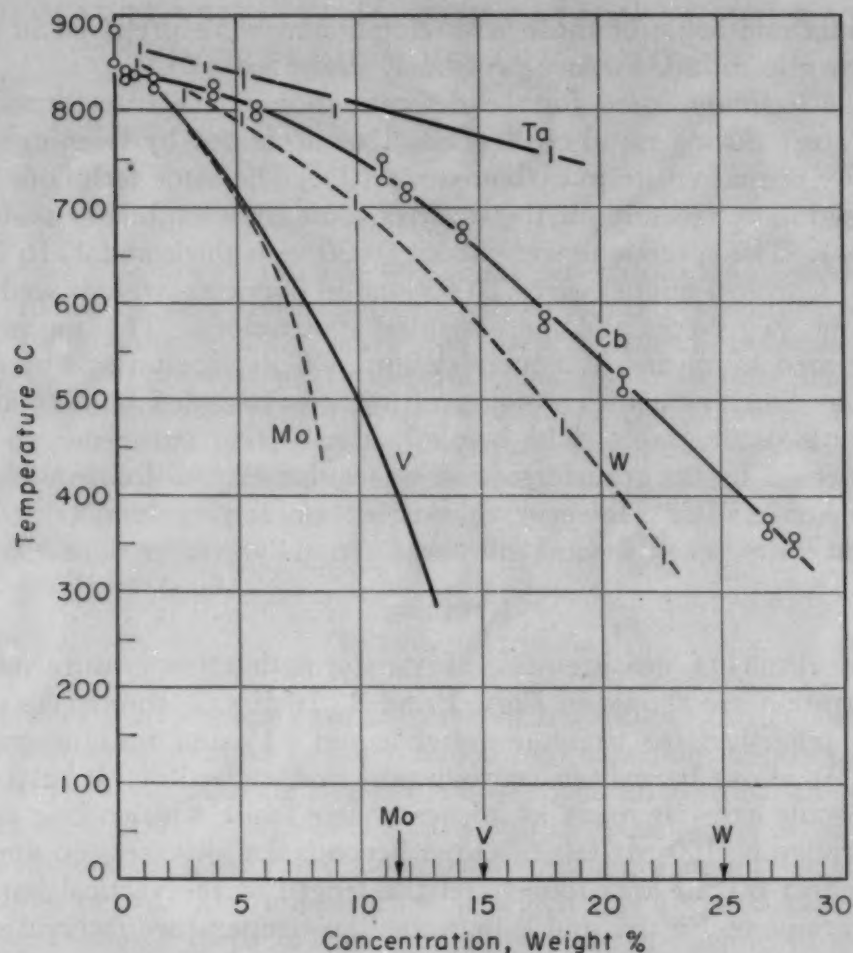


Fig. 1— M_s Curves for Titanium Binary Alloys With Tantalum, Columbium, Tungsten, Vanadium, and Molybdenum.

Table I
Concentration of Alloying Element Above Which Beta Is Retained After Quenching

Alloying Element	Concentration (wt. %)	Reference
molybdenum	12	1
	between 11 and 12	12
tungsten	between 20 and 25	5
columbium	about 36	6
tantalum	between 40 and 50	5
vanadium	14.9	2
	about 15	7
manganese	about 6.4	5
chromium	between 5.4 and 6.5	10
iron	between 3.08 and 4.07	9

abrupt change in curvature is required. For iron, the critical concentration in the range of 3.08 to 4.07% lies definitely on the left side of the intercept of any reasonable extrapolation of the M_s curve with the horizontal axis.

It must be emphasized that the study of the titanium-iron system (9) was made with titanium obtained by the Kroll process and hence the impurities might have been responsible for stabilizing the beta structure. In addition, the titanium-iron alloys containing 4.07 and 5.9% iron were found by Worner (9) to be quite hard in comparison with those containing 8.7% and more of iron, in which the beta structure was retained after quenching. In view of this fact, Worner states,

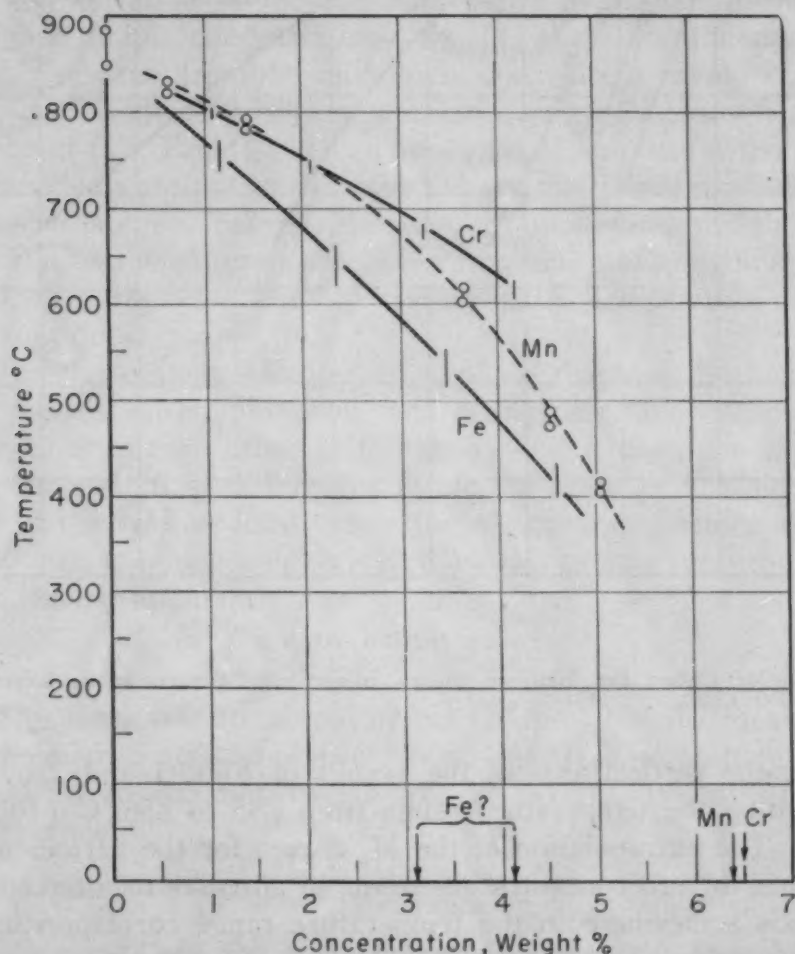


Fig. 2— M_s Curves for Titanium Binary Alloys With Chromium, Manganese, and Iron.

"It would seem that the 4.07 and 5.9% alloys may not actually be strictly unaltered beta solid solutions after the quench, and the evidence obtained from observations under the microscope is inconclusive." On the basis of this statement, and as a result of the present investigation, the critical concentration for retaining beta in titanium-iron alloys is believed to be around 6%.

As shown in a previous paper (1), the beta-to-alpha transformation in pure titanium is progressively lowered when the rate of cooling increases from 10 to 10,000°C per second. This behavior is in-

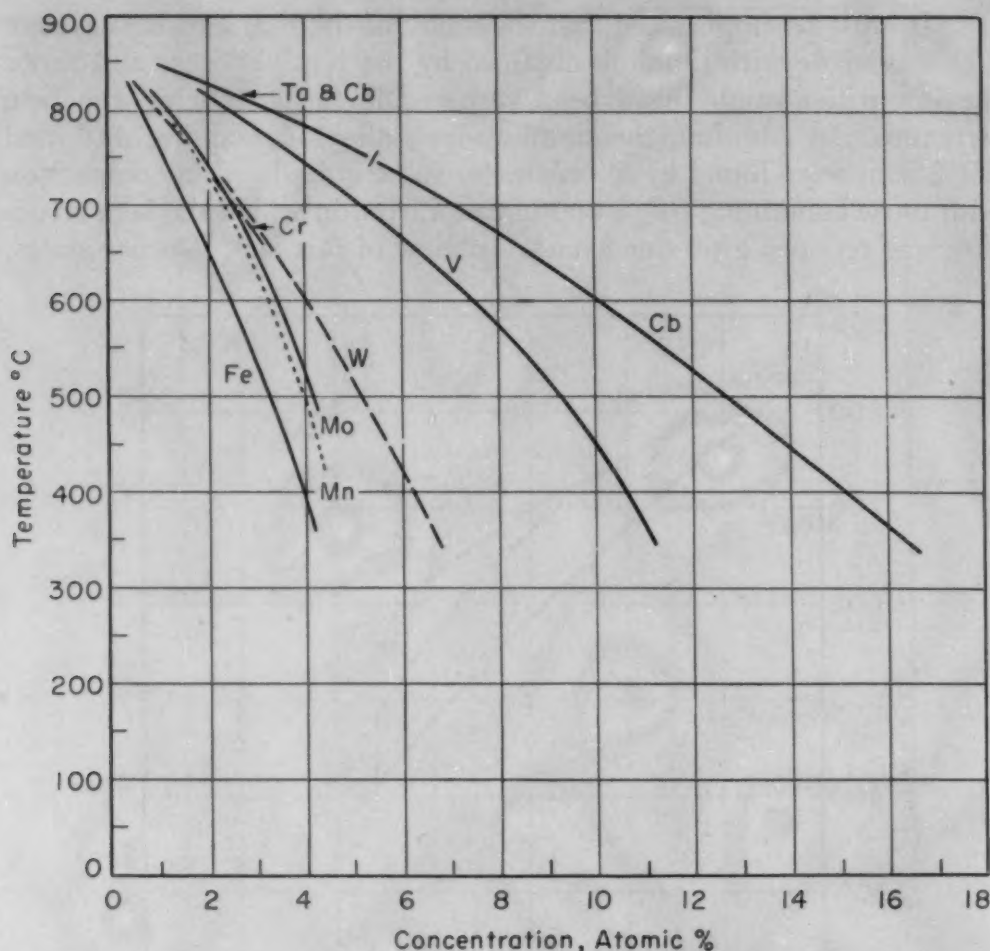


Fig. 3— M_s Curves for Titanium Binary Alloys With Concentrations Expressed in Atomic Per Cent.

dictated on the vertical axis of the graphs of Figs. 1 and 2 by two points limiting the temperature range from 885 to 855 °C (1625 to 1570 °F). The extrapolation of the M_s curves for the various alloying elements to zero concentration seems in all cases to intercept the vertical axis somewhere in the temperature range corresponding to the transformation of pure titanium. A similar result is found in the iron-manganese system, in which a martensite transformation from gamma solid solution to a supersaturated alpha solid solution has been studied by Troiano and McGuire (13).

The alloying elements studied in the present investigation are soluble in beta titanium to various extents; tantalum, columbium, molybdenum, and vanadium form continuous series of solid solutions (1, 2, 5, 6 and 7) whereas iron, chromium, manganese, and tungsten are only partially soluble in titanium. For the elements completely soluble in beta titanium, it might be anticipated that the location of the martensite transformation curve would be somewhat related to the difference in atomic diameter between titanium and the solute element.

To substantiate this hypothesis, tantalum and columbium should have about the same effect on lowering the beta-to-alpha-prime transformation temperature, molybdenum should come next, and vanadium should have the greatest effect of these four elements. When the curves of Fig. 1 are replotted on the basis of atomic concentration (Cf. Fig. 3), the tantalum and columbium curves are very close to each other, at least up to 5.5 atomic per cent, which was the maximum concentration of the tantalum alloys available for this study. At higher atomic concentrations, the M_s curve for tantalum would probably separate from the columbium one, since it should extrapolate to about 17.8 atomic per cent tantalum against 22.5 atomic per cent columbium (Cf. Table I). In addition, the M_s curves for molybdenum and vanadium are not in the expected relative position, since the difference in atomic diameter between titanium and molybdenum is smaller than the difference between titanium and vanadium and yet molybdenum depresses the M_s transformation temperature more than vanadium does.

For the elements leading to a phase diagram of the eutectoid type, namely chromium, iron, and manganese, the M_s curves are rather close to each other (Cf. Fig. 3) and it does not appear that the consideration of differences in atomic diameter is a determining factor in the relative locations of the M_s curves. Factors other than atomic size are obviously involved in the process of beta-to-alpha-prime transformation.

ACKNOWLEDGMENT

This work was sponsored by the Office of Naval Research, U. S. Navy, under contract number N6onr-24430. The author wishes to express his appreciation to Mr. W. V. Wright, Jr., who performed the experiments.

References

1. P. Duwez, "The Effect of the Rate of Cooling on the Alpha-Beta Transformation in Titanium and Titanium-Molybdenum Alloys", *Transactions, American Institute of Mining and Metallurgical Engineers*, Vol. 191, 1951, p. 765-771.
2. P. Pietrokowsky and P. Duwez, "A Partial Titanium-Vanadium Phase Diagram", *Transactions, American Institute of Mining and Metallurgical Engineers*, Vol. 194, 1952, p. 627-630.
3. A. B. Greninger, "The Martensite Thermal Arrest in Iron-Carbon Alloys and Plain Carbon Steels", *TRANSACTIONS, American Society for Metals*, Vol. 30, 1942, p. 1.
4. P. Duwez, "Allotropic Transformation in Titanium-Zirconium Alloys", *Journal, Institute of Metals*, Vol. 19, 1952, p. 525-527.
5. D. J. Maykuth and others, "Titanium Alloy Phase Diagrams for the Systems Titanium-Manganese, Titanium-Tungsten, and Titanium-Tantalum", Summary Report to Wright-Patterson Air Force Base, Jan. 12, 1952.

6. M. Hansen and others, "Systems Titanium-Molybdenum and Titanium-Columbium", *Transactions*, American Institute of Mining and Metallurgical Engineers, Vol. 194, 1951, p. 881-888.
7. H. K. Adenstedt, J. R. Pequignot and J. M. Raymer, "The Titanium-Vanadium System", *TRANSACTIONS*, American Society for Metals, Vol. 44, 1952, p. 990-1003.
8. H. W. Worner, "The Constitution of Titanium-Rich Alloys of Iron and Titanium", *Journal*, Institute of Metals, Vol. 79, 1951, p. 173-188.
9. H. W. Worner, "Heat Treatment of Titanium-Rich Titanium-Iron Alloys", *Journal*, Institute of Metals, Vol. 80, 1952, p. 213-216.
10. P. Duwez and J. L. Taylor, "A Partial Titanium-Chromium Phase Diagram and the Crystal Structure of $TiCr_3$ ", *TRANSACTIONS*, American Society for Metals, Vol. 44, 1952, p. 495-517.
11. M. K. McQuillan, "A Provisional Constitutional Diagram of the Titanium-Chromium System", *Journal*, Institute of Metals, Vol. 79, 1951, p. 379-390.
12. D. J. DeLazaro and others, "Time-Temperature Transformation Characteristics of Titanium-Molybdenum Alloys", *Transactions*, American Institute of Mining and Metallurgical Engineers, Vol. 194, 1952, p. 265-269.
13. A. R. Troiano and F. T. McGuire, "A Study of the Iron-Rich Iron-Manganese Alloys", *TRANSACTIONS*, American Society for Metals, Vol. 31, 1943, p. 340-359.

THE INFLUENCE OF INSOLUBLE PHASES ON THE MACHINABILITY OF TITANIUM

BY R. M. GOLDBOFF, H. L. SHAW, C. M. CRAIGHEAD
AND R. I. JAFFEE

Abstract

The machinability of titanium has been shown to be very sensitive to strength level and to machining conditions. The machinability of titanium doubles when purity is increased from that of the commercial magnesium-reduced grade to that of the high purity iodide titanium grade. Similarly, when the tool-thrust load is increased or the speed of cutting is decreased, the machinability of titanium increases relative to free-cutting steel much more than does, say, 18-8 stainless steel.

In an attempt to improve the machinability of titanium, alloy additions that formed insoluble phases with titanium were investigated. Some, like boron, arsenic, tellurium, sulphur, and selenium, made a moderate improvement in machinability when added in suitable amounts. Others, particularly carbon, were very detrimental to machinability.

INTRODUCTION

TO DATE, very little information concerning the machining characteristics of titanium or its alloys has been published. All of the literature on this subject is very general, and has been mostly concerned with the recommendation of machining practices, such as suggesting the use of high speed tools, heavy cuts, and slow speeds (1, 2).¹ In the past, general statements have been made to the effect that the machining properties of titanium are similar to those of stainless steel or perhaps free-cutting stainless steel. More recently titanium has been described as having machining properties similar to jet-engine alloys (3). It should be pointed out that in almost all instances these conclusions are drawn from the experience of titanium fabricators. Such information is valuable, but its nature certainly points to the obvious need for fundamental machining studies on titanium and its alloys. An enormous effort is being put on the development of titanium and its alloys, and it is essential that so important a phase

¹The figures appearing in parentheses pertain to the references appended to this paper.

A paper presented before the Thirty-fourth Annual Convention of the Society, held in Philadelphia, October 18 to 24, 1952. The authors, R. M. Goldhoff, H. L. Shaw, C. M. Craighead and R. I. Jaffee, are associated with Battelle Memorial Institute, Columbus, Ohio. Manuscript received April 10, 1952.

as machinability keep pace. While no one program can be devised to answer all the questions that might be raised about titanium machinability, much information of limited scope can be provided. The work described here covers the limited field of the effect of insoluble phases on machinability, and attempts to answer the question whether any insoluble phases in titanium cause the marked improvement in machinability that lead does in brass or sulphur or selenium does in steel.

The elements which are commonly used to produce free-machining alloys are effective because they have a relatively low solubility in the base and form inclusions which act as aids to lubrication and lower the shear strength of the chip being cut. They are frequently present in the alloy as elemental phases such as lead in copper-base alloys and steel.

So far as is known, none of the alloying elements, low melting or otherwise, exist as elemental phases in titanium. Many of the common free-machining additions, such as lead, silver, and bismuth, have a relatively high solubility in titanium. Many of them have vapor pressures such that they are quite difficult to introduce into molten titanium. These two factors, high solubility and high vapor pressures, eliminate from consideration in this study many of the elements commonly used to improve machinability in other metals.

When the work began, available information indicated that only a few elements were known to have a low order of solubility in titanium. Falling into this class of additions were carbon, sulphur, silicon, boron, and beryllium. These then were the first additions to be investigated. Sulphur was added as both Ti_3S_4 and MoS_2 . It was thought that the latter compound, providing it could retain its identity and not form Ti_3S_4 on melting, might impart antifriction properties to the titanium, thus improving machining characteristics over and above those due to the sulphur addition. Other possibly insoluble additions added to titanium in this program were germanium, tellurium, selenium, phosphorus, and arsenic. It was necessary to prepare master alloys of titanium and the latter four elements to introduce them into molten titanium.

This study has been directed solely at determining the effects of insoluble phases on the machinability of titanium and its alloys. The results reported here have not been, nor were they intended to be, an exhaustive study of the machining characteristics of titanium. Rather, the work has been directed toward the possible development of a free-machining alloy.

PREPARATION OF ALLOYS

The base material used in this study was magnesium-reduced titanium sponge. Before use, the material was crushed to the proper

Table I
Actual and Intended Compositions of Titanium Alloys Used in Machinability Testing

Alloy No.	Intended Composition, %	Actual Composition, %			
		Alloy	N	W *	Fe C
1	Unalloyed	----	0.023	0.07	0.12 0.05
14	Unalloyed	----	0.023	0.22	0.11 0.07
16	Unalloyed	----	0.023	0.17	0.11 0.08
18	Unalloyed	----	0.023	< 0.01	0.14 0.06
19	Unalloyed	----	0.025	0.20	-----
23	Unalloyed	----	0.023	0.73	-----
27	Unalloyed	----	0.020	0.36	-----
31	Unalloyed	----	0.023	0.01	-----
35	Unalloyed	----	0.023	0.47	-----
39	Unalloyed	----	0.004	0.016	-----
44	Unalloyed	----	0.006	0.27	-----
48	Unalloyed	----	0.007	0.09	-----
53	Unalloyed	----	0.007	0.17	-----
54	Unalloyed	----	0.002	0.028	-----
	Iodide Ti		0.001		0.030
8	0.25C	0.25C	0.021	-----	-----
9	0.50C	0.47C	0.020	-----	-----
49	0.05B	0.067B	0.007	-----	-----
2	0.10B	0.13B	0.028	-----	-----
47	0.10B	0.10B	0.007	-----	-----
10	0.25B	0.29B	0.031	-----	-----
3	0.50B	0.57B	0.023	-----	-----
46	1.00B	0.67B	0.015	-----	-----
4	0.10Be	0.02Be	0.023	-----	-----
5	0.25Be	0.08Be	0.022	-----	-----
11	0.50Be	0.16Be	0.022	-----	-----
6	0.10Si	0.09Si	0.023	-----	-----
15	0.25Si	0.25Si	0.024	-----	-----
7	0.50Si	0.46Si	0.022	-----	-----
41	1.00Si	0.87Si	0.006	-----	-----
12	0.05S*	0.025S	0.020	-----	-----
13	0.10S*	0.035S	0.022	-----	-----
17	0.25S*	0.118S	0.022	-----	-----
20	0.03S†	0.02S	0.025	-----	-----
21	0.10S†	0.10S	0.021	-----	-----
22	0.25S†	0.25S	0.026	-----	-----
43	0.50S†	0.32S	0.009	-----	-----
42	1.00S†	0.68S	0.008	-----	-----
24	0.10Se	0.09Se	0.024	-----	-----
25	0.25Se	0.25Se	0.027	-----	-----
26	0.50Se	0.52Se	0.027	-----	-----
50	1.00Se	0.99Se	0.006	-----	-----
28	0.10P	0.07P	0.025	-----	-----
29	0.25P	0.17P	0.023	-----	-----
30	0.50P	0.39P	0.035	-----	-----
32	0.10Te	0.07Te	0.033	-----	-----
33	0.25Te	0.16Te	0.038	-----	-----
34	0.50Te	0.27Te	0.023	-----	-----
51	1.00Te	0.47Te	0.007	-----	-----
36	0.05Ge	0.03Ge	0.024	-----	-----
37	0.10Ge	0.11Ge	0.025	-----	-----
38	0.25Ge	0.24Ge	0.023	-----	-----
45	0.25As	0.26As	0.007	-----	-----
40	0.50As	0.51As	0.007	-----	-----
52	1.00As	0.67As	0.006	-----	-----

*Sulphur added as MoS₂. †Sulphur added as Ti₃S₄.

size for melting stock and leached in methanol to remove residual magnesium chloride. Analysis of this stock showed the following impurities: approximately 0.05% carbon, 0.15% iron, and 0.03% nitrogen.

For the preparation of alloys, arc-melting techniques were used. This arc furnace was developed at Battelle and has been previously described (4). Its essential features include an inert argon atmos-

phere, a water-cooled copper crucible and an inert, water-cooled tungsten electrode. In the initial melting, two 0.5-pound ingots of each alloy were prepared. Each of these ingots was machined to chips, and the chips were then combined and remelted. The chipping operation was used between melts to insure homogeneous distribution of the alloying additions. The final ingot of each composition weighed about 1 pound.

After melting, the ingots were surface-ground and forged at 1750 °F to 1½-inch square bar stock.

The forged bar stock was sand-blasted, ground, and pickled to remove all scale and surface contamination from the forging operation. The alloys were then hot-rolled at 1450 °F (790 °C) to 7/8-inch diameter bars and given a process anneal which consisted of heating in air for ½ hour at 1450 °F (790 °C) followed by cooling in air. This fabricated and annealed bar stock was the starting point for the machinability tests.

Table I shows the intended and actual compositions of all the alloys studied. Nitrogen analyses are given for all alloys, and tungsten analyses are given for all unalloyed samples. These analyses are included to show the minor variations in composition expected for these elements. The analytical method for oxygen in titanium is in an uncertain state, therefore no oxygen analyses were attempted. Carbon analyses on a number of unalloyed samples, as shown in Table I, were consistent, hence no great variation of carbon content is to be expected in the alloys.

METHODS FOR EVALUATING MACHINABILITY

The important choice of testing methods for studying machinability are mostly dictated by the quantity and shape of available stock. Furthermore, testing methods should simulate machining operations of commercial importance. This latter point is significant because a material superior in one specific test may not fall into the same classification in other cutting operations. Because lathe operations are widely used in evaluating machinability, single-tool lathe tests were used in this study. Saw tests were also included as a means of comparing machinability with another type of cutting operation.

Constant-Pressure Lathe Test

The equipment used for machinability testing is comparatively simple. It was developed at Battelle (5) and, among other things, was instrumental in the development of a superior Bessemer free-cutting steel (6, 7). It consists basically of a lathe with the tool carriage disconnected from the fixed-feed mechanism and mounted on ball bearings; a means of applying a predetermined lateral tool pres-

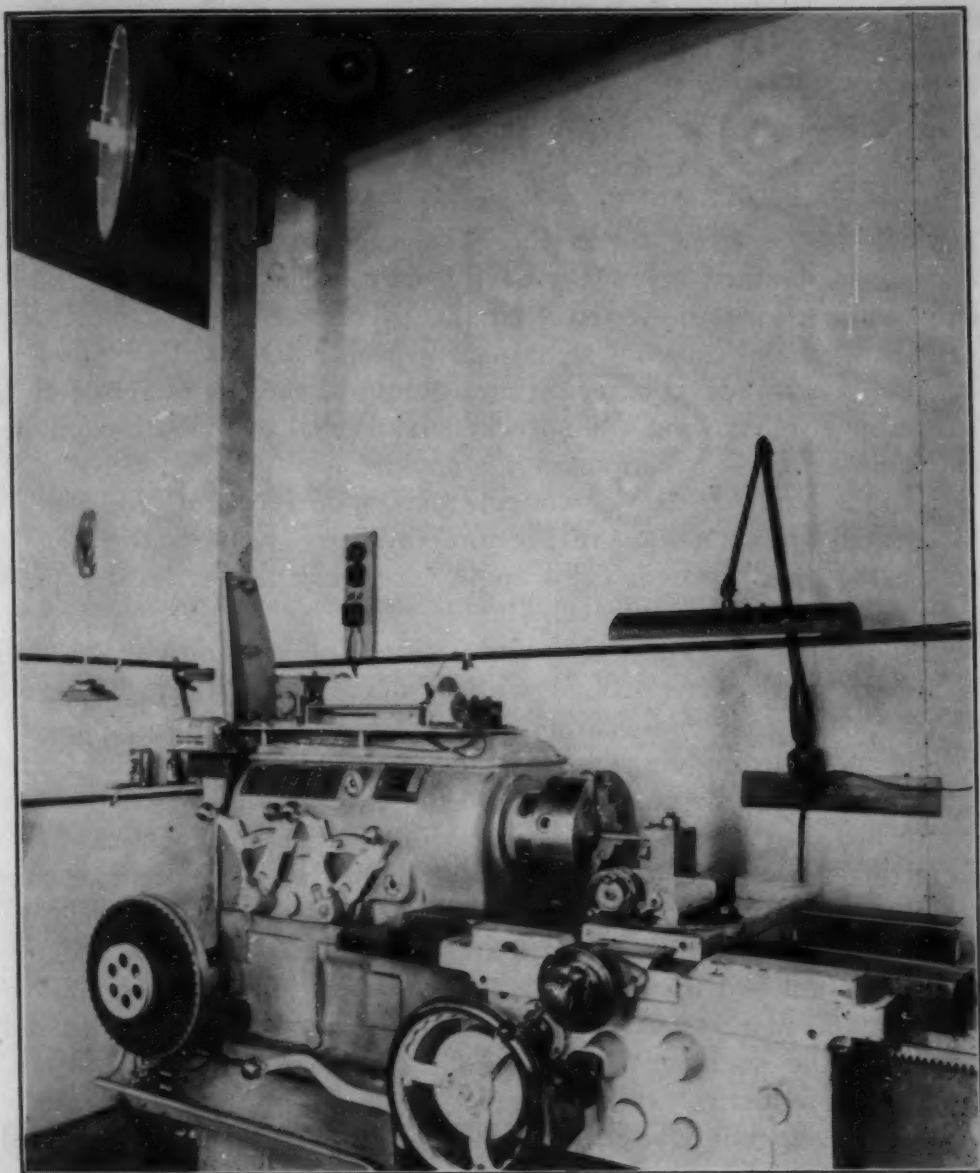


Fig. 1—Machinability Testing Equipment.

sure; and a device for recording the number of spindle revolutions occurring during a certain length of tool travel. Fig. 1 is a photograph of the testing equipment.

The cable attached to the weight shown at the left of the photograph moves the carriage by producing a torque on the drum mounted behind the hand wheel. The drum and hand wheel move the carriage by means of a pinion and rack in front and below the ways. The rate of carriage travel is controlled by the amount of weight used and the resistance of the metal to cutting. Variation in cutting rates among different materials is believed to be controlled by the friction produced between the chip and tool. The small pulley at the lower left is

mounted on ball bearings and its only purpose is to change the direction of the cable.

The black wheel behind the pulley at the lower left of the photograph is connected to the tool carriage by means of a shaft, sprocket, and roller chain. The periphery of the wheel moves 1 inch for each 0.2 inch of tool travel. The cogs on the circumference of the bakelite disk mounted in front of the wheel are spaced uniformly and operate the switch mounted below the device, thereby indicating tool travel. The switch closes an electrical circuit after each 0.2-inch increment of tool travel and causes a signal bell to ring.

The mechanical counter on the column at the left of the lathe is driven by a roller chain and sprockets connected to the lathe spindle, and indicates the revolutions of the spindle.

The special tool holder consists of a solid block of steel rigidly fastened to the compound of the tool carriage. It holds the tool so the cutting edge forms a right angle with the axis of the test piece and the direction of tool travel.

The tools used for testing were $\frac{3}{4}$ -inch square high speed steel tools. The tools were ground with 12-degree side-relief, 12-degree top-rake, 4-degree end-clearance, and 10-degree end-relief angles. A $\frac{1}{16}$ -inch turning cut was used in testing the titanium alloys, and all tests were run dry.

In order to facilitate comparisons between samples tested at different times and to reduce the effect of slight differences in tool conditions, a bar from a lot of Type 304 austenitic stainless steel was tested several times in each series and was used as a reference standard. This standard material was considered to have a machinability rating of 100 in all tests. Materials which cut faster, or had heavier feeds than the standard material under otherwise fixed conditions, were given numerical ratings higher than 100. Conversely, those materials which cut slower, or had lighter feeds than the standard material, were given ratings lower than 100. The ratings may be calculated by either of the following methods:

$$\text{Machinability Index} = 100 \times \frac{\text{Average feed on unknown material}}{\text{Average feed on standard material}}$$

or

$$\text{Machinability Index} = 100 \times \frac{\text{Average number of spindle revolutions for ten 0.2-inch increments of tool travel on the standard material}}{\text{Average number of spindle revolutions for ten 0.2-inch increments of tool travel on the unknown material}}$$

The two methods are equivalent, because feed is defined as the distance of tool advance per spindle revolution. The machinability indexes are usually calculated by the second method because the number of spindle revolutions is available from the primary test record. The original observations of the spindle revolutions, called "R" values, correspond to the number of spindle revolutions for 0.1 inch of tool travel. By definition, the feed equals 0.1 inch divided by "R". Because of this relationship, machinability comparisons can be based on "R" values instead of feeds calculated from them.

Ordinarily, a group of samples is tested with one tool in a series which includes three tests on the standard material. The order of testing each material is varied systematically in different series in order to compensate for any tool wear. To increase the reliability of the machinability ratings and to minimize the effect of different tools, each material is usually included in six series of tests, using a different tool in each series. The machinability rating of a material is based on a comparison with the average feed of the standard material in the same series.

Standard testing conditions include the choice of a testing load (weight plus the weight of the hanger) and a combination of spindle speed and bar size to obtain a given surface speed of cutting. Since prior data on titanium were not available, it was necessary to experiment with this first series of alloys to determine the proper testing conditions. Previous studies on the testing equipment had shown that bar size is important only in determining the surface speeds available for testing. Other factors considered in the choice of testing conditions involved getting a large spread in resulting feed between different materials, consideration of the effects of speed on performance and the sequence of testing, tool-life considerations, and avoidance of excessive temperature changes in tool and workpiece. The selection of these variables is discussed in detail in the section on lathe tests.

Saw Test

The $\frac{5}{8}$ -inch diameter bars, remaining after the turning tests had been completed, were used in saw tests. For this work a Wells band saw, Type 8-M-43, was used. The blade was 11 feet 6 inches long and traveled at a rate of 46 feet per minute. This saw blade was $\frac{3}{4}$ inch wide, of 21-gage material, and had 10 teeth per inch with a "raker" set. The maximum load available with the saw, about 40 pounds, was used in this test work.

In the initial test, alternate cuts were made on Type 304 stainless steel and the various alloys according to the following sequence: stainless steel, test alloy, stainless steel, test alloy, and stainless steel. The time to cut through the bars was recorded. The three values for stainless steel were averaged and a similar average was obtained from the

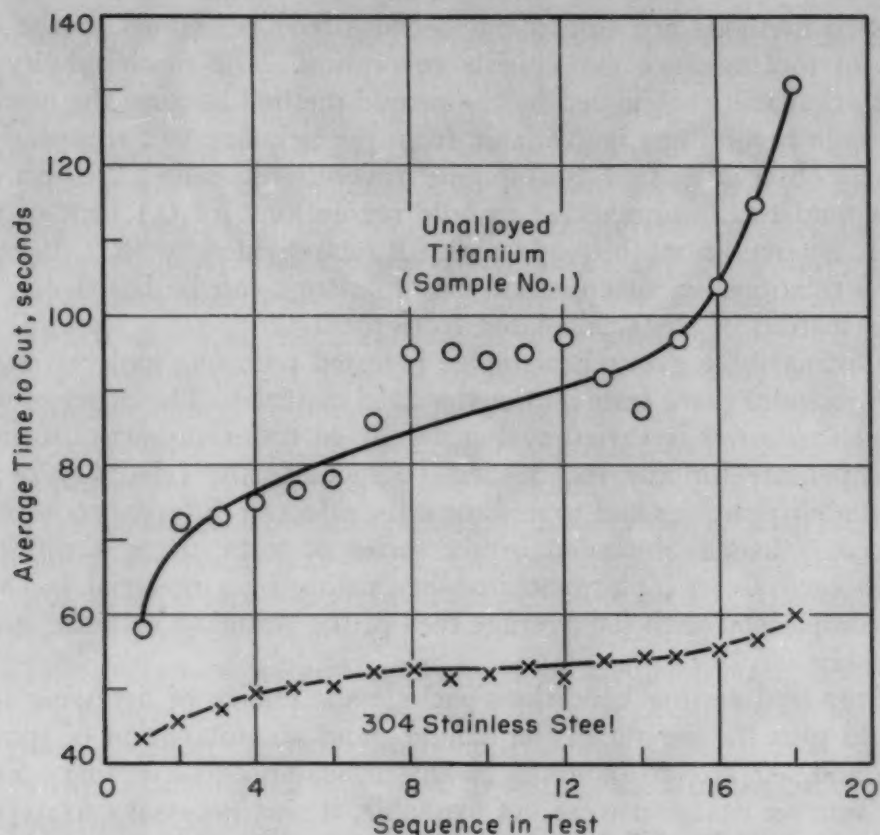


Fig. 2—Relative Effect of Saw Wear on the Cutting Time for Type 304 Stainless Steel and Unalloyed Titanium.

two cuts on each of the various titanium alloys. Using the average time to cut stainless steel as 100, an index was then calculated for each test of the titanium alloys. It was evident from the observed data that Type 304 stainless steel is a relatively insensitive material insofar as saw wear is concerned. The relative effect of saw wear on the cutting time for alternate sawing of Type 304 stainless steel and unalloyed titanium is shown graphically in Fig. 2. The data plotted in this graph are the average times to cut Type 304 stainless steel and unalloyed titanium during a sequence of testing. Obviously titanium is markedly sensitive to saw wear, whereas the stainless steel shows little effect from wear. Because of these diverse characteristics of stainless steel and titanium, comparisons based on sawing stainless steel are meaningless.

Since stainless steel could not be used as a standard material, another saw test was made on the same alloys used previously, but using one of the unalloyed titanium samples as a standard material. In this test a cut was made on the standard, followed by three consecutive cuts on the alloy being tested, and then by a cut on the standard. From this test, using unalloyed titanium as a standard, fairly

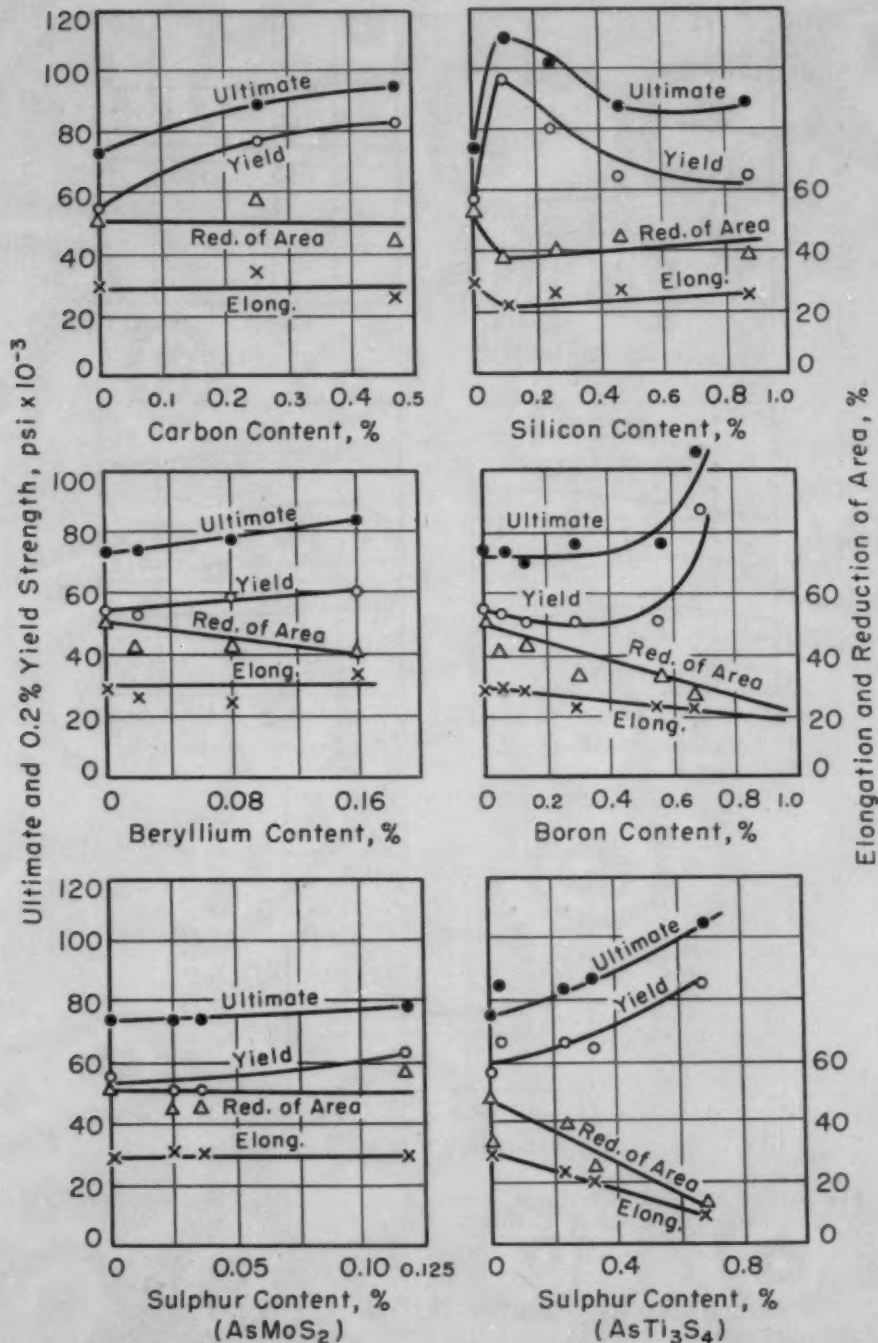


Fig. 3—The Effect of Carbon, Sulphur, Beryllium, Boron, and Silicon on the Mechanical Properties of Titanium.

reproducible ratings were obtained on the various alloys. To show whether position in the test had any effect on the rating in the saw test, the order of testing the alloys was reversed. In general the order seemed immaterial. Therefore, this test using unalloyed titanium as a standard was adopted as a method for evaluating the sawing characteristics of all the alloys.

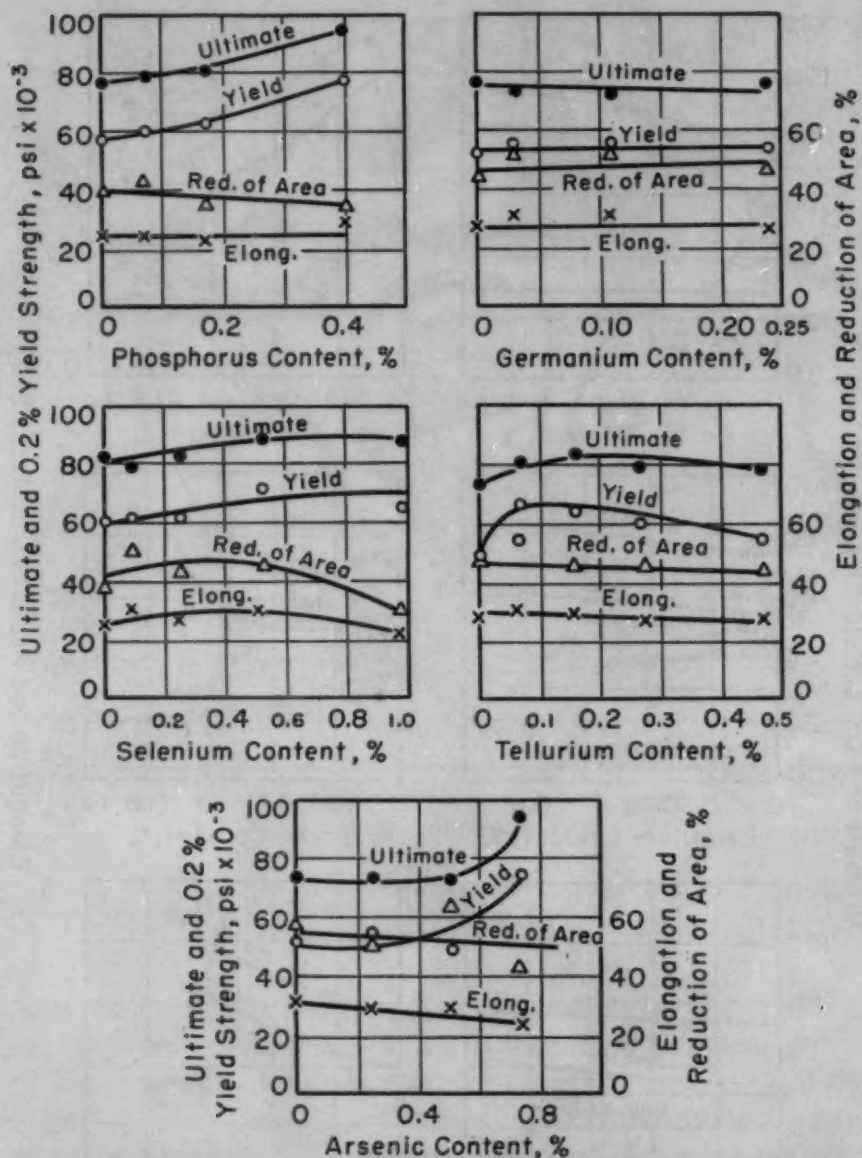


Fig. 4—The Effect of Phosphorus, Germanium, Selenium, Tellurium, and Arsenic on the Mechanical Properties of Titanium.

MECHANICAL PROPERTIES OF ALLOYS TESTED

After completion of the saw test, the remaining $\frac{5}{8}$ -inch rounds of each sample were used to prepare tensile specimens. The standard $\frac{1}{4}$ -inch round specimen with 1-inch gage length was prepared. These specimens were then tested in tension.

The effect of the various additions of alloying elements on the mechanical properties of titanium is shown in Figs. 3 and 4. Generally the trend is for minor increases of strength with corresponding ductility decreases. The best strength increases observed were for the 0.68% S alloy, 0.67% As alloy, 0.39% P alloy, and the 0.09%

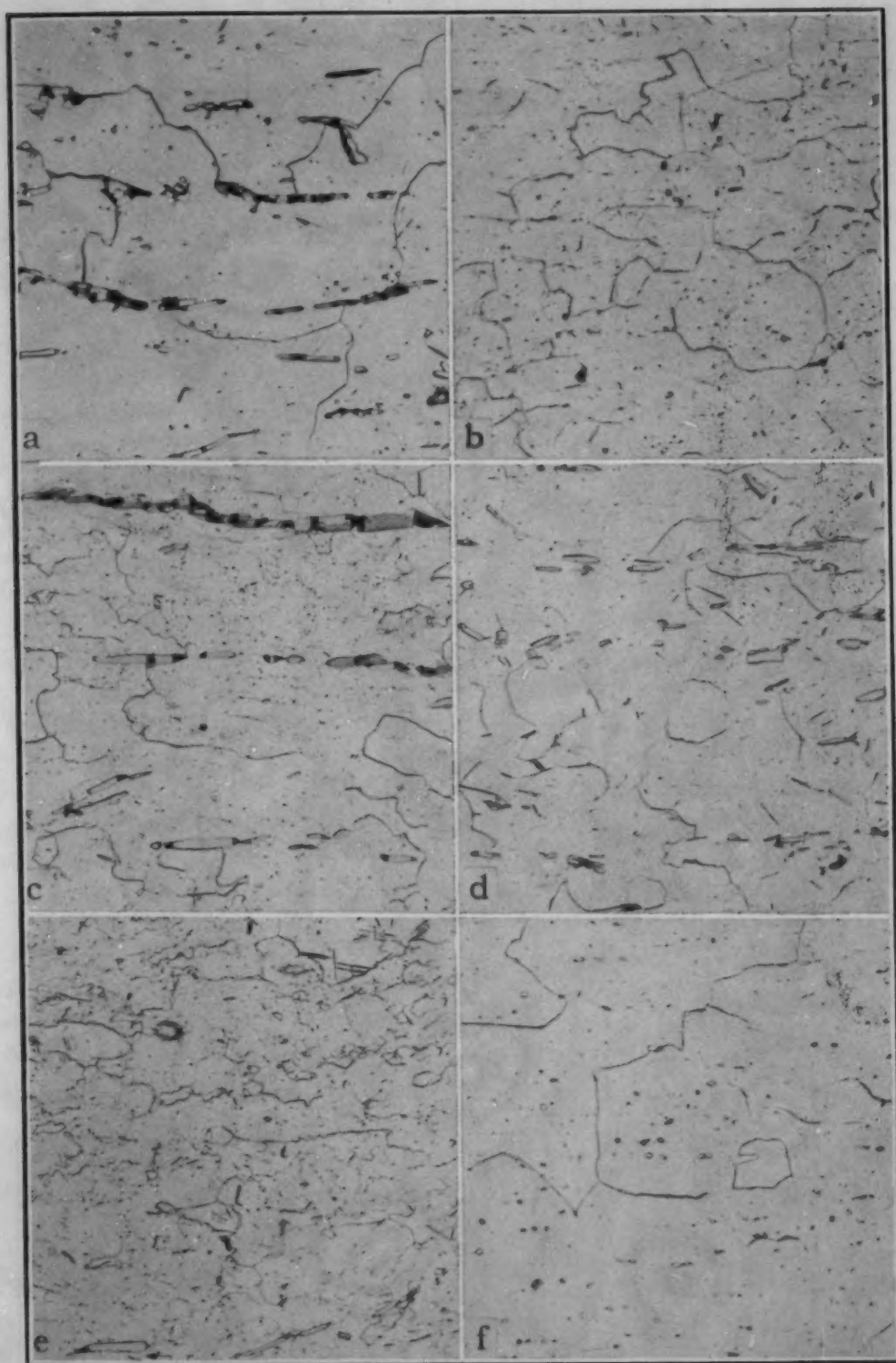


Fig. 5—Representative Microstructures of Titanium Alloys Studied. (a)—0.32% sulphur as TiS_2 . (b)—0.25% silicon. (c)—0.47% carbon. (d)—0.57% boron. (e)—0.118% sulphur as MoS_2 . (f)—0.67% arsenic.

Si alloy. Ultimate strengths of about 100,000 psi and yield strengths of about 80,000 psi were obtained. These values represent increases of about 20,000 psi over the unalloyed ultimate and yield strengths.

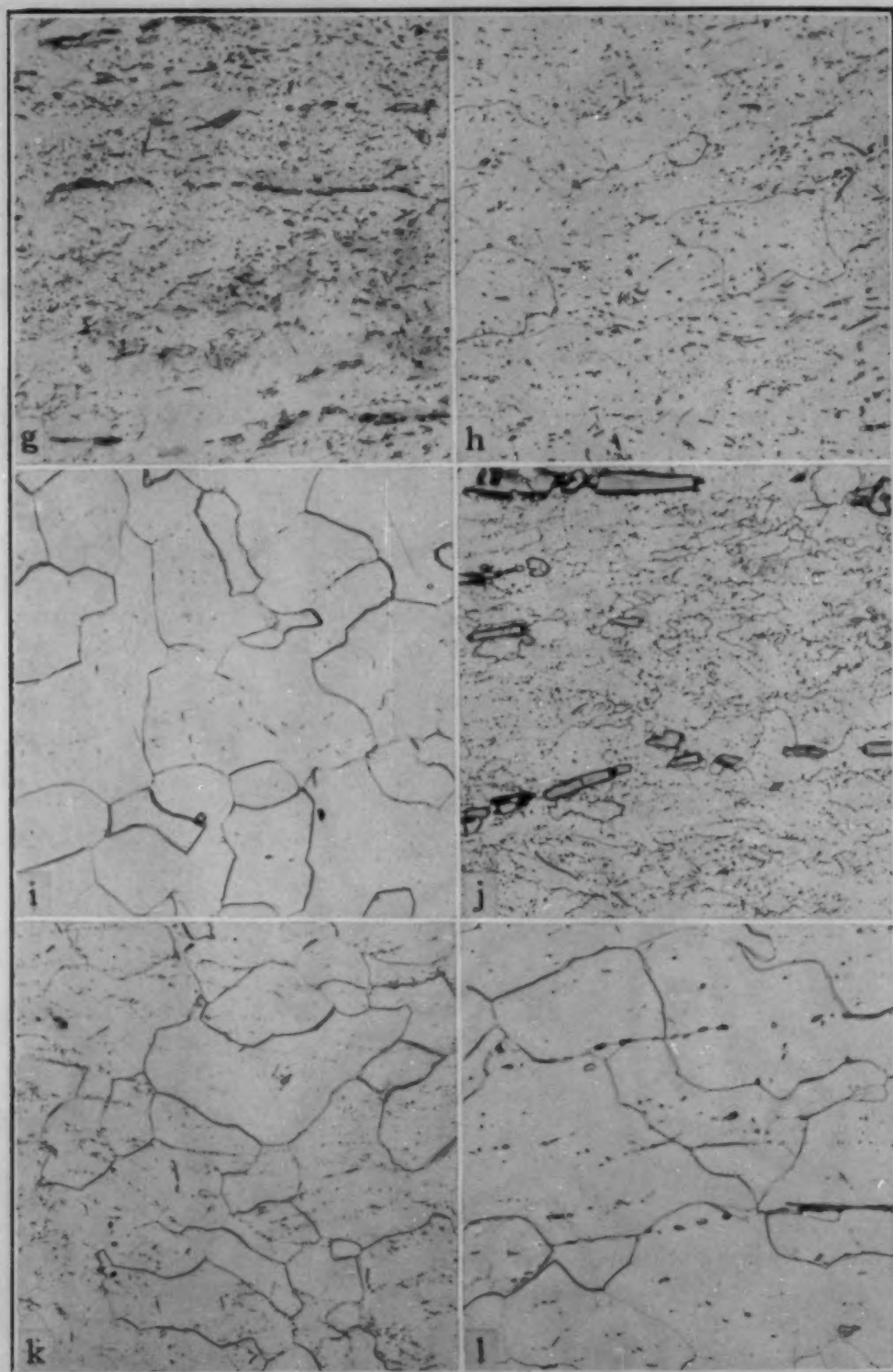


Fig. 5—Representative Microstructures of Titanium Alloys Studied. (g)—0.99% selenium. (h)—0.47% tellurium. (i)—0.25% germanium. (j)—0.39% phosphorus. (k)—0.02% beryllium. (l)—Unalloyed Mg-reduced titanium.

In all cases good ductility was obtained in these alloys. The results for the Ti-Si alloys are anomalous in that there was a maximum in strength at the 0.09% silicon content. The samples were checked

spectrographically to determine the possibility of a mixup, but this was not the case. The maximum strength occurs in the alpha solid-solution region of the Ti-Si phase diagram, and drops off in the two-phase alpha-plus-compound region. The decrease in strength in the region of compound formation is unusual but has been observed before.

MICROSTRUCTURE OF ALLOYS

After completing machinability tests on the alloys, transverse and longitudinal sections were taken from the $\frac{5}{8}$ -inch diameter bars for microscopic examination. Of the ten alloying elements studied, eight produced a discrete, nonallotropic second phase. A representative longitudinal structure for one composition of each of the elements studied is shown in Fig. 5 along with a representative unalloyed titanium structure. Only the beryllium and germanium alloys failed to show an insoluble phase up to the limit of composition studied.

The structures observed are generally equiaxed alpha with a randomly distributed insoluble phase, e.g., titanium carbide, titanium boride, titanium sulphide, etc. The amount of second phase increased with increasing alloy addition and, in some specimens, appeared to have been drawn out and elongated during forging and rolling. Also, most of the specimens have small amounts of beta phase present within the alpha grains or at the grain boundaries. The beta phase is thought to be the result of beta-stabilizing impurities, particularly iron, which is present to the amount of 0.15% in the magnesium-reduced titanium sponge.

Although the same annealing treatment, $\frac{1}{2}$ hour at 1450°F (790°C) following hot rolling, was given to all specimens, some of them apparently were not completely recrystallized. This condition was encountered in several unalloyed specimens as well as a number of the alloys. Consequently, flow lines resulting from residual cold work are quite evident in a number of specimens. This undoubtedly accounts for the range of hardness and mechanical properties observed, particularly among the unalloyed specimens.

Listed below are the elements studied and the lowest per cent addition at which they appear as insoluble compounds in the microstructure:

Element	Composition at Which Insoluble Compound First Noted, %
Carbon	0.25
Boron	0.067
Beryllium	None noted up to 0.15
Silicon	0.09
Sulphur (as MoS_2)	0.025
Sulphur (as Ti_3S_4)	0.02
Selenium	0.25
Phosphorus	0.07
Tellurium	0.47
Germanium	None noted up to 0.24
Arsenic	0.26

LATHE TESTS

The titanium alloy samples ready for machinability testing were in the form of $\frac{7}{8}$ -inch rounds, which had been hot-rolled at 1450°F (790°C), annealed for $\frac{1}{2}$ hour at 1450°F (790°C), and then cooled in air. Before turning tests could be made, it was necessary to machine the samples to $\frac{3}{4}$ -inch rounds. This allowed for two 1/16-inch turning cuts and left a $\frac{1}{2}$ -inch round for use in other work. Actually in testing, only one 1/16-inch cut was taken on the $\frac{3}{4}$ -inch rounds because chatter was encountered at the smaller, $\frac{5}{8}$ -inch diameter. Before proceeding to other tests, the bars were finish turned to $\frac{5}{8}$ -inch diameter.

The original bars for turning were machined on centers. A rough cut was made on the samples to a diameter of 13/16 inch; then the samples were turned in one 1/32-inch cut to $\frac{3}{4}$ -inch diameter. This final cut was made at a surface speed of 32 feet per minute and a feed of 0.0021 inch per revolution. A carbide tool was used for the turning operation. These specimens were then ready for turning evaluation.

Profilometer Measurements

Profilometer surface-roughness measurements were made on all samples and indicated that all alloys could be turned to give a smooth surface finish. The readings were made parallel to the axis of the bar. Results of this test indicate a wide variation among samples including the unalloyed specimens. This is believed to be due to small, unintentional differences in tool contour and conditions. Even though the differences in profilometer readings produced by different tools are greater than the variations among individual samples, there appear to be some differences in profilometric readings resulting from composition. As an example, silicon seems to be detrimental to smoothness while beryllium may be beneficial. Generally the unalloyed titanium specimens, including iodide titanium, varied from 15 to 30 microinches, while the alloy specimens showed no great departure from this range of values. In addition there seems to be no relation between surface finish and hardness.

An interesting note regarding surface finish was made in the case of the 0.10% S (as Ti_3S_4) alloy, Sample No. 21. Trouble was encountered in the melting of this alloy and it undoubtedly had a high degree of oxygen contamination as shown by its comparatively high hardness and mechanical-property values. The surface was quite smooth, being 8 to 9 microinches. No reason is offered for the relatively good finish on this alloy.

Effect of Test Variables

Before turning tests could be made on the titanium alloys, proper testing conditions had to be determined. Testing speed was set to conform to commercial machining practice for titanium. Exploratory tests with a sample of commercial titanium gave a satisfactory feed with a 94-pound thrust and a speed of 27 surface feet per minute. However, under these conditions some of the alloys failed to cut, and the thrust was increased to 107 pounds without changing the speed. Heavier feeds were obtained under these conditions but several samples stopped cutting during the tests. Cutting could only be resumed by increasing the load. Therefore, the thrust load was increased to 120 pounds so that all samples could be tested under the same conditions. At the same time the speed of testing was increased to 56 feet per minute in an effort to reduce the feed and thereby increase the sensitivity of measurement. Under these conditions the small rounds were not stiff enough and excessive chatter accompanied each test. Accordingly, it was decided to standardize the test conditions at a 120-pound thrust load and 27-feet-per-minute surface speed. Nevertheless, the effect of these variables was further checked by running a series of alloys at 27 surface feet per minute over a range of tool-thrust loads consisting of 107, 120, and 134 pounds.

The feed versus load data obtained are plotted on a log-log scale in Fig. 6. Straight lines have been drawn through the data points for each material. This was done because most of the data can best be fitted by a straight line and because it was found in previous work with steel that load-feed data can be fitted on a log-log plot by a straight line.

It is apparent from Fig. 6 that the feeds of the titanium alloys vary much more with tool-thrust load than those of Type 304 stainless steel. The shapes of the log-feed versus log-load lines for the titanium alloys average out to a value of 2.9. This corresponds to a response of feed to almost the cube of the tool thrust. The shapes of the log-feed versus log-load lines for Type 304 stainless steel average out to a value of only 1.5, which is a much smaller response. It should be noted that the data for most steels also correspond to a feed varying with the 1.5 power of the load. Mathematically, these expressions correspond to the following:²

Titanium and titanium alloys:

$$f = K_1 L^{2.9}$$

Type 304 stainless steel:

$$f = K_2 L^{1.5}$$

Most steels:

$$f = K_3 L^{1.45}$$

where f = feed in inches per revolution

L = thrust load in pounds.

The K values for the titanium alloys are very much smaller than

²The customary expression for the load-feed relationship is $L = Kf^r$. The corresponding expressions would be: Ti alloys, $L = K_1' f^{0.34}$; Type 304 stainless steel, $L = K_2' f^{0.66}$; and most steels, $L = K_3' f^{0.69}$.

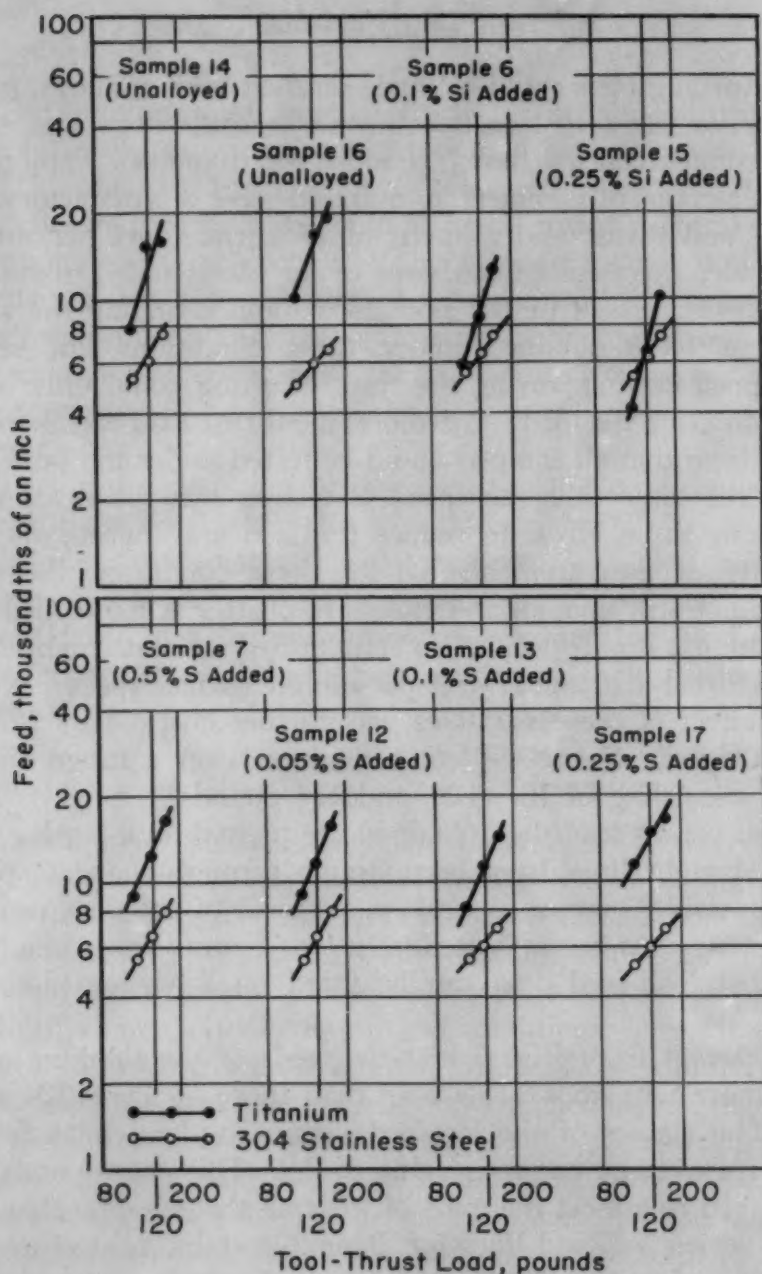


Fig. 6—Feeds Resulting From Various Tool-Thrust Loads for a Number of Titanium Samples and Standard Type 304 Stainless Steel (1/16-Inch Turning Cut at 27 SFM).

those of stainless steel, on the order of 1×10^{-5} as compared with 5×10^{-3} . The tool-thrust loads were of the order of magnitude used in commercial practice. These loads were sufficient that the high exponent values of the titanium alloys overbalanced their low "K" coefficient values. Thus the titanium alloys were found to cut better than the stainless steel under the condition of test.

Effect of Composition

The effect of various alloy additions on the machinability of unalloyed titanium is shown in Figs. 7 through 10. Both turning and saw-test results are shown together.

An outstanding result of the turning tests was the finding that the machinability of iodide titanium was very much better than magnesium-reduced sponge titanium. Using the average of several unalloyed sponge titanium samples as 100, the relative index for the iodide metal was 227. This far exceeds the improvement in turning index resulting from any of the alloying additions added to sponge metal. In addition, benefits were obtained in turning tests from the following additions to magnesium-reduced sponge titanium:

0.05, 0.10, 0.13, and 0.29% boron
0.118% sulphur (as MoS_2)
0.07, 0.27, and 0.47% tellurium
0.26 and 0.51% arsenic
0.03% germanium.

As can be seen from the data, the benefits of these additions are relatively small. From the standpoint of the turning operation, the low concentrations of boron and arsenic seem to have the most promise. Improvements up to 40% are indicated. The carbon alloys are definitely detrimental to turning, and the silicon alloys exhibit a minimum at 0.25% silicon where the relative turning index is very low.

SAW TESTS

Reference is again made to Figs. 7 through 10 where the effect of the various alloying additions on the saw-test rating of titanium is shown. The average ratings have been calculated on the basis of the individual standards having a rating of 100.

As in the turning test, an outstanding result of the saw tests is the superior sawing properties of the high purity iodide titanium as compared with magnesium-reduced metal. Based on the average of the unalloyed magnesium-reduced titanium samples used in the same test as 100, the relative saw rating for iodide titanium is 175. This value is also far above any obtained as a result of alloying magnesium-reduced metal. Benefits in sawing were obtained from the following additions:

0.10 and 0.13% boron
0.02% sulphur (as Ti_2S_3)
0.09% selenium
0.27% tellurium
0.03% germanium
0.26 and 0.51% arsenic.

The improvements noted were relatively small, being a maximum of about 10% for the selenium alloy. The carbon and sulphur additions appear to be definitely detrimental.

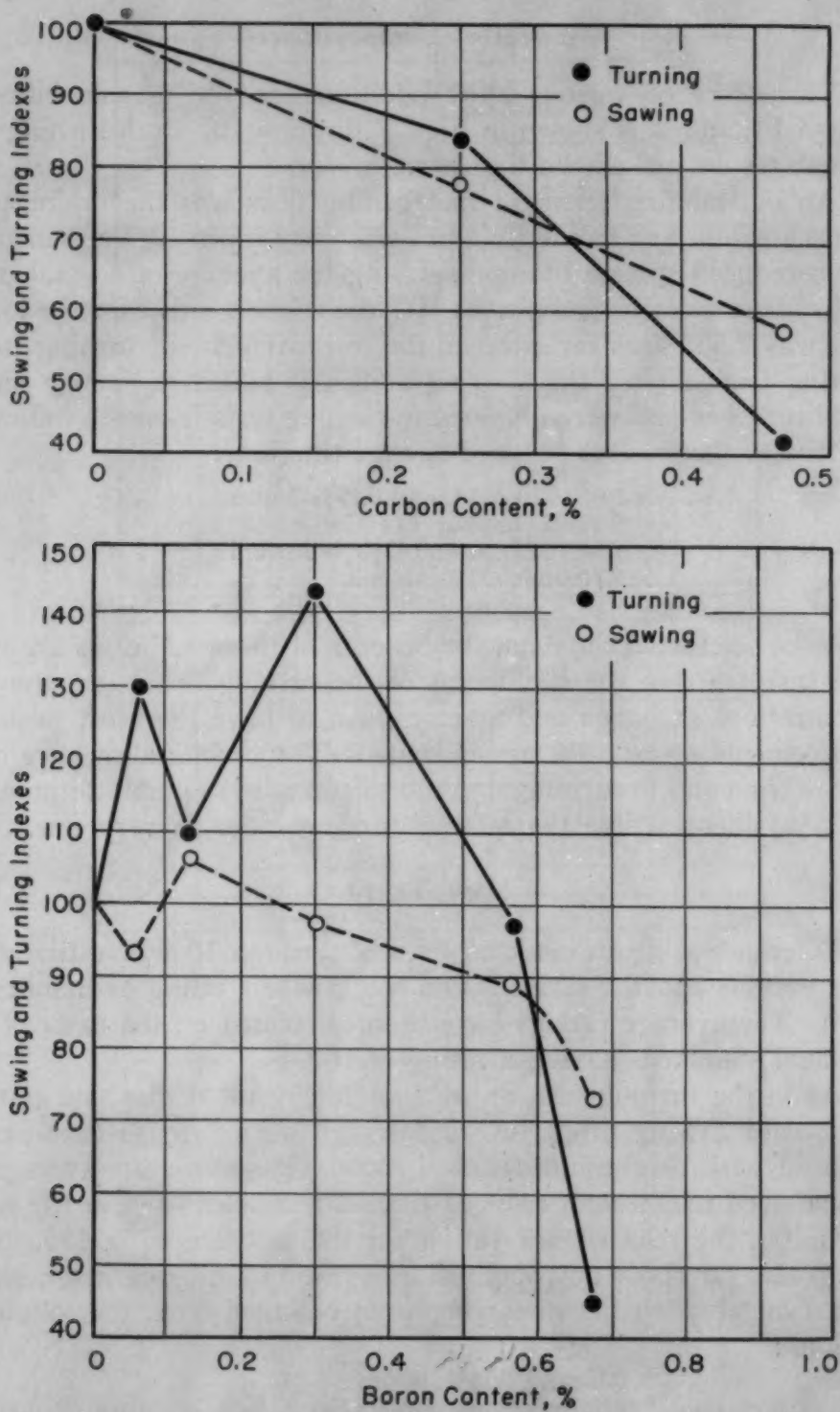


Fig. 7—The Effect of Carbon and Boron on the Machinability of Unalloyed Titanium.

DISCUSSION OF RESULTS

Despite the fact that stainless steel was used as the comparison standard in the turning tests, and unalloyed titanium was used as the

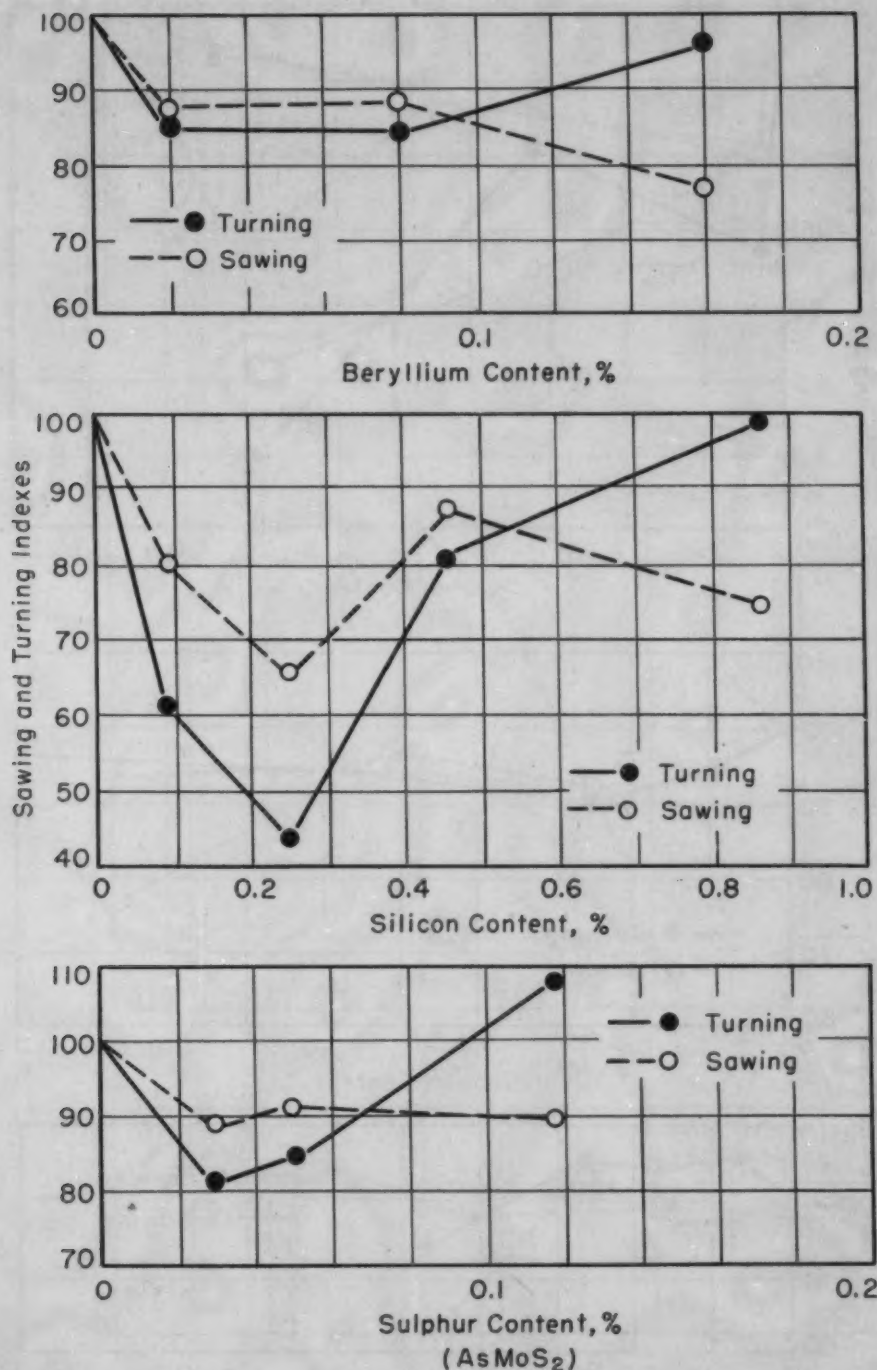


Fig. 8—The Effect of Beryllium, Silicon, and Sulphur on the Machinability of Unalloyed Titanium.

standard in the saw test, there is a considerable degree of correlation in the results from the two tests. Both the turning and saw-test results show that high purity iodide titanium machines better than magnesium-reduced titanium. This result clearly demonstrates that reducing the carbon, oxygen, and nitrogen level, with the corresponding

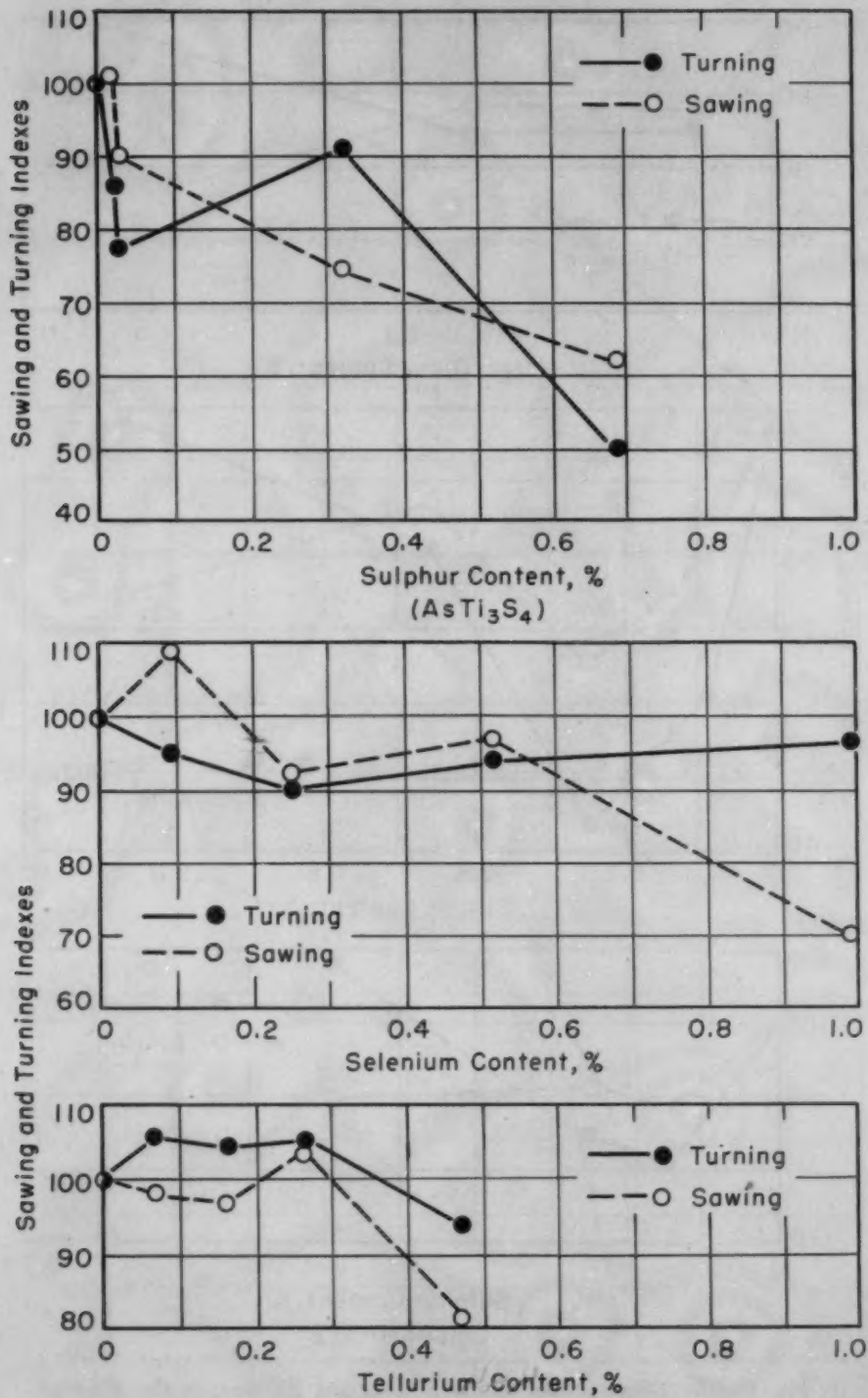


Fig. 9—The Effect of Sulphur, Selenium, and Tellurium on the Machinability of Unalloyed Titanium.

lower hardness and strength level, has a greater effect on machinability than any of the compound-forming additions used in this study. Comparative data on alloys produced from high purity and commercial titanium might very well show a similar trend.

A comparison of the data from the two tests shows that increased

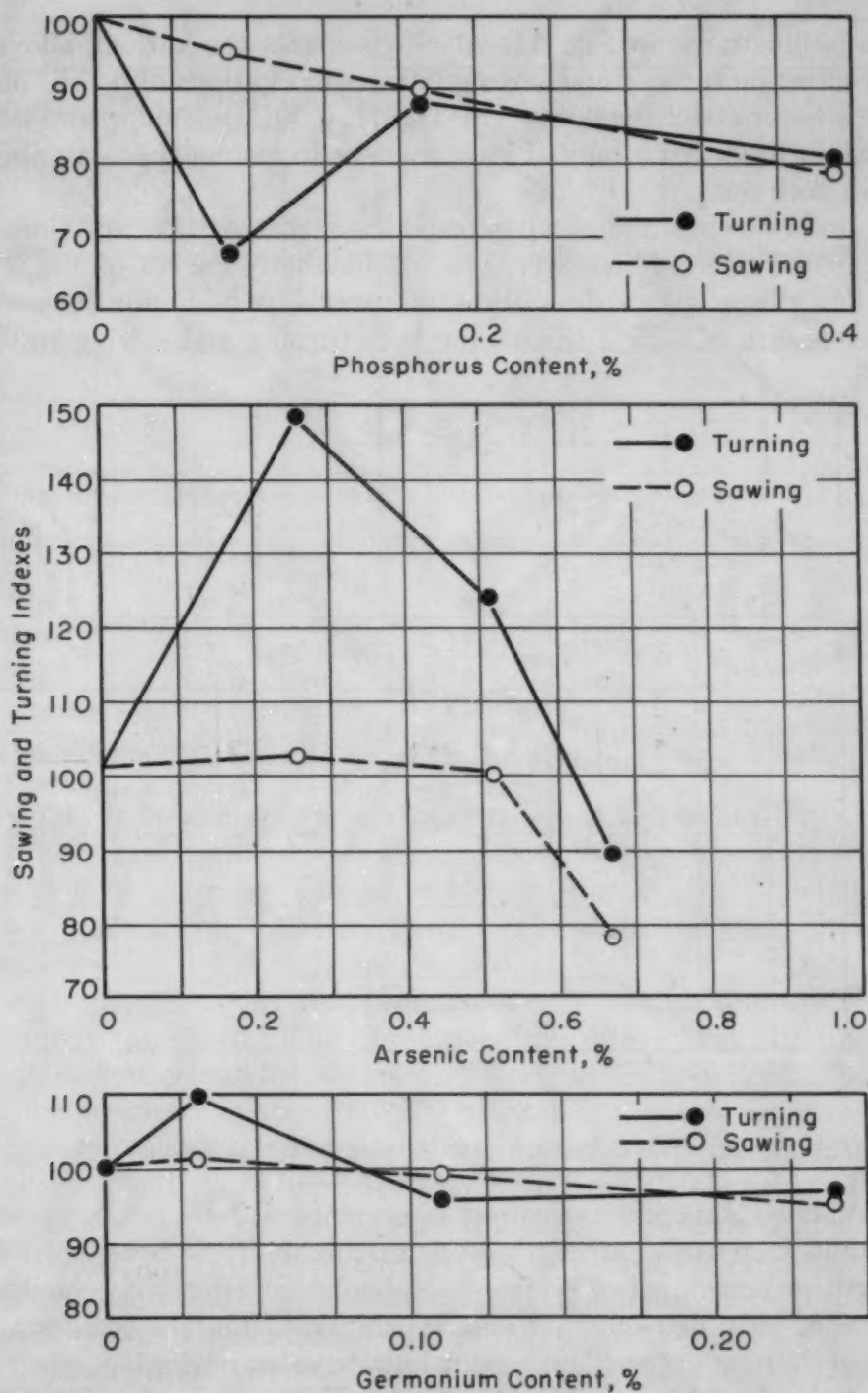


Fig. 10—The Effect of Phosphorus, Arsenic, and Germanium on the Machinability of Unalloyed Titanium.

machinability was obtained in both types of tests from the following additions:

0.10 to 0.13% boron
 0.03% germanium
 0.27% tellurium
 0.26 and 0.51% arsenic.

This is illustrated in Fig. 11, which compares the various alloys for their effect on turning and sawing indexes. Additions of 0.05% boron, 0.29% boron, 0.02% sulphur (as Ti_3S_4), 0.09% selenium, and 0.07% tellurium produced a limited improvement in machinability in one but not in both tests.

Both turning and sawing tests show that carbon additions are detrimental to machinability. The machinability curves of Fig. 8 for titanium-silicon alloys show the same trends: a minimum in machinability occurs at 0.25% silicon, for both turning and sawing tests.

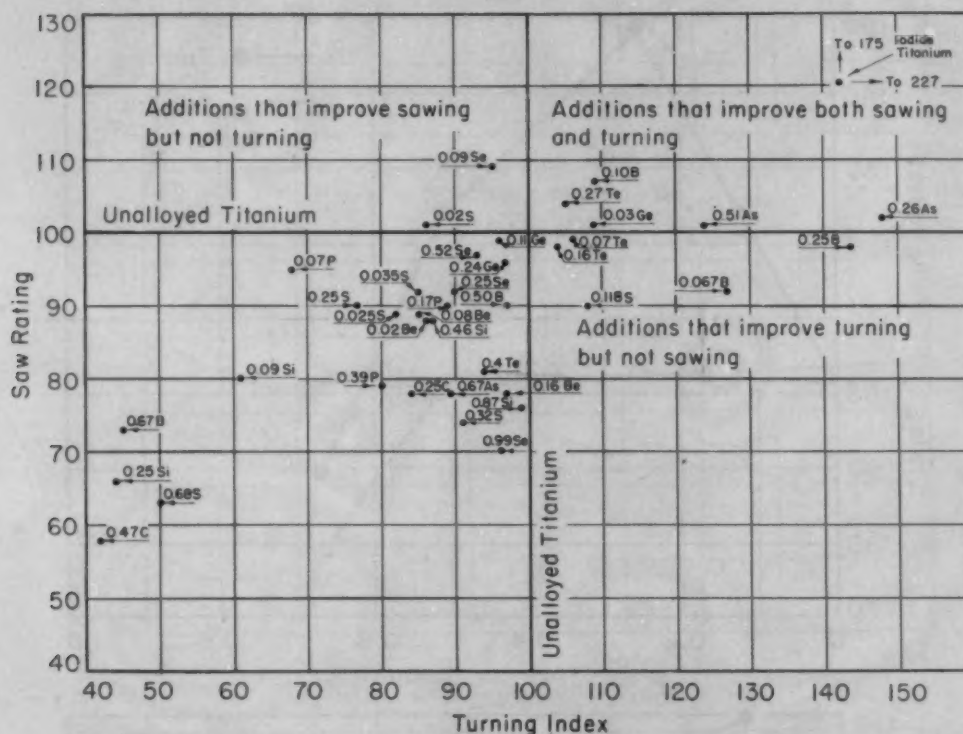


Fig. 11—Plot of Saw Rating Versus Turning Index for Titanium Alloys.

Where compound formation is accompanied by no increase or only mild increase in strength level, machinability is benefited. Any strength increases, whether from solid-solution effects or compound formation, seem detrimental to machinability. Thus, the smaller additions of boron, arsenic, and tellurium have a negligible effect on strength level, and form insoluble phases. They improve machinability. Higher amounts of boron increase strength to a considerable degree, and machinability falls off markedly. The alloys with selenium also bear out this trend insofar as sawability is concerned. Sulphur and phosphorus have definite strengthening effects, and, where these occur, machinability falls off. The two alloys containing carbon both had carbide in the microstructure, and both showed very poor machinability. The increase in strength caused by carbon is moderate, and

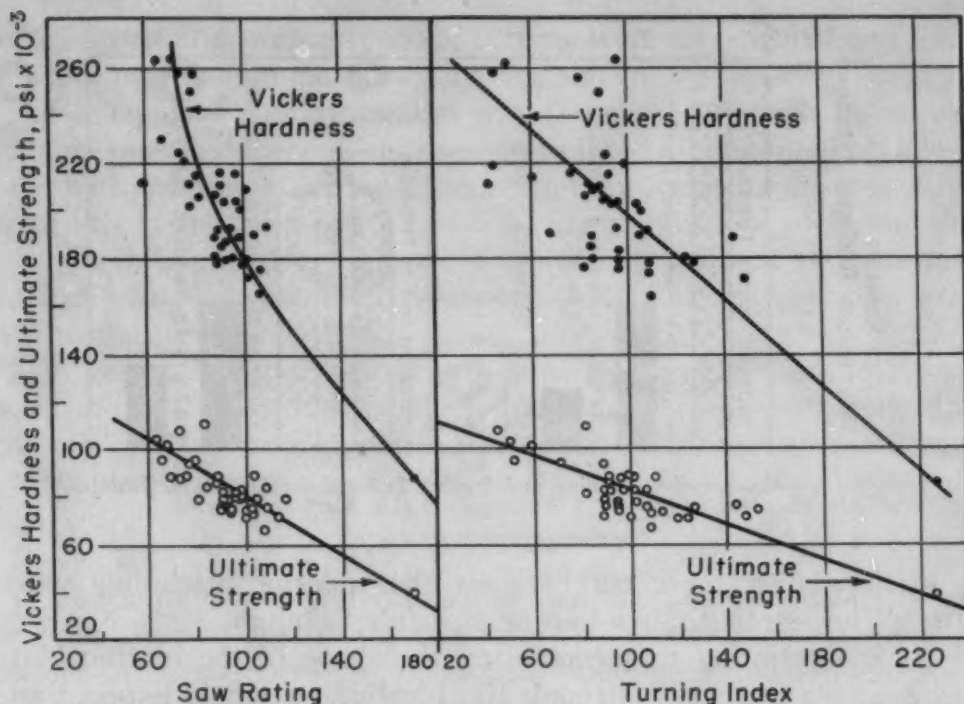


Fig. 12—Correlation of Vickers Hardness and Ultimate Strength With the Saw Rating and Turning Index of Titanium Alloys Based on Unalloyed Titanium.

one would have expected a moderate decrease in machinability. The drastic decrease in machinability appears disproportionate with the strength-level increase. Hence, it appears that the carbide phase is especially detrimental to machinability. The alloys with beryllium and germanium did not show insoluble phases. Strength increases were low with these elements and, correspondingly, machinability was only moderately decreased. The titanium-silicon alloys bear out the contention that machinability varies with strength level. Silicon is soluble in alpha titanium to about 0.4% (8) and is a potent solid-solution strengthener. The low turning rating at the 0.09% silicon addition level corresponds to an increase of strength from 75,000 psi to 110,000 psi. Then as the strength falls off with increasing silicon content, machinability improves. Further evidence of this effect is found in an alloy with an intended composition of 0.1% sulphur, Sample No. 21. This alloy was contaminated in melting when the melting crucible was perforated and water came in contact with the melt. The contamination was most probably oxygen, which is a potent interstitial alpha strengthener. The tensile strength increased from about 80,000 psi to 140,000 psi and the ductility remained excellent, but the turning machinability decreased to very low values. In most cases the alloy bar could not be turned under the test conditions used.

A correlation plot of Vickers hardness and ultimate strength with saw ratings and turning indexes is shown in Fig. 12. In addition to substantiating the foregoing discussion on the effect of strength level

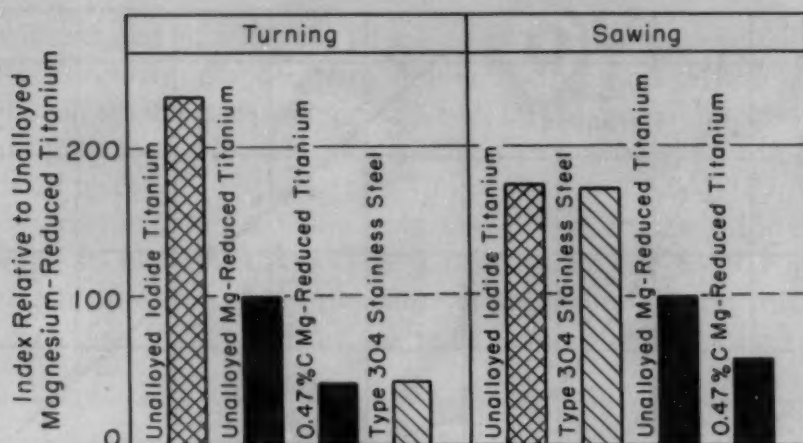


Fig. 13—Comparative Turning and Sawing Indexes for Unalloyed Titanium, Type 304 Stainless Steel, and a Titanium-0.47% Carbon Alloy.

on machinability, these curves show the superior machining properties of low-strength, low-hardness, iodide titanium.

It is interesting to speculate on the shape of the machinability curves shown in Figs. 7 through 10. Ideally, one would expect those additions not appreciably soluble in titanium to show a peak in machinability when an optimum amount of insoluble phase is present, with the benefit falling off when too great a concentration of the insoluble phase is introduced. Where appreciable solubility of the addition in titanium is present, as with silicon, an initial decrease in machinability due to strengthening would be expected, followed by an increase in machinability to a maximum after the appearance of a compound. This theory is borne out at least partially by the experimental work but the data are not extensive enough to make any definite statements as to its general applicability.

In Fig. 13, comparative turning and sawing indexes for stainless steel, unalloyed titanium, and a titanium-0.47% carbon alloy are shown. For the conditions of testing, titanium is shown to be much superior to stainless on turning but inferior to stainless on sawing. This paradoxical situation points up the extreme sensitivity of titanium to testing conditions. It is likely that the titanium could be made to saw better than stainless if higher blade pressures and slower blade speeds were used.

SUMMARY

The influence of insoluble phases on the machinability of titanium has been studied. Turning tests and saw tests were used for the evaluation. The alloying additions studied were boron, carbon, beryllium, silicon, sulphur, selenium, phosphorus, tellurium, germanium, and arsenic.

Titanium was shown to be very sensitive to the conditions of testing, particularly tool thrust. In the turning test, various combinations

of tool thrust and surface speed of turning were investigated and their influence on titanium machinability was shown.

High purity iodide titanium was shown to be much more machinable than commercial, magnesium-reduced titanium. For alloys made with magnesium-reduced titanium, improvements of up to 40% in turning ratings were noted with low concentrations of boron and arsenic, while improvements of up to 10% in saw-test ratings were obtained with low selenium concentrations. Carbon additions were detrimental to machinability.

A good correlation between machinability and strength level was found in these tests. Machinability tends to decrease with increasing strength level. Where the strength level is maintained constant, insoluble phases improve machinability.

ACKNOWLEDGMENTS

The authors are grateful to the Kennecott Copper Corporation for permission to publish the results of this work which was done at Battelle Memorial Institute under their sponsorship. They also wish to thank Dr. Harry P. Croft of the above company for his guidance and cooperation, which greatly facilitated the work. The authors are further indebted to Dr. D. K. Crampton of the Chase Copper and Brass Company of Waterbury, Conn., for supplying the bulk of the analytical results.

References

1. "Handbook on Titanium", Titanium Metals Corporation of America, 3rd printing, March 15, 1951.
2. "Technical Information on Titanium Metal", Remington Arms Company, Technical Bulletin dated April 15, 1950.
3. "Titanium Machines Like Jet-Engine Alloys", Report on Machinability, USAF, reprinted in *Steel*, Oct. 22, 1951, p. 74-77.
4. C. M. Craighead, O. W. Simmons and L. W. Eastwood, "Titanium Binary Alloys", *Journal of Metals*, Vol. 188, March 1950, p. 485-536.
5. F. W. Boulger, H. L. Shaw and H. E. Johnson, "Constant-Pressure Lathe Test for Measuring Machinability", *Transactions, American Society of Mechanical Engineers*, Vol. 71, No. 5, July 1949, p. 431-446.
6. "Free Machining Steel", U. S. Patent No. 2,485,358, Oct. 18, 1949.
7. A. W. McLaren and L. W. Oswald, "Better Machinability with MX Steel", *Iron Age*, Vol. 165, No. 5, 1950, p. 86-88.
8. M. Hansen, H. D. Kessler and D. J. McPherson, "The Titanium-Silicon System", *TRANSACTIONS, American Society for Metals*, Vol. 44, 1952, p. 518.

DISCUSSION

Written Discussion: By Burt H. McKibben, chief metallurgist, Malory-Sharon Titanium Corp., Niles, Ohio.

We wish to congratulate Messrs. R. M. Goldhoff, H. L. Shaw, C. M. Craighead and R. I. Jaffee on their paper. They have done an excellent piece of work, and the report of their findings is quite outstanding.

We at Mallory-Sharon Titanium Corporation feel that these gentlemen have reported a very realistic approach to the machinability problem, and their report on this work is quite timely, inasmuch as machinability is one of the fabricating problems that is outstanding in everyone's mind. They have answered some of the questions that are given to us almost daily by the potential users of this metal, and have backed up their results with some excellent experiments. The effect of carbon, as pointed out in the graph in Fig. 7, is extremely interesting and important to us.

We concur with the findings of the authors and their work, but would comment on the sawing and turning indexes for unalloyed titanium and Type 304 stainless steel as shown in Fig. 13. It has been our observation that this grade of titanium has approximately the same average index of machinability as Type 304 stainless steel.

Again, we wish to congratulate the authors on this outstanding piece of work which, in our opinion, is quite a contribution to the titanium industry.

Written Discussion: By K. W. Stalker, supervisor, Manufacturing Methods, General Electric Co., Aircraft Gas Turbine Dept., Cincinnati.

Improving the machinability of titanium would increase production and lower the cost of jet engine parts made from that material. It appears at this time that there are two ways of accomplishing that end. The first is by developing a new high speed machining alloy. The second answer is to improve machining practice, tool design, and coolant application with respect to presently available forms of titanium and its alloys.

Scientists at Battelle Memorial Institute and Kennecott Copper Company have been conducting an exhaustive study into the problem of developing an alloy with better machining characteristics. Their findings to date, while far from being conclusive, offer considerable hope and encouragement that alloys having insoluble phases will provide the answer to many machining problems. Their studies indicate that many of the soluble elements, often found in commercial titanium, have considerable influence on machining properties.

The importance of developing a high speed machining alloy can be seen when we realize that it takes $1\frac{1}{2}$ times longer to machine a titanium compressor wheel than one made of steel. Furthermore, the titanium requires $1\frac{1}{2}$ times more tool steel.

It should be to their best interests, as well as ours, for the metal producers to carry on the studies that have already been started. They should be eager to develop a machining alloy of titanium and determine its engineering properties. However, that program will necessarily be of a long-range nature.

More immediate benefits should result from studies of tool life and lubrication. It has been observed that the tool cutting edge pits as a result of the ignition of small titanium flakes. This dulls the tool and causes it to overheat, which in turn enables the titanium to literally dissolve and absorb the tool tip.

Development of higher strength tool material, in combination with more effective cooling of the cutting edge, should help to improve the machinability of present production alloys as well as alloys developed in the future.

Machinability tests conducted by General Electric have been limited to forms of titanium that are commercially available today, and more particularly to those alloys that are used to produce jet engines. Our studies have been aimed chiefly at determining the effects of gas contamination, and to date the results have been quite revealing. As an example, in a drilling study it was found that tool life varied as much as 300%, depending on whether the work was being performed on a gas-contaminated or a gas-free material. The difference in hardness of these two materials was only about Rockwell C-5. Similar results were obtained on grinding tests.

On the basis of tests performed by General Electric, it seems questionable whether the constant-weight technique is the best for testing machinability of titanium.³ This is substantiated to some extent by the saw test, which uses a constant-weight technique. Titanium has different machining characteristics from steel, and our tests have shown that a positive feed will generally give more accurate results. For this reason, we prefer a load-temperature recording system for collecting machinability data.

With a 40% increase in machinability, titanium could be worked at approximately the same rate as steel. To get that much increase, it will probably be necessary to develop a new high speed machining alloy and improve presently used tools and lubrication systems. Further, extensive study in both of these fields will be necessary to accomplish the goal, but the rewards will be well worth the efforts.

Written Discussion: By Edward A. Loria, senior engineer, Metallurgy, The Carborundum Co., Niagara Falls, N. Y.

The authors are to be congratulated for presenting the first exploratory paper on the machinability of titanium and titanium alloys. Useful data on turning and sawing tests are presented and one would ask if the study has now been extended to include drilling and grinding tests?

In regard to the effect of constant-pressure test variables, would the authors comment on the scatter in R values with changes in tool-thrust loads and in the speed of testing, also the tendency toward tool wear with these changes?

The individual average constant-pressure indices are not tabulated but are plotted in the diagrams in relation to alloy content. Would the authors include or discuss the data on the coefficients of variation for the different alloys so that one may know the reproducibility of the results?

Perhaps the coefficient of variation may be high in those alloys which have a relatively low machinability rating. Also, in those cases where the alloying element may tend to segregate on casting and forging, the coefficient of variation may be higher than ordinarily.

Battelle has also adapted the constant-pressure lathe test for machinability measurements on gray cast iron.^{3, 4} Small variations in the cutting characteristics produced by variations in gray iron chemistry and microstructure can be detected. As expected, the predominant effect of carbon and silicon in promoting graphitization results in higher indices for irons possessing greater quantities of these elements.

³E. A. Loria, "Machinability of Gray Iron by Constant-Pressure Lathe Tests", *Foundry*, Vol. 80, August 1952, p. 194.

⁴E. A. Loria, F. W. Boulger and H. L. Shaw, "What Constituents Affect Machinability of Gray Irons", *American Machinist*, Vol. 96, October 1952, p. 122.

Written Discussion: By O. W. Simmons and L. W. Berger, metallurgists, Pitman-Dunn Laboratories, Frankford Arsenal, Philadelphia.

During the preparation of certain titanium alloys at Frankford Arsenal it was observed that samples containing sulphur were "easier to saw and drill". Although machinability studies on titanium were not included in the Frankford Arsenal mission to develop titanium casting methods, some simple quantitative tests to substantiate these casual observations were considered to be justified.

To accomplish the above aim in as short a time as possible, the following testing procedure was devised:

1. Titanium alloy ingots (approximately 100 grams in weight) were prepared under an argon atmosphere in a water-cooled copper arc furnace. These ingots, measuring 2 inches in diameter, were fairly uniform in cross section from specimen to specimen, with a maximum thickness of a half inch.

2. Hardness measurements were taken of each ingot with the 3000-kilogram load.

3. The as-cast ingots were then mounted in a mechanical hacksaw (engaged to cut through one edge along the diameter of the button), and sawed for 2 minutes at 100 strokes per minute. The cut was then stopped and the specimen was rotated to present a fresh surface for testing. In all, three cuts were made in each specimen with the same blade, a new blade being used for each new specimen. The blade used was of high speed steel, 12 inches long by 1 inch wide by 0.065 inch thick, containing ten teeth per inch with a raker set.

4. The cross sectional area of each cut was then measured by inserting a piece of graph paper in the cut, and then tracing around the ingot. A planimeter was used to scale the area. Assuming the cut to be of constant width, this area is then a measure of the amount of material removed during each cut. The reduction in amount of material removed in the second cut and the third cut would be a simple indication of blade wear.

5. Some sections of the buttons were examined microscopically.

Results of the above testing procedure are shown in Table II. In general, the amount of material removed had no correlation with the Brinell hardness of the specimens. Considerable improvement in the sawability of certain alloys, however, was effected through sulphur and selenium additions. Moreover, these additions markedly affected blade wear in some cases.

Heats 23 through 27 (Table II) show the effect of iron sulphide additions on a 0.5% carbon alloy. Maximum increase in material removed is noted when adding 0.55% of sulphide (0.2% of sulphur), especially in the second and third cuts, which strongly indicates increased blade life due to the sulphide addition. Improvements in sawability of other alloys upon the addition of 0.2% of sulphur was also observed (Heats 22 and 13, 20 and 18). Heat 13 especially indicates increased blade life in an iron-carbon alloy, which shows almost a four-fold increase in material removed in the third cut over Heat 22. The addition of 0.2% of selenium to the same alloy (Heat 28) shows similar results.

Fig. 14 is a photomicrograph of 2% iron - 0.2% sulphur - titanium alloy. The insoluble phase, to which has been attributed the increase in saw-



Fig. 14—2% Iron—0.2% Sulphur—Titanium Alloy Showing the Insoluble Grain Boundary Constituent. $\times 250$.

ability, appears as a grain boundary constituent. This preferred distribution of insolubles in the cast alloys as opposed to random distribution shown by Goldhoff et al in forged material is expected to have a much more detrimental effect on the mechanical properties of the cast alloys. Thus, such additions to promote machinability are unlikely to be acceptable in cast alloys because of the associated loss in ductility.

Table II
Results of Saw Testing Some Titanium Alloys

Heat No.	Composition, %	BHN 3000 Kg	Cross Sectional Area of Saw-Cut (sq. in.)		
			1st Cut	2nd Cut	3rd Cut
10	Unalloyed	163	0.65	0.61	0.45
11	2 Fe	229	0.60	0.57	0.45
17	2 Fe, 0.05 S	241	0.52	0.50	0.45
22	2 Fe, 0.5 C	229	0.35	0.16	0.12
13	2 Fe, 0.5 C, 0.20 S	229	0.53	0.47	0.43
28	2 Fe, 0.5 C, 0.20 Se	262	0.46	0.40	0.41
14	2 Fe, 2 Al	212	0.39	0.36	0.36
15	2 Fe, 2 Al, 0.20 S	229	0.46	0.41	0.30
21	2 Fe, 2 Al, 0.5 C	269	0.15	0.11	0.08
16	2 Fe, 2 Al, 0.5 C, 0.20 S	255	0.28	0.09	0.09
20	2 Fe, 0.3 Mo	285	0.36	0.35	0.31
18	2 Fe, 0.3 Mo, 0.20 S	241	0.60	0.54	0.49
23	0.5 C	197	0.42	0.16	0.10
24	0.5 C, 0.09 Fe, 0.05 S	212	0.43	0.20	0.11
25	0.5 C, 0.17 Fe, 0.10 S	217	0.36	0.21	0.10
26	0.5 C, 0.35 Fe, 0.20 S	241	0.46	0.34	0.29
27	0.5 C, 0.52 Fe, 0.30 S	229	0.11	0.13	0.12

Note: Dupont Process A titanium sponge used in all heats. Sulphur added as FeS.

Written Discussion: By E. A. Gee, section manager, E. I. du Pont de Nemours & Company, Chemical Division, Newport, Del.

The authors are to be complimented for their effort. It appears to be the first laboratory study of the machinability of titanium. Data are sufficiently detailed to provide an excellent basis for other investigators to initiate further studies of the effects of insoluble phases upon machinability.

The writer is well aware of the difficulty associated with the adoption of a machinability scale. It is felt, however, their use of a constant pressure lathe test does provide practical information in the form of feed-thrust constants.

Unfortunately, the authors have discovered no marked increase in machinability from the addition agents used. If one makes note of the observed solubility of the various elements in relation to turning and sawing, it is seen there is no consistent change in machinability with precipitation of the excess phase. This leads the writer to believe there are other factors operating that have not been considered. The physical properties and dispersion of the insoluble phases may be important factors.

Since carbon and boron form hard insoluble phases in titanium, they would be expected to exhibit the same general behavior. It is difficult to understand the apparent marked improvement in machinability resulting from boron addition compared to carbon.

Since we are sponge producers, we question the validity of selecting magnesium reduced sponge as a machinability standard. Sponge in itself is quite variable in properties. It is indicated in the paper the commercial purity titanium used for the experiments had a yield strength of the order of 55,000 to 60,000 pounds per square inch. This represents sponge of moderate purity. We know sponge more closely approaching iodide titanium can be made with much lower yield strength. Conversely, harder sponge has yield strengths in the range of 80,000 psi. It is believed an effort to investigate the effects of sponge purity alone would be worth-while. If this is done, care should be taken to avoid tungsten variation from electrode burn-off, since it may affect machinability. Consumable electrode melting should be considered for such a study.

The authors by their approach to the problem should most certainly stimulate interest in this field. Their work indicates the complexity of the subject.

Authors' Reply

The authors appreciate the discussions sent in by Gee, McKibben, Stalker, Loria, and Simmons and Berger. We will answer to each of these in turn.

We agree with Mr. Gee that the physical properties and dispersion of the insoluble phases may be important factors in affecting the machinability of titanium. Equally, or perhaps more important than this factor, would be the oxygen and nitrogen contents of the specimens. Solid-solution strengthening by oxygen and nitrogen, as has been shown, has a strong detrimental effect on machinability. The improvement in machinability noted with the low concentrations of boron is more likely the result of the lower yield strength of these alloys, rather than from any contri-

bution from the boride phase itself. The effects of sponge variation were beyond the scope of our investigation, but we agree that such an investigation would be highly desirable.

Mr. McKibben's kind remarks are much appreciated. His comment on the equivalence between the machinability of unalloyed magnesium-reduced titanium and Type 304 stainless steel needs to be qualified by the test method and the conditions under which the test was conducted. As the data in our paper show, depending on the speed and tool thrust used, the machinability rating in turning of this type of titanium can be either less than, the same as, or greater than Type 304 stainless.

The comments made by Mr. Stalker on the experience of the General Electric Co. on machining commercial titanium alloys are a most desirable addition to the discussion. It is unfortunate that sufficient material was not available in our work to include tool life as one of the test results, because there is no doubt that this is one of the most important aspects of the machining of titanium-base materials. We have conducted no machining tests using constant feed, and so cannot comment on Mr. Stalker's opinion that such tests produce more accurate results than the constant-pressure tests used.

Mr. Loria's questions are pertinent to any set of experimental data. A study of the constant-pressure test results indicated that most of the titanium samples showed much greater variations in test data than most steel samples. The Type 304 stainless steel used as an arbitrary standard gave quite reproducible results. The coefficient of variation for thirty-five tests on this material was approximately 11%. Coefficients of variation for four to six tests on each of the titanium samples ranged from 9 to approximately 50%. The higher coefficients of variation are believed to be caused by the higher sensitivity to slight changes in tool conditions. The amount of scatter in test results noted for the various samples did not appear to be influenced by the alloying element nor did it appear to be associated with the relative machinability level.

In tests designed to obtain standard testing conditions, the effects of changes in tool thrust and testing speed on the resulting feed were studied. These tests were of an exploratory nature and were limited because of the small amount of material available for each composition. Changes in tool thrust did not influence the amount of scatter in the test data. Tool wear was not measured in these tests, but heavier tool thrusts and higher testing speeds appeared to give greater tool wear.

The exploratory sawing tests conducted by Messrs. Simmons and Berger were conducted on as-cast material and, as such, cannot be compared conveniently with our results which were conducted on forged material. The improvement noted in the sawability of as-cast Ti-Fe-C and Ti-Fe-Al alloys by sulphur and selenium additions are most interesting. We noted no such improvement in sawing wrought titanium containing such additions.

MECHANICAL PROPERTIES AND STRAIN AGING EFFECTS IN TITANIUM

BY F. D. ROSI AND F. C. PERKINS

Abstract

The tensile properties of titanium of commercial purity were investigated in the temperature range 77 to 925 °K (−196 to 652 °C) at constant strain rates of 0.003 min^{−1} and 0.138 min^{−1}. The results of these tests showed that this material exhibits the usual mechanical effects associated with strain aging. The curves describing the dependence of a number of mechanical properties on temperature indicate that the strain aging is more marked in certain temperature ranges.

Some observations were made on the nature of Lüders' bands in an extended, coarse-grained sheet specimen.

RECENT experiments at this laboratory on the recrystallization of cold-rolled commercially pure titanium suggest that strain aging effects may be anticipated in the plastic deformation of this metal at elevated temperatures. Consequently, it was decided that a study should be made of the gross shape of the stress-strain diagrams for titanium of this purity over a wide temperature range. Such a study would certainly reveal much information regarding the temperature range where one could expect strain aging effects as well as the temperature dependence of such mechanical properties as the yield strength, tensile strength, and ductility.

In general, strain aging is characterized by the yield point phenomenon (double yield point), discontinuous yielding (serrated stress-strain curve), and strengthening. It is noteworthy that these mechanical effects have been observed in a number of metals and alloys which contain small quantities of certain impurities. A classic example is mild steel, where the strain aging effects are associated with the presence of small amounts of carbon and nitrogen (1, 2).¹ In view of this fact alone, it is not altogether surprising that titanium should exhibit strain aging phenomena, since in its commercial form

¹The figures appearing in parentheses pertain to the references appended to this paper.

This work was supported by the United States Air Force, Office of Air Research, Contract No. AF-33-038-16031.

A paper presented before the Eighth Western Metal Congress of the Society, held in Los Angeles, March 23 to 27, 1953. The authors, F. D. Rosi and F. C. Perkins, are associated with the Metallurgical Laboratories, Sylvania Electric Products Inc., Bayside, N. Y. Manuscript received March 19, 1952.

it does contain a number of impurities including carbon and nitrogen. Moreover, these effects have been found to occur more often in metals of the body-centered cubic (Fe, Mo) and hexagonal close-packed (Cd, Zn) types.

EXPERIMENTAL

The material used in this investigation was commercially pure titanium of the following composition: Fe = 0.10%, N = 0.08%, C = 0.05%, Si = 0.04%, W = 0.01%, Ti = remainder. This material was supplied in the form of hot-rolled $\frac{7}{8}$ -inch diameter rods, from which $\frac{1}{2}$ -inch standard tensile specimens were machined.

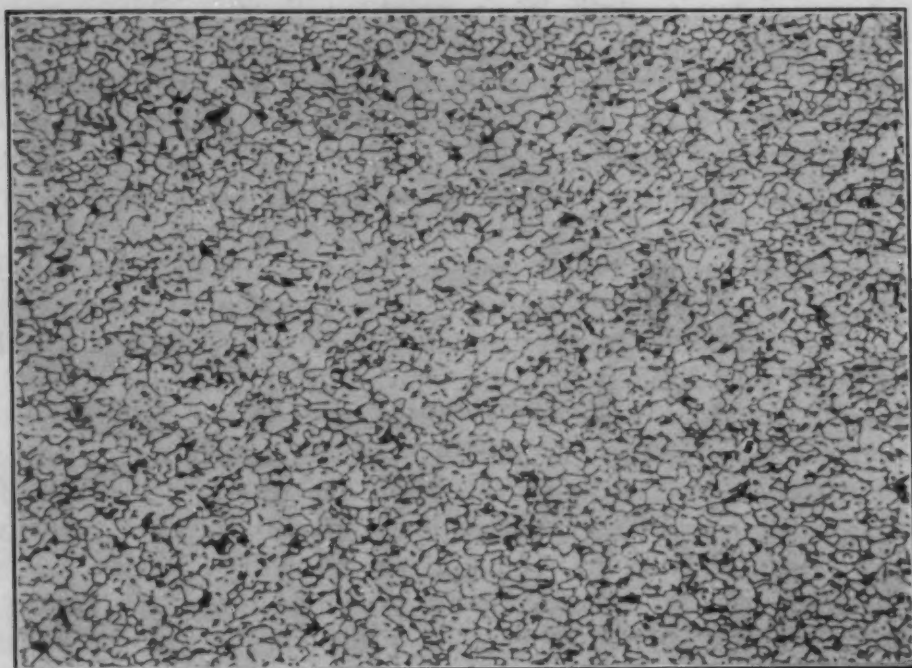


Fig. 1—Grain Structure of Tensile Specimens. 100 X.

Prior to extension, all specimens were annealed in vacuum for 24 hours at 1560 °F (850 °C) in order to produce a uniform structure in all samples. This annealing treatment produced a fine, uniform grain structure, which is shown in the photomicrograph of Fig. 1. Such a structure is desirable, since a fine grain size is known to accentuate strain aging phenomena (3-6).

Tensile tests were made with a Baldwin-Southwark-Tate-Emery hydraulic machine using a dial range of 24,000 pounds. At all temperatures, stress-strain diagrams were obtained at strain rates of 0.003 min⁻¹ and 0.138 min⁻¹. A uniform strain rate was maintained by the use of a pacing instrument which showed the relation between a predetermined uniform rate of crosshead speed and the actual rate at which the test was proceeding. Such a strain device

permitted synchronization of the actual rate to the desired rate by manual control of the application of load.

For the low temperature tests and those up to 230 °C, strain measurements were made using the Baldwin SR-4, bonded, resistance-wire gage and a strain indicator, which permits a reading accuracy of 2 microinches per inch. For extension beyond the 2% limit of these gages, strains were measured with a Starrett dial gage indicator attached to the moving crosshead. With a gage length of 2 inches, this dial extensometer permitted a reading accuracy of 2.5×10^{-5} .

Load and strain readings were taken simultaneously at 30-second intervals, and these data were used to plot the stress-strain diagrams. In a number of tests at room temperature, the stress-strain curve was recorded automatically on a revolving drum. This was made possible by the use of an extensometer attached to the specimen along with a Microformer-type recorder. For the more rapid strain rate tests, the yield point (as well as other mechanical properties) was determined in most cases by visual examination of the loading dial, since the duration of these tests was of the order of several minutes.

The same apparatus was used for the low and high temperature experiments. This consisted of a nichrome-wound stainless steel tube, 2½ inches in diameter, surrounded by another tube 8 inches in diameter. At the bottom of the inner tube was welded a stainless steel plate which contained the lower part of the grip assembly. This assembly, in turn, was fixed to a plate which was welded to the outer tube. Such a design provided a liquid-tight system. The entire apparatus was then mounted to the moving head of the tensile machine. For the liquid nitrogen and powdered dry-ice tests, Santocel powder was used for thermal insulation in addition to a split cork ring at the bottom of the inner tube, while for the tests at elevated temperatures, Silocel powder was used. A heavy oil was used as a medium for testing temperatures up to 660 °F (350 °C), while for higher temperatures, tests were conducted in an atmosphere of argon.

Temperature control for the elevated temperature experiments was obtained by using a powerstat which was connected directly across a 110 A.C. source. With this method of control it was possible to maintain a specimen temperature of ± 3 °C during a complete test to fracture. Temperature readings were obtained with a chromel-alumel thermocouple placed in contact with the specimen at the center of its gage length.

RESULTS AND DISCUSSION

Mechanical Properties—Unless otherwise noted, the tensile test data are presented as curves of stress (psi) versus strain at a constant strain rate of 0.003 min^{-1} . In the absence of a double yield

point, the yield strength was defined as the stress required for a 0.2% offset.

Typical stress-strain diagrams for tensile tests from 77 to 925 °K (−196 to 652 °C) are reproduced in Figs. 2 and 3. It is apparent from Fig. 2 that the gross shape of the stress-strain curves from liquid nitrogen to room temperature are similar in that there is no well-defined yield point, very little strain hardening, and a smooth shape to the curve. Testing at 390 °K (117 °C) produces the first evidence of a double yield point; this persists up to a testing temperature of 555 °K (282 °C). As has been observed with other strain

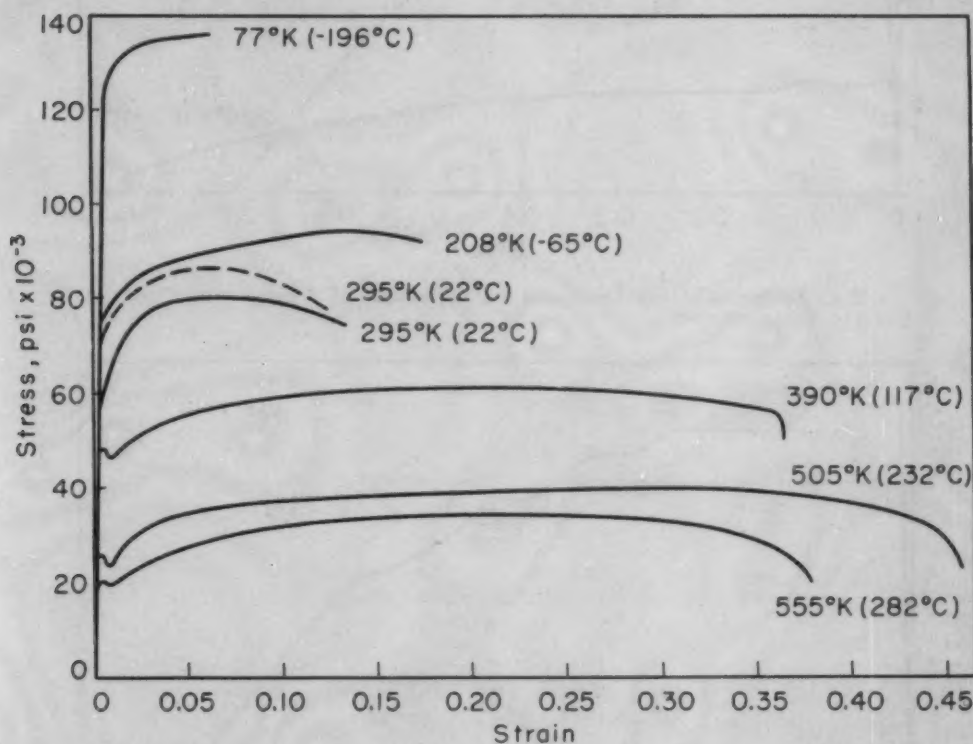


Fig. 2—Stress-Strain Diagrams for Titanium of Commercial Purity at Various Temperatures.

aging effects, the yield point phenomenon, which is characterized by a decrease in stress with strain, occurs within a narrow temperature range and becomes less pronounced (U.Y.P.-L.Y.P.) at both the upper and lower limits of this range.

The first evidence of discontinuous yielding or serration in the stress-strain curve appeared in the test conducted at 725 °K (452 °C) (Fig. 3) in the form of a slight depression in the curve at approximately the ultimate stress. Furthermore, this test appears to have a higher rate of strain hardening and slightly greater yield stress than for that at the lower temperature of testing, 625 °K (352 °C). Examination of the stress-strain diagrams at still higher temperatures shows a definite increase in the degree of serration but no over-all

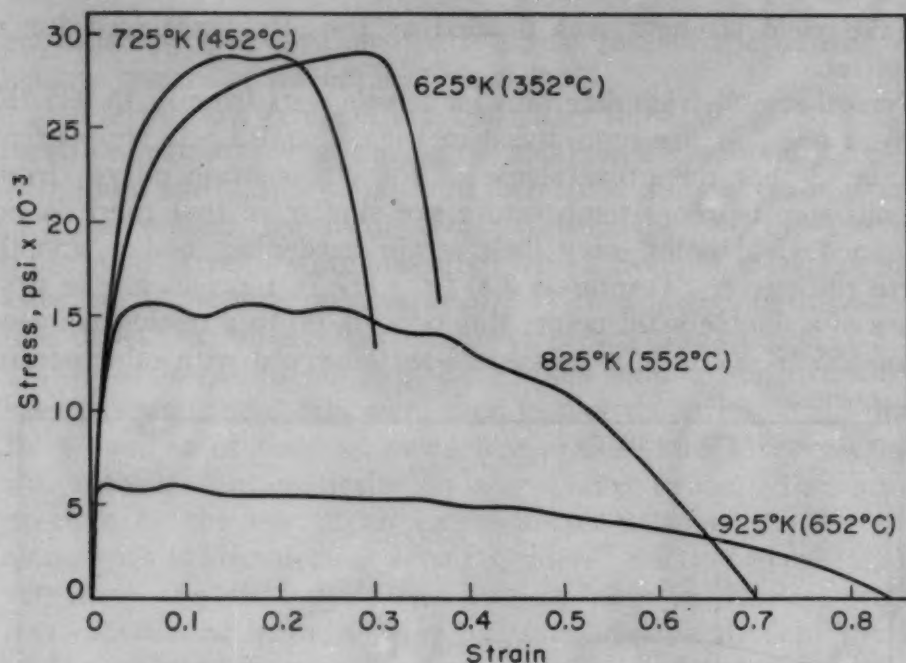


Fig. 3—Stress-Strain Diagrams for Titanium of Commercial Purity at Various Temperatures.

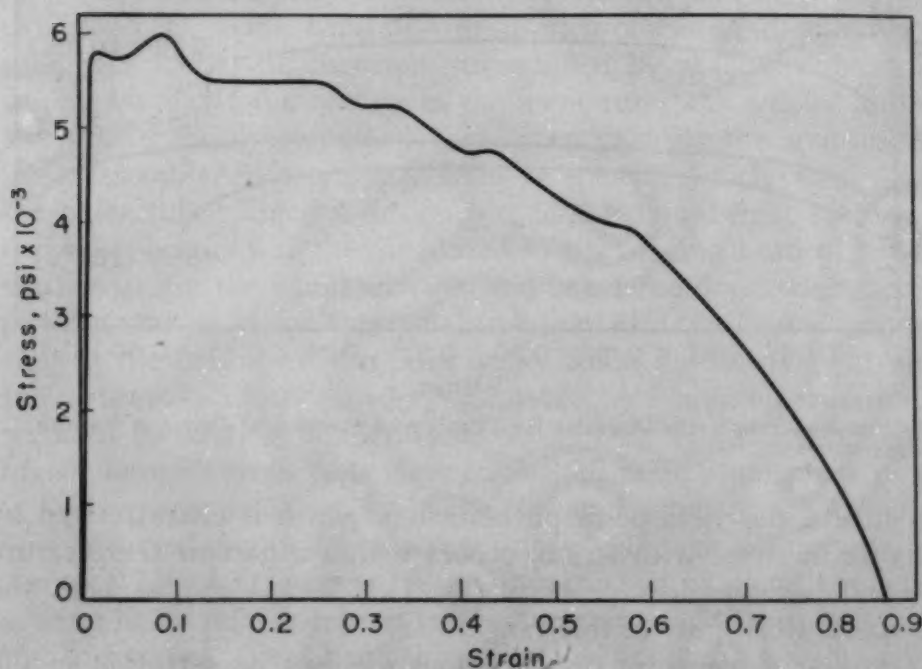


Fig. 4—Stress-Strain Diagram at 925 °K (652 °C).

strain hardening. In fact, it is interesting to note that the discontinuous yielding at the higher strains for the test at 925 °K (652 °C) is not even accompanied by a strengthening effect, which was a characteristic of the curve obtained at 825 °K (552 °C). Instead, the curve takes on the form of a series of steps, which gives the

impression that the drop in stress associated with each increment of strain at constant stress increases with increasing total extension, while the strain increments, themselves, decrease. This effect is better illustrated by the diagram in Fig. 4, which is a magnified plot for the test at 925 °K (652 °C). From the appearance of this curve, one might expect at a still higher temperature of testing that the curve would become smooth.

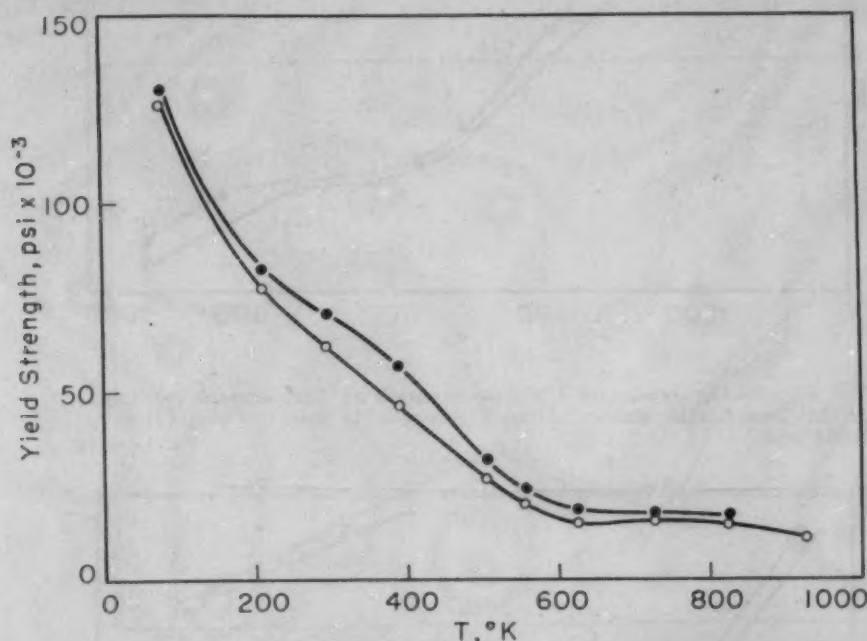


Fig. 5—Dependence of Yield Strength on Temperature for Tests at the Two Strain Rates: Solid Circle = 0.138 min⁻¹; Open Circle = 0.003 min⁻¹.

The effect of increasing the strain rate by a factor of approximately 50 on the gross shape of the stress-strain diagram is illustrated by the dashed curve in Fig. 2 for the test at room temperature. As would be expected, the curve has been displaced upward for the more rapid rate of testing, with the result that both the yield strength and ultimate stress have been increased by 10 to 15%.

Figs. 5 to 9 summarize the data on the general dependence of a number of mechanical properties on temperature for specimens tested at strain rates of 0.003 min⁻¹ and 0.138 min⁻¹. In all cases the curve through the solid points represents the temperature dependence at the larger strain rate.

It may be seen from Fig. 5 that the yield strength increases rapidly with decreasing temperature, reaching a value of 130,000 psi at 77 °K (−196 °C) for the slower strain rate. This is approximately double the value of the yield strength at room temperature. In the temperature range 208 to 555 °K (−65 to 282 °C), the yield strength appears to decrease linearly with rising temperature,

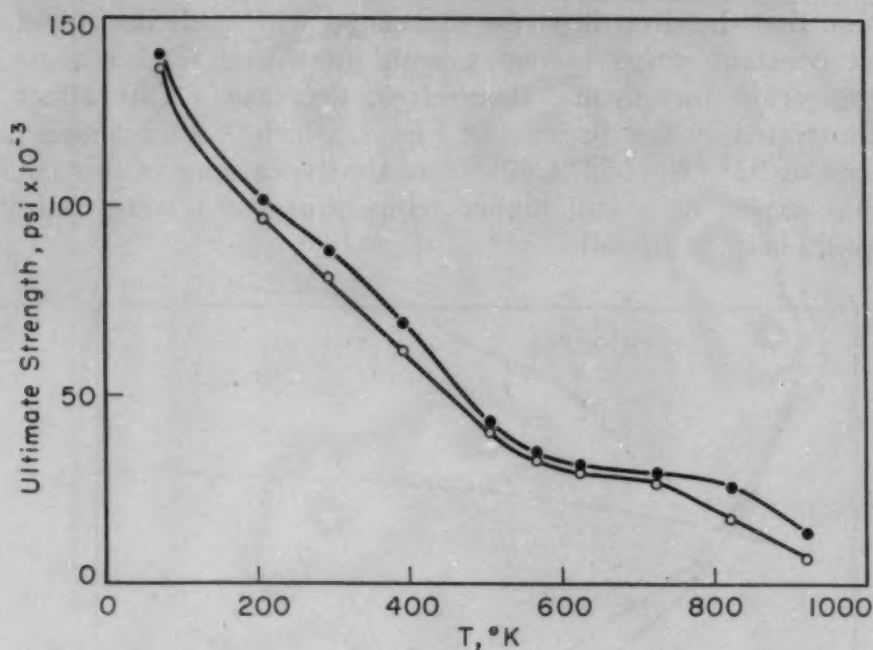


Fig. 6—Dependence of Ultimate Strength on Temperature for Tests at the Two Strain Rates: Solid Circle = 0.138 min⁻¹; Open Circle = 0.003 min⁻¹.

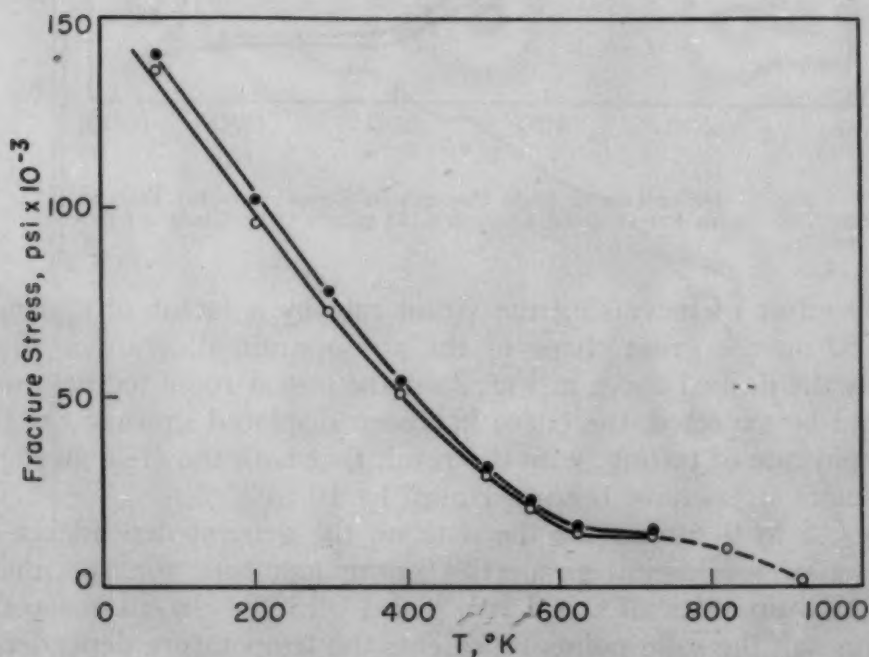


Fig. 7—Dependence of Fracture Stress on Temperature for Tests at the Two Strain Rates: Solid Circle = 0.138 min⁻¹; Open Circle = 0.003 min⁻¹.

whereas for testing temperatures above 555 °K. (282 °C) it remains relatively constant and, in fact, increases slightly at 725 °K (452 °C). On testing at 925 °K (652 °C) the yield stress again decreases with increasing temperature to the low value of 6000 psi. It is

further evident from Fig. 5 that the effect of increasing the strain rate does not significantly change the general temperature dependence of the yield strength. The curve does show, nevertheless, the temperature range in which this property is most sensitive to changes in rate of straining. This rate sensitivity effect reaches a maximum in the neighborhood of 300 to 425 °K (27 to 152 °C), and becomes gradually less pronounced as the temperature both increases and decreases.

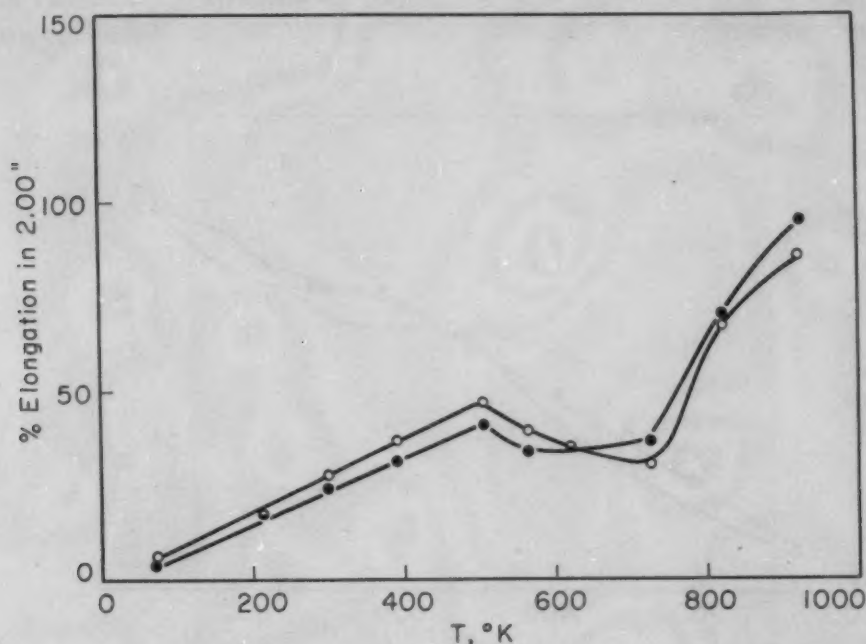


Fig. 8—Dependence of Elongation on Temperature for Tests at the Two Strain Rates: Solid Circle = 0.138 min^{-1} ; Open Circle = 0.003 min^{-1} .

The dependence of the ultimate strength on temperature is given in Fig. 6. A comparison of these curves with those of Fig. 5 shows that the ultimate strength increases with decreasing temperature in a manner very similar to the yield strength for the tests at both strain rates. In the case of the ultimate strength, however, there appears at the higher temperatures of testing a second temperature range where the effect of increasing the strain rate on this property is considerable. For purposes of comparison the mean value of the ultimate strength at the lower strain rate decreases from a value of 137,000 psi at 77 °K (-196°C) to one of 81,000 psi at room temperature, and even more significantly to a value of only 6000 psi for tests at 925 °K (652°C).

Fig. 7 describes the temperature dependence of the fracture stress, which was calculated from the original cross sectional area. As in the case of both the yield and ultimate strengths, the stress at fracture also increases appreciably with decreasing temperature

from 13,000 psi at 725 °K (452 °C) to 137,000 psi at 77 °K (−196 °C). On testing at 925 °K (652 °C), the fracture stress drops almost to zero. It is further apparent from Fig. 7 that the fracture stress is practically insensitive to a variation in the speed of testing.

The effect of temperature on the ductility of these specimens is shown in Figs. 8 and 9, where, respectively, the per cent elongation and reduction in area are plotted against the absolute temperature. It may be seen from Fig. 8 that for both strain rates the elongation

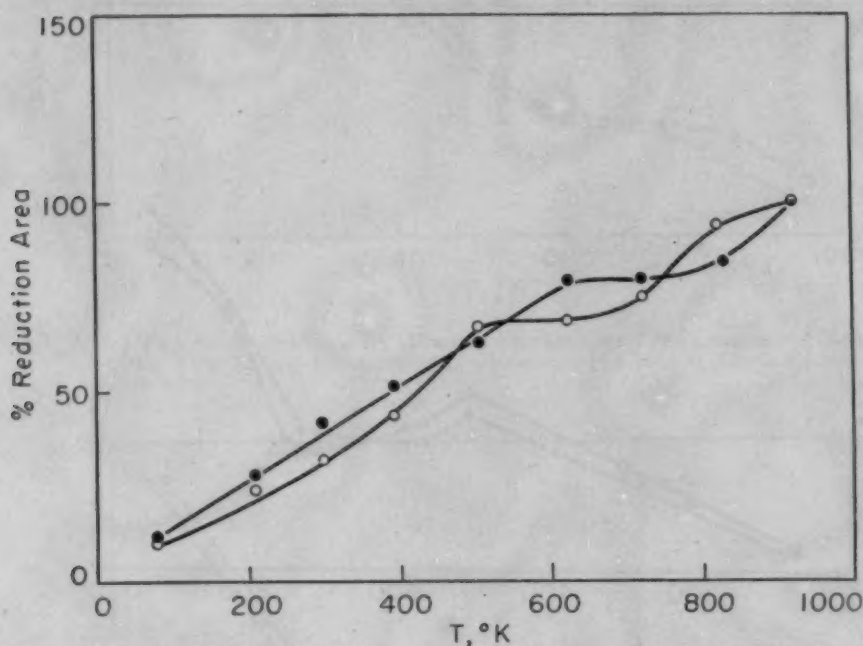


Fig. 9—Dependence of Reduction of Area on Temperature for Tests at the Two Strain Rates: Solid Circle = 0.138 min⁻¹; Open Circle = 0.003 min⁻¹.

increases linearly with rising temperature up to approximately 500 °K (227 °C). In the temperature range 500 to 700 °K (227 to 427 °C), there is a gradual decrease in the elongation despite the higher temperature of testing, and this can be attributed to a strain aging phenomenon. Above 700 °K (427 °C), the elongation once again increases with rising temperature at a more rapid rate. A comparison of the curves shows that the principal effect of increasing the strain rate is to minimize the strain aging effect in the temperature range 500 to 700 °K (227 to 427 °C). An extrapolation of the curves in Fig. 8 to 0% elongation suggests that low temperature brittleness for this material will occur at approximately 25 °K (−248 °C).

The curves of Fig. 9 also demonstrate a possible strain aging effect in the temperature range 500 to 700 °K (227 to 427 °C). In this range the per cent reduction in area no longer increases with increasing temperature, but, instead, remains essentially constant.

It would appear from this constancy that the property of elongation is more sensitive to strain aging. It is evident from Fig. 9 that the singular effect of increasing the strain rate is to shift the temperature range in which strain aging occurs to higher temperatures.

The variation in the elastic modulus with temperature is shown in Fig. 10. As might be expected, this property decreases linearly with increasing temperature from a mean value of 17,300,000 psi at the temperature of liquid nitrogen to one of 11,600,000 psi at 505 °K (232 °C). In determining the elastic modulus in this temperature range, strain measurements were obtained by the use of resistance-

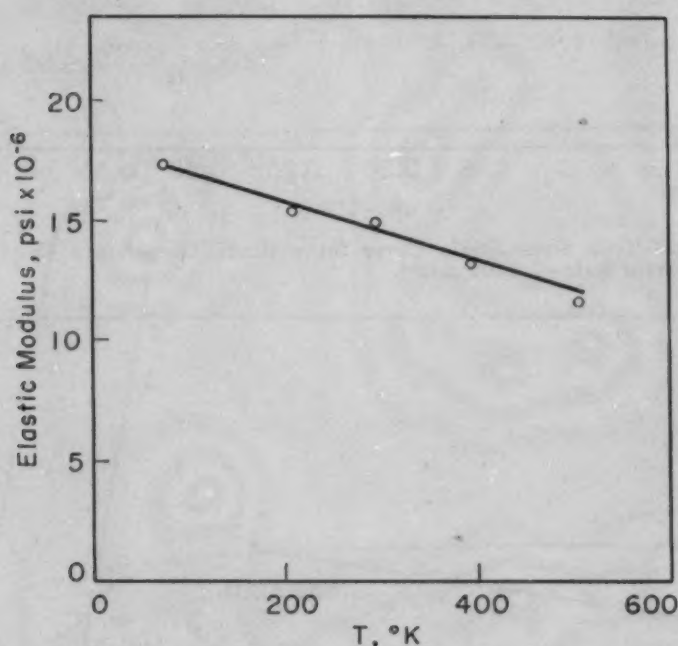


Fig. 10—Dependence of Elastic Modulus on Temperature.

type strain gages, which permit a reading accuracy of 2×10^{-6} . Readings of strain and load were taken simultaneously every 30 seconds on testing at the slow strain rate of 0.003 min^{-1} . Values of the elastic modulus at the higher temperatures of testing were not included in Fig. 10, since the technique used in measuring strain at these temperatures was not considered sufficiently accurate for a reliable comparison with the plotted values.

Fig. 11 shows the plastic portion of the true stress-strain curve for a room temperature test at a constant strain rate of 0.003 min^{-1} . This curve was obtained from simultaneous readings of the axial load and specimen diameter, which permitted a determination of the instantaneous area of the cross section. It may be seen that the curve is linear from approximately the point of maximum load (tensile strength) to the point of fracture. The slope of this straight-

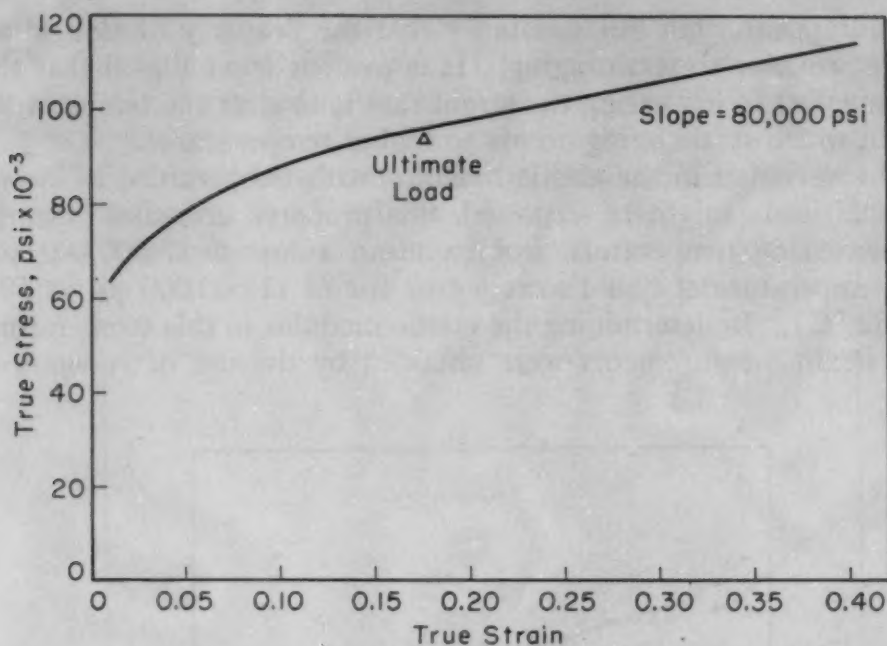


Fig. 11—True Stress-Strain Curve for a Room Temperature Test at a Constant Strain Rate of 0.003 min^{-1} .

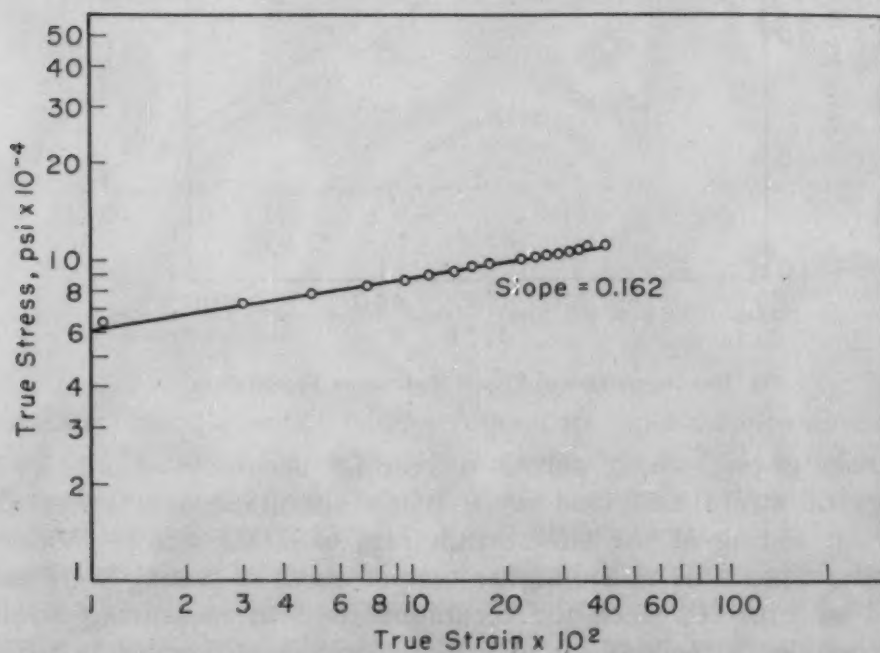


Fig. 12—True Stress-Strain Curve of Fig. 11 Plotted Logarithmically.

line portion of the true stress-strain curve is equal to 80,000 psi, which is the rate of strain hardening for this particular region of the curve (necking region). As might be expected from the work of Ludwik (7) and, more recently, that of Hollomon (8), a plot of true stress σ versus true strain δ on logarithmic coordinates for the curve of Fig. 11 results in a straight line (see Fig. 12) which yields values

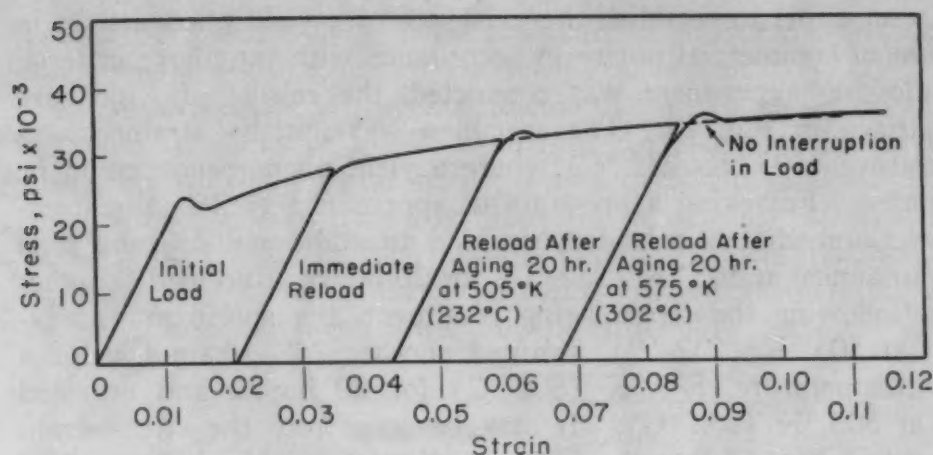


Fig. 13—Stress-Strain Curves at 505°K (232°C) Following Different Aging Treatments.

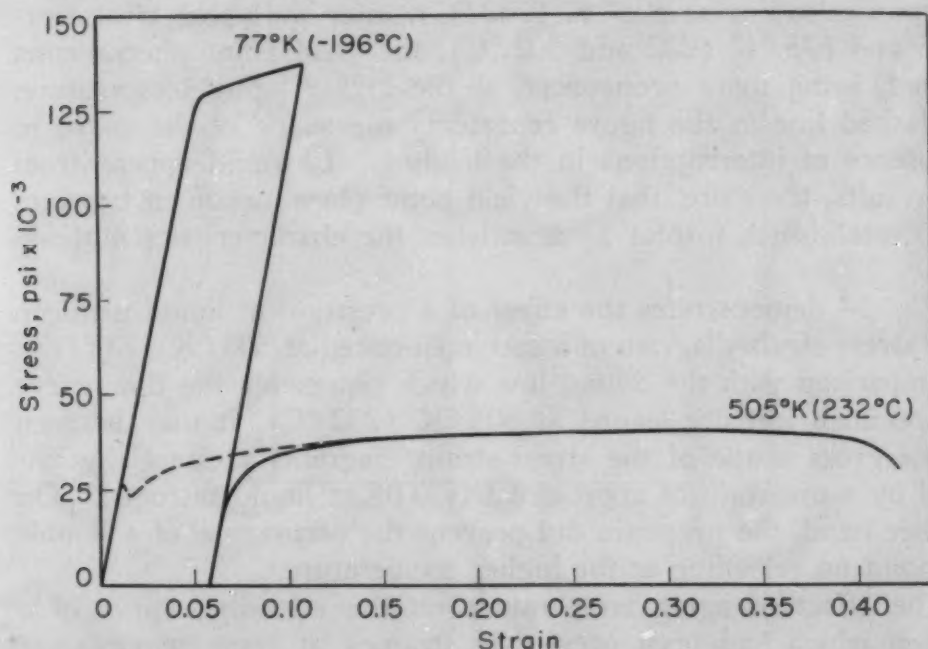


Fig. 14—The Effect of a Pre-Strain at Liquid Nitrogen on the Stress-Strain Diagram at 505°K (232°C).

of 0.162 for the strain hardening coefficient n , and 128,000 psi for the strength coefficient K in the generalized parabola: $\sigma = K \delta^n$.

It has been pointed out by Cottrell (9) that the yield phenomenon is identified by the following characteristics: (a) The yield point exhibits an upper and lower yield stress, or a yield point elongation zone (flow at a constant stress); (b) on immediately retesting a specimen which has been plastically strained, there is a smooth transition from the elastic to the plastic range instead of the yield phenomenon described in (a); and (c) on annealing a prestrained specimen (strain aging), the yield point phenomenon returns.

In an effort to establish the existence of a yield phenomenon in titanium of commercial purity in accordance with the above criteria, the following experiment was conducted, the results of which are summarized in Fig. 13. The specimen was initially strained at a temperature (505°K , 232°C) where a yield phenomenon could be anticipated. Following a prestrain of approximately 2%, the specimen was immediately reloaded, strained an additional 2% and then given an anneal at 505°K (232°C) for 20 hours at no load. Immediately following the strain aging treatment, the specimen was reloaded at 505°K (232°C), strained another 2%, strain-aged at a higher temperature, 575°K (302°C) for 20 hours, and reloaded again at 505°K (232°C). It may be seen from the stress-strain diagrams of Fig. 13 that the initial loading at 505°K (232°C) did produce a double yield point, which disappeared immediately upon reloading after the initial prestrain of 0.02. It is further evident that upon reloading at 505°K (232°C), after the aging treatments at 505 and 575°K (232 and 302°C), the yield point phenomenon returned, being more pronounced at the higher aging temperature. The dashed line in the figure represents the shape of the curve in the absence of interruptions in the loading. It would appear from these results, therefore, that the yield point phenomenon in titanium is well established, insofar as it satisfies the characteristics outlined above.

Fig. 14 demonstrates the effect of a prestrain at liquid nitrogen on the stress-strain diagram of a specimen tested at 505°K (232°C). By comparison with the dotted line which represents the flow curve of a specimen initially loaded at 505°K (232°C), it may be seen that the gross shape of the stress-strain diagram is essentially unaltered by a prestrain of approximately 0.05 at liquid nitrogen. On the other hand, the prestrain did prevent the occurrence of a double yield point on reloading at the higher temperature.

The effect of aging temperature on the reloading curve of a specimen which had been previously strained at room temperature is shown in Fig. 15. Following a preplastic strain of 0.045 at room temperature, the specimens were annealed at various temperatures for 1 hour at no load, and then immediately retested at room temperature. It may be seen that on annealing at 200°C strain aging effects occurred, as evidenced by the appearance of a yield point and a general strengthening of the flow curve on reloading at room temperature. Annealing at 400°C produced a softening effect, despite the appearance of a yield point elongation zone (flow at constant stress), while heating at temperatures of 600 and 800°C apparently results in an over-all recovery. These results further show that the yield point becomes less pronounced as the temperature of annealing increases. Similar observations have recently been re-

ported by Lubahn (10), who conducted similar experiments while studying the strain aging effects in OFHC copper.

As a corollary to the experiments of Fig. 15, the effect of aging at room temperature for 48 hours on the stress-strain curve of a specimen which had also been given a prestrain of 0.045 at room temperature is shown in Fig. 16. As in the case of annealing at 200 °C for 1 hour in Fig. 17, this aging treatment resulted in the appearance of a yield point on reloading at room temperature as well as a slight displacement upward of the entire flow curve.

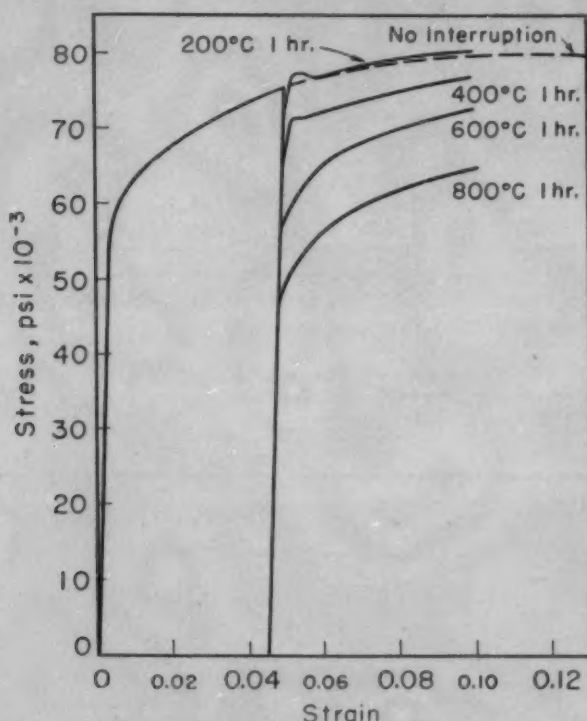


Fig. 15—The Effect of Aging Temperature on the Stress-Strain Curve at Room Temperature.

Fig. 17 demonstrated the effect of increasing strain on the appearance of the yield point on reloading a specimen which had been prestrained at room temperature followed by annealing treatments at 400 °C for 1 hour. It is evident from the two reloading curves following identical heat treatments that the extent of the yield point elongation zone is greater for the test at the higher total extension.

Typical appearance of fractures obtained at the different temperatures of testing at a strain rate of 0.003 min⁻¹ are illustrated in Fig. 18. It is apparent from these photographs that with increasing temperature of testing (right to left) the cross section at fracture tends to become elliptical. At 925 °K (652 °C) the fractured surface has the appearance of a slightly rumpled thin sheet, which results in a maximum reduction in area (Fig. 9). It is

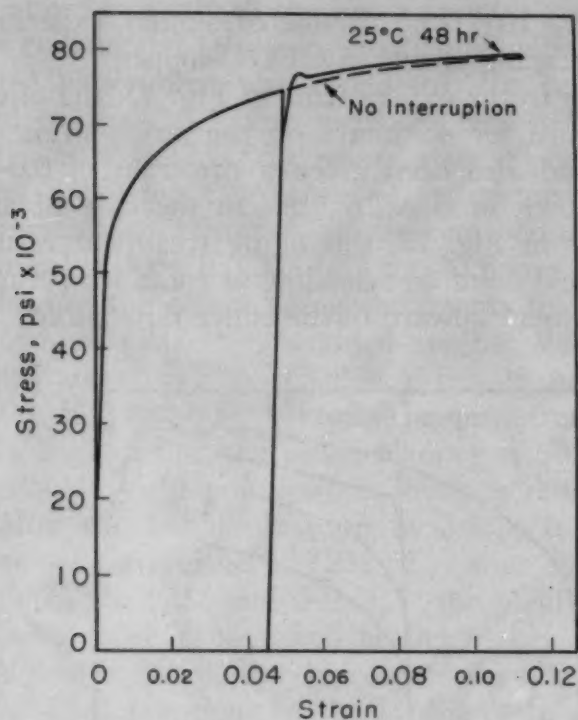


Fig. 16—Effect of Aging at Room Temperature on the Stress-Strain Curve at Room Temperature.

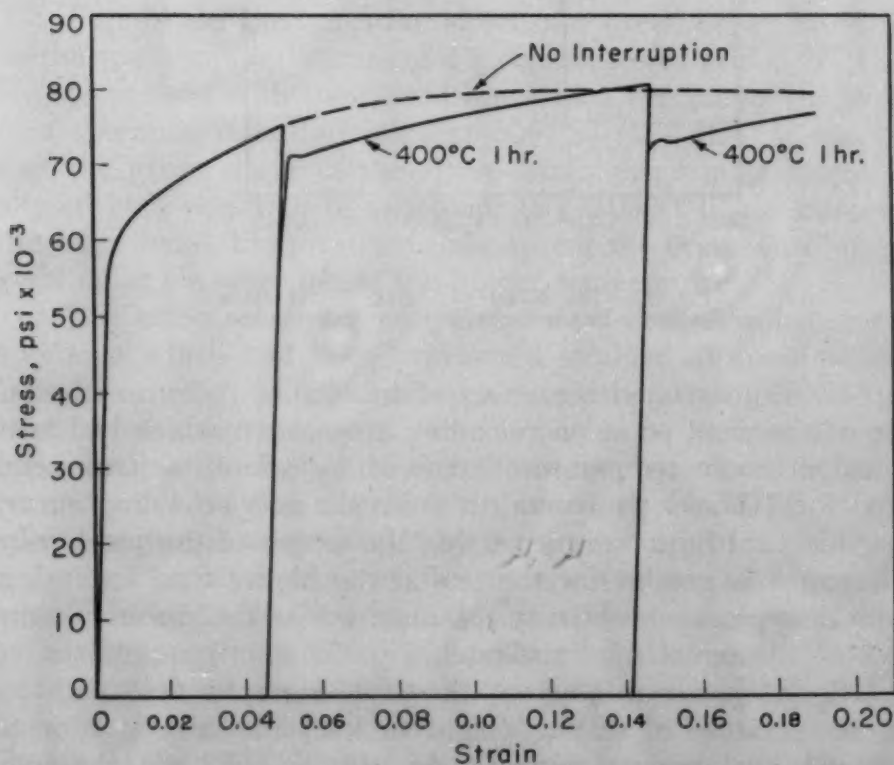


Fig. 17—Effect of Increasing Strain on the Appearance of a Yield Point Following Aging in the Stress-Strain Curve at Room Temperature.

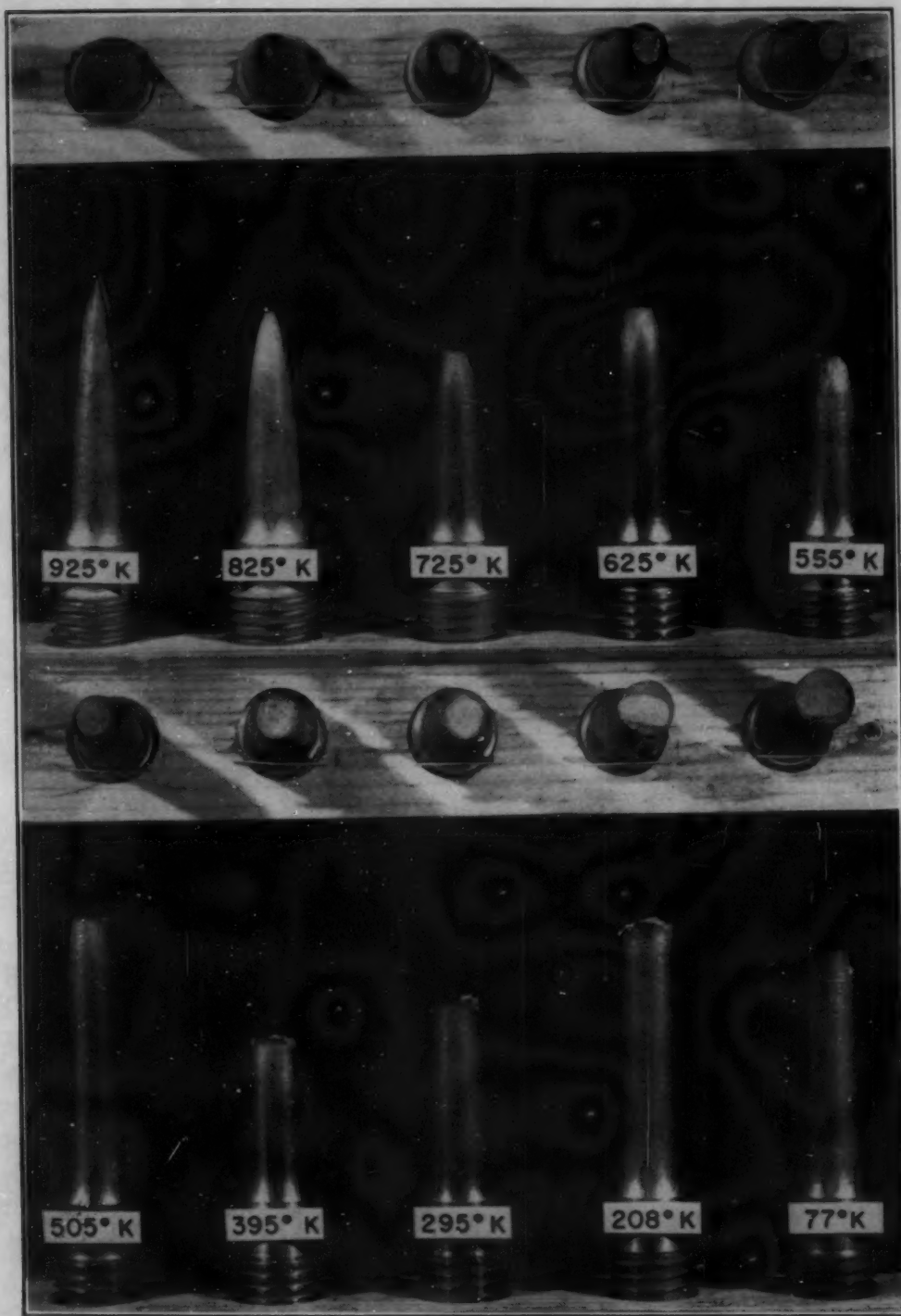


Fig. 18—Appearance of Fractures at Different Temperatures of Testing at a Constant Strain Rate of 0.003 min^{-1} .

interesting to note that for the test at liquid nitrogen (77°K), well-defined, radial cracks, rather uniformly spaced, appear along the entire surface of the specimen. Similar cracks appear on testing at 208 and 295°K (-65 and 22°C), but are not as well defined.

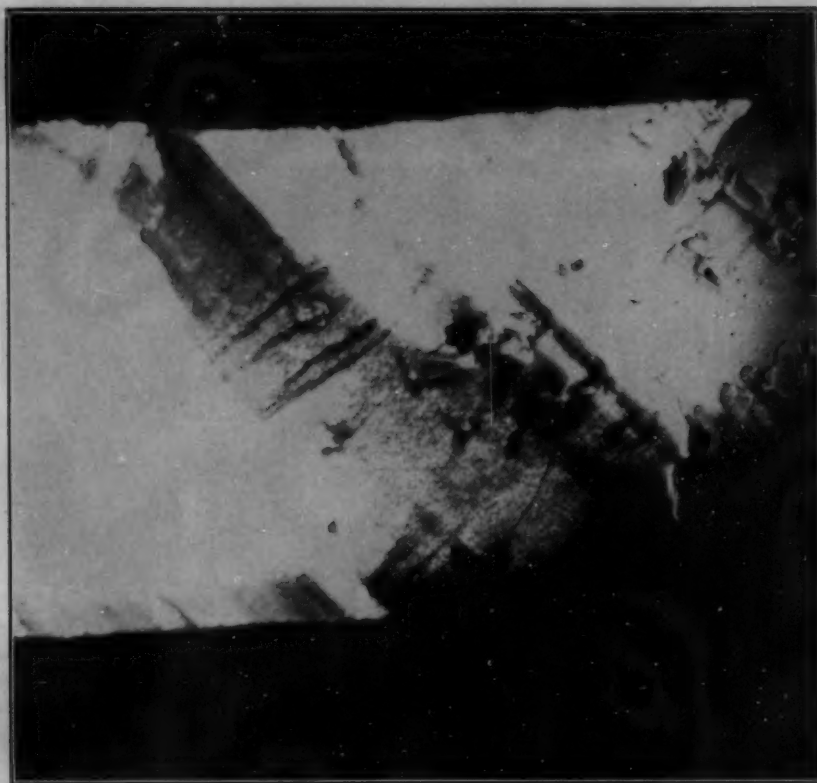


Fig. 19—Appearance of Lüders Bands Near Gripped End in Coarse-Grained Sheet Specimen of Titanium. Arrow indicates direction of applied stress.

With the possible exception of the test at liquid nitrogen, the fracture at all temperatures exhibits those characteristics typical of ductile materials.

Appearance of Lüders' Bands—It is generally accepted that the upper and lower yield points of the stress-strain curve are intimately associated with a localized and discontinuous yielding resulting from the formation and broadening of deformation bands, called Lüders' lines. Since titanium exhibits this yield point phenomenon, the appearance of Lüders' deformation in this material might well be anticipated. Although it is not the purpose of this study to include an investigation of the nature of these bands, an observation of their occurrence in a coarse-grained sheet testpiece is considered worthy of some discussion.

In the course of studies on the plastic flow elements in arc-melted titanium sponge, a sheet specimen ($\frac{1}{4}$ by 0.05 inch), which contained grains ranging from 2 to 5 millimeters in diameter in its gage length of $1\frac{1}{2}$ inches, was extended approximately 5% at room temperature, using conventional methods of gripping. At one end of the gage length (in the vicinity of the grip), Lüders' bands were formed which spread over the specimen in a direction approximately 50 degrees to the specimen axis or direction of applied stress. These

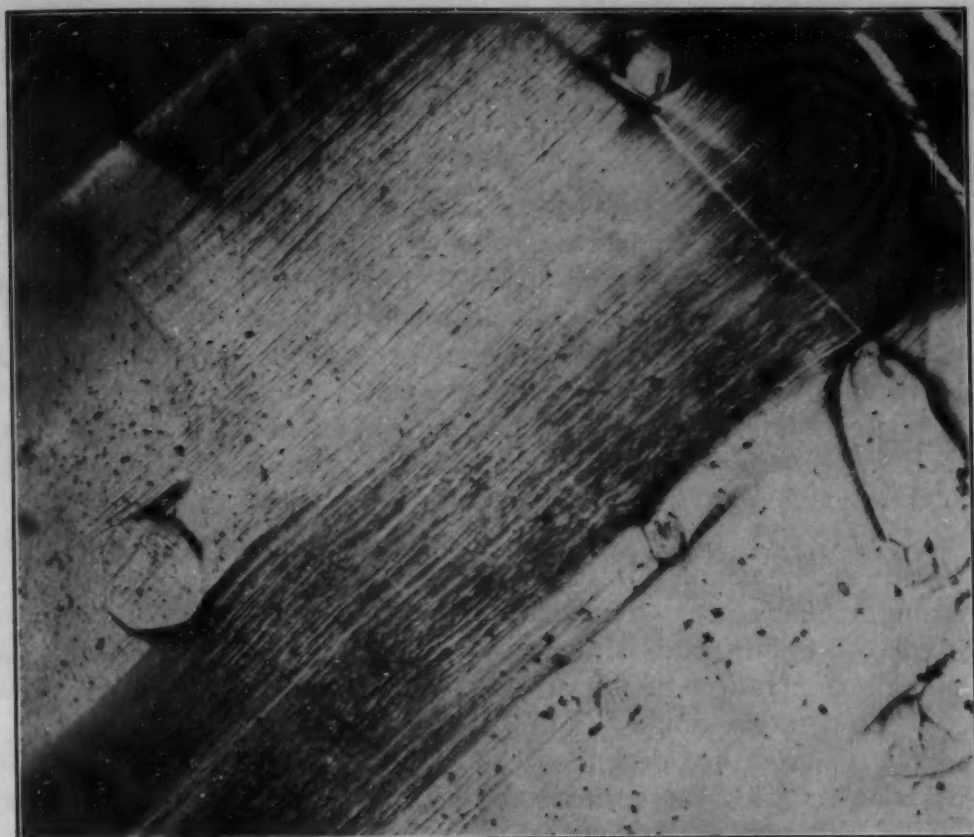


Fig. 20—Appearance of Lüders Bands at Higher Magnification.

bands are shown in Fig. 19, which also reveals a slight necking in the region associated with the bands. It is further evident from this photomicrograph that the deformation within these bands (degree of blackening) varies across the specimen and appears to be a maximum near the edges of the specimen. Careful microscopic examination of the surface on which these bands developed revealed that these bands are actually made up of clusters of fine, parallel lines. This characteristic of Lüders' bands is shown in Fig. 20, which was taken at higher magnification. The round inclusions are simply unabsorbed grains which are frequently observed in the production of coarse grains by the strain-anneal technique, which was used in this case. It is further interesting to note that the deformation in these bands also appears to be greater in the vicinity of such inclusions.

Fortunately, the Lüders' deformation appeared across grains sufficiently large to permit X-ray analysis of the crystallographic nature of the fine, parallel deformation lines. This analysis showed that these fine traces coincided with a prismatic plane $\{10\bar{1}0\}$, which has been found to be the predominant slip plane in titanium at room temperature (14). Thus, it appears that the Lüders' bands observed in this coarse-grained specimen actually consist of clusters of fine slip bands.

Further extension of the sheet specimen resulted in fracture on a plane, which appeared parallel to the prismatic traces of the Lüders' bands.

SUMMARY

The tensile properties of titanium of commercial purity were investigated in the temperature range 77 to 925 °K (−196 to 652 °C) at constant strain rates of 0.003 min^{−1} and 0.138 min^{−1}. The results of these tests showed that this material exhibits the usual mechanical effects associated with the strain aging phenomenon. As mentioned previously, this is not altogether surprising, since this material contains as impurities small amounts of nitrogen and carbon, which are generally associated with the appearance of these effects.

The yield point phenomenon was observed in the temperature range 390 to 555 °K (117 to 282 °C). As is generally the case (15, 16) this phenomenon disappears gradually with increasing or decreasing temperature. The maximum effect (U.Y.P.–L.Y.P.) appeared to occur in the vicinity of 505 °K (232 °C). Discontinuous yielding or serration in the stress-strain curves was observed at a higher temperature range 725 to 925 °K (452 to 652 °C).

The temperature dependence of a number of mechanical properties also revealed the occurrence of strain aging phenomena. For example, the curves showing the effect of temperature on per cent elongation and reduction in area both exhibited discontinuities. In the range 505 to 725 °K (232 to 452 °C) there is actually a decrease in ductility with increasing temperature. In the case of the yield strength, there is no change in this property with increasing temperature in the range 625 to 825 °K (352 to 552 °C), whereas the effect of increasing strain rate on this property is greatest in the range 300 to 400 °K (27 to 127 °C).

Aging at 200 °C resulted in both the appearance of a yield point and a strengthening in the room temperature curve of a specimen which had been given a prestrain of approximately 5%. Aging at higher temperatures brought about the disappearance of the yield point and a softening resulting from a recovery effect.

Some observations were made on the nature of Lüders' bands in an extended, coarse-grained sheet specimen. These bands were found to consist of clusters of fine, parallel lines, which were identified by X-ray analysis to be traces of prismatic {10 $\bar{1}$ 0} planes.

ACKNOWLEDGMENT

The authors wish to express their gratitude to B. H. Alexander for his constructive criticism throughout the course of this investigation, and to O. W. Haines, Jr., for his valuable assistance in performing the tests at the different temperatures.

References

1. C. A. Edwards, D. L. Phillips and H. N. Jones, "The Influence of Some Special Elements on the Strain-Aging and Yield Point Characteristics of Low Carbon Steels", *Journal, Iron and Steel Institute*, Vol. 142, 1940, p. 199.
2. J. R. Low, Jr., and M. Gensamer, "Aging and the Yield Point in Steel", *Transactions, American Institute of Mining and Metallurgical Engineers*, Vol. 158, 1944, p. 207.
3. C. A. Edwards and L. B. Pfeil, "The Tensile Properties of Single Crystals of Iron and the Influence of Crystal Size on the Tensile Properties of Iron", *Journal, Iron and Steel Institute*, Vol. 112, 1925, p. 79.
4. R. Arrowsmith, "A Note on the Effect of Grain Size on the Extension of the Yield Point in Armco Iron", *Journal, Iron and Steel Institute*, Vol. 11, 1924, p. 317.
5. J. Winlock and R. Leiter, "Some Factors Affecting the Plastic Deformation of Sheet and Strip Steel and Their Relation to Deep Drawing Qualities", *TRANSACTIONS, American Society for Metals*, Vol. 25, 1937, p. 163.
6. C. W. Fell, "Yielding Phenomena in Iron, Steel, Aluminum Alloys and Other Metals Under Stress", *Iron and Steel Institute, Carnegie Scholarship Memoirs*, Vol. 26, 1937, p. 123.
7. P. Ludwik, *Elemente der technologischen Mechanik*, Julius Springer, Berlin, 1909.
8. J. H. Hollomon, "Tensile Deformation", *Transactions, American Institute of Mining and Metallurgical Engineers*, Vol. 162, 1945, p. 268.
9. A. H. Cottrell, "The Yield Point in Single Crystal and Polycrystalline Metals", *Symposium on the Plastic Deformation of Crystalline Solids*, Pittsburgh, 1950.
10. J. D. Lubahn, "Strain Aging Effect", General Electric Research Laboratory Report No. RL-467, Contract No. AF-33 (038)-11773, December 1950.
11. J. H. Hollomon, *The Problem of Fracture*, American Welding Society, New York, 1946.
12. W. Sylwestrowicz and E. O. Hall, "The Deformation and Aging of Mild Steel", I, II, III, *Proceedings, Physical Society*, Vol. B-64, June 1951, p. 495; Vol. B-64, September 1951, p. 742.
13. A. Nadai, *Theory of Flow and Fracture of Solids*, McGraw-Hill, N. Y., 1950.
14. C. A. Dube, F. D. Rosi, B. H. Alexander and F. Perkins, "The Mechanism of Plastic Flow in Titanium", Sylvania Electric Products Inc. Report No. YE-51-0445, Contract AF-33-038-16031, May-August, 1951.
15. C. Bach and R. Baumann, *Festigkeitseigenschaften und Gefugebilder der Konstruktions-Materialien*, 2nd Edition, Julius Springer, Berlin, 1921, p. 11.
16. R. L. Kenyon and R. S. Burns, "Aging in Iron and Steel", *Symposium on Age Hardening of Metals*, American Society for Metals, 1940, p. 262.

DISCUSSION

Written Discussion: By A. N. Holden, Knolls Atomic Power Laboratory, General Electric Co., Schenectady, N. Y.

I congratulate the authors for their fine study of the discontinuous yielding and strain aging effects in titanium. These effects are becoming

more the rule than the exception as careful studies are made of commercial metals.

I know the authors, in common with many of us, would like to know what alloying element is causing strain aging effects in titanium, and it seems to me this information might be obtained by either of two alternate means.

The most direct method would be to eliminate in some fashion certain elements from the metal, and I would certainly begin, as the authors suggest, with carbon and nitrogen. It seems unlikely that substitutional elements will be effective in causing strain aging at room temperature in any reasonable time. The second approach would be to measure the rate of occurrence of some comparable manifestation of strain aging at several temperatures and determine an activation energy for the process, which of course is only useful if it agrees with a known activation energy for the diffusion of something in titanium. I hope the authors may soon indict the responsible element, although I share their lack of surprise at observing strain aging in a commercially pure material.

I do not fully appreciate Fig. 14. After its deformation at liquid air temperature, was the material aged at 505 °K (232 °C) for a long enough period to acquire the yielding manifestation of strain aging? The shortest effective aging time mentioned in this work for a comparable temperature is 1 hour at 200 °C (see Fig. 15). If the second test in Fig. 14 represents immediate retesting at 232 °C after the liquid air prestrain, the results are in accord with expectation, but if the test was done after aging 1 hour or longer at 232 °C, the absence of a yield point is mildly surprising.

Authors' Reply

In reply to Dr. Holden's question as to the exact significance of the tests in Fig. 14, it should have been emphasized in the manuscript that this experiment was performed to demonstrate simply the effect of a pre-strain at a low temperature on the yield point phenomenon and gross shape of the stress-strain diagram of a specimen tested at an elevated temperature, where a yield point phenomenon could be expected on loading without a prior pre-strain. It was not intended to complicate this test by introducing an intermediate aging treatment. Consequently, the specimen was kept at a temperature of dry ice for approximately 6 hours following the pre-strain at liquid nitrogen, for the expressed purpose of avoiding any strain-aging effect. The observation that discontinuous yielding did not occur on reloading at the elevated temperature suggests that the effect of a pre-strain on the stress-strain characteristics of this material is independent of the temperature of pre-straining (compare Fig. 14 with the initial and second loading in Fig. 13).

With regard to Dr. Holden's comments regarding the methods for isolating the element or elements responsible for the observed strain-aging effects in titanium, the authors are in complete agreement. Unfortunately, however, no work has been done in this direction at the present time.

MECHANICAL PROPERTIES, INCLUDING FATIGUE OF TITANIUM-BASE ALLOYS RC-130-B AND Ti-150-A AT VERY LOW TEMPERATURES

BY S. M. BISHOP, J. W. SPRETNAK AND M. G. FONTANA

Abstract

Titanium alloys RC-130-B and Ti-150-A were subjected to tensile, fatigue, impact, hardness, and dilatometric tests at low temperatures. Data are reported for: tensile and fatigue at 77, -108 and -321 °F (25, -78 and -196 °C); impact and hardness at 77, -108, -197, -321 and -423 °F (25, -78, -127, -196 and -253 °C); dilatometry over the range from room temperature to -321 °F (-196 °C). Some description is given of apparatus and techniques, and an effort is made to explain unusual behaviors.

DURING the past few years titanium and alloys of titanium have received considerable attention from several diverse fields of engineering. Aircraft structures designers and corrosion engineers are particularly interested in these materials because of their remarkably high strength-weight ratios and their phenomenal resistance to certain corrosive environments.

The investigation covered in this paper was undertaken to determine rather completely the low temperature mechanical properties of two recently developed, commercially available titanium alloys, RC-130-B and Ti-150-A. The behavior of metals and alloys at low temperatures is important and must be known for efficient and proper design of aircraft and other structures.

Because of the grossness of most mechanical tests, the lowest practical temperature is the boiling point of liquid hydrogen, -423 °F (-253 °C). Boiling liquid nitrogen, -321 °F (-196 °C), furnishes another datum point for tests, while the melting point of methylcyclohexane, -197 °F (-127 °C), and the sublimation point of dry ice, -108 °F (-78 °C), give two more low temperature levels. For comparison purposes, the materials were run through the complete gamut of tests at a warm room temperature, about 75 to 80 °F (25 °C). Some modifications of standard mechanical testing techniques were required to maintain test specimens at these low

A paper presented before the Eighth Western Metal Congress of the Society, held in Los Angeles, March 23 to 27, 1953. Of the authors, S. M. Bishop is research fellow, Ohio State University Research Foundation, Columbus; J. W. Spretnak is associate professor and M. G. Fontana is professor and chairman, Department of Metallurgy, Ohio State University, Columbus, Ohio. Manuscript received April 22, 1952.

temperatures, but whatever modifications were made were of a superficial nature and did not influence the experimental results.

MATERIALS

Titanium alloys RC-130-B and Ti-150-A are high strength alloys having compositions shown in Table I. Ti-150-A was received as $\frac{5}{8}$ -inch round rod which had been annealed (6 hours at 1200 °F),

Table I
Chemical Composition of Titanium Alloys

Ti-150-A, Heat No. X-1106	RC-130-B, Heat No. B-3084
%	%
Fe — 1.3	C — 0.24
Cr — 2.7	Al — 3.8
N — 0.08 maximum	Mn — 3.8
C — 0.05 maximum	Ti — balance
Ti — balance	

pickled and centerless ground. RC-130-B was purchased as annealed (1 hour at 1300 °F and air-cooled) $\frac{5}{8}$ -inch round rod which had been given no special surface treatment.

APPARATUS

A previous paper on the subject of low temperature testing (1)¹ contains a very thorough description of the apparatus used in these tests, with the exception of the dilatometer.

For thermal expansion measurements a simple setup was constructed as illustrated in Fig. 9. With this equipment it was possible to regulate the temperature of the specimen to within ± 0.5 °C, since the massive aluminum cylinder surrounding the specimen served to minimize thermal gradients. Cold nitrogen gas introduced at the bottom of the vacuum-jacketed cryostat worked its way up past the aluminum cylinder and out a vent at the top. An electrical vibrator was attached to the side of the cryostat to prevent sticking of the quartz rods and the dial gage. Temperature was measured by means of the two thermocouples, shown in Fig. 9, and a Leeds and Northrup potentiometer.

PROCEDURE

No important changes have been made in the procedures described in previous papers (1, 2, 3); however, the details of procedure for thermal expansion measurements must be described.

Liquid nitrogen was fed from a Dewar flask into a "boiler" or chamber whose "heat leak" could be controlled. The cold nitrogen gas thus produced entered the cryostat in Fig. 9 and refrigerated the aluminum cylinder which surrounds the specimen. During the cool-

¹The figures appearing in parentheses pertain to the references appended to this paper.

ing part of the cycle the temperature of the aluminum cylinder was lowered in 10 °C steps. When both thermocouples in the aluminum cylinder gave the same potential reading on the potentiometer, the flow of cold nitrogen was reduced to a level just sufficient to maintain a constant temperature reading on both thermocouples. Temperature was carefully maintained for 5 to 8 minutes before dial gage readings were taken to permit the specimen to come to equilibrium with the aluminum cylinder. It is believed that this procedure reduced thermal gradients in the specimen to a minimum, and helped reduce hysteresis in the thermal expansion curve. In order to obtain the temperature of liquid nitrogen, boiling liquid nitrogen was fed into the cryostat until it overflowed at the top vent. The entire setup was maintained at this temperature for at least 10 minutes. For the heating part of the cycle, the nitrogen was shut off, and the aluminum cylinder and specimen were very gradually warmed by heat transfer through the vacuum-jacketed cryostat. In order to obtain room temperature in the cryostat it was necessary to force warm air into the outlet vent.

TEST SPECIMENS

Tensile—Standard 0.250-inch diameter tensile specimens with a 1-inch gage length were used for the polished tensile tests. Notched specimens had a 0.300-inch major diameter and a 0.250-inch root diameter. The notch flank angle was 60 degrees, with a root radius of 0.010 inch. Two gage lengths were used on notched specimens—a 1-inch gage length and a 1/4-inch gage length in order to indicate what fraction of the total elongation was localized in the region of the notch.

Fatigue—Polished fatigue specimens were machined with a 0.250-inch critical section which was polished through 000 emery paper. Notched fatigue specimens were made with a notch of the same dimensions as that employed in the notched tensile tests.

Impact and Hardness—Standard Charpy keyhole-notch impact specimens were used in impact tests and as hardness specimens. Hardness readings were taken on the flat sides of the impact specimen away from the notch by means of a Vickers hardness tester.

Dilatometry—3-inch by 5/8-inch round rods were machined for thermal expansion readings. Care was taken to machine the ends of these specimens perfectly flat.

RESULTS AND DISCUSSION

Tensile Tests—As might be expected, both alloys were embrittled by a drop in temperature. Table II affords a comparison between room temperature and low temperature tensile properties. As temperature was lowered, the nominal tensile strength of RC-130-B,

Table II
Tensile Properties of RC-130-B and Ti-150-A at Various Temperatures

	Polished			Notched		
	77 °F (25 °C)	-108 °F (-78 °C)	-321 °F (-196 °C)	77 °F (25 °C)	-108 °F (-78 °C)	-321 °F (-196 °C)
<i>RC-130-B</i>						
Modulus of Elasticity (psi) . . .	16.8×10^6	17.3×10^6	18.9×10^6
Yield Strength (psi)	143,000	169,000	254,000	183,000	200,000	177,000
Ultimate Strength (psi)	149,000	172,000	256,000	186,000	200,000	177,000
Elongation (% in 1 inch)* . . .	19.6	15.0	2.1	0.9	0.2	0.1
Elongation (% in 1/4 inch)*	3.7	0.5	1.1
Reduction of Area (%)	41.3	25.5	4.9
Root	3.2	0	0
Major	0	0	0
<i>Ti-150-A</i>						
Modulus of Elasticity (psi) . . .	15.9×10^6	16.2×10^6	19.0×10^6
Yield Strength (psi)	144,000	171,000	246,000	184,000	185,000	154,000
Ultimate Strength (psi)	153,000	175,000	246,000	186,000	185,000	154,000
Elongation (% in 1 inch)* . . .	6.5	5.6	0.8	0.4	0.3	0.1
Elongation (% in 1/4 inch)*	1.5	0.3	0.6
Reduction of Area (%)	9.1	12.1	1.6
Root	1.9	0	0
Major	0	0	0

*See text for significance of these data for notched specimens.

which was less than that of Ti-150-A at room temperature, approached and finally, at -321°F (-196°C), exceeded the tensile strength of Ti-150-A. RC-130-B is a slightly more ductile material at all temperatures.

The notched tensile tests gave a good example of the effect of low temperatures on notch sensitivity. Referring to Table II it is observed that the notched tensile strength of RC-130-B rises to a maximum at -108°F (-78°C) and then drops again at -321°F (-196°C), while the corresponding value for Ti-150-A is not changed at -108°F (-78°C), but drops sharply between -108 and -321°F (-78 and -196°C). The reduction of the notched fracture stress at -321°F (-196°C) is unusual among the various engineering alloys studied in this program.

Both materials are notch-sensitive at all temperatures, as can be seen from the low elongation and reduction of area figures for notched tensile tests. Elastic moduli rise gradually with falling temperature, the increase being greater in the case of Ti-150-A.

Figs. 1 and 2 are stress-strain curves for the two alloys. The notched stress-strain curves represent the nominal stress in the cross section of the notch root versus the strain over the 1-inch gage length. Such curves can be considered only as schematic representations of deformation under load. The stress-strain curves for polished specimens are without a doubt the most interesting. These materials have a very pronounced yield point and a "drop-of-the-beam" which is characteristic of mild steel. As the temperature is lowered, the drop-of-the-beam effect disappears, but the yield point is still well defined. In general, lower temperatures raise the tensile and yield strengths

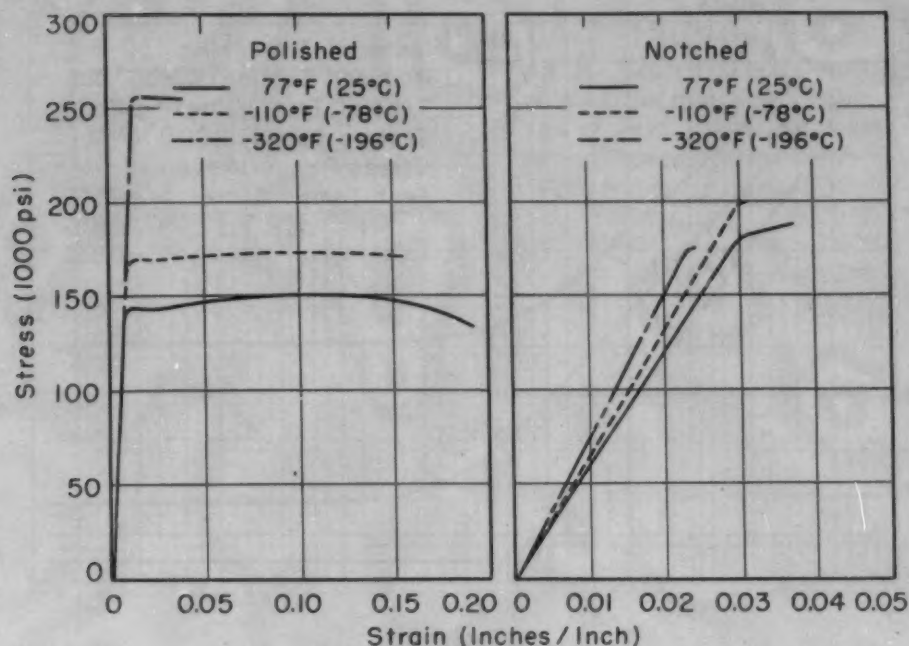


Fig. 1—Tensile Stress-Strain Curves for RC-130-B.

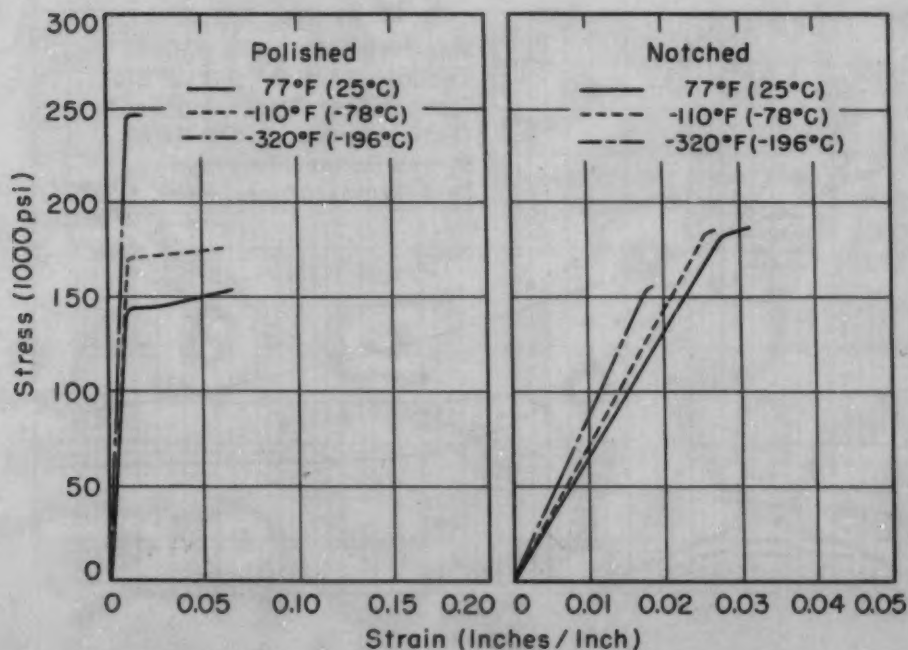


Fig. 2—Tensile Stress-Strain Curves for Ti-150-A.

and decrease the amount of plastic deformation prior to fracture. It was determined that these alloys are two-phased in structure, containing both alpha and beta forms of titanium. It is believed that the yield point results from interstitial atoms in solution in the body-centered beta phase analogous to the behavior of alpha iron. Commercially pure titanium does not show this yield point.

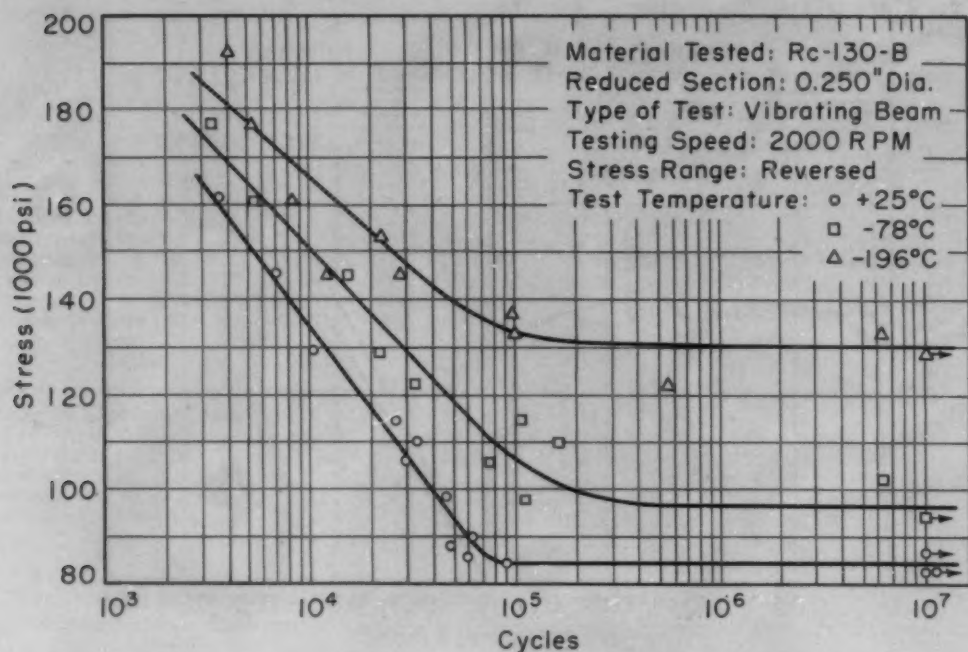


Fig. 3—Fatigue Results for RC-130-B, Unnotched.

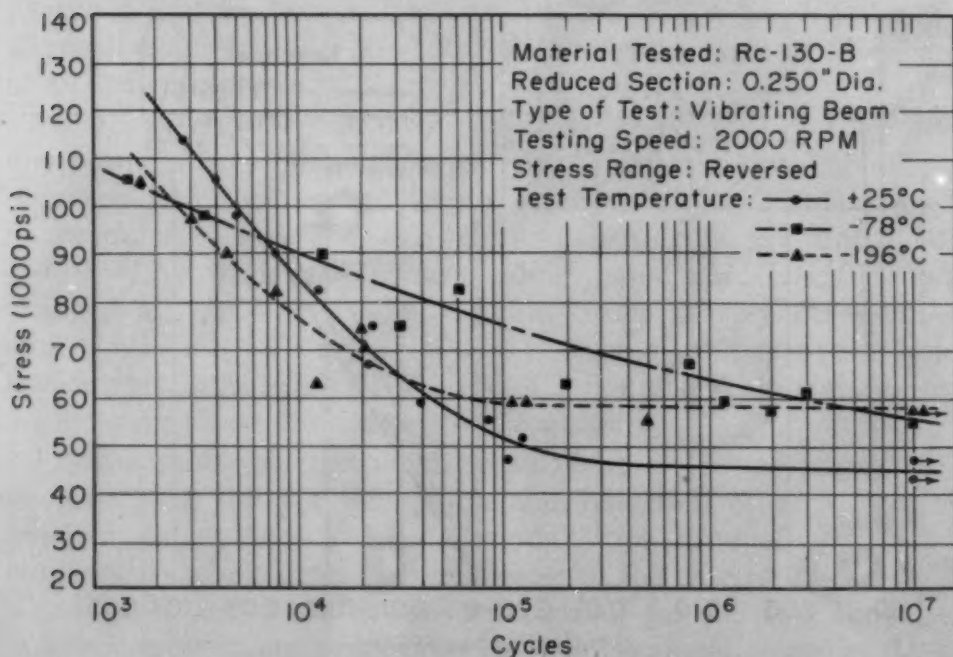


Fig. 4—Fatigue Results for RC-130-B, Notched.

Fatigue Tests—S-N curves shown in Figs. 3, 4, 5 and 6 illustrate the phenomenal increase in fatigue strength which occurs at low temperatures. Cycles-to-fracture is increased over the entire range of stress except in the case of notched specimens at high stresses.

One possible explanation of this behavior is that local yielding

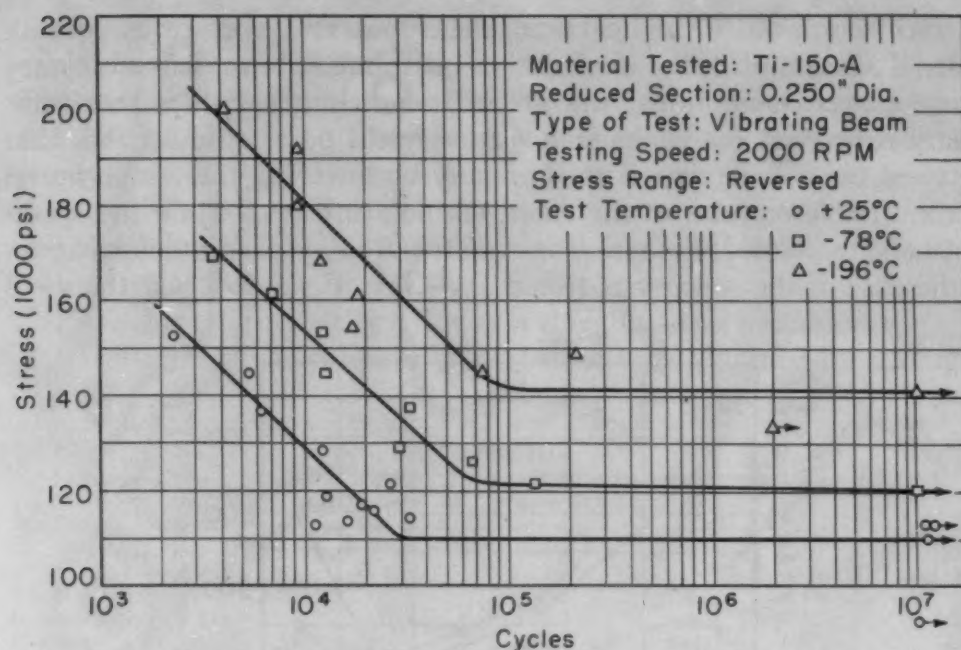


Fig. 5—Fatigue Results for Ti-150-A, Unnotched.

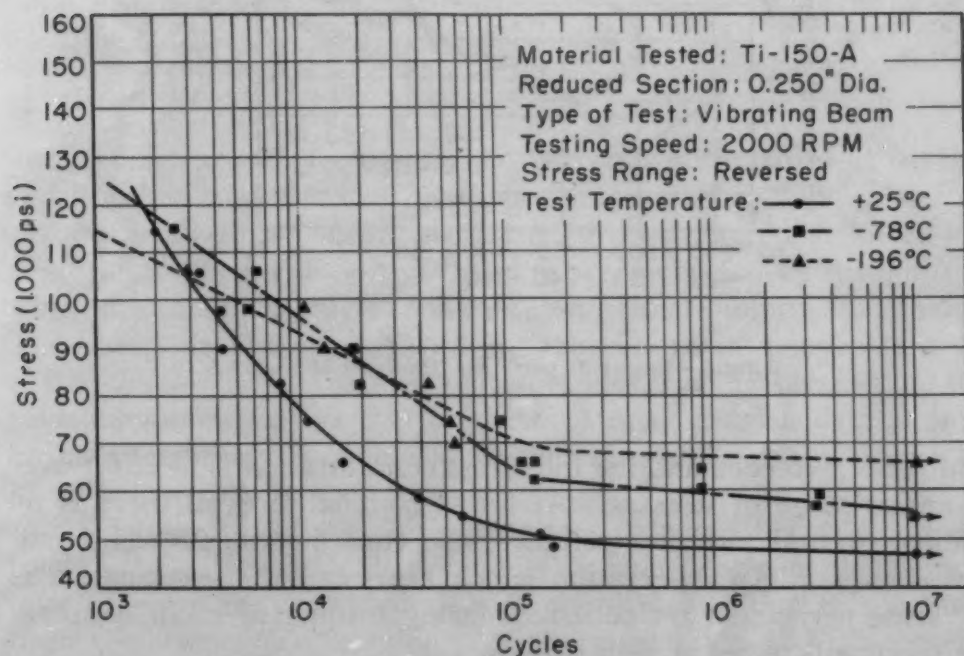


Fig. 6—Fatigue Results for Ti-150-A, Notched.

in the region of the notch root sets up a residual stress pattern which tends to reduce the maximum stress. For example, referring to Fig. 6, at a nominal maximum stress of 110,000 psi, the fatigue life of the material tested at room temperature appears to exceed the fatigue life of the material tested at -321°F (-196°C). But the reverse is true at lower stresses, and the endurance limit at -321°F

(-196°C) is 40% higher than the room temperature endurance limit. To accomplish the explanation mentioned above, it is necessary to make two assumptions: first, that the notch raises the stress sufficiently to exceed the room temperature yield point, and second, that the yield point is increased substantially by lowering the temperature. In the first few cycles of the room temperature test, while the specimen is being loaded, the stress is redistributed by plastic deformation. In the case of the specimens tested at -321°F (-196°C) the yield

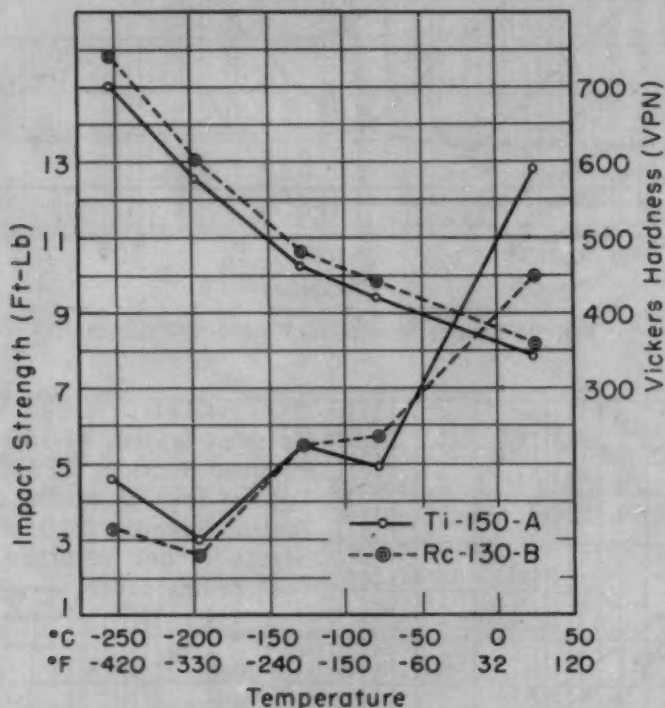


Fig. 7—Impact Strength and Hardness of Ti-150-A and RC-130-B.

point is not exceeded and the full stress concentration is in effect over the entire range of stresses. At lower nominal stresses there is no yielding, even at room temperature, and consequently no redistribution of stress. An observation which bears out this explanation is that some permanent set occurred during loading of room temperature specimens tested at high stresses.

Apparently these alloys possess a rather definite endurance limit, as shown by the flatness of the S-N curves beyond 10^5 cycles. This is another property they have in common with steels.

Ti-150-A has a room temperature endurance limit which is approximately 72% of its room temperature tensile strength. However, this remarkably high endurance ratio falls off rapidly at lower temperatures, and at -321°F (-196°C) the endurance ratio is only 57%.

Impact Tests—Results of impact tests were contrary to what would be expected from the tensile data. Ti-150-A, the slightly softer and more brittle of the two alloys, gave higher impact values than RC-130-B, even though it showed somewhat greater notch sensitivity than RC-130-B in the tensile tests. One possible explanation of this effect is that the RC-130-B alloy is more sensitive to strain rate than the Ti-150-A. At the higher rates of strain encountered in the impact test the RC-130-B becomes less ductile than the Ti-150-A, giving, therefore, lower values of absorbed energy.

Table III gives values of absorbed energy obtained by averaging

Table III
Charpy Impact Strength, Vickers Hardness, and Endurance Limits of RC-130-B and Ti-150-A at Various Temperatures

	77 °F (25 °C)	-108 °F (-78 °C)	-197 °F (-127 °C)	-321 °F (-196 °C)	-423 °F (-253 °C)
<i>RC-130-B</i>					
Impact Strength (ft.-lb.)	10.0	5.7	5.3	2.6	3.3
Hardness (VPN)	358	442	481	602	742
Polished Endurance Limit (psi)	84,000	98,000	...	130,000	...
Notched Endurance Limit (psi)	44,000	55,000	...	57,000	...
<i>Ti-150-A</i>					
Impact Strength (ft.-lb.)	12.8	4.9	5.5	3.0	4.6
Hardness (VPN)	342	421	462	578	703
Polished Endurance Limit (psi)	110,000	120,000	...	141,000	...
Notched Endurance Limit (psi)	47,000	56,000	...	67,000	...

five readings at each temperature. Also shown are hardness readings and polished and notched endurance limits. Fig. 7 illustrates the changes in hardness and impact strength encountered at lower temperatures. The points in this diagram are connected by straight lines which are intended only to indicate approximate intermediate values. The sharp drop in impact values between room temperature and -108 °F (-78 °C) implies that the alloys have a transition temperature somewhat like that of carbon steels. Impact data at intermediate temperatures would show whether the transition range is a narrow or a wide temperature interval.

Dilatometry—Table IV summarizes data on thermal expansion coefficients. Previously determined (4) coefficients for commercially pure titanium are presented also for comparison. Fig. 8 is a plot of these coefficients as a function of temperature. RC-130-B apparently has a much greater thermal expansion than Ti-150-A, especially in the higher temperature range. These values were obtained by drawing tangents to the dilation curves at 20 °C intervals of temperature. The slopes of these tangents were taken as the specific coefficients at the temperatures listed.

PHOTOGRAPHS

Fig. 10 is a photograph of fatigue fractures which are typical

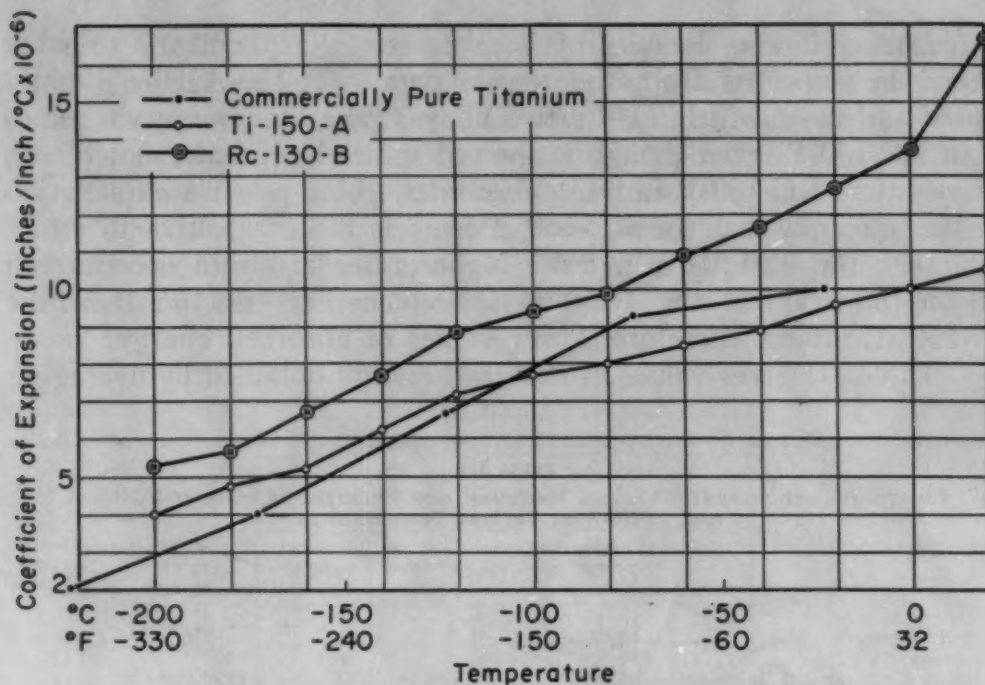


Fig. 8—Coefficients of Expansion at Various Temperatures.

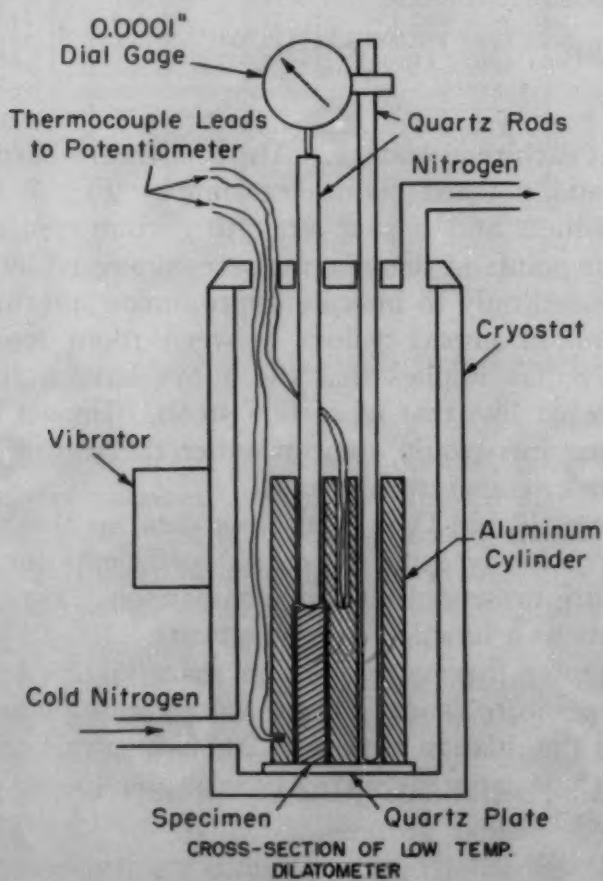


Fig. 9—Cross Section of Low Temperature Dilatometer.



Fig. 10—Typical Fatigue Fractures of Polished Fatigue Specimens.

Table IV
Coefficients of Thermal Expansion of Ti-150-A, RC-130-B and
Commercially Pure Titanium (4)

Titanium		Ti-150-A		RC-130-B	
Temp. °C	Coefficient inches/inch/°C	Temp. °C	Coefficient inches/inch/°C	Temp. °C	Coefficient inches/inch/°C
...	20	10.6×10^{-6}	20	16.7×10^{-6}
...	0	10.0×10^{-6}	0	13.7×10^{-6}
-23	10.0×10^{-6}	-20	9.6×10^{-6}	-20	12.7×10^{-6}
...	-40	8.9×10^{-6}	-40	11.6×10^{-6}
-73	9.3×10^{-6}	-60	8.5×10^{-6}	-60	10.9×10^{-6}
...	-80	8.0×10^{-6}	-80	9.9×10^{-6}
-123	6.7×10^{-6}	-100	7.7×10^{-6}	-100	9.4×10^{-6}
...	-120	7.2×10^{-6}	-120	8.9×10^{-6}
-173	4.0×10^{-6}	-140	6.2×10^{-6}	-140	7.7×10^{-6}
...	-160	5.2×10^{-6}	-160	6.7×10^{-6}
-223	2.0×10^{-6}	-180	4.8×10^{-6}	-180	5.7×10^{-6}
...	-200	4.0×10^{-6}	-200	5.3×10^{-6}

of all those observed during fatigue tests of both materials. The fracture at the left is jagged and rough, and the conchoidal markings which define the progress of the crack are clearly visible. The fracture at the right occurred in more than half of the specimens tested, and is characterized by a very smooth fracture surface and a symmetrical ridge parallel to the neutral plane of stress. Specimens showing higher-than-average fatigue strength had the smooth fracture surface, while specimens of below-average strength fractured as shown at the left in Fig. 10. It is thought that segregation or banding in the axial direction of the rods was responsible for this phenomenon, since some segregation was observed during polishing of hardness test surfaces.

Fig. 11 is a photograph of unusual impact fractures encountered in both alloys at the temperature of liquid nitrogen. Specimens which broke in this manner showed high impact strength when compared



Fig. 11—Unusual Impact Fractures Encountered at -320°F (-196°C).

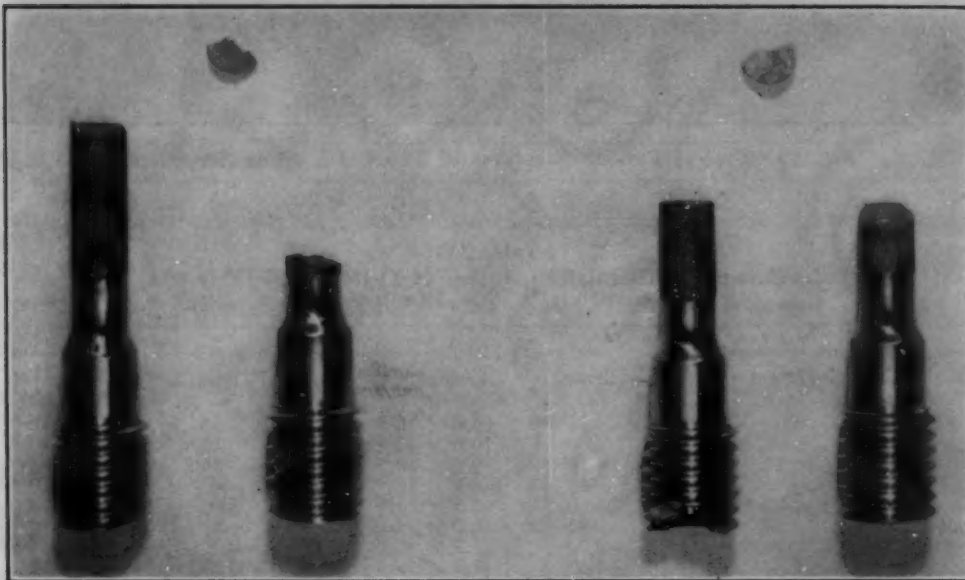


Fig. 12—Unusual Tensile Fractures Encountered at -320°F (-196°C).

with other specimens of the same material broken at the same temperature. Apparently this phenomenon is also caused by segregation on a macroscopic scale.

The tensile fractures illustrated in Fig. 12 occurred at -321°F (-196°C). The specimen at the left is RC-130-B and the one at the right is Ti-150-A. The chips shown at the top of the photograph fit between the fractured ends, and many other much smaller chips were lost. The materials seemed to fracture with almost explosive violence at -321°F (-196°C), implying that more than one crack was responsible for failure. No explanation can be offered for such behavior, except to say that both materials were very brittle at the temperature of liquid nitrogen.

SUMMARY

Fatigue, tensile and dilatometric tests were made at temperatures from 77 to -321°F (25 to -196°C) on two titanium-base alloys,

Ti-150-A and RC-130-B. Impact and hardness tests were performed at temperatures down to -423°F (-253°C).

Fatigue tests using both polished and notched specimens were run at room temperature, at -108°F (-78°C), and at -321°F (-196°C). The endurance limits of both alloys were raised at low temperatures, but RC-130-B showed the greater increase percentage-wise. Ti-150-A suffers a greater loss in fatigue strength as a result of notching than RC-130-B, but Ti-150-A has a substantially higher fatigue strength at all test temperatures.

Ti-150-A had slightly higher yield and ultimate strengths than RC-130-B except at the temperature of liquid nitrogen, -321°F (-196°C); at this temperature, RC-130-B showed a slight gain in yield and tensile strength. Elastic moduli of both materials increased at low temperatures, the increase being greater in Ti-150-A. Elongation and reduction of area were decreased at low temperatures, and there was an increase in notch sensitivity as the temperature was lowered to -321°F (-196°C).

Absorbed energy values, in impact tests, of both alloys were low at all temperatures, considering their tensile strengths, but there was a considerable decrease as temperature was lowered below room temperature.

RC-130-B is slightly harder than Ti-150-A at all temperatures. The hardness of both materials was increased about 107% at the temperature of liquid hydrogen, -423°F (-253°C).

Dilatometry revealed that the thermal expansion coefficient of RC-130-B is greater than that of Ti-150-A over the range from room temperature to -321°F (-196°C). Thermal expansion decreases markedly as the temperature is lowered.

ACKNOWLEDGMENT

The authors express their gratitude for the valuable assistance of Howard E. Brooks. In addition, thanks are due the Ohio State University Cryogenic Laboratory for its cooperation in supplying liquid hydrogen and liquid nitrogen.

The work reported in this paper was carried out at the Engineering Experiment Station under a contract between the Ohio State University Research Foundation and the Materials Laboratory, Research Division, Wright Air Development Center, Wright-Patterson Air Force Base, Mr. Edward Dugger acting as Project Engineer.

References

1. M. G. Fontana and J. L. Zambrow, "Impact Strength and Hardness of Aircraft Alloys Down to -423°F ", *METAL PROGRESS*, January 1948, p. 97.
2. J. L. Zambrow and M. G. Fontana, "Mechanical Properties, Including Fatigue, of Aircraft Alloys at Very Low Temperatures", *TRANSACTIONS, American Society for Metals*, Vol. 41, 1949, p. 480.

3. J. W. Spretnak, M. G. Fontana and H. E. Brooks, "Notched and Unnotched Tensile and Fatigue Properties of Ten Engineering Alloys at 25 °C and -196 °C", *TRANSACTIONS, American Society for Metals*, Vol. 43, 1951, p. 547.
4. Unpublished Master's Thesis by C. H. Philleo of Ohio State University, "Dilatometric Measurements of Aircraft Alloys at Very Low Temperatures", Library of the Department of Metallurgy, Ohio State University, 1951.

DISCUSSION

Written Discussion: By Edward Dugger, materials engineer, Wright Air Development Center, Wright-Patterson Air Force Base, Ohio.

The authors of this paper are to be congratulated on their investigation of a material which is being considered for many aircraft applications and on which much information is needed.

It has been the privilege of this writer to cooperate with the authors in their study. The purpose of this discussion is to make a few supplementary remarks not covered by the paper and to compare some of the results of the investigation on the two titanium alloys with other materials.

Notch sensitivity of titanium alloys has been the subject of considerable discussion and, in general, both notched tension and notched fatigue tests have been used in an attempt to establish the notch sensitivity of materials. Notched tension and notched fatigue tests on these titanium alloys have resulted in apparently contradictory results relative to notch sensitivity effects at low temperatures when compared to results obtained on other metallic materials investigated under the same conditions of test. These other materials included 24S-T4 and 75S-T6 aluminum alloys, AZ31 magnesium alloy, commercially pure titanium and several steels used in structural aircraft applications ranging from 150,000 to 230,000 psi tensile strength.

In tension, these materials (a) increase in the notch strength as the temperature decreases and (b) the notch strength at -321 °F (-196 °C) is greater than the unnotched strength and the ratio of the notched to unnotched strength increases as the temperature decreases. The two titanium alloys do not follow either of these patterns and, in this respect, act in the same manner as SAE 4340 steel heat treated to 230,000 psi, which was the single previous exception of the materials so investigated. The "nonconformity" of RC-130-B and Ti-150-A, coupled with the low elongation and reduction of area values for the notched tensile tests, tends to substantiate the adverse notch sensitivity of these materials. It might also be pointed out that the notch tensile strengths of the two alloys at -321 °F (-196 °C) are less than for commercially pure titanium.

In fatigue, on the other hand, the two alloys appear to compare favorably with the other materials in notch sensitivity at -321 °F (-196 °C). At that temperature, the ratio of the notched to unnotched endurance limit (at 10^7 cycles of stress) for both alloys is greater than the same ratio for the materials previously mentioned, since there is less percentage decrease in the notched endurance limit of the titanium alloys at that temperature as compared to the other materials. Of more importance is the fact that the notched endurance limit of these two materials at -321 °F (-196

°C) is appreciably greater than the endurance limit of the other materials thus investigated.

Using the notch sensitivity index "q" as given in the ASM METALS HANDBOOK for twelve materials or conditions so investigated at -321°F (-196°C), Ti-150-A and RC-130-B are the second and fourth least notch sensitive materials respectively at 10^7 cycles of stress and rank better than commercially pure titanium in this respect. At the higher stress levels (lower cycles of stress to failure, i.e. 10^5 and 10^4) these materials are approximately in the middle of the range with the Ti-150-A being the better of the two at any cycles of stress at that temperature but lower than commercially pure titanium. In addition, at generally all stress levels, these titanium alloys improved in their relative standings to the other materials from 77 to -321°F (25 to -196°C).

The authors have commented on the higher notched fatigue strengths at 77°F (25°C) as compared to -321°F (-196°C) at high stresses. It is noted that this parallels the pattern found on steels above 150,000 psi tensile strength and having the same notch geometry.

The significance of the notch sensitivity difference as shown by the tensile and fatigue tests is not clear at this writing insofar as the use of the material is concerned. It is apparent, however, that these properties will necessitate more consideration than is now given to other materials.

Written Discussion: By L. R. Frazier, Metallurgy Section, Thomson Laboratory, General Electric Co., West Lynn, Mass.

We felt that the work reported was a valuable contribution to the technology of titanium, particularly for the RC-130-B alloy. We felt that an unfortunate choice was made in the particular lot of Ti-150-A alloy. To be representative of the Ti-150-A alloy the investigation should have been made on a lot having 15 to 20% elongation at 77°F for rolled bar or 12 to 17% for a typical forging. The low elongation of the material used, 6.5%, either masks a transition at lower temperatures or is reflected in lower-than-typical low temperature values throughout the work on Ti-150-A.

Authors' Reply

The authors are grateful to Mr. Dugger for his pertinent comments on the test results and his interesting discussion of notch sensitivity.

Mr. Frazier's point concerning the ductility of the Ti-150-A alloy is well taken, and it is admitted that the lot which was used in these tests may not be representative of the material which is being produced at the present time. The order was placed in May 1951 and included a request for a typical lot of material. The manufacturer later informed the authors that some early heats of Ti-150-A were substandard with regard to ductility.

THE TITANIUM-OXYGEN SYSTEM

By E. S. BUMPS, H. D. KESSLER AND M. HANSEN

Abstract

The partial phase diagram is based principally on the results of micrographic analysis of arc-melted alloys containing up to 30% (56 atomic %) oxygen. The diagram has the following principal features—two peritectic reactions: $\text{Melt} + \alpha \rightleftharpoons \beta$, and $\text{Melt} + \alpha \rightleftharpoons \text{TiO}$, at 1740 and 1770 °C, respectively; and a peritectoid reaction: $\alpha + \text{TiO} \rightleftharpoons \delta$, at approximately 925 °C. Alpha titanium has a maximum melting temperature of about 1900 °C at 10% oxygen. The maximum solubility of oxygen in beta titanium is approximately 1.8% at 1740 °C, whereas the solubility in alpha titanium is about 14.5% between 700 and 1600 °C. The intermediate phase, TiO, extends between 20.5 and 29.5% oxygen at 1400 °C, and from about 23.5 to 29.5% oxygen at 800 °C. The existence of a newly discovered delta phase was confirmed by X-ray studies in the composition range of the stoichiometric ratios for Ti_3O_2 and Ti_4O_3 . Lattice parameter measurements are presented for both the alpha and TiO phases, and hardness test results are presented for alloys containing up to 30% oxygen.

INTRODUCTION

THE titanium-oxygen system is one of great importance to the titanium industry. The metal oxidizes rapidly above 650 °C (1200 °F); therefore in such operations as the production of sponge and the melting, forging, and heat treatment of titanium above this temperature, oxygen must be considered as a possible source of contamination. Also, information on the constitution of the titanium-oxygen system is required to throw more light on the mechanism of oxidation and scaling. Because small additions considerably increase the strength of titanium, oxygen is purposely added to several commercial alloys. Thus, whether oxygen reacts deleteriously as a

This paper is based on a portion of the work carried out by Armour Research Foundation for the Wright Air Development Center, Materials Laboratory, under Contract No. AF 33(038)-8708.

A paper presented before the Eighth Western Metal Congress of the Society, held in Los Angeles, March 23 to 27, 1953. Of the authors, E. S. Bumps is metallurgist, Studebaker Corp., South Bend, Ind.; H. D. Kessler is supervisor, Nonferrous Metals Research; and M. Hansen is chairman, Metals Research, Armour Research Foundation, Chicago. Manuscript received April 1, 1952.

contaminant or beneficially as an alloy addition, knowledge of the titanium-oxygen phase relationships can help solve many of the problems related to the development and application of the metal and its alloys.

The literature contains several papers concerning the compounds existing in the titanium-oxygen system (1-4).¹ The bulk of this information is concerned with chemical and structural identification of the following phases:

1. TiO, having a crystal lattice of the NaCl type with a melting point of 1750 °C (3180 °F).
2. Ti₂O₃, having a corundum-type crystal lattice.
3. TiO₂, which has the following naturally occurring modifications: rutile and anatase I and II, which are tetragonal; brookite, which has an orthorhombic structure and melts at 1900 °C (3450 °F).

Ehrlich determined the phases present in the system up to the composition of the dioxide TiO₂, and their approximate ranges of homogeneity (2, 3, 4). These data were obtained by X-ray analysis of samples prepared by sintering mixtures of titanium with TiO and/or TiO₂ at 1500 to 1600 °C (2730 to 2910 °F) in vacuum, followed by furnace cooling and a two-day anneal at 750 °C (1380 °F).

Ehrlich showed that approximately 12.5 weight % oxygen (30 atomic %) is soluble in alpha titanium. The first intermediate phase, TiO, was shown to have a homogeneity range from 17 to 29.3 weight % (38 to 55.5 atomic %) oxygen. The next intermediate phase, based on the composition Ti₂O₃ (33.3 weight % O), was stable between 32.5 and 34.5 weight % (59.3 and 61.3 atomic %) oxygen. A new phase, having a heavily distorted rutile lattice, was placed between 36 and 37.2 weight % (63 and 64.2 atomic %) oxygen. The lower limit of TiO₂ (40 weight % O) was located at 38.7 weight % (65.5 atomic %) oxygen.

The phase relationships in titanium-rich alloys containing up to 1 weight % (3 atomic %) oxygen have been studied by Jaffee, Ogden and Maykuth (5) by micrographic analysis of annealed and quenched alloys. They found that the α/β transformation temperature is raised with increasing oxygen content.

Studies of the effects of small oxygen additions on the mechanical properties of iodide titanium have been published by Jaffee and Campbell (6), Findlay and Snyder (7), and Jaffee et al (5). It was reported that oxygen refines the structure, making the plates of alpha titanium smaller and the Widmanstätten pattern more regular. This was also confirmed by Sutcliffe (8).

Using X-ray diffraction and micrographic methods, Worner (9) confirmed Ehrlich's value of approximately 12.5 weight % (30 atomic %) oxygen being soluble in alpha titanium. He also observed that

¹The figures appearing in parentheses pertain to the references appended to this paper.

oxygen additions increased the transformation temperature. More recently, Jenkins and Worner (10) established the limits of the $\alpha + \beta$ region up to 1.7 weight % oxygen (5 atomic %) by means of measurements of thermoelectric power at various temperatures, and verified their results by micrographic analysis.

EXPERIMENTAL PROCEDURE

Preparation of Alloys

The alloys were prepared by the water-cooled copper block, tungsten electrode arc melting method described in a previous paper (11). The charges consisted of $\frac{1}{4}$ -inch sections of iodide titanium (99.9+ % pure) previously rolled to $\frac{1}{16}$ -inch sheet, and $\frac{1}{4}$ -inch lumps of fractured compacts of high purity TiO_2 (99.9+ % pure). It was found that by proper placing of the charge in the copper block, the arc (previously started against the tungsten insert) could be easily transferred to the charge. Even pure TiO_2 could be melted by this method. Weight losses were not used as a basis for judging the possible variance in composition on melting, because ingots of the brittle high-oxygen alloys spalled badly when the arc was struck during the remelting operations. However, analytical results² for a number of alloys (see Table I) showed good agreement with nom-

Table I
Chemical Analysis of As-Cast Titanium-Oxygen Alloys

Heat No.	Nominal % Oxygen	Analyzed % Oxygen
1198	3.0	3.3
1199	4.0	4.2
1208	10	9.9
1212	14	14.0
1213	15	15.5
1215	17	16.4
1217	19	18.5
1218	20	20.1
1219	21	21.6
1222	24	23.7

inal compositions. As these values are well within the accuracy of the analytical results, the phase diagram as presented is based on nominal compositions. Alloys were prepared having the following nominal oxygen contents: 0.2, 0.4, 0.6, 0.8, 1 . . . 40 (1% increments).

The color variations shown in Table II were recorded by visual observation of the as-cast surface of the ingots.

Annealing Treatments—Annealing treatments consisted of sealing samples in Vycor or quartz capsules, heating to temperatures ranging from 700 to 1500 °C (1290 to 2730 °F), followed by water

²Oxygen by difference using the liquid amalgam reduction method developed by the National Lead Company.

Table II
Appearance of Titanium-Oxygen Alloy Ingots

Composition Range, % O	Color
1-11	Shiny metallic luster (silvery)
12-19	Dull metallic luster (silvery)
20-21	Dull metallic luster (possible tinge of yellow)
22-30	Shiny metallic luster changing from tinge of yellow at 22% to deep gold at 30% oxygen
31-33	Shiny metallic luster changing from gold to purple (mixture) with increasing oxygen contents
34-36	Frangible shiny shell rubbed off easily, leaving dull nonmetallic purple substance
37-38	Nonmetallic blue
39-40	Bluish rutile luster (almost metallic)

Table III
Annealing Conditions for Titanium-Oxygen Alloys

Annealing Temperature, °C	Time, Hours	Container	Atmosphere
700	300	Vycor	Vacuum
800	120	Vycor	Vacuum
800	500	Vycor	Vacuum
900	70	Vycor	Vacuum
900	24	Vycor	Vacuum
950	72	Vycor	Vacuum
1000	24	Vycor	Vacuum
1100	24	Quartz	Argon
1200	4	Quartz	Argon
1300	1	Quartz	Argon
1400	2	Quartz	Argon
1500	$\frac{1}{2}$	Quartz	Argon

quenching (see Table III). Short-time annealing treatments at 1600 °C (2910 °F) and above were accomplished by heating a series of samples in a molybdenum sheet container in a high frequency induction furnace under vacuum conditions and quenching onto a water-cooled brass plate at the bottom of the furnace. The temperature control at these high temperatures was of the order of ± 25 °C. The rate of heating varied considerably with the age of the tantalum heater of the furnace, with an approximate average rate of 20 °C per minute in the temperature range 1500 to 1900 °C (2730 to 3450 °F). At these high temperatures, the holding times were quite short and were limited by the accuracy of control of the induction unit. Therefore, the metallographic results obtained on samples treated above 1500 °C (2730 °F) may not be as accurate as those at lower temperatures. The accuracy is restricted by the short heating times (questionable equilibrium conditions) and limited temperature control.

It had been suspected that titanium-oxygen alloys lose oxygen at elevated temperatures. A check was made to verify this by weighing samples before and after annealing. This was done for a complete series of alloys from 1 to 40% oxygen annealed at 1200 and 1400 °C (2190 and 2550 °F) for 4 hours and 1 hour, respectively. Weight

losses after annealing at these temperatures varied from 0 to 3% of the total weight of the specimen with no apparent correlation with the composition of the alloy. This same amount of weight loss was obtained for unalloyed titanium control samples included with the series. It was concluded from these data that little, if any, oxygen was lost during annealing treatments up to 1400 °C (2550 °F), under the conditions of testing used.

A further and more conclusive check of possible oxygen losses at elevated temperatures was made by X-ray diffraction methods. Diffraction patterns for 5, 7, and 11% oxygen alloys quenched from 1850 °C (3360 °F) showed identical lattice parameter measurements for the same series of alloys quenched from 900 °C (1650 °F).

Melting Range Determinations—Solidus data were obtained by incipient melting techniques (11, 12) and by the metallographic examination of alloys annealed as described in the previous section. The accuracy of the incipient melting data, which were obtained by observing the first visual indications of melting using an optical pyrometer, is estimated to be ± 25 °C.

X-Ray Diffraction Techniques—Lattice parameters were determined for the alpha solid solution and the intermediate phase, TiO. The structure of a newly discovered phase, delta, was also investigated. The diffraction patterns were taken with a 14-centimeter diameter Debye-Scherrer powder camera, using filtered characteristic copper radiation. Specimens were prepared by crushing and screening through a 200-mesh screen. Exposure times of about 4 hours were used, and the parameters were obtained by the solution of simultaneous equations for the spacings of the six high angle lines. The accuracy of the data is about ± 0.005 Å.

DISCUSSION OF RESULTS

The Phase Diagram—The phase diagram as presented in Figs. 1 and 2 was determined by micrographic analysis of alloys containing between 0.2 and 30.0 weight % oxygen, annealed at and quenched from temperatures between 700 and 1850 °C (1290 and 3360 °F). In addition, solidus determinations and X-ray diffraction analyses were used to study portions of the system.

Structural Characteristics—Microscopic studies involved the evaluation of both etched and unetched structures as revealed by means of ordinary reflected light and polarized light, respectively. Typical microstructures illustrating various phase fields depicted in the diagram are shown in Figs. 3-13.

Illustrations of structures characteristic of alloys quenched from the beta field are shown in Figs. 3 and 4. A 0.2% oxygen alloy quenched after 48 hours at 950 °C (1740 °F) revealed a serrated

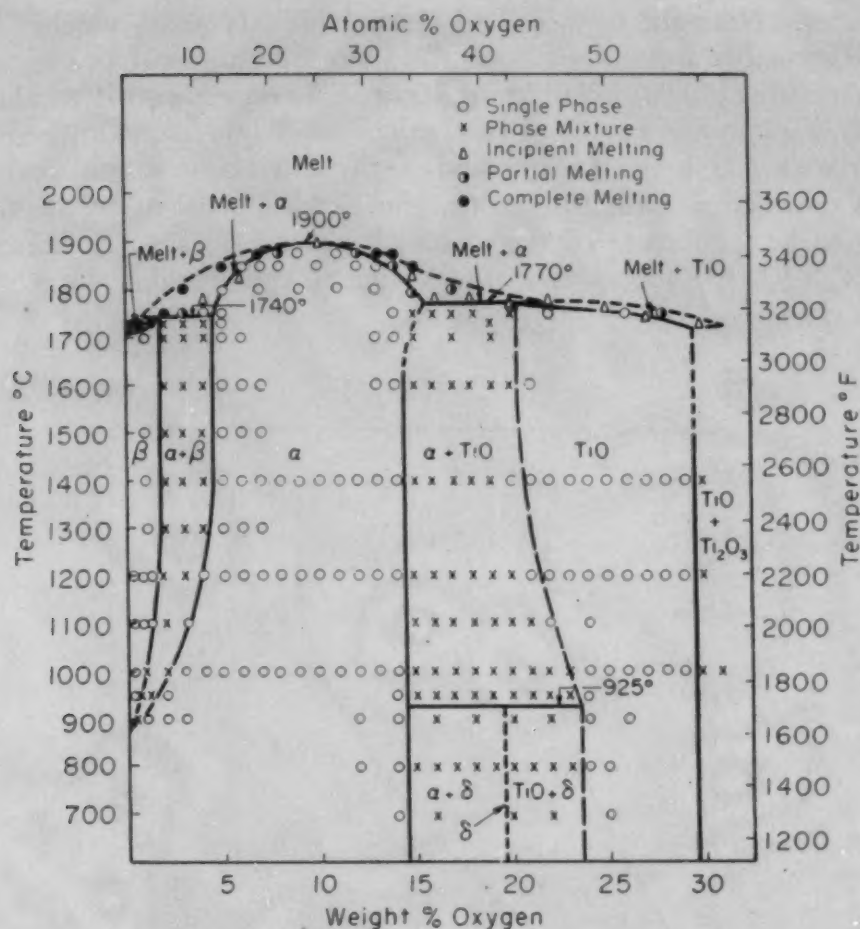


Fig. 1—Partial Phase Diagram of the Titanium-Oxygen System.

alpha transformation structure, as shown in Fig. 3. Specimens quenched from the beta field but with compositions nearer the $\beta/\alpha + \beta$ boundary showed a basket-weave type of transformation structure (Fig. 4). This transformed beta structure was coarser, the higher the temperature of the treatment.

Microstructures of alloys quenched from the $\alpha + \beta$ field are shown in Figs. 5 and 6. At 1000 °C (1830 °F), the amount of alpha phase in a 1.0% alloy was estimated as approximately 30%. The $\alpha + \beta$ structure, as shown in Fig. 5, indicates that the white alpha phase was present at the temperature of treatment and the dark structure in the interstices was formed by the transformation of the beta phase during the quench. Aside from extensive growth of constituents, the high temperature $\alpha + \beta$ structures (Fig. 6) are similar to those of alloys quenched from the lower temperature. The structure of the alpha phase of a 12% oxygen alloy quenched from 1200 °C (2190 °F) is shown in Fig. 7.

The $\alpha + \text{TiO}$ mixture is characterized by banded twin-like

structures. Near the $\alpha/\alpha + \text{TiO}$ phase boundary small patches of a banded structure were observed in the alpha titanium matrix (Fig. 8). The structures of alloys containing 16 to 18% oxygen consisted almost entirely of plate-like bands, as shown in Figs. 9 and 10. On the basis of Ehrlich's (3) investigations and X-ray diffraction studies carried out in connection with this work, the banded structure was interpreted to be a mixture of the alpha phase and TiO. Annealing at 1700 °C (3090 °F) coarsened the structure considerably (Fig. 10),

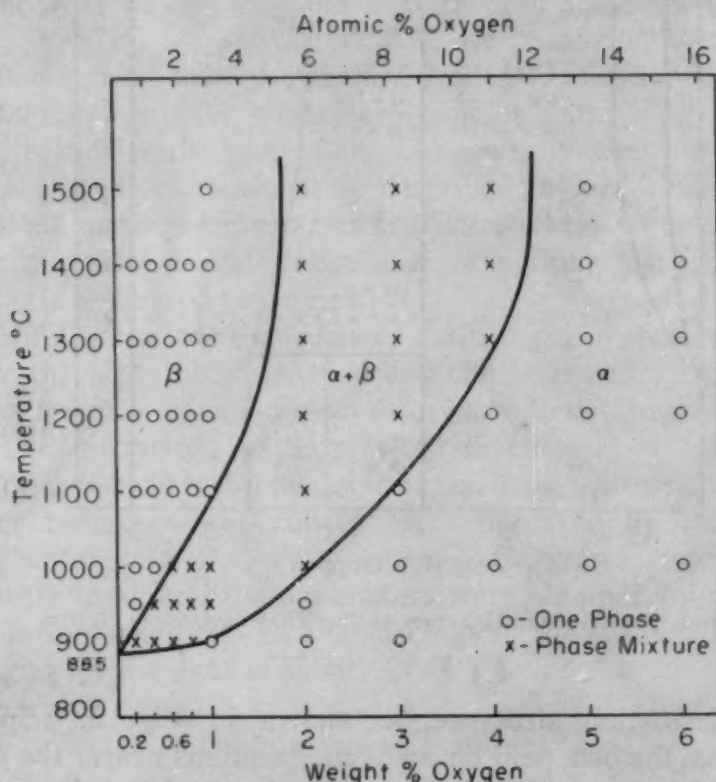


Fig. 2—Titanium-Rich Portion of the Titanium-Oxygen System.

but there was no tendency for the phases to coagulate. At higher oxygen contents, the amount of the banded structures decreased, with the last traces of alpha showing up at the grain boundaries.

The twin-like structure of the $\alpha + \text{TiO}$ alloys is very similar to the banded $\alpha + \kappa$ structure in copper-silicon alloys investigated by Smith (13), who advanced a theory of matching crystallographic planes to account for the unusual stability of this structure. Calculations along this line were made from lattice parameter measurements of the titanium-oxygen system.

When a face-centered cubic precipitate is rejected from the hexagonal close-packed matrix, the information available suggests that the crystallographic relationship is such that the $\{0001\}$ planes of

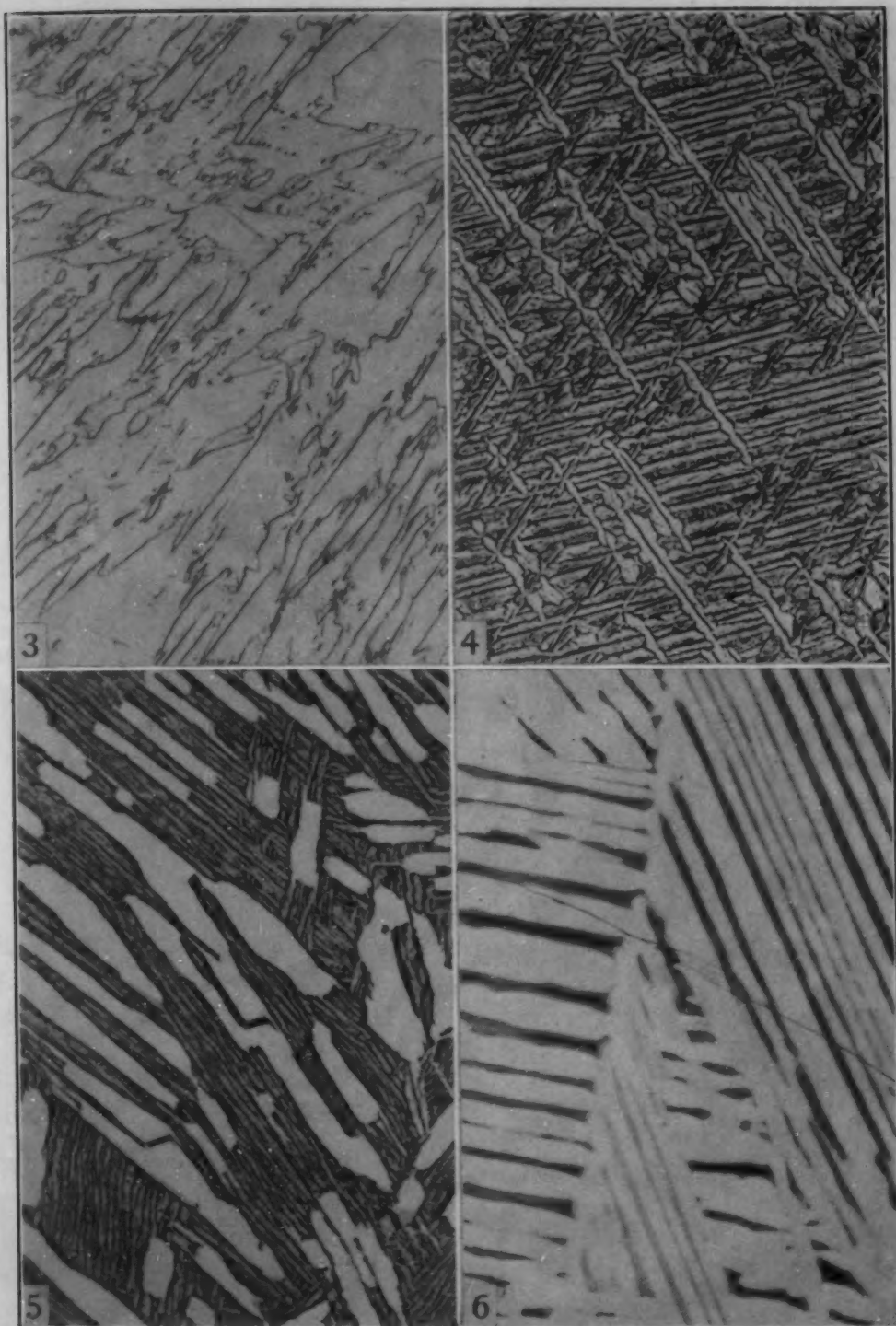


Fig. 3—A 0.2% Oxygen Alloy Quenched After 48 Hours at 950 °C (1740 °F), Showing a Serrated Alpha Transformation Structure. Etchant: 20% HF, 20% HNO₃ in glycerine. $\times 150$.

Fig. 4—A 1.0% Oxygen Alloy Quenched After 4 Hours at 1200 °C (2190 °F); Structure Reveals a Typical Basket-Weave Type of Transformation Structure. Etchant: 20% HF, 20% HNO₃ in glycerine. $\times 150$.

Fig. 5—A 1.0% Oxygen Alloy Quenched After 24 Hours at 1000 °C (1830 °F); Structure Shows Approximately 35% Alpha in Transformed Beta Matrix. Etchant: 20% HF, 20% HNO₃ in glycerine. $\times 150$.

Fig. 6—A 3.0% Oxygen Alloy Quenched From 1700 °C (3090 °F); Structure Shows Duplex Alpha (White) Plus Transformed Beta (Dark). Note the large grain growth. Etchant: 20% HF, 20% HNO₃ in glycerine. $\times 75$.

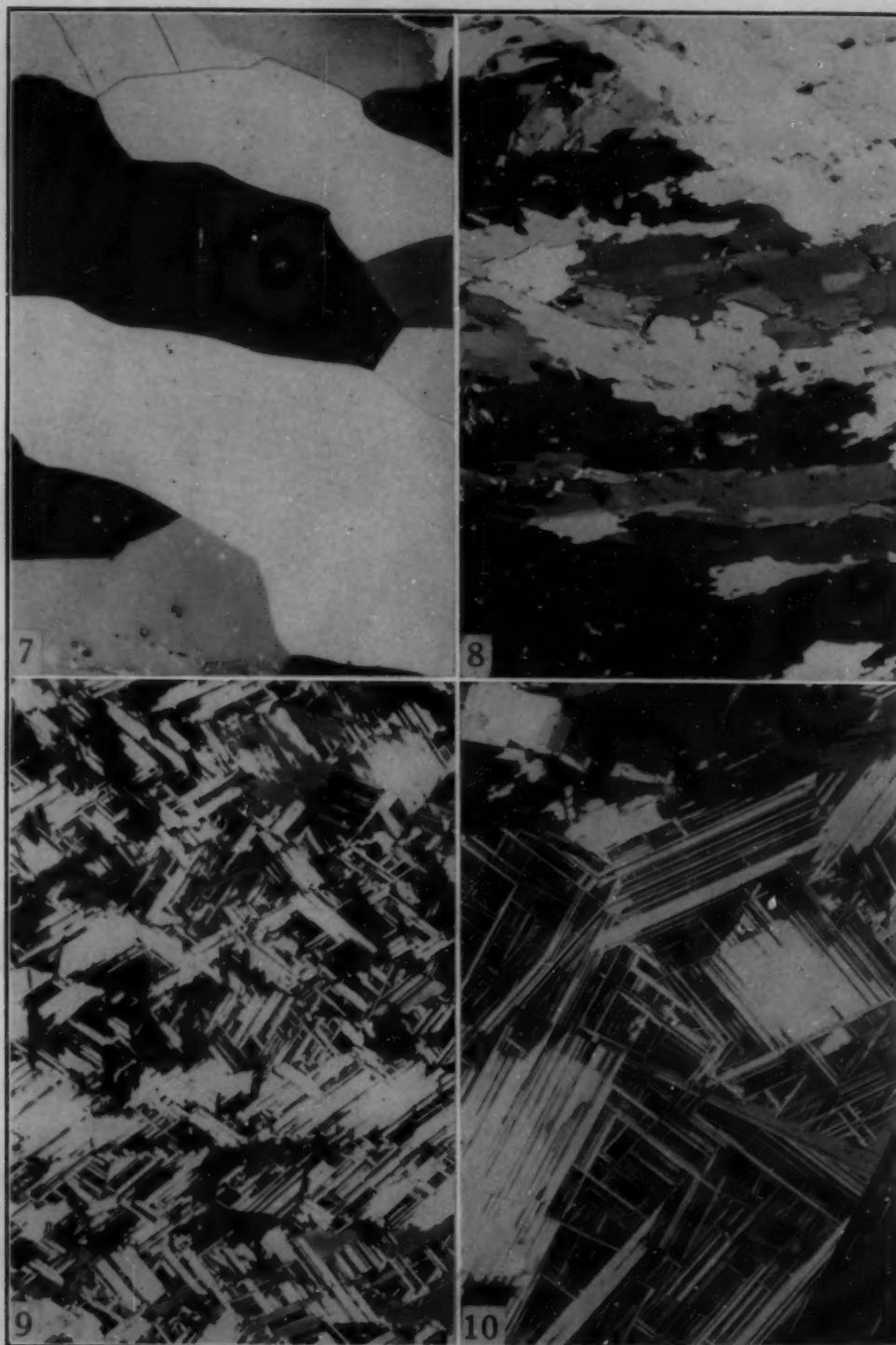


Fig. 7—A 12% Oxygen Alloy Quenched After 4 Hours at 1200 °C (2190 °F). Structure shows polyhedral grains of alpha titanium solid solution. Polarized light, unetched. $\times 75$.

Fig. 8—A 15% Oxygen Alloy Quenched After 4 Hours at 1200 °C (2190 °F). Structure shows patches of a banded alpha plus TiO phase mixture in a titanium solid solution matrix. Polarized light, unetched. $\times 75$.

Fig. 9—A 17% Oxygen Alloy Quenched After 4 Hours at 1200 °C (2190 °F). Nearly 100% twinned structure of a two-phase mixture of alpha plus TiO. Polarized light, unetched. $\times 75$.

Fig. 10—A 17% Oxygen Alloy Quenched From 1700 °C (3090 °F). Coarse banded structure characteristic of the alpha plus TiO field. Polarized light, unetched. $\times 75$.

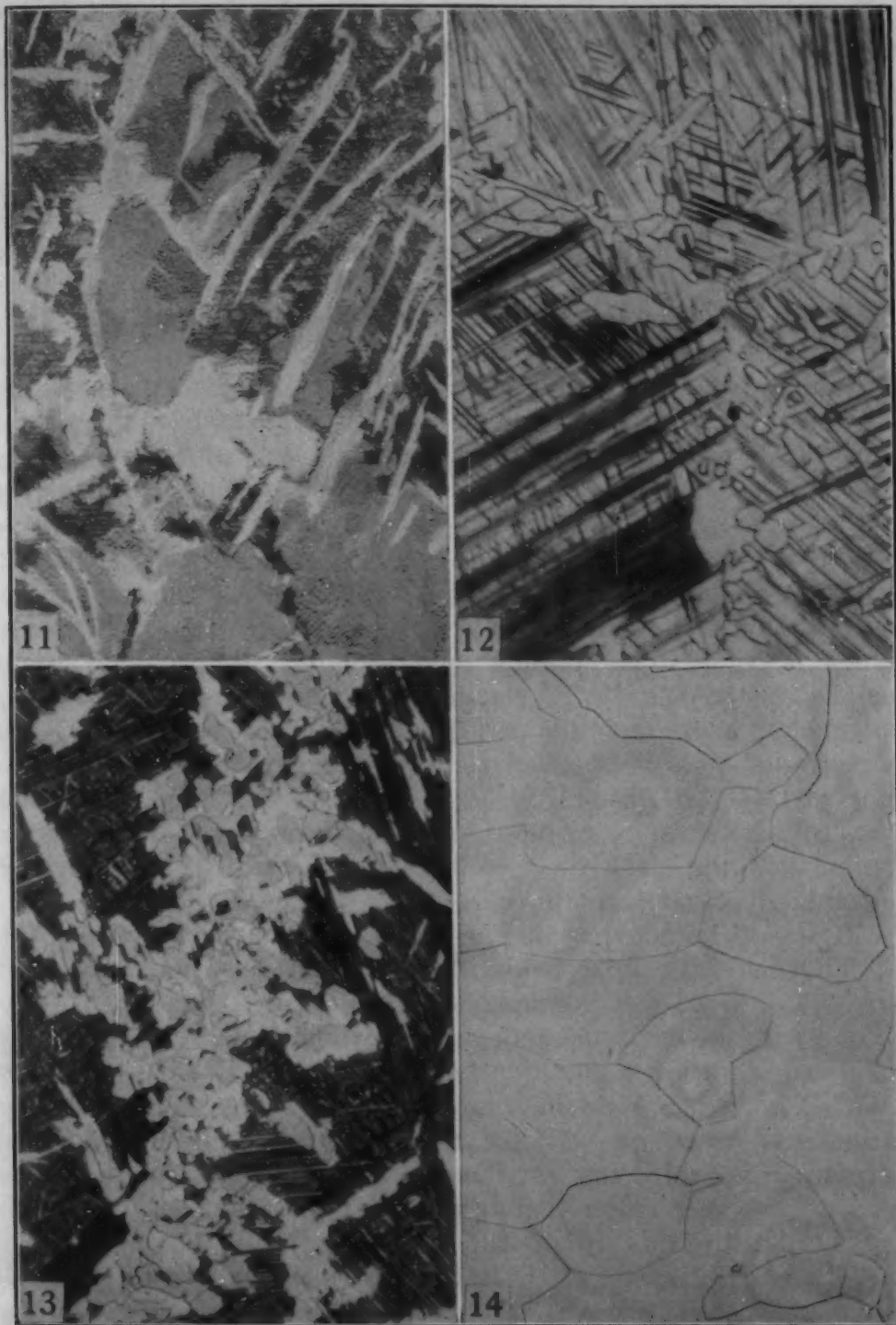


Fig. 11—A 20% Oxygen Alloy Quenched After 500 Hours at 800 °C (1470 °F). Delta precipitate in matrix of partially decomposed banded structure and lamellar areas mostly in grain boundaries. 20% HF, 20% HNO₃ in glycerine. $\times 250$.

Fig. 12—A 19% Oxygen Alloy Quenched After 24 Hours at 1000 °C (1830 °F). Grain boundary alpha and the banded alpha plus TiO matrix. 20% HF, 20% HNO₃ in glycerine. $\times 750$.

Fig. 13—A 19% Oxygen Sample Initially Treated as the Specimen of Fig. 12, Then Subsequently Annealed at 800 °C (1470 °F) for 168 Hours. Grain boundary alpha (gray) having reacted with the TiO of the banded structure to give a delta rim (white). Also delta precipitated in the matrix. 20% HF, 20% HNO₃ in glycerine. $\times 750$.

Fig. 14—A 29% Oxygen Alloy Quenched After 4 Hours at 1200 °C (2190 °F). Polyhedral grains of TiO phase. 20% HF, 20% HNO₃ in 60 glycerine. $\times 150$.

the matrix face the $\{111\}$ planes of the precipitate. Whether this condition actually obtains in the precipitation of TiO from alpha cannot be easily verified, but certainly it is a reasonable assumption. The atomic array in both (0001) and (111) planes follows hexagonal close packing. The interatomic distance in the (0001) plane of the alpha phase at saturation has been measured as 2.955 Å. If one considers the NaCl structure of TiO to be two interlocking face-centered cubic structures of titanium atoms and oxygen atoms, the interatomic spacing of the titanium atoms on the (111) planes is $0.707a$ Å. From the lines of TiO in the phase mixture of $\alpha + \text{TiO}$, the lattice parameter of the TiO was calculated to be 4.176 Å. Accordingly, the interatomic spacing of the titanium atoms on the (111) plane is 2.952 Å. This corresponds very closely to the atomic spacing in the (0001) planes of alpha. The degree of disregistry is about 0.1%. Therefore, it would appear that Smith's explanation for the origin of the stable banded structure is applicable to the case under discussion.

If the above explanation for the formation of the banded structure is accepted (i.e., the precipitation of a face-centered cubic phase from a hexagonal close-packed solid solution), the phase diagram should show the $\alpha/\alpha + \text{TiO}$ boundary curving toward higher oxygen contents and intersecting the peritectic horizontal at a greater oxygen concentration than is obtained at lower temperatures. Actual data points at 1600, 1700, and 1750 °C (2910, 3090, and 3180 °F) do not indicate such curvature of the $\alpha/\alpha + \text{TiO}$ boundary; but it is quite possible that the alpha phase could not be retained on quenching from these higher temperatures.

It should be noted from Fig. 1 that the boundary between the $\alpha + \text{TiO}$ and TiO phase fields is broken and does not correspond perfectly with the metallographic data. For this boundary to correspond with the data points above approximately 925 °C (1695 °F) would require a large inflection between 1000 to 1200 °C (1830 to 2190 °F). Such a bend in this line would not seem theoretically justifiable. As it was difficult to metallographically identify the composition at which the last trace of alpha disappeared, the phase boundary has been placed as indicated in Fig. 1, and no great accuracy is claimed in this region of the diagram.

The phase diagram (Fig. 1) indicates the presence of the hitherto unknown delta phase at approximately 18 to 20% oxygen below 925 °C (1695 °F). Only traces of this phase were observed in the 18, 20, and 22% oxygen alloys annealed at 900 °C (1650 °F). After annealing at 800 °C (1470 °F) for 120 hours, the amount of delta phase increased from a small quantity in the 15% alloy to more than 20% in the 19 and 20% oxygen alloys, and subsequently decreased until no trace was found in the 24% oxygen sample. Treatment for

500 hours at 800 °C (1470 °F) increased the size of the massive delta phase and extended the area covered by the surrounding lamellar precipitate. The banded structure decomposes with the appearance of the delta phase at 800 and 900 °C (1470 and 1650 °F). Fig. 11 is presented to show the appearance of the new phase as revealed in a 20% oxygen alloy annealed at 800 °C (1470 °F).

Figs. 12 and 13 give evidence that the delta phase is formed by the peritectoid reaction, $\alpha + \text{TiO} \rightleftharpoons \delta$. Fig. 12 shows the banded $\alpha + \text{TiO}$ structure of a 19% oxygen alloy with alpha phase in the grain boundaries. This sample was treated above the peritectoid temperature and showed no trace of decomposition. The grain boundary alpha constituent was rejected from the supersaturated cast alloy during the 1000 °C (1830 °F) annealing treatment. Upon re-annealing the above sample at 800 °C (1470 °F) the alpha in the grain boundaries reacted with TiO giving a delta phase reaction rim, see Fig. 13. The peritectoid reaction was also nucleated within the lamellar matrix with the formation of many irregularly shaped white areas of the delta phase. The composition range in which the delta phase occurs includes the stoichiometric ratios for Ti_3O_2 and Ti_4O_3 .

Fig. 14 depicts the single-phase TiO structure of a 29% oxygen alloy. Although of variable composition, this phase has been designated as TiO because the crystal structure is based on this composition.

The determination of phase relationships for alloys containing 30 to 40 weight % oxygen was not attempted because most of these alloys were too friable to prepare by metallographic techniques after heat treatment. By extremely careful handling, a series of samples of as-cast alloys from 30 to 40% oxygen were prepared for examination.

A phase mixture of $\text{TiO} + \text{Ti}_2\text{O}_3$ was observed in the as-cast 31 to 32% oxygen alloys, while the 33% alloy appeared to be a single-phase, corresponding to Ti_2O_3 . A mixture of $\text{Ti}_2\text{O}_3 + \text{TiO}_2$ was revealed in 34 to 37% oxygen alloys, and the as-cast 38 to 40% oxygen alloys appeared to be cored single-phase structures of TiO_2 . These phases and phase ranges confirm, in general, X-ray diffraction studies reported by Ehrlich.

Melting-Range Determinations

Solidus data for this system as determined by incipient melting techniques are shown in Table IV, and also in Fig. 1, together with melting-range data obtained by annealing treatments. These results indicate whether the specimens were completely melted, partially melted, or unmelted. As shown in the diagram, the microscopically determined melting data are in fairly close agreement with the incipient melting results.

The temperature of the peritectic reaction: $\text{Melt} + \alpha \rightleftharpoons \beta$ was

Table IV
Melting Temperatures of Iodide Titanium-Oxygen Alloys

Weight % Oxygen	Melting Point, °C*	Weight % Oxygen	Melting Point, °C*
0	1725	14	1840
2	1750	15	1830
3	1750	16	1780
4	1775	18	1780
6	1820	20	1770
8	1850	22	1765
10	1905	25	1760
11	1875	26	1770
12	1875	27	1740
13	1870	30	1725

*Accuracy of determination approximately $\pm 25^\circ\text{C}$.

placed between 1730 and 1750 °C (3145 and 3180 °F), because after annealing at 1730 °C (3145 °F) the 2, 3, and 4% oxygen alloys show an $\alpha + \beta$ structure with no evidence of melting, whereas the treatments at 1750 °C (3180 °F) gave microstructures showing complete melting, $\alpha +$ partial melting, and unmelted α , respectively, for the same alloys. Similarly, the peritectic temperature of the Melt + $\alpha \rightleftharpoons \text{TiO}$ reaction was placed at 1770 °C (3220 °F) as determined by examination of a series of specimens which showed various amounts of melting at 1800 °C (3270 °F) and did not exhibit melting when treated at 1750 °C (3180 °F). Typical peritectic microstructures were not obtained in any of the alloys at either of the indicated peritectics. Between the two peritectics, a maximum melting point of approximately 1900 °C (3450 °F) at 10% oxygen was obtained for the alpha phase.

The incipient melting temperature for a 25 weight % oxygen alloy, corresponding to the theoretical composition TiO, was determined to be 1760 °C (3200 °F), which is in very close agreement with a previously reported melting point of 1750 °C (3180 °F) (14).

As the accuracy of the melting determinations was of the order of $\pm 25^\circ\text{C}$, it was not possible to show whether TiO has a maximum melting temperature or melts over a temperature range. A maximum melting point would require a eutectic rather than the peritectic reaction at 1770 °C (3220 °F). As the data indicated a downward slope of the solidus line with increasing oxygen content, a peritectic reaction and a melting range are shown in Fig. 1.

X-Ray Diffraction Studies

X-ray diffraction studies were undertaken to determine the structure of the intermediate phase TiO and, by means of the parametric method, to check certain points on solubility boundaries as established by metallographic observations.

Alpha Solid Solution—This phase possesses the hexagonal close-

packed structure of the low temperature allotropic modification of titanium. The lattice parameters as a function of oxygen content are presented in Fig. 15. The pronounced increase in the "c" parameter would tend to confirm that this is an interstitial type of solid solution. The fact that the "c" parameter shows a much greater increase than "a" corroborates the work of Clark (15) for compositions of up to 0.5 weight % oxygen.

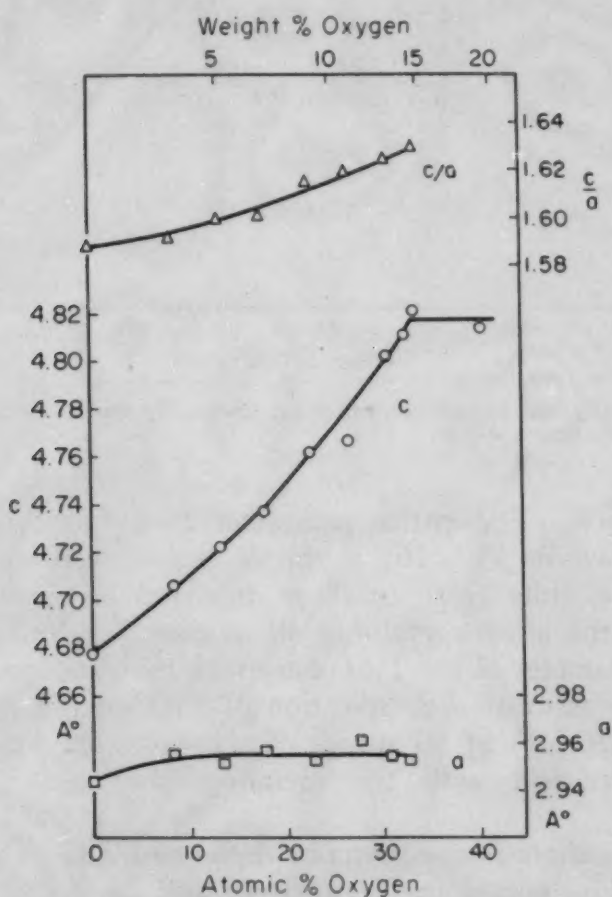


Fig. 15—Lattice Parameter-Composition Curves for the Alpha Phase in Titanium-Oxygen Alloys.

In general, there is some deviation from the results of Ehrlich's work, especially at low oxygen contents. The direction of the deviation points to the relative impurity of the titanium metal he used. From the "c" parameter of the alpha phase in the phase mixture with TiO as quenched below 900 °C (1650 °F), the saturation composition of alpha was determined as 34 atomic % (14.5 weight %) oxygen. This is in exact agreement with the value established by metallographic examination.

The Intermediate Phase, TiO—Ehrlich has reported this phase to have a cubic structure of the NaCl type. This was confirmed by

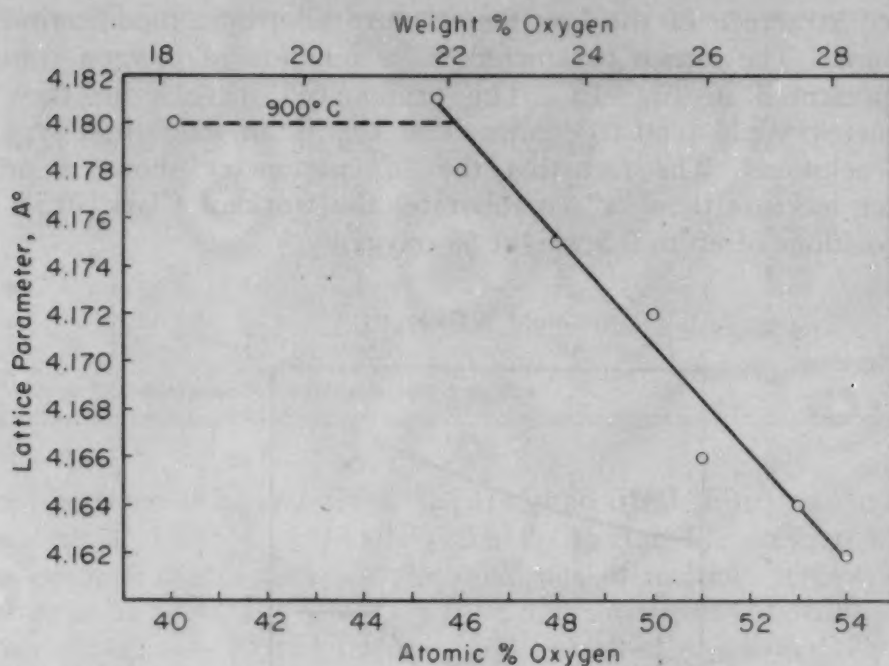


Fig. 16—Lattice Parameter-Composition Curves for the TiO Solid Solution Titanium-Oxygen Alloys.

the present work. The lattice parameter as a function of oxygen content is shown in Fig. 16; a simple linear relationship occurs. The results are quite close to those reported by Ehrlich. From the pattern of the alloy containing 40 atomic % (18.3 weight %) oxygen, the parameter of the TiO phase was calculated to be 4.180 Å. This places the saturation composition of TiO on the titanium side for 900 °C (1650 °F) at 46 atomic % (approx. 22 weight %), in reasonable agreement with the metallographic estimate of 23.5 weight %.

The Intermediate Phase Between Alpha and TiO—On long-term annealing of alloys containing between 15 and 23 weight % oxygen below 900 °C (1650 °F), metallographic examination disclosed the presence of a new phase tentatively named delta. Diffraction patterns of these structures showed a large number of new faint lines which could not be accounted for by either alpha or TiO. Although the determination of the structure of a new phase is best performed when the phase has been isolated, this was not possible. As an alternative, which can only provide tentative results, the extra lines were examined as a group. It was found possible to index all but one of these lines on a Hull-Davy chart for the tetragonal system. The lattice parameters calculated for this tetragonal lattice are: $c = 6.645$ Å, $a = 5.333$ Å, $c/a = 1.246$. The measure of success in relating calculated to observed spacings is shown in Table V. The check is quite close.

Table V
Summary of Observed and Calculated Data on the Delta Phase

Observed Intensity	hkl	dobserved	dcalculated
vw	112	2.474 Å	2.493 Å
vw	120	2.373	2.385
vft	?	2.324
vft	202	2.058	2.079
ft	220	1.874	1.885
vvft	221	1.805	1.814
vw	301	1.716	1.717
vvft	004	1.655	1.661
vw	223	1.432	1.435
vw	204	1.414	1.410
vvft	303	1.386	1.386
vvft	105	1.293	1.289
vw	115	1.242	1.253
vvft	304	1.219	1.214
vft	240	1.191	1.193
ft	324	1.102	1.104
ft	502	1.014	1.016
ft	334	0.9999	1.002

vw = very weak.
ft = faint.
vft = very faint.
vvft = very very faint.

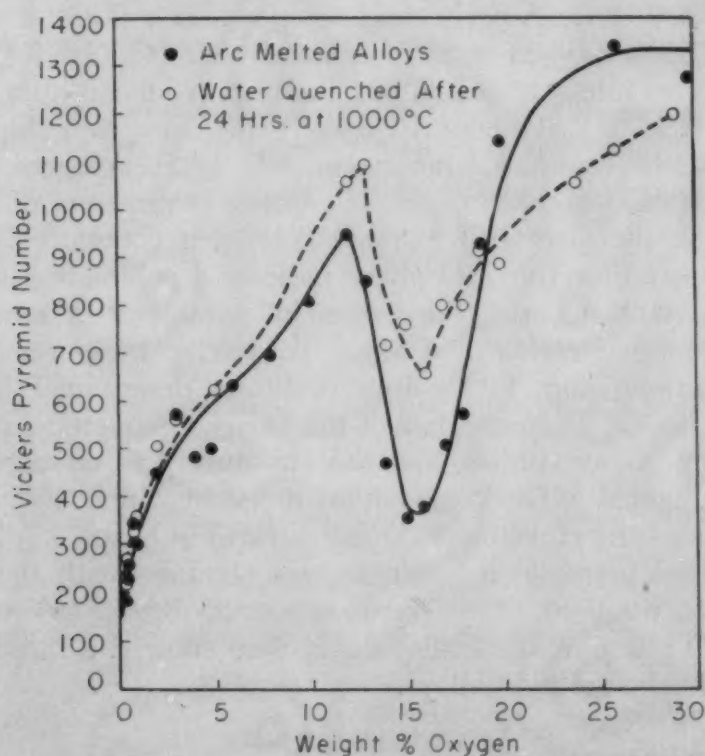


Fig. 17—Vickers Diamond Pyramid Hardness Versus Oxygen Content.

Hardness Determinations

Vickers pyramid hardness data (5-kg. load) for alloys with from 0.2 to 30% oxygen are presented graphically in Fig. 17. Two curves are shown, one representing the hardness of as-cast alloys and the

other, the hardness of a series of alloys annealed at 1000 °C (1830 °F).

The hardness curves show an increase from approximately 170 to 950 and 1100 Vickers in the alpha solid solution range of 0.2 to 13% oxygen. The impressions in specimens of this range of composition were of uniform shape, despite cracks and chipping due to brittleness, which usually accompanies extremely high hardness. On the other hand, impressions in specimens in the 14 to 20% oxygen range of composition were surrounded by deformation bands. This evidence of ductility supports the drop in hardness for alloys which microscopically revealed the banded $\alpha + \text{TiO}$ phase mixture. From 20 to 30% oxygen, hardness again increases to extremely high values.

SUMMARY

The titanium-oxygen phase diagram has the following features: A peritectic reaction: $\text{Melt} + \alpha \rightleftharpoons \beta$, between 1 and 5% oxygen, at approximately 1740 °C (3165 °F). A second peritectic reaction: $\text{Melt} + \alpha \rightleftharpoons \text{TiO}$, between 14.5 and 20.5% oxygen at approximately 1770 °C (3220 °F). A peritectoid reaction: $\alpha + \text{TiO} \rightleftharpoons \delta$, between 14.5 and 23.5% oxygen at approximately 925 °C (1695 °F). The alpha phase exhibits a maximum melting point of approximately 1900 °C (3450 °F) at about 10% oxygen. The solubility limit of oxygen in alpha titanium is approximately 14.5% oxygen from 800 to 1700 °C (1470 to 3090 °F). The lattice parameters of the alpha solid solution increase with increasing oxygen content. X-ray diffraction patterns for the TiO phase indicate a cubic structure of the NaCl type, with a linear decrease in parameter constants with increasing oxygen content. Lattice parameter measurements confirmed the alpha and TiO solubility limits determined by micrographic methods. The existence of the newly discovered δ phase was confirmed by X-ray studies, and the structure was tentatively identified as tetragonal. The composition range in which the new phase occurs includes the stoichiometric ratios for Ti_3O_2 and Ti_4O_3 .

A marked increase in hardness was obtained with the addition of oxygen to titanium. The hardness curve dipped to a minimum for $\alpha + \text{TiO}$ phase mixture alloys, and then showed a rapid increase for the TiO solid solution alloys.

ACKNOWLEDGMENTS

The authors are indebted to the Materials Laboratory, Wright Air Development Center, by whom the research was sponsored and permission granted to publish this paper. The help of the many associates at the Armour Research Foundation is greatly appreciated; thanks are particularly due to Mr. R. J. Van Thyne for the preparation of alloys, Mr. C. A. Johnson for the metallographic work, and Dr. W. Rostoker for the X-ray diffraction analysis.

References

1. C. W. Carstens, "The Behavior of Titanium in the Titanium-Bearing Slags (With Special Reference to TiO)", *Zeitschrift für Kristallographie*, Vol. 67, 1928, p. 260.
2. P. Ehrlich, "Phase Relationships and Magnetic Properties in the System Titanium-Oxygen", *Zeitschrift für Elektrochemie*, Vol. 45, 1939, p. 362.
3. P. Ehrlich, "The Solubility of Oxygen in Metallic Titanium", *Zeitschrift für anorganische und allgemeine Chemie*, Vol. 247, 1941, p. 53.
4. P. Ehrlich, "The Binary Systems of Titanium With the Elements Nitrogen, Carbon and Beryllium", *Zeitschrift für anorganische und allgemeine Chemie*, Vol. 259, 1949, p. 1.
5. R. I. Jaffee, H. R. Ogden and D. J. Maykuth, "Alloys of Titanium With Carbon, Oxygen and Nitrogen", *Transactions, American Institute of Mining and Metallurgical Engineers*, Vol. 188, 1950, p. 1261.
6. R. I. Jaffee and I. E. Campbell, "The Effect of Oxygen, Nitrogen and Hydrogen on Iodide Refined Titanium", *Transactions, American Institute of Mining and Metallurgical Engineers*, Vol. 185, 1949, p. 646; *Journal of Metals*, September 1949, T.P. 2681.
7. W. L. Finlay and J. A. Snyder, "Effects of Three Interstitial Solutes (Nitrogen, Oxygen and Carbon) on the Mechanical Properties of High Purity, Alpha Titanium", *Transactions, American Institute of Mining and Metallurgical Engineers*, Vol. 188, 1950; *Journal of Metals*, February 1950, p. 277.
8. D. A. Sutcliffe, Royal Aircraft Establishment, RAE Technical Note No. MET 141.
9. H. W. Worner, *Australasian Engineer*, Vol. 152, November 1950.
10. A. E. Jenkins and H. W. Worner, "The Structure and Some Properties of Titanium-Oxygen Alloys Containing 0.5 Atomic Per Cent Oxygen", *Journal, Institute of Metals*, Vol. 80, December 1951, p. 157.
11. M. Hansen, H. D. Kessler and D. J. McPherson, "The Titanium-Silicon System", *TRANSACTIONS, American Society for Metals*, Vol. 44, 1952, p. 518.
12. M. Hansen, E. L. Kamen, H. D. Kessler and D. J. McPherson, "Systems Titanium-Molybdenum and Titanium-Columbium", *Journal of Metals*, Vol. 3, 1951, p. 881.
13. C. S. Smith, "Constitution and Microstructure of Copper-Rich Silicon-Copper Alloys", *Transactions, American Institute of Mining and Metallurgical Engineers*, Vol. 137, 1940, p. 313.
14. J. W. Hickman and E. A. Gulbransen, "Oxide Films Formed on Titanium, Zirconium and Their Alloys With Nickel, Copper and Cobalt", *Analytical Chemistry*, Vol. 20, 1948, p. 158.
15. H. T. Clark, Jr., "The Lattice Parameters of High Purity Alpha Titanium and the Effects of Oxygen and Nitrogen on Them", *Transactions, American Institute of Mining and Metallurgical Engineers*, Vol. 185, 1949, p. 588.

DISCUSSION

Written Discussion: By A. E. Jenkins, Commonwealth Scientific and Industrial Research Organization, Physical Metallurgy Section, University of Melbourne, Carlton, Australia.

As part of a recent investigation into the high temperature oxidation of titanium now nearing completion in this laboratory, a full series of titanium-oxygen alloys has been prepared in a manner identical with that

outlined in the present paper, the alloys having been used as a basis for a full X-ray diffraction analysis of various products formed during the oxidation of titanium under different conditions.

During the production of the alloys it was found advisable to use a TiO_2 charge which had previously been pressed and arc-melted in order to avoid the subsequent loss of this material. Little difficulty was experienced in producing satisfactory melts right up to the composition TiO_2 , although, as mentioned by the authors, extreme care had to be exercised from Ti_2O_3 onward. In this range it was found that there was a tendency toward "wetting" the copper hearth with a consequent risk of contaminating the melt. Again, there appeared to be a pronounced immiscibility in the liquid melts between TiO and the higher oxides because solidified ingots tended to show the gold-colored TiO resting in contact with the hearth of the furnace and surmounted by the less dense higher oxides. This latter point has given rise to some interest in this laboratory and is being further investigated.

Did the authors notice any gas evolution during the melting of these high oxygen alloys, especially in those represented by the compositions $\text{TiO}_{1.6} \rightarrow \text{TiO}_2$? It is believed that there is an oxygen loss from these melts in the arc furnace. Pure white TiO_2 when heated in the arc appears to evolve gas, and certainly the black product obtained did not give a very satisfactory X-ray pattern, although one could recognize the characteristic rutile lines.

Regarding the authors' X-ray diffraction results, the somewhat unexpected appearance of the δ phase is most interesting. On the other hand, have the authors noted any structural change in stoichiometric TiO as a result of heat treatment? Results from this laboratory would tend to indicate that some change does occur. TiO which had been produced in the arc furnace from refined iodide titanium and TiO_2 was homogenized for 72 hours at 1030°C and water-quenched. A piece from the same original ingot was heated at 870°C for 48 hours and slow-cooled in air, both treatments being carried out in sealed evacuated silica tubes, the specimens resting on molybdenum boats. X-ray diffraction of the former specimen produced a sharp ideal body-centered cubic pattern giving a result for $a = 4.180 \text{ \AA}$ which is in exact agreement with the authors' value. However, the X-ray pattern from the latter specimen showed a breakdown from the original set of sharp lines into two distinct but less well-defined sets of lines. The patterns were those from two distinct body-centered cubic structures with $a = 4.179 \text{ \AA}$ and 4.143 \AA .

The following parameters have also been determined for the rhombohedral purple-colored sesquioxide of titanium,

$$a = 5.454 \text{ \AA}$$

$$\alpha = 59^\circ 6'$$

The oxide sample was prepared in a similar manner to the TiO .

Apart from these two points, the X-ray diffraction results for both phase boundaries and parameter changes agree very well with those obtained in this laboratory, and which will be published in the very near future.

In conclusion, may I congratulate the authors on presenting this quite valuable and most interesting paper. As they have stressed in their intro-

duction, it will fill a hitherto large gap in the ever-widening range of investigations connected with titanium.

Written Discussion: By R. I. Jaffee, Battelle Memorial Institute, Columbus, Ohio.

The authors have again done the able job of phase-equilibria studies that we have come to expect from them, and are to be congratulated. There are only a few minor points that I would like to have amplified. The drawing of the liquidus line appears to be too high in view of the data points showing complete melting. Apparently, the freezing range is much narrower than is indicated by the dotted line. This has a bearing on the segregation expected in melted ingots and in weldments. It would be helpful if the dotted line, which admittedly indicates some uncertainty, were drawn with more cognizance for the data points obtained. The bracketing of the peritectic temperature between 1730 and 1750 °C depends on the identification of liquid in the alloys containing 2 and 3% oxygen. However, at 1750 °C, the 4% oxygen alloy is indicated to be all alpha. This is anomalous, and makes one wonder how firm is the peritectic temperature of 1740 °C. The dip in hardness in the alpha-plus-TiO field is most interesting. Could the authors offer some speculation about the cause of this, perhaps employing the "matching plane" argument used in discussing the banded structure of these alloys?

Authors' Reply

The authors thank Dr. Jenkins for his comments and are looking forward to reading the complete results of his oxidation studies. With regard to the preparation of compositions between TiO and TiO₂, gravity segregation similar to that observed at the University of Melbourne was noted. However, as this high oxygen portion of the system was of secondary interest, no further investigation was made of the phase relationships involved on solidification of the melts. For the same reason, plus the fact that the ingots generally spalled badly on cooling after the melting operation, no check was made of possible oxygen evolution during the melting process in the region between TiO_{1.6} and TiO₂.

The X-ray diffraction results for TiO reported in the paper were obtained on samples previously annealed for 72 hours at 900 °C, as compared to the 48 hours at 870 °C used by Dr. Jenkins. The X-ray pattern of the stoichiometric TiO showed only the ideal body-centered cubic structure of this phase with $a = 4.172 \text{ \AA}$. Also, no indication of decomposition of TiO was observed metallographically. The authors have noted that the as-cast structures of alloys in the TiO region showed considerable coring. It may be possible that the relatively short annealing time at 870 °C used by Dr. Jenkins was not sufficient to eliminate the coring and thus somehow accounted for the two sets of lines obtained.

Dr. Jaffee's comments are appreciated. The authors are certain that he realizes the experimental difficulties involved in obtaining accurate liquidus data for titanium-base alloys at temperatures above 1700 °C. As admitted by Dr. Jaffee, the fact that the liquidus lines were dotted indicates that no high accuracy is claimed for their exact location. Actually, these tentative phase boundaries were placed on the basis of metallographic ob-

servations made on all samples quenched from the melting region; therefore, the authors feel justified in their interpretation of the results.

With regard to the location of the peritectic temperature questioned by Dr. Jaffee, 1740 °C was selected on the basis of the six data points obtained at the 1725 and 1750 °C temperature levels. One of the three samples at 1750 °C indicated no melting, another showed partial melting and the third melted completely. As two of the samples showed melting and the third which did not was the one immediately adjacent to the alpha field where it would be difficult to observe the first traces of melting, the authors believe they are completely justified in placing the peritectic temperature at 1740 °C.

Regarding the dip in the hardness curve at the alpha plus TiO field, the authors agree that the phenomenon is of considerable interest. As no specific investigation was made of this anomaly, since the primary object of the study was the determination of the phase diagram, the authors would prefer not to make speculative comments on the cause of this strange change in hardness.

THE ORDER-DISORDER TRANSFORMATION VIEWED AS A CLASSICAL PHASE CHANGE

BY F. N. RHINES AND J. B. NEWKIRK

Abstract

The question whether order-disorder transformations are normal Gibbsian phase changes, or are second-order transformations, is reviewed by means of a re-examination of the published evidence and by means of new resistivity and X-ray diffraction observations on copper-gold and copper-zinc alloys. It is concluded that all of the evidence, based upon equilibrium studies, supports the view that order-disorder transformations are normal phase changes.

IT HAS BEEN asserted and widely accepted that some, or all, of the order-disorder transformations found in alloy systems are not phase changes in the classical sense, but are, instead, homogeneous changes of state, sometimes described as second-order transformations. The present paper sets forth the argument against this viewpoint, endeavoring to demonstrate that order-disorder transformations are true heterogeneous phase changes in the full sense of the classical meaning.

This distinction is of critical scientific importance, because the two viewpoints lead to quite different predictions, with regard to the physical behavior of ordering systems. Among the predictions of the classical viewpoint (meaning the "Gibbs Phase Rule viewpoint" and so used throughout this paper) are some that provide an unambiguous basis for distinguishing between the modern and classical modes of behavior: First, the classical viewpoint predicts that, at equilibrium, the structure-sensitive physical properties undergo discontinuous change with temperature; where the equilibrium is univariant the property change occurs isothermally; where the equilibrium is divariant the change occurs within a sharply defined temperature interval. Second, the classical viewpoint predicts that the phases concerned are capable of coexistence, at equilibrium, within the temperature interval of transformation and should there be distinguishable as individually homogeneous masses of finite size, separated by sharply defined interfaces. These characteristics, which are contrary to the predictions of the modern viewpoint on order-disorder transforma-

A paper presented before the Thirty-fourth Annual Convention of the Society, held in Philadelphia, October 18 to 24, 1952. Of the authors, F. N. Rhines is professor of metallurgy, and J. B. Newkirk was formerly research assistant, Metals Research Laboratory, Carnegie Institute of Technology, Pittsburgh. At present Dr. Newkirk is research associate, Research Laboratory, General Electric Co., Schenectady, N. Y. Manuscript received April 17, 1952.

tions, will be used, in the argument that follows, as primary criteria of classical transformation.

It will not be necessary here to describe the modern viewpoint¹ in its many ramifications, because the entire structure of modern order-disorder transformation theory (as distinguished from theory dealing with the degree of order alone) is based upon, and hence must stand or fall with the validity of a single fundamental concept which presumes that:

"An alloy phase has two characteristics. The first is the pattern of sites occupied by atoms irrespective of their nature. Each phase of an alloy system has a different pattern of sites, and and therefore a change from one phase to another involves their complete rearrangement. The second characteristic is the distribution of the atoms among these sites. This distribution may vary continuously, without change of phase, from being random at high temperatures to being partially regular at low temperature."

This statement, from the works of Bragg and Williams (3), being a tentative proposal, was presumably not intended as a denial of the classical nature of the order-disorder transformation, but has been interpreted as such in the subsequent development of the modern theory. Thus, the modern viewpoint predicts a continuous change of the structure-sensitive properties, resulting from a continuous change in the atomic arrangement, such that segregation into distinct ordered and disordered masses is not admissible, even though equilibrium be maintained.

Upon this basis it seems needless to prove that ordering occurs as a classical phase change in those systems in which the ordered and disordered states differ in their crystal structure (although even this is denied by Harker's definition). Moreover, a careful survey of the experimental observations that are recorded in the literature has shown that the distinguishing criteria for classical transformation are fulfilled, beyond reasonable doubt, for all systems in which a change in crystal structure accompanies ordering and for which the results of extensive equilibrium studies have been presented. Only in the cases of systems, such as Cu_3Au and β -brass, wherein the ordering transformation proceeds without any change in the pattern of lattice sites, does the existing information leave room for doubt concerning the applicability of the classical viewpoint. For this reason, the argument presented herewith has been fortified by a careful restudy of the progress of equilibrium ordering in Cu_3Au and β -brass alloys. This study has demonstrated clearly the classical nature of the ordering transformation in these, as in other ordering alloys.

¹Excellent reviews setting forth the modern viewpoint in all of its detail are available in references 1 and 2 which are appended to this paper.

EVIDENCE IN SUPPORT OF THE CLASSICAL VIEWPOINT

The temperature variation of electrical resistance has been re-examined in a series of copper-gold alloys near the Cu_3Au composition (Fig. 1) and in copper-zinc alloys in the β , and $\alpha + \beta$ and the $\beta + \gamma$ ranges (Fig. 2). For these measurements, high purity alloys were prepared, the gold alloys by melting under argon in silica, and

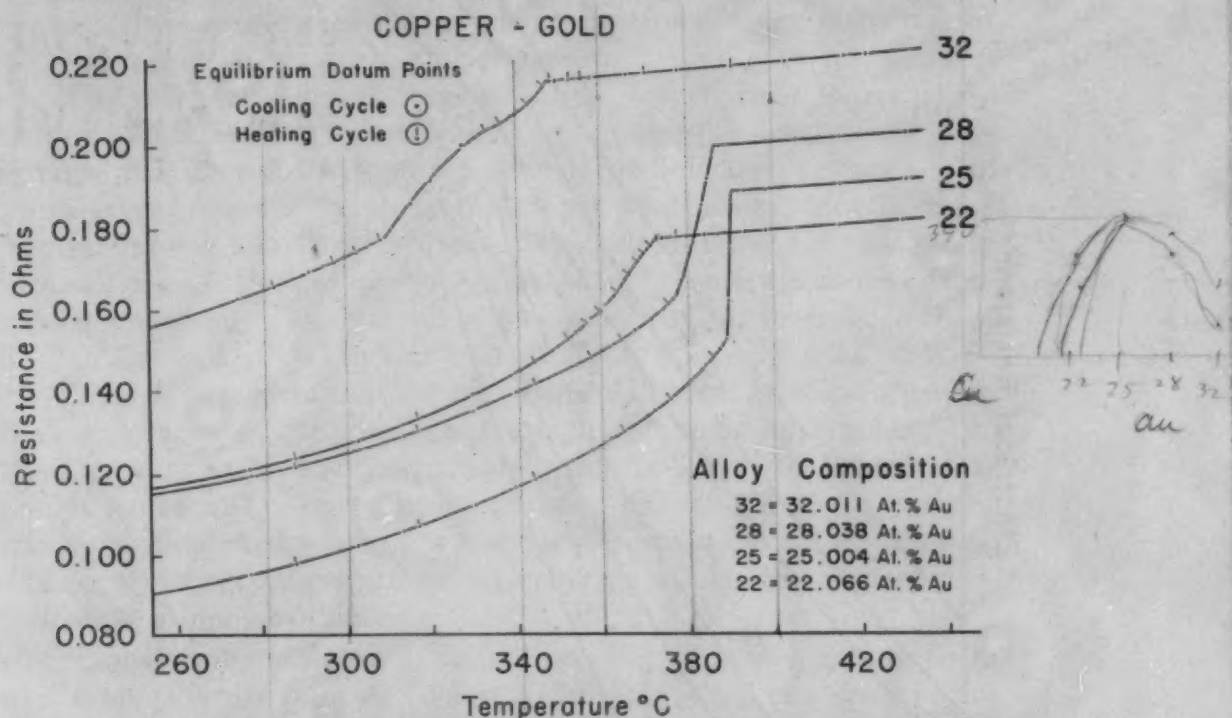


Fig. 1—Equilibrium Resistance-temperature Curves for Four Cu-Au Alloys Neighboring Upon Cu_3Au . It is to be noted that each curve displays two discontinuities corresponding to the beginning and ending of the transformation; these bound the temperature range of the two-phase equilibrium. The peculiar form of Curve 32 in the transformation interval has yet to be explained.

the brasses by melting in graphite under a cover of borax. The billets were homogenized and worked into wires, which, with the necessary electrical connections, were sealed into small glass capsules containing argon at low pressure. These were enclosed within holes in large aluminum temperature-equalizing blocks which, in turn, were wrapped in asbestos and heated in electric muffle furnaces with automatic temperature control. Resistance was measured with a sensitive galvanometer and Type K potentiometer to a reproducible precision of 0.1% including all variables. The total temperature oscillation under constant temperature control was, at best, about 0.3°C ; somewhat larger deviations occurred at some times during the tests. Copper-gold specimens exhibited no detectable deterioration in 11 months of continuous testing at temperature; copper-zinc samples exhibited a barely detectable permanent increase in resistance and some darkening of the glass after one month at temperature.

COPPER - ZINC

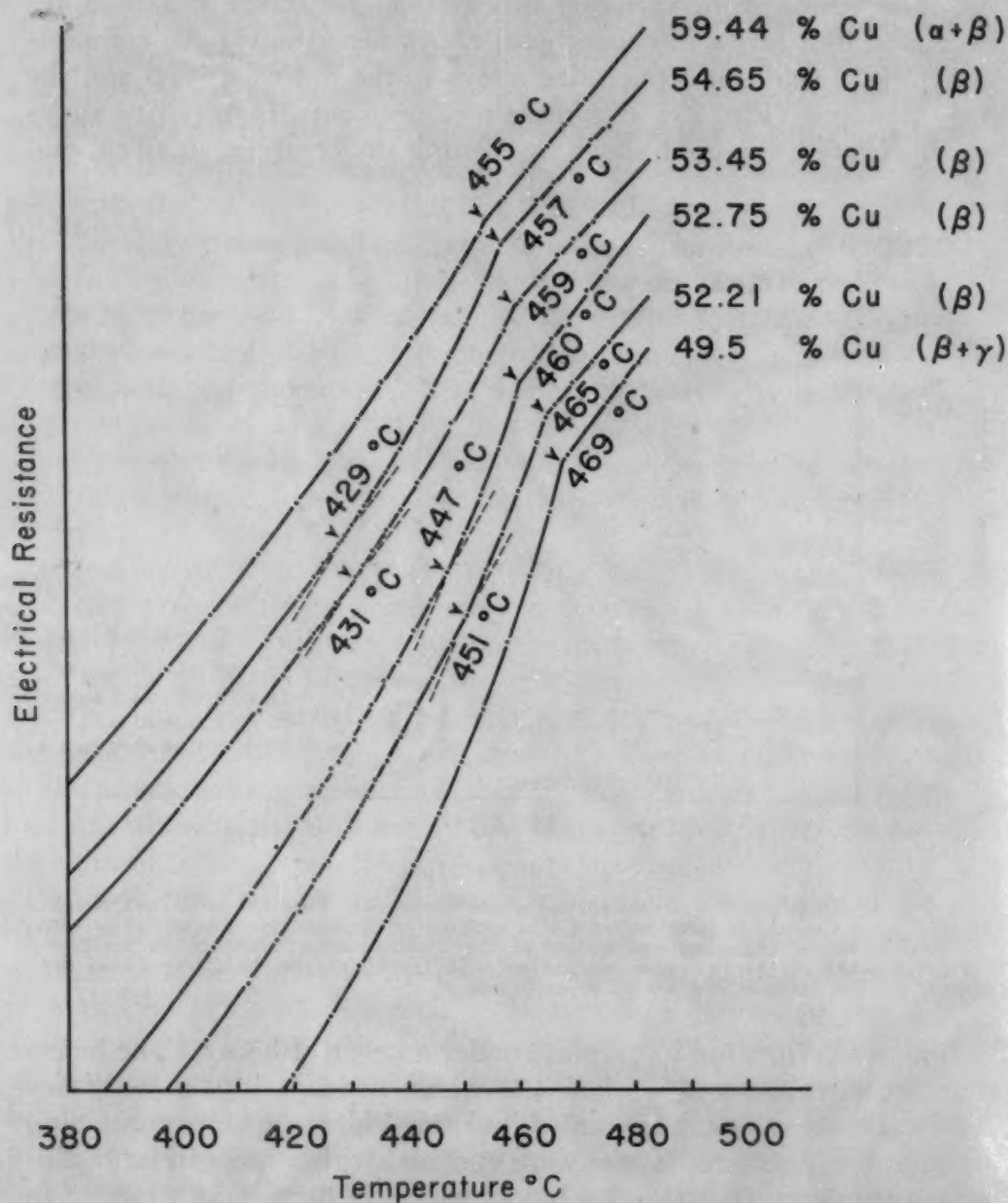


Fig. 2—Resistance-temperature Curves for β -brass Alloys Taken at a Heating Rate of Approximately $\frac{1}{2}$ Degree Per Minute. Essentially identical curves are obtained for heating and cooling rates ranging from 10 degrees per minute to stepwise equilibrium observations with a dwell of 2 or 3 days at each temperature, but the lower break is slightly less distinct in cooling curves, and long-time equilibrium studies cause a slight zinc loss that tends to blur the inflections. All dots on the curves are data points.

In the Cu_3Au series, observations were begun at the maximum temperature reported and the temperature was lowered only after a constant value of resistance had been found over a period of at least 24 hours. At temperatures above that of the beginning of or-

dering, the steady-state resistance reading was always found by the time of the first reading after the new temperature was attained. Within the transformation range a steady state was approached very slowly, frequently requiring several weeks. Immediately below the transformation range, a steady state was reached, usually after about a day at temperature, but the time requirement diminished with lowering temperature. A period in excess of 6 months was required to complete a single traverse of the temperature range surveyed in the copper-gold alloys.

The resistance curves shown in Fig. 1 each have two sharply defined inflections, the upper one of these corresponding in temperature to the previously reported transformation temperature. The temperature interval between the upper and lower inflections is shortest for the alloy nearest the Cu_3Au composition, Curve 25, and becomes progressively longer in alloys that are more removed from this composition. This interval is less than 1°C in Curve 25, about 8°C in Curve 22, 7°C in Curve 28, and 42°C in Curve 32.

Thus, it is evident that the temperature interval of transformation is nearing zero as the ideal Cu_3Au composition is approached, i.e., there appears to be a singular composition at which the transformation is isothermal. At compositions upon either side of Cu_3Au , the transformation occurs within a sharply defined temperature interval. This is all in accord with the first criterion of classical phase transformation as set forth above.

Transformation in the β -CuZn alloy, Fig. 2, is seen also to occur over a temperature interval (about 30°C). It is not expected, in this case, that any composition of the β -CuZn series will exhibit isothermal transformation, because the 50/50 atomic ratio occurs outside the β field and, hence, cannot be produced for study. The behavior of those alloys which can be studied, being divariant, is in full accord with the first criterion of classical phase transformation. The behavior of the alloys in the $\alpha + \beta$ and $\beta + \gamma$ ranges is also normal; here the transformation equilibrium, involving three phases, should be univariant and should occur isothermally, as is observed. This case differs from that of Cu_3Au mainly in its speed of transformation. Equilibrium is approached in the transformation range in a matter of minutes, instead of days.

Evidence that true equilibrium was attained in the resistance studies is to be derived from the fact that data points obtained with the temperature descending superimpose upon those later obtained with the temperature ascending. Additional confirmation is to be had from a group of observations in which, after a data point had been established isothermally, the temperature was set far downward, or far upward, for brief periods, and then returned to its former level; in each case, the original resistance value was eventually resumed.

Published Evidence of a Discontinuous Ordering Transformation

Resistivity Measurements—The finding of similar discontinuities in electrical resistance upon ordering has been reported for other systems, including some in which the crystal structure changes at the transformation. Sharp resistance discontinuities were found in AgPt and NiPt by Esch and Schneider (4) and in Cu_3Pd by Taylor (5). These observations were distinguished by the care with which equilibrium was established before making the measurements, a circumstance by no means common to all of the resistivity studies upon record. Nonequilibrium resistivity measurements on CuAu and Cu_3Au by Grube, Schonmann, Vaupel and Weber (6), on MgCd and Mg_3Cd by Grube and Schiedt (7), and on CuPd by Borelius, Johansson and Linde (8), have all shown double inflections. The latter studies were all similar, in that the observations referred to were made with the temperature rising. This condition is, of course, more favorable for the detection of divariant transformation inflections than are observations made with the temperature falling. It is further to be noted that, in every case in which a variety of compositions was examined, the temperature interval of transformation was smaller the closer the composition of the alloy to stoichiometric proportions.

Dilatometric Observations—Another kind of evidence of discontinuity in the ordering transformation is to be found in dilatometric studies upon copper-gold alloys by Kurnakow and Ageew (9). Two sharp inflections were found in the dilatometric curve of each alloy examined in the composition ranges near CuAu and Cu_3Au . A similar result was obtained by Owen and Liu (10), who measured the lattice parameter of Cu_3Au as a function of temperature and found an abrupt increase in its value at the disordering temperature. Again equilibrium conditions have been established with care in these experiments. Kurnakow and Ageew permitted the volume change to cease at each temperature of observation before proceeding to the next. Owen and Liu employed annealing treatments of 6 hours, or longer duration, at each temperature of observation. Grube and Scheidt's (7) dilatometric studies upon MgCd and Mg_3Cd revealed sharp transformation inflections although a relatively rapid heating rate (1°C per minute) was used.

New Evidence of the Equilibrium Coexistence of Two Phases in the Ordering Transformation Interval

Direct proof of the coexistence of an ordered and a disordered phase at equilibrium within the temperature interval of transformation has been found, by X-ray diffraction means, in copper-gold alloys neighboring upon Cu_3Au . In a typical case, a wire containing 28.038 atomic percentage of gold was stabilized at $383 \pm 1^\circ\text{C}$ (725°F),



Fig. 3—Debye-Scherrer Patterns of Alloy 28 (see Fig. 1) Brought to Equilibrium at (a) 390 °C (Disordered Phase), (b) 383 °C (Disordered + Ordered), and (c) 375 °C (Ordered). Filtered copper radiation was used. Attention is directed to the fact that the 400, 331 and 420 reflections, which are common to the ordered (c) and disordered (a) patterns, do not exactly superimpose in pattern (b); these reflections appear in (b) as triple lines representing the superimposition of the $K\alpha_1$ reflection of the ordered phase upon the $K\alpha_2$ of the disordered phase. The order lines 401, 411 and 421 appear as simple $K\alpha$ doublets in both the ordered (a) and partially ordered (b) patterns. The prints have been enlarged for clarity, but have not been retouched beyond exposing more deeply in the region of the 331 and 420 reflections in (b), to bring out the resolution of these lines.

by holding at this temperature for 352 hours and then quenching in ice water. With this specimen, a Debye-Scherrer pattern was made, using filtered $\text{CuK}\alpha_{1-2}$ radiation and a specimen-to-film distance of 5 centimeters (Fig. 3b). For purposes of comparison, similar patterns were made from the same alloy stabilized at 390 °C (735 °F) (completely disordered), Fig. 3a, and stabilized at 375 °C (705 °F) (fully ordered), Fig. 3c.

The central pattern, (b) in Fig. 3, is seen to be composed of all of the lines of both the disordered pattern (a) and the ordered pattern (c), showing that, at equilibrium at 383 °C (725 °F), this alloy is composed of two distinct states of crystalline matter, one ordered and the other disordered. This satisfies the second criterion of classical phase equilibrium and serves to differentiate between the classical and the modern viewpoints in favor of the former.

That the principal face-centered cubic reflections of the ordered and disordered phases are separately resolved in Fig. 3b is to be ascribed both to the larger lattice parameter of the ^{dis}ordered state and to its higher gold content, which contributes a further spread between the two parameters. Attempts to obtain a similar differentiation between the order and disorder reflections in an alloy on the other side

of Cu_3Au (22.066 atomic percentage gold) failed, presumably because the disordered phase is here poorer in gold than is the ordered phase. In this case, the lattice parameter difference associated with ordering is cancelled by the opposite parameter change resulting from the inverted composition difference.

Published Evidence of Ordered and Disordered Phase Coexistence

X-Ray Evidence—X-ray diffraction demonstrations of the coexistence of ordered and disordered states, under equilibrium conditions, have been reported for a number of other alloy systems. Hultgren and Jaffee (11), and more recently Newkirk, Geisler, Martin and Smoluchowski (12), have found superimposed order and disorder patterns in well-stabilized alloys near the CoPt composition. Similar evidence has been presented for near-NiPt alloys by Esch and Schneider (4) and for near-CuAu alloys by Johansson and Linde (13).

Further X-ray evidence, but of a less positive nature, because equilibrium conditions were not clearly established, has been presented for the case of CuAu alloys by Gorsky (14) and by Ohshima and Sachs (15), and for the FePd alloys by Hultgren and Zapffe (16). Equilibrium studies upon copper-gold-silver alloys, near the CuAu composition, by Hultgren and Tarnopol (17), showed order-disorder coexistence, but this case is complicated by the finding of a third structure of doubtful stability.

Metallographic Evidence—Probably the most unassailable metallographic evidence of the coexistence of ordered and disordered phases is that of Newkirk, Geisler, Martin and Smoluchowski (12), in alloys near CoPt. Here, a clearly defined Widmanstätten pattern of ordered platelets (acicular crosssection) was found disposed parallel to the dodecahedral planes in the disordered matrix crystal. Coincident X-ray evidence (quoted above) was provided to establish the identity of the two phases, so that there can be little doubt of the interpretation of the microstructure in this respect.

A microstructure closely resembling that found in CoPt alloys has been reported by Haughton and Payne (18), for a near-CuAu alloy, quenched from a temperature just below the upper critical. No claim of having established equilibrium is made by these authors, and the observation has been challenged for this reason; but this visual demonstration of the existence of a sharp interface between ordered and disordered particles in CuAu is, nevertheless, worthy of consideration.

Only Kurnakow, Zemczuzny and Zasedatelev (19) have claimed to have shown any detail in the structure of Cu_3Au , and their photomicrographs are far from convincing. It is interesting, however, that Guinier and Griffoul (20) have interpreted diffuse X-ray scattering

patterns of partially ordered Cu_3Au as indicating the initial growth of platelets of an ordered phase upon the $\{100\}$ planes of the disordered matrix. Thus, if a suitable metallographic technique is found, it seems likely that the structure revealed in partially ordered Cu_3Au will be seen to be composed of two separate phases.

New Observations on the Rate of the Ordering Transformation

When a transformation is divariant, the classical viewpoint requires that the conjugate phases differ in composition. It is apparent that a structural change, requiring a change in composition, must proceed by diffusion, which is commonly a slow process. Where particles of a new phase form, some kind of nucleation process must operate and this also may be expected to require substantial time. Hence, it is to be anticipated, from the classical viewpoint, that ordering transformations should be slow in the attainment of equilibrium, particularly within the temperature interval of two-phase coexistence. There is less basis for predicting the speed of transformation according to the modern viewpoint, but it seems reasonable to expect a rather high rate of attainment of equilibrium in a homogeneous-type transformation, due to the short distance required for diffusion.

In the course of the present studies, observations were made upon the rate of attainment of equilibrium in the Cu-Au alloys. Typical results are presented in Fig. 4. When the alloy nearest the composition of Cu_3Au was first stabilized just above the transformation temperature and was then held at a temperature midway in the transformation interval, it was found that its resistance did not change (i.e., no transformation) for several days, after which the resistance began to fall at an accelerating pace, then at a diminishing rate, until equilibrium had been attained (Fig. 4). This is typical of nucleation and growth transformation, even to the long induction period preceding nucleation.

When the same alloy was held at a temperature below the transformation range, after stabilization at a high temperature, the resistance began to fall immediately and attained a steady value within a few hours. In this case, no extensive diffusion is required, and the rate of nucleation should be greater at this lower temperature. Similar behavior was found in all of the other copper-gold alloys, except that the induction periods were generally of shorter duration in alloys away from the stoichiometric composition.

With β -brass, the transformation was found to be much more rapid, too rapid indeed, to permit rate studies such as those just described. However, with increasing rates of heating and cooling through the transformation range, the heating and cooling curves of electrical resistance are found to deviate from each other more and more, indicating the requirement of a significant time for the attain-

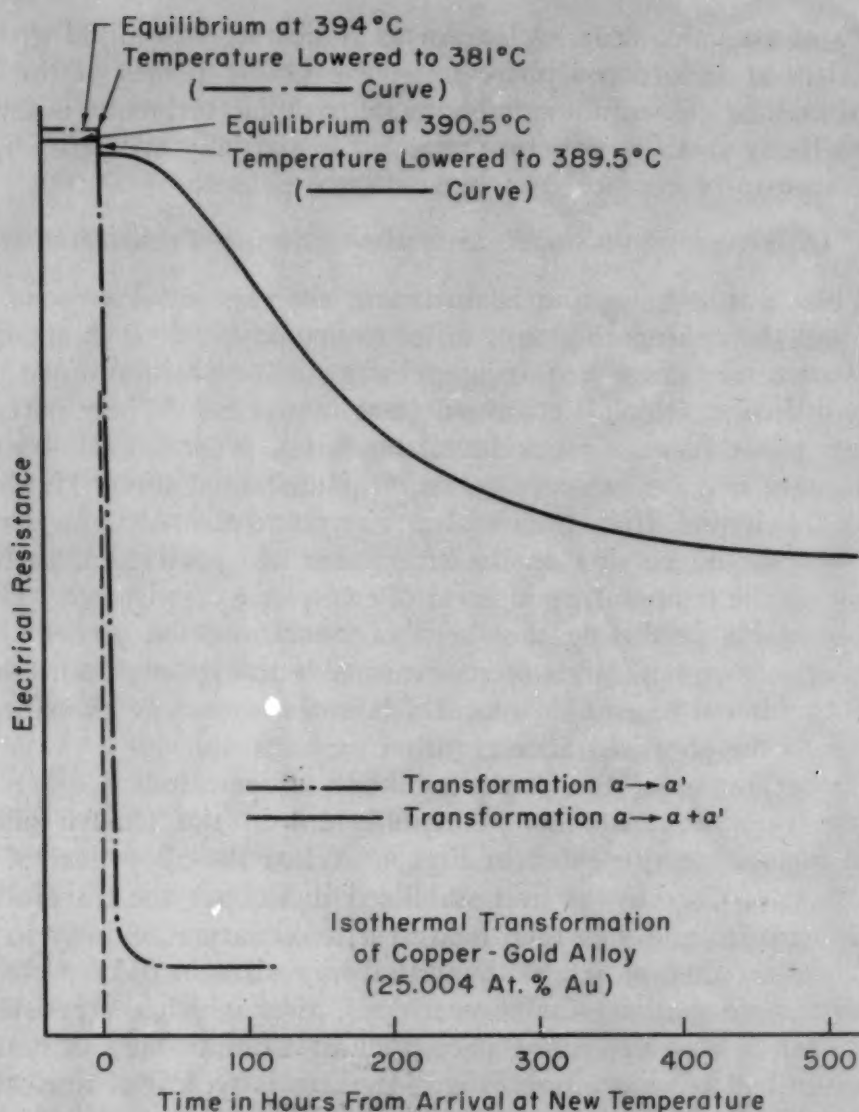


Fig. 4—Dependence upon Temperature of the Rate of Isothermal Transformation of an Alloy Near Cu_3Au . A very slow approach to equilibrium is found when the temperature of reaction is within the range of coexistence of the ordered and disordered phases (solid curve), while a relatively fast rate of transformation is found when the temperature of the ordered alloy is changed directly into the range of equilibrium existence of the ordered phase alone (dash-dot curve).

ment of equilibrium. It is suggested that the relatively rapid transformation of β -brass is to be associated with the comparatively low degree of order that exists in the ordered phase at the lower limit of the transformation range, i.e., the change that takes place in the ordering transformation is small.

Published Observations on Rates of Ordering

Slow rates of approach to a steady state, in the transformation interval, as measured by resistivity, dilatometry, diffraction line sharpening and mechanical tests, have been reported by a number of

investigators for a variety of systems, cf. (Cu_3Au) Sykes and Evans (21), Kurnakow and Ageew (9), Siegel (22), and Borelius (23); (CuAu) Kallback et al. (24), Kurnakow and Ageew (9), Hultgren and Tarnopol (17); ($\beta\text{-CuZn}$) Anastasevich and Frenkel (25); (Ni_3Fe) Kallback (26), and (FePd) Hultgren and Zapffe (16). Within the transformation interval, the rates are generally from one-tenth to one-hundredth as fast as above or below this temperature range.

A case of rather special interest has been presented by Smith (27), who observed that a β -brass is hardened by quenching from a series of temperatures encompassing the transformation range. Soon after quenching, the hardness begins to decline, but the rate of its lowering is sharply dependent upon the temperature from which the metal was quenched. For quenching temperatures above that of the beginning of ordering, a stable low hardness value is reached within 24 hours. Quenching temperatures below the transformation interval lead to a slower rate of hardness decrease; but the slowest rate, by far, is found in alloys quenched from within the transformation range.

The present authors suggest that the retardation of β -brass softening, when quenched from the transformation range, is to be associated with composition differences established by the formation of conjugate ordered and disordered phase particles in this temperature range. Thus, to reach the soft equilibrium state at room temperature, β -brass so treated must not only become fully ordered, but must re-establish a homogeneous distribution of its component elements by a relatively slow diffusion process. Samples quenched from higher and lower temperature need only complete the ordering reaction to arrive at an equilibrium state; this should be a much faster process.

ARGUMENTS AGAINST THE CLASSICAL VIEWPOINT AND REBUTTAL

The evidence and corresponding arguments set forth below include all of the kinds of arguments known to the present authors to have been cited against the classical viewpoint.

Electrical Resistance—It has been argued that, because resistance-temperature curves, such as those of Sykes and Evans (21) for Cu_3Au and those of Matsuda (28) and Imai (29) for $\beta\text{-CuZn}$, exhibit a continuous rise of the resistivity to a single inflection, at what has been called the critical temperature of transformation, the ordering process is, therefore, not discontinuous, as it should be if the classical viewpoint were correct.

From the studies reported in the present paper, it is apparent that discontinuous property change can be observed in these systems if adequate precautions are taken to ensure equilibrium. It has been contended that Sykes and Evans (21) did establish equilibrium for

their measurements and it is true that these authors present a sequence of resistivity observations for which equilibrium was established isothermally and which are virtually identical with those from which Curve 25 of Fig. 1 of the present paper was constructed. These authors chose, however, to place their faith in the results of their nonequilibrium measurements, made with constantly falling or rising temperature, and drew their conclusions accordingly.

Resistance-temperature measurements, made with constantly falling or rising temperatures, do not ordinarily show the discontinuous nature of the reaction clearly, because the second inflection in the property curve represents the termination of a diffusion process which will not have come to an end unless the rate of temperature change is extremely slow. Heating curves are somewhat more likely to show both inflections, because the diffusion velocity is increased by overheating, thus accelerating the change toward equilibrium.

Specific Heat—Another leading argument against the classical viewpoint is based upon specific heat curves, such as those obtained for β -CuZn by Tammann and Heusler (30), Sykes and Wilkinson (31), and Moser (32), and for Cu_3Au and Cu_3Pd by Jones and Sykes (33) and by Mott (34), respectively. It is argued that such curves are wrong for the classical transformation, because a simple isothermal rise and fall, representing the evolution of a latent heat of transformation, is presumed to be required in a classical phase change, and this is not observed; the specific heat is found rather to rise over a long temperature range to a maximum at one temperature.

Specific heat measurements are poorly suited to the detection of phase equilibrium, because the experimental techniques that must be used lose sensitivity as the rate of heating, or cooling, becomes slow, while equilibrium cannot be approached in most of the ordering systems (within the transformation range) unless the rate of temperature change is extremely slow. It is hardly to be expected, therefore, that specific heat curves would reveal the nature of the ordering transformation at equilibrium, i.e., would show either a latent heat evolution or the limits of divariant transformation. Moreover, it should be appreciated that the classical viewpoint does not predict an isothermal latent heat evolution for alloys of the β -brass type, nor indeed for any alloys except those of stoichiometric composition which transform congruently.

X-Ray Diffraction—Harker (35) has reported that certain cubic lines of the Debye-Scherrer pattern of CuAu broaden and resolve into multiple tetragonality lines during ordering at subcritical temperatures. He concludes from this that the ordering of CuAu is a continuous process of the modern type.

This argument is again subject to the objection that a transformation proceeding under nonequilibrium conditions (subcritical trans-

formation) is not expected, necessarily, to exhibit the same characteristics as one proceeding under conditions of near equilibrium. Owen and Sim (36) have, in fact, shown that diffraction effects, like those reported by Harker, are to be accounted for by a process of nucleation and growth, through which the ordered structure is developed at subcritical temperatures. The line broadening, according to these authors, reveals the formation of very small nuclei of the ordered state, while the subsequent sharpening of the order lines denotes the growth of the fine nuclei into ordered domains of sufficient size to produce a sharply defined diffraction pattern. Debye-Scherrer patterns have been published (12), which provide definite X-ray evidence of the coexistence of ordered and disordered phases in Co-Pt alloys after an equilibrium heat treatment.

Hysteresis—It was at one time thought that there is a real hysteresis in the resistivity and elastic property changes accompanying ordering (cf. Borelius and co-workers (23), and Siegel (22), respectively). This would be unnatural to classical phase changes, but normal for second-order transformation. Sykes and Evans (21), showed that the so-called "hysteresis" in Cu_3Au diminishes with a decreasing rate of transformation and is therefore unreal. Others have verified this conclusion with regard to other ordering systems. No further rebuttal of this point is required.

It will be recognized that the "false hysteresis" is nothing more than the inevitable chemical segregation effect accompanying non-equilibrium phase change.

Microstructure—The lack of positive microstructural evidence of the coexistence of an ordered and a disordered phase in such alloys as $\beta\text{-CuZn}$ and Cu_3Au has occasionally been cited against the classical viewpoint. Kaya and Kussman (37) comment to the effect that the ordering of Ni_3Mn must be regarded as a continuous process, because no detectable change in microstructure accompanies ordering in this instance. It hardly seems necessary to point out that such negative metallographic evidence must always be inconclusive, because there remains the possibility that some untried metallographic technique would have reversed the conclusion.

Analogy With Established Second-Order Transformations—Several investigators, including Tammann and co-workers (30), Potter (38) and Moser (32), have pointed out the similarity between the specific heat and resistivity curves of $\beta\text{-CuZn}$ and those of iron and of nickel near the Curie points of these metals. It is inferred by analogy that, since the magnetic transformation is of the second order, the order-disorder transformation must be likewise. A parallel argument has been presented by Fowler (39), comparing the property changes accompanying ordering with those observed in certain halide crystals, which exhibit a "Curie temperature", associated with

the change of vibration and rotation of the molecules at high temperatures to simple oscillation at lower temperature.

The rebuttal of these arguments has been covered by the demonstrations, above, that the supposedly homogeneous property changes referred to by these writers are those produced in nonequilibrium transformation and do not portray the true heterogeneous nature of the equilibrium transformation.

Summary of Rebuttal—A critical examination of the positive evidence cited against the classical viewpoint shows that, without exception, the necessary condition of equilibrium has been lacking. Since the Phase Rule deals only with equilibrium states, arguments based upon such evidence are inapplicable. It has been possible to show also that the observed deviations from equilibrium are of types familiar in other kinds of classical phase changes.

With no unassailable evidence against the classical viewpoint and with much clear evidence in its support, the conclusion seems inevitable that the ordering transformations studied thus far may all be regarded as normal Gibbsian phase changes.

SOME CONSEQUENCES OF THE CLASSICAL VIEWPOINT

While it is not the primary mission of this paper to explore the consequences of applying the Phase Rule to order-disorder transformations, there are a few general comments that should be made, to show that the viewpoint advocated in this paper is a constructive one.

Nature of the Ordered and Disordered Phases—The usual definitions of short-range order and long-range order are inadequate, in themselves, to define the ordered or the disordered phase. Above the disordering transformation, where the disordered phase alone exists at equilibrium, long-range order is absent, but some short-range order may, and usually does, occur. Below the transformation range, where only the ordered phase is found, there is always some degree of long-range order, but the ordering is rarely, if ever, perfect. Upon this basis, the following definitions are proposed:

A *disordered phase* is a crystalline state characterized by the absence of stable long-range order, but which may possess some degree of short-range order.

An *ordered phase* is a crystalline state characterized by the presence of some degree of stable long-range order.

As an interpretation of the latter definition, it is suggested that the ordered phase, at equilibrium, may be composed wholly of domains of long-range order and that departures from perfect ordering result from the existence of interdomain boundaries and of "wrong atoms" within the domains. When the grain size is small, it may be supposed that the intercrystalline boundaries would also contribute to the imperfections of ordering.

The Phase Diagram—The state of confusion in the construction of phase diagrams, which has resulted from the conflict between the classical and modern viewpoint, is well illustrated by the 1948 Edition of the METALS HANDBOOK (American Society for Metals) which includes binary diagrams of almost three dozen alloy systems known to involve ordering. About half of these are drawn in accord with the Phase Rule; the rest show "critical temperatures of ordering", without associated two-phase regions. Had the compilers of these diagrams been required to adhere consistently to the modern viewpoint, it is difficult to understand how they could have done so in all cases. The modern viewpoint, for example, makes no provision for dealing with cases in which ordering proceeds as a three-phased (univariant) reaction, with the ordered and disordered phases existing within wholly different composition ranges; nor does it provide for the transformation from order to disorder with falling temperature. Some examples of three-phased ordering transformations that have been reported are listed below. Primed Greek letters designate ordered phases; the arrows indicate falling temperature.

Disorder (1) \rightarrow Disorder (2) + Order
Example: Cu-Zn, $\beta \rightarrow \alpha + \beta'$

Disorder \rightarrow Order (1) + Order (2)
Example: Au-Zn, $\gamma \rightarrow \beta' + \gamma'$

Order (1) \rightarrow Order (2) + Order (3)
Example: Au-Zn, $\alpha'_1 \rightarrow \alpha'_2 + \beta'$

Order (1) \rightarrow Disorder + Order (2)
Example: Au-Zn, $\gamma'_1 \rightarrow \gamma'_2 + \delta$

Disorder (1) + Disorder (2) \rightarrow Order
Example: Ni-Zn, $\alpha + \beta \rightarrow \beta'$

Disorder + Order (1) \rightarrow Order (2)
Example: Cd-Mg, $\alpha + \gamma' \rightarrow \beta'$

Liquid \rightarrow Disorder + Order
Example: Li-Mg, $L \rightarrow \alpha + \beta'$

Liquid + Disorder \rightarrow Order
Example: Sb-Sn, $L + \beta \rightarrow \beta'$

Liquid + Order \rightarrow Disorder
Example: Be-Cu, $L + \gamma' \rightarrow \beta$

A return to the classical viewpoint will bring all of the combinations of ordering transformations into harmony and make possible the construction of self-consistent phase diagrams of ordering systems.

It should be pointed out that the occurrence of the ordering transformation as a discontinuous phase change, in the systems examined thus far, does not necessarily rule out the possibility that some system may be found in which long-range order develops continuously out of disorder. Like the liquid and gas phases, the ordered

and disordered phases might become indistinguishable above some critical value of pressure and temperature. Were this to occur, however, it is to be anticipated that the physical property curves would exhibit no inflection whatever during the development of long-range order, i.e., exhibit no "critical temperature".

Impact Upon Ordering Theory—In considering the nature of the conflict between the present conclusions and the leading theories of ordering, such as those of Bragg and Williams (3), Bethe (40) and Kirkwood (41), it is important to observe that the classical viewpoint is not concerned with the degree of order in either phase; it deals only with the equilibrium between the ordered and disordered phases. There is, for each ordering alloy, a temperature, or temperature range, within which a simple statement of the degree of order, such as is offered by the modern theories, is not adequate to describe the system, because two different degrees of order are coexistent as separate phases; at other temperatures a single state of order may be presumed to exist. Hence, the classical viewpoint raises no objection to any portions of the modern theory, except those dealing with the so-called transformation itself. It seems at least possible that the modern theory can be so modified as to avoid this conflict with the Phase Rule and yet retain its main strength in its ability to predict the degree of order above and below the phase transformation.

SUMMARY

It has been shown that order-disorder transformations proceed as normal phase changes in accordance with Gibbs Phase Rule. Presumed evidence to the contrary is found to have been based upon observations made without the necessary condition of equilibrium. It is proposed that the *disordered phase* be defined as a crystalline state characterized by the absence of stable long-range order and that the *ordered phase* be defined as a crystalline state characterized by the presence of some degree of stable long-range order.

ACKNOWLEDGMENTS

This research has been supported, in part, by funds placed with the Metals Research Laboratory by the General Motors Corporation. Much of the experimental work reported herein has been conducted by Donald L. Wood of the Metals Research Laboratory.

References

1. A. Boule, "Superstructures and Order-Disorder Transformations in Metallic Alloy", *Bulletin, société chimique de France*, Pt. I, Vol. 12, 1945, p. 169-188.
2. Foster C. Nix and W. Shockley, "Order-Disorder Transformations In Alloys", *Review of Modern Physics*, Vol. 10, 1938, p. 1.

3. William L. Bragg and E. J. Williams, "The Effect of Thermal Agitation on Atomic Arrangement in Alloys", *Proceedings, Royal Society*, Vol. A-145, 1934, p. 699.
4. U. Esch and A. Schneider, "The Nickel-Platinum System", *Zeitschrift für Elektrochemie*, Vol. 50, 1944, p. 268.
5. R. Taylor, "Transformations in the Copper-Palladium Alloys", *Journal, Institute of Metals*, Vol. 54, 1934, p. 255.
6. G. Grube, G. Schonmann, F. Vaupel and W. Weber, "The Constitution Diagram of Copper-Gold Alloys", *Zeitschrift für anorganische Chemie*, Vol. 201, 1931, p. 41.
7. G. Grube and E. Scheidt, "Electrical Conductivity and Thermal Expansion of Magnesium-Cadmium Alloys", *Zeitschrift für anorganische und allgemeine Chemie*, Vol. 194, 1930, p. 190.
8. G. Borelius, C. H. Johansson and J. O. Linde, "Lattice Changes in Metallic Solid Solutions", *Annalen der Physik*, Vol. 86, 1928, p. 291.
9. N. S. Kurnakow and N. W. Ageew, "Physico-Chemical Study of the Gold-Copper Solid Solutions", *Journal, Institute of Metals*, Vol. 46, 1931, p. 481.
10. E. A. Owen and Y. H. Liu, "The Thermal Expansion of the AuCu₃ Alloy", *Philosophical Magazine*, Vol. VII, 38, 1947, p. 354.
11. Ralph Hultgren and R. I. Jaffee, "A Preliminary X-Ray Study of Binary Alloys of Platinum With Cobalt, Molybdenum and Tungsten", *Journal of Applied Physics*, Vol. 12, 1941, p. 501.
12. J. B. Newkirk, A. H. Geisler, D. L. Martin and R. Smoluchowski, "Ordering Reaction in Cobalt-Platinum Alloys", *Transactions, American Institute of Mining and Metallurgical Engineers*, Vol. 188, 1950, p. 1249.
13. C. H. Johansson and J. O. Linde, "X-Ray Studies of Transformations in the CuAu Alloy", *Zeitschrift für Physik*, Vol. 50, 1928, p. 64.
14. W. Gorsky, "X-ray Studies of Transformations in the CuAu Alloy", *Zeitschrift für Physik*, Vol. 50, 1928, p. 64.
15. K. Oshima and G. Sachs, "X-ray Studies on the AuCu Alloy", *Zeitschrift für Physik*, Vol. 63, 1930, p. 210.
16. Ralph Hultgren and Carl A. Zapffe, "An X-ray Study of the Iron-Palladium and Nickel-Palladium System", *Transactions, American Institute of Mining and Metallurgical Engineers*, Vol. 133, 1939, p. 658.
17. Ralph Hultgren and Lester Tarnopol, "The Effect of Silver on the AuCu Superlattice", *Transactions, American Institute of Mining and Metallurgical Engineers*, Vol. 133, 1939, p. 228.
18. J. L. Haughton and R. J. M. Payne, "Transformations in the Copper-Gold Alloys", *Journal, Institute of Metals*, Vol. 46, 1931, p. 457.
19. N. Kurnakow, S. F. Zemczuzny and M. Zasedatelev, "The Transformations in Alloys of Gold With Copper", *Journal, Institute of Metals*, Vol. 15, 1916, p. 305.
20. A. Guinier and R. Griffoul, "Study of the Order-Disorder Transformation in the AuCu₃ Solid Solution", *Revue de Metallurgie*, Vol. 45, 1948, p. 487-396.
21. C. Sykes and H. Evans, "The Transformation in the Copper-Gold Alloy Cu₃Au", *Journal, Institute of Metals*, Vol. 58, 1936, p. 255; Vol. 59, p. 257.
22. Sidney Siegel, "Physical Properties of CuAu", *Journal of Chemical Physics*, Vol. 8, 1940, p. 860.
23. G. Borelius, "On the Equilibrium and Kinetics of Order-Disorder Transformations in Alloys", *Journal, Institute of Metals*, Vol. 74, 1948, p. 17; *Physica*, Vol. 15, 1949, p. 135.
24. O. Kallback, J. Nystron and G. Borelius, "Kinetics of the Order-Disorder

- Transformations in CuAu", *Ingeniors Vetenskaps Akademien, Handlingar*, Vol. 157, 1941 (in English).
25. V. Anastasevich and J. Frenkel, "Formation of Ordered Condition in a Binary Alloy", *Journal of Experimental and Theoretical Physics*, USSR, Vol. 9, 1939, p. 586 (in Russian).
 26. O. Kallback, "Determination of the Order-Disorder Transition Point in FeNi", *Arkiv for Matematik, Astronomi och Fysik*, Vol. 34B, 1947, p. 17 (in English).
 27. C. S. Smith, "Hardness Changes Accompanying the Ordering of Beta Brass", *Transactions*, American Institute of Mining and Metallurgical Engineers, Vol. 152, 1943, p. 144.
 28. T. Matsuda, "On the Transformations in Bronze, Aluminum-Bronze and Brass", *Science Reports*, Tohoku Imperial University, Vol. 11, 1922, p. 223.
 29. H. Imai, "On the Equilibrium Diagram of the Copper-Zinc System", *Science Reports*, Tohoku Imperial University, Vol. 11, 1922, p. 313.
 30. G. Tammann and O. Heusler, "Transformations Occurring in Homogeneous Anisotropic Phase Without Recrystallization", *Zeitschrift für anorganische und allgemeine Chemie*, Vol. 158, 1926, p. 349.
 31. C. Sykes and H. Wilkenson, "The Transformation in the β -Brasses", *Journal*, Institute of Metals, Vol. 61, 1937, p. 223.
 32. H. Moser, "Specific Heat Measurements", *Physikalische Zeitschrift*, Vol. 37, 1936, p. 737.
 33. F. W. Jones and C. Sykes, "Atomic Rearrangement Process in the Copper-Gold Alloy CuAu, II", *Proceedings*, Royal Society, Series A, Vol. 166, 1938, p. 376.
 34. N. F. Mott, "Discussion of Papers by Borelius, Bragg and Desch", *Proceedings*, Physical Society (extra part), Vol. 49, 1937, p. 108.
 35. David Harker, "Order Hardening: Its Mechanism and Recognition", *TRANSACTIONS*, American Society for Metals, Vol. 32, 1944, p. 210.
 36. E. A. Owen and G. M. Sim, "Superlattice Formation (in the Alloy AuCu)", *Philosophical Magazine*, Vol. VII, 38, 1947, p. 342.
 37. S. Kaya and A. Kussmann, "Ferromagnetics and Phase State in the Binary System Ni-Mn", *Zeitschrift für Physik*, Vol. 72, 1931, p. 293.
 38. H. H. Potter, "The Electrical Resistance of Ferromagnetics", *Proceedings*, Physical Society (London), Vol. 49, 1937, p. 671.
 39. R. H. Fowler, "Rotation of Molecules in Solid", *Proceedings*, Royal Society, Vol. 149, 1935, p. 1.
 40. H. A. Bethe, "Statistical Theory of Superlattices", *Proceedings*, Royal Society, Vol. 150, 1935, p. 552.
 41. J. G. Kirkwood, "Statistical Mechanics of Cooperative Phenomena", *Journal of Chemical Physics*, Vol. 8, 1940, p. 623.

DISCUSSION

Written Discussion: By Ralph Hultgren, professor of metallurgy, University of California, Berkeley, Calif.

The authors are to be congratulated on their lucid discussion of an important question of superlattice formation which has been largely ignored by exponents of the "modern viewpoint" of order-disorder transformations. It can be said, at the very least, that experimental evidence that the order-disorder transformation is not a classical phase change is unconvincing. Nevertheless, the experiment I describe below convinced

me many years ago that the experimental evidence in favor of the classical theory is also questionable.

As the authors correctly point out, the principal point at issue is whether or not there is a region of temperature and composition where a disordered and an ordered phase (of differing chemical compositions) are in equilibrium with one another.

They present X-ray diffraction pictures showing the co-existence of ordered and disordered phase after 352 hours at temperature. They cite ample proof from the literature that other authors, including myself, have also found two phases to be present in metal systems at certain temperatures.

While the fact that two phases existed together for 15 days at temperatures where diffusion is comparatively rapid creates a strong presumption of equilibrium, it by no means proves it. Even after 15 years (or 15 centuries) it might logically be maintained that equilibrium had not been reached. The demonstration becomes convincing only when it can be shown that the final state may be reached from both sides.

With this in mind I conducted the following experiment (Ref. 16 and Ralph Hultgren, "Concerning the Existence of a Two-Phase Region in the Ordering Process", *Journal of Chemical Physics*, March 1939). An alloy containing 51.9 atomic % palladium and 48.1 atomic % iron in the powdered form was heated for two days in a furnace at 750 °C, a treatment sufficient to make it completely disordered. The furnace was then slowly cooled to 690 °C. At this point a completely ordered sample of the same composition was inserted.

The ordered and disordered specimens were held at this temperature with a maximum fluctuation of $\frac{1}{2}$ °C for 15 days (360 hours), then quenched.

While the initially ordered specimen showed the familiar two-phase pattern, the disordered one remained completely disordered. Two interpretations of this result are possible, namely: (a) Two phases are truly in equilibrium but 15 days has not been sufficient time for nucleation to occur in the disordered phase, or (b) the single, disordered phase is the equilibrium phase, but 15 days is not sufficient time for disordering to occur in the phase which was initially ordered.

I do not see how a choice can be made between these, and I prefer not to make one. The only conclusion that seems to me certain is that the X-ray pictures proving the co-existence of two phases do *not* prove they are in equilibrium.

Written Discussion: By W. Shockley, Bell Telephone Laboratories, Murray Hill Laboratory, Murray Hill, N. J., and F. C. Nix, Franklin Institute, Philadelphia.

Although Rhines and Newkirk are correct in stressing the emphasis currently placed upon theories of the order-disorder transformation involving a single composition, they give an erroneous impression about the scope of past theoretical work. In particular they imply that the "modern viewpoint" excludes the idea that different states of order may be regarded as different phases. In stating that this "modern viewpoint" has been set forth in particular, Nix and Shockley, *Review of Modern Physics*, Vol. 10, 1938, p. 1-71, the authors might have made reference to the section on the "Phase Diagrams for the Order-Disorder Phenomenon" and perhaps have

quoted the paragraph which states: "No experimental work has as yet shown the occurrence of two phases with different compositions, one ordered and one not, in equilibrium with each other. Although such situations seem inevitable on basic thermodynamic grounds, they may be very difficult to realize in practice, owing to the slowness of obtaining equilibrium." It appears that in practice the slowness has led to a time lag of over 14 years.

In their closing discussion on the "Impact Upon Ordering Theory" the authors refer to three of the better-known approximate treatments. It should be emphasized that mathematically exact treatments have been given by L. Onsager, *Physical Review*, Vol. 65, 1944, p. 117; D. Kaufman, *Physical Review*, Vol. 76, 1949, p. 1232; and C. N. Yang, *Physical Review*, Vol. 85, 1952, p. 808. These start with the same approximate and idealized model as do Bethe and Kirkwood. It may also be appropriate to remark that the connection between order-disorder and phase changes in the face-centered cubic lattice and definitions of ordered phases was presented by W. Shockley, *Journal of Chemical Physics*, Vol. 6, 1938, p. 130-144. (Perhaps this reference is of an awkward age and qualifies neither as "classical" nor "modern".)

Written Discussion: By R. Smoluchowski, Carnegie Institute of Technology, Pittsburgh.

The authors' paper is a very interesting and stimulating survey of the ordering phenomena, and it points out that much of the existing differences of opinion and many of the past arguments seem to be based on insufficiently critical experimental data and on too dogmatic interpretation of statements in the literature. Sweeping generalizations in this field are dangerous and unconvincing.

The existence of two-phase regions at equilibrium in ordering alloys seems to be well established in such alloys as CoPt and AuCu where ordering produces a change in the symmetry of the crystal lattice. Recently one of the authors² was able to measure the width of the two-phase regions in the AuCu system. In the CoPt system, evidence indicates that ordering proceeds as a nucleation and growth process, the size and orientation of the ordered regions being measurable by means of X-rays.³

The authors' evidence for the existence of two-phase regions in AuCu, and in beta brass, in which only a minor change of density occurs, is based on X-ray and on resistivity data. However, the interpretation of the resistivity data, especially for beta brass for which no X-ray data are given, is not as certain as it is assumed. Contrary to the usual point of view, resistivity in ordering alloys depends, in general, not only upon the degree of periodicity of the lattice (domain size and order within the domains) but also upon the thermal scattering which is affected by ordering and upon some possible changes in the band structure. The latter probably do not play an important role for the present discussion. On the other hand, the change of the thermal scattering which depends upon the stiffness of the lattice, i.e. upon the characteristic Debye temperature θ_D , may be quite significant. One expects an ordered lattice to have a higher θ_D and thus a lower thermal scattering of the conduction electrons than

²J. B. Newkirk, private communication.

³J. B. Newkirk, R. Smoluchowski, A. H. Geisler and D. L. Martin, *Journal of Applied Physics*, Vol. 22, 1951, p. 290; *Acta Crystallographica*, Vol. 4, 1951, p. 507.

in a disordered lattice. The local θ_D will depend upon the local degree of order and may vary quite rapidly below the critical ordering temperature T_c . The breaks in the curves obtained by the authors with AuCu_3 are too big and too rapid to be accounted for by a change in θ_D alone, and thus the explanation in terms of a two-phase region seems correct. However, the small changes of slope obtained for beta brass, if at all real, can be equally well interpreted as changes in the vibration spectrum, i.e. in θ_D , of a uniformly ordered lattice. It is well known that elastic constants of beta brass vary in the region below T_c very rapidly⁴ and can easily produce an apparent break in the slope of the resistance curve. A rough estimate indicates that the variation of θ_D in this region could affect the resistivity by as much as 1% per 10 °C, which is just of the order of magnitude of the "irregularities" in the authors' Fig. 2. In that connection it should be pointed out that X-ray⁵ and metallographic⁶ analysis indicates—with experimental points spaced about 25 and 10 degrees apart respectively—an absence of a two-phase region in beta brass. Such a region should exist in the whole range of the boundary between the ordered and disordered beta brass, since this boundary never reaches the stoichiometric composition 50:50. It appears that until more convincing data, especially diffraction data, are available, the beta brass transformation should be regarded as of second order. Electrical conductivity, though often measurable with great accuracy, is far from being an ideal tool for a detailed study of the mechanism of phase transformations in solids.

Written Discussion: By W. D. Bennett, Physical Metallurgy Division, Department of Mines and Technical Surveys, Ottawa, Ont., Canada.

The authors' arguments and evidence in support of the classical viewpoint are valuable and interesting. Their remarks on the following three aspects of the so-called "modern" viewpoint would be appreciated:

(a) Much of the experimental evidence presented is based on an A_3B type of alloy for which it is implied that the Bragg-Williams and Bethe theories predict a continuous decrease of order with increasing temperature. This tangential approach to the critical temperature is only true for an AB type of alloy: for the A_3B type, a definite discontinuity is predicted by the modern theory, purely from energy considerations. Curve 25 shown by the authors for Cu_3Au would, therefore, seem to be in direct support of the modern viewpoint.

(b) Many order-disorder transformations are accompanied by a simultaneous change in the structure of the lattice. This fact makes it difficult to interpret the order-disorder transformations such as those occurring in cobalt-platinum alloys where there is a change from a face-centered cubic to a face-centered tetragonal lattice. It is not easy to see how experimental results on such systems can be used in a discussion of the order-disorder transformation as a classical phase change.

(c) The sluggishness of some order-disorder transformations, notably those occurring in iron-nickel alloys, and their dependence on the rate of cooling, does seem to support the classical viewpoint. However, theories

⁴W. A. Good, *Physical Review*, Vol. 60, 1941, p. 605; R. A. Artman, *Journal of Applied Physics*, Vol. 23, 1951, p. 475.

⁵D. T. Keating and B. E. Warren, "Long-Range Order in Beta-Brass and Cu_3Au ", *Journal of Applied Physics*, Vol. 22, 1951, p. 286.

⁶L. H. Beck and C. S. Smith, *Journal of Metals*, Vol. 4, 1952, p. 1079.

such as those suggested by Sykes and Evans (*Proceedings*, Royal Society, A 157, 1936, p. 213) should be borne in mind. The growth of order in anisotropic domains, which are "out of phase" with each other, seems quite plausible and explains many of these time-dependent phenomena.

Written Discussion: By W. J. Wrazej, Physical Metallurgy Division, Department of Mines and Technical Surveys, Ottawa, Ont., Canada.

It is the greatest pleasure to find that the question of order-disorder transformation has been so successfully treated by the authors. They conclude that all of the evidence, based upon equilibrium studies, supports the view that order-disorder transformations are normal phase changes.

It would be of great interest to hear the authors' expert opinion on how their theory would be effective in the case of iron alloys. There are numerous indications that even small quantities of alloying elements in iron alloys result in the formation of richer and poorer domains, differing with the quantity of the alloying elements.

We know that any atoms in a solution, whether in substitutional or interstitial positions, will upset the lattice of the solvent, i.e. displace the neighboring atoms not only in the unit cell but also in a surrounding group of cells. Owing to that, the state of the lowest distortion which is achieved in a certain "cell group" will be the approach to the state of equilibrium. The distortion of the lattice will be lowest in the case of the ordered state.

Because, as generally accepted, quenching retains the atoms in the positions attained by them at higher temperatures, there is no foundation to assume that even when the lattice configuration changes, say, during the allotropic transformation, the solute atoms will assume other locations except some minute linear movements.

There are many indications that iron-carbon alloys, depending on the quantity of carbon dissolved in the gamma iron phase, are heterogeneous.⁷ Many attempts based on the application of long heating periods at very high temperatures of various iron-carbon alloys remained without effect upon the heterogeneity. The structure resulting from the treatment before quenching remained unaltered, according to the X-ray and micro-examinations. The structure in quenched samples, in spite of the grain growth due to overheating, remained the same, i.e. the proportion of the phases was always the same and in domain-like form.

The distribution of carbon atoms responsible for the existence of the domains differing in carbon content in gamma iron solid solution does not appear, at first sight, to be directly the same process as the order-disorder reaction. It is a fact, however, that in both the cases the distribution of the atoms is connected basically with the distortion of the lattice.

The ordered phase is always, as we know from the lattice interpretation, a structure component approximately stable in composition and is, therefore, usually expressed by chemical formulas, e.g.: Fe_2Al , Fe_2Si , Fe_2Ni , etc. Any deviation from that composition, however, does not change the distribution of the atoms but results in a quantity of depleted solid solution. In other words, at equilibrium there will be as much of the ordered phase produced as the chemical composition will allow.

⁷W. J. Wrazej, "Gamma-Alpha Transformation in Iron-Carbon Alloys", *Nature*, Vol. 158, August 1946, p. 308.

The pseudo-phases which are assumed to exist in iron-carbon alloys in the gamma region are phases varying in carbon content. Between pure gamma iron (γ_0) and saturated solid solution (γ_E) an intermediate phase (γ_S) exists. All of them having a stable composition will differ in proportion only with varying content of carbon in the alloy. In other words, the variation of carbon in iron alloys will be exhibited in the proportion of the pseudo-phases.

It is natural to assume that a phase with no carbon (γ_0) and a phase saturated with carbon (γ_E) will always be parted by an intermediate phase (γ_S). The surplus of one of the phases can delete the co-existence of another phase but that which mostly differs in carbon only. Therefore, the superabundance of carbon-free (γ_0) can delete the existence of the fully saturated pseudo-phase (γ_E) in low carbon alloys, and vice versa, whereas the intermediate phase (γ_S) can still exist as being the resultant from that reaction. The experiments have shown that in samples below 0.4% carbon the traces of retained austenite cannot be seen and in the samples above 0.89% carbon the traces of ferrite (bainite) are removed in quenched iron-carbon alloys as experienced by my own micro- and X-ray examinations.

Written Discussion: By A. H. Geisler, General Electric Research Laboratory, The Knolls, Schenectady, N. Y.

The authors have performed an admirable service in clarifying certain lore which has arisen during the last 20 years regarding the ordering transformation and which has tended to produce a rather stagnant condition in the advancement of an understanding of this solid-state reaction in metals. The inadequacies of the earlier modern theory apparently are of somewhat evasive origin. An obvious one, however, is well illustrated by the use of the term "Curie temperature" in referring to the equilibrium transformation temperatures, an example of which is evident in a very recent dissertation (C. A. Wert, "Modern Research Techniques in Physical Metallurgy", published by the American Society for Metals, 1953). The convention originated in the supposedly analogous temperature dependence of the degree of long-range order and the extent of electron spin alignment revealed by the magnetic induction for saturation of a ferromagnetic material. The latter decreases in a continuous manner on heating and reaches zero at the magnetic Curie temperature where paramagnetic behavior transcends ferromagnetic behavior. If the magnetic transition is a second-order transformation in a single phase, continued usage of the term "Curie temperature" in referring to the temperature range of the ordering transformation with the inference of an analogy to the magnetic transition can only be misleading, for experience now shows that ordering is not always a second-order transformation.

The authors have pointed out that mathematical treatments of the changing degree of equilibrium long-range order with temperature below the transformation range and the changing degree of short-range order in the disordered phase are not being questioned. Such theories should be adequate to explain the observed gradual change in long-range order of a phase such as NiAl which forms in the ordered condition from a liquid solution (I. Isaichev and V. M. Iretsky, "X-Ray Study of the β -Phase in the System Ni-Al at High Temperatures", *Zhurnal Tekhnicheskoi Fiziki*,

Vol. 10, 1940, p. 316), much the same as a structurally analogous phase, ordered β -CuZn, forms from a solid solution. If there be allowed any credence in reasoning by analogy, however, then in these cases one must conclude that the ordering of a solution occurs consistently by first-order transformations, for the solidification of NiAl can hardly be viewed as any process other than a classical phase change. Perhaps the authors should have pointed out that the so-called modern theory is modern only from

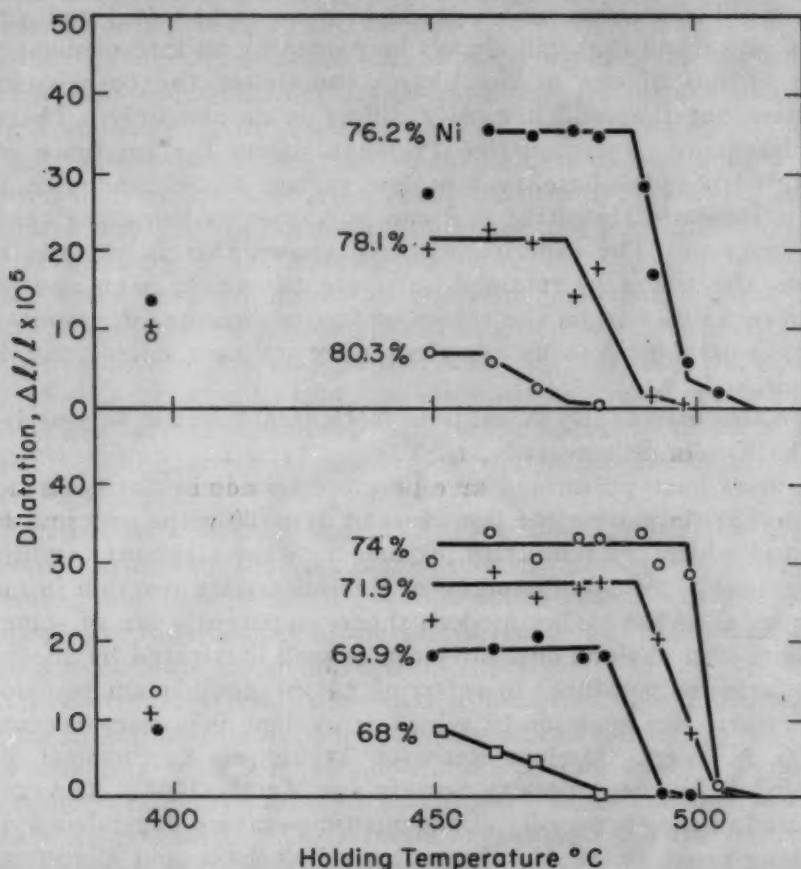


Fig. 5—Dilatometric Measurements on Nickel-Iron Alloys According to Josso.

the standpoint that prior to the period 1934 to 1938 the classical viewpoint had been considered adequate and two-phase equilibria between ordered and disordered phases had been proposed. (See, for example, the variously proposed copper-gold phase diagrams in M. Hansen's book, "Aufbau der Zweistofflegierungen", 1936.)

Further evidence for a heterogeneous transformation in a cubic ordering system should be noted. The nickel-iron alloy system is one of practical interest from the standpoint of magnetic materials. Near the composition Ni_3Fe an ordered phase of the Cu_3Au type forms without change in crystal structure. Dilatometric measurements by Josso (E. Josso, "Equilibrium Diagram of the Order-Disorder Transformation of Fe-Ni Alloys in the Vicinity of Ni_3Fe ", *Comptes rendus*, Vol. 230, 1950, p. 1467), on samples that had been held for 100 hours at temperature after quenching from 1000 °C, have been replotted in Fig. 5. There is little doubt that the equilibrium transformation is accompanied by a discontinuous change in length

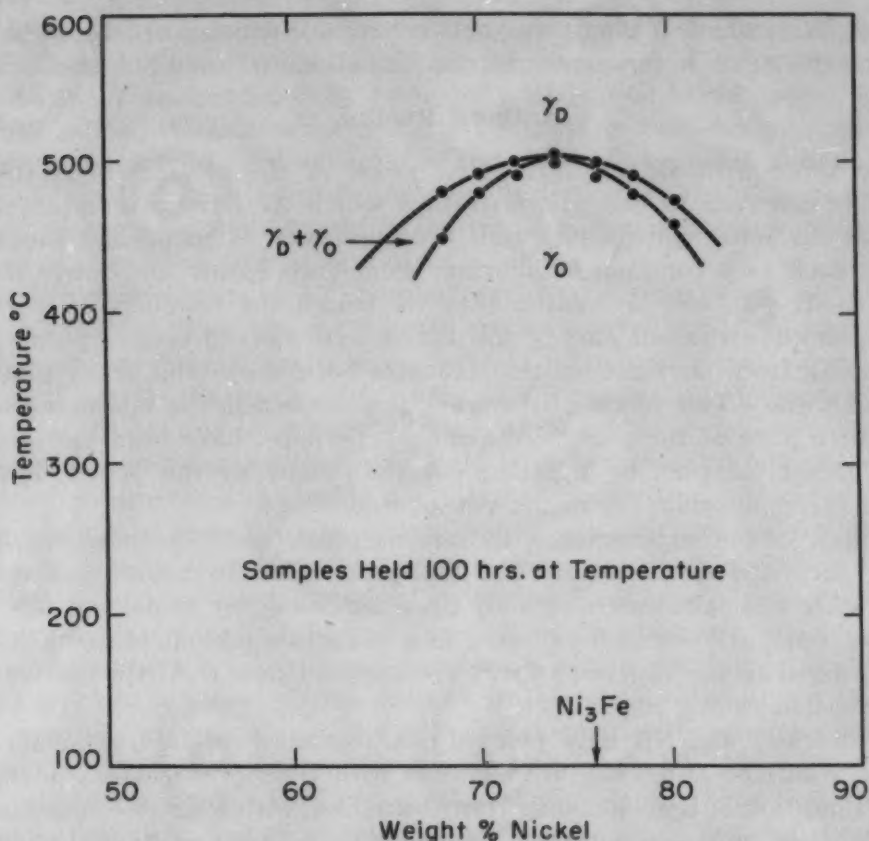


Fig. 6—Phase Fields for Ordering Reaction in Nickel-Iron Phase Diagrams.

with two inflections in the range 450 to 510 °C. Josso has pointed out that the samples which were held at 400 °C had not attained equilibrium. Thus they should not be employed in drawing the curves. The influence of the so-called modern theory is evident in Josso's work, for he considered only the upper inflections and drew a single line separating the disordered field from the ordered in the phase diagram, while completely ignoring the lower temperature inflections. When both inflections are used, a two-phase field required by classical theory can be shown as in Fig. 6, although the dilatometric data lack sufficient detail to permit the accurate locating of the boundaries. It is unfortunate that part of the results shown by the data had to be overlooked by Josso in order to conform with the theory of long-range order of Bragg and Williams.

Although the authors have been concerned mainly with the equilibrium transformation, it should be pointed out that a heterogeneous mechanism is also associated with the course of the changes in physical properties when supercooled alloys are ordered at temperatures below the equilibrium range. Only such a mechanism based on coherent nucleation and particle growth of the ordered phase at the expense of the disordered phase seems to provide an explanation of the transient values of properties such as permeability and coercive force of a large group of ordering magnetic alloys of practical interest. A heterogeneous mechanism for ordering in supercooled disordered alloys is attractive, for it permits the application of theories of nucleation, interfacial energy, orientation rela-

tionship, Widmanstätten patterns and coherency which have been developed for the other heterogeneous transformations in solid solutions.

Authors' Reply

We agree with Dr. Hultgren that proof of the attainment of equilibrium is essential to the demonstration which we have attempted, and also that the most convincing proof of equilibrium is to be had through the approach to a common equilibrium from both higher and lower temperature. It was for this reason that we traced the conductivity curves both up and down in our survey and that we re-checked certain points by approaching from far-removed temperatures both above and below that of the equilibrium. This phase of the work is described in the last paragraph on the fifth page of the paper. We should, perhaps, have been more specific in this discussion, by pointing out that many of the points double checked for equilibrium lay in the two-phased range.

In view of our experience with various copper-gold compositions, we are not surprised to learn that Dr. Hultgren failed to achieve an equilibrium state in a palladium-iron alloy upon annealing for 15 days at 690 °C. We have frequently encountered very long induction periods in going from the disordered to the ordered state. We suppose that this is a matter of low nucleation rate.

As Shockley and Nix have pointed out, the more recent treatments of Onsager, Kaufman and Yang are identical with their predecessors in their basic assumption of homogeneous transformation, with which we find fault. We take issue, however, with the statement that Shockley offered a definition of the ordered phase and with the implication that the discussers have presented a proof of the classical nature of the order-disorder transformation. What Shockley did was offer a definition of "the ordered state", which is an entirely different concept from a phase definition. This and other questionable conventions led to a derivation of a "connection between order-disorder and phase changes", actually to a sort of phase diagram, that was both of a high degree of thermodynamic improbability and counter to the then-known experimental facts.

The really important thing to be noted, however, is that it has been overlooked that there are points of incompatibility between the modern and classical viewpoints. The experimental evidence is clear in showing that AB and A_3B -type alloys both undergo discontinuous property change isothermally in their transformations, which may be interpreted consistently as univariant behavior for both, while the modern theory is a quite different behavior between the AB and A_3B types, providing discontinuous change only for the A_3B type.

All of the experimental evidence bearing upon nonisothermal ordering transformation applies to cases of divariant equilibrium, i.e., to non-stoichiometric, incongruent compositions such as β -brass. Here the physical measurements report a progressive change in the property under examination, only because, in the measurements, the property values of the conjugate phases are averaged; the observed change must, accordingly, be associated primarily with the relative proportions of the two phases. Whether the transformation is univariant, or divariant, however, the ordered phase must appear as a distinct entity, having a degree of order

and physical properties that are sharply distinguishable from those of the disordered phase. Hence, the successful prediction of the course of non-isothermal transformation by means of a derivation based upon a homogeneous model, if such can truthfully be said to have been accomplished, must be regarded by the adherent of the classical viewpoint as being wholly coincidental. In other words, the modern derivation of the degree of order may properly be applied only to individual phases and never to an aggregate of phases considered as a unit.

While it is true, as Dr. Smoluchowski points out, that the inflections in the resistivity curves for β -brass are very small, small enough perhaps to represent thermal scattering effects, it is also true that the inflections are sharp, too sharp, we feel, to be accounted for by thermal scattering effects. With respect to the absence of X-ray evidence of a two-phase region in the β -brass alloys, it should be noted that the effects upon the lattice parameter of ordering and of the composition difference between the conjugate phases are in mutual opposition. Hence, a shift in the lattice parameter with ordering, such as was observed in the Cu-28% Au alloy, is not to be anticipated. This makes it especially difficult to obtain X-ray evidence for the β -brass case. There is obviously much more that must be learned before the case for β -brass can be considered finally settled one way or the other. If the present studies serve to point out the danger of error in assuming that the β - β' transformation is homogeneous, however, they will have accomplished a useful purpose.

Dr. Bennett is, of course, quite right in pointing out that the Bragg degree of order curve is qualitatively correct for the A_3B -type alloys. Our objection in this case is not, however, with the shape of the curve for the stoichiometric alloy, but with the assumption of homogeneous transformation used as a model for its derivation and with the failure of the Bragg model to reveal the divariant nature of nonstoichiometric transformation in alloys infinitesimally adjacent to Cu_3Au . The degree of order prediction of the modern viewpoint is, of course, wrong for the AB case, in so far as one may judge from existing data.

We agree altogether with Dr. Bennett's second point and on the second page of our paper have remarked upon the inconsistency of basing any discussion of homogeneous ordering upon systems in which a crystallographic symmetry change accompanies ordering. So far as the Sykes and Evans growth of order picture is concerned, we are inclined to regard this as another of the many inconsistencies that have been superimposed upon the modern viewpoint. A growth process, per se, is out of place in a homogeneous transformation, but is all right for a heterogeneous phase change.

In reply to the question raised by Dr. Wrazej it can be said only that the Phase Rule is not concerned with concentration fluctuations that may occur within a phase, so long as these do not give rise to the existence of discrete particles of substances that have sharp differences in composition, or structure, or both, at their mutual interfaces. Neither does the Phase Rule apply where a state of homogeneous equilibrium has not been established within each phase of the system.

We thank Dr. Geisler for his comments. We agree that the term "Curie temperature" should not be applied to order-disorder phenomena.

AN END-QUENCH TEST FOR DETERMINING THE HARDENABILITY OF CARBURIZED STEELS

BY F. X. KAYSER, R. F. THOMSON AND A. L. BOEGEHOLD

Abstract

This report describes a new type of end-quench bar which was developed specifically for measuring the hardenability of case-treated steels. This bar, called the trapezoidal bar, was designed such that (a) hardness impressions can be made at any point in the case or in the core over the entire quenched length of the bar without the necessity of grinding, (b) hardness impressions are made perpendicular to the concentration gradient, and (c) the hardenability results are directly comparable to those obtained by using a standard Jominy bar. A résumé is given of its development, and data are presented from experimental work in measuring the hardenability of seven grades of carburizing steels (8117, 81B17, 8620, 3310, 4620, 4815, and 50B20). Conclusions are drawn regarding the case and core hardenability of these steels, and data are presented which indicate that the case hardenability of the boron steels goes through a maximum at about 0.70% carbon.

WHILE the development and application of the hardenability concept has made possible a quantitative index of the response of engineering steels to hardening in various section sizes, the extension of this concept to case-carburized steels has not been fully realized because of the lack of a simple method for measuring the hardenability of these steels. Prior to this investigation, the common method used consisted of carburizing and end quenching a cylindrical bar, and then grinding to predetermined case depths in order to determine the hardenability at the various carbon levels. The principal objections to this procedure were the length of time required and the number of operations involved, the possibility of tempering during the repeated grinding operations, and the fact that hardness impressions were made parallel rather than perpendicular to the concentration gradient. As a result of this situation, there is a scarcity of accurate information now available on the hardenability of carburized steels. However, the necessity of obtaining and using this type of information has become increasingly urgent in recent

A paper presented before the Thirty-fourth Annual Convention of the Society, held in Philadelphia, October 18 to 24, 1952. Of the authors, F. X. Kayser is research metallurgist, R. F. Thomson is head of the Metallurgy Department, and A. L. Boegehold is assistant to the General Manager of the Research Laboratories Division, General Motors Corp., Detroit. Manuscript received April 9, 1952.

years, especially as the demands for alloy conservation have necessitated the intelligent use of all steels on a hardenability basis.

The object of this investigation was

- (a) To develop an end-quench bar which could be used to accurately determine the hardenability of case-carburized steels, and
- (b) To use this bar in studies on the hardenability of seven grades of commercial steels: AISI 3310, AISI 4620, AISI 4815, AISI 50B20, AISI TS8117, AISI 81B17, and AISI 8620.

The first part of this paper includes a complete discussion of the end-quench bar which was developed, and this is followed by a presentation of the data obtained from the commercial steels.

THE TRAPEZOIDAL END-QUENCH BAR

In developing a bar for measuring the hardenability of carburized steels, it was considered essential that three conditions be satisfied. These were:

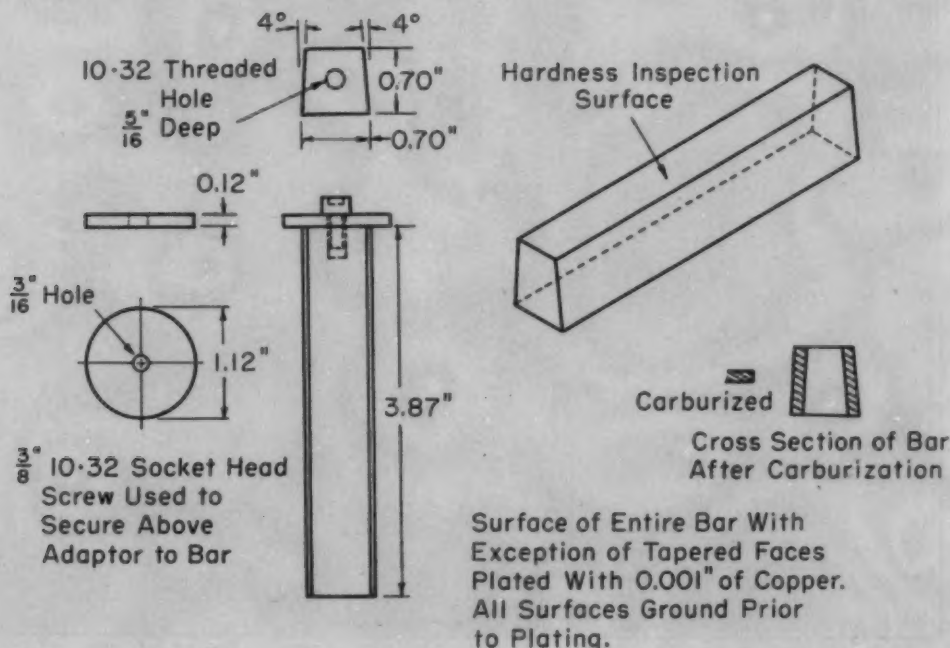


Fig. 1—The Trapezoidal End-Quench Bar for Measuring the Hardenability of Carburized Steels.

- (a) that the bar have a hardness inspection surface providing access to any point in the case or in the core over the entire quenched length of the bar without the necessity of repeated grinding operations,
- (b) that the hardness inspection surface section the case in such a manner that hardness impressions can be made perpendicular (or as nearly perpendicular as possible) to the carbon gradient, and
- (c) that the physical shape of the bar be such as to produce cooling conditions during end quenching equivalent to those produced in end quenching the standard Jominy bar.

The trapezoidal bar illustrated in Fig. 1 meets each of these requirements. Essentially it consists of a $3\frac{7}{8}$ -inch length with a trapezoidal cross section to which an adapter ($1\frac{1}{8}$ inches in diameter by $\frac{1}{8}$ inch thick) is fastened to facilitate end quenching. Its over-all length (4 inches) is equivalent to the over-all length of the standard Jominy bar. In this investigation the bar's entire surface with the exception of the two 4-degree taper faces was plated with 0.001 inch of copper to selectively prevent the diffusion of carbon during the

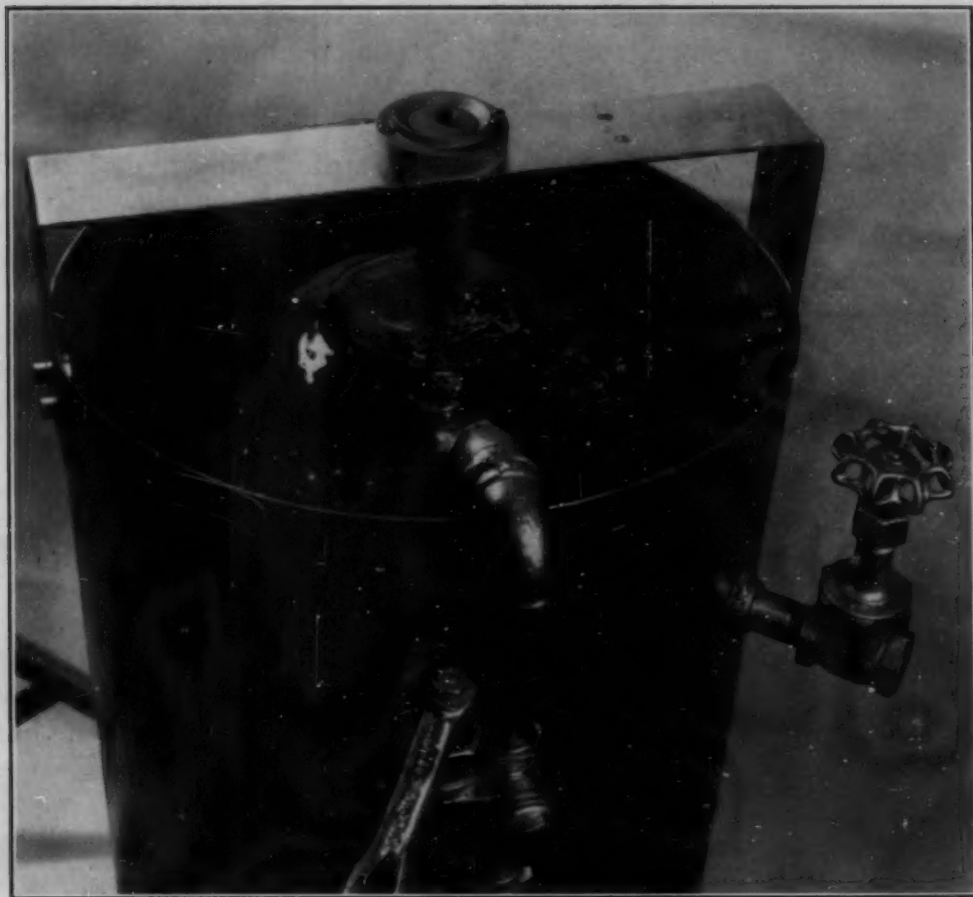


Fig. 2—End Quenching the Trapezoidal Bar.

carburizing operation. As a result, only the two taper faces were subjected to carburization. After hardening by end quenching, and after the hardness inspection surface was prepared (see Fig. 1), it was possible to examine any point in the case or in the core over the entire quenched length of the bar without the necessity of repeated grinding operations, and in a direction nearly perpendicular to the concentration gradient.

The procedure adopted in end quenching the trapezoidal bar was exactly the same as that followed in end quenching the standard Jominy bar (i.e., with regard to the orifice diameter, height of the

water column, etc.). Fig. 2 is an illustration of the quenching operation.

Uniformity of Cooling Across the Bar

Because of the new bar's shape, experiments were conducted to determine the uniformity of cooling across the bar at given distances from the quenched end. For this purpose a number of bars of AISI 8642 and AISI 80B40 were prepared with the entire surface of each bar (including the taper faces) plated with copper. These were austenitized at 1550 °F (845 °C) for 30 minutes at temperature and end-quenched from the austenitizing temperature. The hardness inspection surface of each bar was polished, and Rockwell C as well as Tukon (3000-gram load) readings were obtained at a number of Jominy distances. These impressions were made at selected intervals across the bar from positions within 0.005 inch of each edge. From these data it was concluded that the cooling rate across the trapezoidal bar at any given distance from the quenched end was sufficiently uniform for test purposes.

Comparison of Cooling in New and Standard Bar

A final set of experiments was conducted in order to obtain a comparison of cooling conditions in Jominy and trapezoidal bars during end quenching. The experimental procedure consisted of preparing both types of bars from the same steel and comparing their measured hardenability after austenitizing and end quenching. It was reasoned that if the hardenability of a given steel could be measured in quantitative equivalence by either bar, then, since the conditions of heat transfer were similar, equal hardnesses could be used as a criterion of similar cooling conditions.

The trapezoidal and Jominy bars prepared for this experiment were carefully machined from alternate positions along the length of a 1½-inch diameter bar of AISI 8642. The position of each bar within the original round is illustrated in Fig. 3. Each set of Jominy and trapezoidal bars was aligned such that the edge of the surface of inspection of the trapezoidal bar was in longitudinal alignment with hardness inspection flats ground along the Jominy bar. All of the bars were completely copper plated, austenitized at 1550 °F (845 °C) for 30 minutes at temperature and end-quenched from the austenitizing temperature. Rockwell C hardness readings were taken on these bars, and a typical set of results comparing the hardenability as measured by each bar is presented in Fig. 3. These data indicated conclusively that the physical shape of the trapezoidal bar is such as to produce conditions during end quenching equivalent to those in the standard Jominy bar.

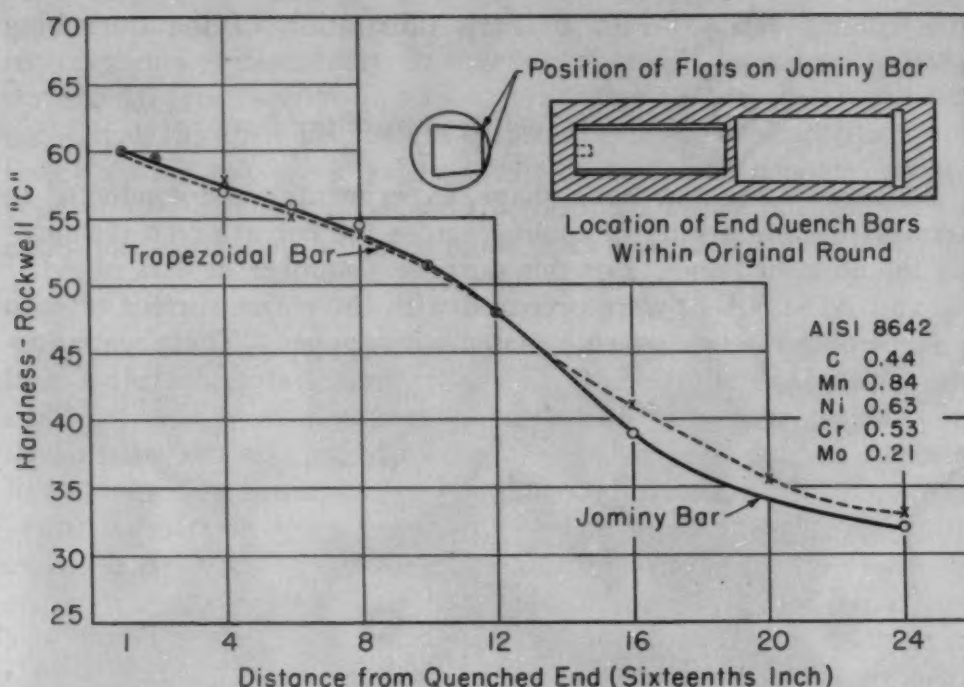


Fig. 3—A Comparison of the Hardenability of AISI 8642 as Measured by the Jominy and Trapezoidal Bars.

EXPERIMENTAL PROBLEMS—HARDNESS TESTING AND UNIFORMITY OF CARBURIZATION

The actual use of the bar for hardenability measurements presented several problems. The first concerned the mode of hardness testing, and the second the uniformity of carbon in the case.

As regards the first, it will be remembered that one of the features of this type of bar is that hardness impressions are made essentially perpendicular to the carbon gradient. While this must be regarded as a major asset, it presented a dilemma to the hardness tester, since impressions taken in this manner must necessarily span a portion of the concentration gradient. Thus, it was necessary, for the sake of accuracy, to take microhardness readings, since the actual change in carbon concentration across these smaller impressions could be regarded as minimal. Experimental work has indicated that the best results are obtained by using the Tukon hardness tester with a Vickers diamond pyramid indenter and a 3000-gram load. The trapezoidal cross section provides excellent "seating" for the hardness impressions. In order to prepare the hardness inspection surface the copper plate is removed after end quenching and this surface polished through at least a 0 to 6-micron diamond impregnated wheel.

With regard to uniformity, reference is made to the amount of carbon present at a given depth below the surface of either taper face after a carburizing treatment. Two methods were used to determine uniformity; the first involved the microscopic examination

of a number of cross sections throughout the bar parallel to the quenched end, and the second compared hardenability results from the case on one side of the bar with those from the opposite case. This work was carried out on both gas and pack-carburized bars and provided conclusive evidence that excellent uniformity had been achieved.

METHOD OF OBTAINING HARDENABILITY DATA FROM THE TRAPEZOIDAL BAR

In Table I, data are presented from a trapezoidal bar of AISI 8117 which had been pack-carburized in a commercial carburizing

Table I
The Hardness Survey* From Both Cases of a Trapezoidal Bar of AISI 8117
Pack-Carburized for 16 Hours at 1700 °F (925 °C) and End-Quenched

Distance Below Carburized Face Inches	1/16 Inch	2/16 Inch	4/16 Inch	6/16 Inch	8/16 Inch	12/16 Inch	1 Inch	1½ Inches	2 Inches
0.010	59†	60	56	45	47	40
0.020	61	62	60	50	45	42
0.030	64	64	61	53	44	38
0.040	63	62	58	43	40	35
0.050	62	52	47	34	34	30
0.060	58	..	57	49	38	31	28	27	27
0.070	54	..	51	41	32	28	20	21	21
0.080	51	50	42	31	25	19	15	15	15
0.090	47	47	37	31	23	21	15
Core	45	41	27	23	16	14	11
0.090	48	47	35	29	27	23	15
0.080	52	49	42	31	26	23	18	17	15
0.070	56	..	52	39	31	30	23	21	20
0.060	60	..	56	49	42	31	28	28	26
0.050	63	52	45	34	35	30
0.040	63	62	54	43	37	35
0.030	63	64	63	54	45	39
0.020	61	61	60	48	45	42
0.010	58	59	58	46	45	41

*For the sake of brevity, data from the 3/16, 5/16, 7/16, 10/16, 14/16, 1½, and 1¾-inch positions are omitted.

†Rockwell C hardness units converted from Vickers diamond pyramid hardness.

compound for 16 hours at 1700 °F (925 °C) and end-quenched directly from the box. Microhardness readings were taken on both cases of the bar at various "J" distances with the Wilson Tukon tester (Vickers diamond pyramid indenter, 3000-gram load) and then converted to the Rockwell C scale.¹ These readings are listed in Table I as a function of case depth and "J" distance.

In order to convert these data to specific carbon levels, a carbon gradient specimen was prepared from the bar as illustrated in Fig. 4. After softening and straightening to within ± 0.0005 inch, millings were obtained from this specimen at various case depths and analyzed to determine the carbon as a function of case depth (this procedure

¹A comparison of actual with converted Rockwell C values indicated that this conversion was accurate at least to $\pm 1\frac{1}{2}$ units from 65 to 20 on the Rockwell C scale.

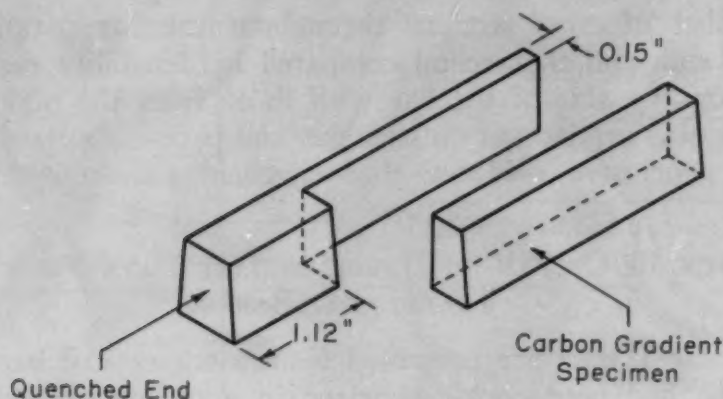


Fig. 4—The Location of the Carbon Gradient Specimen in the Trapezoidal Bar.

Table II
The Case* and Core Hardenability of AISI 8117 Carburized at 1700 °F (925 °C) for 16 Hours and End-Quenched

% Carbon	1/16 Inch	2/16 Inch	4/16 Inch	6/16 Inch	8/16 Inch	12/16 Inch	1 Inch	1½ Inches	2 Inches
1.00	60.5	61	59.5	48	45	42
0.90	62.5	63	62	52.5	44.5	40
0.80	63	63	60	48.5	41.5	37
0.70	63	59	53	40	37.5	33
0.60	62	63	59	48.5	42.5	33	32	29
0.50	59	57	49	40	33.5	28	26.5	25
0.40	56	57.5	51.5	41.5	32	28	22	21.5	21
0.30	51.5	49.5	40	31	25.5	21	17.5	17.5	15
Core	45	41	27	23	16	14	10.5

*The data from both sides of the bar are averaged to determine the case hardenability.

was adopted as the standard method of determining weight per cent carbon versus case depth for the trapezoidal bar). The hardness values at each "J" distance in Table I were then used to determine the hardness at each specific carbon level (0.90, 0.80, 0.70%, core), and these data are presented in Table II. This method of analysis was followed in all of the experimental work presented in this paper.

USING THE TRAPEZOIDAL BAR TO DETERMINE THE HARDENABILITY OF SEVEN GRADES OF COMMERCIAL CARBURIZING STEELS

Steels—Experimentally, the trapezoidal bar was used to determine the case and core hardenability of the seven grades of commercial carburizing steels whose chemical analyses and austenite grain sizes are listed in Table III. These steels were received as 1¼ to 1½-inch diameter rounds and were forged at approximately 1900 °F (1040 °C) to square bar stock having a 1-inch flat. These lengths were then normalized at 1700 °F (925 °C) for 1½ hours. The trapezoidal bars used in this investigation were prepared from the center of the normalized material.

Table III
Chemical Analysis* and Austenite Grain Size of Carburizing Steels

GMR No.	AISI Type	C	Mn	P	S	Si	Ni	Cr	Mo	B	ASTM Austenite Grain Size
27	8620	0.20	0.86	0.029	0.026	0.27	0.53	0.57	0.19	7-8
33	8117	0.20	0.77	0.016	0.029	0.29	0.42	0.39	0.10	7-8
34	81B17	0.19	0.74	0.010	0.028	0.30	0.41	0.40	0.10	0.0012	7-8
40	50B20	0.20	0.94	0.015	0.028	0.31	0.06	0.47	0.01	0.0013	6-8
43	3310	0.13	0.54	0.005	0.010	0.28	3.46	1.68	0.06	7-8
44	4620	0.18	0.57	0.017	0.035	0.31	1.96	0.21	0.25	7-8
45	4815	0.13	0.43	0.015	0.020	0.25	3.58	0.16	0.26	4-5

*Obtained from round bar stock.

Carburizing Treatment—The data reported in this section were all obtained from bars which were pack-carburized in a commercial carburizing compound.

EXPERIMENTAL PROCEDURE

The experimental procedure was conducted as follows:

(a) Two bars of each steel were pack-carburized for 16 hours at $1695 \pm 5^\circ\text{F}$ (925°C) and end-quenched directly from the box. These were packed in separate carburizing boxes (3 inches in diameter and 5 inches high), new carburizing compound being used for each bar. Bars of the same steel were carburized on different days to evaluate the reproducibility of the carburizing treatment. Several trapezoidal bars of AISI 8117 were carburized for 12 hours and end-quenched to determine the reproducibility of the hardenability data when the specific carbon levels occurred at different case depths in the bar. The case depth in the bars carburized 16 hours approximated 0.100 inch with a surface carbon of 1.0 to 1.2%.

(b) A hardness survey was completed on each bar using the Wilson Tukon tester (Vickers diamond pyramid hardness indenter, 3000-gram load). These readings were converted to Rockwell C units. The hardenability of the core of each bar was also determined by actual Rockwell C readings.

(c) Carbon gradient specimens were prepared from each end-quench bar in a manner previously described. After softening and straightening to within ± 0.0005 inch, the chemical analyses of millings obtained at the 0.010, 0.020, 0.040, 0.060, 0.080 and 0.100-inch case depths provided an accurate carbon gradient of each case.

(d) The case hardenability of each bar was determined at a number of specific carbon levels (including 0.20, 0.30, 0.40, 0.50, 0.60, 0.70, 0.80, 0.90%, and in some cases 1.0% carbon) using the data obtained from (b) and (c).

EXPERIMENTAL RESULTS

The experimental results are presented graphically in Figs. 5 through 14. These include a complete summary of the case and core

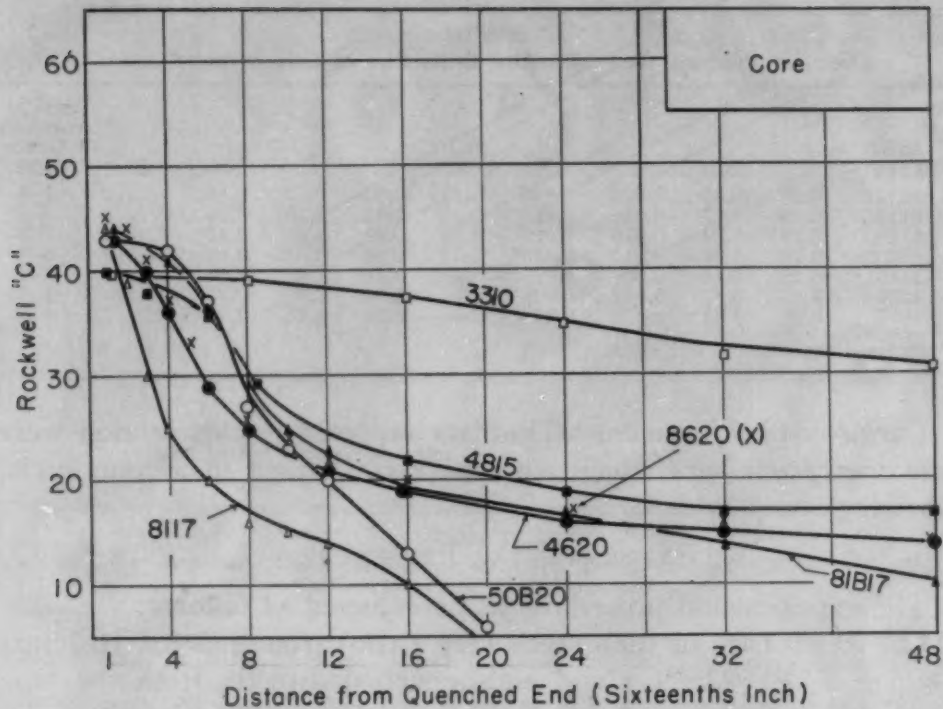


Fig. 5—The Core Hardenability of Seven Commercial Carburizing Steels.

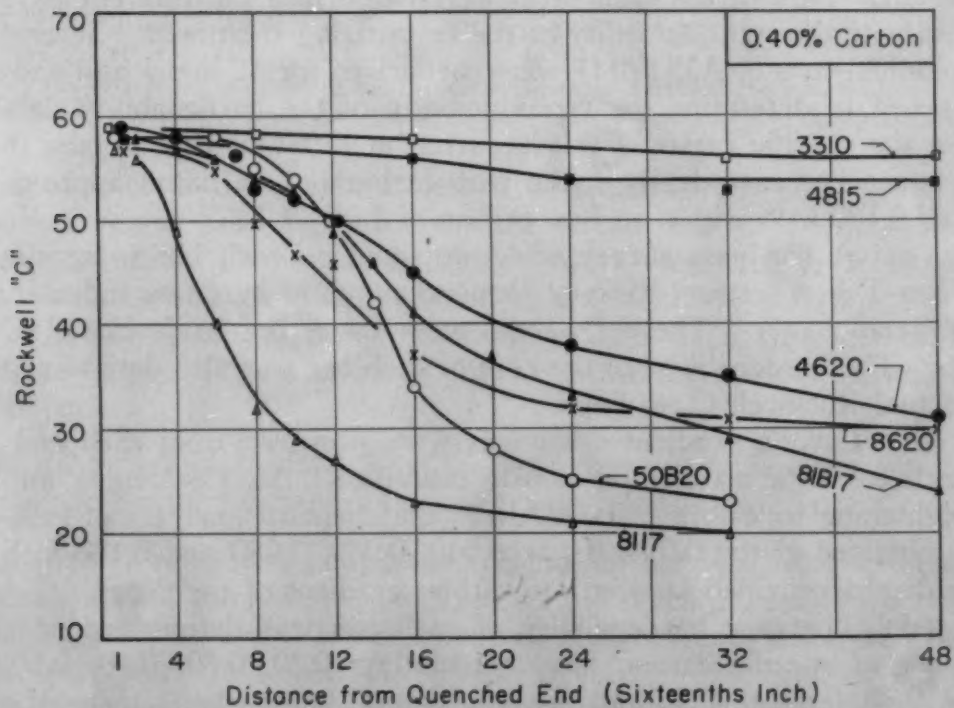


Fig. 6—The Case Hardenability of Seven Commercial Carburizing Steels at the 0.40% Carbon Level (End-Quenched From 1700 °F or 925 °C).

hardenability of each steel, and for any one steel represent an average of the results from the several trapezoidal bars studied.

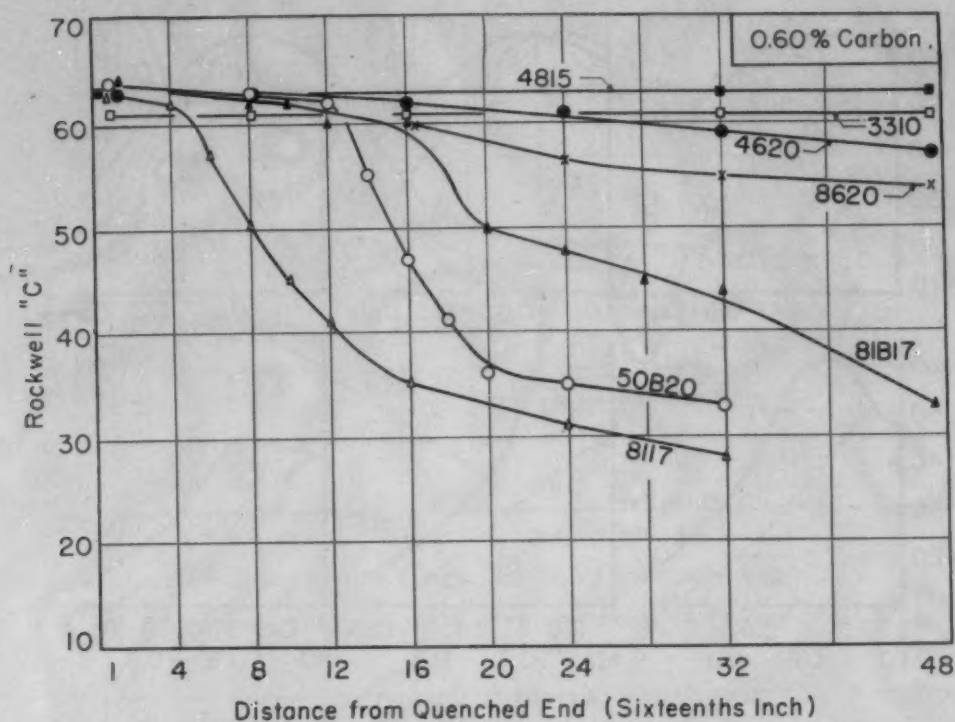


Fig. 7—The Case Hardenability of Seven Grades of Carburizing Steels at the 0.60% Carbon Level (End-Quenched From 1700 °F or 925 °C).

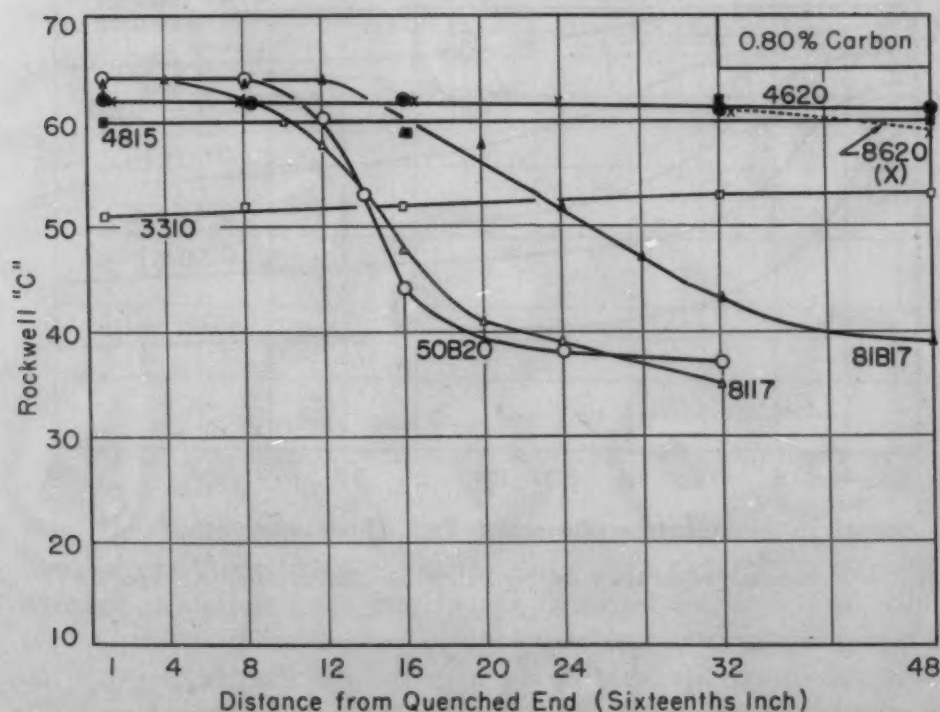


Fig. 8—The Case Hardenability of Seven Commercial Carburizing Steels at the 0.80% Carbon Level (End-Quenched From 1700 °F or 925 °C).

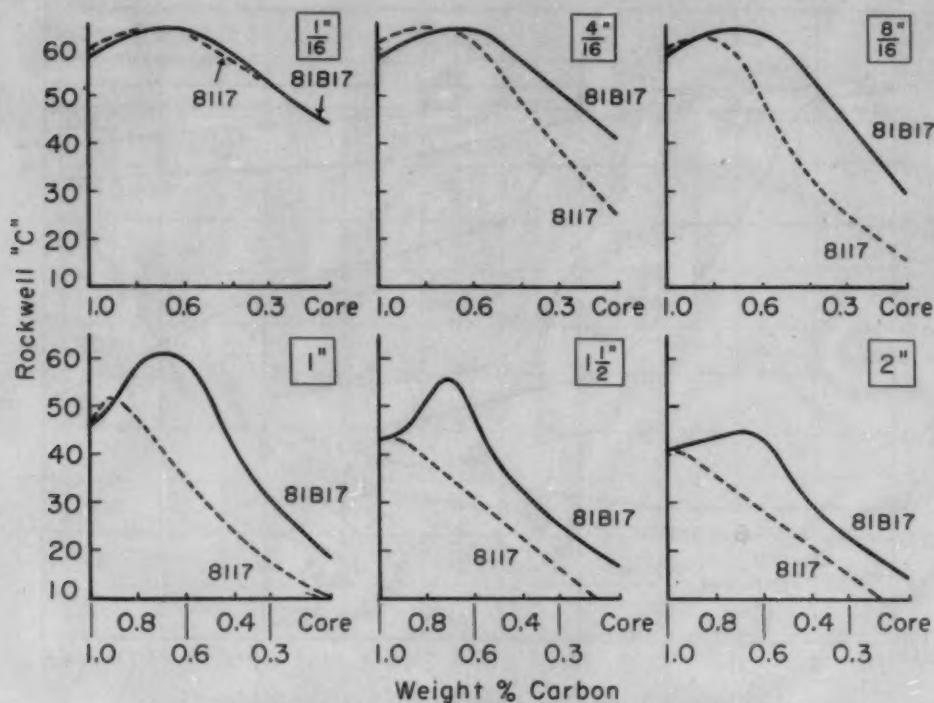


Fig. 9—The Effect of Boron on the Hardenability of a Carburized AISI 8117 Steel at Fixed "J" Distances.

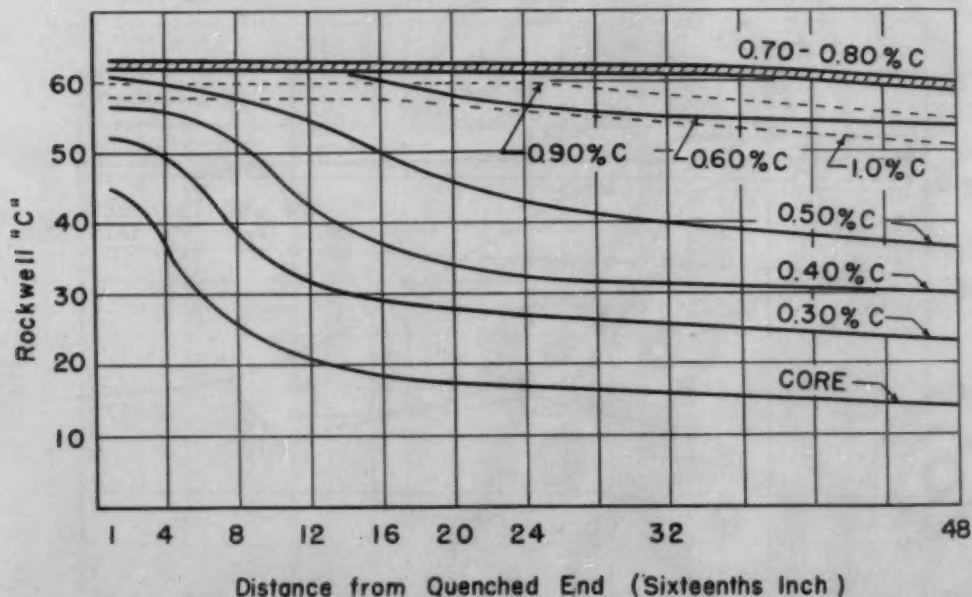


Fig. 10—A Summary of the Hardenability Data From GMR 27 Steel (AISI 8620).

Discussion of Results

Since this investigation served as the initial testing grounds for the trapezoidal end-quench bar, in examining the experimental results particular emphasis was placed on the reproducibility of the hardenability data. Without exception it was found that for a given

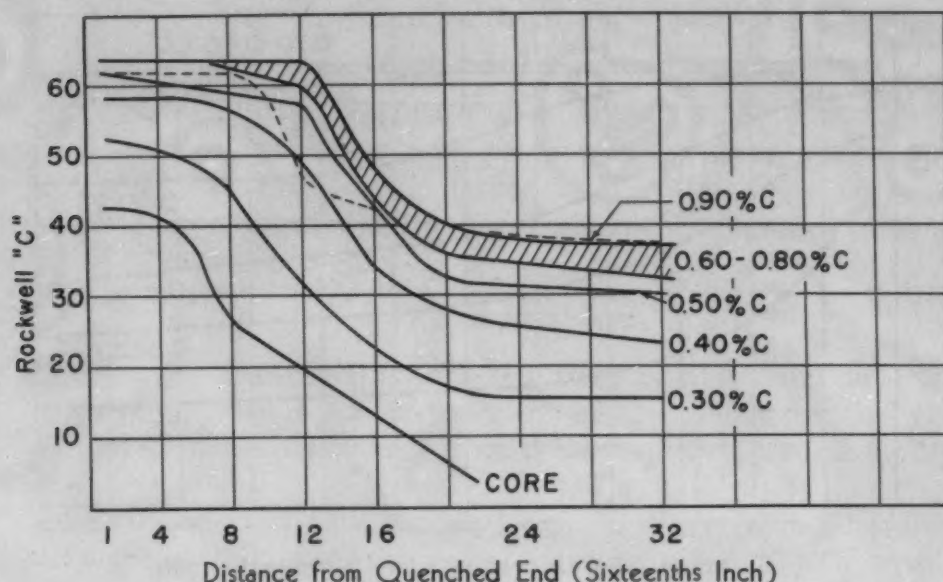


Fig. 11—A Summary of the Hardenability Data From GMR 40 Steel (AISI 50B20).

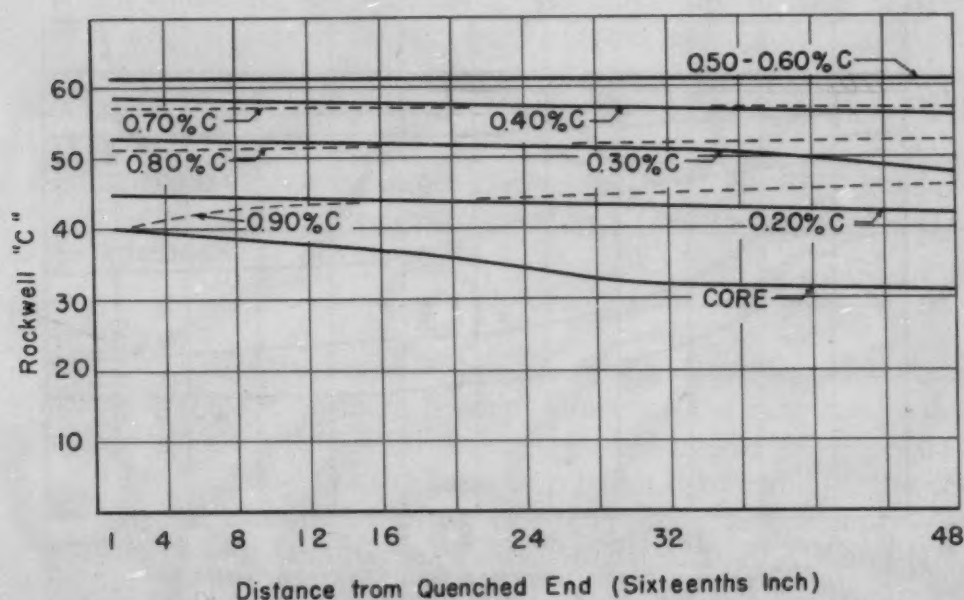


Fig. 12—A Summary of the Hardenability Data From GMR 43 Steel (AISI 3310).

steel the hardenability of the core, and of all carbon levels in the case except those in excess of 0.90%, was accurately reproduced, the average deviation from bar to bar being of the order of ± 1 Rockwell C unit. This degree of accuracy was encouraging in that the carbon gradients produced in a given steel in day-to-day operation did not check any closer than 0.02% carbon at equal case depths.

The order of variation of the measured hardenability of carbon levels in excess of 0.90% was normally of the order of ± 2 Rockwell C units over the entire quenched length of the bar. Since there

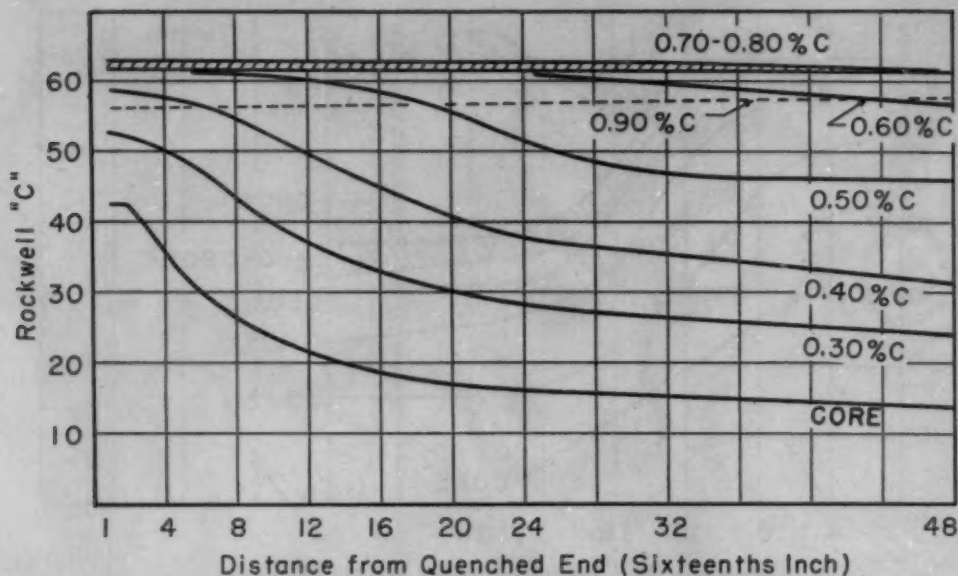


Fig. 13—A Summary of the Hardenability Data From GMR 44 Steel (AISI 4620).

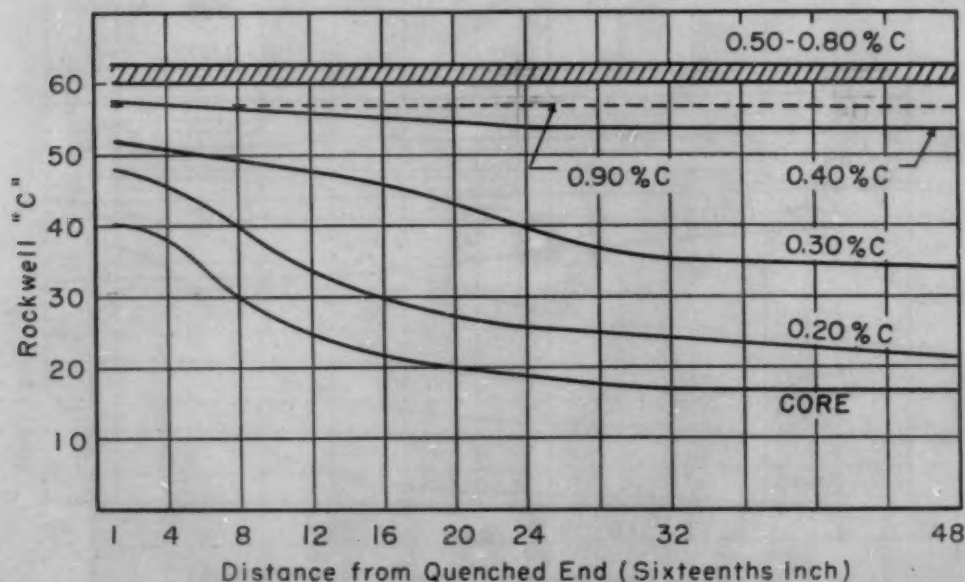


Fig. 14—A Summary of the Hardenability Data From GMR 45 Steel (AISI 4815).

was some possibility that this variation could be attributed to unfavorable cooling effects at the edge of the bar, several bars of 8117 were carburized to a surface carbon of about 0.90% (treatment: 12 hours at 1695 °F or 925 °C). However, the hardenability data at all carbon levels in these bars were in close agreement with the data from 8117 bars whose equivalent carbon levels occurred at much greater case depths. It was concluded that the variation in hardenability in the hypereutectoid regions of the case was due to variations in the transformation characteristics of these regions.

Carbon Gradients

An indication of the order of accuracy with which the carbon levels were located in the bars can be arrived at by comparing the hardness values at the 1/16-inch position in the seven steels at 0.20, 0.30, 0.40, 0.50 and 0.60% carbon. These readings correspond closely with the maximum hardness obtainable on quenching as a function of carbon content.²

Core Hardenability

The core hardenability of each steel is illustrated in Fig. 5. The hardness values are an average of the actual and converted Rockwell C readings obtained from the end-quench bars of the seven steels.

On the basis of core hardenability, these steels may be divided into three groups: (a) high core hardenability—3310; (b) medium core hardenability—4815, 4620, 8620 and 81B17; (c) low core hardenability—8117 and 50B20. Actually, the 50B20 has medium core hardenability for quenching velocities up to the 8/16-inch position on the trapezoidal bar, but at slower cooling velocities drops sharply into the third class. The results suggest that if core hardenability were used as the sole criterion, 8620, 4620, and possibly 81B17 could be used interchangeably.

The effect of boron on the hardenability of the 8117 base composition is seen to be very great, causing a two- to threefold increase in the hardenability of this steel.

Case Hardenability

The effect of increased carbon on the hardenability of each steel is shown in Figs. 6 through 9 which illustrate the case hardenability of each steel at the 0.40, 0.60 and 0.80% carbon levels.

0.40% Carbon—On the basis of relative hardenability, the seven steels may be classified as follows: (a) high hardenability—3310 and 4815; (b) medium hardenability—4620, 8620, 81B17 and 50B20, and (c) low hardenability—8117. The boron has a greater effect in the 50B20 and 81B17 than it had in the core, which is indicative of the variation in the multiplying factor for this element as a function of carbon content.

0.60% Carbon—The relative hardenability of the seven steels at this carbon concentration (see Fig. 7) suggests the following division: (a) high hardenability—4815, 3310, 4620, 8620; (b) medium hardenability—81B17 and 50B20; (c) low hardenability—8117. Although the boron steels cannot be placed in the first group at this carbon level, they are capable of producing as-quenched hard-

²J. L. Burns, T. L. Moore and E. S. Archer, "Quantitative Hardenability", *TRANSACTIONS, American Society for Metals*, Vol. 26, 1938, p. 1-36.

nesses equal to the steels in this group for cooling conditions up to the 12/16-inch position on the trapezoidal bar. However, this does not qualify these steels as potential substitutes for 3310 or 4815, since at lower carbon percentages, for example 0.40%, the boron steels were capable of matching the hardness of the higher alloy steels only over the first 6/16 inch of the end-quench bar. The same type of criticism must be applied to suggestions that the case hardenability of 4620 is equal to that of either 3310 or 4815.

0.80% Carbon—Fig. 8 illustrates the relative hardenability of the seven steels at 0.80% carbon, and from this the following classification is possible: (a) high hardenability—4620, 4815, 8620 and 3310; (b) medium hardenability—81B17; (c) low hardenability—50B20 and 8117. The case hardenability of the 50B20 at 0.80% carbon was slightly less than that at the 0.60% level, while the 81B17 has greater hardenability at 0.80 than at 0.60% carbon. An examination of the data indicates that both steels reached their maximum hardenability at 0.70% carbon, having less hardenability for carbon concentrations either below or above 0.70%. The 50B20 loses enough hardenability in going from 0.70 to 0.80% that it falls slightly below that at 0.60%, while the 81B17 also loses in going from 0.70 to 0.80% carbon but still has hardenability in excess of that at 0.60%. Although the case hardenability of 3310 is high at this carbon concentration, the presence of substantial quantities of retained austenite has effected a decrease in its as-quenched hardness as compared with that at lower carbon percentages.

Carbon Over 0.80%—For increases in carbon over 0.80%, the 4815, 3310 and 4620 all retain their high hardenability, although the as-quenched hardness of each (particularly 3310) is lowered by the presence of retained austenite. At about 1.0%, the 8117 and 81B17 have equivalent hardenability and, more important, the 81B17 has much less hardenability as the carbon increases over 0.80%. Also noteworthy is the fact that the 8620 suffers a decrease in hardenability at carbon percentages in excess of 0.80%. This effect is at direct variance with the use of the multiplying factor for carbon which purports that the hardenability increases with the addition of carbon.

Summary—From these data it is possible to classify the seven steels in the following manner:

(a) 3310—high case and core hardenability. The effect of retained austenite on the hardness becomes progressively greater at carbon concentrations over 0.60%.

(b) 4815—high case and medium core hardenability, with the case hardenability being excellent to 0.40% carbon. The effect of retained austenite on the quenched hardness was observed at carbon levels in excess of 0.90%.

(c) 4620 and 8620—medium case and core hardenability.

(d) 81B17—medium core hardenability. Its case hardenability curves match those of 4620 and 8620 over approximately the first 1 to $1\frac{1}{2}$ inches of the end-quench bar. At positions beyond this they fall sharply below those of 4620 and 8620.

(e) 50B20—hardenability curves for all carbon levels are similar to those of 4620 over about the first $12/16$ inch. Beyond this point, they lie below those of 4620, 8620 and 81B17.

(f) 8117—low case and core hardenability.

Effect of Boron

Although the amount of data on boron grades obtained in this investigation is admittedly small, its significance was such that further consideration seemed justified. In Fig. 9, a comparison is made of the case and core hardenability of 8117 and 81B17 at a number of constant "J" distances. At the $1/16$ -inch position the difference in hardness is of course a straight function of carbon, and no significant differences are observed. However, at the $4/16$ -inch and still more at the $8/16$ -inch position, the effect of boron becomes great, first causing an increase in hardness in the core and in the lower carbon regions, and then at slower cooling conditions, having its greatest effect at progressively higher carbon concentrations. It appears to have its maximum effect on the hardenability of 81B17 at about 0.70% carbon. This figure clearly indicates that at 1% carbon both steels are of comparable hardenability. Also a comparison of the 81B17 hardness gradients at the $1/16$ and 1-inch position strikingly points up the decrease in hardenability at carbon contents over 0.70%.

THE USE OF HARDENABILITY DATA FOR CARBURIZED STEELS

While there is genuine interest in the hardenability of carburized steels, there are complexities involved in the actual application of the hardenability data which must be surmounted. One of the initial steps must be the adoption of a standard method of reporting case and core hardenability, one which will give the greatest amount of information in the most desirable manner. Curves such as those illustrated in Figs. 10 through 14 are suggested for this purpose. First of all, they provide a clear-cut means of classifying case and core hardenability. Also, taking Fig. 14, for example, which shows the hardenability at various carbon levels in the 4815 steel used in this investigation, one finds that a case carburized to a surface carbon 0.70 to 0.80% can be expected to harden to better than Rockwell C-50, at least to the 0.40% carbon level. Also, Fig. 12 warns of the large amount of retained austenite which will be found in a 3310 case carburized to 0.90%.

While there may be some objections that curves of this type necessitate establishing hardenability bands at the various carbon

contents, this task might not be too difficult. In reviewing the curves presented, one observes a tendency for the 0.60 to 0.80% carbon levels to attain maximum hardness over the entire quenched length of the bar. It would not appear that slight changes in the alloying chemistry could decrease the hardenability of these regions.

Experiments are now in progress concerning the application of these data. Although the results are as yet meager, they do indicate that surface hardness and even hardness gradients can be accurately predicted across carburized cases when the surface carbon does not exceed 0.90%.

CONCLUSIONS

1. An end-quench test has been developed which is capable of accurately measuring the case and core hardenability of a carburized steel either at individual carbon levels or as a simple function of case depth.

2. The data obtained from the bar in an investigation of seven grades of commercial carburizing steels indicated the following classification; (a) 3310—high case and core hardenability; (b) 4815—high case hardenability above 0.40% carbon and medium core hardenability; (c) 4620, 8620 and 81B17—medium case and core hardenability. However, the 81B17 case hardenability curves fall below those of 4620 and 8620 at "J" distances beyond 1 to 1½ inches; (d) 50B20—hardenability curves for all carbon levels are similar to 4620 out to about 12/16 inch. Beyond this they fall sharply below; (e) 8117—had the lowest hardenability of all steels tested.

3. The case hardenability of the boron steels was observed to reach a maximum at about 0.70% carbon. Significant decreases were observed at concentrations in excess of this amount.

ACKNOWLEDGMENTS

The authors wish to thank Erwin R. Cprek, whose technical assistance in the experimental work and in the preparation of the final report contributed substantially to the success of this investigation. They are also grateful to William Small and Clark Hathaway of the Chevrolet Forge Division of General Motors Corporation for assistance in the steel procurement program and for forging all of the as-received steels, and the International Nickel Company and the Republic Steel Corporation for providing most of the steel used in this investigation.

DISCUSSION

Written Discussion: By D. Niconoff, Metallurgical Laboratory, Republic Steel Corp., Canton, Ohio.

The authors are to be complimented for developing an ingenious and

much needed method for evaluation of hardenability of carburized steels.

The new method offers obviously numerous advantages over the common procedure of measuring the hardness at several predetermined levels below the carburized surface, and for this reason it will probably find a wide application, at least in the laboratories equipped with the micro-hardness testing machines.

However, the equivalency of the cooling rates obtained on quenching the new trapezoidal bar and the conventional round end-quench bar appears to be somewhat less obvious: Because of greater ratio of its surface area to volume, the trapezoidal bar could be expected to be more susceptible to the air cooling effect prevailing at the upper part of the end-quenched specimens, where the dissipation of heat through thermal conductivity becomes progressively less while the heat loss through convection remains the same.

A reference to Fig. 3 showing the end-quench hardenability curves for both types of specimens clearly indicates that at distances above 14/16 inch from the quenched end the trapezoidal bar gave readings 1 to 3 Rockwell C points higher than the standard specimen.

It would be interesting to know whether the relative position of the curves shown in Fig. 3 is largely accidental, or whether it is indicative of a certain variation in the cooling rates of the end-quench specimens involved in this paper.

Written Discussion: By W. H. Bruckner, research associate professor of metallurgical engineering, Department of Mining and Metallurgical Engineering, University of Illinois.

The concept of hardenability evaluation of one gradient, represented in the carburized case, by means of another gradient, represented by the variation in cooling rate, was originally presented to the ASM by W. E. Jominy and A. L. Boegehold. Shortly after the original paper appeared the discussor made a detailed study of the problem and attempted to show the many facets of the interrelationship involved. The results of that study were contained in the University of Illinois Bulletin No. 13, dated November 21, 1939, with the title "The Hardenability of Carburizing Steels". The large amount of work required to establish the data in the reference cited lends a personal appreciation of the advances made by the authors in their proposed modification of the original Jominy bar as applied specifically to testing carburized steels. The access they have to any point in the bar representing the end-result of imposing the effects of one gradient upon another greatly simplifies the operations required in gathering the data.

In the reference cited the effects of stress upon the transformation characteristics of austenite were considered. It was also considered that the Jominy bar during cooling has instantaneous isotherms practically equivalent to surfaces normal to the bar length; thus stresses could not be developed to the level or complexity of those which would be encountered in actual quenching of steel fully immersed in the quenchant. It was postulated that differences in the transformation behavior of austenite in the Jominy bar and in the immersion-quenched object could exist even when the same composition and cooling rate were involved. The stress history during transformation could not be the same, thus the postulate. The ASM literature has for some time past been concerned with measurement

of the effects of stress upon the transformation; the data may in the near future make it possible to predict the effects of a known stress parameter. It is visualized by the discussor that the excellent method described by the authors when coupled with quantitative knowledge of the specific effect of stress could extend considerably the usefulness of the test. Possibly the greatest present need for consideration of the stress would be where the authors' test specimens have retained austenite. Could the authors cite some values of their "batting average" in predicting hardenability of immersion-quenched rounds or other shapes?

Written Discussion: By Harry B. Knowlton, chief engineer, Materials Engineering, International Harvester Co., Chicago.

The authors are to be complimented upon the very timely presentation of a paper covering an improved method for determining the hardenability of carburized cases of various types of alloy steel. Experiences of the past two years have shown that boron steels and other low alloy steels can usually be substituted satisfactorily for older types of alloy steel containing 0.40 to 0.60% carbon, on the basis of duplicating the hardenability of the original steel. It has been found, however, that carburizing grades of boron steel cannot be substituted satisfactorily for conventional types of steel, on the basis of duplicating the hardenability of the core. As illustrated by the data in this paper, the hardenability of the case cannot be predicted from the hardenability of the core. It has been found that boron has a much greater effect upon the hardenability of low carbon than of high carbon steel.

It has been the writer's experience, during many years of dynamometer testing of case-hardened gears, that at least 90% of the gear failures, either in pitting or breaking, fall within the case. In some exceptional instances, particularly where the case depth is very thin, the properties of the core may be responsible for failure. It is also true that the residual stresses produced by case hardening have an enormous effect upon the performance of the gear. These residual stresses are dependent upon the properties of both case and core, the depth of case and, probably of greatest importance, the relative time at which the case and the core reach their respective M_s points. The M_s point of the core is likely to be several hundred degrees higher than that of the case; consequently it is entirely possible for the outer layers of the core to reach their M_s point before the case hardens.

Without going into great details, suffice it to say that while core properties and stresses set up by hardening of the core may be of some importance, it is still true that the properties of the case are of equal, or greater, importance. The authors of this paper have devised a practical method for the measuring of the hardenability of the case. One of our laboratories has investigated this method, and has reported no difficulty in carrying out the test in this way. The data obtained from such tests should be very valuable in determining steels, which will be satisfactory for case-hardened gears. It may be that other discussors will prefer some other variation of this method. Regardless of which method is used, however, the important point is that we must use some method for determining the hardenability of the case, if we are to effect any conservation in alloying elements for case-hardened gears.

Considering that, in a case-hardened gear, the stress decreases from a maximum at the surface to a minimum (probably near zero) at the neutral axis, it follows that there is definite stress at each depth below the surface. We would prefer to plot the results of the end-quench carburized bar in terms of hardenability at positive depths below the surface, rather than in terms of carbon content. It is granted that the carbon content at different depths below the surface may be different for different steels, but we are still confronted with the necessity for comparing properties of competing steels at positive depths below the surface.

Fig. 15 illustrates our scheme for plotting end-quench hardenability of different layers within the carburized case. It happens this illustration was made from specimens which were tested in the old manner of carbu-

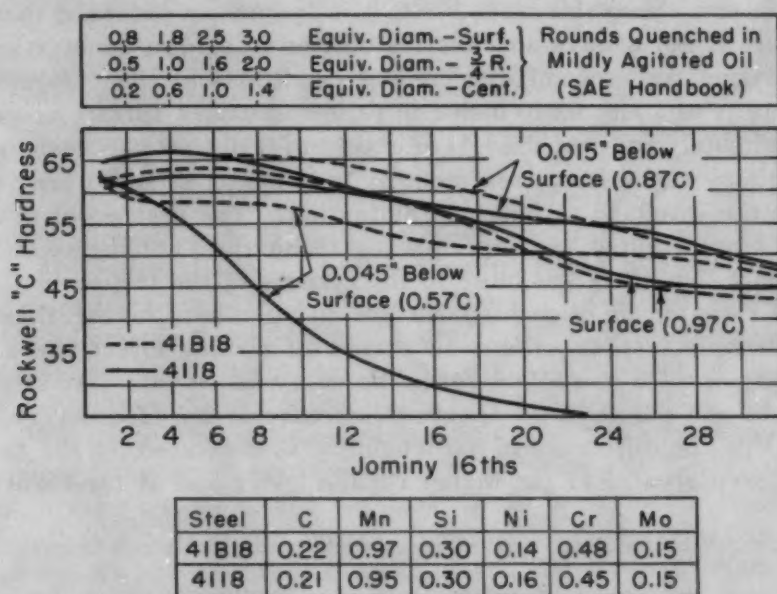


Fig. 15—End-Quench Hardenability of Different Layers Within the Carburized Case of Steels 4118 and 41B18.

riding, hardening and grinding off successive layers. We have since done similar work with the trapezoidal bar, but have not had time to make lantern slides from these data as yet.

We would also call attention to the fact that in our newest hardenability forms, we have placed Boegehold's data on the correlation of Jominy distance with diameters of oil-quenched rounds at the top of the chart. While there is considerable variation in the speed of different oil quenching equipments, we believe that this chart is very helpful in making rough approximations. This particular chart was made to show the effect of boron on 4118 steel. The dotted lines are 41B18, while the solid lines represent 4118. The base heat of steel was the same for both samples.

It will be noted that the boron has a pronounced effect upon the hardenability of the layer at 0.045 inch below the surface. This may be of considerable importance, as we have found that certain heavy duty pinions are inclined to fail within the case, at about a depth of 0.040 to 0.050 beneath the surface. It will be noted that 4118 steel would probably show a

hardness of Rockwell C-55 at 0.045 inch below the surface of a 1 $\frac{3}{4}$ -inch round, while 41B18 would show a similar hardness for sections well over 3 inches in diameter. The hardenability of the surface layers is almost identical for the two steels, but the layer at 0.015 inch below the surface shows an advantage for the boron steel.

Written Discussion: By C. F. Jatzak and A. L. Christenson, research metallurgists, The Timken Roller Bearing Co., Canton, Ohio.

We believe the authors have presented a very useful end-quench test for the measurement of hardenability of carburized steels. Our own limited experience with the trapezoidal end-quench method indicates the test is very reproducible, adequately sensitive and more rapidly performed than the standard carburized Jominy test. It, likewise, presents the good attribute of freedom from grinding. There are, however, two precautions to be observed in employing this test. First, it is frequently observed that a thin copper plate is not always an effective barrier to carbon penetration when gas carburizing, and second, the cooling conditions in the trapezoidal bar at case depths of about 0.040 inch from the carburized surface corresponding approximately to carbon levels in excess of 0.75 to 0.80% carbon (based on the authors' carburizing treatment of 16 hours at 1700 °F) are not comparable to the standard carburized Jominy bar. The first problem may, of course, be circumvented by proper plating techniques, but the second arises from the fact that the areas close to the corners of the trapezoidal section, where the ratio of air quenching surface to volume is higher than in the standard Jominy test, experience increased air cooling effect and a resulting over-all increase in cooling rate. Some evidence that this increase in cooling rate will result in an apparent increase in hardenability is shown in Table IV. The difference in hardenability as measured by the two tests should be even greater at the higher carbon levels and at the higher hard-

Table IV
Comparison of Hardenability Results on Trapezoidal Vs. Standard Jominy End-Quench Bars
Hardenability Expressed as 16's on End-Quench Bar to Rockwell C-60 Position

		Carbon Level					
		4118 Steel*					
		1.10	1.00	0.90	0.80	0.70	0.60
Trapezoidal Bar Run No. 1..	11.0	16.5	14.5	10.0	6.5
Standard Bar Run No. 1.....	9.2	13.5	12.2	8.5	6.0
Trapezoidal Bar Run No. 2..	9.0	13.0	15.5	14.5	10.0	6.0
Standard Bar Run No. 2.....	10.0	13.0	12.0	10.0	6.3
		41B18 Steel					
		1.10	1.00	0.90	0.80	0.70	0.60
Trapezoidal Bar Run No. 1..	15.0	19.0	19.5	13.5	6.0
Standard Bar Run No. 1.....	(9.0)†	16.5	17.0	15.0	7.5
						(0.64 C)	
Trapezoidal Bar Run No. 2..	11.5	15.5	22.0	25.0	17.0	13.0
Standard Bar Run No. 2.....	12.7	19.0	20.0	17.5	13.0
		50B20 Steel					
		1.10	1.00	0.90	0.80	0.70	0.60
Trapezoidal Bar Run No. 1..	15.5	16.5	18.0	16.2	11.5
Standard Bar Run No. 1.....	(11.0)†	14.2	15.0	14.0	10.0
Trapezoidal Bar Run No. 2..	9.2	15.0	16.5	19.0	16.0	12.5
Standard Bar Run No. 2.....	12.0	14.2	14.0	14.2	11.0

*Each steel gas carburized 18 hours at 1700 °F, quenched directly, hardness surveys by Tukon 1 KGM method.

†1.05% carbon level.

Table V
Comparison Cooling Rates in Trapezoidal and Standard End-Quench Bars*

Distance From Quenched End, 16's	ASTM Standard Rates °/Second, 1300 °F	Standard Jominy °/Second, 1300 °F	Test Results†	
			Trapezoidal Bar Distance From Edge	
			0.015	0.040
2	305	550	625°	580°
3	195	150°
4	125	150°	170	144°
5	77
6	56	58°	69	68°
7	42
8	33	34°	39	35
9	26
10	21.4	20.5	24.3	...
11	18.0
12	16.4	16.5	20.3	19.0
13	14.0
14	12.4
16	10.0	9.8	12.6	11.4

*8122 steel type used in test.

†Results standard bar average —2 separate runs.

Results trapezoidal bar (0.015) average—3 separate runs.

(0.040) average—2 separate runs.

enability levels as is indicated by the cooling rate data³ shown in Table V and by the authors' own data on the 8640 steel in their Fig. 3.

The difference shown by our cooling rate and hardenability data, of course, conflicts somewhat with the authors' conclusions that the trapezoidal bar is comparable in cooling characteristics to the standard Jominy. This, we believe, may have arisen from the authors' choice of the 8640 steel for the evaluation of the cooling rate factors in each bar. We realize, of course, that from the authors' standpoint, the 8640 type was an ideal choice since this steel approximates in general the hardenability end-quench curves of most of the carburizing steels evaluated by the authors at carbon levels of 0.80 and lower. However, for an evaluation of cooling rate differences between the trapezoidal and the standard round bar, it is not the best steel type to employ. This steel is bainitic in transformation characteristics and is, therefore, not too sensitive to hardness differences of the type necessary to judge cooling rates from end-quench data. It would seem more appropriate to use a pearlitic-type steel which would show a definite inflection point, since then a horizontal displacement of the inflection point representing a difference in cooling rate would be easily distinguished from end-quench data. We believe that if this were done, the difference in cooling rate which the authors show to exist for the two 8640 end-quench bars in Fig. 3 at 14/16's and beyond, would have been brought closer to the quenched end, say 10/16's. Consequently, their data would have agreed with our cooling rate data of Table V and hardenability data of Table IV.

In closing, it must be emphasized that the above comments concerning the probable differences in cooling conditions of the two test pieces do not infer any loss in usefulness of the trapezoidal test, but only that results from the two tests may be somewhat different, depending on the location of the desired carbon level from the surface. If one is interested only

³Obtained by use of a Hathaway S5-1 Oscillograph (twelve-element high sensitivity galvanometer unit).

in hardenability below the 0.80% carbon level, it is very likely that the trapezoidal results will be close to those of the carburized Jominy end-quench test for most carburizing steels, except perhaps those showing extremely high hardenability potential. Above this carbon level, the hardenability results may be expected to be somewhat greater at all times.

Regardless of this comparison, it is believed that the trapezoidal bar shows enough desirable characteristics over the standard carburized Jominy to warrant full expansion of its use on these merits alone.

Authors' Reply

The authors wish to thank Mr. Niconoff, Professor Bruckner, Mr. Knowlton, and Messrs. Jatczak and Christenson for their comments and discussions on this paper.

In reply to Mr. Niconoff, the curves presented in the paper comparing the hardenability of an 8642 steel as measured by the Jominy and trapezoidal bars were chosen as being typical of the data. On other bars of the same steel which were run but were not reported in the paper, there are a number of instances where the curve from one bar fell just slightly above or below that of the other bar at some point along the quenched length of the bar. This area of discrepancy, which seldom exceeded 3 Rockwell C units, was not observed to fall repeatedly at any one place along the bar. Minor variations in hardenability measurements such as these are easily explained on the basis of normal variations to be expected from bar to bar. The fact, that in all of the experiments completed, the curves from both bars matched so closely, led us to conclude that the cooling conditions during end quenching were the same in each bar.

Professor Bruckner properly points out the difference in stress states between quenched rounds and end-quench bars. We have some work under way at the present time in correlating hardness in carburized quenched rounds and end-quench bars, but do not have sufficient data at this time to determine the "batting average" Professor Bruckner has requested. We hope to have some of these data in the near future. It appears that a somewhat different type of correlation is required than has previously been used on the round end-quench bar due to the presence of the carburized case.

Mr. Knowlton has pointed out the fact that the case hardenability cannot be predicted from core hardenability, and complete hardenability surveys are necessary to aid the alloy conservation program. We were pleased to learn that the trapezoidal bar has been successfully used in the International Harvester Company laboratories. The 4118 and 41B18 hardenability data presented by Mr. Knowlton in Fig. 15 illustrates again the large effect of boron on the hardenability at the lower carbon levels. We have since completed hardenability surveys on trapezoidal bars of the two steels described by Mr. Knowlton. They were from the same heats as used by Mr. Knowlton. The quenching temperature covered a range from 1550 to 1700 °F. We detect a maximum in the 41B18 case hardenability at about 0.80% carbon.

Messrs. Jatczak and Christenson have listed two precautions to be observed in using the trapezoidal bar. The first, regarding the possibility

of carbon leakage through thin copper plate, has been the object of special attention in all of our work to date. We have found that no detectable carbon leakage will occur if the copper plate is properly applied. In work covering the study of over seventy trapezoidal bars, only two were found with carbon leakage, and this was traced to faulty plating. In these bars, the leakage was easily detected by variations in microstructure and hardness. We strongly recommend etching the hardness inspection surface prior to completing the hardness survey. This is the simplest method of detecting such things as carbon leakage and nonuniform carburization.

With regards to the second precaution, since we did not determine cooling rates we appreciate the data which Messrs. Jatzak and Christenson have presented. Further work will be necessary to determine how significant these differences are in relation to the hardenability of steels to be subjected to this test. We agree with Jatzak and Christenson that even though this difference may be real and significant, it does not destroy the usefulness of the trapezoidal bar. Further work on correlation of quenched rounds and the end-quench trapezoidal bar may provide either new correlation charts, or suggest slight dimensional modifications in order to use the older correlation charts.

TRANSVERSE MECHANICAL PROPERTIES IN AN SAE 1045 FORGING STEEL

BY ARTHUR H. GROBE, CYRIL WELLS AND ROBERT F. MEHL

Abstract

Tensile test data for specimens from a high quality SAE forging steel have been accumulated and analyzed statistically. Specimens were cut from the original ingot and from forgings that were reduced 2 to 1, 4 to 1, and 10 to 1. Approximately sixty transverse or ten longitudinal values per each property investigated constituted a sample. The investigation included a study of tensile properties associated with two pearlite and ferrite structures—annealed and air-cooled—and four quenched and tempered structures—quenched to martensite and tempered at 750, 950, 1100 and 1250 °F (400, 510, 595 and 675 °C). Individual tensile blanks were heat treated to have uniformity among specimens and to obtain essentially 100% martensite in the quenched specimens. Sections from the ingot and forgings were given homogenization treatments at 2280 and 2400 °F (1250 and 1315 °C), and tensile specimens were cut and then tested in the annealed condition. The effect of angle of test from the transverse to the longitudinal direction on the tensile properties was determined for the 10 to 1 reduction for specimens in the annealed and quenched and tempered state. Tensile test data are presented for commercial forgings.

THIS laboratory has been engaged for some years in a systematic study of the mechanical properties of forging steels, especially the transverse properties. A summary paper, including in brief form much of the work that has been done, appeared recently (1).^{1, 2} The steels employed were gun steel compositions, for which the

¹The figures appearing in parentheses pertain to the references appended to this paper.

²This reference includes an extended bibliography on the subject; it points out the applicability of the data, applying as well to the data given in the present paper.

This paper is part of a thesis presented by A. H. Grobe to the graduate committee of the Carnegie Institute of Technology in partial fulfillment of the requirements for the degree of Doctor of Science. The research was done for the Office of Scientific Research and Development under Contract No. OEM-956 with the Carnegie Institute of Technology in Pittsburgh.

A paper presented before the Thirty-fourth Annual Convention of the Society, held in Philadelphia, October 18 to 24, 1952. Of the authors, Arthur H. Grobe is research metallurgist, Vanadium-Alloys Steel Co., Latrobe, Pa., Cyril Wells is a member of the staff and Robert F. Mehl is director, Metals Research Laboratory, and head, Department of Metallurgy, Carnegie Institute of Technology, Pittsburgh. Manuscript received April 10, 1952.

composition SAE 4340 may be taken as a prototype. Most of the important metallurgical (and mill) variables were included in the study. In general, it was shown that the reduction in area in the transverse direction (hereinafter designated as RAT) is not a single-valued property, but a statistical one, and must therefore be represented by a distribution curve, characterized by an average, \bar{X} , and a standard deviation, σ ; the spread of values was found to range from 18% RAT in the best case to 40% in the worst, with the value of σ varying from 3% to 8%. Both statistical values and the skewness of the distribution curve vary with change in metallurgical (and mill) variables.

These studies related to alloy steels in the quenched and tempered condition. The present paper extends this earlier work to plain carbon hypoeutectoid steels of the composition SAE 1045. It includes similar studies on this steel in the quenched and tempered condition, and also studies on this steel in the normalized and in the annealed conditions. It comprises a study of the effect of different degrees of reduction by forging in the steps of 2 to 1, 4 to 1, and 10 to 1; the effect of heat treatment, including (a) annealing from 1500 °F (815 °C), (b) normalizing from 1500 °F (815 °C), (c) homogenization for 12 and 48 hours, respectively, at 2280 and 2400 °F (1250 and 1315 °C), followed by furnace cooling from 1500 °F (815 °C), and (d) quenching from 1500 °F (815 °C) followed by tempering at 1250, 1100, 950 and 750 °F (675, 595, 510 and 400 °C), respectively; (e) the effect of angle of test piece with respect to forging-fiber direction. These studies should be of interest to those concerned with the engineering behavior of forgings of this familiar composition.

MATERIALS

The earlier work demonstrated that furnace practice is an important variable. In particular, the presence of idiomorphic crystalline inclusions such as alumina ("refractory inclusions") provides a marked skewness to the distribution curve of RAT, that is, gives a large number of values of low RAT which provides a "tail" to the distribution curve. For this reason it is particularly important to give details concerning the practice employed in making the steel.

Three commercial ingots, 18 by 18 inches weighing 5500 pounds each, were made at the Homestead Works of the Carnegie-Illinois Steel Corporation. These were basic open-hearth steel, of commercial grade. The ingots were numbers 11, 12, and 13 from a total of 34 ingots. They were big-end-up ingots, with hot-top; they tapered from 18 by 18 inches at the top to 14 by 14 inches (in 58½ inches) at the bottom.⁽¹⁾ The materials charged in the furnace are given in Table I, together with the furnace additions.

The heat of SAE 1045 steel, from which the three ingots were

Table 1
Materials Charged and Added in Open-Hearth and in Ladle

Materials Charged			Pounds
Limestone			13,600
Ore			35,000
Scrap, heavy			98,600
Scrap, light			200
Iron, hot			150,000
Iron, cold			31,300
Total Metal Charged			280,100
Total Iron			181,300
Per Cent Iron			64.9%
Additions			
	Furnace-Pounds	Ladle-Pounds	
Ore	3,500	...	
Staflux	5,000	...	
Ferro-Silicon 50%	850	
Silico-Manganese	2,000	...	
Ferro-Manganese	800	50	
Coal	125	
Aluminum Shot	150	

taken, took 3 hours to charge; 5 hours and 55 minutes to melt down; 2 hours and 51 minutes later the heat was blocked. Twelve hours and 5 minutes after the beginning of charging, the heat was tapped, at 2960 °F (1625 °C), into a clean ladle. The ladle analysis was: 0.48% carbon, 0.86% manganese, 0.018% phosphorus, 0.027% sulphur, 0.20% silicon, 0.03% nickel, 0.02% chromium and 0.01% copper; the materials had been so selected as to provide a steel with low percentages of residual metals. The molds used were cold, coated with tar. The average time for filling the mold was 30 seconds; the hot-top was filled 30 to 37 seconds later. The metal was active in the mold.

The ingots stood for 1½ hours and then, in a further period of 1½ hours, were put in the soaking pits, and held at 2350 °F (1290 °C) for 5¼ hours. Ingot No. 13 was removed for cooling, while ingots Nos. 11 and 12 were immediately rolled on an open-pass 40-inch mill to 12¾ by 12¾-inch blooms. Ingot No. 13 and the blooms from ingots Nos. 11 and 12 were cooled to 1200 °F (650 °C) and then covered with slag until they reached 200 °F (93 °C), requiring 8 days. The blooms were then cropped and chipped.

The two 12¾ by 12¾-inch blooms were forged on a 1000-ton steam press to a reduction in section area of (very nearly) 2 to 1 (12¾-inch round), 4 to 1 (9½-inch round), and 10 to 1 (6-inch round). In heating for forging, one end was put in the furnace and forged when it had reached 2100 to 2200 °F (1150 to 1205 °C), and then that section hot-cut; this was continued, in similar steps, until the whole of the piece had been forged, thus providing essentially equal heating times for all sections. The pieces were given a "hydrogen-removal" treatment, consisting of holding at 1300 °F

(705 °C) followed by a furnace cool to below 750 °F (400 °C), followed then by a reheating to 1300 °F (705 °C) and a subsequent slow cooling to room temperature.

Macro- and microexaminations were made on each end of each forging, on the unforged ingot No. 13, from pieces cut from the ends of the cropped forgings, and 3 inches below the hot-top of the ingot. Each of these sections was sulphur-printed and macroetched, and samples were taken for microscopic examination for inclusions. Chemical analyses were made to appraise chemical heterogeneity.

The sulphur prints on all samples exhibited the same general pattern, showing an even distribution with only a very slight tendency to concentration at the center. This effect was slightly greater in the large forgings and the ingot than in the small forgings. The macroetch tests showed no forging defects, flakes, or large pits; the dendritic pattern was pronounced in the 12¾-inch forgings, diminished with increasing forging reduction, and was undetectable in the smallest forging. Evidently this was a good quality commercial forging steel. An attempt was made to rate the samples for cleanliness by the SAE method, but the steel was almost too clean to furnish a rating; only very infrequent inclusions ½ inch long at 100 diameters could be found, and these were disjointed. The average rating for the background of the edge and half-radius was A; centers occasionally gave a B rating; yet inclusions ½ inch long were still very infrequent.

From the several forgings, longitudinal and transverse tensile specimen blanks with the dimensions 5/8 by 5/8 by 4 inches were cut as near to the half-radius of the forging as possible; similar pieces were cut from the ingot. Four transverse and 4 longitudinal specimens were cut from a single section of the 6-inch forging; 10 transverse and 12 longitudinal specimens from the 9½-inch forging, 22 transverse and 44 longitudinal specimens from the 12¾-inch forging, and 52 transverse and 80 longitudinal specimens were cut from a section of the ingot. All of the specimens were taken from sections of the forgings originating in the upper two-thirds of the original ingot (1); the specimens from the ingot were taken from an 8-inch slice cut 3 inches below the hot-top. Sixty transverse and at least 10 longitudinal specimens were used to provide data for each sample as noted below. In all, approximately 3000 tensile tests were made.

SPECIMEN PREPARATION

The heat treating of these forgings was performed on small pieces, for this is a shallow hardening forging steel. In order to produce uniform ferrite-pearlite structures in annealing but especially in normalizing and also to produce a fully martensite structure (through hardening) on quenching prior to tempering, small pieces

were necessarily employed. In order to appraise the depth of hardening, a series of rounds of various sizes was quenched into an iced 5% NaOH solution after austenitizing at 1500 °F (815 °C); it was found that a 1/2-inch round would quench to martensite throughout the cross section—this size was adequate for the preparation of a 0.357-inch diameter tensile bar employed throughout the work. All quenching was done in this way; tempering was conducted at the temperatures indicated for periods of 2 hours. Annealing and normalizing treatments were performed on the blanks as noted above.

The quenching operations were performed as follows:

A rack was devised consisting of two bricks standing parallel in the furnace; across the tops of these bricks were laid steel rods. These rods were threaded through holes drilled in the ends of the sample blanks, which thus hung from the rods; each rod held five sample blanks; after heating, a rod with its five pendant bars was removed and the assembly quenched; the quenched sample blanks were then placed immediately in a salt tempering bath, holding thirty specimens at a time.

The normalizing treatment was performed with the same type of rack; 30 sample blanks were austenitized for 1 1/2 hours, and the whole rack removed to cool in air; a thermocouple was inserted into the center of one specimen, and the following temperature course noted: the temperature fell from 1500 to 1245 °F (815 to 675 °C) in 3 3/4 minutes, then a slight recalescence occurred, with the fall in temperature recurring after 6 minutes. Between 1380 and 1245 °F (750 and 675 °C) the rate of temperature change was 55 degrees per minute. The annealing treatments were performed in a similar fashion, the racks were left in the furnace and the specimens cooled with the furnace; thermocouple readings showed the rate of cooling between 1380 and 1245 °F (750 and 675 °C) to be 3 degrees per minute. A protective atmosphere consisting chiefly of CO was employed for all austenitizing treatments.

The quench-and-temper treatment and the normalizing treatment were each done on batches of 30 specimens. Two such batches, 60 specimens, provided data for one distribution curve. In the quenching operation, at least one specimen blank from each batch was examined for through-quenching.

After heat treatment, the sample blanks were cut to a length of 3 1/2 inches and machined to a tensile specimen of 0.357 inch diameter with a 1.4-inch gage length. Tensile data were taken on a 60,000-pound Southwark-Emery testing machine, using a Selsyn recording extensometer; the following data were recorded: yield strength at 0.01% offset, tensile strength and percentage elongation in 1.4 inches. The percentage reduction in area was measured on the fractured sample, and the nature of the fracture observed.

STATISTICAL INTERPRETATION OF RESULTS

Because of space restriction, an account of the statistical interpretation of results must of necessity be quite superficial. Actually this interpretation is based on results of intense statistical studies; these involve applications of tests of significant differences as well as (a) determinations of whether from a practical point of view sampled populations may be considered normal and sampling random, and (b) determinations of limits between which sampled population statistics

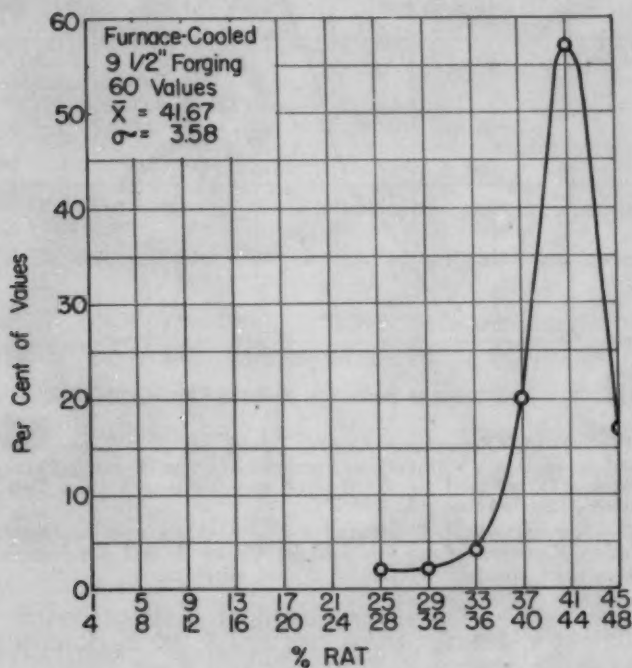


Fig. 1—RAT Frequency Curve for the Furnace-Cooled Specimens From the 9½-Inch Forging.

—average, standard deviation, etc.—are expected to fall with a given certainty. In addition, these studies included estimates of sampled population statistics taking into account sample size effect; they also involved sampling experiments utilizing thousands of data to indicate at least approximately the degree of confidence justified in conclusions given in this paper.

The importance of certain statistics for use in summarizing and interpreting a large amount of data, such as have been accumulated in the present investigation, is apparent from results and discussions in earlier publications (1, 2). Of the statistical methods employed in this research for evaluating quality and the influence of various factors on that quality, some have been described by Olds and Wells (2); others by Snedecor (3) and Ezekiel (4). Sample average, \bar{X} , which measures central tendency, and sample standard deviation, σ , which measures dispersion, together give an estimate of quality.

Thus the estimated RAT quality of furnace-cooled specimens from the 9½-inch forging (Fig. 1) is indicated by $\bar{X} = 41.67\%$ and $\sigma = 3.58\%$ taken together; a better estimate is the frequency curve. Curves A and B (Fig. 2) are both estimates of the RAT quality of quenched and tempered specimens from a forging; frequency

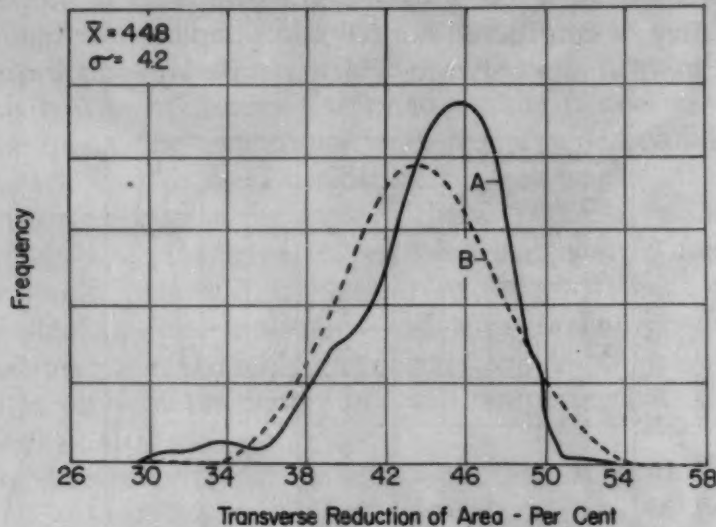


Fig. 2—A—Frequency Curve Based on 277 Transverse Reduction of Area Values for Specimens From a High Quality Forging Quenched to Martensite and Tempered to a Tensile Strength of About 165,000 Psi.

B—Normal Curve Computed From Average and Standard Deviation Figures. Area enclosed by Curve A and abscissa is equal to area enclosed by Curve B and abscissa.

Curve A is a better estimate than normal Curve B, computed from average and standard deviation values.

It is assumed, and with sufficient justification for most practical purposes, that for each sampled population (a) the true average falls between $\bar{X} + (3\sigma/\sqrt{n})$ and $\bar{X} - (3\sigma/\sqrt{n})$, (b) the true standard deviation between $\sigma + (3\sigma/\sqrt{2n})$ and $\sigma - (3\sigma/\sqrt{2n})$ and (c) almost all individual values between $\bar{X} + 3\sigma$ and $\bar{X} - 3\sigma$, where n is the number of values in the sample.

CORRELATION AND REGRESSION

In order to obtain information about the relation between yield strength and longitudinal reduction of area, and yield strength and transverse reduction of area in materials investigated, correlation coefficients and regression line equations have been computed (Table II). In addition, limits between which correlation coefficients and linear regression lines for sampled populations are expected to fall have been calculated, as have also the limits between which practically all individual values in each of several sampled populations probably fall (Table III).

Table II

Results of Correlation and Regression Studies of Yield Strength and Longitudinal Reduction of Area Values for Specimens Containing Mixtures of Ferrite and Pearlite and Coming From an SAE 1045 Steel Reduced 10 to 1, 4 to 1, 2 to 1, and 1 to 1 by Forging

Reduction by Forging	No. of Tests	Correlation Coefficient r	Limits Between Which ρ Is Expected to Fall		Equation of Regression Line ($Y_s = a + bX$)	Limits Between Which β in Equation $Y = a + \beta X$ Is Expected to Fall	
			Max.	Min.		Max.	Min.
10 to 1	54	0.73	0.86	0.56	$Y_s = 33.8 + 0.34X$	0.44	0.24
4 to 1	40	0.92	0.97	0.81	$Y_s = 26.0 + 0.46X$	0.55	0.37
2 to 1	60	0.44	0.67	0.13	$Y_s = 29.2 + 0.37X$	0.63	0.11
1 to 1	24	-0.13	0.43	-0.79	$Y_s = 38.9 - 0.05X$	0.27	-0.37

Note: Each unit of yield strength, X , is 1000 psi. Each unit of longitudinal reduction of area, Y , is 1%.

r = correlation coefficient for sample.

ρ = correlation coefficient for sampled population.

$Y_s = a + bX$ is the regression line equation for the sample.

$Y = a + \beta X$ is the regression line equation for the sampled population.

Y_s , a , and b are estimates of Y , a , and β ; a , b , a , and β are constants.

For any given value of yield strength, X , the best estimate of longitudinal reduction of area, Y , would be Y (true average of all Y values in sampled population associated with the given value of X) if a and β were known; the best estimate of Y is Y_s .

To assist interpretation, results such as presented in Table III may be plotted to indicate graphically the limits between which the sampled population regression line is expected to fall and practically all individual longitudinal reduction of area values fall when yield strength lies between 82,000 psi and 182,000 psi.

TENSILE TEST RESULTS FOR THE ANNEAL AND NORMALIZE TREATMENTS

Two different heat treatments were used to produce ferrite and pearlite structures: a furnace cool with a cooling rate of approximately 3 °F per minute and an air cool with a cooling rate of approximately 55 °F per minute. The structures obtained from the 9½-inch forging after furnace cooling and after air cooling are illustrated in Figs. 3 and 4, respectively. The air-cooled specimens have less fer-

Table III

Data Showing Limits Between Which (A) Points on the Regression Line $Y = a + \beta X$ and (B) Practically All Individual Values of Longitudinal Reduction of Area Are Expected to Fall When Values Are for Specimens From a Unit Quenched to Martensite and Tempered to Yield Strength Values As Indicated

Forging Reduction	No. of Tests	Selected Values of Yield Strength (X (1 unit = 1000 psi))	Limits Between Which Y Probably Falls When the Selected Values of X Are as Indicated		Limits Between Which Practically All Individual Values of Longitudinal Reduction of Area Probably Fall	
			Max. (%)	Min. (%)	Max. (%)	Min. (%)
10 to 1	39	182.1	53.8	50.8	58.1	46.5
		162.1	56.1	53.7	60.4	49.4
		142.1	58.4	56.6	62.7	52.3
		122.1	60.9	59.3	65.2	55.0
		102.1	63.6	61.8	67.9	57.5
		82.1	66.5	64.1	70.8	59.8

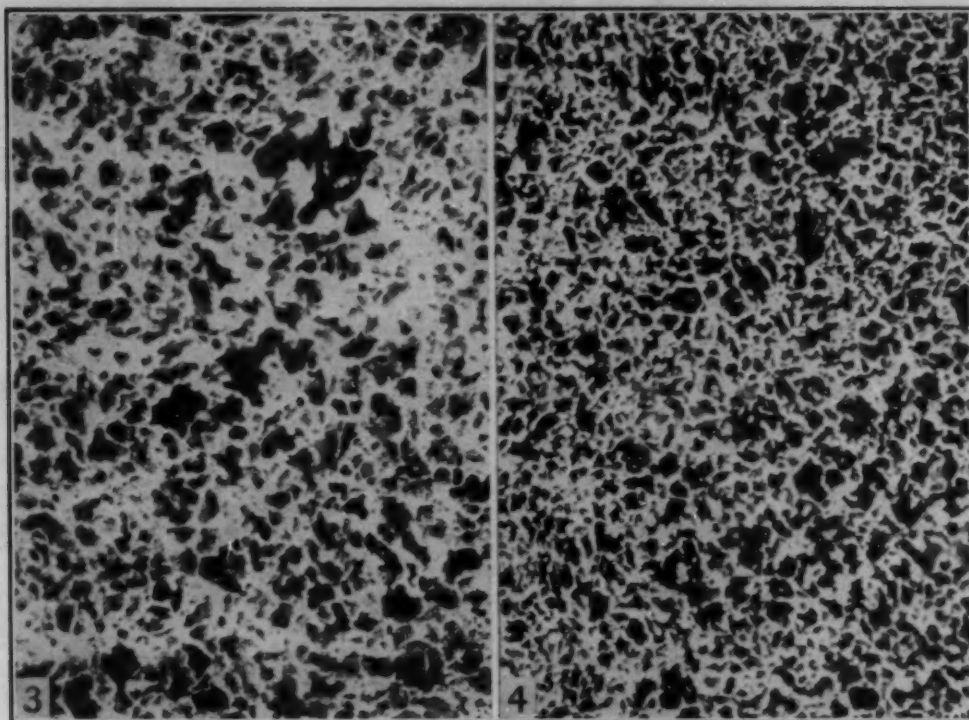


Fig. 3—Microstructure of the Furnace-Cooled Specimens From the $9\frac{1}{2}$ -Inch Forging. Picral etch. $\times 100$.

Fig. 4—Microstructure of the Air-Cooled Specimen From the $9\frac{1}{2}$ -Inch Forging.

rite and finer pearlite than the furnace-cooled blanks. Although these photomicrographs are for the $9\frac{1}{2}$ -inch forging, they are representative of all of the forgings and the ingot.

The results obtained from the tensile tests on the ferrite and pearlite structures resulting from furnace-cool and air-cool treatments of unhomogenized material are listed in the first two major columns of Tables IV and V.

Yield strength is affected more by conditions of testing, such as specimen alignment, than is tensile strength. The variation among yield strength values is normally much higher than that among tensile strength values; standard deviation, σ , is on the average about twice as large for yield strength as for tensile strength. Transverse tensile strength data (Table IV) show the maximum difference among \bar{X} values for the furnace-cooled specimens to be 3100 psi and for the air-cooled specimens to be 3800 psi. Transverse yield strength data show the maximum difference among \bar{X} values for the furnace-cooled specimens to be 6900 psi and for the air-cooled specimens to be 9100 psi. One significant fact revealed by these data is that the ingot has a lower yield strength average than any of the forged reductions. Transverse elongation and transverse reduction of area curves (5) based on data given in Table IV are similar; when a RAT curve has a "tail", a skewness toward lower values, as does

Table IV
Tensile Test Results for Transverse Specimens Containing Ferrite and Pearlite. Approximately 60 Values Constituted a Sample

Property	Reduction by Forging	Furnace-Cooled From 1500 °F					Air-Cooled From 1500 °F					Homogenized 12 Hours at 2280 °F Then Furnace-Cooled From 1500 °F					Homogenized 48 Hours at 2400 °F Then Furnace-Cooled From 1500 °F				
		\bar{X}	σ	$\frac{3\sigma}{\bar{X}}$	$\frac{3\sigma}{\sqrt{n}}$	$\frac{3\sigma}{\sqrt{2n}}$	\bar{X}	σ	$\frac{3\sigma}{\bar{X}}$	$\frac{3\sigma}{\sqrt{n}}$	$\frac{3\sigma}{\sqrt{2n}}$	\bar{X}	σ	$\frac{3\sigma}{\bar{X}}$	$\frac{3\sigma}{\sqrt{n}}$	$\frac{3\sigma}{\sqrt{2n}}$	\bar{X}	σ	$\frac{3\sigma}{\bar{X}}$	$\frac{3\sigma}{\sqrt{n}}$	$\frac{3\sigma}{\sqrt{2n}}$
Yield Strength at 0.01% Offset psi/1000	10 to 1	43.0	2.30	0.90	0.63	0.67	56.9	2.46	0.95	0.67	0.67	42.3	3.38	1.31	0.93	0.93	44.5	2.29	1.22	0.86	0.86
	4 to 1	44.8	1.51	0.59	0.42	0.33	54.9	3.01	1.17	0.83	0.83	41.81	1.58	0.62	0.44	0.44	44.1	2.32	0.92	0.65	0.65
	2 to 1	42.9	2.13	0.82	0.58	0.57	55.2	2.07	0.80	0.57	0.57	41.4	2.96	1.15	0.81	0.81	43.3	2.15	0.83	0.59	0.59
Tensile Strength psi/1000	1 to 1	37.9	3.09	1.21	0.85	0.83	47.8	2.99	1.17	0.83	0.83	41.4	2.45	0.94	0.69	0.69	43.8	2.10	0.81	0.58	0.58
	10 to 1	89.0	1.16	0.46	0.32	0.32	99.8	3.03	1.16	0.83	0.83	93.3	0.74	0.29	0.20	0.20	91.5	0.71	0.37	0.26	0.26
	4 to 1	91.9	0.49	0.19	0.14	0.14	100.4	1.74	0.68	0.48	0.48	91.3	0.48	0.19	0.13	0.13	91.2	0.53	0.21	0.15	0.15
Per Cent Elongation in 1.4 Inches	2 to 1	91.8	0.79	0.31	0.22	0.22	101.3	1.84	0.71	0.50	0.50	93.0	0.85	0.33	0.23	0.23	91.2	0.53	0.21	0.15	0.15
	1 to 1	92.1	0.70	0.27	0.19	0.19	103.6	1.28	0.50	0.36	0.36	91.5	0.82	0.33	0.23	0.23	89.8	1.03	0.40	0.29	0.29
	10 to 1	22.6	2.46	0.96	0.68	0.68	18.5	3.39	1.31	0.93	0.93	18.7	2.45	0.95	0.67	0.67	23.2	2.83	1.50	1.06	1.06
Per Cent Reduction of Area for 0.357- Inch Dia. Specimen	4 to 1	22.6	1.59	0.63	0.44	0.44	21.7	2.24	0.88	0.62	0.62	24.5	2.28	0.90	0.63	0.63	24.1	2.28	0.92	0.65	0.65
	2 to 1	20.9	2.46	0.95	0.68	0.68	16.1	3.26	1.26	0.89	0.89	20.5	1.74	0.67	0.48	0.48	22.7	2.17	0.84	0.60	0.60
	1 to 1	19.8	1.37	0.54	0.38	0.38	16.3	1.81	0.71	0.50	0.50	23.0	1.43	0.58	0.41	0.41	24.2	1.57	0.62	0.44	0.44
	10 to 1	36.7	5.32	2.08	1.47	1.47	32.0	7.56	2.93	1.52	1.52	32.0	6.17	2.39	1.69	1.69	34.9	5.68	3.02	2.13	2.13
	4 to 1	41.7	3.58	1.39	0.98	0.98	44.1	5.60	2.19	1.55	1.55	34.3	5.21	2.05	1.45	1.45	37.1	5.57	2.26	1.59	1.59
	2 to 1	36.4	5.01	1.94	1.37	1.37	29.3	6.92	2.70	1.91	1.91	37.2	4.31	1.67	1.18	1.18	34.4	4.72	1.83	1.29	1.29
	1 to 1	33.2	3.02	1.18	0.83	0.83	30.2	4.33	1.69	1.20	1.20	34.6	2.93	1.17	0.83	0.83	36.5	4.10	1.62	1.14	1.14

Table V
Tensile Test Results for Longitudinal Specimens Containing Ferrite and Pearlite. Each Sample Consisted of at Least 9 Values

Property	Reduction by	Furnace-Cooled From 1500 °F.					Air-Cooled From 1500 °F.					Homogenized 12 Hours at 2280 °F. Then Furnace-Cooled From 1500 °F.					Homogenized 48 Hours at 2400 °F. Then Furnace-Cooled From 1500 °F.				
		\bar{X}	σ	$\frac{3\sigma}{\bar{X}}$	$\frac{\sigma}{\sqrt{n}}$	$\frac{3\sigma}{\sqrt{2n}}$	\bar{X}	σ	$\frac{3\sigma}{\bar{X}}$	$\frac{\sigma}{\sqrt{n}}$	$\frac{3\sigma}{\sqrt{2n}}$	\bar{X}	σ	$\frac{3\sigma}{\bar{X}}$	$\frac{\sigma}{\sqrt{n}}$	$\frac{3\sigma}{\sqrt{2n}}$	\bar{X}	σ	$\frac{3\sigma}{\bar{X}}$	$\frac{\sigma}{\sqrt{n}}$	$\frac{3\sigma}{\sqrt{2n}}$
Yield Strength at 0.01% psi/1000	Forging																				
	10 to 1	41.9	3.12	1.71	1.21	0.86	54.8	0.20	0.12	0.08	0.08	43.6	1.49	1.49	1.05	1.05	42.4	1.20	1.14	0.81	0.81
	4 to 1	41.3	2.21	1.21	0.86	0.61	56.2	0.85	0.81	0.57	0.57	43.4	1.36	1.29	0.91	0.91	43.7	1.42	1.35	0.95	0.95
	2 to 1	43.7	1.57	0.86	0.61	0.42	47.0	4.26	2.33	1.65	1.65	46.3	1.55	1.47	1.04	1.04	42.2	1.17	1.11	0.78	0.78
Tensile Strength psi/1000	1 to 1	42.1	1.14	1.08	0.76	0.54	54.4	1.29	1.04	0.73	0.73	43.1	1.04	0.99	0.70	0.70	44.7	1.55	1.47	1.04	1.04
	10 to 1	90.8	0.79	0.43	0.31	0.23	101.2	1.06	0.64	0.45	0.45	91.8	0.40	0.38	0.27	0.27	90.4	0.80	0.76	0.54	0.54
	4 to 1	92.7	0.60	0.33	0.23	0.16	102.0	0.89	0.85	0.60	0.60	92.8	0.40	0.38	0.27	0.27	91.4	0.49	0.47	0.33	0.33
	2 to 1	92.7	0.53	0.30	0.21	0.16	102.0	0.82	0.45	0.33	0.33	91.2	0.40	0.38	0.27	0.27	90.8	0.60	0.57	0.40	0.40
Per Cent Elongation in 1.4 Inches	1 to 1	91.0	0.45	0.42	0.30	0.21	97.9	0.74	0.60	0.42	0.42	91.1	0.30	0.29	0.20	0.20	91.0	0.00	0.00	0.00	0.00
	10 to 1	25.3	0.72	0.40	0.28	0.15	22.6	0.35	0.21	0.15	0.15	24.0	0.77	0.74	0.52	0.52	26.6	0.49	0.46	0.33	0.33
	4 to 1	23.5	0.42	0.23	0.16	0.10	23.2	0.34	0.33	0.23	0.23	24.0	0.46	0.43	0.31	0.31	25.6	0.49	0.46	0.33	0.33
	2 to 1	22.3	0.81	0.44	0.31	0.25	21.5	0.65	0.35	0.25	0.25	26.1	0.30	0.29	0.20	0.20	25.2	1.33	1.26	0.89	0.89
Per Cent Reduction of Area for 0.357- Inch Dia. Specimen	1 to 1	22.8	0.62	0.58	0.41	0.28	22.4	0.81	0.65	0.46	0.46	24.8	0.60	0.57	0.40	0.40	25.1	0.54	0.51	0.36	0.36
	10 to 1	50.2	1.66	0.91	0.64	0.41	51.3	0.55	0.33	0.23	0.23	40.6	1.11	1.05	0.74	0.74	43.8	1.25	1.19	0.84	0.84
	4 to 1	44.8	0.57	0.31	0.22	0.16	52.3	0.90	0.85	0.60	0.60	38.9	0.54	0.51	0.36	0.36	43.9	1.12	1.07	0.75	0.75
	2 to 1	43.6	2.04	1.12	0.79	0.54	48.6	0.92	0.50	0.36	0.36	45.5	0.92	0.88	0.62	0.62	43.1	0.70	0.66	0.47	0.47
	1 to 1	37.0	0.94	0.90	0.63	0.41	36.3	2.63	2.11	1.49	1.49	39.8	0.87	0.83	0.59	0.59	42.1	0.94	0.90	0.63	0.63

the curve in Fig. 1, a comparable elongation curve has also a tail. The only difference is that the σ values are smaller for the elongation curves than for the RAT curves. The ingot RAT and elongation curves do not have tails, but the frequency curves for the forgings are skewed toward low values. Also the σ 's and, therefore, the total spreads are lower for the ingot than for the forged material. The fact to be noted here is that the ingot does have a spread of transverse ductility values and this spread is quite high.

Data in Tables IV and V, taken together, show that variations among yield strength and tensile strength values for furnace-cooled and air-cooled transverse specimens from unhomogenized material is on the average larger than among comparable yield strength and tensile strength values for furnace-cooled and air-cooled longitudinal specimens. Variations among reduction of area and elongation values for furnace-cooled and air-cooled transverse specimens from unhomogenized material is on the average between 4 and 5 times larger than among reduction of area and elongation values for furnace-cooled and air-cooled longitudinal specimens. A much larger variation of RAT than RAL quality, such as is observed, means that in the determination of RAT and RAL quality, with a given precision, many more RAT than RAL data are needed. This is why, as already pointed out, RAT samples (usually 60 values per sample) obtained are with few exceptions much larger than RAL samples (usually 10 values per sample).

The longitudinal reduction of area (RAL) averages (Table V—first two major columns) for ferrite and pearlite structures reveal an interesting phenomenon: when the tensile strength is increased, the RAL is also increased for the forged steel. This increase in RAL is not accompanied by an observed similar increase in the elongation of the longitudinal test specimens, perhaps partly because the elongation is a less sensitive measure of ductility. In addition, the average RAT (Table IV—first two major columns) is not consistently changed by the increase in tensile strength though in all cases the σ 's are higher for the air-cooled RAT determinations. In brief, the increase in tensile strength by increasing the rate of cooling increases the average RAL for the forged material but does not appear to raise either the average longitudinal elongation or the average RAT. This effect does not extend to the unreduced ingot. Here the increase in tensile strength has little or no effect on the other tensile properties beyond that of increasing the spreads for all properties, except transverse yield strength. Improved RAL quality resulting from increased rate of cooling is found only in ferrite plus pearlite structures. Increased rates of cooling are used commercially, knowingly or unknowingly, to increase RAL values, as is reported in the section on commercial forgings.

The increase of longitudinal reduction of area with an increase of tensile strength produced by a more rapid rate of cooling is not new but is also not generally recognized. Gensamer et al (6 and 7) have shown that the RAL values for a hypoeutectoid steel increase to a maximum and then decrease as the temperature for isothermal reaction to ferrite and pearlite is lowered while the tensile strength increases constantly.

Correlation coefficients and regression line equations have been calculated utilizing RAL and yield strength data for furnace-cooled and air-cooled specimens from unhomogenized material. Results are listed in Table II as are also computed limits between which correlation coefficient, ρ , and regression coefficient, β , for sampled populations are expected to fall. This information justifies confidence in the validity of conclusions which have already been drawn and covers the subject of the effect of cooling rate on RAL quality of material containing ferrite and pearlite. It is not known whether the observed increase of RAL with yield strength, as the cooling rate is increased, is linear. If the relation is linear, then an increase of cooling rate in the range between 3 and 55 °F may be expected to increase average RAL by approximately 0.4% for every 1000-psi increase of tensile strength. Best estimates are that, within the yield strength range studied, a 1000-psi increase of yield strength caused by increased cooling rate is accompanied by an increase of average RAL quality in the material investigated amounting to (a) 0.34%—forging reduction 10 to 1, (b) 0.46%—forging reduction 4 to 1, (c) 0.37%—forging reduction 2 to 1, and (d) 0.05%—unforged ingot. Data listed in Table II justify most confidence in estimate (b) and least—practically none—in (d).

The correlation coefficients and the lines of regression for tensile strength versus RAL exhibit the same trends as those for the yield strength versus RAL. For the yield strength or tensile strength versus RAT there is no correlation.

To show the effect of reduction by forging on both RAT and RAL for both furnace- and air-cool treatments, Figs. 5 and 6 were drawn. Here the reduction of area is plotted against the reduction by forging. These curves have three significant features:

1. As the reduction by forging is increased, the average RAL is increased.
2. The reduction by forging, at least up to 10 to 1, does not lower the average RAT significantly below the reduction of area for the original ingot. In fact at a reduction by forging of 4 to 1 there is considerable improvement.
3. The transverse and longitudinal reduction of area averages from the ingot differ significantly with the longitudinal reduction of area having the higher value.

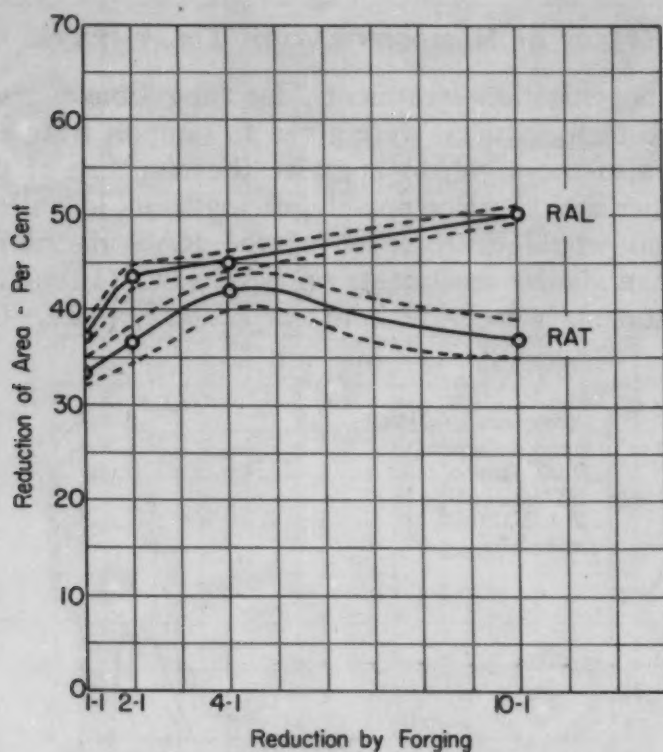


Fig. 5—Reduction of Area Versus the Reduction by Forging Curves for the Furnace-Cooled Tensile Specimens. The dotted lines represent $\bar{X} + 3\sigma/\sqrt{n}$ and $\bar{X} - 3\sigma/\sqrt{n}$ limits.

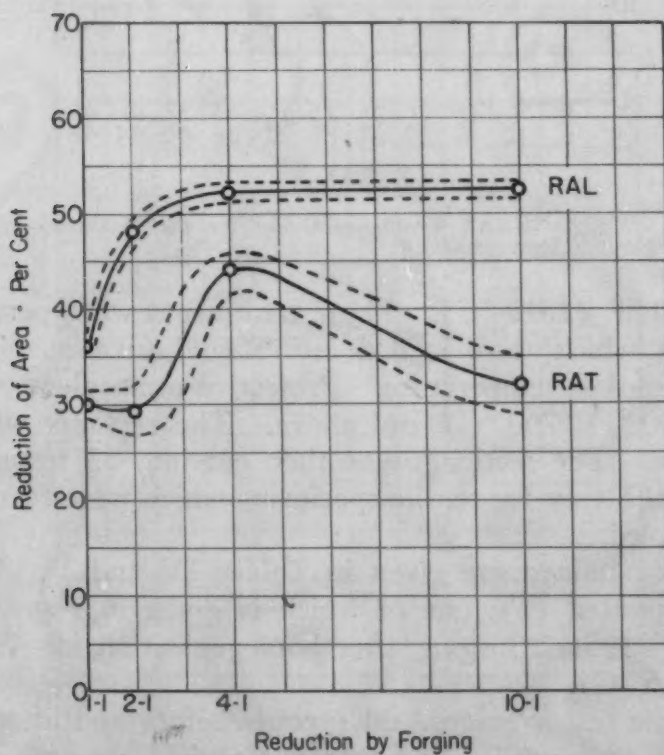


Fig. 6—Reduction of Area Versus Reduction by Forging Curves for the Air-Cooled Tensile Specimens. The dotted lines represent $\bar{X} + 3\sigma/\sqrt{n}$ and $\bar{X} - 3\sigma/\sqrt{n}$ limits.

EFFECT OF HOMOGENIZATION TREATMENTS

Two homogenization treatments, for long time periods and at unusually high temperatures, were given to samples from each of the forgings and also the ingot, to appraise the response of this simple steel to homogenization. Presumably, owing to its low alloy content, homogenization would decrease σ for the RAT distribution more extensively than similar treatments on SAE 4340 (1). The homogenization treatments were: 12 hours at 2280 °F (1250 °C) and 48

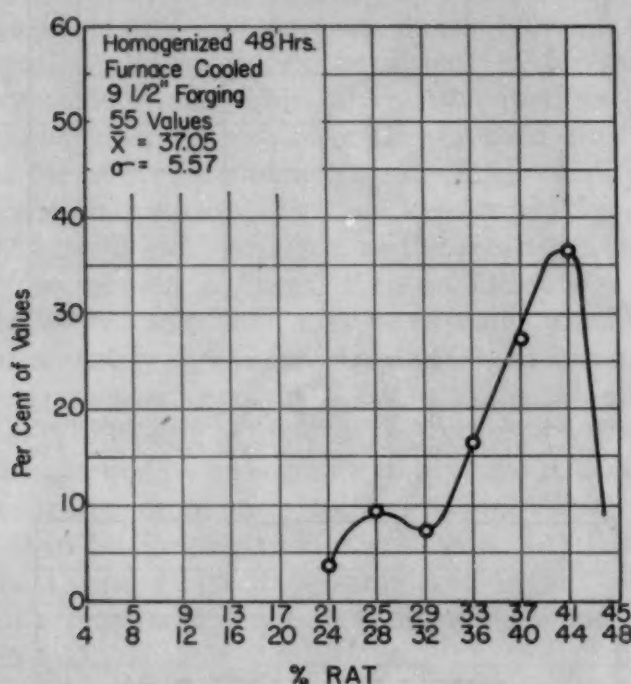


Fig. 7—RAT Frequency Curve for the 9½-Inch Forging Homogenized 48 Hours.

hours at 2400 °F (1315 °C). These treatments were performed on large sections which were loaded into a cold furnace. The times given were times at temperature. Protective atmosphere was maintained at 1400 °F (760 °C) and above. The sections were cooled in the furnace. The sections were then cut into 55 transverse and 10 longitudinal blanks for tensile specimens which were then annealed or furnace-cooled.

The data obtained are given in Tables IV and V. Frequency curves were plotted (5), one of which is given in Fig. 7, a RAT curve for the 9½-inch forging after homogenization for 48 hours at 2400 °F (1315 °C).

The tensile test averages and spreads before and after homogenization agree quite well. The transverse yield strength data have approximately the same values of \bar{X} and σ before and after homoge-

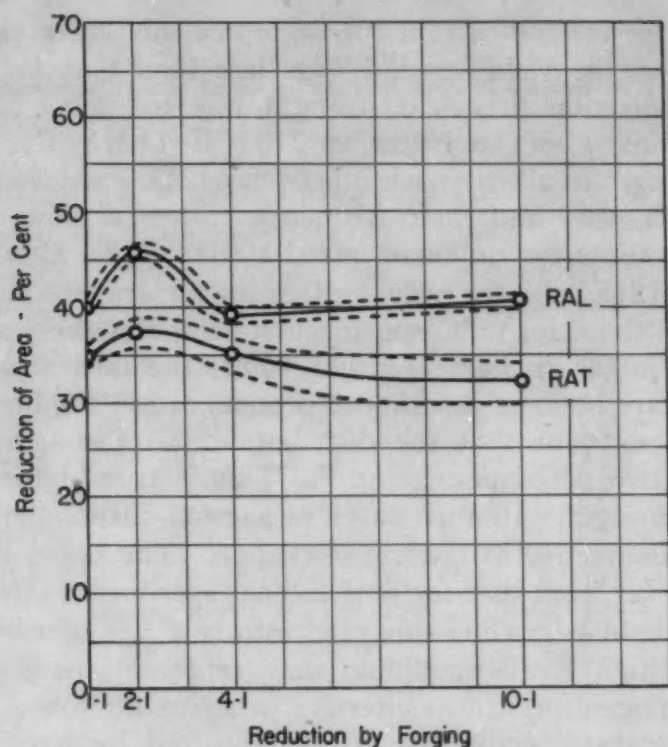


Fig. 8—Reduction of Area Versus Reduction by Forging Curves for the 12-Hour Homogenization Treatment. The dotted lines represent $\bar{X} + 3\sigma/\sqrt{n}$ and $\bar{X} - 3\sigma/\sqrt{n}$ limits.

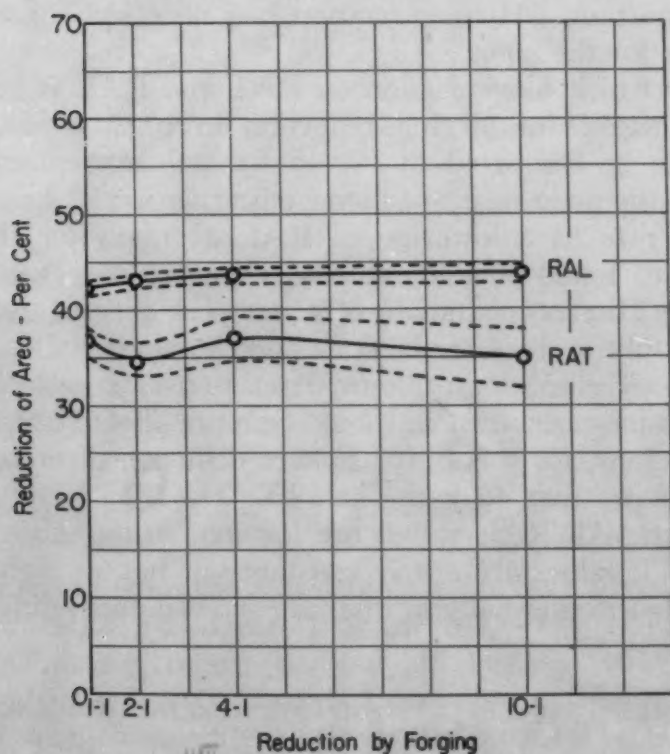


Fig. 9—Reduction of Area Versus Reduction by Forging Curves for the 48-Hour Homogenization Treatment. The dotted lines represent $\bar{X} + 3\sigma/\sqrt{n}$ and $\bar{X} - 3\sigma/\sqrt{n}$ limits.

nization, except for the case of the ingot; in this latter case, before homogenization the yield strength was less than that for forgings; after homogenization the yield strength was the same as that for forgings. Thus, after 48 hours at 2400 °F (1315 °C), the yield strength averages in all cases were between 42,000 and 45,000 psi.

The RAT data and their frequency curves exhibit interesting changes from those for unhomogenized steels. Even after 48 hours at 2400 °F (1315 °C), the values of \bar{X} and σ are not significantly different from those for unhomogenized steels. But there are important changes in the frequency curves (5): the tails and skewness of the curves are in some cases more pronounced in the homogenized steels, to the extreme that the distribution has the appearance of composite of two populations, Fig. 7. This is true of the forgings, but not of the ingot. In such cases in skewed curves the values of \bar{X} and σ are ineffective as criteria of change. The upper maximum, Fig. 7, is not far from that for longitudinal specimens. Presumably, such curves could be further analyzed into two sets of values for \bar{X} and σ . The high RAT maximum may represent those specimens for which homogenization was effective, whereas the low RAT maximum may represent those specimens, impaired by harmful inclusions to the extent that the ductility values could not be improved.

The elongation frequency curves do not have quite the same shape as the RAT curves; but here again homogenization tends to exaggerate the tails. Homogenization had no effect upon the elongation curves for the ingot.

The effect of homogenization on RAT and RAL is summarized for various degrees of forging reduction in Figs. 8 and 9; these figures are to be compared to Fig. 5 for unhomogenized samples. Fig. 8 shows the main result of homogenization for 12 hours at 2280 °F (1250 °C) to be a lowering of RAL averages for the forging reductions 4 to 1 and 10 to 1, without changing the other averages appreciably. Microscopic studies of samples reacted isothermally proved that only at these reductions was homogenization effective. This is to be expected for isothermal reaction rate since homogenization, a diffusion phenomenon, should be more effective at the higher forging reductions, for these give smaller diffusion distances.

Fig. 9 shows that 48 hours at 2400 °F (1315 °C) had a pronounced effect. All RAL values are lowered to an almost constant level; the RAT values are nearly constant but not so high as RAL. Samples reacted isothermally in this case showed apparently complete homogeneity.

TENSILE TEST RESULTS FOR COMMERCIAL FORGINGS

The results recited above were for a special heat of SAE 1045. In order to judge their general commercial validity, comparable

Table VI
Transverse Tensile Tests on the Test Ends of Commercial Forgings

	Heat No. 56446 Air-Cooled	Heat No. 56446 Water-Cooled	Heat No. 83325 Water-Cooled	Heat No. 83325 Air-Cooled
Yield Strength 0.01% Offset				
\bar{X}	43.2	46.7	47.3	45.7
σ	2.34	2.06	2.64	1.41
No. of Tests	58	60	58	59
$3\sigma/\sqrt{n}$	0.92	0.80	1.04	0.55
$3\sigma/\sqrt{2n}$	0.65	0.57	0.74	0.39
Yield Strength 0.1% Offset				
\bar{X}	43.7	45.5	47.6	45.0
σ	1.03	1.33	1.45	1.27
No. of Tests	58	60	58	59
$3\sigma/\sqrt{n}$	0.41	0.52	0.57	0.50
$3\sigma/\sqrt{2n}$	0.29	0.36	0.41	0.35
Tensile Strength				
\bar{X}	83.5	81.5	87.7	84.9
σ	1.25	1.87	1.71	2.24
No. of Tests	58	59	58	59
$3\sigma/\sqrt{n}$	0.49	0.73	0.67	0.87
$3\sigma/\sqrt{2n}$	0.35	0.52	0.48	0.62
Elongation (% in 1.4 Inches)				
\bar{X}	22.1	20.1	21.7	17.2
σ	1.72	3.56	2.25	3.52
No. of Tests	58	52	52	59
$3\sigma/\sqrt{n}$	0.68	1.48	0.94	1.37
$3\sigma/\sqrt{2n}$	0.48	1.05	0.66	0.97
RAT (% for 0.357-Inch Specimen)				
\bar{X}	30.5	31.0	30.3	22.8
σ	3.41	6.52	4.36	4.47
No. of Tests	58	52	52	59
$3\sigma/\sqrt{n}$	1.34	2.71	1.81	1.75
$3\sigma/\sqrt{2n}$	0.95	1.92	1.28	1.24

studies were made on average commercial forgings.

Test ends taken from four 8¼-inch diameter quill shafts, reduced by forging 10 to 1, were obtained. These came from two SAE 1040 basic open hearth heats which were of essentially the same composition, but made by different producers. The compositions were:

	% C	% Mn	% S	% P	% Si
Heat No. 56446	0.42	0.79	0.035	0.016	0.25
Heat No. 83325	0.43	0.79	0.033	0.016

The quill shafts from these two heats each were given the following heat treatments: (a) Heat 10 hours to 1540 °F (840 °C), hold 10 hours, cool in air; reheat 10 hours to 1140 °F (615 °C), hold 10 hours, cool in air; (b) Heat 10 hours to 1600 °F (870 °C), hold 10 hours, quench in water; reheat 10 hours to 1100 °F (595 °C), cool in air. Both heat treatments produced ferrite-pearlite structures.

From each of the four pieces, 60 transverse and 20 longitudinal

Table VII
Longitudinal Tensile Tests on the Test Ends of Commercial Forgings

	Heat No. 56446 Air-Cooled	Heat No. 56446 Water-Cooled	Heat No. 83325 Water-Cooled	Heat No. 83325 Air-Cooled
Yield Strength 0.01% Offset				
\bar{X}	45.0	45.6	49.3	47.6
σ	1.87	1.88	1.61	1.60
No. of Tests	18	20	20	19
$3\sigma/\sqrt{n}$	1.32	1.26	1.08	1.10
$3\sigma/\sqrt{2n}$	0.94	0.89	0.77	0.78
Yield Strength 0.1% Offset				
\bar{X}	44.3	44.6	47.8	46.5
σ	0.85	0.91	0.95	1.25
No. of Tests	18	20	20	19
$3\sigma/\sqrt{n}$	0.60	0.61	0.64	0.86
$3\sigma/\sqrt{2n}$	0.43	0.43	0.45	0.61
Tensile Strength				
\bar{X}	85.00	81.4	89.2	87.0
σ	1.20	0.97	0.96	1.76
No. of Tests	18	20	20	19
$3\sigma/\sqrt{n}$	0.85	0.65	0.65	1.21
$3\sigma/\sqrt{2n}$	0.60	0.46	0.46	0.86
Elongation (% in 1.4 Inches)				
\bar{X}	29.7	34.0	31.0	29.4
σ	1.05	0.52	0.63	0.49
No. of Tests	18	20	20	19
$3\sigma/\sqrt{n}$	0.75	0.35	0.42	0.34
$3\sigma/\sqrt{2n}$	0.53	0.25	0.30	0.24
RAL (% for 0.357-Inch Specimen)				
\bar{X}	53.2	65.6	62.0	54.4
σ	0.53	1.11	2.06	0.58
No. of Tests	18	20	20	19
$3\sigma/\sqrt{n}$	0.37	0.75	1.38	0.40
$3\sigma/\sqrt{2n}$	0.24	0.53	0.98	0.28

blanks for tensile specimens were cut, from approximately the half-radius position. The blanks were machined to 0.357-inch test specimens. The test results are given in Tables VI and VII.

The data show that water quenching increases the RAL average considerably over those for air cooling. In both heats the average longitudinal elongation is somewhat increased by increase in the rate of cooling. For heat No. 56446, the \bar{X} values for RAT and transverse elongation are changed but little, though the change in elongation is significant statistically. The value of σ changes markedly with speed of cooling: it is greater for the faster speed. These results are substantially the same as those obtained for the special SAE 1045 steel. For heat No. 83325, water cooling increases RAT and transverse elongation averages over those for air-cooled forgings, though the values for the air-cooled specimens are low.

The yield strength for both heats is increased by increased rate

of cooling, but the tensile strengths are not changed. The tensile strength for water-cooled specimens of heat No. 56446 is lower than for air-cooled, whereas the reverse is true for heat No. 83325; but the differences are small. This minor anomaly probably originated in the differing tempering treatments.

The data for longitudinal tests on all of the quill shafts from heat No. 56446 were analyzed statistically; the values of \bar{X} and σ were:

	Proof Stress		Tensile Strength		Elongation		RAL	
	\bar{X}	σ	\bar{X}	σ	\bar{X}	σ	\bar{X}	σ
Air-Cooled	50,000	2,200	83,000	2,750	29.8	1.69	52.4	3.7
Water-Cooled	54,000	3,100	87,000	2,700	30.6	1.94	58.8	5.0

These data are for 0.505-inch tensile specimens but should be comparable to those for 0.357-inch specimens since the geometrics of the two types of specimens are similar.

The data for the longitudinal properties of the two sections from heat No. 56446 fit well within the frequency curve for the whole heat; the spread in the latter is greater. This suggests that there is some variation in heat treatment from forging to forging.

These data from the whole heat are in agreement with findings given above for a special heat of SAE 1045: a faster rate of cool gives better RAL values and does not change elongation appreciably.

EFFECT OF ANGLE OF TEST ON THE TENSILE PROPERTIES OF FURNACE-COOLED SPECIMENS FROM THE 6-INCH FORGING

The effect of angle of test on the reduction in area values was appraised from 60 specimen blanks cut from the 6-inch forging at each of the following angles from the transverse direction: 18, 36, 54, and 72 degrees. These blanks were then given the standard furnace cool treatment. The data are given in Table VIII; comparable transverse and longitudinal data have been given in Tables IV and V. The uniformity of the tensile test data demonstrates the uniformity of the heat treatments. The data show that the angle of test has practically no effect on yield strength or tensile strength.

The data on elongation and reduction in area show that at 18 and 36 degrees the total spread is large and the average small as compared to corresponding values at 54 and 72 degrees. Fig. 10 has reduction in area plotted against angle of test. The lowest value for the reduction in area is not in the transverse direction but somewhere between 18 and 36 degrees from this. As noted later, samples from the quenched and tempered 6-inch forging gave somewhat different results.

The spread of values increases from that for the transverse

Table VIII
Results Obtained From the Tensile Tests Taken at Various Angles on the
Furnace-Cooled 6-Inch Forging

	18° From Transverse	36° From Transverse	54° From Transverse	72° From Transverse
Yield Strength Psi/1000				
\bar{X}	43.0	42.6	40.6	42.4
σ	2.92	2.19	3.24	2.77
No. of Tests	58	56	56	60
$3\sigma/\sqrt{n}$	1.15	0.88	1.30	1.07
$3\sigma/\sqrt{2n}$	0.81	0.62	0.92	0.76
Tensile Strength Psi/1000				
\bar{X}	92.4	91.8	92.0	91.8
σ	0.81	1.97	0.61	0.76
No. of Tests	56	56	56	60
$3\sigma/\sqrt{n}$	0.32	0.79	0.25	0.29
$3\sigma/\sqrt{2n}$	0.23	0.56	0.17	0.21
Elongation (% in 1.4 Inches)				
\bar{X}	19.0	20.3	23.1	24.0
σ	2.78	4.14	0.87	0.73
No. of Tests	57	56	53	60
$3\sigma/\sqrt{n}$	1.11	1.66	0.36	0.28
$3\sigma/\sqrt{2n}$	0.78	1.17	0.25	0.20
Reduction in Area % for 0.357-Inch Diameter Specimen				
\bar{X}	30.6	33.9	46.7	48.6
σ	6.05	8.81	1.23	1.54
No. of Tests	58	56	56	60
$3\sigma/\sqrt{n}$	2.38	3.53	0.49	0.60
$3\sigma/\sqrt{2n}$	1.68	2.50	0.35	0.42

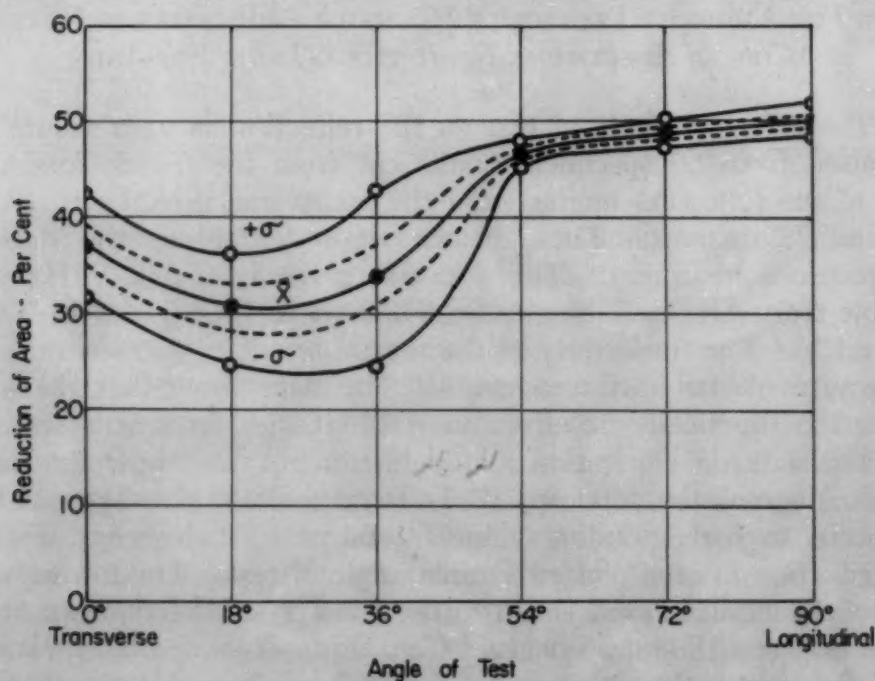


Fig. 10—Reduction of Area Versus Angle of Test for the 6-Inch Forging (10 to 1 Reduction). Dotted lines represent $\bar{X} + 3\sigma/\sqrt{n}$ and $\bar{X} - 3\sigma/\sqrt{n}$ limits.

direction to a maximum ($\sigma = 8.81$) at the 36-degree position, and then drops to a low, almost constant value ($\sigma = 1.2$ to 1.7).

As the angle of test is changed from 0 through 36 degrees, there is a significant change in the type of fracture exhibited. A maximum number of angular-type fractures (1) were obtained at the 18-degree direction, fewer at 36 degrees and in the transverse direction. The fractures at 54, 72 and 90 degrees were almost all cup-and-cone, with a few irregular fractures at 54 degrees. The angular fracture has been associated with the dendritic or fiber pattern, associated with low ductility values (1). In these forgings, apparently, the effective fiber direction lies close to 18 degrees.

TENSILE TEST RESULTS ON QUENCHED AND TEMPERED SPECIMENS

Specimen blanks were quenched completely to martensite and then tempered 2 hours at four different temperatures: 1250, 1100, 950, and 750 °F (675, 595, 510, and 400 °C)—the commercial tempering range. This is a very shallow hardening steel and can be through-hardened only in very small sections. All specimens were tested for through hardening.

The transverse and longitudinal data for the three forging reductions and for the four tempering temperatures are listed in Tables IX and X. Frequency curves were drawn for all data (5). In general, they have the same characteristics as those for ferrite-pearlite structures, in that they are similarly skewed toward low RAT values, except those from the unreduced ingot.

The tensile strength averages at any one tempering temperature are within a range of 4500 psi. The yield strength values are within 12,400 to 31,500 psi of the tensile strength; the yield:tensile ratios are as follows:

LONGITUDINAL YIELD STRENGTH - TENSILE STRENGTH RATIOS

Tempering Temperature	1250 °F	1100 °F	950 °F	750 °F
6-inch forging (10 to 1).....	0.81	0.89	0.88	0.90
9½-inch forging (4 to 1)....	0.87	0.86	0.87	0.89
12¾-inch forging (2 to 1)...	0.79	0.87	0.87	0.89
Ingot (1 to 1).....	0.78	0.80	0.82	0.83

TRANSVERSE YIELD STRENGTH - TENSILE STRENGTH RATIOS

Tempering Temperature	1250 °F	1100 °F	950 °F	750 °F
6-inch forging (10 to 1).....	0.87	0.87	0.89	0.90
9½-inch forging (4 to 1)....	0.85	0.85	0.87	0.88
12¾-inch forging (2 to 1)...	0.78	0.85	0.86	0.88
Ingot (1 to 1).....	0.73	0.82	0.82	0.83

These ratios show the following general tendencies: the ratio for the ingot is always lower than those for the forgings; the ratio tends to increase as the reduction by forging increases; and the ratio tends to increase as the tempering temperature is lowered.

The RAT data have spreads comparable with those for quenched and tempered alloy steels (1); the σ values vary from 3.10 to 8.67.

Table IX
Tensile Test Results for the Transverse Tests on the Quenched and Tempered Structures. Approximately 60 Specimens Were Used for Each Sample

Property	Reduction by Forging	—Tempered at 1250 °F—				—Tempered at 1100 °F—				—Tempered at 950 °F—				—Tempered at 750 °F—			
		\bar{X}	σ	$\frac{3\sigma}{\bar{X}}$	$\frac{\sigma}{\sqrt{2n}}$	\bar{X}	σ	$\frac{3\sigma}{\bar{X}}$	$\frac{\sigma}{\sqrt{2n}}$	\bar{X}	σ	$\frac{3\sigma}{\bar{X}}$	$\frac{\sigma}{\sqrt{2n}}$	\bar{X}	σ	$\frac{3\sigma}{\bar{X}}$	$\frac{\sigma}{\sqrt{2n}}$
Yield Strength at 0.01% Offset psi/1000	10 to 1	83.2	1.94	1.08	0.76	105.7	1.69	0.66	0.46	130.9	1.35	0.52	0.37	174.0	2.38	0.93	0.66
	4 to 1	81.8	2.53	0.99	0.70	101.1	2.27	0.89	0.63	127.0	2.23	0.86	0.61	169.8	3.06	1.19	0.84
	2 to 1	73.8	2.01	1.10	0.78	100.5	2.09	0.81	0.57	125.2	2.32	0.87	0.62	170.0	2.45	0.95	0.67
	1 to 1	71.3	3.63	1.41	1.00	97.6	3.03	1.18	0.83	117.8	3.13	1.28	0.90	158.3	3.39	1.86	1.31
Tensile Strength psi/1000	10 to 1	95.8	0.85	0.47	0.33	120.9	1.09	0.42	0.30	147.2	0.97	0.38	0.27	193.1	1.55	0.61	0.43
	4 to 1	96.3	1.24	0.49	0.34	119.5	1.68	0.66	0.46	146.1	1.37	0.53	0.38	192.8	1.38	0.53	0.38
	2 to 1	95.1	0.89	0.49	0.35	118.3	1.43	0.56	0.39	145.3	1.69	0.67	0.47	193.4	1.63	0.63	0.45
	1 to 1	97.6	1.20	0.46	0.33	119.5	3.10	0.67	0.48	142.9	1.65	0.67	0.48	189.8	2.39	1.31	0.92
Per Cent Elongation in 1.4 Inches	10 to 1	21.5	2.22	1.24	0.88	14.0	1.72	0.67	0.47	10.4	2.35	0.91	0.64	7.6	1.81	0.71	0.50
	4 to 1	24.2	1.70	0.66	0.47	15.7	3.00	1.16	0.82	9.8	2.05	0.79	0.56	7.5	1.98	0.77	0.54
	2 to 1	23.8	1.75	0.96	0.68	16.9	2.05	0.80	0.56	12.0	1.59	0.62	0.44	6.7	1.73	0.67	0.47
	1 to 1	23.2	1.19	0.46	0.33	15.5	0.39	0.15	0.11	12.4	1.62	0.66	0.47	8.2	1.28	0.70	0.49
Per Cent Reduction of Area for 0.357- Inch Dia. Specimen	10 to 1	39.5	6.27	3.44	2.43	33.3	4.70	1.84	1.30	27.2	8.20	3.20	2.26	22.6	7.57	2.96	2.09
	4 to 1	54.4	5.14	2.01	1.42	38.7	7.41	2.87	2.03	28.4	6.97	2.72	1.92	24.8	7.26	2.81	1.99
	2 to 1	50.6	8.67	4.92	3.48	42.7	7.47	2.90	2.05	33.2	6.61	2.58	1.83	20.9	8.21	3.13	2.25
	1 to 1	53.3	3.10	1.20	0.85	41.3	3.71	1.44	1.02	32.3	3.47	1.42	1.00	21.2	4.01	2.20	1.55

Table X
Tensile Test Results for the Longitudinal Tests on the Quenched and Tempered Structures. At Least 10 Specimens Were Used for Each Sample

Property	Reduction by Forging	—Tempered at 1250 °F—				—Tempered at 1100 °F—				—Tempered at 950 °F—				—Tempered at 750 °F—			
		\bar{X}	σ	$\frac{3\sigma}{\bar{X}}$	$\frac{\sigma}{\sqrt{2n}}$	\bar{X}	σ	$\frac{3\sigma}{\bar{X}}$	$\frac{\sigma}{\sqrt{2n}}$	\bar{X}	σ	$\frac{3\sigma}{\bar{X}}$	$\frac{\sigma}{\sqrt{2n}}$	\bar{X}	σ	$\frac{3\sigma}{\bar{X}}$	$\frac{\sigma}{\sqrt{2n}}$
Yield Strength at 0.01% Offset psi/1000	10 to 1	79.9	2.51	2.38	1.68	106.4	1.02	0.97	0.68	130.3	0.82	0.82	0.58	174.6	2.84	2.69	1.90
	4 to 1	85.3	1.56	1.56	1.11	103.3	0.90	0.85	0.60	128.6	1.11	1.06	0.75	171.9	1.52	1.52	1.08
	2 to 1	77.7	2.19	2.08	1.47	103.9	0.94	0.90	0.63	128.4	1.20	1.14	0.81	169.9	2.51	2.51	1.78
	1 to 1	76.1	1.45	1.37	0.97	93.6	2.15	2.04	1.45	117.3	2.33	2.21	1.56	160.7	3.10	2.94	2.08
Tensile Strength psi/1000	10 to 1	98.1	1.81	1.72	1.22	119.7	0.46	0.44	0.31	147.6	1.26	1.26	0.89	193.1	0.70	0.66	0.47
	4 to 1	97.7	0.67	0.67	0.47	119.8	0.62	0.58	0.41	147.5	0.49	0.47	0.33	192.7	1.25	1.25	0.88
	2 to 1	98.3	1.19	1.13	0.80	119.9	0.54	0.51	0.36	147.5	0.50	0.47	0.34	190.8	0.63	0.63	0.45
	1 to 1	97.3	0.64	0.61	0.43	117.6	0.66	0.63	0.45	143.1	0.54	0.51	0.36	192.6	2.50	2.37	1.68
Per Cent Elongation in 1.4 Inches	10 to 1	26.5	1.49	1.42	1.00	21.4	0	0	0	17.1	0.33	0.33	0.23	13.9	1.54	1.46	1.03
	4 to 1	29.9	0.99	0.99	0.70	21.1	1.11	1.05	0.74	16.4	1.71	1.63	1.15	12.5	0.35	0.35	0.25
	2 to 1	25.6	0.49	0.47	0.33	20.6	0.89	0.84	0.59	16.3	2.09	1.98	1.40	12.2	0.42	0.42	0.30
	1 to 1	23.1	1.21	1.15	0.81	19.3	1.95	1.85	1.31	14.8	0.75	0.71	0.50	9.7	0.46	0.44	0.31
Per Cent Reduction of Area for 0.357- Inch Dia. Specimen	10 to 1	67.5	1.77	1.68	1.19	62.0	1.62	1.54	1.09	56.9	1.37	1.37	0.97	54.4	4.03	3.82	2.70
	4 to 1	66.5	0.45	0.45	0.32	60.4	2.25	2.14	1.51	54.8	4.12	3.91	2.76	48.9	0.95	0.95	0.64
	2 to 1	63.5	1.37	1.30	0.92	59.4	2.07	1.96	1.39	53.4	2.99	2.83	2.00	48.2	2.26	2.26	1.60
	1 to 1	54.4	3.77	3.57	2.53	44.8	7.11	6.75	4.77	38.0	2.05	1.94	1.33	26.9	2.34	2.22	1.57

as they do for alloy steels. Frequency curves constructed from the elongation data are similar to those for RAT but skewness is less. Correlation coefficients for longitudinal elongation versus RAL were 0.96 to 0.98, showing almost perfect correlation.

Figs. 11 to 14 show the effect of reduction by forging for the four tempering temperatures. These show that in all cases RAL is increased with increased reduction, with the greatest increase at the

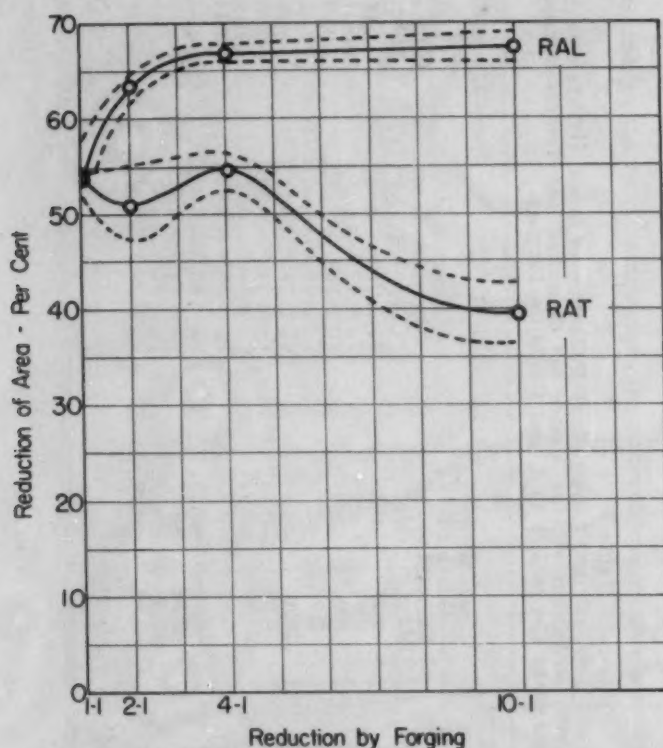


Fig. 11—Reduction of Area Versus the Reduction by Forging Curves for the Specimens Tempered at 1250 °F. The dotted lines represent $\bar{X} + 3\sigma/\sqrt{n}$ and $\bar{X} - 3\sigma/\sqrt{n}$ limits.

reductions 2 to 1 and 4 to 1. The RAT averages at either 2 to 1 or 4 to 1 at all four tempering temperatures are higher than that for the ingot.

The effect of the degree of reduction by forging on RAT and RAL can be shown in a different way: correlation coefficients and lines of regression for yield strength versus RAL, tensile strength versus RAL, and yield strength versus RAT were calculated. These are given in Figs. 15 through 17 and the equations for these lines are given in Table XI. The lines of regression for yield strength versus RAL fall within the range of data for SAE steels given by Janitzky and Baeyertz (8) and are comparable for those reported for SAE 4340 (1). The values of RAT for these plain carbon steels are on the low side of the range for alloy steels.

Table XI

Results of Correlation and Regression Studies of (A) Yield Strength and Longitudinal Reduction of Area, (B) Tensile Strength and Longitudinal Reduction of Area, and (C) Yield Strength and Transverse Reduction of Area Values for Quenched and Tempered Specimens From an SAE 1045 Steel Reduced 10 to 1, 4 to 1, 2 to 1, and 1 to 1 by Forging

Composition of Sampled Population	Reduction by Forging	No. of Tests	Correlation Coefficient r	Limits Between Which ρ Is Expected to Fall		Equation of Regression Line ($Y_s = a + bX$)	Limits Between Which β in Equation $Y = a + \beta X$ Is Expected to Fall		Standard Error of Estimate %
				Max.	Min.		Max.	Min.	
Yield Strength and Longitudinal Reduction of Area Values	10 to 1	39	-0.94	-0.97	-0.86	$Y_s = 76.0 - 0.13X$	-0.15	-0.11	1.70
	4 to 1	38	-0.97	-0.99	-0.93	$Y_s = 82.4 - 0.19X$	-0.21	-0.17	1.64
	2 to 1	39	-0.96	-0.98	-0.91	$Y_s = 76.6 - 0.17X$	-0.19	-0.15	1.74
	1 to 1	40	-0.92	-0.97	-0.82	$Y_s = 76.7 - 0.32X$	-0.38	-0.26	4.38
Tensile Strength and Longitudinal Reduction of Area Values	10 to 1	39	-0.92	-0.97	-0.82	$Y_s = 78.7 - 0.13X$	-0.16	-0.10	2.06
	4 to 1	38	-0.97	-0.99	-0.93	$Y_s = 82.7 - 0.18X$	-0.20	-0.16	1.46
	2 to 1	39	-0.97	-0.99	-0.93	$Y_s = 79.7 - 0.17X$	-0.19	-0.15	1.53
	1 to 1	40	-0.91	-0.96	-0.80	$Y_s = 79.9 - 0.28X$	-0.34	-0.22	4.50
Yield Strength and Transverse Reduction of Area Values	10 to 1	209	-0.70	-0.79	-0.59	$Y_s = 60.7 - 0.23X$	-0.28	-0.18	7.96
	4 to 1	240	-0.77	-0.84	-0.67	$Y_s = 74.0 - 0.31X$	-0.35	-0.27	8.49
	2 to 1	210	-0.84	-0.89	-0.77	$Y_s = 76.3 - 0.33X$	-0.37	-0.29	7.63
	1 to 1	240	-0.93	-0.95	-0.90	$Y_s = 76.0 - 0.35X$	-0.37	-0.33	4.45

For meaning of r , ρ , $Y_s = a + bX$, and $Y = a + \beta X$, see Table II.

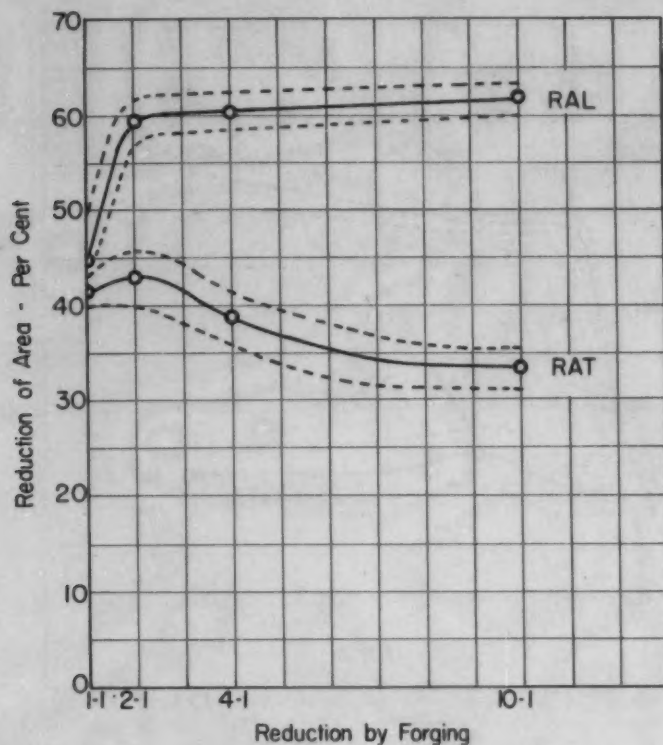


Fig. 12—Reduction of Area Versus the Reduction by Forging Curves for the Specimens Tempered at 1100 °F. The dotted lines represent $\bar{X} + 3\sigma/\sqrt{n}$ and $\bar{X} - 3\sigma/\sqrt{n}$ limits.

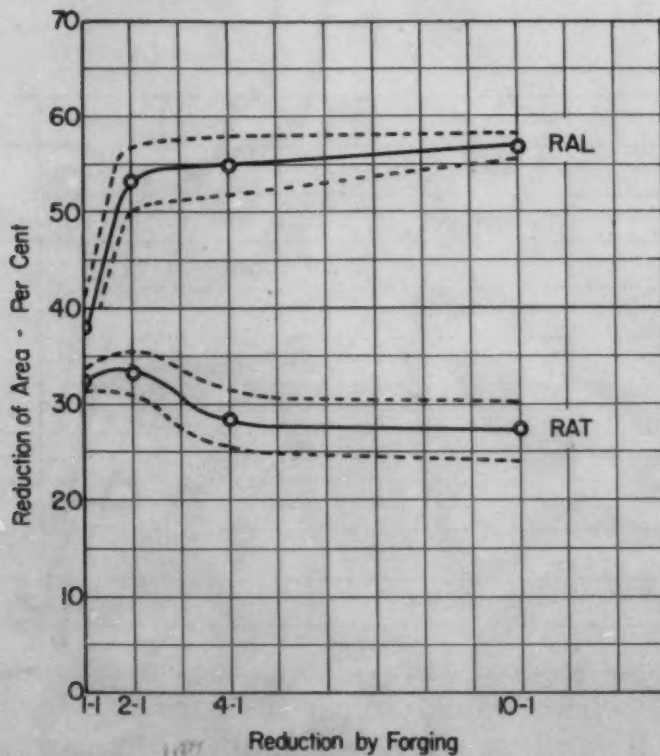


Fig. 13—Reduction of Area Versus the Reduction by Forging Curves for the Specimens Tempered at 950 °F. The dotted lines represent $\bar{X} + 3\sigma/\sqrt{n}$ and $\bar{X} - 3\sigma/\sqrt{n}$ limits.

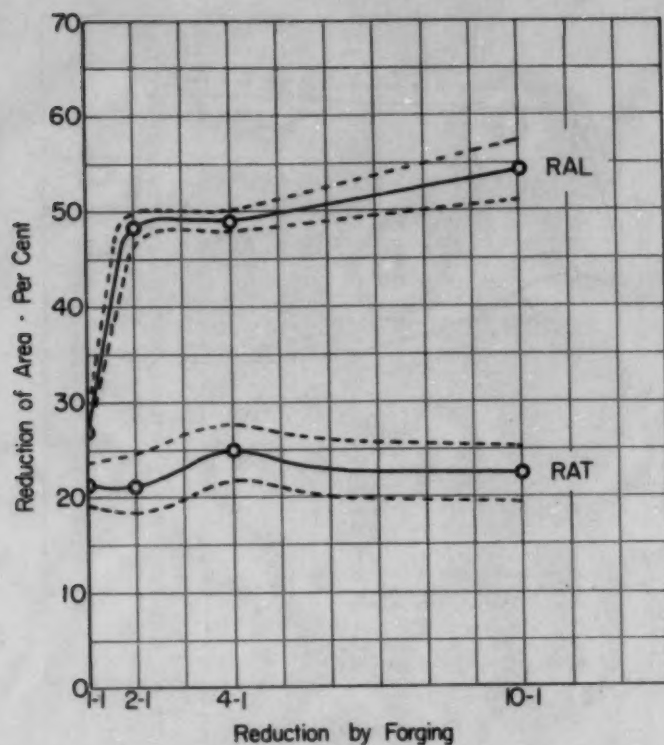


Fig. 14—Reduction of Area Versus the Reduction by Forging Curves for the Specimens Tempered at 750 °F. The dotted lines represent $\bar{X} + 3\sigma/\sqrt{n}$ and $\bar{X} - 3\sigma/\sqrt{n}$ limits.

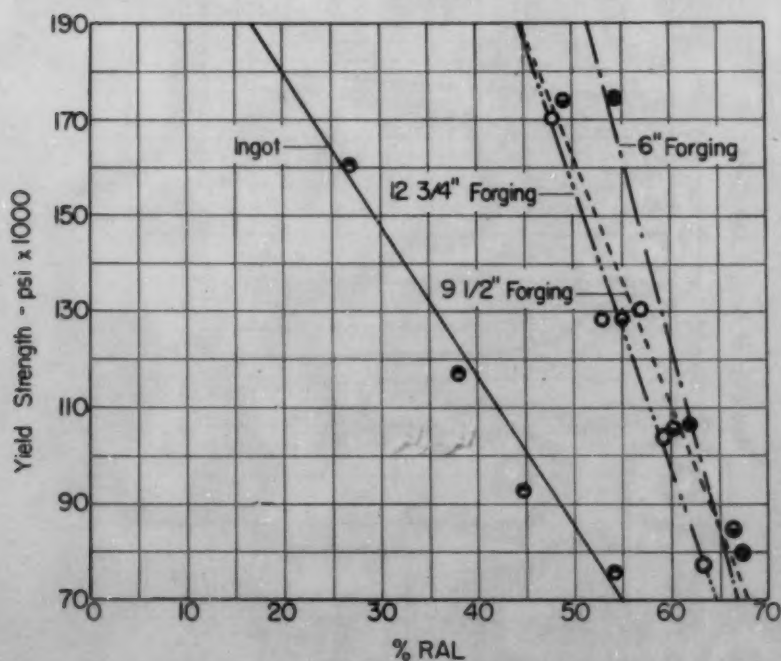


Fig. 15—Lines of Regression for Yield Strength Versus RAL. The points plotted are the average yield strength and average RAL.

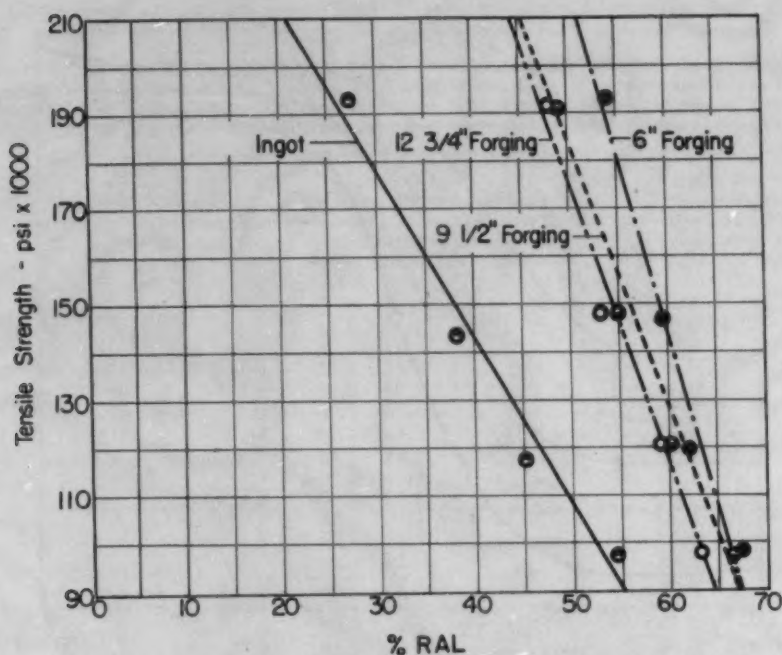


Fig. 16—Lines of Regression for Tensile Strength Versus RAL. The points plotted are the average tensile strength and the average RAL.

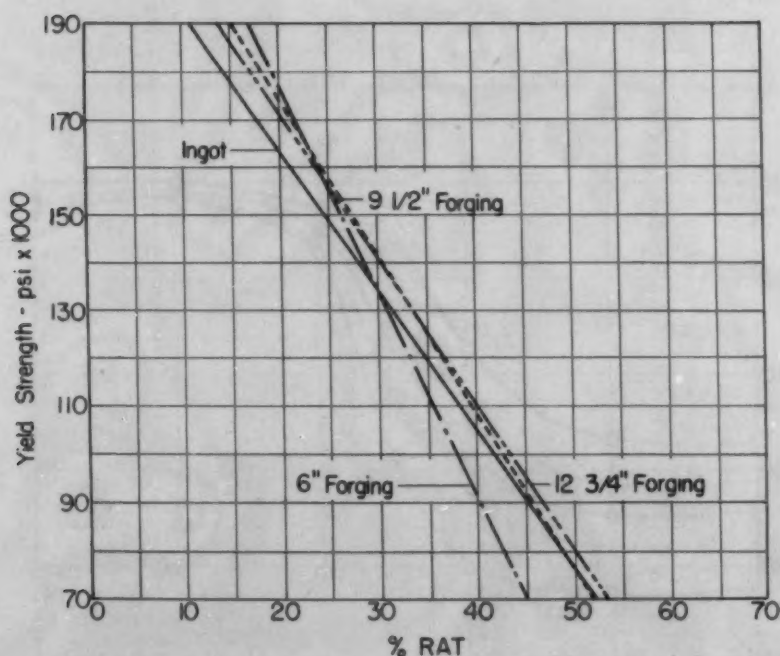


Fig. 17—Lines of Regression for Yield Strength Versus RAT.

The curves and equations for yield strength versus RAL and for tensile strength versus RAL are quite similar. Both illustrate that for a given yield strength or tensile strength, RAL values increase with increasing forging reduction, with the greatest increase between zero reduction (ingot) and 2 to 1. Reduction in area can

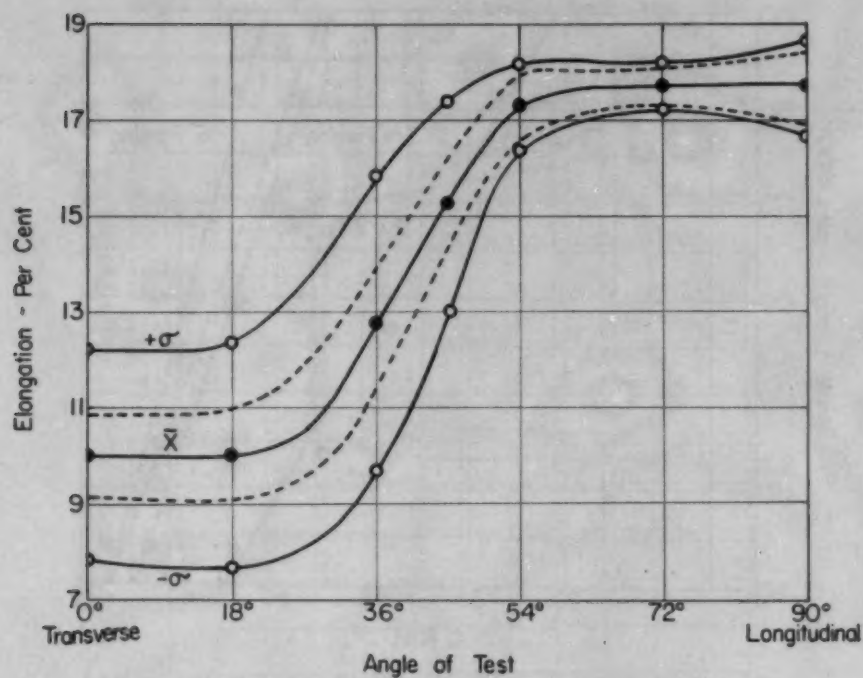


Fig. 18—Elongation Versus Angle of Test for the SAE 1045—6-Inch Forging. Dotted lines represent $\bar{X} + 3\sigma/\sqrt{n}$ and $\bar{X} - 3\sigma/\sqrt{n}$ limits.

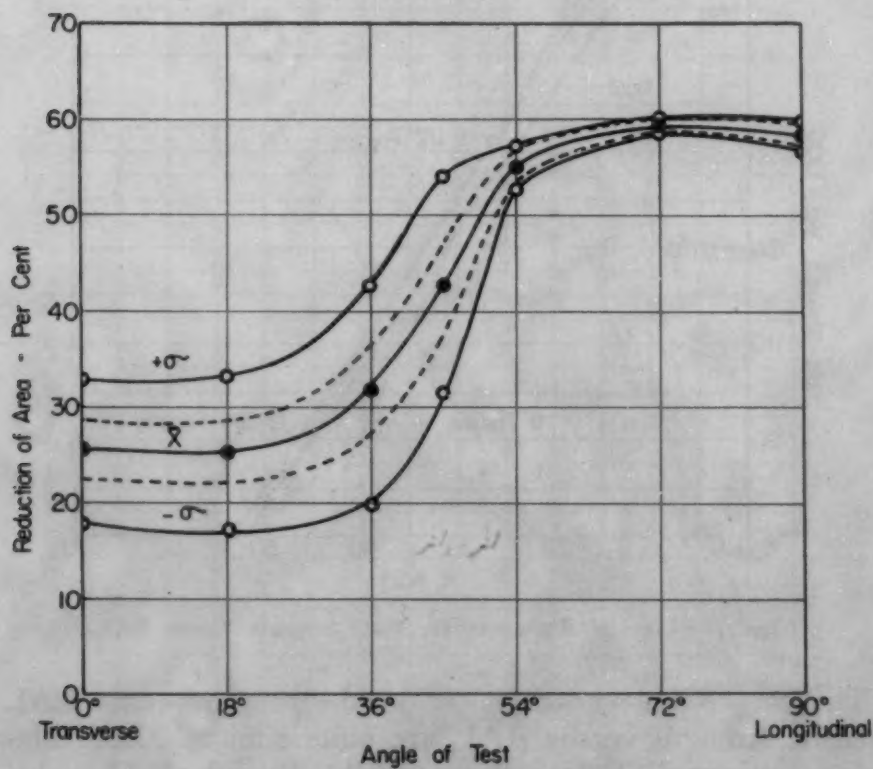


Fig. 19—Reduction of Area Versus Angle of Test for the SAE 1045—6-Inch Forging. Dotted lines represent $\bar{X} + 3\sigma/\sqrt{n}$ and $\bar{X} - 3\sigma/\sqrt{n}$ limits.

¹RAL = longitudinal reduction of area. ²RAT = transverse reduction of area. For meaning of $Y = a + \beta X$, see Table II.

Table XIII
Tensile Test Results Obtained From the Angle Tests on the SAE 1045—6-Inch Forging
in the Quenched and Tempered State (0.252-Inch Diameter Tensile Specimens)

		Yield Strength at 0.01% Offset psi/1000	Yield Strength 0.1% Offset psi/1000	Tensile Strength psi/1000	% Elongation in 1 Inch	% Reduction of Area
Transverse 0°	\bar{X}	130.3	134.7	149.0	10.0	25.3
	σ	2.38	1.62	2.41	2.23	7.4
	No. of Tests	57	57	58	55	55
	$3\sigma/\sqrt{n}$	0.95	0.65	0.96	0.86	2.99
	$3\sigma/\sqrt{2n}$	0.67	0.46	0.68	0.64	2.12
18°	\bar{X}	131.0	135.2	149.8	10.1	25.1
	σ	3.20	2.12	2.00	2.37	8.24
	No. of Tests	53	53	53	55	55
	$3\sigma/\sqrt{n}$	1.32	0.87	0.83	0.96	3.33
	$3\sigma/\sqrt{2n}$	0.93	0.62	0.58	0.68	2.36
36°	\bar{X}	126.9	133.0	147.9	12.8	31.7
	σ	3.24	1.87	1.84	3.13	11.95
	No. of Tests	56	56	56	55	56
	$3\sigma/\sqrt{n}$	1.30	0.75	0.74	1.27	4.79
	$3\sigma/\sqrt{2n}$	0.92	0.53	0.52	0.90	3.39
45°	\bar{X}	126.4	132.2	148.1	15.3	42.7
	σ	3.57	2.31	1.93	2.23	11.26
	No. of Tests	60	60	60	60	60
	$3\sigma/\sqrt{n}$	1.38	0.89	0.75	0.87	4.36
	$3\sigma/\sqrt{2n}$	0.98	0.63	0.53	0.61	3.08
54°	\bar{X}	127.9	132.6	147.7	17.3	54.9
	σ	3.13	1.58	1.19	0.94	2.06
	No. of Tests	15	15	15	15	15
	$3\sigma/\sqrt{n}$	2.42	1.23	0.92	0.73	1.60
	$3\sigma/\sqrt{2n}$	1.71	0.87	0.65	0.52	1.13
72°	\bar{X}	135.5	140.1	154.5	17.7	59.3
	σ	1.78	0.44	0.50	0.44	0.77
	No. of Tests	15	15	15	15	15
	$3\sigma/\sqrt{n}$	1.38	0.34	0.39	0.34	0.60
	$3\sigma/\sqrt{2n}$	0.98	0.24	0.27	0.24	0.42
Longitudinal—90°	\bar{X}	130.8	138.2	152.6	17.73	58.1
	σ	3.47	1.17	1.02	1.00	1.59
	No. of Tests	15	15	15	15	15
	$3\sigma/\sqrt{n}$	2.69	0.90	0.79	0.77	1.23
	$3\sigma/\sqrt{2n}$	1.90	0.64	0.56	0.55	0.87

be plotted against forging reduction at any yield strength level and can be constructed from Figs. 15 and 17, as in Figs. 11 to 14. Each point on any one of the regression lines in Figs. 15 to 17 represents an estimated \bar{Y} value for a given value of X ; \bar{Y} designates the average quality of a unit with respect to either RAL (Figs. 15 and 16) or RAT (Fig. 17) and X designates a selected value of either yield strength (Figs. 15 and 17) or tensile strength (Fig. 16). Limits between which \bar{Y} probably falls for each of a number of selected values of X and limits between which practically all individual \bar{Y} values (RAL or RAT) probably fall are listed in Table XII.

EFFECT OF ANGLE OF TEST ON TENSILE PROPERTIES OF QUENCHED AND TEMPERED SPECIMENS FROM 6-INCH FORGING

Specimen blanks $\frac{1}{2}$ by $\frac{1}{2}$ by $3\frac{1}{2}$ inches were cut from the half-radius position at various angles to the transverse direction. Sixty specimens were cut at each of the following angles: 0, 18, 36, and 45 degrees; 15 specimens were cut at each of the angles: 54, 72, and 90 degrees (longitudinal). These specimens were machined to $\frac{3}{8}$ -inch rounds. They were heat treated as follows: austenitized for $1\frac{1}{2}$ hours at 1500 °F (815 °C), quenched in ice-cold 5% NaOH solution, tempered in a salt bath for 2 hours at 950 °F (510 °C). Tensile test specimens were machined to a diameter of 0.252 inch with a 1-inch gage length. In addition to unusual data, values of yield strength at 0.1% offset were determined.

The data are given in Table XIII. Again, neither yield strength nor tensile strength are substantially affected by variation in angle; this is in conformity with findings on quenched and tempered SAE 4340 (1). The effect of angle on elongation and reduction in area may be observed in Table XIII and in Figs. 18 and 19. It is evident that: (a) the average and the spread for ductility (reduction in area and elongation) does not change appreciably from the transverse direction up to 20 degrees from that direction; (b) the average and the spread for ductility do not change appreciably from the longitudinal direction up to 20 degrees from that direction; (c) the greatest change in ductility occurs in the range 18 to 54 degrees from the transverse direction.

SUMMARY AND CONCLUSIONS

This investigation was designed to study the transverse and longitudinal tensile properties of an SAE 1045 forging steel at reductions by forging of 10 to 1, 4 to 1, 2 to 1, and the unreduced ingot after the following heat treatments on individual tensile specimens:

1. Anneal from 1500 °F (815 °C).
2. Normalize from 1500 °F (815 °C).
3. Two homogenizing treatments on sections from the forgings and ingot for 12 hours at 2280 °F (1250 °C) and 48 hours at 2400 °F (1315 °C) followed by an anneal of individual test specimens at 1500 °F (815 °C).
4. Quench to martensite and then temper at 750, 950, 1100 and 1250 °F (400, 510, 595 and 675 °C).

In addition, the effect of angle of test on the tensile properties was determined for the forging with the 10 to 1 reduction in the furnace-cooled and in the quenched and tempered state.

All of the tensile test results from these heat treatments were analyzed statistically and the limits of accuracy have been stated.

Each sample usually consisted of 60 values for any transverse property and 10 values for any longitudinal property studied.

From the results of the anneal and normalize treatments, the following conclusions were reached:

1. The mean values of the yield strength, tensile strength, and RAL were increased by the increase in the rate of cool from the annealed to the normalized treatment, but the average longitudinal elongation, transverse elongation, and transverse reduction of area (RAT) values were practically not changed. This is true for all three forgings but not for the ingot.

2. The spread of RAT values for both furnace-cooled and air-cooled specimens was from 18 to 40%. Even the ingot had a spread of RAT values from 18 to 24%.

3. The increase in reduction by forging continuously increases the average RAL over the range studied, with the greatest change coming at reductions by forging from zero to 4 to 1.

4. The reduction by forging does not lower the average RAT below the reduction in area for the ingot. In fact, at the reduction by forging of 4 to 1 there is a considerable improvement.

5. The transverse and longitudinal reduction of area averages from the ingot differ significantly, with the longitudinal reduction of area having the higher values.

The conclusion reached as a result of the homogenization treatments was that homogenization is not desirable commercially because: the RAT averages or standard deviation (σ) values are not changed appreciably and the RAL averages are lowered to a constant value.

The testing of commercial forgings in the ferrite and pearlite condition showed: that a faster rate of cool yields higher RAL values without appreciably changing the longitudinal elongation, transverse elongation and RAT; and there are variations from forging to forging in one heat probably due to heat treatment differences.

The conclusions obtained from the work done on the effect of the angle of test on the tensile properties for ferrite and pearlite structures are as follows:

1. The transverse reduction of area (\bar{X}) value is not the lowest obtainable value, but the lowest average reduction of area is between 18 and 36 degrees from the transverse direction for this steel.

2. The greatest change in ductility values comes between 36 and 54 degrees from the transverse direction.

3. The yield strength and tensile strength are practically unaffected by the angle of test.

The conclusions reached from the study of quenched and tempered structures are as follows:

1. The RAT frequency curves for the forgings are all skewed

toward lower values while the RAT frequency curves for the ingot are not skewed.

2. The transverse elongation curves for all forgings are similar to the RAT curves, but the skewness is less pronounced.

3. The yield strength – tensile strength ratios show a tendency to increase as the reduction by forging is increased, with the ratio for the ingot always lower than the ratio for the forgings.

4. The RAT averages for either reductions by forging of 2 to 1 or 4 to 1 are always better than the RAT average for the ingot.

5. The RAL average increases as the reduction by forging is increased with the greatest change before a reduction of 4 to 1.

The conclusions from the study of effect of the angle of test on the tensile properties of the quenched and tempered specimens are:

1. The angle of test practically does not affect either the yield strength or the tensile strength.

2. The average and spread for the transverse ductility and for angles to 18 degrees from this direction do not vary significantly.

3. The average and spread for the longitudinal ductility and for angles up to 30 degrees from this direction do not vary significantly.

4. The greatest change in reduction of area and elongation takes place at angles of 20 to 54 degrees from the transverse direction.

References

1. Cyril Wells and R. F. Mehl, "Transverse Mechanical Properties of Heat Treated Wrought Steel Products", *TRANSACTIONS, American Society for Metals*, Vol. 41, 1949, p. 717.
2. Edwin G. Olds and Cyril Wells, "Statistical Methods for Evaluating the Quality of Certain Wrought Steel Products", *TRANSACTIONS, American Society for Metals*, Vol. 42, 1950, p. 845.
3. G. W. Snedecor, *Statistical Methods*, Fourth Edition, 1946, Iowa State College Press, Ames, Iowa.
4. M. J. B. Ezekiel, *Methods of Correlation Analysis*, John Wiley and Sons, New York, Second Edition, 1941.
5. R. F. Mehl and A. H. Grobe, "Final Report on Acceptance Tests for Plain Carbon Steel Gun Forgings and Other Ordnance Forgings", Serial No. M-466, May 3, 1945, published by the Office of Technical Services, Department of Commerce, Washington 25, D. C.
6. M. Gensamer, E. B. Pearsall, W. S. Pellini and J. R. Low, Jr., "The Tensile Properties of Pearlite, Bainite, and Spheroidite", *TRANSACTIONS, American Society for Metals*, Vol. 30, 1942, p. 983.
7. Maxwell Gensamer, "Strength and Ductility", *TRANSACTIONS, American Society for Metals*, Vol. 36, 1946, p. 30.
8. E. J. Janitzky and M. Baeyertz, "The Marked Similarity in Tensile Properties of Several Heat Treated SAE Steels", *METALS HANDBOOK*, American Society for Metals, 1939, p. 515.
9. *ASTM Manual on the Presentation of Data*, American Society for Testing Materials, 1916 Race Street, Philadelphia 3, Pa. Reprinted July 1947.

DISCUSSION

Written Discussion: By Edward A. Loria, senior engineer, Metallurgy, The Carborundum Co., Niagara Falls.

This study is based primarily on forgings produced from three relatively small ingots taken from one heat of SAE 1045 steel which turned out to be an exceptionally good heat. In view of their statements on the macro- and micro-examinations, one might consider it unfortunate that the authors did not work with forgings taken from larger ingots in which the effects of ingot heterogeneity would become more acute. Notwithstanding the apparent lack of structural anisotropy (factors) that would produce transverse weakness in their forgings, they were still able to obtain significant variations in the transverse mechanical properties of the most commonly used plain carbon forging steel.

At the outset the authors recognize that the steelmaking practice is an important variable and give some details on their heat which produced "a good quality commercial forging steel and one that was almost too clean to furnish an inclusion rating by the SAE method". They should go further and state the tapping and pouring temperatures, the pouring time, and give further details on the control of the oxidizing power of the slag in this particular heat. Different methods of liquid steel refining which are encountered in various plants might produce different effects on the mechanical properties of the resultant steels. For example, in acid open-hearth practice, the state of oxidation is not only interesting at the "melt-down" or "start of carbon boil" period, but throughout the heat as well. The rate of carbon drop at the "go-ahead" or refining period must also be controlled, and such control can produce steel of higher ductility at a given hardness level.

Up to a certain ingot size, a rather homogeneous metal structure can be obtained (as shown in the longitudinal section of the small ingots cast several years ago by the British Heterogeneity of Steel Ingots Committee). Very large ingots, however, cool so slowly that the sluggishness of the solidifying materials prevents the liquid from flowing freely enough into the ingot end cavities, and spongy zones are still formed in the center of the upper portion of the ingot.³ The extension of the original porous area by actual tearing into an originally sound adjacent area during the course of hot working is a good possibility. Moreover, on solidifying, the impurities and alloying elements in the steel segregate in zones which may cause weaknesses in the forging. Shrinkage cavities and mushy material in the ingot are rare in carbon and low alloy steel, but are more frequent in higher alloyed steels. Segregations are more serious the larger the ingot and in the higher alloyed steels. The degree of forging reduction can accentuate these phenomena, especially if the sulphur and phosphorus contents are not sufficiently low or the test pieces are taken from segregation zones. Correct forging may improve the qualities of the poorer zones, but it cannot prevent single test pieces from sometimes giving brittle results.

In view of the above ingot heterogeneity factors, could the authors differentiate between the RAT values and the ingot position in which the test specimens were taken? In relation to their forgings made from 18-

³E. A. Loria, "Internal Structure of Killed Steel Ingots on the Basis of Relative Rates of Solidification", *Blast Furnace and Steel Plant*, Vol. 39, 1951, p. 1333, and "Solidification and Segregation in Killed Steel Ingots", *Blast Furnace and Steel Plant*, Vol. 40, 1952, p. 410.

inch basic open-hearth ingots, a recent study by the writer⁴ on forgings made from 36-inch acid open-hearth ingots produced some variations in the RAT values for test specimens taken from sections corresponding to the bottom, middle and top sections of the ingot, as shown in Fig. 20. The greatest number of low values occur in the forged sections corresponding to the bottom portions of the ingots. Perhaps this variation in RAT with

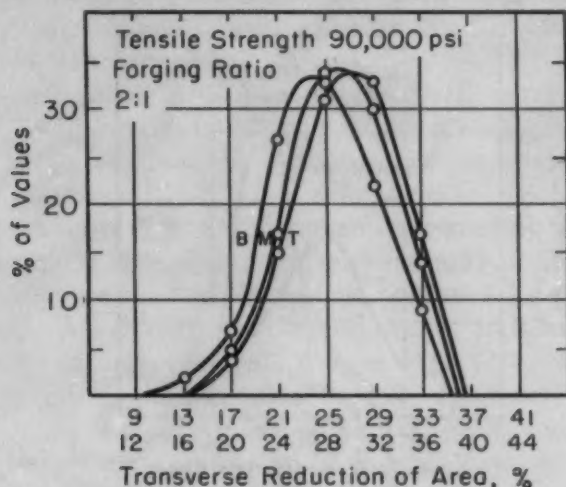


Fig. 20—Frequency Curves for 30-Inch Diameter Solid Shaft Forgings Made From 48-Inch Acid Ingots of 0.35 to 0.42% Carbon, 0.60 to 0.90% Manganese, 0.15 to 0.30% Silicon, 0.040% Phosphorus, 0.040% Sulphur. Curves are based on 110 values. B—Bottom of ingot. M—Middle of ingot. T—Top of ingot. (After Loria.⁴)

ingot position cannot be shown in forgings processed from smaller ingots.

Other unpublished data⁵ on RAT frequency curves for test specimens of the top part of hollow forgings are about equal on the outside and inside of the cylinders. At the bottom of the forging the values for the inside are somewhat lower, as shown in Fig. 21. Microscopic examination of the tensile fractures reveals that this occurrence is likely to be caused by the higher content of nonmetallic inclusions in the respective ingot zone. Bartocci⁶ has obtained the same results and extended his study to the tensile testing of specimens taken at various depths below the surface from the top and bottom ends of the forging. He found that the mean elongation and reduction of area values for transverse test specimens are practically uniform across the top part of the forging, but, at the bottom part, the value decreases from the outside toward the inside wall. In part, he attributes these variations in the RAT frequency curves and mean values on the difference in dendritic structure that was observed between the outside and inside zones. Would the authors state the location of the cuts, with respect to the original ingot, that were processed into forgings for study and the height of their 18-inch square ingots?

⁴E. A. Loria, "Transverse Ductility Variations in Large Steel Forgings", *TRANSACTIONS, American Society for Metals*, Vol. 42, 1950, p. 486.

⁵E. A. Loria, unpublished data.

⁶A. Bartocci, "Comments on the Characteristics of the Transverse Mechanical Properties of Forgings", *La Metallurgia Italiana*, Vol. 42, 1950, p. 289.

The authors state that the dendritic pattern was pronounced in the 12¾-inch forgings. This raises the question of whether or not the presence of dendritic segregation has an influence on the transverse mechanical properties of forgings. Would the authors reproduce the RAT frequency curves for the 12¾-inch forgings for comparison purposes and comments on the percentage of angular fractures producing low values or the skewed portion of their curve? In view of their statement that their steel was

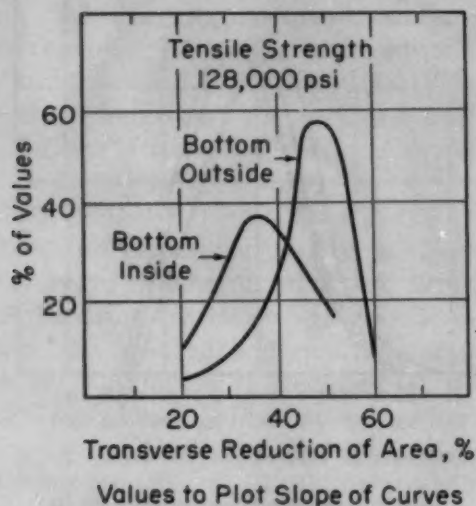


Fig. 21—Frequency Curves for Bottom Part of Cylindrical Forging of 11.8-Inch OD, 2.95-Inch ID, 16 Feet Long. Alloy steel of 0.30% carbon, 0.60% manganese, 2.80% nickel, 0.90% chromium, 0.45% molybdenum, 0.015% phosphorus, 0.015% sulphur. Curves are based on over 100 values. (After Bartocci.)

relatively free of inclusions, would they attach more significance to the dendritic structure in producing the low RAT values in the 12¾-inch forgings? Also, it would be worthwhile if the authors would state the percentages of angular fracture in the transverse tensile test specimen for the 9½-inch and 6-inch round forgings and the 8¾-inch round quill shafts.

Extensive unpublished results⁵ on forgings of 0.21 to 0.29% carbon, 2.50 to 3.00% nickel, 0.40 to 0.60% molybdenum, 0.06 to 0.12% vanadium steel, after normalizing at 1525 °F, tempering at 1125 °F and stress relief at 500 °F, showed entirely cup-cone fractures in longitudinal test specimens and a 50-50 distribution between angular and cup-cone fractures in transverse test specimens. The RAL values ranged from 50 to 55%, whereas the

RAT values ranged from 20 to 30%. This steel grade was deoxidized with ferrosilicon in the ladle (no aluminum) and the forging reduction was 2.5 to 1. The test specimens were trepanned at the ends of each forging. Etch tests made on these forgings showed striking dendritic patterns on some and none on others. In nickel alloyed steels, the dendritic pattern can be pronounced and shown vividly in longitudinal ingot sections. Were the authors able to make photomicrographs of the dendritic pattern in their 12¼-inch forging specimens possessing angular fractures in the manner shown in Fig. 23 (Reference 1)?

No mention is made of a banded structure, not even for the 10-to-1 forging ratio. Apparently, banding was not a problem in their well-made heat of SAE 1045 steel, and the authors conclude that "homogenization is not desirable commercially". On the other hand, Schwartzbart⁷ recently showed the pronounced effect of manganese banding in lowering RAT of (heavily reduced) heat treated steel plate of 0.21% carbon, 1.47% manganese and the very marked improvement produced by a prior homogenization treatment. A banded structure originates from dendritic or globular primary crystals of heterogeneous composition. Normal or inverted ingot segregation comprises additional sources.⁸ However, the most harmful causes of banding are plastic nonmetallic inclusions, such as silicates, which act as nuclei for primary and secondary crystallization. A pronounced ferrite precipitation always takes place on the elongated silicate inclusions, and the transverse "sensitivity" of the material is greatly increased. With very little gross chemical segregation, excellent inclusion ratings, and good sulphur distribution in the one heat of steel studied, these factors were not prominent. The authors state that "microscopic studies of samples reacted isothermally were made in connection with heterogeneity and banding". To make this phase of their study more complete, it would be well to include any TTT-curve determination and a discussion of ferrite banding with different rates of cooling and degrees of forging. Perhaps they may wish to consider this as the subject of a separate paper for future presentation.

The data for the reduction of area versus reduction by forging curves for the quenched and tempered specimens, shown in Figs. 11 to 13, are plotted in a single diagram, Fig. 22, employing the ratio RAL/RAT to illustrate the transverse weakness of the forging. It can be seen that the difference between RAT and RAL becomes less as the tempering temperature was raised. An examination of other data on large forgings⁴ reveals that the maximum beneficial effect of forging on RAL is reached between 2-to-1 and 4-to-1 reduction. Also, the beneficial effect of forging on RAT is reached in the same range. One would expect the optimum reduction to give the best combination of RAL/RAT to depend a good deal on the thoroughness of the forging operation and the size of the forging. In connection with the latter, the change in slope in two of the curves to poorer quality at the 10-to-1 reduction is noteworthy. This may tie in with the RAT frequency curves for the angle tests for the 6-inch forgings which show that the marked skewness (or range of low values) is directly related

⁷H. Schwartzbart, "Effect of Manganese Banding on Mechanical Properties of Heat Treated Steel Plate in the Thickness Direction", *TRANSACTIONS, American Society for Metals*, Vol. 44, 1952, p. 845.

⁸E. A. Loria and H. D. Shephard, "Some Factors Affecting Subsurface Defects in Large Forging Steel Ingots", *TRANSACTIONS, American Society for Metals*, Vol. 41, 1949, p. 328.

to the fiber pattern produced in these heavily reduced (10 to 1) specimens.

In regard to the commercial SAE 1040 quill shafts made by two different producers, it should be stated if they were forged in the same manner. Long experience in forging has shown that finishing at a low temperature is an aid to heat treatment, particularly in attaining improved ductility in the direction of working (better RAL values). The reverse of this is true to a certain extent, and forgings subjected to transverse testing usually are finished at high temperatures. Were the ingot sizes comparable and was the deoxidation practice the same? Ingot design governs cooling conditions and segregation mode. The degree of transverse weakness

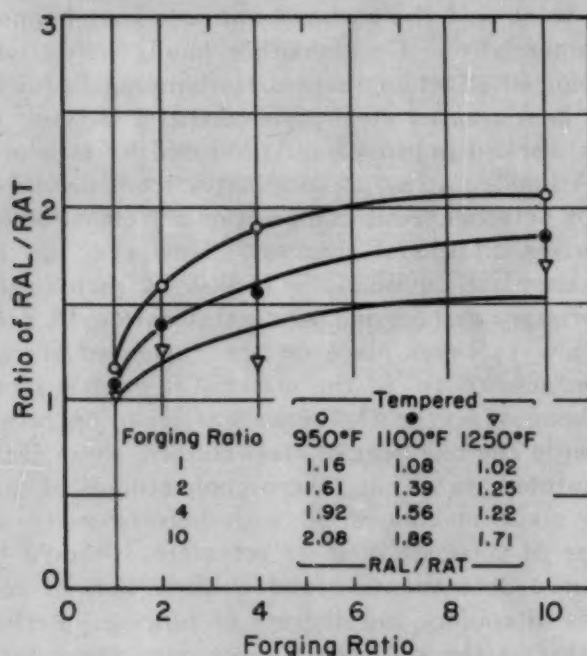


Fig. 22—Effect of Forging Reduction on Ratio of Longitudinal and Transverse Reduction of Area in Quenched and Tempered SAE 1045 Forgings. Plot of Figs. 11 to 13 in a single diagram.

depends on the type of primary crystallization so that a variance in deoxidation practice would not only produce different nonmetallic inclusions, but a different crystalline structure of the ingot. In the treatment of the quill shafts, no mention is made that a coarse microstructure was obtained by the air-cool treatment and a finer and more uniform structure was achieved by the water-cool treatment on the same steel. The carbon content may vary about 10 points between SAE 1045 and SAE 1040 steel, and the manganese may vary a like amount. This extra carbon should yield a slightly less ductile steel.

Deoxidation practice plays an important role on sulphide inclusion types and methods of distribution which, in turn, may produce different transverse properties. Avoiding film-type sulphides is of paramount interest unless the sulphur content of the steel is very low. Has Dr. Wells continued his study of the effect of soft, continuous sulphide stringers on RAT of forgings quenched and tempered to various tensile strength levels?

Unpublished data⁸ for quenched and tempered SAE 1045 forgings from basic open-hearth heats deoxidized with six different silicon-bearing materials showed variations in the average RAT which could be correlated, in most instances, with steel cleanliness, although the types of inclusions were substantially the same in all cases and macro-etch quality was normal, regardless of the type of deoxidizer used. Variations in carbon content from 0.40 to 0.50% in these heats may have affected the results. At 0.40% carbon and above, some heats have a characteristic ductility that is well below the normal expectation. It has been suggested that this effect of carbon is dependent on segregation. Have the authors investigated or extended their work on the effect of carbon in this particular range?

Deoxidation practice will influence directional properties and may not show up in an inclusion count. The low inclusion content of good acid open-hearth steel enables large forgings to be made to specifications requiring high transverse ductility. Low RAT values are due to the spreading out of the original inclusions into flat zones. Therefore, a large piece requiring high transverse ductility should be forged enough to break up the ingot structure, and to promote subsequent heat treatments, but little more. Recently, some measurements of the inclusion contents of acid electric cast steels by point counts were made and correlated with their respective reduction of area values,⁹ but their distribution in chain-like fashion in the grain boundaries produced the most damage. Normal variations in size and quantity of round or angular inclusions had little effect on tensile ductility.

Written Discussion: By John V. Russell, director, Metallurgical Laboratory, Republic Steel Corp., Chicago.

The data presented in the authors' paper are of unusual interest since they represent information about the properties of a very widely used steel but on which, to the best of our knowledge, mechanical properties have never been studied in such detail. Comparison with earlier work from the same laboratory which dealt with heat treated alloy steel forgings of similar size would lead one to believe that the forgings studied here are of quite good quality. Indeed, this is very likely true, but a strict comparison is not justified and we are glad the authors did not attempt to do so.

The fact that large numbers of tensile specimens taken from these forgings show good ductility at the strength levels customary for steel of this type does not mean that the forgings themselves would necessarily be as ductile. It is at this point that the ductility values of tests taken from alloy forgings differ. It has long been customary for many large steel mill parts to be made of plain carbon steel similar to that described in this paper and used in the normalized or annealed condition. We have seen a number of failures of such parts which are completely brittle in character. We have not, on the other hand, observed such failures in similar parts hardened and tempered and of suitable alloy steel. We bring this up for the purpose of emphasizing the fact that tensile tests such as these do not sufficiently describe the expected performance of large forgings and feel that the data shown here may be misleading to some.

A section of the paper describes increases in ductility due to faster

⁸E. A. Loria, "Rating Inclusion Structures in Cast Steels and Their Effects on Tensile Properties", *Electric Furnace Steel Proceedings*, American Institute of Mining and Metallurgical Engineers, Vol. 8, 1950, p. 191.

cooling rates and the effect of this on the pearlite lamellar spacing. Here again we wish to make a precautionary statement. Such faster cooling rates as the authors indicate would have to be obtained by water quenching, thus introducing a considerable hazard. If some hardening occurs on the outer surfaces as a result of this water quenching, and the parts are of sufficient length and mass, there is a possibility that internal cracking could result. If the cracking itself does not occur, one can readily visualize severe residual internal tensile stresses as a result of such quenching. Consequently, it is seldom good practice to quench shallow hardening steels in water in solid sections larger than about 9 inches in diameter.

We wish again to compliment the authors on the quality of the data obtained and the precise manner of presenting them.

Written Discussion: By Daniel J. Girardi and Chester F. Jatczak, research metallurgists, The Timken Roller Bearing Co., Steel and Tube Division, Canton, Ohio.

The authors are to be complimented for another fine contribution to the technical literature on transverse properties. Systematic data on mechanical properties carefully analyzed by statistical methods are very helpful in arriving at more intelligent specifications.

Our own experience on the effect of homogenization treatments of 100 hours at 2200 °F on relatively large section sizes, although based on fewer samples tested, confirms the conclusion that commercial homogenization treatments are not feasible because the RAT values are not improved appreciably.

As shown in the paper, homogenization treatments on SAE 1045, with the exception of the 2280 °F treatment on reductions less than 4 to 1, bring about a lowering of RAL averages. Would the authors care to comment further on this point?

It appears that the intent of the authors in referring to alumina inclusions as "refractory inclusions" is to call attention to their refractory nature or lack of malleability at steel working temperatures. The expression "refractory inclusions" is also used at times to refer to inclusions that are the result of accidental incorporation of refractories or other materials with which molten steel comes in contact.

Written Discussion: By W. J. Wrazej, Physical Metallurgy Division, Department of Mines and Technical Surveys, Ottawa, Ont., Canada.

It is a great pleasure to read such a useful paper based on results from numerous samples carefully chosen for the estimation of how the reduction of forged section influences the mechanical properties and especially the reduction in area in the transverse direction (RAT).

There is one suggestion which I shall be glad if the authors would accept. In my opinion such expressions as "100% martensite in the quenched specimens" (p. 1080); "fully martensite structure (through hardening) on quenching" (p. 1083); "quench to martensite throughout the cross section" (p. 1084); "quenched completely to martensite" (p. 1101); "Quenched to martensite" (p. 1111), and maybe some others not checked by me, as applied to the quenched structure in SAE 1045 should be reworded, for example, as "100% martensitic"; "fully martensitic structure", etc.

The practical metallurgist knows what the authors meant. It is misleading, however, to many others, such as physicists, who are doing useful

work in physical metallurgy. Many of them have no chance and do not feel the necessity to observe "martensitic" structures under the microscope. For them "martensite" is the structure component which will give the tetragonal structure indicated on X-ray films.

In my experience SAE 1045 steel quenched, as we say, "through", owing to a small section (n.b. rightly chosen by the authors $\frac{1}{2}$ -inch diameter), will have a uniform "martensitic structure" without distinct patches of bainite, but this structure component will certainly be present in the form of a few needles in all of the examined grains. Such needles resemble martensite needles in high carbon martensite austenitic structures but appear darkly etched. They cannot be avoided, either by the mode of quenching or by the time and temperature of heating before quenching. After my experience it is a "biological" property of such iron-carbon alloys, even with higher carbon content (up to the eutectoid composition), to show traces of that bainite which increases with a decrease of carbon.

That fact, however, does not deprive the structure of being called "martensitic throughout", i.e., a structure which does not show any separate patches of (darkly etched) bainite.

Written Discussion: By A. O. Schaefer, vice-president in charge of engineering and manufacturing, The Midvale Co., Nicetown, Philadelphia.

The greatest value in a report of this sort is that it supplies factual data supporting what many makers and users of steel forgings have suspected or "known" for a long time.

The greatest danger lies in the temptation to extrapolate from this actual data, and arrive at unwarranted conclusions.

The data represent a specific melting practice, a particular ingot size and design, and simple open-die forging reduction. In practice many similar forgings are made, such as axles for railroad locomotives and cars, shafting, etc. However, the forging practice followed in the manufacture of a great many open-die forgings is complicated by the fact that they are irregular in shape and are consequently forged in several stages. Many shafts have flanges, upset portions, etc. Other forgings may require upsetting as part of the forging process, or they may be forged hollow on mandrels, etc.

So it is apparent that there can be no end to our search for knowledge of forgings until we have investigated every individual forging that has been made. In addition to these complications, if we are to include the ingots used to make forgings, we can predict that they will differ in characteristics from the ingot investigated in this report.

The original great value of this work, and the work that preceded it at the Carnegie Institute of Technology, was the detailed knowledge it gave us of a product that we were turning out in great numbers during the last war, i.e. gun barrels. For the first time it was recognized that the reduction in area in the transverse direction is a statistical property, and is not to be estimated by a single isolated test result.

Painstaking laborious work such as this is warranted in the case of any forging used in large numbers. Much more of this type of investigation is needed before we fully understand open-die forgings. The authors are to be congratulated for adding to our store of knowledge. It is hoped they will continue to investigate and analyze other types of forgings.

Authors' Reply

The authors wish to thank the discussers for their interest, constructive criticisms and additional information.

In answer to E. A. Loria, more complete information concerning the experimental techniques and data are on file at the Carnegie Institute of Technology as the doctorate thesis.

In order that the RAT values would not be influenced by the ingot position, all test specimens were cut from the top two-thirds of the original ingot. It was not possible to correlate RAT values with their position in the portion of the ingot used.

Probably the only way to make an accurate determination of the effect of dendritic structure on the tensile properties would be to study tests from ingots of the same heat of steel cooled in a way to produce a wide variation in dendritic pattern.

Some studies were made concerning "ferrite banding" in this and other SAE 1045 steels. There was no sign of banding in the tensile specimens. The only way that this particular steel could be banded was by an extremely slow rate of cool from the austenitizing temperature. Indications of heterogeneity were present as bands in test samples that were austenitized and then partially reacted isothermally.

The quill shafts were produced from similar ingots forged in approximately the same manner. In this connection, no investigation has been made on the effects of small changes in carbon content.

As stated by J. V. Russel and in another way by A. O. Schaefer, this whole investigation was based on tensile tests cut from forgings from a single heat of steel. These do not necessarily describe the expected performance from large forgings stressed in tension or the properties of tensile test specimens cut from other forgings. Essentially, this study presents the data from one set of forgings from a single heat of steel as a foundation on which it is now possible to build up the knowledge of the tensile properties of plain carbon forging steels. How far this data can be extrapolated will depend on confirming results from other heats of steel of similar compositions.

It is good to have confirmation that homogenization treatments are not commercially feasible to improve RAT values. The homogenization treatments reduced all RAT values for the forgings when this homogenization was complete enough to remove banding in a test specimen which was partially reacted isothermally. In other words, when the "S" curve showed that homogenization was completed, the RAT values were lowered.

No doubt, as stated by W. J. Wrazej, too many different statements were used to describe a fully martensitic condition. In the metallographic examination of the quenched specimens, no traces of bainite were found.

INDEX OF AUTHORS

VOLUME XLV

TRANSACTIONS OF AMERICAN SOCIETY FOR METALS

1953

A

Allten, A. G. 498
Averbach, B. L. 576

B

Beall, R. A. 862
Beattie, H. J., Jr. 397
Bishop, S. M. 993
Boegehold, A. L. 1056
Bowen, K. W. J. 443
Bruckart, W. L. 286, 314
Bucklin, A. G. 151
Buffum, D. C. 725, 732
Bumps, E. S. 1008

C

Carr, F. L. 725, 732
Channon, S. L. 200
Chapman, R. D. 710
Christenson, A. L. 638
Clark, D. S. 620
Cohen, Morris 576
Craighead, C. M. 286, 314, 941

D

Dorn, J. E. 249, 275
Dulis, E. J. 42
Duwez, Pol 934

E

Eichelman, G. H., Jr. 77

F

Fontana, M. G. 993
Furman, D. E. 429

G

Garofalo, F. 377
Giacobbe, J. B. 134
Gilbert, H. L. 862
Goldberg, A. 275
Goldhoff, R. M. 941

Goldman, Manuel 732
Goss, N. P. 333
Grant, N. J. 105, 151
Grobe, A. H. 475, 1080
Grosse, A. V. 758

H

Hamburg, J. F. 686
Hansen, M. 901, 915, 1008
Hayes, E. T. 893
Hoar, T. P. 443
Houston, E. G. 42
Hu, L. W. 686
Hull, F. C. 77
Hum, J. K. Y. 105

J

Jaffe, L. D. 725, 732
Jaffee, R. I. 286, 314, 941
Jatczak, C. F. 771
Jominy, W. E. 710

K

Kayser, F. X. 1056
Kessler, H. D. 1008
Kirshenbaum, A. D. 758

L

LaChance, M. H. 286, 314
Lane, J. R. 177
Liu, T. S. 677
Lubahn, J. D. 787
Lundin, C. E. 901

M

Malenock, P. R. 377
Marin, Joseph 686
McPherson, D. J. 901, 915
Mehl, R. F. 1080

N

Newkirk, J. B. 1029

P

Paasche, O. G.	893	Smith, C. S.	533
Paliwoda, E. J.	344	Smith, G. V.	42, 377
Payson, P.	498	Snyder, H. J.	605
Peretti, E. A.	677	Spretnak, J. W.	993
Perkins, F. C.	972	Starr, C. D.	249, 275
		Stephens, W. W.	862

R

Reynolds, M. B.	839	Talbot, A. M.	429
Rhines, F. N.	1029	Thomson, R. F.	1056
Roberson, A. H.	893	Treco, R. M.	872
Roberts, C. S.	576		
Roberts, G. A.	475		
Rosi, F. D.	972		
Rowland, E. S.	638, 771		

S

Saunders, M. S.	362
Shahinian, Paul	177
Shaw, H. L.	941
Shaw, R. B.	249
Shepard, L. A.	249
Shoenberger, L. R.	344
Sinnott, M. J.	362

T

Talbot, A. M.	429
Thomson, R. F.	1056
Treco, R. M.	872

V

VanVlack, L. H.	741
VerSnyder, F. L.	397
Vicars, E. C.	275
Vreeland, T., Jr.	620

W

Walker, H. L.	200
Wells, Cyril	1080
Westbrook, J. H.	221
Wood, D. S.	620

SUBJECT INDEX

Activation energy

- alpha brass208-211, 215-217
- grain growth215-217
- recrystallization208-211
- aluminum277-283
 - grain boundary relaxation277-283
 - effect of magnesium additions on282-283
- steel593-597
 - first stage of tempering593-594
 - second stage of tempering595-597
 - variation with carbon content596-597

Aluminum

- effect on properties of molybdenum alloys286-313
- effect on recrystallization of molybdenum alloys314-332
- grain boundary migration in560-561, 564
- grain boundary relaxation 275-285
 - activation energy277-283
 - effect of magnesium additions on282-283
 - equation 277
- as a function of the parameter ($D_0 e^{Q/RT}$)..279-280
- correlation of frequency, energy of activation and temperature for277-278
- correlation of grain size, frequency, energy of activation and temperature278-279
- effect of alloying elements on275-285
 - width of relaxation band 284
- effect of frequency of vibration on 276
- effect of temperature .. 276
- hardness 227
- log hardness vs. temperature 227

Aluminum (cont.)

- rigidity relaxation as a function of the parameter ($AD^{1.80} e^{Q/RT}$)280-281, 283

Aluminum alloy, trade designations 14S-T6

- stress-strain relations with biaxial tensile stresses. See Biaxial tensile stresses.

Aluminum-copper alloys

- deformation strength263-270
 - relation to mean free path between $CuAl_2$ particles263-270
 - equation 270
- deformation stress265-270
 - effect of planar mean free path on265-266, 268
 - effect of volume mean free path on265-270
- $CuAl_2$ particle dispersion calculation of mean free path257-262
- equations257-262
- rigidity relaxation as a function of the parameter ($AD^{1.80} e^{Q/RT}$)280-281
- stress-strain curves263-266
 - effect of mean free path of $CuAl_2$ particles on..263-266
 - effect of testing temperature263-266
- tensile properties effect of dispersions on.249-270
- method of determining 254-262

Aluminum-germanium alloys

- rigidity relaxation as a function of the parameter ($AD^{1.80} e^{Q/RT}$)280-281

Aluminum killed steel

- strain aging characteristics 344-361

Aluminum-magnesium alloys	Annual Address of the President	6
grain boundary relaxation 281-282	Annual Dinner of ASM	27
correlation of grain size,	Annual Meeting of ASM ..	5
frequency, energy of	Annual Report of the Secretary	15
activation and temper-	Annual Report of the Treasurer	10
ature for 281-282	Armco iron	
rigidity relaxation	residual stress	
as a function of the	X-ray measurement of .672-673	
parameter ($AD^{1.80} pe^{Q/RT}$)	skewness index as a	
	function of the rotation	
	angle ψ 672-673	
Aluminum-silver alloys	Arsenic-indium system	
rigidity relaxation	See Indium-arsenic system.	
as a function of the	Austenite	
parameter ($AD^{1.80} pe^{Q/RT}$)	in Cr-Ni-Mo-Ti (18-8-3-1) alloy	
..... 280-281	electrolytic separation	
 444-445, 447-449	
Aluminum-tin alloy	properties 449-460	
grains	Austenite to martensite	
frequency of occurrence	transformation	
of various polygonal	stainless steels 77-95	
faces on 539	effect of carbide precipitation	
	on the beginning of	
Aluminum-zinc alloys	transformation .. 82-87, 93-94	
rigidity relaxation	effect of composition on	
as a function of the	temperature of 77-95	
parameter ($AD^{1.80} pe^{Q/RT}$)	procedure for determining 80-85	
	Austenite stabilizers	
	stainless steels	
Anelasticity	chromium or nickel	
boundary between anelastic	equivalents 78-80	
and plastic behavior 827-837	Austenitizing temperature	
definition and characteristics	of high speed steel 18-4-1	
of 787-789	effect on grain size 481	
influence of stress and time	effect on impact strength	
on creep recovery 787-812 486-491	
effect of stress decre-	relationship to hardness 477-484	
ment 807-811	Austenitizing time	
relations between creep	for high speed steel 18-4-1	
and creep recovery ... 800-807	effect on grain size 481	
strain-time relations for	relationship to hardness 477-484	
creep recovery 789-800	Bend test	
influence on tension, creep	for evaluating molybdenum	
and relaxation 812-827	alloys 289	
applications 826	results 295-299	
combination of anelastic		
and plastic behaviors .817-822		
during partial unloading 813-815		
modulus effects 815-817		
relaxation phenomena .. 822-826		
Annealing		
of molybdenum and its alloys		
recrystallization effect		
..... 320-323, 325-332		

Beryllium

- determination of elastic constants 850-852, 855-857
- effect on properties of molybdenum alloys 286-313
- effect on recrystallization of molybdenum alloys .. 314-332

Biaxial tensile stresses

- applied to Alcoa 14S-T6
 - constant stress ratio tests
 - ductility calculations 695, 697, 700, 704-705
 - flow theory substantiation 693-694, 696-697
 - fracture stresses vs. maximum stress
 - theory 694, 696, 704
 - proportional limit vs. maximum stress
 - theory 691-692
 - stress-strain relations 689-691
 - true stress-strain relations 692-697
 - yield strength vs. distortion
 - energy theory 692
- test procedure 687-689
- variable stress ratio tests
 - flow theory substantiation 698-699, 701-705
 - slip theory inconsistencies 705
 - stress-strain relations 695, 697-699, 701

Boron

- effect on properties of molybdenum alloys 286-313
- effect on recrystallization of molybdenum alloys .. 314-332

Brass

- beta phase fractions as a function of composition 556
- determination of elastic constants 847-848, 850-852
- grains
 - frequencies of occurrence of various polygonal faces on 539
 - isolated by fracture .. 539

Brass, alpha

- grain growth 211-218
 - effect of annealing
 - temperature 212-214
 - effect of annealing time 211-214
 - effect of cold work 211-214
 - effect of initial grain
 - size 212-214
 - heat of activation 215-217
 - effect of initial grain
 - size 215-216
 - effect of prior deformation 215-216
- recrystallization 200-211
 - activation energy 208-211
 - schematic representation 209
 - heat of activation 208-211
 - effect of initial grain
 - size 210-211
 - effect of prior deformation 208-211
 - relation between recrystallized grain size and deformation 206-207
 - relation between recrystallized grain size and initial grain
 - size 207-208
 - relation between recrystallized grain size and temperature
 - of annealing 206-207
 - times and temperatures for 204-205, 210

Cadmium

- hardness 229
- log hardness vs temperature 229

Carbon

- effect on case hardenability 781-782
- effect on properties of molybdenum alloys 286-313
- effect on recrystallization of molybdenum alloys .. 314-332
- in high speed steel 18-4-1
 - effect of amount on hardness 477-483
 - effect of amount on impact strength 486-491

Carburization

- contact catalysis theory
 -134, 146-147
- oxidizing potential theory
 -134, 143-144, 146-147
- stainless steels134-148
 - apparatus 135
 - procedure135-137
 - with graphite138-148
 - air atmosphere ..138-141, 143
 - ammonia atmosphere 138-145
 - argon atmosphere 138-141, 143
 - correlation between depth
 - of carburization and
 - corrosion rates
 -139, 143, 146, 148
 - prior oxidized surface
 -138, 141-142, 144
 - Type 304138, 142, 146
 - Type 316138-146
 - Type 347138, 141, 146

Carburized steels

- hardenability1056-1079
 - AISI 33101067, 1071
 - AISI 4620 1068
 - AISI 48151068, 1071
 - AISI 50B20 1067
 - AISI 8117 .1066, 1068-1069, 1071
 - effect of boron on
 -1066, 1069, 1071
 - AISI 8620 1066
- case hardenability at various
 - carbon levels1064-1071
- core hardenability ...1064, 1069
- end-quench test for deter-
 - mining1056-1079
- trapezoidal end-quench
 - bar ...1057-1062, 1076-1077
 - comparison of cooling
 - with standard bar
 -1059-1060, 1077
 - comparison of harden-
 - ability with standard
 - bar1060, 1076-1077
 - experimental problems
 -1060-1061
 - method of obtaining
 - data from1061-1062

Carburizing steels, alloy

- effect of boron on case hard-
 - enability
 - alloys tested772-773
- as function of carbon
 - content781-782
- as function of quench
 - temperature781-782
- hardenability curves for
 - uncarburized steels ..772-773
- multiplying factor for boron 781
- of 4720 steel780-781
- of 8020 steel774-776
- of 9420 steel776-780
 - effect of vanadium ...778, 783

Case hardenability

- of alloy carburizing steels
 - effect of boron on. See
 - Carburizing steels, alloy.

Cells

- in human fat tissue 540

Chromium

- effect on properties of
 - molybdenum alloys286-313
- effect on recrystallization
 - of molybdenum alloys ..314-332

Chromium-nickel-molybdenum-titanium steel

- austenite and sigma separated
 - electrolytically from
 - 18-8-3-1444-449
- characteristics of phases 458-460
- chemical analysis450-451
- electrode potential measure-
 - ments446-447, 451-458
- electronmicrographs
 -450, 455-456
- magnetic examination
 -445-446, 449-450
- photomicrographs. 450, 452-454

Cobalt

- effect on properties of
 - molybdenum alloys286-313
- effect on recrystallization
 - of molybdenum alloys ..314-332

Coefficients of expansion

titanium alloys1001-1003

Columbiumelastic constants determined
.....850-852**Confidential Technical Meeting on
Refractory Type Materials for
High Temperature Applications
—Cleveland, November 24 and
25, 1952 39****Constituents**

in high temperature alloys 397-428

Constitution diagrams

See Phase diagrams.

Copperhardness229-230, 233-235
log hardness vs temperature
.....229-230, 233-235
correlation with tensile
strength229, 233
single and polycrystals
.....229-230, 235
oxygen content
isotopic determination. See
under Isotopic analysis.**Copper-gold alloys**dependence upon temperature
of the rate of isothermal
transformation1037-1038
resistance-temperature
curves1031-1033**Copper-silver alloy**discontinuous precipitation in
.....566-568**Copper-zinc alloys**resistance-temperature
curves1031-1033**Creep**chromium-nickel steels ... 42-76
role of anelasticity in. See
Anelasticity.
total43, 45-46
equation 45**Creep recovery**role of anelasticity in. See
Anelasticity.**Creep-rupture curves**stainless steels ...114-115, 122-123
effect of carbon ...114-115, 122
effect of nitrogen ..114-115, 123**Creep-rupture properties**monel151-169, 181-195
effect of atmosphere on 181
stress vs minimum creep
rate189-195
effect of grain size on 189-195
effect of testing temper-
ature189-195
stress vs rupture life ...182-190
effect of grain size on 182-190
effect of testing temper-
ature182-190
stainless steels105-132
ductility116-117, 119
effect of carbon117, 119
effect of nitrogen117, 119
effect of testing temper-
ature117, 119
effect of carbon105, 108-110
effect of carbon and
nitrogen 111
effect of microstructure
on129-131
effect of nitrogen on
.....105, 111, 113, 115
effect of testing temperature
.....109-112, 114-127, 130-132
minimum creep rates
.....114, 120-121, 127, 130
variation as a function of
carbon plus nitrogen
content
.....114, 120-121, 127, 130
procedure for determining
.....106-108
rupture life 111-114, 118-119, 127
variation as a function
of carbon plus nitrogen
content
.....111-114, 118-119, 127
stress vs. minimum creep
rate111-112, 116

Creep-rupture properties (cont.)

- stainless steels
 - stress vs. rupture life ..
 -109-110, 115
 - stresses for specified rupture
 - times115-117
 - effect of carbon plus
 - nitrogen content ...115-117
 - effect of testing temper-
 - ature115-117

Creep-rupture tests

- monel158-159, 163-164
 - comparison of static recrystallization, equicohesion
 - and hardness163-164
 - oxide penetration during 158-159

Creep strength

- stainless steels 53-56
 - effect of carbon on 54-55
 - effect of columbium on . 55
 - effect of nitrogen on ... 54
 - variation with temperature
 - 53-56
 - Type 303 54
 - Type 304 53-54
 - Type 304L 53-54
 - Type 316 53, 55
 - Type 316L 53, 55
 - Type 32153-54, 56
 - Type 347 53, 56

Deformation strength

- aluminum-copper alloys ..263-270
 - relation to mean free path
 - between CuAl_2 particles
 -263-270
 - equation 270

Deformation stress

- aluminum-copper alloys ..265-270
 - effect of planar mean free
 - path on265-266, 268
 - effect of volume mean free
 - path on265-270
 - correlation with strain hardening index252-253

Delayed yield phenomenon ..620-637

- measurement of plastic and
 - anelastic microstrain .626-628
 - typical record of 626
- mechanism of620-637
- procedure for determining .623-628
- rapid-load tension tests ..624-628
 - delay time vs. stress 624, 627-628
- repeated stress-pulse tests 624-626
 - activation energy for the
 - recovery process 628
 - cumulative time at stress
 - to yield vs. aging time
 -625-626, 628
 - typical record of 625
 - static tension tests 623
 - static stress vs. strain .. 623

Dilatometric measurements

- of steels containing silicon
 - effect of silicon during
 - tempering509-513

Distortion energy theory

- applied to biaxially stressed
 - 14S-T6
 - agreement with yield
 - strength values 602

Ductility

- of biaxially stressed 14S-T6
 -695, 697, 700, 704-705
- monel183-186, 191-197
 - effect of composition ... 193
 - influence of grain size
 -183-186, 191-192, 194, 197
 - influence of stress
 -183-186, 191-192, 194-197
 - influence of testing tempera-
 - ture 183-186, 191-192, 194-197

Elastic constants

- determined by ultrasonics.
 - See under Ultrasonics.

Election of Officers 26**Electrical resistivity measurements**

- of steels containing silicon
 - effect of silicon during
 - tempering513-514

Electrode potential measurements

- of austenite and sigma
separated from Cr-Ni-Mo-Ti
(18-8-3-1) alloy
.....446-447, 451-458

Electrolytic separation

- of austenite and sigma
from Cr-Ni-Mo-Ti (18-8-3-1)
alloy444-445, 447-449

Electron micrographs

- of austenite and sigma
separated from Cr-Ni-Mo-Ti
(18-8-3-1) alloy ..450, 455-456
- iron-carbon alloy 602
- showing interface between
pearlite and tempered
martensite570-571

Elevated temperature hardness

- of binary molybdenum
alloys299-301
- of 8 Cr-1 Mo steel390-391
- relationship to strength 391-393
- of 18 Cr-8 Ni stainless
steels387, 389-390
- relationship to strength
and creep391-393
- hot hardness tester378-383
- influence of duration of
loading on386-389
- influence of specimen prep-
aration on384-386
- of plain carbon steels378-383
- relationship to strength
and creep391-393

Elevated temperature impact properties

- of nodular iron368, 370-371

Elevated temperature properties

- monel
influence of grain size
on177-197
- of nodular iron365-370
- of zirconium-oxygen alloys
.....885-889

Embrittlement

- of Fe-Ni-Cr alloys
by sigma phase437-440

Embrittlement (cont.)

- of SAE 3140 steel
effect of hardness on impact
energy curves. See Impact
energy curves.
- effect of heat treatment on.
See under Temper brittleness.

Endurance limit

- of temper-brittle steel SAE 5140.
See Temper-brittle steel.

Epsilon carbide

- calculation of chemical
composition597-598

Equilibrium diagrams

- See Phase diagrams.

Euler's law 534**Fabricability**

- of binary molybdenum
alloys290-292

Fatigue properties

- titanium alloys998-1001, 1003
- at low temperatures
.....998-1001, 1003
- effect of notch on ...998-1000
- typical fractures ...1001, 1003

Flow stress

- in steels
effect of mean distance
between particles on...250-251

Flow theory

- applicability to biaxially stressed
14S-T6693-699, 701-705

Forgings

- tensile properties1096-1099
- longitudinal1098-1099
- effect of cooling rate
.....1098-1099
- transverse1097-1098
- effect of cooling rate
.....1097-1098

Forging steel

- microstructure 1088
- air-cooled SAE 1045
specimen 1088
- furnace-cooled SAE 1045
specimen 1088

Forging steel (cont.)

- tensile properties
 -1086-1096, 1099-1113
- correlation coefficients
 -1086-1087, 1092, 1103
- effect of angle of test on
 - ..1099-1101, 1108, 1110-1111
- elongation vs. angle of
 - test 1108
- reduction of area vs.
 - angle of test 1108
- effect of homogenization
 - treatment on
 -1088-1089, 1094-1096
- quenched and tempered
 - specimens1101-1111
- effect of angle of test
 - on1108, 1110-1111
- effect of reduction by
 - forging 1101
- reduction of area vs. reduction
 - by forging 1088-1089,
 - 1092-1096, 1103-1107, 1110
- effect of homogenization
 - treatment on
 -1088-1089, 1094-1096
- effect of tempering
 - temperature 1103, 1105-1106
- regression lines
 - 1086-1087, 1092, 1103-
 - 1104, 1106-1107, 1109-1110
- tensile strength vs.
 - longitudinal reduction
 - of area1103-1104, 1107
- yield strength vs.
 - longitudinal reduction
 - of area1103-1104, 1106
- yield strength vs.
 - transverse reduction
 - of area1103-1104, 1107
- specimens containing ferrite
 - and pearlite
 -1088-1096, 1099-1101
- specimens quenched and
 - tempered1101-1113
- transverse mechanical prop-
 - erties in1080-1121
- materials and specimen
 - preparation1081-1085

Forging steel (cont.)

- transverse reduction of area
 - frequency curves ..1085-1086
- furnace-cooled specimens 1085
- quenched and tempered
 - specimens 1086

Fracture, mode of

- stainless steels
 - effect of creep or rupture
 - test exposure on 70, 73

Fracture strength

- of biaxially stressed 14S-T6
 - agreement with maximum
 - stress theory694, 696, 704

Free machining steel

- AISI B-1112 and B-1113 alloys
- machinability742, 747
 - effect of inclusion com-
 - position on750-752
 - effect of inclusion size
 - and shape on742-746
 - effect of mechanical
 - working on 749
 - effect of number of
 - inclusions on 748
 - effect of silicon on ...
 -744, 746-748
 - effect of sulphur content
 - on749-750

Furnace

- for melting zirconium and
 - other refractory metals.862-871

Grain boundary energy

- variation with orientation
 - between crystals545-548
- variation with thickness at
 - various temperatures below
 - melting point554-555

Grain boundary melting551-555

- replacement of grain corners
 - by liquid at temperatures
 - below the melting point
 -552-555
 - equations552-553

Grain boundary melting (cont.)

- volume free energy required
to produce liquid553-555
- as a function of temper-
ature553-555
- as a function of thickness
.....553-555

Grain boundary migration

- in strained aluminum.560-561, 564

Grain boundary relaxation

- aluminum275-285
- activation energy277-283
- effect of magnesium
addition on282-283
- equation 277
- as a function of the
parameter ($D_0 e^{Q/RT}$) ..279-280
- correlation of frequency,
energy of activation and
temperature for277-278
- correlation of grain size,
frequency, energy of
activation and temper-
ature278-279
- effect of alloying elements
on275-285
- width of relaxation band 284
- effect of frequency of
vibration on 276
- effect of temperature .. 276
- aluminum-magnesium alloys
- correlation of grain size,
frequency, energy of
activation and temper-
ature for281-282
- iron
- as a function of the
parameter ($D_0 e^{Q/RT}$) ..279-280

Grain growth

- alpha brass211-218
- effect of annealing tem-
perature212-214
- effect of annealing time.211-214
- effect of cold work211-214
- effect of initial grain
size212-214
- heat of activation215-217

Grain growth (cont.)

- alpha brass
- heat of activation
- effect of initial grain
size215-216
- effect of prior defor-
mation215-216

Grain orientation

- of low carbon steel strip
- effect of rolling temperature
on333-343

Grains

- frequency of occurrence of
various polygonal faces
- on 539
- aluminum-tin alloy 539
- brass 539
- comparison with soap froth 539
- comparison with vegetable
cells 539
- isolated by fracture..... 539

Graphite

- oxygen content
- isotopic determination..762, 766

Hafnium

- furnace for melting862-871

Hardenability

- of alloy carburizing steels.772-773
- carburized steels1056-1079
- AISI 33101067, 1071
- AISI 4620 1068
- AISI 48151068, 1071
- AISI 50B20 1067
- AISI 81171066, 1068
- effect of boron on
.....1066, 1069, 1071
- AISI 8620 1066
- case hardenability at various
carbon levels1064-1071
- core hardenability ...1064, 1069
- end-quench test for deter-
mining1056-1079
- trapezoidal end-quench
bar1057-1060
- comparison of cooling with
standard bar1059-1060

Hardenability (cont.)

- carburized steels
 - trapezoidal end-quench bar
 - experimental problems
 -1060-1061
 - method of obtaining data
 - from1061-1062

Hardness

- of high speed steel 18-4-1
 - effect of carbon content
 - on477-483
 - effect on impact strength
 -488, 490
 - relationship to austenitizing
 - temperature and time.477-484
 - relationship to tempering
 - temperature and time.483-490
- pure metals222-241
 - as a function of the homol-
ogous temperature ...222-223
 - as a function of melting
point222-223
 - correlation between constant
A and the absolute melting
point 233, 235-236
 - correlation between constant
A ($H = Ae^{-BT}$) and heat
content of liquid metal at
melting point 232-233, 235-236
 - correlation between constant
B ($H = Ae^{-BT}$) and the
reciprocal melting point
.....237-240
 - functional relations224-231
 - fundamental correlations
.....231-239
 - hardness-temperature data 234
 - log hardness vs. temperature
.....227-231
 - aluminum 227
 - cadmium 229
 - copper229, 233
 - molybdenum227, 231
 - thallium228, 232
 - tin 230
 - zinc 228
 - qualitative observations 222-223
 - temperature dependence
.....221-241

Hardness (cont.)

- pure metals
 - temperature dependence
 - equation 231, 236-238, 240-241
 - functions proposed for
.....224-225
- of steels containing silicon
 - effect of silicon on501-507
- of temper-brittle steel
 - effect on impact energy curve.
See Impact energy curves.
- titanium
 - effect of impurities on..235-236
- titanium alloys
 - at low temperatures..1000-1001
- titanium-oxygen alloys 1023-1024

Hardness tester

- for elevated temperature
testing378-383

Heat of activation

- See Activation energy.

High speed steel

- W-Cr-V (18-4-1)
 - effect of austenitizing
 - temperature and time
 - on grain size 481
 - on hardness477-484
 - on impact properties..486-491
 - effect of carbon content
 - on hardness477-483
 - on impact strength ..486-491
 - effect of tempering time
and temperature
 - on hardness483-490
 - on impact strength ..486-491
 - effect of vanadium content
 - on hardness480-481, 484
 - impact strength486-491
 - microstructure481-483

High temperature alloys

- alloy M252 (Ni base)
 - microconstituents in ...397-428
- alloy 16-25-6 (Fe base)
 - microconstituents in ...397-428
- alloy 1336 (Co base)
 - microconstituents in ...397-428

High temperature alloys (cont.)

- alloy 1336 (Nb + Ta)
- microconstituents in ...397-428
- Turballoy 13397-428

Hot hardness tester

- results with various steels.377-396

Impact energy curves

- for SAE 3140 steel733-734
- effect of hardness on ...734-735

Impact properties

- of Fe-Ni-Cr alloys
 - effect of sigma phase on.437-440
 - of high speed steel (18-4-1)
 -486-491
 - of nodular iron at elevated temperatures368, 370-371
- of SAE 3140 steel
 - effect of hardness on. See Impact energy curves.
 - effect of heat treatments on725-731
- of steels containing silicon
 - effect of silicon on521-523
- of temper-brittle steel710-724

Impact strength

- titanium alloys
 - at low temperatures
 -1000-1001, 1003-1004
 - typical fractures ...1003-1004

Inclusions

- effect on machinability
- of AISI B-1112 and B-1113 alloys. See under Free machining steel.

Indium

- effect on properties of molybdenum alloys286-313

Indium-arsenic system

- metallographic analysis ..
-678, 681-684
- phase diagram679-680
- thermal analysis678-679
- X-ray analysis679-680

Interface motions

- during transformation ...561-563

Iron

- effect on properties of molybdenum alloys286-313
- effect on recrystallization of molybdenum alloys314-332
- grain boundary relaxation as a function of the parameter ($D_{gr} e^{Q/RT}$) .279-280
- oxygen content
- isotopic determination. See under Isotopic analysis.

Iron-carbon alloys

- single crystals579-582
- method of producing ... 579
- oscillation diffraction patterns581-582
- rotation diffraction patterns 580

Iron-nickel-chromium alloys

- sigma formation in433-437
- effect on impact properties437-440

Isotopic analysis

- of oxygen in metals and metal oxides
 - apparatus760-761
 - copper and iron-oxygen samples analyzed763-765
 - determination of oxygen in graphite762-766
 - other methods of analysis758-759
 - advantages of isotopic method 766
 - preparation of O^{18} master alloys 762
 - principles of method ...759-760
 - procedure761-762

Lattice parameters

- of microconstituents in high temperature alloys400-411

Low carbon steel

- texture of rolled strip
 - effect of rolling temperature on333-343

Lüders bands

- in titanium tensile specimens
.....988-990

Machinability

- of AISI B-1112 and B-1113 alloys
 - correlation with inclusion characteristics. See under Free machining steel.
- stainless steel, Type 304
 - effect of saw wear on cutting time 948
 - comparison with titanium 948
- titanium957-965
 - effect of arsenic on.957, 961-962
 - effect of beryllium on ..
.....957, 959, 963
 - effect of boron on
.....957-958, 961-962
 - effect of carbon on
.....957-958, 962-963
 - effect of germanium on
.....957, 961, 963
 - effect of phosphorus on
.....957, 961-962
 - effect of selenium on ...
.....957, 960, 962
 - effect of silicon on
.....957, 959, 962-963
 - effect of sulphur on
.....957, 959-960, 962-963
 - effect of tellurium on ...
.....957, 960-962
- high purity iodide vs.
magnesium-reduced
titanium957-960
- saw rating vs. turning index
for various titanium
alloys962-964
- correlation with Vickers
hardness and ultimate
strength963-964
- titanium alloys941-971
 - effect of saw wear on cutting
time 948
 - comparison with Type 304
stainless steel 948
 - effect of test variables ..955-956
 - feed vs. load955-956

Machinability (cont.)

- titanium alloys
 - influence of insoluble
phases941-971
 - lathe test944-947, 954-962
 - method of evaluating.946-947
 - profilometer measure-
ments 954
 - testing equipment ...944-946
 - saw test
....947-949, 957-964, 968-969

Magnetic analysis

- of austenite and sigma
separated from Cr-Ni-Mo-Ti
(18-8-3-1) alloy
.....445-446, 449-450

Magnetic permeability

- stainless steels
 - effect of creep or rupture
test exposure on 73-75

Manganese

- effect on properties of
molybdenum alloys286-313
- effect on recrystallization of
molybdenum alloys314-332

Martensite

- tempering of
effect of silicon on498-532

Martensite transformation**temperature**

- in titanium binary alloys..934-939
- concentration vs. transfor-
mation temperature 935-939
- titanium-chromium ..936-939
- titanium-columbium
.....936, 938-939
- titanium-iron935-939
- titanium-manganese .936-938
- titanium-molybdenum
.....935-936, 938-939
- titanium-tantalum ...
.....936, 938-939
- titanium-tungsten ...936, 938
- titanium-vanadium ..
.....935-936, 938-939

Maximum stress theory

- applied to biaxially stressed
14S-T6
- agreement with fracture
stresses694, 696, 704
- agreement with proportional
limit691-692

Mechanical properties

- of binary molybdenum alloys
.....293-299
- of recrystallized molybdenum
.....321-323
- of recrystallized molybdenum
alloys325-332
- stainless steels
 - effect of creep test exposure
on 58-60
- titanium949-953, 972-992
 - dependence of elastic modulus
on temperature 981
 - dependence of elongation
on temperature979-981
 - effect of strain rate on
.....979-981
 - dependence of fracture stress
on temperature978-980
 - effect of strain rate on
.....978, 980
 - dependence of reduction
of area on temperature
.....980-981
 - effect of strain rate on
.....980-981
 - dependence of yield strength
on temperature977-979
 - effect of strain rate on
.....977, 979
 - dependence of ultimate strength
on temperature 978
 - effect of strain rate on 978
 - effect of arsenic on 950
 - effect of beryllium on .. 949
 - effect of boron on 949
 - effect of carbon on 949
 - effect of germanium on . 950
 - effect of phosphorus on. 950
 - effect of selenium on ... 950
 - effect of silicon on950-953
 - effect of sulphur on949-950

Mechanical properties (cont.)

- titanium
 - effect of tellurium on .. 950
 - fracture appearance at
different temperatures
of testing985, 987-988
 - plastic portion of true stress-
strain curve981-983
 - strain aging effects972-992
 - yield point phenomenon 983-984
- titanium alloys993-1007
 - at low temperatures ..993-1007
 - effect on notch sensitivity
.....996-997
 - effect of testing temper-
ature995-997
- of zirconium-oxygen alloys. See
Zirconium-oxygen alloys.

Mechanical properties, transverse

- forging steel, SAE 1045 .1080-1121
- materials and specimen
preparation1081-1085

Mechanical working

- effect on machinability
of free machining steel . 749

Medium alloy steel

- effect of silicon on tempering
.....498-532

Melting temperatures

- titanium-oxygen alloys .1019-1020

Metal oxides

- isotopic determination of oxygen
content. See Isotopic analysis.

Microconstituents

- in high temperature alloys
.....397-428

Microstructure

- of binary molybdenum alloys
.....300-306
- classification557-561
 - types of interfaces between
crystals558-561
 - coherent and incoherent
boundaries558-561

Microstructure (cont.)

- of Cr-Ni-Mo-Ti (18-8-3-1)
 - alloy450, 452-454
- distribution of dihedral angles
 - resulting from random sectioning543-545
- distribution of minor liquid phase in polycrystalline matrix547, 549
- of Fe-Ni-Cr alloys
 - sigma phase432-433
- forging steel, SAE 1045 .1087-1088
 - air-cooled specimen 1088
 - furnace-cooled specimen 1088
- grain boundary energy
 - variation with thickness at various temperatures below melting point554-555
- grain boundary melting ..551-555
- replacement of grain corners by liquid temperatures below the melting point552-555
- equations552-553
- volume free energy required to produce liquid
 - as a function of temperature553-555
 - as a function of thickness553-555
- of high speed steel (18-4-1)481-483
- of high temperature alloys 397-428
- of indium-arsenic alloys ..681-684
- interface motions during trans-formation561-563
- formation of a nucleus by coherent fluctuations in the vicinity of disordered grain boundary562-563
- interfaces and precipitation562-571
- discontinuous precipitation564-571
- measurement of555-557
- brass
 - beta phase fractions as a function of composition 556

Microstructure (cont.)

- measurement of
 - grid for grain boundary area measurement by intercept counting 557
- plane and curved grain boundaries536-545
- grain shape and grain growth536-545
- disappearance of bubbles by diffusion537-538
- polyphase alloys541-545
- variation of dihedral angle with ratio of interface energies541-542
- of recrystallized molybdenum319-321
- of recrystallized molybdenum alloys322-324, 326
- requirements of space-filling534-545
- basic topological relations534-541
- equations ...534-535, 537-538
- stainless steels 60-73
- changes during creep or rupture test exposure .60-73
 - Type 303 61-66
 - Type 30461, 71-73
 - Type 304L60-61, 63-64
 - Type 316CB61-62, 67-68
 - Type 316L61-62, 65-66
 - Type 32161, 64-69, 71-73
 - Type 34761, 71-73
- of steels containing silicon507-509
- structures with anisotropic interfaces545-548
- titanium alloys951-953
 - titanium - 0.67% arsenic 951, 953
 - titanium - 0.02% beryllium952-953
 - titanium - 0.57% boron .951, 953
 - titanium - 0.47% carbon 951, 953
 - titanium - 0.25% germanium952-953
 - titanium - 0.39% phosphorus952-953
 - titanium - 0.99% selenium952-953

Microstructure (cont.)

- titanium alloys
 - titanium - 0.25% silver .951, 953
 - titanium - 0.32% sulphur
 - as Ti_3S_4 951, 953
 - titanium - 0.118% sulphur
 - as MoS_2 951, 953
 - titanium - 0.47% tellurium
 -952-953
 - titanium, unalloyed952-953
- titanium-oxygen alloys .1012-1019
- of two-phase alloy543-544
 - showing different types
 - of grain junction 544
- of zirconium-nickel alloys.897-898
- of zirconium-oxygen alloys
 -883-884
- of zirconium-silicon alloys 906-912
- of zirconium-tin alloys ...921-927

Minimum creep rate intercept

- variations with stress 55-57
 - effect of temperature .. 57
 - Type 304 stainless steel 57
 - Type 304L stainless steel 57
 - Type 316CB stainless steel 57
 - Type 316L stainless steel 57
 - Type 321 stainless steel 57
 - Type 347 stainless steel 57

Modulus of elasticity

- determined ultrasonically for
 - brass847-848, 850-852
 - beryllium850-852
 - columbium850-852
 - thorium850-852
 - titanium850-852
 - Type 347 stainless steel.848-852
 - uranium850-852
 - vanadium850-852
 - zirconium850-852
- influence of anelasticity on
 -815-817

Molybdenum

- elastic constants determined
 -855-857
- furnace for melting862-871
- hardness227, 231
 - log hardness vs. reciprocal
 - temperature227, 231

Molybdenum (cont.)

- hardness
 - log hardness vs. temperature
 -227, 231
- recrystallization of. See under
 - Recrystallization.

Molybdenum alloys, binary

- alloys investigated289-291
- effect of deoxidation312-313
- elevated temperature hard-
 - ness299-301
- fabricability290-292
- microstructure300-306
- most effective alloying
 - additions305-311
- preparation of alloys287-288
- recrystallization of. See under
 - Recrystallization.
- room temperature properties
 -293-299
- strength-elongation
 - correlation305-309
- strength-hardness
 - correlation307-309
- sintering characteristics ..291-292
- test methods287-289

Monel

- creep-rupture properties .
 -151-169, 181-195
- effect of atmosphere on.. 181
- stress vs. minimum creep
 - rate189-195
- effect of grain size on .189-195
- effect of testing tem-
 - perature189-195
- stress vs. rupture life ..182-190
 - effect of grain size on.182-190
 - effect of testing tem-
 - perature182-190
- creep-rupture tests
 -158-159, 163-164
- comparison of static recrystallization, equicohesion
 - and hardness163-164
- oxide penetration during
 -158-159
- ductility183-186, 191-197
 - effect of composition 193

Monel (cont.)

- ductility
 - influence of grain size...
 -183-186, 191-192, 194-197
 - influence of stress
 -183-186, 191-192, 194-197
 - influence of testing temperature
 -183-186, 191-192, 194-197
- high temperature properties177-197
 - influence of grain size on177-197
- recrystallization .158-163, 171-176
 - cold work vs. temperature for159, 161
 - during creep-rupture testing160-163
 - hardness vs. temperature158, 161
- stress-rupture properties152-159, 164-170
 - graphical method of extrapolating and interpolating short-time data ..167-169
 - stress vs. minimum creep rate
 - effect of cold work ..166-167
 - effect of testing temperature166-167
 - stress vs. rupture life..
 - ...152-159, 164-165, 167-170
 - effect of cold work ..
 -153-159, 164-165, 167
 - effect of testing temperature ..153-154, 156-157, 164-165, 167-170

Nickel

- effect on properties of molybdenum alloys286-313
- effect on recrystallization of molybdenum alloys..314-332

Nickel-iron alloys

- order-disorder transformation1051-1054
- dilatometric measurements1052-1053
- phase fields for ordering reaction 1053

Niobium

- furnace for melting.....862-871

Nodular iron

- elevated temperature impact properties ...368, 370-371
- elevated temperature tensile properties .365-367, 369-370
- microstructure
 - annealed364-365
 - as-cast363-364
- stress-rupture data at 1200 °F368-369, 371-373
- fracture structure371-373

Notch sensitivity factor

- of temper-brittle steel ... 718

Order-disorder transformation

- as a classical phase
 - change1029-1055
- arguments against and rebuttal1039-1042
- analogy with established second-order transformations1041-1042
- electrical resistance.1039-1040
- hysteresis 1041
- microstructure 1041
- specific heat 1040
- X-ray diffraction ..1040-1041
- consequences of1042-1044
 - impact upon ordering theory 1044
 - nature of the ordered and disordered phases . 1042
- equilibrium coexistence of two phases in the ordering transformation interval1034-1036
- evidence in support of .1031-1039
- ordered and disordered phase coexistence1036-1037
- metallographic evidence1036-1037
- X-ray evidence 1036
- published evidence of a discontinuous ordering transformation 1034
- dilatometric observations.1034
- resistivity measurements.1034

Order-disorder trans. (cont.)

- as a classical phase change
- rate of the ordering trans-formation1037-1039
- dependence upon temper-ature 1038
- nickel-iron alloys1051-1054
- dilatometric measurements on1052-1053
- phase fields for ordering reaction 1053

Orowan's equation266-270

Oxygen

- effect on properties of zirconium. See Zirconium-oxygen alloys.
- in metals
- isotopic determination. See under Isotopic analysis.

Pearlite

- orientation relationships in568-571

Phase diagrams

- indium-arsenic679-680
- titanium-oxygen1012-1014
- zirconium-nickel, partial .. 895
- beta field 896
- zirconium-silicon903-905
- zirconium-tin918-919

Phosphorus

- effect on properties of molybdenum alloys286-313

Plastic deformation

- role of anelasticity in
- 817-822, 827-837

Poisson's ratio

- determined ultrasonically for
- brass847-848, 850-852
- beryllium850-852, 855-857
- columbium850-852
- molybdenum855-857
- thorium850-852
- titanium850-852, 855-857
- Type 347 stainless steel
- 848-852

Poisson's ratio (cont.)

- determined ultrasonically for
- uranium850-852
- vanadium850-852
- zirconium850-852, 855-857

Precipitation

- discontinuous564-566
- analogy with recrystalli-zation 564
- copper-silver alloy 566
- zinc-copper alloy564-565

President's Annual Address

6

Proportional limit

- of 14S-T6 stressed biaxially
- agreement with maximum stress theory691-692

Recrystallization

- alpha brass201-211
- activation energy208-211
- schematic representation 209
- heat of activation208-211
- effect of initial grain size210-211
- effect of prior defor-mation208-211
- relation between recrystal-lized grain size and de-formation206-207
- relation between recrystal-lized grain size and ini-tial grain size207-208
- relation between recrystal-lized grain size and tem-perature of annealing.206-207
- times and temperatures for204-205, 210
- analogy with discontinuous precipitation 564
- of molybdenum
- effect of annealing temper-ature on microstructure 320-321
- effect on tensile properties321-323
- grain sizes319-321
- recrystallization character-istics320-322

Recrystallization (cont.)

- of molybdenum alloys
 - alloys tested315-317
 - effect of annealing on...325-332
 - effect on tensile properties
 -325-332
 - relationship to alloy con-
 - centration327-329
 - grain refining action of al-
 - loying additions 326
 - microstructures ...322-324, 326
- monel158-163, 171-176
- cold work vs. tempera-
 - ture for159, 161
- during creep-rupture
 - testing160-163
- hardness vs. temperature
 -158, 161

Relaxation

- role of anelasticity in. See
 - Anelasticity.

Relaxation rigidity

- as a function of the
 - parameter ($AD^{1.00} e^{Q/RT}$)
 -280-281, 283
 - aluminum280-281, 283
 - aluminum-copper alloys .280-281
 - aluminum-germanium
 - alloys280-281
 - aluminum-magnesium
 - alloys 283
 - aluminum-silver alloys .280-281
 - aluminum-zinc alloys .. 280

Residual stresses

- Armco iron
 - X-ray measurement of .672-673
 - skewness index as a func-
 - tion of the rotation an-
 - gle ψ 672-673
- in manganese oil hardening
 - tool steel
 - effect of quenching and
 - tempering on605-615
- optical interference method
 - for determining607-612
- curvature measurements 609-611
 - graph showing curvature
 - variation with metal re-
 - moved 610

Residual stresses (cont.)

- optical interference method
 - metal layer removal tech-
 - niques607-609
 - stress calculation611-612
- in steel, FS 1050
 - X-ray measurement of .670-672
 - decrease in the biaxial stress
 - sum as a function of
 - the applied bending
 - stress670-672
 - intensity distribution about
 - the apparent maxi-
 - mum of the broadened
 - 211 K_{α} -doublet670-671
- in steel, high carbon638-676
- stress measurements of
 - martensitic phase .654-661
 - effect of cold work on .655-657
 - effect of electrolytic
 - polishing on657-659
 - effect of stressing be-
 - yond the yield strength
 - on658-660
- X-ray measurement of .638-676
- diffraction pattern obtained
 - using various radia-
 - tions645-646
 - effect of specimen orienta-
 - tion on line sym-
 - metry646-647
- experimental necessities
 - for determining ...642-644
- principles639-642
- technique644-653
- variation of "d" value with
 - orientation of speci-
 - mens652-653
 - variation in relative inten-
 - sity with 2θ 647-651
 - correction factors to com-
 - pensate for intensity
 - variation
 - 647-651, 661-666
- in tool steel607-617
- curvatures induced in
 - specimens607-609
 - by etching607-609
 - by lapping608-609

Residual stresses (cont.)

in tool steel

effect of etching on ...

..... 607-609, 614-615

effect of grinding on

..... 609, 614-615

effect of lapping on....

..... 608-609, 614-615

effect of tempering on sur-

face stress 612-614, 617

equations for determin-

ing 611

Resistivity

of zirconium-oxygen alloys

..... 879-881

Retained austenite

effect of silicon on transition

temperatures 504-505

Rimmed steel

strain aging characteristics

..... 344-361

Rolling temperature

effect on texture

of low carbon steel strip .333-343

Rupture

chromium-nickel steels .. 42-76

Secretary's Annual Report . 15**Shear modulus. See Modulus of elasticity.****Sigma phase**

in Cr-Ni-Mo-Ti (18-8-3-1) alloy

electrolytic separation

..... 444-445, 447-449

properties 449-460

in Fe-Ni-Cr alloys of Types

310, 330 and Incoloy

effect on impact properties

and hardness 437-440

effect of silicon on 434-435

limiting composition free of

sigma 436-437

sigma boundaries 433-436

Silicon

effect on machinability

of free machining steel

..... 744, 746-748

Silicon (cont.)

effect on properties of

molybdenum alloys ...286-313

effect on recrystallization of

molybdenum alloys314-332

effect on tempering of martensite
dilatometric measurements

..... 509-513

electrical resistivity meas-

urements 513-514

hardness effects 501-507

relationship to tempering

time 505-507

microstructures 507-509

properties vs. tempering

time 521-523

specific volume measure-

ments 514-516

steels tested 499-500

theory regarding 520-525

X-ray diffraction meas-

urements 516-520

in Fe-Ni-Cr alloys

effect on sigma formation

..... 434-435

Slip theory

inconsistencies for biaxially

stressed 14S-T6 705

Soap bubbles

disappearance of cells by

diffusion 537-538

with increasing fraction of

liquid phase 549-550

Specific volume measurements

of steels containing silicon

effect of silicon during

tempering 514-516

Stainless steels

austenite to martensite trans-

formation 77-95

effect of carbide precipita-

tion on the beginning of

transformation .. 82-87, 93-94

effect of composition on

temperature of 77-95

procedure for determining .80-85

Stainless steels (cont.)

austenite stabilizers	
chromium or nickel equiv-	
alents	78-80
carburization	134-148
apparatus	135
with graphite	134-147
air atmosphere	138-141, 143
ammonia atmosphere	138-145
argon atmosphere	138-141, 143
correlation between depth	
of carburization and cor-	
rosion rates	
.....	139, 143, 146, 148
prior oxidized surface	
.....	138, 141-142, 144
Type 304	138, 142, 146
Type 316	138-146
Type 347	138, 141, 146
procedure	135-137
chromium-nickel	
creep and rupture	42-76
creep-rupture curves	
effect of carbon ...	114-115, 122
effect of nitrogen ..	114-115, 123
creep-rupture properties ..	105-132
ductility	116-117, 119
effect of carbon	117, 119
effect of nitrogen ...	117, 119
effect of testing tem-	
perature	117, 119
effect of carbon ...	105, 108-110
effect of carbon and ni-	
trogen	111
effect of microstructure	
on	120-131
effect of nitrogen on ..	
.....	105, 111, 113, 115
effect of testing temper-	
ature	100-112, 114-127, 130-132
minimum creep rates ..	
.....	114, 120-121, 127, 130
variation as a function of	
carbon plus nitrogen	
content	
.....	114, 120-121, 127, 130
procedure for determin-	
ing	106-108
rupture life	111-114, 118-119, 127

Stainless steels (cont.)

creep-rupture properties	
rupture life	
variation as a function of	
carbon plus nitrogen	
content	111-114, 118-119, 127
stress vs. minimum creep	
rate	111-112, 116
stress vs. rupture life ..	
.....	109-110, 115
stresses for specified rup-	
ture times	115-117
effect of carbon plus ni-	
trogen content	115-117
effect of testing temper-	
ature	115-117
creep-rupture strength	
effect of molybdenum ..	48-50, 52
creep strength	53-56
effect of carbon on	54-55
effect of columbium on ..	55
effect of nitrogen on ..	54
variation with temperature	
.....	53-56
Type 303	54
Type 304	53-54
Type 304L	53-54
Type 316	53, 55
Type 316L	53, 55
Type 321	53-54, 56
Type 347	53, 56
delta factor vs. M. temper-	
ature	96-97, 101
elongation at rupture vs.	
rupture time	46-55, 57-58
effect of temperature ..	46-55
Type 304	50
Type 304L	47
Type 316CB	49
Type 316L	48
Type 321	51
Type 347	52
hardness vs. hardening tem-	
perature	97-98
431 + Mo alloy	97-98
machinability	948
effect of saw wear on cut-	
ting time	948
comparison with tita-	
nium	948

Stainless steels (cont.)

- magnetic permeability ... 73-75
 - changes during creep or rupture test exposure ... 73-75
- mechanical properties
 - effect of creep test exposure on 58-60
- microstructure
 - changes during creep or rupture test exposure . 60-73
 - Type 303 61-66
 - Type 304 61, 71-73
 - Type 304L 60-61, 63-64
 - Type 316CB 61-62, 67-68
 - Type 316L 60-62, 65-66
 - Type 321 61, 64-69, 71-73
 - Type 347 61, 71-73
- minimum creep rate intercept 55-57
 - effect of temperature .. 57
 - Type 304 57
 - Type 304L 57
 - Type 316CB 57
 - Type 316L 57
 - Type 321 57
 - Type 347 57
- mode of fracture
 - effect of creep or rupture test exposure on 70, 73
- M_s temperature ... 88-93, 102-103
 - effect of annealing temperature on 102-103
 - effect of carbon plus nitrogen on 88
 - effect of chromium 88-90
 - effect of manganese ... 89, 91
 - effect of nickel 88-90
 - effect of quenching rate. 102-103
 - effect of silicon 89, 91-92
 - equation 92
 - measured vs. calculated values 92-93
- precipitated carbide
 - after exposure to elevated temperatures 126-128
- precipitated nitride
 - after exposure to elevated temperatures 126-128
- reduction of area at rupture vs. rupture time 46-55, 57-58

Stainless steels (cont.)

- reduction of area at rupture vs. rupture time
 - effect of temperature .. 46-55
 - Type 304 50
 - Type 304L 47
 - Type 316CB 49
 - Type 316L 48
 - Type 321 51
 - Type 347 52
- retained austenite 117-118, 120-127
 - after creep-rupture tests 120-121, 126-127
 - effect of carbon content 126-127
 - effect of cold work .. 126-127
 - effect of nitrogen content 126-127
 - effect of testing temperature 126
 - after exposure to elevated temperatures 117-118, 120, 122-127
 - effect of carbon content 124
 - effect of cold work 120, 125, 127
 - effect of nitrogen content 124
 - effect of testing temperature 124
- stress vs. minimum creep rate
 - effect of temperature .. 46-55
 - Type 303 53
 - Type 304 50
 - Type 304L 47, 53
 - Type 316CB 49
 - Type 316L 48
 - Type 321 51, 53
 - Type 347 52
- stress vs. ratio of elongation at rupture to time at rupture 46-55
 - effect of temperature .. 46-55
 - Type 304 50
 - Type 304L 47
 - Type 316CB 49
 - Type 316L 48
 - Type 321 51
 - Type 347 52

Stainless steels (cont.)

- stress vs. time for beginning
 - of tertiary creep or time
 - for rupture 46-56
- effect of temperature... 46-55
 - Type 304 50
 - Type 304L 47
 - Type 316CB 49
 - Type 316L 48
 - Type 321 51
 - Type 347 52
- Type 18 Cr-8 Ni
 - hardness at elevated tem-
 - peratures 387-390
 - relationship to strength
 - and creep 391-393
- Type 347
 - elastic constants deter-
 - mined 848-852
- Type 431 + Mo alloy
 - hardness vs. aging time 98-99
 - hardness vs. hardening
 - temperature 97-98
 - microstructure 98-99

Steel

- carburizing
 - effect of boron on case
 - hardenability.
 - See Carburizing steels, alloy.
 - effect of silicon on tempering.
 - See under Silicon.
- flow stress 250-251
 - effect of mean distance
 - between particles on .250-251
- plain carbon
 - hardness at elevated tem-
 - peratures 390-391
 - relationship to strength
 - and creep 391-393
- residual stress in
 - stress measurements of
 - austenitic phase ... 657-661
 - effect of electrolytic pol-
 - ishing 657, 659
 - effect of stressing beyond
 - the yield strength.. 658-660
 - stress measurements of
 - martensitic phase
 - 654-658, 660

Steel (cont.)

- residual stress in
 - stress measurements of
 - martensitic phase
 - effect of cold work on .655-657
 - effect of electrolytic
 - polishing on 657-658
 - effect of stressing beyond
 - yield strength on .. 658-660
 - X-ray measurement of. 638-676
 - decrease in the biaxial stress
 - sum as a function of
 - the applied bending
 - stress 670-672
 - diffraction pattern obtained
 - using various radia-
 - tions 645-646
 - effect of specimen ori-
 - entation on line
 - symmetry 646-647
 - experimental necessities
 - for determining ... 642-644
 - principles 639-642
 - technique 644-653
 - variation of "d" value with
 - orientation of speci-
 - mens 652-653
 - variation in relative in-
 - tensity with 2θ .. 647-651
 - correction factors to com-
 - pensate for intensity
 - variation. 647-651, 661-666
- strain aging of sheet 344-361

Steel, alloy

- 8 Cr-1 Mo type
 - hardness at elevated tem-
 - peratures 390-393

Steel, eutectoid

- tensile properties
 - influence of structure on .252-253

Steel, trade designations

- AISI B-1112 and B-1113 alloys
 - effect of inclusions on machin-
 - ability. See under Free ma-
 - chining steel.
- SAE 3140
 - impact energy curves
 - effect of hardness on. 732-740

Steel, trade designations (cont.)

SAE 3140 temper brittleness
effect of various heat treatments
on. See under Temper brittleness.

SAE 5140
endurance limit710-724

Strain aging

of commercial sheet steels
accelerated test 351
in predicting age hardening352-354
in predicting yield point behavior354-357
factors affecting rimmed steel346-350
factors affecting stabilized steel350-351
natural aging344-346

Strain hardening index

correlation with deformation stress252-253

Stress concentration factor

of temper-brittle steel ...719-721

Stress-rupture properties

monel152-159, 164-170
graphical method of extrapolating and interpolating short-time data167-169
stress vs. minimum creep rate
effect of cold work ..166-167
effect of testing temperature166-167
stress vs. rupture life ..
..... 152-159, 164-165, 167
effect of cold work..
..... 153-159, 164-165, 167
effect of testing temperature ..153-154,
156-157, 164-165, 167-170
of nodular iron at 1200 °F.368-373

Stress-strain relations

for biaxially stressed 14S-T6.
See Biaxial tensile stresses.

Sulphur

effect on machinability
of free machining steel .749-750

Sulphur (cont.)

effect on properties of molybdenum alloys286-313

Surface-tension equilibrium

in polyphase alloys541-545

Tantalum

furnace for melting862-871

Technical Program and Reports of Officers, ASM—34th Annual Convention, Philadelphia, October 18 to 24, 1952 1

Temper brittleness

effect of various heat treatments of SAE 3140 on
heat treatments tested .726-727
impact test results726-730
transition curves727-730
of SAE 3140 steel
effect of hardness on impact
energy curves732-740

Temper-brittle steel

endurance limit of
SAE 5140710-724
heat treatments used ..712-714
impact properties
..... 714-715, 717-719
notch sensitivity factor . 718
stress concentration
factor719-721
tensile properties ..715, 717-719

Tempering

first-stage kinetics582-590
length changes on tempering583-588
effect of carbon content583-588
rate equation585, 587-590
values of m for 589
values of rate constant K589-590
first-stage products of decomposition578-582
 ϵ -iron carbide578,
581, 585, 587-588, 590-591
formula 587

Tempering (cont.)

- of high speed steel 18-4-1
 - effect of time and temperature
 - on hardness .483-486, 488-490
 - on impact strength ..486-491
- low carbon martensitic phase
 - 578-579, 581-582
- carbon content of579, 582
 - effect of tempering
 - temperature on ... 582
- of martensite
 - effect of silicon on. See under Silicon.
- mechanism and kinetics of the
 - first stage576-595
 - model591-594
 - carbon concentration gra-
dients at advancing front
 - 592-593
 - plane-front growth of ag-
gregate at expense of
primary martensite 592
 - rate constant K592-594
 - composition dependence 594
 - temperature depend-
ence592-594
 - second stage of595-597
 - activation energies for..595-597
 - variation with carbon
content596-597
 - length changes from decom-
position of austenite..595-596

Tempering temperature

- of steels containing silicon
 - effect on properties521-523

Tensile properties

- aluminum-copper alloys ..249-270
 - effect of dispersions on.249-270
 - method of determining
 - 254-262
- eutectoid steel252-253
 - influence of structure on.252-253
- forgings, SAE 10401096-1099
 - longitudinal1098-1099
 - effect of cooling rate
 - 1098-1099
 - transverse1097-1098
 - effect of cooling rate
 - 1097-1098

Tensile properties (cont.)

- forging steel, SAE 1045.1086-1116
 - correlation coefficients
 - 1086-1087, 1092, 1103
 - effect of angle of test on
 - .. 1099-1101, 1108, 1110-1111
 - elongation vs. angle of
test 1108
 - reduction of area vs.
angle of test 1108
 - effect of homogenization
treatments on
..... 1088-1089, 1094-1096
 - quenched and tempered
specimens1101-1113
 - effect of angle of test
on1108, 1110-1111
 - effect of reduction by
forging 1101
 - reduction of area frequency
curves1085-
1086, 1094, 1096, 1115-1116
 - furnace-cooled speci-
mens 1085
 - homogenized speci-
mens1094, 1096
 - quenched and tempered
specimens 1086
 - reduction of area vs. reduc-
tion by forging ...
.....1088-1089,
1092-1096, 1103-1107, 1110
 - effect of homogenization
treatment on
..... 1088-1089, 1094-1096
 - effect of tempering tem-
perature ...1103, 1105-1106
 - regression lines
1086-1087, 1092, 1103-
1104, 1106-1107, 1109-1110
 - tensile strength vs. longi-
tudinal reduction of
area1103-1104, 1107
 - yield strength vs. longi-
tudinal reduction of
area1103-1104, 1106
 - yield strength vs. trans-
verse reduction of
area1103-1104, 1107

Tensile properties (cont.)

- forging steel, SAE 1045
 - specimens containing ferrite and pearlite 1088-1096, 1099-1101
- of temper-brittle steel
 - SAE 5140 715, 717-719

Test

- for strain aging of steel .. 351-357

Thallium

- hardness
 - log hardness vs. temperature 228, 232
 - showing allotropic transformation 228, 232

Thorium

- effect on properties of
 - molybdenum alloys 286-313
- effect on recrystallization of
 - molybdenum alloys 314-332
- elastic constants determined 850-852
- furnace for melting 862-871

Tin

- effect on properties of
 - molybdenum alloys 286-313
- hardness
 - log hardness vs. temperature 230

Titanium

- elastic constants determined 850-852, 855-857
- furnace for melting 862-871
- hardness 235-236
 - effect of impurities on .. 235-236
- Lüders bands in tensile
 - specimens 988-990
- machinability 957-965
 - effect of arsenic on. 957, 961-962
 - effect of beryllium on 957, 959, 963
 - effect of boron on 957-958, 961-962
 - effect of carbon on 957-958, 962-963
 - effect of germanium on 957, 961, 963

Titanium (cont.)

- machinability
 - effect of phosphorus on 957, 961-962
 - effect of selenium on 957, 960, 962
 - effect of silicon on 957, 959, 962-963
 - effect of sulphur on 957, 959-960, 962-963
 - effect of tellurium on 957, 960-962
- high purity iodide vs. magnesium-reduced titanium 957-960
- mechanical properties 949-953, 972-992
 - dependence of elastic modulus on temperature 981
 - dependence of elongation on temperature 979-981
 - effect of strain rate on 979-981
 - dependence of fracture stress on temperature 978-980
 - effect of strain rate on 978, 980
 - dependence of reduction of area on temperature 980-981
 - effect of strain rate on 980-981
 - dependence of yield strength on temperature 977-979
 - effect of strain rate on 977, 979
 - dependence of ultimate strength on temperature 978
 - effect of strain rate on 978
 - effect of arsenic on 950
 - effect of beryllium on .. 949
 - effect of boron on 949
 - effect of carbon on 949
 - effect of germanium on. 950
 - effect of phosphorus on. 950
 - effect of selenium on ... 950
 - effect of silicon on 950-953
 - effect of sulphur on 949-950
 - effect of tellurium on .. 950

Titanium (cont.)

- mechanical properties
 - fracture appearance at
 - different temperatures
 - of testing985, 987-988
 - plastic portion of true stress-strain curve981-983
 - strain aging effects972-992
 - yield point phenomenon.983-984
- stress-strain diagrams ...
 -975-977, 983-986
- effect of aging temperature
 - on984-986
- effect of increasing strain
 - on the appearance of a yield point following aging985-986
- effect of a prestrain at
 - liquid nitrogen on983-984
- effect of strain rate on..975, 977
- effect of testing temperature on975-977

Titanium alloys

- coefficients of expansion at
 - various temperatures.1001-1003
- fatigue properties..998-1001, 1003
 - at low temperatures ...
 -998-1001, 1003
 - effect of notch on ...998-1000
 - typical fractures ...1001, 1003
- hardness1000-1001
 - at low temperatures ..1000-1001
- impact strength
 -1000-1001, 1003-1004
 - at low temperatures ..1000-1001
 - typical fractures ...1003-1004
- machinability941-971
 - effect of saw wear on cutting
 - time 948
 - comparison with Type 304
 - stainless steel 948
 - effect of test variables..955-956
 - feed vs. load955-956
 - influence of insoluble
 - phases941-971
 - lathe test944-947, 954-962
 - method of evaluating.946-947
 - profilometer measurements 954

Titanium alloys (cont.)

- machinability
 - saw rating vs. turning index
 - for various titanium alloys962-964
 - correlation with Vickers
 - hardness and ultimate strength963-964
 - saw test
 -947-949, 957-964, 968-969
- mechanical properties
 - at low temperatures ..993-1007
 - effect on notch sensitivity
 -996-997
 - effect of testing temperature on995-997
- microstructure951-953
 - titanium - 0.67% arsenic
 -951, 953
 - titanium - 0.02% beryllium
 -952-953
 - titanium - 0.57% boron .951, 953
 - titanium - 0.47% carbon 951, 953
 - titanium - 0.25% germanium
 -952-953
 - titanium - 0.39% phosphorus
 -952-953
 - titanium - 0.99% selenium
 -952-953
 - titanium - 0.25% silver .951, 953
 - titanium - 0.32% sulphur
 - as Ti_3S_4 951, 953
 - titanium - 0.118% sulphur
 - as MoS_2 951, 953
 - titanium - 0.47% tellurium
 -952-953
 - titanium, unalloyed952-953

Titanium binary alloys

- martensite transformation
 - temperature934-939
- concentration vs. transformation temperature 935-939
 - titanium-chromium ..936-939
 - titanium-columbium
 -936, 938-939
 - titanium-iron935-939
 - titanium-manganese .936-938
 - titanium-molybdenum
 -935-936, 938-939

Titanium binary alloys (cont.)

- martensite transformation temp.
concentration vs. trans. temp.
titanium-tantalum ...
.....936, 938-939
- titanium-tungsten ...936, 938
- titanium-vanadium ..
.....935-936, 938-939

Titanium-oxygen

- phase diagram1012-1014

Titanium-oxygen alloys

- hardness1023-1024
- microstructures1012-1019

Titanium-oxygen system 1008-1028

- annealing treatments ..1010-1011
- appearance of ingots..1010-1011
- melting-range determinations
.....1019-1020
- melting temperatures .. 1020
- preparation of alloys ...1010-1012
- X-ray diffraction studies of
.....1020-1022
- alpha solid solution ..1020-1021
- lattice parameter-
composition curves 1021
- intermediate phase between
alpha and TiO ...1022-1023
- delta phase1022-1023
- intermediate phase TiO
.....1021-1022
- lattice parameter-
composition curves 1022

Tool steel

- residual stresses in605-617
- curvatures induced in
specimens607-609
- by etching607-609
- by lapping608-609
- effect of etching on
.....607-609, 614-615
- effect of grinding on ...
.....609, 614-615
- effect of lapping on
.....608-609, 614-615
- effect of quenching and
tempering on605-615
- effect of tempering on
surface stress612-614, 617

Tool steel (cont.)

- residual stresses in
stress distribution611-613
- equation for determining 611

Transition temperatures

- of SAE 3140 steel
after various heat treat-
ments727-730

Treasurer's Annual Report.. 10**Tungsten**

- effect on properties of
molybdenum alloys286-313
- effect on recrystallization of
molybdenum alloys314-332

Tungsten-chromium-vanadium steel

- high speed steel 18-4-1. See
under High speed steel.

Ultrasonics

- use in determining elastic
constants
apparatus and experimental
technique845-849
- of beryllium ...850-852, 855-857
- of brass847-848, 850-852
- of columbium850-852
- elastic constant equations 845
- of molybdenum855-857
- possible reasons for dis-
crepancies856-859
- of thorium850-852
- of titanium850-852, 855-857
- of Type 317 stainless steel
.....848-852
- types of elastic waves prop-
agated in solids ...839-840
- wave reflections at bound-
aries840-841
- of uranium850-852
- of vanadium850-852
- wave propagation between
parallel faces of solids 841-842
- wave propagation in cylin-
drical rods842-844
- measurement of wave
velocities844-845
- of zirconium ...850-852, 855-857

Uranium

- elastic constants determined
.....850-852
- furnace for melting862-871

Vanadium

- in carburizing steels
 - effect with boron on case
hardness778, 783
- elastic constants determined
.....850-852
- in high speed steel 18-4-1
 - effect on hardness
.....480-481, 484

Vanadium rimmed steel

- strain aging characteristics
.....344-361

X-ray diffraction study

- of austenite and sigma
 - separated from Cr-Ni-Mo-Ti
(18-8-3-1) alloy 445
- of microconstituents in high
temperature alloys397-428
- of rolled low carbon steel
 - effect of rolling temperature
on texture333-343
- of steels containing silicon
 - effect of silicon during
tempering516-520

Yield strength

- of 14S-T6 stressed biaxially
agreement with distortion
energy theory 692

Young's modulus

- See Modulus of elasticity.

Zinc

- hardness
 - log hardness vs. temper-
ature 228

Zinc-copper alloy

- discontinuous precipitation in
.....564-565

Zirconium

- arc melting furnace for
 - advantages 870
 - applicability to other
metals869-870
 - design of furnace864-866
 - operation of furnace ...865-869
 - pressed zirconium electrodes
used863-864
- elastic constants determined
.....850-852, 855-857
- properties of high purity
zirconium. See Zirconium-
oxygen alloys.

Zirconium-nickel system

- microstructures897-899
- phase diagram, partial ... 895

Zirconium-oxygen alloys

- effect of oxygen on hardness
.....881-882
- effect of oxygen on recrystal-
lization 884
- effect of oxygen on resistivity
.....879-881
- effect of oxygen on tensile
properties882-883
- effect of oxygen on thermal
conductivity 881
- elevated temperature tensile
properties885-889
- hydrogen content of zirconium
.....876-877
- microstructure883-884
- oxygen diffusion rate in
zirconium884-885
- preparation of alloys877-878
- stress-strain curves at various
temperatures886, 888-889
- table of physical and
mechanical properties .. 880
- workability883-884

Zirconium-silicon system

- microstructures906-912
- phase diagram903-905

Zirconium-tin system

- microstructures921-927
- phase diagram918-919

